UNITED STATES DISTRICT COURT
FOR THE DISTRICT OF MASSACHUSETTS

PROGENICS PHARMACEUTICALS, INC., and EXINI DIAGNOSTICS AB, Plaintiffs, v. MIM SOFTWARE INC., Defendant.	Civil Action No. 1:24-cv-10437-PBS **JURY TRIAL DEMANDED**

SECOND AMENDED COMPLAINT

Plaintiffs Progenics Pharmaceuticals, Inc. ("Progenics") and EXINI Diagnostics AB ("EXINI") (collectively, "Plaintiffs") hereby file this Second Amended Complaint for patent infringement against Defendant MIM Software Inc. ("MIM"), alleging as follows:

NATURE OF THE ACTION

1. This case is about medical imaging technology that enables improved diagnosis and treatment of cancer and other serious diseases. Plaintiffs pioneered techniques to advance the reliability and accuracy of diagnostic imaging tests like computed tomography (CT) scans or positron emission tomography (PET) scans. More specifically, the inventors developed and patented new systems and methods to help physicians more consistently and accurately interpret the images produced by those types of scans.

2. Plaintiffs own numerous patents that claim inventions in the field of medical imaging analysis and interpretation, specifically including U.S. Patent No. 10,665,346 ("the '346 patent"), U.S. Patent No. 10,973,486 ("the '486 patent"), U.S. Patent No. 11,424,035 ("the '035 patent"), U.S. Patent No. 11,894,141 ("the '141 patent"), U.S. Patent No. 11,657,508 ("the '508

patent"), U.S. Patent No. 11,721,428 ("the '428 patent"), and U.S. Patent No. 11,941,817 ("the '817 patent") (the "Asserted Patents").

3. Through this case, Plaintiffs seek to protect their significant investment in medical imaging technology, which facilitates their commitment to the advancement of disease diagnosis and treatment.

4. In doing so, Plaintiffs aim to redeem the basic principle that Defendant MIM cannot infringe Plaintiffs' patents simply because MIM would prefer not to pay for a license to Plaintiffs' coveted, patented technology.

5. Defendant MIM sells imaging tools for radiation oncology, radiology, and nuclear medicine, including software products like Contour ProtégéAI®, MIM SurePlan™ MRT, LesionID®, and LesionID Pro® (the "Infringing Products") that analyze and display scan results to physicians, and which are part of MIM's broader software suite along with MIM Encore®, PET Edge®, MIM Assistant®, and MIMcloud®. In 2020, MIM and Plaintiffs began discussing potentially integrating the inventions claimed in the Asserted Patents (amongst other technological advances) into MIM's nuclear imaging software platform. Pursuant to a Confidential Disclosure Agreement signed in 2021, Plaintiffs agreed to explore a possible integration with MIM. In other words, MIM was considering licensing Plaintiffs' patented technology so that the two companies could partner. As part of that effort, Plaintiffs shared their patented inventions with MIM and helped MIM consider how those inventions could improve MIM's software. An inventor of the '486 patent (Karl Sjöstrand) and an inventor of the '508 and '817 patents (Aseem Undvall Anand) even agreed to work with MIM on that project.

6. In October 2022, about two years after the partnership discussions began, Plaintiffs sent MIM a draft Collaboration Agreement. The Collaboration Agreement included a list of Plaintiffs' relevant patents and patent applications—including nearly all of the Asserted Patents.

7. Months went by, and Plaintiffs heard nothing back from MIM about the draft Collaboration Agreement, even though MIM continued to emphasize its interest in incorporating Plaintiffs' patented technology into MIM's software.

8. Clouds gathered around June 2023 when Plaintiffs discovered that MIM had begun publishing articles and website materials describing new features included in multiple MIM products, including the Infringing Products. MIM's publications were and are troubling to Plaintiffs. They plainly show that MIM took the inventions claimed in the Asserted Patents and, instead of licensing the technology from Plaintiffs, simply integrated the inventions into the Infringing Products without Plaintiffs' permission.

9. Making matters worse, MIM relied on Plaintiffs' patented innovations to induce GE HealthCare to acquire MIM in January of this year. Apparently, MIM had been pursuing acquisition by GE HealthCare for months while simultaneously incorporating Plaintiffs' patented inventions into MIM's software. GE HealthCare announced the official close of the acquisition on April 1, 2024.

10. Upon information and belief, MIM disregarded the Asserted Patents after deciding that paying for a license would be inconvenient. MIM infringed the Asserted Patents to both improve its software and market itself to its eventual acquirer, GE HealthCare.

11. Plaintiffs thus bring this suit to put a stop to MIM's illegal conduct and obtain compensation for MIM's intentional wrongdoing.

THE PARTIES

12. Plaintiff Progenics is a corporation organized and existing under the laws of the State of Delaware, having its principal place of business at 201 Burlington Road, South Building, Bedford, Massachusetts 01730. Progenics is an oncology company focused on the development and commercialization of innovative targeted medicines and artificial intelligence to find, fight, and follow cancer. Progenics is a subsidiary of Lantheus Holdings, Inc., along with EXINI.

13. Plaintiff EXINI is a corporation organized and existing under the laws of Sweden, having its principal place of business at Scheelevägen 27, Ideon Science Park, Gateway, 223 70 Lund, Sweden. EXINI develops advanced software for medical image analysis. EXINI's products are developed using unique image analysis derived from expert knowledge in nuclear medicine, image analysis, handling of large databases, and machine learning. Like Progenics, EXINI is a subsidiary of Lantheus Holdings, Inc.

14. Defendant MIM is a corporation organized and existing under the laws of the State of Ohio, having its principal place of business at 25800 Science Park Drive, Suite 180, Cleveland, Ohio, 44122. MIM sells imaging tools for radiation oncology, radiology, nuclear medicine, urology, neuroimaging, and cardiac imaging.

JURISDICTION AND VENUE

15. This action arises under the patent laws of the United States, 35 U.S.C. § 100 *et seq.*, and this Court has jurisdiction over the subject matter of this action under 28 U.S.C. §§ 1331 and 1338(a).

16. This Court has personal jurisdiction over MIM because, upon information and belief, MIM, directly or through its affiliates, develops, manufactures, imports, markets, offers to sell, sells, and/or distributes its software products throughout the United States, including in Massachusetts (including to various renowned Massachusetts-based hospitals and cancer centers,

including, upon information and belief, Dana Farber, Massachusetts General Hospital, and Harvard Medical School). MIM, therefore, does business in Massachusetts, derives revenue from conducting business in Massachusetts, and maintains continuous and systematic contacts with Massachusetts. The Court also has personal jurisdiction over MIM because MIM has committed, induced, or contributed to acts of patent infringement in Massachusetts by selling its infringing software products throughout the United States, including in this judicial district.

17. Venue is proper in this district under 28 U.S.C. §§ 1391 and 1400.

FACTUAL BACKGROUND

A. Medical Imaging for Cancer and Other Serious Diseases.

18. One major challenge in treating and managing cancer (and other serious diseases) has long been the difficulty of accurately and consistently interpreting the diagnostic images produced by medical imaging tools.

19. Both anatomical scans (like X-rays or CT) and functional scans (like PET or single-photon emission computed tomography (SPECT)) are valuable tools. But before the inventions claimed in the Asserted Patents, physicians faced major obstacles in using those scans to form a complete and trustworthy picture of a patient's disease.

20. One difficulty was that each type of scan could only capture part of the relevant picture for any given patient. Anatomical scans capture images of the anatomy or structure of organs and tissues within the body (but not the function); functional scans capture the activity and function of those organs or tissues (but not the anatomy/structure). As applied to cancer, an anatomical scan thus cannot reliably detect the activity of a tumor, whereas a functional scan can struggle to differentiate between the organs and tissue surrounding a tumor. Physicians were left to parse two different types of scans to try to piece together the full picture, and this often led to inaccurate or inconsistent diagnoses or treatments.

21. More broadly, the traditional process for interpreting medical imaging—which involved a physician receiving one or more different scan images prepared by a computer—left room for human error. Without any automated integration, mapping, and assessment of those scan results, a physician might misinterpret a PET scan (or a combination of a CT scan and a PET scan) and miss a critical diagnostic insight that could save a patient's life.

22. Plaintiffs' claimed inventions were therefore major advances in overcoming the limitations of medical imaging interpretation, including in the field of (but not limited to) cancer diagnosis and treatment.

B. Plaintiffs' Asserted Patents Claim Major Advances in the Interpretation of Medical Imaging for Cancer and Other Diseases.

23. Plaintiffs spent at least five years and millions of dollars to develop solutions that unlock medical imaging's full potential. Plaintiffs' efforts culminated in the inventions claimed in the Asserted Patents (as well as other patents).

24. Plaintiffs' patented innovations improved the reliability and accuracy of medical imaging interpretation by (amongst other things): (a) using artificial intelligence-based ("AI") algorithms to reliably segment the organs and lesions captured in scans; (b) using a two-step segmentation technique to identify and flag organs, lesions, and/or other points of interest on a scan; (c) creating graphical interfaces, including overlays such as risk maps, that report scan results in a way that benefits from AI-based segmentation and/or two-step segmentation; and (d) automating Prostate Specific Membrane Antigen (PSMA) (or other biomarker) detection while compensating for normal physiological uptake to automatically assess the severity of identified lesions and overall disease burden, progression, and/or response to treatment. These innovations provide reliable risk insights to help ensure accurate diagnosis and treatment by physicians.

25. U.S. Patent No. 10,665,346 ("the '346 patent"), entitled "Network for Medical Image Analysis, Decision Support System, and Related Graphical User Interface (GUI) Applications," was duly and legally issued by the Patent Office on May 26, 2020, and has not expired. The '346 patent is assigned to Progenics. This patent claims, *inter alia*, a platform and supported graphical user interface (GUI) decision-making tools for use by medical practitioners (and/or their patients) to aid in the process of making decisions about a course of cancer treatment (and/or to track treatment and/or the progress of the disease). A true and correct copy of this patent is attached as Exhibit 1.

26. U.S. Patent No. 10,973,486 ("the '486 patent"), entitled "Systems and Methods for Rapid Neural Network-based Image Segmentation and Radiopharmaceutical Uptake Determination," was duly and legally issued by the Patent Office on April 13, 2021, and has not expired. The '486 patent is assigned to Progenics and EXINI. This patent claims, *inter alia*, systems and methods that provide for automated analysis of 3D medical images of a patient in order to automatically identify specific 3D volumes within the 3D images that correspond to specific organs and/or tissue. This kind of accurate identification of 3D volumes allows one to determine quantitative metrics that measure uptake of tracers in particular organs/tissues, which can in turn be used to assess disease state in a patient (including, but not limited to, prostate cancer). A true and correct copy of this patent is attached as Exhibit 2.

27. U.S. Patent No. 11,424,035 ("the '035 patent"), entitled "Network for Medical Image Analysis, Decision Support System, and Related Graphical User Interface (GUI) Applications," was duly and legally issued by the Patent Office on August 23, 2022, and has not expired. The '035 patent is assigned to Progenics. This patent claims, *inter alia*, a platform and supported graphical user interface (GUI) decision-making tools for use by medical practitioners

and/or their patients to aid in the process of making decisions about a course of cancer treatment and/or to track treatment and/or the progress of the disease. A true and correct copy of this patent is attached as Exhibit 3.

28. U.S. Patent No. 11,894,141 ("the '141 patent"), entitled "Network for Medical Image Analysis, Decision Support System, and Related Graphical User Interface (GUI) Applications," was duly and legally issued by the Patent Office on February 6, 2024, and has not expired. The '141 patent is assigned to Progenics. This patent also claims, *inter alia*, a platform and supported GUI decision-making tools for use by medical practitioners and/or their patients to help make decisions about cancer treatment and/or to track treatment and/or the progress of the disease. A true and correct copy of this patent is attached as Exhibit 4.

29. U.S. Patent No. 11,657,508 ("the '508 patent"), entitled "Systems and Methods for Platform Agnostic Whole Body Image Segmentation," was duly and legally issued by the Patent Office on May 23, 2023, and has not expired. The '508 patent is assigned to EXINI. This patent claims, *inter alia*, systems and methods that provide for automated analysis of 3D medical images to automatically identify certain volumes within the images that correspond to specific anatomical regions (e.g., organs and/or tissue), thereby providing for consistent, efficient, and accurate detection of anatomical regions (including soft tissue organs) in the entire body, as well as use of these identified anatomical regions together with detected "hotspots" that represent potential cancerous lesions in nuclear medicine images to accurately assess disease burden in patients. A true and correct copy of this patent is attached as Exhibit 5.

30. U.S. Patent No. 11,721,428 ("the '428 patent"), entitled "Systems and Methods for Artificial Intelligence-Based Image Analysis for Detection and Characterization of Lesions," was duly and legally issued by the Patent Office on August 8, 2023, and has not expired. The '428

patent is assigned to EXINI. This patent claims, *inter alia*, systems and methods that provide for improved detection and characterization of lesions within a subject via automated analysis of nuclear medicine images, such PET or SPECT images. These approaches leverage AI to detect regions of 3D nuclear medicine images corresponding to "hotspots" that represent potential cancerous lesions in the subject, along with techniques for improving the accuracy with which background radiopharmaceutical uptake in reference organs, such as a liver, can be automatically assessed and used to evaluate disease burden and progression in patients. A true and correct copy of this patent is attached as Exhibit 6.

31. U.S. Patent No. 11,941,817 ("the '817 patent"), entitled "Systems and Methods for Platform Agnostic Whole Body Image Segmentation," was duly and legally issued by the Patent Office on March 26, 2024, and has not expired. The '817 patent is assigned to EXINI. This patent claims, *inter alia*, systems and methods that provide for automated analysis of 3D medical images of a subject in order to automatically identify cancerous lesions within the subject. A true and correct copy of this patent is attached as Exhibit 7.

32. The Asserted Patents generally describe inventions for improving the reliability, usability, and accuracy of medical imaging, including by: (a) using AI-based algorithms to help segment the 3D image into different organs (or tissues), thus allowing for clearer differentiation of organs, tissues, and lesions; (b) using a two-step segmentation technique, whereby volumes of interest (e.g., the pelvic region) are first localized within a large and complex 3D image, and are then analyzed by fine-grained segmentation modules, allowing those segmentation modules to efficiently and accurately identify critical organs, and tissue regions, such as the prostate, in medical images; (c) analyzing scan results to prepare a risk map that analyzes areas of importance of concern for physician and patient review; and (d) automating PSMA (or other biomarker)

detection while compensating for normal physiological uptake by using anatomical context provided by AI-based organ segmentation, in order to accurately assess lesion severity and overall disease burden, progression, and/or response to treatment.

33. The inventions claimed in the Asserted Patents improve upon prior art by increasing the reliability, accuracy, and usability of medical imaging for cancer diagnoses and treatment.

34. For example, representative claim 1 of the ’346 patent recites:

A network-based system for generating a disease risk map for use as a decision-making support for evaluating risk of cancer or risk of recurrence of cancer, the system comprising:

a processor; and

a memory having instructions stored thereon, wherein the instructions, when executed by the processor, cause the processor to:

(i) access one or more medical images associated with a particular patient from a database;

(ii) perform an analysis of the one or more medical images associated with the particular patient using a machine learning algorithm, to generate the risk map, wherein the risk map comprises a visual representation of tissue overlaid with graphical denotations marking one or more regions of risk of cancer or risk of recurrence of cancer; and

(iii) cause display of risk map via a graphical user interface (GUI) for presentation or review of the risk map by a user,

wherein the analysis of the one or more medical images comprises creation of a 3D image of the one or more regions of risk of cancer or risk of recurrence of cancer overlaid on the one or more medical images, and wherein the 3D image comprises geographic identification of one or more specific tissue region(s) overlaid on the one or more medical images.

35. Representative claim 42 of the ’486 patent recites:

A method for automatically processing 3D images to identify 3D volumes within the 3D images that correspond to a prostate of a subject and determining one or more uptake metrics indicative of radiopharmaceutical uptake therein, the method comprising:

(a) receiving, by a processor of a computing device, a 3D anatomical image of the subject obtained using an anatomical imaging modality, wherein the 3D anatomical image comprises a graphical representation of tissue within a subject, at least a portion of which corresponds to a pelvic region of the subject;

(b) receiving, by the processor, a 3D functional image of the subject obtained using a functional imaging modality, wherein the 3D functional image comprises a plurality of voxels, each representing a particular physical volume within the subject and having an intensity value that represents detected radiation emitted from the particular physical volume, wherein at least a portion of the plurality of voxels of the 3D functional image represent physical volumes within the pelvic region of the subject;

(c) determining, by the processor, using a first module, an initial volume of interest (VOI) within the 3D anatomical image, the initial VOI corresponding to tissue within the pelvic region of the subject and excluding tissue outside the pelvic region of the subject;

(d) identifying, by the processor, using a second module, a prostate volume within the initial VOI corresponding to the prostate of the subject;

(e) determining, by the processor, the one or more uptake metrics using the 3D functional image and the prostate volume identified within the initial VOI of the 3D anatomical image;

(f) causing, by the processor, display of an interactive graphical user interface (GUI) for presentation to the user of a visual representation of the 3D anatomical image and/or the 3D functional image; and

(g) causing, by the processor, graphical rendering of, within the GUI, the 3D anatomical image and/or the 3D functional image as selectable and superimposable layers, such that either can be selected for display and rendered separately, or both selected for display and rendered together by overlaying the 3D anatomical image with the 3D functional image.

36. Representative claim 1 of the ’035 patent recites:

A network-based decision support system comprising: a processor; and a memory having instructions stored thereon, wherein the instructions, when executed by the processor, cause the processor to:

(i) receive and store a plurality of medical images in a database, each medical image associated with a corresponding patient;

(ii) access one or more of the medical images associated with a particular patient from the database upon user request for transmission to the user for display on a user computing device;

(iii) automatically analyze the one or more medical images using a machine learning algorithm; and

(iv) generate a radiologist report for the particular patient according to the one or more medical images for the patient,

wherein the one or more medical images comprise a composite image of the particular patient, the composite image comprising a CT scan overlaid with a nuclear medicine image

obtained at a substantially same time as the CT scan and following administration to the patient of an imaging agent comprising a Prostate Specific Membrane Antigen (PSMA) binding agent comprising a radionuclide, wherein the instructions cause the processor to automatically analyze the composite image by:

(a) using the composite image to geographically identify a 3D boundary for each of one or more regions of imaged tissue within the nuclear medicine image; and

(b) computing, using the nuclear medicine image with the identified 3D boundary(ies) of the one or more region(s) a risk map comprising a graphical denotation marking a region of risk of cancer or risk of recurrence of cancer.

37. Representative claim 1 of the ’141 patent recites:

A network-based decision support system comprising: a processor; and a memory having instructions stored thereon, wherein the instructions, when executed by the processor, cause the processor to:

(i) receive and store a plurality of medical images in a database, each medical image associated with a corresponding patient;

(ii) access one or more of the medical images associated with a particular patient from the database;

(iii) automatically analyze the one or more medical images using a machine learning algorithm; and

(iv) generate a radiologist report for the particular patient according to the one or more medical images for the patient,

wherein the one or more medical images comprise a composite image of the particular patient, the composite image comprising a CT scan overlaid with a nuclear medicine image obtained at a substantially same time as the CT scan and following administration to the patient of an imaging agent comprising a Prostate Specific Membrane Antigen (PSMA) binding agent comprising a radionuclide, wherein the instructions cause the processor to automatically analyze the composite image by:

(a) using the composite image to geographically identify a 3D boundary for each of one or more regions of imaged tissue within the nuclear medicine image; and

(b) computing, using the nuclear medicine image with the identified 3D boundary(ies) of the one or more region(s), a value of each of one or more risk indices, each risk index value indicative of cancer state or progression in the patient, and wherein the system is a cloud-based system.

38. Representative claim 1 of the ’508 patent recites:

A method for automatically processing 3D images to identify, and measure uptake of radiopharmaceutical in, cancerous lesions within a subject having or at risk for a cancer, the method comprising:

(a) receiving, by a processor of a computing device, a 3D anatomical image of a subject obtained using an anatomical imaging modality, wherein the 3D anatomical image comprises a graphical representation of tissue within the subject;

(b) automatically identifying, by the processor, using one or more machine learning modules, within the 3D anatomical image: a first skeletal volume comprising a graphical representation of one or more bones of the subject; a first aorta volume comprising a graphical representation of at least a portion of an aorta of the subject; and a first liver volume comprising a graphical representation of a liver of the subject;

(c) determining, by the processor, a 3D segmentation map representing a plurality of 3D segmentation masks, including a skeletal mask representing the identified first skeletal volume, an aorta mask representing the identified first aorta volume, and a liver mask representing the identified first liver volume;

(d) receiving, by the processor, a 3D functional image of the subject obtained using a functional imaging modality;

(e) automatically identifying, within the 3D functional image, using the 3D segmentation map: a second skeletal volume corresponding to the first identified skeletal volume, within the 3D anatomical image; a second aorta volume corresponding to the first aorta volume, identified within the 3D anatomical image; and a second liver volume corresponding to the first liver volume, identified within the 3D anatomical image;

(f) automatically detecting, by the processor, within the second skeletal volume, one or more hotspots determined to represent lesions based on intensities of voxels within the second skeletal volume; and

(g) determining, by the processor, for each of the one or more detected hotspots, an individual hotspot index value by: determining an aorta reference intensity level based on a measure of intensity of voxels within the second aorta volume; determining a liver reference intensity level based on a measure of intensity of voxels within the second liver volume; and for each individual detected hotspot: determining a corresponding individual hotspot intensity level based on a measure of intensity of voxels of the detected hotspot; and determining a corresponding individual hotspot index level from the individual hotspot intensity level, the aorta reference intensity level, and the liver reference intensity level.

39. Representative claim 1 of the ’428 patent recites:

A method of measuring intensity values within a reference volume corresponding to a reference tissue region so as to avoid impact from tissue regions associated with low radiopharmaceutical uptake, the method comprising:

(a) receiving, by a processor of a computing device, a 3D functional image of a subject, said 3D functional image obtained using positron emission tomography (PET) and/or single-photon emission computed tomography (SPECT);

(b) identifying, by the processor, the reference volume within the 3D functional image;

(c) fitting, by the processor, a multi-component mixture model to a distribution of intensities of voxels within the reference volume;

(d) identifying, by the processor, a major mode of the multi-component model;

(e) determining, by the processor, a measure of intensities corresponding to the major mode, thereby determining a reference intensity value corresponding to a measure of intensity of voxels that are (i) within the reference tissue volume and (ii) associated with the major mode;

(f) detecting, by the processor, within the functional image, one or more hotspots corresponding potential cancerous lesions; and

(g) determining, by the processor, for each particular hotspot of at least a portion of the detected hotspots, a lesion index value indicative of: (I) a level of radio-pharmaceutical uptake within and underlying lesion to which the particular hotspot corresponds and/or (II) a size of an underlying lesion to which the particular hotspot corresponds, wherein the lesion index value is determined based on (i) a measure of intensity of the particular hotspot and (ii) the reference intensity value.

40. Representative claim 1 of the ’817 patent recites:

A method for automatically processing 3D images to automatically identify cancerous lesions within a subject, the method comprising:

(a) receiving, by a processor of a computing device, a 3D anatomical image of a subject obtained using an anatomical imaging modality, wherein the 3D anatomical image comprises a graphical representation of tissue within the subject;

(b) automatically identifying, by the processor, using one or more machine learning modules, for each of a plurality of target tissue regions, a corresponding target volume of interest (VOI) within the 3D anatomical image;

(c) determining, by the processor, a 3D segmentation map representing a plurality of 3D segmentation masks, each 3D segmentation mask representing a particular identified target VOI;

(d) receiving, by the processor, a 3D functional image of the subject obtained using a functional imaging modality;

(e) identifying, within the 3D functional image, one or more 3D volume(s), each corresponding to an identified target VOI, using the 3D segmentation map; and

(f) automatically detecting, by the processor, within at least a portion of the one or more 3D volumes identified within the 3D functional image, one or more hotspots determined to represent lesions based on intensities of voxels within the 3D functional image.

41. The inventions of the Asserted Patents address technological limitations of medical imaging interpretation that were not routine or conventional at the time of the invention. A person of ordinary skill in the art reading the Asserted Patents and their claims would understand that (a) the Asserted Patents' disclosures and claims solve specific problems, and (b) the claimed inventions represent significant advances in the technical field.

C. 2020-2022: Plaintiffs and MIM Explore Possible Collaboration Involving the Inventions Claimed in Plaintiffs' Asserted Patents.

42. Upon information and belief, MIM infringed (and is infringing) the Plaintiffs' Asserted Patents because MIM decided—after years of negotiations with Plaintiffs about a possible collaboration—that it wanted to use Plaintiffs' patented inventions without paying for them.

43. Around June 2020, MIM and EXINI (and Plaintiffs' parent company, Lantheus Holdings, Inc.) began discussions about a potential collaboration involving (amongst other things) the inventions claimed by the Asserted Patents. More specifically, MIM was interested in integrating the claimed inventions into MIM's nuclear imaging software.

44. The following year, MIM worked with Karl Sjöstrand at EXINI (an inventor on the '486 patent) and Aseem Undvall Anand at EXINI (an inventor on the '508 and '817 patents) to explore powering MIM's systems with Plaintiffs' patented algorithms (including the inventions in the Asserted Patents).

45. Reflecting the substantiveness and seriousness of these discussions, the parties entered into a Confidential Disclosure Agreement in October 2021.

46. These discussions continued into 2022 and included giving MIM access to Plaintiffs' systems to review the capabilities and function of Plaintiffs' patented inventions.

47. Around October 2022, Plaintiffs sent MIM a draft Collaboration Agreement.

48. The draft Collaboration Agreement included a list of Plaintiffs' patents and patent applications that claimed the inventions that the parties had discussed sharing.

49. Nearly all of the Asserted Patents were on that list, indicating that MIM was considering implementing and using Plaintiffs' patented technology. Plaintiffs, too, were considering a collaboration—*but only if* MIM agreed to partnership terms.

50. Plaintiffs followed up with MIM a few times in late 2022 and 2023, as Plaintiffs waited to hear back from MIM about the draft Collaboration Agreement.

51. Plaintiffs never heard back.

D. MIM Markets and Sells Infringing Products and Pursues Acquisition by GE HealthCare.

52. Instead, Plaintiffs discovered around June 2023 that MIM was publishing articles, brochures, and website information about the Infringing Products (Contour ProtégéAI®, MIM SurePlan™ MRT, LesionID®, and LesionID Pro®), as well as other products which are part of MIM's broader software suite including MIM Encore®, PET Edge®, MIM Assistant®, and MIMcloud®. These materials plainly indicate that the Infringing Products practice the inventions claimed in the Asserted Patents as discussed below.

53. MIM is making, using, offering to sell, and selling products that infringe the Asserted Patents.

54. Not only did MIM develop through imitation, market, and sell the Infringing Products, MIM also benefited from the Infringing Products because (upon information and belief) those products—and Plaintiffs' patented inventions embodied in those Infringing Products—

enticed GE HealthCare to acquire MIM. *See* "GE HealthCare Announces Agreement to Acquire MIM Software" (Jan. 8, 2024), *available at* https://www.gehealthcare.com/about/newsroom/press-releases/ge-healthcare-announces-agreement-to-acquire-mim software.

55. GE HealthCare announced in a recent press release its plan to acquire MIM. In that press release, GE HealthCare emphasized how the inventions claimed by the Asserted Patents—which MIM integrated into the Infringing Products—were a main reason GE HealthCare decided to acquire MIM.

56. The press release states, in relevant part:

> MIM Software's portfolio of innovative imaging solutions provides a variety of beneficial features, including: **the integration of diagnostic images from multiple modalities into treatment plans**; **automation to help reduce repetitive tasks and manual interventions**; **quantitation and advanced processing in diagnostic imaging** and nuclear medicine to help determine therapy response . . . GE HealthCare expects to integrate MIM Software solutions into its advanced visualizations to facilitate **AI-based segmentation and contouring** as well as dosimetry analysis for patients across their treatment journeys and in the growing fields of radiology, molecular imaging, and radiation oncology.

Id. (emphasis added).

57. The release is replete with references to Plaintiffs' inventions. For example, the reference to "integration of diagnostic images from multiple modalities" is captured, *inter alia*, by claim 42 of the '486 patent, which describes integrating anatomical and functional diagnostic images into the creation of treatment plans. The reference to "quantitation and advanced processing in diagnostic imaging" refers to, *inter alia*, claim 1 of the '346 patent and the use of AI to create tailored risk maps of cancer/disease risk based on analysis of medical images. The reference to "automation to help reduce repetitive tasks and manual interventions" refers to, *inter alia*, claim 1 of the '508 patent, which describes the use of automation to identify specific 3D

volumes and calculate radiopharmaceutical uptake. And the reference to "AI-based segmentation and contouring" refers to the AI-assisted organ segmentation described across multiple claims of the Asserted Patents. All of these GE HealthCare statements indicate that MIM's use of the patented inventions in its software was a key driver of GE HealthCare's decision to acquire MIM.

58. Upon closing its acquisition of MIM, GE HealthCare issued yet another press release that further reinforces how MIM's infringement of the Asserted Patents played a critical role in GE HealthCare's decision to acquire MIM. *See* "GE HealthCare Closes MIM Software Acquisition, Bolstering Its Portfolio and Advancing Its Precision Care Strategy," GE HealthCare (Apr. 1, 2024), *available at* https://www.gehealthcare.com/about/newsroom/press-releases/ge-healthcare-closes-mim-software-acquisition-bolstering-its-portfolio-and-advancing-its-precision-care-strategy. For example, the press release emphasizes GE HealthCare's desire to use MIM's "**AI-enabled image analysis** and workflow tools spanning multiple care areas, including oncology, urology, neurology, and cardiology." *Id.* (emphasis added). The press release also highlights how acquiring the Infringing Products and their associated software—including "MIM SurePlan and MIM Symphony families, MIM Maestro, MIM Encore, and more"—aligns with GE HealthCare's strategy of "deliver[ing] innovative digital solutions across care pathways for more precise, connected, and efficient care across disease states." *Id.* These statements further indicate that MIM's use of the patented inventions in its software played a key role in GE HealthCare's decision to acquire MIM.

59. The GE HealthCare press releases, however, are not the only public sources that reveal MIM's unlawful use of the Asserted Patents in the Infringing Products.

60. MIM publishes information about the Infringing Products on its website, including via product brochures. MIM's website explains that the brochures "[t]ake a closer look at MIM's

solutions and products in downloadable PDFs." *See* MIM Brochures, *available at* https://www.mimsoftware.com/literature/brochures (accessed on Mar. 14, 2024). MIM also publishes information about the Infringing Products in industry publications and on social media platforms like LinkedIn.

61. These publications reflect several ways that the Infringing Products practice the inventions claimed by the Asserted Patents.

62. For example, MIM's publications show that the Infringing Products possess each element of representative claim 1 of the '346 patent.

63. The preamble to claim 1 of the '346 patent describes "[a] network-based system for generating a disease risk map for use as a decision-making support for evaluating risk of cancer of risk of recurrence of cancer, the system comprising: a processor; and a memory having instructions stored thereon, wherein the instructions, when executed by the processor, cause the processor to:" (*see* '346 patent, at col. 35:46-49) (claim 1 preamble). MIM's brochure entitled "Molecular Radiotherapy Dosimetry" describes how the Infringing Products "Deliver AI on Premise or in the Cloud"—in other words, on a "network-based system." *See* "Molecular Radiotherapy Dosimetry" brochure, *available at* https://go.mimsoftware.com/hubfs/00_Website/02_Literature_Case_Studies/Brochures/TD1000-MIM_Nuclear_Medicine_MRT_Brochure-20230608.pdf, at 6 (accessed on Mar. 14, 2024). The brochure also describes how the Infringing Products provide a decision-support tool that "allow[s] for effective communication with patients and referring physicians," and for "track[ing] dose across therapy cycles and quickly review tumor progression." *Id*. at 10. A different MIM brochure entitled "Molecular Imaging and Nuclear Medicine Diagnostic Solutions" describes how the Infringing Products "Empower Clinical Decisions" by "mak[ing] capturing dosimetry information clinically feasible," and "offer[ing] deep-learning

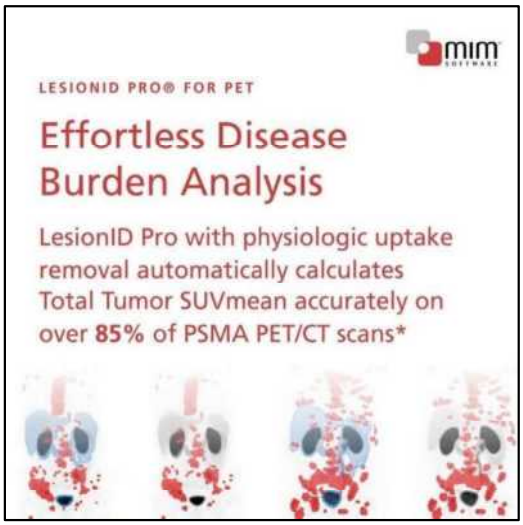
algorithms that expedite the segmentation process." *See* "Molecular Imaging and Nuclear Medicine Diagnostic Solutions", *available at* https://go.mimsoftware.com/hubfs/_Market/MIM%20General/Brochures /Radiology%20and%20Nuclear%20Medicine/MIM%20Nuclear%20Medicine%20Diagnostic%20Solutions%20Brochure.pdf, at 10 (accessed on Mar. 14, 2024). MIM's website also indicates that LesionID® is a component of MIM Encore®, which in turn includes the MIM Assistant® module that allows users to "access data off-site with VPN or other network extensions." *See* MIM Encore®, MIM Software Inc., *available at* https://www.mimsoftware.com/nuclear-medicine/mim-encore (accessed on Mar. 14, 2024); MIM Assistant®, MIM Software Inc., *available at* https://www.mimsoftware.com/remote-access/pacs (accessed on Mar. 14, 2024). These disclosures illustrate that the Infringing Products possess the preamble of claim 1.

64. The Infringing Products also possess the first limitation of claim 1 of the '346 patent[1] because the Infringing Products access scan images for particular patients from an electronic database, and then present those images to clinicians and patients. A MIM brochure, for example, notes how "Contour ProtégéAI for MIM SurePlan MRT has flexible deployment models that allow for easier adoption across any institution." *See* "Molecular Radiotherapy Dosimetry" brochure, *supra* ¶ 63, at 6. The brochure also shows an image of a patient scan presented on a screen. *Id*. MIM's website also refers to how MIMcloud can "push and pull images, and easily share studies . . . " *See* MIMcloud, *available at* https://www.mimsoftware.com/remote-access/mimcloud (accessed on Mar. 14, 2024). According to MIM's publications, MIM Assistant® (which, as discussed above, is packaged with LesionID® in MIM Encore®) includes the capability to "[a]ccess patient studies with fast searching and

[1] *See* '346 patent, claim 1(i) ("access one or more medical images associated with a particular patient from a database").

viewing" and "[a]ccess data off-site with VPN or other network extensions." MIM Assistant®, *supra* ¶ 63.

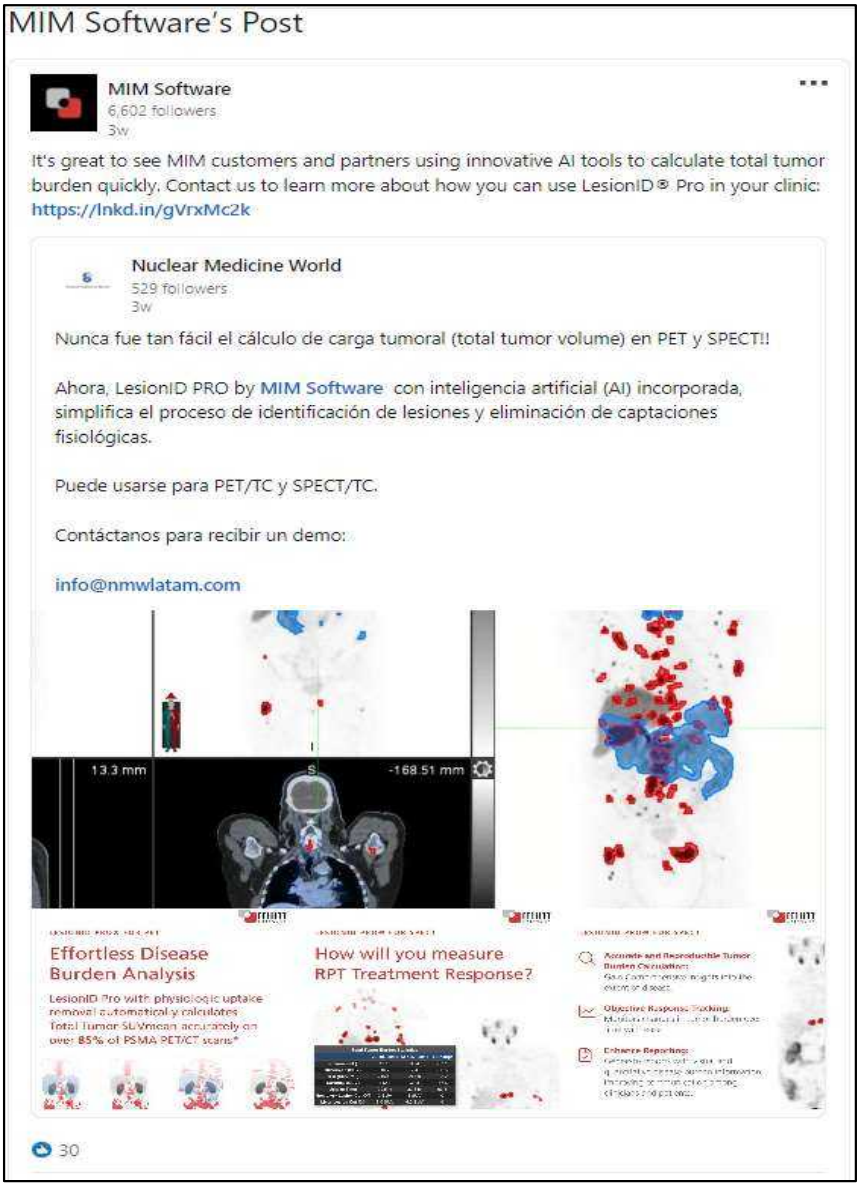
65. The Infringing Products also possess the second limitation of claim 1 of the '346 patent[2] because MIM SurePlan™ MRT uses Contour ProtégéAI® which, according to a MIM brochure, "Segment[s] Normal Structures with Artific[i]al Intelligence." *See* "Molecular Radiotherapy Dosimetry" brochure, *supra* ¶ 63, at 6; *see also id.* ("Triggered automatically upon image arrival, Contour ProtégéAI for MIM SurePlan MRT uses a neural network for segmenting normal structures on CT images. Results are more accurate than atlas-based approaches so users spend less time editing."). The same brochure also discusses how MIM SurePlan™ MRT uses PET Edge® to create contoured tumor regions that are overlaid on a SPECT/CT image. *Id*. MIM's LinkedIn post states that LesionID Pro® can be used to calculate total tumor SUVmean from PET/CT scans:



MIM Software Inc., LinkedIn, https://www.linkedin.com/posts/mim-software-inc%2E_nunca-fue-tan-f%C3%A1cil-el-c%C3%A1lculo-de-carga-tumoral-activity-7157842399761731585-

[2] *See* claim 1(ii) ("perform an analysis of the one or more medical images associated with the particular patient using a machine learning algorithm, to generate a risk map, wherein the risk map comprises a visual representation of tissue overlaid with graphical denotations marking one or more regions of risk of cancer …").

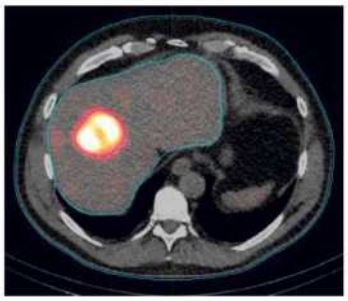
27Bn (Feb. 2024) ("LinkedIn Post"). MIM also commented on the post by Nuclear Medicine World:



Id. Nuclear Medicine World's post translates as, "It has never been so easy to calculate tumor load (total tumor volume) in PET and SPECT!! Now, LesionID PRO by MIM Software with built-in artificial intelligence (AI), simplifies the process of identifying lesions and eliminating physiological uptakes. It can be used for PET/CT and SPECT/CT." MIM reposted this post, commenting, "It's great to see MIM customers and partners using innovative AI tools to calculate

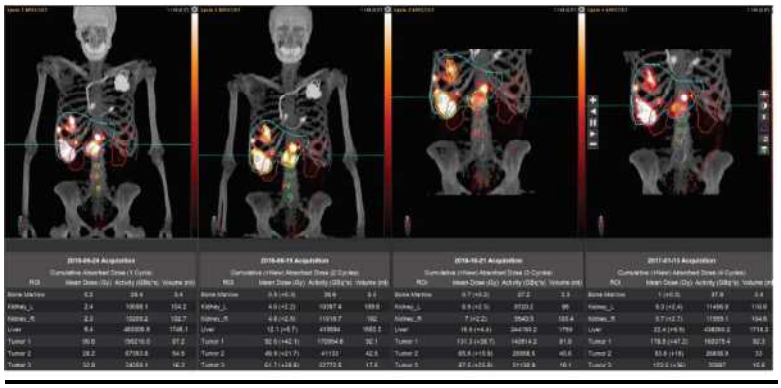
total tumor burden quickly. Contact us to learn more about how you can use LesionID® Pro in your clinic." The post also shows tissue images with markings in red that denote regions identified as a potential tumor, i.e., regions of risk of cancer.

66. The Infringing Products also possess the third limitation of claim 1 of the '346 patent[3] because, as reflected in the image below from a MIM brochure, MIM SurePlan™ MRT displays the risk map (i.e., tumor segmentation) via a graphical user interface (GUI):



Id. at 7. The same image also reveals that the Infringing Products display normal organ contours and tumor contours overlaid on medical images. *See id*. (blue color outlining an organ, and red color outlining a tumor). Another image in the same brochure also shows images of a SPECT/CT with organs and tumors outlined:

[3] *See* claim 1(iii) ("cause display of the risk map via a graphical user interface (GUI) for presentation or review of the risk map by a user, wherein the analysis of one or more medical images comprises creation of a 3D image of the one or more regions of risk of cancer or risk of recurrence of cancer overlaid on the one or more medical images, and wherein the 3D image comprises geographic identification of one or more specific tissue region(s) overlaid on the one or more medical images").



Id. at 10. The MIM LinkedIn post above shows GUI displays for presentation and review by a user, as well as markings identifying potential tumors as overlaid on PET/CT scan images, which are 3D medical images. LinkedIn Post, *supra* ¶ 65.

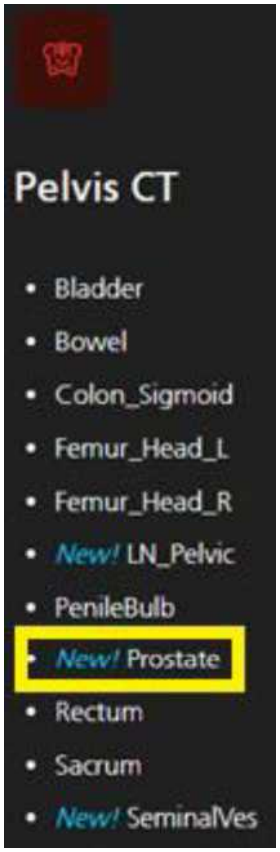
67. Turning next to the '486 patent, the Infringing Products also possess all the elements of exemplary claim 42.

68. The preamble to claim 42 describes "[a] method for automatically processing 3D images to identify 3D volumes within the 3D images that correspond to a prostate of a subject and determining one or more uptake metrics indicative of radiopharmaceutical uptake therein, the method comprising:" (*see* '486 patent, at col. 80:33-37) (claim 42 preamble). The Infringing Products possess this limitation because: (a) MIM SurePlan™ MRT uses Contour ProtégéAI® to perform organ segmentation (*see* "Molecular Radiotherapy Dosimetry" brochure, *supra* ¶ 63, at 6); (b) MIM SurePlan™ MRT provides dose accumulation statistics (*id*. at 10) ("Dose accumulation runs in the background through MIM Assistant®. Cumulative doses and volume changes across cycles can be reviewed."); and (c) Contour ProtégéAI® segments a variety of organs, including the prostate, listing "Prostate" as one of the "Available Structures for Organ Contouring" (*see* "Contour ProtégéAI+™: Zero-Click AI Auto-Contouring", *available at* https://www.mimsoftware.com/radiation-oncology/contour-protegeai-plus (accessed on Mar. 14, 2024)). The brochure also refers to how "MIM SurePlan™ MRT has been helping institutions

drastically reduce the clinical requirements for dosimetry by including AI-based auto-segmentation and support for quantitative SPECT reconstruction with existing SPECT/CT cameras," with CT providing 3D anatomical images. *See* "Molecular Radiotherapy Dosimetry" brochure, *supra* ¶ 63, at 2.

69. The Infringing Products also possess the first limitation of claim 42 of the '486 patent[4] because, as MIM's brochures proclaim, "MIM SurePlan™ MRT has been helping institutions drastically reduce the clinical requirements for dosimetry by including AI-based auto-segmentation and support for quantitative SPECT reconstruction with existing SPECT/**CT cameras**." *Id*. at 2 (emphasis added). CT cameras provide anatomical images. And, as discussed above, MIM directs that physicians and patients can use the Infringing Products on images relating to the patient's pelvic region. *Supra* at ¶ 68. The Contour ProtégéAI® website lists several applications in the pelvic region, including (but not limited to) the prostate:

[4] *See* '486 patent, claim 42(a) ("receiving, by a processor of a computing device, a 3D anatomical image of the subject obtained using an anatomical imaging modality, wherein the 3D anatomical image comprises a graphical representation of tissue within a subject, at least a portion of which corresponds to a pelvic region of the subject").



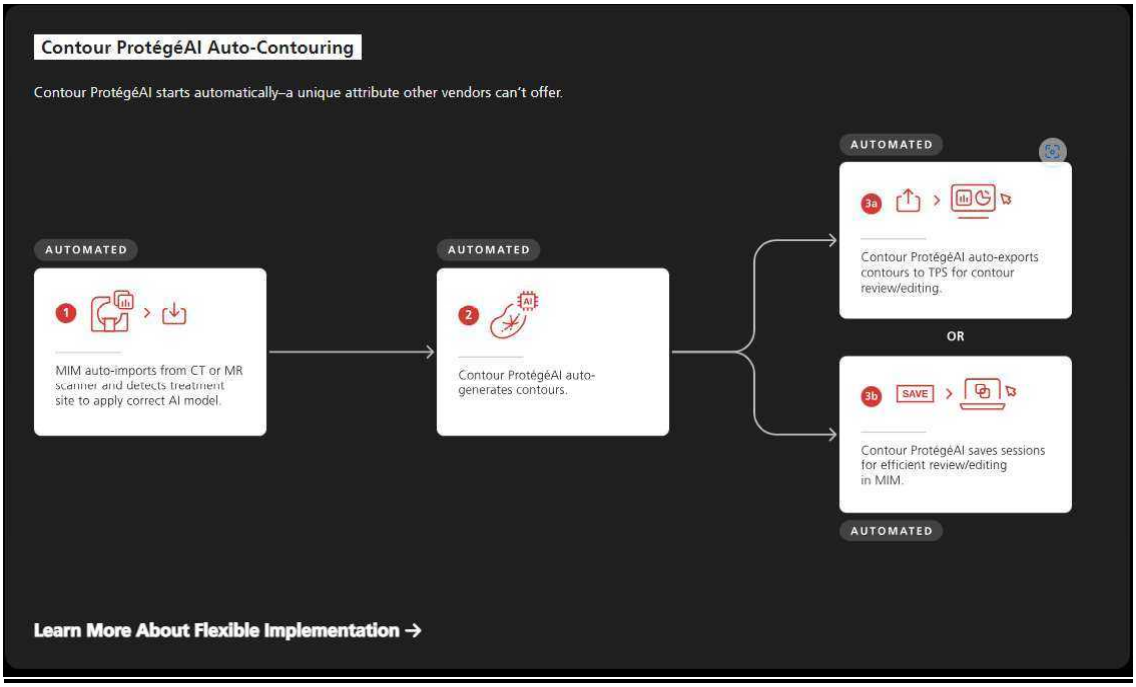
See "Contour ProtégéAI+™: Zero-Click AI Auto-Contouring", *supra* ¶ 68 (yellow box added).

70. The Infringing Products also possess the second limitation of claim 42 of the '486 patent[5] for the reasons already discussed above. The MIM brochure refers to how "MIM SurePlan™ MRT has been helping institutions drastically reduce the clinical requirements for dosimetry by including AI-based auto-segmentation and support for quantitative SPECT reconstruction with existing SPECT/CT cameras," with CT cameras providing 3D anatomical images. *See* "Molecular Radiotherapy Dosimetry" brochure, *supra* ¶ 63, at 2. SPECT imaging is

[5] *See* claim 42(b) ("receiving, by the processor, a 3D functional image of the subject obtained using a functional imaging modality, wherein the 3D functional image comprises a plurality of voxels, each representing a particular physical volume within the subject and having an intensity value that represents detected radiation emitted from the particular physical volume, wherein at least a portion of the plurality of voxels of the 3D functional image represent physical volumes within the pelvic region of the subject").

a 3D functional image. And, as discussed above, the Infringing Products are targeted at multiple applications within the pelvic region. *Supra* at ¶ 68.

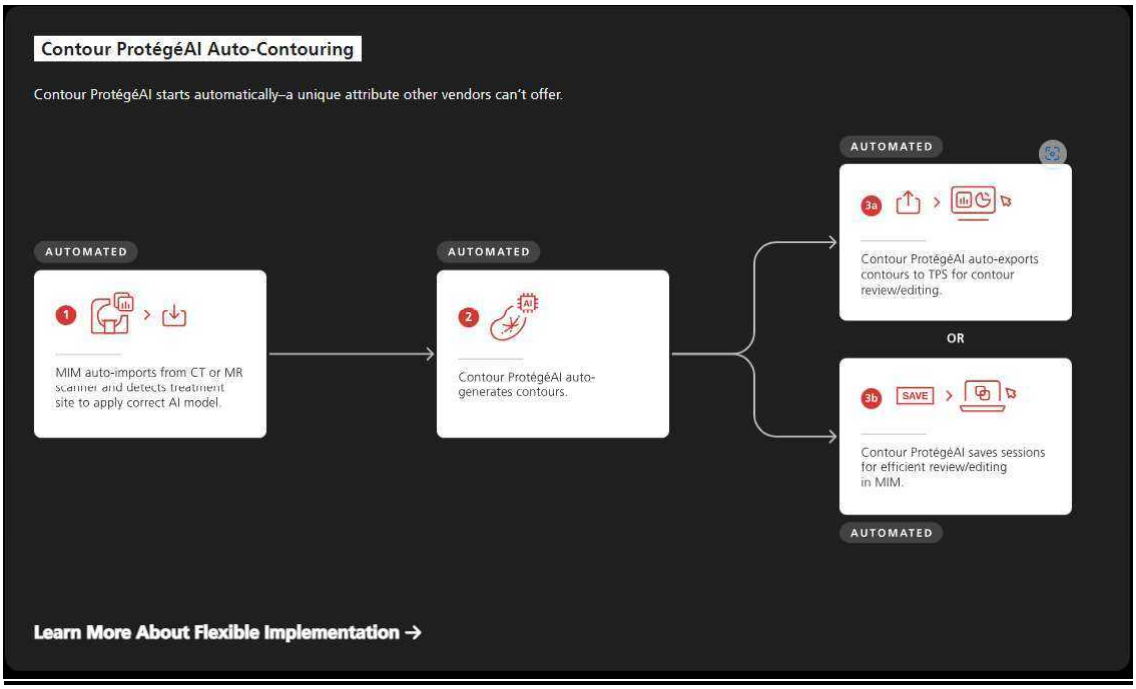
71. The Infringing Products also possess the third limitation of claim 42 of the '486 patent[6] because MIM SurePlan™ MRT uses Contour ProtégéAI® to segment normal structures in a CT image. In other words, when Contour ProtégéAI® "detects [the] treatment site to apply correct AI model" as described in the image below, it is determining, using a first module, an initial volume of interest ("VOI"):



See "Contour ProtégéAI+™: Zero-Click AI Auto-Contouring", *supra* ¶ 68. As discussed above, Contour ProtégéAI® includes a "Pelvis CT" model for segmenting organs within the pelvic region, i.e., where the initial VOI corresponds to a pelvic region. *Id.*

[6] *See* claim 42(c) ("determining, by the processor, using a first module, an initial volume of interest (VOI) within the 3D anatomical image, the initial VOI corresponding to tissue within the pelvic region of the subject and excluding tissue outside the pelvic region of the subject").

72. The Infringing Products also possess the fourth limitation of claim 42 of the '486 patent[7] because, when Contour ProtégéAI® uses the "Pelvis CT" model to segment the prostate, *supra* at ¶ 68, it uses a second module to identify a prostate volume within the initial VOI:



See id. In other words, the left-most box in the image above shows the initial segmentation step (as discussed in the preceding paragraph), and then the reference in the center box to "auto-generat[ing] contours" refers to the Infringing Products' use of the Pelvic CT model to segment the prostate.

73. The Infringing Products also possess the fifth limitation of claim 42 of the '486 patent[8] because, as discussed above, the MIM brochure shows uptake measurements (in bone, kidneys, liver, and tumors):

[7] *See* claim 42(d) ("identifying, by the processor, using a second module, a prostate volume within the initial VOI corresponding to the prostate of the subject").
[8] *See* claim 42(e) ("determining, by the processor, the one or more uptake metrics using the 3D functional image and the prostate volume identified within the initial VOI of the 3D anatomical image").



See "Molecular Radiotherapy Dosimetry" brochure, *supra* ¶ 63, at 10. As discussed above, Contour ProtégéAI® also includes a specific model that segments these organs, as well as the prostate. *Id*. Therefore, the Infringing Products calculate dose within a prostate volume segmented by the Pelvic CT model of Contour ProtégéAI®.

74. The Infringing Products also possess the sixth limitation of claim 42 of the '486 patent[9] as reflected in the image immediately above, which displays SPECT/CT image overlays, which are, respectively, 3D functional and anatomical images. *See id*.

75. The Infringing Products also possess the seventh limitation of claim 42 of the '486 patent[10] as reflected by the same image above, which shows that SurePlan™ MRT displays SPECT/CT image overlays. *Id*.

76. Turning next to the '035 patent, the Infringing Products also possess all the limitations of exemplary claim 1.

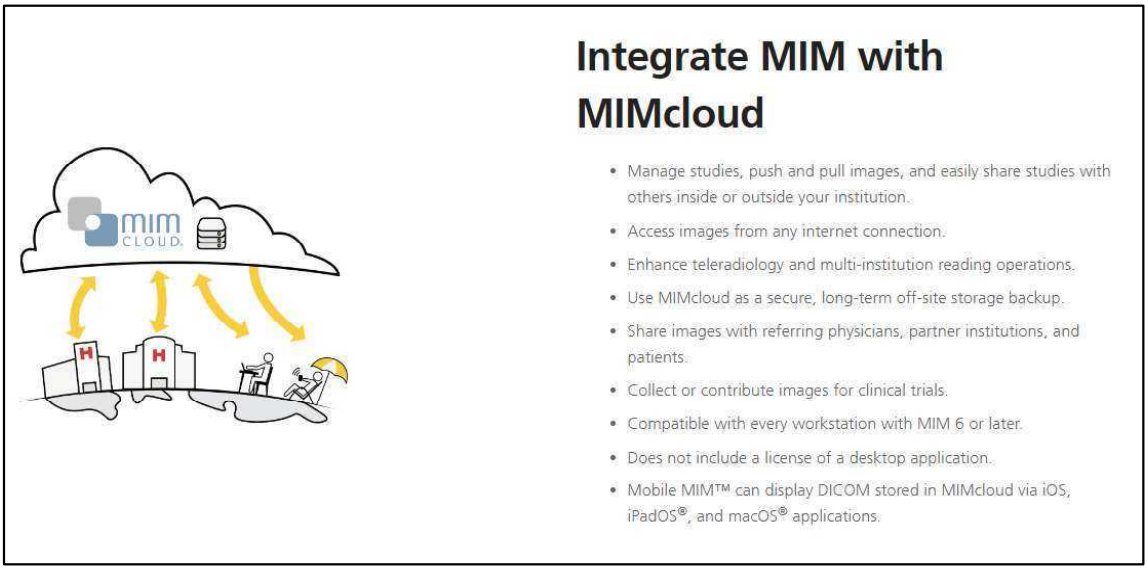
[9] *See* claim 42(f) ("causing, by the processor, display of an interactive graphical user interface (GUI) for presentation to the user of a visual representation of the 3D anatomical image and/or the 3D functional image").
[10] *See* claim 42(g) ("causing, by the processor, graphical rendering of, within the GUI, the 3D anatomical image and/or the 3D functional image as selectable and superimposable layers, such that either can be selected for display and rendered separately, or both selected for display and rendered together by overlaying the 3D anatomical image with the 3D functional image.").

77. The preamble to claim 1 of the '035 patent describes "[a] network-based decision support system comprising: a processor; and a memory having instructions stored thereon, wherein the instructions, when executed by the processor, cause the processor to:" (*see* '035 patent, at col. 36:18-20) (claim 1 preamble). MIM's brochure entitled "Molecular Radiotherapy Dosimetry" describes how the Infringing Products "Deliver AI on Premise or in the Cloud"—in other words, on a 'network-based system':



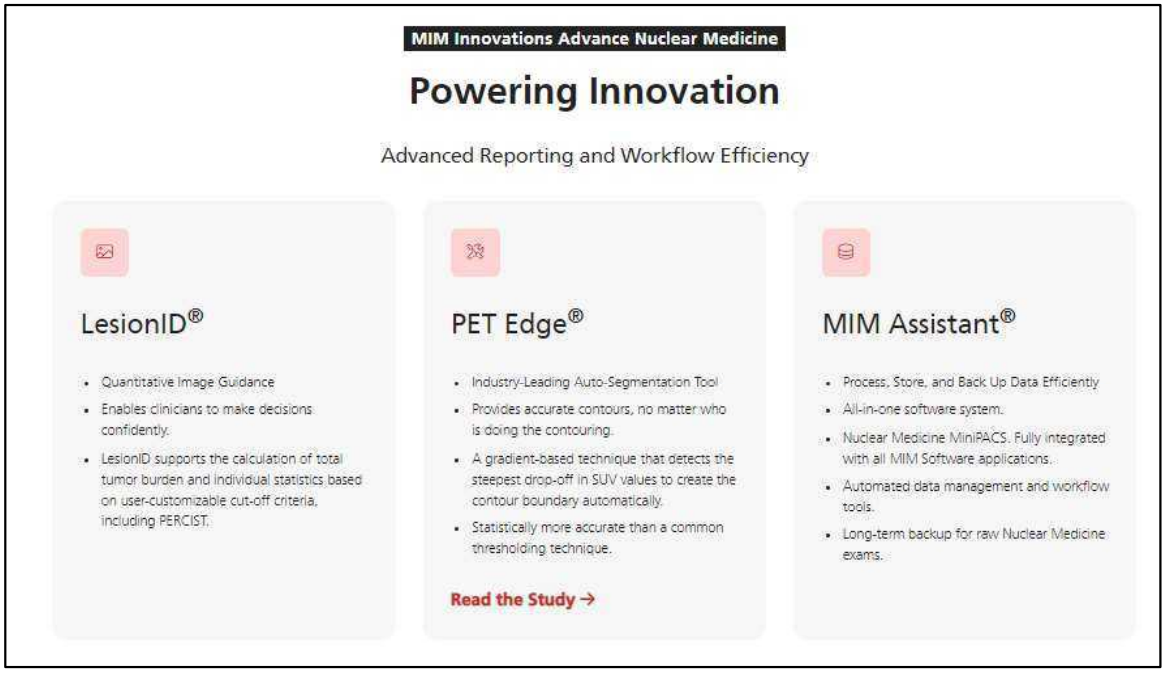
See "Molecular Radiotherapy Dosimetry" brochure, *supra* ¶ 63, at 6. MIM's website also notes that the Infringing Products leverage MIM Assistant®, which allows users to "[a]ccess data off-site with VPN or other network extensions," and/or MIMcloud®, which provides "a secure, internet-based medical image service that provides an easily accessible resource for storing, sharing, and viewing your data." *See* MIM Assistant®, *supra* ¶ 63; MIMcloud®, *supra* ¶ 64; *see also* 510(k) Summary of Safety and Effectiveness, Food & Drug Admin., No. K231765 (Nov. 8, 2023), *available at* https://www.accessdata.fda.gov/cdrh_docs/pdf23/K231765.pdf, at 2 ("Contour ProtégéAI is deployed on a remote server using the MIMcloud service for data management and transfer . . . ").

78. The Infringing Products possess the first limitation of claim 1 of the '035 patent[11] because MIM's Molecular Radiotherapy Dosimetry brochure refers to how the Infringing Products "Deliver AI on Premise or in the Cloud." *See* "Molecular Radiotherapy Dosimetry" brochure, *supra* ¶ 63, at 6. MIMcloud® provides an "easily accessible resource for storing, sharing, and viewing your data," and "secure, long-term off-site storage backup." MIMcloud®, *supra* ¶ 64. MIM's website represents it as follows:



Id. MIM's website also reflects that LesionID® is packaged with MIM Assistant® as part of MIM Encore®:

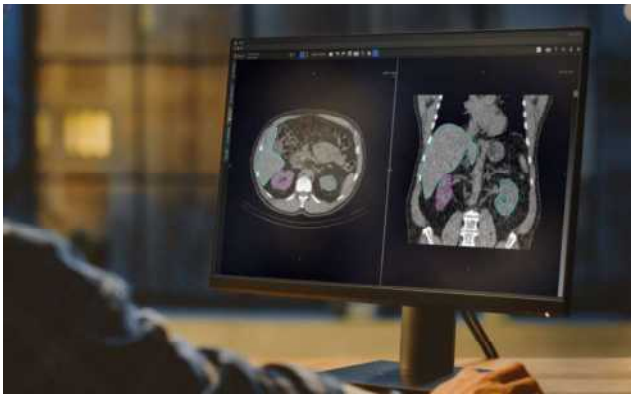
[11] *See* '035 patent, claim 1(i) ("receive and store a plurality of medical images in a database, each medical image associated with a corresponding patient").



MIM's website states that MIM Assistant® "function[s] as an imaging server," "cache[s] a subset of data for mobile access," and "[k]eep[s] data within your local network." MIM Assistant®, *supra* ¶ 63.

79. The Infringing Products also possess the second limitation of claim 1 of the '035 patent[12] because the Infringing Products access scan images for particular patients upon request from an electronic database, and then present those images to clinicians and patients. A MIM brochure, for example, notes how "Contour ProtégéAI for MIM SurePlan MRT has flexible deployment models that allow for easier adoption across any institution." *See* "Molecular Radiotherapy Dosimetry" brochure, *supra* ¶ 63, at 6. The brochure also shows an image of a patient scan presented on a screen, reflecting how the Infringing Products allow for access to such images upon request for display on a computer:

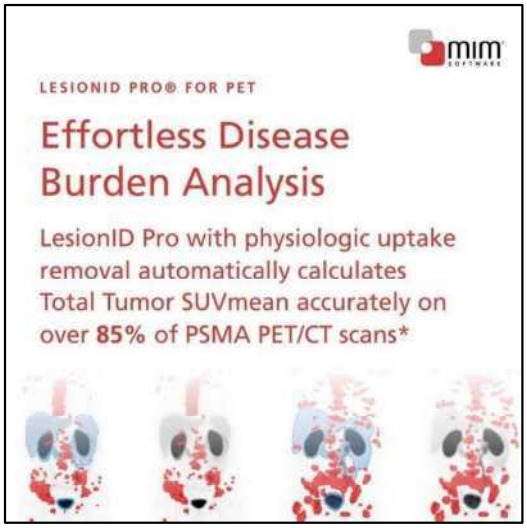
[12] *See* claim 1(ii) ("access one or more of the medical images associated with a particular patient from the database upon user request for transmission to the user for display on a user computing device").



Id. MIM's website also refers to how MIMcloud® can "push and pull images, and easily share studies . . ." *See* MIMcloud®, *supra* ¶ 64. Furthermore, according to MIM's website, MIM Assistant® lets users "[a]ccess patient studies with fast searching and viewing" and "[a]ccess data off-site with VPN or other network extensions," thereby indicating the transmission of patient medical images upon request for display on a computing device. MIM Assistant®, *supra* ¶ 63.

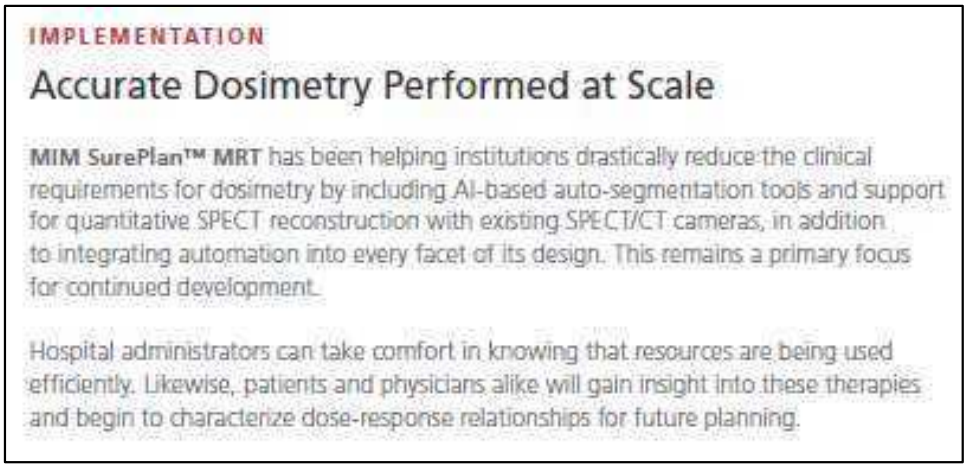
80. The Infringing Products possess the third limitation of claim 1 of the '035 patent[13] because MIM SurePlan™ MRT uses Contour ProtégéAI® which, according to a MIM brochure, "segment[s] normal structures with artificial intelligence." *See* "Molecular Radiotherapy Dosimetry" brochure, *supra* ¶ 63, at 6; *see also id.* ("Triggered automatically upon image arrival, Contour ProtégéAI™ and MIM SurePlan MRT uses a neural network for segmenting normal structures on CT images. Results are more accurate than atlas-based approaches so users spend less time editing."). The same brochure also discusses how MIM SurePlan™ MRT uses PET Edge® to create contour tumor regions that are then overlaid on a SPECT/CT image. *Id.* at 7. Further, MIM posted on LinkedIn a graphic indicating that LesionID Pro® for PET can be used to calculate total tumor SUVmean from PSMA PET/CT scans, which MIM described as an "innovative AI tool." LinkedIn Post, *supra* ¶ 65.

[13] *See* claim 1(iii) ("automatically analyze the one or more medical images using a machine learning algorithm").



81. The Infringing Products possess the fourth limitation of claim 1 of the '035 patent[14] because the MIM website describes LesionID® as being used for "Advanced Reporting and Workflow Efficiency" and explains how it "[e]nables clinicians to make decisions confidently." MIM Encore®, *supra* ¶ 63. Additionally, the MIM Molecular Radiotherapy Dosimetry brochure indicates that MIM SurePlan™ MRT generates a customizable dosimetry report that "allows for effective communication with patients and referring physicians." *See* "Molecular Radiotherapy Dosimetry" brochure, *supra* ¶ 63, at 10. Further, the MIM Molecular Radiotherapy Dosimetry brochure contains the following section indicating that SurePlan™ MRT perform dosimetry analysis on SPECT/CT images:

[14] *See* claim 1(iv) ("generate a radiologist report for the particular patient according to the one or more medical images for the patient, wherein the one or more medical images comprise a composite image of the particular patient, the composite image comprising a CT scan overlaid with a nuclear medicine image obtained at a substantially same time as the CT scan and following administration to the patient of an imaging agent comprising a Prostate Specific Membrane Antigen (PSMA) binding agent comprising a radionuclide, wherein the instructions cause the processor to automatically analyze the composite image by: (a) using the composite image to geographically identify a 3D boundary for each of one or more regions of imaged tissue within the nuclear medicine image; and (b) computing, using the nuclear medicine image with the identified 3D boundary(ies) of the one or more region(s) a risk map comprising a graphical denotation marking a region of risk of cancer or risk of recurrence of cancer.").


IMPLEMENTATION

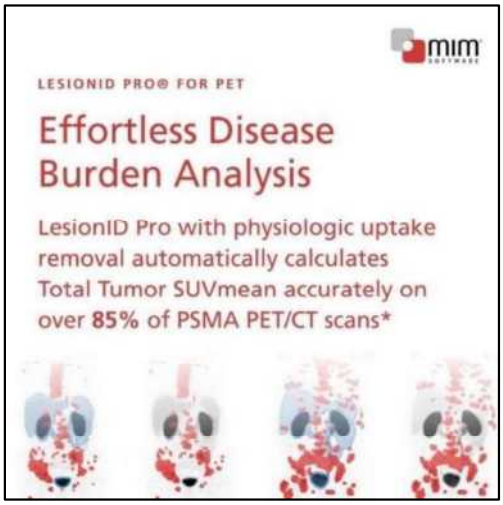
Accurate Dosimetry Performed at Scale

MIM SurePlan™ MRT has been helping institutions drastically reduce the clinical requirements for dosimetry by including AI-based auto-segmentation tools and support for quantitative SPECT reconstruction with existing SPECT/CT cameras, in addition to integrating automation into every facet of its design. This remains a primary focus for continued development.

Hospital administrators can take comfort in knowing that resources are being used efficiently. Likewise, patients and physicians alike will gain insight into these therapies and begin to characterize dose-response relationships for future planning.

Id. at 2. A SPECT/CT image is a composite image comprising a CT scan overlaid with a nuclear medicine image (since a SPECT image is a nuclear medicine image). Other publications indicate that the Infringing Products are used in connection with a PSMA-binding agent therapeutic that can be imaged via SPECT/CT to monitor its biodistribution. A 2023 article co-authored by a group including multiple MIM employees examined this kind of imaging with PSMA-binding agent-based therapeutics. In particular, the article describes performing CT-based deep learning (Convolutional Neural Network) segmentation of organs with physiological uptake to identify and remove VOIs (e.g., representing lesions) within those physiological uptake-associated organs. *See* Wilson et al., "Automating Total Tumor Volume (TTV) Generation on 177Lu-PSMA SPECT/CT Using Deep Learning to Create Normal Organs on the CT for Automatic Physiological Uptake Removal in Patients with Metastatic Castration Resistant Prostate Cancer (mCRPC)," J. of Nuclear Med. (2023), *available at* https://jnm.snmjournals.org/content/64/supplement_1/P914, at 1-3 ("Wilson (2023)"). The authors analyzed 177Lu-PSMA SPECT/CT images, which are composite images comprising a CT scan overlaid with a nuclear medicine image (i.e., a PET image), where the nuclear medicine image is obtained after administering a PSMA binding agent, which is a molecule designed to target and bind to PSMA proteins to detect the presence and location of prostate cancer cells in the body. MIM also published an article discussing the use of SurePlan™

MRT in connection with PSMA binding agents like 177Lu (Pluvicto). *See* David Mirando, "How Will You Handle the Rise in MRT Patient Volumes?", 3 European Fed'n of Orgs. for Med. Physicians 72, 72-73, *available at* https://www.efomp.org/uploads/702479dc-a5a8-45d3-9e15-9670c9a949bd/EFOMP%20Newsletter%20Autumn%202023.pdf (accessed on March 14, 2024). As further evidence, the MIM LinkedIn graphic below states that LesionID Pro® can be used to "calculate[] Total Tumour SUVmean accurately on . . . PSMA PET/CT scans":

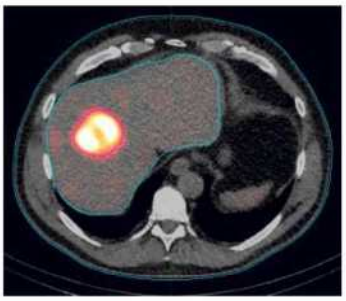


LinkedIn Post, *supra* ¶ 65. The PSMA PET/CT scans illustrated above are composite images comprising a CT scan overlaid with a nuclear medicine image obtained at a substantially same time as the CT scan. The images follow administration to the patient of a PSMA imaging agent.

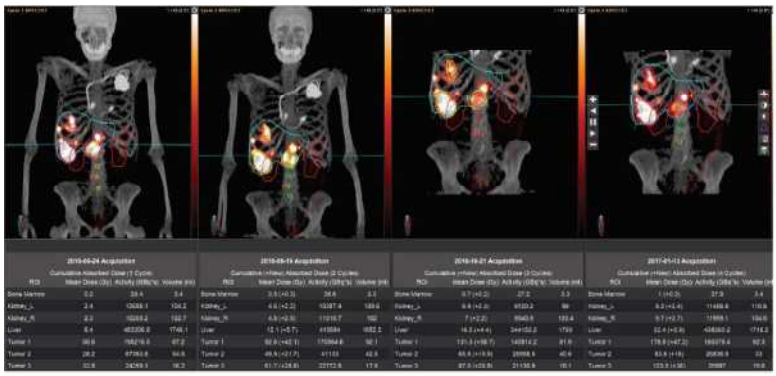
82. The fourth limitation of claim 1 of the '035 patent also includes two sub-steps performed in automatically analyzing the aforementioned composite image. These are: "(a) using the composite image to geographically identify a 3D boundary for each of one or more regions of imaged tissue within the nuclear medicine image; and (b) computing, using the nuclear medicine image with the identified 3D boundary(ies) of the one or more region(s) a risk map comprising a graphical denotation marking a region of risk of cancer or risk of recurrence of cancer." The Infringing Products practice both steps.

83. With regard to sub-step (a), several MIM employee-authored articles describe using a composite image to geographically identify a 3D boundary within tissue in a nuclear medicine image. The articles discuss identifying boundaries of particular organs—i.e., specific tissue region(s)—via segmentation of a CT image. *See* Wilson (2023) at 1-3; James Patrick Buteau et al., "Time-Savings Analysis of Total Tumor Burden Quantification on 68Ga-PSMA-11 PET/CT with Deep Learning Auto-Segmentation of Organs for Automatic Physiological Uptake Removal in Men with Metastatic Castration-Resistant Prostate Cancer (mCRPC)", J. of Nuclear Medicine (2022), available at https://jnm.snmjournals.org/content/63/supplement_2/2205, at 1-3 ("Buteau (2022)"). These identified contours are then transferred to PET images and compared with segmented VOIs representing potential lesions to remove physiological uptake, which can hinder accurate reading of the images. Additionally, a MIM brochure states that MIM SurePlan™ MRT uses Contour ProtégéAI® to identify 3D boundaries of an imaged tissue. *See* "Molecular Radiotherapy Dosimetry" brochure, *supra* ¶ 63, at 6. Therefore, when LesionID Pro® transfers organ contours identified in CT images to a PET image and compares segmented VOIs with these contours, LesionID Pro® is "using the composite image to geographically identify a 3D boundary for each of one or more regions of imaged tissue within the nuclear medicine image" as in claim 1 of the '035 patent.

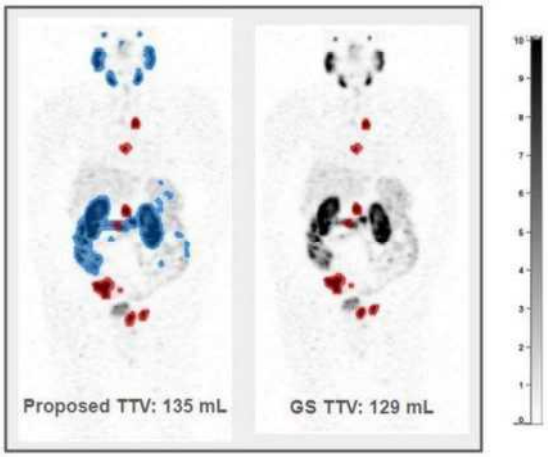
84. Sub-step (b) describes "computing, using the nuclear medicine image with the identified 3D boundary(ies) of the one or more region(s) a risk map comprising a graphical denotation marking a region of risk of cancer or risk of recurrence of cancer." The Infringing Products possess the claimed invention because, as reflected in the image below from a MIM brochure, MIM SurePlan™ MRT displays the risk map (i.e., tumor segmentation) via a graphical user interface (GUI):



See "Molecular Radiotherapy Dosimetry" brochure, *supra* ¶ 63, at 7. The same image also reveals that the Infringing Products display normal organ contours and tumor contours overlaid on medical images. *See id.* (blue color outlining an organ, and red color outlining a tumor). Another image in the same brochure also shows images of a SPECT/CT with organs and tumors outlined:



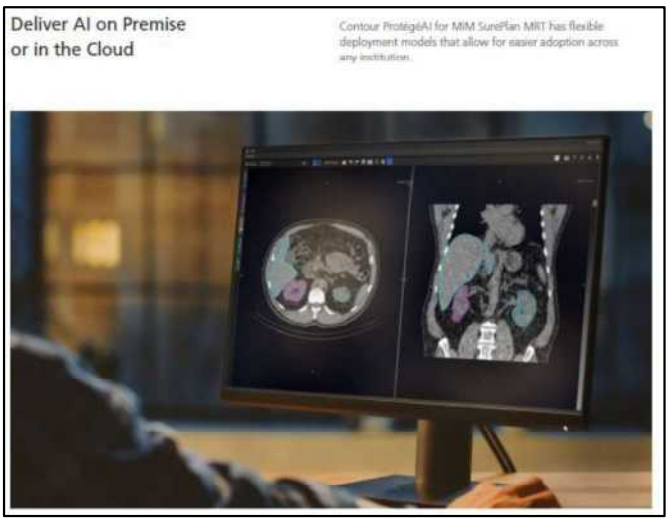
Id. at 10. Further, as described in the MIM employee-authored articles, LesionID Pro® removes VOIs (prospective lesions) that overlap with organs associated with physiological uptake. For example, Wilson (2023) shows red and blue masks, representing identified VOIs (prospective lesions) outside and within regions associated with physiological uptake, followed by removal of the blue portion, to leave a final mask (right hand side of the below)—i.e., a risk map:



Wilson (2023) at 3.

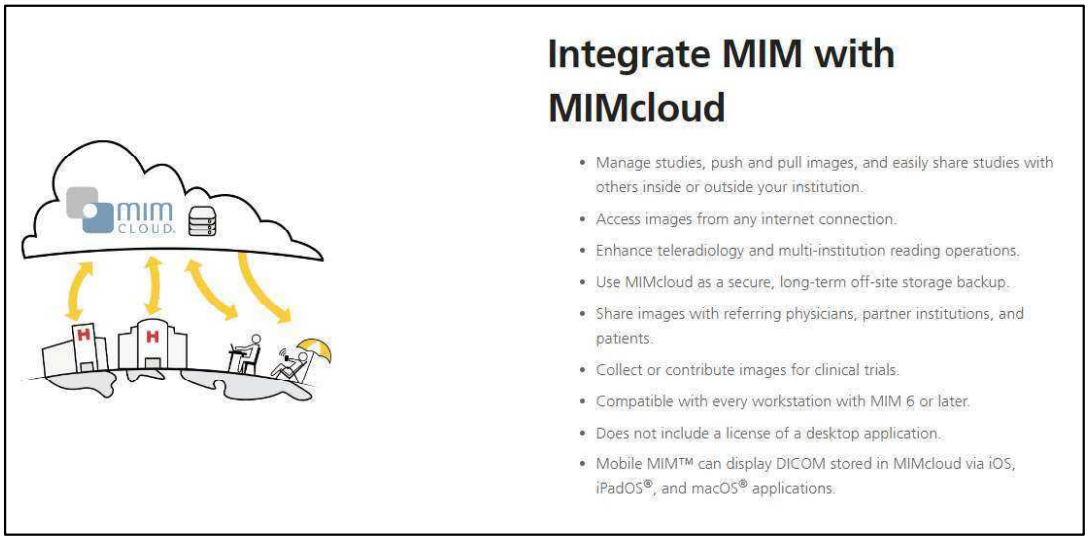
85. Turning next to the '141 patent, the Infringing Products also possess all the elements of exemplary claim 1.

86. The preamble to claim 1 of the '141 patent describes "[a] network-based decision support system comprising: a processor; and a memory having instructions stored thereon, wherein the instructions, when executed by the processor, cause the processor to:" (*see* '141 patent, at col. 37:8-12) (claim 1 preamble). MIM's brochure entitled "Molecular Radiotherapy Dosimetry" describes how the Infringing Products "Deliver AI on Premise or in the Cloud"—in other words, on a 'network-based system':



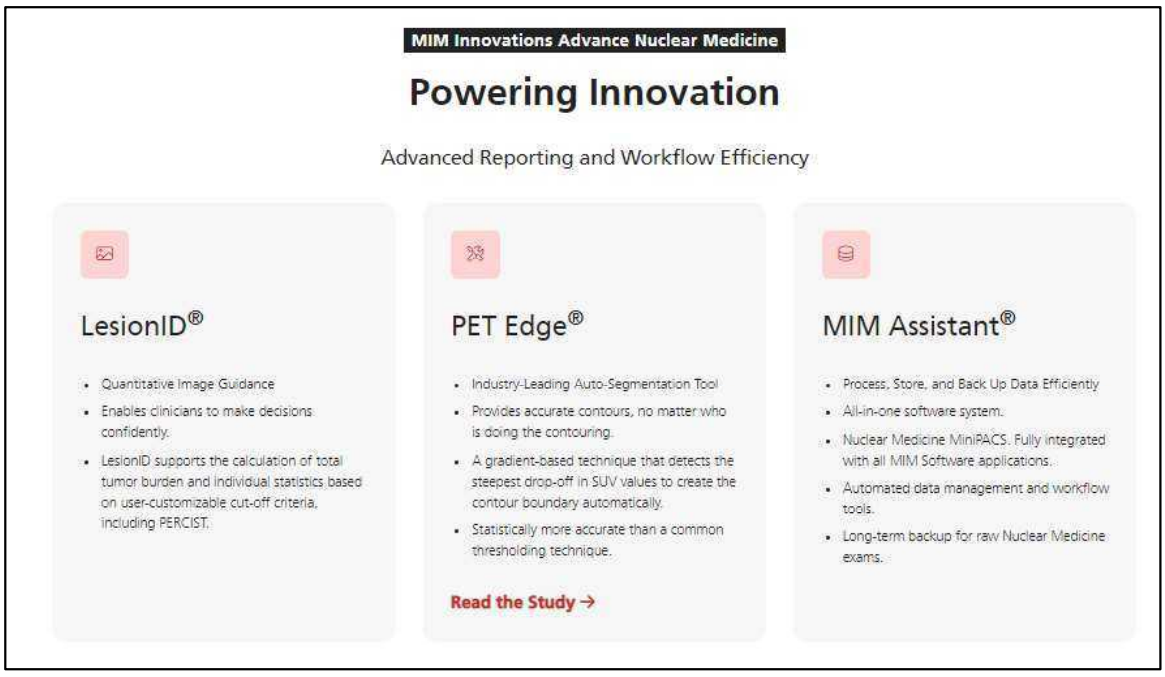
See "Molecular Radiotherapy Dosimetry" brochure, *supra* ¶ 63, at 6. MIM's website also notes that the Infringing Products leverage MIM Assistant®, which allows users to "[a]ccess data off-site with VPN or other network extensions," and/or MIMcloud®, which provides "a secure, internet-based medical image service that provides an easily accessible resource for storing, sharing, and viewing your data." *See* MIM Assistant®, *supra* ¶ 63; MIMcloud®, *supra* ¶ 64; *see also* 510(k) Summary of Safety and Effectiveness, *supra* ¶ 77, at 2 ("Contour ProtégéAI is deployed on a remote server using the MIMcloud service for data management and transfer . . . ").

87. The Infringing Products possess the first limitation of claim 1 of the '141 patent[15] because MIM's Molecular Radiotherapy Dosimetry brochure refers to how the Infringing Products "Deliver AI on Premise or in the Cloud." *See* "Molecular Radiotherapy Dosimetry" brochure, *supra* ¶ 63, at 6. MIMcloud® provides an "easily accessible resource for storing, sharing, and viewing your data," and "secure, long-term off-site storage backup." MIMcloud®, *supra* ¶ 64. MIM's website represents it as follows:



[15] *See* '141 patent, claim 1(i) ("receive and store a plurality of medical images in a database, each medical image associated with a corresponding patient").

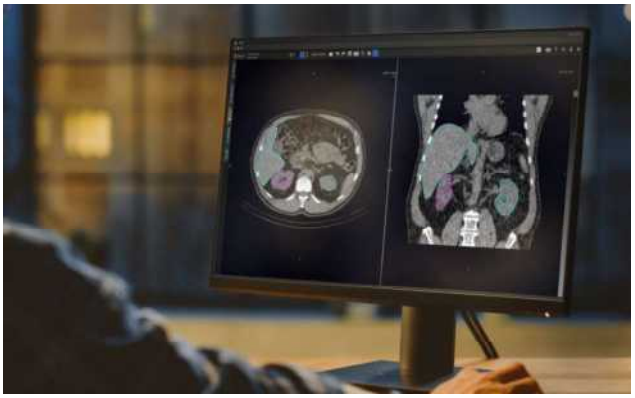
Id. MIM's website also reflects that LesionID® is packaged with MIM Assistant® as part of MIM Encore®:



MIM Encore®, *supra* ¶ 63. MIM's website also states that MIM Assistant® "function[s] as an imaging server," "cache[s] a subset of data for mobile access," and "[k]eep[s] data within your local network." MIM Assistant®, *supra* ¶ 63.

88. The Infringing Products also possess the second limitation of claim 1 of the '141 patent[16] because the Infringing Products access scan images for particular patients from a database. A MIM brochure, for example, notes how "Contour ProtégéAI for MIM SurePlan MRT has flexible deployment models that allow for easier adoption across any institution." *See* "Molecular Radiotherapy Dosimetry" brochure, *supra* ¶ 63, at 6. The brochure also shows an image of a patient scan presented on a screen, reflecting how the Infringing Products allow for access to such images in a database:

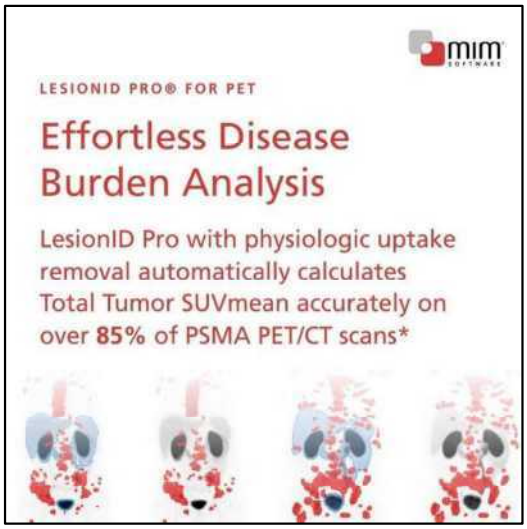
[16] *See* claim 1(ii) ("access one or more of the medical images associated with a particular patient from the database").



Id. MIM's website also refers to how MIMcloud® can "push and pull images, and easily share studies . . ." *See* MIMcloud®, *supra* ¶ 64. Moreover, MIM's website states that MIM Assistant® lets users "[a]ccess patient studies with fast searching and viewing" and "[a]ccess data off-site with VPN or other network extensions," thereby indicating MIM provides access to a database that stores patient data. MIM Assistant®, *supra* ¶ 63.

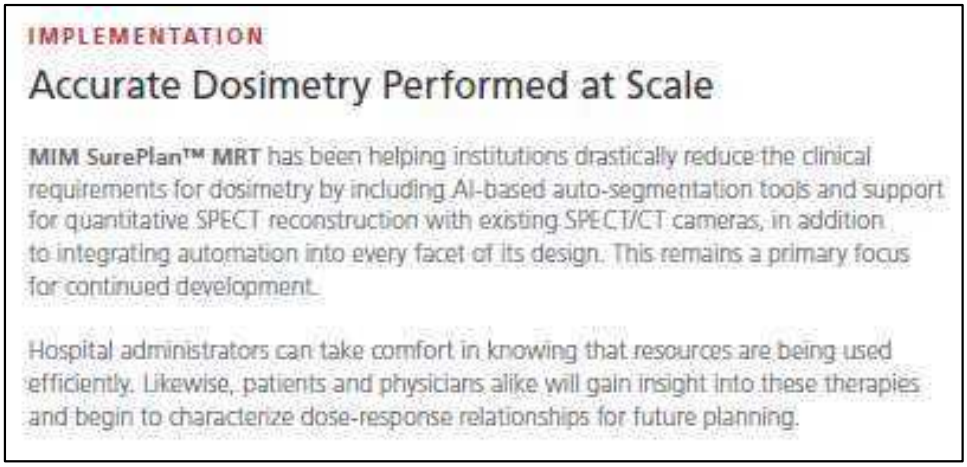
89. The Infringing Products possess the third limitation of claim 1 of the '141 patent[17] because MIM SurePlan™ MRT uses Contour ProtégéAI® which, according to a MIM brochure, "segment[s] normal structures with artificial intelligence." *See* "Molecular Radiotherapy Dosimetry" brochure, *supra* ¶ 63, at 6; *see also id.* ("Triggered automatically upon image arrival, Contour ProtégéAI for MIM SurePlan MRT uses a neural network for segmenting normal structures on CT images. Results are more accurate than atlas-based approaches so users spend less time editing."). The same brochure also discusses how MIM SurePlan™ MRT uses PET Edge® to create contour tumor regions that are then overlaid on a SPECT/CT image. *Id.* Further, MIM posted on LinkedIn a graphic that indicates LesionID Pro® for PET can be used to calculate total tumor SUVmean from PSMA PET/CT scans, which MIM described as an "innovative AI tool." LinkedIn Post, *supra* ¶ 65.

[17] *See* claim 1(iii) ("automatically analyze the one or more medical images using a machine learning algorithm").



90. The Infringing Products possess the fourth limitation of claim 1 of the '141 patent[18] because the MIM website describes LesionID® as being used for "Advanced Reporting and Workflow Efficiency" and explains how it "[e]nables clinicians to make decisions confidently." MIM Encore®, *supra* ¶ 63. Additionally, the MIM Molecular Radiotherapy Dosimetry brochure indicates that MIM SurePlan™ MRT generates a customizable dosimetry report that "allows for effective communication with patients and referring physicians." *See* "Molecular Radiotherapy Dosimetry" brochure, *supra* ¶ 63, at 10. Further, the MIM Molecular Radiotherapy Dosimetry brochure contains the following section indicating that SurePlan™ MRT performs dosimetry analysis on SPECT/CT images:

[18] *See* claim 1(iv) ("generate a radiologist report for the particular patient according to the one or more medical images for the patient, wherein the one or more medical images comprise a composite image of the particular patient, the composite image comprising a CT scan overlaid with a nuclear medicine image obtained at a substantially same time as the CT scan and following administration to the patient of an imaging agent comprising a Prostate Specific Membrane Antigen (PSMA) binding agent comprising a radionuclide, wherein the instructions cause the processor to automatically analyze the composite image by: (a) using the composite image to geographically identify a 3D boundary for each of one or more regions of imaged tissue within the nuclear medicine image; and (b) computing, using the nuclear medicine image with the identified 3D boundary(ies) of the one or more region(s), a value of each of one or more risk indices, each risk index value indicative of cancer state or progression in the patient, and wherein the system is a cloud-based system.").

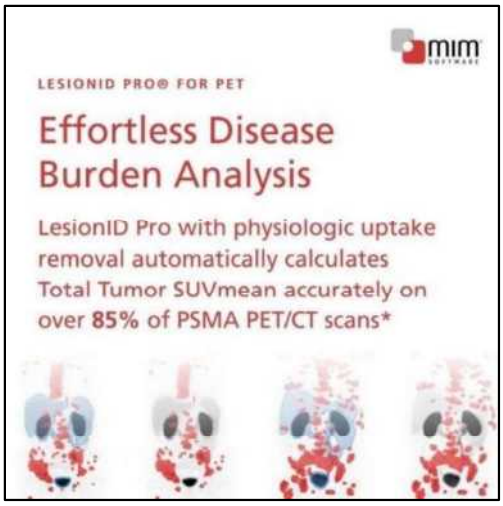

IMPLEMENTATION

Accurate Dosimetry Performed at Scale

MIM SurePlan™ MRT has been helping institutions drastically reduce the clinical requirements for dosimetry by including AI-based auto-segmentation tools and support for quantitative SPECT reconstruction with existing SPECT/CT cameras, in addition to integrating automation into every facet of its design. This remains a primary focus for continued development.

Hospital administrators can take comfort in knowing that resources are being used efficiently. Likewise, patients and physicians alike will gain insight into these therapies and begin to characterize dose-response relationships for future planning.

Id. at 2. A SPECT/CT image is a composite image comprising a CT scan overlaid with a nuclear medicine image (since a SPECT image is a nuclear medicine image). Other publications indicate that the Infringing Products are used in connection with a PSMA-binding agent therapeutic that can be imaged via SPECT/CT to monitor its biodistribution. Wilson (2023) examined this kind of imaging with PSMA-binding agent-based therapeutics. Wilson (2023) at 1-3. In particular, the article describes performing CT-based deep learning (Convolutional Neural Network) segmentation of organs with physiological uptake to identify and remove VOIs (e.g., representing lesions) within those physiological uptake-associated organs. *Id.* at 1-2. The authors analyzed 177Lu-PSMA SPECT/CT images, which are composite images comprising a CT scan overlaid with a nuclear medicine image (i.e., a PET image), where the nuclear medicine image is obtained after administering a PSMA binding agent. MIM also published an article discussing the use of SurePlan™ MRT in connection with PSMA binding agents like 177Lu (Pluvicto). *See* David Mirando, "How Will You Handle the Rise in MRT Patient Volumes?", 3 European Fed'n of Orgs. For Med. Physicians 72, 72-73, *available at* https://www.efomp.org/uploads/702479dc-a5a8-45d3-9e15-9670c9a949bd/EFOMP%20Newsletter%20Autumn%202023.pdf (accessed on March 14, 2024). As further evidence, the MIM LinkedIn graphic below states that LesionID Pro® can be used to "calculate[] Total Tumour SUVmean accurately on . . . PSMA PET/CT scans":



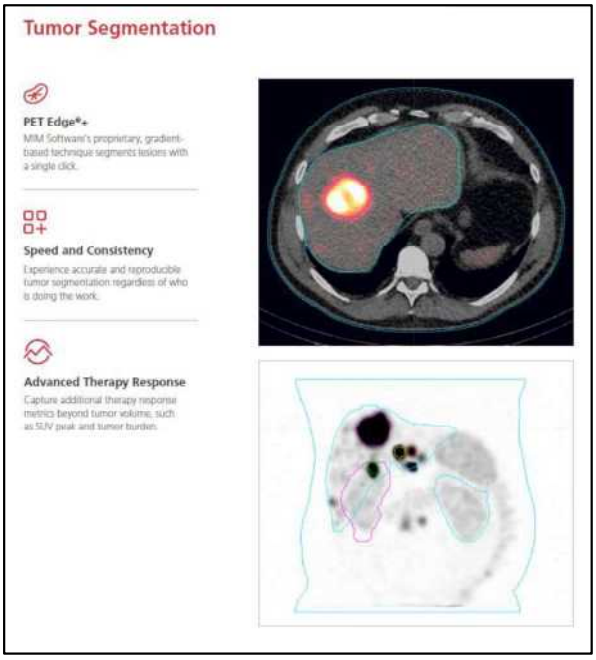
LinkedIn Post, *supra* ¶ 65. The PSMA PET/CT scans here are composite images comprising a CT scan overlaid with a nuclear medicine image obtained at a substantially same time as the CT scan; here, they follow administration to the patient of a PSMA imaging agent.

91. The fourth limitation of claim 1 of the '141 patent also includes two sub-steps to be performed in automatically analyzing the aforementioned composite image. These are: "(a) using the composite image to geographically identify a 3D boundary for each of one or more regions of imaged tissue within the nuclear medicine image; and (b) computing, using the nuclear medicine image with the identified 3D boundary(ies) of the one or more region(s), a value of each of one or more risk indices, each risk index value indicative of cancer state or progression in the patient, and wherein the system is a cloud-based system." The Infringing Products practice both steps.

92. With regard to sub-step (a), "using the composite image to geographically identify a 3D boundary for each of one or more regions of imaged tissue within the nuclear medicine image," several MIM employee-authored articles describe using a composite image to geographically identify a 3D boundary within tissue in a nuclear medicine image. The articles discuss identifying boundaries of particular organs—i.e., specific tissue region(s)—via segmentation of a CT image. *See* Wilson (2023) at 1-3; Buteau (2022) at 1-3. These identified

contours are then transferred to PET images and compared with segmented VOIs representing potential lesions to remove physiological uptake, which can hinder accurate reading of the images. Additionally, a MIM brochure states that MIM SurePlan™ MRT uses Contour ProtégéAI® to identify 3D boundaries of an imaged tissue. *See* "Molecular Radiotherapy Dosimetry" brochure, *supra* ¶ 63, at 6. Therefore, when LesionID Pro® transfers organ contours identified in CT images to a PET image and comparing segmented VOIs with these contours, it is "using the composite image to geographically identify a 3D boundary for each of one or more regions of imaged tissue within the nuclear medicine image" as in claim 1 of the '141 patent.

93. Sub-step (b) of the '141 patent describes "computing, using the nuclear medicine image with the identified 3D boundary(ies) of the one or more region(s), a value of each of one or more risk indices, each risk index value indicative of cancer state or progression in the patient[.]" The Infringing Products possess the claimed invention because MIM SurePlan™ MRT also segments tumors along with the 3D boundaries of tissue, and uses those segmentations to compute "Advanced Therapy Response" statistics like SUV peak and tumor burden:

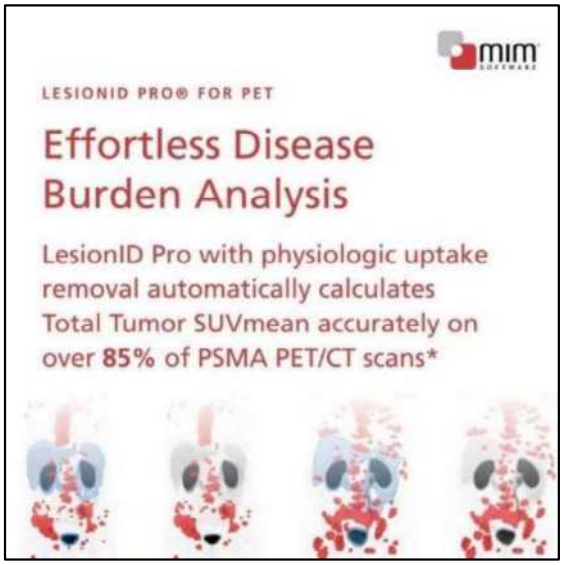


See "Molecular Radiotherapy Dosimetry" brochure, *supra* ¶ 63, at 7. This reflects that, when the Infringing Products calculate a therapy response like tumor burden, the Infringing Products calculate risk index values that indicate cancer state or progression. Wilson (2023) also describes how the Infringing Products remove VOIs (prospective lesions) that overlap with organs associated with physiological uptake, and then use the final set of VOIs (once those overlapping with organs associated with physiological uptake have been removed) to compute Total Tumor Volume (TTV) and Whole Body SUVmean. Wilson (2023) at 1-2. TTV and SUVmean are risk indices that indicate cancer state or progression in a patient. *Id*. Furthermore, with regard to the final wherein clause of the fourth limitation of the '141 patent, "wherein the system is a cloud-based system," the Contour ProtégéAI® 510(k) states that "Contour ProtégéAI is deployed on a remote server using the MIMcloud® service for data management and transfer; or locally on the workstation or server running MIM software." 510(k) Summary of Safety and Effectiveness, *supra* ¶ 77, at 2. MIM SurePlan™ MRT uses Contour ProtégéAI® to perform organ segmentation in CT images. *See* "Molecular Radiotherapy Dosimetry" brochure, *supra* ¶ 63, at 6. MIMcloud®, as discussed above, is a cloud-based system. MIMcloud®, *supra* ¶ 64. LesionID Pro® uses Contour ProtégéAI® in order to segment organs using AI, which is part of LesionID Pro®'s physiological uptake removal approach.

94. Turning next to the '508 patent, the Infringing Products also possess all the elements of exemplary claim 1.

95. The preamble to claim 1 describes "[a] method for automatically processing 3D images to identify, and measure uptake of radiopharmaceutical in, cancerous lesions within a subject having or at risk for a cancer, the method comprising:" (*see* '508 patent, at col. 79:64-67) (claim 1 preamble). MIM's LinkedIn post regarding "LesionID Pro® for PET" states that

"LesionID Pro with physiologic uptake removal automatically calculates Total Tumor SUVmean on . . . PET/CT scans":



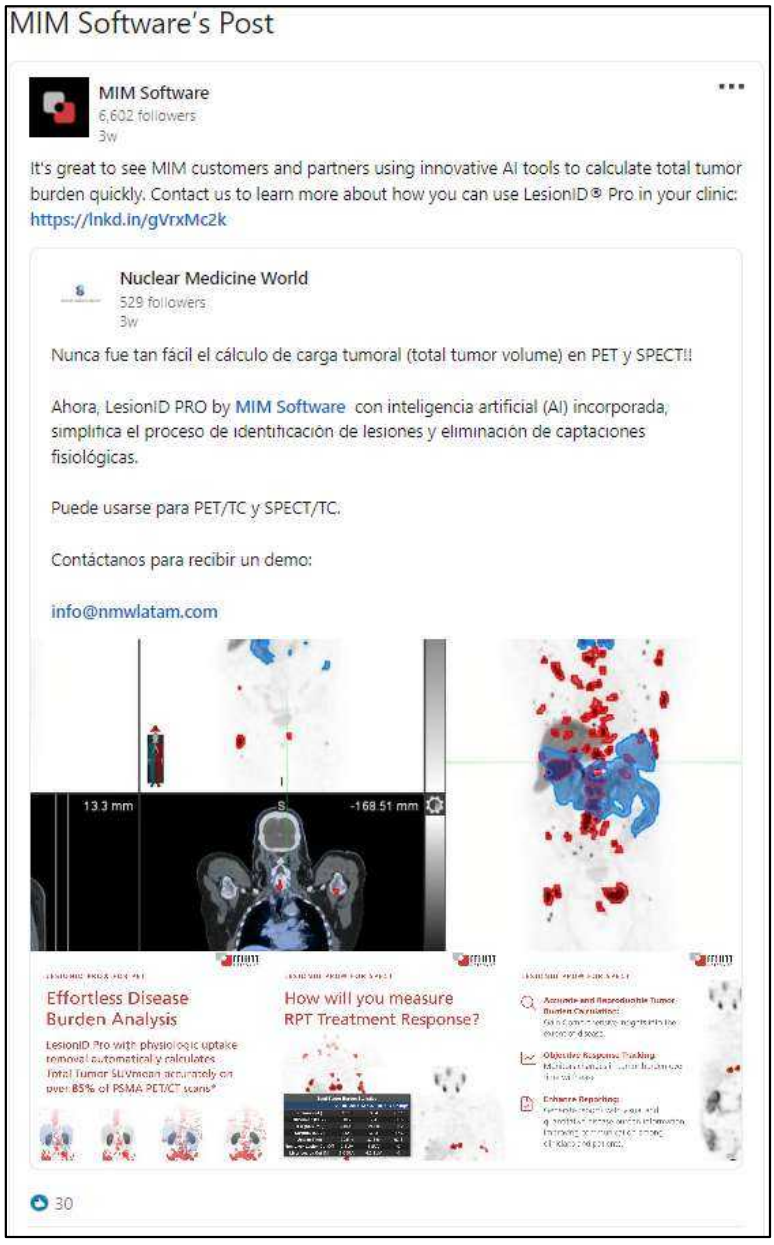
See LinkedIn Post, *supra* ¶ 65. PET and CT scans are 3D images. Tumors are cancerous lesions. These disclosures illustrate that the Infringing Products possess the preamble of claim 1.

96. The Infringing Products also possess the first limitation of claim 1 of the '508 patent[19] because, as indicated in the paragraph immediately above, the LesionID® software involves receiving a PET or CT scan image, which are types of "3D anatomical image[s]." *Id.* And, as indicated above, the same image presents a graphical representation of a subject's tissue.

97. The Infringing Products also possess the second limitation of claim 1 of the '508 patent[20] because, as discussed in the two paragraphs above, LesionID® analyzes 3D anatomical images. A MIM LinkedIn post also demonstrates that the Infringing Products use machine

[19] *See* '508 patent, claim 1(a) ("receiving, by a processor of a computing device, a 3D anatomical image of a subject obtained using an anatomical imaging modality, wherein the 3D anatomical image comprises a graphical representation of tissue within a subject").
[20] *See* claim 1(b) ("automatically identifying, by the processor, using one or more machine learning modules, within the 3D anatomical image: a first skeletal volume comprising a graphical representation of one or more bones of the subject; a first aorta volume comprising a graphical representation of at least portion of an aorta of the subject; and a first liver volume comprising a graphical representation of a liver of the subject").

learning modules. The post states that "[i]t's great to see MIM customers and partners using innovative **AI tools to calculate tumor burden quickly**. Contact us to learn more about how you can use LesionID Pro® in your clinic." LinkedIn Post, *supra* ¶ 65 (emphasis added). Machine learning is a form of AI:



Id. Wilson (2023) also describes approaches for removing physiological uptake, including machine learning-based organ segmentation. The publication states that "**utilizing normal**

structures created by a CT-based deep learning convolutional neural network, VOIs [volumes of interest] contained within organs with physiological uptake were removed from the proposed segmentation. **Organ contours used in the algorithm included**: **liver**, kidneys, parotids, submandibular glands, lacrimal glands, **bone,** bowel, pelvic lymph nodes, prostate, and bladder[.]" Wilson (2023) at 2 (emphasis added). This indicates that the Infringing Products focus on both the skeleton/bones, as well as the liver. MIM's November 2023 510(k) for Contour ProtégéAI® also indicates that its module for "Whole Body – Physiological Uptake Organs" segments the heart, which includes at least a portion of the aorta (an artery originating, and partially contained within, the heart):

Whole Body - Physiological Uptake Organs	Bladder	N/A	95
	Bone	N/A	100
	Bowel	N/A	100
	BowelBag	N/A	100
	Brain	N/A	100
	Cavity_Oral	N/A	100
	Glnd_Lacrimal_L	N/A	100
	Glnd_Lacrimal_R	N/A	100
	Glnd_Submand_L	N/A	100
	Glnd_Submand_R	N/A	100
	Heart	N/A	100
	Kidney_L	N/A	95
	Kidney_R	N/A	100
	Liver	N/A	100
	LN_Iliac	N/A	64

510(k) Summary of Safety and Effectiveness, *supra* ¶ 77, at 18 (also noting the reference to bone/skeleton, and liver) (highlighting added). The same 510(k) also reflects the connection between Contour ProtégéAI® and the "Whole Body – Physiological Uptake Organs" module:

ITEM	Subject Device: Contour ProtégéAI (K231765)	Predicate Device: Contour ProtégéAI (K223774)	Reference Predicate: MIM 4.1 SEASTAR [i.e., MIM Maestro] (K071964)
	SurePlan MRT CT **(4.1.0 models)** Head and Neck CT Thorax CT Whole Body – Physiological Uptake Organs CT	SurePlan MRT CT	

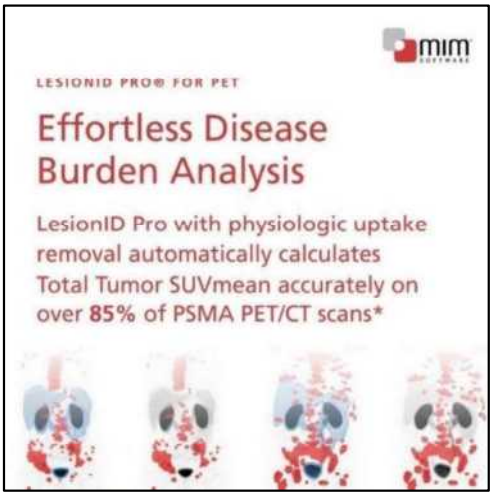
Id.

98. The Infringing Products also possess the third limitation of claim 1 of the '508 patent[21] because, as reflected in both Wilson (2023)[22] and Buteau (2022)[23], the Infringing Products involve a physiological uptake removal technique that creates organ contours and transfers them to nuclear medicine (e.g., SPECT and/or PET) images. The articles expressly reference organ contours including "bone" and "liver." *See* Wilson (2023) at 2 and Buteau (2022) at 2. As referenced above, the Contour ProtégéAI® 510(k) references "bone," "liver," and "heart" (which would necessarily include the aorta) as organs segmented by the "Whole

[21] *See* claim 1(c) ("determining, by the processor, a 3D segmentation map representing a plurality of 3D segmentation masks, including a skeletal mask representing the identified first skeletal volume, an aorta mask representing the identified first aorta volume, and a liver mask representing the identified first liver volume").
[22] Wilson (2023) at 2 ("The proposed algorithm segmented all VOIs in the image with a 3 SUV threshold. Then, utilizing normal structures created by a CT-based deep learning convolutional neural network, VOIs contained within organs with physiological uptake were removed from the proposed segmentation. Organ contours used in the algorithm included: liver, kidneys, parotids, submandibular glands, lacrimal glands, bone, bowel, pelvic lymph nodes, prostate, and bladder . . .").
[23] Buteau 2022 at 2 ("The second method (PUR) involved the same semi-automatic segmentation tool, with the addition of PUR-specific steps, to automatically remove physiological uptake before the reader started editing. These steps included running a deep learning organ segmentation algorithm to create CT-based organ VOIs for areas of physiological uptake (submandibular glands, parotid glands, lacrimal glands, spleen, kidneys, bowel, and bladder) and organs in which PSMA-avid lesions are expected (liver, brain, bone, pelvic lymph nodes, and prostate) . . . The contours were rigidly transferred from the CT to the PET and automatically modified to better adhere to the PET organ borders. Lesions that significantly overlapped the physiological uptake organs were removed automatically."). Buteau (2022) is another article with many MIM co-authors.

Body – Physiological Uptake Organs" model. 510(k) Summary of Safety and Effectiveness, *supra* ¶ 77, at 18.

99. The Infringing Products also possess the fourth limitation of claim 1 of the '508 patent[24] because, as discussed above, the MIM post describing the Infringing Products below expressly references the calculation of "Tumor SUVmean" on a PET/CT scan. PET/CT scans are both types of 3D functional images from a subject:



LinkedIn Post, *supra* ¶ 65. MIM's Molecular Radiotherapy Dosimetry brochure also describes how MIM SurePlan™ MRT operates in relation to SPECT scans, which produce 3D functional images:

[24] *See* '508 patent, claim 1(d) ("receiving, by the processor, a 3D functional image of the subject obtained using a functional imaging modality").



IMPLEMENTATION

Accurate Dosimetry Performed at Scale

MIM SurePlan™ MRT has been helping institutions drastically reduce the clinical requirements for dosimetry by including AI-based auto-segmentation tools and support for quantitative SPECT reconstruction with existing SPECT/CT cameras, in addition to integrating automation into every facet of its design. This remains a primary focus for continued development.

Hospital administrators can take comfort in knowing that resources are being used efficiently. Likewise, patients and physicians alike will gain insight into these therapies and begin to characterize dose-response relationships for future planning.

"Molecular Radiotherapy Dosimetry" brochure, *supra* ¶ 63, at 2.

100. The Infringing Products also possess the fifth limitation of claim 1 of the '508 patent[25] because, as described in Buteau (2022), organ contours for bone, liver, and other regions are transferred to a PET image, thereby identifying corresponding volumes in the PET image (i.e., within the functional image). *See* Buteau (2022) at 2 ("The contours were rigidly transferred from the CT to the PET and automatically modified to better adhere to the PET organ borders."). Additionally, the Contour ProtégéAI® "Whole Body – Physiological Uptake Organs" model references the heart (and thus at least a portion of the aorta) as one of the applicable organs:

[25] *See* claim 1(e) ("automatically identifying, within the 3D functional image, using the 3D segmentation map: a second skeletal volume corresponding to the first identified skeletal volume, within the 3D anatomical image; a second aorta volume corresponding to the first aorta volume, identified within the 3D anatomical image; and a second liver volume corresponding to the first liver volume, identified within the 3D anatomical image").

Whole Body - Physiological Uptake Organs	Bladder	N/A	95
	Bone	N/A	100
	Bowel	N/A	100
	BowelBag	N/A	100
	Brain	N/A	100
	Cavity_Oral	N/A	100
	Glnd_Lacrimal_L	N/A	100
	Glnd_Lacrimal_R	N/A	100
	Glnd_Submand_L	N/A	100
	Glnd_Submand_R	N/A	100
	Heart	N/A	100
	Kidney_L	N/A	95
	Kidney_R	N/A	100
	Liver	N/A	100
	LN_Iliac	N/A	64

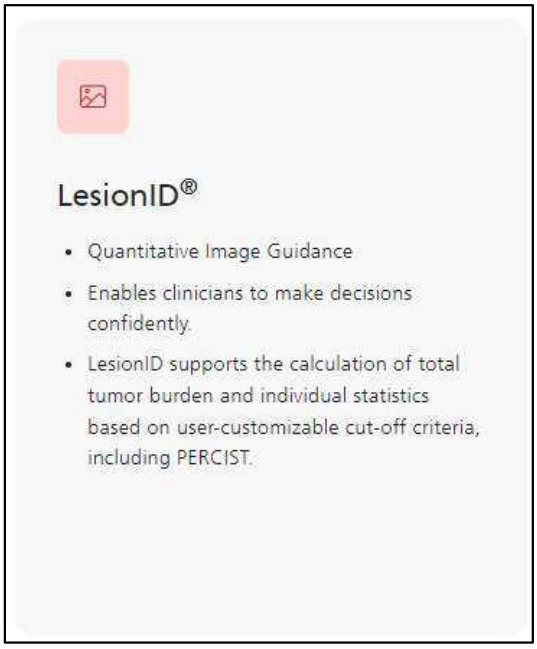
510(k) Summary of Safety and Effectiveness, *supra* ¶ 77, at 18 (highlighting added). The 510(k) reflects that the Infringing Products also transfer organ contours from the CT image to the PET image for the aorta, thereby identifying corresponding volumes in the PET image. *Id*. at 1-2.

101. The Infringing Products also possess the sixth limitation of claim 1 of the '508 patent[26] because the Infringing Products' technique for removal of physiological uptake involves detecting lesions within PET or SPECT images (i.e., 'hotspots'). *See, e.g.*, Wilson (2023) at 2; Buteau (2022) at 2. Buteau (2022) describes the Infringing Products' technique for removal of physiological uptake segments organ VOIs for (i) areas of physiological uptake (submandibular glands, parotid glands, lacrimal glands, spleen, kidneys, bowel, and bladder), and (ii) organs in which PSMA-avid lesions are expected (liver, brain, bone, pelvic lymph nodes, and prostate). Buteau (2022) at 2. The publication then states that "[l]esions that significantly overlapped the physiological uptake organs were removed automatically," which indicates that the Infringing Products retain lesions that are detected within identified bone contours (i.e., "in which PSMA-

[26] *See* claim 1(f) ("automatically detecting, by the processor, within the second skeletal volume, one or more hotspots determined to represent lesions based on intensities of voxels within the second skeletal volume").

avid lesions are expected"). *Id.* The Infringing Products thus detect and retain hotspots within bone regions in a PET or SPECT image.

102. The Infringing Products also possess the seventh limitation of claim 1 of the '508 patent[27] because the Infringing Products compute various metrics, such as tumor burden, volume, SUV mean, and so forth. For example, the MIM Encore® webpage lists LesionID® as a tool/component of MIM Encore® that "supports the calculation of total tumor burden and individual statistics based on user-customizable cut-off criteria, including PERCIST":



MIM Encore®, *supra* ¶ 63. PERCIST is an approach for measuring and tracking tumor burden over time. PERCIST involves, among other things, comparing lesion peak standardized update values (SUV's) to cut-off thresholds derived from liver and/or aorta reference intensities, and then

[27] *See* claim 1(g) ("determining, by the processor, for each of the one or more detected hotspots, an individual hotspot index value by: determining an aorta reference intensity level based on a measure of intensity of voxels with the second aorta volume; determining a liver reference intensity level based on a measure of intensity of voxels within the second liver volume; and for each individual detected hotspot: determining a corresponding individual hotspot intensity level based on a measure of intensity of voxels of the detected hotspot; and determining a corresponding individual hotspot index level from the individual hotspot intensity level, the aorta reference intensity level, and the liver reference intensity level.").

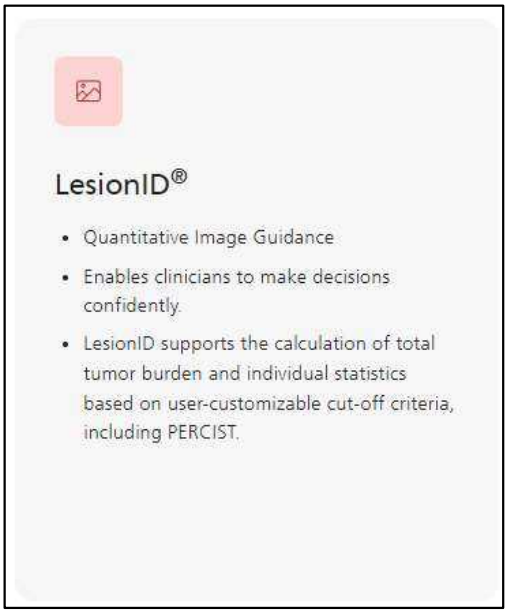
measuring the peak intensities of detected hotspots to identify the intensities that satisfy (i.e., exceed) the cut-off thresholds. *See, e.g.*, Joo Hyun O et al., "Practical PERCIST: A Simplified Guide to PET Response Criteria in Solid Tumors 1.0", 280 Radiology 576, 577 (2016). PERCIST criteria involve measuring an aorta reference intensity, *see id*. at 578 (col. 1) ("If the liver is diseased, the mean background SUL[28] and standard deviation can be measured in a cylindrical VOI with a diameter of 1 cm and a long axis (parallel to the descending aorta) of 2 cm in the center of the descending thoracic **aorta** . . ") (emphasis added), and a liver reference intensity. *See id*. at 577 ("For background activity, a 3-cm diameter spherical volume of interest (VOI) is placed in the right side of **liver**, midway between the dome and inferior margin, excluding central ducts and vessels") (emphasis added). PERCIST also requires at baseline the "measurement of the 'hottest' single tumor and background area on images[.]" *Id*. at 577. To identify the 'hottest' single tumor, PERCIST performs two steps for each detected hotspot: (1) PERCIST evaluates a peak SUL intensity for each hotspot (which will be compared with liver or aorta references (*see id*. at 578 (third column)) ("For a tumor to be measurable at baseline, the **SULpeak** must be greater than or equal to one and a half times the mean SUL in the 3-cm diameter spherical VOI plus two times its standard deviation to have a minimum threshold for evaluation . . . . When the SULpeak of the tumor at baseline is lower than this threshold, the tumor is considered not measurable with PERCIST 1.0.") (emphasis added); and (2) PERCIST compares the peak SUL intensity for each hotspot with liver or aorta references, retaining those hotspots with SULpeak values above the liver and aorta-derived thresholds and recording their SULpeak (e.g., to identify a maximum). *See id*. ("When the activity in the descending thoracic aorta is measured instead of that in the liver, the minimum threshold for evaluation is two times the mean SUL of the thoracic aorta in a tubular

[28] SUL is standardized uptake value (SUV) corrected for lean body mass.

VOI plus two times its standard deviation. This is proposed because blood SUL is typically lower than liver SUL."). Therefore, the Infringing Products possess the seventh limitation of claim 1 of the '508 patent.

103. Turning next to the '428 patent, the Infringing Products also possess all the elements of exemplary claim 1.

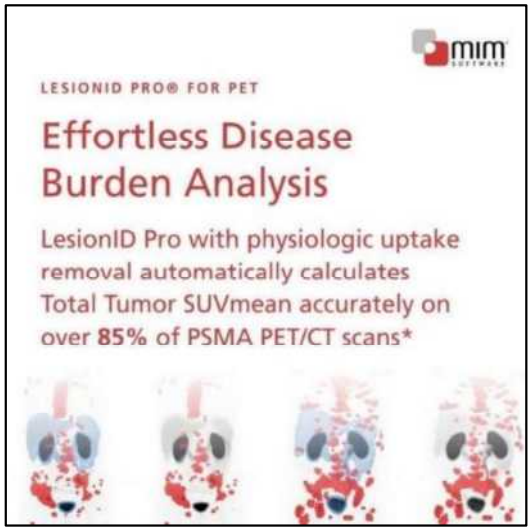
104. The preamble to claim 1 of the '428 patent describes "[a] method of measuring intensity values within a reference volume corresponding to a reference tissue region so as to avoid impact from tissue regions associated with low radiopharmaceutical uptake, the method comprising:" (*see* '428 patent, at col. 48:62-65) (claim 1 preamble). The Infringing Products compute various metrics, such as tumor burden, volume, SUV mean, and so forth. For example, the MIM Encore® webpage lists LesionID® as a component of MIM Encore® that "supports the calculation of total ***tumor burden*** and individual statistics based on user-customizable cut-off criteria, including PERCIST":



MIM Encore®, *supra* ¶ 63 (emphasis added). PERCIST is an approach for measuring and tracking tumor burden over time. PERCIST involves, among other things, comparing lesion peak SUV's

to cut-off thresholds derived from liver and/or aorta reference intensities and then measuring peak intensities of detected hotspots for those satisfying (i.e., exceeding) the cut-off thresholds. *See, e.g.*, Hyun O (2016) at 576-84. These disclosures illustrate that the Infringing Products possess the preamble of claim 1.

105. The Infringing Products also possess the first limitation of claim 1 of the '428 patent.[29] As demonstrated by the MIM LinkedIn post graphic below, LesionID Pro® "automatically calculates Total Tumor SUVmean accurately on . . . PET/CT scans":



LinkedIn Post, *supra* ¶ 65. A PET scan image is a 3D functional image of a subject. Therefore, the Infringing Products implement a method that receives a 3D functional image of a subject using PET and/or SPECT.

106. The Infringing Products also possess the second limitation of claim 1 of the '428 patent[30] because, as discussed immediately above, the Infringing Products involve the use of 3D functional images. Furthermore, the MIM Encore® webpage lists LesionID® as a component of

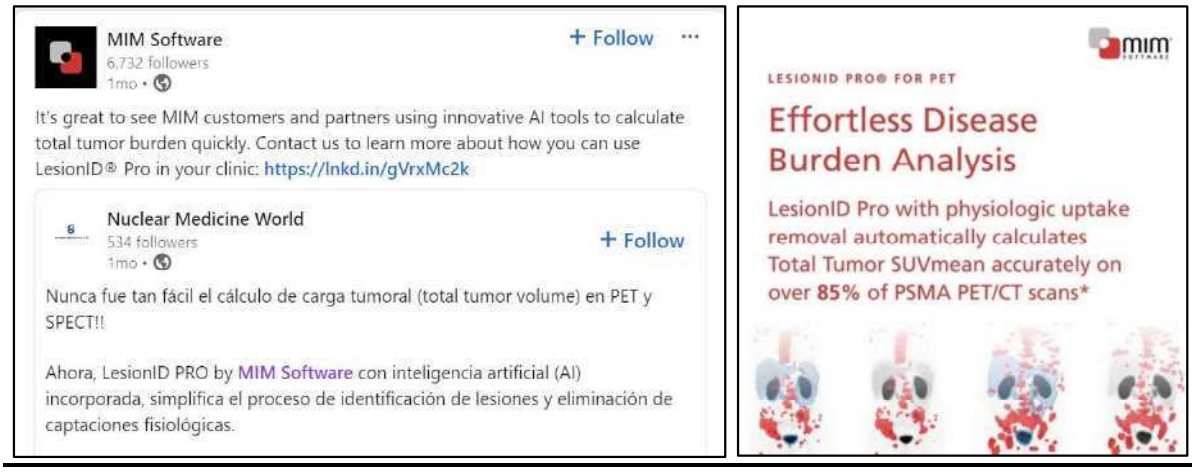
[29] *See* '428 patent, claim 1(a) ("receiving, by a processor of a computing device, a 3D functional image of a subject, said 3D functional image obtained using positron emission tomography (PET) and/or single-photon emission computed tomography (SPECT)").
[30] *See* claim 1(b) ("identifying, by the processor, the reference volume within the 3D functional image").

MIM Encore® that "supports the calculation of total tumor burden and individual statistics based on user-customizable cut-off criteria, including PERCIST." MIM Encore®, *supra* ¶ 63. PERCIST is a reporting method that utilizes (i.e., compares hotspot intensities to) reference volumes that are determined using regions within the liver and/or aorta reference regions. *See, e.g.*, Hyun O (2016) at 576-84.

107. The Infringing Products also possess the third, fourth, and fifth limitations of claim 1 of the '428 patent.[31] As discussed above, the MIM Encore® webpage lists LesionID® as a tool/component of MIM Encore® that "supports the calculation of total tumor burden and individual statistics based on user-customizable cut-off criteria, including PERCIST." MIM Encore®, *supra* ¶ 63. Implementing PERCIST involves manually placing or drawing a marker—such as a "3-cm diameter spherical volume of interest (VOI) in the right side of a liver"—to define a selection of voxels to compute a liver reference intensity (e.g., an average, peak, or other distributional statistic of intensity). *See, e.g.*, Hyun O (2016) at 577-78. The VOI marker is necessary to exclude irrelevant anatomy and/or diseased tissue (e.g., "central ducts and vessels," obvious metastatic tumor present in the liver, and other diseased tissue). *Id*. Measured liver references can thus be compromised by user placement of VOI markers and/or subject to inter-operator variability. *Id*. MIM lists LesionID® as a component of MIM Encore® that "supports the calculation of total tumor burden and individual statistics based on user-customizable cut-off criteria, including PERCIST." *See* MIM Encore®, *supra* ¶ 63. As a result, LesionID® also uses liver references and implements a technique that involves measuring reference intensities within

[31] *See* claim 1(c) ("fitting, by the processor, a multi-component mixture model to a distribution of intensities of voxels within the reference volume"); claim 1(d) ("identifying, by the processor, a major mode of the multi-component model"); and claim 1(e) ("determining, by the processor, a measure of intensities corresponding to the major mode, thereby determining a reference intensity value corresponding to a measure of intensity of voxels that are (i) within the reference tissue volume and (ii) associated with the major mode").

liver or other reference tissue, as claimed by the patent. MIM also indicates in public posts that LesionID Pro® utilizes AI tools to segment organs in CT images, including the liver, and transfers those segmentations to functional (e.g., PET, SPECT) images in order to compute tumor burden measurements:



See LinkedIn Post, *supra* ¶ 65. This reflects that LesionID® and LesionID Pro® use reference organs (such as the liver) to determine reference intensities for evaluating and calibrating radiopharmaceutical uptake and lesion severity. LesionID Pro® also uses AI tools to automate lesion identification and calculation of disease burden statistics.

108. The Infringing Products also possess the sixth limitation of claim 1 of the '428 patent[32] because, as described in Wilson (2023) and Buteau (2022), LesionID® identifies volumes of interest ("VOIs") that represent potential lesions (i.e., hotspots) within PET and/or SPECT images. *See, e.g.*, Wilson (2023) at 2 ("The proposed algorithm segmented all VOIs in the image with a 3 SUV threshold. Then, utilizing normal structures created by a CT-based deep learning convolutional neural network, VOIs contained within organs with physiological uptake were removed from the proposed segmentation. Organ contours used in the algorithm included: liver,

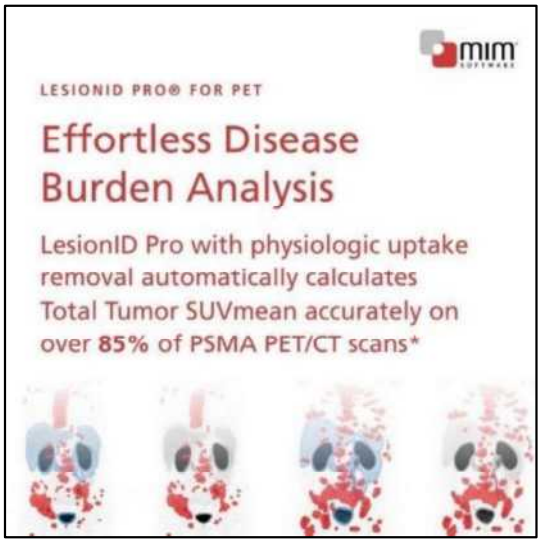
[32] *See* claim 1(f) ("detecting, by the processor, within the functional image, one or more hotspots corresponding potential cancerous lesions").

kidneys, parotids, submandibular glands, lacrimal glands, bone, bowel, pelvic lymph nodes, prostate, and bladder."); Buteau (2022) at 2 ("The second method (PUR) involved the same semi-automatic segmentation tool, with the addition of PUR-specific steps, to automatically remove physiological uptake before the reader started editing. These steps included running a deep learning organ segmentation algorithm to create CT-based organ VOIs for areas of physiological uptake (submandibular glands, parotid glands, lacrimal glands, spleen, kidneys, bowel, and bladder) and organs in which PSMA-avid lesions are expected (liver, brain, bone, pelvic lymph nodes, and prostate) . . . The contours were rigidly transferred from the CT to the PET and automatically modified to better adhere to the PET organ borders. Lesions that significantly overlapped the physiological uptake organs were removed automatically.").

109. The Infringing Products also possess the seventh limitation of claim 1 of the '428 patent[33] because, as discussed above, the Infringing Products use PERCIST criteria to identify and select lesions for inclusion in tumor burden analysis. For example, in PERCIST, "[m]easurement of the 'hottest' single tumor and background area on images, usually of the liver, is required at baseline." *See* Hyun O (2016) at 577 (first and second columns). To identify the 'hottest' single tumor using PERCIST criteria, one must perform two steps for each detected hotspot. First, evaluate a peak SUL intensity for each hotspot, and compare it with liver or aorta references. *Id*. at 578 (third column) ("For a tumor to be measurable at baseline, the SULpeak must be greater than or equal to one and a half times the mean SUL in the 3-cm diameter spherical VOI plus two times its standard deviation to have a minimum threshold for evaluation."). Second,

[33] *See* claim 1(g) ("determining, by the processor, for each particular hotspot of at least a portion of the detected hotspots, a lesion index value indicative of: (I) a level of radiopharmaceutical uptake within and underlying lesion to which the particular hotspot corresponds and/or (II) a size of an underlying lesion to which the particular hotspot corresponds, wherein the lesion index value is determined based on (i) a measure of intensity of the particular hotspot and (ii) the reference intensity value.").

"[w]hen the SULpeak of the tumor at baseline is lower than this threshold, the tumor is considered not measurable with PERCIST 1.0." *Id*. Therefore, when the Infringing Products evaluate whether a hotspot is considered a detectable lesion according to PERCIST, the Infringing Products compare the hotspot intensity with a reference intensity, and then store (for that hotspot) its intensity and/or volume in order to compute its tumor burden (e.g., SUVmean, total tumor volume). This approach is an example of automating tumor burden analysis in a manner that accounts for physiological uptake. MIM has touted the use of LesionID Pro® to account for physiological uptake, for example, in the MIM image below:



LinkedIn Post, *supra* ¶ 65; *see also* MIM Encore®, *supra* ¶ 63 (referencing LesionID®'s use of PERCIST).

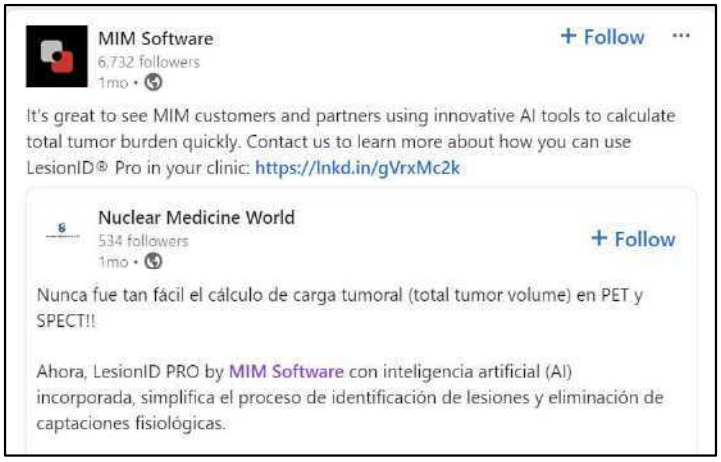
110. Turning next to the '817 patent, the Infringing Products also possess all the limitations of exemplary claim 1.

111. The preamble to claim 1 of the '817 patent describes "[a] method for automatically processing 3D images to automatically identify cancerous lesions within a subject, the method comprising:" (*see* '817 patent, at col. 79:5-7) (claim 1 preamble). Per MIM's LinkedIn post above, "LesionID Pro . . . automatically calculates Total Tumor SUVmean on . . . PET/CT scans."

LinkedIn Post, *supra* ¶ 65. This illustrates that the Infringing Products possess the preamble of claim 1.

112. The Infringing Products also possess the first limitation of claim 1 of the '817 patent[34] because, as MIM disclosed in its LinkedIn post, the Infringing Products "calculate[] Total Tumor SUVmean accurately on . . . PET/CT scans." *Id.* A CT scan is a 3D anatomical image of a subject's tissue. Therefore, the Infringing Products receive a 3D anatomical image of a subject, and thus possess the first limitation of claim 1.

113. The Infringing Products also possess the second limitation of claim 1 of the '817 patent[35] because, as MIM disclosed in its LinkedIn post, "MIM customers and partners [are] using innovative **AI tools to calculate total tumor burden quickly**":



Id. This post therefore discloses that the Infringing Products, like LesionID Pro®, use AI tools like machine learning modules. Furthermore, Wilson (2023) discloses that "[t]he proposed algorithm segmented all **VOIs** in the image with a 3 SUV threshold. Then, utilizing normal

[34] *See* '817 patent, claim 1(a) ("receiving, by a processor of a computing device, a 3D anatomical image of a subject obtained using an anatomical imaging modality, wherein the 3D anatomical image comprises a graphical representation of tissue within the subject").
[35] *See* claim 1(b) ("automatically identifying, by the processor, using one or more machine learning modules, for each of a plurality of target tissue regions, a corresponding target volume of interest (VOI) within the 3D anatomical image").

structures created by a **CT-based deep learning convolutional neural network**, VOIs contained within organs with physiological uptake were removed from the proposed segmentation." Wilson (2023) at 2 (emphasis added). Therefore, the Infringing Products possess the second limitation of claim 1.

114. The Infringing Products also possess the third limitation of claim 1 of the '817 patent[36] because, as discussed in Wilson (2023) and Buteau (2022), the LesionID Pro® physiological uptake removal technique involves creating 3D organ contours that represent and delineate particular organs, for example, in order to transfer them to 3D nuclear medicine (e.g., SPECT and/or PET) images. *See, e.g.*, Wilson (2023) at 2 ("The proposed algorithm segmented all VOIs in the image with a 3 SUV threshold. Then, utilizing normal structures created by a CT-based deep learning convolutional neural network, VOIs contained within organs with physiological uptake were removed from the proposed segmentation. Organ contours used in the algorithm included: liver, kidneys, parotids, submandibular glands, lacrimal glands, bone, bowel, pelvic lymph nodes, prostate, and bladder[.]"); Buteau (2022) at 2 ("The second method (PUR) involved the same semi-automatic segmentation tool, with the addition of PUR-specific steps, to automatically remove physiological uptake before the reader started editing. These steps included running a deep learning organ segmentation algorithm to create CT-based organ VOIs for areas of physiological uptake . . . and organs in which PSMA-avid lesions are expected . . . . The contours were rigidly transferred from the CT to the PET and automatically modified to better adhere to the PET organ borders. Lesions that significantly overlapped the physiological uptake organs were removed automatically."). The Infringing Products therefore possess the third limitation of claim 1.

[36] *See* claim 1(c) ("determining, by the processor, a 3D segmentation map representing a plurality of 3D segmentation masks, each 3D segmentation mask representing a particular identified target VOI").

115. The Infringing Products also possess the fourth limitation of claim 1 of the '817 patent[37] because, as MIM disclosed in its LinkedIn post, the Infringing Products "calculate[] Total Tumor SUVmean accurately on . . . PET/CT scans." *Id*. A PET scan is a 3D functional image of a subject's tissue, and thus the Infringing Products receive a patient's 3D functional image. Therefore, the Infringing Products possess the fourth limitation of claim 1.

116. The Infringing Products also possess the fifth limitation of claim 1 of the '817 patent[38] because, as described in Wilson (2023) and Buteau (2022), the LesionID Pro® physiological uptake removal technique includes steps of transferring 3D contours representing identified organs (VOIs) to a 3D nuclear medicine (e.g., SPECT and/or PET) image, thereby identifying corresponding 3D volumes therein. *See, e.g.*, Wilson (2023) at 2 ("The proposed algorithm segmented all VOIs in the image with a 3 SUV threshold. Then, utilizing normal structures created by a CT-based deep learning convolutional neural network, VOIs contained within organs with physiological uptake were removed from the proposed segmentation. Organ contours used in the algorithm included: liver, kidneys, parotids, submandibular glands, lacrimal glands, bone, bowel, pelvic lymph nodes, prostate, and bladder[.]"); Buteau (2022) at 2 ("The second method (PUR) involved the same semi-automatic segmentation tool, with the addition of PUR-specific steps, to automatically remove physiological uptake before the reader started editing. These steps included running a deep learning organ segmentation algorithm to create CT-based organ VOIs for areas of physiological uptake . . . and organs in which PSMA-avid lesions are expected . . . . The contours were rigidly transferred from the CT to the PET and automatically modified to better adhere to the PET organ borders. Lesions that significantly overlapped the

[37] *See* claim 1(d) ("receiving, by the processor, a 3D functional image of the subject obtained using a functional imaging modality").
[38] *See* claim 1(e) ("identifying, within the 3D functional image, one or more 3D volume(s), each corresponding to an identified target VOI, using the 3D segmentation map").

physiological uptake organs were removed automatically."). The Infringing Products therefore possess the fifth limitation of claim 1.

117. The Infringing Products also possess the sixth limitation of claim 1 of the '817 patent[39] because the LesionID Pro® physiological uptake removal technique identifies VOIs that represent potential lesions—i.e., hotspots within PET and/or SPECT images—and evaluates them for overlap with organ contours that were segmented via a machine learning module (a CNN). *See, e.g.*, Wilson (2023) at 2 ("The proposed algorithm segmented all VOIs in the image with a 3 SUV threshold. Then, utilizing normal structures created by a CT-based deep learning convolutional neural network, VOIs contained within organs with physiological uptake were removed from the proposed segmentation. Organ contours used in the algorithm included: liver, kidneys, parotids, submandibular glands, lacrimal glands, bone, bowel, pelvic lymph nodes, prostate, and bladder[.]"); Buteau (2022) at 2 ("The second method (PUR) involved the same semi-automatic segmentation tool, with the addition of PUR-specific steps, to automatically remove physiological uptake before the reader started editing. These steps included running a deep learning organ segmentation algorithm to create CT-based organ VOIs for areas of physiological uptake . . . and organs in which PSMA-avid lesions are expected . . . . The contours were rigidly transferred from the CT to the PET and automatically modified to better adhere to the PET organ borders. Lesions that significantly overlapped the physiological uptake organs were removed automatically."). The Infringing Products therefore possess the sixth limitation of claim 1.

118. MIM has known of the existence of the Asserted Patents. MIM's infringement has been and is willful and in disregard for the Asserted Patents. MIM has no reasonable basis for

[39] *See* claim 1(f) ("automatically detecting, by the processor, within at least a portion of the one or more 3D volumes identified within the 3D functional image, one or more hotspots determined to represent lesions based on intensities of voxels within the 3D functional image.").

believing that it has a right to engage in the infringing conduct. As discussed above, MIM and Plaintiffs negotiated for years about a potential collaboration involving MIM purchasing the right to integrate Plaintiffs' patented inventions into MIM's software. During those negotiations, Plaintiffs even sent MIM, upon agreement to do so, a draft Collaboration Agreement that expressly listed nearly all the Asserted Patents. Yet, MIM willfully developed, marketed, and sold (and continues to market and sell) the Infringing Products containing Plaintiffs' patented inventions.

119. Plaintiffs have suffered substantial damage (and MIM has unlawfully benefitted) from MIM's infringement of the Asserted Patents. As discussed above, GE HealthCare chose to acquire MIM (rather than enter into a profitable commercial relationship of some kind with Plaintiffs) in large part because of MIM's infringing conduct. *Supra* at ¶¶ 54-58. Plaintiffs have also lost substantial advantage in the market as the only companies permitted to use the claimed inventions, which (as discussed above) represent major breakthroughs in the performance, reliability, and usability of nuclear medicine imaging for cancer and other serious ailments. As a result, Plaintiffs have begun to lose both existing and prospective business to MIM. MIM and Plaintiffs continue to compete for specific customers, and Plaintiffs expect future losses of their existing and prospective business unless MIM ceases its unlawful infringement. Plaintiffs have also lost a licensing and partnership opportunity in view of MIM's actions. Plaintiffs are thus entitled to the full measure of their damages from MIM's infringement, including (without limitation) lost profits, a reasonable royalty, and damages for MIM's willful infringement.

COUNT I: INFRINGEMENT OF U.S. PATENT NO. 10,665,346

120. Plaintiffs repeat and re-allege each of the foregoing paragraphs as if fully set forth herein.

121. MIM has been and is directly and/or indirectly infringing the '346 patent, either literally or under the doctrine of equivalents, by making, using, selling, or offering for sale in the United States, including within this judicial district, the Infringing Products, in violation of 35 U.S.C. § 271(a).

122. MIM has been and is inducing infringement of the '346 patent, either literally or under the doctrine of equivalents, by actively and knowingly inducing its customers to use the Infringing Products that embody or use the inventions claimed in the '346 patent, in violation of 35 U.S.C. § 271(b).

123. MIM's infringement has been, and continues to be knowing, intentional, and willful.

124. MIM's infringement of the '346 patent has caused, and will continue to cause, Plaintiffs damages for which Plaintiffs are entitled to compensation pursuant to 35 U.S.C. § 284.

125. MIM's infringement of the '346 patent has caused, and will continue to cause, Plaintiffs immediate and irreparable harm unless such infringing activities are enjoined by this Court pursuant to 35 U.S.C. § 283. Plaintiffs have no adequate remedy at law.

126. This case is exceptional and Plaintiffs are entitled to an award of attorney fees pursuant to 35 U.S.C. § 285.

COUNT II: INFRINGEMENT OF U.S. PATENT NO. 10,973,486

127. Plaintiffs repeat and re-allege each of the foregoing paragraphs as if fully set forth herein.

128. MIM has been and is directly and/or indirectly infringing the '486 patent, either literally or under the doctrine of equivalents, by making, using, selling, or offering for sale in the

United States, including within this judicial district, the Infringing Products, in violation of 35 U.S.C. § 271(a).

129. MIM has been and is inducing infringement of the '486 patent, either literally or under the doctrine of equivalents, by actively and knowingly inducing its customers to use the Infringing Products that embody or use the inventions claimed in the '486 patent, in violation of 35 U.S.C. § 271(b).

130. MIM's infringement has been, and continues to be knowing, intentional, and willful.

131. MIM's infringement of the '486 patent has caused, and will continue to cause, Plaintiffs damages for which Plaintiffs are entitled to compensation pursuant to 35 U.S.C. § 284.

132. MIM's infringement of the '486 patent has caused, and will continue to cause, Plaintiffs immediate and irreparable harm unless such infringing activities are enjoined by this Court pursuant to 35 U.S.C. § 283. Plaintiffs have no adequate remedy at law.

133. This case is exceptional and Plaintiffs are entitled to an award of attorney fees pursuant to 35 U.S.C. § 285.

COUNT III: INFRINGEMENT OF U.S. PATENT NO. 11,424,035

134. Plaintiffs repeat and re-allege each of the foregoing paragraphs as if fully set forth herein.

135. MIM has been and is directly and/or indirectly infringing the '035 patent, either literally or under the doctrine of equivalents, by making, using, selling, or offering for sale in the United States, including within this judicial district, the Infringing Products, in violation of 35 U.S.C. § 271(a).

136. MIM has been and is inducing infringement of the '035 patent, either literally or under the doctrine of equivalents, by actively and knowingly inducing its customers to use the Infringing Products that embody or use the inventions claimed in the '035 patent, in violation of 35 U.S.C. § 271(b).

137. MIM's infringement has been, and continues to be knowing, intentional, and willful.

138. MIM's infringement of the '035 patent has caused, and will continue to cause, Plaintiffs damages for which Plaintiffs are entitled to compensation pursuant to 35 U.S.C. § 284.

139. MIM's infringement of the '035 patent has caused, and will continue to cause, Plaintiffs immediate and irreparable harm unless such infringing activities are enjoined by this Court pursuant to 35 U.S.C. § 283. Plaintiffs have no adequate remedy at law.

140. This case is exceptional and Plaintiffs are entitled to an award of attorney fees pursuant to 35 U.S.C. § 285.

COUNT IV: INFRINGEMENT OF U.S. PATENT NO. 11,894,141

141. Plaintiffs repeat and re-allege each of the foregoing paragraphs as if fully set forth herein.

142. MIM has been and is directly and/or indirectly infringing the '141 patent, either literally or under the doctrine of equivalents, by making, using, selling, or offering for sale in the United States, including within this judicial district, the Infringing Products, in violation of 35 U.S.C. § 271(a).

143. MIM has been and is inducing infringement of the '141 patent, either literally or under the doctrine of equivalents, by actively and knowingly inducing its customers to use the

Infringing Products that embody or use the inventions claimed in the '141 patent, in violation of 35 U.S.C. § 271(b).

144. MIM's infringement has been, and continues to be knowing, intentional, and willful.

145. MIM's infringement of the '141 patent has caused, and will continue to cause, Plaintiffs damages for which Plaintiffs are entitled to compensation pursuant to 35 U.S.C. § 284.

146. MIM's infringement of the '141 patent has caused, and will continue to cause, Plaintiffs immediate and irreparable harm unless such infringing activities are enjoined by this Court pursuant to 35 U.S.C. § 283. Plaintiffs have no adequate remedy at law.

147. This case is exceptional and Plaintiffs are entitled to an award of attorney fees pursuant to 35 U.S.C. § 285.

COUNT V: INFRINGEMENT OF U.S. PATENT NO. 11,657,508

148. Plaintiffs repeat and re-allege each of the foregoing paragraphs as if fully set forth herein.

149. MIM has been and is directly and/or indirectly infringing the '508 patent, either literally or under the doctrine of equivalents, by making, using, selling, or offering for sale in the United States, including within this judicial district, the Infringing Products, in violation of 35 U.S.C. § 271(a).

150. MIM has been and is inducing infringement of the '508 patent, either literally or under the doctrine of equivalents, by actively and knowingly inducing its customers to use the Infringing Products that embody or use the inventions claimed in the '508 patent, in violation of 35 U.S.C. § 271(b).

151. MIM's infringement has been, and continues to be knowing, intentional, and willful.

152. MIM's infringement of the '508 patent has caused, and will continue to cause, Plaintiffs damages for which Plaintiffs are entitled to compensation pursuant to 35 U.S.C. § 284.

153. MIM's infringement of the '508 patent has caused, and will continue to cause, Plaintiffs immediate and irreparable harm unless such infringing activities are enjoined by this Court pursuant to 35 U.S.C. § 283. Plaintiffs have no adequate remedy at law.

154. This case is exceptional and Plaintiffs are entitled to an award of attorney fees pursuant to 35 U.S.C. § 285.

COUNT VI: INFRINGEMENT OF U.S. PATENT NO. 11,721,428

155. Plaintiffs repeat and re-allege each of the foregoing paragraphs as if fully set forth herein.

156. MIM has been and is directly and/or indirectly infringing the '428 patent, either literally or under the doctrine of equivalents, by making, using, selling, or offering for sale in the United States, including within this judicial district, the Infringing Products, in violation of 35 U.S.C. § 271(a).

157. MIM has been and is inducing infringement of the '428 patent, either literally or under the doctrine of equivalents, by actively and knowingly inducing its customers to use the Infringing Products that embody or use the inventions claimed in the '428 patent, in violation of 35 U.S.C. § 271(b).

158. MIM's infringement has been, and continues to be knowing, intentional, and willful.

159. MIM's infringement of the '428 patent has caused, and will continue to cause, Plaintiffs damages for which Plaintiffs are entitled to compensation pursuant to 35 U.S.C. § 284.

160. MIM's infringement of the '428 patent has caused, and will continue to cause, Plaintiffs immediate and irreparable harm unless such infringing activities are enjoined by this Court pursuant to 35 U.S.C. § 283. Plaintiffs have no adequate remedy at law.

161. This case is exceptional and Plaintiffs are entitled to an award of attorney fees pursuant to 35 U.S.C. § 285.

COUNT VII: INFRINGEMENT OF U.S. PATENT NO. 11,941,817

162. Plaintiffs repeat and re-allege each of the foregoing paragraphs as if fully set forth herein.

163. MIM has been and is directly and/or indirectly infringing the '817 patent, either literally or under the doctrine of equivalents, by making, using, selling, or offering for sale in the United States, including within this judicial district, the Infringing Products, in violation of 35 U.S.C. § 271(a).

164. MIM has been and is inducing infringement of the '817 patent, either literally or under the doctrine of equivalents, by actively and knowingly inducing its customers to use the Infringing Products that embody or use the inventions claimed in the '817 patent, in violation of 35 U.S.C. § 271(b).

165. MIM's infringement has been, and continues to be knowing, intentional, and willful.

166. MIM's infringement of the '817 patent has caused, and will continue to cause, Plaintiffs damages for which Plaintiffs are entitled to compensation pursuant to 35 U.S.C. § 284.

167. MIM's infringement of the '817 patent has caused, and will continue to cause, Plaintiffs immediate and irreparable harm unless such infringing activities are enjoined by this Court pursuant to 35 U.S.C. § 283. Plaintiffs have no adequate remedy at law.

168. This case is exceptional and Plaintiffs are entitled to an award of attorney fees pursuant to 35 U.S.C. § 285.

PRAYER FOR RELIEF

WHEREFORE, Plaintiffs respectfully request the following relief:

(A) A judgment that MIM has infringed the Asserted Patents;

(B) A judgment that MIM's infringement of the Asserted Patents has been willful;

(C) An award against MIM of damages sufficient to compensate Plaintiffs for MIM's infringement of the Asserted Patents;

(D) An award against MIM of all other damages permitted by 35 U.S.C. § 284, including increased damages up to three times the amount of compensatory damages found;

(E) A declaration that this is an exceptional case and an award against MIM and to Plaintiffs of their reasonable attorneys' fees incurred in this action as provided by 35 U.S.C. § 285;

(F) An order preliminarily and permanently enjoining MIM, and its officers, directors, agents, employees, affiliates, and all others acting in privity or in concert with it, and its parents, subsidiaries, divisions, successors, and assigns from further acts of infringement of the Asserted Patents; and

(G) All such other relief that this Court deems just and proper.

JURY DEMAND

Pursuant to Fed. R. Civ. P. 38(b), Plaintiffs hereby demand a jury trial on all issues triable of right by a jury.

Dated: April 5, 2024

Respectfully submitted,

/s/ Michael H. Bunis

Michael H. Bunis (BBO #566839)
Anita M. C. Spieth (BBO #676302)
John C. Calhoun (BBO #694479)
CHOATE, HALL & STEWART LLP
Two International Place
Boston, MA 02110
(617) 248-5000
mbunis@choate.com
aspieth@choate.com
jcalhoun@choate.com

Attorneys for Plaintiffs Progenics Pharmaceuticals, Inc. and EXINI Diagnostics AB.

CERTIFICATE OF SERVICE

I hereby certify that this document filed through the ECF system will be sent electronically to the registered participants as identified on the Notice of Electronic Filing (NEF).

Dated: April 5, 2024

/s/ *Michael H. Bunis*

Michael H. Bunis
CHOATE, HALL & STEWART LLP
Two International Place
Boston, MA 02110
(617) 248-5000
mbunis@choate.com

EXHIBIT 1

US010665346B2

(12) **United States Patent**
Baker

(10) **Patent No.: US 10,665,346 B2**
(45) **Date of Patent: *May 26, 2020**

(54) **NETWORK FOR MEDICAL IMAGE ANALYSIS, DECISION SUPPORT SYSTEM, AND RELATED GRAPHICAL USER INTERFACE (GUI) APPLICATIONS**

(71) Applicant: **Progenics Pharmaceuticals, Inc.**, New York, NY (US)

(72) Inventor: **Mark R. Baker**, New York, NY (US)

(73) Assignee: **Progenics Pharmaceuticals, Inc.**, New York, NY (US)

(*) Notice: Subject to any disclaimer, the term of this patent is extended or adjusted under 35 U.S.C. 154(b) by 0 days.

This patent is subject to a terminal disclaimer.

(21) Appl. No.: **16/718,839**

(22) Filed: **Dec. 18, 2019**

(65) **Prior Publication Data**

US 2020/0126666 A1 Apr. 23, 2020

Related U.S. Application Data

(63) Continuation of application No. 16/418,527, filed on May 21, 2019, which is a continuation of application (Continued)

(51) **Int. Cl.**
G06Q 10/00 (2012.01)
G06K 9/00 (2006.01)
(Continued)

(52) **U.S. Cl.**
CPC ***G16H 50/20*** (2018.01); ***G01N 33/57434*** (2013.01); ***G16H 15/00*** (2018.01);
(Continued)

(58) **Field of Classification Search**
USPC 382/100, 103, 128–134, 154–158, 162, 382/168, 173, 181, 206, 209, 220, 224,
(Continued)

(56) **References Cited**

U.S. PATENT DOCUMENTS

7,450,747 B2 11/2008 Jabri et al.
7,970,194 B2 6/2011 Kimura
(Continued)

FOREIGN PATENT DOCUMENTS

EP 1426903 A2 6/2004
EP 1508872 A1 2/2005
(Continued)

OTHER PUBLICATIONS

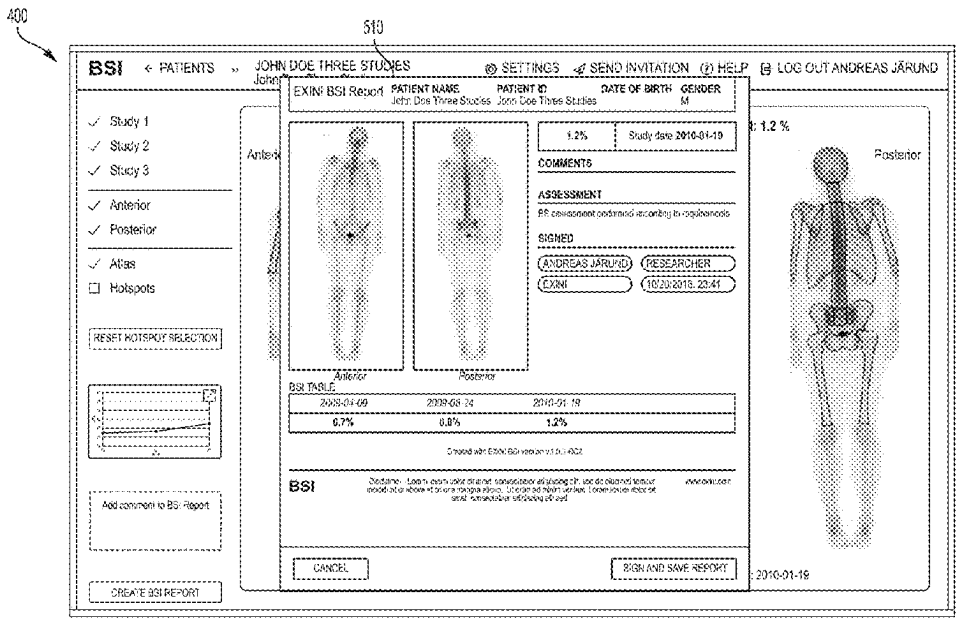
Anand, A. et al., Analytic Validation of the Automated Bone Scan Index as an Imaging Biomarker to Standardize Quantitative Changes in Bone Scans of Patients with Metastatic Prostate Cancer, J. Nucl. Med., 57(1):41-45 (2016).
(Continued)

Primary Examiner — Seyed H Azarian
(74) *Attorney, Agent, or Firm* — Ronen Adato; William R. Haulbrook; Choate, Hall and Stewart LLP

(57) **ABSTRACT**

Described herein is a platform and supported graphical user interface (GUI) decision-making tools for use by medical practitioners and/or their patients, e.g., to aide in the process of making decisions about a course of cancer treatment and/or to track treatment and/or the progress of a disease.

13 Claims, 11 Drawing Sheets



Related U.S. Application Data

No. 15/794,220, filed on Oct. 26, 2017, now Pat. No. 10,340,046.

(60) Provisional application No. 62/413,936, filed on Oct. 27, 2016.

(51) **Int. Cl.**

G16H 50/20	(2018.01)
G16H 30/20	(2018.01)
G16H 30/40	(2018.01)
G16H 50/70	(2018.01)
G16H 50/30	(2018.01)
G16H 15/00	(2018.01)
G01N 33/574	(2006.01)

(52) **U.S. Cl.**

CPC ***G16H 30/20*** (2018.01); ***G16H 30/40*** (2018.01); ***G16H 50/30*** (2018.01); ***G16H 50/70*** (2018.01)

(58) **Field of Classification Search**

USPC 382/232, 254, 286–295, 305, 312; 705/2

See application file for complete search history.

(56) **References Cited**

U.S. PATENT DOCUMENTS

8,211,401	B2	7/2012	Babich et al.	
8,538,166	B2	9/2013	Gordon et al.	
8,705,887	B2	4/2014	Ma et al.	
8,778,305	B2	7/2014	Pomper et al.	
8,855,387	B2	10/2014	Hamadeh et al.	
8,962,799	B2	2/2015	Babich et al.	
9,002,081	B2 *	4/2015	Brown	G06T 7/0014 382/128
RE47,609	E	9/2019	Hamadeh et al.	
2003/0215120	A1	11/2003	Uppaluri et al.	
2006/0062425	A1 *	3/2006	Shen	G06T 15/08 382/100
2007/0081712	A1 *	4/2007	Huang	G06T 7/38 382/128
2007/0081713	A1	4/2007	Jerebko	
2007/0100225	A1	5/2007	Maschke	
2015/0110716	A1	4/2015	Armor	
2015/0331995	A1 *	11/2015	Zhao	G16Z 99/00 705/2
2016/0203263	A1 *	7/2016	Maier	G16H 50/30 705/2
2016/0335395	A1 *	11/2016	Wu	G06F 19/321
2017/0083682	A1 *	3/2017	McNutt	G16H 50/30
2018/0144828	A1	5/2018	Baker	

FOREIGN PATENT DOCUMENTS

WO	WO-9905503	A2	2/1999
WO	WO-2007/062135	A2	5/2007
WO	WO-2009/084995	A1	7/2009
WO	WO-2018/081354	A1	5/2018

OTHER PUBLICATIONS

Anand, A. et al., Automated Bone Scan Index as a quantitative imaging biomarker in metastatic castration-resistant prostate cancer patients being treated with enzalutamide, EJNMMI Research, 6:23, 7 pages (2016).

Anand, A. et al., Translating Prostate Cancer Working Group 2 (PCWG2) Progression Criteria into a Quantitative Response Biomarker in Metastatic Castration Resistant Prostate Cancer (mCRPC), ASCO GU Conference, Poster, presented Feb. 16, 2017.

Anand, A. et al., Translating Prostate Cancer Working Group 2 (PCWG2) progression criteria into a quantitative response biomarker in metastatic castration-resistant prostate cancer (mCRPC), Journal of Clinical Oncology, 35(6):170 (2017).

Armstrong, A. et al., Assessment of the bone scan index in a randomized placebo-controlled trial of tasquinimod in men with metastatic castration-resistant prostate cancer (mCRPC), Urologic Oncology: Seminars and Original Investigations, 32:1308-1316 (2014).

Armstrong, A. et al., Development and validation of a prognostic model for overall survival in chemotherapy-naive men with metastatic castration-resistant prostate cancer (mCRPC) from the phase 3 prevail clinical trial, Journal of Clinical Oncology, 35(Suppl. 6):Abstract 138 (2017).

Armstrong, A. J. et al., Phase 3 prognostic analysis of the automated bone scan index (aBSI) in men with bone-metastatic castration-resistant prostate cancer (CRPC), Meeting Library ASC University, 1 page abstract, (2017).

Belal, S. et al., Association of PET Index quantifying skeletal uptake in NaF PET/CT images with overall survival in prostate cancer patients, ASCO GU 2017, Poster 178, presented Feb. 16, 2017.

Belal, S. et al., PET Index quantifying skeletal uptake in NaF PET/CT images with overall survival in prostate cancer patients, ASCO GU 2017, Abstract (Feb. 13, 2017).

Belal, S. L. et al, 3D skeletal uptake of ^{18}F sodium fluoride in PET/CT images is associate with overall survival in patients with prostate cancer, EJNMMI Research, 7(15):1-8 (2017).

Belal, S.L. et al., Automated evaluation of normal uptake in different skeletal parts in 18F-sodium fluoride (NaF) PET/CT using a new convolutional neural network method, EJNMMI, EANM '17, 44(Suppl 2):S119-S956, Abstract EP-0116 (2017).

Bushberg, J. T. et al., Essential Physics of Medical Imaging, Essential Physics of Medical Imaging, 19.3: p. 581 (table 15-3), p. 713 paragraph 6, section 19.3 and p. 720, (2011).

Dennis, E. et al., Bone Scan Index: A Quantitative Treatment Response Biomarker for Castration-Resistant Metastatic Prostate Cancer, Journal of Clinical Oncology, 30(5):519-524 (2012).

Eiber, M. et al., Prostate Cancer Molecular Imaging Standardized Evaluation (PROMISE): Proposed miTNM Classification for the Interpretation of PSMA-Ligand PET/CT, The Journal of Nuclear Medicine, 59(3):469-478, (2018).

GE Healthcare, SPECT/CT Cameras, retrieved Oct. 25, 2017: <http://www3.gehealthcare.com.sg/en-gb/products/categories/nuclear_medicine/spect-ct_cameras>.

Giesel, F. L. et al., F-18 labelled PSMA-1007: biodistribution, radiation dosimetry and histopathological validation of tumor lesions in prostate cancer patients, Eur. J. Nucl. Med. Mol. Imaging, 44:678-688 (2017).

Goffin, K. E. et al., Phase 2 Study of 99mTc-trofolastat SPECT/CT to identify and localize prostate cancer in intermediate- and high-risk patients undergoing radical prostatectomy and extended pelvic lymph node dissection, Journal of Nuclear Medicine, pp. 1-22 with supplemental data included, (2017).

Guimond, A. et al., Average Brain Models: A Convergence Study, Computer Vision and Image Understanding, 77:192-210 (2000).

Hajnal, J. et al., 4.4 Intensity, Size, and Skew Correction; 7.1 Introduction; 7.2 Methods; 7.3 Image Interpretation—General, In: Medical Image Registration, CRC Press LLC, 80-81:144-148 (2001).

Hiller, S. M. et al., 99mTc-Labeled Small-Molecule Inhibitors of Prostate-Specific Membrane Antigen for Molecular Imaging of Prostate Cancer, Journal of Nuclear Medicine, 54(8):1369-1376 (2013) retrieved Oct. 25, 2017: <http://jnm.snmjournals.org/content/54/8/1369.full>.

Horikoshi, H. et al., Computer-aided diagnosis system for bone scintigrams from Japanese patients: importance of training database, Annals of Nuclear Medicine, 26(8):622-626 (2012).

Huang, J.-H. et al., A Set of Image Processing Algorithms for Computer-Aided Diagnosis in Nuclear Medicine Whole Body Bone Scan Images, IEEE Transactions on Nuclear Science, 54(3):514-522 (2007).

International Search Report, International Application No. PCT/US2017/058418 (Network for Medical Image Analysis, Decision Support System, and Related Graphical User Interface (GUI) Applications, filed Oct. 26, 2017), issued by ISA/European Patent Office, 4 pages, dated Feb. 27, 2018.

(56) **References Cited**

OTHER PUBLICATIONS

Kaboteh R. et al., Progression of bone metastases in patients with prostate cancer—automated detection of new lesions and calculation of bone scan index, EJNMMI Research, 3:64 (2013).
Kaboteh, R. et al., Convolutional neural network based quantification of choline uptake in PET/CT studies is associated with overall survival in patents with prostate cancer, EJNMMI, EANM '17, 44(Suppl 2):S119-S956, Abstract EP-0642 (2017).
Keiss, et al., Prostate-specific membrane antigen and a target for cancer imaging and therapy, The Quarterly Journal of Nuclear Medicine and Molecular Imaging, 59(3):241-268 (2015).
Kikuchi, A. et al., Automated segmentation of the skeleton in whole-body bone scans: influence of difference in atlas, Nuclear Medicine Communications, 33(9):947-953 (2012).
Kinahan, P.E. et al., PET/CT Standardized Update Values (SUVs) in Clinical Practice and Assessing Response to Therapy, Semin Ultrasuond CT MR 31(6):496-505 (2010) retrieved Oct. 25, 2017: <https://www.ncbi.nlm.nih.gov/pmc/articles/PMC3026294/>.
Knutsson, H., and Andersson, M., Morphons: Segmentation using Elastic Canvas and Paint on Priors, IEEE International Conference on Image Processing (ICIP 2005), Genova, Italy, 4 pages. (2005).
Kopka, K. et al., Glu-Ureido-Based Inhibitors of Prostate-Specific Membrane Antigen: Lessons Learned During the Development of a Novel Class of Low-Molecular-Weight Theranostic Radiotracers, The Journal of Nuclear Medicine, 58(9)(Suppl. 2):17S-26S, (2017).
Litjens, G. et al., A survey on deep learning in medical image analysis, Medical Image Analysis, 42:60-88, (2017).
Liu, L. et al., Computer-Aided Detection of Prostate Cancer with MRI: Technology and Applications, Acad Radiol. Author manuscript, 50 pages 2016.
Ma, L. et al., Automatic segmentation of the prostate on CT images using deep learning and multi-atlas fusion, Proc. of SPIE vol. 10133:101332O-1-101332O-9 (2017).
Ma, L. et al., Combining Population and Patient-Specific Characteristics for Prostate Segmentation on 3D CT Images, Proc of SPIE 9784:978427-1-8 (2016).
Ma, L. et al., Random Walk Based Segmentation for the Prostate on 3D Transrectal Ultrasound Images, Proc SPIE Int Soc Opt Eng. Author manuscript, 13 pages (2016).
Mayo Clinic Staff, Choline C-11 PET scan, Overview, Mayo Clinic, 4 pages (2017), retrieved Oct. 25, 2017: <https://www.mayoclinic.org/tests-procedures/choline-c-11-pet-scan/home/ovc-20156994>.
Nakajima, K. et al., Enhanced diagnostic accuracy for quantitative bone scan using an artificial neural network system: a Japanese multi-center database project, EJNMMI Research, 3:83 (2013).
National Cancer Institute, NCI Drug Dictionary: gallium Ga 68-labeled PSMA-11, retrieved Oct. 25, 2017: <https://www.cancer.gov/publications/dictionaries/cancer-drug?cdrid=766400>.
National Cancer Institute, NCI Drug Dictionary: technetium Tc 99m methylene diphosphonate, retrieved Oct. 25, 2017: <https://www.cancer.gov/publications/dictionaries/cancer-drug?cdrid=537722>.
Perera, M. et al., Sensitivity, Specificity, and Predictors of Positive 68Ga-Prostate-specific Membrane Antigen Positron Emission Tomography in Advanced Prostate Cancer: A Systematic Review and Meta-analysis, European Urology, 70(6):926-937 (2016).
Polymeri, E. et al., Analytical validation of an automated method for segmentation of the prostate gland in CT images, EJNMMI, EANM '17, 44(Suppl 2):S119-S956, Abstract EP-0641 (2017).
radiologyinfo.org for Patients, Computed Tomography (CT), retrieved Oct. 25, 2017: <https://www.radiologyinfo.org/en/submenu.cfm?pg=ctscan>.
Rowe, S. P. et al., PET Imaging of prostate-specific membrane antigen in prostate cancer: current state of the art and future challenges, Prostate Cancer and Prostatic Diseases, 1-8 (2016).
Rowe, S. P. et al., PSMA-Based [^{18}F]DCFPyL PET/CT Is Superior to Conventional Imaging for Lesion Detection in Patients with Metastatic Prostate Cancer, Mol Imaging Biol, 18:411-419, (2016).
Sabbatini, P. et al., Prognostic Significance of Extent of Disease in Bone in Patients With Androgen-Independent Prostate Cancer, Journal of Clinical Oncology, 17(3):948-957 (1999).
Sadik, M. et al., 3D prostate gland uptake of 18F-choline—association with overall survival in patients with hormone-naïve prostate cancer, The Journal of Nuclear Medicine, 58(Suppl. 1):Abstract 544 (2017).
Sadik, M. et al., A new computer-based decision-support system for the interpretation of bone scans, Nuclear Medicine Communications, 27(5):417-423 (2006).
Sadik, M. et al., Automated 3D segmentation of the prostate gland in CT images—a first step towards objective measurements of prostate uptake in PET and SPECT images, Journal of Nuclear Medicine, 58(1):1074, (2017).
Sadik, M. et al., Automated quantification of reference levels in liver and mediastinum (blood pool) for the Deauville therapy response classification using FDG-PET/CT in lymphoma patients, EJNMMI, EANM '17, 44(Suppl 2):S119-S956, Abstract EP-0770 (2017).
Sadik, M. et al., Computer-assisted interpretation of planar whole-body bone scans, Journal Nuclear Medicine, 49(12):1958-65, 2008.
Sadik, M. et al., Convolutional neural networks for segmentation of 49 selected bones in CT images show high reproducibility, EJNMMI, EANM '17, 44(Suppl 2):S119-S956, Abstract OP-657 (2017).
Sadik, M. et al., Improved classifications of planar whole-body bone scans using a computer-assisted diagnosis system: a multicenter, multiple-reader, multiple-case study, Journal of Nuclear Medicine, 50(3): 368-75, 2009.
Sadik, M. et al., Variability in reference levels for Deauville classifications applied to lymphoma patients examined with 18F-FDG-PET/CT, EJNMMI, EANM '17, 44(Suppl 2):S119-S956, Abstract EP-0771 (2017).
Sajn, L. et al., Computerized segmentation of whole-body bone scintigrams and its use in automated diagnostics, Computer Methods and Programs in Biomedicine, 80:47-55 (2005).
Salerno, J. et al., Multiparametric magnetic resonance imaging for pre-treatment local staging of prostate cancer: A Cancer Care Ontario clinical practice guideline, Canadian Urological Association Journal, 10(9-10):332-339 (2016).
Sjöstrand K. et al., Statistical regularization of deformation fields for atlas-based segmentation of bone scintigraphy images, MICCAI 5761:664-671 (2009).
Sluimer, I. et al., Toward Automated Segmentation of the Pathological Lung in CT, IEEE Transactions on Medical Imaging, 24(8):1025-1038 (2005).
Tian, Z. et al., A fully automatic multi-atlas based segmentation method for prostate MR images, Proc SPIE Int Soc Opt Eng. Author manuscript, 12 pages (2015).
Tian, Z. et al., A supervoxel-based segmentation method for prostate MR images, Med. Phys., 44(2):558-569 (2017).
Tian, Z. et al., Deep convolutional neural network for prostate MR segmentation, Proc. of SPIE 10135:101351L-1-101351L-6 (2017).
Tian, Z., et al., Superpixel-based Segmentation for 3D Prostate MR Images, IEEE Trans Med Imaging, Author manuscript, 32 pages, (2016).
Ulmert, D. et al., A Novel Automated Platform for Quantifying the Extent of Skeletal Tumour Involvement in Prostate Cancer Patients Using the Bone Scan Index, European Urology, 62(1):78-84 (2012).
Wrangsjo, A. et al., Non-rigid Registration Using Morphons, Proceedings of the 14th Scandinavian Conference on Image Analysis (SCIA '05), pp. 501-510 (2005).
Written Opinion, International Application No. PCT/US2017/058418 (Network for Medical Image Analysis, Decision Support System, and Related Graphical User Interface (GUI) Applications, filed Oct. 26, 2017), issued by ISA/European Patent Office, 9 pages, dated Feb. 27, 2018.
Yin, T.-K., A Computer-Aided Diagnosis for Locating Abnormalities in Bone Scintigraphy by a Fuzzy System With a Three-Step Minimization Approach, IEEE Transactions on Medical Imaging, 23(5):639-654 (2004).

* cited by examiner

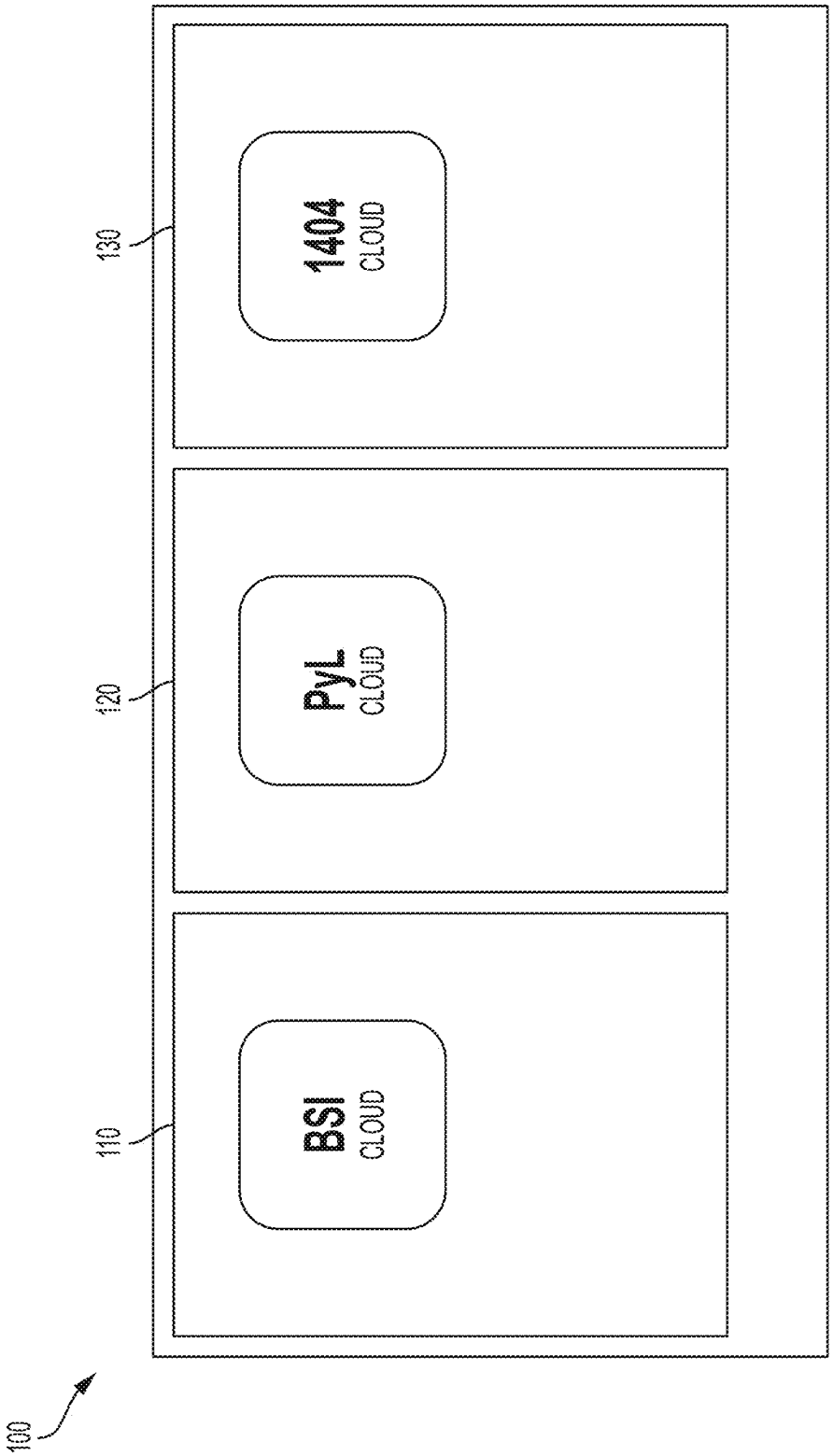


FIG. 1

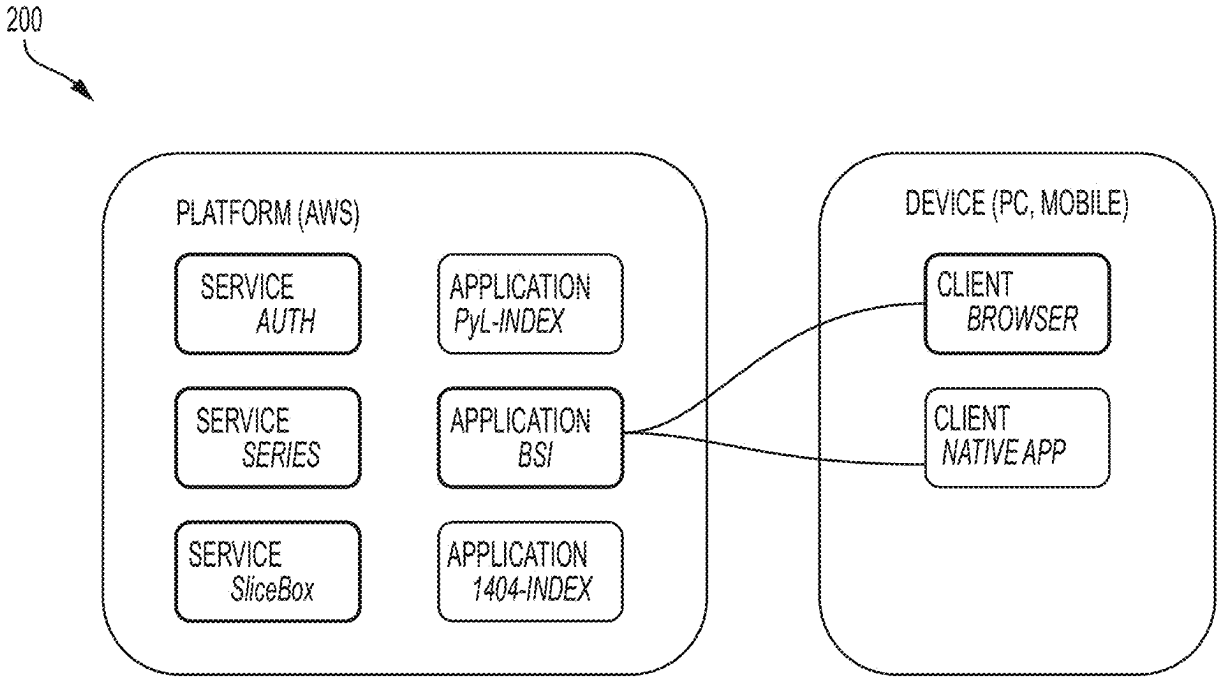

200
PLATFORM (AWS)
SERVICE
AUTH
APPLICATION
PyL-INDEX
SERVICE
SERIES
APPLICATION
BSI
SERVICE
SliceBox
APPLICATION
1404-INDEX
DEVICE (PC, MOBILE)
CLIENT
BROWSER
CLIENT
NATIVE APP

FIG. 2

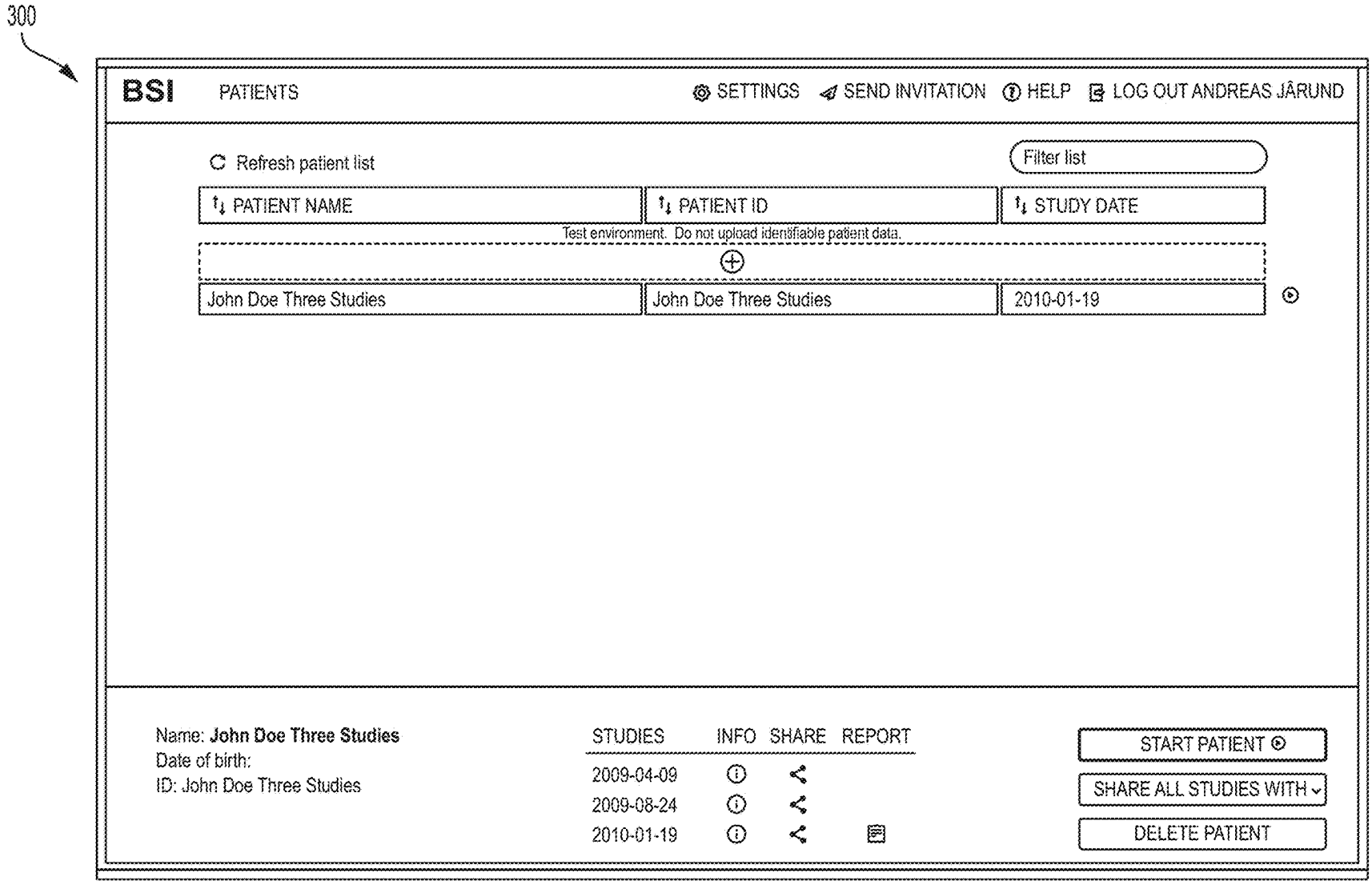

300
BSI
PATIENTS
SETTINGS
SEND INVITATION
HELP
LOG OUT ANDREAS JÅRUND
Refresh patient list
Filter list
PATIENT NAME
PATIENT ID
STUDY DATE
Test environment. Do not upload identifiable patient data.
John Doe Three Studies
John Doe Three Studies
2010-01-19
Name: John Doe Three Studies
Date of birth:
ID: John Doe Three Studies
STUDIES
INFO
SHARE
REPORT
2009-04-09
2009-08-24
2010-01-19
START PATIENT
SHARE ALL STUDIES WITH
DELETE PATIENT

FIG. 3

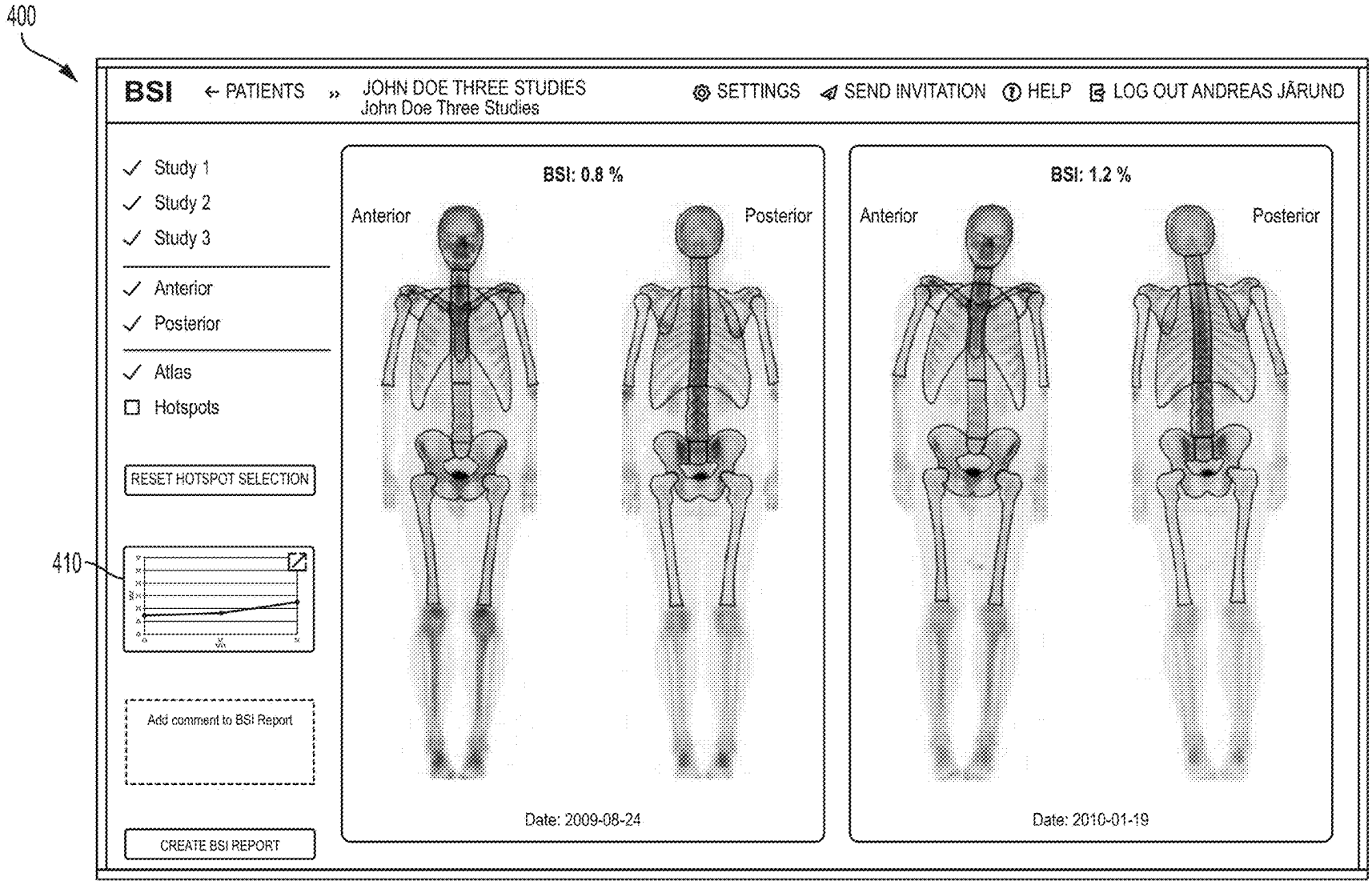

400
BSI
← PATIENTS
»
JOHN DOE THREE STUDIES
John Doe Three Studies
SETTINGS
SEND INVITATION
HELP
LOG OUT ANDREAS JÄRUND
Study 1
Study 2
Study 3
Anterior
Posterior
Atlas
Hotspots
RESET HOTSPOT SELECTION
410
Add comment to BSI Report
CREATE BSI REPORT
BSI: 0.8 %
Anterior
Posterior
Date: 2009-08-24
BSI: 1.2 %
Anterior
Posterior
Date: 2010-01-19

FIG. 4

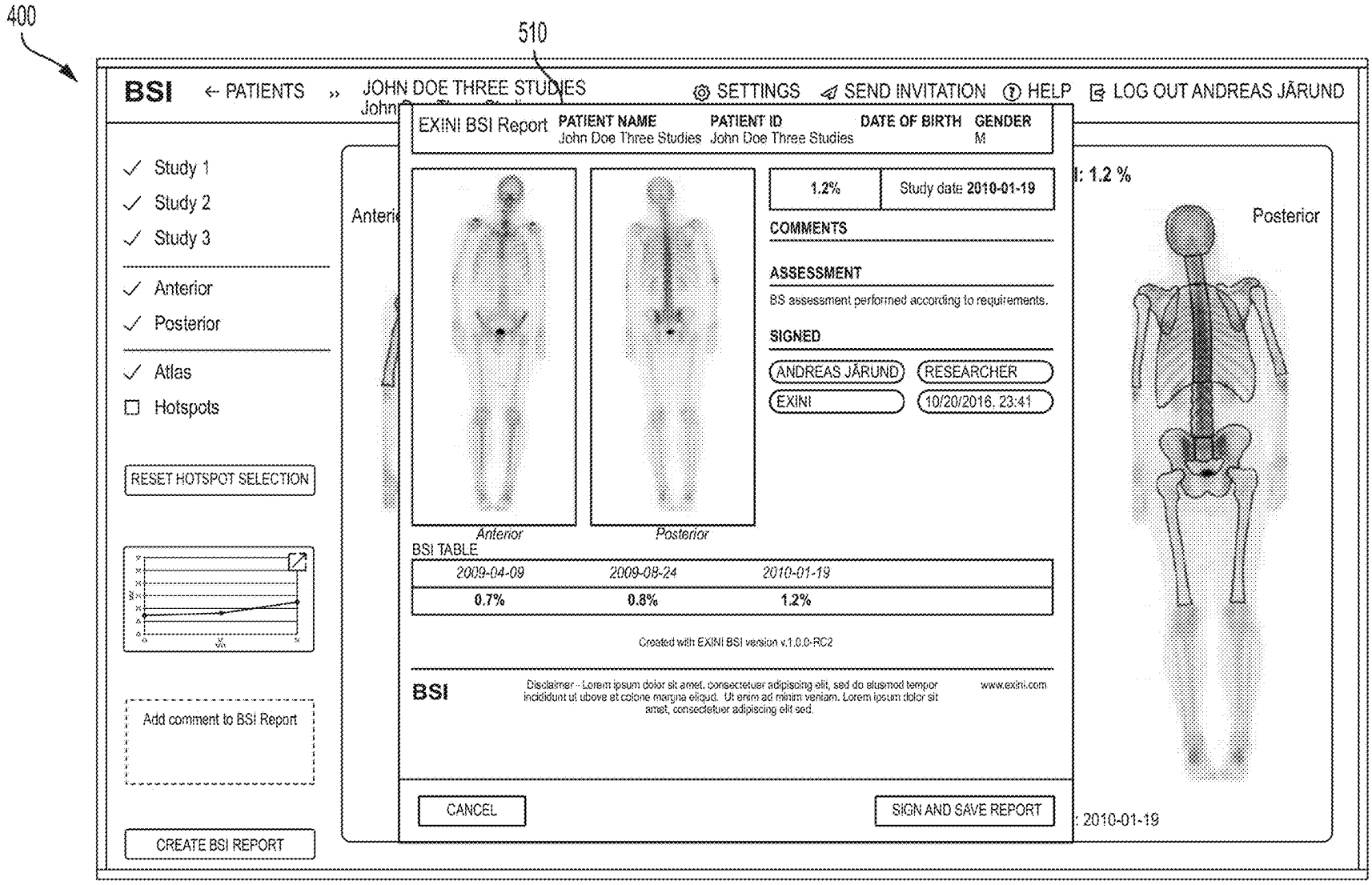

400
510
BSI
← PATIENTS
JOHN DOE THREE STUDIES
SETTINGS
SEND INVITATION
HELP
LOG OUT ANDREAS JÄRUND
Study 1
Study 2
Study 3
Anterior
Posterior
Atlas
Hotspots
RESET HOTSPOT SELECTION
Add comment to BSI Report
CREATE BSI REPORT
EXINI BSI Report
PATIENT NAME
John Doe Three Studies
PATIENT ID
John Doe Three Studies
DATE OF BIRTH
GENDER
M
1.2%
Study date 2010-01-19
COMMENTS
ASSESSMENT
BS assessment performed according to requirements.
SIGNED
ANDREAS JÄRUND
RESEARCHER
EXINI
10/20/2016, 23:41
Anterior
Posterior
BSI TABLE
2009-04-09
2009-08-24
2010-01-19
0.7%
0.8%
1.2%
Created with EXINI BSI version v.1.0.0-RC2
BSI
Disclaimer – Lorem ipsum dolor sit amet, consectetuer adipiscing elit, sed do eiusmod tempor incididunt ut ubove et colone magna eliqud. Ut enim ad minim veniam. Lorem ipsum dolor sit amet, consectetuer adipiscing elit sed.
www.exini.com
CANCEL
SIGN AND SAVE REPORT
1.2 %
Posterior
2010-01-19

FIG. 5

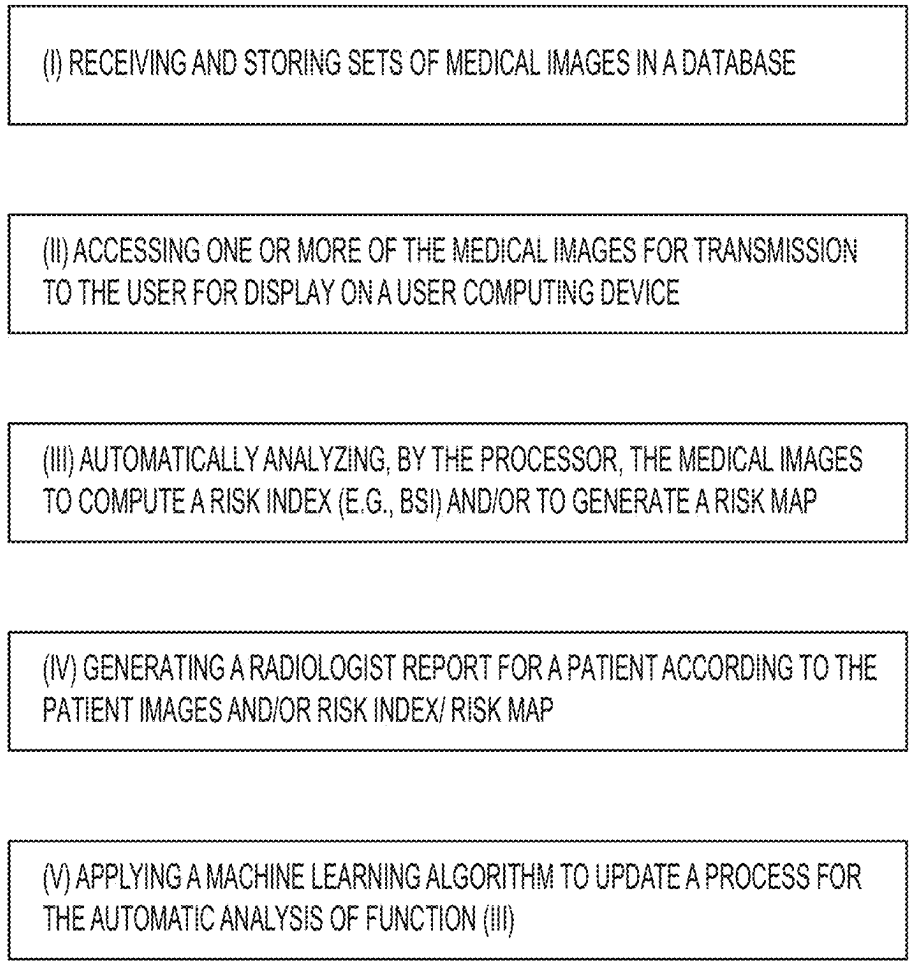

(I) RECEIVING AND STORING SETS OF MEDICAL IMAGES IN A DATABASE
(II) ACCESSING ONE OR MORE OF THE MEDICAL IMAGES FOR TRANSMISSION TO THE USER FOR DISPLAY ON A USER COMPUTING DEVICE
(III) AUTOMATICALLY ANALYZING, BY THE PROCESSOR, THE MEDICAL IMAGES TO COMPUTE A RISK INDEX (E.G., BSI) AND/OR TO GENERATE A RISK MAP
(IV) GENERATING A RADIOLOGIST REPORT FOR A PATIENT ACCORDING TO THE PATIENT IMAGES AND/OR RISK INDEX/ RISK MAP
(V) APPLYING A MACHINE LEARNING ALGORITHM TO UPDATE A PROCESS FOR THE AUTOMATIC ANALYSIS OF FUNCTION (III)

FIG. 6

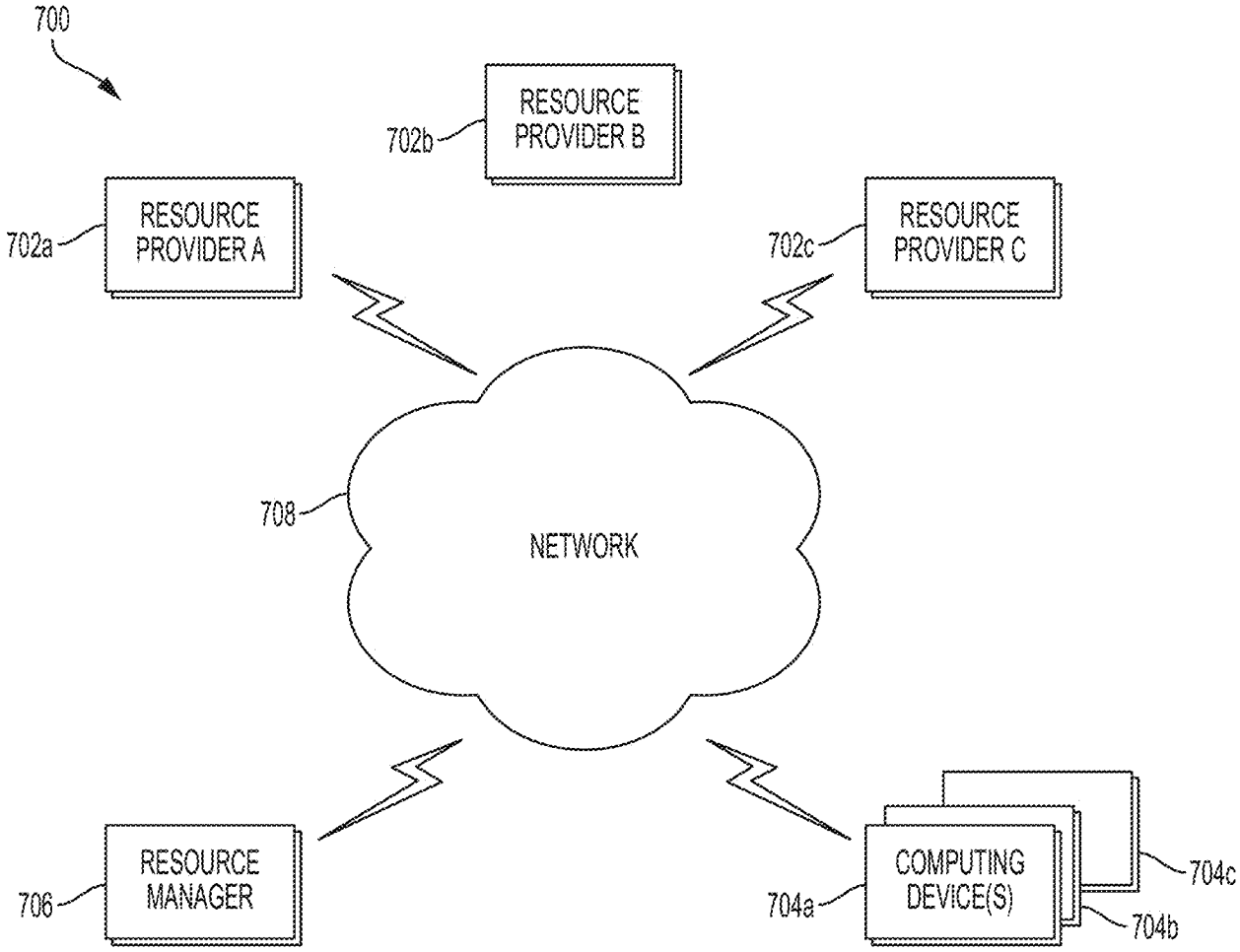

700
RESOURCE PROVIDER B
702b
RESOURCE PROVIDER A
702a
RESOURCE PROVIDER C
702c
708
NETWORK
RESOURCE MANAGER
706
COMPUTING DEVICE(S)
704a
704b
704c

FIG. 7

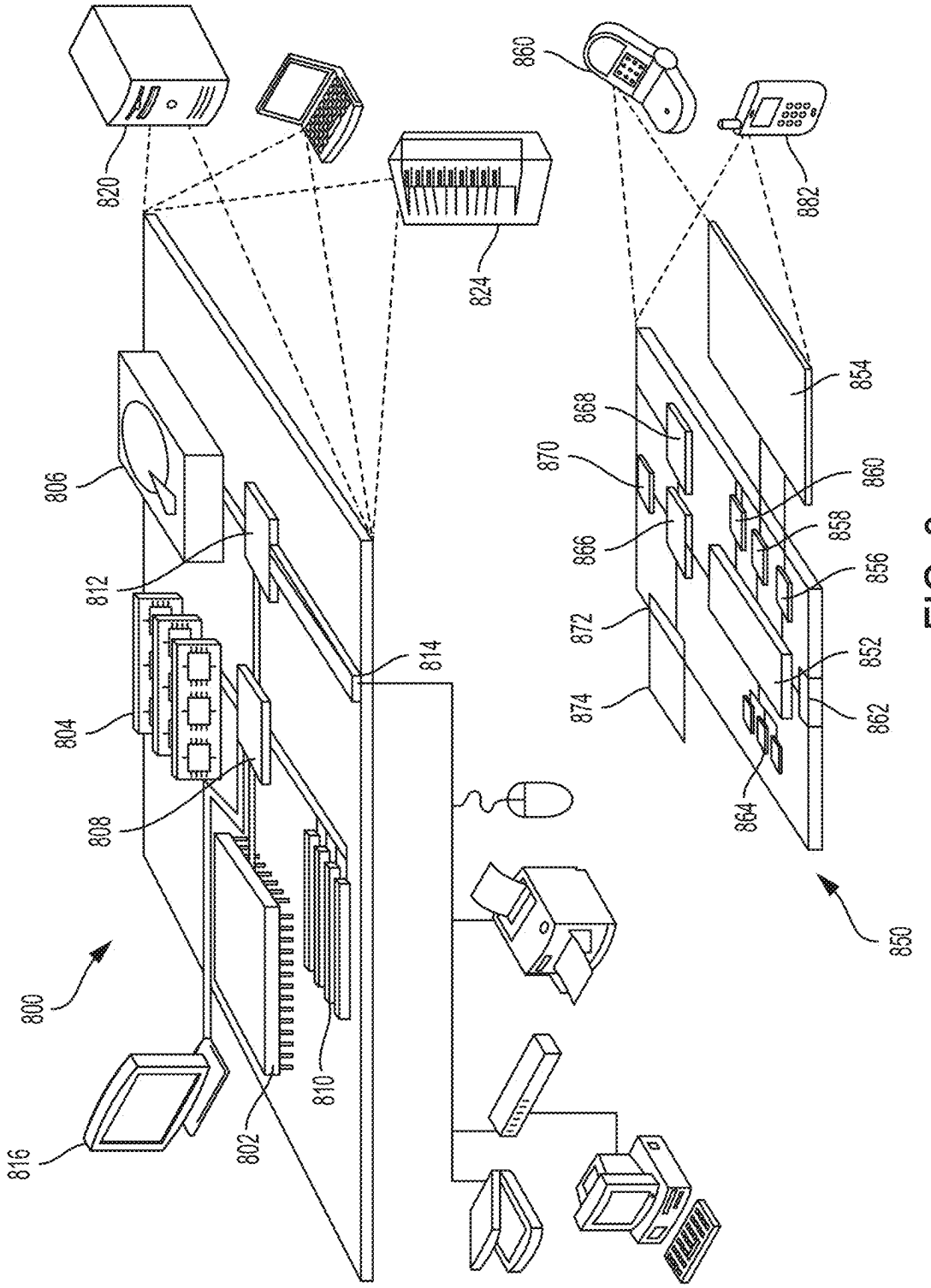

820
824
860
882
806
812
804
808
814
800
816
802
810
854
868
870
866
872
874
858
856
852
862
864
850

FIG. 8

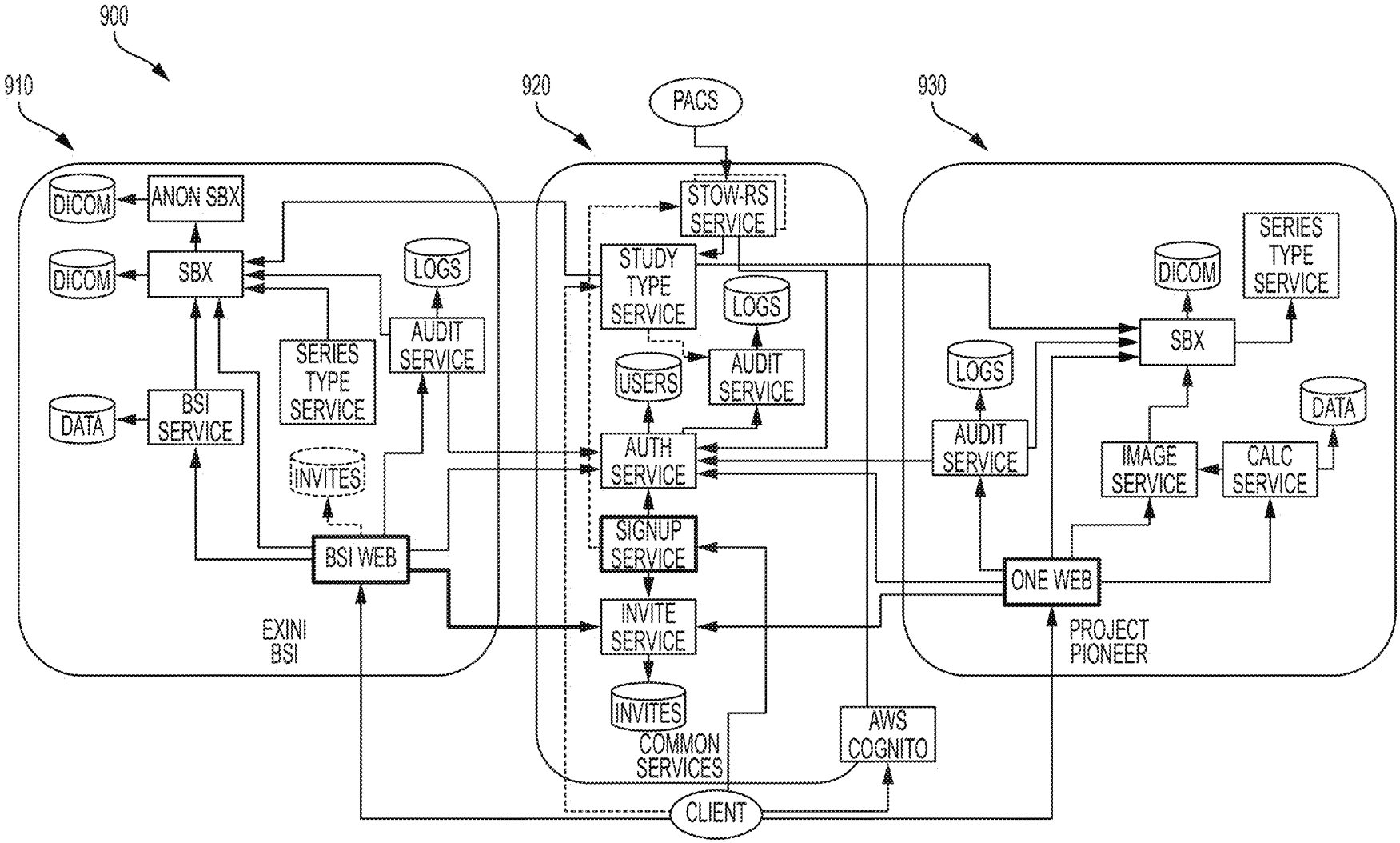

900
910
920
930
PACS
DICOM
ANON SBX
DICOM
SBX
LOGS
AUDIT SERVICE
SERIES TYPE SERVICE
DATA
BSI SERVICE
INVITES
BSI WEB
EXINI BSI
STOW-RS SERVICE
STUDY TYPE SERVICE
LOGS
AUDIT SERVICE
USERS
AUTH SERVICE
SIGNUP SERVICE
INVITE SERVICE
INVITES
COMMON SERVICES
AWS COGNITO
CLIENT
LOGS
AUDIT SERVICE
DICOM
SBX
SERIES TYPE SERVICE
DATA
IMAGE SERVICE
CALC SERVICE
ONE WEB
PROJECT PIONEER

FIG. 9

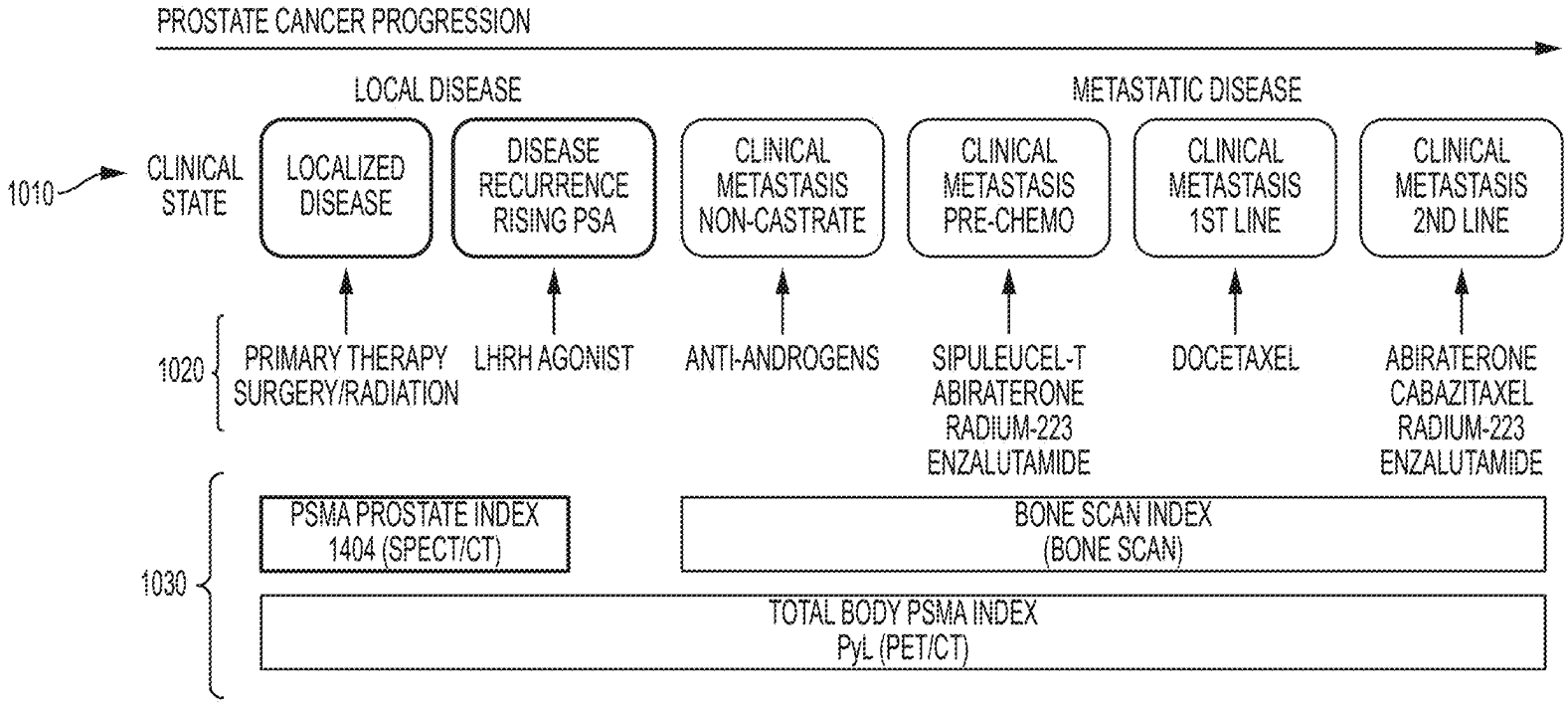

PROSTATE CANCER PROGRESSION
LOCAL DISEASE
METASTATIC DISEASE
1010
CLINICAL STATE
LOCALIZED DISEASE
DISEASE RECURRENCE RISING PSA
CLINICAL METASTASIS NON-CASTRATE
CLINICAL METASTASIS PRE-CHEMO
CLINICAL METASTASIS 1ST LINE
CLINICAL METASTASIS 2ND LINE
1020
PRIMARY THERAPY SURGERY/RADIATION
LHRH AGONIST
ANTI-ANDROGENS
SIPULEUCEL-T ABIRATERONE RADIUM-223 ENZALUTAMIDE
DOCETAXEL
ABIRATERONE CABAZITAXEL RADIUM-223 ENZALUTAMIDE
1030
PSMA PROSTATE INDEX 1404 (SPECT/CT)
BONE SCAN INDEX (BONE SCAN)
TOTAL BODY PSMA INDEX PyL (PET/CT)

FIG. 10

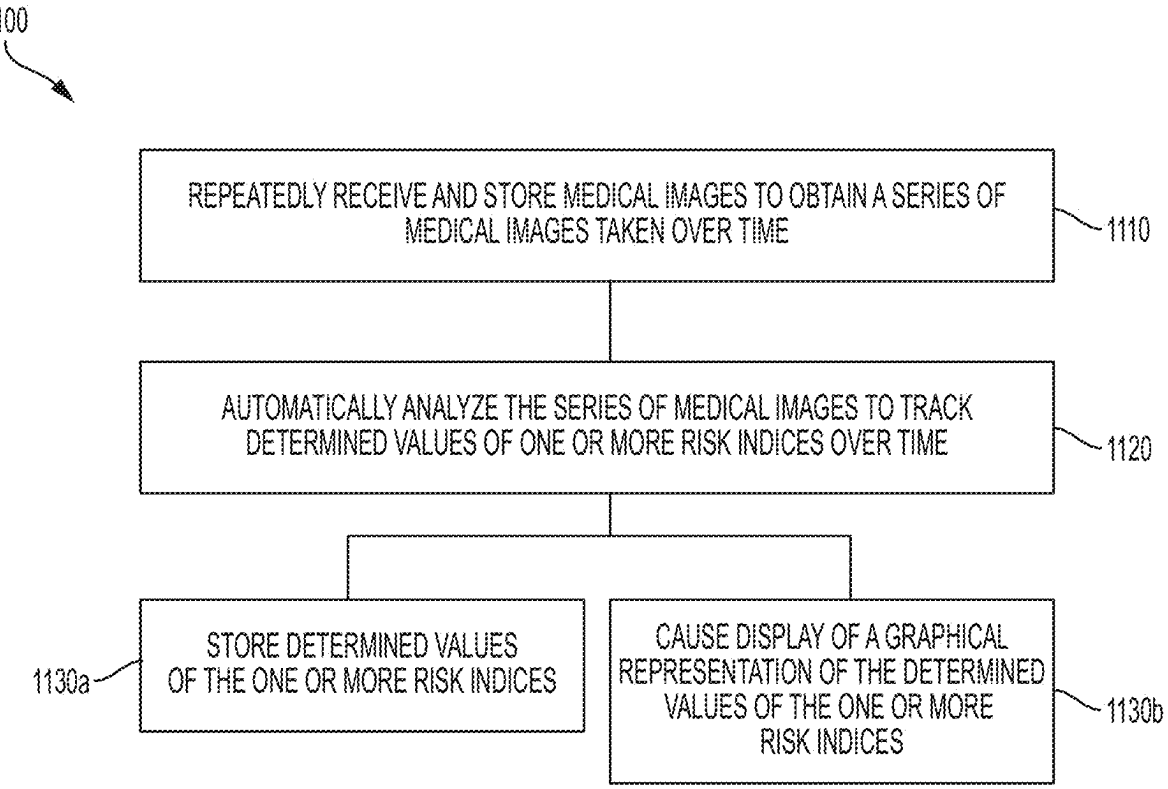

1100
REPEATEDLY RECEIVE AND STORE MEDICAL IMAGES TO OBTAIN A SERIES OF MEDICAL IMAGES TAKEN OVER TIME
1110
AUTOMATICALLY ANALYZE THE SERIES OF MEDICAL IMAGES TO TRACK DETERMINED VALUES OF ONE OR MORE RISK INDICES OVER TIME
1120
STORE DETERMINED VALUES OF THE ONE OR MORE RISK INDICES
1130a
CAUSE DISPLAY OF A GRAPHICAL REPRESENTATION OF THE DETERMINED VALUES OF THE ONE OR MORE RISK INDICES
1130b

FIG. 11

NETWORK FOR MEDICAL IMAGE ANALYSIS, DECISION SUPPORT SYSTEM, AND RELATED GRAPHICAL USER INTERFACE (GUI) APPLICATIONS

CROSS REFERENCE TO RELATED APPLICATIONS

This application is a continuation of U.S. application Ser. No. 16/418,527, filed May 21, 2019, which is a continuation of U.S. application Ser. No. 15/794,220, filed Oct. 26, 2017 (now U.S. Pat. No. 10,340,046, issued Jul. 2, 2019), which claims the benefit of U.S. Provisional Application 62/413,936, filed on Oct. 27, 2016, the content of each of which are hereby incorporated by reference herein in their entirety.

TECHNICAL FIELD

This invention relates generally to systems and methods for creation, analysis, and/or presentation of medical image data. More particularly, in certain embodiments, the invention relates to a cloud-based platform and supported GUI decision-making tools for use by medical practitioners and/or their patients, e.g., to aide in the process of making decisions about a course of cancer treatment and/or to track treatment and/or the progress of a disease.

BACKGROUND

Targeted image analysis involves the use of radiolabeled small molecules that bind to specific receptors, enzymes and proteins in the body that are altered during the evolution of disease. After administration to a patient, these molecules circulate in the blood until they find their intended target. The bound radiopharmaceutical remains at the site of disease, while the rest of the agent clears from the body. The radioactive portion of the molecule serves as a beacon so that an image may be obtained depicting the disease location and concentration using commonly available nuclear medicine cameras, known as single-photon emission computerized tomography (SPECT) or positron emission tomography (PET) cameras, found in most hospitals throughout the world. Physicians can then use this information to determine the presence and the extent of disease in a patient. The physician can use this information to provide a recommended course of treatment to the patient and to track the progression of disease.

There are a variety of software-based analytical techniques available for analysis and enhancement of PET and SPECT images that can be used by a radiologist or physician. There are also a number of radiopharmaceuticals available for imaging particular kinds of cancer. For example, the small molecule diagnostic 1404 targets the extracellular domain of prostate specific membrane antigen (PSMA), a protein amplified on the surface of >95% of prostate cancer cells and a validated target for the detection of primary and metastatic prostate cancer. 1404 is labeled with technetium-99m, a gamma-emitter isotope that is widely available, relatively inexpensive, facilitates efficient preparation, and has spectrum characteristics attractive for nuclear medicine imaging applications.

Another example radiopharmaceutical is PyL™ (also known as [^{18}F]DCFPyL), which is a clinical-stage, fluorinated PSMA-targeted PET imaging agent for prostate cancer. A proof-of-concept study published in the April 2015 issue of the Journal of Molecular Imaging and Biology demonstrated that PET imaging with PyL™ showed high levels of PyL™ uptake in sites of putative metastatic disease and primary tumors, suggesting the potential for high sensitivity and specificity in detecting prostate cancer.

An oncologist may use images from a targeted PET or SPECT study of a patient as input in her assessment of whether the patient has a particular disease, e.g., prostate cancer, what stage of the disease is evident, what the recommended course of treatment (if any) would be, whether surgical intervention is indicated, and likely prognosis. The oncologist may use a radiologist report in this assessment. A radiologist report is a technical evaluation of the PET or SPECT images prepared by a radiologist for a physician who requested the imaging study and includes, for example, the type of study performed, the clinical history, a comparison between images, the technique used to perform the study, the radiologist's observations and findings, as well as overall impressions and recommendations the radiologist may have based on the imaging study results. A signed radiologist report is sent to the physician ordering the study for the physician's review, followed by a discussion between the physician and patient about the results and recommendations for treatment.

Thus, the process involves having a radiologist perform an imaging study on the patient, analyzing the images obtained, creating a radiologist report, forwarding the report to the requesting physician, having the physician formulate an assessment and treatment recommendation, and having the physician communicate the results, recommendations, and risks to the patient. The process may also involve repeating the imaging study due to inconclusive results, or ordering further tests based on initial results.

If an imaging study shows that the patient has a particular disease or condition (e.g., cancer), the physician discusses various treatment options, including surgery, as well as risks of doing nothing or adopting a watchful waiting or active surveillance approach, rather than having surgery.

There are limitations associated with this process, both from the perspective of the physician and from the perspective of the patient. While the radiologist's report is certainly helpful, the physician must ultimately rely on her experience in formulating an assessment and recommendation for her patient. Furthermore, the patient must place a great deal of trust in his physician. The physician may show the patient his PET/SPECT images and may tell the patient a numerical risk associated with various treatment options or likelihood of a particular prognosis, but the patient may very well struggle to make sense of this information. Moreover, the patient's family will likely have questions, particularly if cancer is diagnosed but the patient opts not to have surgery. The patient and/or his family members may search online for supplemental information and may become misinformed about risks of the diagnosed condition. A difficult ordeal may become more traumatic.

Thus, there remains a need for systems and methods for improved analysis of medical imaging studies and communication of those results, diagnoses, prognoses, treatment recommendations, and associated risks to a patient.

SUMMARY OF THE INVENTION

Presented herein is a cloud-based platform and supported graphical user interface (GUI) decision-making tools for use by medical practitioners and/or their patients, e.g., to aide in the process of making decisions about a course of cancer treatment and/or to track treatment and/or the progress of a disease.

For example, presented herein is a network-based (e.g., cloud-based) support platform allowing multiple users to store, access, analyze, and/or provide feedback regarding a given set of image data for a patient; platform supports software tools for automated analysis of targeted PET/SPECT/or other image(s), generation of radiologist reports, and application of machine learning algorithms to update process by which images are analyzed (e.g. updating segmentation and/or classification routines based on growing image database). In certain embodiments, the targeted PET/SPECT image(s) may be obtained using PyL™ and/or 1404 as the radiopharmaceutical(s). In certain embodiments, multiple (accredited) users can access the information, e.g., to weigh in on data interpretation.

Also presented herein is a software tool (e.g., mobile app) featuring a graphical user interface (GUI) element with controls for adjusting presentation of a 3D risk image corresponding to a patient organ (and/or other tissue) for comparison with reference images (e.g., for use in communication of results to patient as a decision-making support). For example, the tool may be supported by the network-based support platform above. This tool can provides an easily-understood, user-friendly, interactive, controllable pictorial display to communicate information about a patient's condition to the patient (and/or to the physician, or to the patient's family with the patient's permission). For example, a patient for whom a risk of cancer is detected can display a map indicating areas and/or degrees of risk and can compare this risk map with those of others for whom a given course of treatment is recommended. For instance, this tool can help a patient in his decision whether or not to have surgery (e.g., for a detected risk of prostate cancer). The patient can visually compare his risk map with a map representing a typical risk-level for which surgery would be recommended, below which it may be reasonable to opt not to have surgery and engage in watchful waiting or active surveillance. Thus, a low-risk patient who is told by his physician that he has a non-zero risk of cancer may find comfort in a visual, controllable comparison between his situation and that of someone (e.g., where the reference to which the patient's risk situation is compared can be tuned for age, weight, and/or other risk factors of the patient).

In one aspect, the invention is directed to a network-based (e.g., cloud based) decision support system comprising: a processor (e.g., of a network or Internet host server); and a memory having instructions stored thereon, wherein the instructions, when executed by the processor, cause the processor to perform one or more of functions (i) to (v) as follows: (i) receive and store medical images [e.g., comprising one or more of the following: targeted PET images, targeted SPECT images, computed tomography (CT) images, magnetic resonance (MR) images, ultrasound (US) images, gamma camera (i.e. scintillation camera) images, and combinations, fusions, or derivatives of any of the above] in a database [e.g., wherein the targeted PET/SPECT/gamma camera image(s) are obtained using one or more radiopharmaceuticals (e.g., [18F]DCFPyL and/or 1404 and/or a composition comprising technetium 99m, {e.g., technetium 99m methylenediphosphonate (^{99m}Tc MDP)}), and/or wherein the medical images are obtained using non-radioactive agents or no agents], each medical image associated with a particular patient; (ii) access one or more of the medical images and/or related data associated with a particular patient from the database upon user request (e.g., following automated verification that the user is properly credentialed for receiving the requested images and/or data) for transmission to the user for display on a user computing device; (iii) automatically analyze one or more of the medical images [e.g., to generate a risk index (e.g., BSI) and/or a risk map, e.g., a visual representation (e.g., 3D representation) of tissue (e.g., an organ or other part of the body) with graphical denotations (e.g., texture- or color-coding) marking regions of risk of current disease or risk of recurrence of disease, e.g., cancer, e.g., wherein the risk map is displayed as an overlay of the PET/SPECT/CT/MRI/US/combined/derived/fused image of the tissue, or is in place of the image of the tissue]; (iv) generate a radiologist report for a patient according to one or more of the medical images for the patient; and (v) apply a machine learning algorithm to update a process for automatically analyzing one or more of the medical images using accumulated image data in the database [e.g., wherein the automatic analysis of the one or more medical images in (iii) and/or (v) above comprises any one or more of (a) to (d) as follows: (a) automated fusion of the (e.g., PET, SPECT, CT, Mill, and/or US) image(s) of the tissue; (b) geographic identification of one or more organs, organ structures, sub-organs, organ regions, and/or other regions of the imaged tissue of the patient and production of a 3D image of the geographically identified tissue with PET, SPECT, CT, MM, and/or US data overlaid; (c) computation of risk information comprising one or more risk indices, a risk field, or a risk map using data from the database, the image(s) of the tissue, and/or the 3D image in (b); and (d) use of the risk information computed in (c) (e.g., and data from the database) to produce a 3D risk picture for the patient].

In certain embodiments, the medical images in the database comprise a series of medical images of a first patient taken over time (e.g., over the course of multiple visits to one or more doctors), and wherein the instructions cause the processor to determine a value of at least a first risk index for each medical image of the series, thereby tracking determined values of at least the first risk index for the first patient over time.

In certain embodiments, the medical images comprise a single-photon emission computerized tomography (SPECT) scan of a first patient obtained (e.g., to identify one or more hotspots) following administration to the first patient of an imaging agent comprising 1404 labeled with ^{99m}Tc, and a computed tomography (CT) scan (e.g., to identify anatomical features) of the first patient, wherein the instructions cause the processor to overlay the SPECT scan with the CT scan to create a composite image (SPECT-CT) of the first patient.

In certain embodiments, the medical images comprise a positron emission tomography (PET) scan of a first patient obtained (e.g., to identify one or more hotspots) following administration to the first patient of an imaging agent comprising [18F]DCFPyL (DCFPyL labeled with ^{18}F), and a CT scan of the first patient, wherein the instructions cause the processor to overlay the PET scan with the CT scan to create a composite image (PET-CT) of the first patient.

In certain embodiments, the medical images comprise a whole-body scan (e.g., including anterior and posterior views) of a first patient made with a gamma camera following administration to the first patient of an imaging agent comprising technetium 99m methylenediphosphonate (^{99m}Tc MDP).

In certain embodiments, the medical images comprise a composite image of a first patient, the composite image comprising a CT scan overlaid with a nuclear medicine image (e.g., a SPECT scan; e.g., a PET scan) obtained at substantially the same time as the CT scan and following administration to the first patient of an imaging agent

comprising a Prostate Specific Membrane Antigen (PSMA) binding agent comprising (e.g., labelled with) a radionuclide, and the instructions cause the processor to automatically analyze the composite image by: (a) using the composite image to geographically identify a 3D boundary for each of one or more regions of imaged tissue [e.g., organs (e.g., a prostate; e.g., a liver; e.g., lungs or a lung; e.g., lymph nodes), organ structures, sub-organs, organ regions, and/or other regions (e.g., one or more particular bones; e.g., a skeletal region of the patient), e.g., regions of interest] within the nuclear medicine image (e.g., such that portions of the nuclear medicine image falling within and/or outside of the 3D boundaries can be differentiated from each other); and (c) computing (i) a value of each of one or more risk indices and/or (ii) a risk map using the nuclear medicine image with the identified 3D boundaries of the one or more region(s).

In certain embodiments, the instructions cause the processor to, for at least one risk index of the one or more risk indices, compute the value of the risk index by: determining, for each of the one or more regions, a corresponding cancerous tissue level within the region based on intensity values of the nuclear medicine image within the 3D boundary of the region (e.g., by identifying within the nuclear medicine image, a plurality of hotspots within the 3D boundary of the region and computing a total number of and/or a total volume of the identified hotspots); and computing the value of the risk index based on the determined cancerous tissue levels within the one or more regions.

In certain embodiments, the nuclear medicine image is a SPECT scan.

In certain embodiments, the imaging agent comprises a metal chelated to the PSMA binding agent, and wherein the metal is the radionuclide [e.g., wherein the metal is a radioisotope of technetium (Tc) (e.g., wherein the metal is technetium-99m (^{99m}Tc)); e.g., wherein the metal is a radioisotope of rhenium (Re) (e.g., wherein the metal is rhenium-188 (^{188}Re); e.g., wherein the metal is rhenium-186 (^{86}Re)); e.g., wherein the metal is a radioisotope of yttrium (Y) (e.g., wherein the metal is ^{90}Y); e.g., wherein the metal is a radioisotope of lutetium (Lu)(e.g., wherein the metal is ^{177}Lu); e.g., wherein the metal is a radioisotope of gallium (Ga) (e.g., wherein the metal is ^{68}Ga; e.g., wherein the metal is ^{67}Ga); e.g., wherein the metal is a radioisotope of indium (e.g., ^{111}In); e.g., wherein the metal is a radioisotope of copper (Cu) (e.g., wherein the metal is ^{67}Cu].

In certain embodiments, the imaging agent comprises ^{99m}Tc-MIP-1404.

In certain embodiments, the nuclear medicine image is a PET scan.

In certain embodiments, the radionuclide is a radioisotope of a halogen [e.g., a radioisotope of fluorine (e.g., ^{18}F); e.g., a radioisotope of iodine (e.g., ^{123}I; e.g., ^{124}I; e.g., ^{125}I; e.g., ^{126}I; e.g., ^{131}I); e.g., a radioisotope of bromine (e.g., ^{75}Br; e.g., ^{76}Br; e.g., ^{77}Br; e.g., ^{80}Br; e.g., ^{80m}Br; e.g., ^{82}Br; e.g., ^{83}Br), e.g., a radioisotope of astatine (e.g., ^{211}At)].

In certain embodiments, the imaging agent comprises [18F]DCFPyL (DCFPyL labeled with ^{18}F).

In certain embodiments, the radionuclide is a radioisotope of gallium (Ga) (e.g., ^{68}Ga).

In certain embodiments, the medical images comprise a nuclear medicine image (e.g., a whole-body scan made with a gamma camera) of a first patient following administration to the first patient of an imaging agent comprising a radionuclide (e.g., ^{99m}Tc)(e.g., wherein the imaging agent comprises ^{99m}Tc MDP), wherein the instructions cause the processor to automatically analyze the nuclear medicine image by: (a) geographically identifying a boundary (e.g., a 2D boundary; e.g., a 3D boundary) for each of one or more regions of imaged tissue [e.g., organs (e.g., a prostate; e.g., a liver; e.g., lungs or a lung; e.g., lymph nodes), organ structures, sub-organs, organ regions, and/or other regions (e.g., one or more particular bones; e.g., a skeletal region of the patient), e.g., regions of interest] within the nuclear medicine image (e.g., such that portions of the nuclear medicine image falling within and/or outside of the boundaries can be differentiated from each other); and (c) computing (i) a value of each of one or more risk indices and/or (ii) a risk map using the nuclear medicine image with the identified boundaries of the one or more region(s).

In certain embodiments, the instructions cause the processor to, for at least one risk index of the one or more risk indices, compute the value of the risk index by: determining, for each of the one or more regions, a corresponding cancerous tissue level within the region based on intensity values of the nuclear medicine image within the boundary of the region (e.g., by identifying within the nuclear medicine image, a plurality of hotspots within the boundary of the region and computing a total number of and/or a total volume of the identified hotspots); and computing the value of the risk index based on the determined cancerous tissue levels within the one or more regions.

In certain embodiments, the system is a cloud-based system.

In certain embodiments, the processor is a processor of one or more network or Internet host servers.

In another aspect, the invention is directed to a method comprising any one or more of (i) to (v) as follows: (i) receiving and storing, by a processor of a server computing device (e.g., received over a network from a client computing device) medical images [e.g., comprising one or more of the following: targeted PET images, targeted SPECT images, computed tomography (CT) images, magnetic resonance (MR) images, ultrasound (US) images, gamma camera (i.e. scintillation camera) images, and combinations, fusions, or derivatives of any of the above] in a database [e.g., wherein the targeted PET/SPECT/gamma camera image(s) are obtained using one or more radiopharmaceuticals, e.g., [18F]DCFPyL and/or 1404 and/or a composition comprising technetium 99m, e.g., technetium 99m methylenediphosphonate (^{99m}Tc MDP), and/or wherein the medical images are obtained using non-radioactive agents or no agents], each medical image associated with a particular patient; (ii) accessing, by the processor, one or more of the medical images and/or related data associated with a particular patient from the database upon user request (e.g., following automated verification that the user is properly credentialed for receiving the requested images and/or data) for transmission to the user for display on a user computing device; (iii) automatically analyzing, by the processor, one or more of the medical images[e.g., to generate a risk map, e.g., a visual representation (e.g., 3D representation) of tissue (e.g., an organ or other part of the body) with graphical denotations (e.g., texture- or color-coding) marking regions of risk of current disease or risk of recurrence of disease, e.g., cancer, e.g., wherein the risk map is displayed as an overlay of the PET/SPECT/CT/MRI/US/combined/derived/fused image of the tissue, or is in place of the image of the tissue]; (iv) generating, by the processor, a radiologist report for a patient according to one or more of the medical images for the patient; and (v) applying, by the processor, a machine learning algorithm to update a process for automatically analyzing one or more of the medical images using accumulated image data in the database, [e.g., wherein the

automatically analyzing the one or more medical images in (iii) and/or (v) above comprises any one or more of (a) to (d) as follows: (a) automatically fusing the (e.g., PET, SPECT, CT, Mill, and/or US) image(s) of the tissue; (b) geographically identifying one or more organs, organ structures, sub-organs, organ regions, and/or other regions of the imaged tissue of the patient and production of a 3D image of the geographically identified tissue with PET, SPECT, CT, MM, and/or US data overlaid; (c) computing risk information comprising one or more risk indices, a risk field, or a risk map using data from the database, the image(s) of the tissue, and/or the 3D image in (b); and (d) using the risk information computed in (c) (e.g., and data from the database) to produce a 3D risk picture for the patient].

In certain embodiments, the medical images in the database comprise a series of medical images of a first patient taken over time (e.g., over the course of multiple visits to one or more doctors), and wherein the method comprises determining a value of at least a first risk index for each medical image of the series, thereby tracking determined values of at least the first risk index over time.

In certain embodiments, the receiving and storing of the medical images comprises repeatedly receiving and storing, over time, a plurality of medical images of the first patient, each obtained at a different time (e.g., at a different visit to one or more doctors), to obtain the series of medical images of the first patient.

In certain embodiments, the medical images comprise a single-photon emission computerized tomography (SPECT) scan of a first patient obtained (e.g., to identify one or more hotspots) following administration to the first patient of an imaging agent comprising 1404 labeled with ^{99m}Tc, and a computed tomography (CT) scan (e.g., to identify anatomical features) of the first patient, wherein the method comprises overlaying the SPECT scan with the CT scan to create a composite image (SPECT-CT) of the first patient.

In certain embodiments, the medical images comprises a positron emission tomography (PET) scan of a first patient obtained following administration to the first patient of an imaging agent comprising [18F]DCFPyL (DCFPyL labeled with ^{18}F), and a CT scan of the first patient, wherein the method comprises overlaying the PET scan with the CT scan to create a composite image (PET-CT) of the first patient.

In certain embodiments, the medical images comprise a whole-body scan (e.g., including anterior and posterior views) of a first patient made with a gamma camera following administration to the first patient of an imaging agent comprising technetium 99m methylenediphosphonate (^{99m}Tc MDP).

In certain embodiments, the medical images comprise a composite image of a first patient, the composite image comprising a CT scan overlaid with a nuclear medicine image (e.g., a SPECT scan; e.g., a PET scan) acquired at substantially the same time and following administration to the first patient of an imaging agent comprising a Prostate Specific Membrane Antigen (PSMA) binding agent comprising a radionuclide, wherein the method comprises automatically analyzing the composite image by: (a) using the composite image to geographically identify a 3D boundary for each of one or more regions of imaged tissue [e.g., organs (e.g., a prostate; e.g., a liver; e.g., lungs or a lung; e.g., lymph nodes), organ structures, sub-organs, organ regions, and/or other regions (e.g., one or more particular bones; e.g., a skeletal region of the patient), e.g., regions of interest] within the nuclear medicine image (e.g., such that portions of the nuclear medicine image falling within and/or outside of the 3D boundaries can be differentiated from each other); and (c) computing (i) a value of each of one or more risk indices and/or a (ii) risk map using the nuclear medicine image with the identified 3D boundaries of the one or more region(s).

In certain embodiments, step (c) comprises, for at least one risk index of the one or more risk indices, computing the value of the risk index by: determining, for each of the one or more regions, a corresponding cancerous tissue level within the region based on intensity values of the nuclear medicine image within the 3D boundary of the region (e.g., by identifying within the nuclear medicine image, a plurality of hotspots within the 3D boundary of the region and computing a total number of and/or a total volume of the identified hotspots); and computing the value of the risk index based on the determined cancerous tissue levels within the one or more regions.

In certain embodiments, the nuclear medicine image is a SPECT scan.

In certain embodiments, the imaging agent comprises a metal chelated to the PSMA binding agent, and wherein the metal is the radionuclide [e.g., wherein the metal is a radioisotope of technetium (Tc) (e.g., wherein the metal is technetium-99m (^{99m}Tc)); e.g., wherein the metal is a radioisotope of rhenium (Re) (e.g., wherein the metal is rhenium-188 (^{188}Re); e.g., wherein the metal is rhenium-186 (^{86}Re)); e.g., wherein the metal is a radioisotope of yttrium (Y) (e.g., wherein the metal is ^{90}Y); e.g., wherein the metal is a radioisotope of lutetium (Lu)(e.g., wherein the metal is ^{177}Lu); e.g., wherein the metal is a radioisotope of gallium (Ga) (e.g., wherein the metal is ^{68}Ga; e.g., wherein the metal is ^{67}Ga); e.g., wherein the metal is a radioisotope of indium (e.g., ^{111}In); e.g., wherein the metal is a radioisotope of copper (Cu) (e.g., wherein the metal is ^{67}Cu)].

In certain embodiments, the imaging agent comprises ^{99m}Tc-MIP-1404.

In certain embodiments, the nuclear medicine image is a PET scan.

In certain embodiments, the radionuclide is a radioisotope of a halogen [e.g., a radioisotope of fluorine (e.g., ^{18}F); e.g., a radioisotope of iodine (e.g., ^{123}I; e.g., ^{124}I; e.g., ^{125}I; e.g., ^{126}I; e.g., ^{131}I); e.g., a radioisotope of bromine (e.g., ^{75}Br; e.g., ^{76}Br; e.g., ^{77}Br; e.g., ^{80}Br; e.g., ^{80m}Br; e.g., ^{82}Br; e.g., ^{83}Br), e.g., a radioisotope of astatine (e.g., ^{211}At)].

In certain embodiments, the imaging agent comprises [18F]DCFPyL (DCFPyL labeled with ^{18}F).

In certain embodiments, the radionuclide is a radioisotope of gallium (Ga)(e.g., ^{68}Ga)

In certain embodiments, the medical images comprise a nuclear medicine image (e.g., a whole-body scan made with a gamma camera) of a first patient obtained following administration to the first patient of an imaging agent comprising a radionuclide (e.g., ^{99m}Tc)(e.g., wherein the imaging agent comprises ^{99m}Tc MDP), wherein the method comprises automatically analyzing the nuclear medicine image by: (a) geographically identifying a boundary (e.g., a 2D boundary; e.g., a 3D boundary) for each of one or more regions of imaged tissue [e.g., organs (e.g., a prostate; e.g., a liver; e.g., lungs or a lung; e.g., lymph nodes), organ structures, sub-organs, organ regions, and/or other regions (e.g., one or more particular bones; e.g., a skeletal region of the patient), e.g., regions of interest] within the nuclear medicine image (e.g., such that portions of the nuclear medicine image falling within and/or outside of the 3D boundaries can be differentiated from each other); and (c) computing (i) a value of each of one or more risk indices and/or (ii) a risk map using the nuclear medicine image with the identified boundaries of the one or more region(s).

In certain embodiments, step (c) comprises, for at least one risk index of the one or more risk indices, computing the value of the risk index by: determining, for each of the one or more regions, a corresponding cancerous tissue level within the region based on intensity values of the nuclear medicine image within the boundary of the region (e.g., by identifying within the nuclear medicine image, a plurality of hotspots within the 3D boundary of the region and computing a total number of and/or a total volume of the identified hotspots); and computing the value of the risk index based on the determined cancerous tissue levels within the one or more regions.

In certain embodiments, the processor is a processor of a cloud-based system.

In certain embodiments, the processor is a processor of one or more network or Internet host servers.

In another aspect, the invention is directed to a system comprising: a processor (e.g., of a network or Internet host server or of a portable computing device); and a memory having instructions stored thereon, wherein the instructions, when executed by the processor, cause the processor to generate and cause display of an interactive graphical user interface (GUI) element (e.g., cause display of the GUI element on a laptop computer or on a remote computing device, e.g., via a mobile app), the GUI element having user-selectable and/or user-adjustable graphical controls (e.g., slider bars, option buttons, text bars, drop-down boxes, windows, animations, and/or any other GUI widget) for selecting and/or adjusting a digital presentation of a 3D risk picture of a patient for comparison with reference images (e.g., for use in communication of results to patient as a decision-making support) caused to be displayed by the processor (e.g., wherein the reference images displayed to the user or presented for selection by the user are tunable according to one or more predetermined variables associated with the patient, e.g., patient age, time since diagnosis, prior treatment, and/or future treatment).

In certain embodiments, the interactive GUI element is produced from medical images of the patient [e.g., comprising one or more of the following: targeted PET images, targeted SPECT images, magnetic resonance (MR) images, ultrasound (US) images, gamma camera (i.e. scintillation camera) images, and combinations, fusions, or derivatives of any of the above] and/or other images or information (e.g., other images received and stored in the database of the network-based decision support system of any of the aspects and/or embodiments described herein).

In another aspect, the invention is directed to a method for tracking prostate cancer progression and treatment efficacy over time, for one or more patient(s), the method comprising: (a) repeatedly receiving and storing in a database, over time, by a processor of a computing device (e.g., a server computing device), a plurality of medical images for each of the one or more patient(s) to obtain, for each of the one or more patient(s), a series of medical images taken over time (e.g., over the course of multiple visits to one or more doctors); (b) for each of the one or more patient(s), automatically analyzing, by the processor, the series of medical images for the patient to determine values of one or more risk indices [e.g., the values of the one or more risk indices corresponding to numeric values indicative of prostate cancer state and/or progression in the patient (e.g., numeric values identifying a particular cancer stage; e.g., numeric values corresponding to a determined overall survival rate for the patient)] for each medical image of the series, thereby tracking determined values of the one or more risk indices over a course prostate cancer progression and treatment for the patient; and (c) for each of the one or more patient(s), storing, by the processor, the determined values of the one or more risk indices for the patient for further processing and/or causing, by the processor, display of a graphical representation of the determined values of the one or more risk indices for the patient (e.g., causing display of a graph showing variation in the determined values of the one or more risk indices for the patient over time).

In certain embodiments, the series of medical images for a particular patient of the one or more patient(s) comprises: (i) a first image subseries comprising one or more medical images obtained using a first nuclear imaging modality (e.g., SPECT scans; e.g., composite SPECT-CT images) each following administration to the particular patient of a first radiopharmaceutical (e.g., ^{99m}Tc-MIP-1404) (e.g., wherein the first radiopharmaceutical facilitates imaging of localized disease, e.g., localized prostate cancer); and (ii) a second image subseries comprising one or more medical images obtained using a second nuclear imaging modality (e.g., PET scans; e.g., composite PET-CT images; e.g., whole-body scans) each following administration to the particular patient of a second radiopharmaceutical (e.g., [18F]DCF-PyL; e.g., ^{99m}Tc MDP) (e.g., wherein the second radiopharmaceutical facilitates imaging of metastatic disease, e.g., metastatic prostate cancer), such that the values of the one or more risk indices determined in step (b) for the particular patient comprise a first subseries of values of a first risk index determined by automated analysis of the first image subseries and a second subseries of values of a second risk index determined by automated analysis of the second image subseries.

In certain embodiments, the medical images of first image subseries are obtained over a first period of time, when prostate cancer of the particular patient is localized (e.g., substantially localized to a prostate of the particular patient), and the medical images of the second image subseries are obtained over a second period of time, when prostate cancer of the particular patient is metastatic (e.g., having spread to regions of the patient outside of the prostate).

In certain embodiments, the first image subseries comprises one or more composite SPECT-CT image(s), each composite SPECT-CT image comprising a CT scan overlaid with a SPECT scan acquired at substantially the same time; the second image subseries comprises one or more composite PET-CT image(s), each composite PET-CT image comprising a CT scan overlaid with a PET scan acquired at substantially the same time; and step (b) comprises: automatically analyzing each of the one or more composite SPECT-CT images by: using the composite SPECT-CT image to geographically identify a 3D boundary of a prostate region (e.g., corresponding to a prostate of the patient) within the SPECT scan of the composite SPECT-CT image (e.g., such that portions of the nuclear medicine image falling within and/or outside of the 3D boundary of the prostate region can be differentiated from each other); and computing a value of the first risk index using the SPECT scan with the identified 3D boundary of the prostate region (e.g., computed based on a region of the SPECT scan corresponding to the identified 3D boundary of the prostate region); and automatically analyzing each of the one or more composite PET-CT images by: using the composite PET-CT image to geographically identify a 3D boundary of one or more metastatic regions within the PET scan of the composite PET-CT image, the one or metastatic regions including regions corresponding to patient tissue locations outside of the prostate [e.g., organs (e.g., a prostate; e.g., a liver; e.g., lungs or a lung; e.g., lymph nodes), organ structures, sub-

organs, organ regions, and/or other regions (e.g., one or more particular bones; e.g., a skeletal region corresponding to the patient's skeleton), e.g., regions of interest] (e.g., such that portions of the PET imaging scan falling within and/or outside of the 3D boundaries of the one or more metastatic region(s) can be differentiated from each other); and computing a value of the second risk index using the PET scan with the identified 3D boundaries of the one or more metastatic region(s).

In certain embodiments, the first image subseries comprises one or more composite SPECT-CT image(s), each composite SPECT-CT image comprising a CT scan overlaid with a SPECT scan acquired at substantially the same time; the second image subseries comprises one or more whole-body scan(s); and step (b) comprises: automatically analyzing each of the one or more composite SPECT-CT images by: using the composite SPECT-CT image to geographically identify a 3D boundary of a prostate region (e.g., corresponding to a prostate of the patient) within the SPECT scan of the composite SPECT-CT image (e.g., such that portions of the nuclear medicine image falling within and/or outside of the 3D boundary of the prostate region can be differentiated from each other); and computing a value of the first risk index using the SPECT scan with the identified 3D boundary of the prostate region (e.g., computed based on a region of the SPECT scan corresponding to the identified 3D boundary of the prostate region); and automatically analyzing each of the one or more whole-body scan(s) by: geographically identifying a boundary of one or more metastatic regions within the whole-body scan, the one or metastatic regions including regions corresponding to patient tissue locations outside of the prostate [(e.g., one or more particular bones; e.g., a skeletal region corresponding to the patient's skeleton), e.g., regions of interest] (e.g., such that portions of the whole-body scan falling within and/or outside of the boundaries of the one or more metastatic region(s) can be differentiated from each other); and computing a value of the second risk index using the PET scan with the identified 3D boundaries of the one or more metastatic region(s).

In another aspect, the invention is directed to a system for tracking prostate cancer progression and treatment efficacy over time, for one or more patient(s), the system comprising: a processor (e.g., of a network or Internet host server); and a memory having instructions stored thereon, wherein the instructions, when executed by the processor, cause the processor to: (a) repeatedly receive and store in a database, over time, a plurality of medical images for each of the one or more patient(s) to obtain, for each of the one or more patient(s), a series of medical images taken over time (e.g., over the course of multiple visits to one or more doctors); (b) for each of the one or more patient(s), automatically analyze the series of medical images for the patient to determine values of one or more risk indices [e.g., the values of the one or more risk indices corresponding to numeric values indicative of prostate cancer state and/or progression in the patient (e.g., numeric values identifying a particular cancer stage; e.g., numeric values corresponding to a determined overall survival rate for the patient)] for each medical image of the series, thereby tracking determined values of the one or more risk indices over a course prostate cancer progression and treatment for the patient; and (c) for each of the one or more patient(s), store the determined values of the one or more risk indices for the patient for further processing and/or cause display of a graphical representation of the determined values of the one or more risk indices for the patient (e.g., causing display of a graph showing variation in the determined values of the one or more risk indices for the patient over time).

In certain embodiments, the series of medical images for a particular patient of the one or more patient(s) comprises: (i) a first image subseries comprising one or more medical images obtained using a first nuclear imaging modality (e.g., SPECT scans; e.g., composite SPECT-CT images) each following administration to the particular patient of a first radiopharmaceutical (e.g., ^{99m}Tc-MIP-1404) (e.g., wherein the first radiopharmaceutical facilitates imaging of localized disease, e.g., localized prostate cancer); and (ii) a second image subseries comprising one or more medical images obtained using a second nuclear imaging modality (e.g., PET scans; e.g., composite PET-CT images; e.g., whole-body scans) each following administration to the particular patient of a second radiopharmaceutical (e.g., [18F]DCF-PyL; e.g., ^{99m}Tc MDP) (e.g., wherein the second radiopharmaceutical facilitates imaging of metastatic disease, e.g., metastatic prostate cancer), such that the values of the one or more risk indices determined in step (b) for the particular patient comprise a first subseries of values of a first risk index determined by automated analysis of the first image subseries and a second subseries of values of a second risk index determined by automated analysis of the second image subseries.

In certain embodiments, the medical images of first image subseries are obtained over a first period of time, when prostate cancer of the particular patient is localized (e.g., substantially localized to a prostate of the particular patient), and the medical images of the second image subseries are obtained over a second period of time, when prostate cancer of the particular patient is metastatic (e.g., having spread to regions of the patient outside of the prostate).

In certain embodiments, the first image subseries comprises one or more composite SPECT-CT image(s), each composite SPECT-CT image comprising a CT scan overlaid with a SPECT scan acquired at substantially the same time; the second image subseries comprises one or more composite PET-CT image(s), each composite PET-CT image comprising a CT scan overlaid with a PET scan acquired at substantially the same time; and the instructions cause the processor to, at step (b): automatically analyze each of the one or more composite SPECT-CT images by: using the composite SPECT-CT image to geographically identify a 3D boundary of a prostate region (e.g., corresponding to a prostate of the patient) within the SPECT scan of the composite SPECT-CT image (e.g., such that portions of the nuclear medicine image falling within and/or outside of the 3D boundary of the prostate region can be differentiated from each other); and computing a value of the first risk index using the SPECT scan with the identified 3D boundary of the prostate region (e.g., computed based on a region of the SPECT scan corresponding to the identified 3D boundary of the prostate region); and automatically analyze each of the one or more composite PET-CT images by: using the composite PET-CT image to geographically identify a 3D boundary of one or more metastatic regions within the PET scan of the composite PET-CT image, the one or metastatic regions including regions corresponding to patient tissue locations outside of the prostate [e.g., organs (e.g., a prostate; e.g., a liver; e.g., lungs or a lung; e.g., lymph nodes), organ structures, sub-organs, organ regions, and/or other regions (e.g., one or more particular bones; e.g., a skeletal region corresponding to the patient's skeleton), e.g., regions of interest] (e.g., such that portions of the PET imaging scan falling within and/or outside of the 3D boundaries of the one or more metastatic region(s) can be differentiated from each other); and computing a value of the second risk index using the PET scan with the identified 3D boundaries of the one or more metastatic region(s).

In certain embodiments, the first image subseries comprises one or more composite SPECT-CT image(s), each composite SPECT-CT image comprising a CT scan overlaid with a SPECT scan acquired at substantially the same time; the second image subseries comprises one or more whole-body scan(s); and the instructions cause the processor to, at

step (b): automatically analyze each of the one or more composite SPECT-CT images by: using the composite SPECT-CT image to geographically identify a 3D boundary of a prostate region (e.g., corresponding to a prostate of the patient) within the SPECT scan of the composite SPECT-CT image (e.g., such that portions of the nuclear medicine image falling within and/or outside of the 3D boundary of the prostate region can be differentiated from each other); and computing a value of the first risk index using the SPECT scan with the identified 3D boundary of the prostate region (e.g., computed based on a region of the SPECT scan corresponding to the identified 3D boundary of the prostate region); and automatically analyze each of the one or more whole-body scan(s) by: geographically identifying a boundary of one or more metastatic regions within the whole-body scan, the one or metastatic regions including regions corresponding to patient tissue locations outside of the prostate [(e.g., one or more particular bones; e.g., a skeletal region corresponding to the patient's skeleton), e.g., regions of interest] (e.g., such that portions of the whole-body scan falling within and/or outside of the boundaries of the one or more metastatic region(s) can be differentiated from each other); and computing a value of the second risk index using the PET scan with the identified 3D boundaries of the one or more metastatic region(s).

Embodiments described with respect to one aspect of the invention may be, applied to another aspect of the invention (e.g., features of embodiments described with respect to one independent claim, e.g., a method claim, are contemplated to be applicable to other embodiments of other independent claims, e.g., a system claim, and vice versa).

BRIEF DESCRIPTION OF THE DRAWINGS

The foregoing and other objects, aspects, features, and advantages of the present disclosure will become more apparent and better understood by referring to the following description taken in conjunction with the accompanying drawings, in which:

FIG. **1** is a screenshot of a graphical user interface (GUI) showing mobile app icons for three cloud-based services, according to illustrative embodiments.

FIG. **2** is a schematic showing the relationship between a platform and a computing device (e.g., personal computer or mobile computing device, e.g., smart phone) running an application, according to illustrative embodiments of the invention.

FIG. **3** is a screenshot of a GUI window in the BSI Cloud application (displayed to a user) that allows a user to enter information about a patient and upload and/or access medical images for the patient, e.g., series of images obtained over a period of time, according to an illustrative embodiment.

FIG. **4** is a screenshot of a GUI window in the BSI Cloud application showing representative full body gamma camera images showing hotspots automatically identified by the system, with corresponding overall computed BSI values for a particular image set obtained at a given time, according to an illustrative embodiment.

FIG. **5** is a screenshot of a GUI window in the BSI Cloud application showing an automatically or semi-automatically generated radiologist report, which can be signed and dated by a radiologist, according to an illustrative embodiment.

FIG. **6** is a block diagram showing a set of functionalities offered by the a cloud-based platform and supported graphical user interface (GUI) decision-making tools described herein, according to an illustrative embodiment.

FIG. **7** is a block diagram of an exemplary cloud computing environment, used in certain embodiments.

FIG. **8** is a block diagram of an example computing device and an example mobile computing device used in certain embodiments.

FIG. **9** is block diagram of an example architecture for implementing the cloud based platform described herein, according to an illustrative embodiment.

FIG. **10** is a schematic showing stages of prostate cancer progression, along with various therapies and diagnostic imaging modalities appropriate for various disease states, according to an illustrative embodiment.

FIG. **11** is a block flow diagram of a process for tracking prostate cancer progression and treatment efficacy over time, according to an illustrative embodiment.

The features and advantages of the present disclosure will become more apparent from the detailed description set forth below when taken in conjunction with the drawings, in which like reference characters identify corresponding elements throughout. In the drawings, like reference numbers generally indicate identical, functionally similar, and/or structurally similar elements.

DETAILED DESCRIPTION

It is contemplated that systems, devices, methods, and processes of the claimed invention encompass variations and adaptations developed using information from the embodiments described herein. Adaptation and/or modification of the systems, devices, methods, and processes described herein may be performed by those of ordinary skill in the relevant art.

Throughout the description, where articles, devices, and systems are described as having, including, or comprising specific components, or where processes and methods are described as having, including, or comprising specific steps, it is contemplated that, additionally, there are articles, devices, and systems of the present invention that consist essentially of, or consist of, the recited components, and that there are processes and methods according to the present invention that consist essentially of, or consist of, the recited processing steps.

It should be understood that the order of steps or order for performing certain action is immaterial so long as the invention remains operable. Moreover, two or more steps or actions may be conducted simultaneously.

The mention herein of any publication, for example, in the Background section, is not an admission that the publication serves as prior art with respect to any of the claims presented herein. The Background section is presented for purposes of clarity and is not meant as a description of prior art with respect to any claim.

Headers are provided for the convenience of the reader—the presence and/or placement of a header is not intended to limit the scope of the subject matter described herein.

A. Medical Imaging Modalities, Associated Radiopharmaceuticals, and Computed Risk Indices

FIG. **1** shows mobile app icons **100** for three cloud-based services, according to illustrative embodiments. As described in the following, the cloud-based services of the platform described herein provide for processing and analysis of medical images in a fully automated fashion and/or in combination with a user interaction (e.g., in a semi-automated fashion). The medical images include nuclear medicine images, obtained using a nuclear imaging modality such as whole-body scans with a gamma camera, Positron Emission Tomography (PET) scans, and Single-Photon Emission Tomography (SPECT) scans.

In certain embodiments, nuclear medicine images use imaging agents comprising radiopharmaceuticals. Nuclear medicine images are obtained following administration of a radiopharmaceutical to a patient, and provide information

regarding the distribution of the radiopharmaceutical within the patient. Radiopharmaceuticals are compounds that comprise a radionuclide.

As used herein, "radionuclide" refers to a moiety comprising a radioactive isotope of at least one element. Exemplary suitable radionuclides include but are not limited to those described herein. In some embodiments, a radionuclide is one used in positron emission tomography (PET). In some embodiments, a radionuclide is one used in single-photon emission computed tomography (SPECT). In some embodiments, a non-limiting list of radionuclides includes ^{99m}Tc, ^{64}Cu, ^{67}Ga, ^{68}Ga, ^{186}Re, ^{188}Re, ^{1535}m, ^{177}Lu, ^{67}Cu, ^{123}I, ^{124}I, ^{125}I, ^{126}I, ^{131}I, ^{11}C, ^{13}N, ^{15}O, ^{18}F, ^{153}Sm, ^{166}Ho, ^{177}Lu, ^{149}Pm, ^{90}Y, ^{213}Bi, ^{103}Pd, ^{109}Pd, ^{159}Gd, ^{140}La, ^{198}Au, ^{199}Au, ^{169}Yb, ^{175}Yb, ^{165}Dy, ^{166}Dy, ^{105}Rh, ^{111}Ag, ^{89}Zr, ^{225}Ac, ^{82}Rb, ^{75}Br, ^{76}Br, ^{77}Br, ^{80}Br, ^{80m}Br, ^{82}Br, ^{83}Br, ^{211}At and ^{192}Ir.

As used herein, the term "radiopharmaceutical" refers to a compound comprising a radionuclide. In certain embodiments, radiopharmaceuticals are used for diagnostic and/or therapeutic purposes. In certain embodiments, radiopharmaceuticals include small molecules that are labeled with one or more radionuclide(s), antibodies that are labeled with one or more radionuclide(s), and antigen-binding portions of antibodies that are labeled with one or more radionuclide(s).

Nuclear medicine images (e.g., PET scans; e.g., SPECT scans; e.g., whole-body scans; e.g. composite PET-CT images; e.g., composite SPECT-CT images) detect radiation emitted from the radionuclides of radiopharmaceuticals to form an image. The distribution of a particular radiopharmaceutical within a patient may be determined by biological mechanisms such as blood flow or perfusion, as well as by specific enzymatic or receptor binding interactions. Different radiopharmaceuticals may be designed to take advantage of different biological mechanisms and/or particular specific enzymatic or receptor binding interactions and thus, when administered to a patient, selectively concentrate within particular types of tissue and/or regions within the patient. Greater amounts of radiation are emitted from regions within the patient that have higher concentrations of radiopharmaceutical than other regions, such that these regions appear brighter in nuclear medicine images. Accordingly, intensity variations within a nuclear medicine image can be used to map the distribution of radiopharmaceutical within the patient. This mapped distribution of radiopharmaceutical within the patient can be used to, for example, infer the presence of cancerous tissue within various regions of the patient's body.

For example, upon administration to a patient, technetium 99m methylenediphosphonate (^{99m}Tc MDP) selectively accumulates within the skeletal region of the patient, in particular at sites with abnormal osteogenesis associated with malignant bone lesions. The selective concentration of radiopharmaceutical at these sites produces identifiable hotspots—localized regions of high intensity in nuclear medicine images. Accordingly, presence of malignant bone lesions associated with metastatic prostate cancer can be inferred by identifying such hotspots within a whole-body scan of the patient. As described in the following, risk indices that correlate with patient overall survival and other prognostic metrics indicative of disease state, progression, treatment efficacy, and the like, can be computed based on automated analysis of intensity variations in whole-body scans obtained following administration of ^{99m}Tc MDP to a patient. In certain embodiments, other radiopharmaceuticals can also be used in a similar fashion to ^{99m}Tc MDP.

In certain embodiments, the particular radiopharmaceutical used depends on the particular nuclear medicine imaging modality used. For example ^{18}F sodium fluoride (NaF) also accumulates in bone lesions, similar to ^{99m}Tc MDP, but can be used with PET imaging. In certain embodiments, PET imaging may also utilize a radioactive form of the vitamin choline, which is readily absorbed by prostate cancer cells.

In certain embodiments, radiopharmaceuticals that selectively bind to particular proteins or receptors of interest—particularly those whose expression is increased in cancerous tissue may be used. Such proteins or receptors of interest include, but are not limited to tumor antigens, such as CEA, which is expressed in colorectal carcinomas, Her2/neu, which is expressed in multiple cancers, BRCA 1 and BRCA 2, expressed in breast and ovarian cancers; and TRP-1 and -2, expressed in melanoma.

For example, human prostate-specific membrane antigen (PSMA) is upregulated in prostate cancer, including metastatic disease. PSMA is expressed by virtually all prostate cancers and its expression is further increased in poorly differentiated, metastatic and hormone refractory carcinomas. Accordingly, radiopharmaceuticals corresponding to PSMA binding agents (e.g., compounds that a high affinity to PSMA) labelled with one or more radionuclide(s) can be used to obtain nuclear medicine images of a patient from which the presence and/or state of prostate cancer within a variety of regions (e.g., including, but not limited to skeletal regions) of the patient can be assessed. In certain embodiments, nuclear medicine images obtained using PSMA binding agents are used to identify the presence of cancerous tissue within the prostate, when the disease is in a localized state. In certain embodiments, nuclear medicine images obtained using radiopharmaceuticals comprising PSMA binding agents are used to identify the presence of cancerous tissue within a variety of regions that include not only the prostate, but also other organs and tissue regions such as lungs, lymph nodes, and bones, as is relevant when the disease is metastatic.

In particular, upon administration to a patient, radionuclide labelled PSMA binding agents selectively accumulate within cancerous tissue, based on their affinity to PSMA. In a similar manner to that described above with regard to ^{99m}Tc MDP, the selective concentration of radionuclide labelled PSMA binding agents at particular sites within the patient produces detectable hotspots in nuclear medicine images. As PSMA binding agents concentrate within a variety of cancerous tissues and regions of the body expressing PSMA, localized cancer within a prostate of the patient and/or metastatic cancer in various regions of the patient's body can be detected, and evaluated. As described in the following, risk indices that correlate with patient overall survival and other prognostic metrics indicative of disease state, progression, treatment efficacy, and the like, can be computed based on automated analysis of intensity variations in nuclear medicine images obtained following administration of a PSMA binding agent radiopharmaceutical to a patient.

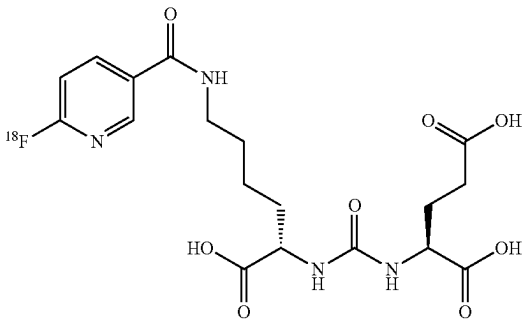
A variety of radionuclide labelled PSMA binding agents may be used as radiopharmaceutical imaging agents for nuclear medicine imaging to detect and evaluate prostate cancer. In certain embodiments, the particular radionuclide labelled PSMA binding agent that is used depends on factors such as the particular imaging modality (e.g., PET; e.g., SPECT) and the particular regions (e.g., organs) of the patient to be imaged. For example, certain radionuclide labelled PSMA binding agents are suited for PET imaging, while others are suited for SPECT imaging. For example, certain radionuclide labelled PSMA binding agents facilitate imaging a prostate of the patient, and are used primarily when the disease is localized, while others facilitate imaging organs and regions throughout the patient's body, and are useful for evaluating metastatic prostate cancer.

A variety of PSMA binding agents and radionuclide labelled versions thereof are described in U.S. Pat. Nos. 8,778,305, 8,211,401, and 8,962,799, each of which are incorporated herein by reference in their entireties.

A.i PET Imaging Radionuclide Labelled PSMA Binding Agents

In certain embodiments, the radionuclide labelled PSMA binding agent is a radionuclide labelled PSMA binding agent appropriate for PET imaging.

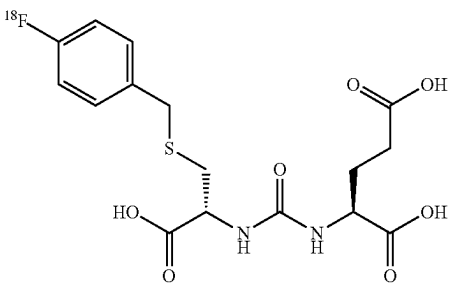
In certain embodiments, the radionuclide labelled PSMA binding agent comprises [18F]DCFPyL (also referred to as PyL™; also referred to as DCFPyL-18F):



[18F]DCFPyL,

or a pharmaceutically acceptable salt thereof.

In certain embodiments, the radionuclide labelled PSMA binding agent comprises [18F]DCFBC:



[18F]DCFBC,

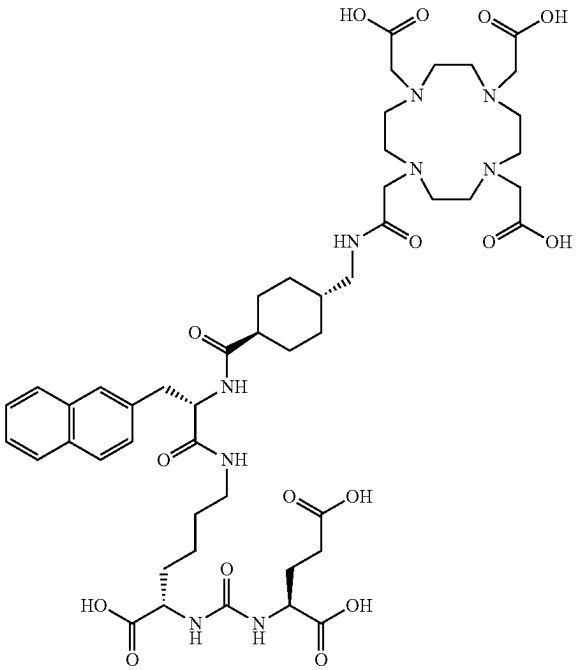
or a pharmaceutically acceptable salt thereof.

In certain embodiments, the radionuclide labelled PSMA binding agent comprises ^{68}Ga-PSMA-HBED-CC (also referred to as ^{68}Ga-PSMA-11):

^{68}Ga-PSMA-HBED-CC,

or a pharmaceutically acceptable salt thereof.

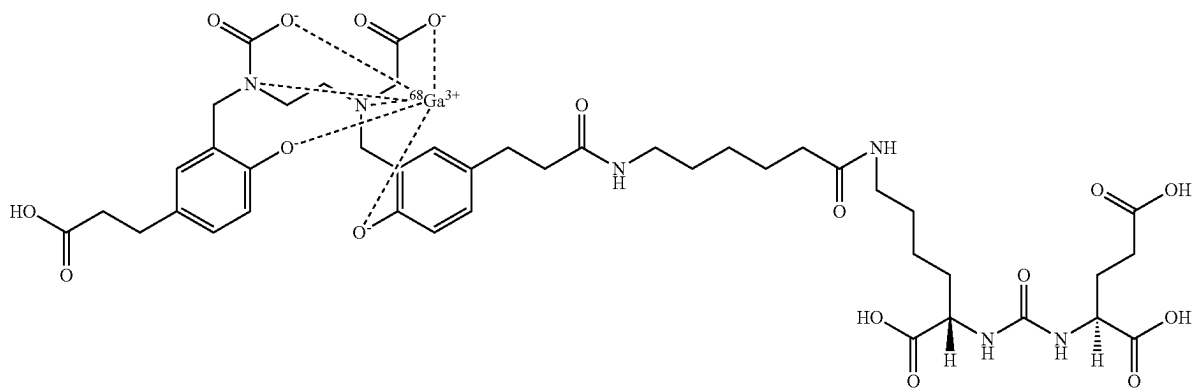
In certain embodiments, the radionuclide labelled PSMA binding agent comprises PSMA-617:

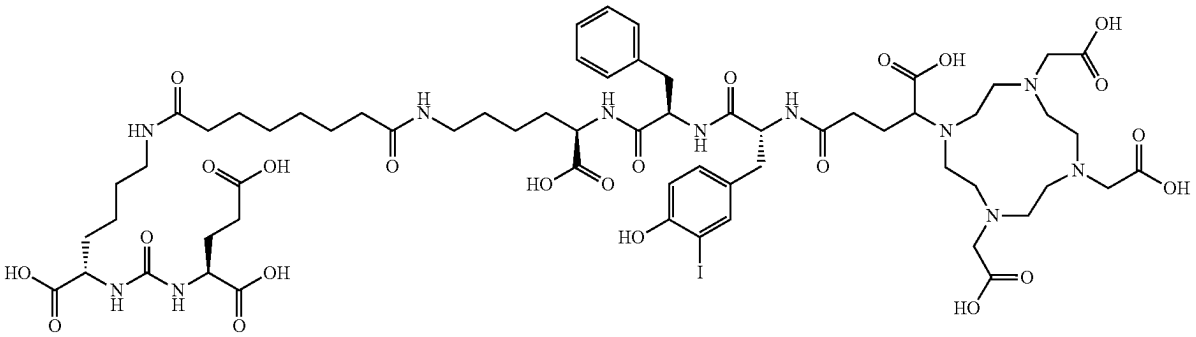


PSMA-617,

or a pharmaceutically acceptable salt thereof. In certain embodiments, the radionuclide labelled PSMA binding agent comprises ^{68}Ga-PSMA-617, which is PSMA-617 labelled with ^{68}Ga, or a pharmaceutically acceptable salt thereof. In certain embodiments, the radionuclide labelled PSMA binding agent comprises ^{177}Lu-PSMA-617, which is PSMA-617 labelled with ^{177}Lu, or a pharmaceutically acceptable salt thereof.

In certain embodiments, the radionuclide labelled PSMA binding agent comprises PSMA-I&T:

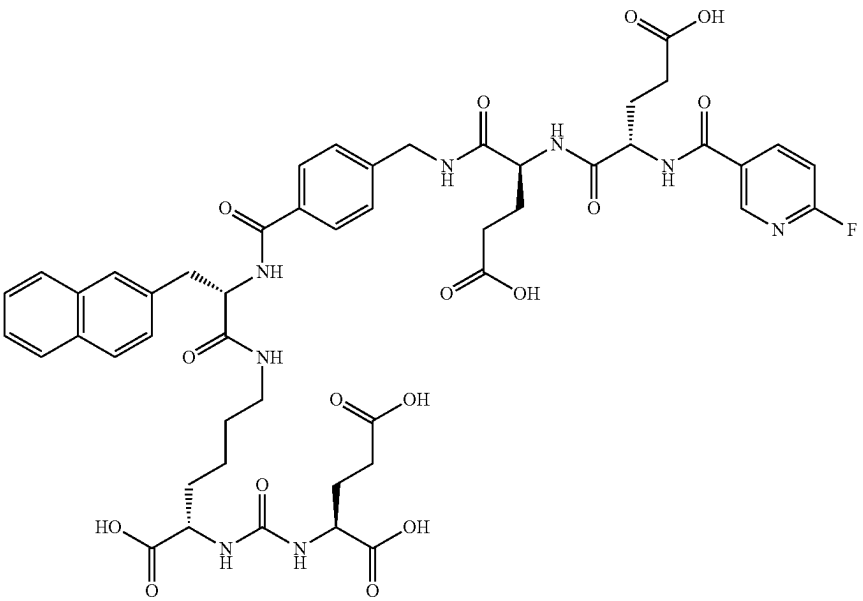




PSMA-I&T,

or a pharmaceutically acceptable salt thereof. In certain embodiments, the radionuclide labelled PSMA binding agent comprises ^{68}Ga-PSMA-I&T, which is PSMA-I&T labelled with ^{68}Ga, or a pharmaceutically acceptable salt thereof.

In certain embodiments, the radionuclide labelled PSMA binding agent comprises PSMA-1007:



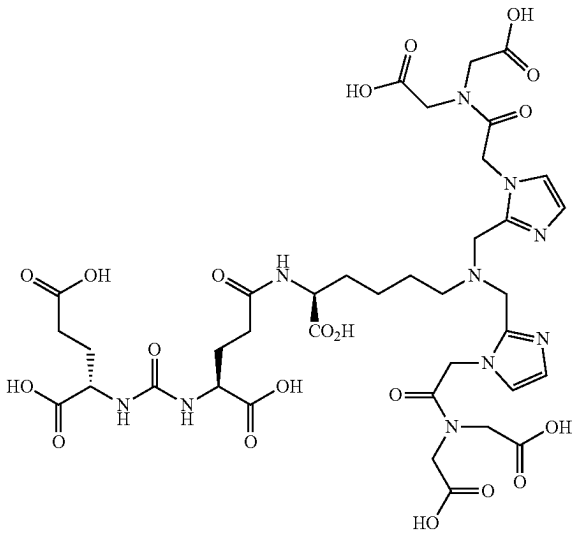
PSMA-1007,

or a pharmaceutically acceptable salt thereof. In certain embodiments, the radionuclide labelled PSMA binding agent comprises ^{18}F-PSMA-1007, which is PSMA-1007 labelled with ^{18}F, or a pharmaceutically acceptable salt thereof.

A.ii SPECT Imaging Radionuclide Labelled PSMA Binding Agents

In certain embodiments, the radionuclide labelled PSMA binding agent is a radionuclide labelled PSMA binding agent appropriate for SPECT imaging.

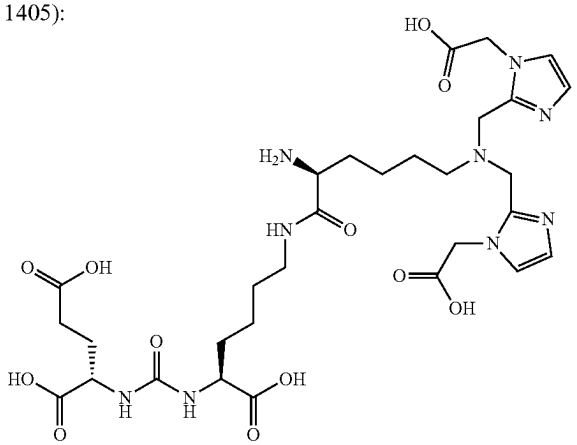
In certain embodiments, the radionuclide labelled PSMA binding agent comprises 1404 (also referred to as MIP-1404):



1404,

or a pharmaceutically acceptable salt thereof.

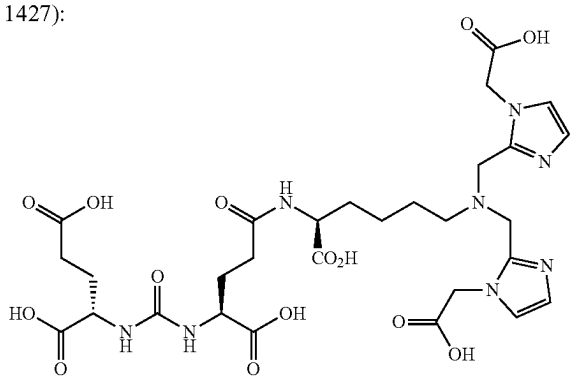
In certain embodiments, the radionuclide labelled PSMA binding agent comprises 1405 (also referred to as MIP-1405):



1405,

or a pharmaceutically acceptable salt thereof.

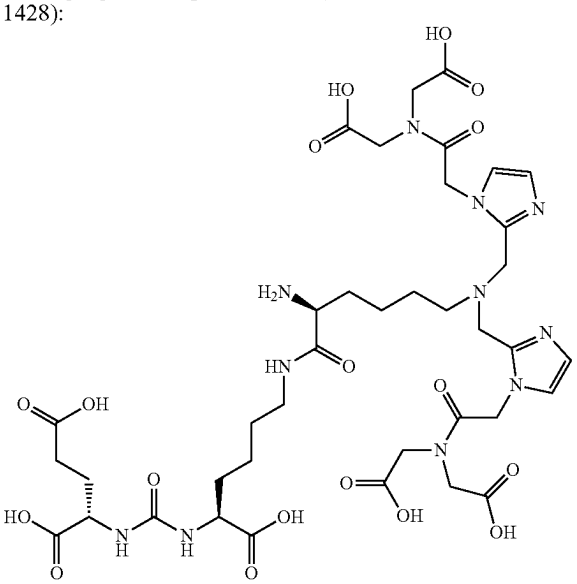
In certain embodiments, the radionuclide labelled PSMA binding agent comprises 1427 (also referred to as MIP-1427):



1427,

or a pharmaceutically acceptable salt thereof.

In certain embodiments, the radionuclide labelled PSMA binding agent comprises 1428 (also referred to as MIP-1428):

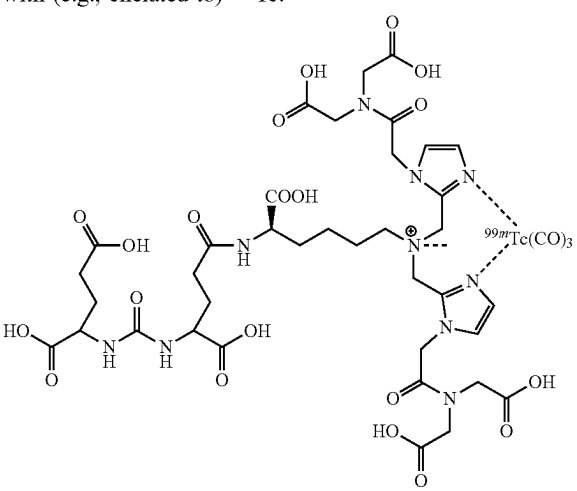


1428,

or a pharmaceutically acceptable salt thereof.

In certain embodiments, the PSMA binding agent is labelled with a radionuclide by chelating it to a radioisotope of a metal [e.g., a radioisotope of technetium (Tc) (e.g., technetium-99m (^{99m}Tc)); e.g., a radioisotope of rhenium (Re) (e.g., rhenium-188 (^{188}Re); e.g., rhenium-186 (^{186}Re)); e.g., a radioisotope of yttrium (Y) (e.g., ^{90}Y); e.g., a radioisotope of lutetium (Lu) (e.g., ^{177}Lu); e.g., a radioisotope of gallium (Ga) (e.g., ^{68}Ga; e.g., ^{67}Ga); e.g., a radioisotope of indium (e.g., ^{111}In); e.g., a radioisotope of copper (Cu) (e.g., ^{67}Cu)].

In certain embodiments, **1404** is labelled with a radionuclide (e.g., chelated to a radioisotope of a metal). In certain embodiments, the radionuclide labelled PSMA binding agent comprises ^{99m}Tc-MIP-1404, which is 1404 labelled with (e.g., chelated to)^{99m}Tc:

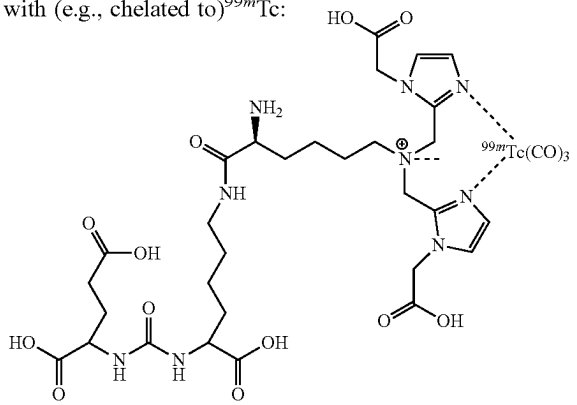


^{99m}Tc-MIP-1404,

or a pharmaceutically acceptable salt thereof. In certain embodiments, 1404 may be chelated to other metal radioisotopes [e.g., a radioisotope of rhenium (Re) (e.g., rhenium-188 (^{188}Re); e.g., rhenium-186 (^{186}Re)); e.g., a radioisotope of yttrium (Y) (e.g., ^{90}Y); e.g., a radioisotope of lutetium

(Lu)(e.g., ^{177}Lu); e.g., a radioisotope of gallium (Ga) (e.g., ^{68}Ga; e.g., ^{67}Ga); e.g., a radioisotope of indium (e.g., ^{111}In); e.g., a radioisotope of copper (Cu) (e.g., ^{67}Cu)] to form a compound having a structure similar to the structure shown above for ^{99m}Tc-MIP-1404, with the other metal radioisotope substituted for ^{99m}Tc.

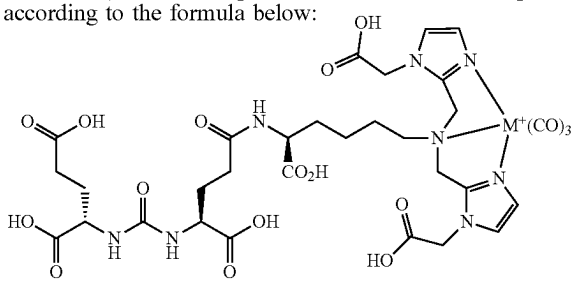
In certain embodiments, **1405** is labelled with a radionuclide (e.g., chelated to a radioisotope of a metal). In certain embodiments, the radionuclide labelled PSMA binding agent comprises ^{99m}Tc-MIP-1405, which is 1405 labelled with (e.g., chelated to)^{99m}Tc:



^{99m}Tc-MIP-1405,

or a pharmaceutically acceptable salt thereof. In certain embodiments, 1405 may be chelated to other metal radioisotopes [e.g., a radioisotope of rhenium (Re) (e.g., rhenium-188 (^{188}Re); e.g., rhenium-186 (^{186}Re)); e.g., a radioisotope of yttrium (Y) (e.g., ^{90}Y); e.g., a radioisotope of lutetium (Lu) (e.g., ^{177}Lu); e.g., a radioisotope of gallium (Ga) (e.g., ^{68}Ga; e.g., ^{67}Ga); e.g., a radioisotope of indium (e.g., ^{111}In); e.g., a radioisotope of copper (Cu) (e.g., ^{67}Cu)] to form a compound having a structure similar to the structure shown above for ^{99m}Tc-MIP-1405, with the other metal radioisotope substituted for ^{99m}Tc.

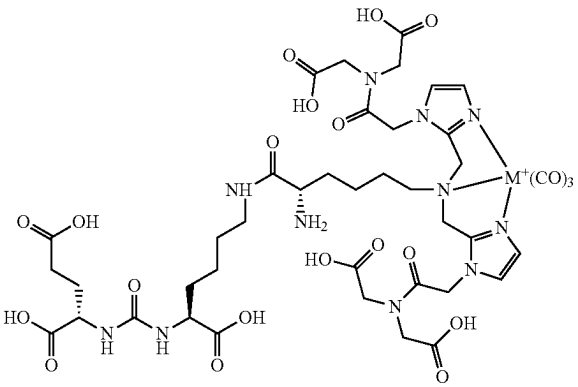
In certain embodiments, 1427 is labelled with (e.g., chelated to) a radioisotope of a metal, to form a compound according to the formula below:



1427 chelated to a metal,

or a pharmaceutically acceptable salt thereof, wherein M is a metal radioisotope [e.g., a radioisotope of technetium (Tc) (e.g., technetium-99m (^{99m}Tc)); e.g., a radioisotope of rhenium (Re) (e.g., rhenium-188 (^{188}Re); e.g., rhenium-186 (^{186}Re)); e.g., a radioisotope of yttrium (Y) (e.g., ^{90}Y); e.g., a radioisotope of lutetium (Lu)(e.g., ^{177}Lu); e.g., a radioisotope of gallium (Ga) (e.g., ^{68}Ga; e.g., ^{67}Ga); e.g., a radioisotope of indium (e.g., In); e.g., a radioisotope of copper (Cu) (e.g., ^{67}Cu)] with which 1427 is labelled.

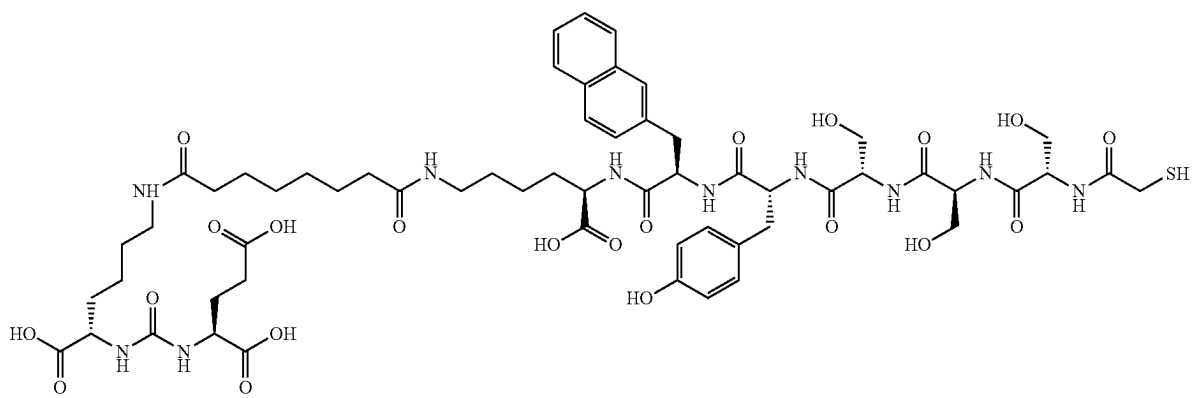
In certain embodiments, 1428 is labelled with (e.g., chelated to) a radioisotope of a metal, to form a compound according to the formula below:



1428 chelated to a metal,

or a pharmaceutically acceptable salt thereof, wherein M is a metal radioisotope [e.g., a radioisotope of technetium (Tc) (e.g., technetium-99m (^{99m}Tc)); e.g., a radioisotope of rhenium (Re) (e.g., rhenium-188 (^{188}Re); e.g., rhenium-186 (^{186}Re)); e.g., a radioisotope of yttrium (Y) (e.g., ^{90}Y); e.g., a radioisotope of lutetium (Lu)(e.g., ^{177}Lu); e.g., a radioisotope of gallium (Ga) (e.g., ^{68}Ga; e.g., ^{67}Ga); e.g., a radioisotope of indium (e.g., In); e.g., a radioisotope of copper (Cu) (e.g., ^{67}Cu)] with which 1428 is labelled.

In certain embodiments, the radionuclide labelled PSMA binding agent comprises PSMA I&S:



PSMA I& S,

or a pharmaceutically acceptable salt thereof. In certain embodiments, the radionuclide labelled PSMA binding agent comprises ^{99m}Tc-PSMA I&S, which is PSMA I&S labelled with ^{99m}Tc, or a pharmaceutically acceptable salt thereof.

A.iii Whole-Body Bone Scans

Turning to FIG. **1**, BSI Cloud **130** refers to a cloud-based decision support system that implements BSI values. BSI refers to bone scan index, which is a value computed from a method for detecting skeletal lesions from whole-body scanning (and anterior and posterior views) with a gamma camera following administration of the radionuclide technetium 99m methylenediphosphonate (^{99m}Tc MDP). Further explanation of BSI is provided, for example, in U.S. Pat. No. 8,855,387, which is incorporated herein by reference in its entirety, as well as in U.S. patent application Ser. No. 15/282,422, filed Sep. 30, 2016, which is incorporated herein by reference in its entirety.

In particular, BSI is computed from whole-body scans by segmenting anterior and posterior views of the whole-body scan of the patient to geographically identify boundaries of regions within the views that correspond to various portions of the patient's skeleton. Segmentation of the patient's skeleton can be performed using a variety of approaches, such as the Active Shape Model-based approach and the atlas image registration approach (which registers the anterior and posterior views of a whole body scan with reference anterior and posterior views of a reference whole body scan that have already been segmented (referred to as an atlas image)) described in U.S. Pat. No. 8,855,387. Other approaches, based on machine learning techniques (e.g., artificial neural networks (ANNs); e.g., convolutional neural networks (CNNs)) may also be used.

The BSI value is computed based on the intensity values of whole-body scan within the identified boundaries of the various skeletal regions. As discussed above, hotspots that correspond to localized regions of high intensity within the views (anterior and/or posterior views) of the whole-body scan can be detected. Hotspots may be detected and/or classified as corresponding to cancerous lesions (e.g., metastases) using a variety of approaches, including, as described in U.S. Pat. No. 8,855,387, machine learning techniques such as ANNs.

Hotspots corresponding to cancerous tissue lesions within the patient's skeleton, once detected, can be used to determine a risk index that provides a measure of disease state for the patient. For example, cancerous tissue levels within one or more regions, such as particular bones and/or the overall skeletal region, can be determined based on features of detected hotspots (e.g., detected hotspots classified as metastases). For example, a cancerous tissue level within a region (e.g., a particular bone; e.g., the overall skeletal region) may be determined based on (e.g., as a function of) a total number of detected hotspots within the region, a total volume of detected hotspots within the region, an average intensity of detected hotspots, a maximal intensity of detected hotspots, and the like, as well as combinations thereof. Properties of the one or more regions, such as their area or volume may also be used. For example, a total number and/or total volume of detected hotspots may be normalized (e.g., divided) by a volume and/or area of the region in which they are detected. A risk index may be determined based on the determined cancerous tissue levels within one or more regions, directly, e.g., as the cancerous tissue level within a single region, or determined from cancerous tissue levels in multiple regions (e.g., as an average; e.g., as a scaled sum; e.g., as a ratio; etc.), or even using machine learning approaches.

For example, the BSI value is a risk index that is a numeric value that quantifies the fraction of the total skeleton of the patient that is involved by cancerous tissue (e.g., tumors), based on the detected hotspots. The BSI value can be compared between different patients, and used as an objective measure of disease state and risk for a particular patient. Notably, since BSI is computed in an automated fashion, variability due to human factors such as radiologist interpretation of images is avoided.

Moreover, a variety of actionable information can be obtained from a patient's BSI value. For example, BSI can be correlated with prognostic values that provide a measure of disease state, progression, life expectancy (e.g., overall survival), treatment efficacy, and the like for the patient. Accordingly, a patient's BSI value can be used and tracked over time (e.g., over the course of multiple visits to one or more doctors) to provide them or their physician with an objective metric of what state their cancer is in, how fast it is progressing, what their outlook is, and whether one or more particular treatments are proving effective.

A.iv Positron Emission Tomography (PET) Scans

PyL Cloud **120** refers to a cloud-based system that uses medical images obtained with the agent PyL™, which is DCFPyL labeled with ^{18}F ([18F]DCFPyL). The patient, after injection of the imaging agent, receives a positron emission tomography (PET) scan to identify hot spots, and a CT scan. Further information about the PyL™ imaging agent is provided above, and, for example, in U.S. Pat. No. 8,778,305, which is incorporated herein by reference in its entirety.

In certain embodiments, the PET scan and the CT scan are combined as a composite image comprising the CT scan overlaid with the PET scan. As used herein, overlaying one image (e.g., a CT scan) with another (e.g., a PET scan) refers to establishing a mapping between coordinates and/or pixels or voxels of the two images that that represent the same physical locations (e.g., within the patient). CT scans provide accurate anatomical information in the form of detailed three-dimensional (3D) images of internal organs, bones, soft tissue, and blood vessels. Accordingly, 3D boundaries of specific regions of imaged tissue can be accurately identified by analysis of CT scans. For example, automated segmentation of CT scans can be performed to identify 3D boundaries of specific organs (e.g., a prostate, lymph nodes, a lung or lungs), sub-organs, organ regions, as well as other regions of imaged tissue, such as particular bones and an overall skeletal region of the patient. Automated segmentation of CT scans can be accomplished via a variety of approaches, include machine learning techniques [e.g., ANN-based approaches (including, e.g., convolutional neural networks (CNNs))], atlas image registration, and combinations thereof. In certain embodiments, manual segmentation of CT images can also be utilized, alone or in combination with automated segmentation approaches (e.g., to refine 3D boundaries identified via automated segmentation; e.g., to provide an initial starting point for an automated segmentation approach).

Once the 3D boundaries of various regions are identified within a CT scan of a composite image, by virtue of the mapping between the CT scan and PET scan of the composite image, the identified 3D boundaries can be transferred to the PET image. Accordingly, regions of the PET image falling within and/or outside of the identified 3D boundaries can be accurately identified.

In certain embodiments, composite images comprising CT scans overlaid with PET scans are obtained using dedicated PET-CT scanner instruments common in many hospitals, and are uploaded as medical images to the cloud-based platform described herein. In certain embodiments, a PET scan and a corresponding CT scan are obtained separately (but at substantially the same time), and uploaded to the cloud-based platform described herein. In such cases, the separately obtained PET and CT scans can be automatically fused to create a composite image.

In certain embodiments, once the 3D boundaries of the various regions are identified within the PET scan, one or more risk indices can be computed in a similar fashion to that described above with regard to BSI. In particular, in certain embodiments, intensity values of the PET scan in relation to (e.g., within and/or outside of) the 3D boundaries of the identified regions can be used to determine levels of cancerous tissue within the identified regions, e.g., based on features of detected hotspots (e.g., detected hotspots corresponding to metastases). Risk indices can then be computed based on the determined cancerous tissue levels. For example, hotspots within the PET scan can be identified, and, based on features such as their size, number, and distribution with respect to the identified regions, used to compute one or more risk indices. As with BSI, risk indices determined from PET scans can be correlated with prognostic values and tracked over time (e.g., over the course of multiple visits to one or more doctors) to provide patients or their physician with an objective metric of what state their cancer is in, how fast it is progressing, what their outlook is, and whether one or more particular treatments are proving effective. The approaches described herein with regard to PET imaging using PyL™ as a radiopharmaceutical can be applied to a variety of other radiopharmaceuticals, such as those described above, including, without limitation NaF, radioisotopes of choline, and any of the PSMA binding agents described in section A.i above.

A.v Single-Photon Emission Computerized Tomography (SPECT) Scans

1404 Cloud **130** refers to a cloud-based system that uses medical images obtained with the agent ^{99m}Tc-MIP-1404, which, as described above, is 1404 labeled with Tc^{99m}. After injection of the imaging agent, the patient receives a single-photon emission computerized tomography (SPECT) scan, e.g., to identify hot spots, and a computed tomography (CT) scan, e.g., to identify anatomical features. These images are overlaid to make a composite image (SPECT/CT). Further information about ^{99m}Tc-MIP-1404 imaging agent is provided above, and, for example, in U.S. Pat. Nos. 8,211,401 and 8,962,799, both of which are incorporated herein by reference in their entireties.

SPECT and CT scans can be analyzed in a manner similar to that described above with respect to PET and CT scans, in order to determine one or more risk indices. In particular, as with PET and CT scans, the SPECT scan and the CT scan can be combined in a composite image in which the CT scan is overlaid with the SPECT scan—a composite SPECT-CT image. As with composite PET-CT images, composite SPECT-CT images may be directly received as medical images by the cloud-based platform described herein (e.g., having been obtained via dedicated SPECT-CT imager in a hospital), or may be created by the cloud-based platform following receipt of separate SPECT scans and CT scans.

Similar to PET-CT images, 3D boundaries of various regions of imaged tissue can be identified within the SPECT image by virtue of the overlay with the CT image of the composite image. Intensity variations within the SPECT image, in relation to the 3D boundaries can be used to compute one or more risk indices. As with the approaches for computing risk indices from composite PET-CT images, this may comprise determine levels of cancerous tissue within the identified regions, for example by detecting hotspots within the 3D boundaries of the identified regions. Such risk indices can be correlated with prognostic values and tracked over time (e.g., over the course of multiple visits to one or more doctors) to provide patients or their physician with an objective metric of what state their cancer is in, how fast it is progressing, what their outlook is, and whether one or more particular treatments are proving effective. The approaches described herein with regard to SPECT imaging using ^{99m}Tc-MIP-1404 as a radiopharmaceutical can be applied to a variety of other radiopharmaceuticals, such as those described above, including, without limitation, any of the PSMA binding agents described in section A.ii above

B. Platform Services and Computing Device Components

FIG. **2** is a schematic **200** showing the relationship between a platform and a computing device (e.g., personal computer or mobile computing device, e.g., smart phone) running an application, according to illustrative embodiments of the invention. The platform performs various services, for example, user authentication ("Auth"), image and other data storage ("SliceBox), and the like—many more services than those shown may be provided. The applications may have both a platform component and a device component (e.g., native app on the client device).

FIG. **9** shows an example architecture **900** for implementing the cloud-based platform described herein, and providing various services such as the BSI Cloud, PyL Cloud, and 1404 Cloud services described above. The architecture shown in FIG. **9** can be used to implement the platform described herein on a variety of datacenters, including publicly available datacenters. The datacenter provides infrastructure in the form of servers and networks and provides services for e.g. networking, messaging, authentication, logging and storage. The architecture **900** for the platform uses a series of functional units with limited scope referred to as microservices. Each microservice handles an isolated set of tasks such as image storage, calculation of a risk index, identification of medical image type, and other tasks. Services (e.g., microservices) can communicate with each other using standard protocols such as Hypertext Transfer Protocol (HTTP). Organizing the platform into a network of microservices, as shown in the architecture **900** of FIG. **9**, allows for parts of the platform to be scaled individually to meet high demand and to ensure minimal downtime.

In certain embodiments, such an architecture allows for components to be improved or replaced without affecting other parts of the platform. The example architecture **900** shown in FIG. **9** includes a set **920** of microservices that that are common to two or more applications in the platform. The left **910** and right **930** panels show microservices in two applications. The microservice network shown in the left panel **910** implements a version of the BSI Cloud service, as described above, and provides for calculation of an automated BSI index (aBSI), which is a risk index derived from automated analysis of whole-body scans obtained with a gamma camera. The microservice network shown in the right panel **930** implements a version of the 1404 Cloud service, as described above, and provides for automated calculation of a SPECT index, which is a risk index derived from automated analysis of composite SPECT-CT images.

C. Image Collection, Analysis, and Result Presentation

FIG. **3** is a GUI window **300** in the BSI Cloud application (displayed to a user) that allows a user to enter information about a patient and upload and/or access medical images for the patient, e.g., series of images obtained over a period of time.

FIG. **4** is a GUI window **400** in the BSI Cloud application showing representative full body gamma camera images showing hotspots automatically identified by the system, with corresponding overall computed BSI values for a particular image set obtained at a given time. A graph **410** at left shows how the BSI value has changed over time (increase) for this particular patient.

FIG. **5** is a GUI window in the BSI Cloud application showing an automatically or semi-automatically generated radiologist report **510**, which can be signed and dated by a radiologist. In certain embodiments, the automatically identified hotspots may be adjusted by the radiologist (or other medical practitioner attending to the patient), with the change(s) reflected in the report. For example, an identified hotspot may be deactivated by the radiologist, or a new hotspot may be activated by the radiologist, such changes possibly affecting the computed BSI value, displayed in the report.

FIG. **6** is a block flow diagram of an illustrative network-based (e.g., cloud based) decision support system, according to an illustrative embodiment of the invention. FIG. **6** shows various functions that may be performed by the cloud based services described herein. These include: (i) receiving and storing sets of medical images in a database; (ii) accessing one or more of the medical images for transmission to the user for display on a user computing device; (iii) automatically analyzing, by the processor, the medical images to compute a risk index (e.g., BSI) and/or to generate a risk map; (iv) generating a radiologist report for a patient according to the patient images and/or risk index/risk map; and applying a machine learning algorithm to update a process for the automatic analysis of function (iii).

FIG. **10** is a schematic showing clinical stages **1010** of prostate cancer progression, along with various therapies **1020** and diagnostic imaging modalities **1030** appropriate for various disease states. As shown in the schematic, depending on the clinical state of a patient's prostate cancer, different imaging modalities and/or different radiopharmaceuticals may be appropriate. Similarly, different risk indices computed based on different imaging modalities and/or different radiopharmaceuticals may most appropriate, depending on the state of the patient's prostate cancer.

For example, in certain embodiments, when a patient either has, or is suspected of having prostate cancer in a localized state, composite SPECT-CT imaging may be used. SPECT scans of composite SPECT-CT images used for evaluation of localized prostate cancer can be obtained following administration of a particular radiopharmaceutical, such as ^{99m}Tc-MIP-1404, that facilitates imaging of localized prostate cancer. Any of the SPECT-CT images themselves, derivatives thereof, and risk indices computed from the SPECT-CT images can be used, accordingly, to assess risk, disease state, progression, treatment efficacy and the like for localized prostate cancer.

In certain embodiments, when a patient has or is suspected of having metastatic prostate cancer, that has metastasized outside of the prostate, other imaging techniques may be used. For example, whole-body scans obtained following administration of ^{99m}Tc-MDP can be used to assess tumor burden in a patient's skeleton. As discussed above, BSI values computed from whole-body scans can be used to assess risk, disease state, progression, treatment efficacy and the like when a patient's prostate cancer has metastasized to their skeleton. In certain embodiments, certain imaging modalities and/or radiopharmaceuticals can be used for evaluate of prostate cancer in both localized and metastatic states. For example, as illustrated in FIG. **10**, PET-CT imaging can be used for evaluating prostate cancer in both localized and metastatic states. As shown in the figure, such PET-CT images may be obtained using an appropriate radiopharmaceutical, such as PyL™, that facilitates imaging of both localized and metastatic prostate cancer.

In certain embodiments, the cloud-based platform facilitates evaluating prostate cancer progression and treatment efficacy over time. For example, as shown in the example process **1100** of the block flow diagram of FIG. **11**, in certain embodiments medical images of a particular patient are repeatedly received and stored over time **1110**, over the course of multiple visits to one or more doctors and/or clinical specialists (e.g., radiologists) by the patient. In this manner, a series of medical images for the patient are obtained. The series of medical images can be automatically analyzed to determine values of one or more risk indices, so as to track changes in the determined values over time **1120**. The determined risk index values may be stored **1130***a* (e.g., for further processing). In certain embodiments, the process causes a graphical representation of the determined risk index values, such as a graph, to be displayed (e.g., on a user computing device; e.g., via a web-based portal) **1130***b*.

Notably, by virtue of the capability of the cloud-based platform described herein to receive, store, and analyze a variety of different medical image types, such as composite SPECT-CT images, whole-body scans, and composite PET-CT images, the medical images need not be of the same type.

For example, a first subseries of medical images may be obtained using a first imaging modality and a first radiopharmaceutical, such as SPECT-CT imaging with ^{99m}Tc-MIP-1404, when the patient's prostate cancer is in a localized state. If the patient's prostate cancer progresses to a metastatic state, a second subseries of images may comprise images obtained via a different, second imaging modality and/or a different, second radiopharmaceutical. For example, the second subseries of medical images may be PET-CT images obtained using PyL™ For example, the second subseries of medical images may be whole-body scans obtained using ^{99m}Tc-MDP.

Risk indices can be computed for the first image subseries and for the second image subseries to provide a unified picture of the patient's prostate cancer progression and treatment over time. This approach can be performed for multiple patients, not only for decision making purposes with regard to each patient's disease progression and particular course of treatment, but also in the context of clinical trials, for example to compare efficacy of a particular treatment with others or a control.

D. Computer System and Network Environment

FIG. **7** shows an illustrative network environment **700** for use in the methods and systems described herein. In brief overview, referring now to FIG. **7**, a block diagram of an exemplary cloud computing environment **700** is shown and described. The cloud computing environment **700** may include one or more resource providers **702***a*, **702***b*, **702***c* (collectively, **702**). Each resource provider **702** may include computing resources. In some implementations, computing resources may include any hardware and/or software used to process data. For example, computing resources may include hardware and/or software capable of executing

algorithms, computer programs, and/or computer applications. In some implementations, exemplary computing resources may include application servers and/or databases with storage and retrieval capabilities. Each resource provider **702** may be connected to any other resource provider **702** in the cloud computing environment **700**. In some implementations, the resource providers **702** may be connected over a computer network **708**. Each resource provider **702** may be connected to one or more computing device **704***a*, **704***b*, **704***c* (collectively, **704**), over the computer network **708**.

The cloud computing environment **700** may include a resource manager **706**. The resource manager **706** may be connected to the resource providers **702** and the computing devices **704** over the computer network **708**. In some implementations, the resource manager **706** may facilitate the provision of computing resources by one or more resource providers **702** to one or more computing devices **704**. The resource manager **706** may receive a request for a computing resource from a particular computing device **704**. The resource manager **706** may identify one or more resource providers **702** capable of providing the computing resource requested by the computing device **704**. The resource manager **706** may select a resource provider **702** to provide the computing resource. The resource manager **706** may facilitate a connection between the resource provider **702** and a particular computing device **704**. In some implementations, the resource manager **706** may establish a connection between a particular resource provider **702** and a particular computing device **704**. In some implementations, the resource manager **706** may redirect a particular computing device **704** to a particular resource provider **702** with the requested computing resource.

FIG. **8** shows an example of a computing device **800** and a mobile computing device **850** that can be used in the methods and systems described in this disclosure. The computing device **800** is intended to represent various forms of digital computers, such as laptops, desktops, workstations, personal digital assistants, servers, blade servers, mainframes, and other appropriate computers. The mobile computing device **850** is intended to represent various forms of mobile devices, such as personal digital assistants, cellular telephones, smart-phones, and other similar computing devices. The components shown here, their connections and relationships, and their functions, are meant to be examples only, and are not meant to be limiting.

The computing device **800** includes a processor **802**, a memory **804**, a storage device **806**, a high-speed interface **808** connecting to the memory **804** and multiple high-speed expansion ports **810**, and a low-speed interface **812** connecting to a low-speed expansion port **814** and the storage device **806**. Each of the processor **802**, the memory **804**, the storage device **806**, the high-speed interface **808**, the high-speed expansion ports **810**, and the low-speed interface **812**, are interconnected using various busses, and may be mounted on a common motherboard or in other manners as appropriate. The processor **802** can process instructions for execution within the computing device **800**, including instructions stored in the memory **804** or on the storage device **806** to display graphical information for a GUI on an external input/output device, such as a display **816** coupled to the high-speed interface **808**. In other implementations, multiple processors and/or multiple buses may be used, as appropriate, along with multiple memories and types of memory. Also, multiple computing devices may be connected, with each device providing portions of the necessary operations (e.g., as a server bank, a group of blade servers, or a multi-processor system). Thus, as the term is used herein, where a plurality of functions are described as being performed by "a processor", this encompasses embodiments wherein the plurality of functions are performed by any number of processors (one or more) of any number of computing devices (one or more). Furthermore, where a function is described as being performed by "a processor", this encompasses embodiments wherein the function is performed by any number of processors (one or more) of any number of computing devices (one or more) (e.g., in a distributed computing system).

The memory **804** stores information within the computing device **800**. In some implementations, the memory **804** is a volatile memory unit or units. In some implementations, the memory **804** is a non-volatile memory unit or units. The memory **804** may also be another form of computer-readable medium, such as a magnetic or optical disk.

The storage device **806** is capable of providing mass storage for the computing device **800**. In some implementations, the storage device **806** may be or contain a computer-readable medium, such as a floppy disk device, a hard disk device, an optical disk device, or a tape device, a flash memory or other similar solid state memory device, or an array of devices, including devices in a storage area network or other configurations. Instructions can be stored in an information carrier. The instructions, when executed by one or more processing devices (for example, processor **802**), perform one or more methods, such as those described above. The instructions can also be stored by one or more storage devices such as computer- or machine-readable mediums (for example, the memory **804**, the storage device **806**, or memory on the processor **802**).

The high-speed interface **808** manages bandwidth-intensive operations for the computing device **800**, while the low-speed interface **812** manages lower bandwidth-intensive operations. Such allocation of functions is an example only. In some implementations, the high-speed interface **808** is coupled to the memory **804**, the display **816** (e.g., through a graphics processor or accelerator), and to the high-speed expansion ports **810**, which may accept various expansion cards (not shown). In the implementation, the low-speed interface **812** is coupled to the storage device **806** and the low-speed expansion port **814**. The low-speed expansion port **814**, which may include various communication ports (e.g., USB, Bluetooth®, Ethernet, wireless Ethernet) may be coupled to one or more input/output devices, such as a keyboard, a pointing device, a scanner, or a networking device such as a switch or router, e.g., through a network adapter.

The computing device **800** may be implemented in a number of different forms, as shown in the figure. For example, it may be implemented as a standard server **820**, or multiple times in a group of such servers. In addition, it may be implemented in a personal computer such as a laptop computer **822**. It may also be implemented as part of a rack server system **824**. Alternatively, components from the computing device **800** may be combined with other components in a mobile device (not shown), such as a mobile computing device **850**. Each of such devices may contain one or more of the computing device **800** and the mobile computing device **850**, and an entire system may be made up of multiple computing devices communicating with each other.

The mobile computing device **850** includes a processor **852**, a memory **864**, an input/output device such as a display **854**, a communication interface **866**, and a transceiver **868**, among other components. The mobile computing device **850** may also be provided with a storage device, such as a

micro-drive or other device, to provide additional storage. Each of the processor **852**, the memory **864**, the display **854**, the communication interface **866**, and the transceiver **868**, are interconnected using various buses, and several of the components may be mounted on a common motherboard or in other manners as appropriate.

The processor **852** can execute instructions within the mobile computing device **850**, including instructions stored in the memory **864**. The processor **852** may be implemented as a chipset of chips that include separate and multiple analog and digital processors. The processor **852** may provide, for example, for coordination of the other components of the mobile computing device **850**, such as control of user interfaces, applications run by the mobile computing device **850**, and wireless communication by the mobile computing device **850**.

The processor **852** may communicate with a user through a control interface **858** and a display interface **856** coupled to the display **854**. The display **854** may be, for example, a TFT (Thin-Film-Transistor Liquid Crystal Display) display or an OLED (Organic Light Emitting Diode) display, or other appropriate display technology. The display interface **856** may comprise appropriate circuitry for driving the display **854** to present graphical and other information to a user. The control interface **858** may receive commands from a user and convert them for submission to the processor **852**. In addition, an external interface **862** may provide communication with the processor **852**, so as to enable near area communication of the mobile computing device **850** with other devices. The external interface **862** may provide, for example, for wired communication in some implementations, or for wireless communication in other implementations, and multiple interfaces may also be used.

The memory **864** stores information within the mobile computing device **850**. The memory **864** can be implemented as one or more of a computer-readable medium or media, a volatile memory unit or units, or a non-volatile memory unit or units. An expansion memory **874** may also be provided and connected to the mobile computing device **850** through an expansion interface **872**, which may include, for example, a SIMM (Single In Line Memory Module) card interface. The expansion memory **874** may provide extra storage space for the mobile computing device **850**, or may also store applications or other information for the mobile computing device **850**. Specifically, the expansion memory **874** may include instructions to carry out or supplement the processes described above, and may include secure information also. Thus, for example, the expansion memory **874** may be provided as a security module for the mobile computing device **850**, and may be programmed with instructions that permit secure use of the mobile computing device **850**. In addition, secure applications may be provided via the SIMM cards, along with additional information, such as placing identifying information on the SIMM card in a non-hackable manner.

The memory may include, for example, flash memory and/or NVRAM memory (non-volatile random access memory), as discussed below. In some implementations, instructions are stored in an information carrier and, when executed by one or more processing devices (for example, processor **852**), perform one or more methods, such as those described above. The instructions can also be stored by one or more storage devices, such as one or more computer- or machine-readable mediums (for example, the memory **864**, the expansion memory **874**, or memory on the processor **852**). In some implementations, the instructions can be received in a propagated signal, for example, over the transceiver **868** or the external interface **862**.

The mobile computing device **850** may communicate wirelessly through the communication interface **866**, which may include digital signal processing circuitry where necessary. The communication interface **866** may provide for communications under various modes or protocols, such as GSM voice calls (Global System for Mobile communications), SMS (Short Message Service), EMS (Enhanced Messaging Service), or MMS messaging (Multimedia Messaging Service), CDMA (code division multiple access), TDMA (time division multiple access), PDC (Personal Digital Cellular), WCDMA (Wideband Code Division Multiple Access), CDMA2000, or GPRS (General Packet Radio Service), among others. Such communication may occur, for example, through the transceiver **868** using a radio-frequency. In addition, short-range communication may occur, such as using a Bluetooth®, Wi-Fi™, or other such transceiver (not shown). In addition, a GPS (Global Positioning System) receiver module **870** may provide additional navigation- and location-related wireless data to the mobile computing device **850**, which may be used as appropriate by applications running on the mobile computing device **850**.

The mobile computing device **850** may also communicate audibly using an audio codec **860**, which may receive spoken information from a user and convert it to usable digital information. The audio codec **860** may likewise generate audible sound for a user, such as through a speaker, e.g., in a handset of the mobile computing device **850**. Such sound may include sound from voice telephone calls, may include recorded sound (e.g., voice messages, music files, etc.) and may also include sound generated by applications operating on the mobile computing device **850**.

The mobile computing device **850** may be implemented in a number of different forms, as shown in the figure. For example, it may be implemented as a cellular telephone **880**. It may also be implemented as part of a smart-phone **882**, personal digital assistant, or other similar mobile device.

Various implementations of the systems and techniques described here can be realized in digital electronic circuitry, integrated circuitry, specially designed ASICs (application specific integrated circuits), computer hardware, firmware, software, and/or combinations thereof. These various implementations can include implementation in one or more computer programs that are executable and/or interpretable on a programmable system including at least one programmable processor, which may be special or general purpose, coupled to receive data and instructions from, and to transmit data and instructions to, a storage system, at least one input device, and at least one output device.

These computer programs (also known as programs, software, software applications or code) include machine instructions for a programmable processor, and can be implemented in a high-level procedural and/or object-oriented programming language, and/or in assembly/machine language. As used herein, the terms machine-readable medium and computer-readable medium refer to any computer program product, apparatus and/or device (e.g., magnetic discs, optical disks, memory, Programmable Logic Devices (PLDs)) used to provide machine instructions and/or data to a programmable processor, including a machine-readable medium that receives machine instructions as a machine-readable signal. The term machine-readable signal refers to any signal used to provide machine instructions and/or data to a programmable processor.

To provide for interaction with a user, the systems and techniques described here can be implemented on a com-

puter having a display device (e.g., a CRT (cathode ray tube) or LCD (liquid crystal display) monitor) for displaying information to the user and a keyboard and a pointing device (e.g., a mouse or a trackball) by which the user can provide input to the computer. Other kinds of devices can be used to provide for interaction with a user as well; for example, feedback provided to the user can be any form of sensory feedback (e.g., visual feedback, auditory feedback, or tactile feedback); and input from the user can be received in any form, including acoustic, speech, or tactile input.

The systems and techniques described here can be implemented in a computing system that includes a back end component (e.g., as a data server), or that includes a middleware component (e.g., an application server), or that includes a front end component (e.g., a client computer having a graphical user interface or a Web browser through which a user can interact with an implementation of the systems and techniques described here), or any combination of such back end, middleware, or front end components. The components of the system can be interconnected by any form or medium of digital data communication (e.g., a communication network). Examples of communication networks include a local area network (LAN), a wide area network (WAN), and the Internet.

The computing system can include clients and servers. A client and server are generally remote from each other and typically interact through a communication network. The relationship of client and server arises by virtue of computer programs running on the respective computers and having a client-server relationship to each other. In some implementations, the modules and/or services (e.g. cloud based services, such as BSI Cloud **110**, PyL Cloud **120**, 1404 Cloud **130**; e.g., any of the microservices described herein) described herein can be separated, combined or incorporated into single or combined modules and/or services. The modules and/or services depicted in the figures are not intended to limit the systems described herein to the software architectures shown therein

While the invention has been particularly shown and described with reference to specific preferred embodiments, it should be understood by those skilled in the art that various changes in form and detail may be made therein without departing from the spirit and scope of the invention as defined by the appended claims.

What is claimed is:

1. A network-based system for generating a disease risk map for use as a decision-making support for evaluating risk of cancer or risk of recurrence of cancer, the system comprising:

a processor; and

a memory having instructions stored thereon, wherein the instructions, when executed by the processor, cause the processor to:

(i) access one or more medical images associated with a particular patient from a database;

(ii) perform an analysis of the one or more medical images associated with the particular patient using a machine learning algorithm, to generate the risk map, wherein the risk map comprises a visual representation of tissue overlaid with graphical denotations marking one or more regions of risk of cancer or risk of recurrence of cancer; and

(iii) cause display of the risk map via a graphical user interface (GUI) for presentation or review of the risk map by a user,

wherein the analysis of the one or more medical images comprises creation of a 3D image of the one or more regions of risk of cancer or risk of recurrence of cancer overlaid on the one or more medical images, and wherein the 3D image comprises geographic identification of one or more specific tissue region(s) overlaid on the one or more medical images.

2. The system of claim **1**, wherein the one or more medical images comprise one or more magnetic resonance images (MRIs).

3. The system of claim **1**, wherein the one or more medical images comprise (i) one or more PET/CT image(s) or (ii) one or more SPECT/CT image(s).

4. The system of claim **1**, wherein the visual representation of tissue is at least a portion of one of the one or more medical images of the particular patient.

5. The system of claim **1**, wherein the cancer is prostate cancer.

6. The system of claim **1**, wherein the visual representation of tissue comprises a visual representation of bone.

7. The system of claim **1**, wherein the one or more specific tissue region(s) comprise one or more members selected from the group consisting of organs, organ structures, sub-organs, and organ regions.

8. The system of claim **1**, wherein the one or more specific tissue region(s) comprise one or more particular bones.

9. The system of claim **1**, wherein the instructions cause the processor to generate a radiologist report for the particular patient based at least in part on the analysis of the one or more medical images.

10. The system of claim **9**, wherein the radiologist report comprises the one or more medical images and the risk map.

11. The system of claim **9**, wherein the radiologist report comprises one or more reference images or reference risk maps.

12. The system of claim **1**, wherein the instructions cause the processor to apply a machine learning algorithm to update a process for automatically analyzing the one or more medical images using accumulated image data in the database.

13. A method for generating a disease risk map for use as a decision-making support for evaluating risk of cancer or risk of recurrence of cancer, the method comprising:

(i) accessing, by a processor, one or more medical images associated with a particular patient from a database;

(ii) automatically analyzing, by the processor, using a machine learning algorithm, the one or more medical images to generate the risk map, wherein the risk map comprises a visual representation of tissue overlaid with graphical denotations marking one or more regions of risk of cancer or risk of recurrence of cancer; and

(iii) causing, by the processor, display of the risk map via a graphical user interface (GUI) for presentation or review of the risk map by a user,

wherein step (ii) comprises creation of a 3D image of the one or more regions of risk of cancer or risk of recurrence of cancer overlaid on the one or more medical images, and wherein the 3D image comprises geographic identification of one or more specific tissue region(s) overlaid on the one or more medical images.

* * * * *

EXHIBIT 2

US010973486B2

(12) United States Patent

Sjöstrand et al.

(10) Patent No.: US 10,973,486 B2
(45) Date of Patent: Apr. 13, 2021

(54) **SYSTEMS AND METHODS FOR RAPID NEURAL NETWORK-BASED IMAGE SEGMENTATION AND RADIOPHARMACEUTICAL UPTAKE DETERMINATION**

(71) Applicants: **Progenics Pharmaceuticals, Inc.**, New York, NY (US); **EXINI Diagnostics AB**, Lund (SE)

(72) Inventors: **Karl Vilhelm Sjöstrand**, New York, NY (US); **Jens Filip Andreas Richter**, Lund (SE); **Kerstin Elsa Maria Johnsson**, Lund (SE); **Erik Konrad Gjertsson**, Lund (SE)

(73) Assignees: **Progenics Pharmaceuticals, Inc.**, New York, NY (US); **EXINI Diagnostics AB**, Lund (SE)

(*) Notice: Subject to any disclaimer, the term of this patent is extended or adjusted under 35 U.S.C. 154(b) by 259 days.

(21) Appl. No.: **16/003,006**

(22) Filed: **Jun. 7, 2018**

(65) **Prior Publication Data**

US 2019/0209116 A1 Jul. 11, 2019

Related U.S. Application Data

(60) Provisional application No. 62/614,935, filed on Jan. 8, 2018.

(51) **Int. Cl.**
G06K 9/46 (2006.01)
A61B 6/00 (2006.01)
(Continued)

(52) **U.S. Cl.**
CPC ***A61B 6/5217*** (2013.01); ***A61B 6/037*** (2013.01); ***A61B 6/465*** (2013.01); ***A61B 6/466*** (2013.01);
(Continued)

(58) **Field of Classification Search**
CPC A61B 6/037; A61B 6/465; A61B 6/466; A61B 6/467; A61B 6/50; A61B 6/5217;
(Continued)

(56) **References Cited**

U.S. PATENT DOCUMENTS

7,450,747 B2 11/2008 Jabri et al.
7,751,605 B2 7/2010 Gündel et al.
(Continued)

FOREIGN PATENT DOCUMENTS

CN 101528267 A 9/2009
CN 102361594 A 2/2012
(Continued)

OTHER PUBLICATIONS

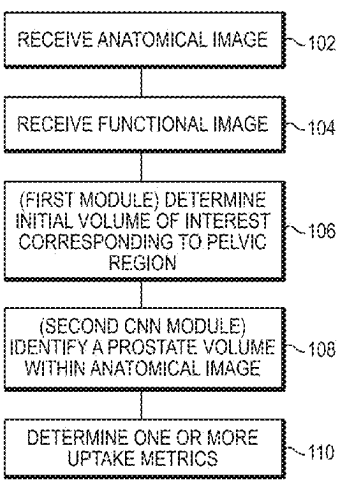
Cha, Kenny H., et al. "Urinary bladder segmentation in CT urography using deep-learning convolutional neural network and level sets." Medical physics 43.4 (2016): 1882-1896. (Year: 2016).*
(Continued)

Primary Examiner — Nirav G Patel
(74) *Attorney, Agent, or Firm* — William R. Haulbrook; Ronen Adato; Choate, Hall & Stewart LLP

(57) **ABSTRACT**

Presented herein are systems and methods that provide for automated analysis of three-dimensional (3D) medical images of a subject in order to automatically identify specific 3D volumes within the 3D images that correspond to specific organs and/or tissue. In certain embodiments, the accurate identification of one or more such volumes can be used to determine quantitative metrics that measure uptake of radiopharmaceuticals in particular organs and/or tissue regions. These uptake metrics can be used to assess disease state in a subject, determine a prognosis for a subject, and/or determine efficacy of a treatment modality.

55 Claims, 83 Drawing Sheets
(30 of 83 Drawing Sheet(s) Filed in Color)



(51) **Int. Cl.**

G06T 7/00	(2017.01)
G06T 5/30	(2006.01)
A61B 6/03	(2006.01)
A61K 51/04	(2006.01)
G06T 15/08	(2011.01)
G06T 7/143	(2017.01)
G06T 7/11	(2017.01)
G06N 3/08	(2006.01)
G06F 3/0484	(2013.01)
G06N 3/04	(2006.01)

(52) **U.S. Cl.**

CPC ***A61B 6/467*** (2013.01); ***A61B 6/50*** (2013.01); ***A61B 6/5223*** (2013.01); ***A61B 6/5229*** (2013.01); ***A61B 6/5258*** (2013.01); ***A61K 51/0478*** (2013.01); ***G06K 9/4647*** (2013.01); ***G06T 5/30*** (2013.01); ***G06T 7/0012*** (2013.01); ***G06T 7/0014*** (2013.01); ***G06T 7/11*** (2017.01); ***G06T 7/143*** (2017.01); ***G06T 15/08*** (2013.01); *G06F 3/04842* (2013.01); *G06K 2209/051* (2013.01); *G06N 3/04* (2013.01); *G06N 3/0454* (2013.01); *G06N 3/08* (2013.01); *G06T 2200/24* (2013.01); *G06T 2207/10081* (2013.01); *G06T 2207/10088* (2013.01); *G06T 2207/10104* (2013.01); *G06T 2207/10108* (2013.01); *G06T 2207/20081* (2013.01); *G06T 2207/30008* (2013.01); *G06T 2207/30081* (2013.01); *G06T 2207/30096* (2013.01)

(58) **Field of Classification Search**

CPC ... A61B 6/5223; A61B 6/5229; A61B 6/5258; A61K 51/0478; G06F 3/04842; G06K 2209/051; G06K 9/00201; G06K 9/4647; G06K 9/6271; G06N 3/04; G06N 3/0454; G06N 3/08; G06N 3/082; G06T 15/08; G06T 2200/24; G06T 2207/10081; G06T 2207/10088; G06T 2207/10104; G06T 2207/10108; G06T 2207/20081; G06T 2207/30008; G06T 2207/30081; G06T 2207/30096; G06T 5/30; G06T 7/0012; G06T 7/0014; G06T 7/11; G06T 7/143

See application file for complete search history.

(56) **References Cited**

U.S. PATENT DOCUMENTS

7,935,055	B2	5/2011	Burckhardt
7,970,194	B2	6/2011	Kimura
8,211,401	B2	7/2012	Babich et al.
8,467,856	B2	6/2013	Renisch et al.
8,538,166	B2	9/2013	Gordon et al.
8,705,887	B2	4/2014	Ma et al.
8,778,305	B2	7/2014	Pomper et al.
8,855,387	B2	10/2014	Hamadeh et al.
8,962,799	B2	2/2015	Babich et al.
9,002,081	B2	4/2015	Brown
9,710,915	B2	7/2017	Firouzian et al.
9,721,340	B2	8/2017	Gillies et al.
10,223,610	B1	3/2019	Akselrod-Ballin et al.
10,311,971	B2	6/2019	Opfer et al.
10,339,653	B2	7/2019	Gillies et al.
10,340,044	B2	7/2019	Yao et al.
10,340,046	B2	7/2019	Baker
RE47,609	E	9/2019	Hamadeh et al.
10,600,184	B2	3/2020	Golden et al.
10,665,346	B2	5/2020	Baker
10,748,652	B2	8/2020	Yao et al.
10,762,993	B2	9/2020	Baker
2003/0215120	A1	11/2003	Uppaluri et al.
2005/0281381	A1	12/2005	Guendel
2006/0062425	A1	3/2006	Shen et al.
2006/0064396	A1	3/2006	Wei et al.
2007/0081712	A1	4/2007	Huang et al.
2007/0081713	A1	4/2007	Jerebko
2007/0100225	A1	5/2007	Maschke
2007/0115204	A1	5/2007	Budz et al.
2008/0027315	A1	1/2008	McGinnis
2009/0309874	A1	12/2009	Salganicoff et al.
2010/0215581	A1	8/2010	Hoffmann
2011/0063288	A1	3/2011	Valadez
2011/0255763	A1	10/2011	Bogoni et al.
2012/0123253	A1	5/2012	Renisch et al.
2013/0038707	A1	2/2013	Cunningham et al.
2013/0211231	A1	8/2013	Sundarapandian et al.
2013/0281841	A1	10/2013	Everett et al.
2015/0110716	A1	4/2015	Armor
2015/0331995	A1	11/2015	Zhao et al.
2016/0203263	A1	7/2016	Maier et al.
2016/0335395	A1	11/2016	Wu et al.
2017/0083682	A1	3/2017	McNutt et al.
2018/0144828	A1	5/2018	Baker
2018/0259608	A1	9/2018	Golden et al.
2018/0360402	A1	12/2018	Carmi
2019/0038239	A1	2/2019	Flohr et al.
2019/0105009	A1	4/2019	Siemionow et al.
2019/0388049	A1	12/2019	Gupta et al.
2020/0027559	A1	1/2020	Baker
2020/0051238	A1	2/2020	El Harouni et al.
2020/0074634	A1	3/2020	Kecskemethy et al.
2020/0085382	A1	3/2020	Taerum et al.
2020/0126666	A1	4/2020	Baker
2020/0193594	A1	6/2020	Georgescu et al.
2020/0193603	A1	6/2020	Golden et al.
2020/0245960	A1	8/2020	Richter et al.
2020/0337658	A1	10/2020	Sjostrand et al.
2020/0342600	A1	10/2020	Sjostrand et al.
2020/0357521	A1	11/2020	Baker

FOREIGN PATENT DOCUMENTS

EP	1426903	A2	6/2004
EP	1508872	A1	2/2005
WO	WO-9905503	A2	2/1999
WO	WO-2007/062135	A2	5/2007
WO	WO-2009/084995	A1	7/2009
WO	WO-2011/077303	A1	6/2011
WO	WO-2018/081354	A1	5/2018
WO	WO-2019/103912	A2	5/2019
WO	WO-2019/136349	A2	7/2019
WO	WO-2020/144134	A1	7/2020
WO	WO-2020/146032	A1	7/2020
WO	WO-2020/190821	A1	9/2020
WO	WO-2020/219620	A1	10/2020

OTHER PUBLICATIONS

Santos-Cuevas, Clara, et al. "99mTc-labeled PSMA inhibitor: Biokinetics and radiation dosimetry in healthy subjects and imaging of prostate cancer tumors in patients." Nuclear Medicine and Biology 52 (2017): 1-6. (Year: 2017).*

Ciernik, I. Frank, et al. "3D-segmentation of the 18F-choline PET signal for target volume definition in radiation therapy of the prostate." Technology in cancer research & treatment 6.1 (2007): 23-30. (Year: 2007).*

Gjertsson, K., Segmentation in Skeletal Scintigraphy Images using Convolutional Neural Networks, Master's Theses in Mathematical Sciences, pp. 39-58, (2017), <https://lup.lub.lu.se/student-papers/search/publication/8916406>. Retrieved on Feb. 24, 2020.

Sjöstrand, K., et al., Automated detection and quantification of Prostatic PSMA uptake in SPECT/CT using a Deep Learning Algorithm for Segmentation of Pelvic Anatomy, The Journal of Nuclear Medicine, 59(1):p. 30, (2018).

Anand, A. et al., Analytic Validation of the Automated Bone Scan Index as an Imaging Biomarker to Standardize Quantitative Changes in Bone Scans of Patients with Metastatic Prostate Cancer, J. Nucl. Med., 57(1):41-45 (2016).

(56) **References Cited**

OTHER PUBLICATIONS

Anand, A. et al., Automated Bone Scan Index as a quantitative imaging biomarker in metastatic castration-resistant prostate cancer patients being treated with enzalutamide, EJNMMI Research, 6:23, 7 pages (2016).

Anand, A. et al., Translating Prostate Cancer Working Group 2 (PCWG2) Progression Criteria into a Quantitative Response Biomarker in Metastatic Castration Resistant Prostate Cancer (mCRPC), ASCO GU Conference, Poster, presented Feb. 16, 2017.

Anand, A. et al., Translating Prostate Cancer Working Group 2 (PCWG2) progression criteria into a quantitative response biomarker in metastatic castration-resistant prostate cancer (mCRPC), Journal of Clinical Oncology, 35(6):170 (2017).

Armstrong, A. et al., Assessment of the bone scan index in a randomized placebo-controlled trial of tasquinimod in men with metastatic castration-resistant prostate cancer (mCRPC), Urologic Oncology: Seminars and Original Investigations, 32:1308-1316 (2014).

Armstrong, A. et al., Development and validation of a prognostic model for overall survival in chemotherapy-naive men with metastatic castration-resistant prostate cancer (mCRPC) from the phase 3 prevail clinical trial, Journal of Clinical Oncology, 35(Suppl. 6):Abstract 138 (2017).

Armstrong, A. J. et al., Phase 3 prognostic analysis of the automated bone scan index (aBSI) in men with bone-metastatic castration-resistant prostate cancer (CRPC), Meeting Library ASC University. 1 page abstract, (2017).

Belal, S. et al., Association of PET Index quantifying skeletal uptake in NaF PET/CT images with overall survival in prostate cancer patients, ASCO GU 2017, Poster 178, presented Feb. 16, 2017.

Belal, S. et al., PET Index quantifying skeletal uptake in NaF PET/CT images with overall survival in prostate cancer patients, ASCO GU 2017, Abstract (Feb. 13, 2017).

Belal, S. L. et al, 3D skeletal uptake of ^{18}F sodium fluoride in PET/CT images is associate with overall survival in patients with prostate cancer, EJNMMI Research, 7(15):1-8 (2017).

Belal, S.L. et al., Automated evaluation of normal uptake in different skeletal parts in 18F-sodium fluoride (NaF) PET/CT using a new convolutional neural network method, EJNMMI, EANM '17, 44(Suppl 2):S119-S956, Abstract EP-0116 (2017).

Bushberg, J. T. et al., Essential Physics of Medical Imaging, Essential Physics of Medical Imaging, 19.3: p. 581 (table 15-3), p. 713 paragraph 6, section 19.3 and p. 720, (2011).

Dennis, E. et al., Bone Scan Index: A Quantitative Treatment Response Biomarker for Castration-Resistant Metastatic Prostate Cancer, Journal of Clinical Oncology. 30(5):519-524 (2012).

GE Healthcare, SPECT/CT Cameras, retrieved Oct. 25, 2017: <http://www3.gehealthcare.com.sg/en-gb/products/categories/nuclear_medicine/spect-ct_cameras>.

Giesel, F. L. et al., F-18 labelled PSMA-1007: biodistribution, radiation dosimetry and histopathological validation of tumor lesions in prostate cancer patients, Eur. J. Nucl. Med. Mol. Imaging, 44:678-688 (2017).

Goffin, K. E. et al., Phase 2 study of ^{99m}Tc-trofolastat SPECT/CT to identify and localize prostate cancer in intermediate- and high-risk patients undergoing radical prostatectomy and extended pelvic lymph node dissection, J. Nucl. Med., 27 pages. (2017).

Goffin, K. E. et al., Phase 2 Study of 99mTc-trofolastat SPECT/CT to identify and localize prostate cancer in intermediate- and high-risk patients undergoing radical prostatectomy and extended pelvic lymph node dissection, Journal of Nuclear Medicine, pp. 1-22 with supplemental data included, (2017).

Guimond, A. et al., Average Brain Models: A Convergence Study, Computer Vision and Image Understanding, 77:192-210 (2000).

Hajnal, J. et al., 4.4 Intensity, Size, and Skew Correction; 7.1 Introduction; 7.2 Methods; 7.3 Image Interpretation—General, In: Medical Image Registration, CRC Press LLC, 80-81:144-148 (2001).

Hiller, S. M. et al., 99mTc-Labeled Small-Molecule Inhibitors of Prostate-Specific Membrane Antigen for Molecular Imaging of Prostate Cancer, Journal of Nuclear Medicine, 54(8):1369-1376 (2013) retrieved Oct. 25, 2017: <http://jnm.snmjournals.org/content/54/8/1369.full>.

Horikoshi, H. et al., Computer-aided diagnosis system for bone scintigrams from Japanese patients: importance of training database, Annals of Nuclear Medicine, 26(8):622-626 (2012).

Huang, J.-H. et al., A Set of Image Processing Algorithms for Computer-Aided Diagnosis in Nuclear Medicine Whole Body Bone Scan Images, IEEE Transactions on Nuclear Science, 54(3):514-522 (2007).

Kaboteh R. et al., Progression of bone metastases in patients with prostate cancer—automated detection of new lesions and calculation of bone scan index, EJNMMI Research, 3:64 (2013).

Kaboteh, R. et al., Convolutional neural network based quantification of choline uptake in PET/CT studies is associated with overall survival in patents with prostate cancer, EJNMMI. EANM '17, 44(Suppl 2):S119-S956, Abstract EP-0642 (2017).

Keiss, et al., Prostate-specific membrane antigen and a target for cancer imaging and therapy, The Quarterly Journal of Nuclear Medicine and Molecular Imaging, 59(3):241-268 (2015).

Kikuchi, A. et al., Automated segmentation of the skeleton in whole-body bone scans: influence of difference in atlas, Nuclear Medicine Communications, 33(9):947-953 (2012).

Kinahan, P.E. et al., PET/CT Standardized Update Values (SUVs) in Clinical Practice and Assessing Response to Therapy, Semin Ultrasuond CT MR 31(6):496-505 (2010) retrieved Oct. 25, 2017: <https://www.ncbi.nlm.nih.gov/pmc/articles/PMC3026294/>.

Knutsson, H., and Andersson, M., Morphons: Segmentation using Elastic Canvas and Paint on Priors, IEEE International Conference on Image Processing (ICIP 2005), Genova, Italy, 4 pages (2005).

Kopka, K. et al., Glu-Ureido-Based Inhibitors of Prostate-Specific Membrane Antigen: Lessons Learned During the Development of a Novel Class of Low-Molecular-Weight Theranostic Radiotracers, The Journal of Nuclear Medicine, 58(9)(Suppl. 2):17S-26S, (2017).

Liu, L. et al., Computer-Aided Detection of Prostate Cancer with MRI: Technology and Applications, Acad Radiol. Author manuscript, 50 pages 2016.

Ma, L. et al., Automatic segmentation of the prostate on CT images using deep learning and multi-atlas fusion, Proc. of SPIE vol. 10133:101332O-1-101332O-9 (2017).

Ma, L. et al., Combining Population and Patient-Specific Characteristics for Prostate Segmentation on 3D CT Images, Proc of SPIE 9784:978427-1-8 (2016).

Ma, L. et al., Random Walk Based Segmentation for the Prostate on 3D Transrectal Ultrasound Images, Proc SPIE Int Soc Opt Eng. Author manuscript, 13 pages (2016).

Mayo Clinic Staff, Choline C-11 PET scan, Overview, Mayo Clinic, 4 pages (2017), retrieved Oct. 25, 2017: <https://www.mayoclinic.org/tests-procedures/choline-c-11-pet-scan/home/ovc-20156994>.

Nakajima, K. et al., Enhanced diagnostic accuracy for quantitative bone scan using an artificial neural network system: a Japanese multi-center database project, EJNMMI Research, 3:83 (2013).

National Cancer Institute, NCI Drug Dictionary: gallium Ga 68-labeled PSMA-11, retrieved Oct. 25, 2017: <https://www.cancer.gov/publications/dictionaries/cancer-drug?cdrid=766400>.

National Cancer Institute, NCI Drug Dictionary: technetium Tc 99m methylene diphosphonate, retrieved Oct. 25, 2017: <https://www.cancer.gov/publications/dictionaries/cancer-drug?cdrid=537722>.

Perera, M. et al., Sensitivity, Specificity, and Predictors of Positive 68Ga-Prostate-specific Membrane Antigen Positron Emission Tomography in Advanced Prostate Cancer: A Systematic Review and Meta-analysis, European Urology, 70(6):926-937 (2016).

Polymeri, E. et al., Analytical validation of an automated method for segmentation of the prostate gland in CT images, EJNMMI, EANM '17, 44(Suppl 2):S119-S956, Abstract EP-0641 (2017).

radiologyinfo.org for Patients, Computed Tomography (CT), retrieved Oct. 25, 2017: <https://www.radiologyinfo.org/en/submenu.cfm?pg=ctscan>.

Rowe, S. P. et al., PET Imaging of prostate-specific membrane antigen in prostate cancer: current state of the art and future challenges, Prostate Cancer and Prostatic Diseases, 1-8 (2016).

(56) **References Cited**

OTHER PUBLICATIONS

Sabbatini, P. et al., Prognostic Significance of Extent of Disease in Bone in Patients With Androgen-Independent Prostate Cancer, Journal of Clinical Oncology, 17(3):948-957 (1999).
Sadik, M. et al., 3D prostate gland uptake of 18F-choline—association with overall survival in patients with hormone-naïve prostate cancer, The Journal of Nuclear Medicine, 58(Suppl. 1):Abstract 544 (2017).
Sadik, M. et al., A new computer-based decision-support system for the interpretation of bone scans, Nuclear Medicine Communications. 27(5):417-423 (2006).
Sadik, M. et al., Automated 3D segmentation of the prostate gland in CT images—a first step towards objective measurements of prostate uptake in PET and SPECT images, Journal of Nuclear Medicine, 58(1) (2017).
Sadik, M. et al., Automated quantification of reference levels in liver and mediastinum (blood pool) for the Deauville therapy response classification using FDG-PET/CT in lymphoma patients, EJNMMI, EANM '17, 44(Suppl 2):S119-S956, Abstract EP-0770 (2017).
Sadik, M. et al., Computer-assisted interpretation of planar whole-body bone scans, Journal Nuclear Medicine, 49(12):1958-65, 2008.
Sadik, M. et al., Convolutional neural networks for segmentation of 49 selected bones in CT images show high reproducibility, EJNMMI, EANM '17, 44(Suppl 2):S119-S956, Abstract OP-657 (2017).
Sadik, M. et al., Improved classifications of planar whole-body bone scans using a computer-assisted diagnosis system: a multicenter, multiple-reader, multiple-case study, Journal of Nuclear Medicine, 50(3): 368-75, 2009.
Sadik, M. et al., Variability in reference levels for Deauville classifications applied to lymphoma patients examined with 18F-FDG-PET/CT, EJNMMI, EANM '17, 44(Suppl 2):S119-S956, Abstract EP-0771 (2017).
Sajn, L. et al., Computerized segmentation of whole-body bone scintigrams and its use in automated diagnostics, Computer Methods and Programs in Biomedicine, 80:47-55 (2005).
Salerno, J. et al., Multiparametric magnetic resonance imaging for pre-treatment local staging of prostate cancer: A Cancer Care Ontario clinical practice guideline, Canadian Urological Association Journal, 10(9-10):332-339 (2016).
Sjöstrand K. et al., Statistical regularization of deformation fields for atlas-based segmentation of bone scintigraphy images, MICCAI 5761:664-671 (2009).
Sluimer, I. et al., Toward Automated Segmentation of the Pathological Lung in CT, IEEE Transactions on Medical Imaging, 24(8):1025-1038 (2005).
Tian, Z. et al., A fully automatic multi-atlas based segmentation method for prostate MR images, Proc SPIE Int Soc Opt Eng. Author manuscript, 12 pages (2015).
Tian, Z. et al., A supervoxel-based segmentation method for prostate MR images, Med. Phys., 44(2):558-569 (2017).
Tian, Z. et al., Deep convolutional neural network for prostate MR segmentation, Proc. of SPIE 10135:101351L-1-101351L-6 (2017).
Tian, Z., et al., Superpixel-based Segmentation for 3D Prostate MR Images, IEEE Trans Med Imaging, Author manuscript, 32 pages, (2016).
Ulmert, D. et al., A Novel Automated Platform for Quantifying the Extent of Skeletal Tumour Involvement in Prostate Cancer Patients Using the Bone Scan Index, European Urology, 62(1):78-84 (2012).
Wrangsjo, A. et al., Non-rigid Registration Using Morphons, Proceedings of the 14th Scandinavian Conference on Image Analysis (SCIA '05), pp. 501-510 (2005).
Yin, T.-K., A Computer-Aided Diagnosis for Locating Abnormalities in Bone Scintigraphy by a Fuzzy System With a Three-Step Minimization Approach, IEEE Transactions on Medical Imaging, 23(5):639-654 (2004).
Litjens, G. et al., A survey on deep learning in medical image analysis, Medical Image Analysis, 42:60-88, (2017).
Partial Search Report and Provisional Opinion, International Application No. PCT/US2019/012486 (Systems and Methods for Rapid Neural Network-Based Image Segmentation and Radiopharmaceutical Uptake Determination, filed Jan. 7, 2019), issued by ISA/European Patent Office, 16 pages, dated May 7, 2019.
Rowe, S. P. et al., PSMA-Based [^{18}F]DCFPyL PET/CT is Superior to Conventional Imaging for Lesion Detection in Patients with Metastatic Prostate Cancer, Mol Imaging Biol, 18:411-419, (2016).
Eiber, M. et al., Prostate Cancer Molecular Imaging Standardized Evaluation (PROMISE): Proposed miTNM Classification for the Interpretation of PSMA-Ligand PET/CT, The Journal of Nuclear Medicine, 59(3):469-478, (2018).
International Search Report, International Application No. PCT/US2019/012486 (Systems and Methods for Rapid Neural Network-Based Image Segmentation and Radiopharmaceutical Uptake Determination, filed Jan. 7, 2019), issued by ISA/European Patent Office, 6 pages, dated Jul. 2, 2019.
Written Opinion, International Application No. PCT/US2019/012486 (Systems and Methods for Rapid Neural Network-Based Image Segmentation and Radiopharmaceutical Uptake Determination, filed Jan. 7, 2019), issued by ISA/European Patent Office, 13 pages, dated Jul. 2, 2019.
American College of Radiology (ACR) and the Society for Pediatric Radiology (SPR), ACR-SPR Practice Parameter for the Performance of Skeletal Scintigraphy (Bone Scan), Resolution 28, (2013-Revused2017), available from: http://www.acr.org.
Anand, A. et al., A Pre-Analytical Validation Study of Automated Bone Scan Index: Effect on Accuracy and Reproducibility Due to the Procedural Variabilities in Bone Scan Image Acquisition. J Nucl Med. Jul. 21, 2016. [Epub ahead of print].
Armstrong, A. J. et al., Phase 3 Assessment of the Automated Bone Scan Index as a Prognostic Imaging Biomarker of Overall Survival in Men with Metastatic Castration-Resistant Prostate Cancer: A Secondary Analysis of a Randomized Clinical Trial. JAMA Oncology 4:944-951, (2018).
Bai, P. et. al., Body region localization in whole-body low-dose CT images of PET/CT scans using virtual landmarks, Medical Physics Wiley USA, 46(3): 1286-1299 (2019).
Bombardieri, E. et al., Bone scintigraphy: procedure guidelines for tumour imaging, Eur J. Nucl. Med. Mol. Imaging, 30:BP99-BP106, (2003).
Brynolfsson, J., et. al., Deep Learning based urinary bladder segmentation using 18FDCFPyL (PyL-PSMA) PET/CT images, EPS-145, European Association of Nuclear Medicine, (2020), <http://link.springer.com/article/10.1007/s00259-020-04988-4>. Retrieved Sep. 18, 2020.
Brynolfsson, J., et. al., Deep Learning-Enabled comprehensive detection and quantification of 18FDCFPyL (PyL-PSMA) PET/CT, OP-548, European Association of Nuclear Medicine, (2020), <http://link.springer.com/article/10.1007/s00259-020-04988-4>. Retrieved Sep. 18, 2020.
Dertat, A., Applied Depp Learning—Part 4: Convolutional Neural Networks, Towards Data Science,<http://towardsdatascience.com/applied-deep-learning-part-4-convolutional-neural-networks-584bc134c1e2> (2017).
Gjertsson, K., et. al., A Novel Automated Deep Learning Algorithm for Segmentation of the Skeleton in Low-Dose CT for [(18)F] DCFPyL PET/CT Hybrid Imaging in Patients with Metastatic Prostate Cancer, Annual Congress of the European Association of Nuclear Medicine Oct. 12-16, 2019 Barcelona, Spain. Eur J Nucl Med Mol Imaging 46 (Suppl 1), S1-S952 (2019). Abstract EP-0823, p. S765.
Johnsson, K., et. al., miPSMA Index: Comprehensive and Automated Quantification of 18F-DCFPyL (PyL-PSMA) PET/CT for Prostate Cancer Staging, J Nucl Med., 61: (Supplement 1): 1435, (2020).
Lin, T.Y. et. al., Feature Pyramid Networks for object detection, FAIR, (2016), <https://arxiv.org/abs/1612.03144v1>.
Meyer, A., et. al., Deep learning algorithm improves identification of men with low-risk prostate cancer using PSMA targeted 99mTc-MIP-1404 SPECT/CT, Journal of Clinical Oncology, 37:(15), (2019).
Nickols, N.G., et. al., A deep learning algorithm to predict coexisting metastatic disease using intraprostatic [F18]DCFPYL PSMA image alone in veterans with prostate cancer, Journal of Clinical Oncology 38, (Supplement 6), 2020.

(56) **References Cited**

OTHER PUBLICATIONS

Ohlsson, M., et. al., Automated decision support for bone scintigraphy, Computer-based medical systems, pp. 1-6, (2009).

Pouliot, F., et. al., Prospective evaluation of a Novel Deep Learning Algorithm (PSMA-AI) in the assessment of 99mTc-MIP-1404 SPECT/CT in patients with low or intermediate risk prostate cancer, Annual Congress of the European Association of Nuclear Medicine Oct. 12-16, 2019 Barcelona, Spain. Eur J Nucl Med Mol Imaging 46 (Suppl 1), S1-S952 (2019). Abstract EP-0804, p. S765.

Ren, S., et. al., Faster R-CNN: Towards Real-Time Object Detection with Region Proposal Networks, (2015), <http://image-net.org/challenges/LSVRC/2015/results>.

Ronneberger, O., et. al., U-Net: Convolutional Networks for Biomedical Image Segmentation, Springer International Publishing, (2015), <http://lmb.informatik.uni-freiburg.de/>. Retrieved on Nov. 18, 2015.

Sjostrand, K., et. al., Automated Assessment of Prostatic PSMA Expression in SPECT/CT using Deep Convolutional Neural Networks—A Prospectively Planned Retrospective Analysis of Phase 3 Study MIP-1404-3301, The Journal of Nuclear Medicine, 60 (Supplement 1): Abstract 401, (2019).

* cited by examiner

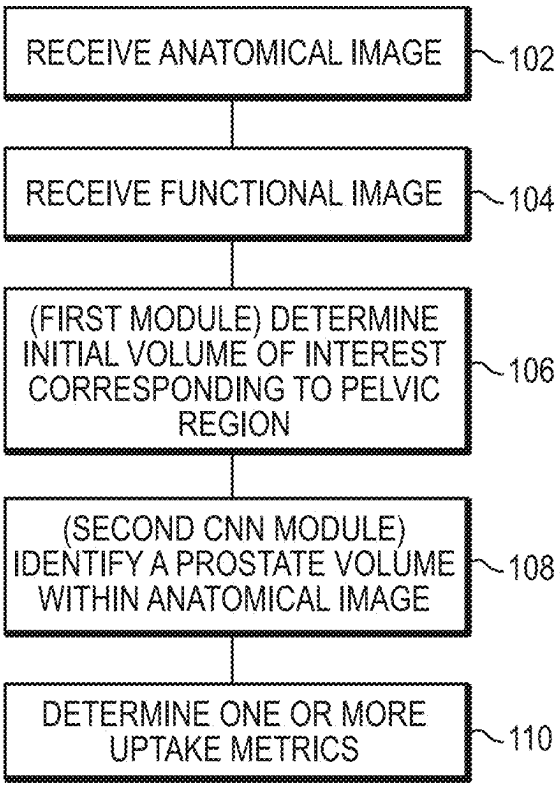

RECEIVE ANATOMICAL IMAGE
102
RECEIVE FUNCTIONAL IMAGE
104
(FIRST MODULE) DETERMINE INITIAL VOLUME OF INTEREST CORRESPONDING TO PELVIC REGION
106
(SECOND CNN MODULE) IDENTIFY A PROSTATE VOLUME WITHIN ANATOMICAL IMAGE
108
DETERMINE ONE OR MORE UPTAKE METRICS
110

FIG. 1

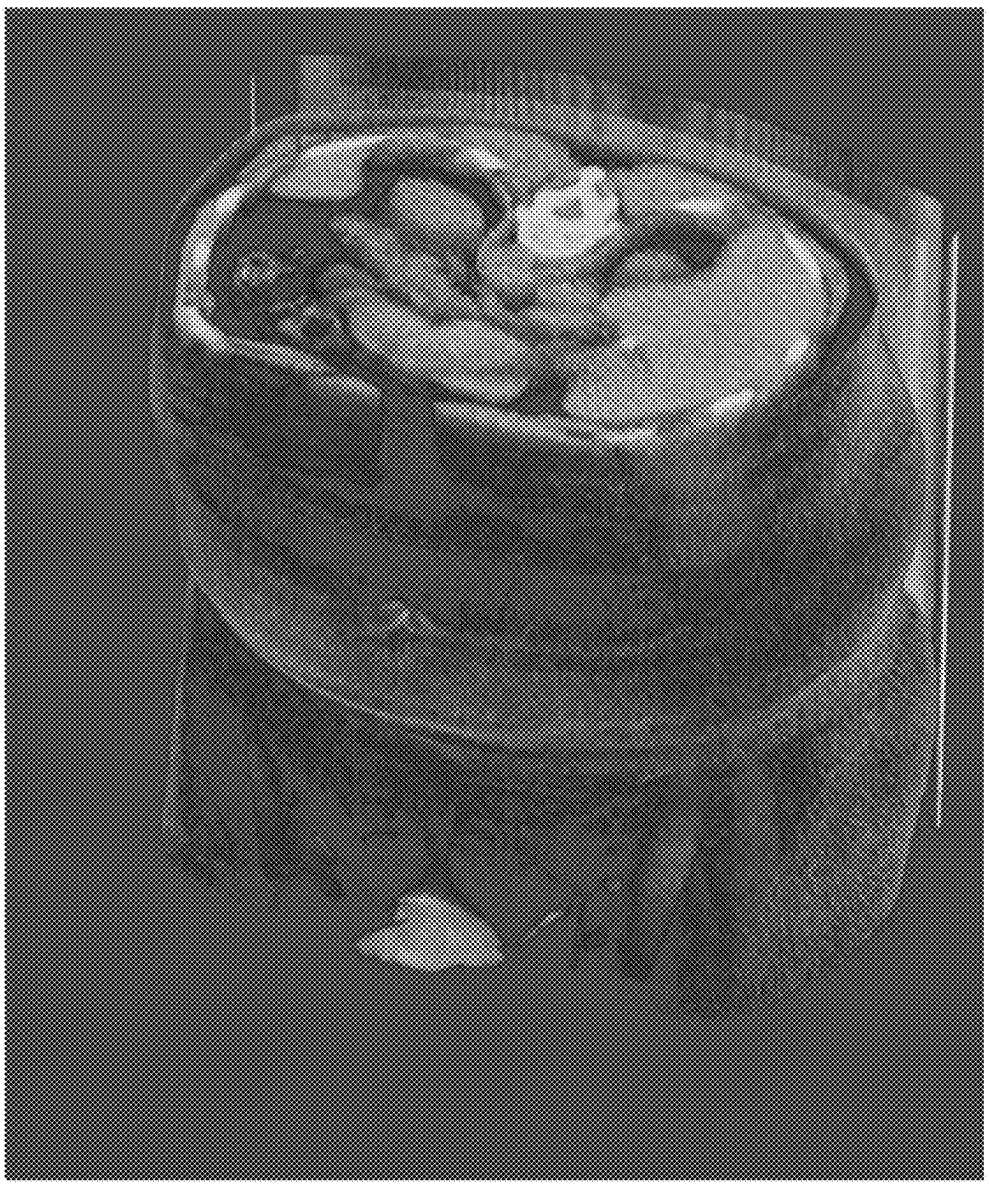


FIG. 2A



FIG. 2B

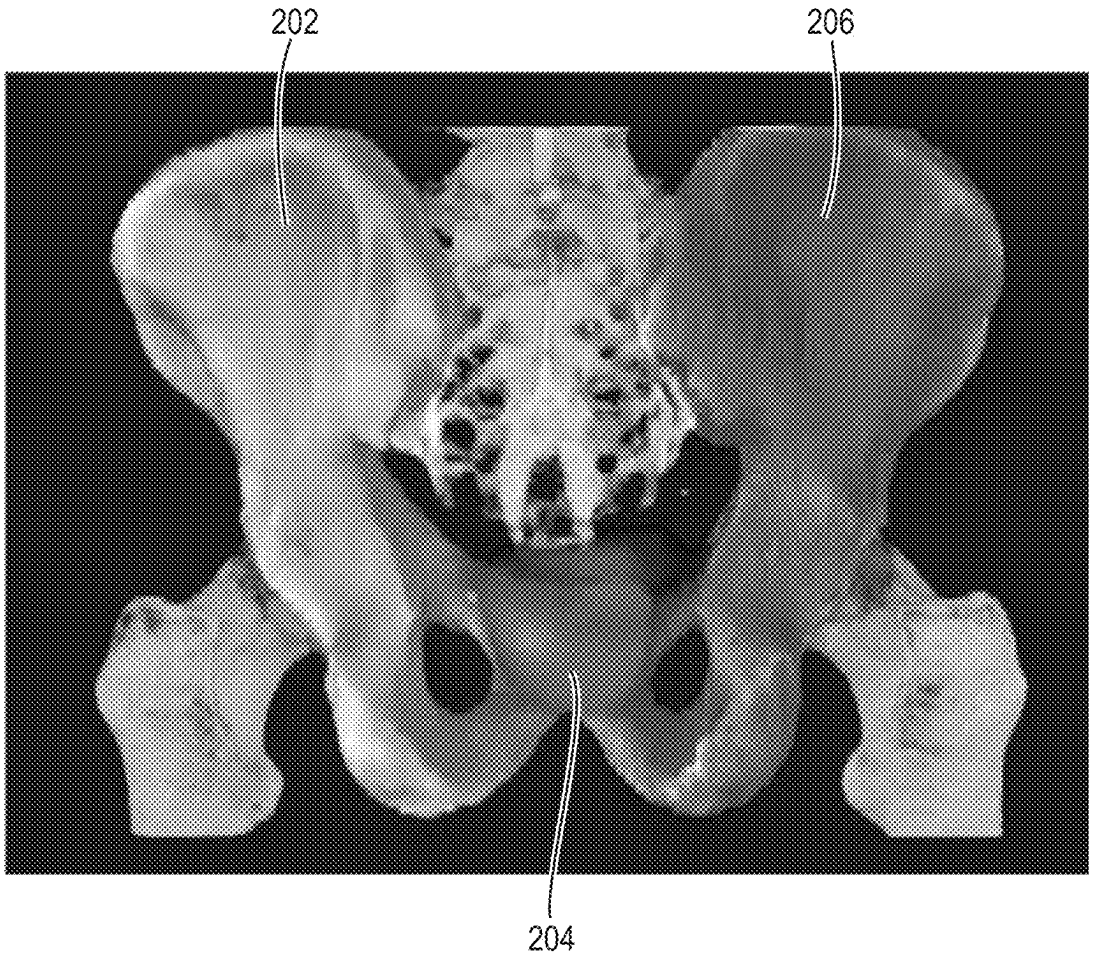


FIG. 2C

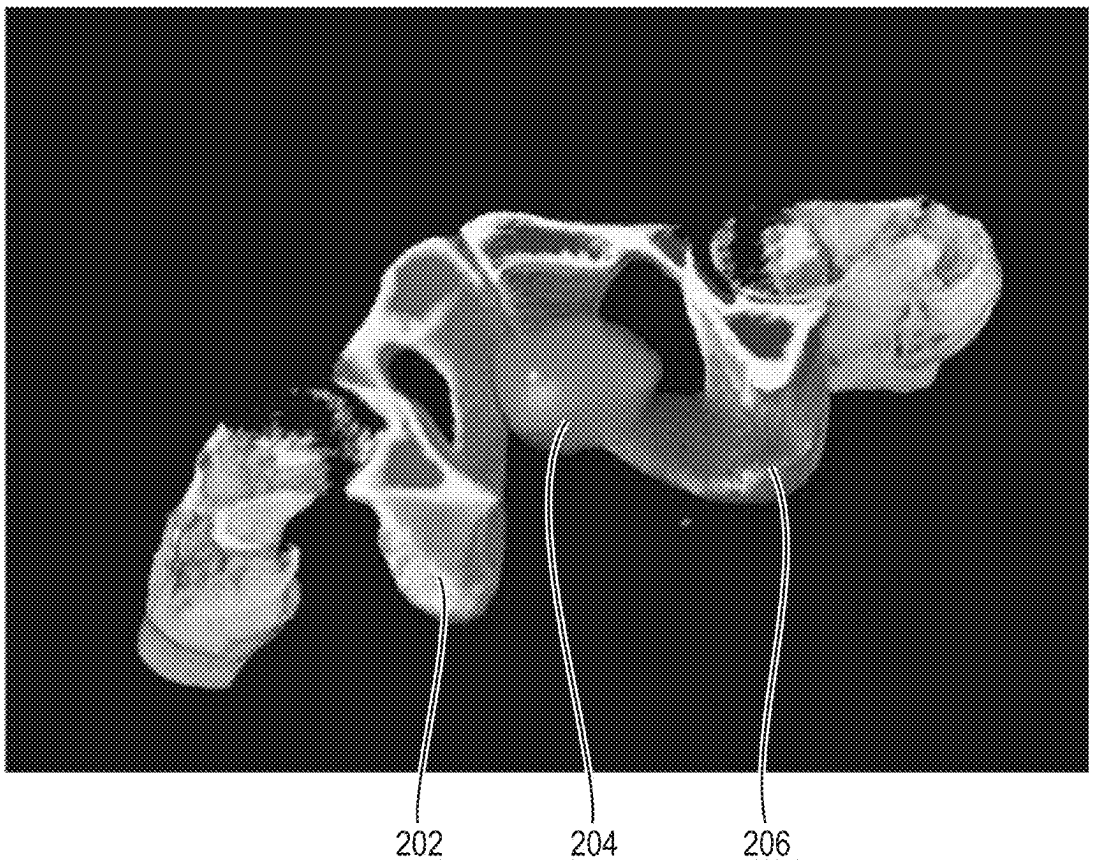


FIG. 2D

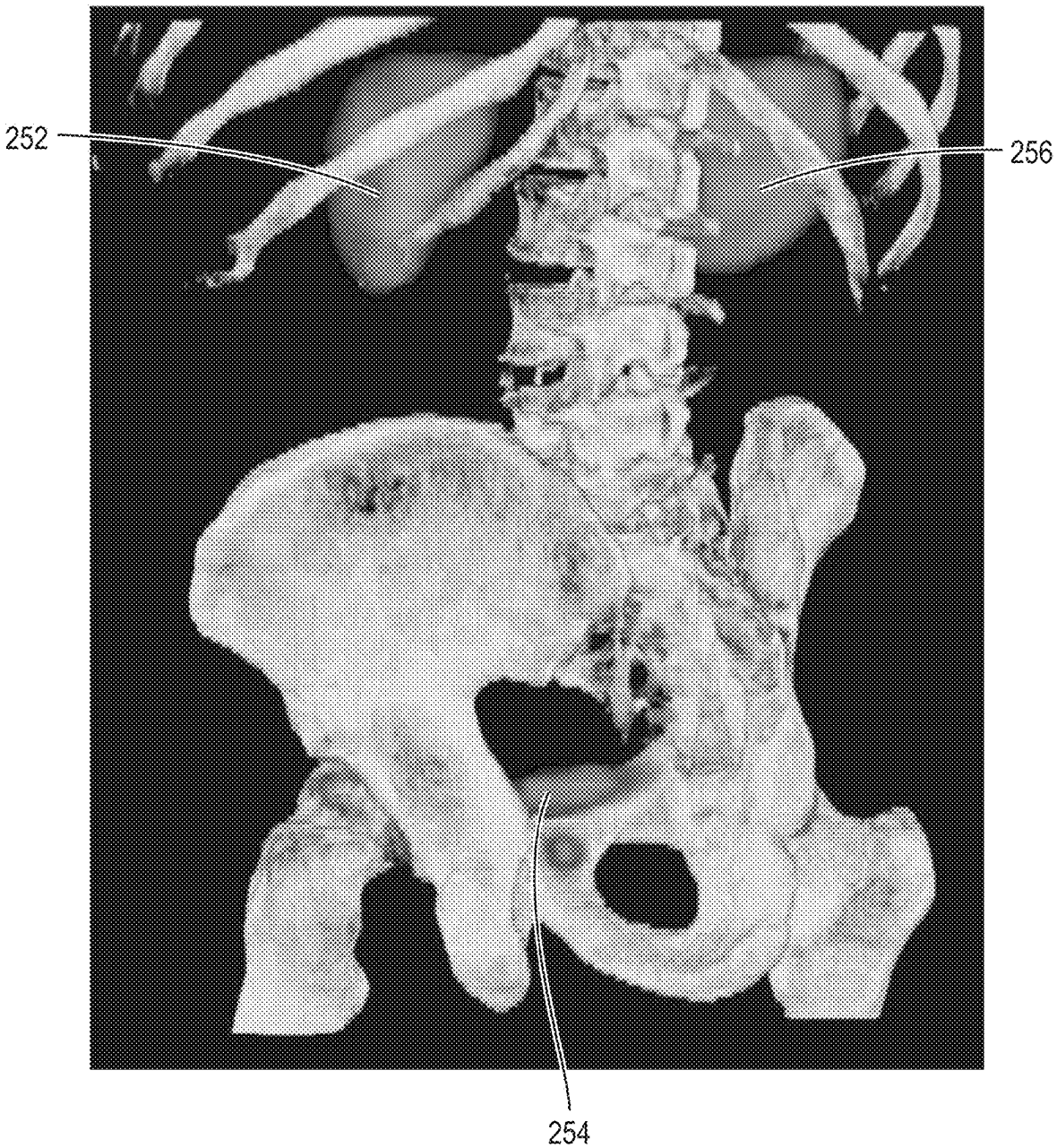


FIG. 2E

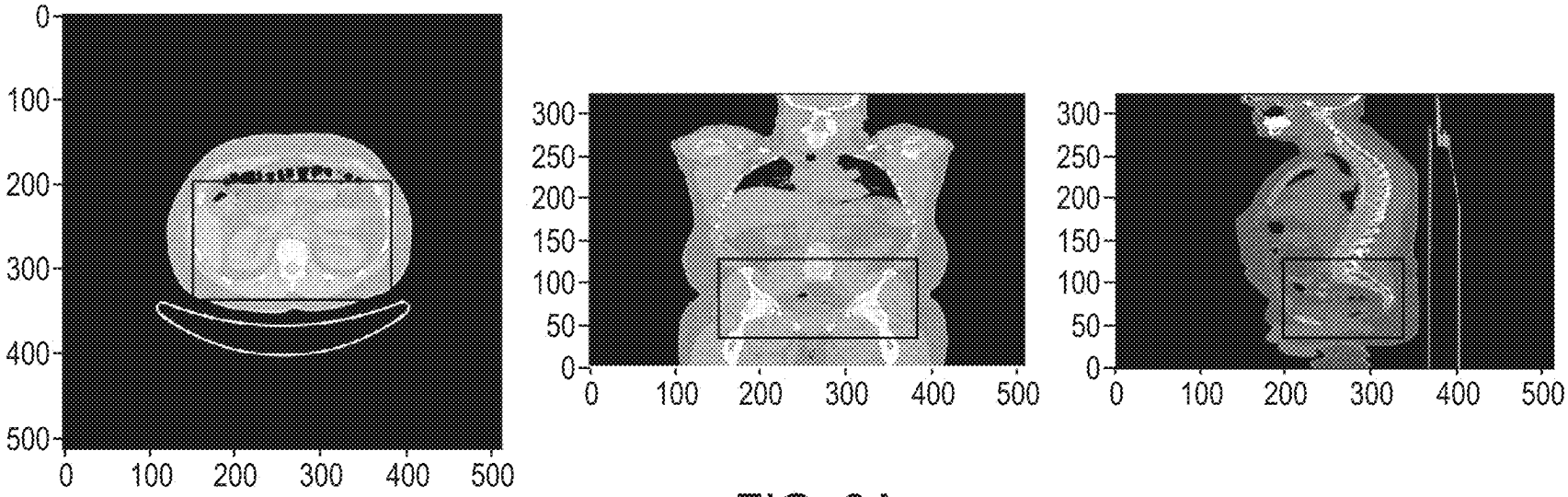

0
100
200
300
400
500
0 100 200 300 400 500
300
250
200
150
100
50
0
0 100 200 300 400 500
300
250
200
150
100
50
0
0 100 200 300 400 500

FIG. 3A

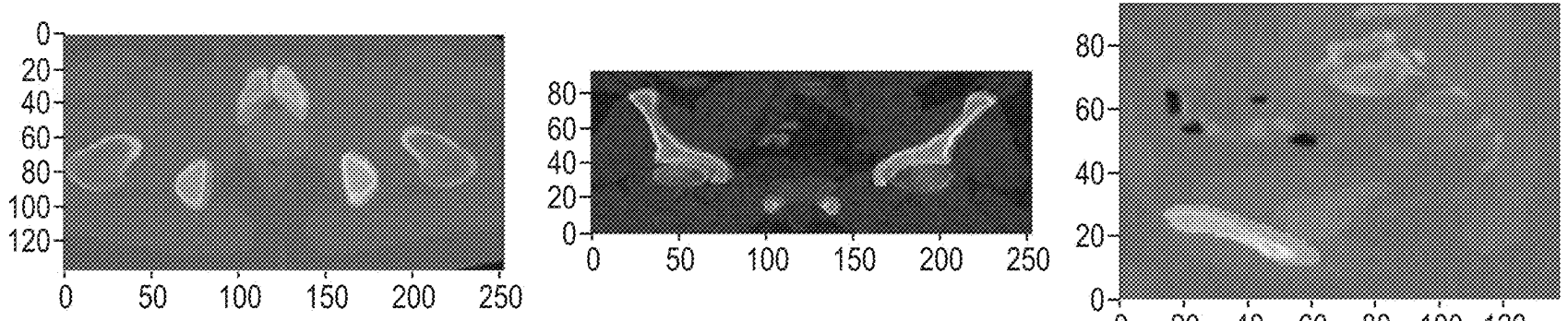

0
20
40
60
80
100
120
0 50 100 150 200 250
80
60
40
20
0
0 50 100 150 200 250
80
60
40
20
0
0 20 40 60 80 100 120

FIG. 3B

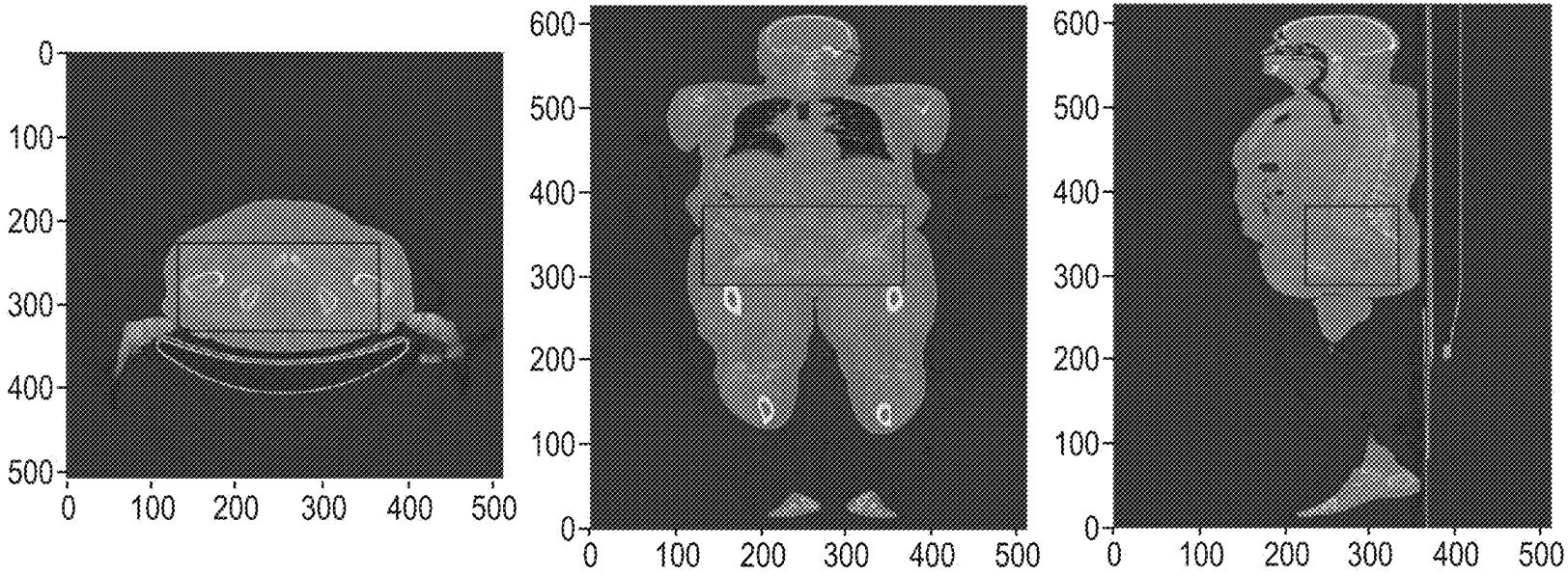

0
100
200
300
400
500
0 100 200 300 400 500
600
500
400
300
200
100
0
0 100 200 300 400 500
600
500
400
300
200
100
0
0 100 200 300 400 500

FIG. 4A

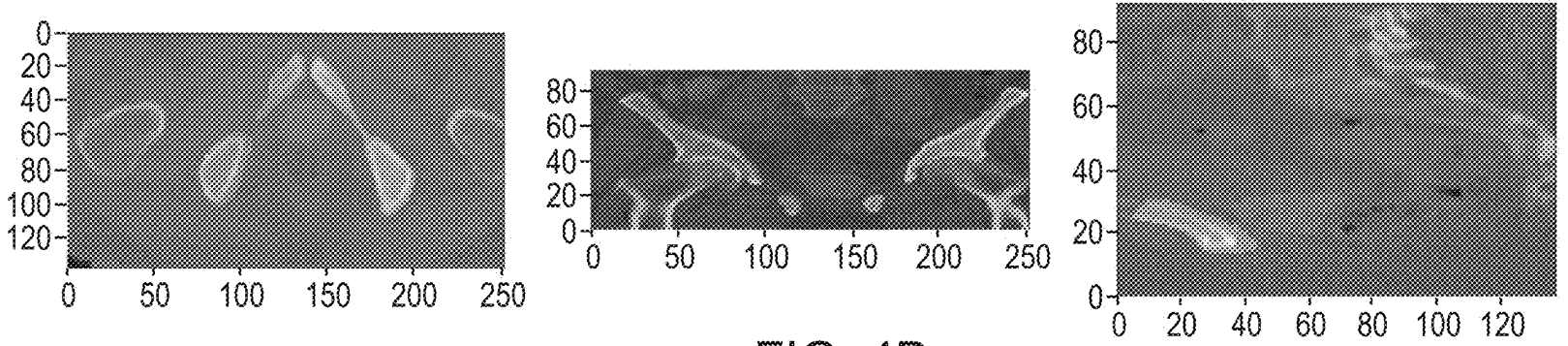

0
20
40
60
80
100
120
0 50 100 150 200 250
80
60
40
20
0
0 50 100 150 200 250
80
60
40
20
0
0 20 40 60 80 100 120

FIG. 4B

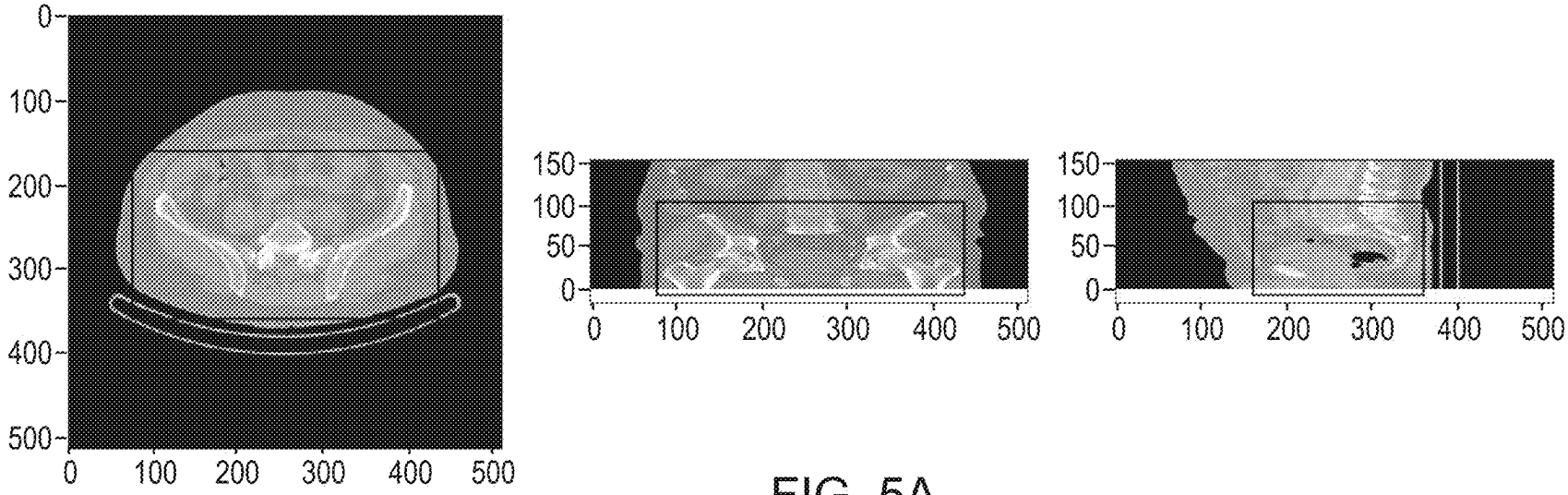

0
100
200
300
400
500
0 100 200 300 400 500
150
100
50
0
0 100 200 300 400 500
150
100
50
0
0 100 200 300 400 500

FIG. 5A

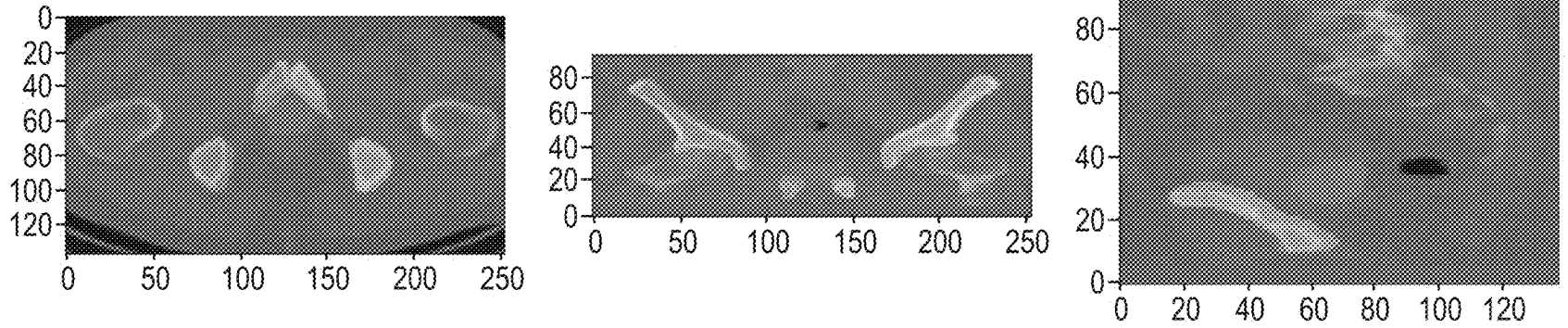

0
20
40
60
80
100
120
0 50 100 150 200 250
80
60
40
20
0
0 50 100 150 200 250
80
60
40
20
0
0 20 40 60 80 100 120

FIG. 5B

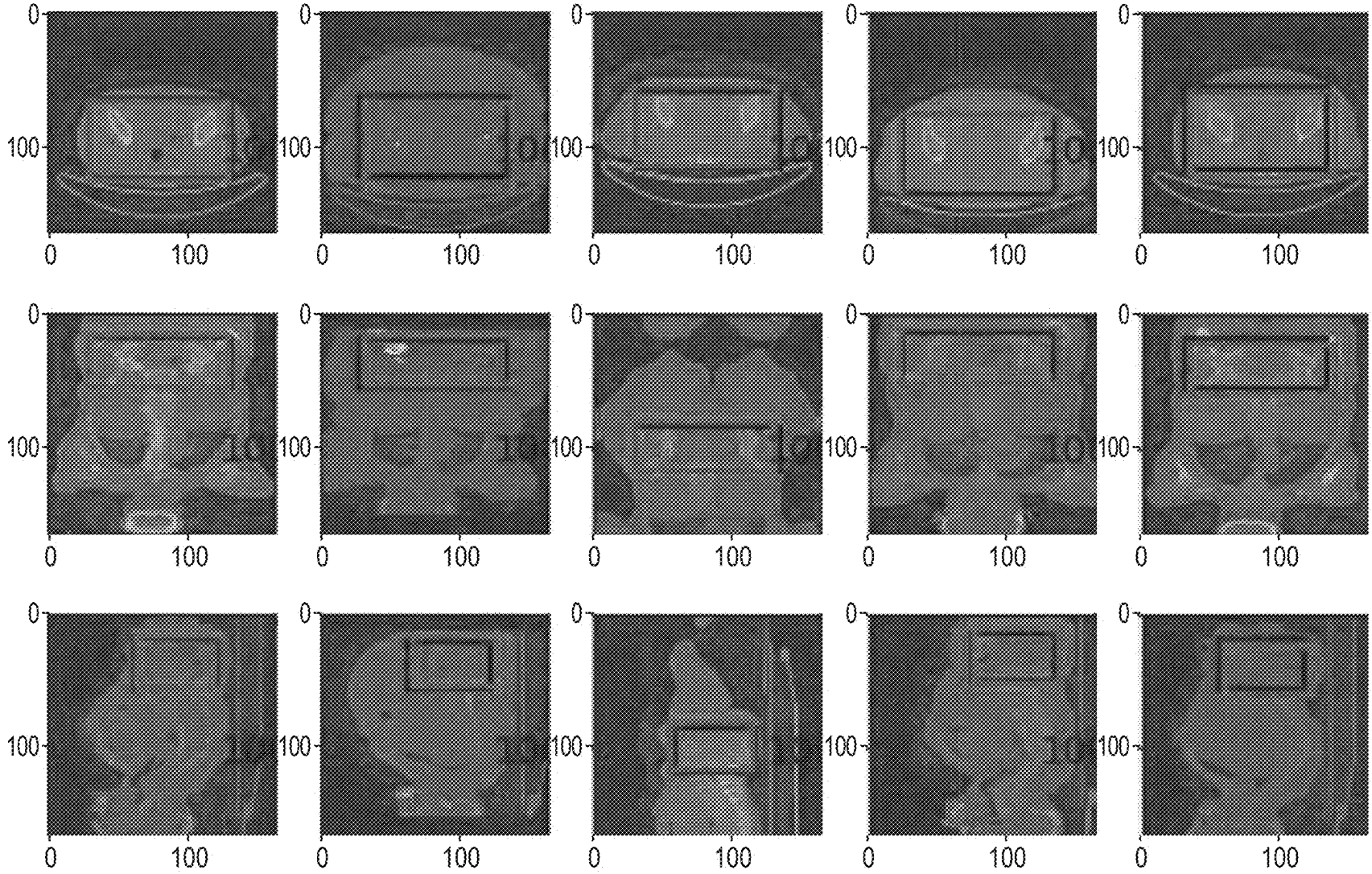
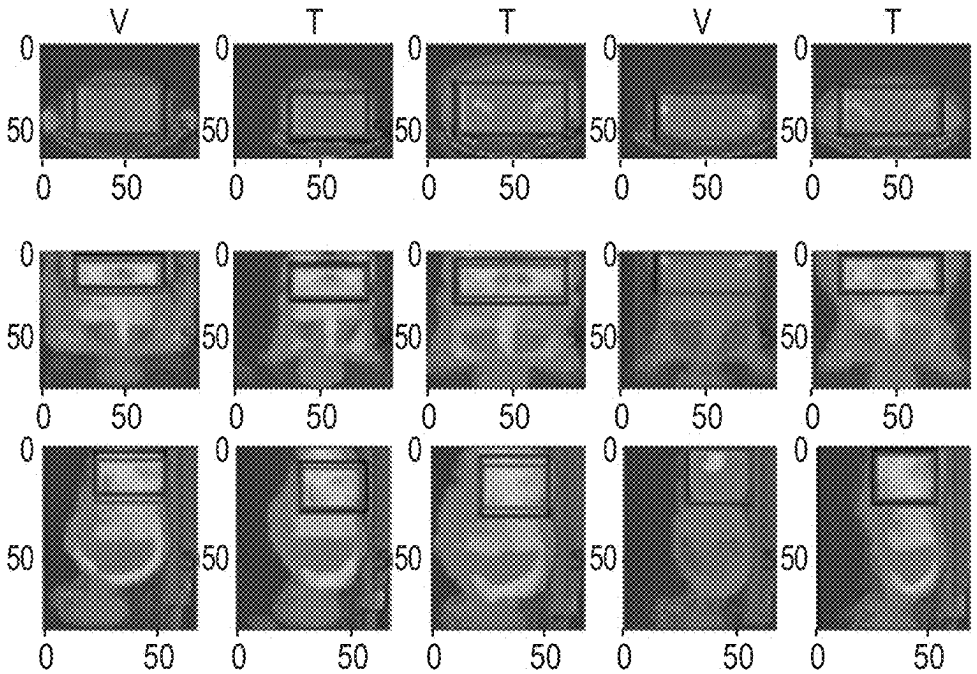
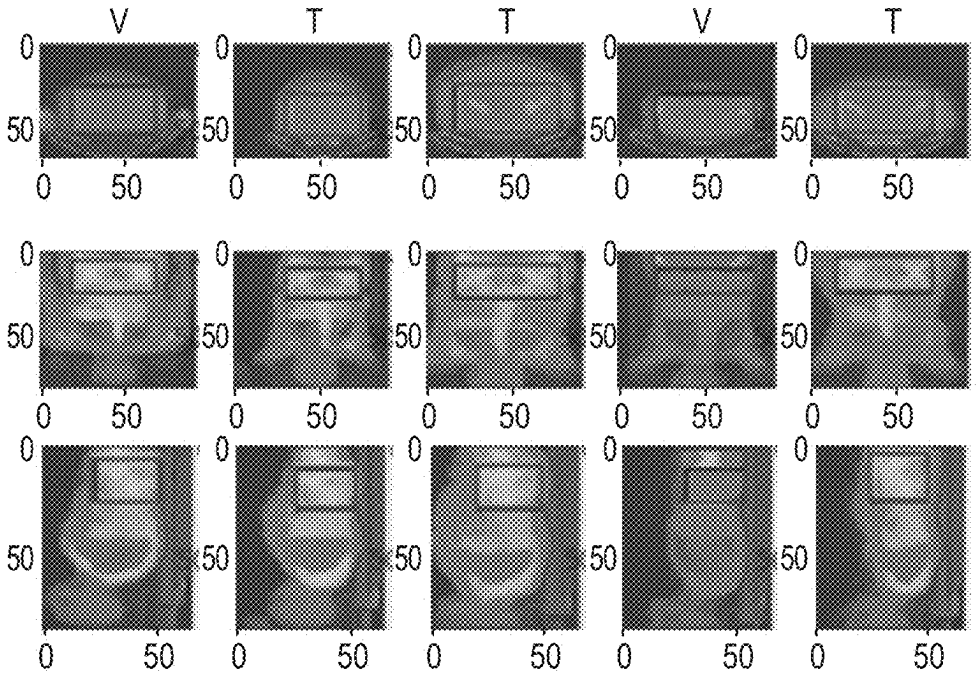


FIG. 6A



TRAD. LOCALIZATION
(MEDIAN CROP SIZE = 94 x 130 x 221)

FIG. 6B



TRAD. LOCALIZATION
(MEDIAN CROP SIZE = 74 x 116 x 205)

FIG. 6C

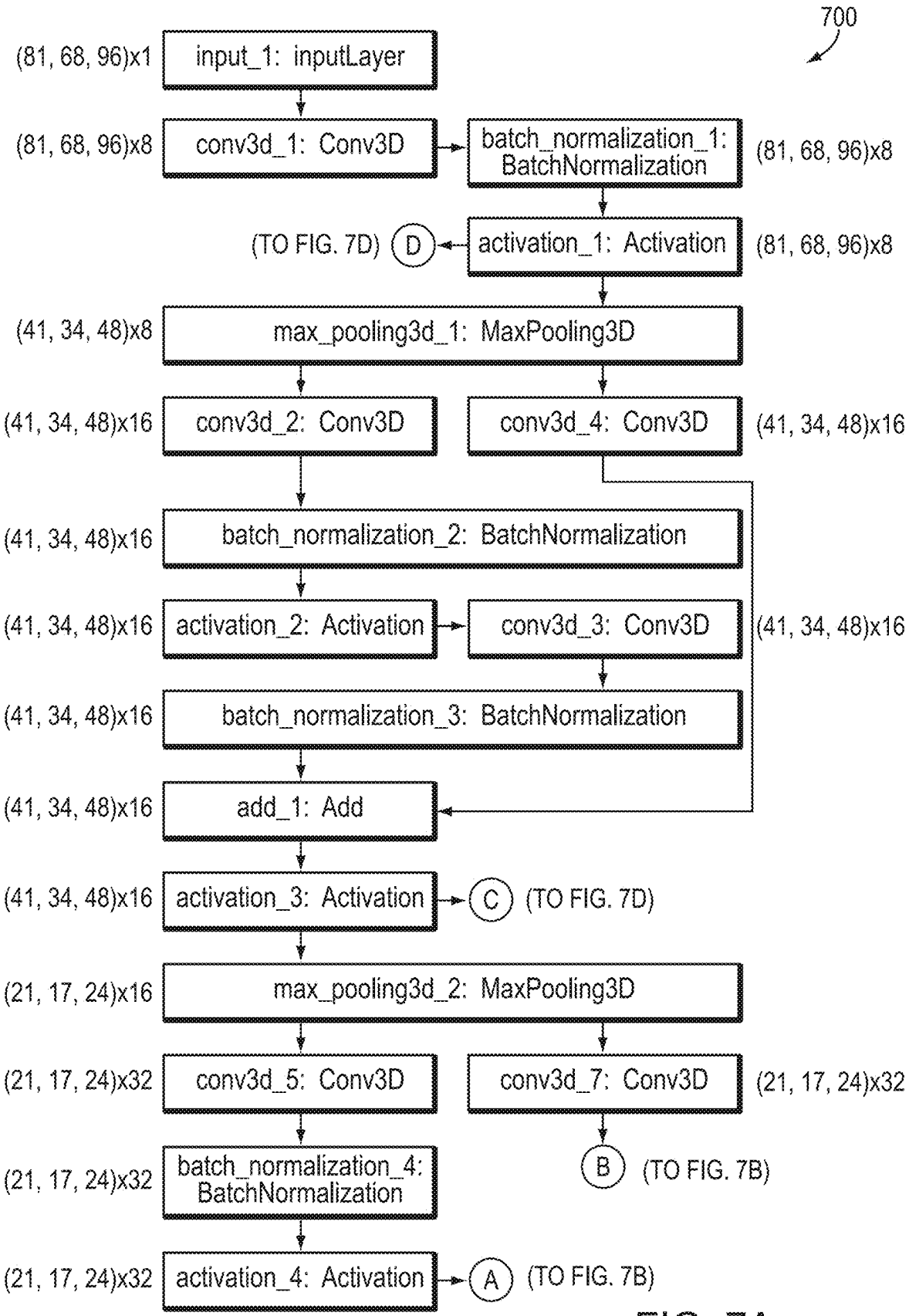

700
(81, 68, 96)x1
input_1: inputLayer
(81, 68, 96)x8
conv3d_1: Conv3D
batch_normalization_1: BatchNormalization
(81, 68, 96)x8
(TO FIG. 7D)
D
activation_1: Activation
(81, 68, 96)x8
(41, 34, 48)x8
max_pooling3d_1: MaxPooling3D
(41, 34, 48)x16
conv3d_2: Conv3D
conv3d_4: Conv3D
(41, 34, 48)x16
(41, 34, 48)x16
batch_normalization_2: BatchNormalization
(41, 34, 48)x16
activation_2: Activation
conv3d_3: Conv3D
(41, 34, 48)x16
(41, 34, 48)x16
batch_normalization_3: BatchNormalization
(41, 34, 48)x16
add_1: Add
(41, 34, 48)x16
activation_3: Activation
C
(TO FIG. 7D)
(21, 17, 24)x16
max_pooling3d_2: MaxPooling3D
(21, 17, 24)x32
conv3d_5: Conv3D
conv3d_7: Conv3D
(21, 17, 24)x32
(21, 17, 24)x32
batch_normalization_4: BatchNormalization
B
(TO FIG. 7B)
(21, 17, 24)x32
activation_4: Activation
A
(TO FIG. 7B)

FIG. 7A

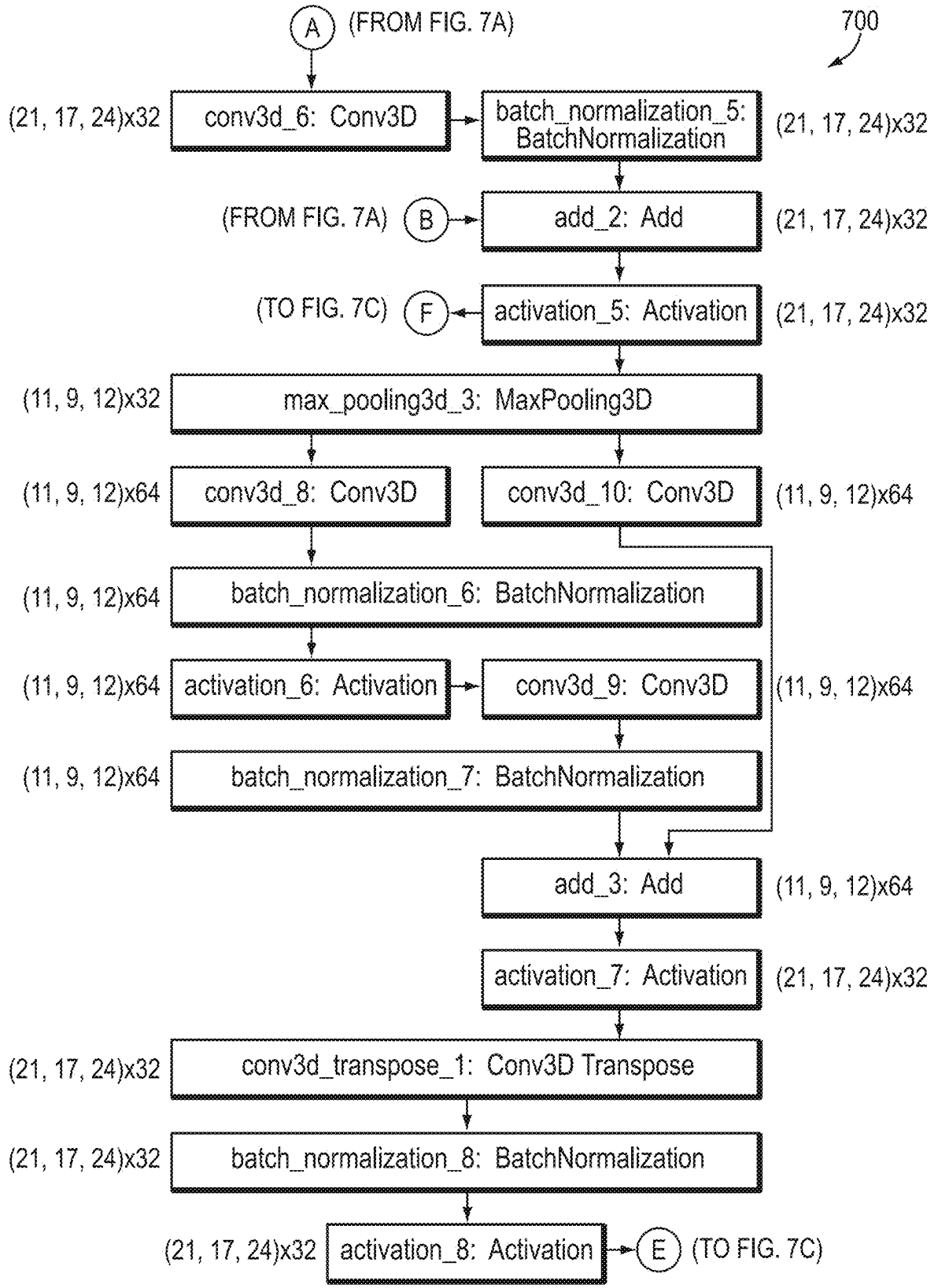

A
(FROM FIG. 7A)
700
(21, 17, 24)x32
conv3d_6: Conv3D
batch_normalization_5: BatchNormalization
(21, 17, 24)x32
(FROM FIG. 7A)
B
add_2: Add
(21, 17, 24)x32
(TO FIG. 7C)
F
activation_5: Activation
(21, 17, 24)x32
(11, 9, 12)x32
max_pooling3d_3: MaxPooling3D
(11, 9, 12)x64
conv3d_8: Conv3D
conv3d_10: Conv3D
(11, 9, 12)x64
(11, 9, 12)x64
batch_normalization_6: BatchNormalization
(11, 9, 12)x64
activation_6: Activation
conv3d_9: Conv3D
(11, 9, 12)x64
(11, 9, 12)x64
batch_normalization_7: BatchNormalization
add_3: Add
(11, 9, 12)x64
activation_7: Activation
(21, 17, 24)x32
(21, 17, 24)x32
conv3d_transpose_1: Conv3D Transpose
(21, 17, 24)x32
batch_normalization_8: BatchNormalization
(21, 17, 24)x32
activation_8: Activation
E
(TO FIG. 7C)

FIG. 7B

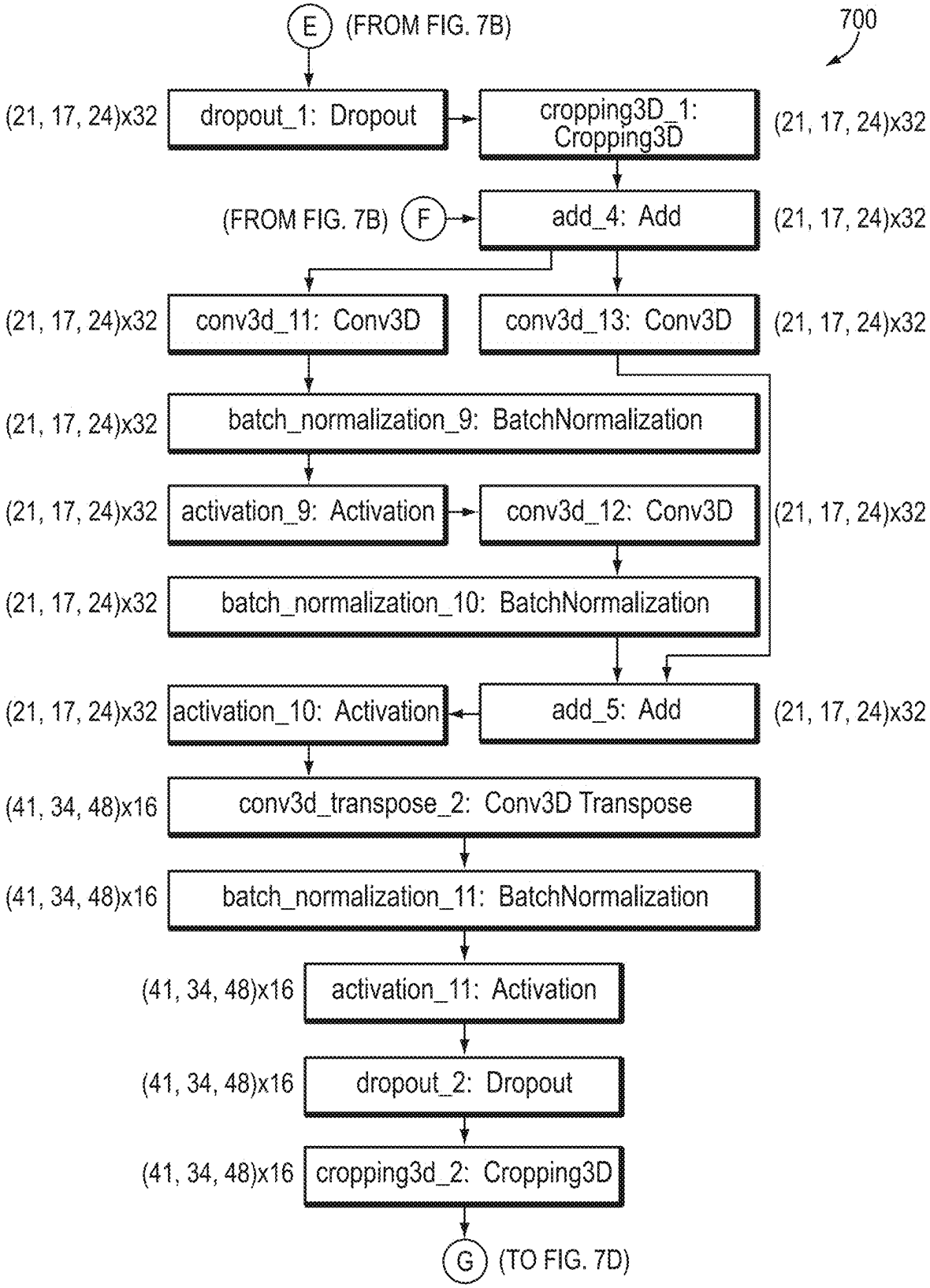

E
(FROM FIG. 7B)
700
(21, 17, 24)x32
dropout_1: Dropout
cropping3D_1: Cropping3D
(21, 17, 24)x32
(FROM FIG. 7B)
F
add_4: Add
(21, 17, 24)x32
(21, 17, 24)x32
conv3d_11: Conv3D
conv3d_13: Conv3D
(21, 17, 24)x32
(21, 17, 24)x32
batch_normalization_9: BatchNormalization
(21, 17, 24)x32
activation_9: Activation
conv3d_12: Conv3D
(21, 17, 24)x32
(21, 17, 24)x32
batch_normalization_10: BatchNormalization
(21, 17, 24)x32
activation_10: Activation
add_5: Add
(21, 17, 24)x32
(41, 34, 48)x16
conv3d_transpose_2: Conv3D Transpose
(41, 34, 48)x16
batch_normalization_11: BatchNormalization
(41, 34, 48)x16
activation_11: Activation
(41, 34, 48)x16
dropout_2: Dropout
(41, 34, 48)x16
cropping3d_2: Cropping3D
G
(TO FIG. 7D)

FIG. 7C

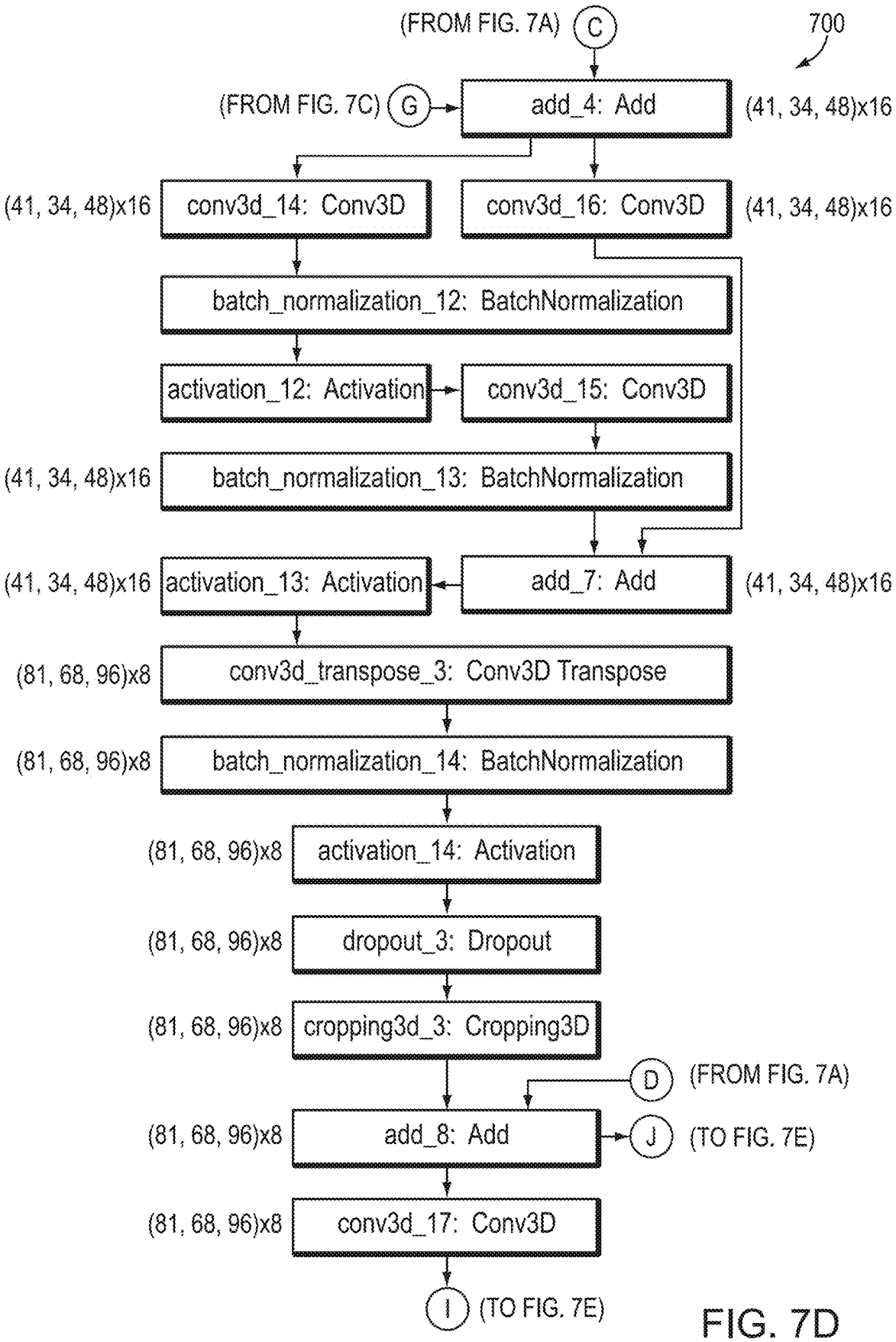

(FROM FIG. 7A) C
700
(FROM FIG. 7C) G
add_4: Add
(41, 34, 48)x16
(41, 34, 48)x16
conv3d_14: Conv3D
conv3d_16: Conv3D
(41, 34, 48)x16
batch_normalization_12: BatchNormalization
activation_12: Activation
conv3d_15: Conv3D
(41, 34, 48)x16
batch_normalization_13: BatchNormalization
(41, 34, 48)x16
activation_13: Activation
add_7: Add
(41, 34, 48)x16
(81, 68, 96)x8
conv3d_transpose_3: Conv3D Transpose
(81, 68, 96)x8
batch_normalization_14: BatchNormalization
(81, 68, 96)x8
activation_14: Activation
(81, 68, 96)x8
dropout_3: Dropout
(81, 68, 96)x8
cropping3d_3: Cropping3D
D
(FROM FIG. 7A)
(81, 68, 96)x8
add_8: Add
J
(TO FIG. 7E)
(81, 68, 96)x8
conv3d_17: Conv3D
I
(TO FIG. 7E)

FIG. 7D

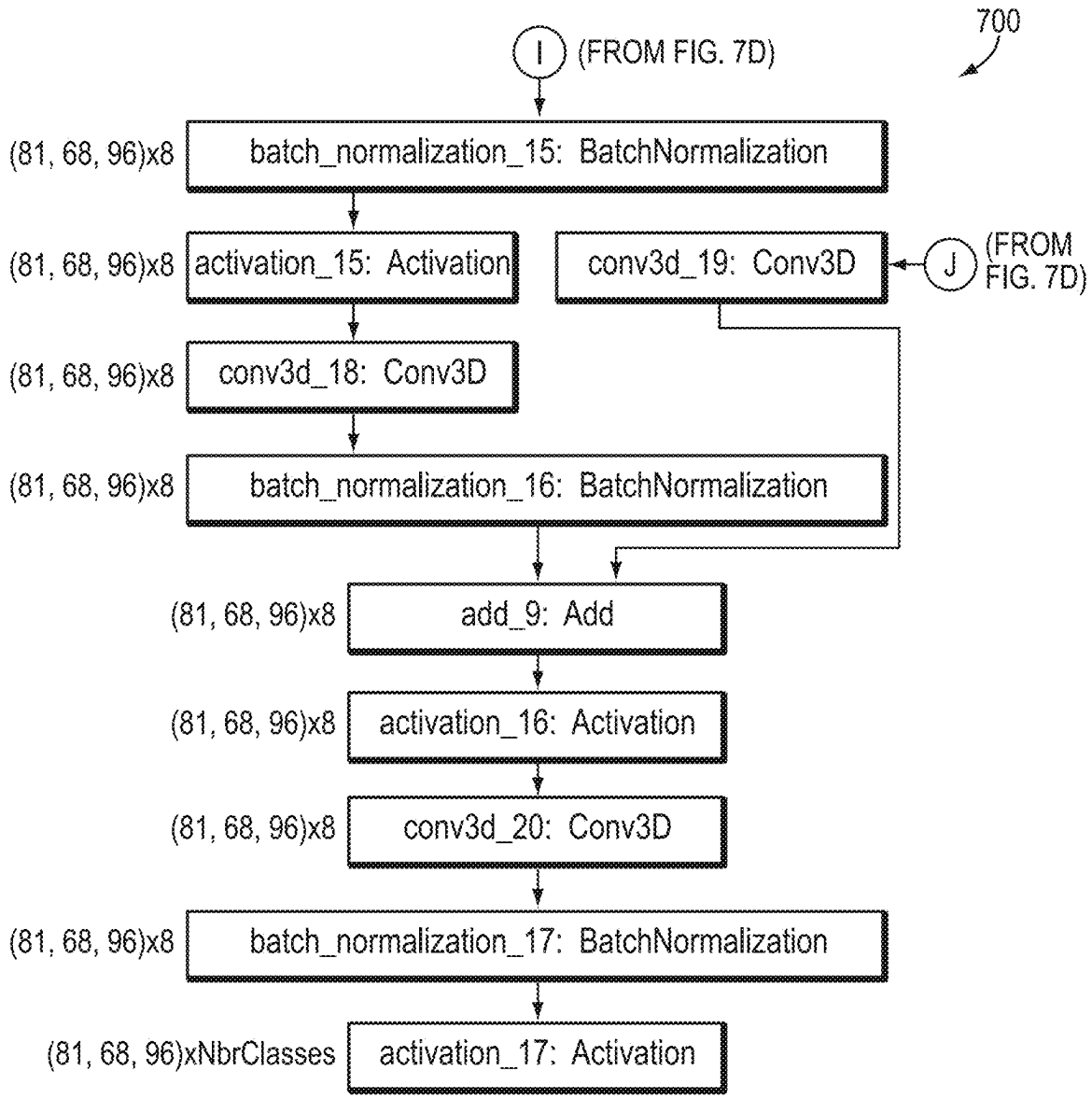

700
I
(FROM FIG. 7D)
(81, 68, 96)x8
batch_normalization_15: BatchNormalization
(81, 68, 96)x8
activation_15: Activation
conv3d_19: Conv3D
J
(FROM FIG. 7D)
(81, 68, 96)x8
conv3d_18: Conv3D
(81, 68, 96)x8
batch_normalization_16: BatchNormalization
(81, 68, 96)x8
add_9: Add
(81, 68, 96)x8
activation_16: Activation
(81, 68, 96)x8
conv3d_20: Conv3D
(81, 68, 96)x8
batch_normalization_17: BatchNormalization
(81, 68, 96)xNbrClasses
activation_17: Activation

FIG. 7E

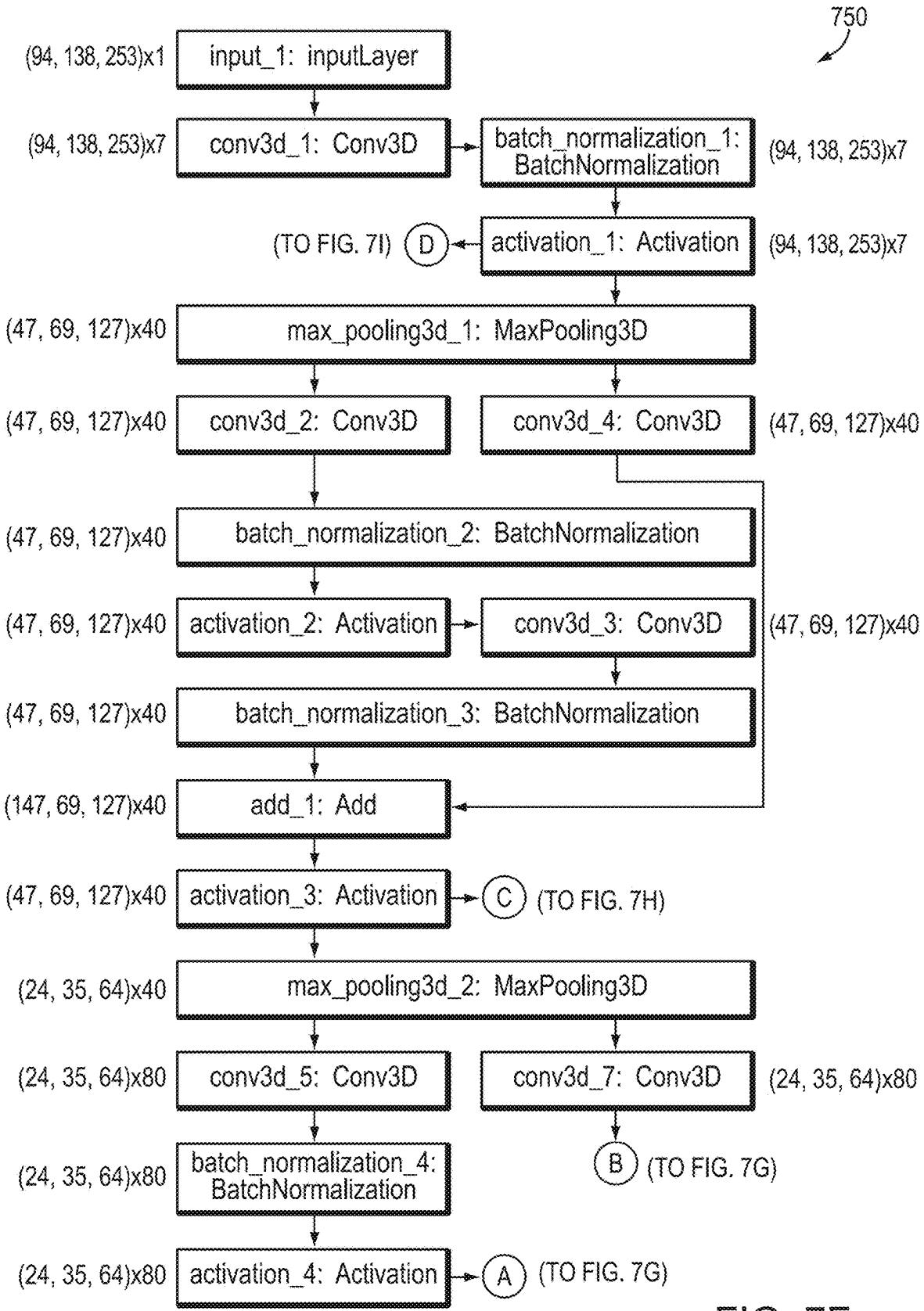

750
(94, 138, 253)x1
input_1: inputLayer
(94, 138, 253)x7
conv3d_1: Conv3D
batch_normalization_1: BatchNormalization
(94, 138, 253)x7
(TO FIG. 7I)
D
activation_1: Activation
(94, 138, 253)x7
(47, 69, 127)x40
max_pooling3d_1: MaxPooling3D
(47, 69, 127)x40
conv3d_2: Conv3D
conv3d_4: Conv3D
(47, 69, 127)x40
(47, 69, 127)x40
batch_normalization_2: BatchNormalization
(47, 69, 127)x40
activation_2: Activation
conv3d_3: Conv3D
(47, 69, 127)x40
(47, 69, 127)x40
batch_normalization_3: BatchNormalization
(147, 69, 127)x40
add_1: Add
(47, 69, 127)x40
activation_3: Activation
C
(TO FIG. 7H)
(24, 35, 64)x40
max_pooling3d_2: MaxPooling3D
(24, 35, 64)x80
conv3d_5: Conv3D
conv3d_7: Conv3D
(24, 35, 64)x80
(24, 35, 64)x80
batch_normalization_4: BatchNormalization
B
(TO FIG. 7G)
(24, 35, 64)x80
activation_4: Activation
A
(TO FIG. 7G)

FIG. 7F

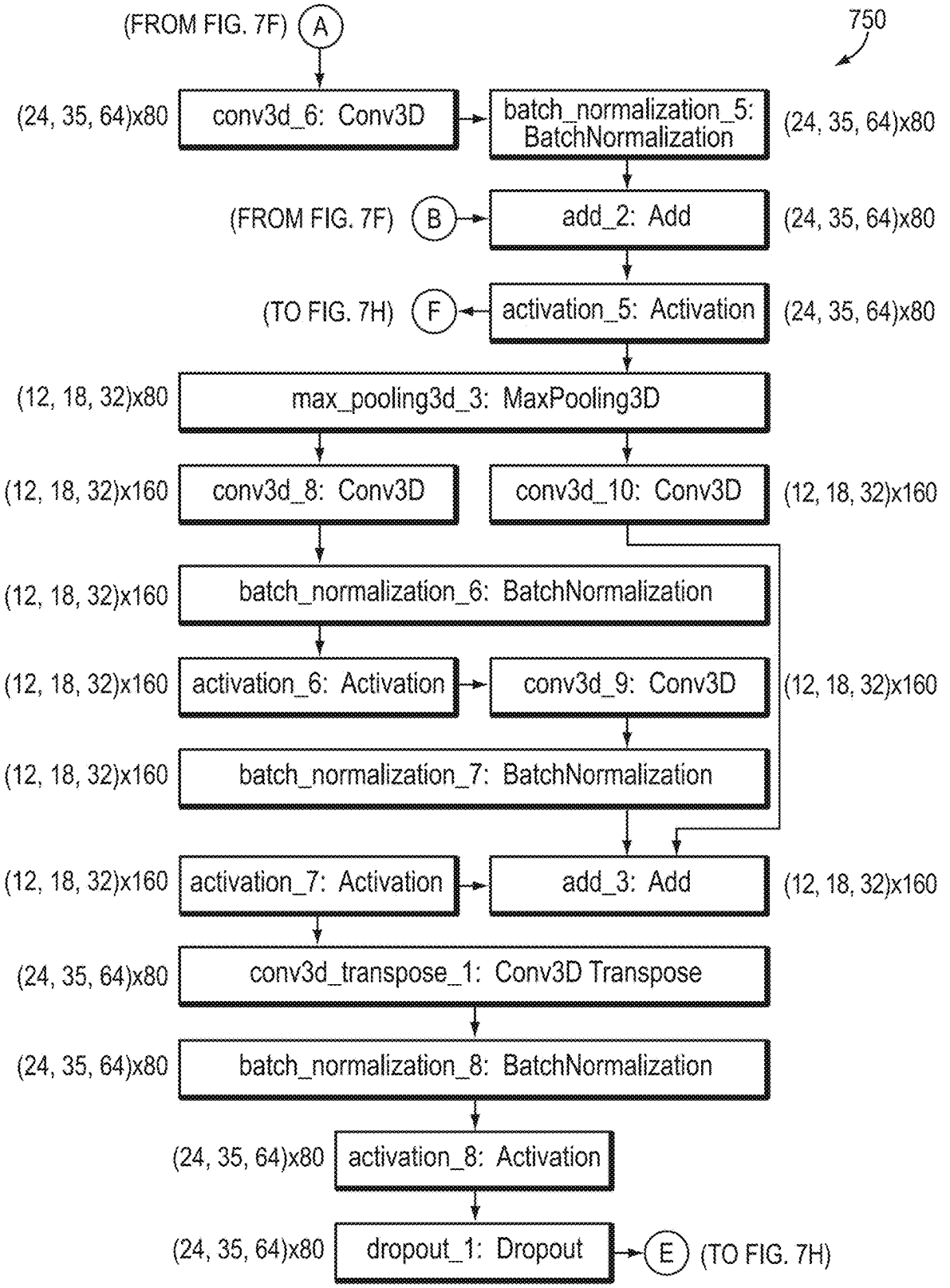

(FROM FIG. 7F) A
750
(24, 35, 64)x80
conv3d_6: Conv3D
batch_normalization_5: BatchNormalization
(24, 35, 64)x80
(FROM FIG. 7F) B
add_2: Add
(24, 35, 64)x80
(TO FIG. 7H) F
activation_5: Activation
(24, 35, 64)x80
(12, 18, 32)x80
max_pooling3d_3: MaxPooling3D
(12, 18, 32)x160
conv3d_8: Conv3D
conv3d_10: Conv3D
(12, 18, 32)x160
(12, 18, 32)x160
batch_normalization_6: BatchNormalization
(12, 18, 32)x160
activation_6: Activation
conv3d_9: Conv3D
(12, 18, 32)x160
(12, 18, 32)x160
batch_normalization_7: BatchNormalization
(12, 18, 32)x160
activation_7: Activation
add_3: Add
(12, 18, 32)x160
(24, 35, 64)x80
conv3d_transpose_1: Conv3D Transpose
(24, 35, 64)x80
batch_normalization_8: BatchNormalization
(24, 35, 64)x80
activation_8: Activation
(24, 35, 64)x80
dropout_1: Dropout
E
(TO FIG. 7H)

FIG. 7G

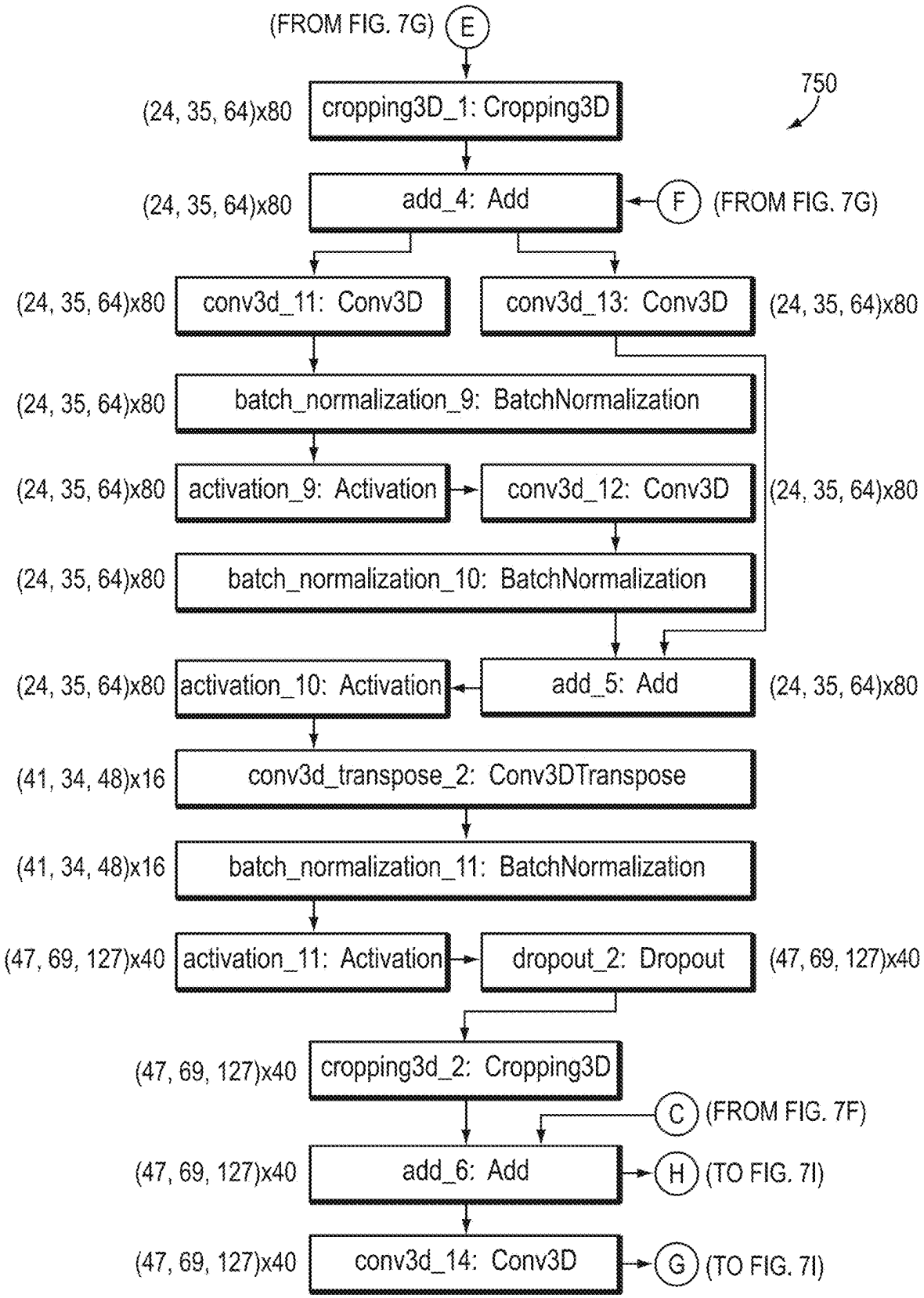

(FROM FIG. 7G)
E
750
(24, 35, 64)x80
cropping3D_1: Cropping3D
(24, 35, 64)x80
add_4: Add
F
(FROM FIG. 7G)
(24, 35, 64)x80
conv3d_11: Conv3D
conv3d_13: Conv3D
(24, 35, 64)x80
(24, 35, 64)x80
batch_normalization_9: BatchNormalization
(24, 35, 64)x80
activation_9: Activation
conv3d_12: Conv3D
(24, 35, 64)x80
(24, 35, 64)x80
batch_normalization_10: BatchNormalization
(24, 35, 64)x80
activation_10: Activation
add_5: Add
(24, 35, 64)x80
(41, 34, 48)x16
conv3d_transpose_2: Conv3DTranspose
(41, 34, 48)x16
batch_normalization_11: BatchNormalization
(47, 69, 127)x40
activation_11: Activation
dropout_2: Dropout
(47, 69, 127)x40
(47, 69, 127)x40
cropping3d_2: Cropping3D
C
(FROM FIG. 7F)
(47, 69, 127)x40
add_6: Add
H
(TO FIG. 7I)
(47, 69, 127)x40
conv3d_14: Conv3D
G
(TO FIG. 7I)

FIG. 7H

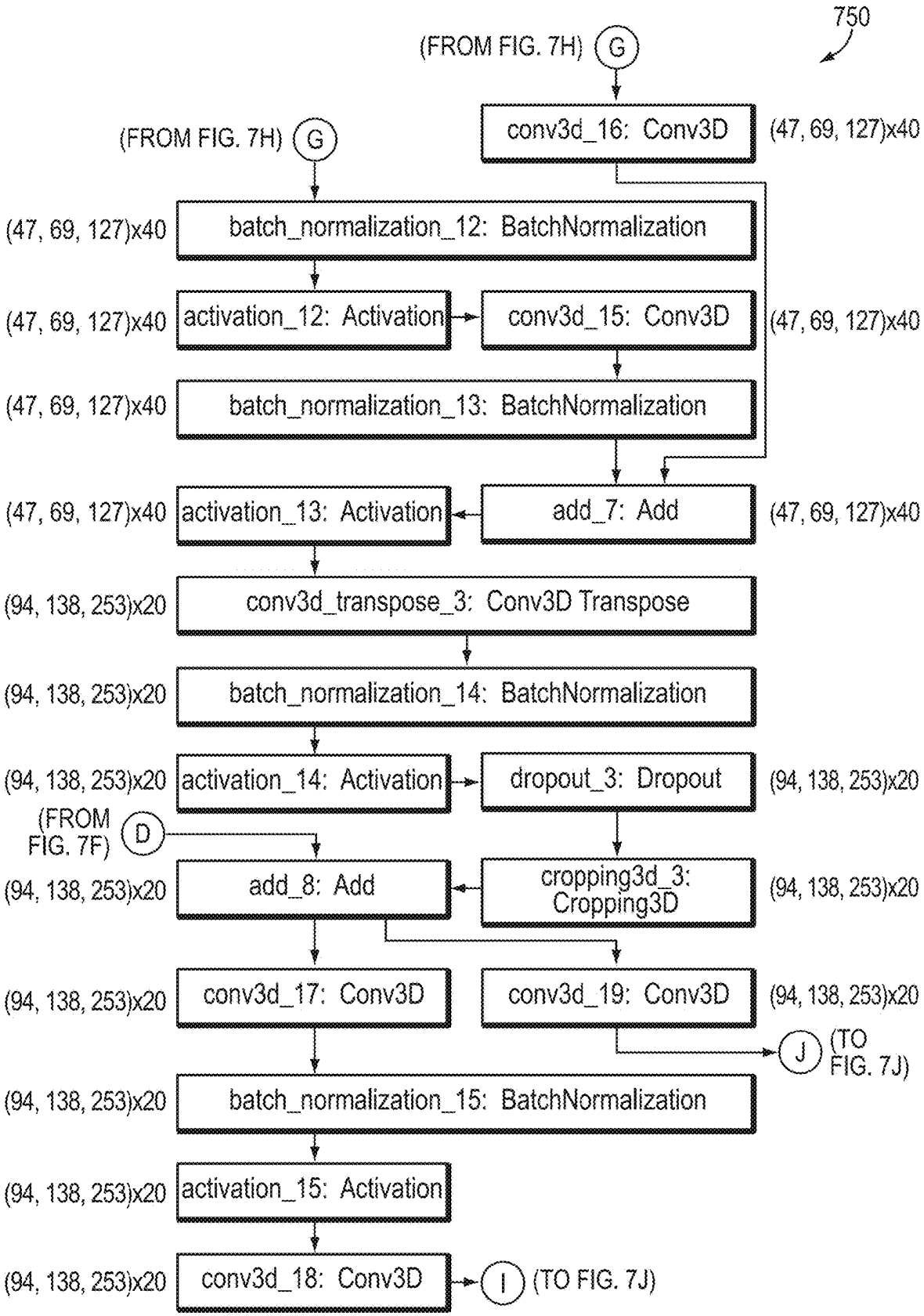

750
(FROM FIG. 7H) G
(FROM FIG. 7H) G
conv3d_16: Conv3D
(47, 69, 127)x40
(47, 69, 127)x40
batch_normalization_12: BatchNormalization
(47, 69, 127)x40
activation_12: Activation
conv3d_15: Conv3D
(47, 69, 127)x40
(47, 69, 127)x40
batch_normalization_13: BatchNormalization
(47, 69, 127)x40
activation_13: Activation
add_7: Add
(47, 69, 127)x40
(94, 138, 253)x20
conv3d_transpose_3: Conv3D Transpose
(94, 138, 253)x20
batch_normalization_14: BatchNormalization
(94, 138, 253)x20
activation_14: Activation
dropout_3: Dropout
(94, 138, 253)x20
(FROM FIG. 7F) D
(94, 138, 253)x20
add_8: Add
cropping3d_3: Cropping3D
(94, 138, 253)x20
(94, 138, 253)x20
conv3d_17: Conv3D
conv3d_19: Conv3D
(94, 138, 253)x20
J (TO FIG. 7J)
(94, 138, 253)x20
batch_normalization_15: BatchNormalization
(94, 138, 253)x20
activation_15: Activation
(94, 138, 253)x20
conv3d_18: Conv3D
I (TO FIG. 7J)

FIG. 7I

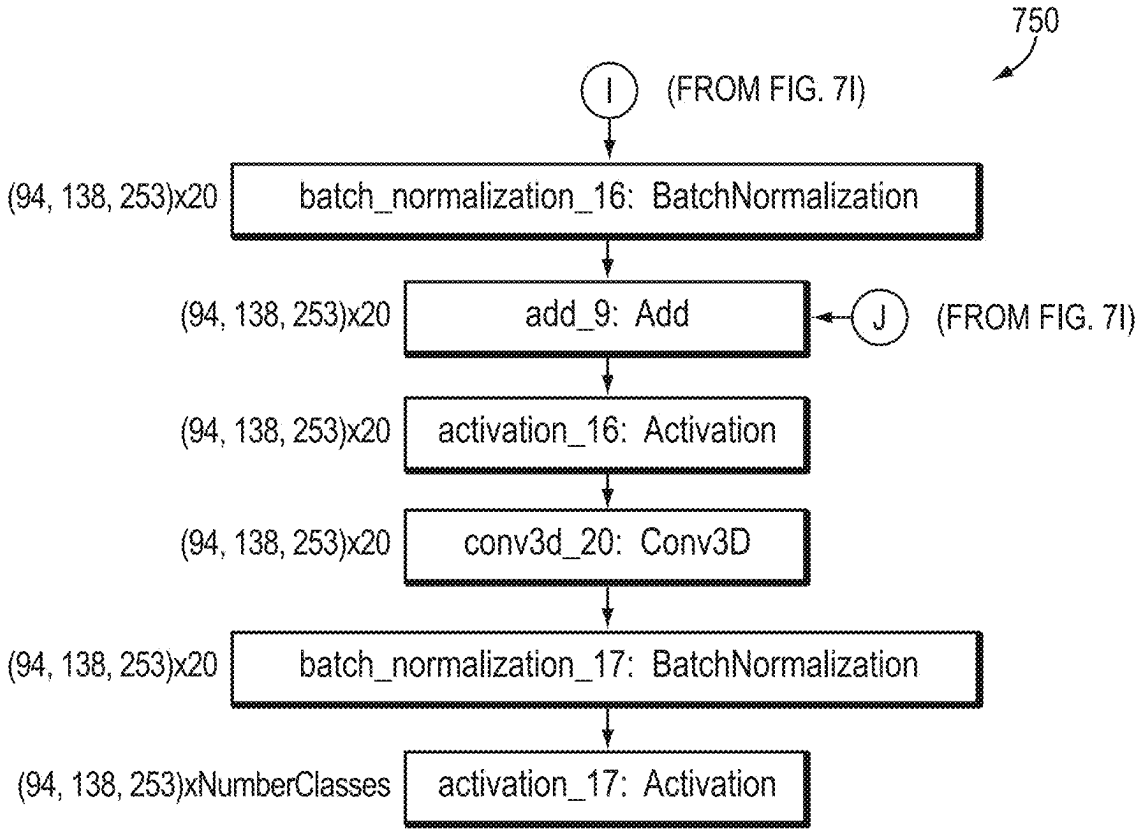

750
I
(FROM FIG. 7I)
(94, 138, 253)x20
batch_normalization_16: BatchNormalization
(94, 138, 253)x20
add_9: Add
J
(FROM FIG. 7I)
(94, 138, 253)x20
activation_16: Activation
(94, 138, 253)x20
conv3d_20: Conv3D
(94, 138, 253)x20
batch_normalization_17: BatchNormalization
(94, 138, 253)xNumberClasses
activation_17: Activation

FIG. 7J

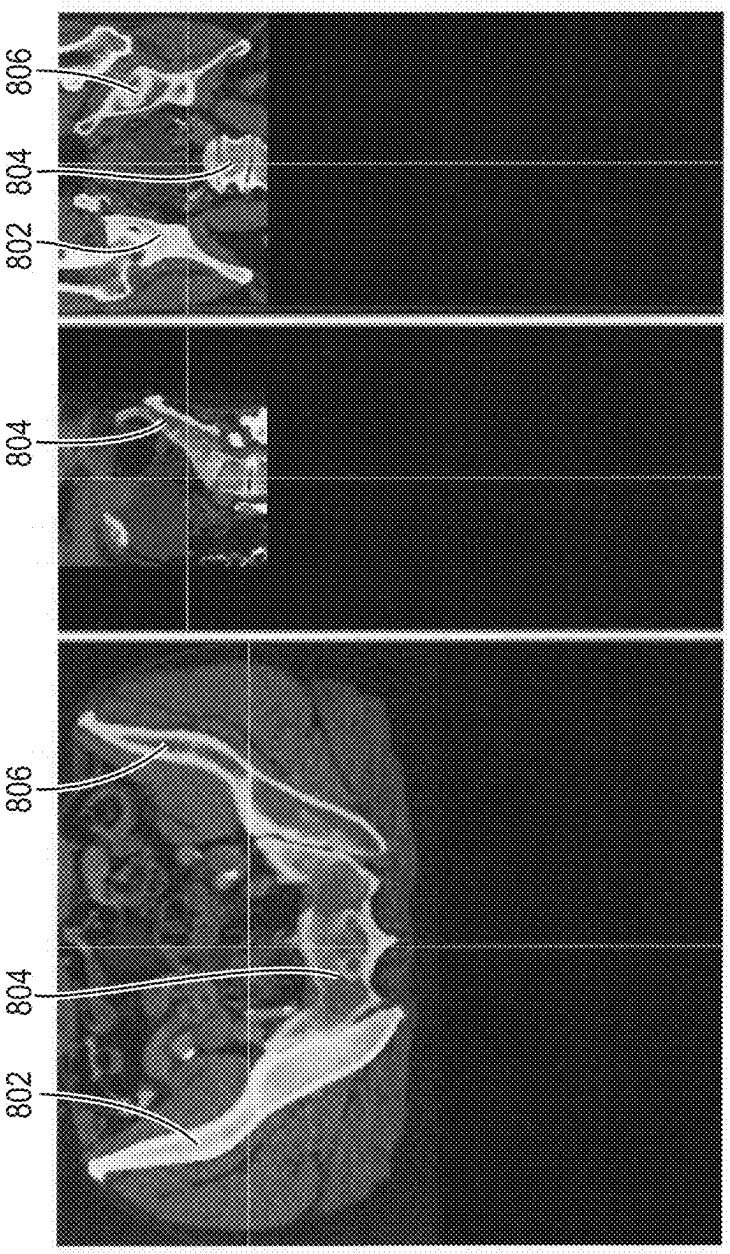


FIG. 8A

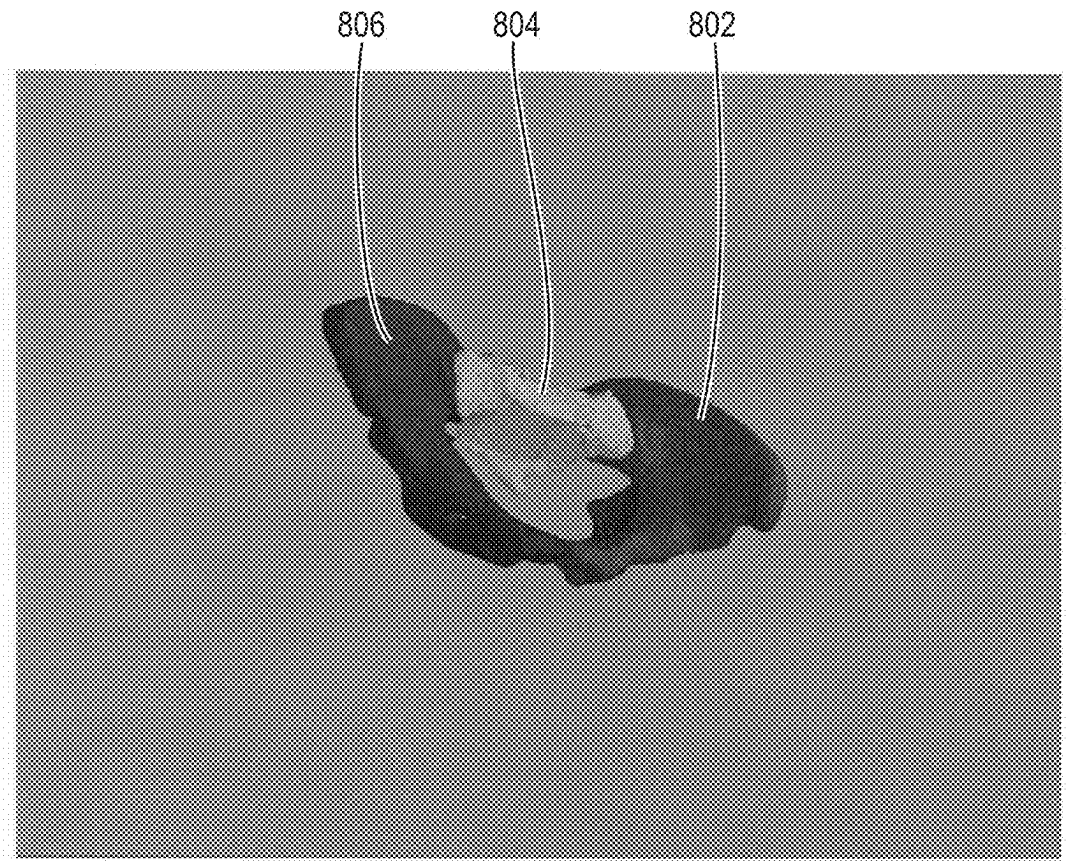


FIG. 8B

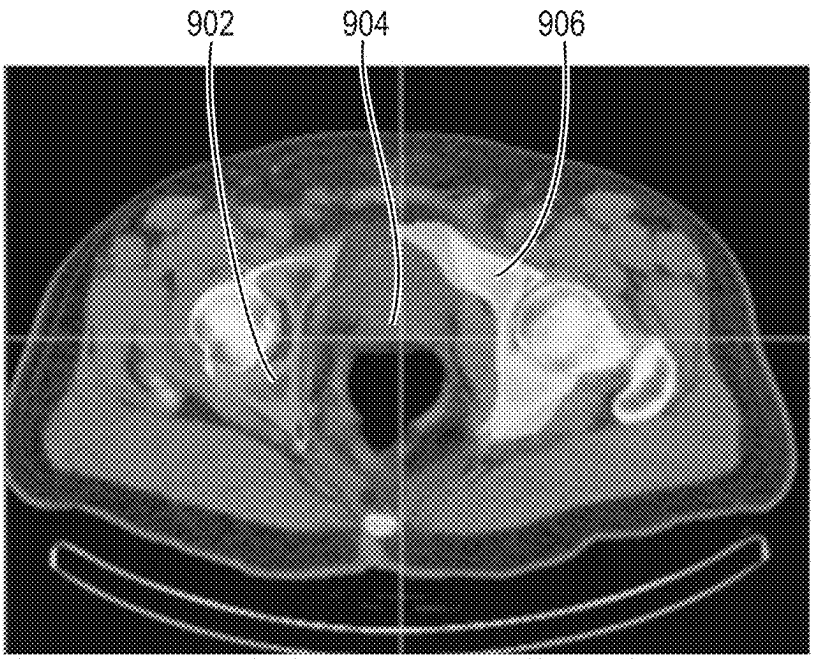


FIG. 9A

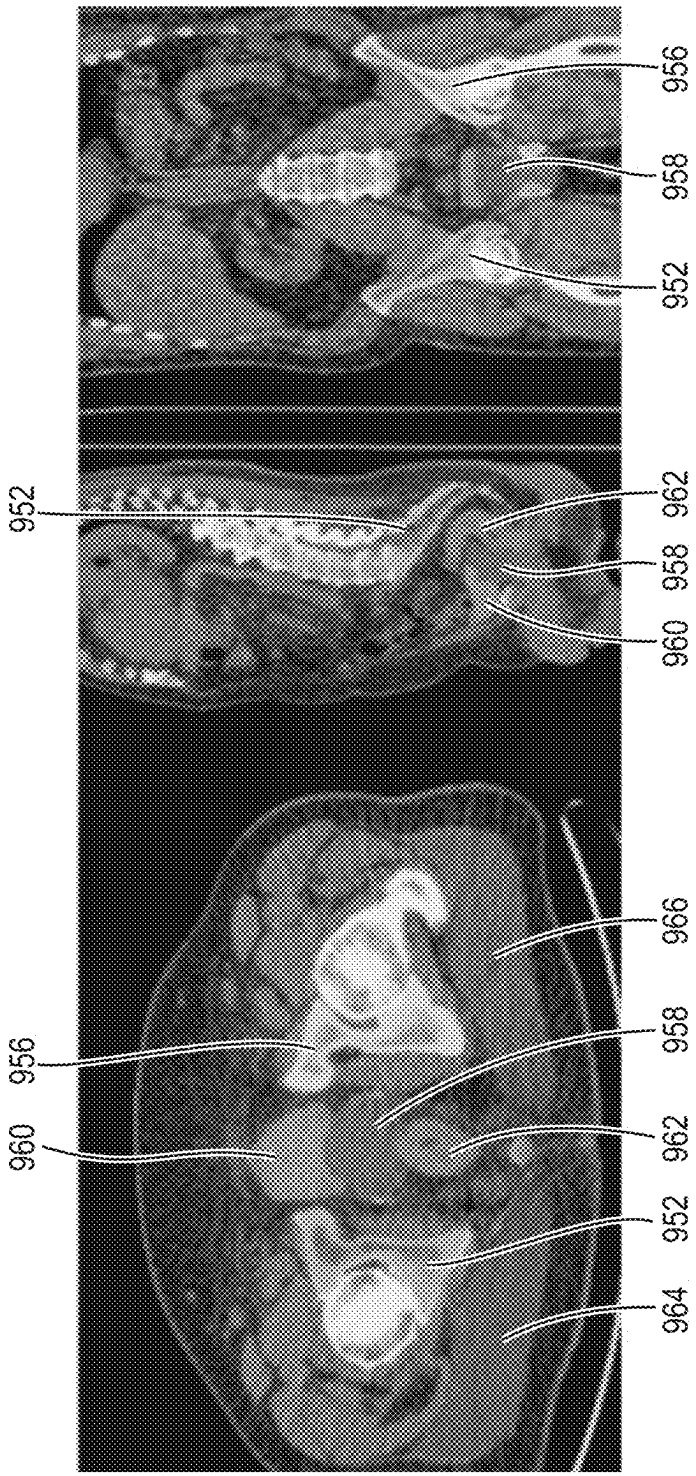


FIG. 9B



FIG. 10

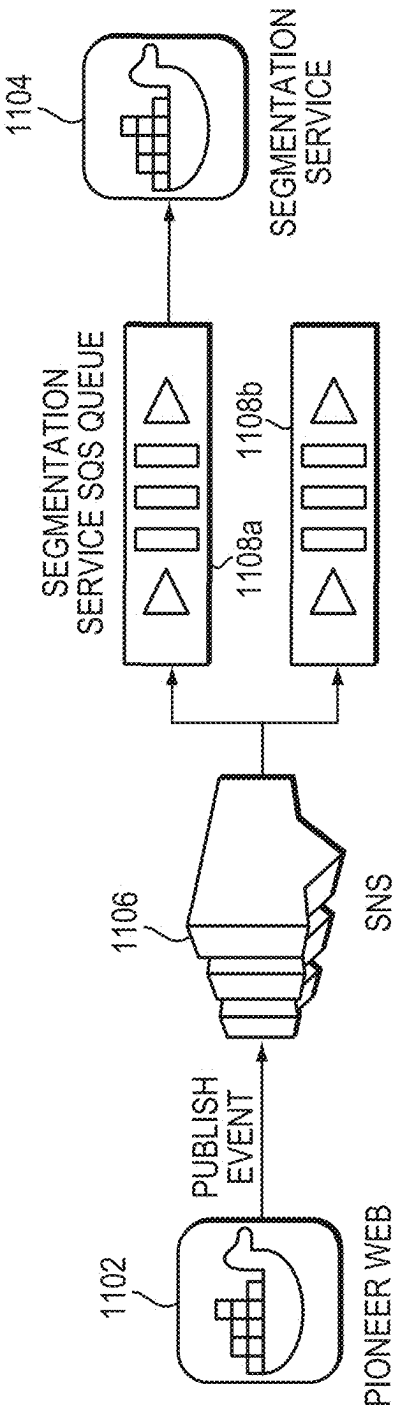

1104
SEGMENTATION SERVICE
SEGMENTATION SERVICE SQS QUEUE
1108a
1108b
1106
SNS
PUBLISH EVENT
1102
PIONEER WEB

FIG. 11

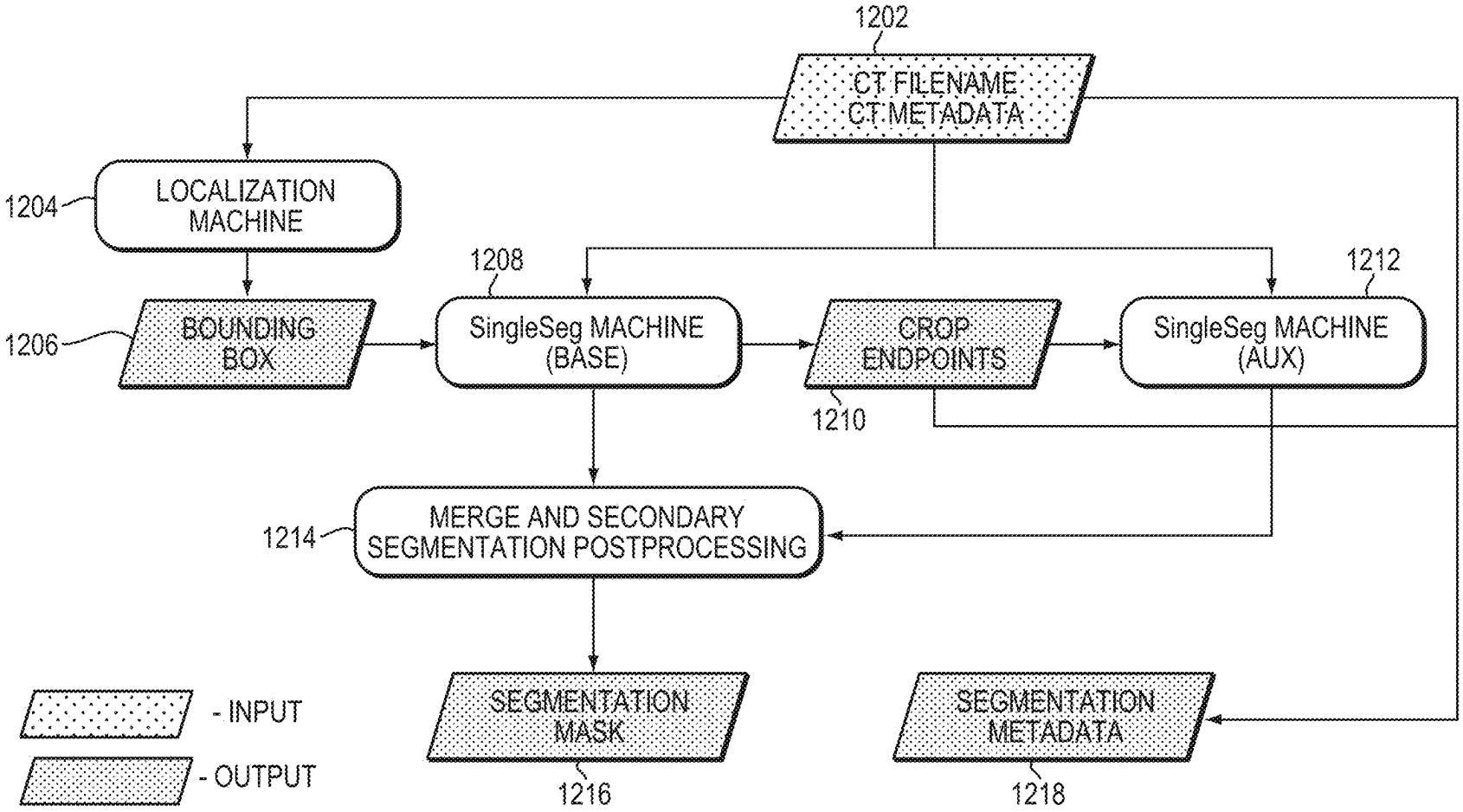

1202
CT FILENAME
CT METADATA
1204
LOCALIZATION MACHINE
1206
BOUNDING BOX
1208
SingleSeg MACHINE (BASE)
CROP ENDPOINTS
1210
1212
SingleSeg MACHINE (AUX)
1214
MERGE AND SECONDARY SEGMENTATION POSTPROCESSING
SEGMENTATION MASK
1216
SEGMENTATION METADATA
1218
- INPUT
- OUTPUT

FIG. 12

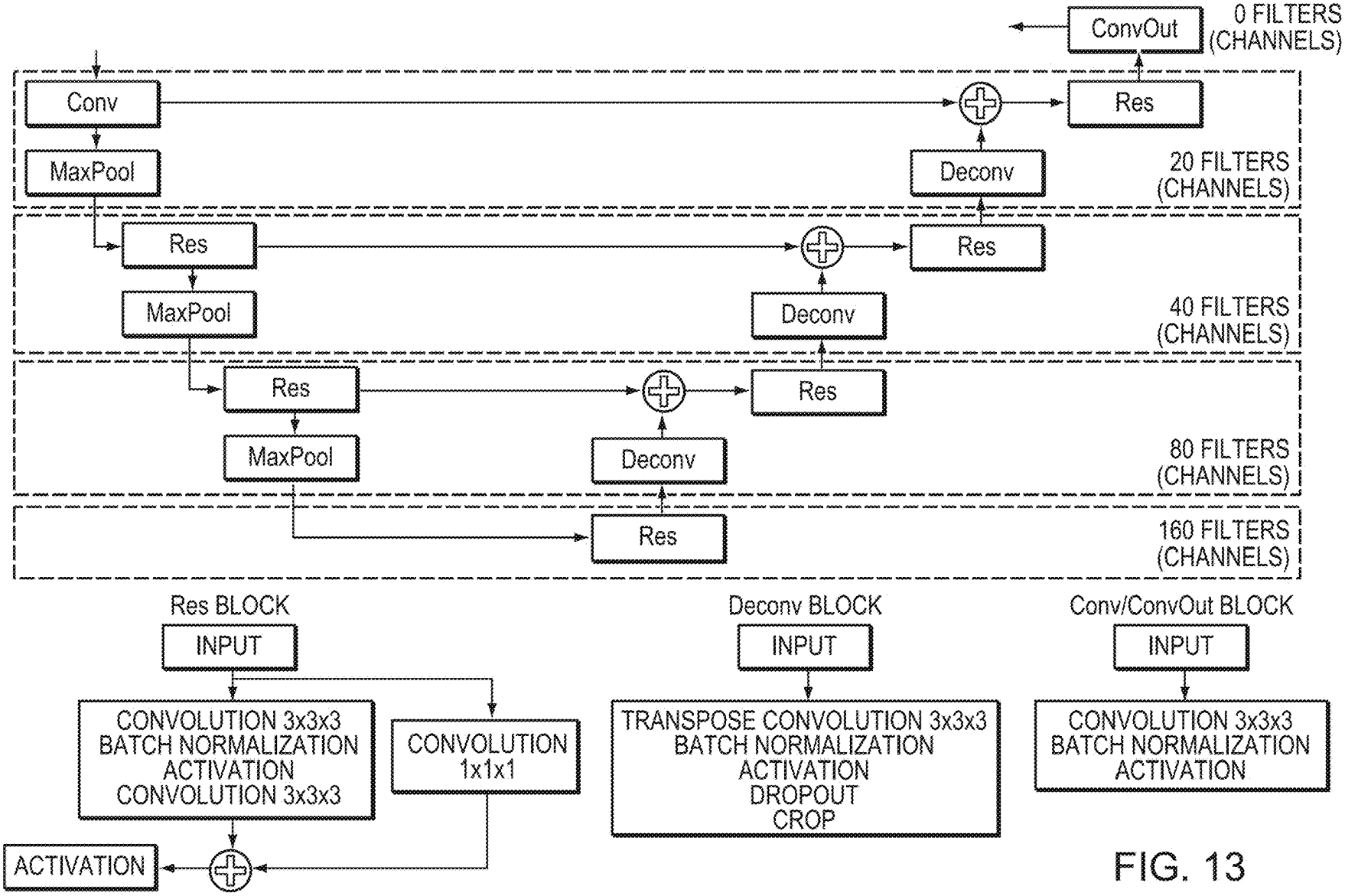

ConvOut
0 FILTERS (CHANNELS)
Conv
Res
MaxPool
Deconv
20 FILTERS (CHANNELS)
Res
Res
MaxPool
Deconv
40 FILTERS (CHANNELS)
Res
Res
MaxPool
Deconv
80 FILTERS (CHANNELS)
Res
160 FILTERS (CHANNELS)
Res BLOCK
INPUT
CONVOLUTION 3x3x3
BATCH NORMALIZATION
ACTIVATION
CONVOLUTION 3x3x3
CONVOLUTION 1x1x1
ACTIVATION
Deconv BLOCK
INPUT
TRANSPOSE CONVOLUTION 3x3x3
BATCH NORMALIZATION
ACTIVATION
DROPOUT
CROP
Conv/ConvOut BLOCK
INPUT
CONVOLUTION 3x3x3
BATCH NORMALIZATION
ACTIVATION

FIG. 13

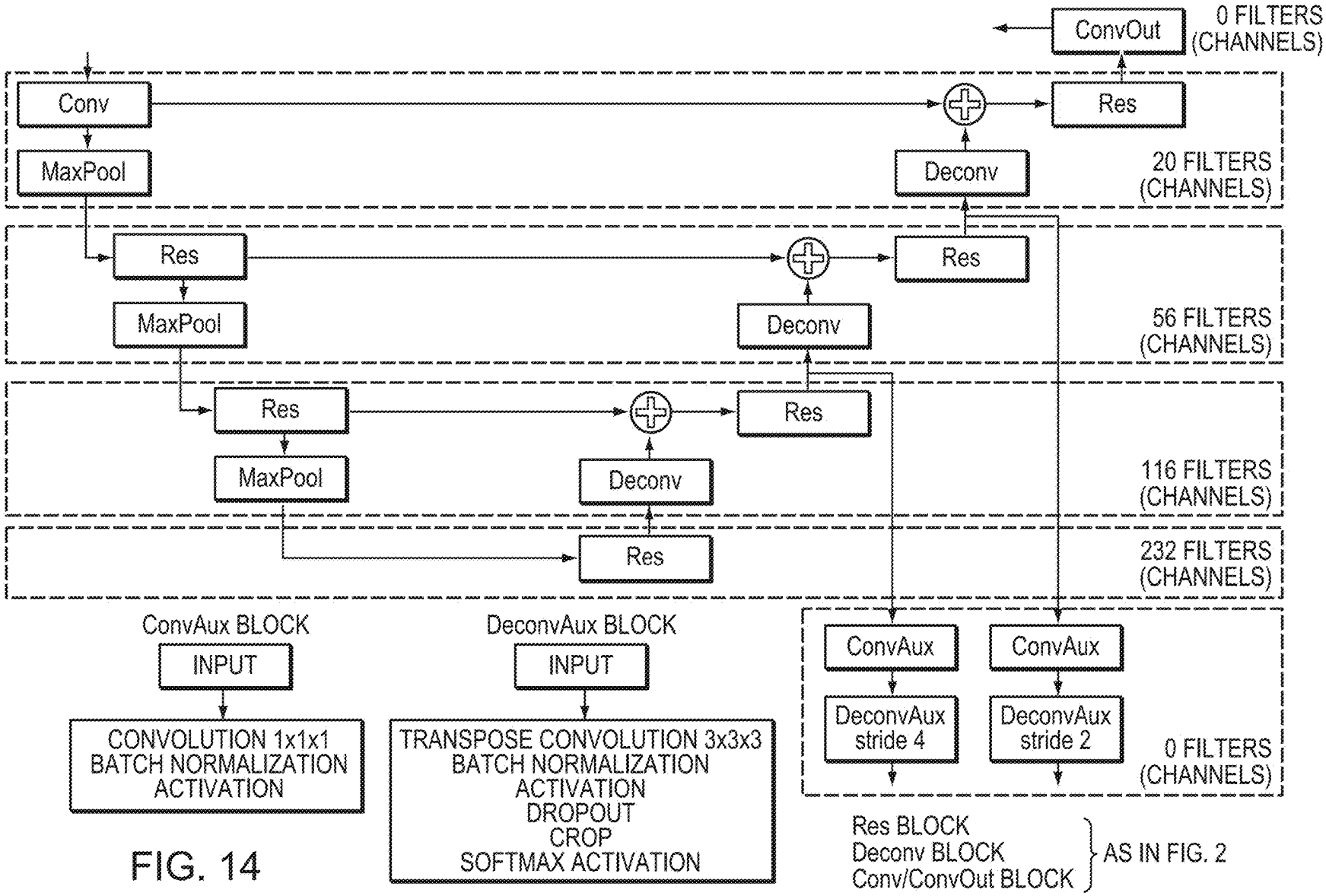

ConvOut
0 FILTERS (CHANNELS)
Conv
Res
MaxPool
Deconv
20 FILTERS (CHANNELS)
Res
Res
MaxPool
Deconv
56 FILTERS (CHANNELS)
Res
Res
MaxPool
Deconv
116 FILTERS (CHANNELS)
Res
232 FILTERS (CHANNELS)
ConvAux BLOCK
INPUT
CONVOLUTION 1x1x1
BATCH NORMALIZATION
ACTIVATION
DeconvAux BLOCK
INPUT
TRANSPOSE CONVOLUTION 3x3x3
BATCH NORMALIZATION
ACTIVATION
DROPOUT
CROP
SOFTMAX ACTIVATION
ConvAux
ConvAux
DeconvAux stride 4
DeconvAux stride 2
0 FILTERS (CHANNELS)
Res BLOCK
Deconv BLOCK
Conv/ConvOut BLOCK
AS IN FIG. 2

FIG. 14

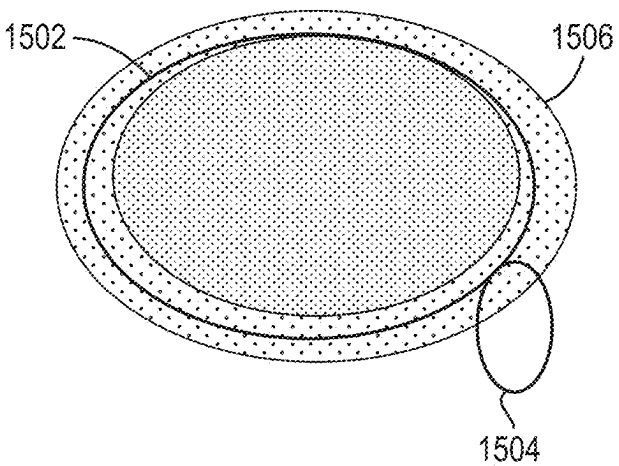


FIG. 15

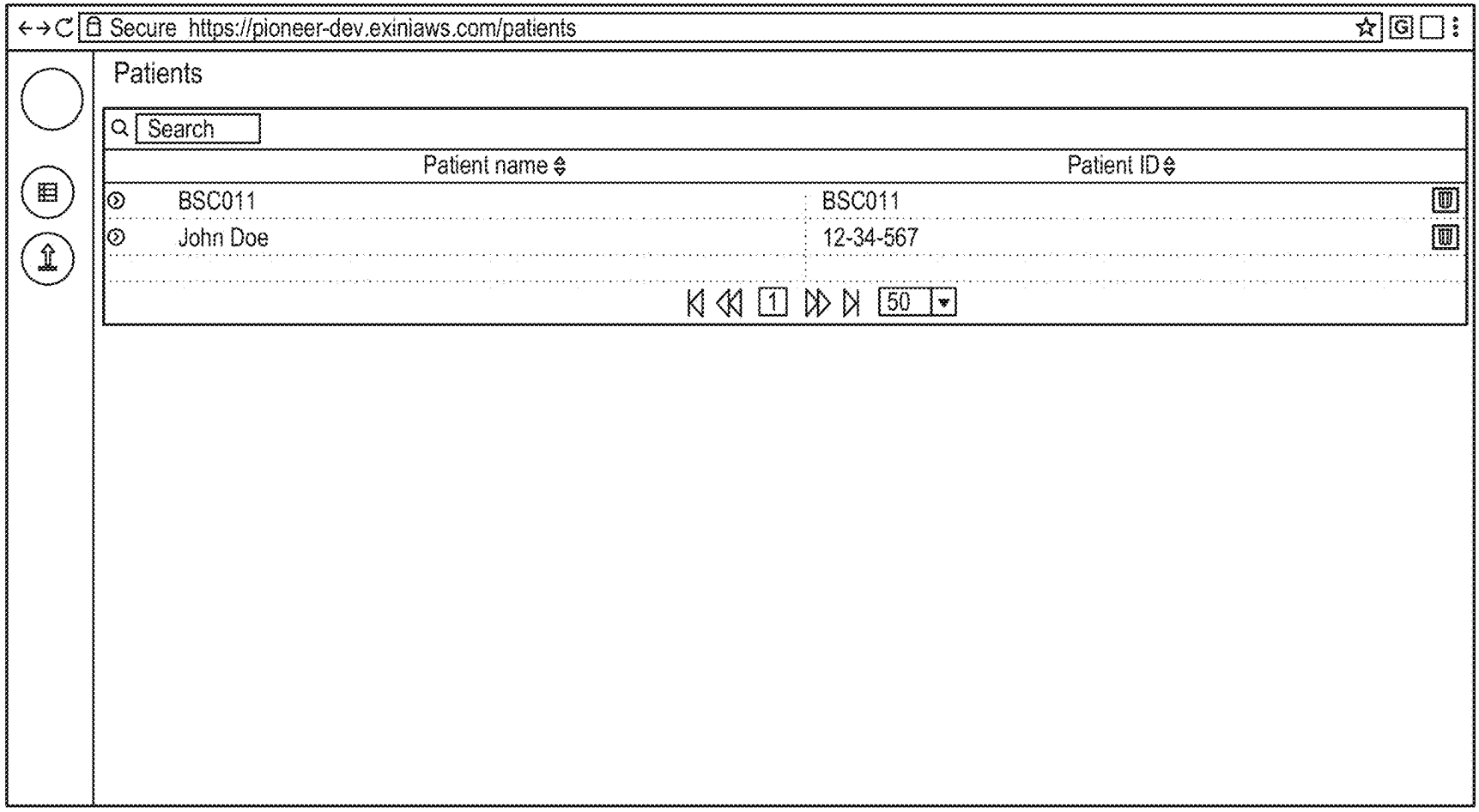

Secure https://pioneer-dev.exiniaws.com/patients
Patients
Search
Patient name
Patient ID
BSC011
BSC011
John Doe
12-34-567
1
50

FIG. 16A

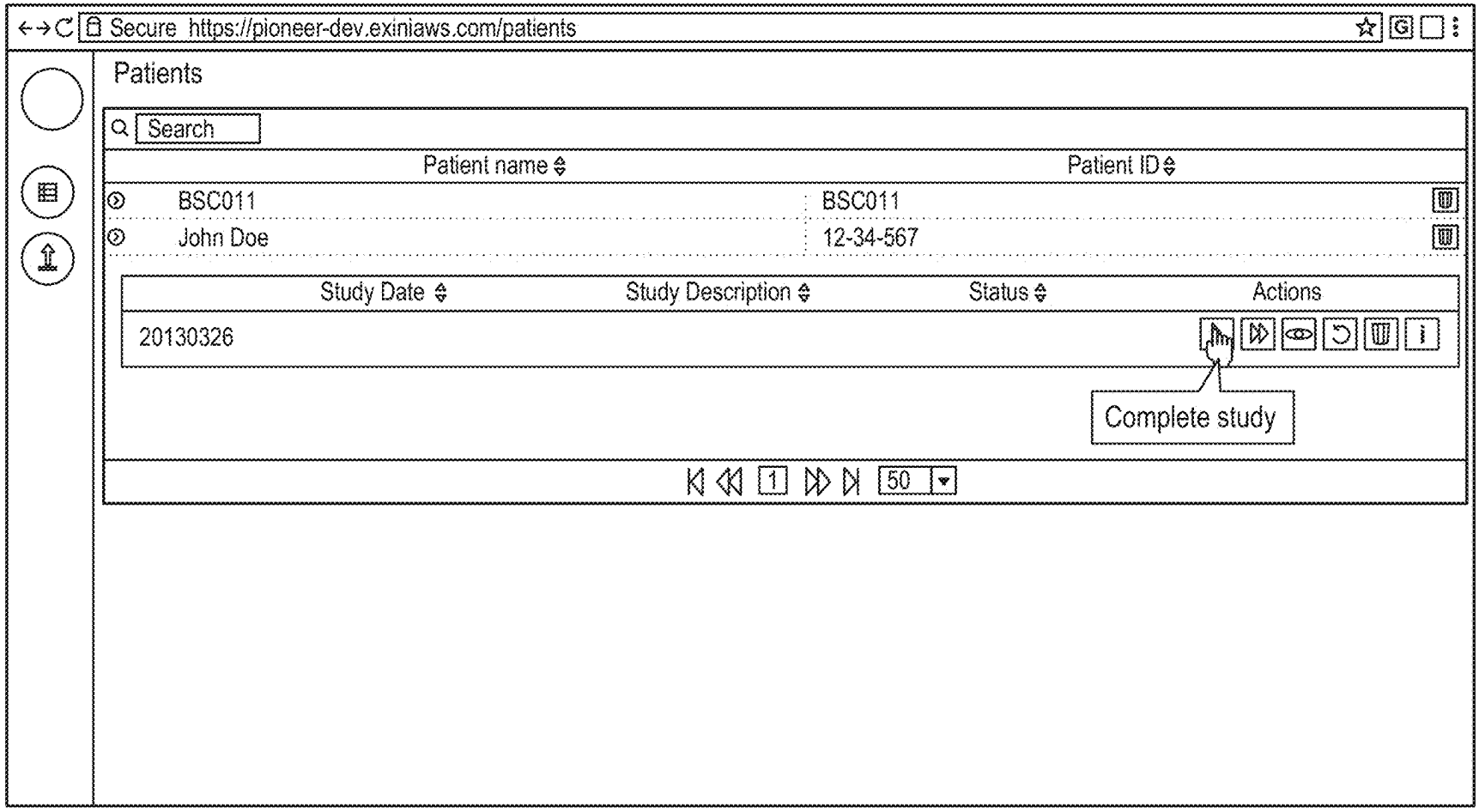

Secure https://pioneer-dev.exiniaws.com/patients
Patients
Search
Patient name
Patient ID
BSC011
BSC011
John Doe
12-34-567
Study Date
Study Description
Status
Actions
20130326
Complete study
1
50

FIG. 16B

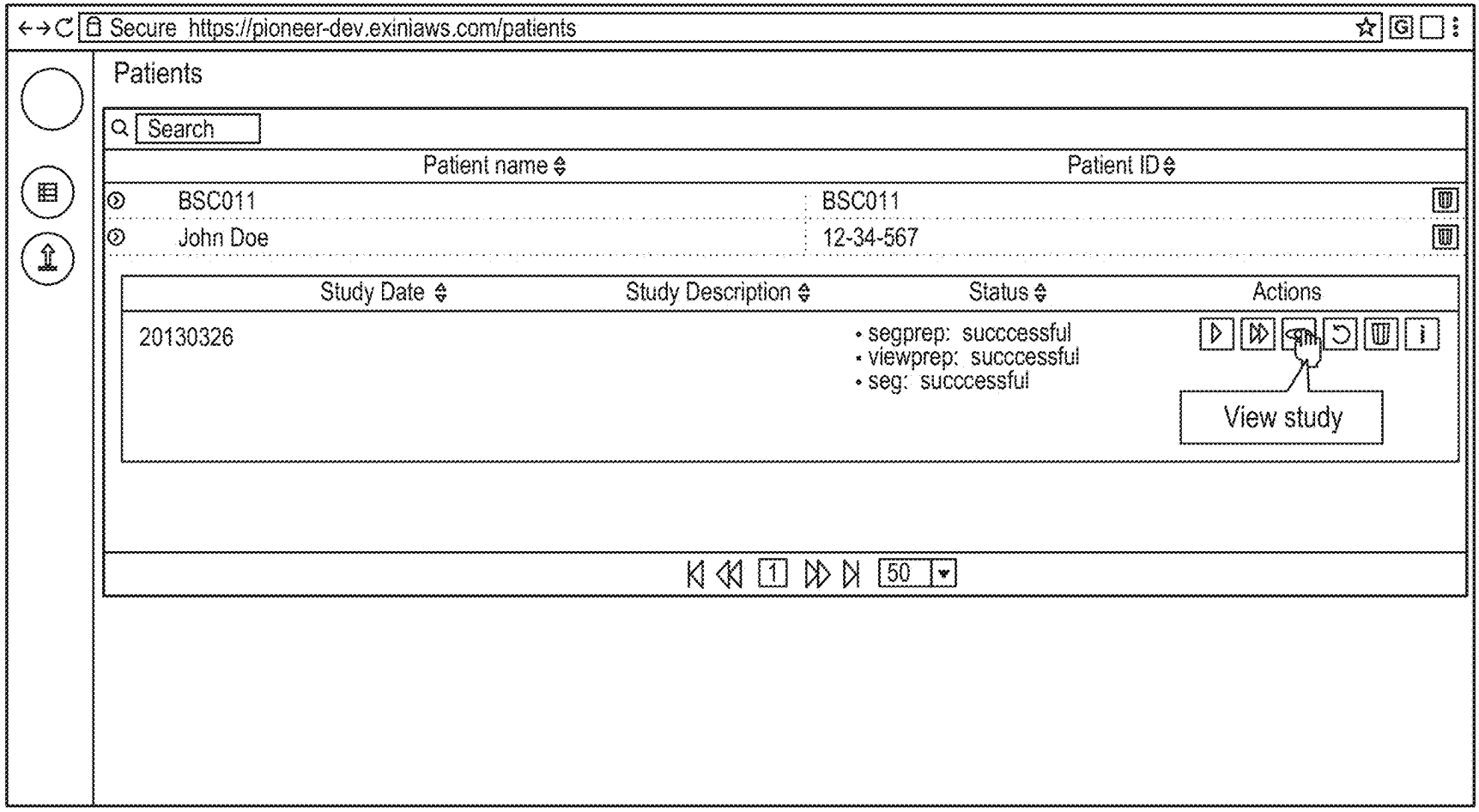

Secure https://pioneer-dev.exiniaws.com/patients
Patients
Search
Patient name
Patient ID
BSC011
BSC011
John Doe
12-34-567
Study Date
Study Description
Status
Actions
20130326
• segprep: successful
• viewprep: successful
• seg: successful
View study
1
50

FIG. 16C

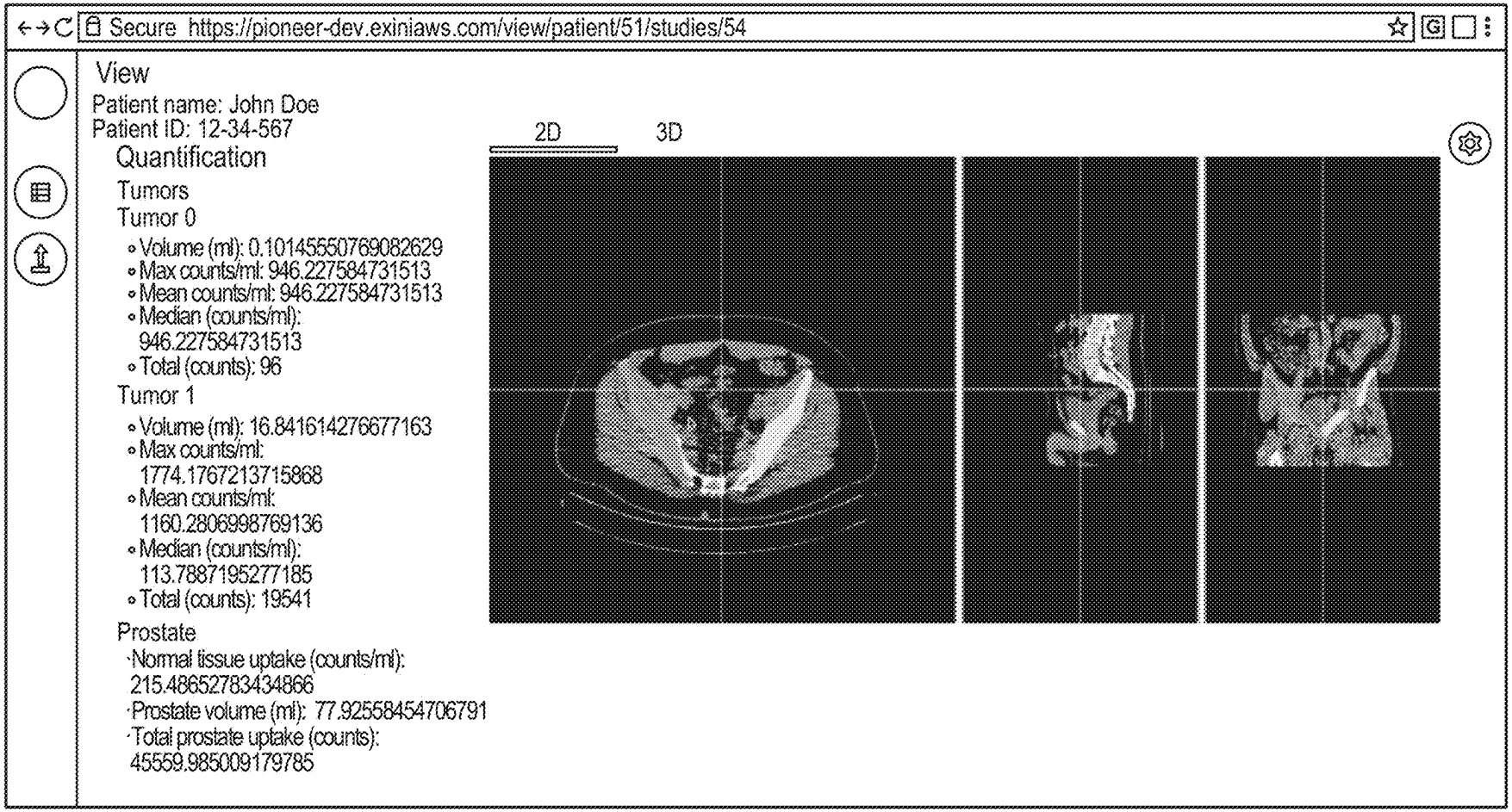

Secure https://pioneer-dev.exiniaws.com/view/patient/51/studies/54
View
Patient name: John Doe
Patient ID: 12-34-567
Quantification
Tumors
Tumor 0
Volume (ml): 0.10145550769082629
Max counts/ml: 946.227584731513
Mean counts/ml: 946.227584731513
Median (counts/ml): 946.227584731513
Total (counts): 96
Tumor 1
Volume (ml): 16.841614276677163
Max counts/ml: 1774.1767213715868
Mean counts/ml: 1160.2806998769136
Median (counts/ml): 113.78871952771 85
Total (counts): 19541
Prostate
Normal tissue uptake (counts/ml): 215.48652783434866
Prostate volume (ml): 77.92558454706791
Total prostate uptake (counts): 45559.985009179785
2D
3D

FIG. 17A


Secure https://pioneer-dev.exiniaws.com/view/patient/51/studies/54
View
Patient name: John Doe
Patient ID: 12-34-567
Quantification
Tumors
Tumor 0
Volume (ml): 0.10145550769082629
Max counts/ml: 946.227584731513
Mean counts/ml: 946.227584731513
Median (counts/ml): 946.227584731513
Total (counts): 96
Tumor 1
Volume (ml): 16.841614276677163
Max counts/ml: 1774.1767213715868
Mean counts/ml: 1160.2806998769136
Median (counts/ml): 113.78871952771 85
Total (counts): 19541
Prostate
Normal tissue uptake (counts/ml): 215.48652783434866
Prostate volume (ml): 77.92558454706791
Total prostate uptake (counts): 45559.985009179785
2D
3D

FIG. 17B

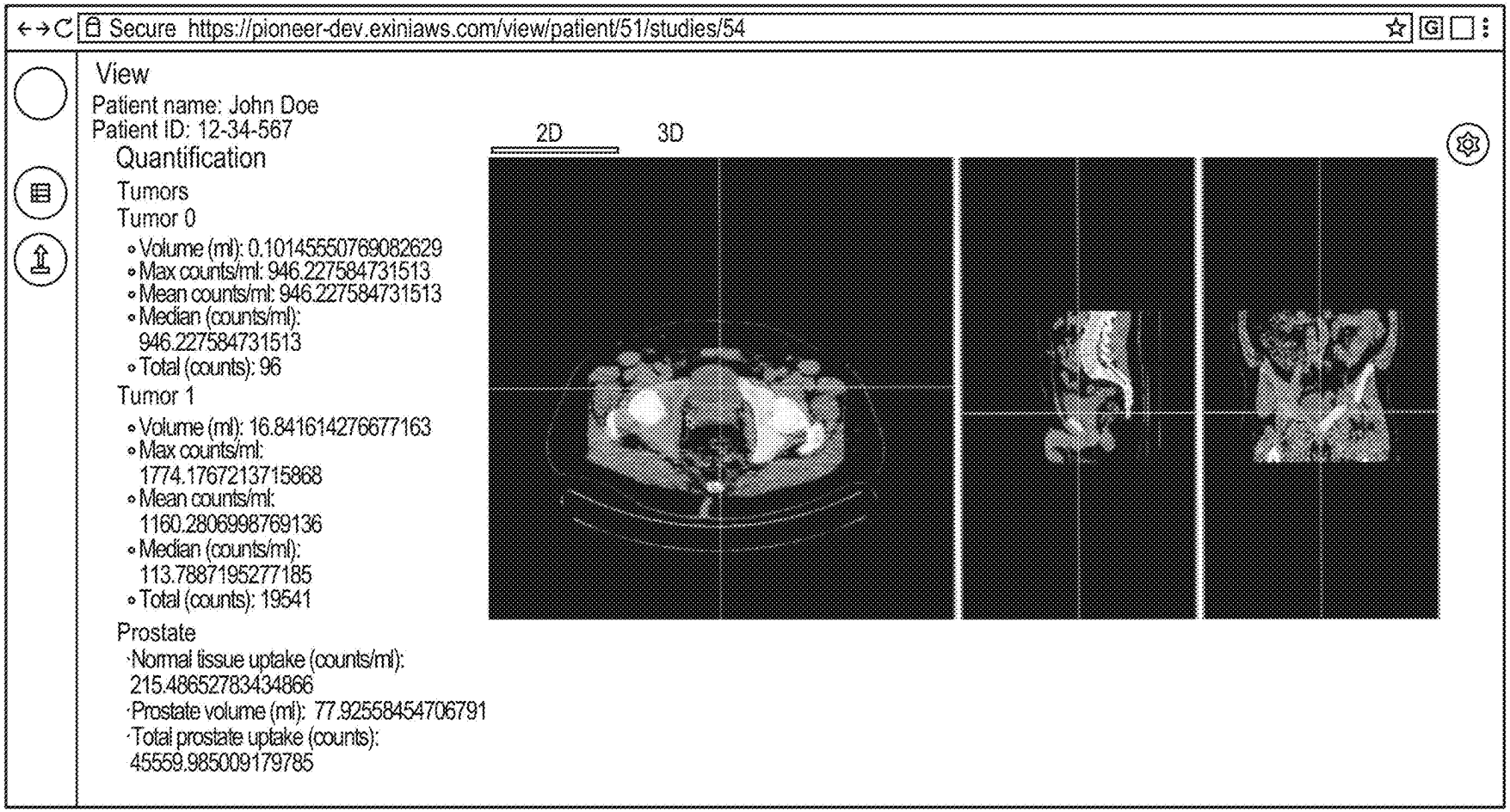

Secure https://pioneer-dev.exiniaws.com/view/patient/51/studies/54
View
Patient name: John Doe
Patient ID: 12-34-567
Quantification
Tumors
Tumor 0
Volume (ml): 0.10145550769082629
Max counts/ml: 946.227584731513
Mean counts/ml: 946.227584731513
Median (counts/ml): 946.227584731513
Total (counts): 96
Tumor 1
Volume (ml): 16.841614276677163
Max counts/ml: 1774.1767213715868
Mean counts/ml: 1160.2806998769136
Median (counts/ml): 113.78871952771185
Total (counts): 19541
Prostate
Normal tissue uptake (counts/ml): 215.48652783434866
Prostate volume (ml): 77.92558454706791
Total prostate uptake (counts): 45559.985009179785
2D
3D

FIG. 17C

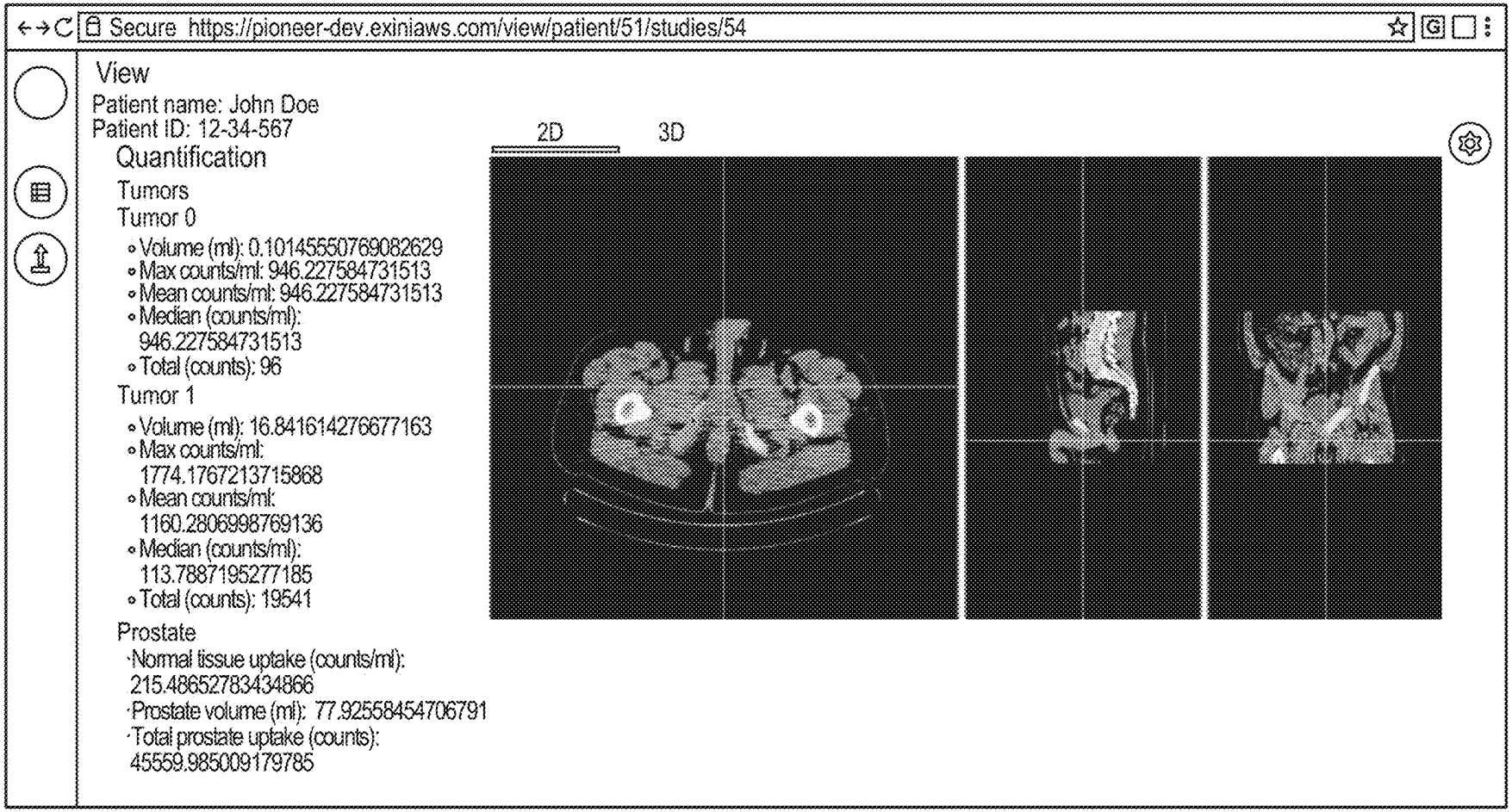

Secure https://pioneer-dev.exiniaws.com/view/patient/51/studies/54
View
Patient name: John Doe
Patient ID: 12-34-567
Quantification
Tumors
Tumor 0
Volume (ml): 0.10145550769082629
Max counts/ml: 946.227584731513
Mean counts/ml: 946.227584731513
Median (counts/ml): 946.227584731513
Total (counts): 96
Tumor 1
Volume (ml): 16.841614276677163
Max counts/ml: 1774.1767213715868
Mean counts/ml: 1160.2806998769136
Median (counts/ml): 113.78871952771 85
Total (counts): 19541
Prostate
Normal tissue uptake (counts/ml): 215.48652783434866
Prostate volume (ml): 77.92558454706791
Total prostate uptake (counts): 45559.985009179785
2D
3D

FIG. 17D

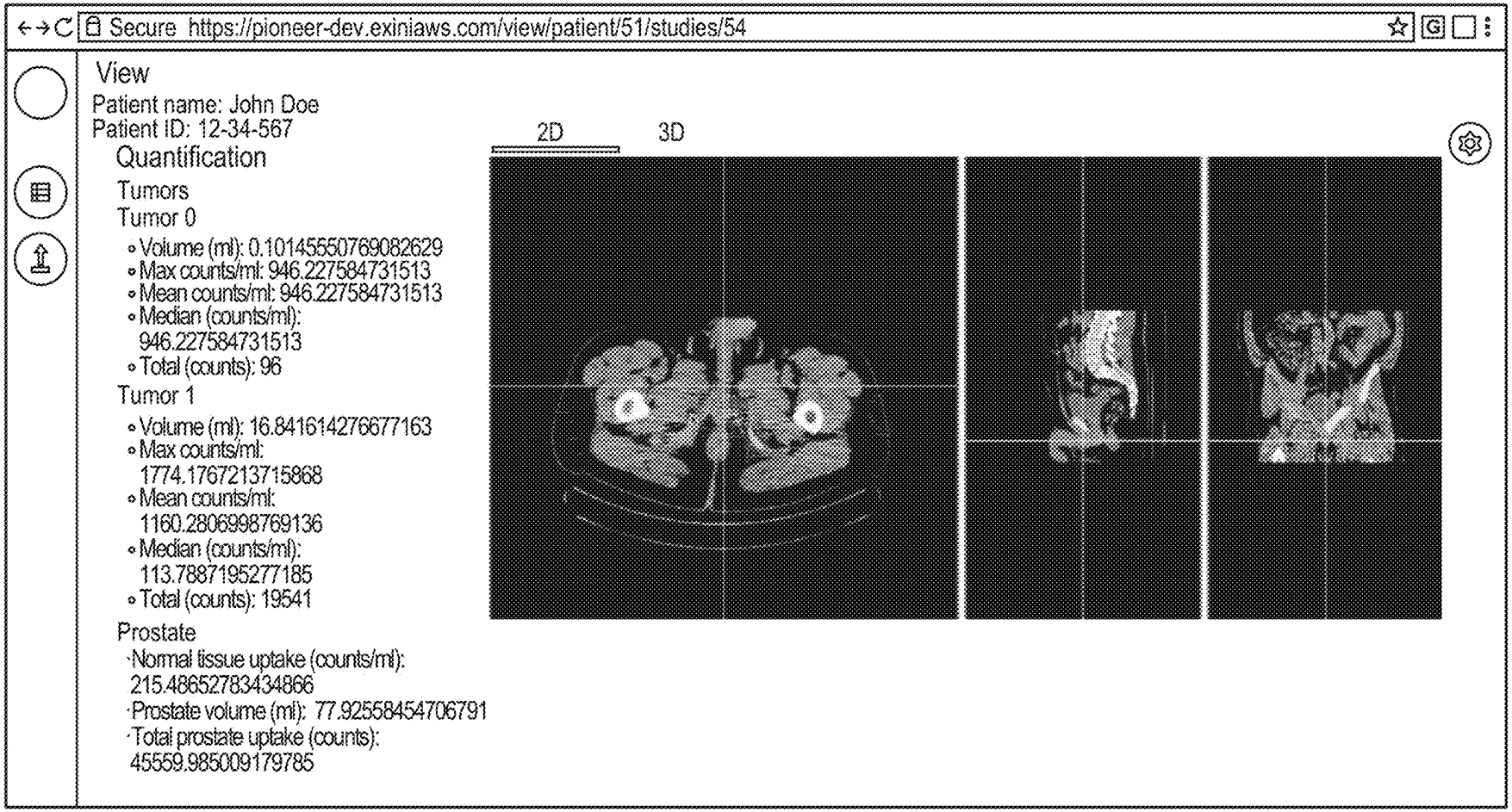

Secure https://pioneer-dev.exiniaws.com/view/patient/51/studies/54
View
Patient name: John Doe
Patient ID: 12-34-567
Quantification
Tumors
Tumor 0
Volume (ml): 0.10145550769082629
Max counts/ml: 946.227584731513
Mean counts/ml: 946.227584731513
Median (counts/ml): 946.227584731513
Total (counts): 96
Tumor 1
Volume (ml): 16.841614276677163
Max counts/ml: 1774.1767213715868
Mean counts/ml: 1160.2806998769136
Median (counts/ml): 113.78871952771 85
Total (counts): 19541
Prostate
Normal tissue uptake (counts/ml): 215.48652783434866
Prostate volume (ml): 77.92558454706791
Total prostate uptake (counts): 45559.985009179785
2D
3D

FIG. 17E

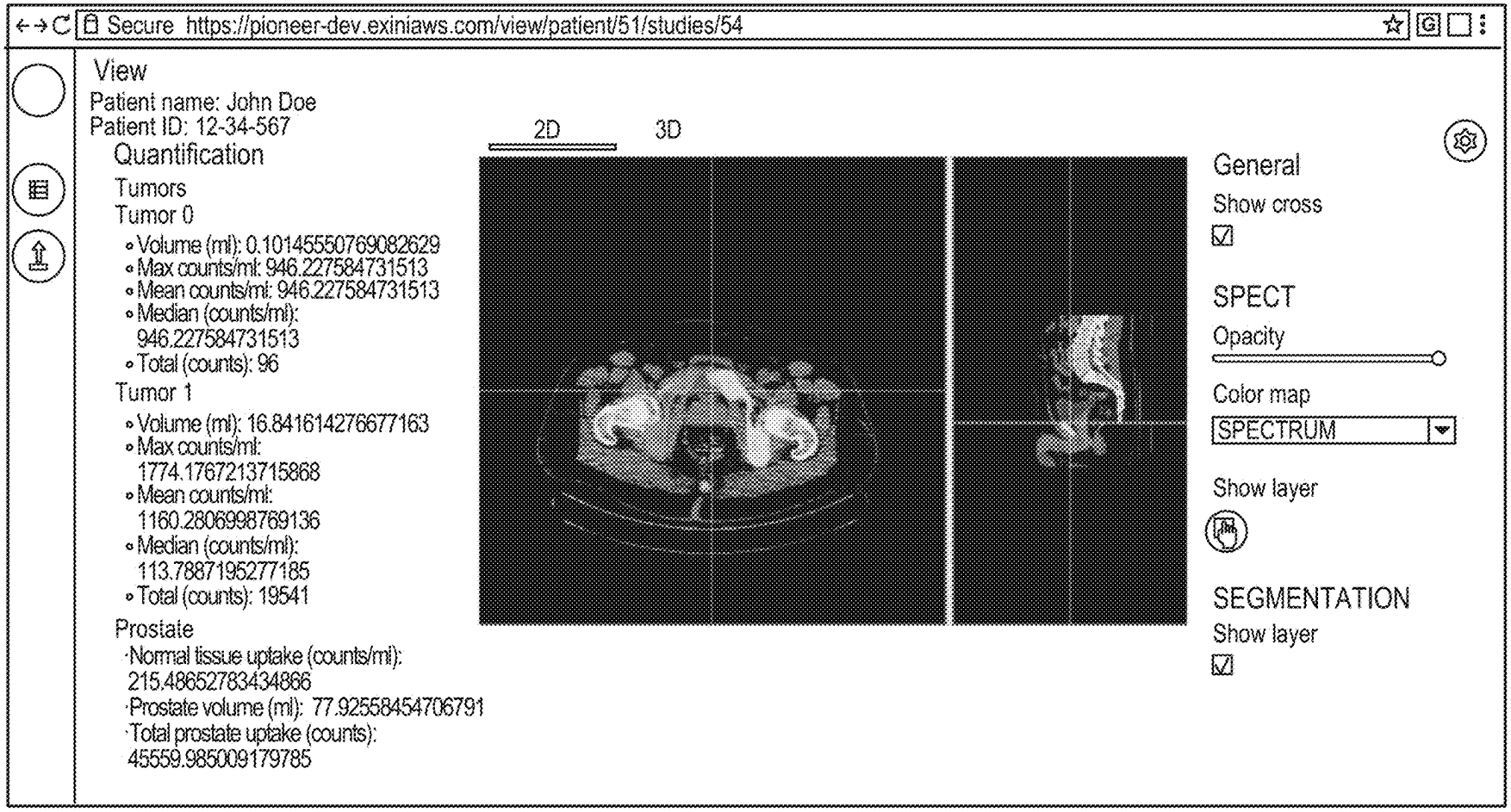

Secure https://pioneer-dev.exiniaws.com/view/patient/51/studies/54
View
Patient name: John Doe
Patient ID: 12-34-567
Quantification
Tumors
Tumor 0
Volume (ml): 0.10145550769082629
Max counts/ml: 946.227584731513
Mean counts/ml: 946.227584731513
Median (counts/ml): 946.227584731513
Total (counts): 96
Tumor 1
Volume (ml): 16.841614276677163
Max counts/ml: 1774.1767213715868
Mean counts/ml: 1160.2806998769136
Median (counts/ml): 113.7887195277185
Total (counts): 19541
Prostate
Normal tissue uptake (counts/ml): 215.48652783434866
Prostate volume (ml): 77.92558454706791
Total prostate uptake (counts): 45559.985009179785
2D
3D
General
Show cross
SPECT
Opacity
Color map
SPECTRUM
Show layer
SEGMENTATION
Show layer

FIG. 18A

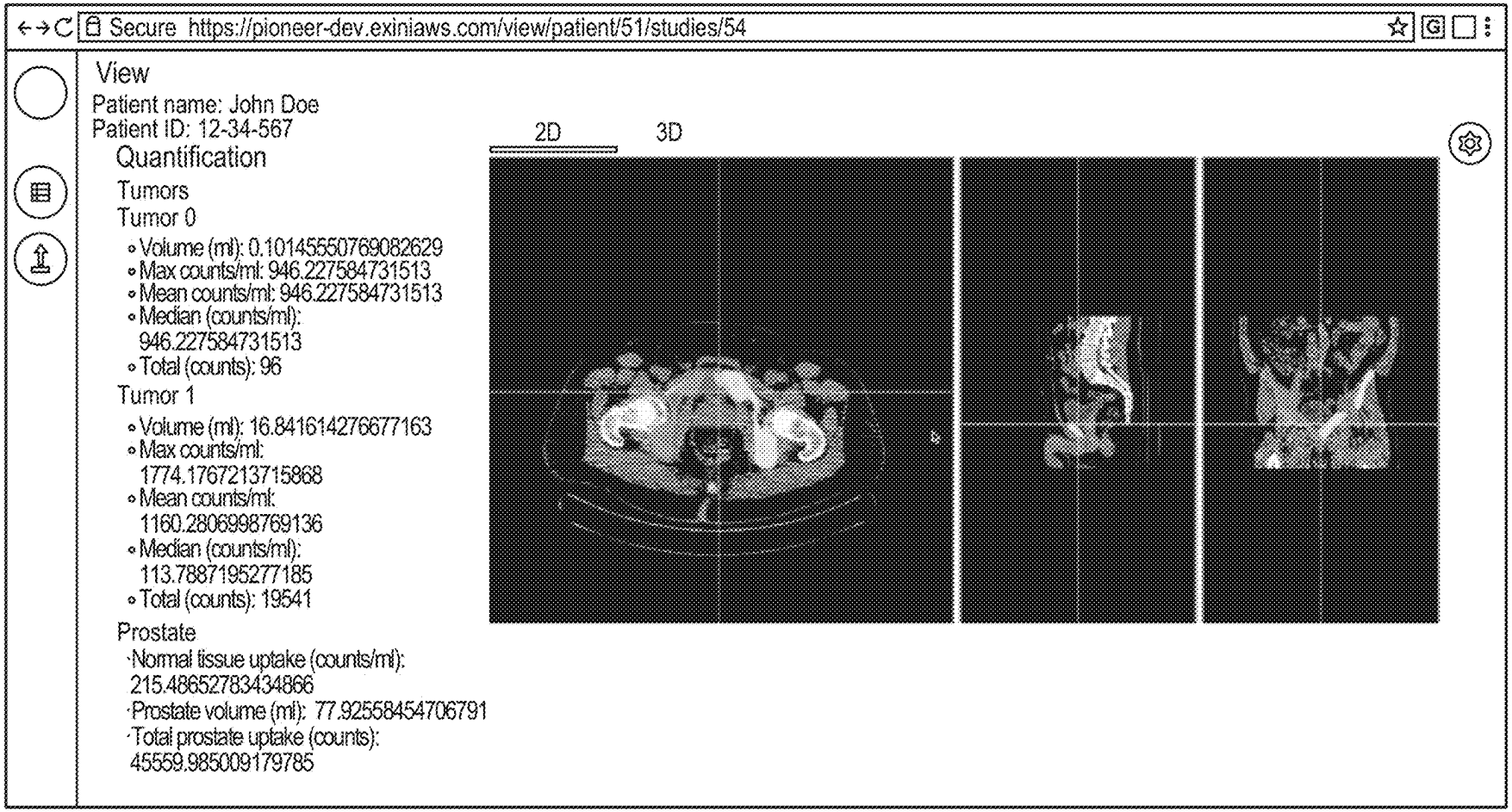

Secure https://pioneer-dev.exiniaws.com/view/patient/51/studies/54
View
Patient name: John Doe
Patient ID: 12-34-567
Quantification
Tumors
Tumor 0
Volume (ml): 0.10145550769082629
Max counts/ml: 946.227584731513
Mean counts/ml: 946.227584731513
Median (counts/ml): 946.227584731513
Total (counts): 96
Tumor 1
Volume (ml): 16.841614276677163
Max counts/ml: 1774.1767213715868
Mean counts/ml: 1160.2806998769136
Median (counts/ml): 113.78871952771 85
Total (counts): 19541
Prostate
Normal tissue uptake (counts/ml): 215.48652783434866
Prostate volume (ml): 77.92558454706791
Total prostate uptake (counts): 45559.985009179785
2D
3D

FIG. 18B

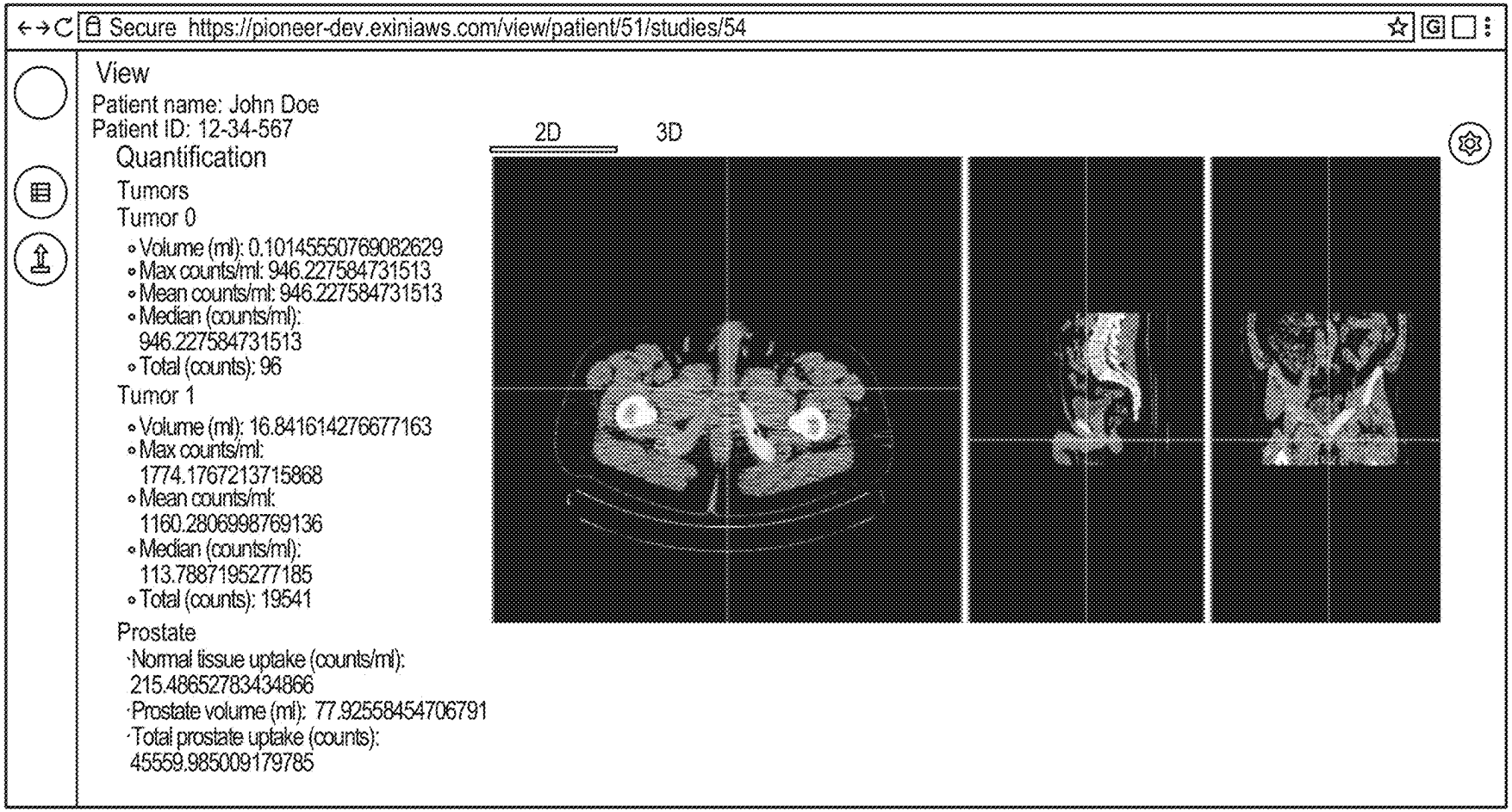

Secure https://pioneer-dev.exiniaws.com/view/patient/51/studies/54
View
Patient name: John Doe
Patient ID: 12-34-567
Quantification
Tumors
Tumor 0
Volume (ml): 0.10145550769082629
Max counts/ml: 946.227584731513
Mean counts/ml: 946.227584731513
Median (counts/ml): 946.227584731513
Total (counts): 96
Tumor 1
Volume (ml): 16.841614276677163
Max counts/ml: 1774.1767213715868
Mean counts/ml: 1160.2806998769136
Median (counts/ml): 113.78871952771 85
Total (counts): 19541
Prostate
Normal tissue uptake (counts/ml): 215.48652783434866
Prostate volume (ml): 77.92558454706791
Total prostate uptake (counts): 45559.985009179785
2D
3D

FIG. 18C

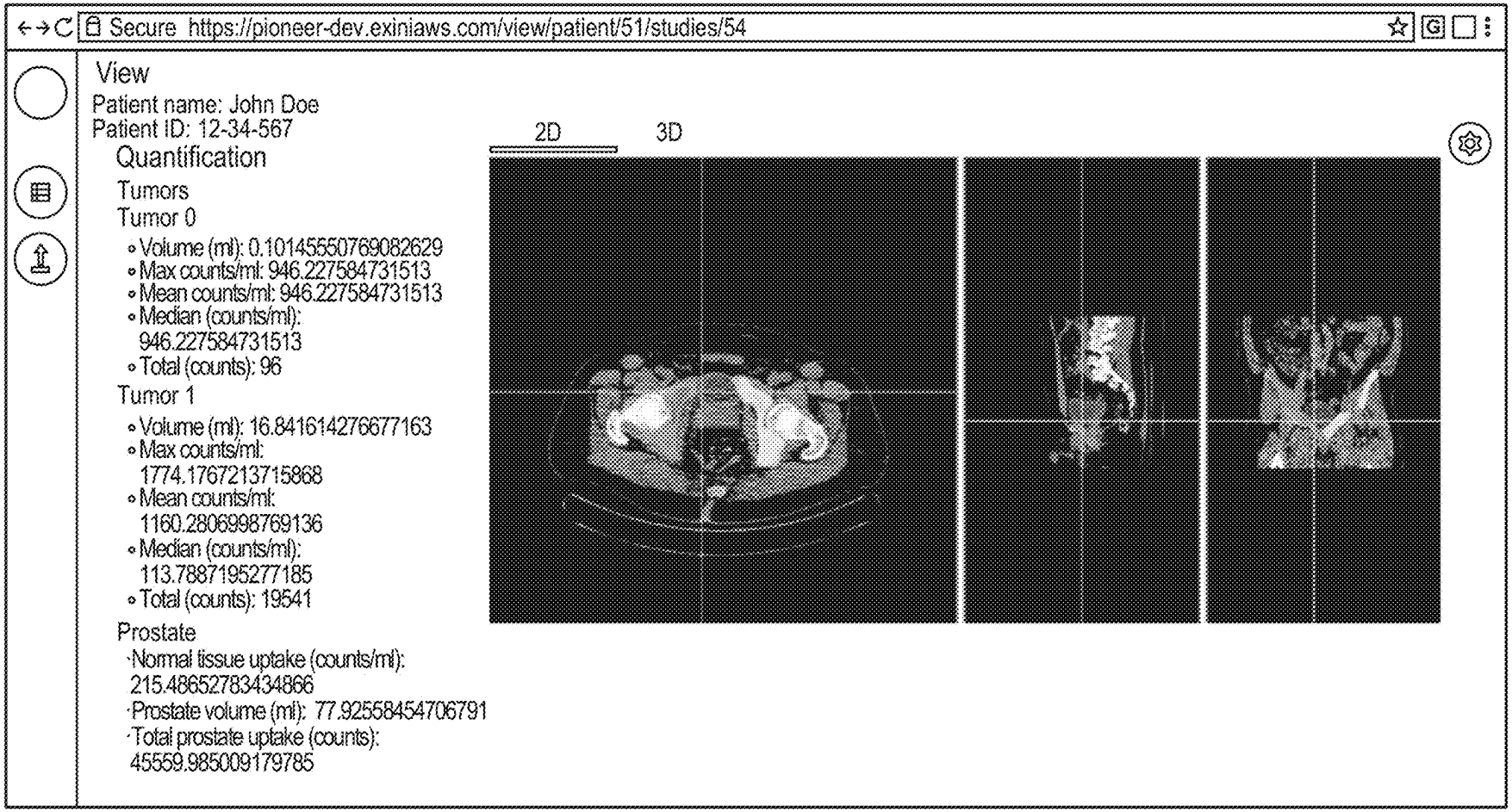

Secure https://pioneer-dev.exiniaws.com/view/patient/51/studies/54
View
Patient name: John Doe
Patient ID: 12-34-567
Quantification
Tumors
Tumor 0
Volume (ml): 0.10145550769082629
Max counts/ml: 946.227584731513
Mean counts/ml: 946.227584731513
Median (counts/ml): 946.227584731513
Total (counts): 96
Tumor 1
Volume (ml): 16.841614276677163
Max counts/ml: 1774.1767213715868
Mean counts/ml: 1160.2806998769136
Median (counts/ml): 113.78871952771185
Total (counts): 19541
Prostate
Normal tissue uptake (counts/ml): 215.48652783434866
Prostate volume (ml): 77.92558454706791
Total prostate uptake (counts): 45559.985009179785
2D
3D

FIG. 18D

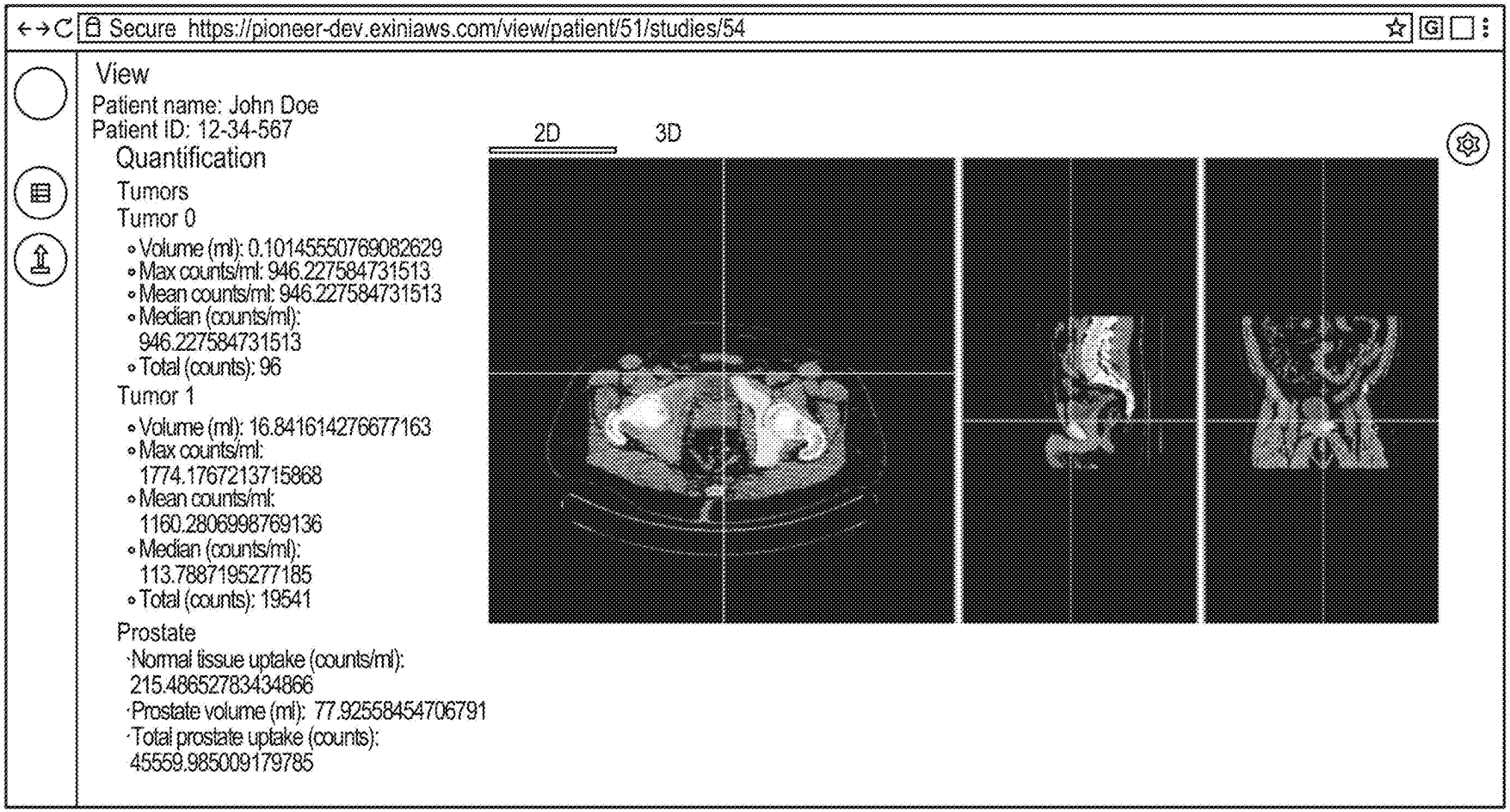

Secure https://pioneer-dev.exiniaws.com/view/patient/51/studies/54
View
Patient name: John Doe
Patient ID: 12-34-567
Quantification
Tumors
Tumor 0
Volume (ml): 0.10145550769082629
Max counts/ml: 946.227584731513
Mean counts/ml: 946.227584731513
Median (counts/ml): 946.227584731513
Total (counts): 96
Tumor 1
Volume (ml): 16.841614276677163
Max counts/ml: 1774.1767213715868
Mean counts/ml: 1160.2806998769136
Median (counts/ml): 113.78871952771 85
Total (counts): 19541
Prostate
Normal tissue uptake (counts/ml): 215.48652783434866
Prostate volume (ml): 77.92558454706791
Total prostate uptake (counts): 45559.985009179785
2D
3D

FIG. 18E

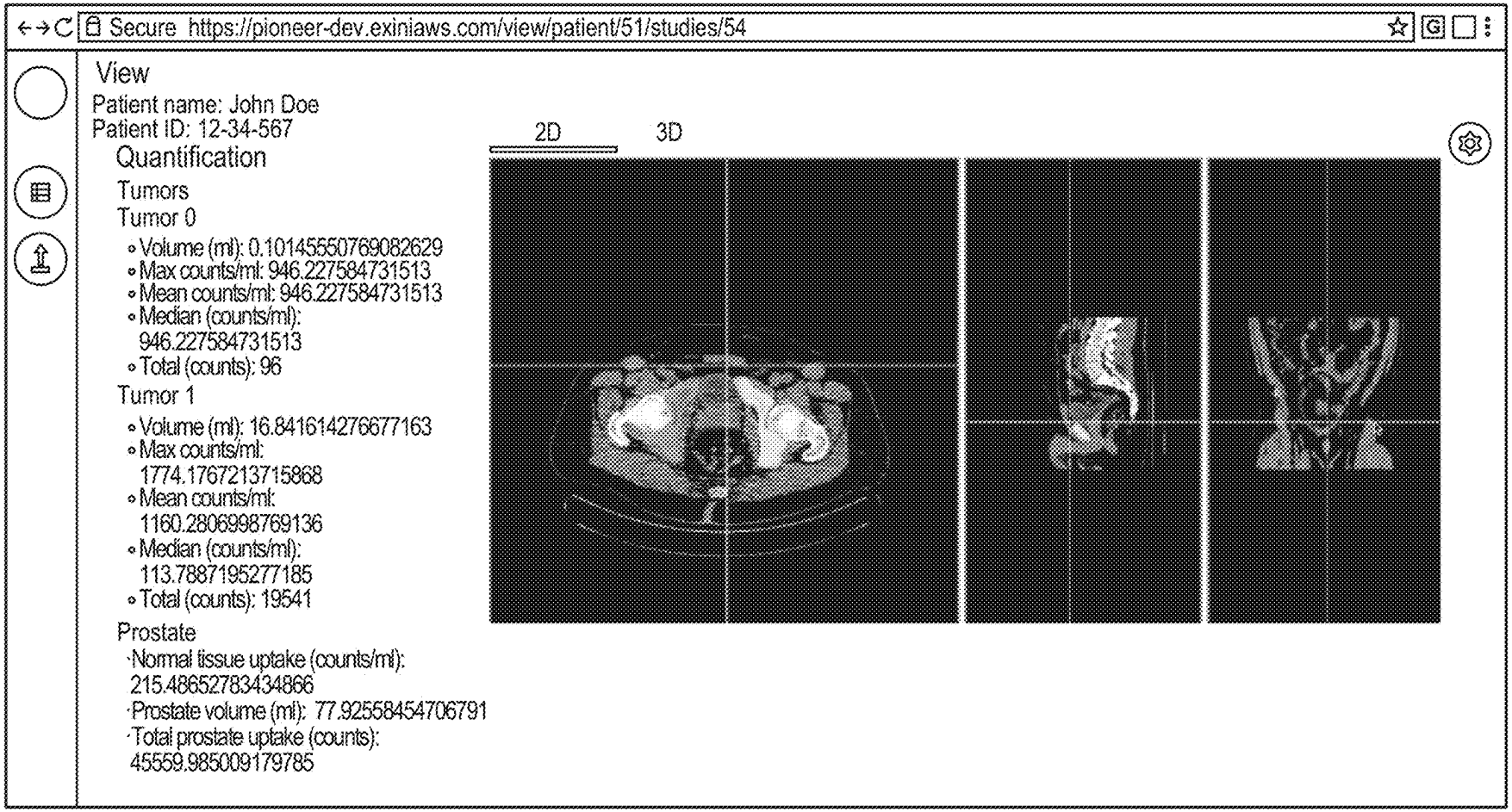

Secure https://pioneer-dev.exiniaws.com/view/patient/51/studies/54
View
Patient name: John Doe
Patient ID: 12-34-567
Quantification
Tumors
Tumor 0
Volume (ml): 0.10145550769082629
Max counts/ml: 946.227584731513
Mean counts/ml: 946.227584731513
Median (counts/ml): 946.227584731513
Total (counts): 96
Tumor 1
Volume (ml): 16.841614276677163
Max counts/ml: 1774.1767213715868
Mean counts/ml: 1160.2806998769136
Median (counts/ml): 113.78871952771 85
Total (counts): 19541
Prostate
Normal tissue uptake (counts/ml): 215.48652783434866
Prostate volume (ml): 77.92558454706791
Total prostate uptake (counts): 45559.985009179785
2D
3D

FIG. 18F

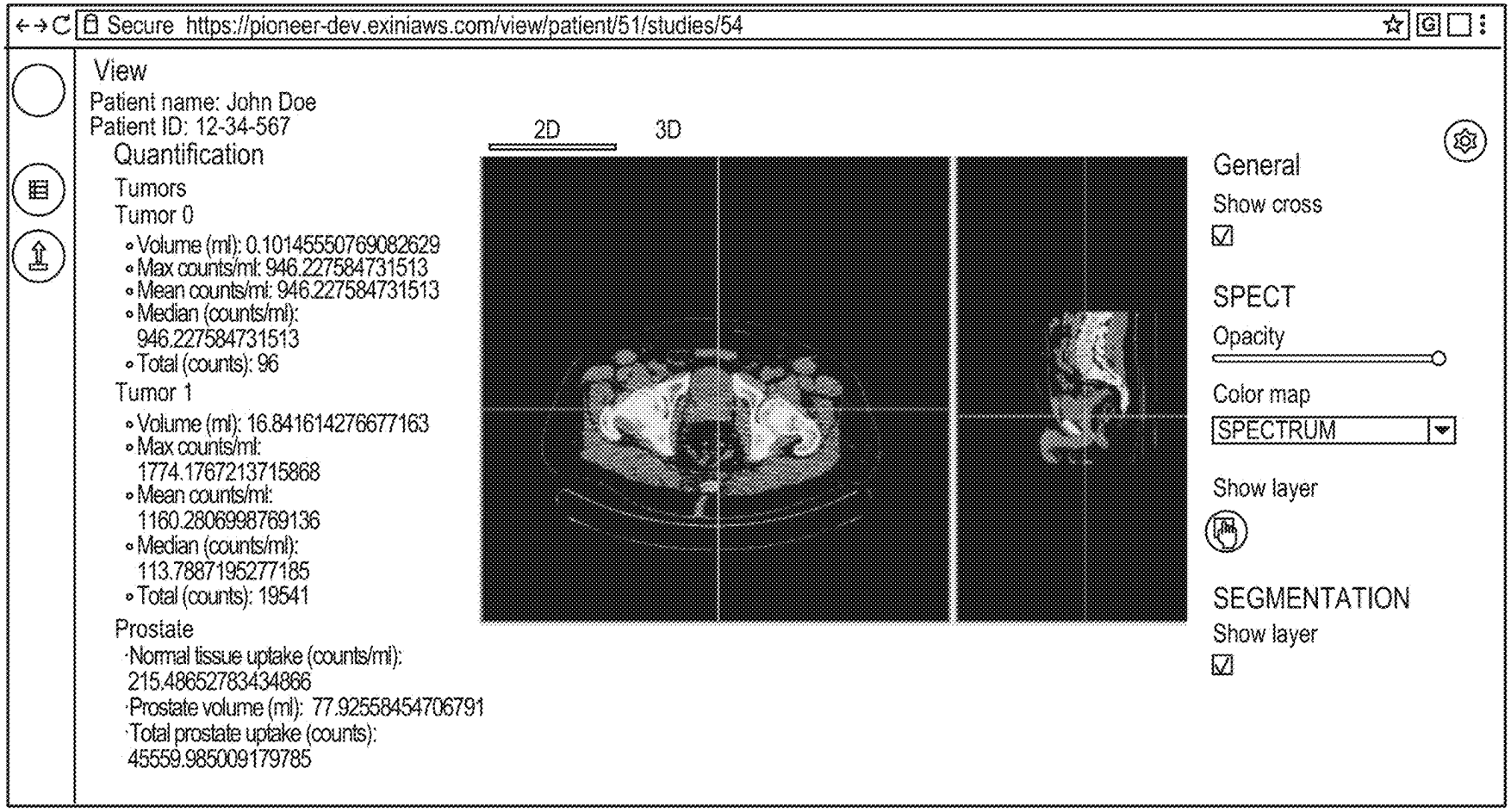

Secure https://pioneer-dev.exiniaws.com/view/patient/51/studies/54
View
Patient name: John Doe
Patient ID: 12-34-567
Quantification
Tumors
Tumor 0
Volume (ml): 0.10145550769082629
Max counts/ml: 946.227584731513
Mean counts/ml: 946.227584731513
Median (counts/ml): 946.227584731513
Total (counts): 96
Tumor 1
Volume (ml): 16.841614276677163
Max counts/ml: 1774.1767213715868
Mean counts/ml: 1160.2806998769136
Median (counts/ml): 113.7887195277185
Total (counts): 19541
Prostate
Normal tissue uptake (counts/ml): 215.48652783434866
Prostate volume (ml): 77.92558454706791
Total prostate uptake (counts): 45559.985009179785
2D
3D
General
Show cross
SPECT
Opacity
Color map
SPECTRUM
Show layer
SEGMENTATION
Show layer

FIG. 19A

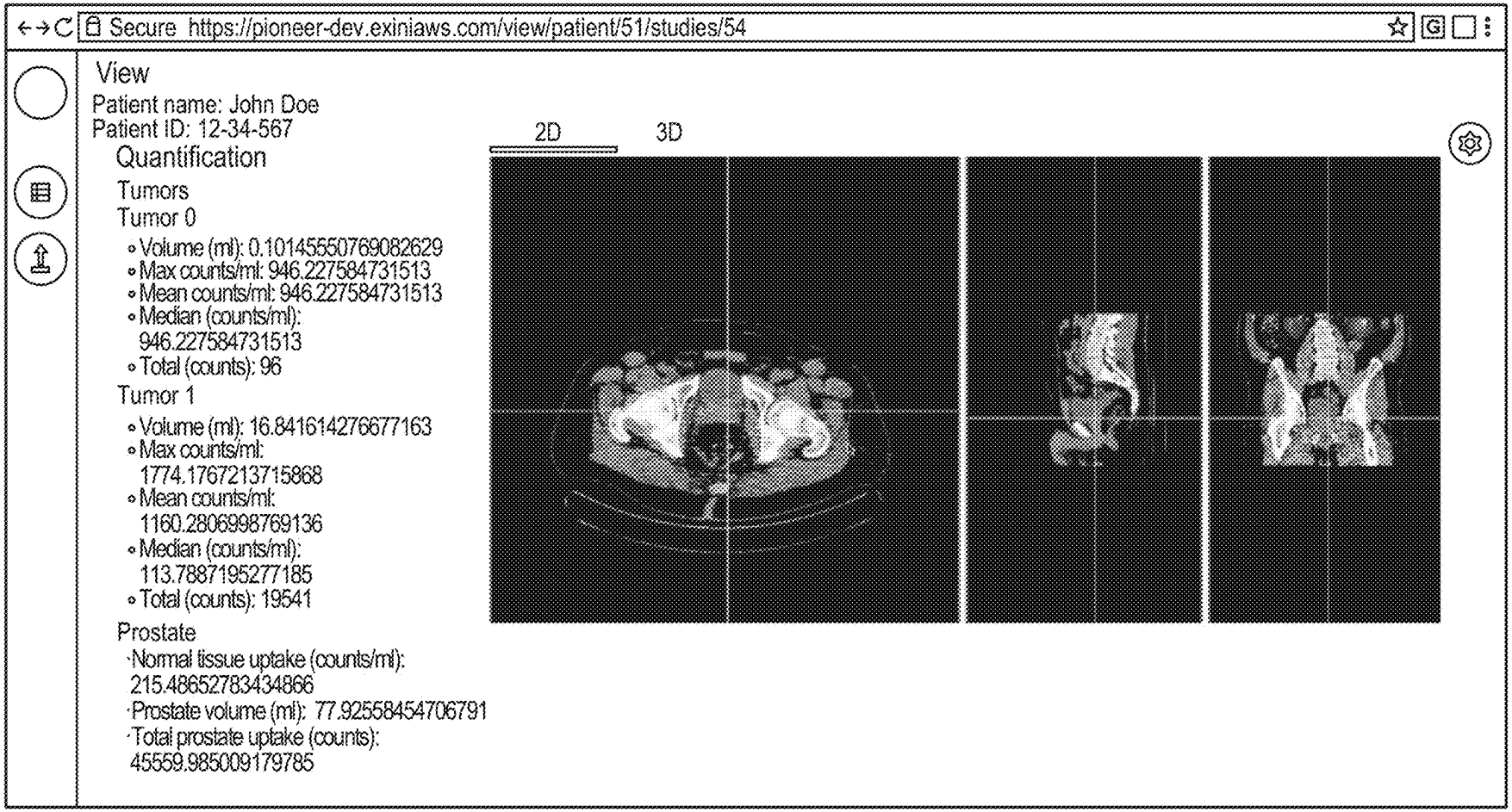

Secure https://pioneer-dev.exiniaws.com/view/patient/51/studies/54
View
Patient name: John Doe
Patient ID: 12-34-567
Quantification
Tumors
Tumor 0
Volume (ml): 0.10145550769082629
Max counts/ml: 946.227584731513
Mean counts/ml: 946.227584731513
Median (counts/ml): 946.227584731513
Total (counts): 96
Tumor 1
Volume (ml): 16.841614276677163
Max counts/ml: 1774.1767213715868
Mean counts/ml: 1160.2806998769136
Median (counts/ml): 113.78871952771 85
Total (counts): 19541
Prostate
Normal tissue uptake (counts/ml): 215.48652783434866
Prostate volume (ml): 77.92558454706791
Total prostate uptake (counts): 45559.985009179785
2D
3D

FIG. 19B

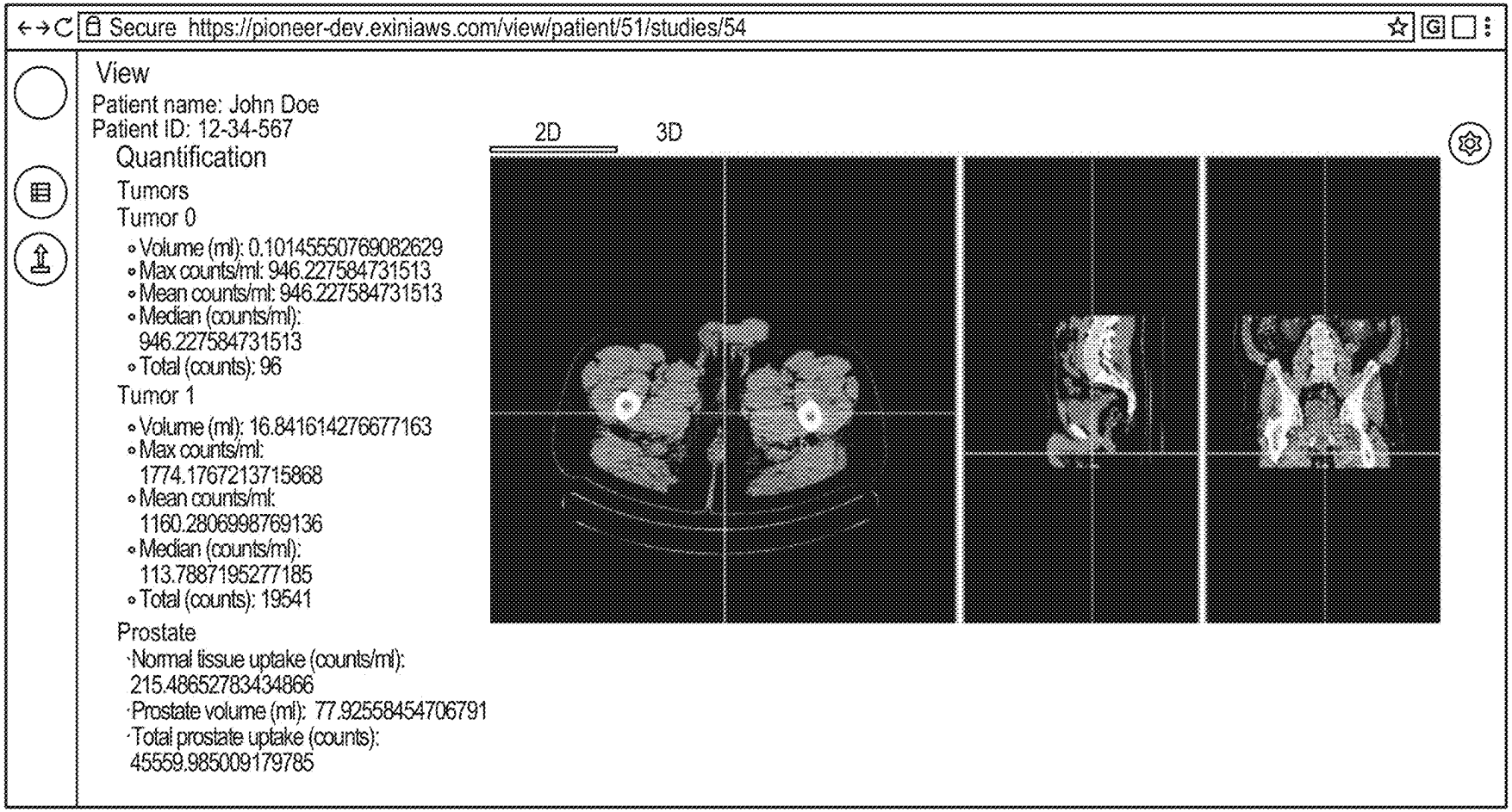

Secure https://pioneer-dev.exiniaws.com/view/patient/51/studies/54
View
Patient name: John Doe
Patient ID: 12-34-567
Quantification
Tumors
Tumor 0
Volume (ml): 0.10145550769082629
Max counts/ml: 946.227584731513
Mean counts/ml: 946.227584731513
Median (counts/ml): 946.227584731513
Total (counts): 96
Tumor 1
Volume (ml): 16.841614276677163
Max counts/ml: 1774.1767213715868
Mean counts/ml: 1160.2806998769136
Median (counts/ml): 113.78871952771185
Total (counts): 19541
Prostate
Normal tissue uptake (counts/ml): 215.48652783434866
Prostate volume (ml): 77.92558454706791
Total prostate uptake (counts): 45559.985009179785
2D
3D

FIG. 19C

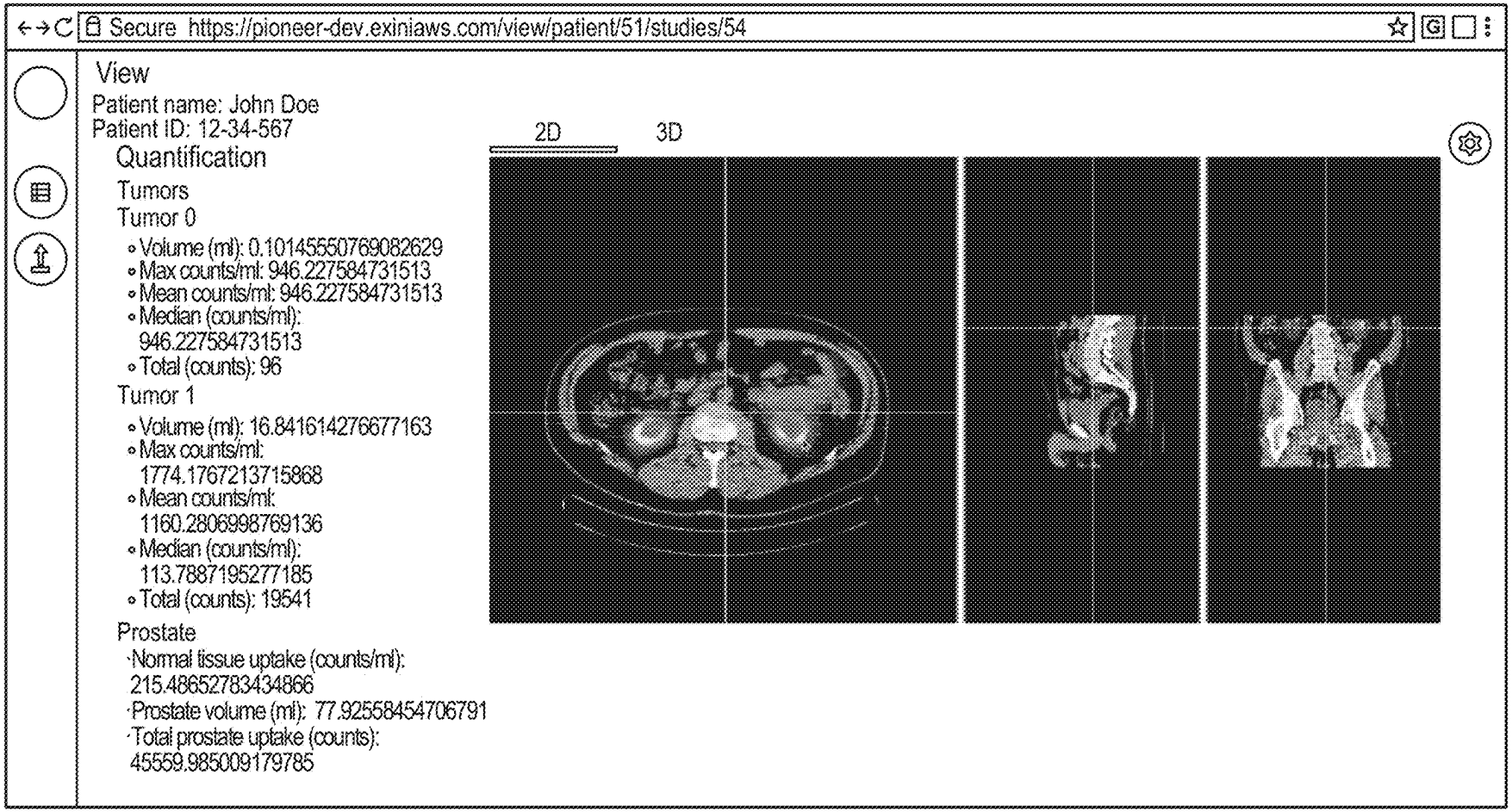

Secure https://pioneer-dev.exiniaws.com/view/patient/51/studies/54
View
Patient name: John Doe
Patient ID: 12-34-567
Quantification
Tumors
Tumor 0
Volume (ml): 0.10145550769082629
Max counts/ml: 946.227584731513
Mean counts/ml: 946.227584731513
Median (counts/ml): 946.227584731513
Total (counts): 96
Tumor 1
Volume (ml): 16.841614276677163
Max counts/ml: 1774.1767213715868
Mean counts/ml: 1160.2806998769136
Median (counts/ml): 113.78871952771 85
Total (counts): 19541
Prostate
Normal tissue uptake (counts/ml): 215.48652783434866
Prostate volume (ml): 77.92558454706791
Total prostate uptake (counts): 45559.985009179785
2D
3D

FIG. 19D



FIG. 20A



FIG. 20B

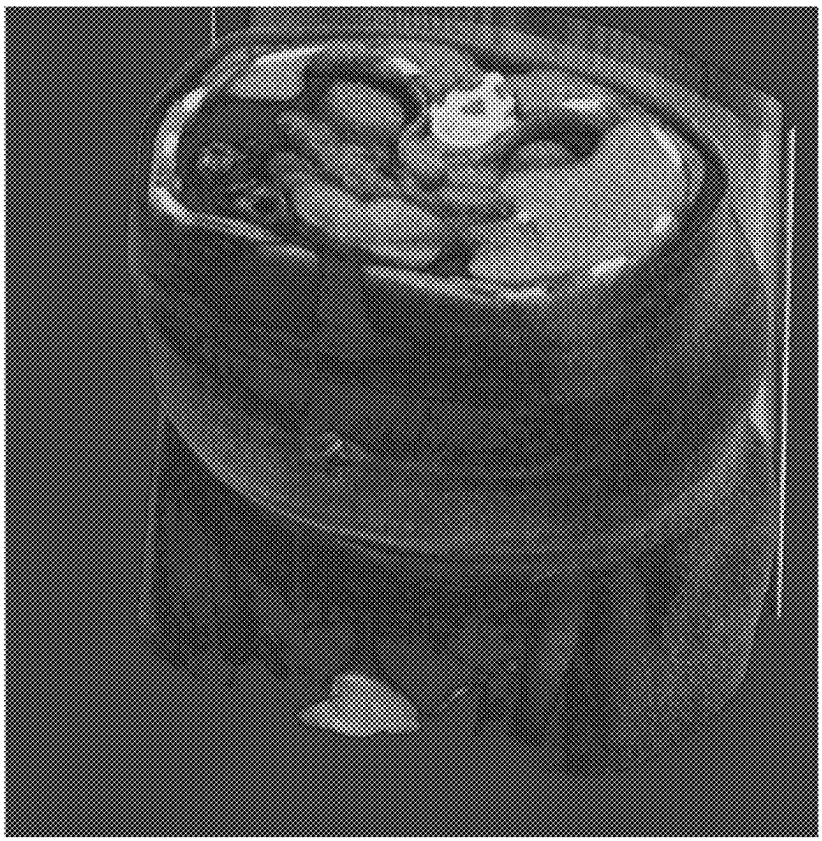


FIG. 20C

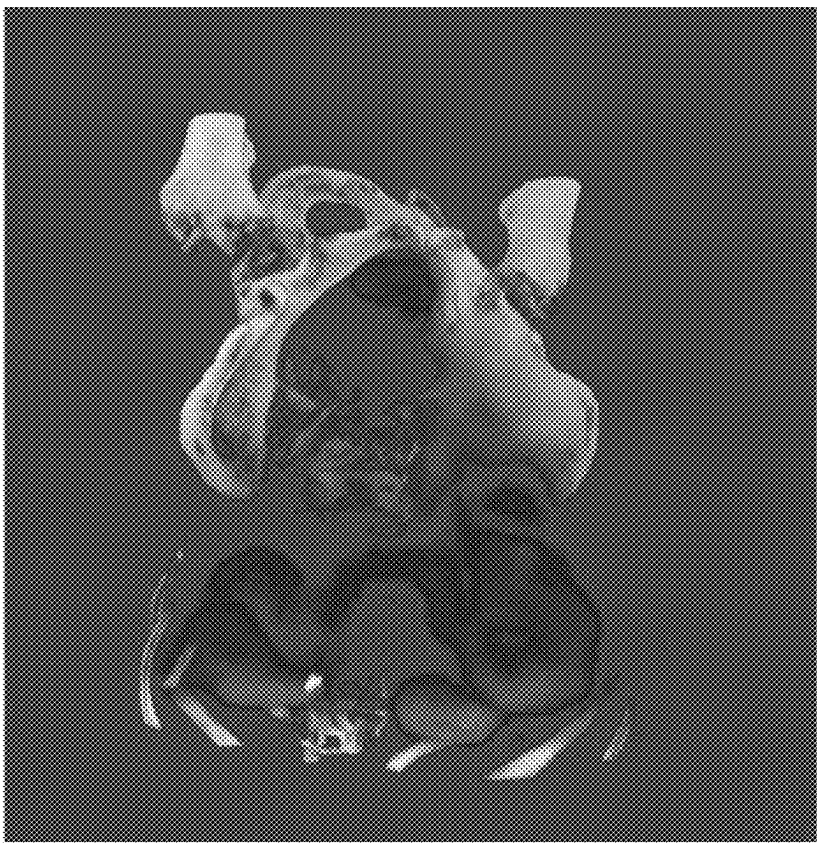


FIG. 21A



FIG. 21B

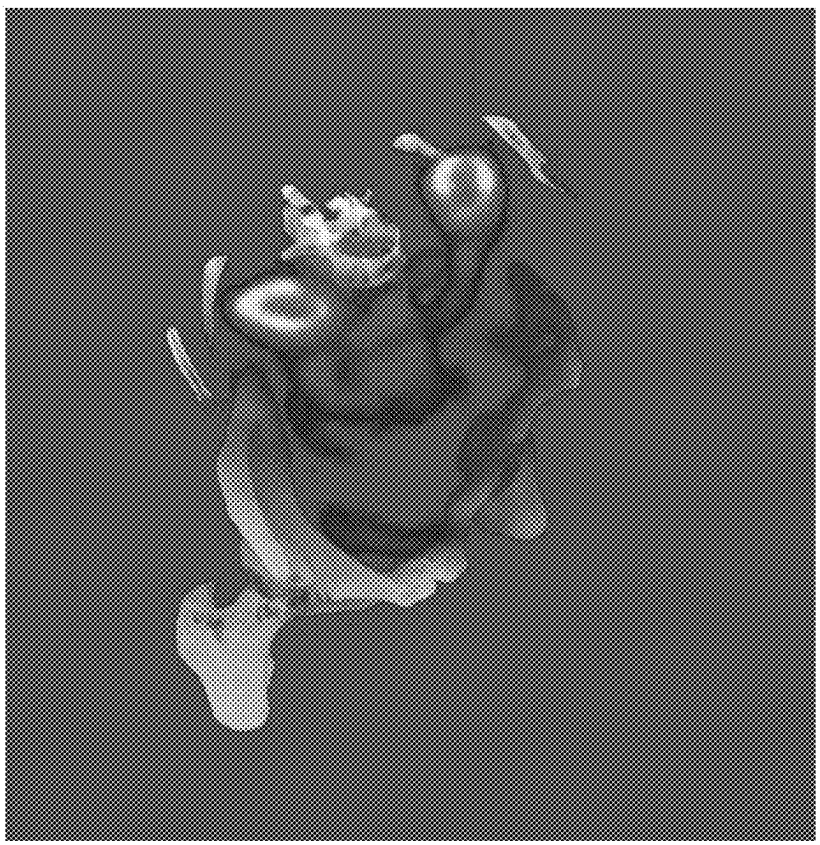


FIG. 22A

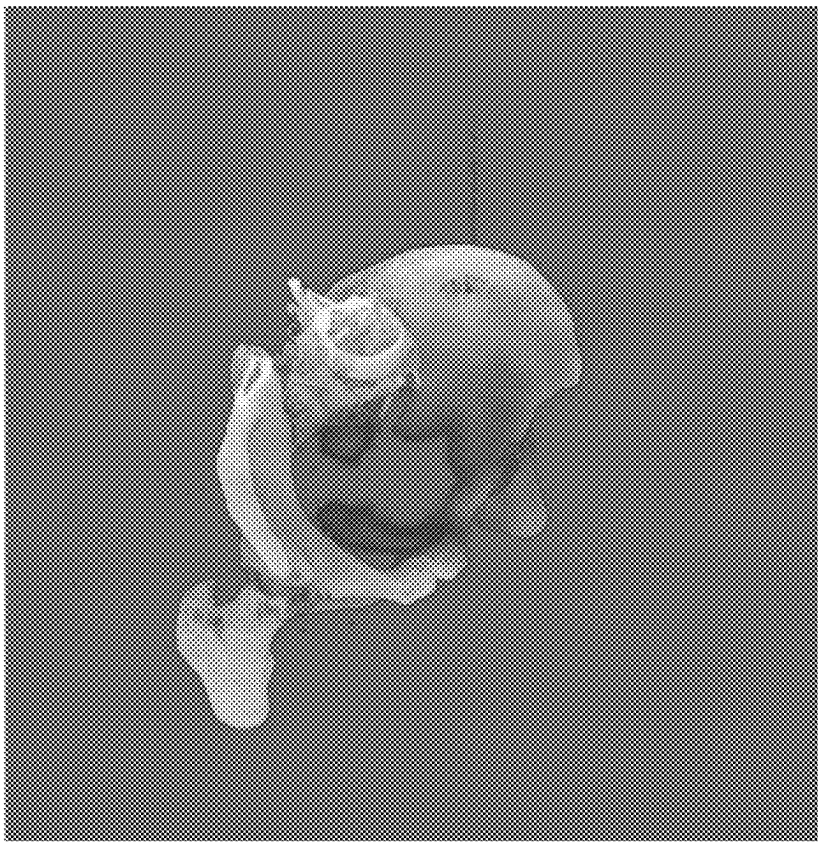


FIG. 22B

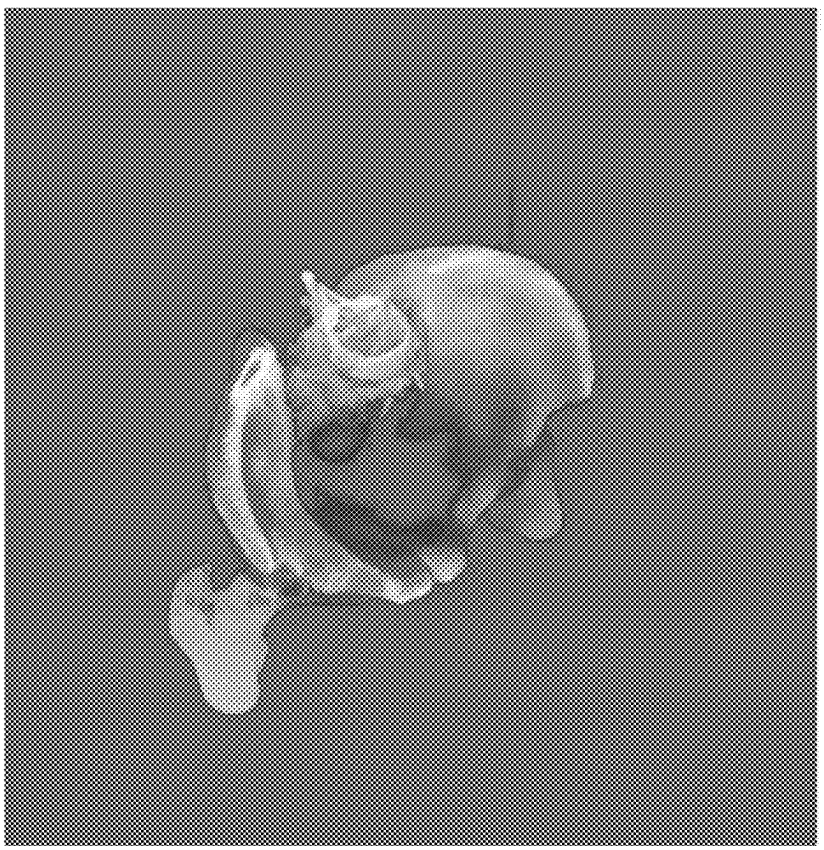


FIG. 22C



FIG. 22D

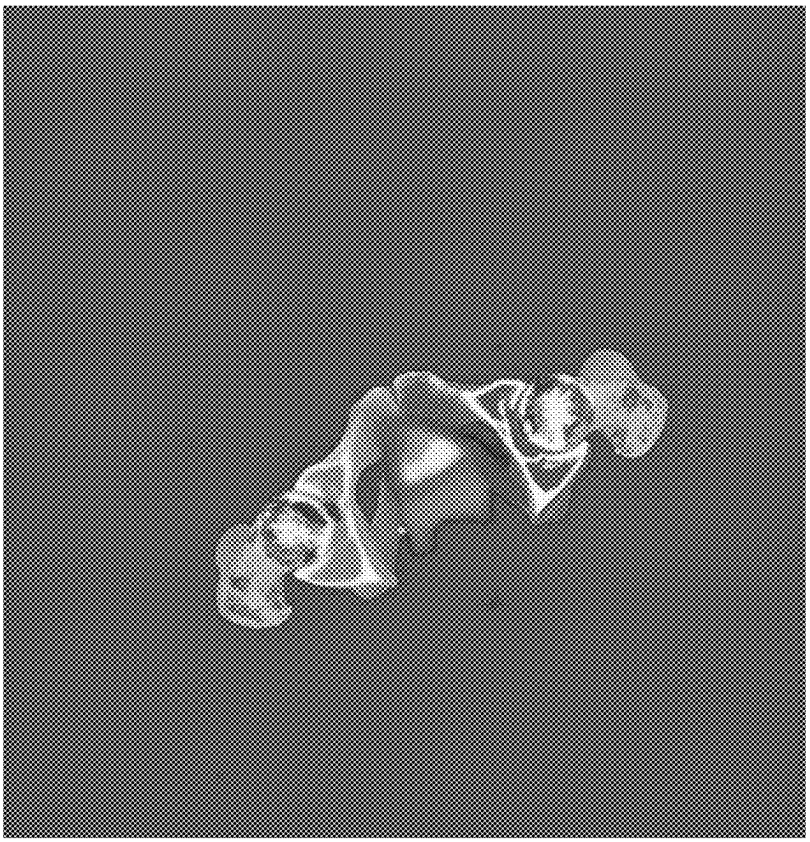


FIG. 22E

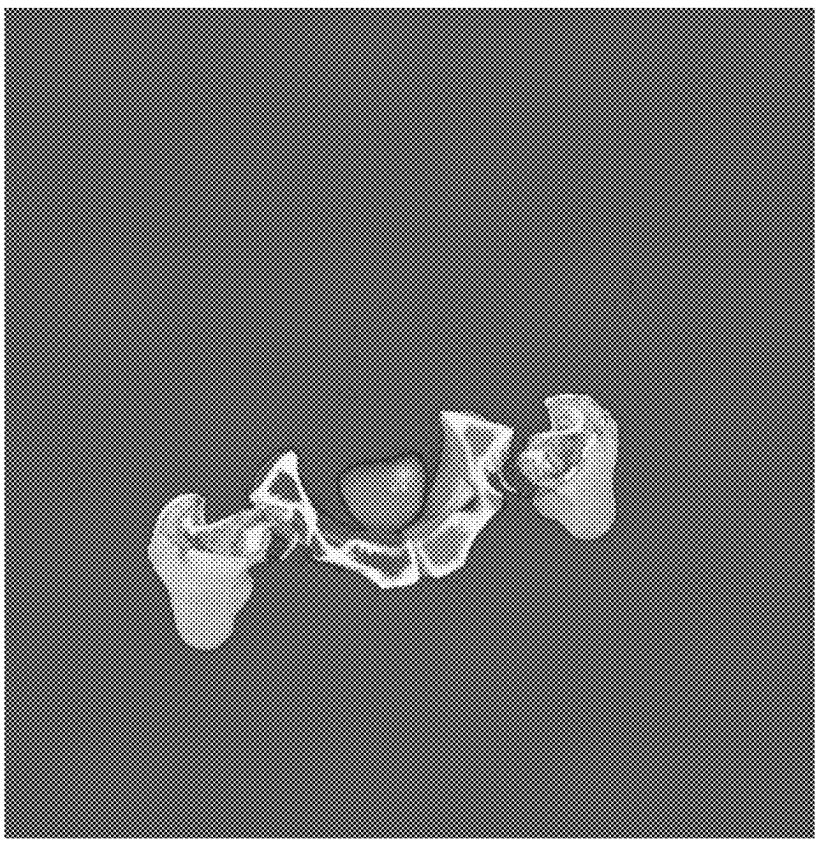


FIG. 22F



FIG. 23A

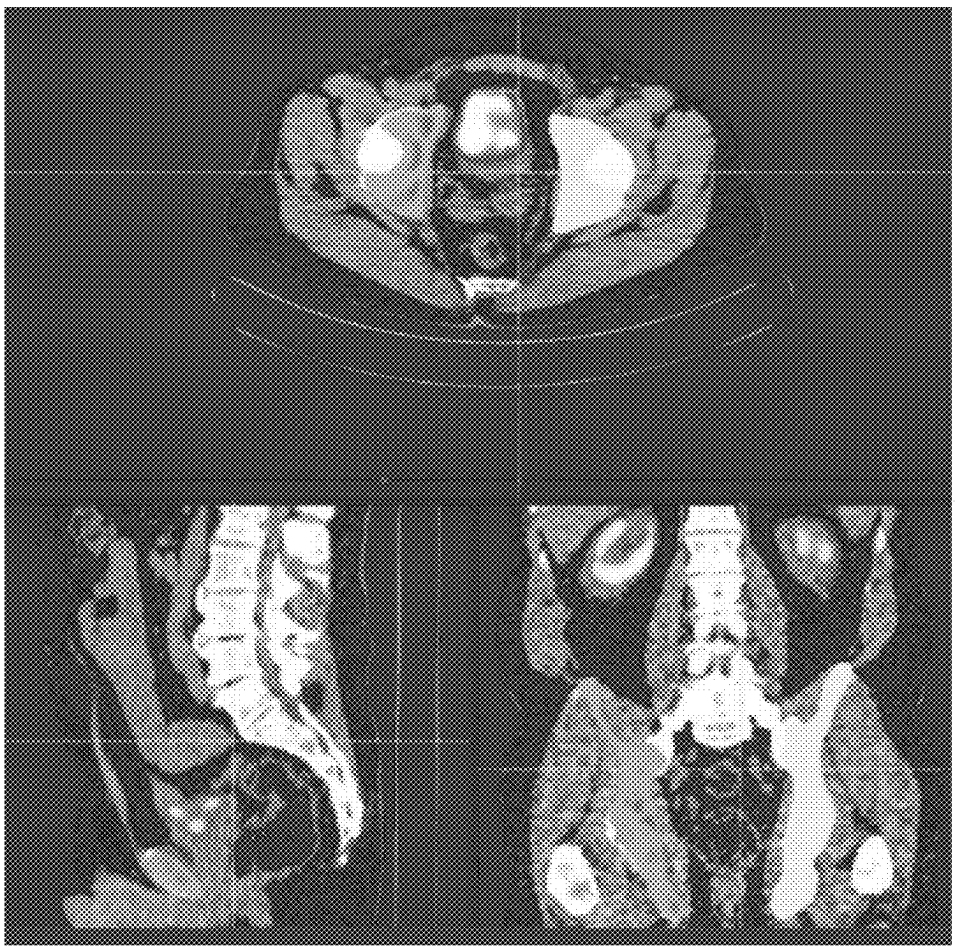


FIG. 23B

Report

REPORT DATE

DIAGNOSTIC DEVICE
Pioneer Web 1404 CADx

esc

Patient

PATIENT NAME

PATIENT ID

AGE <BIRTH DATE>

Study data

STUDY DATE

INDEX
1.24

PREVIOUS STUDY INDEX
2.62

TECHNICIAN

PHYSICIAN

COMMENT
Lorem ipsum dolor sit amet, consectetur adipiscing elit. Morbi cursus nisi enim, ac fringilla sem accumsan quis. Cras nec arcu sed nulla elementum tinidunt faucibus a felis. Aenean a convallis arcu. Cras ac leo at leo bibendum placerat ac sit

STUDY DESCRIPTION
Lorem ipsum dolor sit amet ads

Tumor data

	TUMOR #1	TUMOR #2
Volume (ml)	7.7	7.7
Max (counts/ml)	29.312	29.312
Mean (counts/ml)	17.336	17.336
Median (counts/ml)	16.402	16.402
Max voxel intensity	3.232	3.232
Total (counts)	133.808	133.808

Prostate data

NORMAL TISSUE UPTAKE (COUNTS/ML)
731.8

PROSTATE VOLUME (ML)
80.7

TOTAL PROSTATE UPTAKE (COUNTS)
386.933

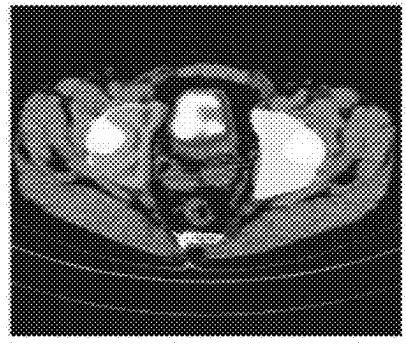


FIG. 24

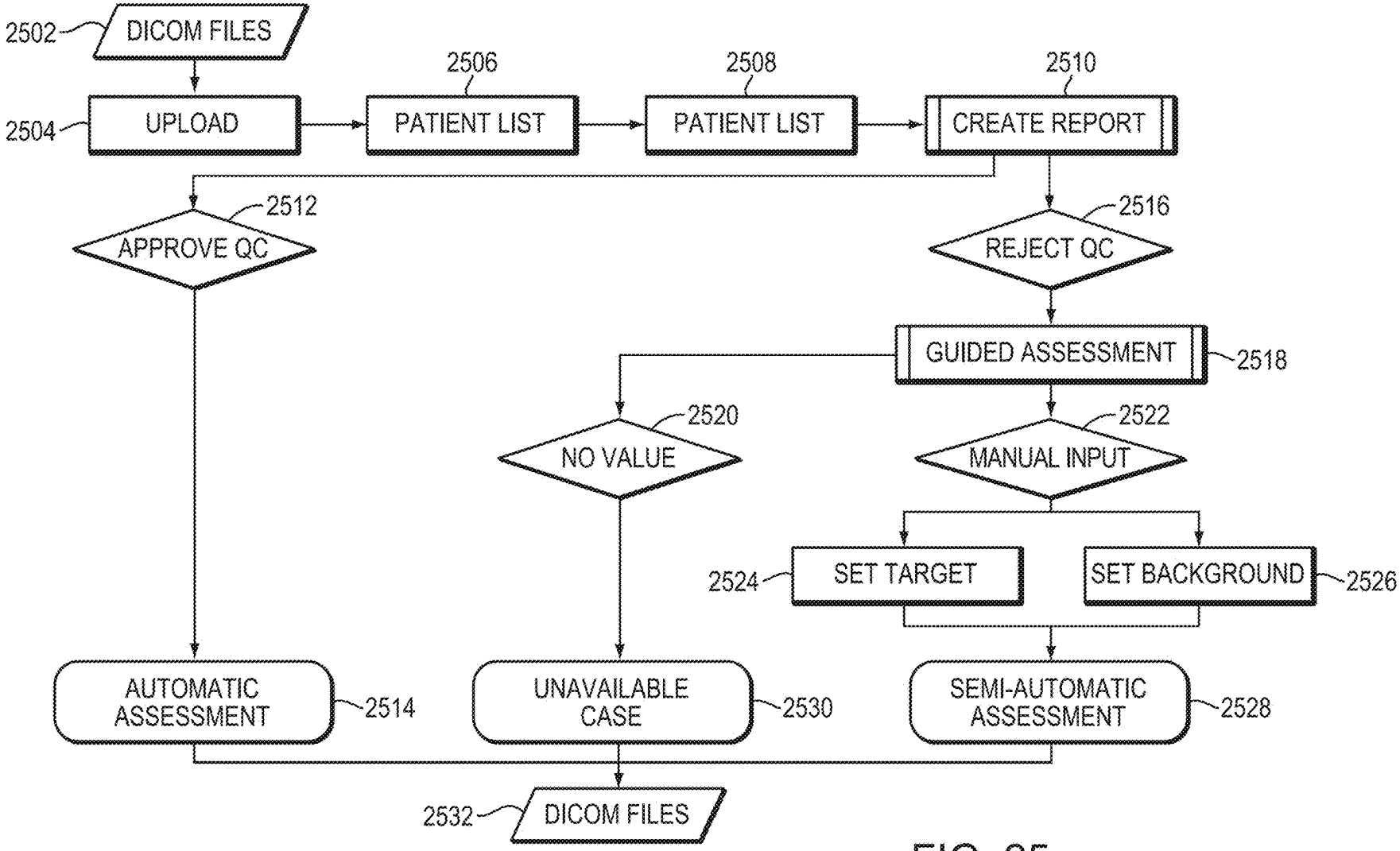

2502
DICOM FILES
2504
UPLOAD
2506
PATIENT LIST
2508
PATIENT LIST
2510
CREATE REPORT
2512
APPROVE QC
2516
REJECT QC
GUIDED ASSESSMENT
2518
2520
NO VALUE
2522
MANUAL INPUT
2524
SET TARGET
SET BACKGROUND
2526
AUTOMATIC ASSESSMENT
2514
UNAVAILABLE CASE
2530
SEMI-AUTOMATIC ASSESSMENT
2528
2532
DICOM FILES

FIG. 25

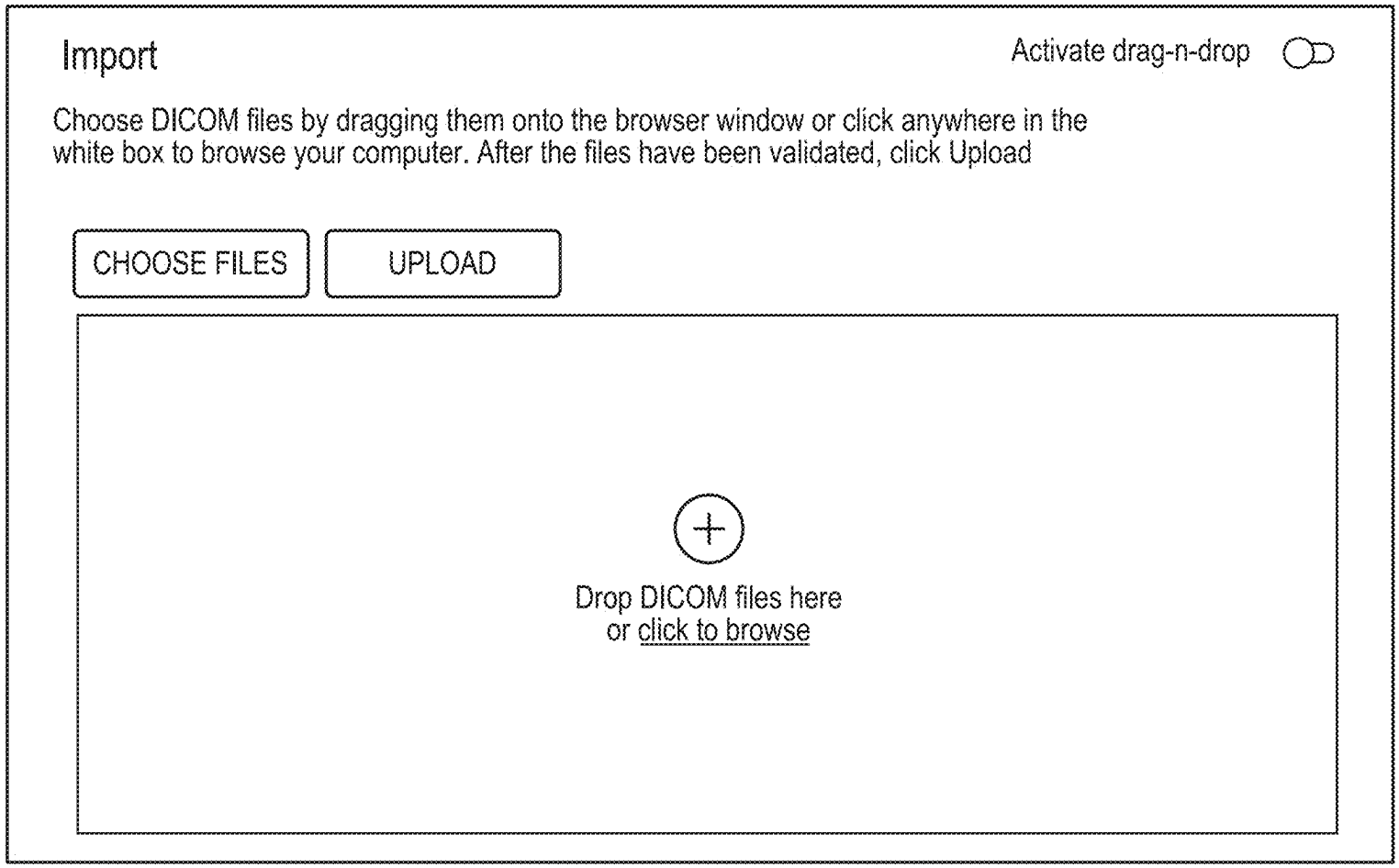

2600a
Import
Activate drag-n-drop
Choose DICOM files by dragging them onto the browser window or click anywhere in the white box to browse your computer. After the files have been validated, click Upload
CHOOSE FILES
UPLOAD
Drop DICOM files here
or click to browse

FIG. 26A

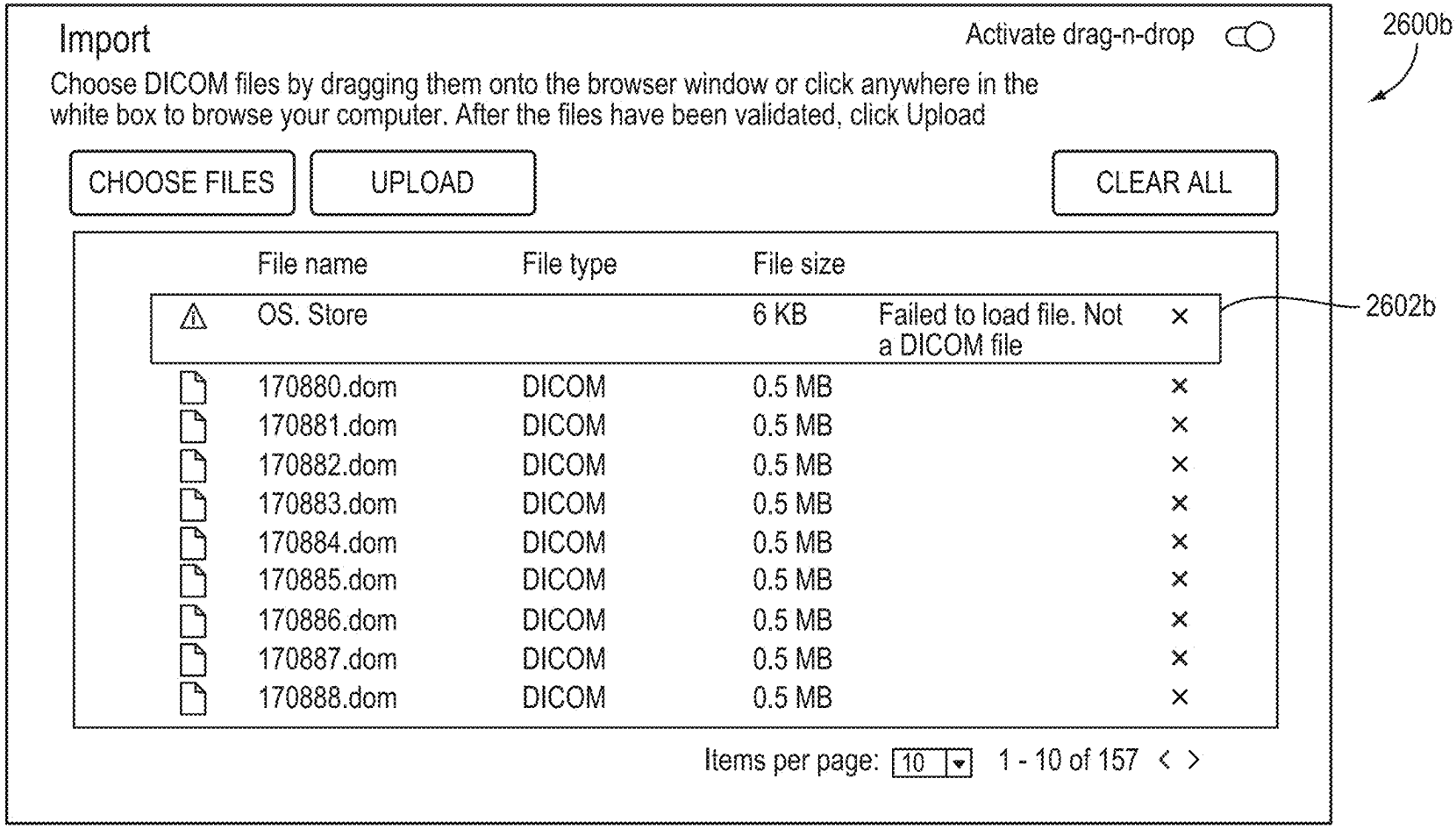

Import
Activate drag-n-drop
Choose DICOM files by dragging them onto the browser window or click anywhere in the white box to browse your computer. After the files have been validated, click Upload
CHOOSE FILES
UPLOAD
CLEAR ALL
File name
File type
File size
OS. Store
6 KB
Failed to load file. Not a DICOM file
170880.dom DICOM 0.5 MB
170881.dom DICOM 0.5 MB
170882.dom DICOM 0.5 MB
170883.dom DICOM 0.5 MB
170884.dom DICOM 0.5 MB
170885.dom DICOM 0.5 MB
170886.dom DICOM 0.5 MB
170887.dom DICOM 0.5 MB
170888.dom DICOM 0.5 MB
Items per page: 10
1 - 10 of 157
2600b
2602b

FIG. 26B

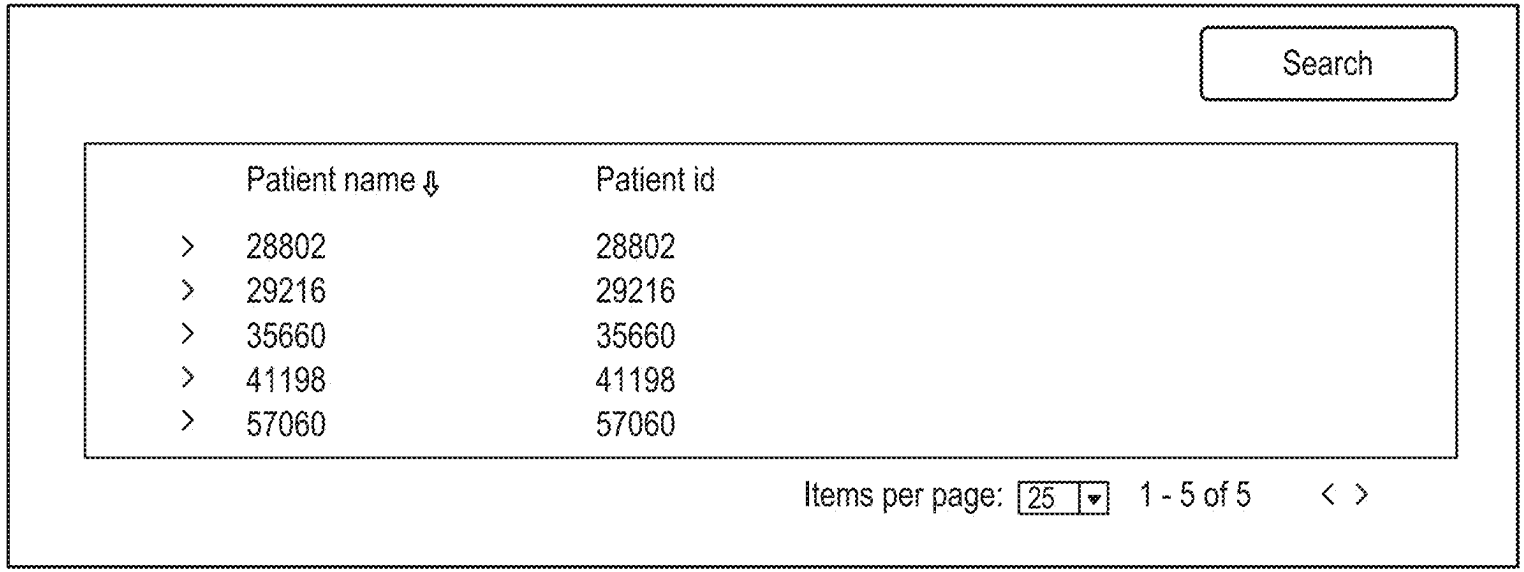


FIG. 27A

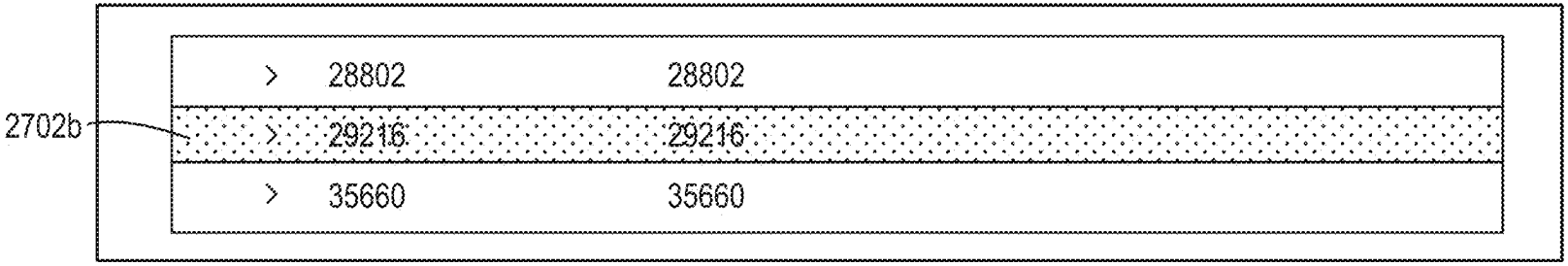


FIG. 27B

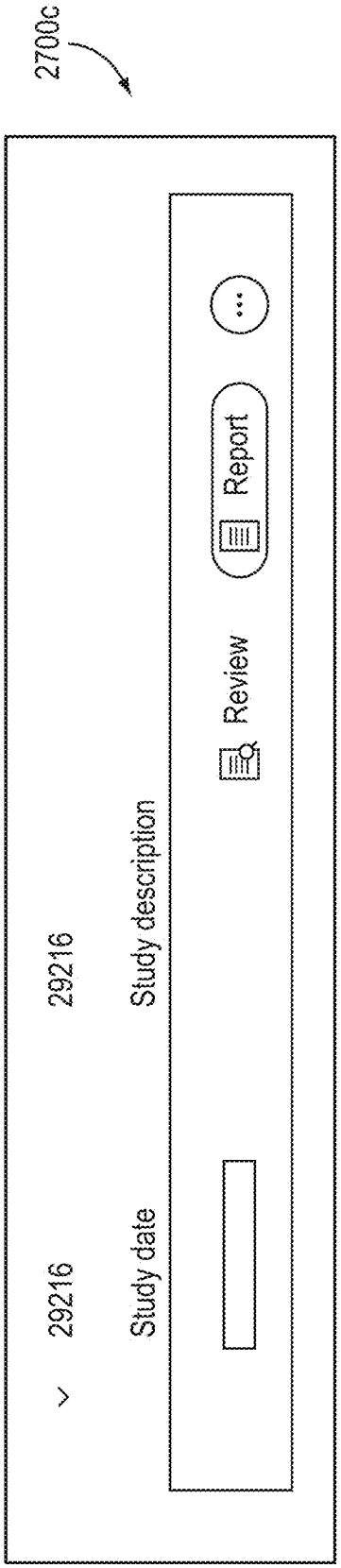

2700c
29216
Study description
Review
Report
29216
Study date

FIG. 27C

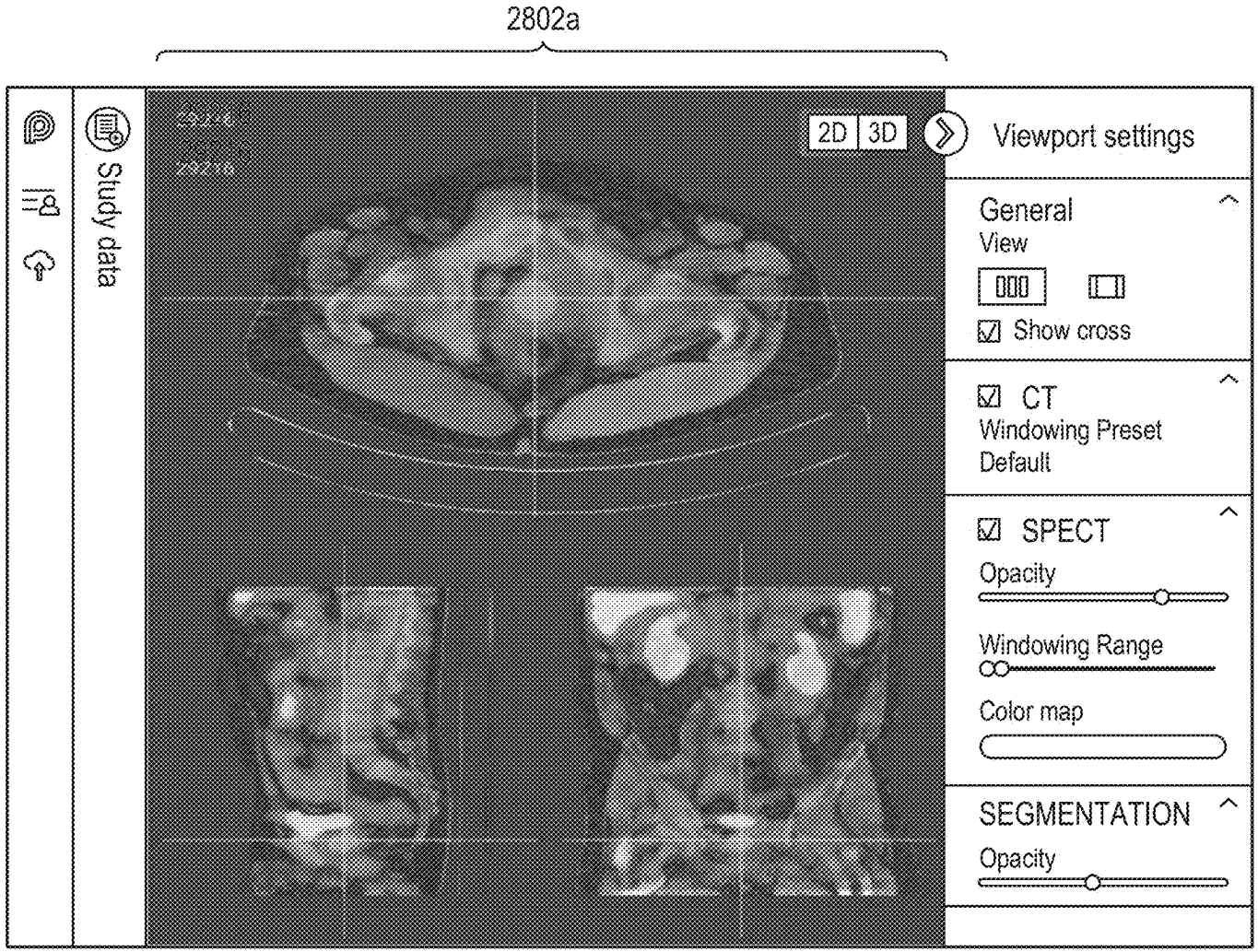

2802a
2800
Study data
2D
3D
Viewport settings
General
View
Show cross
CT
Windowing Preset
Default
SPECT
Opacity
Windowing Range
Color map
SEGMENTATION
Opacity

FIG. 28A

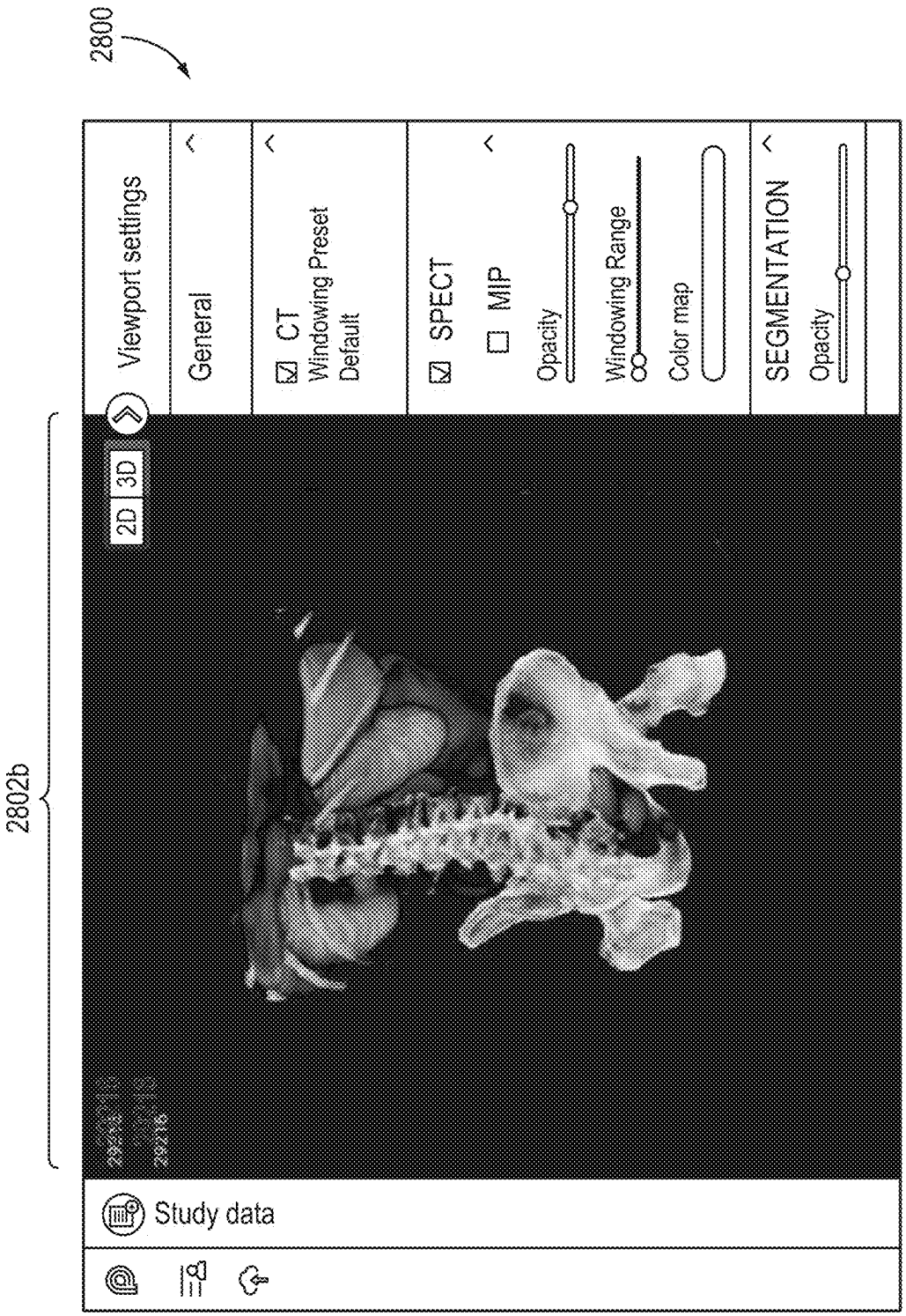

2800
2802b
Viewport settings
General
CT
Windowing Preset
Default
SPECT
MIP
Opacity
Windowing Range
Color map
SEGMENTATION
Opacity
2D
3D
Study data

FIG. 28B

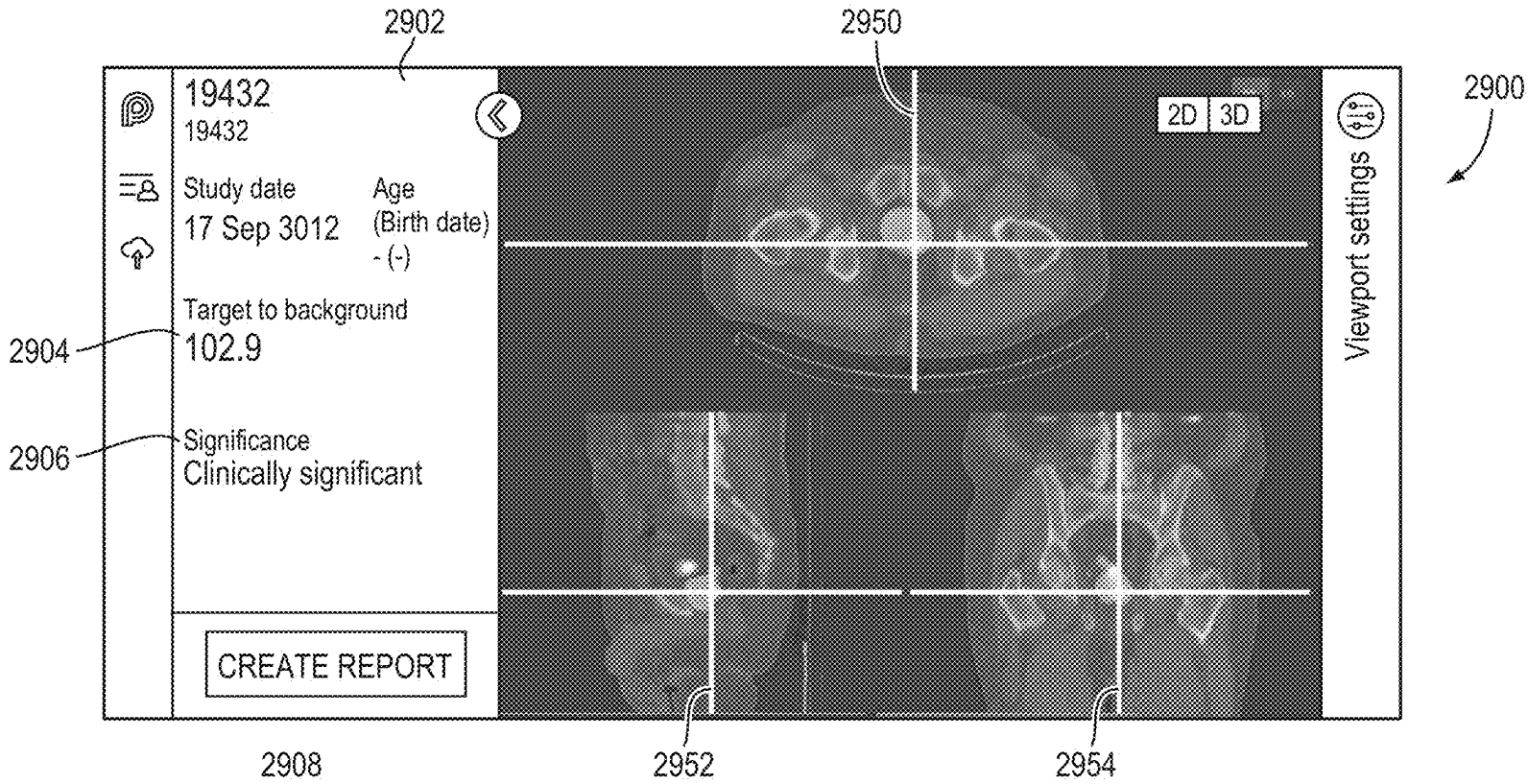

2902
2950
2900
19432
19432
Study date
17 Sep 3012
Age
(Birth date)
- (-)
Target to background
102.9
2904
2906
Significance
Clinically significant
CREATE REPORT
2D
3D
Viewport settings
2908
2952
2954

FIG. 29A

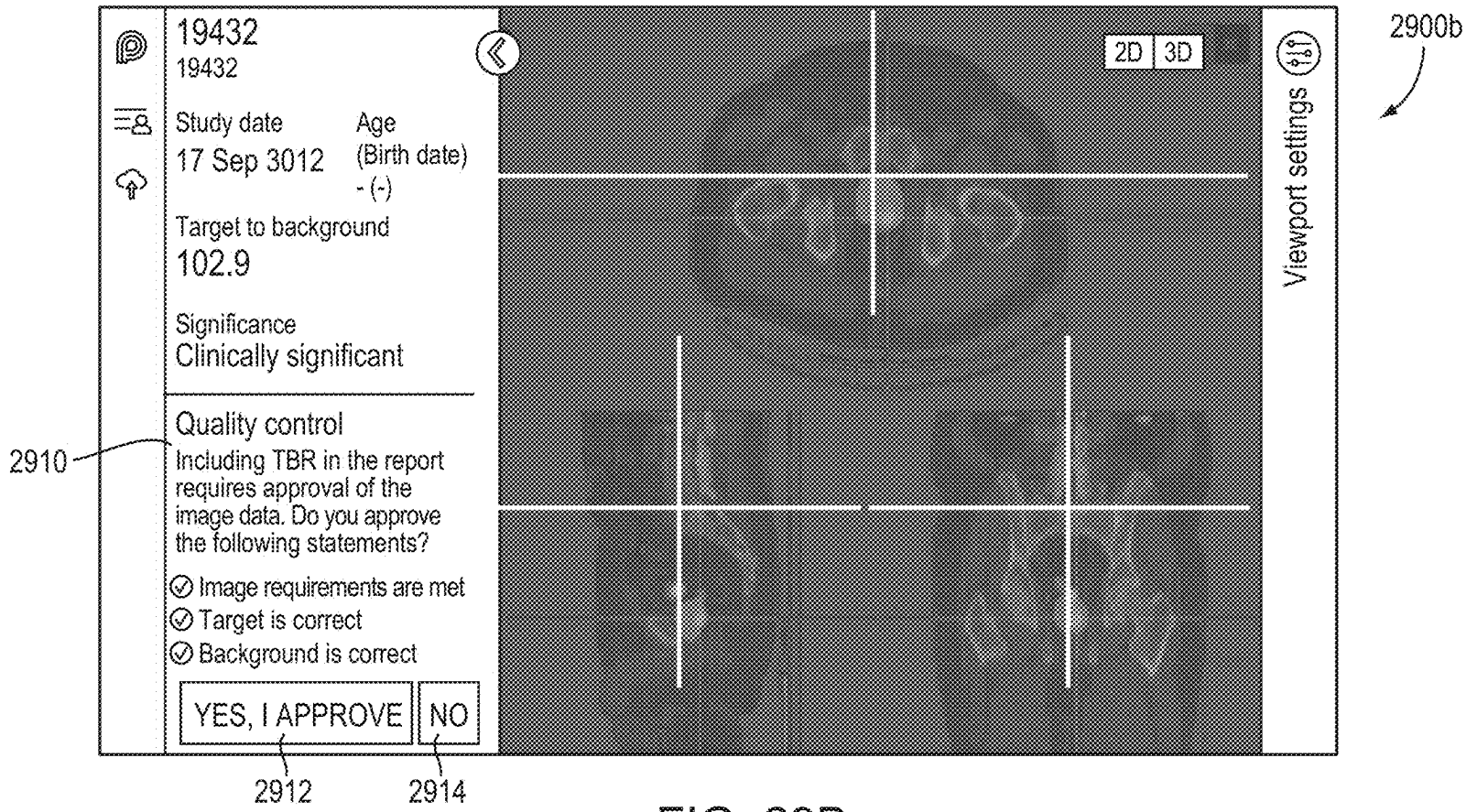

19432
19432
Study date
17 Sep 3012
Age
(Birth date)
- (-)
Target to background
102.9
Significance
Clinically significant
Quality control
Including TBR in the report requires approval of the image data. Do you approve the following statements?
Image requirements are met
Target is correct
Background is correct
YES, I APPROVE
NO
2910
2912
2914
2D
3D
Viewport settings
2900b

FIG. 29B

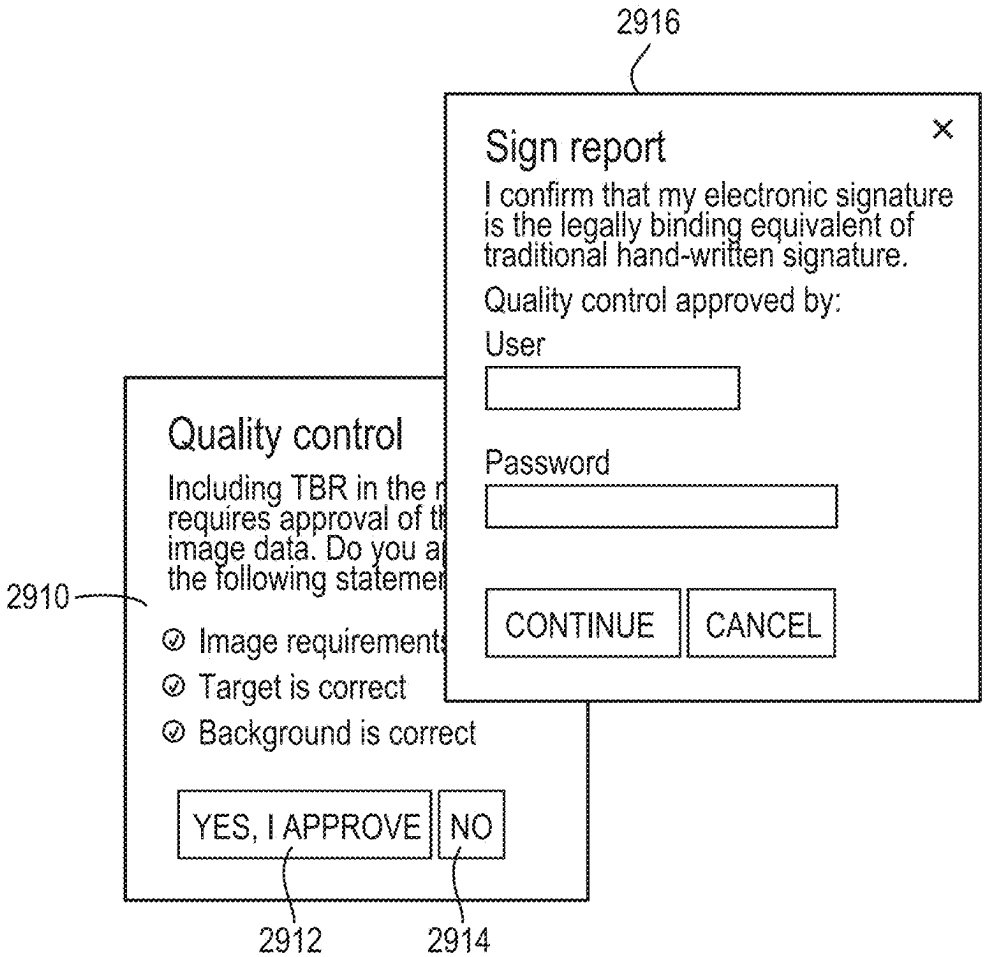

2916
Sign report
I confirm that my electronic signature is the legally binding equivalent of traditional hand-written signature.
Quality control approved by:
User
Password
CONTINUE
CANCEL
Quality control
Including TBR in the r
requires approval of t
image data. Do you a
the following statemer
2910
Image requirement
Target is correct
Background is correct
YES, I APPROVE
NO
2912
2914

FIG. 29C

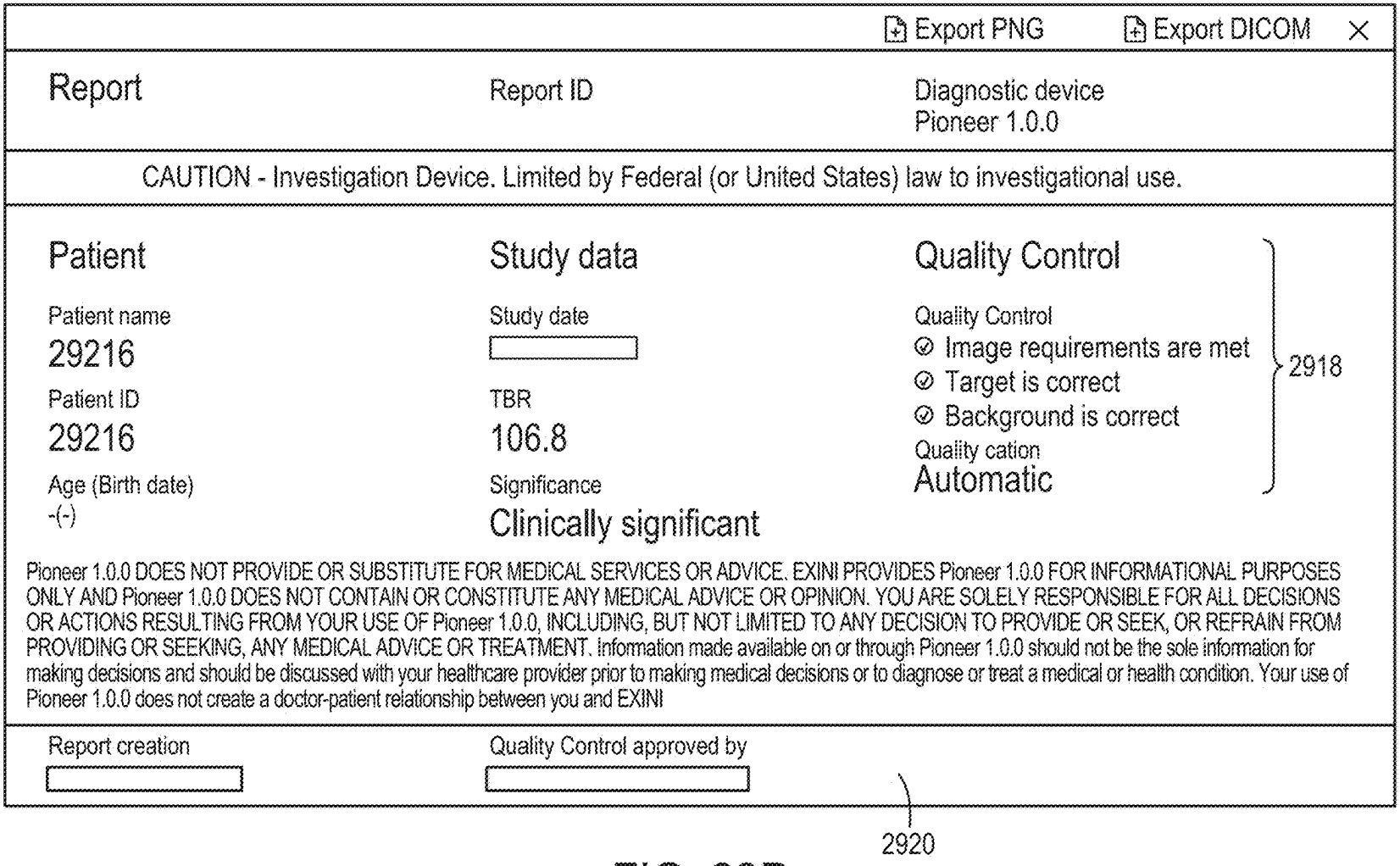

2900d
Export PNG
Export DICOM
Report
Report ID
Diagnostic device
Pioneer 1.0.0
CAUTION - Investigation Device. Limited by Federal (or United States) law to investigational use.
Patient
Patient name
29216
Patient ID
29216
Age (Birth date)
-(-)
Study data
Study date
TBR
106.8
Significance
Clinically significant
Quality Control
Quality Control
Image requirements are met
Target is correct
Background is correct
Quality cation
Automatic
2918
Pioneer 1.0.0 DOES NOT PROVIDE OR SUBSTITUTE FOR MEDICAL SERVICES OR ADVICE. EXINI PROVIDES Pioneer 1.0.0 FOR INFORMATIONAL PURPOSES ONLY AND Pioneer 1.0.0 DOES NOT CONTAIN OR CONSTITUTE ANY MEDICAL ADVICE OR OPINION. YOU ARE SOLELY RESPONSIBLE FOR ALL DECISIONS OR ACTIONS RESULTING FROM YOUR USE OF Pioneer 1.0.0, INCLUDING, BUT NOT LIMITED TO ANY DECISION TO PROVIDE OR SEEK, OR REFRAIN FROM PROVIDING OR SEEKING, ANY MEDICAL ADVICE OR TREATMENT. Information made available on or through Pioneer 1.0.0 should not be the sole information for making decisions and should be discussed with your healthcare provider prior to making medical decisions or to diagnose or treat a medical or health condition. Your use of Pioneer 1.0.0 does not create a doctor-patient relationship between you and EXINI
Report creation
Quality Control approved by
2920

FIG. 29D

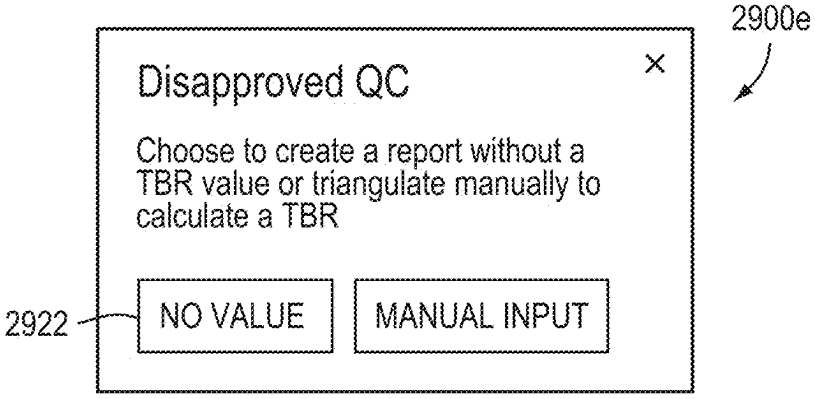


FIG. 29E

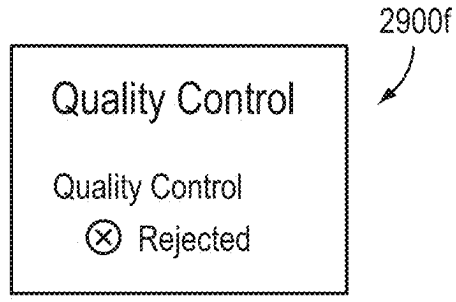


FIG. 29F

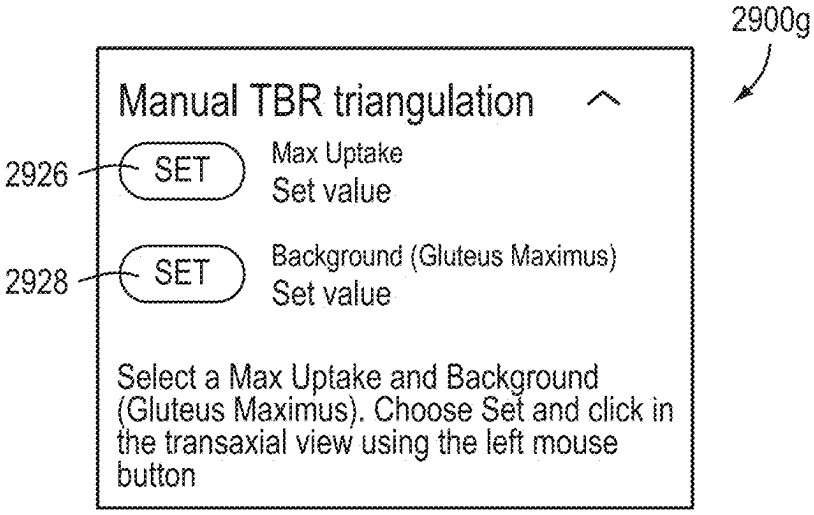


FIG. 29G

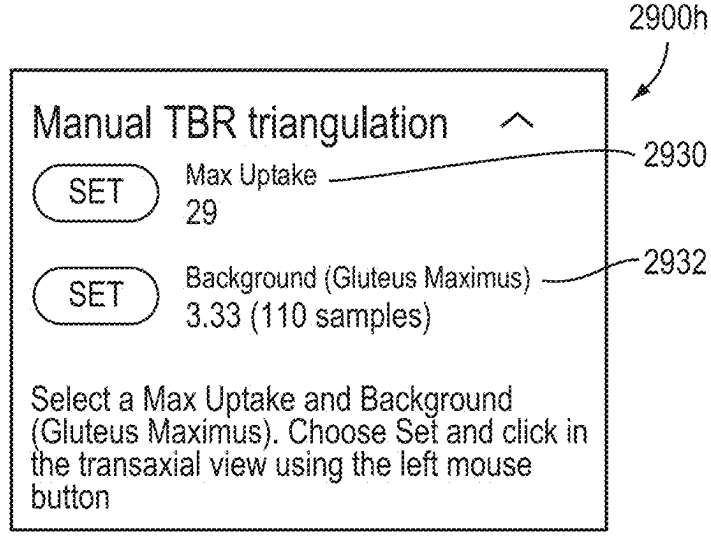


FIG. 29H

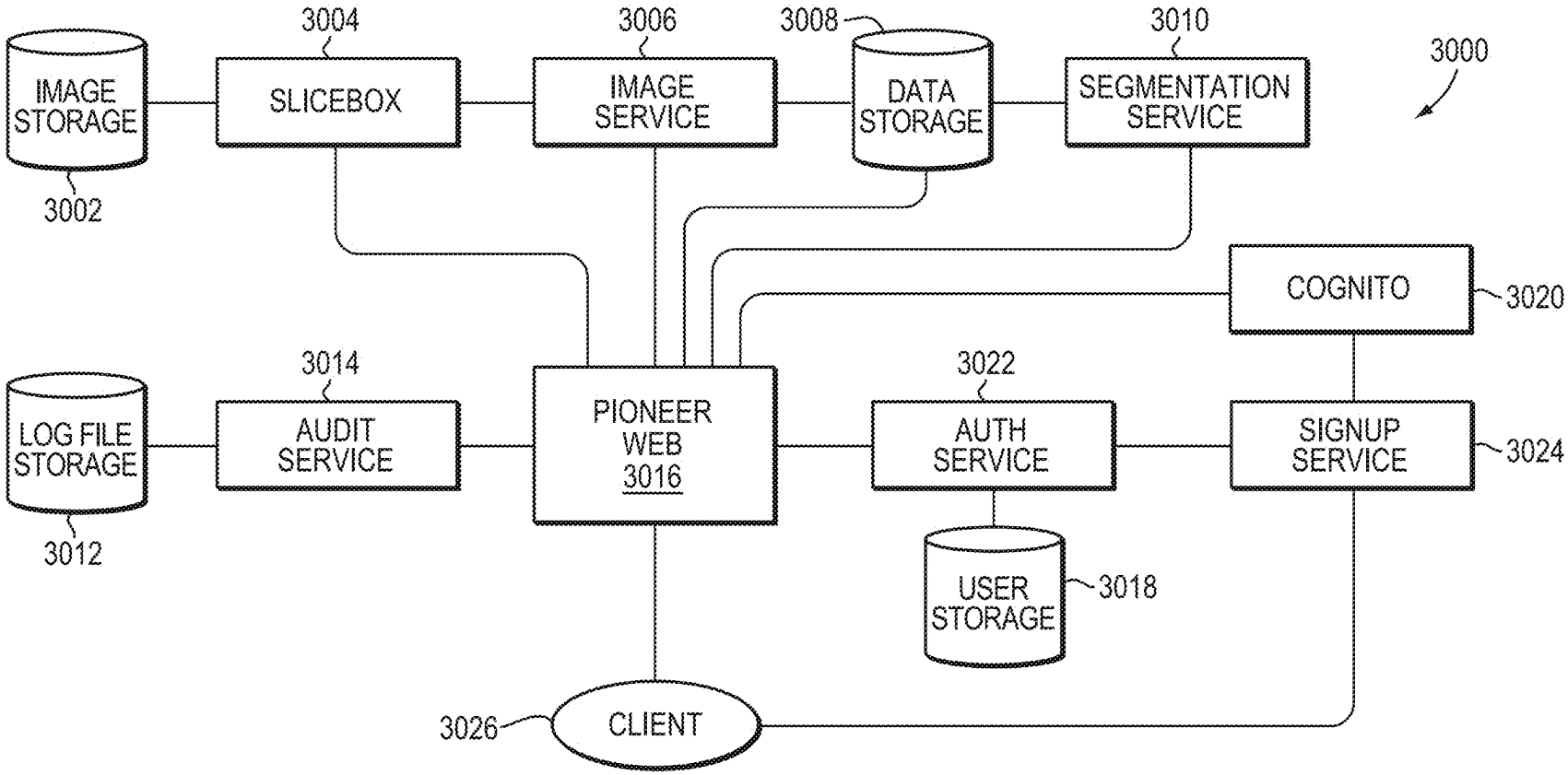

IMAGE STORAGE
3002
3004
SLICEBOX
3006
IMAGE SERVICE
3008
DATA STORAGE
3010
SEGMENTATION SERVICE
3000
COGNITO
3020
LOG FILE STORAGE
3012
3014
AUDIT SERVICE
PIONEER WEB 3016
3022
AUTH SERVICE
SIGNUP SERVICE
3024
USER STORAGE
3018
3026
CLIENT

FIG. 30

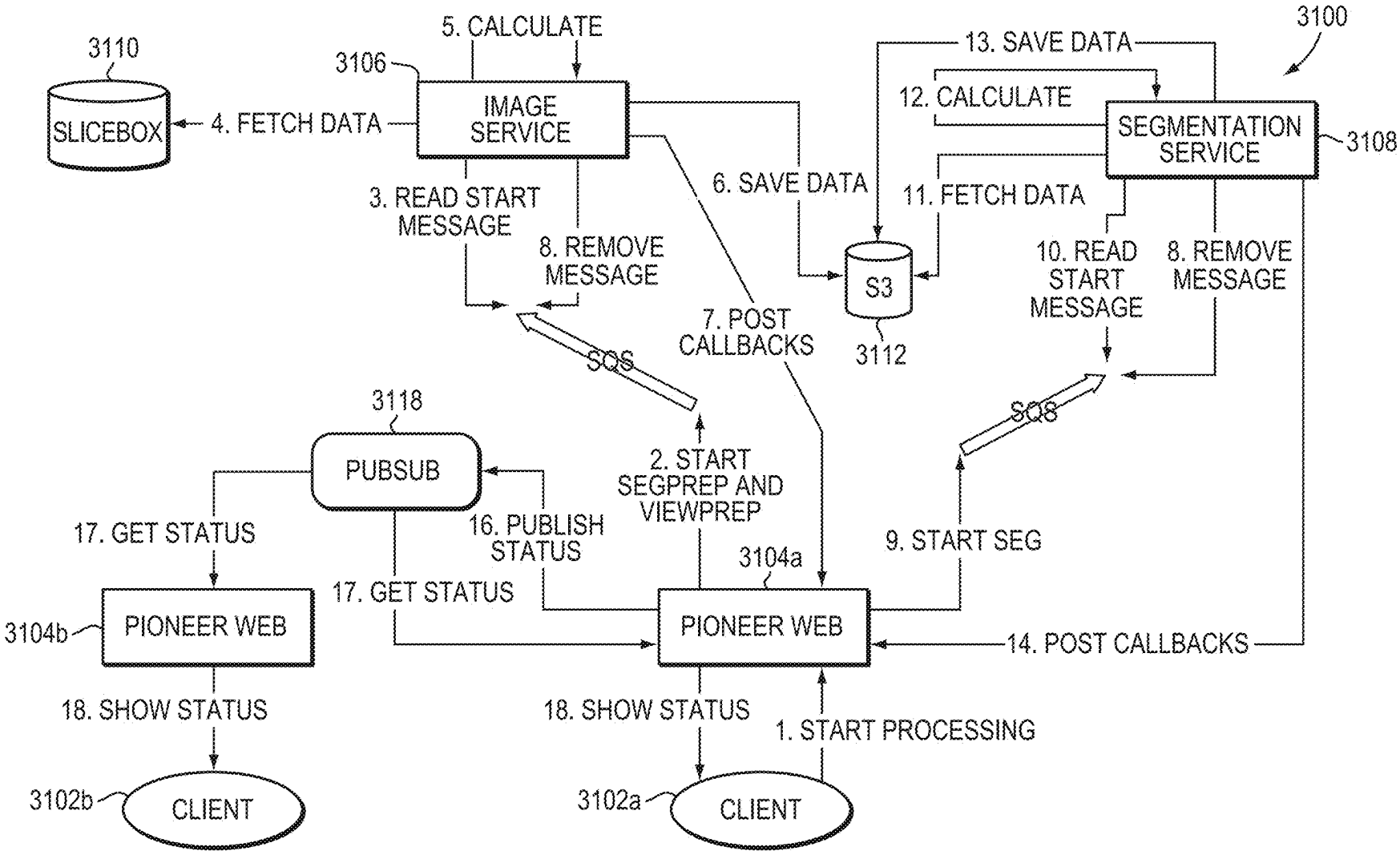

3110
SLICEBOX
4. FETCH DATA
5. CALCULATE
3106
IMAGE SERVICE
3. READ START MESSAGE
8. REMOVE MESSAGE
6. SAVE DATA
13. SAVE DATA
12. CALCULATE
3100
SEGMENTATION SERVICE
3108
11. FETCH DATA
10. READ START MESSAGE
8. REMOVE MESSAGE
S3
3112
7. POST CALLBACKS
SQS
SQS
3118
PUBSUB
2. START SEGPREP AND VIEWPREP
17. GET STATUS
16. PUBLISH STATUS
9. START SEG
3104a
17. GET STATUS
3104b
PIONEER WEB
PIONEER WEB
14. POST CALLBACKS
18. SHOW STATUS
18. SHOW STATUS
1. START PROCESSING
3102b
CLIENT
3102a
CLIENT

FIG. 31

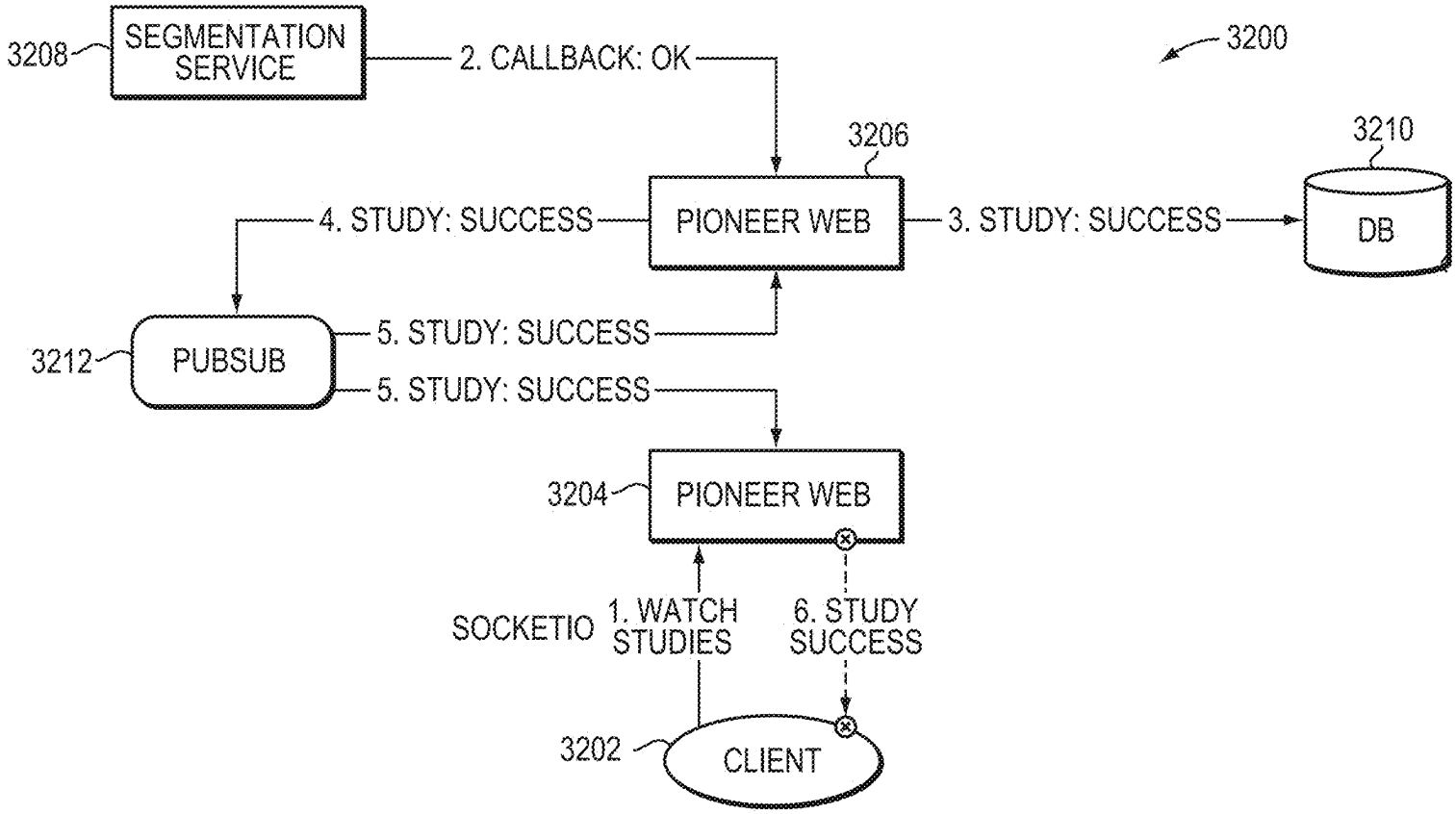

3208
SEGMENTATION SERVICE
2. CALLBACK: OK
3200
3206
3210
4. STUDY: SUCCESS
PIONEER WEB
3. STUDY: SUCCESS
DB
3212
PUBSUB
5. STUDY: SUCCESS
5. STUDY: SUCCESS
3204
PIONEER WEB
SOCKETIO
1. WATCH STUDIES
6. STUDY SUCCESS
3202
CLIENT

FIG. 32

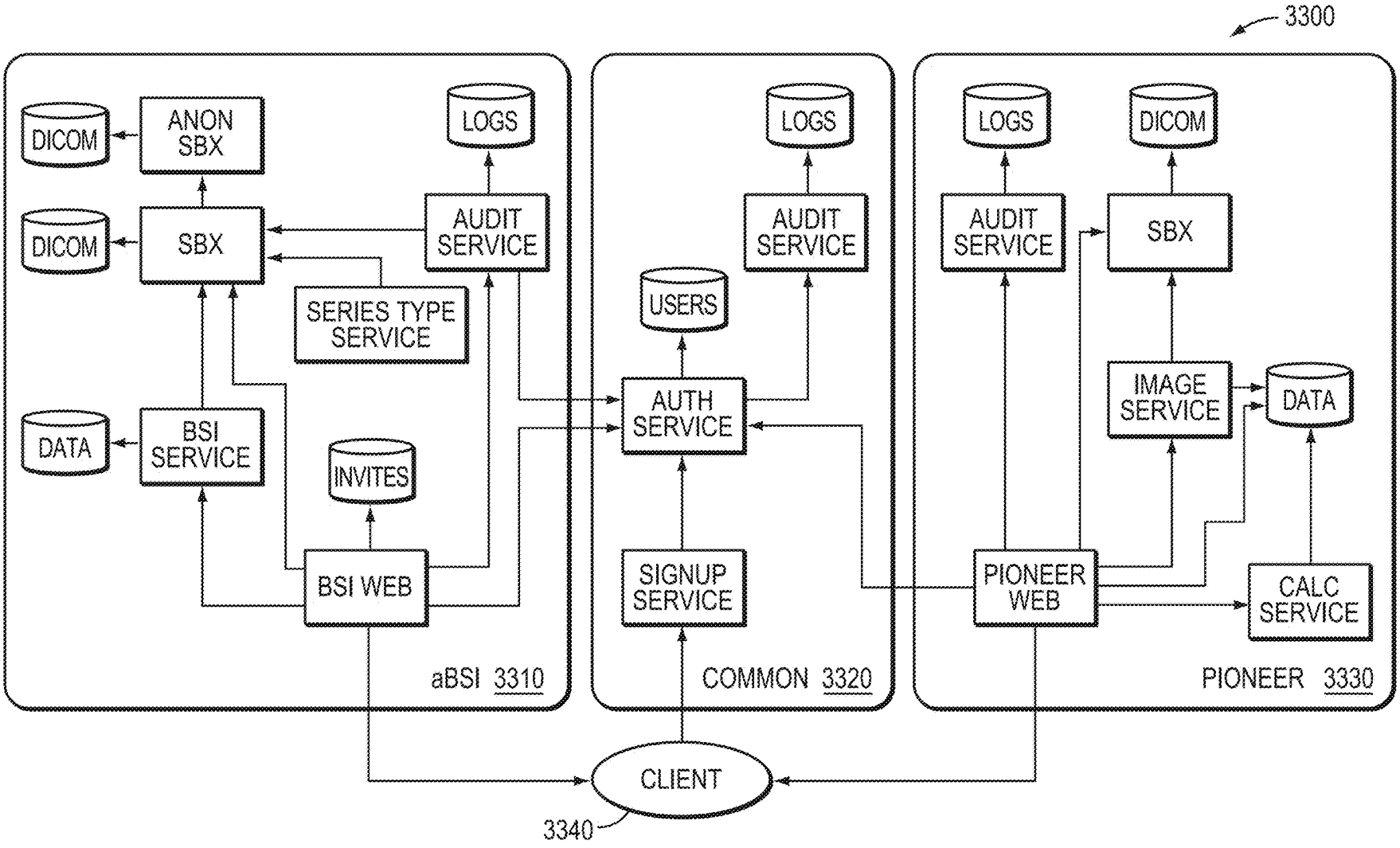

3300
DICOM
ANON SBX
LOGS
DICOM
SBX
AUDIT SERVICE
SERIES TYPE SERVICE
DATA
BSI SERVICE
INVITES
BSI WEB
aBSI 3310
LOGS
AUDIT SERVICE
USERS
AUTH SERVICE
SIGNUP SERVICE
COMMON 3320
LOGS
DICOM
AUDIT SERVICE
SBX
IMAGE SERVICE
DATA
PIONEER WEB
CALC SERVICE
PIONEER 3330
CLIENT
3340

FIG. 33

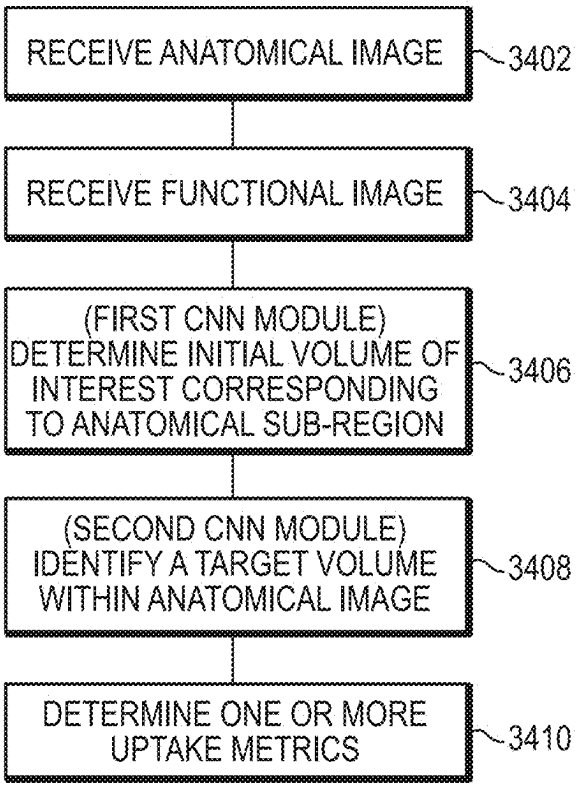

RECEIVE ANATOMICAL IMAGE
3402
RECEIVE FUNCTIONAL IMAGE
3404
(FIRST CNN MODULE) DETERMINE INITIAL VOLUME OF INTEREST CORRESPONDING TO ANATOMICAL SUB-REGION
3406
(SECOND CNN MODULE) IDENTIFY A TARGET VOLUME WITHIN ANATOMICAL IMAGE
3408
DETERMINE ONE OR MORE UPTAKE METRICS
3410

FIG. 34

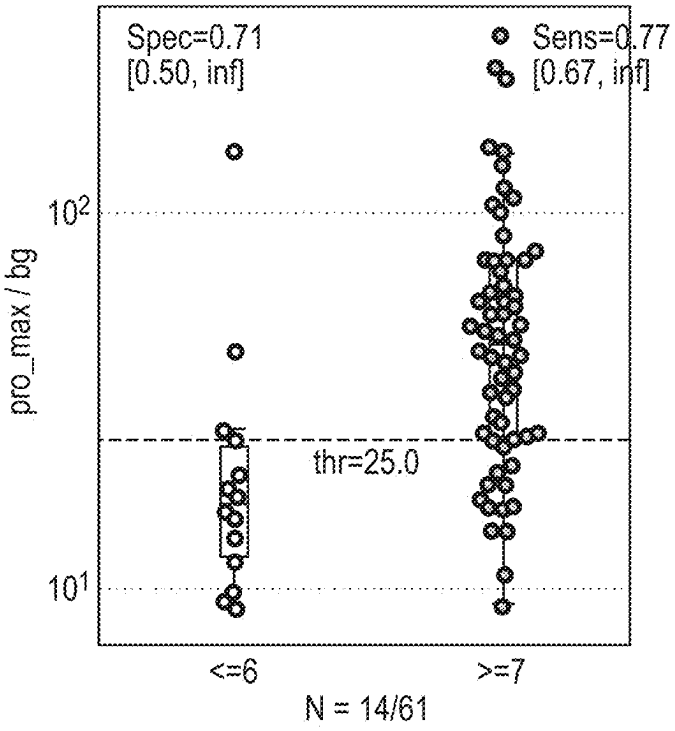


FIG. 35A

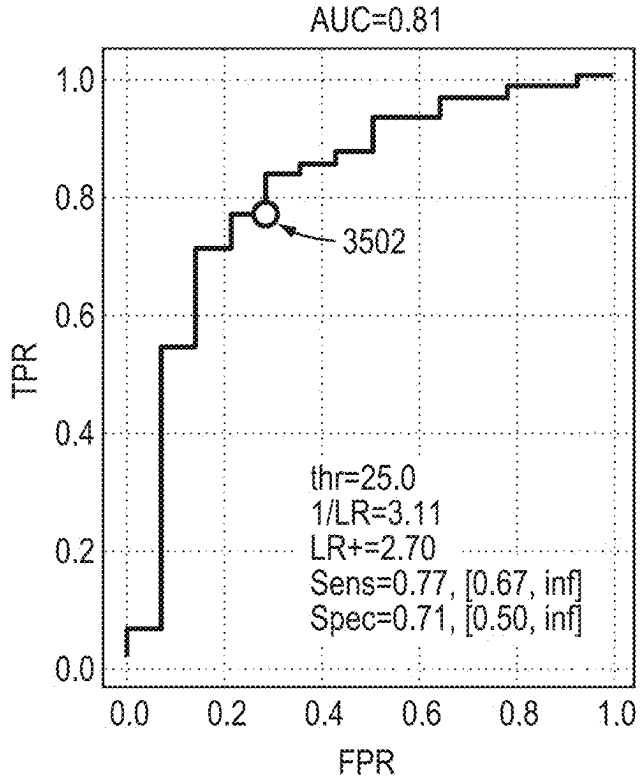


FIG. 35B

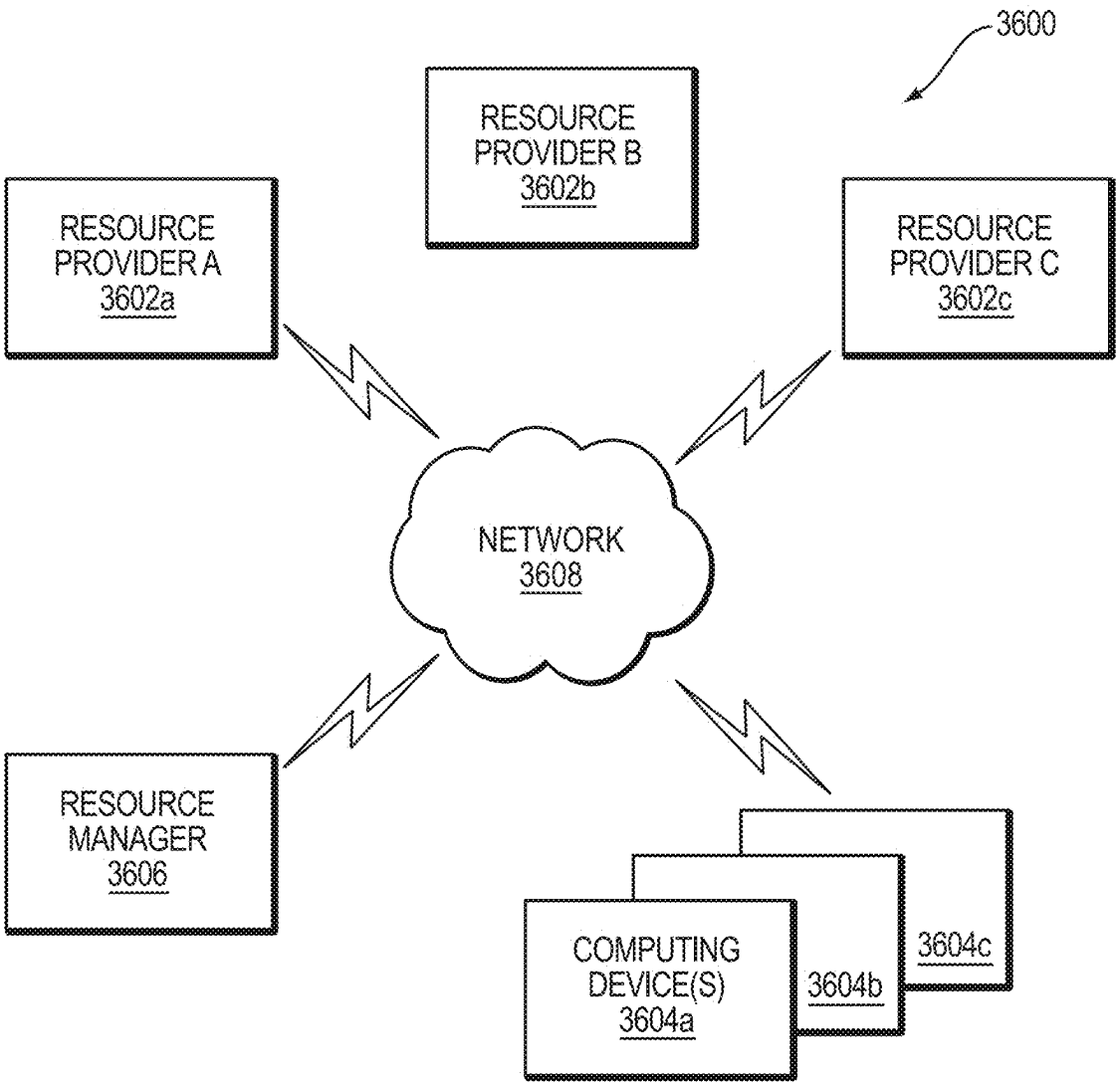

3600
RESOURCE PROVIDER B 3602b
RESOURCE PROVIDER A 3602a
RESOURCE PROVIDER C 3602c
NETWORK 3608
RESOURCE MANAGER 3606
COMPUTING DEVICE(S) 3604a
3604b
3604c

FIG. 36

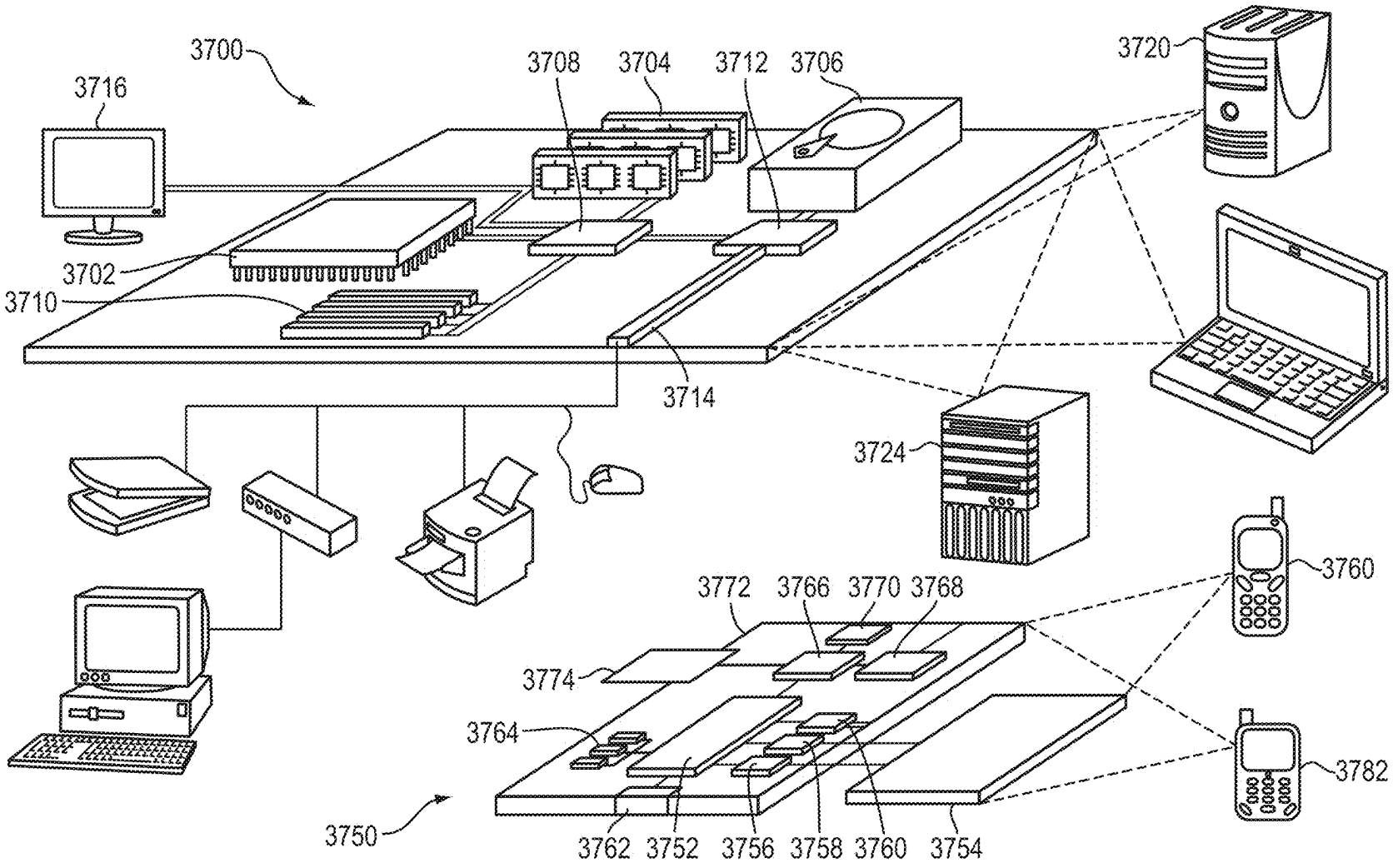

3700
3716
3708
3704
3712
3706
3720
3702
3710
3714
3724
3760
3772
3766
3770
3768
3774
3764
3782
3750
3762
3752
3756
3758
3760
3754

FIG. 37

SYSTEMS AND METHODS FOR RAPID NEURAL NETWORK-BASED IMAGE SEGMENTATION AND RADIOPHARMACEUTICAL UPTAKE DETERMINATION

CROSS REFERENCE TO RELATED APPLICATIONS

This application claims priority to and benefit of U.S. Provisional Application No. 62/614,935, filed Jan. 8, 2018, the content of which is hereby incorporated by reference in its entirety.

FIELD OF THE INVENTION

This invention relates generally to methods, systems, and architectures for automated analysis and/or presentation of medical image data. More particularly, in certain embodiments, the invention relates to automated identification of one or more particular regions of interest (e.g., corresponding to specific organs or tissue) within images of a subject and determination of radiopharmaceutical uptake within such region(s), e.g., for identification and/or staging of disease, e.g., prostate cancer.

BACKGROUND OF THE INVENTION

Targeted image analysis involves the use of radiolabeled small molecules that bind to specific receptors, enzymes and proteins in the body that are altered during the evolution of disease. After administration to a patient, these molecules circulate in the blood until they find their intended target. The bound radiopharmaceutical remains at the site of disease, while the rest of the agent clears from the body. The radioactive portion of the molecule serves as a beacon so that an image may be obtained depicting the disease location and concentration using commonly available nuclear medicine cameras, known as single-photon emission computerized tomography (SPECT) or positron emission tomography (PET) cameras, found in most hospitals throughout the world. Physicians can then use this information to determine the presence and the extent of disease in a patient. The physician can use this information to provide a recommended course of treatment to the patient and to track the progression of disease.

There are a variety of software-based analytical techniques available for analysis and enhancement of PET and SPECT images that can be used by a radiologist or physician. There are also a number of radiopharmaceuticals available for imaging particular kinds of cancer. For example, the small molecule diagnostic 1404 targets the extracellular domain of prostate specific membrane antigen (PSMA), a protein amplified on the surface of >95% of prostate cancer cells and a validated target for the detection of primary and metastatic prostate cancer. 1404 is labeled with technetium-99m, a gamma-emitter isotope that is widely available, relatively inexpensive, facilitates efficient preparation, and has spectrum characteristics attractive for nuclear medicine imaging applications.

Another example radiopharmaceutical is PyL™ (also known as [^{18}F]DCFPyL), which is a clinical-stage, fluorinated PSMA-targeted PET imaging agent for prostate cancer. A proof-of-concept study published in the April 2015 issue of the Journal of Molecular Imaging and Biology demonstrated that PET imaging with PyL™ showed high levels of PyL™ uptake in sites of putative metastatic disease and primary tumors, suggesting the potential for high sensitivity and specificity in detecting prostate cancer.

An oncologist may use images from a targeted PET or SPECT study of a patient as input in her assessment of whether the patient has a particular disease, e.g., prostate cancer, what stage of the disease is evident, what the recommended course of treatment (if any) would be, whether surgical intervention is indicated, and likely prognosis. The oncologist may use a radiologist report in this assessment. A radiologist report is a technical evaluation of the PET or SPECT images prepared by a radiologist for a physician who requested the imaging study and includes, for example, the type of study performed, the clinical history, a comparison between images, the technique used to perform the study, the radiologist's observations and findings, as well as overall impressions and recommendations the radiologist may have based on the imaging study results. A signed radiologist report is sent to the physician ordering the study for the physician's review, followed by a discussion between the physician and patient about the results and recommendations for treatment.

Thus, the process involves having a radiologist perform an imaging study on the patient, analyzing the images obtained, creating a radiologist report, forwarding the report to the requesting physician, having the physician formulate an assessment and treatment recommendation, and having the physician communicate the results, recommendations, and risks to the patient. The process may also involve repeating the imaging study due to inconclusive results, or ordering further tests based on initial results.

If an imaging study shows that the patient has a particular disease or condition (e.g., cancer), the physician discusses various treatment options, including surgery, as well as risks of doing nothing or adopting a watchful waiting or active surveillance approach, rather than having surgery.

There are limitations associated with this process, both from the perspective of the physician and from the perspective of the patient. While the radiologist's report is certainly helpful, the physician must ultimately rely on her experience in formulating an assessment and recommendation for her patient. Furthermore, the patient must place a great deal of trust in his physician. The physician may show the patient his PET/SPECT images and may tell the patient a numerical risk associated with various treatment options or likelihood of a particular prognosis, but the patient may very well struggle to make sense of this information. Moreover, the patient's family will likely have questions, particularly if cancer is diagnosed but the patient opts not to have surgery. The patient and/or his family members may search online for supplemental information and may become misinformed about risks of the diagnosed condition. A difficult ordeal may become more traumatic.

Thus, there remains a need for systems and methods for improved analysis of medical imaging studies and communication of those results, diagnoses, prognoses, treatment recommendations, and associated risks to a patient.

SUMMARY OF THE INVENTION

Presented herein are systems and methods that provide for automated analysis of three-dimensional (3D) medical images of a subject in order to automatically identify specific 3D volumes within the 3D images that correspond to specific organs and/or tissue. In certain embodiments, the accurate identification of one or more such volumes are used to automatically determine quantitative metrics that represent uptake of radiopharmaceuticals in particular organs

and/or tissue regions. These uptake metrics can be used to assess disease state in a subject, determine a prognosis for a subject, and/or determine efficacy of a treatment modality.

For example, the systems and methods described herein can be used for automated analysis of medical images in order to determine uptake metrics that provide a quantitative measure of uptake of a radiopharmaceutical such as a radionuclide labelled PSMA binding agent (e.g., ^{99m}Tc-MIP-1404, e.g., [^{18}F]DCFPyL) within a prostate of the subject. Such uptake metrics are of relevance for evaluating patient risk for prostate cancer and/or prostate cancer severity/stage within a subject. For example, it has been found that high sensitivities and specificities can be achieved for the automated classification of clinically significant prostate cancer vs. clinically non-significant prostate cancer.

In certain embodiments, the image analysis approaches described herein utilize a combination of 3D anatomical and functional images obtained for the subject. Anatomical images, such as x-ray computed tomography (CT) images, provide detailed anatomical/structural information. Functional images convey information relating to physiological activities within specific organs and/or tissue, such as metabolism, blood flow, regional chemical composition, and/or absorption. Of particular relevance are nuclear medicine images, such as single photon emission computed tomography (SPECT) and/or positron emission tomography (PET) images, which are acquired by detecting emitted radiation from the subject and which can be used to infer spatial distributions of administered radiopharmaceuticals within the subject.

For example, SPECT imaging can be used to evaluate uptake of the radiopharmaceutical ^{99m}Tc-MIP-1404 (which is 1404 labelled with ^{99m}Tc). In certain embodiments, in order to evaluate ^{99m}Tc-MIP-1404 uptake in a prostate of a subject, a CT image and a corresponding SPECT image are obtained for the subject, such that the anatomical/structural information of the CT image can be correlated with the functional information of the corresponding SPECT image. Often the CT and SPECT images are acquired via two separate scans (e.g., a first scan for the CT image and a second scan for the SPECT image) using a single multi-modal imaging system, such that the subject is a substantially fixed position over the duration of the two scans. In this manner, a mapping between voxels of the CT image and those of the SPECT image is established, and volumes identified within the CT image as corresponding to specific organs and/or tissue regions can be used to identify those voxels the SPECT image that correspond to those same specific organs/and or tissue regions.

Accordingly, in certain embodiments, the image analysis approaches described herein utilize convolutional neural networks (CNNs) to accurately identify a prostate volume within the CT image that corresponds to the prostate of the subject. The identified prostate volume can be used to identify those voxels of the SPECT image that also correspond to the subject's prostate. Uptake metrics that provide a measure of uptake of the imaging agent (e.g., a labelled PSMA binding agent, e.g., ^{99m}Tc-MIP-1404 or [^{18}F]DCFPyL) in the prostate can thus be computed using the intensities of SPECT image voxels corresponding to the prostate of the subject. The uptake metrics, then, can be converted to an identification of whether or not the subject has prostate cancer and/or a quantification of risk that the subject has prostate cancer, and/or a staging of the disease (e.g., as part of disease tracking over time), which may be used by the medical practitioner in advising treatment options, and/or monitoring efficacy of administered therapy, for example.

Various advances are described herein that improve the performance of the automated measurement of uptake metrics in the prostate (or, more broadly, a particular organ or tissue region of interest) via this multi-image approach, i.e., analysis of a 3D anatomical image in combination with a 3D functional image. These advances include, for example, the automated identification of a bounding box in the 3D anatomical image (e.g., using a first convolutional neural network, CNN) to identify a pelvic region within which the prostate lies.

For example, a set of 3D anatomical images with identified physiology (e.g., identified pelvic regions) is used to train a first CNN on points representing the boundaries of the pelvic region (e.g., the vertices of a cuboid bounding box) such that the first CNN can be used to automatically identify the pelvic region in a 3D anatomical image of a subject. This provides a more standard-sized initial volumetric region of the 3D anatomical image to be subsequently processed (e.g., via a second CNN) for detailed segmentation of regions of interest within the initial volumetric region—e.g., where the bounding box bounds regions of the image corresponding to the prostate and/or the bladder and/or the rectum, and/or gluteal muscles of the subject. Imaging agent uptake metrics may then be determined from the portions of the 3D functional image that map to one or more of the identified regions of the 3D anatomical image. Note that, as used herein, the 'bounding box' isn't necessarily a cuboid, but may have other shapes. In certain embodiments, the bounding box is a cuboid.

The determination of the bounding box via the first CNN may use, as input, a significantly less dense resolution than is used for segmentation of the prostate and/or other organs within the bounding box by the second CNN. For example, a whole body 3D anatomical image having a first number of voxels (e.g., 81×68×96 voxels) may be processed via the first CNN to find the bounding box, then the second CNN may process an image corresponding to the bounding box region but having a more dense resolution, e.g., many more voxels (e.g., 94×138×253 voxels) than the first number of voxels.

The 'bounding box' approach of identifying one or more portions of a 3D anatomical image that is/are relevant to the analysis at hand, e.g., prior to applying a second CNN (for detailed segmentation), improves computational efficiency by removing a large portion of the initial 3D anatomical image prior to the more computationally intensive subsequent processing. This approach is more computationally efficient than performing the detailed segmentation on the entire initial 3D anatomical image since, for example, identification of the pelvic region (e.g., the vertices of a cuboid bounding box) is simpler than detailed segmentation of a prostate, bladder, and/or other tissues of interest. Not only is this approach more computationally efficient, it also may result in more accurate subsequent processing, e.g., the more detailed segmentation provided by the second CNN. This is because, for example, 3D anatomical images obtained at different medical institutions using different machines vary in size (e.g., where varying size means there are different numbers of voxels of the images, and/or different volumes of the patient tissue represented in the images), and training the second CNN for automated detailed segmentation of the prostate using portions of 3D anatomical training images having a more standardized image volume size, and within

which the organs and other tissue regions of interest lie, results in a more robust, accurate segmentation.

Another advance described herein that improves the performance of the automated measurement of uptake metrics in the prostate (or, more broadly, a particular organ or tissue region of interest) via this multi-image approach (i.e., analysis of a 3D anatomical image in combination with a 3D functional image) is the accurate identification of one or more tissue regions in addition to the prostate, and the accounting for imaging agent uptake in those regions in the determination of (i) uptake metrics in the prostate and/or (ii) an identification and/or staging of prostate cancer. Certain imaging agents comprising a PSMA binding agent have high uptake in certain organs, which may affect the identification of diseased tissue (e.g., prostate cancer). For example, uptake of a radionuclide labelled PSMA binding agent by the bladder may result in scattering in the 3D functional image, and may reduce accuracy of the measured imaging agent intensity in the prostate, which is located near the bladder. By training a second CNN for detailed segmentation of both the prostate and the bladder of a subject, it is possible to accurately, automatically account for a 'bleed through' or 'cross-talk' effect and/or other effects caused by uptake of the imaging agent by the bladder. Furthermore, by training the second CNN for identification of a reference region in the 3D anatomical image, e.g., the gluteal muscles, it is possible to more accurately weight/normalize imaging agent intensity measurements and improve the accuracy and diagnostic value of the uptake measurements in the prostate of the subject.

Thus, in certain embodiments, the systems and methods described herein utilize a unique combination of two CNN modules, wherein a first CNN module identifies an initial volume of interest (VOI) within the CT image and a second receives the VOI as input and identifies the prostate volume therein. As described herein, this approach allows the second CNN module to operate on a smaller input size (e.g., the VOI as opposed to the full CT image). The savings in computational resources (e.g., memory; e.g., processing time) by reducing the input size in this manner can be allocated to improving the accuracy of the second CNN module and/or used to improve the speed of the image processing approach.

In certain embodiments, the systems and methods described herein identify, along with the prostate, various additional tissue volumes within the CT image. For example, additional tissue volumes corresponding to pelvic bones, a bladder, a rectum, and gluteal muscles of the subject may be identified in addition to the prostate. As described herein, the identification of such additional tissue volumes can be used for a variety of functions and confers advantages over other approaches, such as a binary classification approach wherein voxels of the CT image are either identified as corresponding to prostate or not. In particular, identification of additional tissue volumes can, for example, (i) improve the accuracy with which the CNN module identifies the prostate volume within the CT image, (ii) provide for identification of reference regions that can be used to compute normalization values for uptake metric calculation, and (iii) allow for intensities of SPECT image voxels corresponding to prostate to be corrected for cross-talk that results, for example, from the accumulation of radiopharmaceutical within the bladder.

In certain embodiments, the image analysis approaches described herein can be used for analysis of a variety of anatomical and functional images and are not limited CT and SPECT images. For example, positron emission tomography (PET) is another functional imaging modality that provides information about the distribution of radiopharmaceutical within a subject. As with SPECT images, PET images can be used in combination with CT images to determine uptake metrics for various organs and tissue regions of interest. The approaches described herein may also be applied to a variety of organs and/or tissue regions of interest, such as bone, lymph nodes, liver, and lungs.

Accordingly, by providing for rapid and accurate identification of specific organs and tissue regions within medical images, the systems and method described herein provide for accurate and automated determination of uptake metrics that provide quantitative measures of radiopharmaceutical uptake within various organs and tissue regions within a subject. Uptake metrics determined in this automated manner provide valuable tools for assessing disease risk, state, and progression within patients, as well as treatment efficacy.

In one aspect, the invention is directed to a method for automatically processing 3D images to identify 3D volumes within the 3D images that correspond to a prostate of a subject and determining one or more uptake metrics indicative of radiopharmaceutical uptake therein (i.e., in the prostate), the method comprising: (a) receiving, by a processor of a computing device, a 3D anatomical image of the subject obtained using an anatomical imaging modality [e.g., x-ray computed tomography (CT) (e.g., a whole-body CT image; e.g., a partial body CT image); e.g., magnetic resonance imaging (MRI); e.g., 3D ultra-sound], wherein the 3D anatomical image comprises a graphical representation of tissue (e.g., soft-tissue and/or bone) within a subject, at least a portion of which corresponds to a pelvic region of the subject; (b) receiving, by the processor, a 3D functional image of the subject obtained using a functional imaging modality [e.g., single-photon emission computed tomography (SPECT); e.g., positron emission tomography (PET)], wherein the 3D functional image comprises a plurality of voxels, each representing a particular physical volume within the subject and having an intensity value that represents detected radiation emitted from the particular physical volume, wherein at least a portion of the plurality of voxels of the 3D functional image represent physical volumes within the pelvic region of the subject; (c) determining, by the processor, using a first module (e.g., a first machine learning module), an initial volume of interest (VOI) within the 3D anatomical image (e.g., a parallelepiped, e.g., a cuboid), the initial VOI corresponding to tissue within the pelvic region of the subject and excluding tissue outside the pelvic region of the subject (e.g., wherein the VOI excludes more voxels of the 3D anatomical image than it includes; e.g., wherein the VOI includes less than 25% of the voxels of the 3D anatomical image; e.g., wherein a majority of voxels within the VOI represent physical volumes within the pelvic region of the subject); (d) identifying, by the processor, using a second module (e.g., a second machine learning module), a prostate volume within the initial VOI corresponding to the prostate of the subject; and (e) determining, by the processor, (e.g., and displaying) the one or more uptake metrics using the 3D functional image and the prostate volume identified within the initial VOI of the 3D anatomical image [e.g., computing a quantity of radiopharmaceutical in the prostate of the subject based on intensity values of voxels of the 3D functional image that correspond to the prostate volume identified within the initial VOI of the 3D anatomical image; e.g., computing a sum (e.g., a weighted sum), an average, and/or a maximum of intensities of voxels of the 3D functional image representing a physical

volume occupied by the prostate of the subject] [e.g., wherein the one or more uptake metrics comprises a tumor to background ratio (TBR) value and/or wherein the method comprises determining (e.g., and displaying) a prostate cancer classification status of either (i) clinically significant or (ii) clinically non-significant based at least in part on the TBR value].

In certain embodiments, the first module receives the 3D anatomical image as input and outputs a plurality of coordinate values representing opposite corners of a rectangular volume within the 3D anatomical image (e.g., two sets of coordinate values that represent the opposite corners of the rectangular volume).

In certain embodiments, step (c) comprises determining, using the first module, a 3D pelvic bone mask that identifies a volume of the 3D anatomical image corresponding to pelvic bones (e.g., one or more (up to all) of a sacrum, a coccyx, a left hip bone, and a right hip bone) of the subject.

In certain embodiments, the first module is a Convolutional Neural Network (CNN) module (e.g., a Neural Network module that utilizes one or more convolution layers).

In certain embodiments, step (d) comprises using the second module to identify one or more additional tissue volumes within the 3D anatomical image, each volume corresponding to a specific tissue region within the subject, wherein the one or more additional tissue volumes correspond(s) to one or more specific tissue regions selected from the group consisting of: a pelvic bone (e.g., a sacrum; e.g., a coccyx; e.g., a left hip bone; e.g., a right hip bone) of the subject; a bladder of the subject; a rectum of the subject; and a gluteal muscle (e.g., a left gluteal muscle; e.g., a right gluteal muscle) of the subject.

In certain embodiments, step (d) comprises using the second module to classify each voxel within the initial VOI as corresponding a particular tissue region of a set of (predetermined) different tissue regions {e.g., the set comprising the prostate and, optionally, one or more additional tissue regions [e.g., a pelvic bone (e.g., a sacrum; e.g., a coccyx; e.g., a left hip bone; e.g., a right hip bone) of the subject; a bladder of the subject; a rectum of the subject; and a gluteal muscle (e.g., a left gluteal muscle; e.g., a right gluteal muscle]} within the subject. In certain embodiments, classifying each voxel within the initial VOI comprises: determining, via the second module, for each of a plurality of voxels within the initial VOI, a set of likelihood values, wherein the set of likelihood values comprises, for each of one or more tissue regions of the tissue region set, a corresponding likelihood value that represents a likelihood (e.g., as computed by the second module) that the voxel represents a physical volume within the tissue region; and for each of the plurality of voxels within the initial VOI, classifying the voxel as corresponding to the particular tissue region based on the set of likelihood values determined for the voxel. In certain embodiments, the second module receives as input the initial VOI (e.g., the entire initial VOI) and outputs a plurality of values comprising, for each voxel within the initial VOI, at least one of (i), (ii), and (iii) as follows: (i) a value classifying the voxel [e.g., classifying the voxel as corresponding to a specific tissue region, e.g., a region selected from a predetermined set of different tissue regions, e.g., the prostate of the subject; e.g., a pelvic bone (e.g., a sacrum; e.g., a coccyx; e.g., a left hip bone; e.g., a right hip bone) of the subject; a bladder of the subject; a rectum of the subject; and a gluteal muscle (e.g., a left gluteal muscle; e.g., a right gluteal muscle) of the subject]; (ii) a set of likelihood values for the voxel [e.g., a likelihood the voxel corresponds to a specific tissue region, e.g., a region selected from a predetermined set of different tissue regions, e.g., the prostate of the subject; e.g., a pelvic bone (e.g., a sacrum; e.g., a coccyx; e.g., a left hip bone; e.g., a right hip bone) of the subject; a bladder of the subject; a rectum of the subject; and a gluteal muscle (e.g., a left gluteal muscle; e.g., a right gluteal muscle) of the subject]; and (iii) a value identifying the voxel as not corresponding to (e.g., or as likely not corresponding to, or identifying a likelihood the voxel does not correspond to) any of a predetermined set of different tissue regions (e.g., identifying the voxel as corresponding to or as likely corresponding to, or a likelihood the voxel corresponds to, a background area, e.g., that is not of diagnostic interest) (e.g., such that the second module classifies and/or computes likelihood values for the entire VOI in one round, as opposed to operating on each voxel one at a time). In certain embodiments, the (predetermined) set of different tissue regions comprises one or more tissue regions selected from the group consisting of: the prostate of the subject; a pelvic bone (e.g., a sacrum; e.g., a coccyx; e.g., a left hip bone; e.g., a right hip bone) of the subject; a bladder of the subject; a rectum of the subject; and a gluteal muscle (e.g., a left gluteal muscle; e.g., a right gluteal muscle) of the subject.

In certain embodiments, step (d) comprises using the second module to identify a set of one or more base tissue volumes, the one or more base tissue volumes comprising the identified prostate volume and the one or more additional tissue volumes, and wherein the method further comprises: identifying, by the processor, using one or more auxiliary modules (e.g., auxiliary machine learning modules), one or more auxiliary tissue volumes within the 3D anatomical image, each auxiliary tissue volume corresponding [e.g., representing a same specific tissue region [e.g., the prostate of the subject; e.g., a pelvic bone (e.g., a sacrum; e.g., a coccyx; e.g., a left hip bone; e.g., a right hip bone) of the subject; a bladder of the subject; a rectum of the subject; and a gluteal muscle (e.g., a left gluteal muscle; e.g., a right gluteal muscle) of the subject] to a base tissue volume identified by the second module; and merging, by the processor, each auxiliary tissue volume with the corresponding base tissue volume identified by the second module (e.g., adding to the corresponding base tissue volume by incorporating portions of the corresponding auxiliary tissue volume not included in the original base tissue volume).

In certain embodiments, the method comprises: identifying, by the processor, (e.g., using the second module) a reference volume within the 3D anatomical image (e.g., within the initial VOI), the reference volume corresponding to a reference tissue region within the subject (e.g., a gluteal muscle); and at step (e), determining at least one of the one or more uptake metrics using the 3D functional image and the reference volume identified within the 3D anatomical image (e.g., computing a normalization value based on intensity values of voxels of the 3D functional image that correspond to the reference volume identified within the 3D anatomical image). In certain embodiments, the at least one of the one or more uptake metrics determined using the 3D functional image and the reference volume comprises a tumor to background ratio (TBR) value, wherein determining the TBR value comprises: determining a target intensity value using intensity values of one or more voxels of the 3D functional image that correspond to the prostate volume identified within the initial VOI of the 3D anatomical image (e.g., wherein the target intensity value is a maximum of intensities of the voxels of the 3D functional image that correspond to the prostate volume); determining a background intensity value using intensity values of one or more

voxels of the 3D functional image that correspond to the reference volume identified within the 3D anatomical image [e.g., wherein the background intensity value is an average intensity of a plurality (e.g., all) of the voxels of the 3D functional image that correspond to the identified reference volume; and determining, as the TBR value, a ratio of the target intensity value to the background intensity value. In certain embodiments, the method comprises determining a prostate cancer status for the subject based on the TBR value in comparison with one or more threshold values (e.g., predetermined threshold values). In certain embodiments, the one or more threshold values are determined using a plurality of reference TBR values [e.g., each reference TBR value having been determined from a corresponding set of reference images (e.g., a reference 3D anatomical image and a reference 3D functional image; e.g., a CT/SPECT image set)], each reference TBR value associated with a particular classification prostate cancer status (e.g., assigned by a medical practitioner)[e.g., a Gleason grade having been determined (e.g., based on histopathology from a radical prostatectomy) for a same subject for which the reference TBR value was determined]. In certain embodiments, the one or more threshold values are determined using a receiver operating characteristic (ROC) curve [e.g., using area under the curve (AUC) analysis; e.g., to provide a specific sensitivity value and/or a specific specificity value]. In certain embodiments, the method comprises determining the prostate cancer status for the subject to be (i) clinically significant if the TBR value is above a cutoff threshold or (ii) clinically non-significant if the TBR value is below the cutoff threshold.

In certain embodiments, the method comprises identifying, by the processor, (e.g., using the second module) a bladder volume within the 3D anatomical image (e.g., within the initial VOI) corresponding to a bladder of the subject; and at step (e), correcting for cross-talk from the bladder (e.g., scattering and/or partial volume effects through which radiopharmaceutical uptake in the bladder influences intensity values of voxels of the 3D functional image that represent physical volumes within the prostate) using intensities of voxels of the 3D functional image corresponding to the identified bladder volume within the 3D anatomical image [e.g., by adjusting intensities of voxels of the 3D functional image that correspond to the prostate volume based on their proximity to the identified bladder volume and/or a bladder uptake (e.g., determined based on intensities of voxels of the 3D functional image that correspond to the bladder volume); e.g., by using intensities of voxels of the 3D functional image to establish a model of radiation scattering from the bladder and adjusting intensities of voxels of the 3D functional image based on the model]. In certain embodiments, correcting for cross-talk from the bladder comprises: determining one or more bladder intensity bleed functions that model a contribution of intensity originating from radiopharmaceutical within the bladder of the subject to intensity of one or more voxels of the 3D functional image corresponding to one or more regions of the 3D anatomical image that are outside of the identified bladder volume, wherein the one or more bladder intensity bleed functions model said contribution as a function of distance from the identified bladder volume [e.g., wherein each of the one or more bladder intensity bleed functions models intensity bleed along a particular direction and is obtained by fitting a template function (e.g., an n-th degree polynomial) to intensities of voxels of the 3D functional image corresponding to the identified bladder volume within the 3D anatomical image and lying along the particular direction]; and for each of one or more voxels of the 3D functional image corresponding to the identified prostate volume within the 3D anatomical image, adjusting an intensity of the voxel for bladder cross-talk using the one or more bladder intensity bleed functions [e.g., by evaluating the one or more bladder intensity bleed functions to determine a bladder intensity bleed value for the voxel and subtracting the bladder intensity bleed value from the intensity of the voxel to obtain a corrected voxel intensity].

In certain embodiments, the method comprises: identifying, by the processor, (e.g., using the second module) a bladder volume within the 3D anatomical image (e.g., within the initial VOI) corresponding to a bladder of the subject; determining, by the processor, a dilated bladder volume by applying a morphological dilation operation to the identified bladder volume; and at step (e), determining the one or more uptake metrics using intensity values of voxels of the 3D functional image that (i) correspond to the prostate volume identified within the VOI of the 3D anatomical image, but (ii) do not correspond to regions of the 3D anatomical image within the dilated bladder volume (e.g., thereby omitting from the computation of the one or more uptake metrics those voxels of the 3D functional image that correspond to locations in the 3D anatomical image within a predefined distance from the identified bladder volume; e.g., and, accordingly, are excessively close to the identified bladder volume).

In certain embodiments, the 3D functional image is a nuclear medicine image (e.g., a single-photon emission computerized tomography (SPECT) scan; e.g., an positron emission tomography (PET) scan) of the subject following administration to the subject of the radiopharmaceutical. In certain embodiments, the radiopharmaceutical comprises a PSMA binding agent (e.g., ^{99m}Tc-MIP-1404; e.g., [^{18}F] DCFPyL). In certain embodiments, the nuclear medicine image is a single-photon emission computerized tomography (SPECT) scan of the subject obtained following administration to the subject of the radiopharmaceutical. In certain embodiments, the radiopharmaceutical comprises ^{99m}Tc-MP-1404.

In certain embodiments, the method comprises determining, based on at least a portion of the one or more uptake metrics, one or more diagnostic or prognostic values [e.g., a value that provides a measure of disease state, progression, life expectancy (e.g., overall survival), treatment efficacy, and the like for the subject (e.g., Gleason score)] for the subject. In certain embodiments, determining at least one of the one or more diagnostic or prognostic values comprises comparing an uptake metric to one or more threshold value(s). In certain embodiments, at least one of the one or more diagnostic or prognostic values estimates a risk for clinically significant prostate cancer in the subject.

In certain embodiments, the method comprises: (f) causing, by the processor, display of an interactive graphical user interface (GUI) for presentation to the user of a visual representation of the 3D anatomical image and/or the 3D functional image; and (g) causing, by the processor, graphical rendering of, within the GUI, the 3D anatomical image and/or the 3D functional image as selectable and superimposable layers, such that either can be selected for display (e.g., via a corresponding user-selectable graphical control element (e.g., a toggle element)) and rendered separately, or both selected for display and rendered together by overlaying the 3D anatomical image with the 3D functional image. In certain embodiments, step (g) comprises causing graphical rendering of a selectable and superimposable segmentation layer comprising one or more identified specific tissue

volumes within the 3D anatomical image, wherein upon selection of the segmentation layer for display, graphics representing the one or more specific tissue volumes are overlaid on the 3D anatomical image and/or the 3D functional image (e.g., as outlines; e.g., as semi-transparent color-coded volumes). In certain embodiments, the one or more specific tissue volumes comprise(s) the identified prostate volume. In certain embodiments, the method comprises, at step (g), causing rendering of a 2D cross sectional view of the 3D anatomical image and/or the 3D functional image within an interactive 2D viewer, such that a position of the 2D cross sectional view is adjustable by the user. In certain embodiments, the method comprises, at step (g), causing rendering of an interactive (e.g., rotatable; e.g., sliceable) 3D view of the 3D anatomical image and/or the 3D functional image. In certain embodiments, the method comprises causing display of, within the GUI, a graphical element (e.g., a cross-hair, a target, a colored marker, etc.) indicating a location corresponding to a voxel of the identified prostate volume (e.g., said location also corresponding to a voxel of the 3D functional image having a maximal intensity, e.g., a maximal corrected intensity, in comparison with other voxels of the 3D functional image corresponding to the identified prostate volume), thereby facilitating user review and/or quality control of the method (e.g., allowing a medical practitioner to verify the identified location corresponds to an expected physical location of the prostate of the subject). In certain embodiments, the method comprises causing display of, within the GUI, text and/or graphics representing the one or more uptake metrics determined in step (e) (e.g., and, optionally, one or more prognostic values determined therefrom) along with a quality control graphical widget for guiding the user through a quality control and reporting workflow for review and/or updating of the one or more uptake metrics (e.g., wherein the quality control graphical widget comprises a selectable graphical control element for receipt of a user input corresponding to (i) approval of the one or more uptake metrics as determined, automatically, by the processor or (ii) disapproval of the automated determination of the one or more uptake metrics). In certain embodiments, the method comprises: receiving, via the quality control graphical widget, a user input corresponding to an approval of automated determination of the one or more uptake metrics (e.g., and any prognostic values determined therefrom); and responsive to the receipt of the user input corresponding to the approval of the automated determination of the one or more uptake metrics, generating, by the processor, a report for the subject comprising a representation of the one or more automatically determined uptake metrics [e.g., the report comprising: an identification of the subject (e.g., an anonymized patient ID number); a representation (e.g., text) of the one or more determined uptake metrics (e.g., and any prognostic values determined therefrom); and a representation (e.g., graphics and/or text) of the user approval the automated determination of the one or more uptake metrics (e.g., and any prognostic values determined therefrom)].

In certain embodiments, the method comprises: receiving, via the quality control graphical widget, a user input corresponding to disapproval of automated determination of the one or more uptake metrics (e.g., and any prognostic values determined therefrom); responsive to receipt of the user input corresponding to the disapproval of the automated determination of the one or more uptake metrics, causing, by the processor, display of a voxel selection graphical element (e.g., a cursor; e.g., an adjustable cross-hair) for user selection of one or more voxels of the 3D functional image (e.g., directly or indirectly, e.g., through selection of voxels of the 3D anatomical image and subsequent determination of corresponding voxels of the 3D functional image) for use in determining updated values of the one or more uptake metrics; receiving, via the voxel selection graphical element, the user selection of one or more voxels of the 3D functional image for use in determining updated values of the one or more uptake metrics [e.g., wherein the user selection is one or more corrected background intensity measurement location(s) and/or one or more corrected prostate intensity location(s), e.g., where a user overrides automated identification of a location of the prostate and/or where the user overrides automated identification of a location of a background area, e.g., gluteal muscle]; updating, by the processor, values of the one or more uptake metrics using the user selected voxels; and generating, by the processor, a report for the subject comprising a representation (e.g., text) of the one or more updated uptake metrics [e.g., the report comprising: an identification of the subject (e.g., an anonymized patient ID number); a representation (e.g., text) of the one or more determined uptake metrics (e.g., and any prognostic values determined therefrom); and a representation (e.g., graphics and/or text) of the user approval of the determination of the one or more uptake metrics (e.g., and any prognostic values determined therefrom) using the user selected voxels (e.g., text indicating that the uptake metrics were determined via semi-automated analysis, with manual selection of voxels from the user)].

In certain embodiments, the method comprises: receiving, via the quality control graphical widget, a user input corresponding to disapproval of automated determination of the one or more uptake metrics (e.g., and any prognostic values determined therefrom); receiving, via the quality control graphical widget, a user input corresponding to a rejection of quality control (e.g., due to low image quality); and generating, by the processor, a report for the subject, wherein the report comprises an identification of the rejection of quality control.

In certain embodiments, voxels of the 3D functional image are related to voxels of the 3D anatomical image via a known relationship [e.g., each voxel of the 3D functional image is associated with one or more voxels of the 3D anatomical image; e.g., each of a plurality of sets of one or more voxels of the 3D functional image is associated with a set of one or more voxels of the 3D anatomical image; e.g., coordinates associated with voxels of the 3D functional image are related to coordinates associated with voxels of the anatomical 3D image via a known functional relationship (e.g., via a known spatial relationship between the first and second imaging modalities)].

In certain embodiments, the first module is a first CNN (convolutional neural network) module and the second module is a second CNN module, wherein the second CNN module comprises a greater number of convolutional filters than the first CNN module (e.g., at least 1.5 times as many, e.g., at least twice as many, e.g., approximately twice as many, e.g., at least three times as many, e.g., approximately three times as many).

In certain embodiments, the method comprises performing steps (a) and (c) for each of a plurality of 3D anatomical images to determine a plurality of initial VOIs, each within one of the plurality of 3D anatomical images, wherein a variability in sizes of the initial VOIs is less than (e.g., substantially less than) a variability in sizes of the 3D anatomical images (e.g., wherein variability in "sizes" means either or both of (i) and (ii) as follows: (i) variability in one or more dimensions of the anatomical volume rep-

resented in the image, e.g., as measured in mm, and (ii) variability in the number of voxels in the image along each of one or more dimensions of the image) (e.g., wherein the sizes of the 3D anatomical images (each full image from which each VOI is determined) vary by at least 200 mm, and/or by at least 300 mm, and/or by at least 400 mm, and/or by at least 500 mm, and/or by as much as 400 mm, and/or by as much as 500 mm, and/or by as much as 1000 mm, and/or by as much as 1500 mm) along each of one or more dimensions; e.g., wherein the sizes of the 3D anatomical images (each full image from which each VOI is determined) vary by at least 25 voxels, and/or by at least 50 voxels, and/or by at least 100 voxels, and/or by at least 250 voxels, and/or by at least 300 voxels, and/or by as much as 250 voxels, and/or by as much as 300 voxels, and/or by as much as 500 voxels) along each of one or more dimensions; e.g., wherein the sizes of the VOIs vary by less than or equal to 200 mm (e.g., less than or equal to 100 mm; e.g., less than or equal to 50 mm) along each of one or more dimensions; e.g. wherein the sizes of the VOIs vary by less than or equal to 250 voxels (e.g., less than or equal to 200 voxels; e.g., less than or equal to 150 voxels) along each of one or more dimensions].

In another aspect, the invention is directed to a method for automatically processing 3D images to identify 3D volumes within the 3D images that correspond to a target tissue region within a subject and determining one or more uptake metrics indicative of radiopharmaceutical uptake therein, the method comprising: (a) receiving, by a processor of a computing device, a 3D anatomical image of the subject obtained using an anatomical imaging modality [e.g., x-ray computed tomography (CT); e.g., magnetic resonance imaging (MRI); e.g., ultra-sound], wherein the 3D anatomical image comprises a graphical representation of tissue (e.g., soft-tissue and/or bone) within a pelvic region of the subject; (b) receiving, by the processor, a 3D functional image of the subject obtained using a functional imaging modality [e.g., single-photon emission computed tomography (SPECT); e.g., positron emission tomography (PET)], wherein the 3D functional image comprises a plurality of voxels, each representing a particular physical volume within the subject and having an intensity value that represents detected radiation emitted from a the particular physical volume, wherein at least a portion of the plurality of voxels of the 3D functional image represent physical volumes within the pelvic region of the subject; (c) determining, by the processor, using a first module (e.g., a first machine learning module), an initial volume of interest (VOI) within the 3D anatomical image (e.g., a rectangular prism), the initial VOI corresponding to an anatomical sub-region (e.g., a group of related tissue, such as a pelvic region, a chest region, a head and/or neck region, and the like) comprising the target region (e.g., wherein the VOI excludes more voxels of the 3D anatomical image than it includes; e.g., wherein the VOI includes less than 25% of the voxels of the 3D anatomical image; e.g., wherein a majority of voxels within the VOI represent physical volumes within the anatomical sub-region); (d) identifying, by the processor, using a second module (e.g., a second machine learning module), a target volume within the initial VOI corresponding to the target tissue region of the subject; and (e) determining, by the processor, the one or more uptake metrics using the 3D functional image and the target volume identified within the VOI of the 3D anatomical image [e.g., computing a quantity of radiopharmaceutical in the target tissue region of the subject based on intensity values of voxels of the 3D functional image that correspond to the target volume identified within the VOI of the 3D anatomical image; e.g., computing a sum (e.g., a weighted sum), an average, and/or a maximum of intensities of voxels of the 3D functional image representing a physical volume occupied by the target tissue region of the subject].

In certain embodiments, the method has one or more of the features articulated in paragraphs above.

In another aspect, the invention is directed to a method of automatically analyzing a 3D functional image [e.g., a nuclear medicine image (e.g., a SPECT image; e.g., a PET image)] to correct prostate voxel intensities for cross-talk from radiopharmaceutical uptake into a bladder, the method comprising: (a) receiving, by a processor of a computing device, a 3D anatomical image of the subject obtained using an anatomical imaging modality [e.g., x-ray computed tomography (CT); e.g., magnetic resonance imaging (MRI); e.g., 3D ultra-sound], wherein the 3D anatomical image comprises a graphical representation of tissue (e.g., soft-tissue and/or bone) within a subject, at least a portion of which corresponds to a bladder and a prostate of the subject; (b) receiving, by the processor, the 3D functional image of the subject, wherein the 3D functional image comprises a plurality of voxels, each representing a particular physical volume within the subject and having an intensity value that represents detected radiation emitted from a the particular physical volume, wherein at least a portion of the plurality of voxels of the 3D functional image represent physical volumes within the bladder and/or the prostate of the subject; (c) automatically identifying, by the processor, within the 3D anatomical image: (i) a prostate volume corresponding to a prostate of the subject and (ii) a bladder volume corresponding to a bladder of the subject; (d) automatically identifying, by the processor, within the 3D functional image, (i) a plurality of prostate voxels corresponding to the identified prostate volume and (ii) a plurality of bladder voxels corresponding to the identified bladder volume; (e) adjusting, by the processor, one or more measured intensities of the prostate voxels (e.g., one or more cumulative measurements and/or peak measurements and/or mean measurements and/or median measurements of intensity corresponding to the identified prostate volume and/or corresponding to each of, and/or cumulatively of, a plurality of regions of the identified prostate volume) based on one or more measured intensities of the bladder voxels (e.g., one or more cumulative measurements and/or peak measurements and/or mean measurements and/or median measurements of intensity corresponding to the identified bladder volume and/or corresponding to each of, and/or cumulatively of, a plurality of regions of the identified bladder volume); and (f) determining, by the processor, one or more uptake metrics indicative of radiopharmaceutical uptake within the prostate of the subject using the adjusted intensities of the prostate voxels.

In certain embodiments, the method has one or more of the features articulated in the paragraphs above.

In another aspect, the invention is directed to a method of detecting a prostate cancer status, and/or quantifying a prostate cancer risk, of a subject based on automated analysis of a 3D functional image (e.g., a SPECT image) of a portion of the subject, the method comprising: (a) acquiring, following administration to the subject of a radiopharmaceutical comprising a PSMA binding agent, the 3D functional image (e.g., a SPECT image); (b) identifying, by a processor of a computing device, a 3D target volume within the 3D functional image, the 3D target volume corresponding to a prostate of the subject; (c) determining, by the processor, using intensities of voxels of the 3D target volume, a target to background ratio (TBR) value; and (d)

causing, by the processor, graphical rendering of text and/or graphics representing the determined TBR value for display within an interactive graphical user interface (GUI) [e.g., wherein the method comprises determining (e.g., and displaying) a prostate cancer classification status of either (i) clinically significant or (ii) clinically non-significant based at least in part on the TBR value].

In certain embodiments, the method has one or more of the features articulated in the paragraphs above.

In another aspect, the invention is directed to a system for automatically processing 3D images to identify 3D volumes within the 3D images that correspond to a prostate of a subject and determining one or more uptake metrics indicative of radiopharmaceutical uptake therein (i.e., in the prostate), the system comprising: a processor; and a memory (e.g., external to or embedded in the processor) having instructions stored thereon, wherein the instructions, when executed by the processor, cause the processor to: (a) receive a 3D anatomical image of the subject obtained using an anatomical imaging modality [e.g., x-ray computed tomography (CT) (e.g., a whole-body CT image; e.g., a partial body CT image); e.g., magnetic resonance imaging (MRI); e.g., 3D ultra-sound], wherein the 3D anatomical image comprises a graphical representation of tissue (e.g., soft-tissue and/or bone) within a subject, at least a portion of which corresponds to a pelvic region of the subject; (b) receive a 3D functional image of the subject obtained using a functional imaging modality [e.g., single-photon emission computed tomography (SPECT); e.g., positron emission tomography (PET)], wherein the 3D functional image comprises a plurality of voxels, each representing a particular physical volume within the subject and having an intensity value that represents detected radiation emitted from the particular physical volume, wherein at least a portion of the plurality of voxels of the 3D functional image represent physical volumes within the pelvic region of the subject; (c) determine, using a first module (e.g., a first machine learning module), an initial volume of interest (VOI) within the 3D anatomical image (e.g., a parallelepiped, e.g., a cuboid), the initial VOI corresponding to tissue within the pelvic region of the subject and excluding tissue outside the pelvic region of the subject (e.g., wherein the VOI excludes more voxels of the 3D anatomical image than it includes; e.g., wherein the VOI includes less than 25% of the voxels of the 3D anatomical image; e.g., wherein a majority of voxels within the VOI represent physical volumes within the pelvic region of the subject); (d) identify, using a second module (e.g., a second machine learning module), a prostate volume within the initial VOI corresponding to the prostate of the subject; and (e) determine (e.g., and display) the one or more uptake metrics using the 3D functional image and the prostate volume identified within the initial VOI of the 3D anatomical image [e.g., compute a quantity of radiopharmaceutical in the prostate of the subject based on intensity values of voxels of the 3D functional image that correspond to the prostate volume identified within the initial VOI of the 3D anatomical image; e.g., compute a sum (e.g., a weighted sum) and/or an average and/or a maximum of intensities of voxels of the 3D functional image representing a physical volume occupied by the prostate of the subject] [e.g., wherein the one or more uptake metrics comprises a tumor to background ratio (TBR) value, and wherein the instructions, when executed by the processor, cause the processor to determine (e.g., and display) a prostate cancer classification status of either (i) clinically significant or (ii) clinically non-significant based at least in part on the TBR value].

In certain embodiments, the system has one or more of the features articulated in the paragraphs above.

In another aspect, the invention is directed to a system for automatically processing 3D images to identify 3D volumes within the 3D images that correspond to a target tissue region within a subject and determining one or more uptake metrics indicative of radiopharmaceutical uptake therein (i.e., in the target tissue region), the system comprising: a processor; and a memory (e.g., external to or embedded in the processor) having instructions stored thereon, wherein the instructions, when executed by the processor, cause the processor to: (a) receive a 3D anatomical image of the subject obtained using an anatomical imaging modality [e.g., x-ray computed tomography (CT); e.g., magnetic resonance imaging (MRI); e.g., ultra-sound], wherein the 3D anatomical image comprises a graphical representation of tissue (e.g., soft-tissue and/or bone) within a pelvic region of the subject; (b) receive a 3D functional image of the subject obtained using a functional imaging modality [e.g., single-photon emission computed tomography (SPECT); e.g., positron emission tomography (PET)], wherein the 3D functional image comprises a plurality of voxels, each representing a particular physical volume within the subject and having an intensity value that represents detected radiation emitted from a the particular physical volume, wherein at least a portion of the plurality of voxels of the 3D functional image represent physical volumes within the pelvic region of the subject; (c) determine, using a first module (e.g., a first machine learning module), an initial volume of interest (VOI) within the 3D anatomical image (e.g., a rectangular prism), the initial VOI corresponding to an anatomical sub-region (e.g., a group of related tissue, such as a pelvic region, a chest region, a head and/or neck region, and the like) comprising the target region (e.g., wherein the VOI excludes more voxels of the 3D anatomical image than it includes; e.g., wherein the VOI includes less than 25% of the voxels of the 3D anatomical image; e.g., wherein a majority of voxels within the VOI represent physical volumes within the anatomical sub-region); (d) identify, using a second module (e.g., a second machine learning module), a target volume within the initial VOI corresponding to the target tissue region of the subject; and (e) determine the one or more uptake metrics using the 3D functional image and the target volume identified within the VOI of the 3D anatomical image [e.g., compute a quantity of radiopharmaceutical in the target tissue region of the subject based on intensity values of voxels of the 3D functional image that correspond to the target volume identified within the VOI of the 3D anatomical image; e.g., compute a sum (e.g., a weighted sum), and/or an average, and/or a maximum of intensities of voxels of the 3D functional image representing a physical volume occupied by the target tissue region of the subject] [e.g., wherein the one or more uptake metrics comprises a tumor to background ratio (TBR) value, and wherein the instructions, when executed by the processor, cause the processor to determine (e.g., and display) a cancer classification status of either (i) clinically significant or (ii) clinically non-significant based at least in part on the TBR value].

In certain embodiments, the system has one or more of the features articulated in the paragraphs above .

In another aspect, the invention is directed to a system for detecting a prostate cancer status, and/or quantifying a prostate cancer risk, of a subject based on automated analysis of a 3D functional image (e.g., a SPECT image) of a portion of the subject, the system comprising: a processor; and a memory (e.g., external to or embedded in the proces-

sor) having instructions stored thereon, wherein the instructions, when executed by the processor, cause the processor to: (a) receive the 3D functional image (e.g., a SPECT image) of the portion (e.g., any or all) of the subject following administration to the subject of a radiopharmaceutical comprising a PSMA binding agent; (b) identify a 3D target volume within the 3D functional image, the 3D target volume corresponding to a prostate of the subject; (c) determine, using intensities of voxels of the 3D target volume, a target to background ratio (TBR) value; and (d) cause graphical rendering of text and/or graphics representing the determined TBR value for display within an interactive graphical user interface (GUI) [e.g., wherein the instructions, when executed by the processor, cause the processor to determine (e.g., and display) a prostate cancer classification status of either (i) clinically significant or (ii) clinically non-significant based at least in part on the TBR value].

In certain embodiments, the system has one or more of the features articulated in the paragraphs above.

In certain embodiments, the invention is directed to a computer-aided detection (CADe) device comprising any of the systems described herein. In certain embodiments, the instructions cause the processor to identify a classification of either clinically significant prostate cancer or clinically non-significant prostate cancer for the subject.

In certain embodiments, the invention is directed to a computer-aided diagnostic (CADx) device comprising any of the systems described herein. In certain embodiments, the instructions cause the processor to identify a classification of either clinically significant prostate cancer or clinically non-significant prostate cancer for the subject.

In certain embodiments, the invention is directed to a combination product comprising: (a) a radiolabeled PSMA binding agent (e.g., ^{99m}Tc-MIP-1404; e.g., [^{18}F]DCFPyL, e.g., other known PSMA binding agent); and (b) a computer-aided detection (CADe) device comprising any of the systems described herein. In certain embodiments, the combination product comprises a label specifying usage of the radiolabeled PSMA binding agent with the computer aided detection device.

Features of embodiments described with respect to one aspect of the invention may be applied with respect to another aspect of the invention.

BRIEF DESCRIPTION OF THE FIGURES

The patent or application file contains at least one drawing executed in color. Copies of this patent or patent application publication with color drawing(s) will be provided by the Office upon request and payment of the necessary fee.

The foregoing and other objects, aspects, features, and advantages of the present disclosure will become more apparent and better understood by referring to the following description taken in conjunction with the accompanying drawings, in which:

FIG. **1** is a block diagram showing a process for automatically identifying 3D volumes within 3D images that correspond to a prostate of a subject and determining uptake metrics indicative of radiopharmaceutical uptake therein, according to an illustrative embodiment.

FIG. **2**A is an image showing 3D view of a CT image comprising a graphical representation of soft-tissue, according to an illustrative embodiment.

FIG. **2**B is an image showing a 3D view of a CT image comprising a graphical representation of bone, according to an illustrative embodiment.

FIG. **2**C is an image showing a 3D view of a CT image comprising a graphical representation of bone overlaid with a SPECT image and graphics representing an identified tissue volume corresponding to a prostate organ within pelvic bones of a subject, according to an illustrative embodiment.

FIG. **2**D is an image showing 3D view of a CT image comprising a graphical representation of bone overlaid with a SPECT image and graphics representing an identified tissue volume corresponding to a prostate organ within pelvic bones of a subject, according to an illustrative embodiment.

FIG. **2**E is an image showing a 3D view of a CT image comprising a graphical representation of bone overlaid with a SPECT image, according to an illustrative embodiment.

FIG. **3**A is a set of images, each image showing a 2D cross-sectional view of a 3D CT image overlaid with graphics representing an identified initial volume of interest (VOI) within the 3D CT image, according to an illustrative embodiment.

FIG. **3**B is a set images, each image showing a 2D cross-sectional view of a 3D CT image overlaid with graphics representing an identified initial volume of interest (VOI) within the 3D CT image, according to an illustrative embodiment.

FIG. **4**A is a set of images showing 2D cross sectional views of a CT image of a subject and a cuboidal region identified as an initial volume of interest within the CT image, according to an illustrative embodiment.

FIG. **4**B is a set of images showing 2D cross sectional views of a CT image of a subject along with identified tissue volumes corresponding to pelvic bones and a prostate of the subject.

FIG. **5**A is a set of images showing 2D cross sectional views of a CT image of a subject and a cuboidal region identified as an initial volume of interest within the CT image, according to an illustrative embodiment.

FIG. **5**B is a set of images showing 2D cross sectional views of a CT image of a subject along with identified tissue volumes corresponding to pelvic bones and a prostate of the subject.

FIG. **6**A is a set of images showing 2D cross sectional views of a CT image of a subject and a cuboidal region identified as an initial volume of interest within the CT image, according to an illustrative embodiment.

FIG. **6**B is a set of images, each image showing a 2D cross-sectional view of a 3D CT image overlaid with graphics representing an identified initial volume of interest (VOI) within the 3D CT image, according to an illustrative embodiment.

FIG. **6**C is a set of images, each image showing a 2D cross-sectional view of a 3D CT image overlaid with graphics representing an identified initial volume of interest (VOI) within the 3D CT image, according to an illustrative embodiment.

FIGS. **7**A-**7**E present a block diagram of a CNN module architecture (localization network) for identifying a volume of interest (e.g., VOI) corresponding to a pelvic region within a CT image of a subject (wherein the VOI is subsequently processed by a second CNN module for more detailed segmentation/identification of the prostate and/or other tissues within the pelvic region), according to an illustrative embodiment.

FIGS. **7**F-**7**J present a block diagram of a CNN module architecture (segmentation network) for processing the previously-identified VOI for precise segmentation of the pros-

tate and/or other tissues within the pelvic region, according to an illustrative embodiment.

FIG. **8**A is a set images, each showing a 2D cross-sectional view of a 3D CT image overlaid with graphics representing identified tissue volumes corresponding to three different pelvic bones (left and right hip bones and the sacrum), according to an illustrative embodiment.

FIG. **8**B is an image showing a 3D view of a 3D CT image overlaid with graphics representing identified tissue volumes corresponding to three different pelvic bones (left and right hip bones and the sacrum), according to an illustrative embodiment.

FIG. **9**A is an image showing a 2D cross-sectional view of a 3D CT image overlaid with graphics representing identified tissue volumes corresponding to pelvic bones (left and right hip bones) and a prostate of a subject, according to an illustrative embodiment.

FIG. **9**B is a set of images showing different 2D cross sectional views of a 3D CT image overlaid with graphics representing identified tissue volumes corresponding to pelvic bones, gluteal muscles, a rectum, a prostate, and a bladder of a subject, according to an illustrative embodiment.

FIG. **10** is an image showing a 2D cross sectional view of a low quality 3D CT image overlaid with graphics representing identified tissue volumes corresponding to pelvic bones and a prostate of a subject, according to an illustrative embodiment.

FIG. **11** is a schematic showing an example architecture wherein image segmentation for identification of a prostate volume as described herein is performed by a dedicated module, according to an illustrative embodiment.

FIG. **12** is a block flow diagram showing an example architecture of modules for performing CNN-based image segmentation, according to an illustrative embodiment.

FIG. **13** is a block flow diagram showing a structure of a CNN, according to an illustrative embodiment.

FIG. **14** is a block flow diagram showing a structure of a CNN that performs auxiliary predictions, according to an illustrative embodiment.

FIG. **15** is a schematic illustrating cross-talk between a bladder and a prostate of a subject, according to an illustrative embodiment.

FIG. **16**A is a screenshot of a graphical user interface (GUI) for reviewing patient image data showing a window for selecting subjects for whom to analyze and/or review data, according to an illustrative embodiment.

FIG. **16**B is a screenshot of a graphical user interface (GUI) for reviewing patient image data showing a window for selecting subjects for whom to analyze and/or review data, along with a graphical control element for initiating processing of and reviewing patient image data, according to an illustrative embodiment.

FIG. **16**C is a screenshot of a graphical user interface (GUI) for reviewing patient image data showing a window for selecting subjects for whom to analyze and/or review data, along with a graphical control element for initiating processing of and reviewing patient image data, according to an illustrative embodiment.

FIG. **17**A is a screenshot of a GUI for reviewing patient image data showing a window comprising a set of images each showing a different 2D cross sectional view of a CT image of a subject overlaid with a SPECT image of the subject and graphics representing identified tissue volumes, according to an illustrative embodiment.

FIG. **17**B is a screenshot of a GUI for reviewing patient image data showing a window comprising a set of images each showing a different 2D cross sectional view of a CT image of a subject overlaid with a SPECT image of the subject and graphics representing identified tissue volumes, according to an illustrative embodiment.

FIG. **17**C is a screenshot of a GUI for reviewing patient image data showing a window comprising a set of images each showing a different 2D cross sectional view of a CT image of a subject overlaid with a SPECT image of the subject and graphics representing identified tissue volumes, according to an illustrative embodiment.

FIG. **17**D is a screenshot of a GUI for reviewing patient image data showing a window comprising a set of images each showing a different 2D cross sectional view of a CT image of a subject overlaid with a SPECT image of the subject and graphics representing identified tissue volumes, according to an illustrative embodiment.

FIG. **17**E is a screenshot of a GUI for reviewing patient image data showing a window comprising a set of images each showing a different 2D cross sectional view of a CT image of a subject overlaid with a SPECT image of the subject and graphics representing identified tissue volumes, according to an illustrative embodiment.

FIG. **18**A is a screenshot of a GUI for reviewing patient image data showing a window comprising a graphical control element for toggling display of selectable layers illustrating a user toggling of a SPECT image layer off, according to an illustrative embodiment.

FIG. **18**B is a screenshot of a GUI for reviewing patient image data showing a window comprising a set of images each showing a different 2D cross sectional view of a CT image of a subject overlaid with graphics representing identified tissue volumes, according to an illustrative embodiment.

FIG. **18**C is a screenshot of a GUI for reviewing patient image data showing a window comprising a set of images each showing a different 2D cross sectional view of a CT image of a subject overlaid with graphics representing identified tissue volumes, according to an illustrative embodiment.

FIG. **18**D is a screenshot of a GUI for reviewing patient image data showing a window comprising a set of images each showing a different 2D cross sectional view of a CT image of a subject overlaid with graphics representing identified tissue volumes, according to an illustrative embodiment.

FIG. **18**E is a screenshot of a GUI for reviewing patient image data showing a window comprising a set of images each showing a different 2D cross sectional view of a CT image of a subject overlaid with graphics representing identified tissue volumes, according to an illustrative embodiment.

FIG. **18**F is a screenshot of a GUI for reviewing patient image data showing a window comprising a set of images each showing a different 2D cross sectional view of a CT image of a subject overlaid with graphics representing identified tissue volumes, according to an illustrative embodiment.

FIG. **19**A is a screenshot of a GUI for reviewing patient image data showing a window comprising a graphical control element for toggling display of selectable layers illustrating a user toggling of a SPECT image layer and a segmentation layer on and off, respectively, according to an illustrative embodiment.

FIG. **19**B is a screenshot of a GUI for reviewing patient image data showing a window comprising a set of images each showing a different 2D cross sectional view of a CT

image of a subject overlaid with a SPECT image of the subject, according to an illustrative embodiment.

FIG. **19**C is a screenshot of a GUI for reviewing patient image data showing a window comprising a set of images each showing a different 2D cross sectional view of a CT image of a subject overlaid with a SPECT image of the subject, according to an illustrative embodiment.

FIG. **19**D is a screenshot of a GUI for reviewing patient image data showing a window comprising a set of images each showing a different 2D cross sectional view of a CT image of a subject overlaid with a SPECT image of the subject, according to an illustrative embodiment.

FIG. **20**A is a screenshot of a GUI for reviewing patient image data showing a window comprising an image showing a 3D view of a CT image of a subject comprising a graphical representation of soft tissue overlaid with a SPECT image of the subject, according to an illustrative embodiment.

FIG. **20**B is a screenshot of a GUI for reviewing patient image data showing a window comprising an image showing a 3D view of a CT image of a subject comprising a graphical representation of soft tissue overlaid with a SPECT image of the subject, according to an illustrative embodiment.

FIG. **20**C is a screenshot of a GUI for reviewing patient image data showing a window comprising an image showing a 3D view of a CT image of a subject comprising a graphical representation of soft tissue overlaid with a SPECT image of the subject, according to an illustrative embodiment.

FIG. **21**A is a screenshot of a GUI for reviewing patient image data showing a window comprising an image showing a 3D view of a CT image of a subject comprising a graphical representation of bone overlaid with a SPECT image of the subject, according to an illustrative embodiment.

FIG. **21**B is a screenshot of a GUI for reviewing patient image data showing a window comprising an image showing a 3D view of a CT image of a subject comprising a graphical representation of bone overlaid with a SPECT image of the subject, according to an illustrative embodiment.

FIG. **22**A is a screenshot of a GUI for reviewing patient image data showing a window comprising an image showing a 3D view of a CT image of a subject comprising a graphical representation of bone overlaid with a SPECT image of the subject, according to an illustrative embodiment.

FIG. **22**B is a screenshot of a GUI for reviewing patient image data showing a window comprising an image showing a 3D view of a CT image of a subject comprising a graphical representation of bone overlaid with a SPECT image of the subject, according to an illustrative embodiment.

FIG. **22**C is a screenshot of a GUI for reviewing patient image data showing a window comprising an image showing a 3D view of a CT image of a subject comprising a graphical representation of bone overlaid with a SPECT image of the subject and graphics representing identified tissue volumes, according to an illustrative embodiment.

FIG. **22**D is a screenshot of a GUI for reviewing patient image data showing a window comprising an image showing a 3D view of a CT image of a subject comprising a graphical representation of bone overlaid with a SPECT image of the subject and graphics representing identified tissue volumes, according to an illustrative embodiment.

FIG. **22**E is a screenshot of a GUI for reviewing patient image data showing a window comprising an image showing a 3D view of a CT image of a subject comprising a graphical representation of bone overlaid with a SPECT image of the subject and graphics representing identified tissue volumes, according to an illustrative embodiment.

FIG. **22**F is a screenshot of a GUI for reviewing patient image data showing a window comprising an image showing a 3D view of a CT image of a subject comprising a graphical representation of bone overlaid with a SPECT image of the subject and graphics representing identified tissue volumes, according to an illustrative embodiment.

FIG. **23**A is a screenshot of a GUI for reviewing patient image data showing a window comprising an image showing a 3D view of a CT image of a subject comprising a graphical representation of bone overlaid with a SPECT image of the subject, according to an illustrative embodiment.

FIG. **23**B is a screenshot of a GUI for reviewing patient image data showing a window comprising an image showing a 3D view of a CT image of a subject comprising a graphical representation of bone overlaid with a SPECT image of the subject, according to an illustrative embodiment.

FIG. **24** is a screenshot of a GUI for reviewing patient image data showing a window comprising a generated report for a subject, according to an illustrative embodiment.

FIG. **25** is a block flow diagram showing a workflow for user interaction with a GUI in which the user reviews images, segmentation results, and uptake metrics, and generates reports, according to an illustrative embodiment.

FIG. **26**A is a screenshot of a view of a GUI window that allows a user to upload images, according to an illustrative embodiment.

FIG. **26**B is a screenshot of a view of a GUI window showing a listing of images uploaded by a user, according to an illustrative embodiment.

FIG. **27**A is a screenshot of a view of a GUI window showing a listing of patients, according to an illustrative embodiment.

FIG. **27**B is screenshot of a view of a GUI window showing a listing of patients, according to an illustrative embodiment.

FIG. **27**C is a screenshot of a view of a GUI window showing a selected patient and menu providing a user with options for reviewing study data and generating a report, according to an illustrative embodiment.

FIG. **28**A is a screenshot of a GUI for reviewing patient image data showing a window comprising an image showing a 3D view of a CT image of a subject comprising a graphical representation of bone overlaid with a SPECT image of the subject and graphics representing identified tissue volumes, according to an illustrative embodiment.

FIG. **28**B is a screenshot of a GUI for reviewing patient image data showing a window comprising an image showing a 3D view of a CT image of a subject comprising a graphical representation of bone overlaid with a SPECT image of the subject, according to an illustrative embodiment.

FIG. **29**A is a screenshot of a GUI for reviewing patient image data showing a window for reviewing a determined uptake metric, according to an illustrative embodiment.

FIG. **29**B is a screenshot of a GUI for reviewing patient image data showing a quality control graphical widget, according to an illustrative embodiment.

FIG. **29**C is a screenshot of a view of a quality control graphical widget allowing a user to sign a generated report, according to an illustrative embodiment.

FIG. **29**D is a screenshot showing a generated report (e.g., an auto-generated report), according to an illustrative embodiment.

FIG. **29**E is a screenshot of a view of a quality control graphical widget displayed in respond to a user input of disapproval of automated determination of an uptake metric, according to an illustrative embodiment.

FIG. **29**F is a screenshot of a portion of a generate report showing a graphical indication of rejection of quality control, according to an illustrative embodiment.

FIG. **29**G is a screenshot of a quality control graphical widget allowing a user to manually update one or more values used in determination of an uptake metric, according to an illustrative embodiment.

FIG. **29**H is a screenshot of a quality control graphical widget allowing a user to manually update one or more values used in determination of an uptake metric, according to an illustrative embodiment.

FIG. **30** is a block diagram showing a microservice network architecture for performing image segmentation to identify prostate volumes within images, determine uptake metrics, and provide results to a client, according to an illustrative embodiment.

FIG. **31** is a block flow diagram showing dataflow between microservices of a cloud-based application in order to process a study by performing image segmentation and determining uptake metrics, according to an illustrative embodiment.

FIG. **32** is a block flow diagram showing communication between microservices of a cloud-based application and a client, according to an illustrative embodiment.

FIG. **33** is a block diagram of an example architecture for implementing a cloud-based platform comprising a cloud-based application for performing image segmentation and computing uptake metrics in accordance with the systems and methods described herein, according to an illustrative embodiment.

FIG. **34** is a block diagram showing a process for automatically identifying 3D target volumes within 3D images and determining uptake metrics indicative of radiopharmaceutical uptake therein, according to an illustrative embodiment.

FIG. **35**A is a swarm plot of clinically non-significant and clinically significant images.

FIG. **35**B is an ROC curve determined based on varying a TBR threshold computed in accordance with the systems and methods described herein.

FIG. **36** is a block diagram of an exemplary cloud computing environment, used in certain embodiments.

FIG. **37** is a block diagram of an example computing device and an example mobile computing device used in certain embodiments.

The features and advantages of the present disclosure will become more apparent from the detailed description set forth below when taken in conjunction with the drawings, in which like reference characters identify corresponding elements throughout. In the drawings, like reference numbers generally indicate identical, functionally similar, and/or structurally similar elements.

DETAILED DESCRIPTION

It is contemplated that systems, architectures, devices, methods, and processes of the claimed invention encompass variations and adaptations developed using information from the embodiments described herein. Adaptation and/or modification of the systems, architectures, devices, methods, and processes described herein may be performed, as contemplated by this description.

Throughout the description, where articles, devices, systems, and architectures are described as having, including, or comprising specific components, or where processes and methods are described as having, including, or comprising specific steps, it is contemplated that, additionally, there are articles, devices, systems, and architectures of the present invention that consist essentially of, or consist of, the recited components, and that there are processes and methods according to the present invention that consist essentially of, or consist of, the recited processing steps.

It should be understood that the order of steps or order for performing certain action is immaterial so long as the invention remains operable. Moreover, two or more steps or actions may be conducted simultaneously.

The mention herein of any publication, for example, in the Background section, is not an admission that the publication serves as prior art with respect to any of the claims presented herein. The Background section is presented for purposes of clarity and is not meant as a description of prior art with respect to any claim.

Documents are incorporated herein by reference as noted. Where there is any discrepancy in the meaning of a particular term, the meaning provided in the Definition section above is controlling.

Headers are provided for the convenience of the reader—the presence and/or placement of a header is not intended to limit the scope of the subject matter described herein.

As used herein, "radionuclide" refers to a moiety comprising a radioactive isotope of at least one element. Exemplary suitable radionuclides include but are not limited to those described herein. In some embodiments, a radionuclide is one used in positron emission tomography (PET). In some embodiments, a radionuclide is one used in single-photon emission computed tomography (SPECT). In some embodiments, a non-limiting list of radionuclides includes ^{99m}Tc, ^{111}In, ^{64}Cu, ^{67}Ga, ^{68}Ga, ^{186}Re, ^{188}Re, ^{153}Sm, ^{177}Lu, ^{67}Cu, ^{123}I, ^{124}I, ^{125}I, ^{126}I, ^{131}I, ^{11}C, ^{13}N, ^{15}O, ^{18}F, ^{153}Sm, ^{166}Ho, ^{177}Lu, ^{149}Pm, ^{90}Y, ^{213}Bi, ^{103}Pd, ^{109}Pd, ^{159}Gd, ^{140}La, ^{198}Au, ^{199}Au, ^{169}Yb, ^{175}Yb, ^{165}Dy, ^{166}Dy, ^{105}Ru, ^{111}Ag, ^{89}Zr, ^{225}Ac, ^{82}Rb, ^{75}Br, ^{76}Br, ^{77}Br, ^{80}Br, ^{80m}Br, ^{82}Br, ^{83}Br, ^{211}At and ^{192}Ir.

As used herein, the term "radiopharmaceutical" refers to a compound comprising a radionuclide. In certain embodiments, radiopharmaceuticals are used for diagnostic and/or therapeutic purposes. In certain embodiments, radiopharmaceuticals include small molecules that are labeled with one or more radionuclide(s), antibodies that are labeled with one or more radionuclide(s), and antigen-binding portions of antibodies that are labeled with one or more radionuclide(s).

As used herein, "3D" or "three dimensional" with reference to an "image" means conveying information about three dimensions. A 3D image may be rendered as a dataset in three dimensions and/or may be displayed as a set of two-dimensional representations, or as a three-dimensional representation.

As used herein, an "image"—for example, a 3-D image of a subject—includes any visual representation, such as a photo, a video frame, streaming video, as well as any electronic, digital or mathematical analogue of a photo, video frame, or streaming video. Any apparatus described herein, in certain embodiments, includes a display for displaying an image or any other result produced by the

processor. Any method described herein, in certain embodiments, includes a step of displaying an image or any other result produced via the method.

As used herein, a "subject" means a human or other mammal (e.g., rodent (mouse, rat, hamster), pig, cat, dog, horse, primate, rabbit, and the like).

As used herein, "administering" an agent means introducing a substance (e.g., an imaging agent) into a subject. In general, any route of administration may be utilized including, for example, parenteral (e.g., intravenous), oral, topical, subcutaneous, peritoneal, intraarterial, inhalation, vaginal, rectal, nasal, introduction into the cerebrospinal fluid, or instillation into body compartments.

As used herein, the terms "filter", and "filtering", as in a "filtering function" or a "filter", refer to a function that operates on localized portions of an input array (e.g., a multi-dimensional array) of data (e.g., image data, e.g., values computed by a layer of a CNN), referred to herein as "subpatches", computing, for a given subpatch, a response value. In general, a filter is applied in a sliding window fashion across the array to compute a plurality of response values for the array. In particular, for a given multidimensional array, a subpatch of the array can be a rectangular region of the array having a specific size (e.g., having the same number of dimensions as the array). For example, for a 6×3×3 array, a given 3×3×3 subpatch refers to a given 3×3×3 set of adjacent values (e.g., a neighborhood) of the array, such that there are five distinct 3×3×3 subpatches in the 6×3×3 array (each patch shifted one position over along the first dimension).

For example, a filtering function can compute, for a given subpatch of an array, a response value using the values of the subpatch. A filtering function can be applied in a sliding window fashion across an array, computing, for each of a plurality of subpatches of the array, a response value. The computed response values can be stored in an output array such that the positional correspondence between response values and the subpatches of the input array is maintained.

For example, at a first step, beginning with a subpatch in a corner of an input array, a filter can compute a first response value, and store the first response value in a corresponding corner of an output array. In certain embodiments, at a second step, the filter then computes a second response value for a second subpatch, shifted one position over along a specific dimension of the input array. The second response value can be stored in a corresponding position of the output array—that is, shifted one position over along a same dimension of the output array. The step of shifting position of the subpatch, computing a response value, and storing the response value in a corresponding position of the output array can be repeated for the full input array, along each dimension of the input array. In certain embodiments (e.g., a strided filtering approach), the subpatch for which the filter computes a response value is shifted more than one position at a time along a given dimension, such that response values are not computed for every possible subpatch of the input array.

As used herein, the term "convolutional neural network (CNN)" refers to a type of artificial neural network where at least one layer performs one or more filtering functions. As used herein, the term "convolution layer" refers to a layer of a CNN that receives as input an input array and computes an output array, wherein values of the output array are computed by applying one or more filters to the input array. In particular, in certain embodiments, a convolution layer receives as input an input array having n+1 dimensions and produces an output array also having n+1 dimensions. The first n dimensions of input and output arrays operated on by filtering layers of a CNN are referred to herein as "spatial dimensions". The $(n+1)^{th}$ dimension of the input is referred to herein as the "input channel" dimension. The size of the input channel dimension is referred to herein as the "number of input channels". The $(n+1)^{th}$ dimension of the output is referred to herein as the "output channel" dimension. The size of the input channel dimension is referred to herein as the "number of output channels".

In certain embodiments, a convolution layer computes response values by applying a filter that operates on subpatches that are smaller than the input array along the spatial dimensions, but extend across the full output channel dimension. For example, an $N \times M \times L \times K_0$ size input array, has three spatial dimensions and K_0 output channels. Filters of a convolution layer may operate on subpatches having sizes of $N_f \times M_f \times L_f \times K_0$, where $N_f \leq N$, $M_f \leq M$ and $L_f \leq L$. Often, a filter of a convolutional layer operates on subpatches having sizes where $N_f < N$, $M_f < M$ and/or $L_f < L$. For example, in certain embodiments, $N_f << N$, $M_f << M$ and/or $L_f << L$.

Accordingly, for each of one or more filters applied by a convolution layer, response values computed by a given filter are stored in a corresponding output channel. Accordingly, a convolution layer that receives an input array having n+1 dimensions computes an output array also having n+1 dimensions, wherein the $(n+1)^{th}$ dimension represents the output channels corresponding to the one or more filters applied by the convolution layer. In this manner, an output array computed by a given convolution layer can be received as input by a subsequent convolution layer.

As used herein, the term "size" in reference to a filter of a convolution layer refers to a size along spatial dimensions of subpatches on which the filter operates (e.g., the subpatch size along the output channel dimension is taken as the full number of output channels). As used herein, the term "size", in reference to a convolution layer, as in "size of a convolution layer" refers to a size of filters of the convolution layer (e.g., each filter of the convolution layer having a same size). In certain embodiments, a filter of a convolution layer has a number of variable parameters that are determined via a machine learning training process. In certain embodiments, the number of parameters of a given filter equals the number of values in a subpatch that the given filter operates on. For example, a size $N_f \times M_f \times L_f$ filter that operates on an input array with K_0 output channels has $N_f \times M_f \times L_f \times K_0$ parameters. In certain embodiments, a filter is implemented as an array, and the response value determined by the filter for a given subpatch is computed as a dot product between the filter and the given subpatch.

As used herein, the term "fully convolutional neural network (FCNN)" refers to a CNN wherein each layer of the CNN is a convolution layer.

As used herein, the term "volume", as used in reference to an input or output of a layer of a CNN refers to an input array received or an output array computed by a CNN layer.

As used herein, the term "CNN module" refers to a computer implemented process that implements a specific CNN in order to determine, for a given input, such as an image (e.g., a 2D image; e.g., a 3D image) one or more output values. For example, a CNN module may receive as input a 3D image of a subject (e.g., a CT image; e.g., an MRI), and for each voxel of the image, determine a value that represents a likelihood that the voxel lies within a region of the 3D image that corresponds to a representation of a particular organ or tissue of the subject. A CNN module may be software and/or hardware. For example, a CNN module may be implemented entirely as software, or certain func-

tions of a CNN module may be carried out via specialized hardware (e.g., via an application specific integrated circuit (ASIC)).

As used herein, the term "tissue" refers to bone (osseous tissue) as well as soft-tissue.

The systems and methods described herein provide for automated analysis of medical images of a subject in order to automatically identify regions of interest that correspond to particular organs and/or tissue that are represented in the images. In certain embodiments, convolutional neural network (CNN) modules are employed in order to accurately segment images. In certain embodiments, the accurate automated identification of particular organs and/or tissue in images of a subject allows for quantitative metrics that measure uptake of radiopharmaceuticals (e.g., radiolabeled small molecules; e.g., radiolabeled antibodies; e.g., radiolabeled antigen-binding portions of antibodies) in particular organs to be determined.

In certain embodiments, the systems and methods described herein facilitate automated identification of regions of interest that correspond to particular organs or tissue in which tumors and/or tumor metastases may be present. Radionuclide labelled molecules that selectively bind to specific tumor cell surface proteins may be utilized in combination with the approaches described herein for imaging tumors. For example, the molecule 1404 binds specifically to Prostate Specific Membrane Antigen (PSMA), which is over expressed on many cancer cells. The molecule 1404 may be labelled with a radionuclide, such as ^{99m}Tc, for use in single-photon emission computed tomography (SPECT) imaging.

In certain embodiments, uptake metrics of radiopharmaceuticals are relevant to assessing disease state and prognosis in a subject.

A. Identifying Prostate Volumes and Determining Uptake Metrics

FIG. **1** shows a process **100** for automatically processing 3D images to identify 3D volumes that correspond to a prostate of a subject and determining one or more uptake metrics indicative of radiopharmaceutical uptake therein.

Referring to Steps **102** and **104** of Process **100** in FIG. **1**:

The various panels of FIG. **2** illustrate CT images (FIG. **2**A and FIG. **2**B) showing bone and soft-tissue, and highlight the pelvic bones (green **202** and blue **206** in FIGS. **2**C and **2**D) and prostate (purple **204** in FIGS. **2**C and **2**D). The highlighted regions are automatically generated by the systems and methods described herein, and identify the pelvic bones and prostate. FIG. **2**E shows a SPECT image (the bright pink and purple regions **252**, **254**, and **256**) overlaid on a CT image. As can be seen, the CT image provides detailed anatomical information, while the anatomical/structural information in the SPECT image is more limited. Accordingly, it is possible to segment the CT image, and use a mapping between voxels of the CT image and those of the SPECT image to identify particular voxels of the SPECT image that correspond to tissue volumes of interest, such as the prostate, bladder, rectum, and gluteal muscle, for example.

Referring to Steps **106** and **108** of Process **100** in FIG. **1**:

The approach of identifying the prostate volume within the CT image first uses a first machine learning module (e.g., a CNN module) to identify an initial volume of interest within the CT image. This produces a standardized input to a second machine learning module (e.g., a second CNN module) that is responsible for identifying the prostate volume. The second CNN module may also identify other tissue volumes, such as pelvic bones, gluteal muscles, rectum, and bladder. The first and second machine learning modules may be combined and implemented as a single module and/or a single software application. The first and second machine learning modules may also be implemented separately, e.g., as separate software applications.

i. Bounding Box Generation (Localization Machine)

FIGS. **3**-**5** present examples of the processing of various CT images showing, first, the identification of the initial volume of interest (VOI) (panels A) and, second, the segmentation of the prostate and pelvic bones (the prostate volume is represented by the blue-green volume in the middle). As shown in these examples, the initial CT image size can substantially depending on the imaging system used, the imaging protocol followed by the radiologist, and other factors, but the initial VOI size is fairly standard.

For example, initial 3D anatomical images may range in size from as large as 700 mm×700 mm×1870 mm (depth×width×height) (i.e. a full body scan), or even larger, to as small as 180 mm×240 mm×290 mm (covering the pelvic bone), or even smaller. In the examples described herein, the smallest tested matrix size of an initial 3D anatomical image is 256×256×76 pixels. The bounding boxes (e.g., identified by the first CNN) for the examples described herein have approximate size ranges of 180-220 mm×240-320 mm×290-380 mm. Matrix sizes of the bounding boxes for the example described herein are in the range of 80-220×150-390×50-300 pixels.

In the example, 3D anatomical images for training the first CNN to detect pelvic region bounding boxes had the following image dimensions:

Training Images (3D Anatomical Images):
#rows: 247-512 (sp 1.37), size (mm): 340-700
#columns: 319-512 (sp 1.37), size (mm): 430-700
#slices: 274-624 (sp 3.0), size (mm): 820-1870

In the example, 3D anatomical images for validating the first CNN for detection of bounding boxes had the following image dimensions, with the resulting range in dimensions of bounding boxes identified by the first CNN:

Validation Images (3D Anatomical Images):
#rows: 256-512, size (mm): 500-600
#columns: 256-512, size (mm): 500-600
#slices: 76-427, size (mm): 380-1070
Bounding Boxes:
#rows: 82-222, size (mm): 180-220
#columns: 148-386, size (mm): 240-320
#slices: 50-295, size (mm): 290-380

The following are three example approaches for automatically generating a bounding box (cuboid) for the pelvic region from an initial 3D anatomical image, for use in subsequent processing for detailed identification of the prostate.

In a first approach, the first CNN receives as input the grayscale CT image (a single input channel) and outputs coordinates of the opposite corners of the bounding box.

In a second approach, the grayscale CT image is processed via thresholding to produce a thresholded image with a rough identification of the pelvic region. In this second approach, the first CNN receives two input channels—one being the grayscale CT image and the other being the thresholded image. The second CNN outputs coordinates of opposite corners of the bounding box.

In a third approach, the first CNN is essentially a rough version of the second CNN—that is, the first CNN identifies a prostate, pelvic bones, and a sacrum (and background). The bounding box is generated using the identified pelvic

bones (e.g., by drawing the smallest box that fits the pelvic bones, or maybe adding some buffer distance). A distinction here is that the output of the first CNN is not merely coordinates of cuboid vertices. In this approach, likelihood values are automatically determined for each voxel of the image that give the likelihood as to how the voxel is classified—e.g., whether the voxel is prostate, left/right pelvic bone, sacrum, or background, for example.

In one illustrative embodiment of this third approach, the localization and segmentation networks are very similar. The localization network segments left and right pelvic bones, sacrum and the background (4 classes in all) in very downsampled images. Based on this rough segmentation of the pelvic bones, a bounding box is created. The segmentation network then segments the pelvic bones, the prostate, and the background within this bounding box and at higher resolution. The localization CNN and the segmentation CNN have identical architectures. The differences are in what input shape they require, where the localization network resize images to size (81, 68, 96) and the segmentation CNN resize pelvic images (as output from the localization network) to size (94, 138, 253). Also, the number of convolutional filters differs. The segmentation network has 20 convolutional filters in the first layer whereas the localization network only has 8. The size and number of filters of subsequent layers are scaled, as is shown in the flow charts herein. To create the bounding box after the localization network, the method finds the corners of the first segmentation and draws a square around it with a margin. The input images to the localization network are small because they have been downsampled to a lower resolution, whereas the segmentation process a cropped version of the CT image in the original resolution.

The FIG. **6**A shows an example of approach 1. FIG. **6**B and FIG. **6**C show a comparison between approach 1 and approach 3.

FIGS. **7**A-E show an example architecture **700** of the first CNN network described herein. The CNN module architecture (localization network) is used for identifying a volume of interest (e.g., VOI) corresponding to a pelvic region within a CT image of a subject (wherein the VOI is subsequently processed by a second machine learning module (e.g., a second CNN module) for more detailed segmentation/identification of the prostate and/or other tissues within the pelvic region).

ii. Prostate Volume and Additional Tissue Volume Determination (Single Segmentation Machine)

FIGS. **7**F-J show an example architecture **750** of the second CNN network described herein. As noted above, the second CNN operates on the VOI to identify a prostate volume, as well as various additional tissue volumes. Additional tissue volumes can include left/right pelvic bones, a sacrum, a bladder, gluteal muscles, and a rectum. Identifying multiple tissue volumes, as opposed to performing a binary classification (e.g., where voxels are simply identified as prostate or background) improves the accuracy of the classification approach.

FIG. **8**A shows left and right pelvic bones (blue, **806** and yellow, **802**) and the sacrum (red, **804**) in 2D, and FIG. **8**B shows the same in 3D.

FIG. **9**A shows left and right pelvic bones (red, **902** and yellow, **906**) and a prostate (blue, **904**).

FIG. **9**B shows segmentation of left and right pelvic bones (two lighter green regions, **952** and **956**), prostate (dark green, **958**), bladder (greenish beige, **960**), a rectum (brown, **962**), and gluteal muscles (blue, **964** and red, **966**).

FIG. **10** shows a low quality CT image, where segmentation still worked.

iii. Segmentation Module Architecture

Data Input and Output

FIG. **11** shows an example architecture **1100** in which image segmentation as described herein is performed by a Segmentation Service module **1104** that receives requests to process images (e.g., perform segmentation as described herein) from a client facing module, Pioneer Web **1102**.

The particular example architecture **1100** shown in FIG. **11** is used in an embodiment of the image segmentation and analysis systems and methods described herein, in particular a cloud-based software application, referred to as Pioneer. Pioneer is a software device to assist in the assessment and characterization of prostate cancer in the prostate gland using MIP-1404 SPECT/CT image data. The software uses artificial intelligence to automatically segment the image data into distinct anatomical regions and then analyzes the volumetric regions of interest (ROI). Pioneer extracts quantitative data from ROIs to assist in determining the presence or absence of clinically significant prostate cancer.

The architecture and module organization shown in FIG. **11**, as well as other architectures and module organizations described herein with respect to Pioneer, may be adapted for use with other imaging modalities and/or other radiopharmaceuticals. For example, a variety of radiopharmaceuticals suitable for use with SPECT imaging are described herein, in section M "Imaging Agents" below. Various 3D functional imaging modalities may also be used for imaging radiopharmaceutical uptake in a subject, and combined with a 3D anatomical imaging modality, such as, but not limited to CT imaging, and analyzed via adapted versions of the approached described herein with respect to Pioneer. For example, various nuclear medicine imaging modalities, such as PET imaging may be used to image radiopharmaceutical uptake. Like SPECT imaging, PET imaging may be performed in combination with CT imaging to obtain an image set comprising a PET image and a CT image—a CT/PET image. Accordingly, the approaches described herein with respect to Pioneer, and CT/SPECT images may also be adapted for use with CT/PET images. Various radiopharmaceuticals suitable for use with PET imaging are also described in section M "Imaging Agents", below.

Turning again to FIG. **11**, as shown in FIG. **11**, Pioneer is implemented as a cloud based service using Amazon Web Services, in which Simple Notification Service (SNS) and Simple Queue Service (SQS) messaging is used to handle requests. The Segmentation Service **1104** listens for requests on a dedicated SQS queue. Events that occur in Pioneer Web **1102** are published to a dedicated SNS topic "Pioneer Events" **1106**. To allow for parallel asynchronous processing, a fanout pattern may be used, such that SNS messages are sent to a topic and then replicated and pushed to multiple Amazon SQS queues **1108***a*, **1108***b*, of which the Segmentation Service is a consumer.

The Segmentation Service **1104** may download input data (e.g., image data) from source Uniform Resource Locators (URLs) provided by the requester (e.g., Pioneer Web **1102**) and that link to datasets in a local filesystem. In certain embodiments, the input data comprises a pre-processed 3D anatomical image, such as a CT image and a 3D functional image, such as a SPECT scan. Image metadata may also be included, along with the 3D anatomical and functional images.

In certain embodiments, CT and SPECT images have resolutions meeting particular requirements, established for the system. For example, CT images with resolutions rang-

ing from 1.0 to 2.2 mm in x and y directions and between 1.0 and 5.0 mm in a z (slice) direction may be used. In certain embodiments, SPECT images with resolutions ranging from 2.9 to 4.8 mm in all directions are used.

Once Segmentation Service **1104** has performed image segmentation to identify a prostate volume and any additional tissue volumes in a particular CT image, as described herein, Segmentation Service **1104** provides segmentation output data that identifies the prostate volume within the particular CT image for storage and/or further processing (e.g., display in a GUI; e.g., computation of uptake metrics). In certain embodiments, a request issued to the Segmentation Service **1104** includes a target URL that specifies a storage location for the segmentation output data. Accordingly, the Segmentation Service **1104** may upload segmentation output data to the target URL included in the request.

The segmentation output data may include data such as a segmentation mask set, that identifies each voxel of the 3D anatomical image (e.g., CT image) as corresponding to a particular tissue region or as background, as determined by the second machine learning module described herein. The segmentation mask set may include, or be used to determine, for each particular tissue region, a corresponding segmentation mask that identifies voxels of the CT image classified as belonging to that particular tissue region. For example, a segmentation mask set may be stored in a .tiled.png format, with voxels labelled with different numerical labels identifying different particular tissue regions or background. An example set of labels for various tissue regions is shown below, with voxels identified as background labeled with 0:

```
{'prostate': 1,
'gluteus_maximus_left': 2,
'gluteus_maximus_right': 3,
'rectum': 4,
'urinary_bladder': 5,
'sacrum_and_coccyx': 6,
'hip_bone_left': 7,
'hip_bone_right': 8
}
```

In certain embodiments, the segmentation mask set identifies a prostate volume and a reference volume (e.g., a left gluteal muscle) and labels all other voxels as background.

In certain embodiments, segmentation mask metadata is also included in the segmentation output data. Segmentation mask metadata may be used to store information about the particular image(s) processed, such as a number of voxels in each direction (e.g., a number of rows, columns, and slices) and their spacing.

In certain embodiments, the Segmentation Service **1104** also performs quantification using results of the segmentation, such as identified prostate and reference volumes, and intensities of voxels of the 3D functional image (e.g., SPECT image). This quantification is discussed in more detail herein, for example, in the subsection below entitled, "Uptake metrics". For example, for use in computing a target to background ratio (TBR) value for the subject, as described herein, the Segmentation Service **1104** may identify a prostate maximum intensity voxel, along with a background value. The prostate maximum intensity voxel is a voxel identified as having a maximum intensity within a set of voxels of the 3D functional image corresponding to the identified prostate volume. In certain embodiments, as described herein, voxels of the 3D functional image corresponding to the identified prostate volume are corrected for cross-talk (also referred to as bleed) from a bladder of the subject, and the prostate maximum intensity voxel is identified following correction for bladder cross-talk. The background value used for determination of the TBR value is an average over intensities of a plurality of voxels of the 3D functional image that correspond to a reference volume, such as a volume corresponding to a left gluteal muscle of the subject, within the 3D anatomical image. As described herein, typically all voxels corresponding to the identified reference volume are used to compute the background value.

Data corresponding to the quantification performed by the Segmentation Service **1104** may be included in the segmentation output data. For example, quantification results may be included in a quantification result dictionary, as shown in the .json format example below:

```
{
"prostate_max": 988.0,
"prostate_max_pos": {
"z": 92,
"y": 74,
"x": 67
},
"background": 9.056859205776174,
}
```

Keys of the quantification result dictionary in the above example are as follows: "prostate_max" stores an intensity of the prostate maximum intensity voxel; "prostate_max_pos" stores a location of the prostate maximum intensity voxel in the SPECT image; and "background" stores the background value.

Example Segmentation Service Architecture Including CNN Module Organization and Interaction

FIG. **12** shows an example architecture **1200** of modules for performing the CNN-based image segmentation as described herein. The example architecture **1200** includes a first machine learning module (referred in FIG. **12** as "Localization Machine") **1204** for identifying an initial VOI, and a second machine learning module (referred to as "SingleSegMachine (base)" in FIG. **12**, short for "base Single Segmentation Machine") **1208** for identifying a prostate volume, additional tissue volumes, and a reference volume as described herein. Inputs and outputs of the first and second machine learning modules are also shown, along with several additional modules, including auxiliary machine learning modules (referred to as SingleSegMachine (aux) in FIG. **12**, short for "auxiliary Single Segmentation Machine") **1212** and a module **1214** for merging outputs of the second machine learning module (base Single Segmentation Machine) and any auxiliary machine learning modules (auxiliary Single Segmentation Machines) and performing postprocessing. Outputs generated by the module organization shown in FIG. **12** include a segmentation mask set **1216** that identifies various tissue volumes in a 3D anatomical image (e.g., a CT image) and segmentation metadata **1218**.

As described herein, the first machine learning module **1204** receives as input a CT image **1202** and produces a bounding box that identifies an initial VOI corresponding to a pelvic region of the subject. The second machine learning module **1208** receives, as input, the initial VOI along with the CT image **1202**. The second machine learning module **1208** may add a crop margin to the initial VOI (e.g., add a margin about the initial bounding box to expand the bounding box) and provide the crop endpoints to auxiliary machine learning modules. As described herein, the second machine learning module **1208** identifies a prostate volume within the initial VOI. The second machine learning module

1208 may also identify additional tissue volumes corresponding to additional tissue regions within the subject, such as a left gluteal muscle, a bladder, and left and right hip bones. A tissue volume corresponding to a left gluteal muscle of the subject may be used as a reference volume, for example to compute a background value in determining a TBR value for the subject, as described herein. A tissue volume corresponding to a bladder of the subject may be used for correcting intensity values of voxels of a SPECT image for bladder cross-talk, for example as described herein, in section B "Correcting for Bladder Intensity Bleed Through". Identified tissue volumes corresponding to a left and right hip bone of the subject may be used for postprocessing.

In certain embodiments, as described herein, performance may be improved by using, in addition to the second machine learning module **1208**, one or more auxiliary machine learning modules **1212** that perform image segmentation in a similar fashion to the second machine learning module, identifying a prostate volume and additional tissue volumes (e.g., as shown in FIGS. **12**, **1208** and **1212**). These auxiliary tissue volumes, identified by the auxiliary machine learning modules, may be merged, via module **1214**, with the base tissue volumes (the prostate volume and any additional tissue volumes) identified using the second machine learning module **1208**.

In certain embodiments, the first and second machine learning modules, and any auxiliary machine learning modules, are implemented as trained CNN modules. Each trained CNN module may be represented (e.g., via computer code) as a directory that comprises an associated trained neural network with model structure and weights. Neural network libraries, such as Keras, can be used to represent trained CNN modules in this manner. The dictionary representing a particular CNN module may also include metadata that describes any preprocessing to be performed on an image before it is fed as input to the particular CNN module. Metadata describing how the neural network model was built and trained may also be included.

Accordingly, a particular CNN module may perform steps such as (1) loading and preprocessing an image, given an image file name and image metadata; (2) feeding the preprocessed image through the associated trained neural network (e.g., as included in the directory representing the particular CNN module) to obtain a raw prediction output (e.g., a map that includes, for each of one or more voxels of the CT image, a likelihood (e.g., probability) that that voxel belongs to a particular category as determined by a trained neural network); and (3) postprocess the raw prediction output. As described herein, the first machine learning module **1204** may postprocess the raw prediction output produced by its associated trained neural network to determine crop endpoints of a bounding box corresponding to an initial VOL The second machine learning module **1208** may postprocess the raw prediction output produced by its associated trained neural network to determine a segmentation mask set that labels voxels of the CT image with values (e.g., numerical values) that indicate a particular tissue volume to which they correspond or identify the voxels as background, as determined by the second machine learning module.

An example model structure of a CNN module implementation of the first machine learning module (Localization Machine in FIG. **12**) **1204** is shown in FIG. **13**. An example model structure of a CNN module implementation of the second machine learning module (Single Segmentation Machine in FIG. **12**) **1208** is shown in FIG. **14**.

Example first machine learning module (Localization Machine) Implementation

As described herein, the first machine learning module identifies an initial VOI—e.g., a "bounding box" that identifies a region of the CT image that corresponds to a pelvic region of the subject, which includes pelvic bones of the subject, along with tissue regions such as a prostate, a bladder, a rectum, and left and right gluteal muscles. An identification of the bounding box (e.g., crop endpoints) is provided to the second machine learning module, as well as any auxiliary machine learning modules, allowing them to limit their processing to a small, specific, target region of the CT image as opposed to having to operate on and process the entire CT image. This reduces the amount of data processed by these machine learning modules, which perform computationally intensive fine segmentation, thereby improving their performance and efficiency.

In an example implementation of the first machine learning module in accordance with approach 3 as described herein, Localization Machine **1204** in FIG. **12** extracts a bounding box (to identify the initial VOI) from a coarse segmentation of a CT image performed by its associated trained neural network (a CNN), referred to as a Localization CNN.

In certain embodiments, the CT image is preprocessed to prepare it for segmentation by the Localization CNN. A configuration file may be used to specify the preprocessing steps and parameters. The preprocessing may include steps such as cropping the CT image to remove one or more regions that correspond to surrounding air, normalizing intensities of voxels in the CT image, and resizing the CT image (e.g., to produce a resized CT image that conforms to a fixed input size expected by the Localization CNN). The intensity normalization preprocessing step adjusts intensities of voxels of the CT image to produce a particular mean and standard deviation of intensities over all voxels of the CT image. For example, voxel intensities of the CT image may be normalized by subtracting a first fixed value and then dividing by a second fixed value, to produce a CT image in which a mean intensity over all voxels is specific mean value (e.g., 0) and a standard deviation of intensities over all voxels is a specific standard deviation value (e.g., 1). The resizing step may be performed by sampling the CT image.

The Localization CNN receives the preprocessed CT image as input and passes it through a series of layers as shown in FIG. **13**. The output of the Localization CNN is a coarse segmentation, e.g., represented via a first segmentation mask set, that classifies voxels of the preprocessed CT image as belonging to one of four categories, three representing particular tissue regions: (i) a sacrum and coccyx, (ii) a left hip bone, (iii) a right hip bone, and a fourth category, (iv) background (e.g., everything else). This coarse segmentation is obtained from a raw prediction map generated by the Localization CNN. The raw prediction map has a same shape—that is a same set of voxels as the preprocessed CT image received as input, but with four channels. Each channel corresponds to a particular classification category—(i) sacrum and coccyx, (ii) left hip bone, (iii) right hip bone, and (iv) background. Each channel represents a probability map for the classification category to which it corresponds. That is, each particular channel corresponding to a particular classification category includes, for each voxel of the preprocessed CT image, a likelihood value representing probability that the voxel belongs to that particular category (e.g., represents a physical volume inside the tissue region that the category represents, or represents

background). Accordingly, for each voxel, a sum over the likelihood values for that voxel in each channel is 1.

To determine the first segmentation mask set that classifies each voxel as belonging to a particular category, each voxel of the preprocessed CT image is assigned to the category (e.g., tissue region or background) having a largest likelihood value (e.g., probability) for that voxel. The determined first segmentation mask set has a same shape as the preprocessed CT image, and labels each voxel with a value identifying the category that it is classified as belonging to. For example, a particular voxel may be labeled with a numerical value, such as 1, 2, or 3 corresponding to categories (i), (ii), and (iii) as described above, or a value 0 zero if it is classified as a background voxel.

A bounding box that identifies an initial VOI may be determined from the first segmentation mask set as a smallest box (e.g., rectangular volume) that comprises all voxels labeled as belonging to categories (i)-(iii). Coordinates identifying the bounding box (e.g., coordinates of opposite corners of a rectangular volume corresponding to the bounding box) are determined and output as crop endpoints. In certain embodiments, wherein the preprocessed CT image input to the Localization CNN is a resized version of the original CT image, the coordinates identifying the bounding box are transformed to a coordinate system of the original CT image and output as crop endpoints.

Example Second Machine Learning Module (Segmentation Machine) Implementation

In the example architecture of FIG. **12**, a second machine learning module, also referred to as a base Single Segmentation Machine **1208** (SingleSegMachine (base) in FIG. **12**) performs a high-resolution segmentation of a CT image to identify a prostate volume corresponding to a prostate of the subject, along with additional tissue volumes corresponding to specific tissue regions, such as left and right gluteal muscles, a rectum, a bladder, a sacrum and coccyx, and left and right hip bones.

In certain embodiments, the CT image is preprocessed to prepare it for segmentation by the second machine learning module. As with Localization Machine **1204**, a configuration file may be used to specify preprocessing steps and parameters. Preprocessing steps may include normalizing intensities of the CT image, similar to the approach described above with respect to Localization Machine **1204**. The CT image may also be cropped using the crop endpoints that identify the initial VOI (bounding box) and are output by the Localization Machine **1204**, to produce a reduced, fixed size preprocessed CT image input for providing as input to a trained neural network (a trained CNN) associated with and implemented in Single Segmentation Machine **1208**. Preprocessing may also include a resizing step.

Similar to the Localization CNN of the Localization Machine, the Single Segmentation Machine implements a trained CNN, referred to as a Segmentation CNN, that receives as input the preprocessed CT image. The Segmentation CNN passes the preprocessed CT image through a series of layers, and outputs a second raw prediction map. Similar to the raw prediction map produced by the Localization CNN, the second raw prediction map includes multiple channels, each corresponding to a different particular category into which each voxel of the input CT image is to be classified. Each channel represents a probability map for the classification category to which it corresponds and includes, for each voxel of the preprocessed CT image, a likelihood value corresponding to a probability (as determined by the Segmentation CNN) that the voxel belongs to that category.

As described above, the second raw prediction map output by the Segmentation CNN comprises a channel corresponding to a prostate of the subject. The second raw prediction map may include other channels, corresponding to various additional tissue regions, such as a left gluteal muscle, a right gluteal muscle, a rectum, a urinary bladder, a sacrum and coccyx, a left hip bone, and a right hip bone. The second raw prediction map may also include a background channel.

Certain variants of high-resolution segmentation CNN's give predictions from multiple levels of the network, resulting in multiple probability maps per category. These multiple probability maps are referred to as auxiliary predictions. The CNN model structure shown in FIG. **13** corresponds to a model structure that does not produce auxiliary predictions, and the CNN model structure shown in FIG. **14** is for a model that produces auxiliary predictions. In certain embodiments, while a number of filters in a top layer (e.g., **20** filters in FIGS. **13** and **28** filters in FIG. **14**) may vary, a number of filters in subsequent, lower layers doubles each layer down. In certain embodiments, the Segmentation CNN produces a single probability map, and does not produce any auxiliary predictions. In certain embodiments, the Segmentation CNN produces auxiliary predictions.

In certain embodiments, when the Segmentation CNN produces auxiliary prediction map, likelihood values for each category as included in the second raw prediction map and each auxiliary probability map are averaged together, such that for a particular voxel, a single likelihood value for each category is determined.

In certain embodiments, to determine a second, fine segmentation mask set that classifies each voxel as belonging to a particular category, each voxel of the preprocessed CT image is assigned to the highest probability value. In certain embodiments, a number of labels in the fine segmentation mask set is reduced, such that only certain tissue volumes, such as a prostate volume and a reference volume (e.g., a left gluteal muscle volume) are included in the fine segmentation mask set.

Auxiliary Single Segmentation Machines

In certain embodiments, one or more auxiliary machine learning modules are used to produce auxiliary fine segmentation mask sets, similar to the fine segmentation mask set generated by the second machine learning module. These auxiliary fine segmentation mask sets identify a same set of tissue volumes as the fine segmentation mask set generated by the second machine learning module. In this manner, the second machine learning module generates a base fine segmentation mask set, and the one or more auxiliary machine learning modules each generate an auxiliary fine segmentation mask set, thereby providing a parallel set of classifications for voxels of the CT image.

In certain embodiments, for each category representing a particular tissue region, a corresponding base fine segmentation mask (e.g., that identifies a volume in the CT image determined via the base Single Segmentation Machine as corresponding to the particular tissue region) of or determined using the base fine segmentation mask set and one or more corresponding auxiliary fine segmentation masks (e.g., each identifying a volume of the CT image determined via an auxiliary Single Segmentation Machine as corresponding to the same particular tissue region) are merged, to produce a merged fine segmentation mask. For example, for a particular category, certain voxels in the one or more auxiliary fine segmentation masks may be identified (e.g., labeled) as belonging to the particular category, but not

belong to a set of voxels in the base fine segmentation mask that are identified as belonging to the particular category. These voxels may be added (e.g., by labeling them as such) to the set of voxels identified as belonging to the particular category in the base fine segmentation mask to produce the final merged fine segmentation mask. For example, in the architecture shown in FIG. **12**, base Single Segmentation Machine **1208** produces a base fine segmentation mask and one or more auxiliary Single Segmentation Machine(s) **1212** each produces an auxiliary segmentation mask. The base fine segmentation mask produced by base Single Segmentation Machine **1208** is merged with the one or more auxiliary fine segmentation masks produced by the auxiliary Single Segmentation Machine(s) **1212** by module **1214** to produce a final fine segmentation mask set **1216** comprising a final fine segmentation mask for each category.

In certain embodiments, one or more of the final fine segmentation masks are filtered such that only a largest connected part is retained. In certain embodiments, when filtering to retain only a largest connected component of a prostate segmentation mask (e.g., a final fine segmentation mask that identifies a volume of the CT image corresponding to a prostate of the subject) is performed, a subset of connected components of the prostate segmentation mask is considered. The subset comprises only components that (i) have a center of mass lying in between the hip bones' centers of mass in a left-right direction of an axial plane (x direction) and (ii) lie within a bounding box defined so that the left and right hip bones are just contained.

iv. Uptake Metrics

Referring to step **110** of process **100** in FIG. **1**, one or more uptake metrics are determined, from which diagnosis or staging of a condition (e.g., prostate cancer) may be informed or automatically rendered. The one or more uptake metrics are determined using the 3D functional image and the prostate volume identified within the VOI of the 3D anatomical image. For example, a quantity of radiopharmaceutical in the prostate of the subject may be computed based on intensity values of voxels of the 3D functional image that correspond to the prostate volume identified within the VOI of the 3D anatomical image. This may involve computing a sum (e.g., a weighted sum), an average, and/or a maximum of intensities of voxels of the 3D functional image representing a physical volume occupied by the prostate of the subject. In certain embodiments, this involves computing a normalization value based on intensity values of voxels of the 3D functional image that correspond to a reference volume identified within the 3D anatomical image. For example, the normalization value for intensities identified in the prostate may be normalized using intensity values of one or more voxels that correspond to the gluteal muscles, or another reference volume within the VOI (or, in certain embodiments, elsewhere within the 3D anatomical image). The uptake metrics, then, can be converted to an identification of whether or not the subject has prostate cancer and/or a quantification of risk that the subject has prostate cancer, and/or a staging of the disease (e.g., as part of disease tracking over time), which may be used by the medical practitioner in advising treatment options, and/or monitoring efficacy of administered therapy, for example.

Target to Background Ratio

In certain embodiments, one or more uptake metrics determined include(s) a target to background ratio (TBR) value for the subject. Determining the TBR value comprises determining (i) a target intensity value using intensity values of one or more voxels of the 3D functional image (e.g., PET or SPECT image) that correspond to the prostate volume identified within the initial VOI of the 3D anatomical image (e.g., CT image), and (ii) determining a background intensity value using intensity values of one or more voxels of the 3D functional image that correspond to an identified reference volume. The TBR value is computed as a ratio of the target intensity value to the background intensity value.

In particular, in certain embodiments, the target intensity value is a maximum of intensities of the voxels of the 3D functional image (e.g., PET or SPECT image) that correspond to the identified prostate volume. As described above, a prostate maximum intensity voxel corresponding to a voxel identified as having a maximum intensity within a set of voxels of the 3D functional image corresponding to the identified prostate volume. The target value may then be taken as the intensity of the prostate maximum intensity voxel. The background intensity value may be computed as an average over intensities of a plurality of voxels of the 3D functional image that correspond to the identified reference volume. As described herein, a gluteal muscle, such as a left gluteal muscle, or a portion thereof, may be used as the identified reference volume.

For example, TBR values may be computed from a SPECT/CT image for a subject recorded following administration of a radiopharmaceutical such as 1404 to the subject. The SPECT image corresponds to the 3D functional image and the CT image corresponds to the anatomical image. The image segmentation approaches described herein may be used to identify, within the CT image, a prostate volume along with a reference volume corresponding to a left gluteal muscle of the subject. A prostate segmentation mask and a left gluteal muscle segmentation mask may be used to identify the prostate volume and the left gluteal reference volume, respectively.

The prostate volume segmentation mask identifies voxels of the CT image that are classified as belonging to a prostate of the subject via the machine learning segmentation approaches described herein. In certain embodiments, in order to identify voxels of the SPECT image that correspond to the identified prostate volume within the CT image, voxels of the prostate segmentation mask are mapped to corresponding voxels of the SPECT image. Since the prostate segmentation mask identifies voxels in the CT image, it may have a different resolution from the SPECT image (e.g., since the SPECT and CT images may have different resolutions). Interpolation (e.g., bilinear interpolation) and/or sampling may be used to match a resolution of the prostate segmentation mask to the resolution of the SPECT image, such that each voxel of the prostate segmentation mask maps to a particular corresponding voxel of the SPECT image. In this manner, a SPECT prostate mask that identifies voxels in the SPECT image that correspond to the prostate volume identified within the CT image is obtained. A SPECT left gluteal muscle mask that identifies those voxels in the SPECT image that correspond to the identified left gluteal muscle reference volume in the CT image may be obtained in a similar fashion.

The SPECT left gluteal muscle mask may be used to determine the background intensity value. In particular, intensities of voxels in the SPECT image identified by the SPECT left gluteal muscle mask are extracted and partitioned into quartiles. The background value is computed as a mean over the extracted left gluteal muscle voxel intensities that fall within a first and third quartile. Other approaches for computing a background value, such as computing an overall mean or a median over all extracted left gluteal muscle voxel intensities, may also be used. The above described approach of partitioning the extracted left

gluteal muscle voxel intensities into quartiles, was found to be more stable against outliers than computing an overall mean and more precise than a median (e.g., since the intensities are discretized and many of them have a same value). The determined background intensity value may be output and stored in a result dictionary, e.g., under a key 'background'.

The target intensity value may be computed using the SPECT prostate mask. A prostate maximum intensity voxel may be identified as a voxel of the SPECT prostate mask and having a maximal SPECT image intensity. The target intensity value is determined as the intensity of the prostate maximum intensity voxel. Both the target value intensity value and a location of the prostate maximum intensity voxel may be stored. For example, a result dictionary may store the target intensity value and the prostate maximum intensity voxel location under keys such as "prostate_max" and "prostate_max_position", respectively. In certain embodiments, intensities of voxels of the SPECT image corresponding to the identified prostate volume are corrected for bladder "cross-talk" or "bleed" as described in section B below, prior to determining the target intensity value, such that, for example, the maximum intensity stored is a maximum corrected intensity and the prostate maximum intensity voxel is a voxel of the SPECT prostate mask having a maximum corrected intensity.

In certain embodiments, a prostate cancer status for a subject may be determined by comparing a determined TBR value for the subject with one or more threshold values. In particular, a determined TBR value may be compared with a particular threshold value (e.g., a cutoff threshold) to distinguish between patients who have clinically significant prostate cancer (e.g., assigned a status of clinically significant) from those who do not (e.g., assigned a status of clinically non-significant). Example 4 below shows an example approach for determining a TBR threshold value based on TBR values computed from reference images, in order to obtain a desired sensitivity and specificity.

B. Correcting for Bladder Intensity Bleed Through

FIG. **15**. is a schematic illustrating cross-talk of imaging agent intensity from a bladder to a prostate of a subject. In the figure, reference **1502** is a bladder, **1506** is the cross-talk/intensity that bleeds from the bladder, and **1504** is the prostate. Certain imaging agents comprising a PSMA binding agent have high uptake in the bladder, which may affect the identification of diseased tissue (e.g., prostate cancer). For example, uptake of a radionuclide labelled PSMA binding agent by the bladder may result in scattering in the 3D functional image, and may reduce accuracy of the measured imaging agent intensity in the prostate, which is located near the bladder. By training a second CNN for detailed segmentation of both the prostate and the bladder of a subject, it is possible to accurately, automatically account for a 'bleed through' or 'cross-talk' effect and/or other effects caused by uptake of the imaging agent by the bladder. Furthermore, by training the second CNN for identification of a reference region in the 3D anatomical image, e.g., the gluteal muscles, it is possible to more accurately weight/normalize imaging agent intensity measurements and improve the accuracy and diagnostic value of the uptake measurements in the prostate of the subject.

i. Bladder Dilation

In certain embodiments, bladder cross-talk correction includes a step wherein an identified bladder volume is dilated (e.g., via morphological dilation) with two iterations. This dilation may be used to prohibit high intensities very close to the segmented urinary bladder to be used for determination of a target intensity value in computing a TBR value (e.g., selected as a maximal intensity), and also to stabilize a bladder suppression approach described below.

ii. Bladder Suppression Computation

In certain embodiments, a bladder suppression method is used to remove intensity bleed from the bladder to other regions of the functional image. An amount of suppression, that is, intensity bleed to remove from a particular voxel of the functional image is dependent on a distance from that voxel to a core bladder region, corresponding to a region of the bladder having high intensity voxels.

In certain embodiments, bladder suppression is made if a maximum functional image intensity within a volume of the functional image identified as corresponding to a bladder (e.g., corresponding to a bladder volume identified within a 3D anatomical image; e.g. as identified via a urinary bladder mask) is more than a specific multiplier value times a determined background intensity value. As described herein, a background intensity value may be determined based on intensities of voxels of the 3D functional image corresponding to a reference volume identified within the 3D anatomical image, for example a gluteal muscle volume. For example, bladder suppression may be performed if a maximum functional image intensity within a region corresponding to the identified bladder volume is 15 times a determined background value (e.g., the bladder-to-background ratio should be at least 15).

In certain embodiments, bladder suppression is computed from and applied to a portion of the 3D functional image that lies within a bladder suppression bounding box of a specific size about the identified bladder volume. For example, a bladder suppression bounding box that contains the urinary bladder with a margin of a predetermined size in a particular direction (e.g., 40 mm in the vertical direction) and is a same number of voxels in the other directions may be determined.

For example, after masking out a region of the 3D functional image corresponding the prostate, the core bladder region may be determined as a region of the 3D functional image within the bladder suppression bounding box comprising voxels having intensities within a specific fraction of a maximum intensity within the bounding box (e.g., not including voxels of the masked out prostate region). For example, the core bladder region may be determined as the region comprising voxels having intensities greater than or equal to 50% of the maximum intensity within the bladder suppression bounding box. The core bladder region may include high-intensity regions that were not included in the original bladder mask.

In certain embodiments, one or more bladder intensity bleed functions are determined to perform bladder suppression and thereby correct intensities of voxels of the 3D functional image for bladder cross-talk. For example, the 3D functional image may be cropped using the bladder suppression bounding box and a determined background intensity value subtracted from intensities of voxels within the cropped image region. Sample intensities are then collected to determine how bladder intensity (e.g., intensity originating from radiopharmaceutical uptake within a bladder of the subject) decreases as one moves away from the bladder. The samples are collected starting at an extreme top, an extreme front, an extreme right and an extreme left of the core bladder region and then moving straight up, forward, right or left respectively, one voxel at a time. If an edge of the cropped image region is encountered, extrapolated intensi-

ties may be used as samples, for example linear extrapolation from a previous two or more samples.

The intensity samples provide four curves of intensity (e.g., sets of sampled intensity data points) decrease from the bladder core, to each of which a template function may be fit to establish four bladder intensity bleed functions that model bladder intensity variation as a function of distance from the core bladder region. Before further analysis, such as fitting, outlier removal may be performed, for example to remove the curve farthest away from the others. A template function such as an n-th degree polynomial (e.g., a 5th degree polynomial) is fitted to the data points in the remaining three curves, resulting in a function modelling the bladder intensity bleed as a function of the distance to the core bladder. This bladder intensity bleed function describes how much should be subtracted from the original intensities to obtain corrected intensities, depending on the distance to the core bladder region.

In certain embodiments, to decrease a risk that the bladder intensity bleed function underestimates bleed in the direction of the bladder (the bleed might vary to some extent between different directions), before fitting to the sampled intensity data points, the distances are multiplied with an expansion factor (e.g., ranging from 1 to 2; e.g., 1.2), so that the fit bladder intensity bleed function is stretched out. Risk of underestimating bladder intensity bleed may also be reduced by multiplying the sampled intensity data points by a scaling factor. The scaling factor may be variable scaling factor having a value that depends on the bladder-to-background intensity ratio. For example, a scaling factor that has a particular value when the bladder to background ratio is sufficiently high and increases (e.g., linearly) with lower bladder-to-background ratios may be used. For example, the sample intensities may be multiplied with a factor that is 1.2 when the bladder-to background ratio is sufficiently high and for lower bladder-to-background ratios increases linearly from 0 for a bladder-to-background ratio of 15. This approach of multiplying the sampled intensity data points with a scaling factor also improves robustness of the bladder suppression approach.

In certain embodiments, a reach of bladder suppression, that is, a farthest distance from the bladder where it is applied, is based on where the decay rate of the function is sufficiently small. If the decay rate never gets sufficiently small then the distance is chosen as a length of the intensity sample vectors. In certain embodiments, it is ensured that bladder suppression at all distances is non-negative.

Once determined, the bladder intensity bleed function may be evaluated at locations of various voxels of the 3D functional image, for example at voxel locations corresponding to locations within the prostate of the subject, to determine a bladder intensity bleed value for each particular voxel location. Accordingly, an intensity of a particular voxel may be corrected for bladder cross-talk by subtracting, from the intensity of the particular voxel, a determined bladder intensity bleed value at a location of the particular voxel. Intensities of voxels at various locations within the 3D functional image, for example at locations corresponding to an identified prostate volume (e.g., identified within a 3D anatomical image), may be corrected for bladder cross-talk in this manner.

iii. Corrected Prostate Maximal Intensity and Location

In certain embodiments, the bladder suppression approach described herein is used to correct intensity values of voxels of the 3D functional image that correspond a prostate volume identified within the 3D anatomical image, and uptake metrics, such as a TBR value, are determined using the corrected intensity values.

C. Visualizing Image Data and Computed Uptake Metrics

FIG. **16**A shows a window of the GUI interface with two subjects (patients) listed. The user can select a desired subject to process and view their image data.

FIG. **16**B shows an exemplary GUI with graphical control elements for processing and navigating subject data, which appears after the user selected the subject "John Doe". The user clicks a selectable button element to complete processing of image data for the selected subject.

In FIG. **16**C, after processing of the selected subject's image data is complete, the user clicks another selectable button to view the processed image data and computed uptake metrics.

In FIGS. **17**A-**17**E a 2D viewer is displayed. FIGS. **17**A-**17**E show a set of 2D cross-sectional views of CT image data overlaid with the SPECT image as well as graphics representing identified tissue volumes—specifically, a prostate and pelvic bones. The user can scan through the cross sectional slices as shown in the figures.

The CT image and SPECT image are rendered as selectable layers which can be toggled on and off. The graphics representing identified tissue volumes are also rendered as a selectable segmentation layer. In FIG. **18**A the user toggles display of the SPECT image layer off, such that only the CT image and segmentation layers are displayed. In FIGS. **18**B-**18**F the user scans through the cross sections.

In FIG. **19**A the user toggles display of the SPECT image layer on, and the segmentation layer off. FIGS. **19**B-**19**D show the user scanning through the cross-sectional views again, this time with only the CT image and the SPECT image layers displayed.

FIGS. **20**A-**20**C show a rotatable and sliceable 3D viewer for viewing the CT image along with overlaid with SPECT image data, wherein the CT image comprises a graphical representation of soft-tissue.

FIGS. **21**A-**21**B also show the rotatable and sliceable 3D viewer, this time with only a graphical representation of bone in the CT image displayed.

FIGS. **22**A-**22**F show how a user can use the 3D viewer to inspect the image data and automated identification of the prostate and other additional tissue regions. The user slices down to focus on the pelvic region in FIG. **22**B and turns on the segmentation layer to display graphics representing the identified prostate volume and pelvic bone volumes overlaid on the CT image as colorized regions. The user can slice and rotate the image to view the bright spots of the SPECT image intensity in the prostate region (purple volume).

FIGS. **23**A and **23**B show the viewer, but with a black background to improve contrast and mimic a radiologist scan.

FIG. **24** shows a report (e.g., an auto-generated report) with various uptake metrics.

D. User Interface, Quality Control, and Reporting

In certain embodiments, the systems and methods described herein are implemented as part of a GUI-based workflow that allows a user, such as a medical practitioner (e.g., a radiologist, a technician) to upload images of patients (subjects), initiate an automated analysis in accordance with the approaches described herein, in which a prostate volume is identified in a 3D anatomical image and used to determine

uptake metrics using corresponding voxels of a 3D functional image. The user may then view results of the automated analysis, including the determined uptake metrics and any prognostic values determined therefrom. The user may be guided through a quality control workflow, in which they choose to approve or disapprove the results of the automated analysis, and, if the results are approved, generate a report for the patient. The quality control workflow may also allow the user to manually adjust and update the results of the automated analysis, for example via an interaction with the GUI, and generate a report based on the manually updated results.

FIG. **25** shows an example workflow **2500**, used in certain embodiments for analysis of SPECT/CT images. As shown in FIG. **25**, the user may upload 2504 SPECT/CT images that conform to a specific accepted standard format **2502**, specifically the DICOM standard in the example of FIG. **25**. FIG. **26**A shows an example GUI window **2600***a* of a web-based portal that allows a user to upload 2504 images. FIG. **26**B shows an updated view **2600***b* of the GUI window shown in FIG. **26**A, in which several images have been selected for upload, and checked for conformance with the DICOM standard. One image is identified as not conforming to the DICOM standard, and indicated as failed to upload **2602***b*.

Returning to FIG. **25**, in another step **2506**, the user may view a list of patients for which images have been uploaded. FIG. **27**A shows a view **2700***a* of a GUI window listing patients via anonymized numerical identifiers. FIG. **27**B shows another view **2700***b* of the GUI window shown in FIG. **27**A, in which a row of the patient list corresponding to a specific patient is highlighted for selection. FIG. **27**C shows another view **2700***c* of the GUI, wherein upon selection of the row corresponding to the specific patient, a menu listing studies performed for the specific patient is displayed, including selectable buttons that allow the user to review image data for the study and generate a report.

In certain embodiments, the user review of the image data, along with any automated analysis results performed using the image data, is a prerequisite for generating a report. The user review of image data and automated analysis may be required to validate accuracy of image segmentation. For example, as shown in FIG. **25**, following viewing of the patient list **2506** and selection of a patient, in a next step **2508**, the user reviews the image data for the patient and results of automated processing as described herein.

In particular, in the review step **2508** of the workflow **2500** shown in FIG. **25**, a user examines SPECT/CT image data for the selected patient using a GUI based viewer. The user may select to view and examine the SPECT/CT image data as a set of 2D slices or as a 3D rendering. FIG. **28**A shows a view of the GUI viewer **2800** in which the SPECT/CT image data is displayed as a set of 2D slices **2802***a*. FIG. **28**B shows a view of the GUI based viewer **2800** in which the SPECT/CT image data is displayed as a 3D rendering **2802***b*.

As shown in FIG. **28**A and FIG. **28**B, GUI viewer **2800** displays the SPECT image and the CT image as selectable layers, overlaid on each other. The user may select one layer at a time, to view the SPECT and/or CT image alone, or may select both a CT layer and a SPECT layer to view the SPECT image overlaid on the CT image. The user may adjust an opacity of the SPECT image, e.g., to emphasize or deemphasize the SPECT image features overlaid on the CT image. The user may also view a segmentation layer that shows locations of various tissue regions identified via the second machine learning module within the CT image, as described herein. In this manner, the user may, for example, validate the image segmentation performed by the second machine learning module via visual inspection of the CT image layer and the segmentation layer.

The user may also view and validate the one or more uptake metrics determined via the automated image analysis approaches described herein. For example, FIG. **29**A shows a GUI view **2900** in which a panel **2902** of the GUI displays an automatically determined TBR value **2904** for the patient. The panel also displays a determined TBR based classification **2906**, indicating that the TBR value is associated with clinically significant prostate cancer.

In certain embodiments, in order to aid in the user validation of the determined uptake metrics, a graphical element is displayed within the GUI to indicate a location of a voxel of the identified prostate volume. For example, as described herein, when a TBR value is computed as a ratio of a target intensity value to a background intensity value, a maximal intensity of voxels in the SPECT image corresponding to the identified prostate volume is identified. Accordingly, the GUI may display a graphical element that indicates a location of a voxel of the SPECT image corresponding to the identified prostate volume and having a maximal intensity in comparison with other voxels of the SPECT image that correspond to the identified prostate volume. In this manner, a position of a maximum SPECT intensity voxel corresponding to a location within the prostate volume is displayed to the user. The user may then visually verify, for example by inspection of the relation of the graphical element in comparison with the CT image, that this maximum SPECT intensity voxel indeed lies within the prostate of the subject. For example, as shown in FIG. **29**A, a set of cross-hair graphical elements **2950**, **2952**, and **2954** identifying a location of the maximum SPECT intensity voxel are overlaid on the 2D slices shown in the image viewer.

Returning to FIG. **25**, in another step **2510**, the user may choose to generate a report summarizing analysis performed for the patient using the uploaded SPECT/CT images, and be guided through a quality control workflow. For example, as shown in FIG. **29**A, the user may select (e.g., click) a create report button **2908** of the GUI. Upon the user selection of the create report button **2908**, a quality control graphical widget **2910** is displayed as shown in FIG. **29**B. The quality control graphical widget **2910** may guide a user to check if various acceptance criteria are met. For example, the quality control graphical widget **2910** guides a user to check that image requirements are met, and that a target value and background value, as used in determining a TBR value, are correct. The user may approve the automated analysis results, via selection of button **2912**, or may disapprove the automated analysis results, via selection of button **2914**.

As shown in FIG. **25**, following user approval of the quality control check **2512**, the automated assessment results **2514** are used to generate a report **2532** for the patient. As shown in FIG. **29**C, prior to generation a report, the user may be presented with a widget **2916** requesting their confirmation of approval of the quality control. FIG. **29**D shows an example report **2900***d*. The report may include an identification of the quality control criteria **2918**, along with an identification of the user that approved the quality control and signed the report **2920**.

As shown in FIG. **25**, if the user disapproves **2516** the automated determination of the uptake metric (e.g., TBR), the quality control widget may begin a guided assessment **2518** workflow. In the guided assessment workflow, the user may manually update values used in determining the one or

more uptake metrics via a manual interaction with the GUI. The user may also provide an input that indicates that the images for the patient cannot be used for accurately determining uptake metrics may also be received via the quality control widget. For example, following a user input corresponding to disapproval of the quality control, a GUI element such as that shown in FIG. **29**E may be presented to the user. The GUI element **2900***e* shown in FIG. **29**E allows the user to select whether no TBR value can be determined for the patient, via selection of button **2922**, or whether they would like to manually update the target and background intensity values used for the TBR value calculation, via selection of button **2924**.

For example, if the user determines (e.g., via visual inspection of the images) that the images are of too poor quality to use for accurate determination of a TBR value, the user may select button **2922** in GUI element **2900***e* to identify the case as unevaluable. As shown in FIG. **25**, follow receipt of the user identification of the case as unevaluable **2520**, the case is marked as unevaluable **2530**, and a report **2532** is produced that identifies quality control as rejected. FIG. **29**F shows an example of graphics and text **2900***f* that may be included in such a report to identify the quality control as rejected.

In certain embodiments, the user may elect to update the target and/or background intensity values used for determining the TBR value via a manual interaction with the GUI. Once a user input indicating that they wish to update the target and/or background intensity values is received **2522**, they are guided to manually set a target value **2524** and/or a background value **2526**. FIG. **29**G shows a view **2900***g* of a manual input graphical widget displayed to the user to allow them to set a target and/or background value. The user may click on button **2926** to manually set the target intensity value via interaction with the GUI. Upon selection of button **2926**, the user is presented with a voxel selection graphical element that allows them to select a voxel of the SPECT image to use as the maximum intensity voxel in computing the TBR value. For example, the user may be provided with a movable cross-hair that allows them to locate positions in the SPECT and CT images, such as the cross-hairs shown in FIG. **29**A. The user may move the cross-hairs and/or click on locations within the viewer to select a particular voxel to use as the maximum intensity voxel. As shown in FIG. **29**H, an updated view **2900***h* of the manual input graphical widget may show an intensity value **2930** of the selected maximum intensity voxel that will be used as an updated target intensity value for computing an updated TBR value.

The user may also select button **2928** to set a background value to use in computing the TBR value. Upon selection of button **2928**, the user may be presented with a voxel selection element and guided to select multiple voxels that they identify (e.g., based on visual inspection of the CT image layer and/or segmentation layer displayed in the GUI viewer) as belonging to the left gluteal muscle. Since the background intensity value for computing TBR is an average over intensities of multiple voxels of the SPECT image corresponding to physical locations within the left gluteal muscle, the user may be guided to select a sufficient number of voxels to ensure an accurate background intensity value is determined. For example, as shown in the view **2900***h* of the manual input graphical widget shown in FIG. **29**H, when the user is selecting voxels to use in determining an update background intensity value, a number of samples may be displayed along with the updated value of the background intensity **2932**. In certain embodiments, the user is required to select at least a predefined number of samples (e.g., 100), and the displayed background intensity value and number of samples **2932** includes a visual indication (e.g., color change) to let the user know once a sufficient number of samples has been selected.

Returning to FIG. **25**, once the user has completed manual input of an updated target value and/or an updated background intensity value, an updated TBR value is computed using the updated values and stored as a semi-automatic assessment **2528**. A report **2532** may then be generate using the semi-automatic assessment results.

E. Example Cloud-Based Architecture and Service Organization

In certain embodiments, the systems and methods described herein are implemented as a cloud-based application. The cloud-based application may use multiple modules to implement various functionalities, such as a client facing module that provides an interface for receiving input from a user and presenting them with image data and results. The client facing module may, in turn, interface with other modules, such as a segmentation service module that performs automated image segmentation to identify a prostate volume and compute uptake metrics as described herein.

FIG. **30** shows an example microservice network architecture **3000** for implementing the systems and methods described herein as a cloud-based application. The particular example microservice network is used in the example cloud-based application referred to as Pioneer, as described herein. In the example microservice network architecture **3000** of FIG. **30**, microservice Pioneer web **3016** is a client facing module that serves a client **3026** to provide them with an interface (e.g., by serving code instruction such as javascript and HTML) for interacting with stored images and analysis results. Pioneer web **3016** also communicates with other microservices, as shown in FIG. **30**. Audit service **3014** logs events and saves event logs in a log file storage database **3012**. Cognito **3020** stores and authenticates users. Auth service **3022** tracks user groups and customer product registrations. Signup service **3024** is a front-end service that allows users to sign up, e.g., for use of the cloud-based system. Slicebox **3004** stores image files in a standardized DICOM format, including 3D anatomical images such as CT images, and 3D functional images such as SPECT and PET images. Images are stored in image storage database **3002**. Image service **3006** reads images (e.g, DICOM files) and stores images and image metadata in a specific (e.g., convenient; e.g., standardized) format. Segmentation service **3010** performs automated image segmentation and uptake metric determination as described herein. Segmentation service **3010** fetches image data prepared by image service **3006** from data storage database **3008**, performs image segmentation and uptake metric determination, and stores results in the data storage database **3008**.

The architecture shown in FIG. **30** can be used to implement applications and platforms described herein on a variety of datacenters, including publicly available datacenters. The datacenter provides infrastructure in the form of servers and networks and provides services for e.g. networking, messaging, authentication, logging and storage. The architecture **3000** for the application uses a series of functional units with limited scope referred to as microservices. Each microservice handles an isolated set of tasks such as image storage, calculation of a risk index, identification of medical image type, and other tasks. Services (e.g., microservices) can communicate with each other using standard protocols such as Hypertext Transfer Protocol (HTTP).

Organizing the application into a network of microservices, as shown in the architecture **3000** of FIG. **30**, allows for parts of the platform to be scaled individually to meet high demand and to ensure minimal downtime. In certain embodiments, such an architecture allows for components to be improved or replaced without affecting other parts of the application, or platforms that include the application along with others.

FIG. **31** is a block flow diagram showing an example dataflow **3100** for performing automated segmentation and analysis of CT/SPECT images using a microservice network such as the one shown in FIG. **30**. Images uploaded by a user are stored in slicebox **3110**. A user may initiate processing of a study (e.g., images for a patient) to initiate automated image segmentation and analysis, for example via an interaction with Pioneer web **3104***a* via a client **3102***a*. Processing of a study may also begin automatically (e.g., following uploading of images; e.g., at regular time intervals). As shown in FIG. **31**, once processing of a study is initiated, Pioneer web **3104***a* interacts with Image service **3106** to initiate preparation (e.g., preprocessing; e.g., formatting) of image data for automated segmentation and analysis. Image service **3106** saves preprocessed images in database S3 **3112**. Pioneer web **3104***a* initiates image segmentation and analysis by Segmentation service (e.g., by sending a SQS message). Segmentation service **3108** fetches image data comprising a 3D anatomical image and a 3D functional image, such as a CT/SPECT image, from S3 **3112**. Segmentation service **3108** performs image segmentation to identify tissue volumes, including a prostate volume, within the 3D anatomical image, and uses the identified tissue volumes and the 3D functional image to compute one or more uptake metrics as described herein. Results of the automated image segmentation and uptake metric determination are saved in S3 **3112**. Segmentation service posts a callback to Pioneer web **3104***a* indicating whether results were successfully obtained or if an error/exception occurred. Upon receipt of the callback, Pioneer web **3104***a* publishes an updated status for the study on channel Pubsub **3118**. Multiple Pioneer web services **3104***a* and **3104***b* may receive the status update for the study and notify clients **3102***a* and **3102***b* with which they interact of the status update.

FIG. **32** shows a data flow **3200** between microservices showing how a client may request statuses of studies and be notified of study status updates in a manner similar to that described above with reference to FIG. **31**. As shown in FIG. **32**, a client **3202** may send study ids to a Pioneer web service instance **3204** that receives status updates via Pub/Sub channel **3212**. Callbacks for completed calculations (e.g., completed image segmentation and uptake metric analysis as described herein) may enter Pioneer web from any Segmentation service **3208**. A status for a completed calculation for a study may be saved in a database **3210** and an updated status for the study is sent to the Pub/Sub channel **3212**. All Pioneer web instances (e.g., **3204** and **3206**) subscribe to the status updates and may provide a status update (e.g., a notification of a completed calculation for the study) to a client **3202** with which they interact.

In certain embodiments, for example as described above with respect to FIG. **30** and FIG. **31**, implementations of the systems and methods described herein may include an Image service module that performs image data preprocessing and formatting, for example to provide appropriately formatted image data to a Segmentation service that performs automated image segmentation and uptake metric determination.

The image service module may preprocess different images from various modalities, including 3D functional and 3D anatomical images, to standardize and format the images. For example, preprocessing of a 3D functional image (e.g., a nuclear medicine image, such as a SPECT image), may include performing basic compliance checks and interpreting voxel intensity values as specified in a standard format (e.g., DICOM PS3 NM Image IOD). Frames of the 3D functional image may be arranged in a particular order corresponding to a direction along the subject, such as a head-to-feet order. A position may be adjusted to represent an outer corner of a first voxel. Attributes from the 3D functional image that may be needed in further processing may also be extracted.

Preprocessing of a 3D anatomical image, such as a CT image, may also include performing basic compliance checks and interpreting voxel intensity values as specified in a standard format (e.g., DICOM PS3 NM Image IOD). Slices of the 3D anatomical image may be arranged in a particular order corresponding to a direction along the subject, such as a head-to-feet order. Cropping bounds to remove one or more regions of the 3D anatomical image that correspond to air around an imaged patient may also be determined. A position may be adjusted to represent an outer corner of a first voxel. Attributes from the 3D anatomical image that may be needed in further processing may also be extracted.

FIG. **33** shows an architecture **3300** illustrating how a cloud-based application implementing the image segmentation and analysis approaches described herein, may be combined with other systems for performing other types of image analysis, to provide a cloud-based platform that a client/user may use to multiple image analysis applications. The architecture **3300** shown in FIG. **33** includes a set **3320** of microservices that are common between two or more applications. The left **3310** and right **3330** panels show microservices in two applications. Microservice network **3330** implements a version of the Pioneer cloud-based application, as described herein, and provides for automated analysis of CT/SPECT images, calculation of uptake metrics, such as TBR, and generation of reports. The microservice network **3310** shown in the left panel implements web-based application, referred to as aBSI, that analyzes whole-body scans obtained with a gamma camera, and computes an automated bone scan index (BSI). Further details regarding aBSI and automated BSI determination are provided in U.S. patent application Ser. No. 15/794,220, filed Oct. 10, 2017, the content of which is hereby incorporated by reference in its entirety.

F. Identifying Other Target Volumes of Interest and Computing Uptake Metrics

With regard to FIG. **34**, the approaches described herein can be used to identify other target volumes, e.g., lungs, lymph nodes, bone, liver. Other image types can be used. Various radiopharmaceuticals can be used to generate 3D functional images. For example, in certain embodiments, 1404 is the imaging agent used for SPECT images, and, in certain embodiments, PyL is the imaging agent used for PET images. In one embodiment, imaging is performed over the whole body of the subject for detection of disease (e.g., tumors) in tissue, e.g., in lymph nodes. The total number of tumors and/or the size and/or another metric associated with the spreading and/or quantity of diseased tissue (e.g., cancer) is/are determined automatically using methods described herein. For example, in process **3400** a 3D anatomical image

and a corresponding 3D functional image are received at steps **3402** and **3404**, respectively. A first CNN may be used to efficiently identify **3406** one or more sub-regions of an initial 3D anatomical image for more detailed segmentation by a second CNN **3408**, and the corresponding 3D functional image is analyzed within the identified one or more sub-regions to quantify overall imaging agent uptake and/or to provide a computed metric indicative of the level and/or extent of disease in the subject **3410**.

G. Example 1: Automated Detection and Quantification of Prostatic PSMA Uptake from SPECT/CT Imaging

In this example, 99mTc MIP-1404, a small-molecule inhibitor of prostate-specific membrane antigen (PSMA) was used to detect clinically significant disease in prostate cancer. An objective of this example was to develop a deep learning model for the automatic detection and quantification of prostatic MIP-1404 uptake in SPECT/CT images.

A deep-learning algorithm was developed based on convolutional neural networks for automatically segmenting the prostate and pelvic bones from CT images. The algorithm as designed to process both high- and low-dose CT images as well as whole and part body field of views, with no manual interaction necessary. The training material consisted of 100 diagnostic CT images (all male) with complete and distinct segmentations, performed manually, for relevant anatomical regions. The algorithm was validated on the MIP-1404 phase II study including 102 high-risk prostate cancer patients who all underwent PSMA imaging prior to radical prostatectomy. All validation scans were quantified manually using the OsiriX medical image viewer (Pixmeo SARL), by measuring the maximum uptake in a circular ROI placed inside the prostate in the slice and region with highest uptake values determined visually. The automatic algorithm uses its volumetric segmentations to measure uptake at every voxel in the prostate, and registers the maximum uptake. The Pearson correlation coefficient was used to assess the concordance between manual and automated quantification of prostatic uptake.

The algorithm based on the lining material had 2.7 million parameters and was optimized using Adam, a variant of gradient descent. In the test set, 1404 images of 34 patients (33%; 34/102) were excluded due to excessive CT artifacts, incomplete data and/or data format problems. Computation time on the evaluable patients (N=68) was 13 seconds (per case) on commodity hardware. The automated maximum uptake value was significantly correlated to the manually obtained in the prostate ($r=0.95$, 95% CI=[0.91,0.97]; slope=0.89, 95% CI=[0.80,0.98]; $p<0.0001$). The algorithm was fully automated and deterministic, resulting in 100% repeatability.

This example demonstrates the feasibility of an objective and automated measure of MIP-1404 uptake in the prostate.

H. Example 2: Technical and Clinical Performance of Automated Segmentation and Uptake Metric Determination

Example 2 shows evaluation of technical and clinical performance of an embodiment automated image segmentation and uptake metric determination approaches described herein implement via an example cloud-based application referred to as Pioneer. To establish the hypothesis generating algorithm for Pioneer, MIP-1404 SPECT/CT image data from two clinical studies were used, including healthy volunteers (a phase 1 study: MIP-1404-1301) and patients with prostate cancer who had histopathology data available following radical prostatectomy (a phase 2 study: MIP-1404-201). Data comparing the receiver operating characteristic plot (ROC), sensitivity, specificity, positive and negative predictive values produced by Pioneer with those obtained by traditional manual reads, showed that Pioneer could be a useful tool to assist radiologists in MIP-1404 image interpretation; thereby facilitating the evaluation of patients with prostate cancer.

i. Technical Performance

The analytical verification of the algorithm's segmentation and quantification performance criteria and the motivation was prospectively defined as detailed in OTHA-2262 and OTHA-2263, respectively. Total of sixty-one 1404 SPECT/CT images and standard for care read from nuclear medicine physician was used as benchmark to evaluate the analytical performance. All manual reads were done independently and blindly to the technical performance acceptance criteria.

The prostate segmentation performance test demonstrated mean dice of 0.77 and a standard deviation of 0.012. The lower endpoint of the one sided 95% confidence interval was 0.75, higher than the pre-defined threshold in OTHA-2262 (0.70). The background (gluteus maximus left) segmentation performance test demonstrated mean dice of 0.94 and a standard deviation of 0.002. The lower endpoint of the one sided 95% confidence interval was 0.94, higher than the pre-defined threshold in OTHA-2262 (0.80).

Only in four of the total 61 (6.6%) of the target locations predicted by the automated Pioneer software were classified by the human expert (nuclear medicine reader) as faulty. The outcome was better than that specified in OTHA-2263.

ii. Clinical Performance

In a retrospective ad hoc analysis of clinical performance, fourteen healthy volunteers (phase 1 study MIP-1404-1301) and 105 subjects with prostate cancer patients (phase 2 study MIP-1404-201) were combined in a single cohort for analysis with Pioneer. Subjects in MIP-1404-201 who received prior therapy for prostate cancer were excluded.

Images that had CT artifacts or could not be reconstructed for automated analysis were also excluded. A total of 75 images were evaluated from 61 subjects with prostate cancer and 14 normal volunteers.

Pioneer's automated assessment was evaluated against the histopathological truth standard for those who had been diagnosed with prostate cancer and had undergone radical prostatectomy following MIP-1404 SPECT/CT imaging. For healthy volunteers the assumption was made that they had no prostate cancer based on their normal PSA and pelvic MRI at the time of study. Spearman's rho was used to assess the correlation with Gleason score. Area under the receiver operating characteristic (ROC) curve was employed to determine the performance of the algorithm in detecting prostate cancer in the prostate gland. Sensitivity and specificity was determined from the optimal threshold/cutoff value from the ROC curve.

The automated quantitative assessment of the 1404 images correlated with Gleason score (rho: 0.54; $p<0.0001$). The ROC curve demonstrated an AUC of 0.80 (95% CI: 67-94). The optimal threshold for the binary TBR-based result in distinguishing clinically significant prostate cancer from clinically non-significant cancer or normal prostate was determined to be 25. Using this threshold, Pioneer distinguished clinically significant from clinically non-significant prostate cancer or normal prostates with a sensitivity

of 75% and specificity of 80% using 1404 SPECT/CT images from the MIP-1404-1301 and MIP-1404-201 studies.

Accordingly, Pioneer improves on manual reads by providing (i) more objective and reproducible read performance across all diagnostic endpoints, and (ii) point estimates for key diagnostic performance parameters, e.g. sensitivity, specificity, that have been shown to be consistently >70% using histopathology as the truth standard.

I. Example 3: Example Cloud Based Software for Automated and Semi-Automated Analysis of 1404 CT/SPECT Images

Example 3 is an example of a cloud-based software platform, referred to as Pioneer that implements an embodiment of the automated image analysis approaches described herein. Pioneer is a cloud-based software platform, implemented according to regulatory and data safety standards, where users can upload 1404 SPECT/CT image data, view it using 2-dimensional and 3-dimensional medical image viewers accessed through the user's ordinary internet browser, and review and export TBR values. The software also provides a quality control workflow where users can assess the quality of the analysis with options to reject and/or adjust the automated analysis.

Thus, under the supervision of the user, the software employs an artificial intelligence algorithm to automatically identify and analyze the regions of interest (ROIs). Pioneer extracts image data from the ROIs to provide an objective analysis—Target to background (TBR)—based on uptake in the prostate and background. Since signals in the prostate are often obscured by signals from the urinary bladder (MIP-1404 being excreted in urine), capability was also built in the software to segment the bladder and suppress bladder associated signals, thus enabling prostatic signals to be measured more accurately.

The non-clinical performance data of Pioneer include verification and validation (V&V) assessments, including definition of test methods. Pre-determined acceptance criteria were designed to ensure, at a minimum, equivalent performance with state of the art (manual assessment). The verification included software unit testing, integration testing and software system testing with functional testing of all software requirements. The validation process was performed to ensure that the system meets the user requirements specification. The V&V test results showed that Pioneer meets its intended use, user and software requirements.

J. Example 4: Selection of TBR Threshold for Clinically Significant Findings

Example 4 is an example showing how a TBR threshold value for partitioning patient prostate cancer pathology into clinically significant and clinically non-significant classifications can be determined.

Two datasets of SPECT/CT images were combined to select an appropriate threshold value. A first dataset comprised images of healthy individuals, taken from a phase I study of the 1404 drug. This dataset contained originally 14 images. Segmentation of a prostate within the images was performed in accordance with the approaches described herein and two images where segmentation of the prostate clearly failed were excluded, resulting in 12 remaining images. A second data set comprised images of individuals with prostate cancer, originating from a phase II study of the 1404 drug. The images were partitioned based on the subject's Gleason grades on histopathology from radical prostatectomy. A total Gleason Score of 7 or above was considered clinically significant and total Gleason Score 6 or below was considered clinically non-significant. This dataset contained originally 65 images (63 clinically significant, 2 clinically non-significant), after excluding one image where the image did not cover the entire pelvic region and one image where the segmentation of prostate had clearly failed, 63 remained (61 clinically significant, 2 clinically non-significant).

In summary, 14 images without clinically significant pathology and 61 images with clinically significant pathology were used.

A software package implementing an embodiment of the automated image segmentation and uptake metric determination approaches described herein, ctseg package version 1.0.0rcIII, was used to compute TBR values for the images.

FIG. **35**A shows a swarm plot of clinically non-significant (<=6 on the x-axis) and clinically significant images (>=7 on the x-axis). A threshold of 25 gives a sensitivity of 0.77 (lower endpoint of Jeffreys one-sided 95% confidence interval is 0.67) and a specificity of 0.71 (lower endpoint of Jeffreys one-sided 95% confidence interval is 0.50) on the test data. FIG. **35**B shows a ROC curve based on varying the TBR threshold. The point for TBR threshold 25 is marked **3502** (red circular marker).

As shown in FIGS. **35** A and **35**B, a threshold value of 25 provided a value for distinguishing between patients who do have clinically significant prostate cancer and those who do not. However, since there are few data points very close to the threshold, the estimates of sensitivity and specificity are not robust to small random variations in data. To get more robust estimates, the R package 'scdensity' was used to estimate smooth unimodal densities for the distribution of log TBR values for clinically non-significant and significant images respectively. From this, estimates for sensitivity and specificity were computed for different TBR thresholds, see Table 1.

TABLE 1

Robust estimates of sensitivity and specificity for different TBR thresholds.

TBR threshold	Specificity	Sensitivity
22	0.68	0.79
23	0.70	0.78
24	0.73	0.76
25	0.75	0.75
26	0.76	0.73
27	0.78	0.72
28	0.79	0.70

Accordingly, based on the analysis described in this example, a TBR threshold of 25 was selected based on a desired specificity and sensitivity. These preliminary studies based on Phase 1 and Phase 2 data have shown improved diagnostic accuracy of MIP-1404 SPECT/CT using the automated method in comparison to manual reads.

K. Example 5: Application of AI to Phase 3 Study MIP-1404-3301 ("proSPECT-AS")

MIP1404-3301 is a pivotal phase 3 multicenter trial of ^{99m}Tc-MIP1404 Injection for the detection of prostate cancer. MIP-1404-3301 is titled "A Phase 3 Study to Evaluate the Safety and Efficacy of 1404 SPECT/CT Imaging to

Detect Clinically Significant Prostate Cancer in Men with Biopsy Proven Low-Grade Prostate Cancer who are Candidates for Active Surveillance". Cohort A patients were men with biopsy-proven low to intermediate grade prostate cancer (Gleason score 3+3 or 3+4) who were candidates for active surveillance but elected to have radical prostatectomy. Cohort B patients were biopsy-proven very low risk prostate cancer patients who scheduled to undergo routine re-biopsy as part or routine active surveillance. The phase 3 study was initiated in December 2015, and enrollment is now complete. The computer-assisted diagnosis (CADx) software device is to be used as the primary reading methodology to analyze the primary end-points in Study MIP-1404-3301.

There are two co-primary endpoints:

Specificity of ^{99m}Tc-MIP1404 to detect clinically significant prostate cancer when compared to histopathology following radical prostatectomy (cohort A) or prostate biopsy (cohort B) using automated reading technology;

Sensitivity of ^{99m}Tc-MIP1404 to detect clinically significant prostate cancer when compared to histopathology following radical prostatectomy (cohort A) or prostate biopsy (cohort B) using automated reading technology.

The 1404 image data from the Phase 3 trial were collected by a central imaging core laboratory. The image analysis is conducted by a radiologist using the automated software device. The medical software device is used in the assessment and characterization of prostate cancer, using a radioactive PSMA targeting imaging agent, for example as a Computer Aided Detection (CADe) device. The analysis is useful in estimating the risk for clinically significant prostate cancer in a patients. The device is also useful as a combination product comprising 1404 radioactive diagnostic agent indicated for the imaging of patients with prostate cancer in combination with the automated software device, for the automated assessment, characterization and diagnosis of prostate cancer, for example as a Computer-aided Diagnostic (CADx) device. The 1404 imaging results help estimate the risk for clinically significant prostate cancer in these patients. The software uses artificial intelligence to automatically segment the image data into distinct anatomical regions and then analyzes the volumetric regions of interest (ROI). The software extracts quantitative data from ROIs to assist in determining the presence or absence of clinically significant prostate cancer. The software device is used to assist radiologist and physicians in the assessment, characterization and quantification of prostate cancer in SPECT/CT and PET/CT images. The device is indicated for evaluation of patients presenting high-risk or low-risk screening, diagnostic imaging workup, or evaluation of extent of disease. The results from the image analysis are useful in guiding treatment decisions for the patients by the physicians.

L. Example 6: Training and Validation of Convolutional Neural Networks Implemented by the First Machine Learning Module (Localization Machine) and Second Machine Learning Module (Segmentation Machine)

Example 5 is an example showing training and validation of CNN modules used to segment CT images to identify various tissue volumes, including a prostate volume, in accordance with the aspects and embodiments described herein. In this example, the neural networks were defined and trained using the Keras framework with the Tensorflow backend.

i. Training and Validation Data

The training and validation data comprised CT images coupled with semi-automated segmentations corrected by a radiologist delineating all or some of the following body parts: (i) a prostate; (ii) a urinary bladder; (iii) a rectum; (iv) a left gluteus maximus; (v) a right gluteus maximus; (vi) a left hip bone; (vii) a right hip bone; and (viii) a sacrum and coccyx

To train a localization CNN, 90 high quality CT images were used with segmentations of all the body parts above. For training a segmentation CNN for high resolution segmentation of left gluteus maximus, these and 10 images of the same type were used. For training a segmentation CNN for high resolution segmentation of the prostate, an additional data set of 73 lower-quality images with more anatomical variation in prostate and urinary bladder (due to disease) was used. These additional images were matched with segmentations of the prostate and the urinary bladder only. Pseudo labels for rectum, left and right hip bone, and sacrum and coccyx were generated for these 73 images. The pseudo labels are predicted labels generated using a previously trained network (a network trained on the 100 high quality CT images). The pseudo labels were merged with the manual labels before training.

ii. Training Configuration

Each training run was defined by a configuration file named config.json. The configuration file included parameters for: (i) which data set is used; (ii) data preprocessing; (iii) partitioning data into training and validation sets; (iv) model structure; and (v) training hyperparameters.

This configuration file is used when the trained model is used for inference, to ensure that the same image preprocessing is done during inference as during training.

iii. Preprocessing

The configuration file defines which preprocessing steps are applied during training. Several preprocessing steps were included. Cropping preprocessing steps were performed to remove surrounding air for localization training and to crop out a bounding box defined by pelvic bones, urinary bladder, rectum and prostate for segmentation. A fixed intensity normalization step was performed by subtraction of a fixed value and then division by another fixed value, where the values are chosen so that on average the intensities of voxels in the images have a mean intensity 0 and a standard deviation 1. Images were also reshaped to a fixed size by resampling. For localization, the resolution in each direction decreased by a factor of 4 for an image with median sizes in each direction. For high-resolution segmentation the resolution does not change for an image with median sizes in each dimension. Other preprocessing steps included one-hot-encoding of segmentation labels, segmentation label reweighting as defined in section iv. "Optimization", below, and data augmentation, as defined in section iv. "Optimization", below.

Some preprocessing steps are performed offline in order to speed up the training, resulting in preprocessed data sets. The config.json that belongs to the training only defines those preprocessing steps that are done online.

For localization training, the preprocessing steps for the offline preprocessing is stored in a separate file meta_data/prep_config.json in the trained CNN directory.

iv. Optimization

The loss function used for training is voxel-wise categorical cross entropy, weighted such that all voxel belonging to one class (in the true labeling) together have the same weight as all voxels belonging to any other class (when the label frequencies equal the median frequencies across the data

set). This approach balances the classes and is important for prostate segmentation since the prostate is very small in comparison to, e.g., the background.

The loss is optimized using mini-batch descent with the Adam optimizer for around 2000-3000 epochs. The batch size equals 1. A batch size of 1 means that batch normalization turns into instance normalization (since the batch is only one sample). For improved performance, instance normalization is enforced also during inference.

The learning rate is determined by a learning rate schedule with a very low learning rate (e.g., 1×10^{-5}) for the first few epochs, then decreasing in steps from a high learning rate (e.g. 1×10^{-2}). After 250 epochs the learning rate is halved, then halved again after 500 more epochs, then halved again after 1000 more epochs. To decrease overfitting, dropout is used. Dropout rates vary between 0.2 and 0.5 for different networks (but the rate same in all places where it is applied for a given network, as shown, for example, in FIG. **13** and FIG. **14**). Appropriate rates of dropout are based on experience from multiple trainings and how it affects the difference in performance on training and validation sets.

A training approach where the training image data is augmented by adding random distortions was used prevent the neural networks from focusing on fine details in the images. Training the neural networks (e.g., the localization CNN and segmentation CNN) in this manner allows them to handle (e.g., perform effective localization and/or segmentation of) images with image artifacts that are not present or not common in the training data.

The random distortions added to augment the training data include additive or multiplicative noise and added smoothed salt noise. These random distortions are applied independently with certain probabilities. These random distortions are scheduled to be not used for the first few hundred epochs so that the network first learns to handle images without artifacts, then the noise level is gradually increased. The intensity distortions are only applied to the 100 high-quality CT images, not the 73 low-quality images since they already have artifacts.

The localization CNN is trained to handle (e.g., receive as input) whole-body images as well as different partial-body images. To this end, augmentation with random crops of the image (always keeping the entire pelvic bounding box) is used.

v. Computational Resources

The localization trainings were done on a Nvidia GeForce GTX 1050, where a training took a few hours.

The high resolution segmentation trainings were done on a Nvidia GeForce GTX 1080 Ti, where training took 2-3 days.

vi. Model Selection

To optimize neural network structures and select hyper parameters for the training it is necessary to have metrics measuring performance. The main metric for evaluating the progress of training is Sorensen-Dice score (referred to hereafter as "Dice score"): the weighted score (weighting described above in section iv. "Optimization") or the score for individual body parts (prostate or left gluteus maximus).

When aggregating results over multiple images, most often averages of evaluated Dice scores are used (e.g., as metrics). In certain cases, a frequency of images with Dice scores below a certain level is used.

For each localization training run, the model that had best average weighted Dice score for the training images was selected. For segmentation trainings used to train the segmentation neural network to segment the prostate, the Dice score for prostate was used as a basis for selection. For segmentation trainings used to train the segmentation neural network to segment the left gluteus maximus the Dice score for left gluteus maximus was a basis for selection. For segmentation trainings with auxiliary predictions, the Dice scores were based on the prediction from the main output—that is, the output which is present also when there are no auxiliary predictions.

When training the localization CNN, 30% of the 90 CT images were reserved for validation, such that performance of the localization CNN could be evaluated using images that it was not trained on. To train the segmentation CNN for high-resolution prostate segmentation, 23 of the low-quality CT images were set aside for validation, such that only 50 of the low quality images were used in training (resulting in 150 CT images for training in total).

Metrics corresponding to a precision in cropping was used when selecting between different localization trainings. Cropping precision was evaluated based on several metrics/aspects. In particular, one metric was that as few images as possible of the 90 training and validation images should need a crop margin above 0.1 to encompass the entire pelvic bones. Another metric was that an error in distance to the bounding box walls should be as small as possible (evaluated by looking at box plots of errors). Another metric was that on 102 low-quality CT images (without ground truth segmentations available), 2D projections of them with the coarse segmentation and final bounding box overlaid should show good agreement between segmentation and anatomy, especially that the appropriate region was covered.

When selecting between different high-resolution segmentation trainings, the following metrics/aspects were considered: (i) Dice scores for training and validation data; (ii) precision and recall for prostate for training and validation data; (iii) overlap between ground-truth bladder and predicted prostate; and (iv) examples of segmentations overlaid on CT-images in a CT image viewer where one can scroll through the slices in the sagittal, axial and coronal planes.

Accordingly, this example provides an example of an approach that can be used to train neural network models used in the localization machine learning module (first machine learning module) and segmentation machine learning modules (second machine learning module and any auxiliary segmentation machine learning modules) described herein.

M. Imaging Agents

In certain embodiments, 3D functional images are nuclear medicine images that use imaging agents comprising radiopharmaceuticals. Nuclear medicine images are obtained following administration of a radiopharmaceutical to a patient, and provide information regarding the distribution of the radiopharmaceutical within the patient. Radiopharmaceuticals are compounds that comprise a radionuclide.

Nuclear medicine images (e.g., PET scans; e.g., SPECT scans; e.g., whole-body scans; e.g. composite PET-CT images; e.g., composite SPECT-CT images) detect radiation emitted from the radionuclides of radiopharmaceuticals to form an image. The distribution of a particular radiopharmaceutical within a patient may be determined by biological mechanisms such as blood flow or perfusion, as well as by specific enzymatic or receptor binding interactions. Different radiopharmaceuticals may be designed to take advantage of different biological mechanisms and/or particular specific enzymatic or receptor binding interactions and thus, when administered to a patient, selectively concentrate within particular types of tissue and/or regions within the patient.

Greater amounts of radiation are emitted from regions within the patient that have higher concentrations of radiopharmaceutical than other regions, such that these regions appear brighter in nuclear medicine images. Accordingly, intensity variations within a nuclear medicine image can be used to map the distribution of radiopharmaceutical within the patient. This mapped distribution of radiopharmaceutical within the patient can be used to, for example, infer the presence of cancerous tissue within various regions of the patient's body.

For example, upon administration to a patient, technetium 99m methylenediphosphonate (^{99m}Tc MDP) selectively accumulates within the skeletal region of the patient, in particular at sites with abnormal osteogenesis associated with malignant bone lesions. The selective concentration of radiopharmaceutical at these sites produces identifiable hotspots—localized regions of high intensity in nuclear medicine images. Accordingly, presence of malignant bone lesions associated with metastatic prostate cancer can be inferred by identifying such hotspots within a whole-body scan of the patient. Risk indices that correlate with patient overall survival and other prognostic metrics indicative of disease state, progression, treatment efficacy, and the like, can be computed based on automated analysis of intensity variations in whole-body scans obtained following administration of ^{99m}Tc MDP to a patient. In certain embodiments, other radiopharmaceuticals can also be used in a similar fashion to ^{99m}Tc MDP.

In certain embodiments, the particular radiopharmaceutical used depends on the particular nuclear medicine imaging modality used. For example ^{18}F sodium fluoride (NaF) also accumulates in bone lesions, similar to ^{99m}Tc MDP, but can be used with PET imaging. In certain embodiments, PET imaging may also utilize a radioactive form of the vitamin choline, which is readily absorbed by prostate cancer cells.

In certain embodiments, radiopharmaceuticals that selectively bind to particular proteins or receptors of interest—particularly those whose expression is increased in cancerous tissue may be used. Such proteins or receptors of interest include, but are not limited to tumor antigens, such as CEA, which is expressed in colorectal carcinomas, Her2/neu, which is expressed in multiple cancers, BRCA 1 and BRCA 2, expressed in breast and ovarian cancers; and TRP-1 and -2, expressed in melanoma.

For example, human prostate-specific membrane antigen (PSMA) is upregulated in prostate cancer, including metastatic disease. PSMA is expressed by virtually all prostate cancers and its expression is further increased in poorly differentiated, metastatic and hormone refractory carcinomas. Accordingly, radiopharmaceuticals corresponding to PSMA binding agents (e.g., compounds that a high affinity to PSMA) labelled with one or more radionuclide(s) can be used to obtain nuclear medicine images of a patient from which the presence and/or state of prostate cancer within a variety of regions (e.g., including, but not limited to skeletal regions) of the patient can be assessed. In certain embodiments, nuclear medicine images obtained using PSMA binding agents are used to identify the presence of cancerous tissue within the prostate, when the disease is in a localized state. In certain embodiments, nuclear medicine images obtained using radiopharmaceuticals comprising PSMA binding agents are used to identify the presence of cancerous tissue within a variety of regions that include not only the prostate, but also other organs and tissue regions such as lungs, lymph nodes, and bones, as is relevant when the disease is metastatic.

In particular, upon administration to a patient, radionuclide labelled PSMA binding agents selectively accumulate within cancerous tissue, based on their affinity to PSMA. In a similar manner to that described above with regard to ^{99m}Tc MDP, the selective concentration of radionuclide labelled PSMA binding agents at particular sites within the patient produces detectable hotspots in nuclear medicine images. As PSMA binding agents concentrate within a variety of cancerous tissues and regions of the body expressing PSMA, localized cancer within a prostate of the patient and/or metastatic cancer in various regions of the patient's body can be detected, and evaluated. As described in the following, risk indices that correlate with patient overall survival and other prognostic metrics indicative of disease state, progression, treatment efficacy, and the like, can be computed based on automated analysis of intensity variations in nuclear medicine images obtained following administration of a PSMA binding agent radiopharmaceutical to a patient.

A variety of radionuclide labelled PSMA binding agents may be used as radiopharmaceutical imaging agents for nuclear medicine imaging to detect and evaluate prostate cancer. In certain embodiments, the particular radionuclide labelled PSMA binding agent that is used depends on factors such as the particular imaging modality (e.g., PET; e.g., SPECT) and the particular regions (e.g., organs) of the patient to be imaged. For example, certain radionuclide labelled PSMA binding agents are suited for PET imaging, while others are suited for SPECT imaging. For example, certain radionuclide labelled PSMA binding agents facilitate imaging a prostate of the patient, and are used primarily when the disease is localized, while others facilitate imaging organs and regions throughout the patient's body, and are useful for evaluating metastatic prostate cancer.

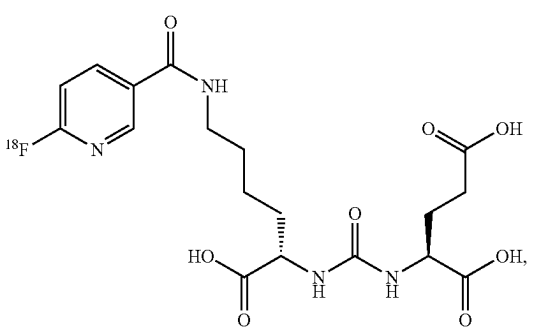
A variety of PSMA binding agents and radionuclide labelled versions thereof are described in U.S. Pat. Nos. 8,778,305, 8,211,401, and 8,962,799, each of which are incorporated herein by reference in their entireties.

i. PET Imaging Radionuclide Labelled PSMA Binding Agents

In certain embodiments, the radionuclide labelled PSMA binding agent is a radionuclide labelled PSMA binding agent appropriate for PET imaging.

In certain embodiments, the radionuclide labelled PSMA binding agent comprises [18F]DCFPyL (also referred to as PyL™; also referred to as DCFPyL-18F):

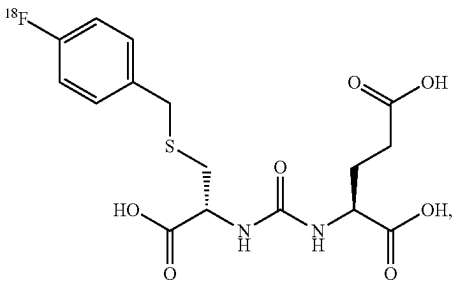
[18F]DCFPyL



or a pharmaceutically acceptable salt thereof.

In certain embodiments, the radionuclide labelled PSMA binding agent comprises [18F]DCFBC:

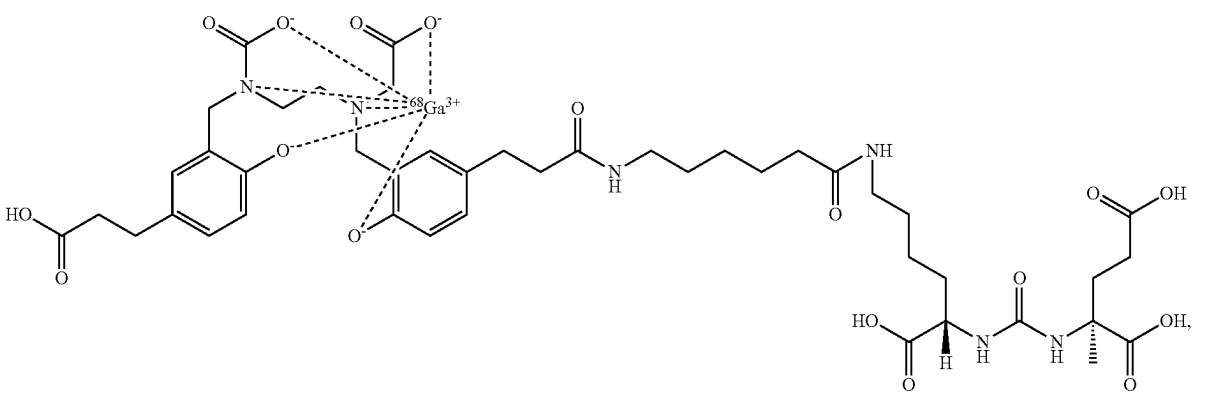
[18F]DCFBC



or a pharmaceutically acceptable salt thereof.

In certain embodiments, the radionuclide labelled PSMA binding agent comprises ^{68}Ga-PSMA-HBED-CC (also referred to as ^{68}Ga-PSMA-11):

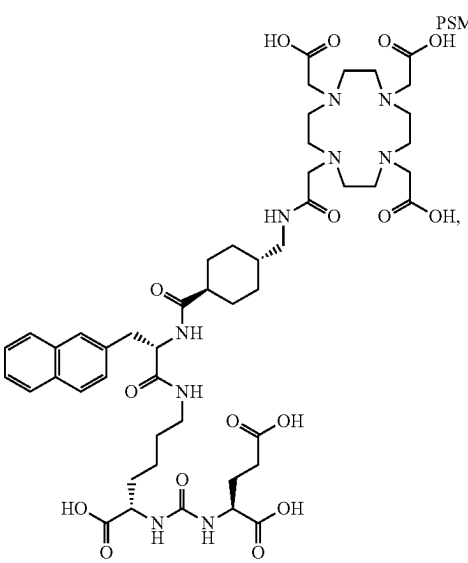
^{68}Ga-PSMA-HBED-CC



or a pharmaceutically acceptable salt thereof.

In certain embodiments, the radionuclide labelled PSMA binding agent comprises PSMA-617:

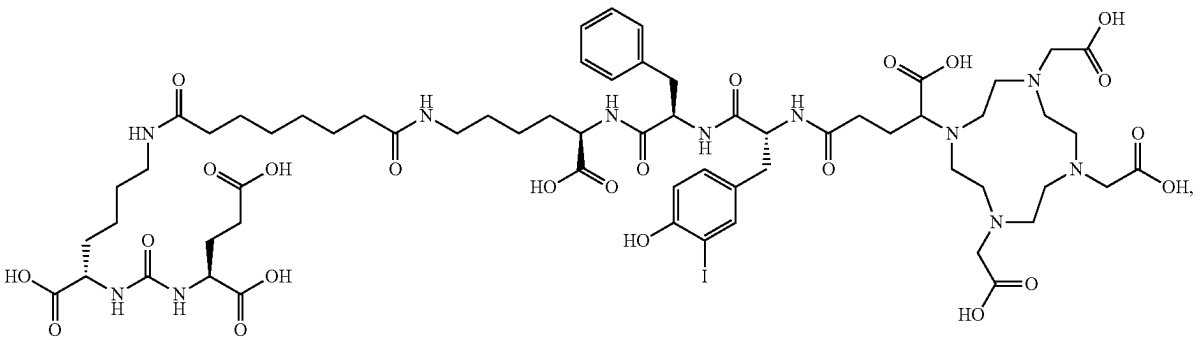
PSMA-617



or a pharmaceutically acceptable salt thereof. In certain embodiments, the radionuclide labelled PSMA binding agent comprises ^{68}Ga-PSMA-617, which is PSMA-617 labelled with ^{68}Ga, or a pharmaceutically acceptable salt thereof. In certain embodiments, the radionuclide labelled PSMA binding agent comprises ^{177}Lu-PSMA-617, which is PSMA-617 labelled with ^{177}Lu, or a pharmaceutically acceptable salt thereof.

In certain embodiments, the radionuclide labelled PSMA binding agent comprises PSMA-I&T:

PSMA-I&T

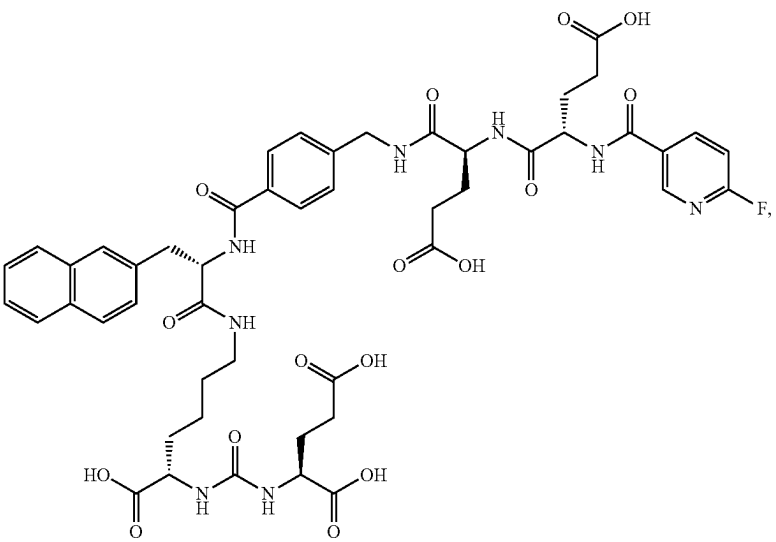


PSMA-I&T

or a pharmaceutically acceptable salt thereof. In certain embodiments, the radionuclide labelled PSMA binding agent comprises ^{68}Ga-PSMA-I&T, which is PSMA-I&T labelled with ^{68}Ga, or a pharmaceutically acceptable salt thereof.

In certain embodiments, the radionuclide labelled PSMA binding agent comprises PSMA-1007:

PSMA-1007



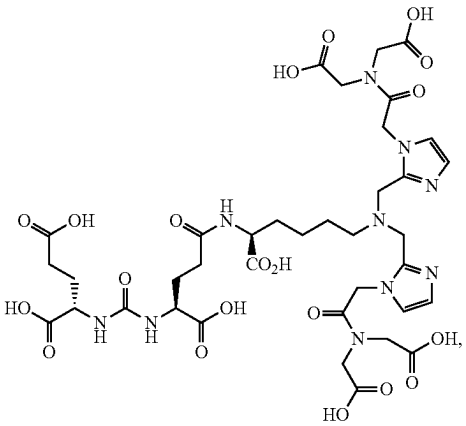
or a pharmaceutically acceptable salt thereof. In certain embodiments, the radionuclide labelled PSMA binding agent comprises ^{18}F-PSMA-1007, which is PSMA-1007 labelled with ^{18}F, or a pharmaceutically acceptable salt thereof.

ii. SPECT Imaging Radionuclide Labelled PSMA Binding Agents

In certain embodiments, the radionuclide labelled PSMA binding agent is a radionuclide labelled PSMA binding agent appropriate for SPECT imaging.

In certain embodiments, the radionuclide labelled PSMA binding agent comprises 1404 (also referred to as MIP-1404):

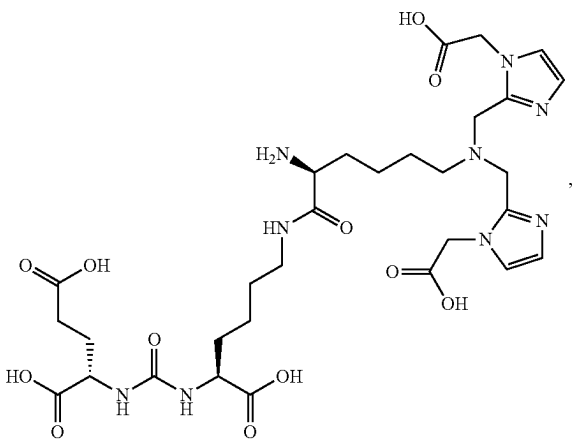
1404



or a pharmaceutically acceptable salt thereof.

In certain embodiments, the radionuclide labelled PSMA binding agent comprises 1405 (also referred to as MIP-1405):

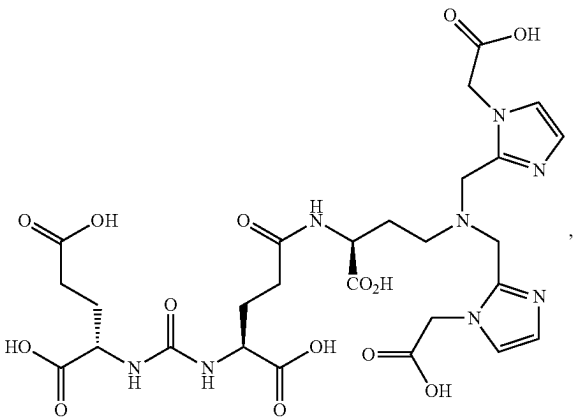
1405



or a pharmaceutically acceptable salt thereof.

In certain embodiments, the radionuclide labelled PSMA binding agent comprises 1427 (also referred to as MIP-1427):

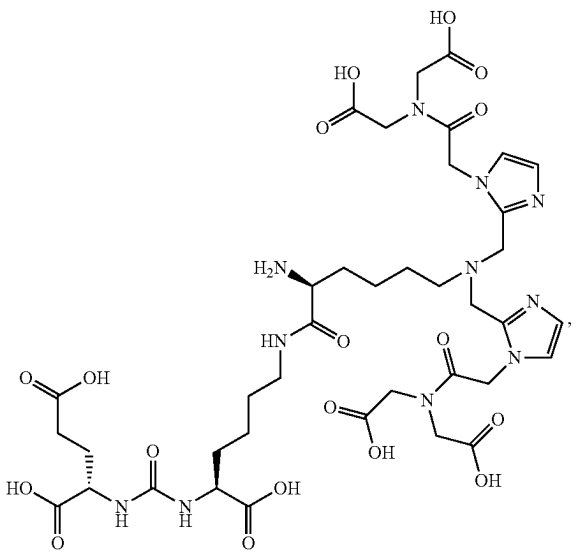
1427



or a pharmaceutically acceptable salt thereof.

In certain embodiments, the radionuclide labelled PSMA binding agent comprises 1428 (also referred to as MIP-1428):

1428

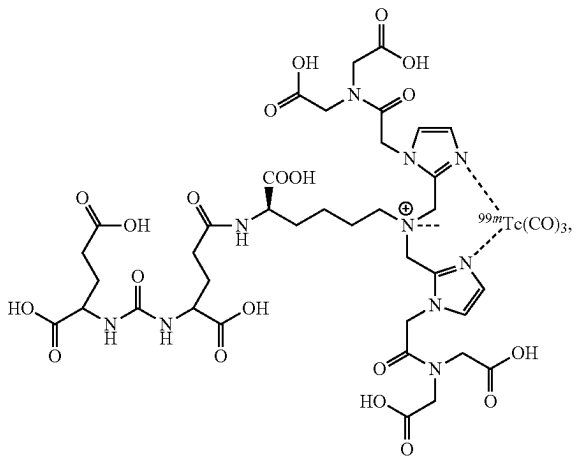


or a pharmaceutically acceptable salt thereof.

In certain embodiments, the PSMA binding agent is labelled with a radionuclide by chelating it to a radioisotope of a metal [e.g., a radioisotope of technetium (Tc) (e.g., technetium-99m (^{99m}Tc)); e.g., a radioisotope of rhenium (Re) (e.g., rhenium-188 (^{188}Re); e.g., rhenium-186 (^{186}Re)); e.g., a radioisotope of yttrium (Y) (e.g., ^{90}Y); e.g., a radioisotope of lutetium (Lu) (e.g., ^{177}Lu); e.g., a radioisotope of gallium (Ga) (e.g., ^{68}Ga; e.g., ^{67}Ga); e.g., a radioisotope of indium (e.g., ^{111}In); e.g., a radioisotope of copper (Cu) (e.g., ^{67}Cu)].

In certain embodiments, 1404 is labelled with a radionuclide (e.g., chelated to a radioisotope of a metal). In certain embodiments, the radionuclide labelled PSMA binding agent comprises ^{99m}Tc-MIP-1404, which is 1404 labelled with (e.g., chelated to)^{99m}Tc:

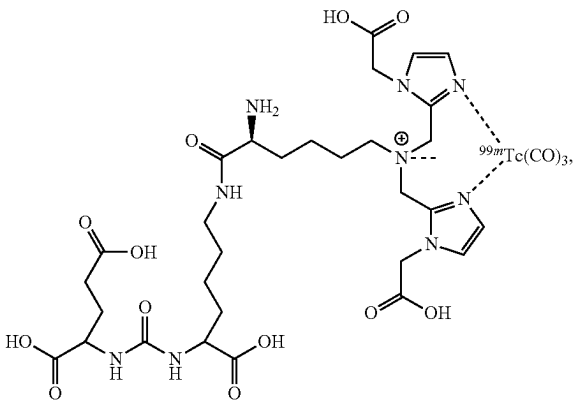
^{99m}Tc-MIP-1404



or a pharmaceutically acceptable salt thereof. In certain embodiments, 1404 may be chelated to other metal radioisotopes [e.g., a radioisotope of rhenium (Re) (e.g., rhenium-188 (^{188}Re); e.g., rhenium-186 (^{186}Re)); e.g., a radioisotope of yttrium (Y) (e.g., ^{90}Y); e.g., a radioisotope of lutetium (Lu)(e.g., ^{177}Lu); e.g., a radioisotope of gallium (Ga) (e.g., ^{68}Ga; e.g., ^{67}Ga); e.g., a radioisotope of indium (e.g., ^{111}In); e.g., a radioisotope of copper (Cu) (e.g., ^{67}Cu)] to form a compound having a structure similar to the structure shown above for ^{99m}Tc-MIP-1404, with the other metal radioisotope substituted for ^{99m}Tc.

In certain embodiments, 1405 is labelled with a radionuclide (e.g., chelated to a radioisotope of a metal). In certain embodiments, the radionuclide labelled PSMA binding agent comprises ^{99m}Tc-MIP-1405, which is 1405 labelled with (e.g., chelated to)^{99m}Tc:

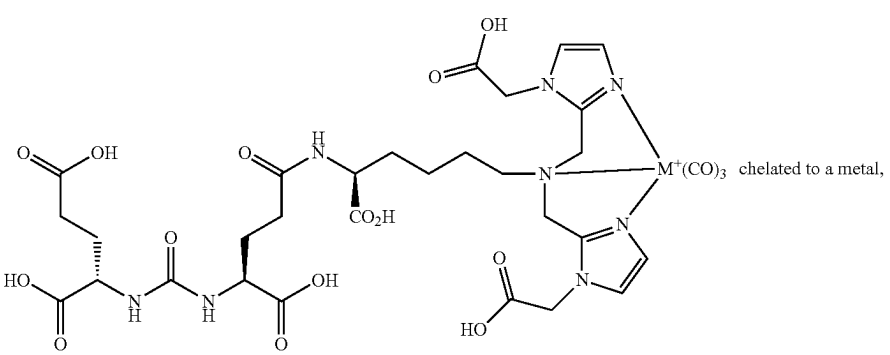
^{99m}Tc-MIP-1405



or a pharmaceutically acceptable salt thereof. In certain embodiments, 1405 may be chelated to other metal radioisotopes [e.g., a radioisotope of rhenium (Re) (e.g., rhenium-188 (^{188}Re); e.g., rhenium-186 (^{186}Re)); e.g., a radioisotope of yttrium (Y) (e.g., ^{90}Y); e.g., a radioisotope of lutetium (Lu)(e.g., ^{177}Lu); e.g., a radioisotope of gallium (Ga) (e.g., ^{68}Ga; e.g., ^{67}Ga); e.g., a radioisotope of indium (e.g., ^{111}In); e.g., a radioisotope of copper (Cu) (e.g., ^{67}Cu)] to form a compound having a structure similar to the structure shown above for ^{99m}Tc-MIP-1405, with the other metal radioisotope substituted for ^{99m}Tc.

In certain embodiments, 1427 is labelled with (e.g., chelated to) a radioisotope of a metal, to form a compound according to the formula below:

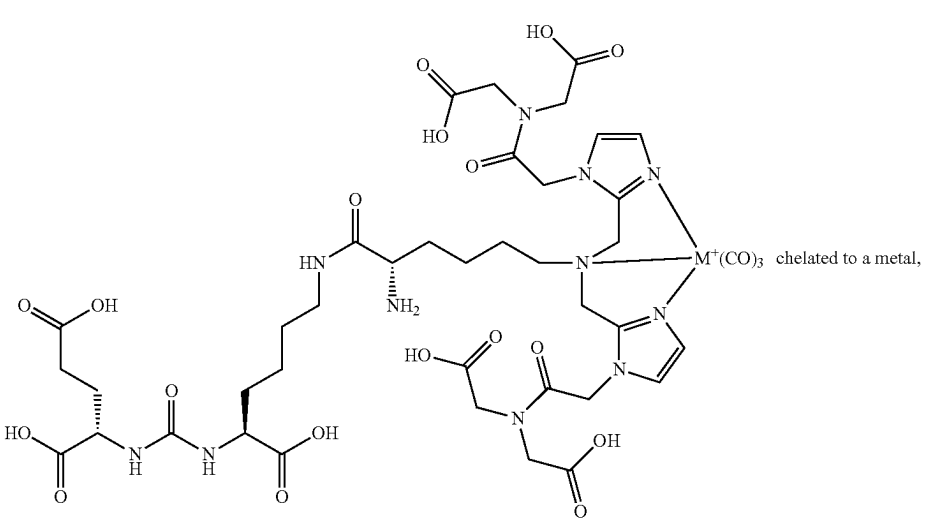
1427



or a pharmaceutically acceptable salt thereof, wherein M is a metal radioisotope [e.g., a radioisotope of technetium (Tc) (e.g., technetium-99m (^{99m}Tc)); e.g., a radioisotope of rhenium (Re) (e.g., rhenium-188 ^{188}Re); (e.g., rhenium-186 (^{186}Re)); e.g., a radioisotope of yttrium (Y) (e.g., ^{90}Y); e.g., a radioisotope of lutetium (Lu)(e.g., ^{177}Lu); e.g., a radioisotope of gallium (Ga) (e.g., ^{68}Ga; e.g., ^{67}Ga); e.g., a radioisotope of indium (e.g., ^{111}In); e.g., a radioisotope of copper (Cu) (e.g., ^{67}Cu)] with which 1427 is labelled.

In certain embodiments, 1428 is labelled with (e.g., chelated to) a radioisotope of a metal, to form a compound according to the formula below:

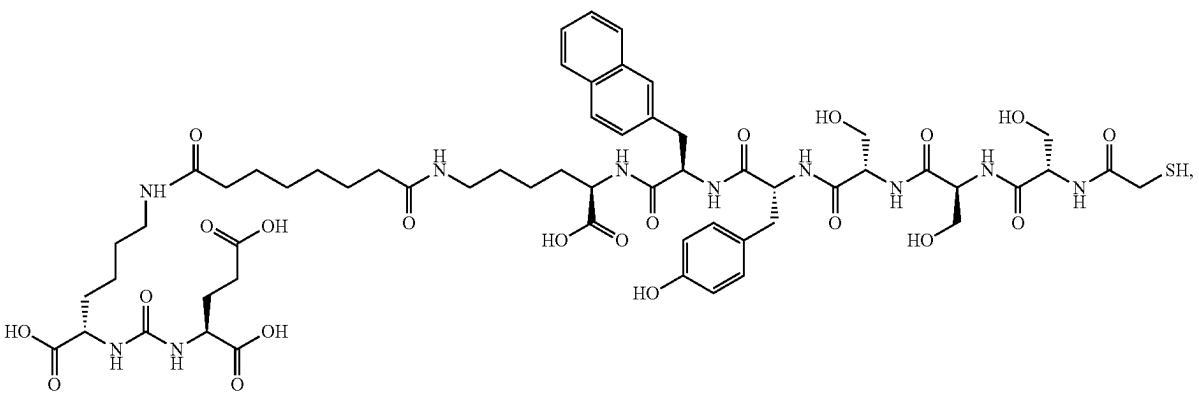
1428



or a pharmaceutically acceptable salt thereof, wherein M is a metal radioisotope [e.g., a radioisotope of technetium (Tc) (e.g., technetium-99m (^{99m}Tc)); e.g., a radioisotope of rhenium (Re) (e.g., rhenium-188 (^{188}Re); e.g., rhenium-186 (^{186}Re)); e.g., a radioisotope of yttrium (Y) (e.g., ^{90}Y); e.g., a radioisotope of lutetium (Lu)(e.g., ^{177}Lu); e.g., a radioisotope of gallium (Ga) (e.g., ^{68}Ga; e.g., ^{67}Ga); e.g., a radioisotope of indium (e.g., ^{111}In); e.g., a radioisotope of copper (Cu) (e.g., ^{67}Cu)] with which 1428 is labelled.

In certain embodiments, the radionuclide labelled PSMA binding agent comprises PSMA I&S:

PSMA I&S



or a pharmaceutically acceptable salt thereof. In certain embodiments, the radionuclide labelled PSMA binding agent comprises ^{99m}Tc-PSMA I&S, which is PSMA I&S labelled with ^{99m}Tc, or a pharmaceutically acceptable salt thereof.

N. Computer System and Network Architecture

As shown in FIG. **36**, an implementation of a network environment **3600** for use in providing systems, methods, and architectures described herein is shown and described. In brief overview, referring now to FIG. **36**, a block diagram of an exemplary cloud computing environment **3600** is shown and described. The cloud computing environment **3600** may include one or more resource providers **3602***a*, **3602***b*, **3602***c* (collectively, **3602**). Each resource provider **3602** may include computing resources. In some implementations, computing resources may include any hardware and/or software used to process data. For example, computing resources may include hardware and/or software capable of executing algorithms, computer programs, and/or computer applications. In some implementations, exemplary computing resources may include application servers and/or databases with storage and retrieval capabilities. Each

resource provider **3602** may be connected to any other resource provider **3602** in the cloud computing environment **3600**. In some implementations, the resource providers **3602** may be connected over a computer network **3608**. Each resource provider **3602** may be connected to one or more computing device **3604***a*, **3604***b*, **3604***c* (collectively, **3604**), over the computer network **3608**.

The cloud computing environment **3600** may include a resource manager **3606**. The resource manager **3606** may be connected to the resource providers **3602** and the computing devices **3604** over the computer network **3608**. In some implementations, the resource manager **3606** may facilitate the provision of computing resources by one or more resource providers **3602** to one or more computing devices **3604**. The resource manager **3606** may receive a request for a computing resource from a particular computing device **3604**. The resource manager **3606** may identify one or more resource providers **3602** capable of providing the computing resource requested by the computing device **3604**. The resource manager **3606** may select a resource provider **3602** to provide the computing resource. The resource manager **3606** may facilitate a connection between the resource provider **3602** and a particular computing device **3604**. In some implementations, the resource manager **3606** may establish a connection between a particular resource provider **3602** and a particular computing device **3604**. In some implementations, the resource manager **3606** may redirect a particular computing device **3604** to a particular resource provider **3602** with the requested computing resource.

FIG. **37** shows an example of a computing device **3700** and a mobile computing device **3750** that can be used to implement the techniques described in this disclosure. The computing device **3700** is intended to represent various forms of digital computers, such as laptops, desktops, workstations, personal digital assistants, servers, blade servers, mainframes, and other appropriate computers. The mobile computing device **3750** is intended to represent various forms of mobile devices, such as personal digital assistants, cellular telephones, smart-phones, and other similar computing devices. The components shown here, their connections and relationships, and their functions, are meant to be examples only, and are not meant to be limiting.

The computing device **3700** includes a processor **3702**, a memory **3704**, a storage device **3706**, a high-speed interface **3708** connecting to the memory **3704** and multiple high-speed expansion ports **3710**, and a low-speed interface **3712** connecting to a low-speed expansion port **3714** and the storage device **3706**. Each of the processor **3702**, the memory **3704**, the storage device **3706**, the high-speed interface **3708**, the high-speed expansion ports **3710**, and the low-speed interface **3712**, are interconnected using various busses, and may be mounted on a common motherboard or in other manners as appropriate. The processor **3702** can process instructions for execution within the computing device **3700**, including instructions stored in the memory **3704** or on the storage device **3706** to display graphical information for a GUI on an external input/output device, such as a display **3716** coupled to the high-speed interface **3708**. In other implementations, multiple processors and/or multiple buses may be used, as appropriate, along with multiple memories and types of memory. Also, multiple computing devices may be connected, with each device providing portions of the necessary operations (e.g., as a server bank, a group of blade servers, or a multi-processor system). Thus, as the term is used herein, where a plurality of functions are described as being performed by "a processor", this encompasses embodiments wherein the plurality of functions are performed by any number of processors (one or more) of any number of computing devices (one or more). Furthermore, where a function is described as being performed by "a processor", this encompasses embodiments wherein the function is performed by any number of processors (one or more) of any number of computing devices (one or more) (e.g., in a distributed computing system).

The memory **3704** stores information within the computing device **3700**. In some implementations, the memory **3704** is a volatile memory unit or units. In some implementations, the memory **3704** is a non-volatile memory unit or units. The memory **3704** may also be another form of computer-readable medium, such as a magnetic or optical disk.

The storage device **3706** is capable of providing mass storage for the computing device **3700**. In some implementations, the storage device **3706** may be or contain a computer-readable medium, such as a floppy disk device, a hard disk device, an optical disk device, or a tape device, a flash memory or other similar solid state memory device, or an array of devices, including devices in a storage area network or other configurations. Instructions can be stored in an information carrier. The instructions, when executed by one or more processing devices (for example, processor **3702**), perform one or more methods, such as those described above. The instructions can also be stored by one or more storage devices such as computer- or machine-readable mediums (for example, the memory **3704**, the storage device **3706**, or memory on the processor **3702**).

The high-speed interface **3708** manages bandwidth-intensive operations for the computing device **3700**, while the low-speed interface **3712** manages lower bandwidth-intensive operations. Such allocation of functions is an example only. In some implementations, the high-speed interface **3708** is coupled to the memory **3704**, the display **3716** (e.g., through a graphics processor or accelerator), and to the high-speed expansion ports **3710**, which may accept various expansion cards (not shown). In the implementation, the low-speed interface **3712** is coupled to the storage device **3706** and the low-speed expansion port **3714**. The low-speed expansion port **3714**, which may include various communication ports (e.g., USB, Bluetooth®, Ethernet, wireless Ethernet) may be coupled to one or more input/output devices, such as a keyboard, a pointing device, a scanner, or a networking device such as a switch or router, e.g., through a network adapter.

The computing device **3700** may be implemented in a number of different forms, as shown in the figure. For example, it may be implemented as a standard server **3720**, or multiple times in a group of such servers. In addition, it may be implemented in a personal computer such as a laptop computer **3722**. It may also be implemented as part of a rack server system **3724**. Alternatively, components from the computing device **3700** may be combined with other components in a mobile device (not shown), such as a mobile computing device **3750**. Each of such devices may contain one or more of the computing device **3700** and the mobile computing device **3750**, and an entire system may be made up of multiple computing devices communicating with each other.

The mobile computing device **3750** includes a processor **3752**, a memory **3764**, an input/output device such as a display **3754**, a communication interface **3766**, and a transceiver **3768**, among other components. The mobile computing device **3750** may also be provided with a storage device, such as a micro-drive or other device, to provide additional storage. Each of the processor **3752**, the memory **3764**, the

display **3754**, the communication interface **3766**, and the transceiver **3768**, are interconnected using various buses, and several of the components may be mounted on a common motherboard or in other manners as appropriate.

The processor **3752** can execute instructions within the mobile computing device **3750**, including instructions stored in the memory **3764**. The processor **3752** may be implemented as a chipset of chips that include separate and multiple analog and digital processors. The processor **3752** may provide, for example, for coordination of the other components of the mobile computing device **3750**, such as control of user interfaces, applications run by the mobile computing device **3750**, and wireless communication by the mobile computing device **3750**.

The processor **3752** may communicate with a user through a control interface **3758** and a display interface **3756** coupled to the display **3754**. The display **3754** may be, for example, a TFT (Thin-Film-Transistor Liquid Crystal Display) display or an OLED (Organic Light Emitting Diode) display, or other appropriate display technology. The display interface **3756** may comprise appropriate circuitry for driving the display **3754** to present graphical and other information to a user. The control interface **3758** may receive commands from a user and convert them for submission to the processor **3752**. In addition, an external interface **3762** may provide communication with the processor **3752**, so as to enable near area communication of the mobile computing device **3750** with other devices. The external interface **3762** may provide, for example, for wired communication in some implementations, or for wireless communication in other implementations, and multiple interfaces may also be used.

The memory **3764** stores information within the mobile computing device **3750**. The memory **3764** can be implemented as one or more of a computer-readable medium or media, a volatile memory unit or units, or a non-volatile memory unit or units. An expansion memory **3774** may also be provided and connected to the mobile computing device **3750** through an expansion interface **3772**, which may include, for example, a SIMM (Single In Line Memory Module) card interface. The expansion memory **3774** may provide extra storage space for the mobile computing device **3750**, or may also store applications or other information for the mobile computing device **3750**. Specifically, the expansion memory **3774** may include instructions to carry out or supplement the processes described above, and may include secure information also. Thus, for example, the expansion memory **3774** may be provide as a security module for the mobile computing device **3750**, and may be programmed with instructions that permit secure use of the mobile computing device **3750**. In addition, secure applications may be provided via the SIMM cards, along with additional information, such as placing identifying information on the SIMM card in a non-hackable manner.

The memory may include, for example, flash memory and/or NVRAM memory (non-volatile random access memory), as discussed below. In some implementations, instructions are stored in an information carrier. that the instructions, when executed by one or more processing devices (for example, processor **3752**), perform one or more methods, such as those described above. The instructions can also be stored by one or more storage devices, such as one or more computer- or machine-readable mediums (for example, the memory **3764**, the expansion memory **3774**, or memory on the processor **3752**). In some implementations, the instructions can be received in a propagated signal, for example, over the transceiver **3768** or the external interface **3762**.

The mobile computing device **3750** may communicate wirelessly through the communication interface **3766**, which may include digital signal processing circuitry where necessary. The communication interface **3766** may provide for communications under various modes or protocols, such as GSM voice calls (Global System for Mobile communications), SMS (Short Message Service), EMS (Enhanced Messaging Service), or MMS messaging (Multimedia Messaging Service), CDMA (code division multiple access), TDMA (time division multiple access), PDC (Personal Digital Cellular), WCDMA (Wideband Code Division Multiple Access), CDMA2000, or GPRS (General Packet Radio Service), among others. Such communication may occur, for example, through the transceiver **3768** using a radio-frequency. In addition, short-range communication may occur, such as using a Bluetooth®, Wi-Fi™, or other such transceiver (not shown). In addition, a GPS (Global Positioning System) receiver module **3770** may provide additional navigation- and location-related wireless data to the mobile computing device **3750**, which may be used as appropriate by applications running on the mobile computing device **3750**.

The mobile computing device **3750** may also communicate audibly using an audio codec **3760**, which may receive spoken information from a user and convert it to usable digital information. The audio codec **3760** may likewise generate audible sound for a user, such as through a speaker, e.g., in a handset of the mobile computing device **3750**. Such sound may include sound from voice telephone calls, may include recorded sound (e.g., voice messages, music files, etc.) and may also include sound generated by applications operating on the mobile computing device **3750**.

The mobile computing device **3750** may be implemented in a number of different forms, as shown in the figure. For example, it may be implemented as a cellular telephone **3780**. It may also be implemented as part of a smart-phone **3782**, personal digital assistant, or other similar mobile device.

Various implementations of the systems and techniques described here can be realized in digital electronic circuitry, integrated circuitry, specially designed ASICs (application specific integrated circuits), computer hardware, firmware, software, and/or combinations thereof. These various implementations can include implementation in one or more computer programs that are executable and/or interpretable on a programmable system including at least one programmable processor, which may be special or general purpose, coupled to receive data and instructions from, and to transmit data and instructions to, a storage system, at least one input device, and at least one output device.

These computer programs (also known as programs, software, software applications or code) include machine instructions for a programmable processor, and can be implemented in a high-level procedural and/or object-oriented programming language, and/or in assembly/machine language. As used herein, the terms machine-readable medium and computer-readable medium refer to any computer program product, apparatus and/or device (e.g., magnetic discs, optical disks, memory, Programmable Logic Devices (PLDs)) used to provide machine instructions and/or data to a programmable processor, including a machine-readable medium that receives machine instructions as a machine-readable signal. The term machine-readable signal refers to any signal used to provide machine instructions and/or data to a programmable processor.

To provide for interaction with a user, the systems and techniques described here can be implemented on a com-

puter having a display device (e.g., a CRT (cathode ray tube) or LCD (liquid crystal display) monitor) for displaying information to the user and a keyboard and a pointing device (e.g., a mouse or a trackball) by which the user can provide input to the computer. Other kinds of devices can be used to provide for interaction with a user as well; for example, feedback provided to the user can be any form of sensory feedback (e.g., visual feedback, auditory feedback, or tactile feedback); and input from the user can be received in any form, including acoustic, speech, or tactile input.

The systems and techniques described here can be implemented in a computing system that includes a back end component (e.g., as a data server), or that includes a middleware component (e.g., an application server), or that includes a front end component (e.g., a client computer having a graphical user interface or a Web browser through which a user can interact with an implementation of the systems and techniques described here), or any combination of such back end, middleware, or front end components. The components of the system can be interconnected by any form or medium of digital data communication (e.g., a communication network). Examples of communication networks include a local area network (LAN), a wide area network (WAN), and the Internet.

The computing system can include clients and servers. A client and server are generally remote from each other and typically interact through a communication network. The relationship of client and server arises by virtue of computer programs running on the respective computers and having a client-server relationship to each other.

In some implementations, the various modules described herein can be separated, combined or incorporated into single or combined modules. The modules depicted in the figures are not intended to limit the systems described herein to the software architectures shown therein.

Elements of different implementations described herein may be combined to form other implementations not specifically set forth above. Elements may be left out of the processes, computer programs, databases, etc. described herein without adversely affecting their operation. In addition, the logic flows depicted in the figures do not require the particular order shown, or sequential order, to achieve desirable results. Various separate elements may be combined into one or more individual elements to perform the functions described herein.

Throughout the description, where apparatus and systems are described as having, including, or comprising specific components, or where processes and methods are described as having, including, or comprising specific steps, it is contemplated that, additionally, there are apparatus, and systems of the present invention that consist essentially of, or consist of, the recited components, and that there are processes and methods according to the present invention that consist essentially of, or consist of, the recited processing steps.

It should be understood that the order of steps or order for performing certain action is immaterial so long as the invention remains operable. Moreover, two or more steps or actions may be conducted simultaneously.

While the invention has been particularly shown and described with reference to specific preferred embodiments, it should be understood by those skilled in the art that various changes in form and detail may be made therein without departing from the spirit and scope of the invention as defined by the appended claims.

What is claimed is:

1. A method for automatically processing 3D images to identify 3D volumes within the 3D images that correspond to a prostate of a subject and determining one or more uptake metrics indicative of radiopharmaceutical uptake therein, the method comprising:

(a) receiving, by a processor of a computing device, a 3D anatomical image of the subject obtained using an anatomical imaging modality, wherein the 3D anatomical image comprises a graphical representation of tissue within a subject, at least a portion of which corresponds to a pelvic region of the subject;

(b) receiving, by the processor, a 3D functional image of the subject obtained using a functional imaging modality, wherein the 3D functional image comprises a plurality of voxels, each representing a particular physical volume within the subject and having an intensity value that represents detected radiation emitted from the particular physical volume, wherein at least a portion of the plurality of voxels of the 3D functional image represent physical volumes within the pelvic region of the subject;

(c) determining, by the processor, using a first module, an initial volume of interest (VOI) within the 3D anatomical image, the initial VOI corresponding to tissue within the pelvic region of the subject and excluding tissue outside the pelvic region of the subject;

(d) identifying, by the processor, using a second module, a prostate volume within the initial VOI corresponding to the prostate of the subject; and

(e) determining, by the processor, the one or more uptake metrics using the 3D functional image and the prostate volume identified within the initial VOI of the 3D anatomical image, and

wherein the method comprises:

identifying, by the processor, a reference volume within the 3D anatomical image, the reference volume corresponding to a reference tissue region within the subject; and

at step (e), determining at least one of the one or more uptake metrics using the 3D functional image and the reference volume identified within the 3D anatomical image.

2. The method of claim **1**, wherein the at least one of the one or more uptake metrics determined using the 3D functional image and the reference volume comprises a tumor to background ratio (TBR) value, and wherein determining the TBR value comprises:

determining a target intensity value using intensity values of one or more voxels of the 3D functional image that correspond to the prostate volume identified within the initial VOI of the 3D anatomical image;

determining a background intensity value using intensity values of one or more voxels of the 3D functional image that correspond to the reference volume identified within the 3D anatomical image; and

determining, as the TBR value, a ratio of the target intensity value to the background intensity value.

3. The method of claim **2**, comprising determining a prostate cancer status for the subject based on the TBR value in comparison with one or more threshold values.

4. The method of claim **3**, wherein the one or more threshold values are determined using a plurality of reference TBR values, each reference TBR value associated with a particular classification prostate cancer status.

5. The method of claim 3, wherein the one or more threshold values are determined using a receiver operating characteristic (ROC) curve.

6. The method of claim 3, comprising determining the prostate cancer status for the subject to be (i) clinically significant if the TBR value is above a cutoff threshold or (ii) clinically non-significant if the TBR value is below the cutoff threshold.

7. The method of claim 1, the method comprising:

identifying, by the processor, a bladder volume within the 3D anatomical image corresponding to a bladder of the subject; and

at step (e), correcting for cross-talk from the bladder using intensities of voxels of the 3D functional image corresponding to the identified bladder volume within the 3D anatomical image.

8. The method of claim 7, wherein correcting for cross-talk from the bladder comprises:

determining one or more bladder intensity bleed functions that model a contribution of intensity originating from radiopharmaceutical within the bladder of the subject to intensity of one or more voxels of the 3D functional image corresponding to one or more regions of the 3D anatomical image that are outside of the identified bladder volume, wherein the one or more bladder intensity bleed functions model said contribution as a function of distance from the identified bladder volume; and

for each of one or more voxels of the 3D functional image corresponding to the identified prostate volume within the 3D anatomical image, adjusting an intensity of the voxel for bladder cross-talk using the one or more bladder intensity bleed functions.

9. The method of claim 1, comprising:

identifying, by the processor, a bladder volume within the 3D anatomical image corresponding to a bladder of the subject;

determining, by the processor, a dilated bladder volume by applying a morphological dilation operation to the identified bladder volume; and

at step (e), determining the one or more uptake metrics using intensity values of voxels of the 3D functional image that (i) correspond to the prostate volume identified within the VOI of the 3D anatomical image, but (ii) do not correspond to regions of the 3D anatomical image within the dilated bladder volume.

10. The method of claim 1, wherein the 3D functional image is a nuclear medicine image of the subject following administration to the subject of the radiopharmaceutical.

11. The method of claim 10, wherein the radiopharmaceutical comprises a PSMA binding agent.

12. The method of claim 10, wherein the nuclear medicine image is a single-photon emission computerized tomography (SPECT) scan of the subject obtained following administration to the subject of the radiopharmaceutical.

13. The method of claim 10, wherein the radiopharmaceutical comprises ^{99m}Tc-MIP-1404.

14. The method of claim 1, the method comprising:

causing, by the processor, display of an interactive graphical user interface (GUI) for presentation to the user of a visual representation of the 3D anatomical image and/or the 3D functional image; and

(g) causing, by the processor, graphical rendering of, within the GUI, the 3D anatomical image and/or the 3D functional image as selectable and superimposable layers, such that either can be selected for display and rendered separately, or both selected for display and rendered together by overlaying the 3D anatomical image with the 3D functional image.

15. The method of claim 14, comprising causing display of, within the GUI, text and/or graphics representing the one or more uptake metrics determined in step (e) along with a quality control graphical widget for guiding the user through a quality control and reporting workflow for review and/or updating of the one or more uptake metrics.

16. The method of claim 15, comprising:

receiving, via the quality control graphical widget, a user input corresponding to an approval of automated determination of the one or more uptake metrics; and

responsive to the receipt of the user input corresponding to the approval of the automated determination of the one or more uptake metrics, generating, by the processor, a report for the subject comprising a representation of the one or more automatically determined uptake metrics.

17. The method of claim 15, comprising:

receiving, via the quality control graphical widget, a user input corresponding to disapproval of automated determination of the one or more uptake metrics;

responsive to receipt of the user input corresponding to the disapproval of the automated determination of the one or more uptake metrics, causing, by the processor, display of a voxel selection graphical element for user selection of one or more voxels of the 3D functional image for use in determining updated values of the one or more uptake metrics;

receiving, via the voxel selection graphical element, the user selection of one or more voxels of the 3D functional image for use in determining updated values of the one or more uptake metrics;

updating, by the processor, values of the one or more uptake metrics using the user selected voxels; and

generating, by the processor, a report for the subject comprising a representation of the one or more updated uptake metrics.

18. The method of claim 15, comprising:

receiving, via the quality control graphical widget, a user input corresponding to disapproval of automated determination of the one or more uptake metrics;

receiving, via the quality control graphical widget, a user input corresponding to a rejection of quality control; and

generating, by the processor, a report for the subject, wherein the report comprises an identification of the rejection of quality control.

19. The method of claim 14, wherein step (g) comprises causing graphical rendering of a selectable and superimposable segmentation layer comprising one or more identified specific tissue volumes within the 3D anatomical image, wherein upon selection of the segmentation layer for display, graphics representing the one or more specific tissue volumes are overlaid on the 3D anatomical image and/or the 3D functional image.

20. The method of claim 19, wherein the one or more specific tissue volumes comprise(s) the identified prostate volume.

21. The method of claim 14, the method comprising, at step (g), causing rendering of a 2D cross sectional view of the 3D anatomical image and/or the 3D functional image within an interactive 2D viewer, such that a position of the 2D cross sectional view is adjustable by the user.

22. The method of claim 14 the method comprising, at step (g), causing rendering of an interactive 3D view of the 3D anatomical image and/or the 3D functional image.

23. The method of claim 14, comprising causing display of, within the GUI, a graphical element indicating a location corresponding to a voxel of the identified prostate volume, thereby facilitating user review and/or quality control of the method.

24. The method of claim 1, wherein the first module receives the 3D anatomical image as input and outputs a plurality of coordinate values representing opposite corners of a rectangular volume within the 3D anatomical image.

25. The method of claim 1, wherein step (c) comprises determining, using the first module, a 3D pelvic bone mask that identifies a volume of the 3D anatomical image corresponding to pelvic bones of the subject.

26. The method of claim 1, wherein the first module is a Convolutional Neural Network (CNN) module.

27. The method of claim 1, wherein step (d) comprises using the second module to identify one or more additional tissue volumes within the 3D anatomical image, each volume corresponding to a specific tissue region within the subject, wherein the one or more additional tissue volumes correspond(s) to one or more specific tissue regions selected from the group consisting of:

a pelvic bone of the subject;

a bladder of the subject;

a rectum of the subject; and

a gluteal muscle of the subject.

28. The method of claim 27, wherein step (d) comprises using the second module to identify a set of one or more base tissue volumes, the one or more base tissue volumes comprising the identified prostate volume and the one or more additional tissue volumes, and wherein the method further comprises:

identifying, by the processor, using one or more auxiliary modules, one or more auxiliary tissue volumes within the 3D anatomical image, each auxiliary tissue volume corresponding to a base tissue volume identified by the second module; and

merging, by the processor, each auxiliary tissue volume with the corresponding base tissue volume identified by the second module.

29. The method of claim 1, wherein step (d) comprises using the second module to classify each voxel within the initial VOI as corresponding a particular tissue region of a set of different tissue regions within the subject.

30. The method of claim 29, wherein classifying each voxel within the initial VOI comprises:

determining, via the second module, for each of a plurality of voxels within the initial VOI, a set of likelihood values, wherein the set of likelihood values comprises, for each of one or more tissue regions of the tissue region set, a corresponding likelihood value that represents a likelihood that the voxel represents a physical volume within the tissue region; and

for each of the plurality of voxels within the initial VOI, classifying the voxel as corresponding to the particular tissue region based on the set of likelihood values determined for the voxel.

31. The method of claim 29, wherein the second module receives as input the initial VOI and outputs a plurality of values comprising, for each voxel within the initial VOI, at least one of (i), (ii), and (iii) as follows:

a value classifying the voxel;

(ii) a set of likelihood values for the voxel; and

(iii) a value identifying the voxel as not corresponding to any of a predetermined set of different tissue regions.

32. The method of claim 29, wherein the set of different tissue regions comprises one or more tissue regions selected from the group consisting of:

the prostate of the subject;

a pelvic bone of the subject;

a bladder of the subject;

a rectum of the subject; and

a gluteal muscle f the subject.

33. The method of claim 1, the method comprising determining, based on at least a portion of the one or more uptake metrics, one or more diagnostic or prognostic values for the subject.

34. The method of claim 33, wherein determining at least one of the one or more diagnostic or prognostic values comprises comparing an uptake metric to one or more threshold value(s).

35. The method of claim 33, wherein at least one of the one or more diagnostic or prognostic values estimates a risk for clinically significant prostate cancer in the subject.

36. The method of claim 1, wherein voxels of the 3D functional image are related to voxels of the 3D anatomical image via a known relationship.

37. The method of claim 1, wherein the first module is a first CNN (convolutional neural network) module and the second module is a second CNN module, wherein the second CNN module comprises a greater number of convolutional filters than the first CNN module.

38. The method of claim 1, comprising performing steps (a) and (c) for each of a plurality of 3D anatomical images to determine a plurality of initial VOIs, each within one of the plurality of 3D anatomical images, wherein a variability in sizes of the initial VOIs is less than a variability in sizes of the 3D anatomical images.

39. A system for automatically processing 3D images to identify 3D volumes within the 3D images that correspond to a prostate of a subject and determining one or more uptake metrics indicative of radiopharmaceutical uptake therein, the system comprising:

a processor; and

a memory having instructions stored thereon, wherein the instructions, when executed by the processor, cause the processor to:

(a) receive a 3D anatomical image of the subject obtained using an anatomical imaging modality, wherein the 3D anatomical image comprises a graphical representation of tissue within a subject, at least a portion of which corresponds to a pelvic region of the subject;

(b) receive a 3D functional image of the subject obtained using a functional imaging modality, wherein the 3D functional image comprises a plurality of voxels, each representing a particular physical volume within the subject and having an intensity value that represents detected radiation emitted from the particular physical volume, wherein at least a portion of the plurality of voxels of the 3D functional image represent physical volumes within the pelvic region of the subject;

(c) determine, using a first module, an initial volume of interest (VOI) within the 3D anatomical image, the initial VOI corresponding to tissue within the pelvic region of the subject and excluding tissue outside the pelvic region of the subject;

(d) identify, using a second module, a prostate volume within the initial VOI corresponding to the prostate of the subject; and

(e) determine the one or more uptake metrics using the 3D functional image and the prostate volume identified within the initial VOI of the 3D anatomical image, and wherein the instructions, when executed by the processor, cause the processor to:

identify a reference volume within the 3D anatomical image, the reference volume corresponding to a reference tissue region within the subject; and

at step (e), determine at least one of the one or more uptake metrics using the 3D functional image and the reference volume identified within the 3D anatomical image.

40. A method for automatically processing 3D images to identify 3D volumes within the 3D images that correspond to a prostate of a subject and determining one or more uptake metrics indicative of radiopharmaceutical uptake therein, the method comprising:

(a) receiving, by a processor of a computing device, a 3D anatomical image of the subject obtained using an anatomical imaging modality, wherein the 3D anatomical image comprises a graphical representation of tissue within a subject, at least a portion of which corresponds to a pelvic region of the subject;

(b) receiving, by the processor, a 3D functional image of the subject obtained using a functional imaging modality, wherein the 3D functional image comprises a plurality of voxels, each representing a particular physical volume within the subject and having an intensity value that represents detected radiation emitted from the particular physical volume, wherein at least a portion of the plurality of voxels of the 3D functional image represent physical volumes within the pelvic region of the subject;

(c) determining, by the processor, using a first module, an initial volume of interest (VOI) within the 3D anatomical image, the initial VOI corresponding to tissue within the pelvic region of the subject and excluding tissue outside the pelvic region of the subject;

(d) identifying, by the processor, using a second module, a prostate volume within the initial VOI corresponding to the prostate of the subject; and

(e) determining, by the processor, the one or more uptake metrics using the 3D functional image and the prostate volume identified within the initial VOI of the 3D anatomical image, and

wherein the method further comprises:

identifying, by the processor, a bladder volume within the 3D anatomical image corresponding to a bladder of the subject; and

at step (e), correcting for cross-talk from the bladder using intensities of voxels of the 3D functional image corresponding to the identified bladder volume within the 3D anatomical image.

41. A method for automatically processing 3D images to identify 3D volumes within the 3D images that correspond to a prostate of a subject and determining one or more uptake metrics indicative of radiopharmaceutical uptake therein, the method comprising:

(a) receiving, by a processor of a computing device, a 3D anatomical image of the subject obtained using an anatomical imaging modality, wherein the 3D anatomical image comprises a graphical representation of tissue within a subject, at least a portion of which corresponds to a pelvic region of the subject;

(b) receiving, by the processor, a 3D functional image of the subject obtained using a functional imaging modality, wherein the 3D functional image comprises a plurality of voxels, each representing a particular physical volume within the subject and having an intensity value that represents detected radiation emitted from the particular physical volume, wherein at least a portion of the plurality of voxels of the 3D functional image represent physical volumes within the pelvic region of the subject;

(c) determining, by the processor, using a first module, an initial volume of interest (VOI) within the 3D anatomical image, the initial VOI corresponding to tissue within the pelvic region of the subject and excluding tissue outside the pelvic region of the subject;

(d) identifying, by the processor, using a second module, a prostate volume within the initial VOI corresponding to the prostate of the subject; and

(e) determining, by the processor, the one or more uptake metrics using the 3D functional image and the prostate volume identified within the initial VOI of the 3D anatomical image, and

wherein the method further comprises:

identifying, by the processor, a bladder volume within the 3D anatomical image corresponding to a bladder of the subject;

determining, by the processor, a dilated bladder volume by applying a morphological dilation operation to the identified bladder volume; and

at step (e), determining the one or more uptake metrics using intensity values of voxels of the 3D functional image that (i) correspond to the prostate volume identified within the VOI of the 3D anatomical image, but (ii) do not correspond to regions of the 3D anatomical image within the dilated bladder volume.

42. A method for automatically processing 3D images to identify 3D volumes within the 3D images that correspond to a prostate of a subject and determining one or more uptake metrics indicative of radiopharmaceutical uptake therein, the method comprising:

(a) receiving, by a processor of a computing device, a 3D anatomical image of the subject obtained using an anatomical imaging modality, wherein the 3D anatomical image comprises a graphical representation of tissue within a subject, at least a portion of which corresponds to a pelvic region of the subject;

(b) receiving, by the processor, a 3D functional image of the subject obtained using a functional imaging modality, wherein the 3D functional image comprises a plurality of voxels, each representing a particular physical volume within the subject and having an intensity value that represents detected radiation emitted from the particular physical volume, wherein at least a portion of the plurality of voxels of the 3D functional image represent physical volumes within the pelvic region of the subject;

(c) determining, by the processor, using a first module, an initial volume of interest (VOI) within the 3D anatomical image, the initial VOI corresponding to tissue within the pelvic region of the subject and excluding tissue outside the pelvic region of the subject;

(d) identifying, by the processor, using a second module, a prostate volume within the initial VOI corresponding to the prostate of the subject;

(e) determining, by the processor, the one or more uptake metrics using the 3D functional image and the prostate volume identified within the initial VOI of the 3D anatomical image;

causing, by the processor, display of an interactive graphical user interface (GUI) for presentation to the user of

a visual representation of the 3D anatomical image and/or the 3D functional image; and

(g) causing, by the processor, graphical rendering of, within the GUI, the 3D anatomical image and/or the 3D functional image as selectable and superimposable layers, such that either can be selected for display and rendered separately, or both selected for display and rendered together by overlaying the 3D anatomical image with the 3D functional image.

43. A method for automatically processing 3D images to identify 3D volumes within the 3D images that correspond to a prostate of a subject and determining one or more uptake metrics indicative of radiopharmaceutical uptake therein, the method comprising:

(a) receiving, by a processor of a computing device, a 3D anatomical image of the subject obtained using an anatomical imaging modality, wherein the 3D anatomical image comprises a graphical representation of tissue within a subject, at least a portion of which corresponds to a pelvic region of the subject;

(b) receiving, by the processor, a 3D functional image of the subject obtained using a functional imaging modality, wherein the 3D functional image comprises a plurality of voxels, each representing a particular physical volume within the subject and having an intensity value that represents detected radiation emitted from the particular physical volume, wherein at least a portion of the plurality of voxels of the 3D functional image represent physical volumes within the pelvic region of the subject;

(c) determining, by the processor, using a first module, an initial volume of interest (VOI) within the 3D anatomical image, the initial VOI corresponding to tissue within the pelvic region of the subject and excluding tissue outside the pelvic region of the subject;

(d) identifying, by the processor, using a second module, a prostate volume within the initial VOI corresponding to the prostate of the subject; and

(e) determining, by the processor, the one or more uptake metrics using the 3D functional image and the prostate volume identified within the initial VOI of the 3D anatomical image;

wherein step (d) comprises using the second module to identify one or more additional tissue volumes within the 3D anatomical image, each volume corresponding to a specific tissue region within the subject, wherein the one or more additional tissue volumes correspond(s) to one or more specific tissue regions selected from the group consisting of:

a pelvic bone of the subject;

a bladder of the subject;

a rectum of the subject; and

a gluteal muscle of the subject; and

wherein the method further comprises:

identifying, by the processor, using one or more auxiliary modules, one or more auxiliary tissue volumes within the 3D anatomical image, each auxiliary tissue volume corresponding to a base tissue volume identified by the second module; and

merging, by the processor, each auxiliary tissue volume with the corresponding base tissue volume identified by the second module.

44. A method for automatically processing 3D images to identify 3D volumes within the 3D images that correspond to a prostate of a subject and determining one or more uptake metrics indicative of radiopharmaceutical uptake therein, the method comprising:

(a) receiving, by a processor of a computing device, a 3D anatomical image of the subject obtained using an anatomical imaging modality, wherein the 3D anatomical image comprises a graphical representation of tissue within a subject, at least a portion of which corresponds to a pelvic region of the subject;

(b) receiving, by the processor, a 3D functional image of the subject obtained using a functional imaging modality, wherein the 3D functional image comprises a plurality of voxels, each representing a particular physical volume within the subject and having an intensity value that represents detected radiation emitted from the particular physical volume, wherein at least a portion of the plurality of voxels of the 3D functional image represent physical volumes within the pelvic region of the subject;

(c) determining, by the processor, using a first module, an initial volume of interest (VOI) within the 3D anatomical image, the initial VOI corresponding to tissue within the pelvic region of the subject and excluding tissue outside the pelvic region of the subject;

(d) identifying, by the processor, using a second module, a prostate volume within the initial VOI corresponding to the prostate of the subject;

(e) determining, by the processor, the one or more uptake metrics using the 3D functional image and the prostate volume identified within the initial VOI of the 3D anatomical image; and

determining, by the processor, based on at least a portion of the one or more uptake metrics, one or more diagnostic or prognostic values for the subject, wherein for at least one of the one or more diagnostic or prognostic values said determining comprises comparing an uptake metric to one or more threshold value(s).

45. A method for automatically processing 3D images to identify 3D volumes within the 3D images that correspond to a prostate of a subject and determining one or more uptake metrics indicative of radiopharmaceutical uptake therein, the method comprising:

(a) receiving, by a processor of a computing device, a 3D anatomical image of the subject obtained using an anatomical imaging modality, wherein the 3D anatomical image comprises a graphical representation of tissue within a subject, at least a portion of which corresponds to a pelvic region of the subject;

(b) receiving, by the processor, a 3D functional image of the subject obtained using a functional imaging modality, wherein the 3D functional image comprises a plurality of voxels, each representing a particular physical volume within the subject and having an intensity value that represents detected radiation emitted from the particular physical volume, wherein at least a portion of the plurality of voxels of the 3D functional image represent physical volumes within the pelvic region of the subject;

(c) determining, by the processor, using a first module, an initial volume of interest (VOI) within the 3D anatomical image, the initial VOI corresponding to tissue within the pelvic region of the subject and excluding tissue outside the pelvic region of the subject;

(d) identifying, by the processor, using a second module, a prostate volume within the initial VOI corresponding to the prostate of the subject;

(e) determining, by the processor, the one or more uptake metrics using the 3D functional image and the prostate volume identified within the initial VOI of the 3D anatomical image; and

determining, by the processor, based on at least a portion of the one or more uptake metrics, one or more diagnostic or prognostic values for the subject, wherein at least one of the one or more diagnostic or prognostic values estimates a risk for clinically significant prostate cancer in the subject.

46. A method for automatically processing 3D images to identify 3D volumes within the 3D images that correspond to a prostate of a subject and determining one or more uptake metrics indicative of radiopharmaceutical uptake therein, the method comprising:

(a) receiving, by a processor of a computing device, a 3D anatomical image of the subject obtained using an anatomical imaging modality, wherein the 3D anatomical image comprises a graphical representation of tissue within a subject, at least a portion of which corresponds to a pelvic region of the subject;

(b) receiving, by the processor, a 3D functional image of the subject obtained using a functional imaging modality, wherein the 3D functional image comprises a plurality of voxels, each representing a particular physical volume within the subject and having an intensity value that represents detected radiation emitted from the particular physical volume, wherein at least a portion of the plurality of voxels of the 3D functional image represent physical volumes within the pelvic region of the subject;

(c) determining, by the processor, using a first module, an initial volume of interest (VOI) within the 3D anatomical image, the initial VOI corresponding to tissue within the pelvic region of the subject and excluding tissue outside the pelvic region of the subject;

(d) identifying, by the processor, using a second module, a prostate volume within the initial VOI corresponding to the prostate of the subject; and

(e) determining, by the processor, the one or more uptake metrics using the 3D functional image and the prostate volume identified within the initial VOI of the 3D anatomical image,

wherein the first module is a first CNN (convolutional neural network) module and the second module is a second CNN module, wherein the second CNN module comprises a greater number of convolutional filters than the first CNN module.

47. A method for automatically processing 3D images to identify 3D volumes within the 3D images that correspond to a prostate of a subject and determining one or more uptake metrics indicative of radiopharmaceutical uptake therein, the method comprising:

(a) receiving, by a processor of a computing device, a 3D anatomical image of the subject obtained using an anatomical imaging modality, wherein the 3D anatomical image comprises a graphical representation of tissue within a subject, at least a portion of which corresponds to a pelvic region of the subject;

(b) receiving, by the processor, a 3D functional image of the subject obtained using a functional imaging modality, wherein the 3D functional image comprises a plurality of voxels, each representing a particular physical volume within the subject and having an intensity value that represents detected radiation emitted from the particular physical volume, wherein at least a portion of the plurality of voxels of the 3D functional image represent physical volumes within the pelvic region of the subject;

(c) determining, by the processor, using a first module, an initial volume of interest (VOI) within the 3D anatomical image, the initial VOI corresponding to tissue within the pelvic region of the subject and excluding tissue outside the pelvic region of the subject;

(d) identifying, by the processor, using a second module, a prostate volume within the initial VOI corresponding to the prostate of the subject; and

(e) determining, by the processor, the one or more uptake metrics using the 3D functional image and the prostate volume identified within the initial VOI of the 3D anatomical image,

wherein the method comprises performing steps (a) and (c) for each of a plurality of 3D anatomical images to determine a plurality of initial VOIs, each within one of the plurality of 3D anatomical images, wherein a variability in sizes of the initial VOIs is less than a variability in sizes of the 3D anatomical images.

48. A system for automatically processing 3D images to identify 3D volumes within the 3D images that correspond to a prostate of a subject and determining one or more uptake metrics indicative of radiopharmaceutical uptake therein, the system comprising:

a processor; and

a memory having instructions stored thereon, wherein the instructions, when executed by the processor, cause the processor to:

(a) receive a 3D anatomical image of the subject obtained using an anatomical imaging modality, wherein the 3D anatomical image comprises a graphical representation of tissue within a subject, at least a portion of which corresponds to a pelvic region of the subject;

(b) receive a 3D functional image of the subject obtained using a functional imaging modality, wherein the 3D functional image comprises a plurality of voxels, each representing a particular physical volume within the subject and having an intensity value that represents detected radiation emitted from the particular physical volume, wherein at least a portion of the plurality of voxels of the 3D functional image represent physical volumes within the pelvic region of the subject;

(c) determine, using a first module, an initial volume of interest (VOI) within the 3D anatomical image, the initial VOI corresponding to tissue within the pelvic region of the subject and excluding tissue outside the pelvic region of the subject;

(d) identify, using a second module, a prostate volume within the initial VOI corresponding to the prostate of the subject; and

(e) determine the one or more uptake metrics using the 3D functional image and the prostate volume identified within the initial VOI of the 3D anatomical image, and

wherein the instructions further cause the processor to:

identify a bladder volume within the 3D anatomical image corresponding to a bladder of the subject; and

at step (e), correct for cross-talk from the bladder using intensities of voxels of the 3D functional image corresponding to the identified bladder volume within the 3D anatomical image.

49. A system for automatically processing 3D images to identify 3D volumes within the 3D images that correspond

to a prostate of a subject and determining one or more uptake metrics indicative of radiopharmaceutical uptake therein, the system comprising:

a processor; and

a memory having instructions stored thereon, wherein the instructions, when executed by the processor, cause the processor to:

(a) receive a 3D anatomical image of the subject obtained using an anatomical imaging modality, wherein the 3D anatomical image comprises a graphical representation of tissue within a subject, at least a portion of which corresponds to a pelvic region of the subject;

(b) receive a 3D functional image of the subject obtained using a functional imaging modality, wherein the 3D functional image comprises a plurality of voxels, each representing a particular physical volume within the subject and having an intensity value that represents detected radiation emitted from the particular physical volume, wherein at least a portion of the plurality of voxels of the 3D functional image represent physical volumes within the pelvic region of the subject;

(c) determine, using a first module, an initial volume of interest (VOI) within the 3D anatomical image, the initial VOI corresponding to tissue within the pelvic region of the subject and excluding tissue outside the pelvic region of the subject;

(d) identify, using a second module, a prostate volume within the initial VOI corresponding to the prostate of the subject; and

(e) determine the one or more uptake metrics using the 3D functional image and the prostate volume identified within the initial VOI of the 3D anatomical image, and

wherein the instructions further cause the processor to:

identify a bladder volume within the 3D anatomical image corresponding to a bladder of the subject;

determine a dilated bladder volume by applying a morphological dilation operation to the identified bladder volume; and

at step (e), determine the one or more uptake metrics using intensity values of voxels of the 3D functional image that (i) correspond to the prostate volume identified within the VOI of the 3D anatomical image, but (ii) do not correspond to regions of the 3D anatomical image within the dilated bladder volume.

50. A system for automatically processing 3D images to identify 3D volumes within the 3D images that correspond to a prostate of a subject and determining one or more uptake metrics indicative of radiopharmaceutical uptake therein, the system comprising:

a processor; and

a memory having instructions stored thereon, wherein the instructions, when executed by the processor, cause the processor to:

(a) receive a 3D anatomical image of the subject obtained using an anatomical imaging modality, wherein the 3D anatomical image comprises a graphical representation of tissue within a subject, at least a portion of which corresponds to a pelvic region of the subject;

(b) receive a 3D functional image of the subject obtained using a functional imaging modality, wherein the 3D functional image comprises a plurality of voxels, each representing a particular physical volume within the subject and having an intensity value that represents detected radiation emitted from the particular physical volume, wherein at least a portion of the plurality of voxels of the 3D functional image represent physical volumes within the pelvic region of the subject;

(c) determine, using a first module, an initial volume of interest (VOI) within the 3D anatomical image, the initial VOI corresponding to tissue within the pelvic region of the subject and excluding tissue outside the pelvic region of the subject;

(d) identify, using a second module, a prostate volume within the initial VOI corresponding to the prostate of the subject;

(e) determine the one or more uptake metrics using the 3D functional image and the prostate volume identified within the initial VOI of the 3D anatomical image;

cause display of an interactive graphical user interface (GUI) for presentation to the user of a visual representation of the 3D anatomical image and/or the 3D functional image; and

(g) cause graphical rendering of, within the GUI, the 3D anatomical image and/or the 3D functional image as selectable and superimposable layers, such that either can be selected for display and rendered separately, or both selected for display and rendered together by overlaying the 3D anatomical image with the 3D functional image.

51. A system for automatically processing 3D images to identify 3D volumes within the 3D images that correspond to a prostate of a subject and determining one or more uptake metrics indicative of radiopharmaceutical uptake therein, the system comprising:

a processor; and

a memory having instructions stored thereon, wherein the instructions, when executed by the processor, cause the processor to:

(a) receive a 3D anatomical image of the subject obtained using an anatomical imaging modality, wherein the 3D anatomical image comprises a graphical representation of tissue within a subject, at least a portion of which corresponds to a pelvic region of the subject;

(b) receive a 3D functional image of the subject obtained using a functional imaging modality, wherein the 3D functional image comprises a plurality of voxels, each representing a particular physical volume within the subject and having an intensity value that represents detected radiation emitted from the particular physical volume, wherein at least a portion of the plurality of voxels of the 3D functional image represent physical volumes within the pelvic region of the subject;

(c) determine, using a first module, an initial volume of interest (VOI) within the 3D anatomical image, the initial VOI corresponding to tissue within the pelvic region of the subject and excluding tissue outside the pelvic region of the subject;

(d) identify, using a second module, a prostate volume within the initial VOI corresponding to the prostate of the subject; and

(e) determine the one or more uptake metrics using the 3D functional image and the prostate volume identified within the initial VOI of the 3D anatomical image;

wherein step (d) comprises using the second module to identify one or more additional tissue volumes

within the 3D anatomical image, each volume corresponding to a specific tissue region within the subject, wherein the one or more additional tissue volumes correspond(s) to one or more specific tissue regions selected from the group consisting of:

a pelvic bone of the subject;

a bladder of the subject;

a rectum of the subject; and

a gluteal muscle of the subject; and

wherein the instructions further cause the processor to:

identify, using one or more auxiliary modules, one or more auxiliary tissue volumes within the 3D anatomical image, each auxiliary tissue volume corresponding to a base tissue volume identified by the second module; and

merge each auxiliary tissue volume with the corresponding base tissue volume identified by the second module.

52. A system for automatically processing 3D images to identify 3D volumes within the 3D images that correspond to a prostate of a subject and determining one or more uptake metrics indicative of radiopharmaceutical uptake therein, the system comprising:

a processor; and

a memory having instructions stored thereon, wherein the instructions, when executed by the processor, cause the processor to:

(a) receive a 3D anatomical image of the subject obtained using an anatomical imaging modality, wherein the 3D anatomical image comprises a graphical representation of tissue within a subject, at least a portion of which corresponds to a pelvic region of the subject;

(b) receive a 3D functional image of the subject obtained using a functional imaging modality, wherein the 3D functional image comprises a plurality of voxels, each representing a particular physical volume within the subject and having an intensity value that represents detected radiation emitted from the particular physical volume, wherein at least a portion of the plurality of voxels of the 3D functional image represent physical volumes within the pelvic region of the subject;

(c) determine, using a first module, an initial volume of interest (VOI) within the 3D anatomical image, the initial VOI corresponding to tissue within the pelvic region of the subject and excluding tissue outside the pelvic region of the subject;

(d) identify, using a second module, a prostate volume within the initial VOI corresponding to the prostate of the subject;

(e) determine the one or more uptake metrics using the 3D functional image and the prostate volume identified within the initial VOI of the 3D anatomical image; and

(f) determine, based on at least a portion of the one or more uptake metrics, one or more diagnostic or prognostic values for the subject, wherein for at least one of the one or more diagnostic or prognostic values said determining comprises comparing an uptake metric to one or more threshold value(s).

53. A system for automatically processing 3D images to identify 3D volumes within the 3D images that correspond to a prostate of a subject and determining one or more uptake metrics indicative of radiopharmaceutical uptake therein, the system comprising:

a processor; and

a memory having instructions stored thereon, wherein the instructions, when executed by the processor, cause the processor to:

(a) receive a 3D anatomical image of the subject obtained using an anatomical imaging modality, wherein the 3D anatomical image comprises a graphical representation of tissue within a subject, at least a portion of which corresponds to a pelvic region of the subject;

(b) receive a 3D functional image of the subject obtained using a functional imaging modality, wherein the 3D functional image comprises a plurality of voxels, each representing a particular physical volume within the subject and having an intensity value that represents detected radiation emitted from the particular physical volume, wherein at least a portion of the plurality of voxels of the 3D functional image represent physical volumes within the pelvic region of the subject;

(c) determine, using a first module, an initial volume of interest (VOI) within the 3D anatomical image, the initial VOI corresponding to tissue within the pelvic region of the subject and excluding tissue outside the pelvic region of the subject;

(d) identify, using a second module, a prostate volume within the initial VOI corresponding to the prostate of the subject;

(e) determine the one or more uptake metrics using the 3D functional image and the prostate volume identified within the initial VOI of the 3D anatomical image; and

(f) determine, based on at least a portion of the one or more uptake metrics, one or more diagnostic or prognostic values for the subject, wherein at least one of the one or more diagnostic or prognostic values estimates a risk for clinically significant prostate cancer in the subject.

54. A system for automatically processing 3D images to identify 3D volumes within the 3D images that correspond to a prostate of a subject and determining one or more uptake metrics indicative of radiopharmaceutical uptake therein, the system comprising:

a processor; and

a memory having instructions stored thereon, wherein the instructions, when executed by the processor, cause the processor to:

(a) receive a 3D anatomical image of the subject obtained using an anatomical imaging modality, wherein the 3D anatomical image comprises a graphical representation of tissue within a subject, at least a portion of which corresponds to a pelvic region of the subject;

(b) receive a 3D functional image of the subject obtained using a functional imaging modality, wherein the 3D functional image comprises a plurality of voxels, each representing a particular physical volume within the subject and having an intensity value that represents detected radiation emitted from the particular physical volume, wherein at least a portion of the plurality of voxels of the 3D functional image represent physical volumes within the pelvic region of the subject;

(c) determine, using a first module, an initial volume of interest (VOI) within the 3D anatomical image, the initial VOI corresponding to tissue within the pelvic region of the subject and excluding tissue outside the pelvic region of the subject;

(d) identify, using a second module, a prostate volume within the initial VOI corresponding to the prostate of the subject; and

(e) determine the one or more uptake metrics using the 3D functional image and the prostate volume identified within the initial VOI of the 3D anatomical image, wherein the first module is a first CNN (convolutional neural network) module and the second module is a second CNN module, wherein the second CNN module comprises a greater number of convolutional filters than the first CNN module.

55. A system for automatically processing 3D images to identify 3D volumes within the 3D images that correspond to a prostate of a subject and determining one or more uptake metrics indicative of radiopharmaceutical uptake therein, the system comprising:

a processor; and

a memory having instructions stored thereon, wherein the instructions, when executed by the processor, cause the processor to:

(a) receive a 3D anatomical image of the subject obtained using an anatomical imaging modality, wherein the 3D anatomical image comprises a graphical representation of tissue within a subject, at least a portion of which corresponds to a pelvic region of the subject;

(b) receive a 3D functional image of the subject obtained using a functional imaging modality, wherein the 3D functional image comprises a plurality of voxels, each representing a particular physical volume within the subject and having an intensity value that represents detected radiation emitted from the particular physical volume, wherein at least a portion of the plurality of voxels of the 3D functional image represent physical volumes within the pelvic region of the subject;

(c) determine, using a first module, an initial volume of interest (VOI) within the 3D anatomical image, the initial VOI corresponding to tissue within the pelvic region of the subject and excluding tissue outside the pelvic region of the subject;

(d) identify, using a second module, a prostate volume within the initial VOI corresponding to the prostate of the subject; and

(e) determine the one or more uptake metrics using the 3D functional image and the prostate volume identified within the initial VOI of the 3D anatomical image, wherein the instructions cause the processor to perform steps (a) and (c) for each of a plurality of 3D anatomical images to determine a plurality of initial VOIs, each within one of the plurality of 3D anatomical images, wherein a variability in sizes of the initial VOIs is less than a variability in sizes of the 3D anatomical images.

* * * * *

EXHIBIT 3

US011424035B2

(12) **United States Patent**
Baker

(10) **Patent No.: US 11,424,035 B2**
(45) **Date of Patent: *Aug. 23, 2022**

(54) **NETWORK FOR MEDICAL IMAGE ANALYSIS, DECISION SUPPORT SYSTEM, AND RELATED GRAPHICAL USER INTERFACE (GUI) APPLICATIONS**

(71) Applicant: **Progenics Pharmaceuticals, Inc.**, N. Billerica, MA (US)

(72) Inventor: **Mark R. Baker**, New York, NY (US)

(73) Assignee: **Progenics Pharmaceuticals, Inc.**, Massachusetts, MA (US)

(*) Notice: Subject to any disclaimer, the term of this patent is extended or adjusted under 35 U.S.C. 154(b) by 167 days.

This patent is subject to a terminal disclaimer.

(21) Appl. No.: **16/938,488**

(22) Filed: **Jul. 24, 2020**

(65) **Prior Publication Data**

US 2020/0357521 A1 Nov. 12, 2020

Related U.S. Application Data

(63) Continuation of application No. 16/418,527, filed on May 21, 2019, now Pat. No. 10,762,993, which is a (Continued)

(51) **Int. Cl.**
G06K 9/00 (2022.01)
G06Q 10/00 (2012.01)
(Continued)

(52) **U.S. Cl.**
CPC ***G16H 50/20*** (2018.01); ***G01N 33/57434*** (2013.01); ***G16H 15/00*** (2018.01);
(Continued)

(58) **Field of Classification Search**
CPC G06K 9/00; G06Q 10/00
(Continued)

(56) **References Cited**

U.S. PATENT DOCUMENTS

7,450,747 B2 11/2008 Jabri et al.
7,751,605 B2 7/2010 Gündel et al.
(Continued)

FOREIGN PATENT DOCUMENTS

CN 101528267 A 9/2009
CN 102361594 A 2/2012
(Continued)

OTHER PUBLICATIONS

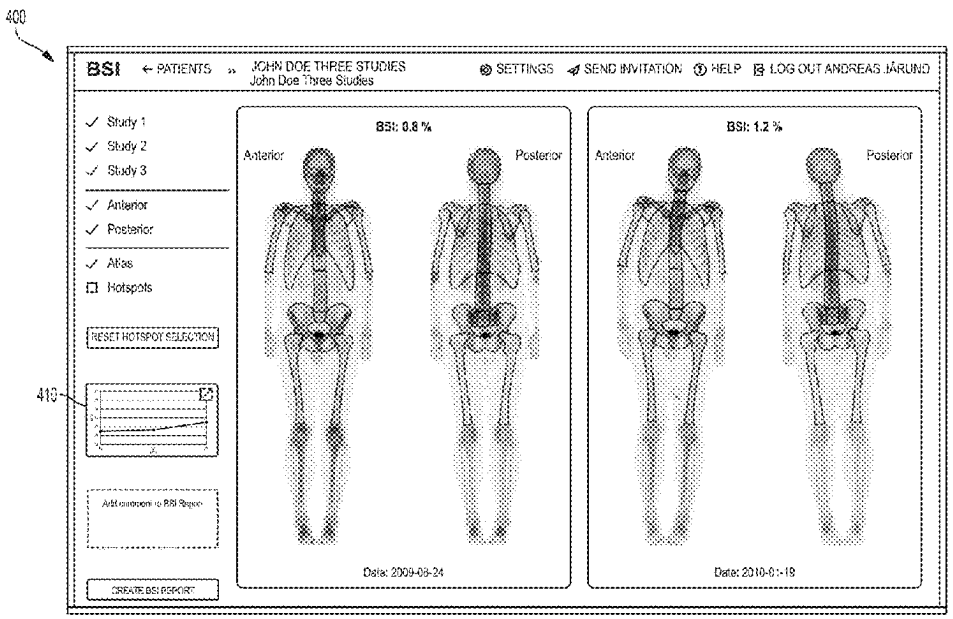
Ali, A. et al., The Automated Bone Scan Index as a Predictor of Response to Prostate Radiotherapy in Men with Newly Diagnosed Metastatic Prostate Cancer: An Exploratory Analysis of STAMPEDE's "M1|RT Comparison", European Urology Oncology 3:412-419. (2020).
(Continued)

Primary Examiner — Seyed H Azarian
(74) *Attorney, Agent, or Firm* — Choate, Hall & Stewart LLP; William R. Haulbrook; Ronen Adato

(57) **ABSTRACT**

Described herein is a platform and supported graphical user interface (GUI) decision-making tools for use by medical practitioners and/or their patients, e.g., to aide in the process of making decisions about a course of cancer treatment and/or to track treatment and/or the progress of a disease.

45 Claims, 11 Drawing Sheets



Related U.S. Application Data

continuation of application No. 15/794,220, filed on Oct. 26, 2017, now Pat. No. 10,340,046.

(60) Provisional application No. 62/413,936, filed on Oct. 27, 2016.

(51) **Int. Cl.**

G16H 50/20	(2018.01)
G16H 30/40	(2018.01)
G16H 50/70	(2018.01)
G16H 15/00	(2018.01)
G16H 30/20	(2018.01)
G16H 50/30	(2018.01)
G01N 33/574	(2006.01)

(52) **U.S. Cl.**

CPC ***G16H 30/20*** (2018.01); ***G16H 30/40*** (2018.01); ***G16H 50/30*** (2018.01); ***G16H 50/70*** (2018.01)

(58) **Field of Classification Search**

USPC 382/100, 103, 128–134, 154–158, 162, 382/168, 173, 181, 206, 209, 220, 224, 382/232, 254, 286–295, 305, 312; 705/2; 378/4, 21

See application file for complete search history.

(56) **References Cited**

U.S. PATENT DOCUMENTS

7,935,055	B2	5/2011	Burckhardt	
7,970,194	B2	6/2011	Kimura	
8,199,985	B2	6/2012	Jakobsson et al.	
8,211,401	B2	7/2012	Babich et al.	
8,467,856	B2	6/2013	Renisch et al.	
8,538,166	B2	9/2013	Gordon et al.	
8,705,887	B2	4/2014	Ma et al.	
8,778,305	B2	7/2014	Pomper et al.	
8,855,387	B2	10/2014	Hamadeh et al.	
8,962,799	B2	2/2015	Babich et al.	
9,002,081	B2 *	4/2015	Brown	G06T 7/0014 382/128
9,710,915	B2	7/2017	Firouzian et al.	
9,721,340	B2	8/2017	Gillies et al.	
10,223,610	B1	3/2019	Akselrod-Ballin et al.	
10,311,971	B2	6/2019	Opfer et al.	
10,339,653	B2	7/2019	Gillies et al.	
10,340,044	B2	7/2019	Yao et al.	
10,340,046	B2	7/2019	Baker	
RE47,609	E	9/2019	Hamadeh et al.	
10,600,184	B2	3/2020	Golden et al.	
10,665,346	B2	5/2020	Baker	
10,748,652	B2	8/2020	Yao et al.	
10,762,993	B2	9/2020	Baker	
10,818,386	B2	10/2020	Yao et al.	
10,943,681	B2	3/2021	Yao et al.	
10,973,486	B2	4/2021	Sjostrand et al.	
11,011,257	B2	5/2021	Lints et al.	
2003/0215120	A1	11/2003	Uppaluri et al.	
2005/0281381	A1	12/2005	Guendel	
2006/0062425	A1 *	3/2006	Shen	G06T 15/08 382/100
2006/0064396	A1	3/2006	Wei et al.	
2006/0078183	A1	4/2006	deCharms	
2007/0081712	A1 *	4/2007	Huang	G06T 7/38 382/128
2007/0081713	A1	4/2007	Jerebko	
2007/0100225	A1	5/2007	Maschke	
2007/0115204	A1	5/2007	Budz et al.	
2008/0027315	A1	1/2008	McGinnis	
2009/0309874	A1	12/2009	Salganicoff et al.	
2010/0215581	A1	8/2010	Hoffmann	
2010/0322488	A1	12/2010	Virtue et al.	
2011/0063288	A1	3/2011	Valadez	
2011/0255763	A1	10/2011	Bogoni et al.	
2012/0123253	A1	5/2012	Renisch et al.	
2013/0038707	A1	2/2013	Cunningham et al.	
2013/0129168	A1	5/2013	Ross	
2013/0211231	A1	8/2013	Sundarapandian et al.	
2013/0281841	A1	10/2013	Everett et al.	
2015/0110716	A1	4/2015	Armor	
2015/0331995	A1 *	11/2015	Zhao	G16H 10/60 705/2
2016/0203263	A1 *	7/2016	Maier	G16H 30/40 705/2
2016/0335395	A1 *	11/2016	Wu	G06Q 10/103
2017/0083682	A1	3/2017	McNutt et al.	
2018/0144828	A1	5/2018	Baker	
2018/0259608	A1	9/2018	Golden et al.	
2018/0360402	A1	12/2018	Carmi	
2019/0038239	A1	2/2019	Flohr et al.	
2019/0105009	A1	4/2019	Siemionow et al.	
2019/0209116	A1	7/2019	Sjostrand et al.	
2019/0388049	A1	12/2019	Gupta et al.	
2020/0027559	A1	1/2020	Baker	
2020/0051238	A1	2/2020	El Harouni et al.	
2020/0074634	A1	3/2020	Kecskemethy et al.	
2020/0085382	A1	3/2020	Taerum et al.	
2020/0126666	A1	4/2020	Baker	
2020/0193594	A1	6/2020	Georgescu et al.	
2020/0193603	A1	6/2020	Golden et al.	
2020/0245960	A1	8/2020	Richter et al.	
2020/0337658	A1	10/2020	Sjostrand et al.	
2020/0342600	A1	10/2020	Sjostrand et al.	
2020/0352518	A1	11/2020	Lyman et al.	
2020/0357117	A1	11/2020	Lyman et al.	
2020/0357118	A1	11/2020	Yao et al.	
2021/0082547	A1	3/2021	Yao et al.	
2021/0093249	A1	4/2021	Anand et al.	
2021/0183485	A1	6/2021	Yao et al.	
2021/0233633	A1	7/2021	Lints et al.	
2021/0334974	A1	10/2021	Johnsson et al.	
2021/0335480	A1	10/2021	Johnsson et al.	

FOREIGN PATENT DOCUMENTS

EP	1426903	A2	6/2004
EP	1508872	A1	2/2005
EP	3043318	A1	7/2016
JP	2010-029481	A	2/2010
JP	6013042	B2	10/2016
JP	6170284	B2	7/2017
SE	524500	C2	8/2004
WO	WO-9905503	A2	2/1999
WO	WO-2007/062135	A2	5/2007
WO	WO-2009/084995	A1	7/2009
WO	WO-2011/077303	A1	6/2011
WO	WO-2015/058151	A2	4/2015
WO	WO-2018/081354	A1	5/2018
WO	WO-2019/103912	A2	5/2019
WO	WO-2019/136349	A2	7/2019
WO	WO-2020/144134	A1	7/2020
WO	WO-2020/146032	A1	7/2020
WO	WO-2020/190821	A1	9/2020
WO	WO-2020/219619	A1	10/2020
WO	WO-2020/219620	A1	10/2020
WO	WO-2021/061315	A1	4/2021

OTHER PUBLICATIONS

Ceci, F. et al., E-PSMA: the EANM standardized reporting guidelines v1.0 for PSMA-PET, European Journal of Nuclear Medicine and Molecular Imaging, 48:1626-1638, (2021).

Johnsson, K. et al., Analytical performance of aPROMISE: automated anatomic contextualization, detection, and quantification of [18F]DCFPyL (PSMA) imaging for standardized reporting, European Journal of Nuclear Medicin and Molecular Imaging, 11 pages, Aug. 31, 2021, doi: 10.1007/s00259-021-05497-8. Epub ahead of print. PMID: 34463809.

(56) **References Cited**

OTHER PUBLICATIONS

Matsubara, N. et al, A Phase II, Randomized, Open-Label, Multi-arm Study of TAS-115 for Castration-Resistant Prostate Cancer Patients With Bone Metastases, Clinical Genitourinary Cancer, 000(xxx):1-10, (2021).

Nickols, N. et al., aPROMISE: A Novel Automated-PROMISE platform to Standardize Evaluation of Tumor Burden in 18F-DCFPyL (PSMA) images of Veterans with Prostate Cancer, Journal of Nuclear Medicine, 26 pages, May 28, 2021, doi: 10.2967/jnumed.120.261863.

Paschalis, A. et al., Prostate-specific Membrane Antigen Heterogeneity and DNA Repair Defects in Prostate Cancer, European Urology, 76(4):469-478, (2019).

American College of Radiology (ACR) and the Society for Pediatric Radiology (SPR), ACR-SPR Practice Parameter for ehe Performance of Skeletal Scintigraphy (Bone Scan), Resolution 28, (2013-Revused2017), available from: http://www.acr.org.

Anand, A. et al., A Pre-Analytical Validation Study of Automated Bone Scan Index: Effect on Accuracy and Reproducibility Due to the Procedural Variabilities in Bone Scan Image Acquisition. J Nucl Med. Jul. 21, 2016. [Epub ahead of print].

Anand, A. et al., Analytic Validation of the Automated Bone Scan Index as an Imaging Biomarker to Standardize Quantitative Changes in Bone Scans of Patients with Metastatic Prostate Cancer, J. Nucl. Med., 57(1):41 -45 (2016).

Anand, A. et al., Automated Bone Scan Index as a quantitative imaging biomarker in metastatic castration-resistant prostate cancer patients being treated with enzalutamide, EJNMMI Research, 6:23, 7 pages (2016).

Anand, A. et al., Translating Prostate Cancer Working Group 2 (PCWG2) Progression Criteria into a Quantitative Response Biomarker in Metastatic Castration Resistant Prostate Cancer (mCRPC), ASCO GU Conference, Poster, presented Feb. 16, 2017.

Anand, A. et al., Translating Prostate Cancer Working Group 2 (PCWG2) progression criteria into a quantitative response biomarker in metastatic castration-resistant prostate cancer (mCRPC), Journal of Clinical Oncology, 35(6):170 (2017).

Armstrong, A. et al., Assessment of the bone scan index in a randomized placebo-controlled trial of tasquinimod in men with metastatic castration-resistant prostate cancer (mCRPC), Urologic Oncology: Seminars and Original Investigations, 32:1308-1316 (2014).

Armstrong, A. et al., Development and validation of a prognostic model for overall survival in chemotherapy-naive men with metastatic castration-resistant prostate cancer (mCRPC) from the phase 3 prevail clinical trial, Journal of Clinical Oncology, 35(Suppl. 6):Abstract 138 (2017).

Armstrong, A. J. et al., Phase 3 prognostic analysis of the automated bone scan index (aBSI) in men with bone-metastatic castration-resistant prostate cancer (CRPC), Meeting Library ASC University (2017).

Belal, S. et al., Association of PET Index quantifying skeletal uptake in NaF PET/CT images with overall survival in prostate cancer patients, ASCO GU 2017, Poster 178, presented Feb. 16, 2017.

Belal, S. et al., PET Index quantifying skeletal uptake in NaF PET/CT images with overall survival in prostate cancer patients, ASCO GU 2017, Abstract (Feb. 13, 2017).

Belal, S. L. et al, 3D skeletal uptake of ^{18} F sodium fluoride in PET/CT images is associate with overall survival in patients with prostate cancer, EJNMMI Research, 7(15):1-8 (2017).

Belal, S.L. et al., Automated evaluation of normal uptake in different skeletal parts in 18F-sodium fluoride (NaF) PET/CT using a new convolutional neural network method, EJNMMI, EANM '17, 44(Suppl 2):S119-S956, Abstract EP-0116 (2017).

Bombardieri, E. et al., Bone scintigraphy: procedure guidelines for tumour imaging, Eur J. Nucl. Med. Mol. Imaging, 30:BP99-BP106, (2003).

Bushberg, J. T. et al., Essential Physics of Medical Imaging, Essential Physics of Medical Imaging, 19.3: p. 581 (table 15-3), p. 713 paragraph 6, section 19.3 and p. 720, (2011).

Cha, K. H., et al. Urinary bladder segmentation in CT urography using deep-learning convolutional neural network and level sets, Medical physics, 43(4):1882-1896, (2016).

Ciernik, I. F., et al. 3D-segmentation of the 18F-choline PET signal for target volume definition in radiation therapy of the prostate, Technology in cancer research & treatment 6(1):23-30, (2007).

Dennis, E. et al., Bone Scan Index: A Quantitative Treatment Response Biomarker for Castration-Resistant Metastatic Prostate Cancer, Journal of Clinical Oncology, 30(5):519-524 (2012).

Eiber, M. et al., Prostate Cancer Molecular Imaging Standardized Evaluation (PROMISE): Proposed miTNM Classification for the Interpretation of PSMA-Ligand PET/CT, The Journal of Nuclear Medicine, 59(3):469-478, (2018).

GE Healthcare, SPECT/CT Cameras, retrieved Oct. 25, 2017: <http://www3.gehealthcare.com.sg/en-gb/products/categories/nuclear_medicine/spect-ct_cameras>.

Giesel, F. L. et al., F-18 labelled PSMA-1007: biodistribution, radiation dosimetry and histopathological validation of tumor lesions in prostate cancer patients, Eur. J. Nucl. Med. Mol. Imaging, 44:678-688 (2017).

Gjertsson, K., Segmentation in Skeletal Scintigraphy Images using Convolutional Neural Networks, Master's Theses in Mathematical Sciences, pp. 39-58, (2017), <https://lup.lub.lu.se/student-papers/search/publication/8916406>.

Goffin, K. E. et al., Phase 2 study of ^{99m}Tc-trofolastat SPECT/CT to identify and localize prostate cancer in intermediate- and high-risk patients undergoing radical prostatectomy and extended pelvic lymph node dissection, J. Nucl. Med., 27 pages (2017).

Guimond, A. et al., Average Brain Models: A Convergence Study, Computer Vision and Image Understanding, 77:192-210 (2000).

Hajnal, J. et al., 4.4 Intensity, Size, and Skew Correction; 7.1 Introduction; 7.2 Methods; 7.3 Image Interpretation—General, In: Medical Image Registration, CRC Press LLC, 80-81:144-148 (2001).

Hiller, S. M. et al., 99mTc-Labeled Small-Molecule Inhibitors of Prostate-Specific Membrane Antigen for Molecular Imaging of Prostate Cancer, Journal of Nuclear Medicine, 54(8):1369-1376 (2013) retrieved Oct. 25, 2017: <http://jnm.snmjournals.org/content/54/8/1369.full>.

Horikoshi, H. et al., Computer-aided diagnosis system for bone scintigrams from Japanese patients: importance of training database, Annals of Nuclear Medicine, 26(8):622-626 (2012).

Huang, J.-H. et al., A Set of Image Processing Algorithms for Computer-Aided Diagnosis in Nuclear Medicine Whole Body Bone Scan Images, IEEE Transactions on Nuclear Science, 54(3):514-522 (2007).

International Search Report, International Application No. PCT/US2017/058418 (Network for Medical Image Analysis, Decision Support System, and Related Graphical User Interface (GUI) Applications, filed Oct. 26, 2017), issued by ISA/European Patent Office, 4 pages, dated Feb. 27, 2018.

Kaboteh R. et al., Progression of bone metastases in patients with prostate cancer—automated detection of new lesions and calculation of bone scan index, EJNMMI Research, 3:64 (2013).

Kaboteh, R. et al., Convolutional neural network based quantification of choline uptake in PET/CT studies is associated with overall survival in patents with prostate cancer, EJNMMI, EANM '17, 44(Suppl 2):S119-S956, Abstract EP-0642 (2017).

Keiss, et al., Prostate-specific membrane antigen and a target for cancer imaging and therapy, The Quarterly Journal of Nuclear Medicine and Molecular Imaging, 59(3):241-268 (2015).

Kikuchi, A. et al., Automated segmentation of the skeleton in whole-body bone scans: influence of difference in atlas, Nuclear Medicine Communications, 33(9):947-953 (2012).

Kinahan, P.E. et al., PET/CT Standardized Update Values (SUVs) in Clinical Practice and Assessing Response to Therapy, Semin Ultrasound CT MR 31(6):496-505 (2010) retrieved Oct. 25, 2017: <https://www.ncbi.nlm.nih.gov/pmc/articles/PMC3026294/>.

Knutsson, H., and Andersson, M., Morphons: Segmentation using Elastic Canvas and Paint on Priors, IEEE International Conference on Image Processing (ICIP 2005), Genova, Italy, 4 pages (2005).

Kopka, K. et al., Glu-Ureido-Based Inhibitors of Prostate-Specific Membrane Antigen: Lessons Learned During the Development of a

(56) **References Cited**

OTHER PUBLICATIONS

Novel Class of Low-Molecular-Weight Theranostic Radiotracers, The Journal of Nuclear Medicine, 58(9)(Suppl. 2):17S-26S, (2017).
Litjens, G. et al., A survey on deep learning in medical image analysis, Medical Image Analysis, 42:60-88, (2017).
Liu, L. et al., Computer-Aided Detection of Prostate Cancer with MRI: Technology and Applications, Acad Radiol. Author manuscript, 50 pages 2016.
Ma, L. et al., Automatic segmentation of the prostate on CT images using deep learning and multi-atlas fusion, Proc. of SPIE vol. 10133:1013320-1-101332O-9 (2017).
Ma, L. et al., Combining Population and Patient-Specific Characteristics for Prostate Segmentation on 3D CT Images, Proc of SPIE 9784:978427-1-8 (2016).
Ma, L. et al., Random Walk Based Segmentation for the Prostate on 3D Transrectal Ultrasound Images, Proc SPIE Int Soc Opt Eng. Author manuscript, 13 pages (2016).
Mayo Clinic Staff, Choline C-11 PET scan, Overview, Mayo Clinic, 4 pages (2017), retrieved Oct. 25, 2017: <https://www.mayoclinic.org/tests-procedures/choline-c-11-pet-scan/home/ovc-20156994>.
Nakajima, K. et al., Enhanced diagnostic accuracy for quantitative bone scan using an artificial neural network system: a Japanese multi-center database project, EJNMMI Research, 3:83 (2013).
National Cancer Institute, NCI Drug Dictionary: gallium Ga 68-labeled PSMA-11, retrieved Oct. 25, 2017: <https://www.cancer.gov/publications/dictionaries/cancer-drug?cdrid=766400>.
National Cancer Institute, NCI Drug Dictionary: technetium Tc 99m methylene diphosphonate, retrieved Oct. 25, 2017: <https://www.cancer.gov/publications/dictionaries/cancer-drug?cdrid=537722>.
Ohlsson, M., et al., Automated decision support for bone scintigraphy, Computer-based medical systems, pp. 1-6, (2009).
Perera, M. et al., Sensitivity, Specificity, and Predictors of Positive 68Ga-Prostate-specific Membrane Antigen Positron Emission Tomography in Advanced Prostate Cancer: A Systematic Review and Meta-analysis, Europeain Urology, 70(6):926-937 (2016).
Polymeri, E. et al., Analytical validation of an automated method for segmentation of the prostate gland in CT images, EJNMMI, EANM '17, 44(Suppl 2):S119-S956, Abstract EP-0641 (2017).
radiologyinfo.org for Patients, Computed Tomography (CT), retrieved Oct. 25, 2017: <https://www.radiologyinfo.org/en/submenu.cfm?pg=ctscan>.
Rowe, S. P. et al., PET Imaging of prostate-specific membrane antigen in prostate cancer: current state of the art and future challenges, Prostate Cancer and Prostatic Diseases, 1 -8 (2016).
Rowe, S. P. et al., PSMA-Based [^{18}F]DCFPyL PET/CT Is Superior to Conventional Imaging for Lesion Detection in Patients with Metastatic Prostate Cancer, Mol Imaging Biol, 18:411-419, (2016).
Sabbatini, P. et al., Prognostic Significance of Extent of Disease in Bone in Patients With Androgen-Independent Prostate Cancer, Journal of Clinical Oncology, 17(3):948-957 (1999).
Sadik, M. et al., 3D prostate gland uptake of 18F-choline—association with overall survival in patients with hormone-naïve prostate cancer, The Journal of Nuclear Medicine, 58(Suppl. 1):Abstract 544 (2017).
Sadik, M. et al., A new computer-based decision-support system for the interpretation of bone scans, Nuclear Medicine Communications, 27(5):417-423 (2006).
Sadik, M. et al., Automated 3D segmentation of the prostate gland in CT images—a first step towards objective measurements of prostate uptake in PET and SPECT images, Journal of Nuclear Medicine, 58(1):1074, (2017).
Sadik, M. et al., Automated quantification of reference levels in liver and mediastinum (blood pool) for the Deauville therapy response classification using FDG-PET/CT in lymphoma patients, EJNMMI, EANM '17, 44(Suppl 2):S119-S956, Abstract EP-0770 (2017).
Sadik, M. et al., Computer-assisted interpretation of planar whole-body bone scans, Journal Nuclear Medicine, 49(12):1958-65, 2008.
Sadik, M. et al., Convolutional neural networks for segmentation of 49 selected bones in CT images show high reproducibility, EJNMMI, EANM '17, 44(Suppl 2):S119-S956, Abstract OP-657 (2017).
Sadik, M. et al., Improved classifications of planar whole-body bone scans using a computer-assisted diagnosis system: a multicenter, multiple-reader, multiple-case study, Journal of Nuclear Medicine, 50(3): 368-75, 2009.
Sadik, M. et al., Variability in reference levels for Deauville classifications applied to lymphoma patients examined with 18F-FDG-PET/CT, EJNMMI, EANM '17, 44(Suppl 2):S119-S956, Abstract EP-0771 (2017).
Sajn, L. et al., Computerized segmentation of whole-body bone scintigrams and its use in automated diagnostics, Computer Methods and Programs in Biomedicine, 80:47-55 (2005).
Salerno, J. et al., Multiparametric magnetic resonance imaging for pre-treatment local staging of prostate cancer: A Cancer Care Ontario clinical practice guideline, Canadian Urological Association Journal, 10(9-10):332-339 (2016).
Santos-Cuevas, C. et al. 99mTc-labeled PSMA inhibitor: Biokinetics and radiation dosimetry in healthy subjects and imaging of prostate cancer tumors in patients, Nuclear Medicine and Biology 52:1-6, (2017).
Sjöstrand K. et al., Statistical regularization of deformation fields for atlas-based segmentation of bone scintigraphy images, MICCAI 5761:664-671 (2009).
Sluimer, I. et al., Toward Automated Segmentation of the Pathological Lung in CT, IEEE Transactions on Medical Imaging, 24(8):1025-1038 (2005).
Tian, Z. et al., A fully automatic multi-atlas based segmentation method for prostate MR images, Proc SPIE Int Soc Opt Eng. Author manuscript, 12 pages (2015).
Tian, Z. et al., A supervoxel-based segmentation method for prostate MR images, Med. Phys., 44(2):558-569 (2017).
Tian, Z et al., Deep convolutional neural network for prostate MR segmentation, Proc. of SPIE 10135:101351L-1-101351L-6 (2017).
Tian, Z., et al., Superpixel-based Segmentation for 3D Prostate MR Images, IEEE Trans Med Imaging, Author manuscript, 32 pages, (2016).
Ulmert, D. et al., A Novel Automated Platform for Quantifying the Extent of Skeletal Tumour Involvement in Prostate Cancer Patients Using the Bone Scan Index, European Urology, 62(1):78-84 (2012).
Wrangsjo, A. et al., Non-rigid Registration Using Morphons, Proceedings of the 14th Scandinavian Conference on Image Analysis (SCIA '05), pp. 501-510 (2005).
Written Opinion, International Application No. PCT/US2017/058418 (Network for Medical Image Analysis, Decision Support System, and Related Graphical User Interface (GUI) Applications, filed Oct. 26, 2017), issued by ISA/European Patent Office, 9 pages, dated Feb. 27, 2018.
Yin, T.-K., A Computer-Aided Diagnosis for Locating Abnormalities in Bone Scintigraphy by a Fuzzy System With a Three-Step Minimization Approach, IEEE Transactions on Medical Imaging, 23(5):639-654 (2004).
Armstrong, A. J et al., Phase 3 Assessment of the Automated Bone Scan Index as a Prognostic Imaging Biomarker of Overall Survival in Men with Metastatic Castration-Resistant Prostate Cancer: A Secondary Analysis of a Randomized Clinical Trial. JAMA Oncology 4:944-951, (2018).
Bai, P et al., Body region localization in whole-body low-dose CT images of PET/CT scans using virtual landmarks, Medical Physics Wiley USA, 46(3): 1286-1299 (2019).
Brynolfsson, J., et al., Deep Learning based urinary bladder segmentation using 18FDCFPyL (PyL-PSMA) PET/CT images, EPS-145, European Association of Nuclear Medicine, (2020), <http://link.springer.com/article/10.1007/s00259-020-04988-4>. Retrieved Sep. 18, 2020.
Brynolfsson, J., et al., Deep Learning-Enabled comprehensive detection and quantification of 18FDCFPyL (PyL-PSMA) PET/CT, OP-548, European Association of Nuclear Medicine, (2020), <http://link.springer.com/article/10.1007/s00259-020-04988-4>. Retrieved Sep. 18, 2020.
Dertat, A., Applied Depp Learning—{art 4: Convolutional Neural Networks, Towards Data Science,<http://towardsdatascience.com/applied-deep-learning-part-4-convolutional-neural-networks-584bc134c1e> (2017).

(56) **References Cited**

OTHER PUBLICATIONS

Gjertsson, K., et al., A Novel Automated Deep Learning Algorithm for Segmentation of the Skeleton in Low-Dose CT for [(18)F] DCFPyL PET/CT Hybrid Imaging in Patients with Metastatic Prostate Cancer, Annual Congress of the European Association of Nuclear Medicine Oct. 12-16, 2019 Barcelona, Spain. Eur J Nucl Med Mol Imaging 46 (Suppl 1), S1-S952 (2019). Abstract EP-0823, p. S765.

Johnsson, K., et al., miPSMA Index: Comprehensive and Automated Quantification of 18F-DCFPyL (PyL-PSMA) PET/CT for Prostate Cancer Staging, J Nucl Med., 61: (Supplement 1): 1435, (2020).

Lin, T.Y. et al., Feature Pyramid Networks for object detection, FAIR, (2016), <https://arxiv.org/abs/1612.03144v1 >.

Meyer, A., et al., Deep learning algorithm improves identification of men with low-risk prostate cancer using PSMA targeted 99mTc-MIP-1404 SPECT/CT, Journal of Clinical Oncology, 37:(15), (2019).

Nickols, N.G., et al., A deep learning algorithm to predict coexisting metastatic disease using intraprostatic [F18]DCFPYL PSMA image alone in veterans with prostate cancer, Journal of Clinical Oncology 38, (Supplement 6), 2020.

Pouliot, F., et al., Prospective evaluation of a Novel Deep Learning Algorithm (PSMA-AI) in the assessment of 99mTc-MIP-1404 SPECT/CT in patients with low or intermediate risk prostate cancer, Annual Congress of the European Association of Nuclear Medicine Oct. 12-16, 2019 Barcelona, Spain. Eur J Nucl Med Mol Imaging 46 (Suppl 1), S1-S952 (2019). Abstract EP-0804, p. S765.

Ren, S., et al., Faster R-CNN: Towards Real-Time Object Detection with Region Proposal Networks, (2015), <http://image-net.org/challenges/LSVRC/2015/results>.

Ronneberger, O., et al., U-Net: Convolutional Networks for Biomedical Image Segmentation, Springer International Publishing, (2015), <http://lmb.informatik.uni-freiburg.de/>. Retrieved on Nov. 18, 2015.

Sjöstrand, K., et al., Automated detection and quantification of Prostatic PSMA uptake in SPECT/CT using a Deep Learning Algorithm for Segmentation of Pelvic Anatomy, The Journal of Nuclear Medicine, 59(1):p. 30, (2018).

Sjostrand, K., et al., Automated Assessment of Prostatic PSMA Expression in SPECT/CT using Deep Convolutional Neural Networks—A Prospectively Planned Retrospective Analysis of Phase 3 Study MIP-1404-3301, The Journal of Nuclear Medicine, 60 (Supplement 1): Abstract 401, (2019).

Capobianco, N. et al., Whole-body uptake classification and prostate cancer staging in ^{68}Ga-PSMA-11 PET/CT using dual-tracer learning, European Journal of Nuclear Medicine and Molecular Imaging, (2021), <https:/doi.org/10.1007/s00259-021-05473-2> 10 pages. Retrieved on Apr. 18, 2021.

Fendler, W.P. et al., ^{68}Ga-PSMA PET/CT: Joint EANM and SNMMI procedure guideline for prostate cancer imaging: version 1.0, Eur J Nucl Med Mol Imaging, DOI 10.1007/s00259-017-3670-z, 11 pages, (2017).

Im, HJ, et al., et al., Current Methods to Define Metabolic Tumor Volume in Positron Emission Tomography: Which One is Better?, Nucl. Med. Mol. Imaging, 52(1):5-15, (2018).

Polymeri, E., et al., Deep learning-based quantification of PET/CT prostate gland uptake: association with overall survival, Clinical Physiology Functional Imaging, DOI: 10.1111/cpf.12611, 40(2):106-113, (2019).

Trägärdh, E., et al., RECOMIA—a cloud-based platform for artificial intelligence research in nuclear medicine and radiology, EJNMMI Physics, <https://doi.org/10.1186/s40658-020-00316-9>, 7:51, 12 pages, (2020).

Wallis, J.W. et al., Three-dimensional display in nuclear medicine, IEEE Trans Med Imaging, 8(4):297-303, (1989).

Communication pursuant to Article 94(3) EPC for European Application No. 17794628.2-1126, 6 pages, (dated Apr. 22, 2021).

* cited by examiner

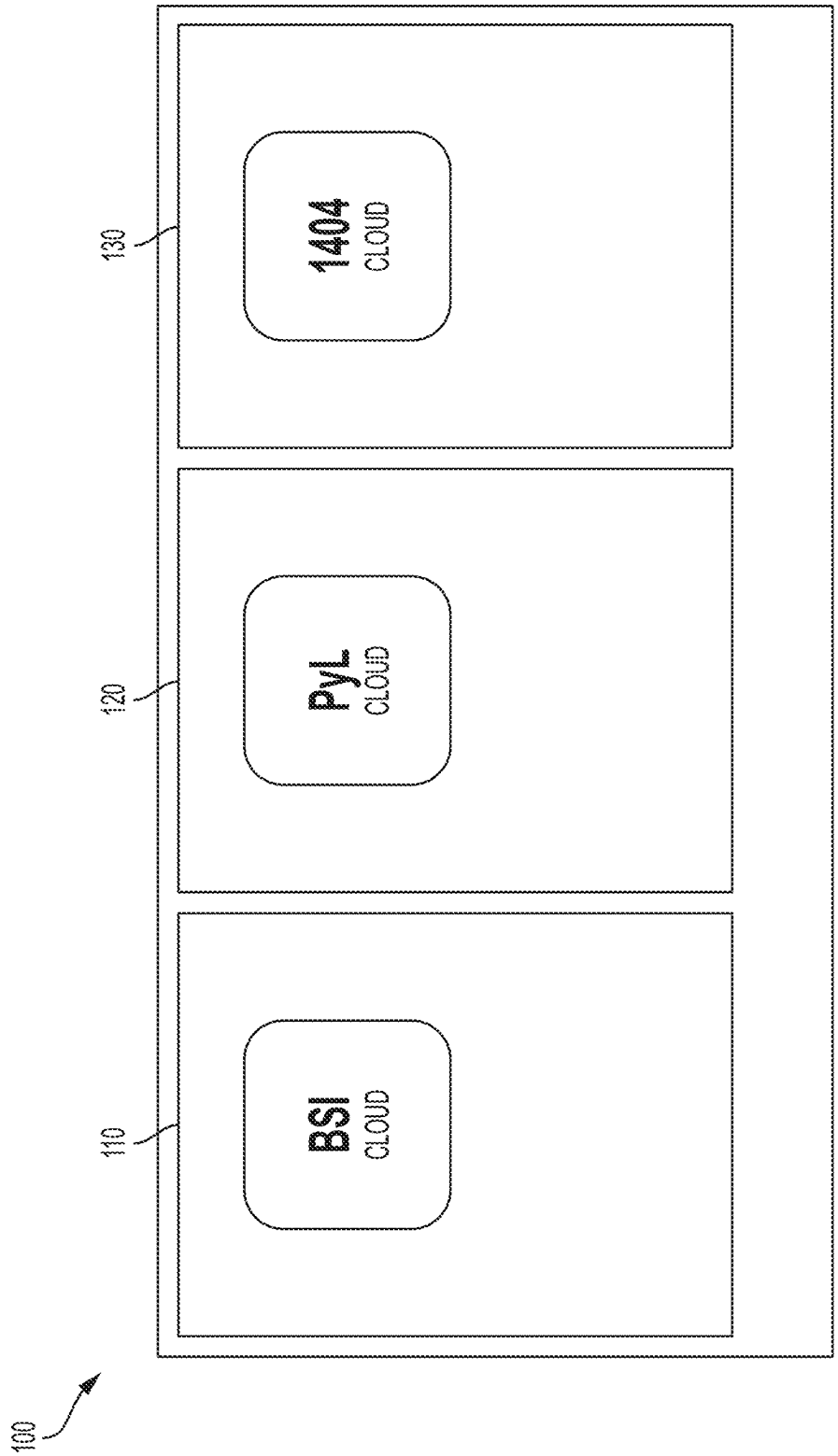


FIG. 1

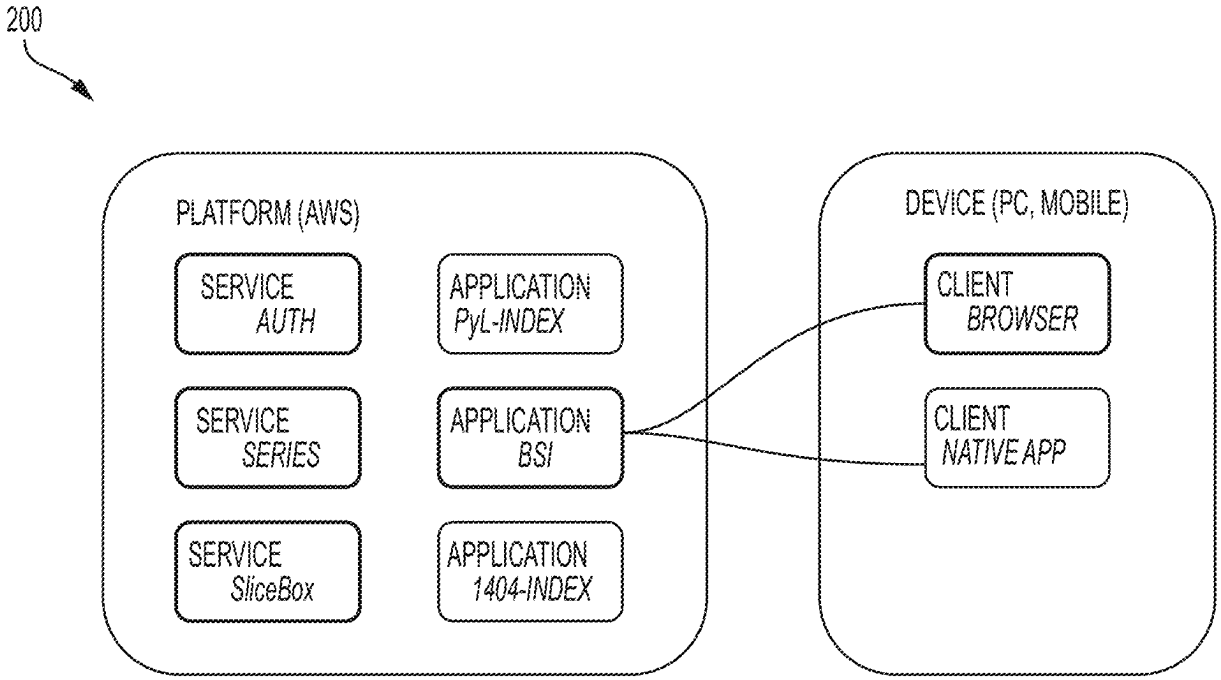

200
PLATFORM (AWS)
SERVICE
AUTH
APPLICATION
PyL-INDEX
SERVICE
SERIES
APPLICATION
BSI
SERVICE
SliceBox
APPLICATION
1404-INDEX
DEVICE (PC, MOBILE)
CLIENT
BROWSER
CLIENT
NATIVE APP

FIG. 2

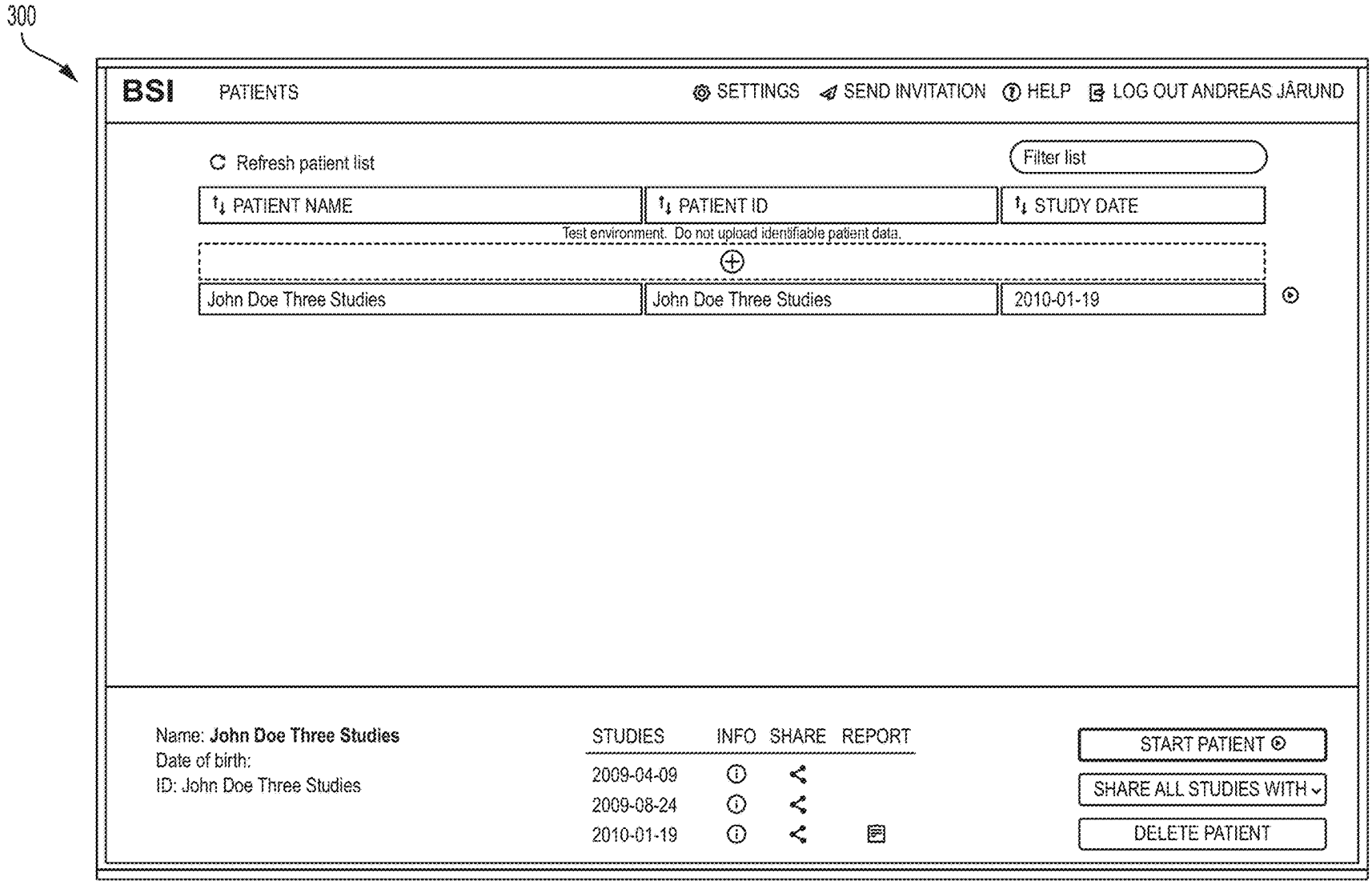

300
BSI
PATIENTS
SETTINGS
SEND INVITATION
HELP
LOG OUT ANDREAS JÅRUND
Refresh patient list
Filter list
PATIENT NAME
PATIENT ID
STUDY DATE
Test environment. Do not upload identifiable patient data.
John Doe Three Studies
John Doe Three Studies
2010-01-19
Name: John Doe Three Studies
Date of birth:
ID: John Doe Three Studies
STUDIES
INFO
SHARE
REPORT
2009-04-09
2009-08-24
2010-01-19
START PATIENT
SHARE ALL STUDIES WITH
DELETE PATIENT

FIG. 3

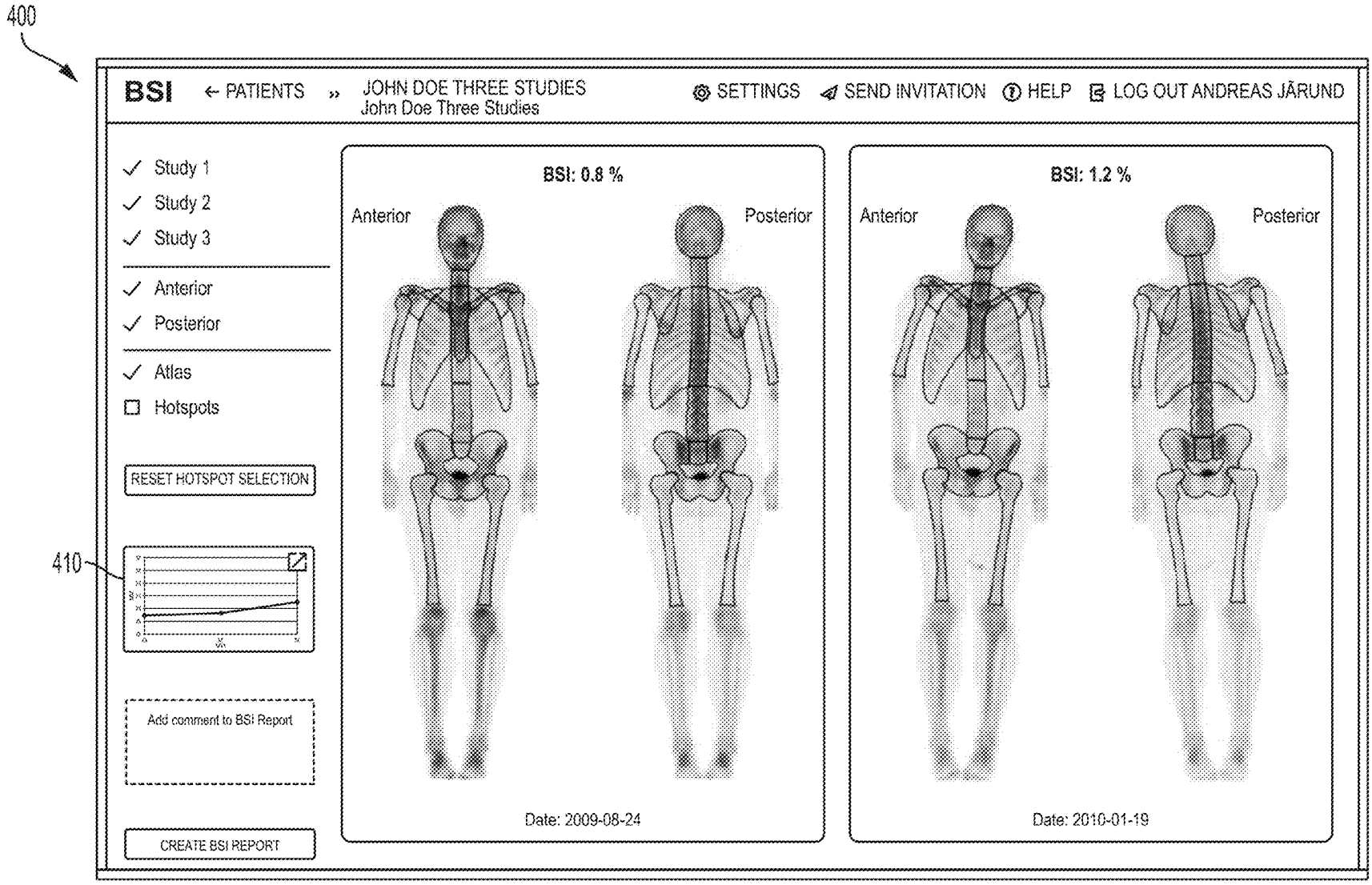

400
BSI
← PATIENTS
»
JOHN DOE THREE STUDIES
John Doe Three Studies
SETTINGS
SEND INVITATION
HELP
LOG OUT ANDREAS JÄRUND
Study 1
Study 2
Study 3
Anterior
Posterior
Atlas
Hotspots
RESET HOTSPOT SELECTION
410
Add comment to BSI Report
CREATE BSI REPORT
BSI: 0.8 %
Anterior
Posterior
Date: 2009-08-24
BSI: 1.2 %
Anterior
Posterior
Date: 2010-01-19

FIG. 4

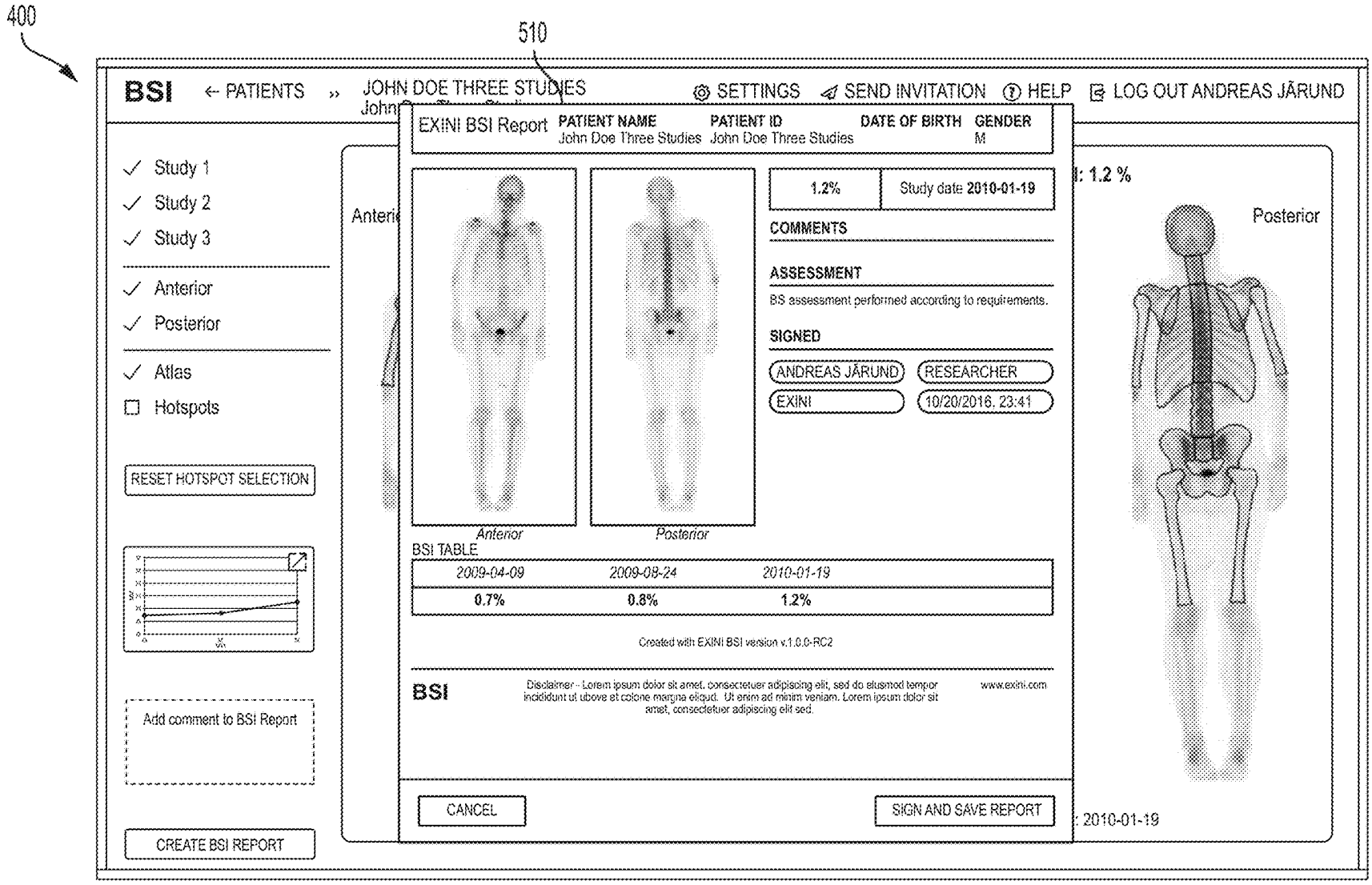

400
510
BSI
← PATIENTS
JOHN DOE THREE STUDIES
SETTINGS
SEND INVITATION
HELP
LOG OUT ANDREAS JÄRUND
Study 1
Study 2
Study 3
Anterior
Posterior
Atlas
Hotspots
RESET HOTSPOT SELECTION
Add comment to BSI Report
CREATE BSI REPORT
EXINI BSI Report
PATIENT NAME
John Doe Three Studies
PATIENT ID
John Doe Three Studies
DATE OF BIRTH
GENDER
M
1.2%
Study date 2010-01-19
COMMENTS
ASSESSMENT
BS assessment performed according to requirements.
SIGNED
ANDREAS JÄRUND
RESEARCHER
EXINI
10/20/2016, 23:41
Anterior
Posterior
BSI TABLE
2009-04-09
2009-08-24
2010-01-19
0.7%
0.8%
1.2%
Created with EXINI BSI version v.1.0.0-RC2
BSI
Disclaimer – Lorem ipsum dolor sit amet, consectetuer adipiscing elit, sed do eiusmod tempor incididunt ut ubove et colone magna eliqud. Ut enim ad minim veniam. Lorem ipsum dolor sit amet, consectetuer adipiscing elit sed.
www.exini.com
CANCEL
SIGN AND SAVE REPORT
1.2 %
Posterior
2010-01-19

FIG. 5

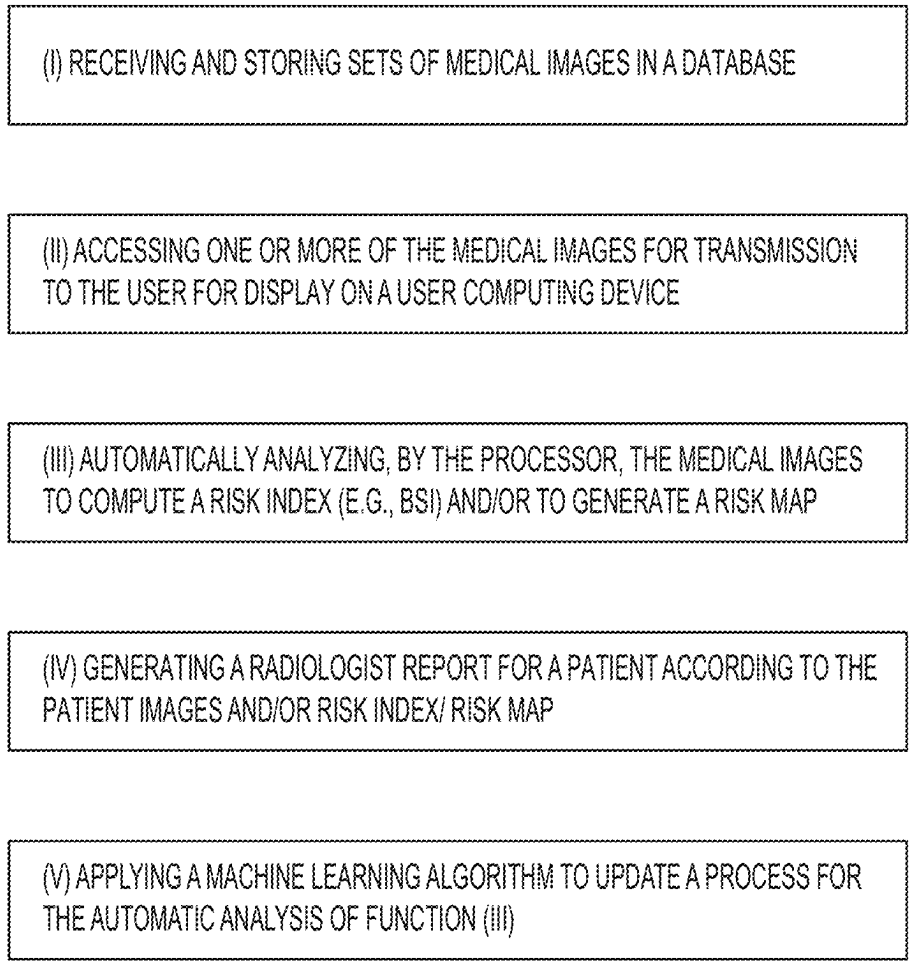

(I) RECEIVING AND STORING SETS OF MEDICAL IMAGES IN A DATABASE
(II) ACCESSING ONE OR MORE OF THE MEDICAL IMAGES FOR TRANSMISSION TO THE USER FOR DISPLAY ON A USER COMPUTING DEVICE
(III) AUTOMATICALLY ANALYZING, BY THE PROCESSOR, THE MEDICAL IMAGES TO COMPUTE A RISK INDEX (E.G., BSI) AND/OR TO GENERATE A RISK MAP
(IV) GENERATING A RADIOLOGIST REPORT FOR A PATIENT ACCORDING TO THE PATIENT IMAGES AND/OR RISK INDEX/ RISK MAP
(V) APPLYING A MACHINE LEARNING ALGORITHM TO UPDATE A PROCESS FOR THE AUTOMATIC ANALYSIS OF FUNCTION (III)

FIG. 6

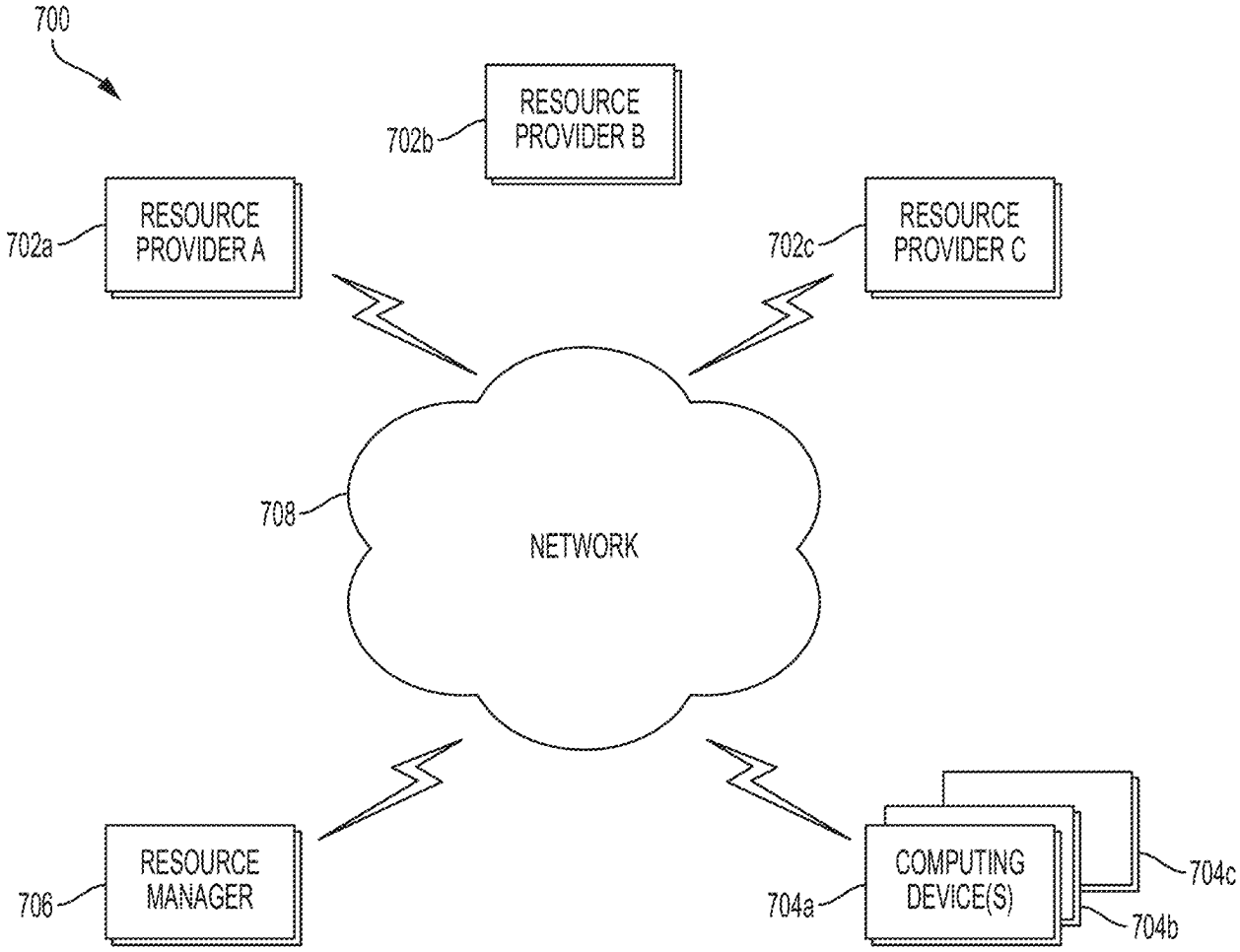

700
RESOURCE PROVIDER B
702b
RESOURCE PROVIDER A
702a
RESOURCE PROVIDER C
702c
708
NETWORK
RESOURCE MANAGER
706
COMPUTING DEVICE(S)
704a
704c
704b

FIG. 7

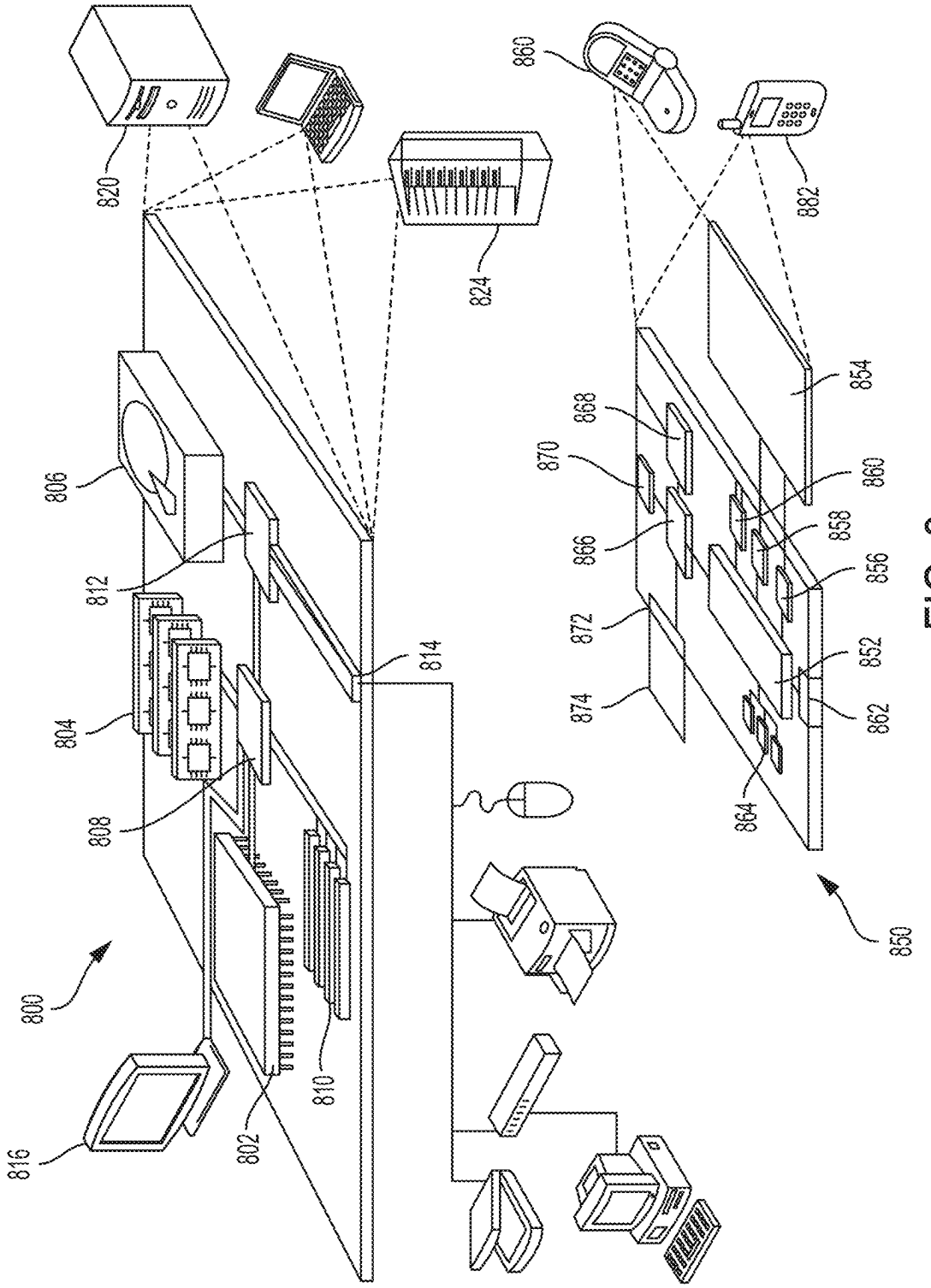

820
824
860
882
806
812
804
808
814
800
816
802
810
854
868
870
866
872
874
858
856
852
862
864
850

FIG. 8

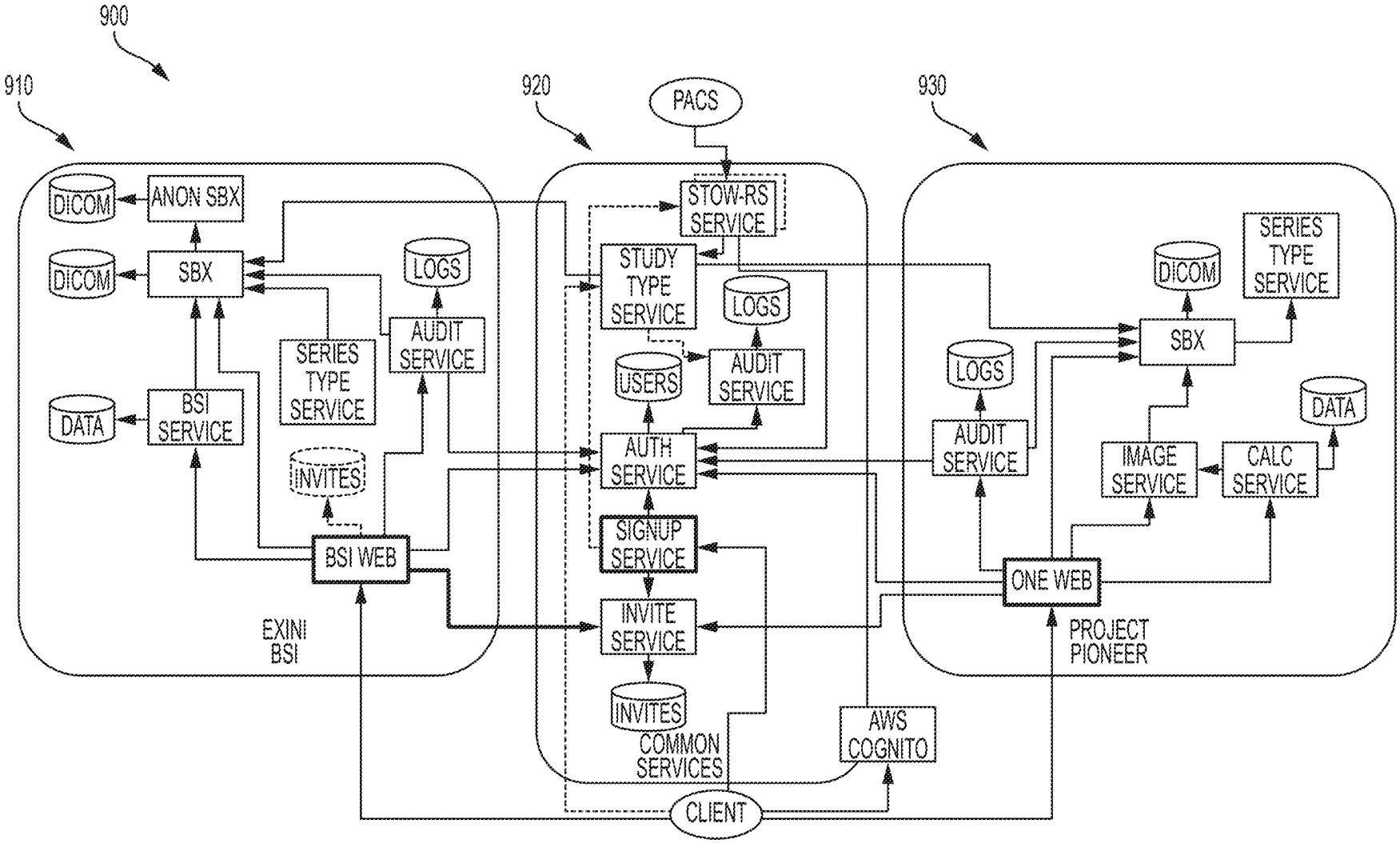

900
910
920
930
PACS
DICOM
ANON SBX
DICOM
SBX
DATA
BSI SERVICE
LOGS
AUDIT SERVICE
SERIES TYPE SERVICE
INVITES
BSI WEB
EXINI BSI
STOW-RS SERVICE
STUDY TYPE SERVICE
LOGS
AUDIT SERVICE
USERS
AUTH SERVICE
SIGNUP SERVICE
INVITE SERVICE
INVITES
COMMON SERVICES
CLIENT
AWS COGNITO
LOGS
AUDIT SERVICE
DICOM
SBX
SERIES TYPE SERVICE
DATA
IMAGE SERVICE
CALC SERVICE
ONE WEB
PROJECT PIONEER

FIG. 9

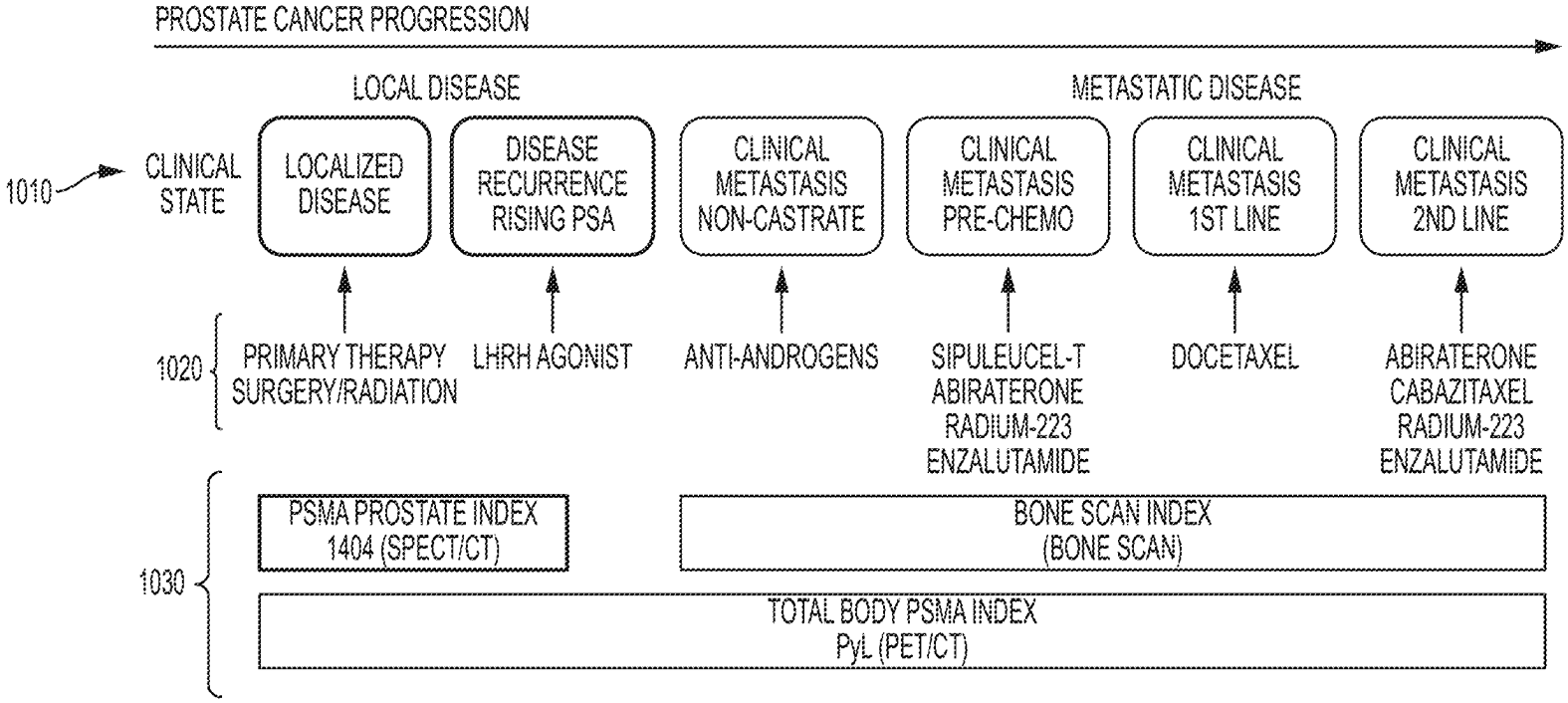

PROSTATE CANCER PROGRESSION
LOCAL DISEASE
METASTATIC DISEASE
1010
CLINICAL STATE
LOCALIZED DISEASE
DISEASE RECURRENCE RISING PSA
CLINICAL METASTASIS NON-CASTRATE
CLINICAL METASTASIS PRE-CHEMO
CLINICAL METASTASIS 1ST LINE
CLINICAL METASTASIS 2ND LINE
1020
PRIMARY THERAPY SURGERY/RADIATION
LHRH AGONIST
ANTI-ANDROGENS
SIPULEUCEL-T ABIRATERONE RADIUM-223 ENZALUTAMIDE
DOCETAXEL
ABIRATERONE CABAZITAXEL RADIUM-223 ENZALUTAMIDE
1030
PSMA PROSTATE INDEX 1404 (SPECT/CT)
BONE SCAN INDEX (BONE SCAN)
TOTAL BODY PSMA INDEX PyL (PET/CT)

FIG. 10

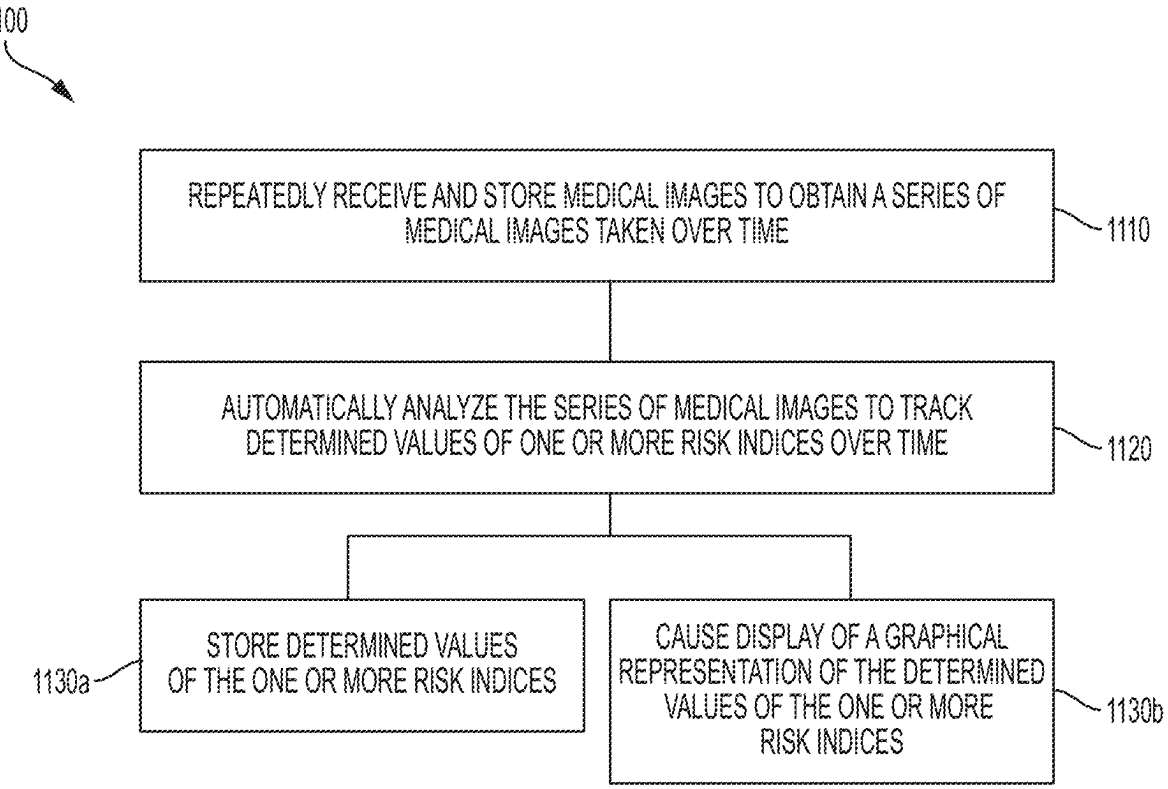

1100
REPEATEDLY RECEIVE AND STORE MEDICAL IMAGES TO OBTAIN A SERIES OF MEDICAL IMAGES TAKEN OVER TIME
1110
AUTOMATICALLY ANALYZE THE SERIES OF MEDICAL IMAGES TO TRACK DETERMINED VALUES OF ONE OR MORE RISK INDICES OVER TIME
1120
STORE DETERMINED VALUES OF THE ONE OR MORE RISK INDICES
1130a
CAUSE DISPLAY OF A GRAPHICAL REPRESENTATION OF THE DETERMINED VALUES OF THE ONE OR MORE RISK INDICES
1130b

FIG. 11

NETWORK FOR MEDICAL IMAGE ANALYSIS, DECISION SUPPORT SYSTEM, AND RELATED GRAPHICAL USER INTERFACE (GUI) APPLICATIONS

CROSS REFERENCE TO RELATED APPLICATIONS

This application is a continuation of U.S. application Ser. No. 16/418,527, filed May 21, 2019 (now U.S. Pat. No. 10,762,993), which is a continuation of U.S. application Ser. No. 15/794,220 filed Oct. 26, 2017 (now U.S. Pat. No. 10,340,046), which claims the benefit of U.S. Provisional Application 62/413,936, filed on Oct. 27, 2016, the contents of each of which are hereby incorporated by reference herein in their entirety.

TECHNICAL FIELD

This invention relates generally to systems and methods for creation, analysis, and/or presentation of medical image data. More particularly, in certain embodiments, the invention relates to a cloud-based platform and supported GUI decision-making tools for use by medical practitioners and/or their patients, e.g., to aide in the process of making decisions about a course of cancer treatment and/or to track treatment and/or the progress of a disease.

BACKGROUND

Targeted image analysis involves the use of radiolabeled small molecules that bind to specific receptors, enzymes and proteins in the body that are altered during the evolution of disease. After administration to a patient, these molecules circulate in the blood until they find their intended target. The bound radiopharmaceutical remains at the site of disease, while the rest of the agent clears from the body. The radioactive portion of the molecule serves as a beacon so that an image may be obtained depicting the disease location and concentration using commonly available nuclear medicine cameras, known as single-photon emission computerized tomography (SPECT) or positron emission tomography (PET) cameras, found in most hospitals throughout the world. Physicians can then use this information to determine the presence and the extent of disease in a patient. The physician can use this information to provide a recommended course of treatment to the patient and to track the progression of disease.

There are a variety of software-based analytical techniques available for analysis and enhancement of PET and SPECT images that can be used by a radiologist or physician. There are also a number of radiopharmaceuticals available for imaging particular kinds of cancer. For example, the small molecule diagnostic 1404 targets the extracellular domain of prostate specific membrane antigen (PSMA), a protein amplified on the surface of >95% of prostate cancer cells and a validated target for the detection of primary and metastatic prostate cancer. 1404 is labeled with technetium-99 m, a gamma-emitter isotope that is widely available, relatively inexpensive, facilitates efficient preparation, and has spectrum characteristics attractive for nuclear medicine imaging applications.

Another example radiopharmaceutical is PyL™ (also known as [^{18}F]DCFPyL), which is a clinical-stage, fluorinated PSMA-targeted PET imaging agent for prostate cancer. A proof-of-concept study published in the April 2015 issue of the Journal of Molecular Imaging and Biology

demonstrated that PET imaging with PyL™ showed high levels of PyL™ uptake in sites of putative metastatic disease and primary tumors, suggesting the potential for high sensitivity and specificity in detecting prostate cancer.

An oncologist may use images from a targeted PET or SPECT study of a patient as input in her assessment of whether the patient has a particular disease, e.g., prostate cancer, what stage of the disease is evident, what the recommended course of treatment (if any) would be, whether surgical intervention is indicated, and likely prognosis. The oncologist may use a radiologist report in this assessment. A radiologist report is a technical evaluation of the PET or SPECT images prepared by a radiologist for a physician who requested the imaging study and includes, for example, the type of study performed, the clinical history, a comparison between images, the technique used to perform the study, the radiologist's observations and findings, as well as overall impressions and recommendations the radiologist may have based on the imaging study results. A signed radiologist report is sent to the physician ordering the study for the physician's review, followed by a discussion between the physician and patient about the results and recommendations for treatment.

Thus, the process involves having a radiologist perform an imaging study on the patient, analyzing the images obtained, creating a radiologist report, forwarding the report to the requesting physician, having the physician formulate an assessment and treatment recommendation, and having the physician communicate the results, recommendations, and risks to the patient. The process may also involve repeating the imaging study due to inconclusive results, or ordering further tests based on initial results.

If an imaging study shows that the patient has a particular disease or condition (e.g., cancer), the physician discusses various treatment options, including surgery, as well as risks of doing nothing or adopting a watchful waiting or active surveillance approach, rather than having surgery.

There are limitations associated with this process, both from the perspective of the physician and from the perspective of the patient. While the radiologist's report is certainly helpful, the physician must ultimately rely on her experience in formulating an assessment and recommendation for her patient. Furthermore, the patient must place a great deal of trust in his physician. The physician may show the patient his PET/SPECT images and may tell the patient a numerical risk associated with various treatment options or likelihood of a particular prognosis, but the patient may very well struggle to make sense of this information. Moreover, the patient's family will likely have questions, particularly if cancer is diagnosed but the patient opts not to have surgery. The patient and/or his family members may search online for supplemental information and may become misinformed about risks of the diagnosed condition. A difficult ordeal may become more traumatic.

Thus, there remains a need for systems and methods for improved analysis of medical imaging studies and communication of those results, diagnoses, prognoses, treatment recommendations, and associated risks to a patient.

SUMMARY OF THE INVENTION

Presented herein is a cloud-based platform and supported graphical user interface (GUI) decision-making tools for use by medical practitioners and/or their patients, e.g., to aide in the process of making decisions about a course of cancer treatment and/or to track treatment and/or the progress of a disease.

For example, presented herein is a network-based (e.g., cloud-based) support platform allowing multiple users to store, access, analyze, and/or provide feedback regarding a given set of image data for a patient; platform supports software tools for automated analysis of targeted PET/SPECT/or other image(s), generation of radiologist reports, and application of machine learning algorithms to update process by which images are analyzed (e.g. updating segmentation and/or classification routines based on growing image database). In certain embodiments, the targeted PET/SPECT image(s) may be obtained using PyL™ and/or 1404 as the radiopharmaceutical(s). In certain embodiments, multiple (accredited) users can access the information, e.g., to weigh in on data interpretation.

Also presented herein is a software tool (e.g., mobile app) featuring a graphical user interface (GUI) element with controls for adjusting presentation of a 3D risk image corresponding to a patient organ (and/or other tissue) for comparison with reference images (e.g., for use in communication of results to patient as a decision-making support). For example, the tool may be supported by the network-based support platform above. This tool can provides an easily-understood, user-friendly, interactive, controllable pictorial display to communicate information about a patient's condition to the patient (and/or to the physician, or to the patient's family with the patient's permission). For example, a patient for whom a risk of cancer is detected can display a map indicating areas and/or degrees of risk and can compare this risk map with those of others for whom a given course of treatment is recommended. For instance, this tool can help a patient in his decision whether or not to have surgery (e.g., for a detected risk of prostate cancer). The patient can visually compare his risk map with a map representing a typical risk-level for which surgery would be recommended, below which it may be reasonable to opt not to have surgery and engage in watchful waiting or active surveillance. Thus, a low-risk patient who is told by his physician that he has a non-zero risk of cancer may find comfort in a visual, controllable comparison between his situation and that of someone (e.g., where the reference to which the patient's risk situation is compared can be tuned for age, weight, and/or other risk factors of the patient).

In one aspect, the invention is directed to a network-based (e.g., cloud based) decision support system comprising: a processor (e.g., of a network or Internet host server); and a memory having instructions stored thereon, wherein the instructions, when executed by the processor, cause the processor to perform one or more of functions (i) to (v) as follows: (i) receive and store medical images [e.g., comprising one or more of the following: targeted PET images, targeted SPECT images, computed tomography (CT) images, magnetic resonance (MR) images, ultrasound (US) images, gamma camera (i.e. scintillation camera) images, and combinations, fusions, or derivatives of any of the above] in a database [e.g., wherein the targeted PET/SPECT/gamma camera image(s) are obtained using one or more radiopharmaceuticals (e.g., [18F]DCFPyL and/or 1404 and/or a composition comprising technetium 99m, {e.g., technetium 99m methylenediphosphonate (^{99m}Tc MDP)}), and/or wherein the medical images are obtained using non-radioactive agents or no agents], each medical image associated with a particular patient; (ii) access one or more of the medical images and/or related data associated with a particular patient from the database upon user request (e.g., following automated verification that the user is properly credentialed for receiving the requested images and/or data) for transmission to the user for display on a user computing device; (iii) automatically analyze one or more of the medical images [e.g., to generate a risk index (e.g., BSI) and/or a risk map, e.g., a visual representation (e.g., 3D representation) of tissue (e.g., an organ or other part of the body) with graphical denotations (e.g., texture- or color-coding) marking regions of risk of current disease or risk of recurrence of disease, e.g., cancer, e.g., wherein the risk map is displayed as an overlay of the PET/SPECT/CT/MRI/US/combined/derived/fused image of the tissue, or is in place of the image of the tissue]; (iv) generate a radiologist report for a patient according to one or more of the medical images for the patient; and (v) apply a machine learning algorithm to update a process for automatically analyzing one or more of the medical images using accumulated image data in the database [e.g., wherein the automatic analysis of the one or more medical images in (iii) and/or (v) above comprises any one or more of (a) to (d) as follows: (a) automated fusion of the (e.g., PET, SPECT, CT, Mill, and/or US) image(s) of the tissue; (b) geographic identification of one or more organs, organ structures, sub-organs, organ regions, and/or other regions of the imaged tissue of the patient and production of a 3D image of the geographically identified tissue with PET, SPECT, CT, MM, and/or US data overlaid; (c) computation of risk information comprising one or more risk indices, a risk field, or a risk map using data from the database, the image(s) of the tissue, and/or the 3D image in (b); and (d) use of the risk information computed in (c) (e.g., and data from the database) to produce a 3D risk picture for the patient].

In certain embodiments, the medical images in the database comprise a series of medical images of a first patient taken over time (e.g., over the course of multiple visits to one or more doctors), and wherein the instructions cause the processor to determine a value of at least a first risk index for each medical image of the series, thereby tracking determined values of at least the first risk index for the first patient over time.

In certain embodiments, the medical images comprise a single-photon emission computerized tomography (SPECT) scan of a first patient obtained (e.g., to identify one or more hotspots) following administration to the first patient of an imaging agent comprising 1404 labeled with ^{99m}Tc, and a computed tomography (CT) scan (e.g., to identify anatomical features) of the first patient, wherein the instructions cause the processor to overlay the SPECT scan with the CT scan to create a composite image (SPECT-CT) of the first patient.

In certain embodiments, the medical images comprise a positron emission tomography (PET) scan of a first patient obtained (e.g., to identify one or more hotspots) following administration to the first patient of an imaging agent comprising [18F]DCFPyL (DCFPyL labeled with ^{18}F), and a CT scan of the first patient, wherein the instructions cause the processor to overlay the PET scan with the CT scan to create a composite image (PET-CT) of the first patient.

In certain embodiments, the medical images comprise a whole-body scan (e.g., including anterior and posterior views) of a first patient made with a gamma camera following administration to the first patient of an imaging agent comprising technetium 99m methylenediphosphonate (^{99m}Tc MDP).

In certain embodiments, the medical images comprise a composite image of a first patient, the composite image comprising a CT scan overlaid with a nuclear medicine image (e.g., a SPECT scan; e.g., a PET scan) obtained at substantially the same time as the CT scan and following administration to the first patient of an imaging agent

comprising a Prostate Specific Membrane Antigen (PSMA) binding agent comprising (e.g., labelled with) a radionuclide, and the instructions cause the processor to automatically analyze the composite image by: (a) using the composite image to geographically identify a 3D boundary for each of one or more regions of imaged tissue [e.g., organs (e.g., a prostate; e.g., a liver; e.g., lungs or a lung; e.g., lymph nodes), organ structures, sub-organs, organ regions, and/or other regions (e.g., one or more particular bones; e.g., a skeletal region of the patient), e.g., regions of interest] within the nuclear medicine image (e.g., such that portions of the nuclear medicine image falling within and/or outside of the 3D boundaries can be differentiated from each other); and (c) computing (i) a value of each of one or more risk indices and/or (ii) a risk map using the nuclear medicine image with the identified 3D boundaries of the one or more region(s).

In certain embodiments, the instructions cause the processor to, for at least one risk index of the one or more risk indices, compute the value of the risk index by: determining, for each of the one or more regions, a corresponding cancerous tissue level within the region based on intensity values of the nuclear medicine image within the 3D boundary of the region (e.g., by identifying within the nuclear medicine image, a plurality of hotspots within the 3D boundary of the region and computing a total number of and/or a total volume of the identified hotspots); and computing the value of the risk index based on the determined cancerous tissue levels within the one or more regions.

In certain embodiments, the nuclear medicine image is a SPECT scan.

In certain embodiments, the imaging agent comprises a metal chelated to the PSMA binding agent, and wherein the metal is the radionuclide [e.g., wherein the metal is a radioisotope of technetium (Tc) (e.g., wherein the metal is technetium-99m (^{99m}Tc)); e.g., wherein the metal is a radioisotope of rhenium (Re) (e.g., wherein the metal is rhenium-188 (^{188}Re); e.g., wherein the metal is rhenium-186 (^{186}Re)); e.g., wherein the metal is a radioisotope of yttrium (Y) (e.g., wherein the metal is ^{90}Y); e.g., wherein the metal is a radioisotope of lutetium (Lu)(e.g., wherein the metal is ^{177}Lu); e.g., wherein the metal is a radioisotope of gallium (Ga) (e.g., wherein the metal is ^{68}Ga; e.g., wherein the metal is ^{67}Ga); e.g., wherein the metal is a radioisotope of indium (e.g., ^{111}In); e.g., wherein the metal is a radioisotope of copper (Cu) (e.g., wherein the metal is ^{67}Cu)].

In certain embodiments, the imaging agent comprises ^{99m}Tc-MIP-1404.

In certain embodiments, the nuclear medicine image is a PET scan.

In certain embodiments, the radionuclide is a radioisotope of a halogen [e.g., a radioisotope of fluorine (e.g., ^{18}F); e.g., a radioisotope of iodine (e.g., ^{123}I; e.g., ^{124}I; e.g., ^{125}I; e.g., ^{126}I; e.g., ^{131}I); e.g., a radioisotope of bromine (e.g., ^{75}Br; e.g., ^{76}Br; e.g., ^{77}Br; e.g., ^{80}Br; e.g., ^{80m}Br; e.g., ^{82}Br; e.g., ^{83}Br), e.g., a radioisotope of astatine (e.g., ^{211}At)].

In certain embodiments, the imaging agent comprises [18F]DCFPyL (DCFPyL labeled with ^{18}F).

In certain embodiments, the radionuclide is a radioisotope of gallium (Ga) (e.g., ^{68}Ga).

In certain embodiments, the medical images comprise a nuclear medicine image (e.g., a whole-body scan made with a gamma camera) of a first patient following administration to the first patient of an imaging agent comprising a radionuclide (e.g., ^{99m}Tc)(e.g., wherein the imaging agent comprises ^{99m}Tc MDP), wherein the instructions cause the processor to automatically analyze the nuclear medicine image by: (a) geographically identifying a boundary (e.g., a 2D boundary; e.g., a 3D boundary) for each of one or more regions of imaged tissue [e.g., organs (e.g., a prostate; e.g., a liver; e.g., lungs or a lung; e.g., lymph nodes), organ structures, sub-organs, organ regions, and/or other regions (e.g., one or more particular bones; e.g., a skeletal region of the patient), e.g., regions of interest] within the nuclear medicine image (e.g., such that portions of the nuclear medicine image falling within and/or outside of the boundaries can be differentiated from each other); and (c) computing (i) a value of each of one or more risk indices and/or (ii) a risk map using the nuclear medicine image with the identified boundaries of the one or more region(s).

In certain embodiments, the instructions cause the processor to, for at least one risk index of the one or more risk indices, compute the value of the risk index by: determining, for each of the one or more regions, a corresponding cancerous tissue level within the region based on intensity values of the nuclear medicine image within the boundary of the region (e.g., by identifying within the nuclear medicine image, a plurality of hotspots within the boundary of the region and computing a total number of and/or a total volume of the identified hotspots); and

computing the value of the risk index based on the determined cancerous tissue levels within the one or more regions.

In certain embodiments, the system is a cloud-based system.

In certain embodiments, the processor is a processor of one or more network or Internet host servers.

In another aspect, the invention is directed to a method comprising any one or more of (i) to (v) as follows: (i) receiving and storing, by a processor of a server computing device (e.g., received over a network from a client computing device) medical images [e.g., comprising one or more of the following: targeted PET images, targeted SPECT images, computed tomography (CT) images, magnetic resonance (MR) images, ultrasound (US) images, gamma camera (i.e. scintillation camera) images, and combinations, fusions, or derivatives of any of the above] in a database [e.g., wherein the targeted PET/SPECT/gamma camera image(s) are obtained using one or more radiopharmaceuticals, e.g., [18F]DCFPyL and/or 1404 and/or a composition comprising technetium 99m, e.g., technetium 99m methylenediphosphonate (^{99m}Tc MDP), and/or wherein the medical images are obtained using non-radioactive agents or no agents], each medical image associated with a particular patient; (ii) accessing, by the processor, one or more of the medical images and/or related data associated with a particular patient from the database upon user request (e.g., following automated verification that the user is properly credentialed for receiving the requested images and/or data) for transmission to the user for display on a user computing device; (iii) automatically analyzing, by the processor, one or more of the medical images[e.g., to generate a risk map, e.g., a visual representation (e.g., 3D representation) of tissue (e.g., an organ or other part of the body) with graphical denotations (e.g., texture- or color-coding) marking regions of risk of current disease or risk of recurrence of disease, e.g., cancer, e.g., wherein the risk map is displayed as an overlay of the PET/SPECT/CT/MM/US/combined/derived/fused image of the tissue, or is in place of the image of the tissue]; (iv) generating, by the processor, a radiologist report for a patient according to one or more of the medical images for the patient; and (v) applying, by the processor, a machine learning algorithm to update a process for automatically analyzing one or more of the medical images using

accumulated image data in the database, [e.g., wherein the automatically analyzing the one or more medical images in (iii) and/or (v) above comprises any one or more of (a) to (d) as follows: (a) automatically fusing the (e.g., PET, SPECT, CT, MRI, and/or US) image(s) of the tissue; (b) geographically identifying one or more organs, organ structures, sub-organs, organ regions, and/or other regions of the imaged tissue of the patient and production of a 3D image of the geographically identified tissue with PET, SPECT, CT, MRI, and/or US data overlaid; (c) computing risk information comprising one or more risk indices, a risk field, or a risk map using data from the database, the image(s) of the tissue, and/or the 3D image in (b); and (d) using the risk information computed in (c) (e.g., and data from the database) to produce a 3D risk picture for the patient].

In certain embodiments, the medical images in the database comprise a series of medical images of a first patient taken over time (e.g., over the course of multiple visits to one or more doctors), and wherein the method comprises determining a value of at least a first risk index for each medical image of the series, thereby tracking determined values of at least the first risk index over time.

In certain embodiments, the receiving and storing of the medical images comprises repeatedly receiving and storing, over time, a plurality of medical images of the first patient, each obtained at a different time (e.g., at a different visit to one or more doctors), to obtain the series of medical images of the first patient.

In certain embodiments, the medical images comprise a single-photon emission computerized tomography (SPECT) scan of a first patient obtained (e.g., to identify one or more hotspots) following administration to the first patient of an imaging agent comprising 1404 labeled with ^{99m}Tc, and a computed tomography (CT) scan (e.g., to identify anatomical features) of the first patient, wherein the method comprises overlaying the SPECT scan with the CT scan to create a composite image (SPECT-CT) of the first patient.

In certain embodiments, the medical images comprises a positron emission tomography (PET) scan of a first patient obtained following administration to the first patient of an imaging agent comprising [18F]DCFPyL (DCFPyL labeled with ^{18}F), and a CT scan of the first patient, wherein the method comprises overlaying the PET scan with the CT scan to create a composite image (PET-CT) of the first patient.

In certain embodiments, the medical images comprise a whole-body scan (e.g., including anterior and posterior views) of a first patient made with a gamma camera following administration to the first patient of an imaging agent comprising technetium 99m methylenediphosphonate (^{99m}Tc MDP).

In certain embodiments, the medical images comprise a composite image of a first patient, the composite image comprising a CT scan overlaid with a nuclear medicine image (e.g., a SPECT scan; e.g., a PET scan) acquired at substantially the same time and following administration to the first patient of an imaging agent comprising a Prostate Specific Membrane Antigen (PSMA) binding agent comprising a radionuclide, wherein the method comprises automatically analyzing the composite image by: (a) using the composite image to geographically identify a 3D boundary for each of one or more regions of imaged tissue [e.g., organs (e.g., a prostate; e.g., a liver; e.g., lungs or a lung; e.g., lymph nodes), organ structures, sub-organs, organ regions, and/or other regions (e.g., one or more particular bones; e.g., a skeletal region of the patient), e.g., regions of interest] within the nuclear medicine image (e.g., such that portions of the nuclear medicine image falling within and/or outside of the 3D boundaries can be differentiated from each other); and (c) computing (i) a value of each of one or more risk indices and/or a (ii) risk map using the nuclear medicine image with the identified 3D boundaries of the one or more region(s).

In certain embodiments, step (c) comprises, for at least one risk index of the one or more risk indices, computing the value of the risk index by: determining, for each of the one or more regions, a corresponding cancerous tissue level within the region based on intensity values of the nuclear medicine image within the 3D boundary of the region (e.g., by identifying within the nuclear medicine image, a plurality of hotspots within the 3D boundary of the region and computing a total number of and/or a total volume of the identified hotspots); and computing the value of the risk index based on the determined cancerous tissue levels within the one or more regions.

In certain embodiments, the nuclear medicine image is a SPECT scan.

In certain embodiments, the imaging agent comprises a metal chelated to the PSMA binding agent, and wherein the metal is the radionuclide [e.g., wherein the metal is a radioisotope of technetium (Tc) (e.g., wherein the metal is technetium-99m (^{99m}Tc)); e.g., wherein the metal is a radioisotope of rhenium (Re) (e.g., wherein the metal is rhenium-188 (^{188}Re); e.g., wherein the metal is rhenium-186 (^{186}Re)); e.g., wherein the metal is a radioisotope of yttrium (Y) (e.g., wherein the metal is ^{90}Y); e.g., wherein the metal is a radioisotope of lutetium (Lu)(e.g., wherein the metal is ^{177}Lu); e.g., wherein the metal is a radioisotope of gallium (Ga) (e.g., wherein the metal is ^{68}Ga; e.g., wherein the metal is ^{67}Ga); e.g., wherein the metal is a radioisotope of indium (e.g., ^{111}In); e.g., wherein the metal is a radioisotope of copper (Cu) (e.g., wherein the metal is ^{67}Cu)].

In certain embodiments, the imaging agent comprises ^{99m}Tc-MIP-1404.

In certain embodiments, the nuclear medicine image is a PET scan.

In certain embodiments, the radionuclide is a radioisotope of a halogen [e.g., a radioisotope of fluorine (e.g., ^{18}F); e.g., a radioisotope of iodine (e.g., ^{123}I; e.g., ^{124}I; e.g., ^{125}I; e.g., ^{126}I; e.g., ^{131}I); e.g., a radioisotope of bromine (e.g., ^{75}Br; e.g., ^{76}Br; e.g., ^{77}Br; e.g., ^{80}Br; e.g., ^{80m}Br; e.g., ^{82}Br; e.g., ^{83}Br), e.g., a radioisotope of astatine (e.g., ^{211}At)].

In certain embodiments, the imaging agent comprises [18F]DCFPyL (DCFPyL labeled with ^{18}F).

In certain embodiments, the radionuclide is a radioisotope of gallium (Ga)(e.g., ^{68}Ga)

In certain embodiments, the medical images comprise a nuclear medicine image (e.g., a whole-body scan made with a gamma camera) of a first patient obtained following administration to the first patient of an imaging agent comprising a radionuclide (e.g., ^{99m}Tc)(e.g., wherein the imaging agent comprises ^{99m}Tc MDP), wherein the method comprises automatically analyzing the nuclear medicine image by: (a) geographically identifying a boundary (e.g., a 2D boundary; e.g., a 3D boundary) for each of one or more regions of imaged tissue [e.g., organs (e.g., a prostate; e.g., a liver; e.g., lungs or a lung; e.g., lymph nodes), organ structures, sub-organs, organ regions, and/or other regions (e.g., one or more particular bones; e.g., a skeletal region of the patient), e.g., regions of interest] within the nuclear medicine image (e.g., such that portions of the nuclear medicine image falling within and/or outside of the 3D boundaries can be differentiated from each other); and (c) computing (i) a value of each of one or more risk indices

and/or (ii) a risk map using the nuclear medicine image with the identified boundaries of the one or more region(s).

In certain embodiments, step (c) comprises, for at least one risk index of the one or more risk indices, computing the value of the risk index by: determining, for each of the one or more regions, a corresponding cancerous tissue level within the region based on intensity values of the nuclear medicine image within the boundary of the region (e.g., by identifying within the nuclear medicine image, a plurality of hotspots within the 3D boundary of the region and computing a total number of and/or a total volume of the identified hotspots); and computing the value of the risk index based on the determined cancerous tissue levels within the one or more regions.

In certain embodiments, the processor is a processor of a cloud-based system.

In certain embodiments, the processor is a processor of one or more network or Internet host servers.

In another aspect, the invention is directed to a system comprising: a processor (e.g., of a network or Internet host server or of a portable computing device); and a memory having instructions stored thereon, wherein the instructions, when executed by the processor, cause the processor to generate and cause display of an interactive graphical user interface (GUI) element (e.g., cause display of the GUI element on a laptop computer or on a remote computing device, e.g., via a mobile app), the GUI element having user-selectable and/or user-adjustable graphical controls (e.g., slider bars, option buttons, text bars, drop-down boxes, windows, animations, and/or any other GUI widget) for selecting and/or adjusting a digital presentation of a 3D risk picture of a patient for comparison with reference images (e.g., for use in communication of results to patient as a decision-making support) caused to be displayed by the processor (e.g., wherein the reference images displayed to the user or presented for selection by the user are tunable according to one or more predetermined variables associated with the patient, e.g., patient age, time since diagnosis, prior treatment, and/or future treatment).

In certain embodiments, the interactive GUI element is produced from medical images of the patient [e.g., comprising one or more of the following: targeted PET images, targeted SPECT images, magnetic resonance (MR) images, ultrasound (US) images, gamma camera (i.e. scintillation camera) images, and combinations, fusions, or derivatives of any of the above] and/or other images or information (e.g., other images received and stored in the database of the network-based decision support system of any of the aspects and/or embodiments described herein).

In another aspect, the invention is directed to a method for tracking prostate cancer progression and treatment efficacy over time, for one or more patient(s), the method comprising: (a) repeatedly receiving and storing in a database, over time, by a processor of a computing device (e.g., a server computing device), a plurality of medical images for each of the one or more patient(s) to obtain, for each of the one or more patient(s), a series of medical images taken over time (e.g., over the course of multiple visits to one or more doctors); (b) for each of the one or more patient(s), automatically analyzing, by the processor, the series of medical images for the patient to determine values of one or more risk indices [e.g., the values of the one or more risk indices corresponding to numeric values indicative of prostate cancer state and/or progression in the patient (e.g., numeric values identifying a particular cancer stage; e.g., numeric values corresponding to a determined overall survival rate for the patient)] for each medical image of the series, thereby tracking determined values of the one or more risk indices over a course prostate cancer progression and treatment for the patient; and (c) for each of the one or more patient(s), storing, by the processor, the determined values of the one or more risk indices for the patient for further processing and/or causing, by the processor, display of a graphical representation of the determined values of the one or more risk indices for the patient (e.g., causing display of a graph showing variation in the determined values of the one or more risk indices for the patient over time).

In certain embodiments, the series of medical images for a particular patient of the one or more patient(s) comprises: (i) a first image subseries comprising one or more medical images obtained using a first nuclear imaging modality (e.g., SPECT scans; e.g., composite SPECT-CT images) each following administration to the particular patient of a first radiopharmaceutical (e.g., ^{99m}Tc-MIP-1404) (e.g., wherein the first radiopharmaceutical facilitates imaging of localized disease, e.g., localized prostate cancer); and (ii) a second image subseries comprising one or more medical images obtained using a second nuclear imaging modality (e.g., PET scans; e.g., composite PET-CT images; e.g., whole-body scans) each following administration to the particular patient of a second radiopharmaceutical (e.g., [18F] DCFPyL; e.g., ^{99m}Tc MDP) (e.g., wherein the second radiopharmaceutical facilitates imaging of metastatic disease, e.g., metastatic prostate cancer), such that the values of the one or more risk indices determined in step (b) for the particular patient comprise a first subseries of values of a first risk index determined by automated analysis of the first image subseries and a second subseries of values of a second risk index determined by automated analysis of the second image subseries.

In certain embodiments, the medical images of first image subseries are obtained over a first period of time, when prostate cancer of the particular patient is localized (e.g., substantially localized to a prostate of the particular patient), and the medical images of the second image subseries are obtained over a second period of time, when prostate cancer of the particular patient is metastatic (e.g., having spread to regions of the patient outside of the prostate).

In certain embodiments, the first image subseries comprises one or more composite SPECT-CT image(s), each composite SPECT-CT image comprising a CT scan overlaid with a SPECT scan acquired at substantially the same time; the second image subseries comprises one or more composite PET-CT image(s), each composite PET-CT image comprising a CT scan overlaid with a PET scan acquired at substantially the same time; and step (b) comprises: automatically analyzing each of the one or more composite SPECT-CT images by: using the composite SPECT-CT image to geographically identify a 3D boundary of a prostate region (e.g., corresponding to a prostate of the patient) within the SPECT scan of the composite SPECT-CT image (e.g., such that portions of the nuclear medicine image falling within and/or outside of the 3D boundary of the prostate region can be differentiated from each other); and computing a value of the first risk index using the SPECT scan with the identified 3D boundary of the prostate region (e.g., computed based on a region of the SPECT scan corresponding to the identified 3D boundary of the prostate region); and automatically analyzing each of the one or more composite PET-CT images by: using the composite PET-CT image to geographically identify a 3D boundary of one or more metastatic regions within the PET scan of the composite PET-CT image, the one or metastatic regions including regions corresponding to patient tissue locations outside

of the prostate [e.g., organs (e.g., a prostate; e.g., a liver; e.g., lungs or a lung; e.g., lymph nodes), organ structures, sub-organs, organ regions, and/or other regions (e.g., one or more particular bones; e.g., a skeletal region corresponding to the patient's skeleton), e.g., regions of interest] (e.g., such that portions of the PET imaging scan falling within and/or outside of the 3D boundaries of the one or more metastatic region(s) can be differentiated from each other); and computing a value of the second risk index using the PET scan with the identified 3D boundaries of the one or more metastatic region(s).

In certain embodiments, the first image subseries comprises one or more composite SPECT-CT image(s), each composite SPECT-CT image comprising a CT scan overlaid with a SPECT scan acquired at substantially the same time; the second image subseries comprises one or more whole-body scan(s); and step (b) comprises: automatically analyzing each of the one or more composite SPECT-CT images by: using the composite SPECT-CT image to geographically identify a 3D boundary of a prostate region (e.g., corresponding to a prostate of the patient) within the SPECT scan of the composite SPECT-CT image (e.g., such that portions of the nuclear medicine image falling within and/or outside of the 3D boundary of the prostate region can be differentiated from each other); and computing a value of the first risk index using the SPECT scan with the identified 3D boundary of the prostate region (e.g., computed based on a region of the SPECT scan corresponding to the identified 3D boundary of the prostate region); and automatically analyzing each of the one or more whole-body scan(s) by: geographically identifying a boundary of one or more metastatic regions within the whole-body scan, the one or metastatic regions including regions corresponding to patient tissue locations outside of the prostate [(e.g., one or more particular bones; e.g., a skeletal region corresponding to the patient's skeleton), e.g., regions of interest] (e.g., such that portions of the whole-body scan falling within and/or outside of the boundaries of the one or more metastatic region(s) can be differentiated from each other); and computing a value of the second risk index using the PET scan with the identified 3D boundaries of the one or more metastatic region(s).

In another aspect, the invention is directed to a system for tracking prostate cancer progression and treatment efficacy over time, for one or more patient(s), the system comprising: a processor (e.g., of a network or Internet host server); and a memory having instructions stored thereon, wherein the instructions, when executed by the processor, cause the processor to: (a) repeatedly receive and store in a database, over time, a plurality of medical images for each of the one or more patient(s) to obtain, for each of the one or more patient(s), a series of medical images taken over time (e.g., over the course of multiple visits to one or more doctors); (b) for each of the one or more patient(s), automatically analyze the series of medical images for the patient to determine values of one or more risk indices [e.g., the values of the one or more risk indices corresponding to numeric values indicative of prostate cancer state and/or progression in the patient (e.g., numeric values identifying a particular cancer stage; e.g., numeric values corresponding to a determined overall survival rate for the patient)] for each medical image of the series, thereby tracking determined values of the one or more risk indices over a course prostate cancer progression and treatment for the patient; and (c) for each of the one or more patient(s), store the determined values of the one or more risk indices for the patient for further processing and/or cause display of a graphical representation of the determined values of the one or more risk indices for the patient (e.g., causing display of a graph showing variation in the determined values of the one or more risk indices for the patient over time).

In certain embodiments, the series of medical images for a particular patient of the one or more patient(s) comprises: (i) a first image subseries comprising one or more medical images obtained using a first nuclear imaging modality (e.g., SPECT scans; e.g., composite SPECT-CT images) each following administration to the particular patient of a first radiopharmaceutical (e.g., ^{99m}Tc-MIP-1404) (e.g., wherein the first radiopharmaceutical facilitates imaging of localized disease, e.g., localized prostate cancer); and (ii) a second image subseries comprising one or more medical images obtained using a second nuclear imaging modality (e.g., PET scans; e.g., composite PET-CT images; e.g., whole-body scans) each following administration to the particular patient of a second radiopharmaceutical (e.g., [18F] DCFPyL; e.g., ^{99m}Tc MDP) (e.g., wherein the second radiopharmaceutical facilitates imaging of metastatic disease, e.g., metastatic prostate cancer), such that the values of the one or more risk indices determined in step (b) for the particular patient comprise a first subseries of values of a first risk index determined by automated analysis of the first image subseries and a second subseries of values of a second risk index determined by automated analysis of the second image subseries.

In certain embodiments, the medical images of first image subseries are obtained over a first period of time, when prostate cancer of the particular patient is localized (e.g., substantially localized to a prostate of the particular patient), and the medical images of the second image subseries are obtained over a second period of time, when prostate cancer of the particular patient is metastatic (e.g., having spread to regions of the patient outside of the prostate).

In certain embodiments, the first image subseries comprises one or more composite SPECT-CT image(s), each composite SPECT-CT image comprising a CT scan overlaid with a SPECT scan acquired at substantially the same time; the second image subseries comprises one or more composite PET-CT image(s), each composite PET-CT image comprising a CT scan overlaid with a PET scan acquired at substantially the same time; and the instructions cause the processor to, at step (b): automatically analyze each of the one or more composite SPECT-CT images by: using the composite SPECT-CT image to geographically identify a 3D boundary of a prostate region (e.g., corresponding to a prostate of the patient) within the SPECT scan of the composite SPECT-CT image (e.g., such that portions of the nuclear medicine image falling within and/or outside of the 3D boundary of the prostate region can be differentiated from each other); and computing a value of the first risk index using the SPECT scan with the identified 3D boundary of the prostate region (e.g., computed based on a region of the SPECT scan corresponding to the identified 3D boundary of the prostate region); and automatically analyze each of the one or more composite PET-CT images by: using the composite PET-CT image to geographically identify a 3D boundary of one or more metastatic regions within the PET scan of the composite PET-CT image, the one or metastatic regions including regions corresponding to patient tissue locations outside of the prostate [e.g., organs (e.g., a prostate; e.g., a liver; e.g., lungs or a lung; e.g., lymph nodes), organ structures, sub-organs, organ regions, and/or other regions (e.g., one or more particular bones; e.g., a skeletal region corresponding to the patient's skeleton), e.g., regions of interest] (e.g., such that portions of the PET imaging scan

falling within and/or outside of the 3D boundaries of the one or more metastatic region(s) can be differentiated from each other); and computing a value of the second risk index using the PET scan with the identified 3D boundaries of the one or more metastatic region(s).

In certain embodiments, the first image subseries comprises one or more composite SPECT-CT image(s), each composite SPECT-CT image comprising a CT scan overlaid with a SPECT scan acquired at substantially the same time; the second image subseries comprises one or more whole-body scan(s); and the instructions cause the processor to, at step (b): automatically analyze each of the one or more composite SPECT-CT images by: using the composite SPECT-CT image to geographically identify a 3D boundary of a prostate region (e.g., corresponding to a prostate of the patient) within the SPECT scan of the composite SPECT-CT image (e.g., such that portions of the nuclear medicine image falling within and/or outside of the 3D boundary of the prostate region can be differentiated from each other); and computing a value of the first risk index using the SPECT scan with the identified 3D boundary of the prostate region (e.g., computed based on a region of the SPECT scan corresponding to the identified 3D boundary of the prostate region); and automatically analyze each of the one or more whole-body scan(s) by: geographically identifying a boundary of one or more metastatic regions within the whole-body scan, the one or metastatic regions including regions corresponding to patient tissue locations outside of the prostate [(e.g., one or more particular bones; e.g., a skeletal region corresponding to the patient's skeleton), e.g., regions of interest] (e.g., such that portions of the whole-body scan falling within and/or outside of the boundaries of the one or more metastatic region(s) can be differentiated from each other); and computing a value of the second risk index using the PET scan with the identified 3D boundaries of the one or more metastatic region(s).

Embodiments described with respect to one aspect of the invention may be, applied to another aspect of the invention (e.g., features of embodiments described with respect to one independent claim, e.g., a method claim, are contemplated to be applicable to other embodiments of other independent claims, e.g., a system claim, and vice versa).

BRIEF DESCRIPTION OF THE DRAWINGS

The foregoing and other objects, aspects, features, and advantages of the present disclosure will become more apparent and better understood by referring to the following description taken in conjunction with the accompanying drawings, in which:

FIG. **1** is a screenshot of a graphical user interface (GUI) showing mobile app icons for three cloud-based services, according to illustrative embodiments.

FIG. **2** is a schematic showing the relationship between a platform and a computing device (e.g., personal computer or mobile computing device, e.g., smart phone) running an application, according to illustrative embodiments of the invention.

FIG. **3** is a screenshot of a GUI window in the BSI Cloud application (displayed to a user) that allows a user to enter information about a patient and upload and/or access medical images for the patient, e.g., series of images obtained over a period of time, according to an illustrative embodiment.

FIG. **4** is a screenshot of a GUI window in the BSI Cloud application showing representative full body gamma camera images showing hotspots automatically identified by the system, with corresponding overall computed BSI values for a particular image set obtained at a given time, according to an illustrative embodiment.

FIG. **5** is a screenshot of a GUI window in the BSI Cloud application showing an automatically or semi-automatically generated radiologist report, which can be signed and dated by a radiologist, according to an illustrative embodiment.

FIG. **6** is a block diagram showing a set of functionalities offered by the a cloud-based platform and supported graphical user interface (GUI) decision-making tools described herein, according to an illustrative embodiment.

FIG. **7** is a block diagram of an exemplary cloud computing environment, used in certain embodiments.

FIG. **8** is a block diagram of an example computing device and an example mobile computing device used in certain embodiments.

FIG. **9** is block diagram of an example architecture for implementing the cloud based platform described herein, according to an illustrative embodiment.

FIG. **10** is a schematic showing stages of prostate cancer progression, along with various therapies and diagnostic imaging modalities appropriate for various disease states, according to an illustrative embodiment.

FIG. **11** is a block flow diagram of a process for tracking prostate cancer progression and treatment efficacy over time, according to an illustrative embodiment.

The features and advantages of the present disclosure will become more apparent from the detailed description set forth below when taken in conjunction with the drawings, in which like reference characters identify corresponding elements throughout. In the drawings, like reference numbers generally indicate identical, functionally similar, and/or structurally similar elements.

DETAILED DESCRIPTION

It is contemplated that systems, devices, methods, and processes of the claimed invention encompass variations and adaptations developed using information from the embodiments described herein. Adaptation and/or modification of the systems, devices, methods, and processes described herein may be performed by those of ordinary skill in the relevant art.

Throughout the description, where articles, devices, and systems are described as having, including, or comprising specific components, or where processes and methods are described as having, including, or comprising specific steps, it is contemplated that, additionally, there are articles, devices, and systems of the present invention that consist essentially of, or consist of, the recited components, and that there are processes and methods according to the present invention that consist essentially of, or consist of, the recited processing steps.

It should be understood that the order of steps or order for performing certain action is immaterial so long as the invention remains operable. Moreover, two or more steps or actions may be conducted simultaneously.

The mention herein of any publication, for example, in the Background section, is not an admission that the publication serves as prior art with respect to any of the claims presented herein. The Background section is presented for purposes of clarity and is not meant as a description of prior art with respect to any claim.

Headers are provided for the convenience of the reader—the presence and/or placement of a header is not intended to limit the scope of the subject matter described herein.

A. Medical Imaging Modalities, Associated Radiopharmaceuticals, and Computed Risk Indices

FIG. **1** shows mobile app icons **100** for three cloud-based services, according to illustrative embodiments. As described in the following, the cloud-based services of the platform described herein provide for processing and analysis of medical images in a fully automated fashion and/or in combination with a user interaction (e.g., in a semi-automated fashion). The medical images include nuclear medicine images, obtained using a nuclear imaging modality such as whole-body scans with a gamma camera, Positron Emission Tomography (PET) scans, and Single-Photon Emission Tomography (SPECT) scans.

In certain embodiments, nuclear medicine images use imaging agents comprising radiopharmaceuticals. Nuclear medicine images are obtained following administration of a radiopharmaceutical to a patient, and provide information regarding the distribution of the radiopharmaceutical within the patient. Radiopharmaceuticals are compounds that comprise a radionuclide.

As used herein, "radionuclide" refers to a moiety comprising a radioactive isotope of at least one element. Exemplary suitable radionuclides include but are not limited to those described herein. In some embodiments, a radionuclide is one used in positron emission tomography (PET). In some embodiments, a radionuclide is one used in single-photon emission computed tomography (SPECT). In some embodiments, a non-limiting list of radionuclides includes ^{99m}Tc, ^{111}In, ^{64}Cu, ^{67}Ga, ^{68}Ga, ^{186}Re, ^{188}Re, ^{153}Sm, ^{177}Lu, ^{67}Cu, ^{12}I, ^{124}I, ^{125}I, ^{126}I, ^{131}I, ^{11}C, ^{13}N, ^{15}O, ^{18}F, ^{153}Sm, ^{166}Ho, ^{177}Lu, ^{149}Pm, ^{90}Y, ^{213}Bi, ^{103}Pd, ^{109}Pd, ^{159}Gd, ^{140}La, ^{198}Au, ^{199}Au, ^{169}Yb, ^{175}Yb, ^{165}Dy, ^{166}Dy, ^{105}Rh, ^{111}Ag, ^{89}Zr, ^{225}Ac, ^{82}Rb, ^{75}Br, ^{76}Br, ^{77}Br, ^{80}Br, ^{80m}Br, ^{82}Br, ^{83}Br, ^{211}At and ^{192}Ir.

As used herein, the term "radiopharmaceutical" refers to a compound comprising a radionuclide. In certain embodiments, radiopharmaceuticals are used for diagnostic and/or therapeutic purposes. In certain embodiments, radiopharmaceuticals include small molecules that are labeled with one or more radionuclide(s), antibodies that are labeled with one or more radionuclide(s), and antigen-binding portions of antibodies that are labeled with one or more radionuclide(s).

Nuclear medicine images (e.g., PET scans; e.g., SPECT scans; e.g., whole-body scans; e.g. composite PET-CT images; e.g., composite SPECT-CT images) detect radiation emitted from the radionuclides of radiopharmaceuticals to form an image. The distribution of a particular radiopharmaceutical within a patient may be determined by biological mechanisms such as blood flow or perfusion, as well as by specific enzymatic or receptor binding interactions. Different radiopharmaceuticals may be designed to take advantage of different biological mechanisms and/or particular specific enzymatic or receptor binding interactions and thus, when administered to a patient, selectively concentrate within particular types of tissue and/or regions within the patient. Greater amounts of radiation are emitted from regions within the patient that have higher concentrations of radiopharmaceutical than other regions, such that these regions appear brighter in nuclear medicine images. Accordingly, intensity variations within a nuclear medicine image can be used to map the distribution of radiopharmaceutical within the patient. This mapped distribution of radiopharmaceutical within the patient can be used to, for example, infer the presence of cancerous tissue within various regions of the patient's body.

For example, upon administration to a patient, technetium 99m methylenediphosphonate (^{99m}Tc MDP) selectively accumulates within the skeletal region of the patient, in particular at sites with abnormal osteogenesis associated with malignant bone lesions. The selective concentration of radiopharmaceutical at these sites produces identifiable hotspots—localized regions of high intensity in nuclear medicine images. Accordingly, presence of malignant bone lesions associated with metastatic prostate cancer can be inferred by identifying such hotspots within a whole-body scan of the patient. As described in the following, risk indices that correlate with patient overall survival and other prognostic metrics indicative of disease state, progression, treatment efficacy, and the like, can be computed based on automated analysis of intensity variations in whole-body scans obtained following administration of ^{99m}Tc MDP to a patient. In certain embodiments, other radiopharmaceuticals can also be used in a similar fashion to ^{99m}Tc MDP.

In certain embodiments, the particular radiopharmaceutical used depends on the particular nuclear medicine imaging modality used. For example ^{18}F sodium fluoride (NaF) also accumulates in bone lesions, similar to ^{99m}Tc MDP, but can be used with PET imaging. In certain embodiments, PET imaging may also utilize a radioactive form of the vitamin choline, which is readily absorbed by prostate cancer cells.

In certain embodiments, radiopharmaceuticals that selectively bind to particular proteins or receptors of interest—particularly those whose expression is increased in cancerous tissue may be used. Such proteins or receptors of interest include, but are not limited to tumor antigens, such as CEA, which is expressed in colorectal carcinomas, Her2/neu, which is expressed in multiple cancers, BRCA 1 and BRCA 2, expressed in breast and ovarian cancers; and TRP-1 and -2, expressed in melanoma.

For example, human prostate-specific membrane antigen (PSMA) is upregulated in prostate cancer, including metastatic disease. PSMA is expressed by virtually all prostate cancers and its expression is further increased in poorly differentiated, metastatic and hormone refractory carcinomas. Accordingly, radiopharmaceuticals corresponding to PSMA binding agents (e.g., compounds that a high affinity to PSMA) labelled with one or more radionuclide(s) can be used to obtain nuclear medicine images of a patient from which the presence and/or state of prostate cancer within a variety of regions (e.g., including, but not limited to skeletal regions) of the patient can be assessed. In certain embodiments, nuclear medicine images obtained using PSMA binding agents are used to identify the presence of cancerous tissue within the prostate, when the disease is in a localized state. In certain embodiments, nuclear medicine images obtained using radiopharmaceuticals comprising PSMA binding agents are used to identify the presence of cancerous tissue within a variety of regions that include not only the prostate, but also other organs and tissue regions such as lungs, lymph nodes, and bones, as is relevant when the disease is metastatic.

In particular, upon administration to a patient, radionuclide labelled PSMA binding agents selectively accumulate within cancerous tissue, based on their affinity to PSMA. In a similar manner to that described above with regard to ^{99m}Tc MDP, the selective concentration of radionuclide labelled PSMA binding agents at particular sites within the patient produces detectable hotspots in nuclear medicine images. As PSMA binding agents concentrate within a variety of cancerous tissues and regions of the body expressing PSMA, localized cancer within a prostate of the patient and/or metastatic cancer in various regions of the patient's body can be detected, and evaluated. As described in the following, risk indices that correlate with patient overall survival and other prognostic metrics indicative of disease state, progression, treatment efficacy, and the like, can be

computed based on automated analysis of intensity variations in nuclear medicine images obtained following administration of a PSMA binding agent radiopharmaceutical to a patient.

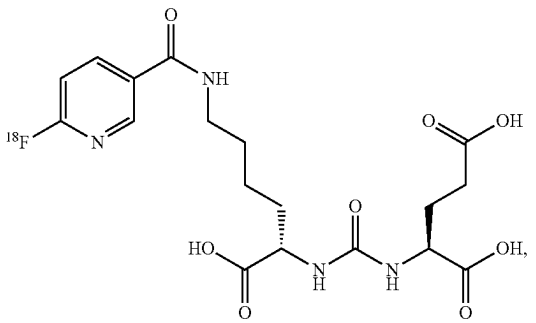
A variety of radionuclide labelled PSMA binding agents may be used as radiopharmaceutical imaging agents for nuclear medicine imaging to detect and evaluate prostate cancer. In certain embodiments, the particular radionuclide labelled PSMA binding agent that is used depends on factors such as the particular imaging modality (e.g., PET; e.g., SPECT) and the particular regions (e.g., organs) of the patient to be imaged. For example, certain radionuclide labelled PSMA binding agents are suited for PET imaging, while others are suited for SPECT imaging. For example, certain radionuclide labelled PSMA binding agents facilitate imaging a prostate of the patient, and are used primarily when the disease is localized, while others facilitate imaging organs and regions throughout the patient's body, and are useful for evaluating metastatic prostate cancer.

A variety of PSMA binding agents and radionuclide labelled versions thereof are described in U.S. Pat. Nos. 8,778,305, 8,211,401, and 8,962,799, each of which are incorporated herein by reference in their entireties.

A.i PET Imaging Radionuclide Labelled PSMA Binding Agents

In certain embodiments, the radionuclide labelled PSMA binding agent is a radionuclide labelled PSMA binding agent appropriate for PET imaging.

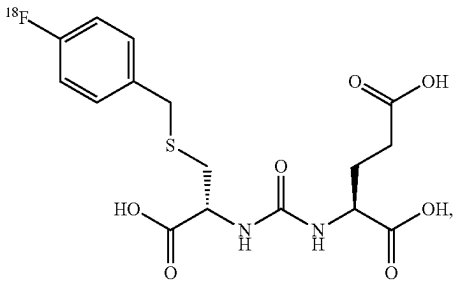
In certain embodiments, the radionuclide labelled PSMA binding agent comprises [18F]DCFPyL (also referred to as PyL™; also referred to as DCFPyL-18F):



[18F]DCFPyL

or a pharmaceutically acceptable salt thereof.

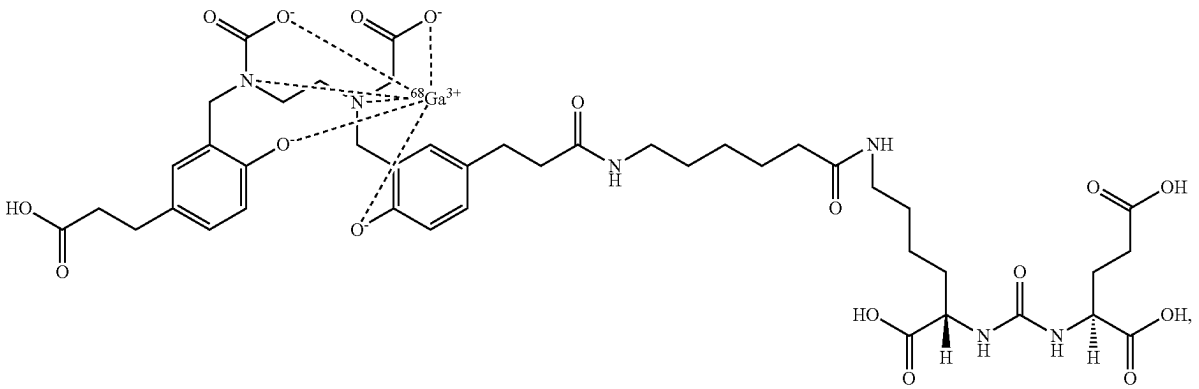
In certain embodiments, the radionuclide labelled PSMA binding agent comprises [18F]DCFBC:



[18F]DCFBC

or a pharmaceutically acceptable salt thereof.

In certain embodiments, the radionuclide labelled PSMA binding agent comprises ^{68}Ga-PSMA-HBED-CC (also referred to as ^{68}Ga-PSMA-11):

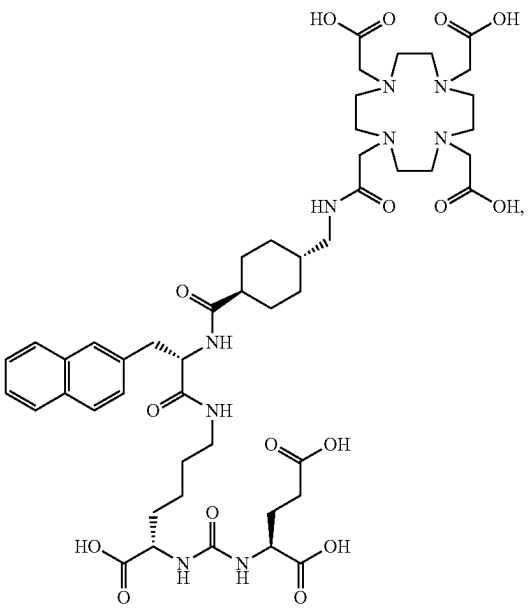


^{68}Ga-PSMA-HBED-CC

or a pharmaceutically acceptable salt thereof.

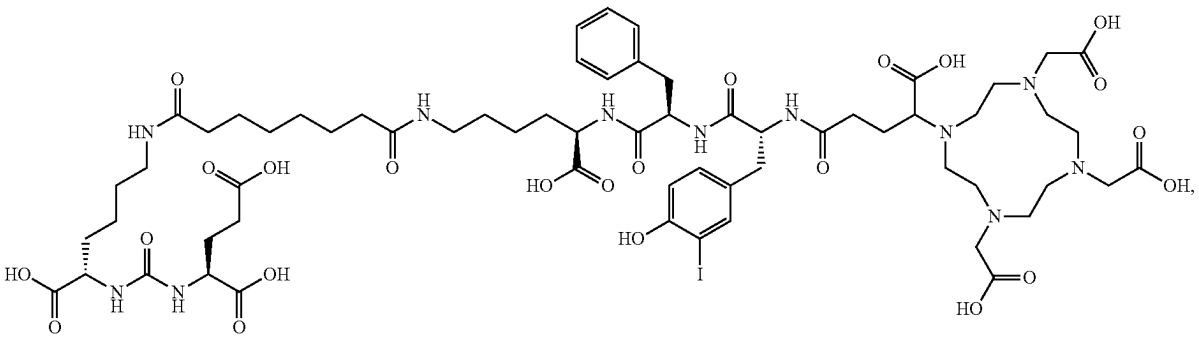
In certain embodiments, the radionuclide labelled PSMA binding agent comprises PSMA-617:

PSMA-617



or a pharmaceutically acceptable salt thereof. In certain embodiments, the radionuclide labelled PSMA binding agent comprises ^{68}Ga-PSMA-617, which is PSMA-617 labelled with ^{68}Ga, or a pharmaceutically acceptable salt thereof. In certain embodiments, the radionuclide labelled PSMA binding agent comprises ^{177}Lu-PSMA-617, which is PSMA-617 labelled with ^{177}Lu, or a pharmaceutically acceptable salt thereof.

In certain embodiments, the radionuclide labelled PSMA binding agent comprises PSMA-I&T:

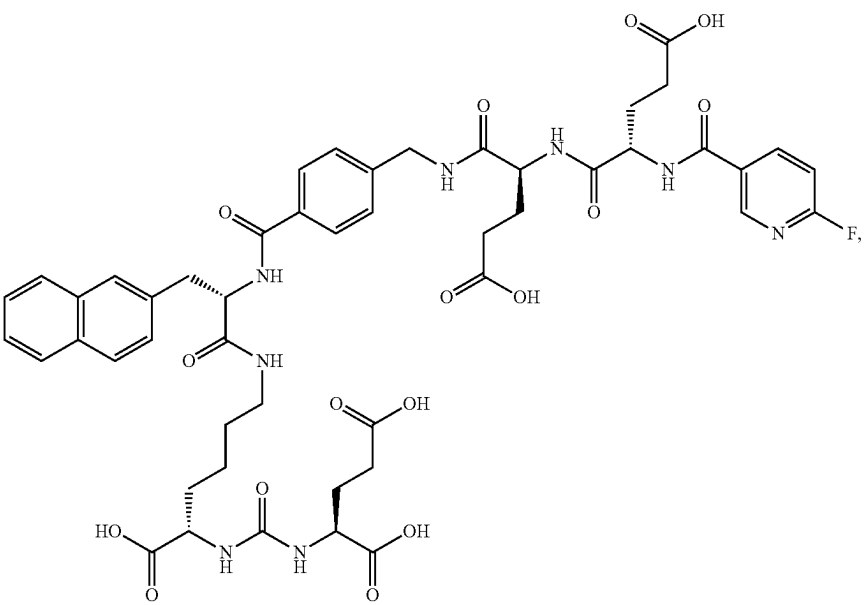


PSMA-I & T

or a pharmaceutically acceptable salt thereof. In certain embodiments, the radionuclide labelled PSMA binding agent comprises ^{68}Ga-PSMA-I&T, which is PSMA-I&T labelled with ^{68}Ga, or a pharmaceutically acceptable salt thereof.

In certain embodiments, the radionuclide labelled PSMA binding agent comprises PSMA-1007:

PSMA-1007



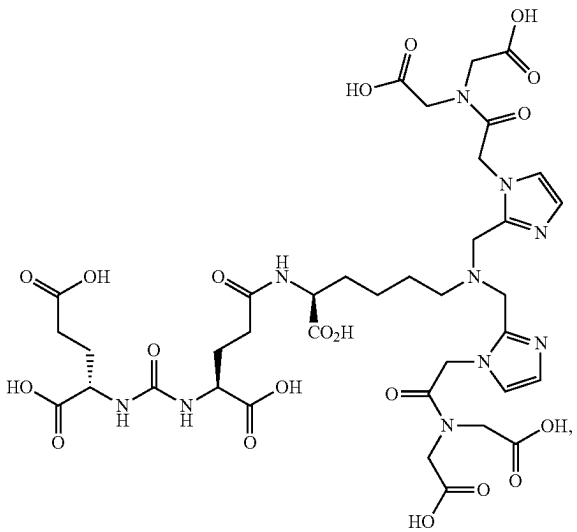
or a pharmaceutically acceptable salt thereof. In certain embodiments, the radionuclide labelled PSMA binding agent comprises ^{18}F-PSMA-1007, which is PSMA-1007 labelled with ^{18}F, or a pharmaceutically acceptable salt thereof.

A.ii SPECT Imaging Radionuclide Labelled PSMA Binding Agents

In certain embodiments, the radionuclide labelled PSMA binding agent is a radionuclide labelled PSMA binding agent appropriate for SPECT imaging.

In certain embodiments, the radionuclide labelled PSMA binding agent comprises 1404 (also referred to as MIP-1404):

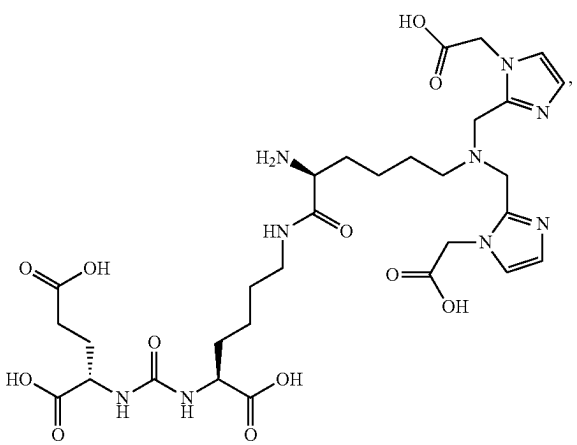
1404



or a pharmaceutically acceptable salt thereof.

In certain embodiments, the radionuclide labelled PSMA binding agent comprises 1405 (also referred to as MIP-1405):

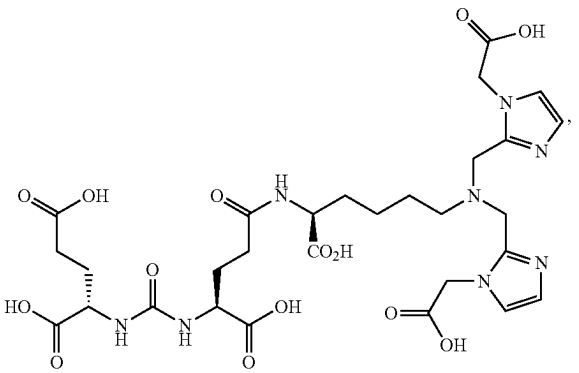
1405



or a pharmaceutically acceptable salt thereof.

In certain embodiments, the radionuclide labelled PSMA binding agent comprises 1427 (also referred to as MIP-1427):

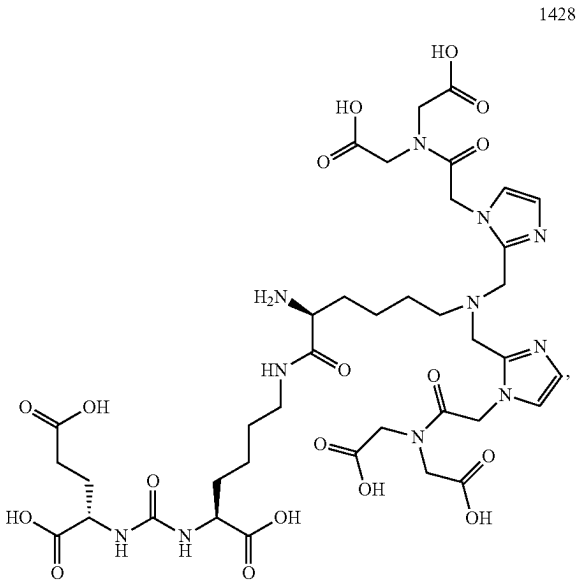
1427



or a pharmaceutically acceptable salt thereof.

In certain embodiments, the radionuclide labelled PSMA binding agent comprises 1428 (also referred to as MIP-1428):

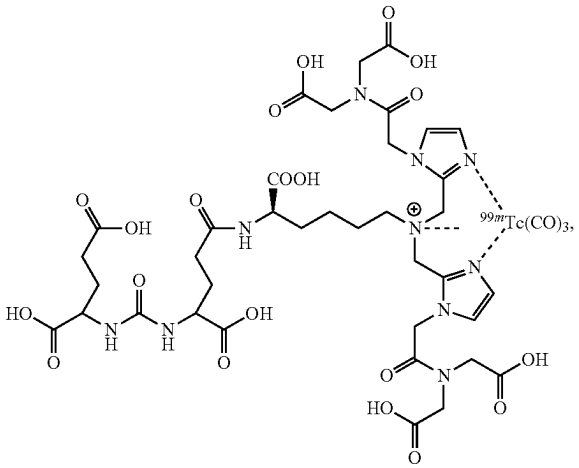
1428



or a pharmaceutically acceptable salt thereof.

In certain embodiments, the PSMA binding agent is labelled with a radionuclide by chelating it to a radioisotope of a metal [e.g., a radioisotope of technetium (Tc) (e.g., technetium-99m (^{99m}Tc)); e.g., a radioisotope of rhenium (Re) (e.g., rhenium-188 (^{188}Re); e.g., rhenium-186 ($^{186}_{Re}$)); e.g., a radioisotope of yttrium (Y) (e.g., ^{90}Y); e.g., a radioisotope of lutetium (Lu)(e.g., ^{177}Lu); e.g., a radioisotope of gallium (Ga) (e.g., ^{68}Ga; e.g., ^{67}Ga); e.g., a radioisotope of indium (e.g., ^{111}In); e.g., a radioisotope of copper (Cu) (e.g., ^{67}Cu)].

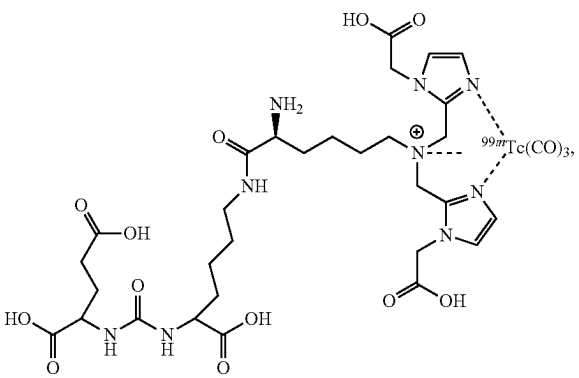
In certain embodiments, 1404 is labelled with a radionuclide (e.g., chelated to a radioisotope of a metal). In certain embodiments, the radionuclide labelled PSMA binding agent comprises ^{99m}Tc-MIP-1404, which is 1404 labelled with (e.g., chelated to) ^{99m}Tc:



^{99m}Tc-MIP-1404

or a pharmaceutically acceptable salt thereof. In certain embodiments, 1404 may be chelated to other metal radioisotopes [e.g., a radioisotope of rhenium (Re) (e.g., rhenium-188 (^{188}Re); e.g., rhenium-186 (^{186}Re)); e.g., a radioisotope of yttrium (Y) (e.g., ^{90}Y); e.g., a radioisotope of lutetium (Lu)(e.g., ^{177}Lu); e.g., a radioisotope of gallium (Ga) (e.g., ^{68}Ga; e.g., ^{67}Ga); e.g., a radioisotope of indium (e.g., ^{111}In); e.g., a radioisotope of copper (Cu) (e.g., ^{67}Cu)] to form a compound having a structure similar to the structure shown above for ^{99m}Tc-MIP-1404, with the other metal radioisotope substituted for ^{99m}Tc.

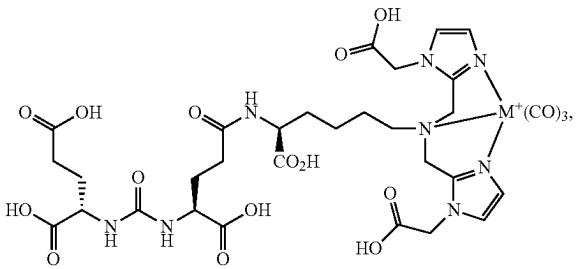
In certain embodiments, 1405 is labelled with a radionuclide (e.g., chelated to a radioisotope of a metal). In certain embodiments, the radionuclide labelled PSMA binding agent comprises ^{99m}Tc-MIP-1405, which is 1405 labelled with (e.g., chelated to)^{99m}Tc:



^{99m}Tc-MIP-1405

or a pharmaceutically acceptable salt thereof. In certain embodiments, 1405 may be chelated to other metal radioisotopes [e.g., a radioisotope of rhenium (Re) (e.g., rhenium-188 (^{188}Re); e.g., rhenium-186 (^{186}Re)); e.g., a radioisotope of yttrium (Y) (e.g., ^{90}Y); e.g. a radioisotope of lutetium (Lu)(e.g., ^{177}Lu); e.g., a radioisotope of gallium (Ga) (e.g., ^{68}Ga; e.g. ^{67}Ga); e.g., a radioisotope of indium (e.g., ^{111}In); e.g., a radioisotope of copper (Cu) (e.g., ^{67}Cu)] to form a compound having a structure similar to the structure shown above for ^{99m}Tc-MIP-1405, with the other metal radioisotope substituted for ^{99m}Tc.

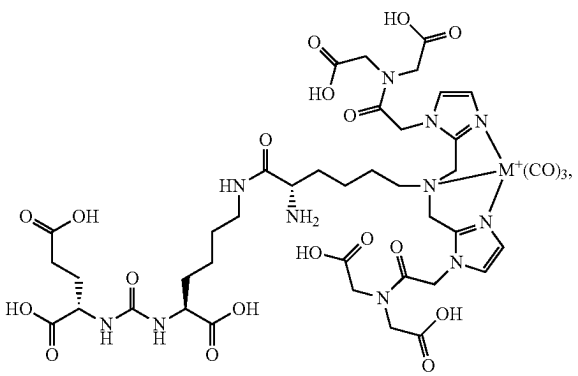
In certain embodiments, 1427 is labelled with (e.g., chelated to) a radioisotope of a metal, to form a compound according to the formula below:



1427 chelated to a metal

or a pharmaceutically acceptable salt thereof, wherein M is a metal radioisotope [e.g., a radioisotope of technetium (Tc) (e.g., technetium-99m (^{99m}Tc)); e.g., a radioisotope of rhenium (Re) (e.g., rhenium-188 (^{188}Re); e.g., rhenium-186 (^{186}Re)); e.g., a radioisotope of yttrium (Y) (e.g., ^{90}Y); e.g., a radioisotope of lutetium (Lu)(e.g., ^{177}Lu); e.g., a radioisotope of gallium (Ga) (e.g., ^{68}Ga; e.g., ^{67}Ga); e.g., a radioisotope of indium (e.g., In); e.g., a radioisotope of copper (Cu) (e.g., ^{67}Cu)] with which 1427 is labelled.

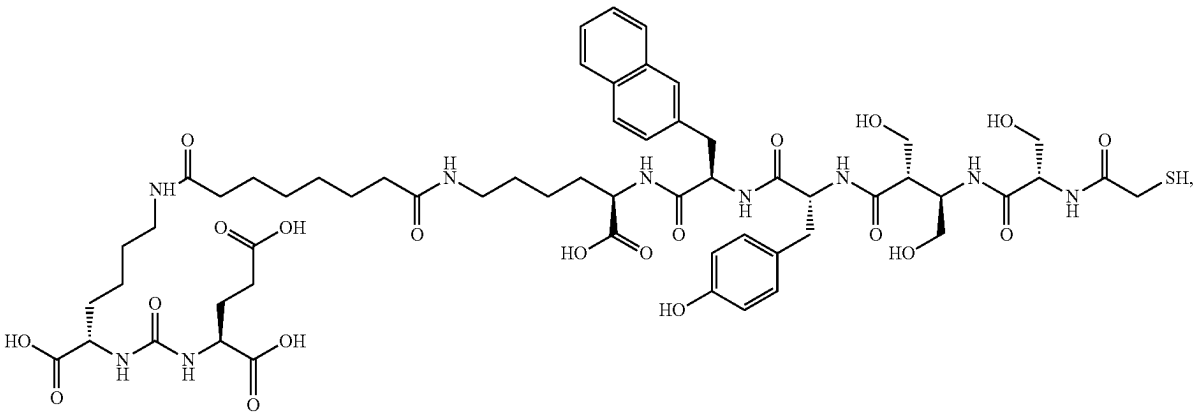
In certain embodiments, 1428 is labelled with (e.g., chelated to) a radioisotope of a metal, to form a compound according to the formula below:



1428 chelated to a metal

or a pharmaceutically acceptable salt thereof, wherein M is a metal radioisotope [e.g., a radioisotope of technetium (Tc) (e.g., technetium-99m (^{99m}Tc)); e.g., a radioisotope of rhenium (Re) (e.g., rhenium-188 (^{188}Re); e.g., rhenium-186 (^{186}Re)); e.g., a radioisotope of yttrium (Y) (e.g., ^{90}Y); e.g., a radioisotope of lutetium (Lu)(e.g., ^{177}Lu); e.g., a radioisotope of gallium (Ga) (e.g., ^{68}Ga; e.g., ^{67}Ga); e.g., a radioisotope of indium (e.g., In); e.g., a radioisotope of copper (Cu) (e.g., ^{67}Cu)] with which 1428 is labelled.

In certain embodiments, the radionuclide labelled PSMA binding agent comprises PSMA I&S:



PSMA I & S

or a pharmaceutically acceptable salt thereof. In certain embodiments, the radionuclide labelled PSMA binding agent comprises ^{99m}Tc-PSMA I&S, which is PSMA I&S labelled with ^{99m}Tc, or a pharmaceutically acceptable salt thereof.

A.iii Whole-Body Bone Scans

Turning to FIG. **1**, BSI Cloud **130** refers to a cloud-based decision support system that implements BSI values. BSI refers to bone scan index, which is a value computed from a method for detecting skeletal lesions from whole-body scanning (and anterior and posterior views) with a gamma camera following administration of the radionuclide technetium 99m methylenediphosphonate (^{99m}Tc MDP). Further explanation of BSI is provided, for example, in U.S. Pat. No. 8,855,387, which is incorporated herein by reference in its entirety, as well as in U.S. patent application Ser. No. 15/282,422, filed Sep. 30, 2016, which is incorporated herein by reference in its entirety.

In particular, BSI is computed from whole-body scans by segmenting anterior and posterior views of the whole-body scan of the patient to geographically identify boundaries of regions within the views that correspond to various portions of the patient's skeleton. Segmentation of the patient's skeleton can be performed using a variety of approaches, such as the Active Shape Model-based approach and the atlas image registration approach (which registers the anterior and posterior views of a whole body scan with reference anterior and posterior views of a reference whole body scan that have already been segmented (referred to as an atlas image)) described in U.S. Pat. No. 8,855,387. Other approaches, based on machine learning techniques (e.g., artificial neural networks (ANNs); e.g., convolutional neural networks (CNNs)) may also be used.

The BSI value is computed based on the intensity values of whole-body scan within the identified boundaries of the various skeletal regions. As discussed above, hotspots that correspond to localized regions of high intensity within the views (anterior and/or posterior views) of the whole-body scan can be detected. Hotspots may be detected and/or classified as corresponding to cancerous lesions (e.g., metastases) using a variety of approaches, including, as described in U.S. Pat. No. 8,855,387, machine learning techniques such as ANNs.

Hotspots corresponding to cancerous tissue lesions within the patient's skeleton, once detected, can be used to determine a risk index that provides a measure of disease state for the patient. For example, cancerous tissue levels within one or more regions, such as particular bones and/or the overall skeletal region, can be determined based on features of detected hotspots (e.g., detected hotspots classified as metastases). For example, a cancerous tissue level within a region (e.g., a particular bone; e.g., the overall skeletal region) may be determined based on (e.g., as a function of) a total number of detected hotspots within the region, a total volume of detected hotspots within the region, an average intensity of detected hotspots, a maximal intensity of detected hotspots, and the like, as well as combinations thereof. Properties of the one or more regions, such as their area or volume may also be used. For example, a total number and/or total volume of detected hotspots may be normalized (e.g., divided) by a volume and/or area of the region in which they are detected. A risk index may be determined based on the determined cancerous tissue levels within one or more regions, directly, e.g., as the cancerous tissue level within a single region, or determined from cancerous tissue levels in multiple regions (e.g., as an average; e.g., as a scaled sum; e.g., as a ratio; etc.), or even using machine learning approaches.

For example, the BSI value is a risk index that is a numeric value that quantifies the fraction of the total skeleton of the patient that is involved by cancerous tissue (e.g., tumors), based on the detected hotspots. The BSI value can be compared between different patients, and used as an objective measure of disease state and risk for a particular patient. Notably, since BSI is computed in an automated fashion, variability due to human factors such as radiologist interpretation of images is avoided.

Moreover, a variety of actionable information can be obtained from a patient's BSI value. For example, BSI can be correlated with prognostic values that provide a measure of disease state, progression, life expectancy (e.g., overall survival), treatment efficacy, and the like for the patient. Accordingly, a patient's BSI value can be used and tracked over time (e.g., over the course of multiple visits to one or more doctors) to provide them or their physician with an objective metric of what state their cancer is in, how fast it is progressing, what their outlook is, and whether one or more particular treatments are proving effective.

A.iv Positron Emission Tomography (PET) Scans

PyL Cloud **120** refers to a cloud-based system that uses medical images obtained with the agent PyL™, which is DCFPyL labeled with ^{18}F ([18F]DCFPyL). The patient,

after injection of the imaging agent, receives a positron emission tomography (PET) scan to identify hot spots, and a CT scan. Further information about the PyL™ imaging agent is provided above, and, for example, in U.S. Pat. No. 8,778,305, which is incorporated herein by reference in its entirety.

In certain embodiments, the PET scan and the CT scan are combined as a composite image comprising the CT scan overlaid with the PET scan. As used herein, overlaying one image (e.g., a CT scan) with another (e.g., a PET scan) refers to establishing a mapping between coordinates and/or pixels or voxels of the two images that that represent the same physical locations (e.g., within the patient). CT scans provide accurate anatomical information in the form of detailed three-dimensional (3D) images of internal organs, bones, soft tissue, and blood vessels. Accordingly, 3D boundaries of specific regions of imaged tissue can be accurately identified by analysis of CT scans. For example, automated segmentation of CT scans can be performed to identify 3D boundaries of specific organs (e.g., a prostate, lymph nodes, a lung or lungs), sub-organs, organ regions, as well as other regions of imaged tissue, such as particular bones and an overall skeletal region of the patient. Automated segmentation of CT scans can be accomplished via a variety of approaches, include machine learning techniques [e.g., ANN-based approaches (including, e.g., convolutional neural networks (CNNs))], atlas image registration, and combinations thereof. In certain embodiments, manual segmentation of CT images can also be utilized, alone or in combination with automated segmentation approaches (e.g., to refine 3D boundaries identified via automated segmentation; e.g., to provide an initial starting point for an automated segmentation approach).

Once the 3D boundaries of various regions are identified within a CT scan of a composite image, by virtue of the mapping between the CT scan and PET scan of the composite image, the identified 3D boundaries can be transferred to the PET image. Accordingly, regions of the PET image falling within and/or outside of the identified 3D boundaries can be accurately identified.

In certain embodiments, composite images comprising CT scans overlaid with PET scans are obtained using dedicated PET-CT scanner instruments common in many hospitals, and are uploaded as medical images to the cloud-based platform described herein. In certain embodiments, a PET scan and a corresponding CT scan are obtained separately (but at substantially the same time), and uploaded to the cloud-based platform described herein. In such cases, the separately obtained PET and CT scans can be automatically fused to create a composite image.

In certain embodiments, once the 3D boundaries of the various regions are identified within the PET scan, one or more risk indices can be computed in a similar fashion to that described above with regard to BSI. In particular, in certain embodiments, intensity values of the PET scan in relation to (e.g., within and/or outside of) the 3D boundaries of the identified regions can be used to determine levels of cancerous tissue within the identified regions, e.g., based on features of detected hotspots (e.g., detected hotspots corresponding to metastases). Risk indices can then be computed based on the determined cancerous tissue levels. For example, hotspots within the PET scan can be identified, and, based on features such as their size, number, and distribution with respect to the identified regions, used to compute one or more risk indices. As with BSI, risk indices determined from PET scans can be correlated with prognostic values and tracked over time (e.g., over the course of multiple visits to one or more doctors) to provide patients or their physician with an objective metric of what state their cancer is in, how fast it is progressing, what their outlook is, and whether one or more particular treatments are proving effective. The approaches described herein with regard to PET imaging using PyL™ as a radiopharmaceutical can be applied to a variety of other radiopharmaceuticals, such as those described above, including, without limitation NaF, radioisotopes of choline, and any of the PSMA binding agents described in section A.i above.

A.v Single-Photon Emission Computerized Tomography (SPECT) Scans

1404 Cloud **130** refers to a cloud-based system that uses medical images obtained with the agent ^{99m}Tc-MIP-1404, which, as described above, is 1404 labeled with Tc^{99m}. After injection of the imaging agent, the patient receives a single-photon emission computerized tomography (SPECT) scan, e.g., to identify hot spots, and a computed tomography (CT) scan, e.g., to identify anatomical features. These images are overlaid to make a composite image (SPECT/CT). Further information about ^{99m}Tc-MIP-1404 imaging agent is provided above, and, for example, in U.S. Pat. Nos. 8,211,401 and 8,962,799, both of which are incorporated herein by reference in their entireties.

SPECT and CT scans can be analyzed in a manner similar to that described above with respect to PET and CT scans, in order to determine one or more risk indices. In particular, as with PET and CT scans, the SPECT scan and the CT scan can be combined in a composite image in which the CT scan is overlaid with the SPECT scan—a composite SPECT-CT image. As with composite PET-CT images, composite SPECT-CT images may be directly received as medical images by the cloud-based platform described herein (e.g., having been obtained via dedicated SPECT-CT imager in a hospital), or may be created by the cloud-based platform following receipt of separate SPECT scans and CT scans.

Similar to PET-CT images, 3D boundaries of various regions of imaged tissue can be identified within the SPECT image by virtue of the overlay with the CT image of the composite image. Intensity variations within the SPECT image, in relation to the 3D boundaries can be used to compute one or more risk indices. As with the approaches for computing risk indices from composite PET-CT images, this may comprise determine levels of cancerous tissue within the identified regions, for example by detecting hotspots within the 3D boundaries of the identified regions. Such risk indices can be correlated with prognostic values and tracked over time (e.g., over the course of multiple visits to one or more doctors) to provide patients or their physician with an objective metric of what state their cancer is in, how fast it is progressing, what their outlook is, and whether one or more particular treatments are proving effective. The approaches described herein with regard to SPECT imaging using ^{99m}Tc-MIP-1404 as a radiopharmaceutical can be applied to a variety of other radiopharmaceuticals, such as those described above, including, without limitation, any of the PSMA binding agents described in section A.ii above

B. Platform Services and Computing Device Components

FIG. **2** is a schematic 200 showing the relationship between a platform and a computing device (e.g., personal computer or mobile computing device, e.g., smart phone) running an application, according to illustrative embodiments of the invention. The platform performs various services, for example, user authentication ("Auth"), image and other data storage ("SliceBox"), and the like—many more services than those shown may be provided. The

applications may have both a platform component and a device component (e.g., native app on the client device).

FIG. **9** shows an example architecture **900** for implementing the cloud-based platform described herein, and providing various services such as the BSI Cloud, PyL Cloud, and 1404 Cloud services described above. The architecture shown in FIG. **9** can be used to implement the platform described herein on a variety of datacenters, including publicly available datacenters. The datacenter provides infrastructure in the form of servers and networks and provides services for e.g. networking, messaging, authentication, logging and storage. The architecture **900** for the platform uses a series of functional units with limited scope referred to as microservices. Each microservice handles an isolated set of tasks such as image storage, calculation of a risk index, identification of medical image type, and other tasks. Services (e.g., microservices) can communicate with each other using standard protocols such as Hypertext Transfer Protocol (HTTP). Organizing the platform into a network of microservices, as shown in the architecture **900** of FIG. **9**, allows for parts of the platform to be scaled individually to meet high demand and to ensure minimal downtime.

In certain embodiments, such an architecture allows for components to be improved or replaced without affecting other parts of the platform. The example architecture **900** shown in FIG. **9** includes a set **920** of microservices that that are common to two or more applications in the platform. The left **910** and right **930** panels show microservices in two applications. The microservice network shown in the left panel **910** implements a version of the BSI Cloud service, as described above, and provides for calculation of an automated BSI index (aBSI), which is a risk index derived from automated analysis of whole-body scans obtained with a gamma camera. The microservice network shown in the right panel **930** implements a version of the 1404 Cloud service, as described above, and provides for automated calculation of a SPECT index, which is a risk index derived from automated analysis of composite SPECT-CT images.

C. Image Collection, Analysis, and Result Presentation

FIG. **3** is a GUI window **300** in the BSI Cloud application (displayed to a user) that allows a user to enter information about a patient and upload and/or access medical images for the patient, e.g., series of images obtained over a period of time.

FIG. **4** is a GUI window **400** in the BSI Cloud application showing representative full body gamma camera images showing hotspots automatically identified by the system, with corresponding overall computed BSI values for a particular image set obtained at a given time. A graph **410** at left shows how the BSI value has changed over time (increase) for this particular patient.

FIG. **5** is a GUI window in the BSI Cloud application showing an automatically or semi-automatically generated radiologist report **510**, which can be signed and dated by a radiologist. In certain embodiments, the automatically identified hotspots may be adjusted by the radiologist (or other medical practitioner attending to the patient), with the change(s) reflected in the report. For example, an identified hotspot may be deactivated by the radiologist, or a new hotspot may be activated by the radiologist, such changes possibly affecting the computed BSI value, displayed in the report.

FIG. **6** is a block flow diagram of an illustrative network-based (e.g., cloud based) decision support system, according to an illustrative embodiment of the invention. FIG. **6** shows various functions that may be performed by the cloud based services described herein. These include: (i) receiving and storing sets of medical images in a database; (ii) accessing one or more of the medical images for transmission to the user for display on a user computing device; (iii) automatically analyzing, by the processor, the medical images to compute a risk index (e.g., BSI) and/or to generate a risk map; (iv) generating a radiologist report for a patient according to the patient images and/or risk index/risk map; and applying a machine learning algorithm to update a process for the automatic analysis of function (iii).

FIG. **10** is a schematic showing clinical stages **1010** of prostate cancer progression, along with various therapies **1020** and diagnostic imaging modalities **1030** appropriate for various disease states. As shown in the schematic, depending on the clinical state of a patient's prostate cancer, different imaging modalities and/or different radiopharmaceuticals may be appropriate. Similarly, different risk indices computed based on different imaging modalities and/or different radiopharmaceuticals may most appropriate, depending on the state of the patient's prostate cancer.

For example, in certain embodiments, when a patient either has, or is suspected of having prostate cancer in a localized state, composite SPECT-CT imaging may be used. SPECT scans of composite SPECT-CT images used for evaluation of localized prostate cancer can be obtained following administration of a particular radiopharmaceutical, such as ^{99m}Tc-MIP-1404, that facilitates imaging of localized prostate cancer. Any of the SPECT-CT images themselves, derivatives thereof, and risk indices computed from the SPECT-CT images can be used, accordingly, to assess risk, disease state, progression, treatment efficacy and the like for localized prostate cancer.

In certain embodiments, when a patient has or is suspected of having metastatic prostate cancer, that has metastasized outside of the prostate, other imaging techniques may be used. For example, whole-body scans obtained following administration of ^{99m}Tc-MDP can be used to assess tumor burden in a patient's skeleton. As discussed above, BSI values computed from whole-body scans can be used to assess risk, disease state, progression, treatment efficacy and the like when a patient's prostate cancer has metastasized to their skeleton. In certain embodiments, certain imaging modalities and/or radiopharmaceuticals can be used for evaluate of prostate cancer in both localized and metastatic states. For example, as illustrated in FIG. **10**, PET-CT imaging can be used for evaluating prostate cancer in both localized and metastatic states. As shown in the figure, such PET-CT images may be obtained using an appropriate radiopharmaceutical, such as PyL™, that facilitates imaging of both localized and metastatic prostate cancer.

In certain embodiments, the cloud-based platform facilitates evaluating prostate cancer progression and treatment efficacy over time. For example, as shown in the example process **1100** of the block flow diagram of FIG. **11**, in certain embodiments medical images of a particular patient are repeatedly received and stored over time **1110**, over the course of multiple visits to one or more doctors and/or clinical specialists (e.g., radiologists) by the patient. In this manner, a series of medical images for the patient are obtained. The series of medical images can be automatically analyzed to determine values of one or more risk indices, so as to track changes in the determined values over time **1120**. The determined risk index values may be stored **1130** e.g., for further processing). In certain embodiments, the process causes a graphical representation of the determined risk

index values, such as a graph, to be displayed (e.g., on a user computing device; e.g., via a web-based portal) **1130***b*.

Notably, by virtue of the capability of the cloud-based platform described herein to receive, store, and analyze a variety of different medical image types, such as composite SPECT-CT images, whole-body scans, and composite PET-CT images, the medical images need not be of the same type.

For example, a first subseries of medical images may be obtained using a first imaging modality and a first radiopharmaceutical, such as SPECT-CT imaging with ^{99m}Tc-MIP-1404, when the patient's prostate cancer is in a localized state. If the patient's prostate cancer progresses to a metastatic state, a second subseries of images may comprise images obtained via a different, second imaging modality and/or a different, second radiopharmaceutical. For example, the second subseries of medical images may be PET-CT images obtained using PyL™ For example, the second subseries of medical images may be whole-body scans obtained using ^{99m}Tc-MDP.

Risk indices can be computed for the first image subseries and for the second image subseries to provide a unified picture of the patient's prostate cancer progression and treatment over time. This approach can be performed for multiple patients, not only for decision making purposes with regard to each patient's disease progression and particular course of treatment, but also in the context of clinical trials, for example to compare efficacy of a particular treatment with others or a control.

D. Computer System and Network Environment

FIG. **7** shows an illustrative network environment **700** for use in the methods and systems described herein. In brief overview, referring now to FIG. **7**, a block diagram of an exemplary cloud computing environment **700** is shown and described. The cloud computing environment **700** may include one or more resource providers **702***a*, **702***b*, **702***c* (collectively, **702**). Each resource provider **702** may include computing resources. In some implementations, computing resources may include any hardware and/or software used to process data. For example, computing resources may include hardware and/or software capable of executing algorithms, computer programs, and/or computer applications. In some implementations, exemplary computing resources may include application servers and/or databases with storage and retrieval capabilities. Each resource provider **702** may be connected to any other resource provider **702** in the cloud computing environment **700**. In some implementations, the resource providers **702** may be connected over a computer network **708**. Each resource provider **702** may be connected to one or more computing device **704***a*, **704***b*, **704***c* (collectively, **704**), over the computer network **708**.

The cloud computing environment **700** may include a resource manager **706**. The resource manager **706** may be connected to the resource providers **702** and the computing devices **704** over the computer network **708**. In some implementations, the resource manager **706** may facilitate the provision of computing resources by one or more resource providers **702** to one or more computing devices **704**. The resource manager **706** may receive a request for a computing resource from a particular computing device **704**. The resource manager **706** may identify one or more resource providers **702** capable of providing the computing resource requested by the computing device **704**. The resource manager **706** may select a resource provider **702** to provide the computing resource. The resource manager **706** may facilitate a connection between the resource provider **702** and a particular computing device **704**. In some implementations, the resource manager **706** may establish a connection between a particular resource provider **702** and a particular computing device **704**. In some implementations, the resource manager **706** may redirect a particular computing device **704** to a particular resource provider **702** with the requested computing resource.

FIG. **8** shows an example of a computing device **800** and a mobile computing device **850** that can be used in the methods and systems described in this disclosure. The computing device **800** is intended to represent various forms of digital computers, such as laptops, desktops, workstations, personal digital assistants, servers, blade servers, mainframes, and other appropriate computers. The mobile computing device **850** is intended to represent various forms of mobile devices, such as personal digital assistants, cellular telephones, smart-phones, and other similar computing devices. The components shown here, their connections and relationships, and their functions, are meant to be examples only, and are not meant to be limiting.

The computing device **800** includes a processor **802**, a memory **804**, a storage device **806**, a high-speed interface **808** connecting to the memory **804** and multiple high-speed expansion ports **810**, and a low-speed interface **812** connecting to a low-speed expansion port **814** and the storage device **806**. Each of the processor **802**, the memory **804**, the storage device **806**, the high-speed interface **808**, the high-speed expansion ports **810**, and the low-speed interface **812**, are interconnected using various busses, and may be mounted on a common motherboard or in other manners as appropriate. The processor **802** can process instructions for execution within the computing device **800**, including instructions stored in the memory **804** or on the storage device **806** to display graphical information for a GUI on an external input/output device, such as a display **816** coupled to the high-speed interface **808**. In other implementations, multiple processors and/or multiple buses may be used, as appropriate, along with multiple memories and types of memory. Also, multiple computing devices may be connected, with each device providing portions of the necessary operations (e.g., as a server bank, a group of blade servers, or a multi-processor system). Thus, as the term is used herein, where a plurality of functions are described as being performed by "a processor", this encompasses embodiments wherein the plurality of functions are performed by any number of processors (one or more) of any number of computing devices (one or more). Furthermore, where a function is described as being performed by "a processor", this encompasses embodiments wherein the function is performed by any number of processors (one or more) of any number of computing devices (one or more) (e.g., in a distributed computing system).

The memory **804** stores information within the computing device **800**. In some implementations, the memory **804** is a volatile memory unit or units. In some implementations, the memory **804** is a non-volatile memory unit or units. The memory **804** may also be another form of computer-readable medium, such as a magnetic or optical disk.

The storage device **806** is capable of providing mass storage for the computing device **800**. In some implementations, the storage device **806** may be or contain a computer-readable medium, such as a floppy disk device, a hard disk device, an optical disk device, or a tape device, a flash memory or other similar solid state memory device, or an array of devices, including devices in a storage area network or other configurations. Instructions can be stored in an information carrier. The instructions, when executed by one or more processing devices (for example, processor **802**),

perform one or more methods, such as those described above. The instructions can also be stored by one or more storage devices such as computer- or machine-readable mediums (for example, the memory **804**, the storage device **806**, or memory on the processor **802**).

The high-speed interface **808** manages bandwidth-intensive operations for the computing device **800**, while the low-speed interface **812** manages lower bandwidth-intensive operations. Such allocation of functions is an example only. In some implementations, the high-speed interface **808** is coupled to the memory **804**, the display **816** (e.g., through a graphics processor or accelerator), and to the high-speed expansion ports **810**, which may accept various expansion cards (not shown). In the implementation, the low-speed interface **812** is coupled to the storage device **806** and the low-speed expansion port **814**. The low-speed expansion port **814**, which may include various communication ports (e.g., USB, Bluetooth®, Ethernet, wireless Ethernet) may be coupled to one or more input/output devices, such as a keyboard, a pointing device, a scanner, or a networking device such as a switch or router, e.g., through a network adapter.

The computing device **800** may be implemented in a number of different forms, as shown in the figure. For example, it may be implemented as a standard server **820**, or multiple times in a group of such servers. In addition, it may be implemented in a personal computer such as a laptop computer **822**. It may also be implemented as part of a rack server system **824**. Alternatively, components from the computing device **800** may be combined with other components in a mobile device (not shown), such as a mobile computing device **850**. Each of such devices may contain one or more of the computing device **800** and the mobile computing device **850**, and an entire system may be made up of multiple computing devices communicating with each other.

The mobile computing device **850** includes a processor **852**, a memory **864**, an input/output device such as a display **854**, a communication interface **866**, and a transceiver **868**, among other components. The mobile computing device **850** may also be provided with a storage device, such as a micro-drive or other device, to provide additional storage. Each of the processor **852**, the memory **864**, the display **854**, the communication interface **866**, and the transceiver **868**, are interconnected using various buses, and several of the components may be mounted on a common motherboard or in other manners as appropriate.

The processor **852** can execute instructions within the mobile computing device **850**, including instructions stored in the memory **864**. The processor **852** may be implemented as a chipset of chips that include separate and multiple analog and digital processors. The processor **852** may provide, for example, for coordination of the other components of the mobile computing device **850**, such as control of user interfaces, applications run by the mobile computing device **850**, and wireless communication by the mobile computing device **850**.

The processor **852** may communicate with a user through a control interface **858** and a display interface **856** coupled to the display **854**. The display **854** may be, for example, a TFT (Thin-Film-Transistor Liquid Crystal Display) display or an OLED (Organic Light Emitting Diode) display, or other appropriate display technology. The display interface **856** may comprise appropriate circuitry for driving the display **854** to present graphical and other information to a user. The control interface **858** may receive commands from a user and convert them for submission to the processor **852**. In addition, an external interface **862** may provide communication with the processor **852**, so as to enable near area communication of the mobile computing device **850** with other devices. The external interface **862** may provide, for example, for wired communication in some implementations, or for wireless communication in other implementations, and multiple interfaces may also be used.

The memory **864** stores information within the mobile computing device **850**. The memory **864** can be implemented as one or more of a computer-readable medium or media, a volatile memory unit or units, or a non-volatile memory unit or units. An expansion memory **874** may also be provided and connected to the mobile computing device **850** through an expansion interface **872**, which may include, for example, a SIMM (Single In Line Memory Module) card interface. The expansion memory **874** may provide extra storage space for the mobile computing device **850**, or may also store applications or other information for the mobile computing device **850**. Specifically, the expansion memory **874** may include instructions to carry out or supplement the processes described above, and may include secure information also. Thus, for example, the expansion memory **874** may be provided as a security module for the mobile computing device **850**, and may be programmed with instructions that permit secure use of the mobile computing device **850**. In addition, secure applications may be provided via the SIMM cards, along with additional information, such as placing identifying information on the SIMM card in a non-hackable manner.

The memory may include, for example, flash memory and/or NVRAM memory (non-volatile random access memory), as discussed below. In some implementations, instructions are stored in an information carrier and, when executed by one or more processing devices (for example, processor **852**), perform one or more methods, such as those described above. The instructions can also be stored by one or more storage devices, such as one or more computer- or machine-readable mediums (for example, the memory **864**, the expansion memory **874**, or memory on the processor **852**). In some implementations, the instructions can be received in a propagated signal, for example, over the transceiver **868** or the external interface **862**.

The mobile computing device **850** may communicate wirelessly through the communication interface **866**, which may include digital signal processing circuitry where necessary. The communication interface **866** may provide for communications under various modes or protocols, such as GSM voice calls (Global System for Mobile communications), SMS (Short Message Service), EMS (Enhanced Messaging Service), or MMS messaging (Multimedia Messaging Service), CDMA (code division multiple access), TDMA (time division multiple access), PDC (Personal Digital Cellular), WCDMA (Wideband Code Division Multiple Access), CDMA2000, or GPRS (General Packet Radio Service), among others. Such communication may occur, for example, through the transceiver **868** using a radio-frequency. In addition, short-range communication may occur, such as using a Bluetooth®, Wi-Fi™, or other such transceiver (not shown). In addition, a GPS (Global Positioning System) receiver module **870** may provide additional navigation- and location-related wireless data to the mobile computing device **850**, which may be used as appropriate by applications running on the mobile computing device **850**.

The mobile computing device **850** may also communicate audibly using an audio codec **860**, which may receive spoken information from a user and convert it to usable digital information. The audio codec **860** may likewise generate audible sound for a user, such as through a speaker,

e.g., in a handset of the mobile computing device **850**. Such sound may include sound from voice telephone calls, may include recorded sound (e.g., voice messages, music files, etc.) and may also include sound generated by applications operating on the mobile computing device **850**.

The mobile computing device **850** may be implemented in a number of different forms, as shown in the figure. For example, it may be implemented as a cellular telephone **880**. It may also be implemented as part of a smart-phone **882**, personal digital assistant, or other similar mobile device.

Various implementations of the systems and techniques described here can be realized in digital electronic circuitry, integrated circuitry, specially designed ASICs (application specific integrated circuits), computer hardware, firmware, software, and/or combinations thereof. These various implementations can include implementation in one or more computer programs that are executable and/or interpretable on a programmable system including at least one programmable processor, which may be special or general purpose, coupled to receive data and instructions from, and to transmit data and instructions to, a storage system, at least one input device, and at least one output device.

These computer programs (also known as programs, software, software applications or code) include machine instructions for a programmable processor, and can be implemented in a high-level procedural and/or object-oriented programming language, and/or in assembly/machine language. As used herein, the terms machine-readable medium and computer-readable medium refer to any computer program product, apparatus and/or device (e.g., magnetic discs, optical disks, memory, Programmable Logic Devices (PLDs)) used to provide machine instructions and/or data to a programmable processor, including a machine-readable medium that receives machine instructions as a machine-readable signal. The term machine-readable signal refers to any signal used to provide machine instructions and/or data to a programmable processor.

To provide for interaction with a user, the systems and techniques described here can be implemented on a computer having a display device (e.g., a CRT (cathode ray tube) or LCD (liquid crystal display) monitor) for displaying information to the user and a keyboard and a pointing device (e.g., a mouse or a trackball) by which the user can provide input to the computer. Other kinds of devices can be used to provide for interaction with a user as well; for example, feedback provided to the user can be any form of sensory feedback (e.g., visual feedback, auditory feedback, or tactile feedback); and input from the user can be received in any form, including acoustic, speech, or tactile input.

The systems and techniques described here can be implemented in a computing system that includes a back end component (e.g., as a data server), or that includes a middleware component (e.g., an application server), or that includes a front end component (e.g., a client computer having a graphical user interface or a Web browser through which a user can interact with an implementation of the systems and techniques described here), or any combination of such back end, middleware, or front end components. The components of the system can be interconnected by any form or medium of digital data communication (e.g., a communication network). Examples of communication networks include a local area network (LAN), a wide area network (WAN), and the Internet.

The computing system can include clients and servers. A client and server are generally remote from each other and typically interact through a communication network. The relationship of client and server arises by virtue of computer programs running on the respective computers and having a client-server relationship to each other. In some implementations, the modules and/or services (e.g. cloud based services, such as BSI Cloud **110**, PyL Cloud **120**, **1404** Cloud **130**; e.g., any of the microservices described herein) described herein can be separated, combined or incorporated into single or combined modules and/or services. The modules and/or services depicted in the figures are not intended to limit the systems described herein to the software architectures shown therein

While the invention has been particularly shown and described with reference to specific preferred embodiments, it should be understood by those skilled in the art that various changes in form and detail may be made therein without departing from the spirit and scope of the invention as defined by the appended claims.

What is claimed is:

1. A network-based decision support system comprising:

a processor; and

a memory having instructions stored thereon, wherein the instructions, when executed by the processor, cause the processor to:

(i) receive and store a plurality of medical images in a database, each medical image associated with a corresponding patient;

(ii) access one or more of the medical images associated with a particular patient from the database upon user request for transmission to the user for display on a user computing device;

(iii) automatically analyze the one or more medical images using a machine learning algorithm; and

(iv) generate a radiologist report for the particular patient according to the one or more medical images for the patient,

wherein the one or more medical images comprise a composite image of the particular patient, the composite image comprising a CT scan overlaid with a nuclear medicine image obtained at a substantially same time as the CT scan and following administration to the patient of an imaging agent comprising a Prostate Specific Membrane Antigen (PSMA) binding agent comprising a radionuclide, wherein the instructions cause the processor to automatically analyze the composite image by:

(a) using the composite image to geographically identify a 3D boundary for each of one or more regions of imaged tissue within the nuclear medicine image; and

(b) computing, using the nuclear medicine image with the identified 3D boundary(ies) of the one or more region(s)

a risk map comprising a graphical denotation marking a region of risk of cancer or risk of recurrence of cancer.

2. The system of claim **1**, wherein the nuclear medicine image is a SPECT scan.

3. The system of claim **2**, wherein the imaging agent comprises a metal chelated to the PSMA binding agent, and wherein the metal is the radionuclide.

4. The system of claim **3**, wherein the imaging agent comprises ^{99m}Tc-MIP-1404.

5. The system of claim **1**, wherein the nuclear medicine image is a PET scan.

6. The system of claim **5**, wherein the radionuclide is a radioisotope of a halogen.

7. The system of claim **5**, wherein the imaging agent comprises [18F]DCFPyL.

8. The system of claim **5**, wherein the radionuclide is a radioisotope of gallium (Ga).

9. The system of claim 1, wherein the system is a cloud-based system.

10. The system of claim 1, wherein the processor is a processor of one or more network or Internet host servers.

11. The method of claim 1, wherein the cancer is prostate cancer.

12. The method of claim 11, wherein the cancer is metastatic prostate cancer.

13. The method of claim 1, wherein the imaged tissue comprises bone.

14. The method of claim 1, wherein the imaged tissue comprises a prostate of the patient.

15. The system of claim 1, wherein at step (b), the instructions cause the processor to compute a value of each of one or more risk indices, each risk index value indicative of cancer state or progression in the patient.

16. The system of claim 15, wherein the plurality of medical images in the database comprise a series of medical images of a first patient taken over time, and wherein the instructions cause the processor to determine a value of at least a first risk index for each medical image of the series, thereby tracking determined values of at least the first risk index for the first patient over time.

17. The system of claim 15, wherein at step (b) the instructions cause the processor to, for at least one risk index of the one or more risk indices, compute the value of the risk index by:

determining, for each of the one or more regions, a corresponding cancerous tissue level within the region based on intensity values of the nuclear medicine image within the 3D boundary of the region; and

computing the value of the risk index based on the determined cancerous tissue levels within the one or more regions.

18. A method comprising performing, by a processor of a server computing device, (i) to (v) as follows:

(i) receiving and storing, by the processor, a plurality of medical images in a database, each medical image associated with a corresponding patient;

(ii) accessing, by the processor, one or more of the medical images associated with a particular patient from the database upon user request for transmission to the user for display on a user computing device;

(iii) automatically analyzing, by the processor, the one or more medical images using a machine learning algorithm; and

(iv) generating, by the processor, a radiologist report for the particular patient according to the one or more medical images for the patient,

wherein the one or more medical images comprise a composite image of the particular patient, the composite image comprising a CT scan overlaid with a nuclear medicine image acquired at a substantially same time as the CT scan and following administration to the patient of an imaging agent comprising a Prostate Specific Membrane Antigen (PSMA) binding agent comprising a radionuclide, wherein the method comprises automatically analyzing the composite image by:

(a) using the composite image to geographically identify a 3D boundary for each of one or more regions of imaged tissue within the nuclear medicine image; and

(b) computing, using the nuclear medicine image with the identified 3D boundary(ies) of the one or more region(s),

a risk map comprising a graphical denotation marking regions of risk of cancer or risk of recurrence of cancer.

19. The method of claim 18, wherein the nuclear medicine image is a SPECT scan.

20. The method of claim 19, wherein the imaging agent comprises a metal chelated to the PSMA binding agent, and wherein the metal is the radionuclide.

21. The method of claim 20, wherein the imaging agent comprises ^{99m}Tc-MIP-1404.

22. The method of claim 18, wherein the nuclear medicine image is a PET scan.

23. The method of claim 22, wherein the radionuclide is a radioisotope of a halogen.

24. The method of claim 23, wherein the imaging agent comprises [18F]DCFPyL.

25. The method of claim 22, wherein the radionuclide is a radioisotope of gallium (Ga).

26. The method of claim 18, wherein the processor is a processor of a cloud-based system.

27. The method of claim 18, wherein the processor is a processor of one or more network or Internet host servers.

28. The method of claim 18, wherein the cancer is prostate cancer.

29. The method of claim 28, wherein the cancer is metastatic prostate cancer.

30. The method of claim 18, wherein the imaged tissue comprises bone.

31. The method of claim 18, wherein the imaged tissue comprises a prostate of the patient.

32. The method of claim 18, wherein step (b) comprises computing a value of each of one or more risk indices, each risk index value indicative of cancer state or progression in the patient.

33. The method of claim 32, wherein the plurality of medical images in the database comprise a series of medical images of a first patient taken over time, and wherein the method comprises determining a value of at least a first risk index for each medical image of the series, thereby tracking determined values of at least the first risk index over time.

34. The method of claim 33, wherein the receiving and storing of the plurality of medical images comprises repeatedly receiving and storing, over time, a plurality of medical images of the first patient, each obtained at a different time, to obtain the series of medical images of the first patient.

35. The method of claim 32, wherein step (b) comprises, for at least one risk index of the one or more risk indices, computing the value of the risk index by:

determining, for each of the one or more regions, a corresponding cancerous tissue level within the region based on intensity values of the nuclear medicine image within the 3D boundary of the region; and

computing the value of the risk index based on the determined cancerous tissue levels within the one or more regions.

36. A method for tracking prostate cancer progression and treatment efficacy over time, for one or more patient(s), the method comprising:

(a) repeatedly receiving and storing in a database, over time, by a processor of a computing device, a plurality of medical images for each of the one or more patient(s) to obtain, for each of the one or more patient(s), a series of medical images taken over time;

(b) for each of the one or more patient(s), automatically analyzing, by the processor, using a machine learning algorithm, the series of medical images for the patient to determine (i) values of one or more risk indices for each medical image of the series, thereby tracking determined values of the one or more risk indices over a course prostate cancer progression and treatment for

the patient and (ii) a risk map comprising a graphical denotation marking a region of risk of cancer or risk of recurrence of cancer; and

(c) for each of the one or more patient(s), storing, by the processor, (i) the determined values of the one or more risk indices, each indicative of prostate cancer state or progression, and (ii) the risk map, for the patient for further processing or causing, by the processor, display of a graphical representation of the determined values of the one or more risk indices for the patient,

wherein the series of medical images for a particular patient of the one or more patient(s) comprises a composite images of the particular patient, each composite image comprising a CT scan overlaid with a corresponding nuclear medicine image acquired at a substantially same time as the CT scan and following administration to the patient of an imaging agent comprising a Prostate Specific Membrane Antigen (PSMA) binding agent comprising a radionuclide, and wherein step (b) comprises:

using the composite image to geographically identify a 3D boundary for each of one or more regions of imaged tissue within the corresponding nuclear medicine image; and

using the corresponding nuclear medicine image with the identified 3D boundary(ies) of the one or more region(s) to compute (i) the value of each of the one or more risk indices and (ii) the risk map.

37. The method of claim **36**, wherein the series of medical images for the particular patient of the one or more patient(s) comprises:

(i) a first image subseries comprising one or more medical images obtained using a first nuclear imaging modality each following administration to the particular patient of a first radiopharmaceutical; and

(ii) a second image subseries comprising one or more medical images obtained using a second nuclear imaging modality each following administration to the particular patient of a second radiopharmaceutical,

such that the values of the one or more risk indices determined in step (b) for the particular patient comprise a first subseries of values of a first risk index determined by automated analysis of the first image subseries and a second subseries of values of a second risk index determined by automated analysis of the second image subseries.

38. The method of claim **37**, wherein the medical images of first image subseries are obtained over a first period of time, when prostate cancer of the particular patient is localized, and the medical images of the second image subseries are obtained over a second period of time, when prostate cancer of the particular patient is metastatic.

39. The method of claim **37**, wherein:

the first image subseries comprises one or more composite SPECT-CT image(s), each composite SPECT-CT image comprising a CT scan overlaid with a SPECT scan acquired at substantially the same time;

the second image subseries comprises one or more composite PET-CT image(s), each composite PET-CT image comprising a CT scan overlaid with a PET scan acquired at substantially the same time; and

step (b) comprises:

automatically analyzing each of the one or more composite SPECT-CT images by:

using the composite SPECT-CT image to geographically identify a 3D boundary of a prostate region within the SPECT scan of the composite SPECT-CT image; and

computing a value of the first risk index using the SPECT scan with the identified 3D boundary of the prostate region; and

automatically analyzing each of the one or more composite PET-CT images by:

using the composite PET-CT image to geographically identify a 3D boundary of one or more metastatic regions within the PET scan of the composite PET-CT image, the one or metastatic regions including regions corresponding to patient tissue locations outside of the prostate; and

computing a value of the second risk index using the PET scan with the identified 3D boundaries of the one or more metastatic region(s).

40. The method of claim **37**, wherein:

the first image subseries comprises one or more composite SPECT-CT image(s), each composite SPECT-CT image comprising a CT scan overlaid with a SPECT scan acquired at substantially the same time;

the second image subseries comprises one or more whole-body scan(s); and

step (b) comprises:

automatically analyzing each of the one or more composite SPECT-CT images by:

using the composite SPECT-CT image to geographically identify a 3D boundary of a prostate region within the SPECT scan of the composite SPECT-CT image; and

computing a value of the first risk index using the SPECT scan with the identified 3D boundary of the prostate region; and

automatically analyzing each of the one or more whole-body scan(s) by:

geographically identifying a boundary of one or more metastatic regions within the whole-body scan, the one or metastatic regions including regions corresponding to patient tissue locations outside of the prostate; and

computing a value of the second risk index using the PET scan with the identified 3D boundaries of the one or more metastatic region(s).

41. A system for tracking prostate cancer progression and treatment efficacy over time, for one or more patient(s), the system comprising:

a processor; and

a memory having instructions stored thereon, wherein the instructions, when executed by the processor, cause the processor to:

(a) repeatedly receive and store in a database, over time, a plurality of medical images for each of the one or more patient(s) to obtain, for each of the one or more patient(s), a series of medical images taken over time;

(b) for each of the one or more patient(s), automatically analyze the series of medical images for the patient using a machine learning algorithm to determine (i) values of one or more risk indices for each medical image of the series, thereby tracking determined values of the one or more risk indices over a course prostate cancer progression and treatment for the patient and (ii) a risk map comprising a graphical denotation marking a region of risk of cancer or risk of recurrence of cancer; and

(c) for each of the one or more patient(s), store (i) the determined values of the one or more risk indices, each indicative of prostate cancer state or progression, and (ii) the risk map, for the patient for further processing or cause display of a graphical representation of the determined values of the one or more risk indices for the patient,

wherein the series of medical images for a particular patient of the one or more patient(s) comprises a composite images of the particular patient, each composite image comprising a CT scan overlaid with a corresponding nuclear medicine image acquired at a substantially same time as the CT scan and following administration to the particular patient of an imaging agent comprising a Prostate Specific Membrane Antigen (PSMA) binding agent comprising a radionuclide, and wherein step (b) comprises:

using the composite image to geographically identify a 3D boundary for each of one or more regions of imaged tissue within the corresponding nuclear medicine image; and

using the corresponding nuclear medicine image with the identified 3D boundary(ies) of the one or more region(s) to compute (i) the value of each of the one or more risk indices and (ii) the risk map.

42. The system of claim **41**, wherein the series of medical images for the particular patient of the one or more patient(s) comprises:

(i) a first image subseries comprising one or more medical images obtained using a first nuclear imaging modality each following administration to the particular patient of a first radiopharmaceutical; and

(ii) a second image subseries comprising one or more medical images obtained using a second nuclear imaging modality each following administration to the particular patient of a second radiopharmaceutical,

such that the values of the one or more risk indices determined in step (b) for the particular patient comprise a first subseries of values of a first risk index determined by automated analysis of the first image subseries and a second subseries of values of a second risk index determined by automated analysis of the second image subseries.

43. The system of claim **42**, wherein the medical images of first image subseries are obtained over a first period of time, when prostate cancer of the particular patient is localized, and the medical images of the second image subseries are obtained over a second period of time, when prostate cancer of the particular patient is metastatic.

44. The system of claim **42**, wherein:

the first image subseries comprises one or more composite SPECT-CT image(s), each composite SPECT-CT image comprising a CT scan overlaid with a SPECT scan acquired at substantially the same time;

the second image subseries comprises one or more composite PET-CT image(s), each composite PET-CT image comprising a CT scan overlaid with a PET scan acquired at substantially the same time; and

the instructions cause the processor to, at step (b):

automatically analyze each of the one or more composite SPECT-CT images by:

using the composite SPECT-CT image to geographically identify a 3D boundary of a prostate region within the SPECT scan of the composite SPECT-CT image; and

computing a value of the first risk index using the SPECT scan with the identified 3D boundary of the prostate region; and

automatically analyze each of the one or more composite PET-CT images by:

using the composite PET-CT image to geographically identify a 3D boundary of one or more metastatic regions within the PET scan of the composite PET-CT image, the one or metastatic regions including regions corresponding to patient tissue locations outside of the prostate; and

computing a value of the second risk index using the PET scan with the identified 3D boundaries of the one or more metastatic region(s).

45. The system of claim **42**, wherein:

the first image subseries comprises one or more composite SPECT-CT image(s), each composite SPECT-CT image comprising a CT scan overlaid with a SPECT scan acquired at substantially the same time;

the second image subseries comprises one or more whole-body scan(s); and

the instructions cause the processor to, at step (b):

automatically analyze each of the one or more composite SPECT-CT images by:

using the composite SPECT-CT image to geographically identify a 3D boundary of a prostate region within the SPECT scan of the composite SPECT-CT image; and

computing a value of the first risk index using the SPECT scan with the identified 3D boundary of the prostate region; and

automatically analyze each of the one or more whole-body scan(s) by:

geographically identifying a boundary of one or more metastatic regions within the whole-body scan, the one or metastatic regions including regions corresponding to patient tissue locations outside of the prostate; and

computing a value of the second risk index using the PET scan with the identified 3D boundaries of the one or more metastatic region(s).

* * * * *

UNITED STATES PATENT AND TRADEMARK OFFICE

CERTIFICATE OF CORRECTION

PATENT NO. : 11,424,035 B2
APPLICATION NO. : 16/938488
DATED : August 23, 2022
INVENTOR(S) : Mark R. Baker

It is certified that error appears in the above-identified patent and that said Letters Patent is hereby corrected as shown below:

On the Title Page

Item [73], "Massachusetts" should be changed to --N. Billerica--

In the Claims

Column 37, Claim 11, Line 5, the word "method" should be changed to --system--

Column 37, Claim 12, Line 7, the word "method" should be changed to --system--

Column 37, Claim 13, Line 9, the word "method" should be changed to --system--

Column 37, Claim 14, Line 11, the word "method" should be changed to --system--

Signed and Sealed this
Twentieth Day of December, 2022

Katherine Kelly Vidal

Katherine Kelly Vidal
Director of the United States Patent and Trademark Office

EXHIBIT 4

US011894141B2

(12) **United States Patent**
Baker

(10) **Patent No.: US 11,894,141 B2**
(45) **Date of Patent: *Feb. 6, 2024**

(54) **NETWORK FOR MEDICAL IMAGE ANALYSIS, DECISION SUPPORT SYSTEM, AND RELATED GRAPHICAL USER INTERFACE (GUI) APPLICATIONS**

(71) Applicant: **Progenics Pharmaceuticals, Inc.**, N. Billerica, MA (US)

(72) Inventor: **Mark R. Baker**, New York, NY (US)

(73) Assignee: **Progenics Pharmaceuticals, Inc.**, N. Billerica, MA (US)

(*) Notice: Subject to any disclaimer, the term of this patent is extended or adjusted under 35 U.S.C. 154(b) by 15 days.

This patent is subject to a terminal disclaimer.

(21) Appl. No.: **17/862,528**

(22) Filed: **Jul. 12, 2022**

(65) **Prior Publication Data**

US 2022/0375612 A1 Nov. 24, 2022

Related U.S. Application Data

(63) Continuation of application No. 16/938,488, filed on Jul. 24, 2020, now Pat. No. 11,424,035, which is a (Continued)

(51) **Int. Cl.**
G06K 9/00 (2022.01)
G06Q 10/00 (2023.01)
(Continued)

(52) **U.S. Cl.**
CPC ***G16H 50/20*** (2018.01); ***G01N 33/57434*** (2013.01); ***G16H 15/00*** (2018.01);
(Continued)

(58) **Field of Classification Search**
CPC G06Q 10/00; G06K 9/00
(Continued)

(56) **References Cited**

U.S. PATENT DOCUMENTS

5,762,608 A 6/1998 Warne et al.
7,450,747 B2 11/2008 Jabri et al.
(Continued)

FOREIGN PATENT DOCUMENTS

CN 1200520 A 12/1998
CN 101528267 A 9/2009
(Continued)

OTHER PUBLICATIONS

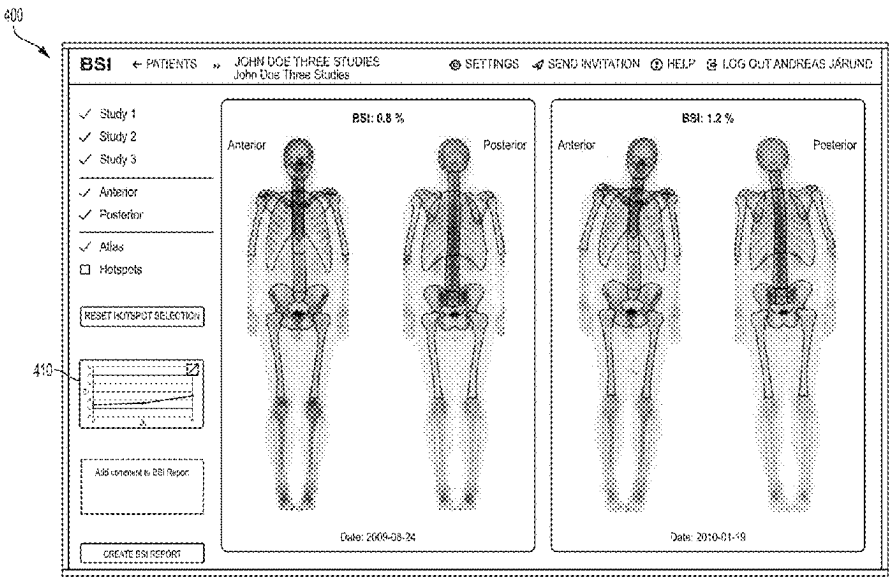
Gorthi, S. et al., Segmentation of Head and Neck Lymph Node Regions for Radiotherapy Planning Using Active Contour-Based Atlas Registration, IEEE Journal of Selected Topics in Signal Processing, 3(1):135-147 (2009).
(Continued)

Primary Examiner — Seyed H Azarian
(74) *Attorney, Agent, or Firm* — Choate, Hall & Stewart LLP; William R. Haulbrook; Ronen Adato

(57) **ABSTRACT**

Described herein is a platform and supported graphical user interface (GUI) decision-making tools for use by medical practitioners and/or their patients, e.g., to aide in the process of making decisions about a course of cancer treatment and/or to track treatment and/or the progress of a disease.

35 Claims, 11 Drawing Sheets



Related U.S. Application Data

continuation of application No. 16/418,527, filed on May 21, 2019, now Pat. No. 10,762,993, which is a continuation of application No. 15/794,220, filed on Oct. 26, 2017, now Pat. No. 10,340,046.

(60) Provisional application No. 62/413,936, filed on Oct. 27, 2016.

(51) **Int. Cl.**

G16H 50/20	(2018.01)
G16H 30/40	(2018.01)
G16H 50/70	(2018.01)
G16H 15/00	(2018.01)
G16H 30/20	(2018.01)
G16H 50/30	(2018.01)
G01N 33/574	(2006.01)

(52) **U.S. Cl.**

CPC ***G16H 30/20*** (2018.01); ***G16H 30/40*** (2018.01); ***G16H 50/30*** (2018.01); ***G16H 50/70*** (2018.01)

(58) **Field of Classification Search**

USPC 382/100, 103, 128–133, 154, 158, 162, 382/168, 173, 181, 206, 209, 220, 224, 382/232, 254, 286–295, 305, 312; 378/4, 378/21; 705/2

See application file for complete search history.

(56) **References Cited**

U.S. PATENT DOCUMENTS

7,751,605	B2	7/2010	Gündel et al.	
7,935,055	B2	5/2011	Burckhardt	
7,970,194	B2	6/2011	Kimura	
8,199,985	B2	6/2012	Jakobsson et al.	
8,211,401	B2	7/2012	Babich et al.	
8,467,856	B2	6/2013	Renisch et al.	
8,538,166	B2	9/2013	Gordon et al.	
8,705,887	B2	4/2014	Ma et al.	
8,778,305	B2	7/2014	Pomper et al.	
8,855,387	B2	10/2014	Hamadeh et al.	
8,962,799	B2	2/2015	Babich et al.	
9,002,081	B2 *	4/2015	Brown	G06T 7/0014 382/128
9,466,133	B2	10/2016	Sowards-Emmerd et al.	
9,710,915	B2	7/2017	Firouzian et al.	
9,721,340	B2	8/2017	Gillies et al.	
10,058,393	B2	8/2018	Bonutti et al.	
10,223,610	B1	3/2019	Akselrod-Ballin et al.	
10,311,971	B2	6/2019	Opfer et al.	
10,330,763	B2	6/2019	James et al.	
10,339,653	B2	7/2019	Gillies et al.	
10,340,044	B2	7/2019	Yao et al.	
10,340,046	B2	7/2019	Baker	
RE47,609	E	9/2019	Hamadeh et al.	
10,492,723	B2	12/2019	Madabhushi et al.	
10,600,184	B2	3/2020	Golden et al.	
10,665,346	B2	5/2020	Baker	
10,748,652	B2	8/2020	Yao et al.	
10,762,993	B2	9/2020	Baker	
10,818,386	B2	10/2020	Yao et al.	
10,943,681	B2	3/2021	Yao et al.	
10,973,486	B2	4/2021	Sjostrand et al.	
11,011,257	B2	5/2021	Lints et al.	
11,321,844	B2	5/2022	Johnsson et al.	
11,386,988	B2	7/2022	Johnsson et al.	
11,424,035	B2	8/2022	Baker	
11,534,125	B2	12/2022	Sjöstrand et al.	
11,564,621	B2	1/2023	Anand et al.	
2003/0215120	A1	11/2003	Uppaluri et al.	
2005/0281381	A1	12/2005	Guendel	
2006/0062425	A1 *	3/2006	Shen	G06T 15/08 382/100
2006/0064396	A1	3/2006	Wei et al.	
2006/0078183	A1	4/2006	deCharms	
2007/0081712	A1 *	4/2007	Huang	G06T 7/38 382/128
2007/0081713	A1	4/2007	Jerebko	
2007/0100225	A1	5/2007	Maschke	
2007/0115204	A1	5/2007	Budz et al.	
2008/0027315	A1	1/2008	McGinnis	
2009/0309874	A1	12/2009	Salganicoff et al.	
2009/0311182	A1	12/2009	Wang et al.	
2010/0215581	A1	8/2010	Hoffmann	
2010/0266170	A1	10/2010	Khamene et al.	
2010/0322488	A1	12/2010	Virtue et al.	
2011/0063288	A1	3/2011	Valadez	
2011/0255763	A1	10/2011	Bogoni et al.	
2012/0123253	A1	5/2012	Renisch et al.	
2013/0038707	A1	2/2013	Cunningham et al.	
2013/0094704	A1	4/2013	Hamadeh et al.	
2013/0129168	A1	5/2013	Ross	
2013/0211231	A1	8/2013	Sundarapandian et al.	
2013/0281841	A1	10/2013	Everett et al.	
2014/0193336	A1	7/2014	Rousso et al.	
2015/0110716	A1	4/2015	Armor	
2015/0119704	A1	4/2015	Roth et al.	
2015/0331995	A1 *	11/2015	Zhao	G16H 50/20 705/2
2016/0203263	A1 *	7/2016	Maier	G16H 30/40 705/2
2016/0335395	A1 *	11/2016	Wu	G16H 30/20
2017/0083682	A1	3/2017	McNutt et al.	
2017/0112577	A1	4/2017	Bonutti et al.	
2018/0144828	A1	5/2018	Baker	
2018/0259608	A1	9/2018	Golden et al.	
2018/0360402	A1	12/2018	Carmi	
2019/0038239	A1	2/2019	Flohr et al.	
2019/0105009	A1	4/2019	Siemionow et al.	
2019/0209116	A1	7/2019	Sjostrand et al.	
2019/0388049	A1	12/2019	Gupta et al.	
2020/0027559	A1	1/2020	Baker	
2020/0051238	A1	2/2020	El Harouni et al.	
2020/0074634	A1	3/2020	Kecskemethy et al.	
2020/0085382	A1	3/2020	Taerum et al.	
2020/0126666	A1	4/2020	Baker	
2020/0170604	A1	6/2020	Yildirim et al.	
2020/0193594	A1	6/2020	Georgescu et al.	
2020/0193603	A1	6/2020	Golden et al.	
2020/0245960	A1	8/2020	Richter et al.	
2020/0311919	A1	10/2020	Grimmer et al.	
2020/0315455	A1	10/2020	Lee et al.	
2020/0337658	A1	10/2020	Sjostrand et al.	
2020/0342600	A1	10/2020	Sjostrand et al.	
2020/0352518	A1	11/2020	Lyman et al.	
2020/0357117	A1	11/2020	Lyman et al.	
2020/0357118	A1	11/2020	Yao et al.	
2020/0357521	A1	11/2020	Baker	
2020/0410672	A1	12/2020	Katscher et al.	
2021/0032206	A1	2/2021	Neumaier et al.	
2021/0082547	A1	3/2021	Yao et al.	
2021/0093249	A1	4/2021	Anand et al.	
2021/0183485	A1	6/2021	Yao et al.	
2021/0233633	A1	7/2021	Lints et al.	
2021/0334974	A1	10/2021	Johnsson et al.	
2021/0335480	A1	10/2021	Johnsson et al.	
2022/0005586	A1	1/2022	Brynolfsson et al.	
2022/0398724	A1	12/2022	Anand et al.	
2023/0115732	A1	4/2023	Brynolfsson et al.	

FOREIGN PATENT DOCUMENTS

CN	102361594	A	2/2012
CN	102947840	A	2/2013
CN	103607954	A	2/2014
CN	106558045	A	4/2017
EP	1426903	A2	6/2004
EP	1508872	A1	2/2005
EP	3043318	A1	7/2016

(56) **References Cited**

FOREIGN PATENT DOCUMENTS

GB	2457577	A	8/2009
JP	2010-029481	A	2/2010
JP	2015-513083	A	4/2015
JP	6013042	B2	10/2016
JP	2017067489	A	4/2017
JP	6170284	B2	7/2017
SE	524500	C2	8/2004
WO	WO-99/05503	A2	2/1999
WO	WO-2007/062135	A2	5/2007
WO	WO-2009/084995	A1	7/2009
WO	WO-2011/077303	A1	6/2011
WO	WO-2011/091378	A1	7/2011
WO	WO-2013/126147	A2	8/2013
WO	WO-2015/058151	A2	4/2015
WO	WO-2018/015953	A1	1/2018
WO	WO-2018/081354	A1	5/2018
WO	WO-2019/103912	A2	5/2019
WO	WO-2019/136349	A2	7/2019
WO	WO-2020/144134	A1	7/2020
WO	WO-2020/146032	A1	7/2020
WO	WO-2020/190821	A1	9/2020
WO	WO-2020/219619	A1	10/2020
WO	WO-2020/219620	A1	10/2020
WO	WO-2021/061315	A1	4/2021
WO	WO-2022/008374	A1	1/2022
WO	WO-2023/057411	A1	4/2023

OTHER PUBLICATIONS

Teng, C. et al., Head and neck lymph node region delineation using a hybrid image registration method, 3rd IEEE International Symposium on Biomedical Imaging: Nano to Macro, 4 pages, (2006).

Ali, A. et al., The Automated Bone Scan Index as a Predictor of Response to Prostate Radiotherapy in Men with Newly Diagnosed Metastatic Prostate Cancer: An Exploratory Analysis of STAMPEDE's "M1|RT Comparison", European Urology Oncology 3:412-419, (2020).

American College of Radiology (ACR) and the Society for Pediatric Radiology (SPR), ACR-SPR Practice Parameter For The Performance Of Skeletal Scintigraphy (Bone Scan), Resolution 28, (2013—Revused2017), available from: <http://www.acr.org>, 9 pages (2017).

Anand, A. et al., A Pre-Analytical Validation Study of Automated Bone Scan Index: Effect on Accuracy and Reproducibility Due to the Procedural Variabilities in Bone Scan Image Acquisition. J Nucl Med. pp. 1865-1871, (2016).

Anand, A. et al., Analytic Validation of the Automated Bone Scan Index as an Imaging Biomarker to Standardize Quantitative Changes in Bone Scans of Patients with Metastatic Prostate Cancer, J. Nucl. Med., 57(1):41-45 (2016).

Anand, A. et al., Automated Bone Scan Index as a quantitative imaging biomarker in metastatic castration-resistant prostate cancer patients being treated with enzalutamide, EJNMMI Research, 6:23, 7 pages (2016).

Anand, A. et al., Translating Prostate Cancer Working Group 2 (PCWG2) Progression Criteria into a Quantitative Response Biomarker in Metastatic Castration Resistant Prostate Cancer (mCRPC), ASCO GU Conference, Poster, 1 page, presented Feb. 16, 2017.

Anand, A. et al., Translating Prostate Cancer Working Group 2 (PCWG2) progression criteria into a quantitative response biomarker in metastatic castration-resistant prostate cancer (mCRPC), Journal of Clinical Oncology, 35(6):170 (2017).

Armstrong, A. et al., Assessment of the bone scan index in a randomized placebo-controlled trial of tasquinimod in men with metastatic castration-resistant prostate cancer (mCRPC), Urologic Oncology: Seminars and Original Investigations, 32:1308-1316 (2014).

Armstrong, A. et al., Development and validation of a prognostic model for overall survival in chemotherapy-naive men with metastatic castration-resistant prostate cancer (mCRPC) from the phase 3 prevail clinical trial, Journal of Clinical Oncology, 35(Suppl. 6):Abstract 138, 5 pages, (2017).

Armstrong, A. J. et al., Phase 3 Assessment of the Automated Bone Scan Index as a Prognostic Imaging Biomarker of Overall Survival in Men with Metastatic Castration-Resistant Prostate Cancer: A Secondary Analysis of a Randomized Clinical Trial. JAMA Oncology 4:944-951, (2018).

Armstrong, A. J. et al., Phase 3 prognostic analysis of the automated bone scan index (aBSI) in men with bone-metastatic castration-resistant prostate cancer (CRPC), Meeting Library ASC University, 11 pages (2017).

Bai, P. et. al., Body region localization in whole-body low-dose CT images of PET/CT scans using virtual landmarks, Medical Physics Wiley USA, 46(3): 1286-1299 (2019).

Belal, S. et al., Association of PET Index quantifying skeletal uptake in NaF PET/CT images with overall survival in prostate cancer patients, ASCO GU 2017, Poster 178, 1 page, presented Feb. 16, 2017.

Belal, S. et al., PET Index quantifying skeletal uptake in NaF PET/CT images with overall survival in prostate cancer patients, ASCO GU 2017, Abstract, 1 page, (Feb. 13, 2017).

Belal, S. L. et al, 3D skeletal uptake of 18F sodium fluoride in PET/CT images is associate with overall survival in patients with prostate cancer, EJNMMI Research, 7(15):1-8 (2017).

Belal, S.L. et al., Automated evaluation of normal uptake in different skeletal parts in 18F-sodium fluoride (NaF) PET/CT using a new convolutional neural network method, EJNMMI, EANM '17, 44(Suppl 2):S119-S956, Abstract EP-0116 (2017).

Bombardieri, E. et al., Bone scintigraphy: procedure guidelines for tumour imaging, Eur J. Nucl. Med. Mol. Imaging, 30:BP99-BP106, (2003).

Brynolfsson, J., et. al., Deep Learning based urinary bladder segmentation using 18FDCFPyL (PyL-PSMA) PET/CT images, EPS-145, European Association of Nuclear Medicine, (2020), <http://link.springer.com/article/10.1007/s00259-020-04988-4>. pp. S1 and S403-S404, Retrieved Sep. 18, 2020.

Brynolfsson, J., et. al., Deep Learning-Enabled comprehensive detection and quantification of 18FDCFPyL (PyL-PSMA) PET/CT, OP-548, European Association of Nuclear Medicine, (2020), <http://link.springer.com/article/10.1007/s00259-020-04988-4>. pp. S1 and S273, Retrieved Sep. 18, 2020.

Bushberg, J. T. et al., Essential Physics of Medical Imaging, Essential Physics of Medical Imaging, 19.3: p. 581 (table 15-3), p. 713 paragraph 6, section 19.3 and p. 720, (2011).

Capobianco, N. et al., Whole-body uptake classification and prostate cancer staging in ^{68}Ga-PSMA-11 PET/CT using dual-tracer learning, European Journal of Nuclear Medicine and Molecular Imaging, (2021), <https:/doi.org/10.1007/s00259-021-05473-2> 10 pages. Retrieved on Apr. 18, 2021.

Ceci, F. et al., E-PSMA: the EANM standardized reporting guidelines v1.0 for PSMA-PET, European Journal of Nuclear Medicine and Molecular Imaging, 48:1626-1638, (2021).

Cha, K. H., et al. Urinary bladder segmentation in CT urography using deep-learning convolutional neural network and level sets, Medical physics, 43(4):1882-1896, (2016).

Christ, P.F. et al., Automatic Liver and Tumor Segmentation of CT and MRI Volumes Using Cascaded Fully Convolutional Neural Networks, Arxiv.org, Cornell University Library, 20 pages, (2017).

Ciernik, I. F., et al. 3D-segmentation of the 18F-choline PET signal for target volume definition in radiation therapy of the prostate, Technology in cancer research & treatment 6(1): 23-30, (2007).

Communication pursuant to Article 94(3) EPC for European Application No. 17794628.2-1126, 6 pages, (dated Apr. 22, 2021).

Dennis, E. et al., Bone Scan Index: A Quantitative Treatment Response Biomarker for Castration-Resistant Metastatic Prostate Cancer, Journal of Clinical Oncology, 30(5):519-524 (2012).

Dertat, A., Applied Deep Learning—Part 4: Convolutional Neural Networks, Towards Data Science,<http://towardsdatascience.com/applied-deep-learning-part-4-convolutional-neural-networks-584bc134c1e2> 26 pages, (2017).

Eiber, M. et al., Prostate Cancer Molecular Imaging Standardized Evaluation (PROMISE): Proposed miTNM Classification for the

(56) **References Cited**

OTHER PUBLICATIONS

Interpretation of PSMA-Ligand PET/CT, The Journal of Nuclear Medicine, 59(3):469-478, (2018).
Fendler, W.P. et. al., ^{68}Ga-PSMA PET/CT: Joint EANM and SNMMI procedure guideline for prostate cancer imaging: version 1.0, Eur J Nucl Med Mol Imaging, DOI 10.1007/s00259-017-3670-z, 11 pages, (2017).
GE Healthcare, SPECT/CT Cameras, 2 pages, retrieved Oct. 25, 2017: <http://www3.gehealthcare.com.sg/en-gb/products/categories/nuclear_medicine/spect-ct_cameras>.
Giesel, F. L. et al., F-18 labelled PSMA-1007: biodistribution, radiation dosimetry and histopathological validation of tumor lesions in prostate cancer patients, Eur. J. Nucl. Med. Mol. Imaging, 44:678-688 (2017).
Gjertsson, K., et. al., A Novel Automated Deep Learning Algorithm for Segmentation of the Skeleton in Low-Dose CT for [(18)F] DCFPyL PET/CT Hybrid Imaging in Patients with Metastatic Prostate Cancer, Annual Congress of the European Association of Nuclear Medicine Oct. 12-16, 2019 Barcelona, Spain. Eur J Nucl Med Mol Imaging 46 (Suppl 1), S1-S952 (2019). Abstract EP-0823, p. S765.
Gjertsson, K., Segmentation in Skeletal Scintigraphy Images using Convolutional Neural Networks, Master's Theses in Mathematical Sciences, pp. 39-58, (2017), <https://lup.lub.lu.se/student-papers/search/publication/8916406>.
Goffin, K. E. et al., Phase 2 study of ^{99m}Tc-trofolastat SPECT/CT to identify and localize prostate cancer in intermediate- and high-risk patients undergoing radical prostatectomy and extended pelvic lymph node dissection, J. Nucl. Med., 27 pages (2017).
Guimond, A. et al., Average Brain Models: A Convergence Study, Computer Vision and Image Understanding, 77:192-210 (2000).
Hajnal, J. et al., 4.4 Intensity, Size, and Skew Correction; 7.1 Introduction; 7.2 Methods; 7.3 Image Interpretation—General, In: Medical Image Registration, CRC Press LLC, 80-81:144-148 (2001).
Hiller, S. M. et al., 99mTc-Labeled Small-Molecule Inhibitors of Prostate-Specific Membrane Antigen for Molecular Imaging of Prostate Cancer, Journal of Nuclear Medicine, 54(8): 1369-1376 (2013) retrieved Oct. 25, 2017: <http://jnm.snmjournals.org/content/54/8/1369.full>.
Horikoshi, H. et al., Computer-aided diagnosis system for bone scintigrams from Japanese patients: importance of training database, Annals of Nuclear Medicine, 26(8):622-626 (2012).
Huang, J.-H. et al., A Set of Image Processing Algorithms for Computer-Aided Diagnosis in Nuclear Medicine Whole Body Bone Scan Images, IEEE Transactions on Nuclear Science, 54(3):514-522 (2007).
Im, HJ, et. al., et. al., Current Methods to Define Metabolic Tumor vol. in Positron Emission Tomography: Which One is Better?, Nucl. Med. Mol. Imaging, 52(1):5-15, (2018).
International Search Report, International Application No. PCT/US2017/058418 (Network for Medical Image Analysis, Decision Support System, and Related Graphical User Interface (GUI) Applications, filed Oct. 26, 2017), issued by ISA/European Patent Office, 4 pages, dated Feb. 27, 2018.
Johnsson, K. et al., Analytical performance of aPROMISE: automated anatomic contextualization, detection, and quantification of [18F]DCFPyL (PSMA) imaging for standardized reporting, European Journal of Nuclear Medicin and Molecular Imaging, 11 pages, Aug. 31, 2021, doi: 10.1007/s00259-021-05497-8. Epub ahead of print. PMID: 34463809.
Johnsson, K., et. al., miPSMA Index: Comprehensive and Automated Quantification of 18F-DCFPyL (PyL-PSMA) PET/CT for Prostate Cancer Staging, J Nucl Med., 61: (Supplement 1): 1435, 5 pages, (2020).
Kaboteh R. et al., Progression of bone metastases in patients with prostate cancer—automated detection of new lesions and calculation of bone scan index, EJNMMI Research, 3:64, 6 pages, (2013).
Kaboteh, R. et al., Convolutional neural network based quantification of choline uptake in PET/CT studies is associated with overall survival in patents with prostate cancer, EJNMMI, EANM '17, 44(Suppl 2):S119-S956, Abstract EP-0642 (2017).
Kiess, et al., Prostate-specific membrane antigen and a target for cancer imaging and therapy, The Quarterly Journal of Nuclear Medicine and Molecular Imaging, 59(3):241-268 (2015).
Kikuchi, A. et al., Automated segmentation of the skeleton in whole-body bone scans: influence of difference in atlas, Nuclear Medicine Communications, 33(9):947-953 (2012).
Kinahan, P.E. et al., PET/CT Standardized Update Values (SUVs) in Clinical Practice and Assessing Response to Therapy, Semin Ultrasound CT MR 31(6):496-505 (2010) retrieved Oct. 25, 2017: <https://www.ncbi.nlm.nih.gov/pmc/articles/PMC3026294/>.
Knutsson, H., and Andersson, M., Morphons: Segmentation using Elastic Canvas and Paint on Priors, IEEE International Conference on Image Processing (ICIP 2005), Genova, Italy, 4 pages (2005).
Kopka, K. et al., Glu-Ureido-Based Inhibitors of Prostate-Specific Membrane Antigen: Lessons Learned During the Development of a Novel Class of Low-Molecular-Weight Theranostic Radiotracers, The Journal of Nuclear Medicine, 58(9)(Suppl. 2):17S-26S, (2017).
Lin, T.Y. et. al., Feature Pyramid Networks for object detection, FAIR, 10 pages, (2016), <https://arxiv.org/abs/1612.03144v1>.
Litjens, G. et al., A survey on deep learning in medical image analysis, Medical Image Analysis, 42:60-88, (2017).
Liu, L. et al., Computer-Aided Detection of Prostate Cancer with MRI: Technology and Applications, Acad Radiol. Author manuscript, 50 pages 2016.
Ma, L. et al., Automatic segmentation of the prostate on CT images using deep learning and multi-atlas fusion, Proc. of SPIE vol. 10133:101332O-1-101332O-9 (2017).
Ma, L. et al., Combining Population and Patient-Specific Characteristics for Prostate Segmentation on 3D CT Images, Proc of SPIE 9784:978427-1-8 (2016).
Ma, L. et al., Random Walk Based Segmentation for the Prostate on 3D Transrectal Ultrasound Images, Proc SPIE Int Soc Opt Eng. Author manuscript, 13 pages (2016).
Matsubara, N. et al, A Phase II, Randomized, Open-Label, Multiarm Study of TAS-115 for Castration-Resistant Prostate Cancer Patients With Bone Metastases, Clinical Genitourinary Cancer, 000(xxx):1-10, (2021).
Mayo Clinic Staff, Choline C-11 PET scan, Overview, Mayo Clinic, 4 pages (2017), retrieved Oct. 25, 2017: <https://www.mayoclinic.org/tests-procedures/choline-c-11-pet-scan/home/ovc-20156994>.
Meyer, A., et. al., Deep learning algorithm improves identification of men with low-risk prostate cancer using PSMA targeted 99mTc-MIP-1404 SPECT/CT, Journal of Clinical Oncology, 37:(15), (2019).
Nakajima, K. et al., Enhanced diagnostic accuracy for quantitative bone scan using an artificial neural network system: a Japanese multi-center database project, EJNMMI Research, 3:83, 9 pages, (2013).
National Cancer Institute, NCI Drug Dictionary: gallium Ga 68-labeled PSMA-11, 1 page, retrieved Oct. 25, 2017: <https://www.cancer.gov/publications/dictionaries/cancer-drug?cdrid=766400>.
National Cancer Institute, NCI Drug Dictionary: technetium Tc 99m methylene diphosphonate, 1 page, retrieved Oct. 25, 2017: <https://www.cancer.gov/publications/dictionaries/cancer-drug?cdrid=537722>.
Nickols, N. et al., aPROMISE: A Novel Automated-PROMISE platform to Standardize Evaluation of Tumor Burden in 18F-DCFPyL (PSMA) images of Veterans with Prostate Cancer, Journal of Nuclear Medicine, 26 pages, May 28, 2021, doi: 10.2967/jnumed.120.261863.
Nickols, N.G., et. al., A deep learning algorithm to predict coexisting metastatic disease using intraprostatic [F18]DCFPYL PSMA image alone in veterans with prostate cancer, Journal of Clinical Oncology 38, (Supplement 6), 2020.
Ohlsson, M., et. al., Automated decision support for bone scintigraphy, Computer-based medical systems, pp. 1-6, (2009).
Paschalis, A. et al., Prostate-specific Membrane Antigen Heterogeneity and DNA Repair Defects in Prostate Cancer, European Urology, 76(4):469-478, (2019).
Perera, M. et al., Sensitivity, Specificity, and Predictors of Positive 68Ga-Prostate-specific Membrane Antigen Positron Emission Tomog-

(56) **References Cited**

OTHER PUBLICATIONS

raphy in Advanced Prostate Cancer: A Systematic Review and Meta-analysis, European Urology, 70(6):926-937 (2016).
Polymeri, E. et al., Analytical validation of an automated method for segmentation of the prostate gland in CT images, EJNMMI, EANM '17, 44(Suppl 2):S119-S956, Abstract EP-0641 (2017).
Polymeri, E., et. al., Deep learning-based quantification of PET/CT prostate gland uptake: association with overall survival, Clinical Physiology Functional Imaging, DOI: 10.1111/cpf.12611, 40(2):106-113, (2019).
Pouliot, F., et al., Prospective evaluation of a Novel Deep Learning Algorithm (PSMA-AI) in the assessment of 99mTc-MIP-1404 SPECT/CT in patients with low or intermediate risk prostate cancer, Annual Congress of the European Association of Nuclear Medicine Oct. 12-16, 2019 Barcelona, Spain. Eur J Nucl Med Mol Imaging 46 (Suppl 1), S1-S952 (2019). Abstract EP-0804, p. S765.
radiologyinfo.org for Patients, Computed Tomography (CT), 2 pages, retrieved Oct. 25, 2017: <https://www.radiologyinfo.org/en/submenu.cfm?pg=ctscan>.
Ren, S., et. al., Faster R-CNN: Towards Real-Time Object Detection with Region Proposal Networks, 14 pages, (2015), <http://image-net.org/challenges/LSVRC/2015/results>.
Ronneberger, O., et. al., U-Net: Convolutional Networks for Biomedical Image Segmentation, Springer International Publishing, pp. 234-241, (2015), <http://lmb.informatik.uni-freiburg.de/>. Published online on Nov. 18, 2015.
Rowe, S. P. et al., PET Imaging of prostate-specific membrane antigen in prostate cancer: current state of the art and future challenges, Prostate Cancer and Prostatic Diseases, pp. 1-8 (2016).
Rowe, S. P. et al., PSMA-Based [^{18}F]DCFPyL PET/CT Is Superior to Conventional Imaging for Lesion Detection in Patients with Metastatic Prostate Cancer, Mol Imaging Biol, 18:411-419, (2016).
Sabbatini, P. et al., Prognostic Significance of Extent of Disease in Bone in Patients With Androgen-Independent Prostate Cancer, Journal of Clinical Oncology, 17(3):948-957 (1999).
Sadik, M. et al., 3D prostate gland uptake of 18F-choline—association with overall survival in patients with hormone-naïve prostate cancer, The Journal of Nuclear Medicine, 58(Suppl. 1):Abstract 544, 2 pages, (2017).
Sadik, M. et al., A new computer-based decision-support system for the interpretation of bone scans, Nuclear Medicine Communications, 27(5):417-423 (2006).
Sadik, M. et al., Automated 3D segmentation of the prostate gland in CT images—a first step towards objective measurements of prostate uptake in PET and SPECT images, Journal of Nuclear Medicine, 58(1):1074, (2017).
Sadik, M. et al., Automated quantification of reference levels in liver and mediastinum (blood pool) for the Deauville therapy response classification using FDG-PET/CT in lymphoma patients, EJNMMI, EANM '17, 44(Suppl 2):S119-S956, Abstract EP-0770 (2017).
Sadik, M. et al., Computer-assisted interpretation of planar whole-body bone scans, Journal Nuclear Medicine, 49(12):1958-65, 2008.
Sadik, M. et al., Convolutional neural networks for segmentation of 49 selected bones in CT images show high reproducibility, EJNMMI, EANM '17, 44(Suppl 2):S119-S956, Abstract OP-657 (2017).
Sadik, M. et al., Improved classifications of planar whole-body bone scans using a computer-assisted diagnosis system: a multicenter, multiple-reader, multiple-case study, Journal of Nuclear Medicine, 50(3): 368-75, 2009.
Sadik, M. et al., Variability in reference levels for Deauville classifications applied to lymphoma patients examined with 18F-FDG-PET/CT, EJNMMI, EANM '17, 44(Suppl 2):S119-S956, Abstract EP-0771 (2017).
Sajn, L. et al., Computerized segmentation of whole-body bone scintigrams and its use in automated diagnostics, Computer Methods and Programs in Biomedicine, 80:47-55 (2005).
Salerno, J. et al., Multiparametric magnetic resonance imaging for pre-treatment local staging of prostate cancer: A Cancer Care Ontario clinical practice guideline, Canadian Urological Association Journal, 10(9-10):332-339 (2016).
Santos-Cuevas, C. et al. 99mTc-labeled PSMA inhibitor: Biokinetics and radiation dosimetry in healthy subjects and imaging of prostate cancer tumors in patients, Nuclear Medicine and Biology 52:1-6, (2017).
Sjöstrand K. et al., Statistical regularization of deformation fields for atlas-based segmentation of bone scintigraphy images, MICCAI 5761:664-671 (2009).
Sjöstrand, K., et al., Automated detection and quantification of Prostatic PSMA uptake in SPECT/CT using a Deep Learning Algorithm for Segmentation of Pelvic Anatomy, The Journal of Nuclear Medicine, 59(1):p. 30, (2018).
Sjostrand, K., et. al., Automated Assessment of Prostatic PSMA Expression in SPECT/CT using Deep Convolutional Neural Networks—A Prospectively Planned Retrospective Analysis of Phase 3 Study MIP-1404-3301, The Journal of Nuclear Medicine, 60 (Supplement 1): Abstract 401, 1 page, (2019).
Sluimer, I. et al., Toward Automated Segmentation of the Pathological Lung in CT, IEEE Transactions on Medical Imaging, 24(8):1025-1038 (2005).
Tian, Z. et al., A fully automatic multi-atlas based segmentation method for prostate MR images, Proc SPIE Int Soc Opt Eng. Author manuscript, 12 pages (2015).
Tian, Z. et al., A supervoxel-based segmentation method for prostate MR images, Med. Phys., 44(2):558-569 (2017).
Tian, Z. et al., Deep convolutional neural network for prostate MR segmentation, Proc. of SPIE 10135:101351L-1-101351L-6 12 pages, (2017).
Tian, Z., et al., Superpixel-based Segmentation for 3D Prostate MR Images, IEEE Trans Med Imaging, Author manuscript, pp. 558-569, (2016).
Trägärdh, E., et. al., RECOMIA—a cloud-based platform for artificial intelligence research in nuclear medicine and radiology, EJNMMI Physics, <https://doi.org/10.1186/s40658-020-00316-9>, 7:51, 12 pages, (2020).
Ulmert, D. et al., A Novel Automated Platform for Quantifying the Extent of Skeletal Tumour Involvement in Prostate Cancer Patients Using the Bone Scan Index, European Urology, 62(1):78-84 (2012).
Wallis, J.W. et. al., Three-dimensional display in nuclear medicine, IEEE Trans Med Imaging, 8(4):297-303, (1989).
Wrangsjo, A. et al., Non-rigid Registration Using Morphons, Proceedings of the 14th Scandinavian Conference on Image Analysis (SCIA '05), pp. 501-510 (2005).
Written Opinion, International Application No. PCT/US2017/058418 (Network for Medical Image Analysis, Decision Support System, and Related Graphical User Interface (GUI) Applications, filed Oct. 26, 2017), issued by ISA/European Patent Office, 9 pages, dated Feb. 27, 2018.
Yin, T.-K., and Chiu, N.T., A Computer-Aided Diagnosis for Locating Abnormalities in Bone Scintigraphy by a Fuzzy System With a Three-Step Minimization Approach, IEEE Transactions on Medical Imaging, 23(5):639-654 (2004).
Inoue, T., What cancers can be understood and not known by "PET"?—Effects of PET scanning by site, Medical Note Interview, 4 pages, (2015), retrieved from the internet at: https://medicalnote.jp/contents/150715-000003-CYJIZE.
Kawakami, K. et al., Introduction of bone scintigraphy diagnosis support software "Bonenavi" (Topics), Journal of Nuclear Medicine (Japanese), 63:41-51 (2011).
Kawakami, K., Evaluation of bone metastasis by bone scintigraphy diagnostic support software BONENAVI, Communication of the Imaging Group of the JSRT, 36(1):74-77 (2013).
Nogi, S. et al., Metastatic bone tumor quantified by computer-assisted diagnosis system of bone scintigraphy, Nuclear Medicine in Clinic, 45(3):35-37 (2012).
US Food and Drug Administration, Clinical Trial Endpoints for the Approval of Cancer Drugs and Biologics, 21 pages, (2018).
Washino, H., Injectable for bone scintigraphy: Technetium hydroxymethylenediphosphonate (99mTc) injection solution (Revised Edition), 9 pages, (2007), retrieved from the internet at:https://rada.or.jp/database/home4/normal/ht-docs/member/synopsis/030292.html#:%7E:text=%E6%A6%82%E8%A6%81).

(56) **References Cited**

OTHER PUBLICATIONS

Grahovac, M. et al., Machine learning predictive performance evaluation of conventional and fuzzy radiomics in clinical cancer imaging cohorts, Eur. J. Med. Mol. Imaging, 50(6):1607-1620 (2023).

International Search Report for PCT/EP2022/077505, filed Oct. 4, 2022, 9 pages, (dated Mar. 23, 2023).

Kertesz, H. et al., Implementation of a Spatially-Variant and Tissue-Dependent Positron Range Correction for PET/CT Imaging, Front. Physiol., 13:818463 (2022).

Kertesz, H. et al., Positron range in combination with point-spread-function correction: an evaluation of different implementations for [124I]-PET imaging, ENJMMI Phys., 9(1):56 (2022).

Khurshid, Z. et al., Role of textural heterogeneity parameters in patient selection for 177Lu-PSMA therapy via response prediction, Oncotarget., 9(70):33312-33321 (2018).

Krajnc, D. et al., Automated data preparation for in vivo tumor characterization with machine learning, Front. Oncol., 12:1017911 (2022).

Papp, L. et al., Glioma Survival Prediction with Combined Analysis of In Vivo 11C-MET PET Features, Ex Vivo Features, and Patient Features by Supervised Machine Learning, J. Nucl. Med., 59(6):892-899 (2018).

Papp, L. et al., Optimized Feature Extraction for Radiomics Analysis of 18F-FDG PET Imaging, J. Nucl. Med., 60(6):864-872 (2019).

Papp, L. et al., Supervised machine learning enables non-invasive lesion characterization in primary prostate cancer with [68Ga]Ga-PSMA-11 PET/MRI, Eur. J. Nucl. Mol. Imaging, 48(6):1795-1805 (2021).

Valladares, A. et al., A multi-modality physical phantom for mimicking tumor heterogeneity patterns in PET/CT and PET/MRI, Med. Phys., 49(9):5819-5829 (2022).

Written Opinion for PCT/EP2022/077505, filed Oct. 4, 2022, 11 pages, (dated Mar. 23, 2023).

* cited by examiner

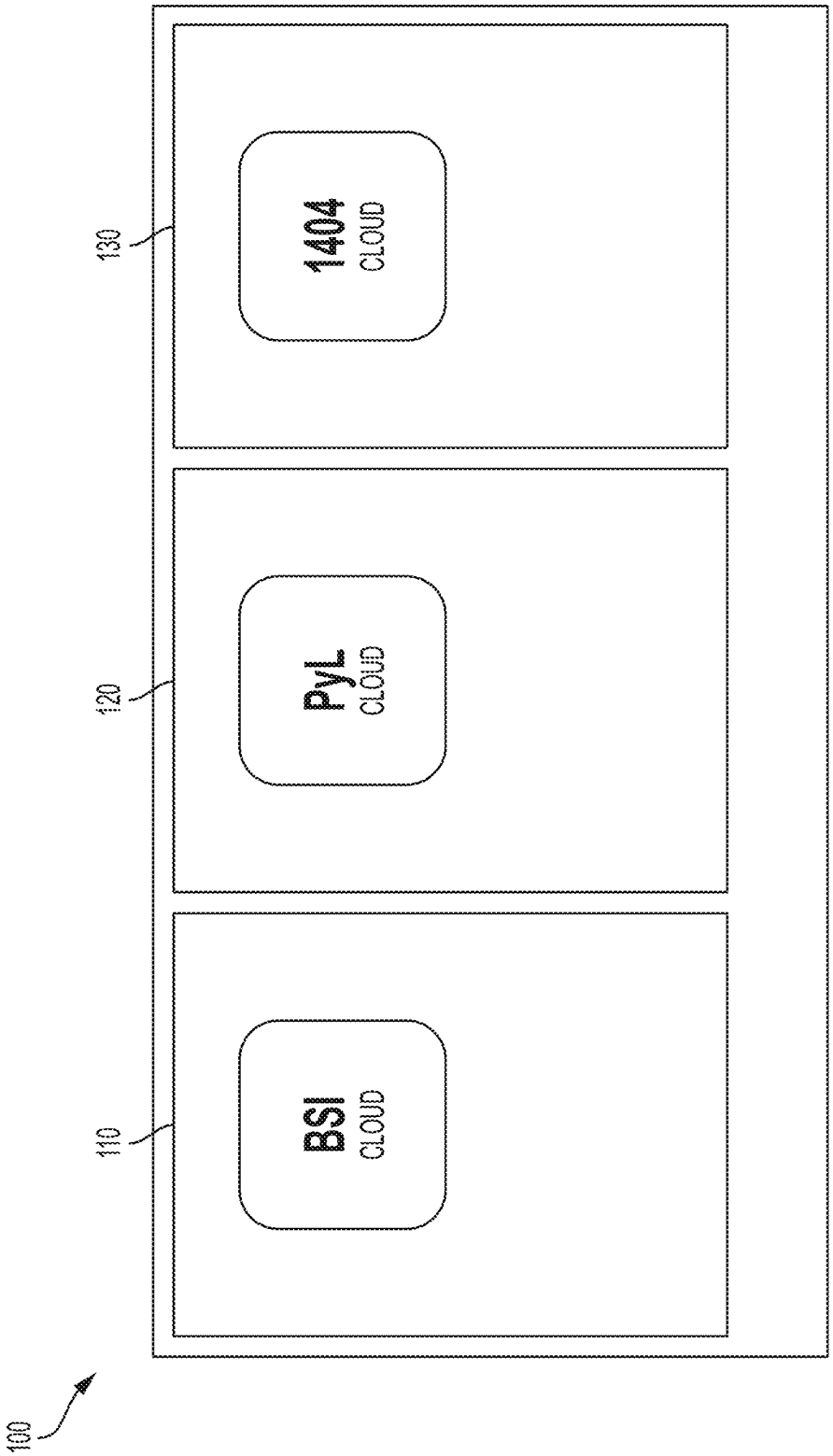


FIG. 1

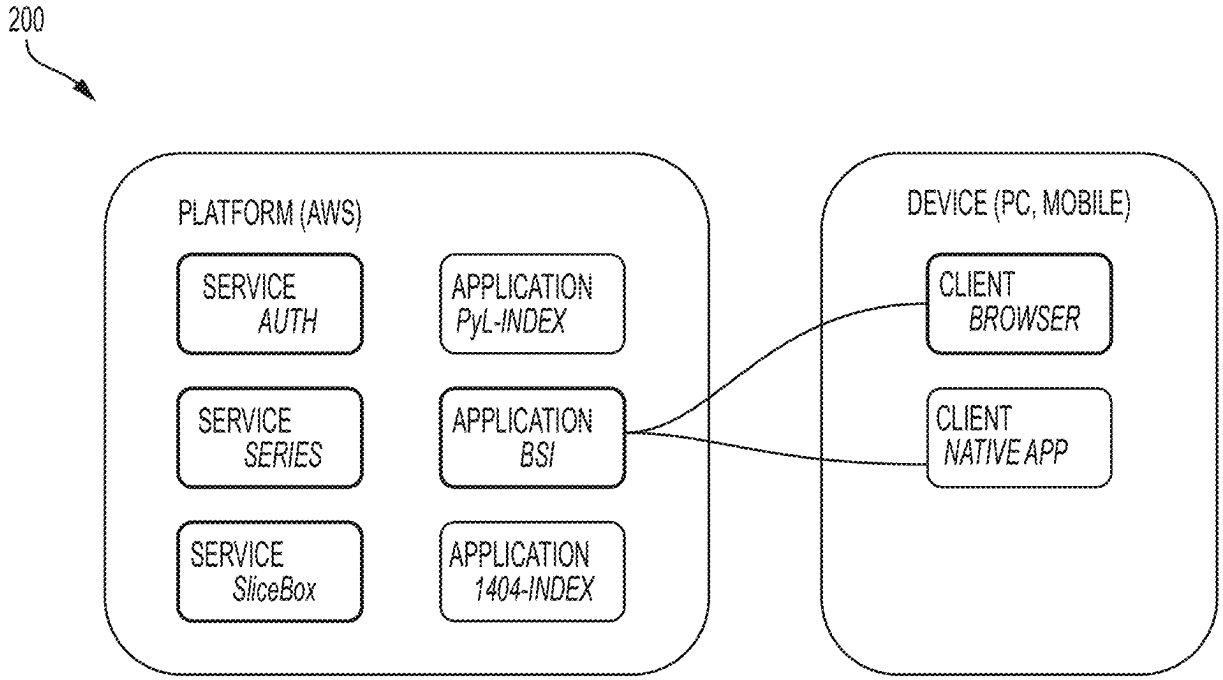

200
PLATFORM (AWS)
SERVICE AUTH
SERVICE SERIES
SERVICE SliceBox
APPLICATION PyL-INDEX
APPLICATION BSI
APPLICATION 1404-INDEX
DEVICE (PC, MOBILE)
CLIENT BROWSER
CLIENT NATIVE APP

FIG. 2

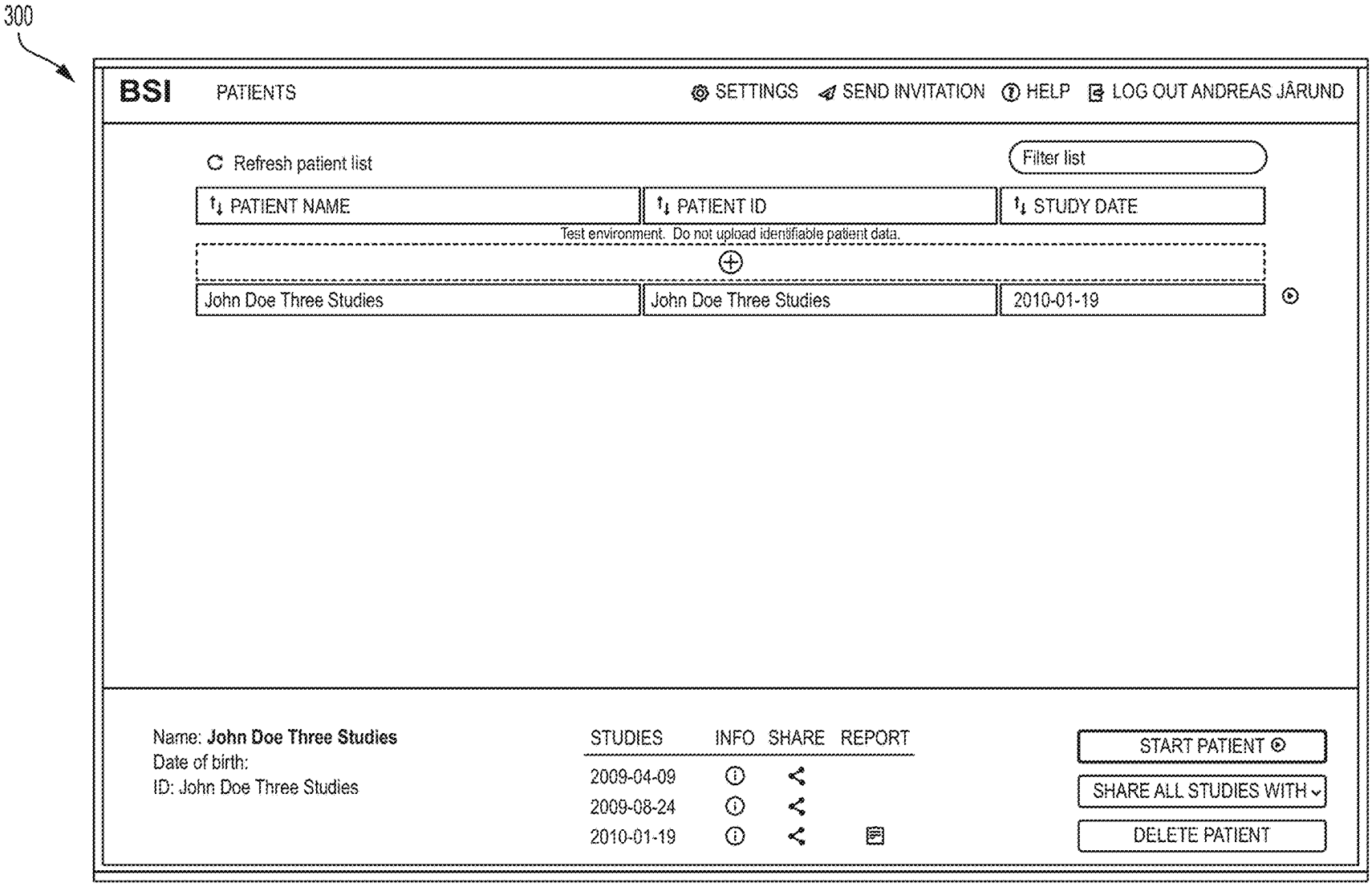

300
BSI
PATIENTS
SETTINGS
SEND INVITATION
HELP
LOG OUT ANDREAS JÅRUND
Refresh patient list
Filter list
PATIENT NAME
PATIENT ID
STUDY DATE
Test environment. Do not upload identifiable patient data.
John Doe Three Studies
John Doe Three Studies
2010-01-19
Name: John Doe Three Studies
Date of birth:
ID: John Doe Three Studies
STUDIES
INFO
SHARE
REPORT
2009-04-09
2009-08-24
2010-01-19
START PATIENT
SHARE ALL STUDIES WITH
DELETE PATIENT

FIG. 3

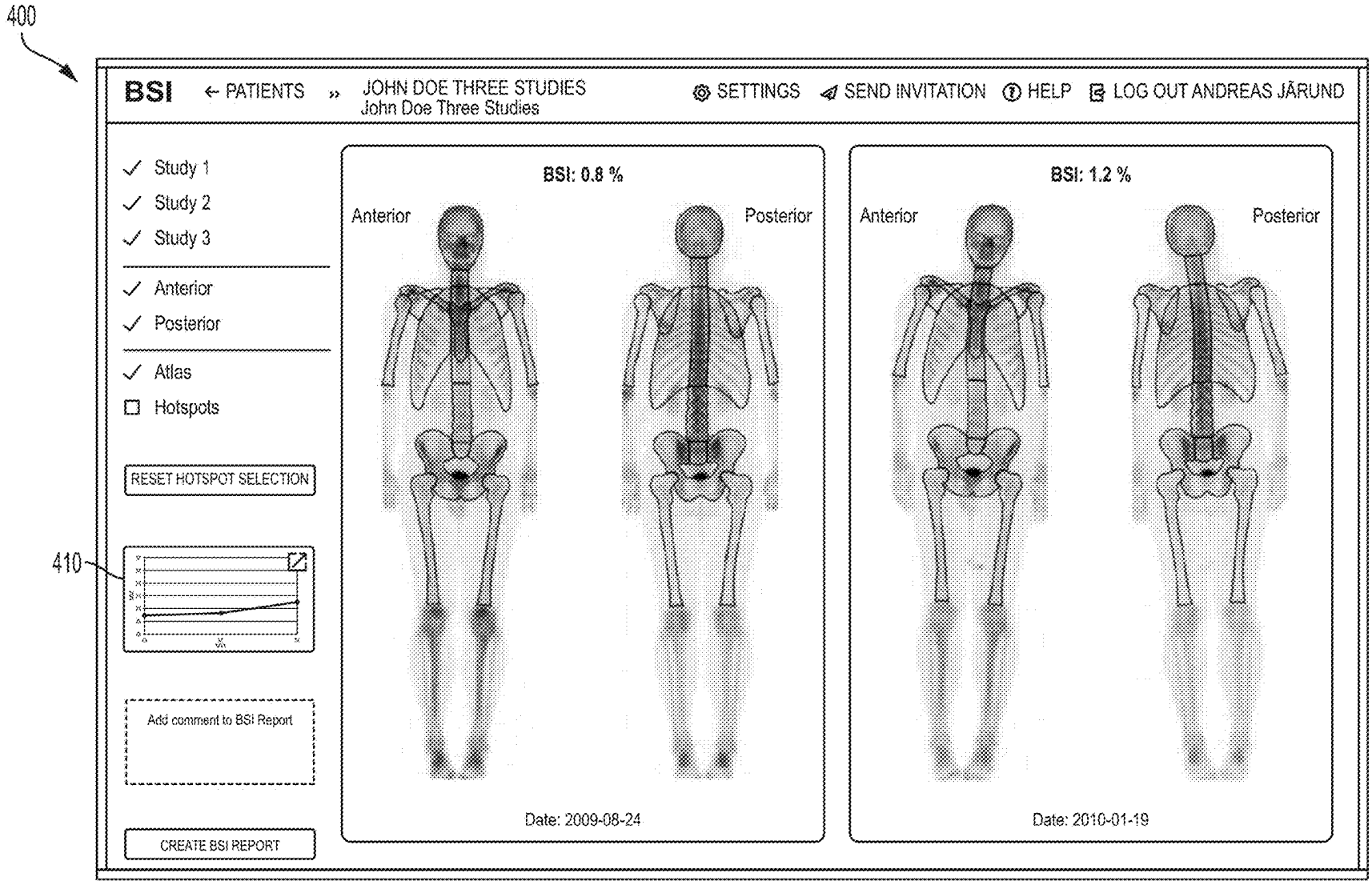

400
BSI
← PATIENTS
»
JOHN DOE THREE STUDIES
John Doe Three Studies
SETTINGS
SEND INVITATION
HELP
LOG OUT ANDREAS JÄRUND
Study 1
Study 2
Study 3
Anterior
Posterior
Atlas
Hotspots
RESET HOTSPOT SELECTION
410
Add comment to BSI Report
CREATE BSI REPORT
BSI: 0.8 %
Anterior
Posterior
Date: 2009-08-24
BSI: 1.2 %
Anterior
Posterior
Date: 2010-01-19

FIG. 4

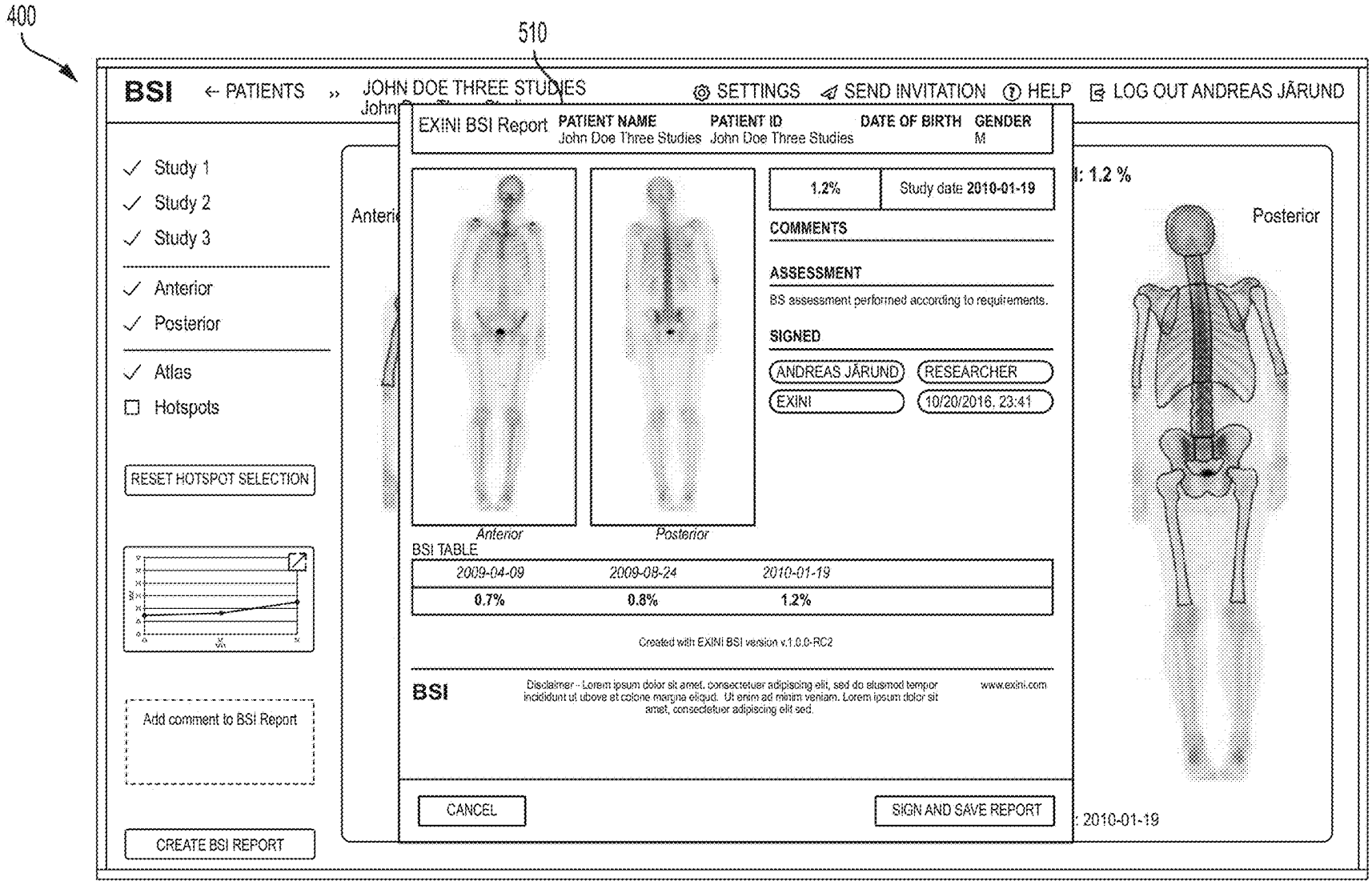

400
510
BSI
← PATIENTS
JOHN DOE THREE STUDIES
SETTINGS
SEND INVITATION
HELP
LOG OUT ANDREAS JÄRUND
Study 1
Study 2
Study 3
Anterior
Posterior
Atlas
Hotspots
RESET HOTSPOT SELECTION
Add comment to BSI Report
CREATE BSI REPORT
EXINI BSI Report
PATIENT NAME
John Doe Three Studies
PATIENT ID
John Doe Three Studies
DATE OF BIRTH
GENDER
M
1.2%
Study date 2010-01-19
COMMENTS
ASSESSMENT
BS assessment performed according to requirements.
SIGNED
ANDREAS JÄRUND
RESEARCHER
EXINI
10/20/2016, 23:41
Anterior
Posterior
BSI TABLE
2009-04-09
2009-08-24
2010-01-19
0.7%
0.8%
1.2%
Created with EXINI BSI version v.1.0.0-RC2
BSI
Disclaimer – Lorem ipsum dolor sit amet, consectetuer adipiscing elit, sed do eiusmod tempor incididunt ut ubove et colone magna eliqud. Ut enim ad minim veniam. Lorem ipsum dolor sit amet, consectetuer adipiscing elit sed.
www.exini.com
CANCEL
SIGN AND SAVE REPORT
1.2 %
Posterior
2010-01-19

FIG. 5

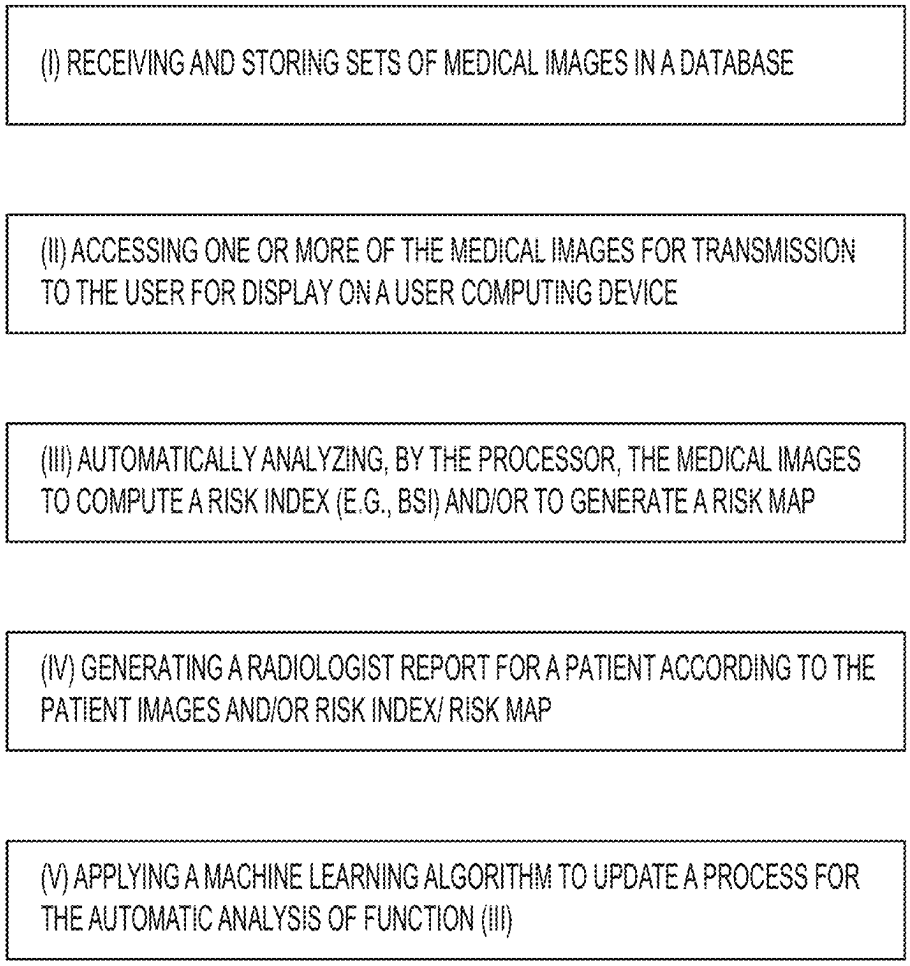

(I) RECEIVING AND STORING SETS OF MEDICAL IMAGES IN A DATABASE
(II) ACCESSING ONE OR MORE OF THE MEDICAL IMAGES FOR TRANSMISSION TO THE USER FOR DISPLAY ON A USER COMPUTING DEVICE
(III) AUTOMATICALLY ANALYZING, BY THE PROCESSOR, THE MEDICAL IMAGES TO COMPUTE A RISK INDEX (E.G., BSI) AND/OR TO GENERATE A RISK MAP
(IV) GENERATING A RADIOLOGIST REPORT FOR A PATIENT ACCORDING TO THE PATIENT IMAGES AND/OR RISK INDEX/ RISK MAP
(V) APPLYING A MACHINE LEARNING ALGORITHM TO UPDATE A PROCESS FOR THE AUTOMATIC ANALYSIS OF FUNCTION (III)

FIG. 6

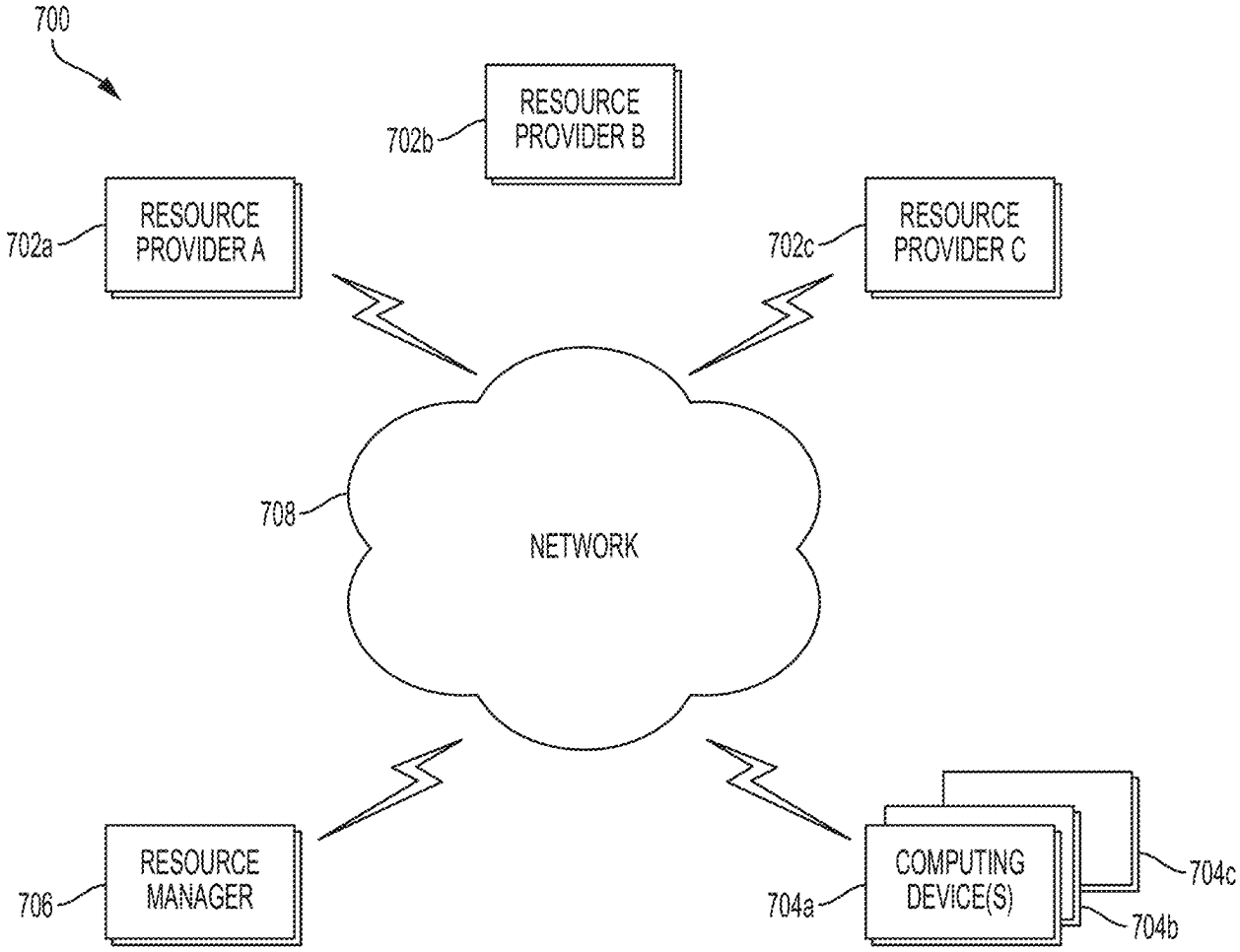

700
RESOURCE PROVIDER B
702b
RESOURCE PROVIDER A
702a
RESOURCE PROVIDER C
702c
708
NETWORK
RESOURCE MANAGER
706
COMPUTING DEVICE(S)
704a
704c
704b

FIG. 7

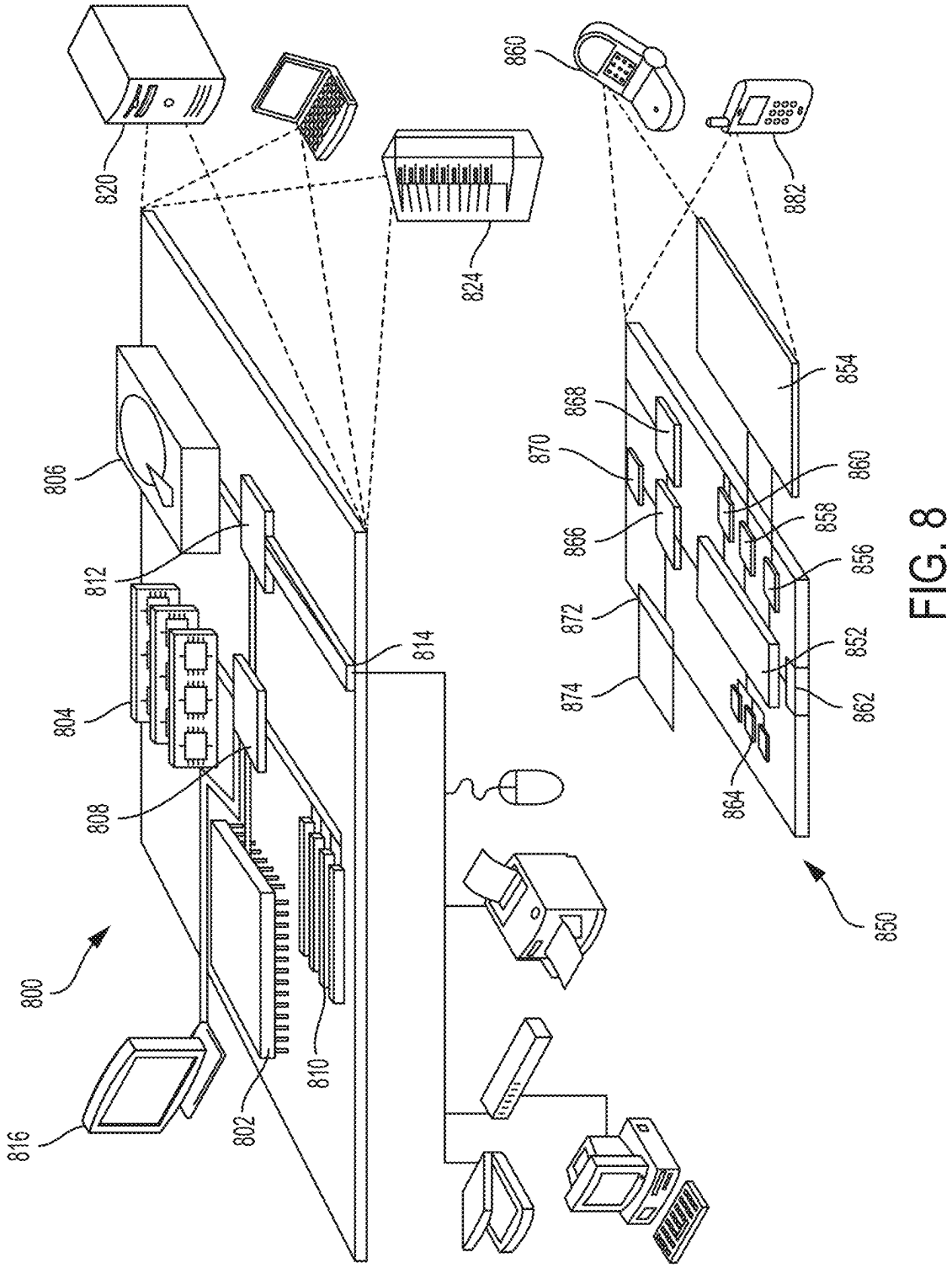

820
824
860
882
806
812
804
808
814
810
802
816
800
850
854
868
870
866
872
874
858
856
852
862
864

FIG. 8

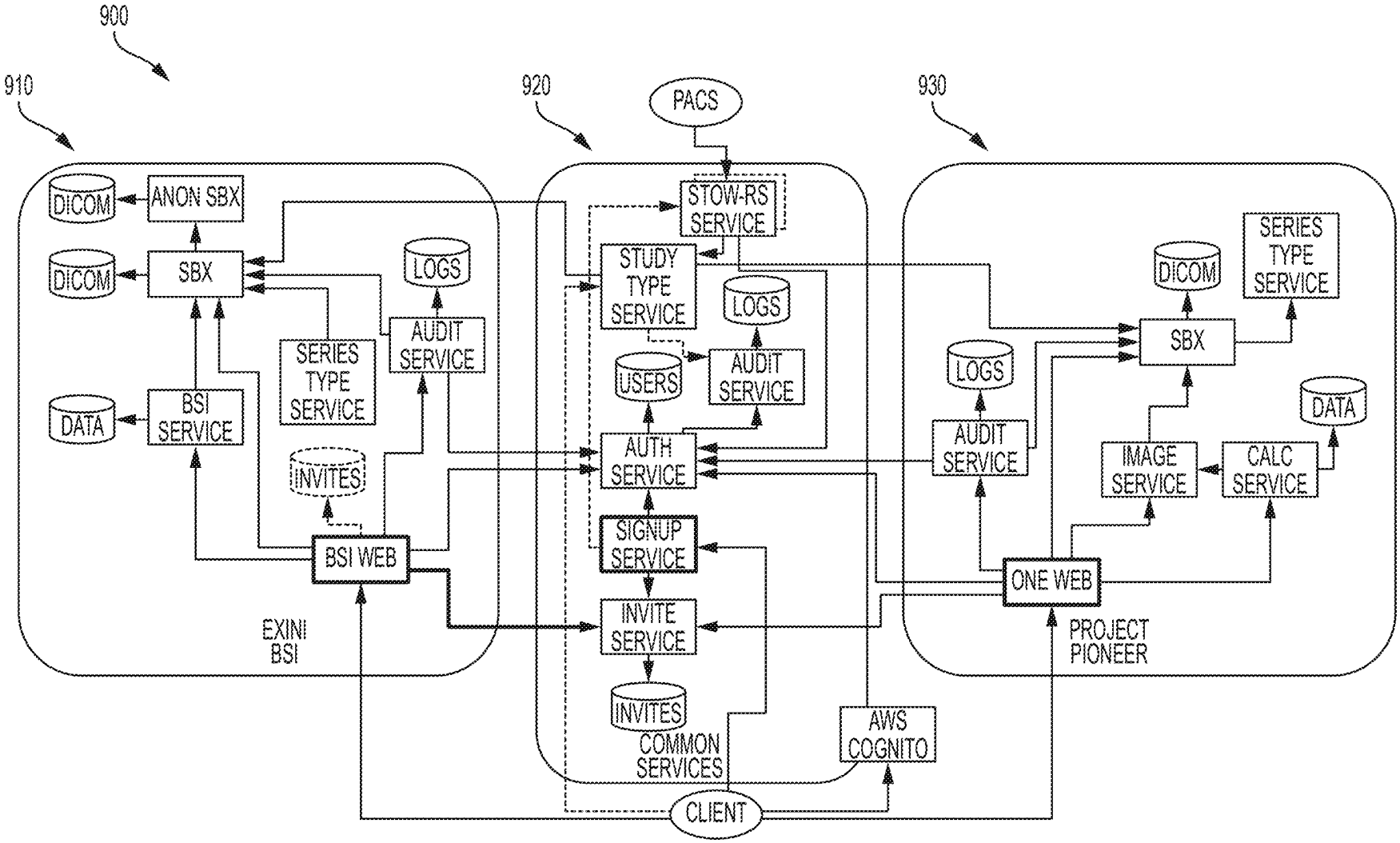

900
910
920
930
PACS
DICOM
ANON SBX
DICOM
SBX
LOGS
AUDIT SERVICE
SERIES TYPE SERVICE
DATA
BSI SERVICE
INVITES
BSI WEB
EXINI BSI
STOW-RS SERVICE
STUDY TYPE SERVICE
LOGS
AUDIT SERVICE
USERS
AUTH SERVICE
SIGNUP SERVICE
INVITE SERVICE
INVITES
COMMON SERVICES
AWS COGNITO
CLIENT
LOGS
AUDIT SERVICE
DICOM
SBX
SERIES TYPE SERVICE
DATA
IMAGE SERVICE
CALC SERVICE
ONE WEB
PROJECT PIONEER

FIG. 9

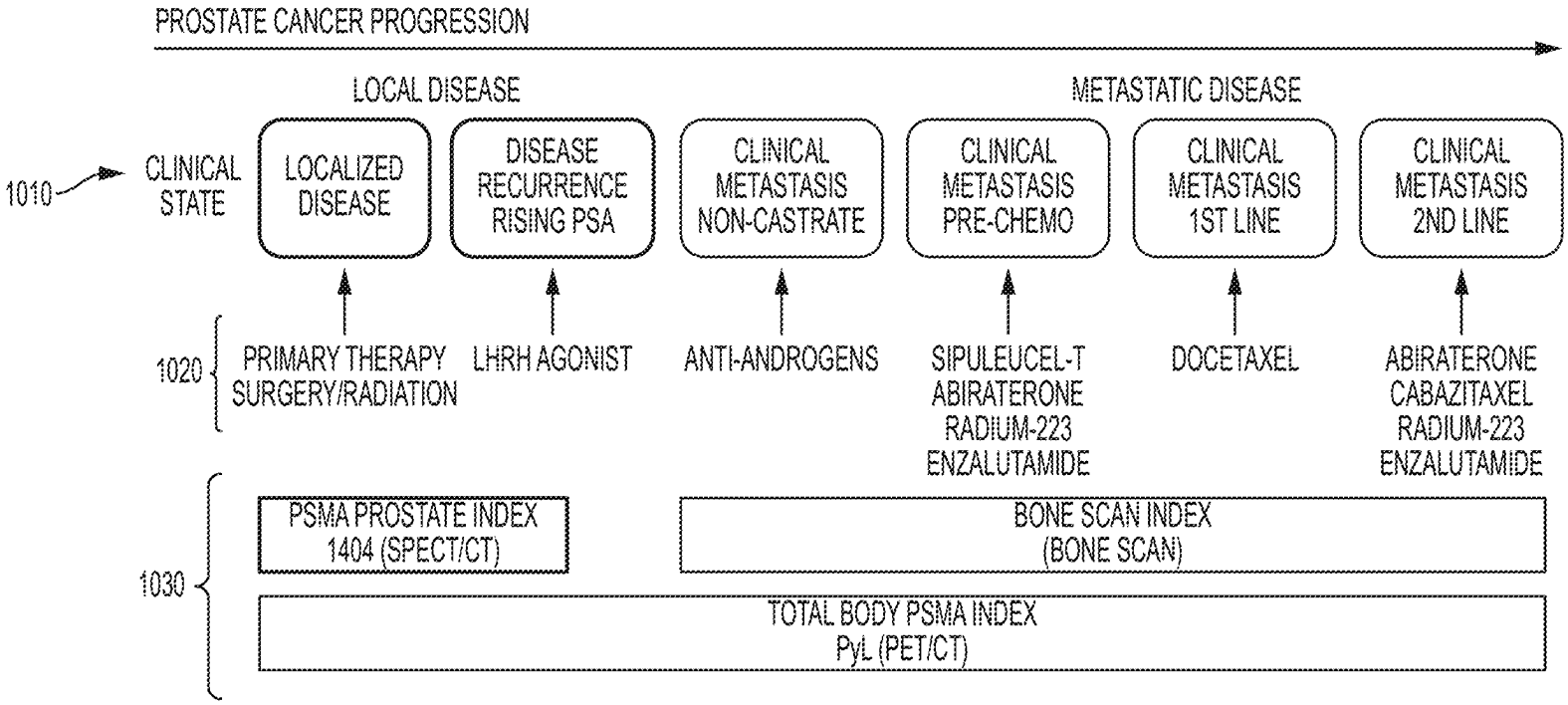

PROSTATE CANCER PROGRESSION
LOCAL DISEASE
METASTATIC DISEASE
1010
CLINICAL STATE
LOCALIZED DISEASE
DISEASE RECURRENCE RISING PSA
CLINICAL METASTASIS NON-CASTRATE
CLINICAL METASTASIS PRE-CHEMO
CLINICAL METASTASIS 1ST LINE
CLINICAL METASTASIS 2ND LINE
1020
PRIMARY THERAPY SURGERY/RADIATION
LHRH AGONIST
ANTI-ANDROGENS
SIPULEUCEL-T ABIRATERONE RADIUM-223 ENZALUTAMIDE
DOCETAXEL
ABIRATERONE CABAZITAXEL RADIUM-223 ENZALUTAMIDE
1030
PSMA PROSTATE INDEX 1404 (SPECT/CT)
BONE SCAN INDEX (BONE SCAN)
TOTAL BODY PSMA INDEX PyL (PET/CT)

FIG. 10

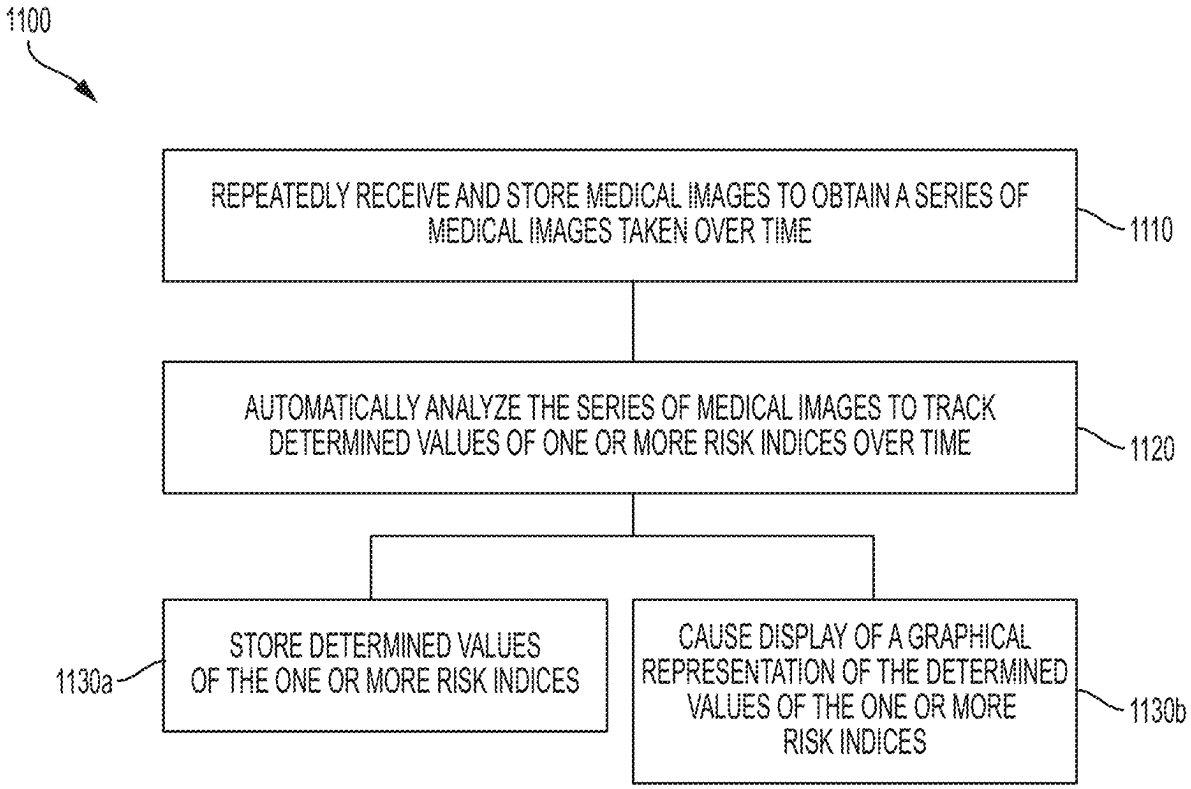

1100
REPEATEDLY RECEIVE AND STORE MEDICAL IMAGES TO OBTAIN A SERIES OF MEDICAL IMAGES TAKEN OVER TIME
1110
AUTOMATICALLY ANALYZE THE SERIES OF MEDICAL IMAGES TO TRACK DETERMINED VALUES OF ONE OR MORE RISK INDICES OVER TIME
1120
STORE DETERMINED VALUES OF THE ONE OR MORE RISK INDICES
1130a
CAUSE DISPLAY OF A GRAPHICAL REPRESENTATION OF THE DETERMINED VALUES OF THE ONE OR MORE RISK INDICES
1130b

FIG. 11

NETWORK FOR MEDICAL IMAGE ANALYSIS, DECISION SUPPORT SYSTEM, AND RELATED GRAPHICAL USER INTERFACE (GUI) APPLICATIONS

CROSS REFERENCE TO RELATED APPLICATIONS

This application is a continuation of U.S. application Ser. No. 16/938,488, filed Jul. 24, 2020 (now U.S. Pat. No. 11,424,035), which is a continuation of U.S. application Ser. No. 16/418,527, filed May 21, 2019 (now U.S. Pat. No. 10,762,993), which is a continuation of U.S. application Ser. No. 15/794,220 filed Oct. 26, 2017 (now U.S. Pat. No. 10,340,046), which claims the benefit of U.S. Provisional Application 62/413,936, filed on Oct. 27, 2016, the contents of each of which are hereby incorporated by reference herein in their entirety.

TECHNICAL FIELD

This invention relates generally to systems and methods for creation, analysis, and/or presentation of medical image data. More particularly, in certain embodiments, the invention relates to a cloud-based platform and supported GUI decision-making tools for use by medical practitioners and/or their patients, e.g., to aide in the process of making decisions about a course of cancer treatment and/or to track treatment and/or the progress of a disease.

BACKGROUND

Targeted image analysis involves the use of radiolabeled small molecules that bind to specific receptors, enzymes and proteins in the body that are altered during the evolution of disease. After administration to a patient, these molecules circulate in the blood until they find their intended target. The bound radiopharmaceutical remains at the site of disease, while the rest of the agent clears from the body. The radioactive portion of the molecule serves as a beacon so that an image may be obtained depicting the disease location and concentration using commonly available nuclear medicine cameras, known as single-photon emission computerized tomography (SPECT) or positron emission tomography (PET) cameras, found in most hospitals throughout the world. Physicians can then use this information to determine the presence and the extent of disease in a patient. The physician can use this information to provide a recommended course of treatment to the patient and to track the progression of disease.

There are a variety of software-based analytical techniques available for analysis and enhancement of PET and SPECT images that can be used by a radiologist or physician. There are also a number of radiopharmaceuticals available for imaging particular kinds of cancer. For example, the small molecule diagnostic 1404 targets the extracellular domain of prostate specific membrane antigen (PSMA), a protein amplified on the surface of >95% of prostate cancer cells and a validated target for the detection of primary and metastatic prostate cancer. 1404 is labeled with technetium-99m, a gamma-emitter isotope that is widely available, relatively inexpensive, facilitates efficient preparation, and has spectrum characteristics attractive for nuclear medicine imaging applications.

Another example radiopharmaceutical is PyL™ (also known as [^{18}F]DCFPyL), which is a clinical-stage, fluorinated PSMA-targeted PET imaging agent for prostate cancer. A proof-of-concept study published in the April 2015 issue of the Journal of Molecular Imaging and Biology demonstrated that PET imaging with PyL™ showed high levels of PyL™ uptake in sites of putative metastatic disease and primary tumors, suggesting the potential for high sensitivity and specificity in detecting prostate cancer.

An oncologist may use images from a targeted PET or SPECT study of a patient as input in her assessment of whether the patient has a particular disease, e.g., prostate cancer, what stage of the disease is evident, what the recommended course of treatment (if any) would be, whether surgical intervention is indicated, and likely prognosis. The oncologist may use a radiologist report in this assessment. A radiologist report is a technical evaluation of the PET or SPECT images prepared by a radiologist for a physician who requested the imaging study and includes, for example, the type of study performed, the clinical history, a comparison between images, the technique used to perform the study, the radiologist's observations and findings, as well as overall impressions and recommendations the radiologist may have based on the imaging study results. A signed radiologist report is sent to the physician ordering the study for the physician's review, followed by a discussion between the physician and patient about the results and recommendations for treatment.

Thus, the process involves having a radiologist perform an imaging study on the patient, analyzing the images obtained, creating a radiologist report, forwarding the report to the requesting physician, having the physician formulate an assessment and treatment recommendation, and having the physician communicate the results, recommendations, and risks to the patient. The process may also involve repeating the imaging study due to inconclusive results, or ordering further tests based on initial results.

If an imaging study shows that the patient has a particular disease or condition (e.g., cancer), the physician discusses various treatment options, including surgery, as well as risks of doing nothing or adopting a watchful waiting or active surveillance approach, rather than having surgery.

There are limitations associated with this process, both from the perspective of the physician and from the perspective of the patient. While the radiologist's report is certainly helpful, the physician must ultimately rely on her experience in formulating an assessment and recommendation for her patient. Furthermore, the patient must place a great deal of trust in his physician. The physician may show the patient his PET/SPECT images and may tell the patient a numerical risk associated with various treatment options or likelihood of a particular prognosis, but the patient may very well struggle to make sense of this information. Moreover, the patient's family will likely have questions, particularly if cancer is diagnosed but the patient opts not to have surgery. The patient and/or his family members may search online for supplemental information and may become misinformed about risks of the diagnosed condition. A difficult ordeal may become more traumatic.

Thus, there remains a need for systems and methods for improved analysis of medical imaging studies and communication of those results, diagnoses, prognoses, treatment recommendations, and associated risks to a patient.

SUMMARY OF THE INVENTION

Presented herein is a cloud-based platform and supported graphical user interface (GUI) decision-making tools for use by medical practitioners and/or their patients, e.g., to aide in

the process of making decisions about a course of cancer treatment and/or to track treatment and/or the progress of a disease.

For example, presented herein is a network-based (e.g., cloud-based) support platform allowing multiple users to store, access, analyze, and/or provide feedback regarding a given set of image data for a patient; platform supports software tools for automated analysis of targeted PET/SPECT/or other image(s), generation of radiologist reports, and application of machine learning algorithms to update process by which images are analyzed (e.g. updating segmentation and/or classification routines based on growing image database). In certain embodiments, the targeted PET/SPECT image(s) may be obtained using PyL™ and/or 1404 as the radiopharmaceutical(s). In certain embodiments, multiple (accredited) users can access the information, e.g., to weigh in on data interpretation.

Also presented herein is a software tool (e.g., mobile app) featuring a graphical user interface (GUI) element with controls for adjusting presentation of a 3D risk image corresponding to a patient organ (and/or other tissue) for comparison with reference images (e.g., for use in communication of results to patient as a decision-making support). For example, the tool may be supported by the network-based support platform above. This tool can provides an easily-understood, user-friendly, interactive, controllable pictorial display to communicate information about a patient's condition to the patient (and/or to the physician, or to the patient's family with the patient's permission). For example, a patient for whom a risk of cancer is detected can display a map indicating areas and/or degrees of risk and can compare this risk map with those of others for whom a given course of treatment is recommended. For instance, this tool can help a patient in his decision whether or not to have surgery (e.g., for a detected risk of prostate cancer). The patient can visually compare his risk map with a map representing a typical risk-level for which surgery would be recommended, below which it may be reasonable to opt not to have surgery and engage in watchful waiting or active surveillance. Thus, a low-risk patient who is told by his physician that he has a non-zero risk of cancer may find comfort in a visual, controllable comparison between his situation and that of someone (e.g., where the reference to which the patient's risk situation is compared can be tuned for age, weight, and/or other risk factors of the patient).

In one aspect, the invention is directed to a network-based (e.g., cloud based) decision support system comprising: a processor (e.g., of a network or Internet host server); and a memory having instructions stored thereon, wherein the instructions, when executed by the processor, cause the processor to perform one or more of functions (i) to (v) as follows: (i) receive and store medical images [e.g., comprising one or more of the following: targeted PET images, targeted SPECT images, computed tomography (CT) images, magnetic resonance (MR) images, ultrasound (US) images, gamma camera (i.e. scintillation camera) images, and combinations, fusions, or derivatives of any of the above] in a database [e.g., wherein the targeted PET/SPECT/gamma camera image(s) are obtained using one or more radiopharmaceuticals (e.g., [18F]DCFPyL and/or 1404 and/or a composition comprising technetium 99m, {e.g., technetium 99m methylenediphosphonate (^{99m}Tc MDP)}), and/or wherein the medical images are obtained using non-radioactive agents or no agents], each medical image associated with a particular patient; (ii) access one or more of the medical images and/or related data associated with a particular patient from the database upon user request (e.g., following automated verification that the user is properly credentialed for receiving the requested images and/or data) for transmission to the user for display on a user computing device; (iii) automatically analyze one or more of the medical images [e.g., to generate a risk index (e.g., BSI) and/or a risk map, e.g., a visual representation (e.g., 3D representation) of tissue (e.g., an organ or other part of the body) with graphical denotations (e.g., texture- or color-coding) marking regions of risk of current disease or risk of recurrence of disease, e.g., cancer, e.g., wherein the risk map is displayed as an overlay of the PET/SPECT/CT/MRI/US/combined/derived/fused image of the tissue, or is in place of the image of the tissue]; (iv) generate a radiologist report for a patient according to one or more of the medical images for the patient; and (v) apply a machine learning algorithm to update a process for automatically analyzing one or more of the medical images using accumulated image data in the database [e.g., wherein the automatic analysis of the one or more medical images in (iii) and/or (v) above comprises any one or more of (a) to (d) as follows: (a) automated fusion of the (e.g., PET, SPECT, CT, Mill, and/or US) image(s) of the tissue; (b) geographic identification of one or more organs, organ structures, sub-organs, organ regions, and/or other regions of the imaged tissue of the patient and production of a 3D image of the geographically identified tissue with PET, SPECT, CT, MRI, and/or US data overlaid; (c) computation of risk information comprising one or more risk indices, a risk field, or a risk map using data from the database, the image(s) of the tissue, and/or the 3D image in (b); and (d) use of the risk information computed in (c) (e.g., and data from the database) to produce a 3D risk picture for the patient].

In certain embodiments, the medical images in the database comprise a series of medical images of a first patient taken over time (e.g., over the course of multiple visits to one or more doctors), and wherein the instructions cause the processor to determine a value of at least a first risk index for each medical image of the series, thereby tracking determined values of at least the first risk index for the first patient over time.

In certain embodiments, the medical images comprise a single-photon emission computerized tomography (SPECT) scan of a first patient obtained (e.g., to identify one or more hotspots) following administration to the first patient of an imaging agent comprising 1404 labeled with ^{99m}Tc, and a computed tomography (CT) scan (e.g., to identify anatomical features) of the first patient, wherein the instructions cause the processor to overlay the SPECT scan with the CT scan to create a composite image (SPECT-CT) of the first patient.

In certain embodiments, the medical images comprise a positron emission tomography (PET) scan of a first patient obtained (e.g., to identify one or more hotspots) following administration to the first patient of an imaging agent comprising [18F]DCFPyL (DCFPyL labeled with ^{18}F), and a CT scan of the first patient, wherein the instructions cause the processor to overlay the PET scan with the CT scan to create a composite image (PET-CT) of the first patient.

In certain embodiments, the medical images comprise a whole-body scan (e.g., including anterior and posterior views) of a first patient made with a gamma camera following administration to the first patient of an imaging agent comprising technetium 99m methylenediphosphonate (^{99m}Tc MDP).

In certain embodiments, the medical images comprise a composite image of a first patient, the composite image comprising a CT scan overlaid with a nuclear medicine

image (e.g., a SPECT scan; e.g., a PET scan) obtained at substantially the same time as the CT scan and following administration to the first patient of an imaging agent comprising a Prostate Specific Membrane Antigen (PSMA) binding agent comprising (e.g., labelled with) a radionuclide, and the instructions cause the processor to automatically analyze the composite image by: (a) using the composite image to geographically identify a 3D boundary for each of one or more regions of imaged tissue [e.g., organs (e.g., a prostate; e.g., a liver; e.g., lungs or a lung; e.g., lymph nodes), organ structures, sub-organs, organ regions, and/or other regions (e.g., one or more particular bones; e.g., a skeletal region of the patient), e.g., regions of interest] within the nuclear medicine image (e.g., such that portions of the nuclear medicine image falling within and/or outside of the 3D boundaries can be differentiated from each other); and (c) computing (i) a value of each of one or more risk indices and/or (ii) a risk map using the nuclear medicine image with the identified 3D boundaries of the one or more region(s).

In certain embodiments, the instructions cause the processor to, for at least one risk index of the one or more risk indices, compute the value of the risk index by: determining, for each of the one or more regions, a corresponding cancerous tissue level within the region based on intensity values of the nuclear medicine image within the 3D boundary of the region (e.g., by identifying within the nuclear medicine image, a plurality of hotspots within the 3D boundary of the region and computing a total number of and/or a total volume of the identified hotspots); and computing the value of the risk index based on the determined cancerous tissue levels within the one or more regions.

In certain embodiments, the nuclear medicine image is a SPECT scan.

In certain embodiments, the imaging agent comprises a metal chelated to the PSMA binding agent, and wherein the metal is the radionuclide [e.g., wherein the metal is a radioisotope of technetium (Tc) (e.g., wherein the metal is technetium-99m (^{99m}Tc)); e.g., wherein the metal is a radioisotope of rhenium (Re) (e.g., wherein the metal is rhenium-188 (^{188}Re); e.g., wherein the metal is rhenium-186 (^{86}Re)); e.g., wherein the metal is a radioisotope of yttrium (Y) (e.g., wherein the metal is ^{90}Y); e.g., wherein the metal is a radioisotope of lutetium (Lu) (e.g., wherein the metal is ^{177}Lu); e.g., wherein the metal is a radioisotope of gallium (Ga) (e.g., wherein the metal is ^{68}Ga; e.g., wherein the metal is ^{67}Ga); e.g., wherein the metal is a radioisotope of indium (e.g., ^{111}In); e.g., wherein the metal is a radioisotope of copper (Cu) (e.g., wherein the metal is ^{67}Cu)].

In certain embodiments, the imaging agent comprises ^{99m}Tc-MIP-1404.

In certain embodiments, the nuclear medicine image is a PET scan.

In certain embodiments, the radionuclide is a radioisotope of a halogen [e.g., a radioisotope of fluorine (e.g., ^{18}F); e.g., a radioisotope of iodine (e.g., ^{123}I; e.g., ^{124}I; e.g., ^{125}I; e.g., ^{126}I; e.g., ^{131}I) e.g., a radioisotope of bromine (e.g., ^{75}Br; e.g., ^{76}Br; e.g., ^{77}Br; e.g., ^{80}Br; e.g., ^{80m}Br; e.g., ^{82}Br; e.g., ^{83}Br), e.g., a radioisotope of astatine (e.g., ^{211}At)].

In certain embodiments, the imaging agent comprises [18F]DCFPyL (DCFPyL labeled with ^{18}F).

In certain embodiments, the radionuclide is a radioisotope of gallium (Ga) (e.g., ^{68}Ga).

In certain embodiments, the medical images comprise a nuclear medicine image (e.g., a whole-body scan made with a gamma camera) of a first patient following administration to the first patient of an imaging agent comprising a radionuclide (e.g., ^{99m}Tc) (e.g., wherein the imaging agent comprises ^{99m}Tc MDP), wherein the instructions cause the processor to automatically analyze the nuclear medicine image by: (a) geographically identifying a boundary (e.g., a 2D boundary; e.g., a 3D boundary) for each of one or more regions of imaged tissue [e.g., organs (e.g., a prostate; e.g., a liver; e.g., lungs or a lung; e.g., lymph nodes), organ structures, sub-organs, organ regions, and/or other regions (e.g., one or more particular bones; e.g., a skeletal region of the patient), e.g., regions of interest] within the nuclear medicine image (e.g., such that portions of the nuclear medicine image falling within and/or outside of the boundaries can be differentiated from each other); and (c) computing (i) a value of each of one or more risk indices and/or (ii) a risk map using the nuclear medicine image with the identified boundaries of the one or more region(s).

In certain embodiments, the instructions cause the processor to, for at least one risk index of the one or more risk indices, compute the value of the risk index by: determining, for each of the one or more regions, a corresponding cancerous tissue level within the region based on intensity values of the nuclear medicine image within the boundary of the region (e.g., by identifying within the nuclear medicine image, a plurality of hotspots within the boundary of the region and computing a total number of and/or a total volume of the identified hotspots); and computing the value of the risk index based on the determined cancerous tissue levels within the one or more regions.

In certain embodiments, the system is a cloud-based system.

In certain embodiments, the processor is a processor of one or more network or Internet host servers.

In another aspect, the invention is directed to a method comprising any one or more of (i) to (v) as follows: (i) receiving and storing, by a processor of a server computing device (e.g., received over a network from a client computing device) medical images [e.g., comprising one or more of the following: targeted PET images, targeted SPECT images, computed tomography (CT) images, magnetic resonance (MR) images, ultrasound (US) images, gamma camera (i.e. scintillation camera) images, and combinations, fusions, or derivatives of any of the above] in a database [e.g., wherein the targeted PET/SPECT/gamma camera image(s) are obtained using one or more radiopharmaceuticals, e.g., [18F]DCFPyL and/or 1404 and/or a composition comprising technetium 99m, e.g., technetium 99m methylenediphosphonate (^{99m}Tc MDP), and/or wherein the medical images are obtained using non-radioactive agents or no agents], each medical image associated with a particular patient; (ii) accessing, by the processor, one or more of the medical images and/or related data associated with a particular patient from the database upon user request (e.g., following automated verification that the user is properly credentialed for receiving the requested images and/or data) for transmission to the user for display on a user computing device; (iii) automatically analyzing, by the processor, one or more of the medical images[e.g., to generate a risk map, e.g., a visual representation (e.g., 3D representation) of tissue (e.g., an organ or other part of the body) with graphical denotations (e.g., texture- or color-coding) marking regions of risk of current disease or risk of recurrence of disease, e.g., cancer, e.g., wherein the risk map is displayed as an overlay of the PET/SPECT/CT/MRI/US/combined/derived/fused image of the tissue, or is in place of the image of the tissue]; (iv) generating, by the processor, a radiologist report for a patient according to one or more of the medical images for the patient; and (v) applying, by the processor, a

machine learning algorithm to update a process for automatically analyzing one or more of the medical images using accumulated image data in the database, [e.g., wherein the automatically analyzing the one or more medical images in (iii) and/or (v) above comprises any one or more of (a) to (d) as follows: (a) automatically fusing the (e.g., PET, SPECT, CT, MRI, and/or US) image(s) of the tissue; (b) geographically identifying one or more organs, organ structures, sub-organs, organ regions, and/or other regions of the imaged tissue of the patient and production of a 3D image of the geographically identified tissue with PET, SPECT, CT, MRI, and/or US data overlaid; (c) computing risk information comprising one or more risk indices, a risk field, or a risk map using data from the database, the image(s) of the tissue, and/or the 3D image in (b); and (d) using the risk information computed in (c) (e.g., and data from the database) to produce a 3D risk picture for the patient].

In certain embodiments, the medical images in the database comprise a series of medical images of a first patient taken over time (e.g., over the course of multiple visits to one or more doctors), and wherein the method comprises determining a value of at least a first risk index for each medical image of the series, thereby tracking determined values of at least the first risk index over time.

In certain embodiments, the receiving and storing of the medical images comprises repeatedly receiving and storing, over time, a plurality of medical images of the first patient, each obtained at a different time (e.g., at a different visit to one or more doctors), to obtain the series of medical images of the first patient.

In certain embodiments, the medical images comprise a single-photon emission computerized tomography (SPECT) scan of a first patient obtained (e.g., to identify one or more hotspots) following administration to the first patient of an imaging agent comprising 1404 labeled with ^{99m}Tc, and a computed tomography (CT) scan (e.g., to identify anatomical features) of the first patient, wherein the method comprises overlaying the SPECT scan with the CT scan to create a composite image (SPECT-CT) of the first patient.

In certain embodiments, the medical images comprises a positron emission tomography (PET) scan of a first patient obtained following administration to the first patient of an imaging agent comprising [18F]DCFPyL (DCFPyL labeled with ^{18}F), and a CT scan of the first patient, wherein the method comprises overlaying the PET scan with the CT scan to create a composite image (PET-CT) of the first patient.

In certain embodiments, the medical images comprise a whole-body scan (e.g., including anterior and posterior views) of a first patient made with a gamma camera following administration to the first patient of an imaging agent comprising technetium 99m methylenediphosphonate (^{99m}Tc MDP).

In certain embodiments, the medical images comprise a composite image of a first patient, the composite image comprising a CT scan overlaid with a nuclear medicine image (e.g., a SPECT scan; e.g., a PET scan) acquired at substantially the same time and following administration to the first patient of an imaging agent comprising a Prostate Specific Membrane Antigen (PSMA) binding agent comprising a radionuclide, wherein the method comprises automatically analyzing the composite image by: (a) using the composite image to geographically identify a 3D boundary for each of one or more regions of imaged tissue [e.g., organs (e.g., a prostate; e.g., a liver; e.g., lungs or a lung; e.g., lymph nodes), organ structures, sub-organs, organ regions, and/or other regions (e.g., one or more particular bones; e.g., a skeletal region of the patient), e.g., regions of interest] within the nuclear medicine image (e.g., such that portions of the nuclear medicine image falling within and/or outside of the 3D boundaries can be differentiated from each other); and (c) computing (i) a value of each of one or more risk indices and/or a (ii) risk map using the nuclear medicine image with the identified 3D boundaries of the one or more region(s).

In certain embodiments, step (c) comprises, for at least one risk index of the one or more risk indices, computing the value of the risk index by: determining, for each of the one or more regions, a corresponding cancerous tissue level within the region based on intensity values of the nuclear medicine image within the 3D boundary of the region (e.g., by identifying within the nuclear medicine image, a plurality of hotspots within the 3D boundary of the region and computing a total number of and/or a total volume of the identified hotspots); and computing the value of the risk index based on the determined cancerous tissue levels within the one or more regions.

In certain embodiments, the nuclear medicine image is a SPECT scan.

In certain embodiments, the imaging agent comprises a metal chelated to the PSMA binding agent, and wherein the metal is the radionuclide [e.g., wherein the metal is a radioisotope of technetium (Tc) (e.g., wherein the metal is technetium-99m (^{99m}Tc)); e.g., wherein the metal is a radioisotope of rhenium (Re) (e.g., wherein the metal is rhenium-188 (^{188}Re); e.g., wherein the metal is rhenium-186 (^{86}Re)); e.g., wherein the metal is a radioisotope of yttrium (Y) (e.g., wherein the metal is ^{90}Y); e.g., wherein the metal is a radioisotope of lutetium (Lu) (e.g., wherein the metal is ^{177}Lu); e.g., wherein the metal is a radioisotope of gallium (Ga) (e.g., wherein the metal is ^{68}Ga; e.g., wherein the metal is ^{67}Ga); e.g., wherein the metal is a radioisotope of indium (e.g., ^{111}In); e.g., wherein the metal is a radioisotope of copper (Cu) (e.g., wherein the metal is ^{67}Cu)].

In certain embodiments, the imaging agent comprises ^{99m}Tc-MIP-1404.

In certain embodiments, the nuclear medicine image is a PET scan.

In certain embodiments, the radionuclide is a radioisotope of a halogen [e.g., a radioisotope of fluorine (e.g., ^{18}F); e.g., a radioisotope of iodine (e.g., ^{123}I; e.g., ^{124}I; e.g., ^{125}I; e.g., ^{126}I; e.g., ^{131}I); e.g., a radioisotope of bromine (e.g., ^{75}Br; e.g., ^{76}Br; e.g., ^{77}Br; e.g., ^{80}Br; e.g., ^{80m}Br; e.g., ^{82}Br; e.g., ^{83}Br), e.g., a radioisotope of astatine (e.g., ^{211}At)].

In certain embodiments, the imaging agent comprises [18F]DCFPyL (DCFPyL labeled with ^{18}F).

In certain embodiments, the radionuclide is a radioisotope of gallium (Ga) (e.g., ^{68}Ga)

In certain embodiments, the medical images comprise a nuclear medicine image (e.g., a whole-body scan made with a gamma camera) of a first patient obtained following administration to the first patient of an imaging agent comprising a radionuclide (e.g., ^{99m}Tc) (e.g., wherein the imaging agent comprises ^{99m}Tc MDP), wherein the method comprises automatically analyzing the nuclear medicine image by: (a) geographically identifying a boundary (e.g., a 2D boundary; e.g., a 3D boundary) for each of one or more regions of imaged tissue [e.g., organs (e.g., a prostate; e.g., a liver; e.g., lungs or a lung; e.g., lymph nodes), organ structures, sub-organs, organ regions, and/or other regions (e.g., one or more particular bones; e.g., a skeletal region of the patient), e.g., regions of interest] within the nuclear medicine image (e.g., such that portions of the nuclear medicine image falling within and/or outside of the 3D boundaries can be differentiated from each other); and (c)

computing (i) a value of each of one or more risk indices and/or (ii) a risk map using the nuclear medicine image with the identified boundaries of the one or more region(s).

In certain embodiments, step (c) comprises, for at least one risk index of the one or more risk indices, computing the value of the risk index by: determining, for each of the one or more regions, a corresponding cancerous tissue level within the region based on intensity values of the nuclear medicine image within the boundary of the region (e.g., by identifying within the nuclear medicine image, a plurality of hotspots within the 3D boundary of the region and computing a total number of and/or a total volume of the identified hotspots); and computing the value of the risk index based on the determined cancerous tissue levels within the one or more regions.

In certain embodiments, the processor is a processor of a cloud-based system.

In certain embodiments, the processor is a processor of one or more network or Internet host servers.

In another aspect, the invention is directed to a system comprising: a processor (e.g., of a network or Internet host server or of a portable computing device); and a memory having instructions stored thereon, wherein the instructions, when executed by the processor, cause the processor to generate and cause display of an interactive graphical user interface (GUI) element (e.g., cause display of the GUI element on a laptop computer or on a remote computing device, e.g., via a mobile app), the GUI element having user-selectable and/or user-adjustable graphical controls (e.g., slider bars, option buttons, text bars, drop-down boxes, windows, animations, and/or any other GUI widget) for selecting and/or adjusting a digital presentation of a 3D risk picture of a patient for comparison with reference images (e.g., for use in communication of results to patient as a decision-making support) caused to be displayed by the processor (e.g., wherein the reference images displayed to the user or presented for selection by the user are tunable according to one or more predetermined variables associated with the patient, e.g., patient age, time since diagnosis, prior treatment, and/or future treatment).

In certain embodiments, the interactive GUI element is produced from medical images of the patient [e.g., comprising one or more of the following: targeted PET images, targeted SPECT images, magnetic resonance (MR) images, ultrasound (US) images, gamma camera (i.e. scintillation camera) images, and combinations, fusions, or derivatives of any of the above] and/or other images or information (e.g., other images received and stored in the database of the network-based decision support system of any of the aspects and/or embodiments described herein).

In another aspect, the invention is directed to a method for tracking prostate cancer progression and treatment efficacy over time, for one or more patient(s), the method comprising: (a) repeatedly receiving and storing in a database, over time, by a processor of a computing device (e.g., a server computing device), a plurality of medical images for each of the one or more patient(s) to obtain, for each of the one or more patient(s), a series of medical images taken over time (e.g., over the course of multiple visits to one or more doctors); (b) for each of the one or more patient(s), automatically analyzing, by the processor, the series of medical images for the patient to determine values of one or more risk indices [e.g., the values of the one or more risk indices corresponding to numeric values indicative of prostate cancer state and/or progression in the patient (e.g., numeric values identifying a particular cancer stage; e.g., numeric values corresponding to a determined overall survival rate for the patient)] for each medical image of the series, thereby tracking determined values of the one or more risk indices over a course prostate cancer progression and treatment for the patient; and (c) for each of the one or more patient(s), storing, by the processor, the determined values of the one or more risk indices for the patient for further processing and/or causing, by the processor, display of a graphical representation of the determined values of the one or more risk indices for the patient (e.g., causing display of a graph showing variation in the determined values of the one or more risk indices for the patient over time).

In certain embodiments, the series of medical images for a particular patient of the one or more patient(s) comprises: (i) a first image subseries comprising one or more medical images obtained using a first nuclear imaging modality (e.g., SPECT scans; e.g., composite SPECT-CT images) each following administration to the particular patient of a first radiopharmaceutical (e.g., ^{99m}Tc-MIP-1404) (e.g., wherein the first radiopharmaceutical facilitates imaging of localized disease, e.g., localized prostate cancer); and (ii) a second image subseries comprising one or more medical images obtained using a second nuclear imaging modality (e.g., PET scans; e.g., composite PET-CT images; e.g., whole-body scans) each following administration to the particular patient of a second radiopharmaceutical (e.g., [18F] DCFPyL; e.g., ^{99m}Tc MDP) (e.g., wherein the second radiopharmaceutical facilitates imaging of metastatic disease, e.g., metastatic prostate cancer), such that the values of the one or more risk indices determined in step (b) for the particular patient comprise a first subseries of values of a first risk index determined by automated analysis of the first image subseries and a second subseries of values of a second risk index determined by automated analysis of the second image subseries.

In certain embodiments, the medical images of first image subseries are obtained over a first period of time, when prostate cancer of the particular patient is localized (e.g., substantially localized to a prostate of the particular patient), and the medical images of the second image subseries are obtained over a second period of time, when prostate cancer of the particular patient is metastatic (e.g., having spread to regions of the patient outside of the prostate).

In certain embodiments, the first image subseries comprises one or more composite SPECT-CT image(s), each composite SPECT-CT image comprising a CT scan overlaid with a SPECT scan acquired at substantially the same time; the second image subseries comprises one or more composite PET-CT image(s), each composite PET-CT image comprising a CT scan overlaid with a PET scan acquired at substantially the same time; and step (b) comprises: automatically analyzing each of the one or more composite SPECT-CT images by: using the composite SPECT-CT image to geographically identify a 3D boundary of a prostate region (e.g., corresponding to a prostate of the patient) within the SPECT scan of the composite SPECT-CT image (e.g., such that portions of the nuclear medicine image falling within and/or outside of the 3D boundary of the prostate region can be differentiated from each other); and computing a value of the first risk index using the SPECT scan with the identified 3D boundary of the prostate region (e.g., computed based on a region of the SPECT scan corresponding to the identified 3D boundary of the prostate region); and automatically analyzing each of the one or more composite PET-CT images by: using the composite PET-CT image to geographically identify a 3D boundary of one or more metastatic regions within the PET scan of the composite PET-CT image, the one or metastatic regions includ-

ing regions corresponding to patient tissue locations outside of the prostate [e.g., organs (e.g., a prostate; e.g., a liver; e.g., lungs or a lung; e.g., lymph nodes), organ structures, sub-organs, organ regions, and/or other regions (e.g., one or more particular bones; e.g., a skeletal region corresponding to the patient's skeleton), e.g., regions of interest] (e.g., such that portions of the PET imaging scan falling within and/or outside of the 3D boundaries of the one or more metastatic region(s) can be differentiated from each other); and computing a value of the second risk index using the PET scan with the identified 3D boundaries of the one or more metastatic region(s).

In certain embodiments, the first image subseries comprises one or more composite SPECT-CT image(s), each composite SPECT-CT image comprising a CT scan overlaid with a SPECT scan acquired at substantially the same time; the second image subseries comprises one or more whole-body scan(s); and step (b) comprises: automatically analyzing each of the one or more composite SPECT-CT images by: using the composite SPECT-CT image to geographically identify a 3D boundary of a prostate region (e.g., corresponding to a prostate of the patient) within the SPECT scan of the composite SPECT-CT image (e.g., such that portions of the nuclear medicine image falling within and/or outside of the 3D boundary of the prostate region can be differentiated from each other); and computing a value of the first risk index using the SPECT scan with the identified 3D boundary of the prostate region (e.g., computed based on a region of the SPECT scan corresponding to the identified 3D boundary of the prostate region); and automatically analyzing each of the one or more whole-body scan(s) by: geographically identifying a boundary of one or more metastatic regions within the whole-body scan, the one or metastatic regions including regions corresponding to patient tissue locations outside of the prostate [(e.g., one or more particular bones; e.g., a skeletal region corresponding to the patient's skeleton), e.g., regions of interest] (e.g., such that portions of the whole-body scan falling within and/or outside of the boundaries of the one or more metastatic region(s) can be differentiated from each other); and computing a value of the second risk index using the PET scan with the identified 3D boundaries of the one or more metastatic region(s).

In another aspect, the invention is directed to a system for tracking prostate cancer progression and treatment efficacy over time, for one or more patient(s), the system comprising: a processor (e.g., of a network or Internet host server); and a memory having instructions stored thereon, wherein the instructions, when executed by the processor, cause the processor to: (a) repeatedly receive and store in a database, over time, a plurality of medical images for each of the one or more patient(s) to obtain, for each of the one or more patient(s), a series of medical images taken over time (e.g., over the course of multiple visits to one or more doctors); (b) for each of the one or more patient(s), automatically analyze the series of medical images for the patient to determine values of one or more risk indices [e.g., the values of the one or more risk indices corresponding to numeric values indicative of prostate cancer state and/or progression in the patient (e.g., numeric values identifying a particular cancer stage; e.g., numeric values corresponding to a determined overall survival rate for the patient)] for each medical image of the series, thereby tracking determined values of the one or more risk indices over a course prostate cancer progression and treatment for the patient; and (c) for each of the one or more patient(s), store the determined values of the one or more risk indices for the patient for further processing and/or cause display of a graphical representation of the determined values of the one or more risk indices for the patient (e.g., causing display of a graph showing variation in the determined values of the one or more risk indices for the patient over time).

In certain embodiments, the series of medical images for a particular patient of the one or more patient(s) comprises: (i) a first image subseries comprising one or more medical images obtained using a first nuclear imaging modality (e.g., SPECT scans; e.g., composite SPECT-CT images) each following administration to the particular patient of a first radiopharmaceutical (e.g., ^{99m}Tc-MIP-1404) (e.g., wherein the first radiopharmaceutical facilitates imaging of localized disease, e.g., localized prostate cancer); and (ii) a second image subseries comprising one or more medical images obtained using a second nuclear imaging modality (e.g., PET scans; e.g., composite PET-CT images; e.g., whole-body scans) each following administration to the particular patient of a second radiopharmaceutical (e.g., [18F] DCFPyL; e.g., ^{99m}Tc MDP) (e.g., wherein the second radiopharmaceutical facilitates imaging of metastatic disease, e.g., metastatic prostate cancer), such that the values of the one or more risk indices determined in step (b) for the particular patient comprise a first subseries of values of a first risk index determined by automated analysis of the first image subseries and a second subseries of values of a second risk index determined by automated analysis of the second image subseries.

In certain embodiments, the medical images of first image subseries are obtained over a first period of time, when prostate cancer of the particular patient is localized (e.g., substantially localized to a prostate of the particular patient), and the medical images of the second image subseries are obtained over a second period of time, when prostate cancer of the particular patient is metastatic (e.g., having spread to regions of the patient outside of the prostate).

In certain embodiments, the first image subseries comprises one or more composite SPECT-CT image(s), each composite SPECT-CT image comprising a CT scan overlaid with a SPECT scan acquired at substantially the same time; the second image subseries comprises one or more composite PET-CT image(s), each composite PET-CT image comprising a CT scan overlaid with a PET scan acquired at substantially the same time; and the instructions cause the processor to, at step (b): automatically analyze each of the one or more composite SPECT-CT images by: using the composite SPECT-CT image to geographically identify a 3D boundary of a prostate region (e.g., corresponding to a prostate of the patient) within the SPECT scan of the composite SPECT-CT image (e.g., such that portions of the nuclear medicine image falling within and/or outside of the 3D boundary of the prostate region can be differentiated from each other); and computing a value of the first risk index using the SPECT scan with the identified 3D boundary of the prostate region (e.g., computed based on a region of the SPECT scan corresponding to the identified 3D boundary of the prostate region); and automatically analyze each of the one or more composite PET-CT images by: using the composite PET-CT image to geographically identify a 3D boundary of one or more metastatic regions within the PET scan of the composite PET-CT image, the one or metastatic regions including regions corresponding to patient tissue locations outside of the prostate [e.g., organs (e.g., a prostate; e.g., a liver; e.g., lungs or a lung; e.g., lymph nodes), organ structures, sub-organs, organ regions, and/or other regions (e.g., one or more particular bones; e.g., a skeletal region corresponding to the patient's skeleton), e.g., regions

of interest] (e.g., such that portions of the PET imaging scan falling within and/or outside of the 3D boundaries of the one or more metastatic region(s) can be differentiated from each other); and computing a value of the second risk index using the PET scan with the identified 3D boundaries of the one or more metastatic region(s).

In certain embodiments, the first image subseries comprises one or more composite SPECT-CT image(s), each composite SPECT-CT image comprising a CT scan overlaid with a SPECT scan acquired at substantially the same time; the second image subseries comprises one or more whole-body scan(s); and the instructions cause the processor to, at step (b): automatically analyze each of the one or more composite SPECT-CT images by: using the composite SPECT-CT image to geographically identify a 3D boundary of a prostate region (e.g., corresponding to a prostate of the patient) within the SPECT scan of the composite SPECT-CT image (e.g., such that portions of the nuclear medicine image falling within and/or outside of the 3D boundary of the prostate region can be differentiated from each other); and computing a value of the first risk index using the SPECT scan with the identified 3D boundary of the prostate region (e.g., computed based on a region of the SPECT scan corresponding to the identified 3D boundary of the prostate region); and automatically analyze each of the one or more whole-body scan(s) by: geographically identifying a boundary of one or more metastatic regions within the whole-body scan, the one or metastatic regions including regions corresponding to patient tissue locations outside of the prostate [(e.g., one or more particular bones; e.g., a skeletal region corresponding to the patient's skeleton), e.g., regions of interest] (e.g., such that portions of the whole-body scan falling within and/or outside of the boundaries of the one or more metastatic region(s) can be differentiated from each other); and computing a value of the second risk index using the PET scan with the identified 3D boundaries of the one or more metastatic region(s).

Embodiments described with respect to one aspect of the invention may be, applied to another aspect of the invention (e.g., features of embodiments described with respect to one independent claim, e.g., a method claim, are contemplated to be applicable to other embodiments of other independent claims, e.g., a system claim, and vice versa).

BRIEF DESCRIPTION OF THE DRAWINGS

The foregoing and other objects, aspects, features, and advantages of the present disclosure will become more apparent and better understood by referring to the following description taken in conjunction with the accompanying drawings, in which:

FIG. **1** is a screenshot of a graphical user interface (GUI) showing mobile app icons for three cloud-based services, according to illustrative embodiments.

FIG. **2** is a schematic showing the relationship between a platform and a computing device (e.g., personal computer or mobile computing device, e.g., smart phone) running an application, according to illustrative embodiments of the invention.

FIG. **3** is a screenshot of a GUI window in the BSI Cloud application (displayed to a user) that allows a user to enter information about a patient and upload and/or access medical images for the patient, e.g., series of images obtained over a period of time, according to an illustrative embodiment.

FIG. **4** is a screenshot of a GUI window in the BSI Cloud application showing representative full body gamma camera images showing hotspots automatically identified by the system, with corresponding overall computed BSI values for a particular image set obtained at a given time, according to an illustrative embodiment.

FIG. **5** is a screenshot of a GUI window in the BSI Cloud application showing an automatically or semi-automatically generated radiologist report, which can be signed and dated by a radiologist, according to an illustrative embodiment.

FIG. **6** is a block diagram showing a set of functionalities offered by the a cloud-based platform and supported graphical user interface (GUI) decision-making tools described herein, according to an illustrative embodiment.

FIG. **7** is a block diagram of an exemplary cloud computing environment, used in certain embodiments.

FIG. **8** is a block diagram of an example computing device and an example mobile computing device used in certain embodiments.

FIG. **9** is block diagram of an example architecture for implementing the cloud based platform described herein, according to an illustrative embodiment.

FIG. **10** is a schematic showing stages of prostate cancer progression, along with various therapies and diagnostic imaging modalities appropriate for various disease states, according to an illustrative embodiment.

FIG. **11** is a block flow diagram of a process for tracking prostate cancer progression and treatment efficacy over time, according to an illustrative embodiment.

The features and advantages of the present disclosure will become more apparent from the detailed description set forth below when taken in conjunction with the drawings, in which like reference characters identify corresponding elements throughout. In the drawings, like reference numbers generally indicate identical, functionally similar, and/or structurally similar elements.

DETAILED DESCRIPTION

It is contemplated that systems, devices, methods, and processes of the claimed invention encompass variations and adaptations developed using information from the embodiments described herein. Adaptation and/or modification of the systems, devices, methods, and processes described herein may be performed by those of ordinary skill in the relevant art.

Throughout the description, where articles, devices, and systems are described as having, including, or comprising specific components, or where processes and methods are described as having, including, or comprising specific steps, it is contemplated that, additionally, there are articles, devices, and systems of the present invention that consist essentially of, or consist of, the recited components, and that there are processes and methods according to the present invention that consist essentially of, or consist of, the recited processing steps.

It should be understood that the order of steps or order for performing certain action is immaterial so long as the invention remains operable. Moreover, two or more steps or actions may be conducted simultaneously.

The mention herein of any publication, for example, in the Background section, is not an admission that the publication serves as prior art with respect to any of the claims presented herein. The Background section is presented for purposes of clarity and is not meant as a description of prior art with respect to any claim.

Headers are provided for the convenience of the reader—the presence and/or placement of a header is not intended to limit the scope of the subject matter described herein.

A. Medical Imaging Modalities, Associated Radiopharmaceuticals, and Computed Risk Indices

FIG. **1** shows mobile app icons **100** for three cloud-based services, according to illustrative embodiments. As described in the following, the cloud-based services of the platform described herein provide for processing and analysis of medical images in a fully automated fashion and/or in combination with a user interaction (e.g., in a semi-automated fashion). The medical images include nuclear medicine images, obtained using a nuclear imaging modality such as whole-body scans with a gamma camera, Positron Emission Tomography (PET) scans, and Single-Photon Emission Tomography (SPECT) scans.

In certain embodiments, nuclear medicine images use imaging agents comprising radiopharmaceuticals. Nuclear medicine images are obtained following administration of a radiopharmaceutical to a patient, and provide information regarding the distribution of the radiopharmaceutical within the patient. Radiopharmaceuticals are compounds that comprise a radionuclide.

As used herein, "radionuclide" refers to a moiety comprising a radioactive isotope of at least one element. Exemplary suitable radionuclides include but are not limited to those described herein. In some embodiments, a radionuclide is one used in positron emission tomography (PET). In some embodiments, a radionuclide is one used in single-photon emission computed tomography (SPECT). In some embodiments, a non-limiting list of radionuclides includes ^{99m}Tc, ^{111}In, ^{64}Cu, ^{67}Ga, ^{68}Ga, ^{186}Re, ^{188}Re, ^{153}Sm, ^{177}Lu, ^{67}Cu, ^{123}I, ^{124}I, ^{125}I, ^{126}I, ^{131}I, ^{11}C, ^{13}N, ^{15}O, ^{18}F, ^{153}Sm, ^{166}Ho, ^{177}Lu, ^{149}Pm, ^{90}Y, ^{213}Bi, ^{103}Pd, ^{109}Pd, ^{159}Gd, ^{140}La, ^{198}Au, ^{199}Au, ^{169}Yb, ^{175}Yb, ^{165}Dy, ^{166}Dy, ^{105}Rh, ^{111}Ag, ^{89}Zr, ^{225}Ac, ^{82}Rb, ^{75}Br, ^{76}Br, ^{77}Br, ^{80}Br, ^{80m}Br, ^{82}Br, ^{83}Br, ^{211}At and ^{192}Ir.

As used herein, the term "radiopharmaceutical" refers to a compound comprising a radionuclide. In certain embodiments, radiopharmaceuticals are used for diagnostic and/or therapeutic purposes. In certain embodiments, radiopharmaceuticals include small molecules that are labeled with one or more radionuclide(s), antibodies that are labeled with one or more radionuclide(s), and antigen-binding portions of antibodies that are labeled with one or more radionuclide(s).

Nuclear medicine images (e.g., PET scans; e.g., SPECT scans; e.g., whole-body scans; e.g. composite PET-CT images; e.g., composite SPECT-CT images) detect radiation emitted from the radionuclides of radiopharmaceuticals to form an image. The distribution of a particular radiopharmaceutical within a patient may be determined by biological mechanisms such as blood flow or perfusion, as well as by specific enzymatic or receptor binding interactions. Different radiopharmaceuticals may be designed to take advantage of different biological mechanisms and/or particular specific enzymatic or receptor binding interactions and thus, when administered to a patient, selectively concentrate within particular types of tissue and/or regions within the patient. Greater amounts of radiation are emitted from regions within the patient that have higher concentrations of radiopharmaceutical than other regions, such that these regions appear brighter in nuclear medicine images. Accordingly, intensity variations within a nuclear medicine image can be used to map the distribution of radiopharmaceutical within the patient. This mapped distribution of radiopharmaceutical within the patient can be used to, for example, infer the presence of cancerous tissue within various regions of the patient's body.

For example, upon administration to a patient, technetium 99m methylenediphosphonate (^{99m}Tc MDP) selectively accumulates within the skeletal region of the patient, in particular at sites with abnormal osteogenesis associated with malignant bone lesions. The selective concentration of radiopharmaceutical at these sites produces identifiable hotspots—localized regions of high intensity in nuclear medicine images. Accordingly, presence of malignant bone lesions associated with metastatic prostate cancer can be inferred by identifying such hotspots within a whole-body scan of the patient. As described in the following, risk indices that correlate with patient overall survival and other prognostic metrics indicative of disease state, progression, treatment efficacy, and the like, can be computed based on automated analysis of intensity variations in whole-body scans obtained following administration of ^{99m}Tc MDP to a patient. In certain embodiments, other radiopharmaceuticals can also be used in a similar fashion to ^{99m}Tc MDP.

In certain embodiments, the particular radiopharmaceutical used depends on the particular nuclear medicine imaging modality used. For example ^{18}F sodium fluoride (NaF) also accumulates in bone lesions, similar to ^{99m}Tc MDP, but can be used with PET imaging. In certain embodiments, PET imaging may also utilize a radioactive form of the vitamin choline, which is readily absorbed by prostate cancer cells.

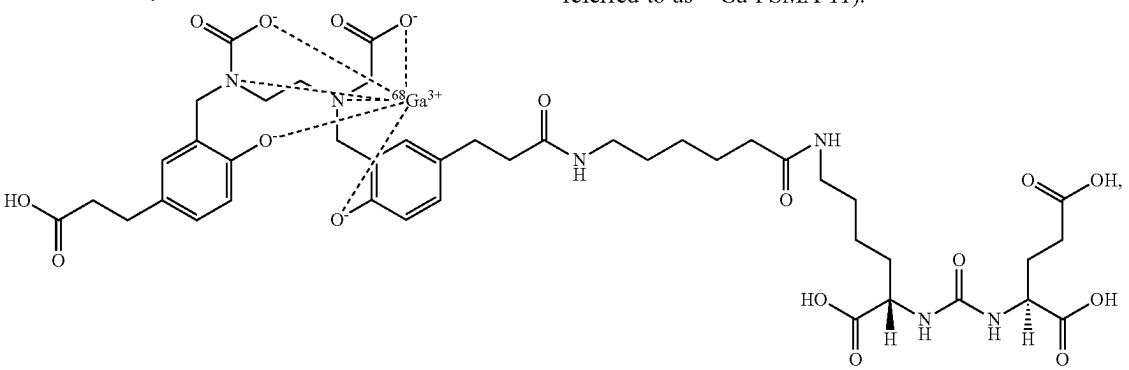
In certain embodiments, radiopharmaceuticals that selectively bind to particular proteins or receptors of interest—particularly those whose expression is increased in cancerous tissue may be used. Such proteins or receptors of interest include, but are not limited to tumor antigens, such as CEA, which is expressed in colorectal carcinomas, Her2/neu, which is expressed in multiple cancers, BRCA 1 and BRCA 2, expressed in breast and ovarian cancers; and TRP-1 and -2, expressed in melanoma.

For example, human prostate-specific membrane antigen (PSMA) is upregulated in prostate cancer, including metastatic disease. PSMA is expressed by virtually all prostate cancers and its expression is further increased in poorly differentiated, metastatic and hormone refractory carcinomas. Accordingly, radiopharmaceuticals corresponding to PSMA binding agents (e.g., compounds that a high affinity to PSMA) labelled with one or more radionuclide(s) can be used to obtain nuclear medicine images of a patient from which the presence and/or state of prostate cancer within a variety of regions (e.g., including, but not limited to skeletal regions) of the patient can be assessed. In certain embodiments, nuclear medicine images obtained using PSMA binding agents are used to identify the presence of cancerous tissue within the prostate, when the disease is in a localized state. In certain embodiments, nuclear medicine images obtained using radiopharmaceuticals comprising PSMA binding agents are used to identify the presence of cancerous tissue within a variety of regions that include not only the prostate, but also other organs and tissue regions such as lungs, lymph nodes, and bones, as is relevant when the disease is metastatic.

In particular, upon administration to a patient, radionuclide labelled PSMA binding agents selectively accumulate within cancerous tissue, based on their affinity to PSMA. In a similar manner to that described above with regard to ^{99m}Tc MDP, the selective concentration of radionuclide labelled PSMA binding agents at particular sites within the patient produces detectable hotspots in nuclear medicine images. As PSMA binding agents concentrate within a variety of cancerous tissues and regions of the body expressing PSMA, localized cancer within a prostate of the patient and/or metastatic cancer in various regions of the patient's body can be detected, and evaluated. As described in the following, risk indices that correlate with patient overall survival and other prognostic metrics indicative of disease state, progression, treatment efficacy, and the like, can be computed based on automated analysis of intensity variations in nuclear medicine images obtained following administration of a PSMA binding agent radiopharmaceutical to a patient.

A variety of radionuclide labelled PSMA binding agents may be used as radiopharmaceutical imaging agents for nuclear medicine imaging to detect and evaluate prostate cancer. In certain embodiments, the particular radionuclide labelled PSMA binding agent that is used depends on factors such as the particular imaging modality (e.g., PET; e.g., SPECT) and the particular regions (e.g., organs) of the patient to be imaged. For example, certain radionuclide labelled PSMA binding agents are suited for PET imaging, while others are suited for SPECT imaging. For example, certain radionuclide labelled PSMA binding agents facilitate imaging a prostate of the patient, and are used primarily when the disease is localized, while others facilitate imaging organs and regions throughout the patient's body, and are useful for evaluating metastatic prostate cancer.

A variety of PSMA binding agents and radionuclide labelled versions thereof are described in U.S. Pat. Nos. 8,778,305, 8,211,401, and 8,962,799, each of which are incorporated herein by reference in their entireties.

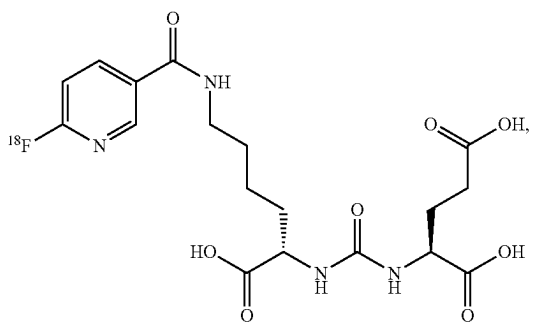


^{68}Ga-PSMA-HBED-CC

A.i PET Imaging Radionuclide Labelled PSMA Binding Agents

In certain embodiments, the radionuclide labelled PSMA binding agent is a radionuclide labelled PSMA binding agent appropriate for PET imaging.

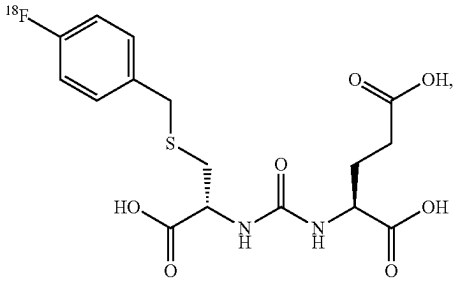
In certain embodiments, the radionuclide labelled PSMA binding agent comprises [18F]DCFPyL (also referred to as PyL™; also referred to as DCFPyL-18F):



[18F]DCFPyL

or a pharmaceutically acceptable salt thereof.

In certain embodiments, the radionuclide labelled PSMA binding agent comprises [18F]DCFBC:



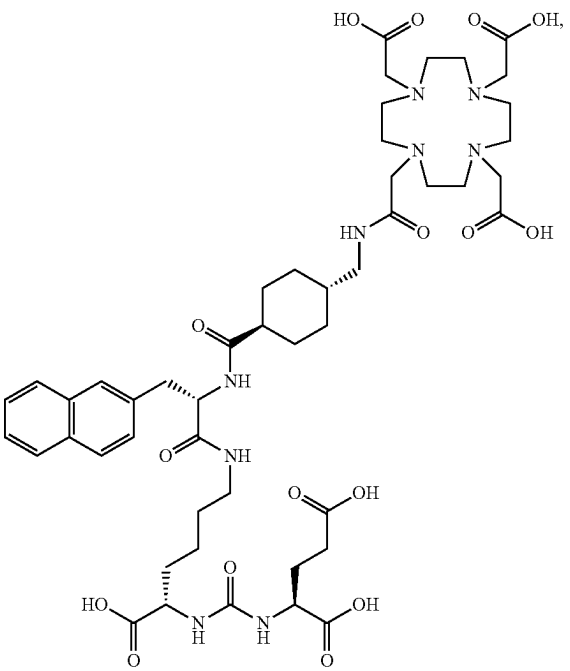
[18F]DCFBC

or a pharmaceutically acceptable salt thereof.

In certain embodiments, the radionuclide labelled PSMA binding agent comprises ^{68}Ga-PSMA-HBED-CC (also referred to as ^{68}Ga-PSMA-11):

or a pharmaceutically acceptable salt thereof.

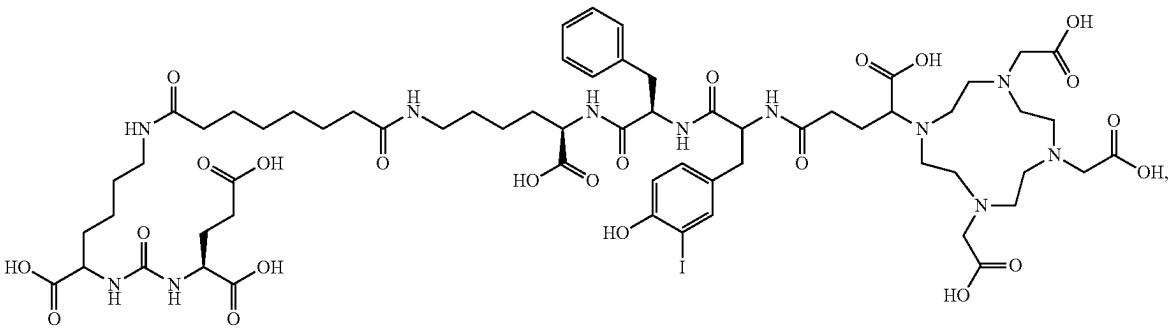
In certain embodiments, the radionuclide labelled PSMA binding agent comprises PSMA-617:



PSMA-617

or a pharmaceutically acceptable salt thereof. In certain embodiments, the radionuclide labelled PSMA binding agent comprises ^{68}Ga-PSMA-617, which is PSMA-617 labelled with ^{68}Ga, or a pharmaceutically acceptable salt thereof. In certain embodiments, the radionuclide labelled PSMA binding agent comprises ^{117}Lu-PSMA-617, which is PSMA-617 labelled with ^{177}Lu, or a pharmaceutically acceptable salt thereof.

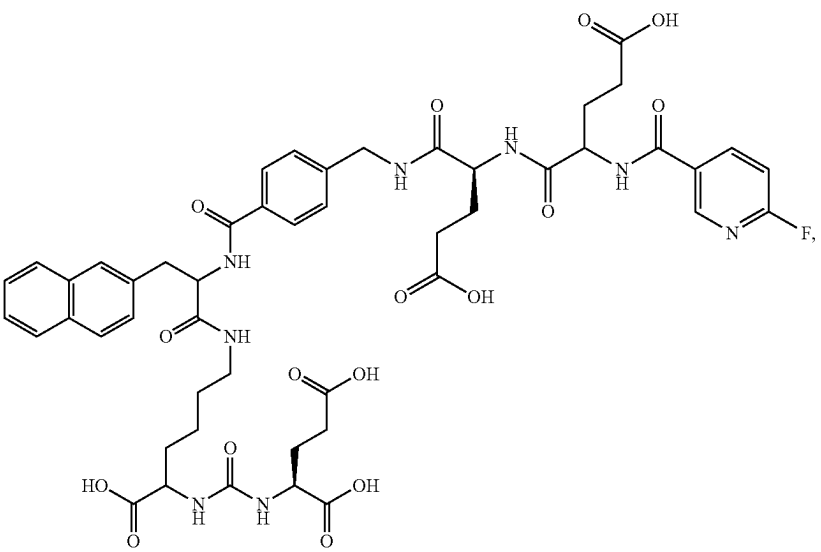
In certain embodiments, the radionuclide labelled PSMA binding agent comprises PSMA-I&T:



PSMA-I&T

or a pharmaceutically acceptable salt thereof. In certain embodiments, the radionuclide labelled PSMA binding agent comprises ^{68}Ga-PSMA-I&T, which is PSMA-I&T labelled with ^{68}Ga, or a pharmaceutically acceptable salt thereof.

In certain embodiments, the radionuclide labelled PSMA binding agent comprises PSMA-1007:



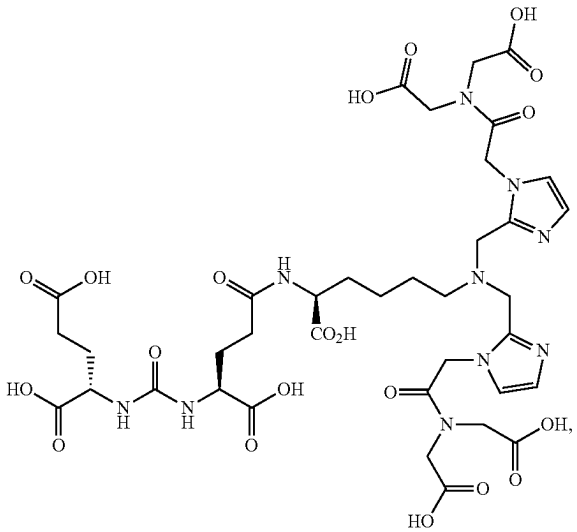
PSMA-1007

or a pharmaceutically acceptable salt thereof. In certain embodiments, the radionuclide labelled PSMA binding agent comprises ^{18}F-PSMA-1007, which is PSMA-1007 labelled with ^{18}F, or a pharmaceutically acceptable salt thereof.

A.ii SPECT Imaging Radionuclide Labelled PSMA Binding Agents

In certain embodiments, the radionuclide labelled PSMA binding agent is a radionuclide labelled PSMA binding agent appropriate for SPECT imaging.

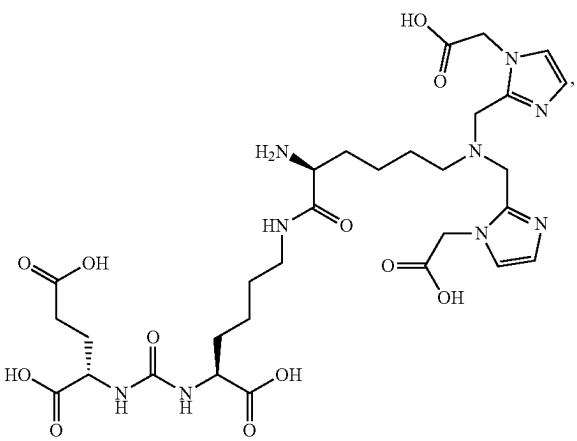
In certain embodiments, the radionuclide labelled PSMA binding agent comprises 1404 (also referred to as MIP-1404):



1404

or a pharmaceutically acceptable salt thereof.

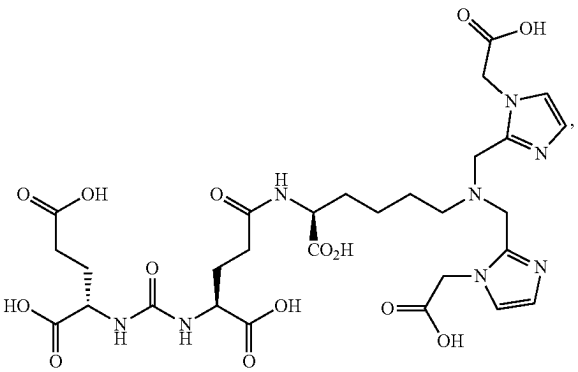
In certain embodiments, the radionuclide labelled PSMA binding agent comprises 1405 (also referred to as MIP-1405):



1405

or a pharmaceutically acceptable salt thereof.

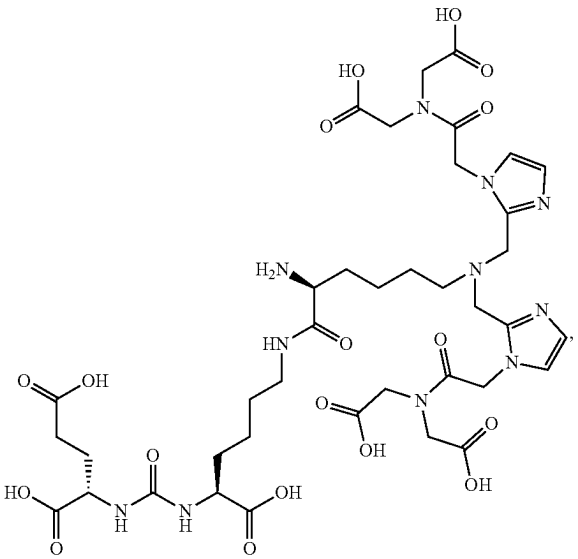
In certain embodiments, the radionuclide labelled PSMA binding agent comprises 1427 (also referred to as MIP-1427):



1427

or a pharmaceutically acceptable salt thereof.

In certain embodiments, the radionuclide labelled PSMA binding agent comprises 1428 (also referred to as MIP-1428):

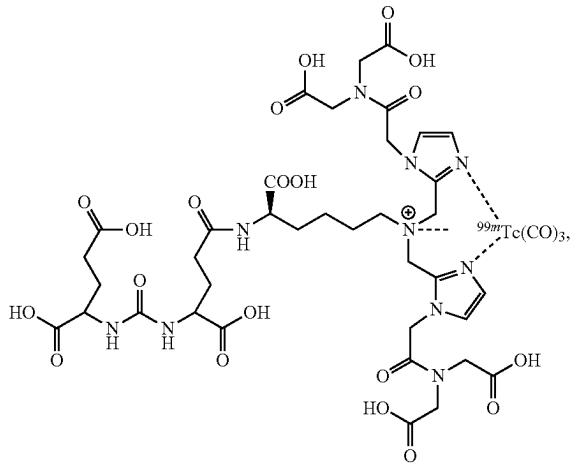


1428

or a pharmaceutically acceptable salt thereof.

In certain embodiments, the PSMA binding agent is labelled with a radionuclide by chelating it to a radioisotope of a metal [e.g., a radioisotope of technetium (Tc) (e.g., technetium-99m (^{99m}Tc)); e.g., a radioisotope of rhenium (Re) (e.g., rhenium-188 (^{188}Re); e.g., rhenium-186 ($^{186}_{Re}$)); e.g., a radioisotope of yttrium (Y) (e.g., ^{90}Y); e.g., a radioisotope of lutetium (Lu) (e.g., ^{177}Lu); e.g., a radioisotope of gallium (Ga) (e.g., ^{68}Ga; e.g., ^{67}Ga); e.g., a radioisotope of indium (e.g., ^{111}In); e.g., a radioisotope of copper (Cu) (e.g., ^{67}Cu)].

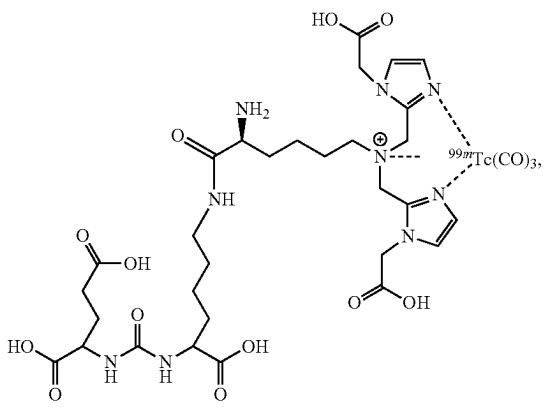
In certain embodiments, 1404 is labelled with a radionuclide (e.g., chelated to a radioisotope of a metal). In certain embodiments, the radionuclide labelled PSMA binding agent comprises ^{99m}Tc-MIP-1404, which is 1404 labelled with (e.g., chelated to) ^{99m}Tc:



^{99m}Tc-MIP-1404

or a pharmaceutically acceptable salt thereof. In certain embodiments, 1404 may be chelated to other metal radioisotopes [e.g., a radioisotope of rhenium (Re) (e.g., rhenium-188 (^{188}Re); e.g., rhenium-186 (^{186}Re)); e.g., a radioisotope of yttrium (Y) (e.g., ^{90}Y); e.g., a radioisotope of lutetium (Lu) (e.g., ^{177}Lu); e.g., a radioisotope of gallium (Ga) (e.g., ^{68}Ga; e.g., ^{67}Ga); e.g., a radioisotope of indium (e.g., ^{111}In); e.g., a radioisotope of copper (Cu) (e.g., 67^{Cu})] to form a compound having a structure similar to the structure shown above for ^{99m}Tc-MIP-1404, with the other metal radioisotope substituted for ^{99m}Tc.

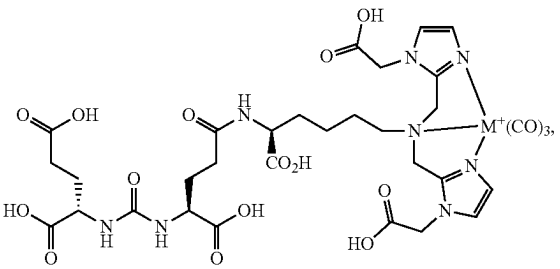
In certain embodiments, 1405 is labelled with a radionuclide (e.g., chelated to a radioisotope of a metal). In certain embodiments, the radionuclide labelled PSMA binding agent comprises ^{99m}Tc-MIP-1405, which is 1405 labelled with (e.g., chelated to) ^{99m}Tc:



^{99m}Tc-MIP-1405

or a pharmaceutically acceptable salt thereof. In certain embodiments, 1405 may be chelated to other metal radioisotopes [e.g., a radioisotope of rhenium (Re) (e.g., rhenium-188 (188Re): e.g., rhenium-186 (^{186}Re)); e.g., a radioisotope of yttrium (Y) (e.g., ^{90}Y); e.g., a radioisotope of lutetium (Lu)(e.g., ^{177}Lu); e.g., a radioisotope of gallium (Ga) (e.g., ^{68}Ga; e.g., ^{67}Ga); e.g., a radioisotope of indium (e.g., ^{111}In); e.g., a radioisotope of copper (Cu) (e.g., ^{67}Cu)] to form a compound having a structure similar to the structure shown above for ^{99m}Tc-MIP-1405, with the other metal radioisotope substituted for ^{99m}Tc.

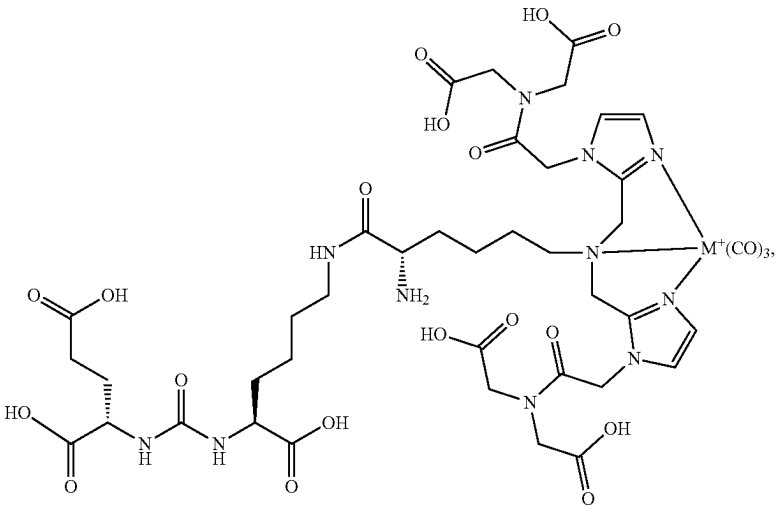
In certain embodiments, 1427 is labelled with (e.g., chelated to) a radioisotope of a metal, to form a compound according to the formula below:



1427 chelated to a metal

or a pharmaceutically acceptable salt thereof, wherein M is a metal radioisotope [e.g., a radioisotope of technetium (Tc) (e.g., technetium-99m (^{99m}Tc)); e.g., a radioisotope of rhenium (Re) (e.g., rhenium-188 (^{188}Re); e.g., rhenium-186 (^{186}Re)); e.g., a radioisotope of yttrium (Y) (e.g., ^{90}Y); e.g., a radioisotope of lutetium (Lu) (e.g., ^{177}Lu); e.g., a radioisotope of gallium (Ga) (e.g., ^{68}Ga; e.g., ^{67}Ga); e.g., a radioisotope of indium (e.g., ^{111}In); e.g., a radioisotope of copper (Cu) (e.g., ^{67}Cu)] with which 1427 is labelled.

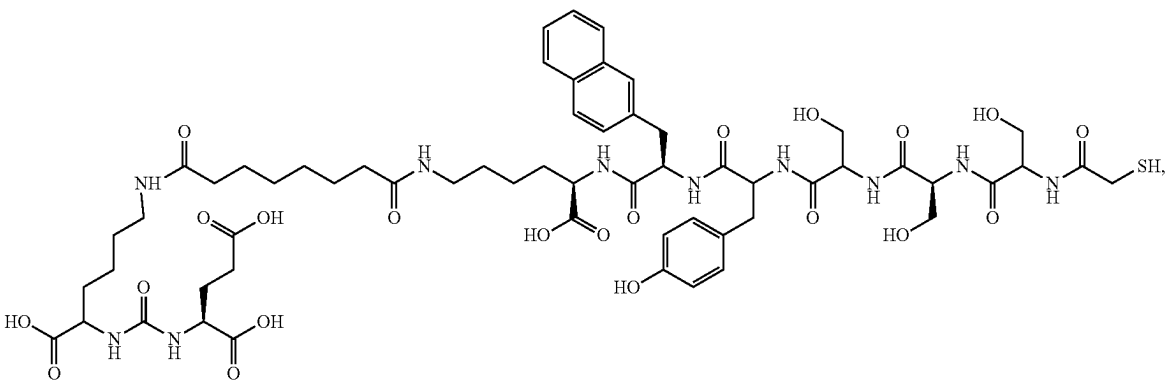
In certain embodiments, 1428 is labelled with (e.g., chelated to) a radioisotope of a metal, to form a compound according to the formula below:



1428 chelated to a metal

or a pharmaceutically acceptable salt thereof, wherein M is a metal radioisotope [e.g., a radioisotope of technetium (Tc) (e.g., technetium-99m (^{99m}Tc)); e.g., a radioisotope of rhenium (Re) (e.g., rhenium-188 (^{188}Re); e.g., rhenium-186 (^{186}Re)); e.g., a radioisotope of yttrium (Y) (e.g., ^{90}Y); e.g., a radioisotope of lutetium (Lu) (e.g., ^{177}Lu); e.g., a radioisotope of gallium (Ga) (e.g., ^{68}Ga; e.g., ^{67}Ga); e.g., a radioisotope of indium (e.g., ^{111}In); e.g., a radioisotope of copper (Cu) (e.g., ^{67}Cu] with which 1428 is labelled.

In certain embodiments, the radionuclide labelled PSMA binding agent comprises PSMA I&S:



PSMA I&S

or a pharmaceutically acceptable salt thereof. In certain embodiments, the radionuclide labelled PSMA binding agent comprises ^{99m}Tc-PSMA I&S, which is PSMA I&S labelled with ^{99m}Tc, or a pharmaceutically acceptable salt thereof.

A.iii Whole-Body Bone Scans

Turning to FIG. **1**, BSI Cloud 130 refers to a cloud-based decision support system that implements BSI values. BSI refers to bone scan index, which is a value computed from a method for detecting skeletal lesions from whole-body scanning (and anterior and posterior views) with a gamma camera following administration of the radionuclide technetium 99m methylenediphosphonate (^{99m}Tc MDP). Further explanation of BSI is provided, for example, in U.S. Pat. No. 8,855,387, which is incorporated herein by reference in its entirety, as well as in U.S. patent application Ser. No. 15/282,422, filed Sep. 30, 2016, which is incorporated herein by reference in its entirety.

In particular, BSI is computed from whole-body scans by segmenting anterior and posterior views of the whole-body scan of the patient to geographically identify boundaries of regions within the views that correspond to various portions of the patient's skeleton. Segmentation of the patient's skeleton can be performed using a variety of approaches, such as the Active Shape Model-based approach and the atlas image registration approach (which registers the anterior and posterior views of a whole body scan with reference anterior and posterior views of a reference whole body scan that have already been segmented (referred to as an atlas image)) described in U.S. Pat. No. 8,855,387. Other approaches, based on machine learning techniques (e.g., artificial neural networks (ANNs); e.g., convolutional neural networks (CNNs)) may also be used.

The BSI value is computed based on the intensity values of whole-body scan within the identified boundaries of the

various skeletal regions. As discussed above, hotspots that correspond to localized regions of high intensity within the views (anterior and/or posterior views) of the whole-body scan can be detected. Hotspots may be detected and/or classified as corresponding to cancerous lesions (e.g., metastases) using a variety of approaches, including, as described in U.S. Pat. No. 8,855,387, machine learning techniques such as ANNs.

Hotspots corresponding to cancerous tissue lesions within the patient's skeleton, once detected, can be used to determine a risk index that provides a measure of disease state for the patient. For example, cancerous tissue levels within one or more regions, such as particular bones and/or the overall skeletal region, can be determined based on features of detected hotspots (e.g., detected hotspots classified as metastases). For example, a cancerous tissue level within a region (e.g., a particular bone; e.g., the overall skeletal region) may be determined based on (e.g., as a function of) a total number of detected hotspots within the region, a total volume of detected hotspots within the region, an average intensity of detected hotspots, a maximal intensity of detected hotspots, and the like, as well as combinations thereof. Properties of the one or more regions, such as their area or volume may also be used. For example, a total number and/or total volume of detected hotspots may be normalized (e.g., divided) by a volume and/or area of the region in which they are detected. A risk index may be determined based on the determined cancerous tissue levels within one or more regions, directly, e.g., as the cancerous tissue level within a single region, or determined from cancerous tissue levels in multiple regions (e.g., as an average; e.g., as a scaled sum; e.g., as a ratio; etc.), or even using machine learning approaches.

For example, the BSI value is a risk index that is a numeric value that quantifies the fraction of the total skeleton of the patient that is involved by cancerous tissue (e.g., tumors), based on the detected hotspots. The BSI value can be compared between different patients, and used as an objective measure of disease state and risk for a particular patient. Notably, since BSI is computed in an automated fashion, variability due to human factors such as radiologist interpretation of images is avoided.

Moreover, a variety of actionable information can be obtained from a patient's BSI value. For example, BSI can be correlated with prognostic values that provide a measure of disease state, progression, life expectancy (e.g., overall survival), treatment efficacy, and the like for the patient. Accordingly, a patient's BSI value can be used and tracked over time (e.g., over the course of multiple visits to one or more doctors) to provide them or their physician with an objective metric of what state their cancer is in, how fast it is progressing, what their outlook is, and whether one or more particular treatments are proving effective.

A.iv Positron Emission Tomography (PET) Scans

PyL Cloud 120 refers to a cloud-based system that uses medical images obtained with the agent PyL™, which is DCFPyL labeled with ^{18}F ([18F]DCFPyL). The patient, after injection of the imaging agent, receives a positron emission tomography (PET) scan to identify hot spots, and a CT scan. Further information about the PyL™ imaging agent is provided above, and, for example, in U.S. Pat. No. 8,778,305, which is incorporated herein by reference in its entirety.

In certain embodiments, the PET scan and the CT scan are combined as a composite image comprising the CT scan overlaid with the PET scan. As used herein, overlaying one image (e.g., a CT scan) with another (e.g., a PET scan) refers to establishing a mapping between coordinates and/or pixels or voxels of the two images that that represent the same physical locations (e.g., within the patient). CT scans provide accurate anatomical information in the form of detailed three-dimensional (3D) images of internal organs, bones, soft tissue, and blood vessels. Accordingly, 3D boundaries of specific regions of imaged tissue can be accurately identified by analysis of CT scans. For example, automated segmentation of CT scans can be performed to identify 3D boundaries of specific organs (e.g., a prostate, lymph nodes, a lung or lungs), sub-organs, organ regions, as well as other regions of imaged tissue, such as particular bones and an overall skeletal region of the patient. Automated segmentation of CT scans can be accomplished via a variety of approaches, include machine learning techniques [e.g., ANN-based approaches (including, e.g., convolutional neural networks (CNNs))], atlas image registration, and combinations thereof. In certain embodiments, manual segmentation of CT images can also be utilized, alone or in combination with automated segmentation approaches (e.g., to refine 3D boundaries identified via automated segmentation; e.g., to provide an initial starting point for an automated segmentation approach).

Once the 3D boundaries of various regions are identified within a CT scan of a composite image, by virtue of the mapping between the CT scan and PET scan of the composite image, the identified 3D boundaries can be transferred to the PET image. Accordingly, regions of the PET image falling within and/or outside of the identified 3D boundaries can be accurately identified.

In certain embodiments, composite images comprising CT scans overlaid with PET scans are obtained using dedicated PET-CT scanner instruments common in many hospitals, and are uploaded as medical images to the cloud-based platform described herein. In certain embodiments, a PET scan and a corresponding CT scan are obtained separately (but at substantially the same time), and uploaded to the cloud-based platform described herein. In such cases, the separately obtained PET and CT scans can be automatically fused to create a composite image.

In certain embodiments, once the 3D boundaries of the various regions are identified within the PET scan, one or more risk indices can be computed in a similar fashion to that described above with regard to BSI. In particular, in certain embodiments, intensity values of the PET scan in relation to (e.g., within and/or outside of) the 3D boundaries of the identified regions can be used to determine levels of cancerous tissue within the identified regions, e.g., based on features of detected hotspots (e.g., detected hotspots corresponding to metastases). Risk indices can then be computed based on the determined cancerous tissue levels. For example, hotspots within the PET scan can be identified, and, based on features such as their size, number, and distribution with respect to the identified regions, used to compute one or more risk indices. As with BSI, risk indices determined from PET scans can be correlated with prognostic values and tracked over time (e.g., over the course of multiple visits to one or more doctors) to provide patients or their physician with an objective metric of what state their cancer is in, how fast it is progressing, what their outlook is, and whether one or more particular treatments are proving effective. The approaches described herein with regard to PET imaging using PyL™ as a radiopharmaceutical can be applied to a variety of other radiopharmaceuticals, such as those described above, including, without limitation NaF, radioisotopes of choline, and any of the PSMA binding agents described in section A.i above.

A.v Single-Photon Emission Computerized Tomography (SPECT) Scans

1404 Cloud 130 refers to a cloud-based system that uses medical images obtained with the agent ^{99m}Tc-MIP-1404, which, as described above, is 1404 labeled with Tc^{99m}. After injection of the imaging agent, the patient receives a single-photon emission computerized tomography (SPECT) scan, e.g., to identify hot spots, and a computed tomography (CT) scan, e.g., to identify anatomical features. These images are overlaid to make a composite image (SPECT/CT). Further information about ^{99m}Tc-MIP-1404 imaging agent is provided above, and, for example, in U.S. Pat. Nos. 8,211,401 and 8,962,799, both of which are incorporated herein by reference in their entireties.

SPECT and CT scans can be analyzed in a manner similar to that described above with respect to PET and CT scans, in order to determine one or more risk indices. In particular, as with PET and CT scans, the SPECT scan and the CT scan can be combined in a composite image in which the CT scan is overlaid with the SPECT scan—a composite SPECT-CT image. As with composite PET-CT images, composite SPECT-CT images may be directly received as medical images by the cloud-based platform described herein (e.g., having been obtained via dedicated SPECT-CT imager in a hospital), or may be created by the cloud-based platform following receipt of separate SPECT scans and CT scans.

Similar to PET-CT images, 3D boundaries of various regions of imaged tissue can be identified within the SPECT image by virtue of the overlay with the CT image of the composite image. Intensity variations within the SPECT image, in relation to the 3D boundaries can be used to compute one or more risk indices. As with the approaches for computing risk indices from composite PET-CT images, this may comprise determine levels of cancerous tissue within the identified regions, for example by detecting hotspots within the 3D boundaries of the identified regions. Such risk indices can be correlated with prognostic values and tracked over time (e.g., over the course of multiple visits to one or more doctors) to provide patients or their physician with an objective metric of what state their cancer is in, how fast it is progressing, what their outlook is, and whether one or more particular treatments are proving effective. The approaches described herein with regard to SPECT imaging using ^{99m}Tc-MIP-1404 as a radiopharmaceutical can be applied to a variety of other radiopharmaceuticals, such as those described above, including, without limitation, any of the PSMA binding agents described in section A.ii above

B. Platform Services and Computing Device Components

FIG. **2** is a schematic **200** showing the relationship between a platform and a computing device (e.g., personal computer or mobile computing device, e.g., smart phone) running an application, according to illustrative embodiments of the invention. The platform performs various services, for example, user authentication ("Auth"), image and other data storage ("SliceBox), and the like—many more services than those shown may be provided. The applications may have both a platform component and a device component (e.g., native app on the client device).

FIG. **9** shows an example architecture **900** for implementing the cloud-based platform described herein, and providing various services such as the BSI Cloud, PyL Cloud, and 1404 Cloud services described above. The architecture shown in FIG. **9** can be used to implement the platform described herein on a variety of datacenters, including publicly available datacenters. The datacenter provides infrastructure in the form of servers and networks and provides services for e.g. networking, messaging, authentication, logging and storage. The architecture **900** for the platform uses a series of functional units with limited scope referred to as microservices. Each microservice handles an isolated set of tasks such as image storage, calculation of a risk index, identification of medical image type, and other tasks. Services (e.g., microservices) can communicate with each other using standard protocols such as Hypertext Transfer Protocol (HTTP). Organizing the platform into a network of microservices, as shown in the architecture **900** of FIG. **9**, allows for parts of the platform to be scaled individually to meet high demand and to ensure minimal downtime.

In certain embodiments, such an architecture allows for components to be improved or replaced without affecting other parts of the platform. The example architecture **900** shown in FIG. **9** includes a set **920** of microservices that that are common to two or more applications in the platform. The left **910** and right **930** panels show microservices in two applications. The microservice network shown in the left panel **910** implements a version of the BSI Cloud service, as described above, and provides for calculation of an automated BSI index (aBSI), which is a risk index derived from automated analysis of whole-body scans obtained with a gamma camera. The microservice network shown in the right panel **930** implements a version of the 1404 Cloud service, as described above, and provides for automated calculation of a SPECT index, which is a risk index derived from automated analysis of composite SPECT-CT images.

C. Image Collection, Analysis, and Result Presentation

FIG. **3** is a GUI window **300** in the BSI Cloud application (displayed to a user) that allows a user to enter information about a patient and upload and/or access medical images for the patient, e.g., series of images obtained over a period of time.

FIG. **4** is a GUI window **400** in the BSI Cloud application showing representative full body gamma camera images showing hotspots automatically identified by the system, with corresponding overall computed BSI values for a particular image set obtained at a given time. A graph **410** at left shows how the BSI value has changed over time (increase) for this particular patient.

FIG. **5** is a GUI window in the BSI Cloud application showing an automatically or semi-automatically generated radiologist report **510**, which can be signed and dated by a radiologist. In certain embodiments, the automatically identified hotspots may be adjusted by the radiologist (or other medical practitioner attending to the patient), with the change(s) reflected in the report. For example, an identified hotspot may be deactivated by the radiologist, or a new hotspot may be activated by the radiologist, such changes possibly affecting the computed BSI value, displayed in the report.

FIG. **6** is a block flow diagram of an illustrative network-based (e.g., cloud based) decision support system, according to an illustrative embodiment of the invention. FIG. **6** shows various functions that may be performed by the cloud based services described herein. These include: (i) receiving and storing sets of medical images in a database; (ii) accessing one or more of the medical images for transmission to the user for display on a user computing device; (iii) automatically analyzing, by the processor, the medical images to compute a risk index (e.g., BSI) and/or to generate a risk map; (iv) generating a radiologist report for a patient according to the patient images and/or risk index/risk map; and applying a machine learning algorithm to update a process for the automatic analysis of function (iii).

FIG. **10** is a schematic showing clinical stages **1010** of prostate cancer progression, along with various therapies **1020** and diagnostic imaging modalities **1030** appropriate for various disease states. As shown in the schematic, depending on the clinical state of a patient's prostate cancer, different imaging modalities and/or different radiopharmaceuticals may be appropriate. Similarly, different risk indices computed based on different imaging modalities and/or different radiopharmaceuticals may most appropriate, depending on the state of the patient's prostate cancer.

For example, in certain embodiments, when a patient either has, or is suspected of having prostate cancer in a localized state, composite SPECT-CT imaging may be used. SPECT scans of composite SPECT-CT images used for evaluation of localized prostate cancer can be obtained following administration of a particular radiopharmaceutical, such as ^{99m}Tc-MIP-1404, that facilitates imaging of localized prostate cancer. Any of the SPECT-CT images themselves, derivatives thereof, and risk indices computed from the SPECT-CT images can be used, accordingly, to assess risk, disease state, progression, treatment efficacy and the like for localized prostate cancer.

In certain embodiments, when a patient has or is suspected of having metastatic prostate cancer, that has metastasized outside of the prostate, other imaging techniques may be used. For example, whole-body scans obtained following administration of ^{99m}Tc-MDP can be used to assess tumor burden in a patient's skeleton. As discussed above, BSI values computed from whole-body scans can be used to assess risk, disease state, progression, treatment efficacy and the like when a patient's prostate cancer has metastasized to their skeleton. In certain embodiments, certain imaging modalities and/or radiopharmaceuticals can be used for evaluate of prostate cancer in both localized and metastatic states. For example, as illustrated in FIG. **10**, PET-CT imaging can be used for evaluating prostate cancer in both localized and metastatic states. As shown in the figure, such PET-CT images may be obtained using an appropriate radiopharmaceutical, such as PyL™, that facilitates imaging of both localized and metastatic prostate cancer.

In certain embodiments, the cloud-based platform facilitates evaluating prostate cancer progression and treatment efficacy over time. For example, as shown in the example process **1100** of the block flow diagram of FIG. **11**, in certain embodiments medical images of a particular patient are repeatedly received and stored over time **1110**, over the course of multiple visits to one or more doctors and/or clinical specialists (e.g., radiologists) by the patient. In this manner, a series of medical images for the patient are obtained. The series of medical images can be automatically analyzed to determine values of one or more risk indices, so as to track changes in the determined values over time **1120**. The determined risk index values may be stored **1130***a* (e.g., for further processing). In certain embodiments, the process causes a graphical representation of the determined risk index values, such as a graph, to be displayed (e.g., on a user computing device; e.g., via a web-based portal) **1130***b*.

Notably, by virtue of the capability of the cloud-based platform described herein to receive, store, and analyze a variety of different medical image types, such as composite SPECT-CT images, whole-body scans, and composite PET-CT images, the medical images need not be of the same type.

For example, a first subseries of medical images may be obtained using a first imaging modality and a first radiopharmaceutical, such as SPECT-CT imaging with ^{99m}Tc-MIP-1404, when the patient's prostate cancer is in a localized state. If the patient's prostate cancer progresses to a metastatic state, a second subseries of images may comprise images obtained via a different, second imaging modality and/or a different, second radiopharmaceutical. For example, the second subseries of medical images may be PET-CT images obtained using PyL™ For example, the second subseries of medical images may be whole-body scans obtained using ^{99m}Tc-MDP.

Risk indices can be computed for the first image subseries and for the second image subseries to provide a unified picture of the patient's prostate cancer progression and treatment over time. This approach can be performed for multiple patients, not only for decision making purposes with regard to each patient's disease progression and particular course of treatment, but also in the context of clinical trials, for example to compare efficacy of a particular treatment with others or a control.

D. Computer System and Network Environment

FIG. **7** shows an illustrative network environment **700** for use in the methods and systems described herein. In brief overview, referring now to FIG. **7**, a block diagram of an exemplary cloud computing environment **700** is shown and described. The cloud computing environment **700** may include one or more resource providers **702***a*, **702***b*, **702***c* (collectively, **702**). Each resource provider **702** may include computing resources. In some implementations, computing resources may include any hardware and/or software used to process data. For example, computing resources may include hardware and/or software capable of executing algorithms, computer programs, and/or computer applications. In some implementations, exemplary computing resources may include application servers and/or databases with storage and retrieval capabilities. Each resource provider **702** may be connected to any other resource provider **702** in the cloud computing environment **700**. In some implementations, the resource providers **702** may be connected over a computer network **708**. Each resource provider **702** may be connected to one or more computing device **704***a*, **704***b*, **704***c* (collectively, **704**), over the computer network **708**.

The cloud computing environment **700** may include a resource manager **706**. The resource manager **706** may be connected to the resource providers **702** and the computing devices **704** over the computer network **708**. In some implementations, the resource manager **706** may facilitate the provision of computing resources by one or more resource providers **702** to one or more computing devices **704**. The resource manager **706** may receive a request for a computing resource from a particular computing device **704**. The resource manager **706** may identify one or more resource providers **702** capable of providing the computing resource requested by the computing device **704**. The resource manager **706** may select a resource provider **702** to provide the computing resource. The resource manager **706** may facilitate a connection between the resource provider **702** and a particular computing device **704**. In some implementations, the resource manager **706** may establish a connection between a particular resource provider **702** and a particular computing device **704**. In some implementations, the resource manager **706** may redirect a particular computing device **704** to a particular resource provider **702** with the requested computing resource.

FIG. **8** shows an example of a computing device **800** and a mobile computing device **850** that can be used in the methods and systems described in this disclosure. The computing device **800** is intended to represent various forms of digital computers, such as laptops, desktops, worksta-

tions, personal digital assistants, servers, blade servers, mainframes, and other appropriate computers. The mobile computing device **850** is intended to represent various forms of mobile devices, such as personal digital assistants, cellular telephones, smart-phones, and other similar computing devices. The components shown here, their connections and relationships, and their functions, are meant to be examples only, and are not meant to be limiting.

The computing device **800** includes a processor **802**, a memory **804**, a storage device **806**, a high-speed interface **808** connecting to the memory **804** and multiple high-speed expansion ports **810**, and a low-speed interface **812** connecting to a low-speed expansion port **814** and the storage device **806**. Each of the processor **802**, the memory **804**, the storage device **806**, the high-speed interface **808**, the high-speed expansion ports **810**, and the low-speed interface **812**, are interconnected using various busses, and may be mounted on a common motherboard or in other manners as appropriate. The processor **802** can process instructions for execution within the computing device **800**, including instructions stored in the memory **804** or on the storage device **806** to display graphical information for a GUI on an external input/output device, such as a display **816** coupled to the high-speed interface **808**. In other implementations, multiple processors and/or multiple buses may be used, as appropriate, along with multiple memories and types of memory. Also, multiple computing devices may be connected, with each device providing portions of the necessary operations (e.g., as a server bank, a group of blade servers, or a multi-processor system). Thus, as the term is used herein, where a plurality of functions are described as being performed by "a processor", this encompasses embodiments wherein the plurality of functions are performed by any number of processors (one or more) of any number of computing devices (one or more). Furthermore, where a function is described as being performed by "a processor", this encompasses embodiments wherein the function is performed by any number of processors (one or more) of any number of computing devices (one or more) (e.g., in a distributed computing system).

The memory **804** stores information within the computing device **800**. In some implementations, the memory **804** is a volatile memory unit or units. In some implementations, the memory **804** is a non-volatile memory unit or units. The memory **804** may also be another form of computer-readable medium, such as a magnetic or optical disk.

The storage device **806** is capable of providing mass storage for the computing device **800**. In some implementations, the storage device **806** may be or contain a computer-readable medium, such as a floppy disk device, a hard disk device, an optical disk device, or a tape device, a flash memory or other similar solid state memory device, or an array of devices, including devices in a storage area network or other configurations. Instructions can be stored in an information carrier. The instructions, when executed by one or more processing devices (for example, processor **802**), perform one or more methods, such as those described above. The instructions can also be stored by one or more storage devices such as computer- or machine-readable mediums (for example, the memory **804**, the storage device **806**, or memory on the processor **802**).

The high-speed interface **808** manages bandwidth-intensive operations for the computing device **800**, while the low-speed interface **812** manages lower bandwidth-intensive operations. Such allocation of functions is an example only. In some implementations, the high-speed interface **808** is coupled to the memory **804**, the display **816** (e.g., through a graphics processor or accelerator), and to the high-speed expansion ports **810**, which may accept various expansion cards (not shown). In the implementation, the low-speed interface **812** is coupled to the storage device **806** and the low-speed expansion port **814**. The low-speed expansion port **814**, which may include various communication ports (e.g., USB, Bluetooth®, Ethernet, wireless Ethernet) may be coupled to one or more input/output devices, such as a keyboard, a pointing device, a scanner, or a networking device such as a switch or router, e.g., through a network adapter.

The computing device **800** may be implemented in a number of different forms, as shown in the figure. For example, it may be implemented as a standard server **820**, or multiple times in a group of such servers. In addition, it may be implemented in a personal computer such as a laptop computer **822**. It may also be implemented as part of a rack server system **824**. Alternatively, components from the computing device **800** may be combined with other components in a mobile device (not shown), such as a mobile computing device **850**. Each of such devices may contain one or more of the computing device **800** and the mobile computing device **850**, and an entire system may be made up of multiple computing devices communicating with each other.

The mobile computing device **850** includes a processor **852**, a memory **864**, an input/output device such as a display **854**, a communication interface **866**, and a transceiver **868**, among other components. The mobile computing device **850** may also be provided with a storage device, such as a micro-drive or other device, to provide additional storage. Each of the processor **852**, the memory **864**, the display **854**, the communication interface **866**, and the transceiver **868**, are interconnected using various buses, and several of the components may be mounted on a common motherboard or in other manners as appropriate.

The processor **852** can execute instructions within the mobile computing device **850**, including instructions stored in the memory **864**. The processor **852** may be implemented as a chipset of chips that include separate and multiple analog and digital processors. The processor **852** may provide, for example, for coordination of the other components of the mobile computing device **850**, such as control of user interfaces, applications run by the mobile computing device **850**, and wireless communication by the mobile computing device **850**.

The processor **852** may communicate with a user through a control interface **858** and a display interface **856** coupled to the display **854**. The display **854** may be, for example, a TFT (Thin-Film-Transistor Liquid Crystal Display) display or an OLED (Organic Light Emitting Diode) display, or other appropriate display technology. The display interface **856** may comprise appropriate circuitry for driving the display **854** to present graphical and other information to a user. The control interface **858** may receive commands from a user and convert them for submission to the processor **852**. In addition, an external interface **862** may provide communication with the processor **852**, so as to enable near area communication of the mobile computing device **850** with other devices. The external interface **862** may provide, for example, for wired communication in some implementations, or for wireless communication in other implementations, and multiple interfaces may also be used.

The memory **864** stores information within the mobile computing device **850**. The memory **864** can be implemented as one or more of a computer-readable medium or media, a volatile memory unit or units, or a non-volatile memory unit or units. An expansion memory **874** may also

be provided and connected to the mobile computing device **850** through an expansion interface **872**, which may include, for example, a SIMM (Single In Line Memory Module) card interface. The expansion memory **874** may provide extra storage space for the mobile computing device **850**, or may also store applications or other information for the mobile computing device **850**. Specifically, the expansion memory **874** may include instructions to carry out or supplement the processes described above, and may include secure information also. Thus, for example, the expansion memory **874** may be provided as a security module for the mobile computing device **850**, and may be programmed with instructions that permit secure use of the mobile computing device **850**. In addition, secure applications may be provided via the SIMM cards, along with additional information, such as placing identifying information on the SIMM card in a non-hackable manner.

The memory may include, for example, flash memory and/or NVRAM memory (non-volatile random access memory), as discussed below. In some implementations, instructions are stored in an information carrier and, when executed by one or more processing devices (for example, processor **852**), perform one or more methods, such as those described above. The instructions can also be stored by one or more storage devices, such as one or more computer- or machine-readable mediums (for example, the memory **864**, the expansion memory **874**, or memory on the processor **852**). In some implementations, the instructions can be received in a propagated signal, for example, over the transceiver **868** or the external interface **862**.

The mobile computing device **850** may communicate wirelessly through the communication interface **866**, which may include digital signal processing circuitry where necessary. The communication interface **866** may provide for communications under various modes or protocols, such as GSM voice calls (Global System for Mobile communications), SMS (Short Message Service), EMS (Enhanced Messaging Service), or MMS messaging (Multimedia Messaging Service), CDMA (code division multiple access), TDMA (time division multiple access), PDC (Personal Digital Cellular), WCDMA (Wideband Code Division Multiple Access), CDMA2000, or GPRS (General Packet Radio Service), among others. Such communication may occur, for example, through the transceiver **868** using a radio-frequency. In addition, short-range communication may occur, such as using a Bluetooth®, Wi-Fi™, or other such transceiver (not shown). In addition, a GPS (Global Positioning System) receiver module **870** may provide additional navigation- and location-related wireless data to the mobile computing device **850**, which may be used as appropriate by applications running on the mobile computing device **850**.

The mobile computing device **850** may also communicate audibly using an audio codec **860**, which may receive spoken information from a user and convert it to usable digital information. The audio codec **860** may likewise generate audible sound for a user, such as through a speaker, e.g., in a handset of the mobile computing device **850**. Such sound may include sound from voice telephone calls, may include recorded sound (e.g., voice messages, music files, etc.) and may also include sound generated by applications operating on the mobile computing device **850**.

The mobile computing device **850** may be implemented in a number of different forms, as shown in the figure. For example, it may be implemented as a cellular telephone **880**. It may also be implemented as part of a smart-phone **882**, personal digital assistant, or other similar mobile device.

Various implementations of the systems and techniques described here can be realized in digital electronic circuitry, integrated circuitry, specially designed ASICs (application specific integrated circuits), computer hardware, firmware, software, and/or combinations thereof. These various implementations can include implementation in one or more computer programs that are executable and/or interpretable on a programmable system including at least one programmable processor, which may be special or general purpose, coupled to receive data and instructions from, and to transmit data and instructions to, a storage system, at least one input device, and at least one output device.

These computer programs (also known as programs, software, software applications or code) include machine instructions for a programmable processor, and can be implemented in a high-level procedural and/or object-oriented programming language, and/or in assembly/machine language. As used herein, the terms machine-readable medium and computer-readable medium refer to any computer program product, apparatus and/or device (e.g., magnetic discs, optical disks, memory, Programmable Logic Devices (PLDs)) used to provide machine instructions and/or data to a programmable processor, including a machine-readable medium that receives machine instructions as a machine-readable signal. The term machine-readable signal refers to any signal used to provide machine instructions and/or data to a programmable processor.

To provide for interaction with a user, the systems and techniques described here can be implemented on a computer having a display device (e.g., a CRT (cathode ray tube) or LCD (liquid crystal display) monitor) for displaying information to the user and a keyboard and a pointing device (e.g., a mouse or a trackball) by which the user can provide input to the computer. Other kinds of devices can be used to provide for interaction with a user as well; for example, feedback provided to the user can be any form of sensory feedback (e.g., visual feedback, auditory feedback, or tactile feedback); and input from the user can be received in any form, including acoustic, speech, or tactile input.

The systems and techniques described here can be implemented in a computing system that includes a back end component (e.g., as a data server), or that includes a middleware component (e.g., an application server), or that includes a front end component (e.g., a client computer having a graphical user interface or a Web browser through which a user can interact with an implementation of the systems and techniques described here), or any combination of such back end, middleware, or front end components. The components of the system can be interconnected by any form or medium of digital data communication (e.g., a communication network). Examples of communication networks include a local area network (LAN), a wide area network (WAN), and the Internet.

The computing system can include clients and servers. A client and server are generally remote from each other and typically interact through a communication network. The relationship of client and server arises by virtue of computer programs running on the respective computers and having a client-server relationship to each other. In some implementations, the modules and/or services (e.g. cloud based services, such as BSI Cloud 110, PyL Cloud 120, 1404 Cloud 130; e.g., any of the microservices described herein) described herein can be separated, combined or incorporated into single or combined modules and/or services. The modules and/or services depicted in the figures are not intended to limit the systems described herein to the software architectures shown therein

While the invention has been particularly shown and described with reference to specific preferred embodiments, it should be understood by those skilled in the art that various changes in form and detail may be made therein without departing from the spirit and scope of the invention as defined by the appended claims.

What is claimed is:

1. A network-based decision support system comprising:

a processor; and

a memory having instructions stored thereon, wherein the instructions, when executed by the processor, cause the processor to:

(i) receive and store a plurality of medical images in a database, each medical image associated with a corresponding patient;

(ii) access one or more of the medical images associated with a particular patient from the database;

(iii) automatically analyze the one or more medical images using a machine learning algorithm; and

(iv) generate a radiologist report for the particular patient according to the one or more medical images for the patient,

wherein the one or more medical images comprise a composite image of the particular patient, the composite image comprising a CT scan overlaid with a nuclear medicine image obtained at a substantially same time as the CT scan and following administration to the patient of an imaging agent comprising a Prostate Specific Membrane Antigen (PSMA) binding agent comprising a radionuclide, wherein the instructions cause the processor to automatically analyze the composite image by:

(a) using the composite image to geographically identify a 3D boundary for each of one or more regions of imaged tissue within the nuclear medicine image; and

(b) computing, using the nuclear medicine image with the identified 3D boundary(ies) of the one or more region(s), a value of each of one or more risk indices, each risk index value indicative of cancer state or progression in the patient, and wherein the system is a cloud-based system.

2. The system of claim **1**, wherein the plurality of medical images in the database comprise a series of medical images of a first patient taken over time, and wherein the instructions cause the processor to determine a value of at least a first risk index for each medical image of the series, thereby tracking determined values of at least the first risk index for the first patient over time.

3. The system of claim **2**, wherein the instructions cause the processor to correlate the determined values of the first risk index with one or more prognostic values, thereby providing an objective metric of cancer state, progression, outlook, or treatment efficacy.

4. The system of claim **3**, wherein the one or more prognostic values comprise a measure of life expectancy.

5. The system of claim **4**, wherein the measure of life expectancy is overall survival.

6. The system of claim **1**, wherein the nuclear medicine image is a PET scan.

7. The system of claim **6**, wherein the radionuclide is a radioisotope of a halogen.

8. The system of claim **7**, wherein the imaging agent comprises [18F]DCFPyL.

9. The system of claim **7**, wherein the halogen is fluorine-18 [18F].

10. The system of claim **6**, wherein the radionuclide is a radioisotope of gallium (Ga).

11. The system of claim **10**, wherein the imaging agent comprises 68Ga-PSMA-11.

12. The system of claim **6**, wherein the imaging agent comprises 18F-PSMA-1007.

13. The system of claim **1**, wherein the instructions cause the processor to, for at least one risk index of the one or more risk indices, compute the value of the risk index by:

determining, for each of the one or more regions, a corresponding cancerous tissue level within the region based on intensity values of the nuclear medicine image within the 3D boundary of the region; and

computing the value of the risk index based on the determined cancerous tissue levels within the one or more regions.

14. The system of claim **1**, wherein the cancer is prostate cancer.

15. The system of claim **14**, wherein the cancer is metastatic prostate cancer.

16. The system of claim **1**, wherein the instructions cause the processor to automatically analyze the composite image by, at step (a):

using the machine learning algorithm to geographically identify, within the CT scan of the composite image, the 3D boundary(ies) for each of the one or more region(s); and

transferring the 3D boundary(ies) to the nuclear medicine image.

17. The system of claim **1**, wherein the nuclear medicine image is a PET scan and the instructions cause the processor to automatically analyze the composite image by, at step (b):

computing the value of at least one particular risk index of the one or more risk indices based on intensity values of the PET scan in relation to the identified 3D boundary(ies).

18. The system of claim **17**, wherein the instructions cause the processor to automatically analyze the composite image by, at step (b):

computing the value of at least one particular risk index of the one or more risk indices based on intensity values of the PET scan within one or more of the identified 3D boundary(ies) within PET scan.

19. The system of claim **17**, wherein the instructions cause the processor to automatically analyze the composite image by:

identifying one or more hotspots within the PET scan; and

at step (b), computing the value of the particular risk index based one or more features of the one or more hotspots together with the identified 3D boundary(ies).

20. The system of claim **19**, wherein the one or more features comprise one or more members selected from the group consisting of: a size of the one or more hotspots, a number of the one or more hotspots, and a distribution of the one or more hotspots.

21. The system of claim **19**, wherein the instructions cause the processor to automatically analyze the composite image by, at step (b):

compute the value of the particular risk index based on one or more members selected from the group consisting of:

a total number of identified hotspots within one or more of the 3D boundary(ies);

a total volume of detected hotspots within one or more of the 3D boundary(ies);

an average intensity of detected hotspots within one or more of the 3D boundary(ies); and

a maximal intensity of detected hotspots within one or more of the 3D boundary(ies).

22. The system of claim 1, wherein the one or more regions of imaged tissue comprise one or more members selected from the group consisting of: organs, organ structures, sub-organs, and organ regions.

23. The system of claim 1, wherein the one or more regions of imaged tissue comprise bone or a prostate of the patient.

24. A method comprising performing, by a processor of a server computing device, (i) to (iv) as follows:

(i) receiving and storing, by the processor of a server computing device, said processor a processor of a cloud-based system, a plurality of medical images in a database, each medical image associated with a particular corresponding patient;

(ii) accessing, by the processor, one or more of the medical images associated with a particular patient from the database;

(iii) automatically analyzing, by the processor, the one or more medical images using a machine learning algorithm; and

(iv) generating, by the processor, a radiologist report for the particular patient according to the one or more medical images for the patient,

wherein the one or more medical images comprise a composite image of the particular patient, the composite image comprising a CT scan overlaid with a nuclear medicine image acquired at a substantially same time as the CT scan and following administration to the patient of an imaging agent comprising a Prostate Specific Membrane Antigen (PSMA) binding agent comprising a radionuclide, wherein the method comprises automatically analyzing the composite image by:

(a) using the composite image to geographically identify a 3D boundary for each of one or more regions of imaged tissue within the nuclear medicine image; and

(b) computing, using the nuclear medicine image with the identified 3D boundary(ies) of the one or more region(s), a value of each of one or more risk indices, each risk index value indicative of cancer state or progression in the patient.

25. The method of claim 24, wherein the plurality of medical images in the database comprise a series of medical images of a first patient taken over time, and wherein the method comprises determining a value of at least a first risk index for each medical image of the series, thereby tracking determined values of at least the first risk index over time.

26. The method of claim 25, wherein the receiving and storing of the plurality of medical images comprises repeatedly receiving and storing, over time, a plurality of medical images of the first patient, each obtained at a different time, to obtain the series of medical images of the first patient.

27. A method for tracking prostate cancer progression and treatment efficacy over time, for one or more patient(s), the method comprising:

(a) repeatedly receiving and storing in a database, over time, by a processor of a computing device, said processor a processor of a cloud-based system, a plurality of medical images for each of the one or more patient(s) to obtain, for each of the one or more patient(s), a series of medical images taken over time;

(b) for each of the one or more patient(s), automatically analyzing, by the processor, using a machine learning algorithm, the series of medical images for the patient to determine values of one or more risk indices for each medical image of the series, thereby tracking determined values of the one or more risk indices over a course prostate cancer progression and treatment for the patient; and

(c) for each of the one or more patient(s), storing, by the processor, the determined values of the one or more risk indices, each indicative of prostate cancer state or progression, for the patient for further processing and/or causing, by the processor, display of a graphical representation of the determined values of the one or more risk indices for the patient,

wherein the series of medical images for a particular patient of the one or more patient(s) comprises a CT scan overlaid with a nuclear medicine image acquired at a substantially same time as the CT scan and following administration to the patient of an imaging agent comprising a Prostate Specific Membrane Antigen (PSMA) binding agent comprising a radionuclide, and wherein step (b) comprises:

using the composite image to geographically identify a 3D boundary for each of one or more regions of imaged tissue within the nuclear medicine image; and

computing the value of each of the one or more risk indices using the nuclear medicine image with the identified 3D boundary(ies) of the one or more region(s).

28. The method of claim 27, wherein the series of medical images for the particular patient of the one or more patient(s) comprises:

(i) a first image subseries comprising one or more medical images obtained using a first nuclear imaging modality each following administration to the particular patient of a first radiopharmaceutical; and

(ii) a second image subseries comprising one or more medical images obtained using a second nuclear imaging modality each following administration to the particular patient of a second radiopharmaceutical,

such that the values of the one or more risk indices determined in step (b) for the particular patient comprise a first subseries of values of a first risk index determined by automated analysis of the first image subseries and a second subseries of values of a second risk index determined by automated analysis of the second image subseries.

29. The method of claim 28, wherein the medical images of first image subseries are obtained over a first period of time, when prostate cancer of the particular patient is localized, and the medical images of the second image subseries are obtained over a second period of time, when prostate cancer of the particular patient is metastatic.

30. The method of claim 29, comprising using PET-CT imaging for evaluating prostate cancer in both localized and metastatic states.

31. A system for tracking prostate cancer progression and treatment efficacy over time, for one or more patient(s), the system comprising:

a processor; and

a memory having instructions stored thereon, wherein the instructions, when executed by the processor, cause the processor to:

(a) repeatedly receive and store in a database, over time, a plurality of medical images for each of the one or more patient(s) to obtain, for each of the one or more patient(s), a series of medical images taken over time;

(b) for each of the one or more patient(s), automatically analyze the series of medical images for the patient, using a machine learning algorithm, to determine values of one or more risk indices for each medical image

of the series, thereby tracking determined values of the one or more risk indices over a course prostate cancer progression and treatment for the patient; and

(c) for each of the one or more patient(s), store the determined values of the one or more risk indices, each indicative of prostate cancer state or progression, for the patient for further processing and/or cause display of a graphical representation of the determined values of the one or more risk indices for the patient

wherein the series of medical images for a particular patient of the one or more patient(s) comprises a CT scan overlaid with a nuclear medicine image acquired at a substantially same time as the CT scan and following administration to the patient of an imaging agent comprising a Prostate Specific Membrane Antigen (PSMA) binding agent comprising a radionuclide, and wherein step (b) comprises:

using the composite image to geographically identify a 3D boundary for each of one or more regions of imaged tissue within the nuclear medicine image; and

computing the value of each of the one or more risk indices using the nuclear medicine image with the identified 3D boundary(ies) of the one or more region(s), and

wherein the system is a cloud-based system.

32. A network-based decision support system comprising:

a processor; and

a memory having instructions stored thereon, wherein the instructions, when executed by the processor, cause the processor to:

(i) receive and store a plurality of medical images in a database, each medical image associated with a corresponding patient;

(ii) access one or more of the medical images associated with a particular patient from the database;

(iii) automatically analyze the one or more medical images using a machine learning algorithm; and

(iv) generate a radiologist report for the particular patient according to the one or more medical images for the patient,

wherein the one or more medical images comprise a composite image of the particular patient, the composite image comprising a CT scan overlaid with a nuclear medicine image obtained at a substantially same time as the CT scan and following administration to the patient of an imaging agent comprising a Prostate Specific Membrane Antigen (PSMA) binding agent comprising a radionuclide, wherein the instructions cause the processor to automatically analyze the composite image by:

(a) using the composite image to geographically identify a 3D boundary for each of one or more regions of imaged tissue within the nuclear medicine image; and

(b) computing, using the nuclear medicine image with the identified 3D boundary(ies) of the one or more region(s), a value of each of one or more risk indices, each risk index value indicative of cancer state or progression in the patient, and

wherein the plurality of medical images in the database comprise a series of medical images of a first patient taken over time, and wherein the instructions cause the processor to determine a value of at least a first risk index for each medical image of the series, thereby tracking determined values of at least the first risk index for the first patient over time.

33. A network-based decision support system comprising:

a processor; and

a memory having instructions stored thereon, wherein the instructions, when executed by the processor, cause the processor to:

(i) receive and store a plurality of medical images in a database, each medical image associated with a corresponding patient;

(ii) access one or more of the medical images associated with a particular patient from the database;

(iii) automatically analyze the one or more medical images using a machine learning algorithm;

And

(iv) generate a radiologist report for the particular patient according to the one or more medical images for the patient,

wherein the one or more medical images comprise a composite image of the particular patient, the composite image comprising a CT scan overlaid with a nuclear medicine image obtained at a substantially same time as the CT scan and following administration to the patient of an imaging agent comprising a Prostate Specific Membrane Antigen (PSMA) binding agent comprising a radionuclide, wherein the instructions cause the processor to automatically analyze the composite image by:

(a) using the composite image to geographically identify a 3D boundary for each of one or more regions of imaged tissue within the nuclear medicine image; and

(b) computing, using the nuclear medicine image with the identified 3D boundary(ies) of the one or more region(s), a value of each of one or more risk indices, each risk index value indicative of cancer state or progression in the patient, and

wherein, for at least one particular risk index of the one or more risk indices, the instructions cause the processor to compute the value of the particular risk index by:

determining, for each of the one or more regions, a corresponding cancerous tissue level within the region based on intensity values of the nuclear medicine image within the 3D boundary of the region; and

computing the value of the particular risk index based on the determined cancerous tissue levels within the one or more regions.

34. A method comprising performing, by a processor of a server computing device, (i) to (iv) as follows:

(i) receiving and storing, by the processor of a server computing device, a plurality of medical images in a database, each medical image associated with a particular corresponding patient;

(ii) accessing, by the processor, one or more of the medical images associated with a particular patient from the database;

(iii) automatically analyzing, by the processor, the one or more medical images using a machine learning algorithm; and

(iv) generating, by the processor, a radiologist report for the particular patient according to the one or more medical images for the patient,

wherein the one or more medical images comprise a composite image of the particular patient, the composite image comprising a CT scan overlaid with a nuclear medicine image acquired at a substantially same time as the CT scan and following administration to the patient of an imaging agent comprising a Prostate Specific Membrane Antigen (PSMA) binding agent comprising a radionuclide, wherein the method comprises automatically analyzing the composite image by:

(a) using the composite image to geographically identify a 3D boundary for each of one or more regions of imaged tissue within the nuclear medicine image; and

(b) computing, using the nuclear medicine image with the identified 3D boundary(ies) of the one or more region(s), a value of each of one or more risk indices, each risk index value indicative of cancer state or progression in the patient, and

wherein the plurality of medical images in the database comprise a series of medical images of a first patient taken over time, and wherein the instructions cause the processor to determine a value of at least a first risk index for each medical image of the series, thereby tracking determined values of at least the first risk index for the first patient over time.

35. A method comprising performing, by a processor of a server computing device, (i) to (iv) as follows:

(i) receiving and storing, by the processor of a server computing device, a plurality of medical images in a database, each medical image associated with a particular corresponding patient;

(ii) accessing, by the processor, one or more of the medical images associated with a particular patient from the database;

(iii) automatically analyzing, by the processor, the one or more medical images using a machine learning algorithm; and

(iv) generating, by the processor, a radiologist report for the particular patient according to the one or more medical images for the patient,

wherein the one or more medical images comprise a composite image of the particular patient, the composite image comprising a CT scan overlaid with a nuclear medicine image acquired at a substantially same time as the CT scan and following administration to the patient of an imaging agent comprising a Prostate Specific Membrane Antigen (PSMA) binding agent comprising a radionuclide, wherein the method comprises automatically analyzing the composite image by:

(a) using the composite image to geographically identify a 3D boundary for each of one or more regions of imaged tissue within the nuclear medicine image; and

(b) computing, using the nuclear medicine image with the identified 3D boundary(ies) of the one or more region(s), a value of each of one or more risk indices, each risk index value indicative of cancer state or progression in the patient, and

wherein, for at least one particular risk index of the one or more risk indices, the method comprises computing, by the processor, the value of the particular risk index by:

determining, for each of the one or more regions, a corresponding cancerous tissue level within the region based on intensity values of the nuclear medicine image within the 3D boundary of the region; and

computing the value of the risk index based on the determined cancerous tissue levels within the one or more regions.

* * * * *

EXHIBIT 5

US011657508B2

(12) United States Patent

Richter et al.

(10) Patent No.: US 11,657,508 B2
(45) Date of Patent: May 23, 2023

(54) **SYSTEMS AND METHODS FOR PLATFORM AGNOSTIC WHOLE BODY IMAGE SEGMENTATION**

(71) Applicant: **EXINI Diagnostics AB**, Lund (SE)

(72) Inventors: **Jens Filip Andreas Richter**, Lund (SE); **Kerstin Elsa Maria Johnsson**, Lund (SE); **Erik Konrad Gjertsson**, Lund (SE); **Aseem Undvall Anand**, Queens, NY (US)

(73) Assignee: **EXINI Diagnostics AB**, Lund (SE)

(*) Notice: Subject to any disclaimer, the term of this patent is extended or adjusted under 35 U.S.C. 154(b) by 717 days.

(21) Appl. No.: **16/734,599**

(22) Filed: **Jan. 6, 2020**

(65) **Prior Publication Data**

US 2020/0245960 A1 Aug. 6, 2020

Related U.S. Application Data

(60) Provisional application No. 62/934,305, filed on Nov. 12, 2019, provisional application No. 62/907,158,
(Continued)

(51) **Int. Cl.**
G06T 7/00 (2017.01)
G06T 7/11 (2017.01)
(Continued)

(52) **U.S. Cl.**
CPC ***G06T 7/11*** (2017.01); ***A61B 6/032*** (2013.01); ***A61B 6/037*** (2013.01); ***A61B 6/463*** (2013.01);
(Continued)

(58) **Field of Classification Search**
CPC G06T 7/11; G16H 50/50; G16H 50/30; G16H 30/20
See application file for complete search history.

(56) **References Cited**

U.S. PATENT DOCUMENTS

7,450,747 B2 11/2008 Jabri et al.
7,751,605 B2 7/2010 Gündel et al.
(Continued)

FOREIGN PATENT DOCUMENTS

CN 101528267 A 9/2009
CN 102361594 A 2/2012
(Continued)

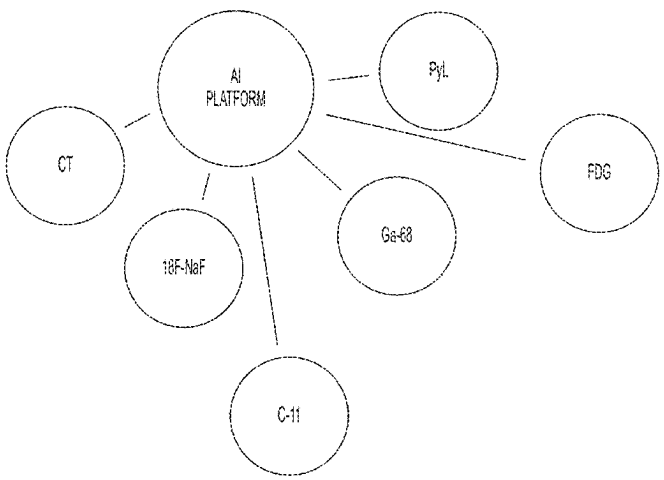
OTHER PUBLICATIONS

Brynolfsson, J., et al., Deep Learning based urinary bladder segmentation using 18FDCFPyL (PyL-PSMA) PET/CT images, EPS-145, European Association of Nuclear Medicine, (2020), <http://link.springer.com/article/10.1007/s00259-020-04988-4>. Retrieved Sep. 18, 2020.
(Continued)

Primary Examiner — Joseph M Santos Rodriguez
(74) *Attorney, Agent, or Firm* — Choate, Hall & Stewart LLP; William R. Haulbrook; Ronen Adato

(57) **ABSTRACT**

Presented herein are systems and methods that provide for automated analysis of three-dimensional (3D) medical images of a subject in order to automatically identify specific 3D volumes within the 3D images that correspond to specific anatomical regions (e.g., organs and/or tissue). Notably, the image analysis approaches described herein are not limited to a single particular organ or portion of the body. Instead, they are robust and widely applicable, providing for consistent, efficient, and accurate detection of anatomical regions, including soft tissue organs, in the entire body. In certain embodiments, the accurate identification of one or more such volumes is used to automatically determine quantitative metrics that represent uptake of radiopharmaceuticals in particular organs and/or tissue regions. These uptake metrics can be used to assess disease state in a
(Continued)



subject, determine a prognosis for a subject, and/or determine efficacy of a treatment modality.

10 Claims, 26 Drawing Sheets
(20 of 26 Drawing Sheet(s) Filed in Color)

Related U.S. Application Data

filed on Sep. 27, 2019, provisional application No. 62/870,210, filed on Jul. 3, 2019, provisional application No. 62/863,608, filed on Jun. 19, 2019, provisional application No. 62/837,941, filed on Apr. 24, 2019, provisional application No. 62/789,155, filed on Jan. 7, 2019.

(51) **Int. Cl.**

G16H 50/50	(2018.01)
G16H 30/20	(2018.01)
G16H 50/30	(2018.01)
G16H 50/20	(2018.01)
G16H 30/40	(2018.01)
A61B 6/03	(2006.01)
A61B 6/00	(2006.01)
A61K 51/04	(2006.01)
G06V 20/64	(2022.01)
G06V 20/69	(2022.01)
G06V 30/24	(2022.01)
G06F 18/214	(2023.01)

(52) **U.S. Cl.**

CPC ***A61B 6/466*** (2013.01); ***A61B 6/481*** (2013.01); ***A61B 6/505*** (2013.01); ***A61B 6/507*** (2013.01); ***A61B 6/5205*** (2013.01); ***A61B 6/5241*** (2013.01); ***A61B 6/5247*** (2013.01); ***A61K 51/0455*** (2013.01); ***G06F 18/214*** (2023.01); ***G06V 20/64*** (2022.01); ***G06V 20/695*** (2022.01); ***G06V 20/698*** (2022.01); ***G06V 30/2504*** (2022.01); ***G16H 30/20*** (2018.01); ***G16H 30/40*** (2018.01); ***G16H 50/20*** (2018.01); ***G16H 50/30*** (2018.01); ***G16H 50/50*** (2018.01); *G06V 2201/031* (2022.01); *G06V 2201/033* (2022.01)

(56) **References Cited**

U.S. PATENT DOCUMENTS

7,935,055	B2	5/2011	Burckhardt
7,970,194	B2	6/2011	Kimura
8,199,985	B2	6/2012	Jakobsson et al.
8,211,401	B2	7/2012	Babich et al.
8,467,856	B2	6/2013	Renisch et al.
8,538,166	B2	9/2013	Gordon et al.
8,705,887	B2	4/2014	Ma et al.
8,778,305	B2	7/2014	Pomper et al.
8,855,387	B2	10/2014	Hamadeh et al.
8,962,799	B2	2/2015	Babich et al.
9,002,081	B2	4/2015	Brown
9,466,133	B2	10/2016	Sowards-Emmerd et al.
9,710,915	B2	7/2017	Firouzian et al.
9,721,340	B2	8/2017	Gillies et al.
10,058,393	B2	8/2018	Bonutti et al.
10,223,610	B1	3/2019	Akselrod-Ballin et al.
10,311,971	B2	6/2019	Opfer et al.
10,330,763	B2	6/2019	James et al.
10,339,653	B2	7/2019	Gillies et al.
10,340,044	B2	7/2019	Yao et al.
10,340,046	B2	7/2019	Baker
RE47,609	E	9/2019	Hamadeh et al.
10,492,723	B2	12/2019	Madabhushi et al.
10,600,184	B2	3/2020	Golden et al.
10,665,346	B2	5/2020	Baker
10,748,652	B2	8/2020	Yao et al.
10,762,993	B2	9/2020	Baker
10,818,386	B2	10/2020	Yao et al.
10,943,681	B2	3/2021	Yao et al.
10,973,486	B2	4/2021	Sjostrand et al.
11,011,257	B2	5/2021	Lints et al.
11,321,844	B2	5/2022	Johnsson et al.
11,386,988	B2	7/2022	Johnsson et al.
11,424,035	B2	8/2022	Baker
11,534,125	B2	12/2022	Sjöstrand et al.
2003/0215120	A1	11/2003	Uppaluri et al.
2005/0281381	A1	12/2005	Guendel
2006/0062425	A1	3/2006	Shen et al.
2006/0064396	A1	3/2006	Wei et al.
2006/0078183	A1	4/2006	deCharms
2007/0081712	A1	4/2007	Huang et al.
2007/0081713	A1	4/2007	Jerebko
2007/0100225	A1	5/2007	Maschke
2007/0115204	A1	5/2007	Budz et al.
2008/0027315	A1	1/2008	McGinnis
2009/0309874	A1	12/2009	Salganicoff et al.
2010/0215581	A1	8/2010	Hoffmann
2010/0266170	A1	10/2010	Khamene et al.
2010/0322488	A1	12/2010	Virtue et al.
2011/0063288	A1	3/2011	Valadez
2011/0255763	A1	10/2011	Bogoni et al.
2012/0123253	A1	5/2012	Renisch et al.
2013/0038707	A1	2/2013	Cunningham et al.
2013/0094704	A1	4/2013	Hamadeh et al.
2013/0129168	A1	5/2013	Ross
2013/0211231	A1	8/2013	Sundarapandian et al.
2013/0281841	A1	10/2013	Everett et al.
2015/0110716	A1	4/2015	Armor
2015/0331995	A1	11/2015	Zhao et al.
2016/0203263	A1	7/2016	Maier et al.
2016/0335395	A1	11/2016	Wu et al.
2017/0083682	A1	3/2017	McNutt et al.
2018/0144828	A1	5/2018	Baker
2018/0259608	A1	9/2018	Golden et al.
2018/0360402	A1	12/2018	Carmi
2019/0038239	A1	2/2019	Flohr et al.
2019/0105009	A1	4/2019	Siemionow et al.
2019/0209116	A1	7/2019	Sjostrand et al.
2019/0388049	A1	12/2019	Gupta et al.
2020/0027559	A1	1/2020	Baker
2020/0051238	A1	2/2020	El Harouni et al.
2020/0074634	A1	3/2020	Kecskemethy et al.
2020/0085382	A1	3/2020	Taerum et al.
2020/0126666	A1	4/2020	Baker
2020/0170604	A1	6/2020	Yildirim et al.
2020/0193594	A1	6/2020	Georgescu et al.
2020/0193603	A1	6/2020	Golden et al.
2020/0315455	A1	10/2020	Lee et al.
2020/0337658	A1	10/2020	Sjostrand et al.
2020/0342600	A1	10/2020	Sjostrand et al.
2020/0352518	A1	11/2020	Lyman et al.
2020/0357117	A1	11/2020	Lyman et al.
2020/0357118	A1	11/2020	Yao et al.
2020/0357521	A1	11/2020	Baker
2021/0032206	A1	2/2021	Neumaier et al.
2021/0082547	A1	3/2021	Yao et al.
2021/0093249	A1	4/2021	Anand et al.
2021/0183485	A1	6/2021	Yao et al.
2021/0233633	A1	7/2021	Lints et al.
2021/0334974	A1	10/2021	Johnsson et al.
2021/0335480	A1	10/2021	Johnsson et al.
2022/0375612	A1	11/2022	Baker
2022/0398724	A1	12/2022	Anand et al.

FOREIGN PATENT DOCUMENTS

CN	102947840	A	2/2013
CN	103607954	A	2/2014
CN	106558045	A	4/2017
EP	1426903	A2	6/2004
EP	1508872	A1	2/2005

(56) **References Cited**

FOREIGN PATENT DOCUMENTS

EP	3043318	A1	7/2016
JP	2010-029481	A	2/2010
JP	6013042	B2	10/2016
JP	6170284	B2	7/2017
SE	524500	C2	8/2004
WO	WO-9905503	A2	2/1999
WO	WO-2007/062135	A2	5/2007
WO	WO-2009/084995	A1	7/2009
WO	WO-2011/077303	A1	6/2011
WO	WO-2011/091378	A1	7/2011
WO	WO-2015/058151	A2	4/2015
WO	WO-2018/015953	A1	1/2018
WO	WO-2018/081354	A1	5/2018
WO	WO-2019/103912	A2	5/2019
WO	WO-2019/136349	A2	7/2019
WO	WO-2020/144134	A1	7/2020
WO	WO-2020/146032	A1	7/2020
WO	WO-2020/190821	A1	9/2020
WO	WO-2020/219619	A1	10/2020
WO	WO-2020/219620	A1	10/2020
WO	WO-2021/061315	A1	4/2021

OTHER PUBLICATIONS

Brynolfsson, J., et al., Deep Learning-Enabled comprehensive detection and quantification of 18FDCFPyL (PyL-PSMA) PET/CT, OP-548, European Association of Nuclear Medicine, (2020), <http://link.springer.com/article/10.1007/s00259-020-04988-4>. Retrieved Sep. 18, 2020.

Cha, K. H., et al. Urinary bladder segmentation in CT urography using deep-learning convolutional neural network and level sets, Medical physics, 43(4):1882-1896, (2016).

Ciernik, I. F., et al. 3D-segmentation of the 18F-choline PET signal for target volume definition in radiation therapy of the prostate, Technology in cancer research & treatment 6(1): 23-30, (2007).

Dertat, A., Applied Depp Learning-{art 4: Convolutional Neural Networks, Towards Data Science, <http://towardsdatascience.com/applied-deep-learning-part-4-convolutional-neural-networks-584bc134de2> (2017).

Johnsson, K., et al., miPSMA Index: Comprehensive and Automated Quantification of 18F-DCFPyL (PyL-PSMA) PET/CT for Prostate Cancer Staging, J Nucl Med., 61: (Supplement 1): 1435, (2020).

Lin, T.Y. et al., Feature Pyramid Networks for object detection, FAIR, (2016), <https://arxiv.org/abs/1612.03144v1>.

Nickols, N.G., et al., A deep learning algorithm to predict coexisting metastatic disease using intraprostatic [F18]DCFPYL PSMA image alone in veterans with prostate cancer, Journal of Clinical Oncology 38, (Supplement 6), 2020.

Ren, S., et al., Faster R-CNN: Towards Real-Time Object Detection with Region Proposal Networks, (2015), <http://image-net.org/challenges/LSVRC/2015/results>.

Ronneberger, O., et al., U-Net: Convolutional Networks for Biomedical Image Segmentation, Springer International Publishing, (2015), <http://lmb.informatik.uni-freiburg.de/>. Published online on Nov. 18, 2015.

Santos-Cuevas, C. et al. 99mTc-labeled PSMA inhibitor: Biokinetics and radiation dosimetry in healthy subjects and imaging of prostate cancer tumors in patients, Nuclear Medicine and Biology 52:1-6, (2017).

Christ, P.F. et al., Automatic Liver and Tumor Segmentation of CT and MRI Volumes Using Cascaded Fully Convolutional Neural Networks, Arxiv.org, Cornell University Library, 20 pages, (2017).

Capobianco, N. et al., Whole-body uptake classification and prostate cancer staging in ^{68}Ga-PSMA-11 PET/CT using dual-tracer learning, European Journal of Nuclear Medicine and Molecular Imaging, (2021), <https:/doi.org/10.1007/s00259-021-05473-2> 10 pages. Retrieved on Apr. 18, 2021.

Fendler, W.P. et al., 68Ga-PSMA PET/CT: Joint EANM and SNMMI procedure guideline for prostate cancer imaging: version 1.0, Eur J Nucl Med Mol Imaging, DOI 10.1007/s00259-017-3670-z, 11 pages, (2017).

Im, HJ, et al., et al., Current Methods to Define Metabolic Tumor Volume in Positron Emission Tomography: Which One is Better?, Nucl. Med. Mol. Imaging, 52(1):5-15, (2018).

Polymeri, E., et al., Deep learning-based quantification of PET/CT prostate gland uptake: association with overall survival, Clinical Physiology Functional Imaging, DOI: 10.1111/cpf.12611, 40(2):106-113, (2019).

Trägärdh, E., et al., RECOMIA—a cloud-based platform for artificial intelligence research in nuclear medicine and radiology, EJNMMI Physics, <https://doi.org/10.1186/s40658-020-00316-9>, 7:51, 12 pages, (2020).

Wallis, J.W. et al., Three-dimensional display in nuclear medicine, IEEE Trans Med Imaging, 8(4):297-230, (1989).

American College of Radiology (ACR) and the Society for Pediatric Radiology (SPR), ACR-SPR Practice Parameter For The Performance Of Skeletal Scintigraphy (Bone Scan), Resolution 28, (2013-Revused2017), available from: http://www.acr.org.

Anand, A. et al., A Pre-Analytical Validation Study of Automated Bone Scan Index: Effect on Accuracy and Reproducibility Due to the Procedural Variabilities in Bone Scan Image Acquisition. J Nucl Med. Jul. 21, 2016. [Epub ahead of print].

Anand, A. et al., Analytic Validation of the Automated Bone Scan Index as an Imaging Biomarker to Standardize Quantitative Changes in Bone Scans of Patients with Metastatic Prostate Cancer, J. Nucl. Med., 57(1):41-45 (2016).

Anand, A. et al., Automated Bone Scan Index as a quantitative imaging biomarker in metastatic castration-resistant prostate cancer patients being treated with enzalutamide, EJNMMI Research, 6:23, 7 pages (2016).

Anand, A. et al., Translating Prostate Cancer Working Group 2 (PCWG2) Progression Criteria into a Quantitative Response Biomarker in Metastatic Castration Resistant Prostate Cancer (mCRPC), ASCO GU Conference, Poster, presented Feb. 16, 2017.

Anand, A. et al., Translating Prostate Cancer Working Group 2 (PCWG2) progression criteria into a quantitative response biomarker in metastatic castration-resistant prostate cancer (mCRPC), Journal of Clinical Oncology, 35(6):170 (2017).

Armstrong, A. et al., Assessment of the bone scan index in a randomized placebo-controlled trial of tasquinimod in men with metastatic castration-resistant prostate cancer (mCRPC), Urologic Oncology: Seminars and Original Investigations, 32:1308-1316 (2014).

Armstrong, A. et al., Development and validation of a prognostic model for overall survival in chemotherapy-naive men with metastatic castration-resistant prostate cancer (mCRPC) from the phase 3 prevail clinical trial, Journal of Clinical Oncology, 35(SuppL6):Abstract 138 (2017).

Armstrong, A. J. et al., Phase 3 Assessment of the Automated Bone Scan Index as a Prognostic Imaging Biomarker of Overall Survival in Men with Metastatic Castration-Resistant Prostate Cancer: A Secondary Analysis of a Randomized Clinical Trial. JAMA Oncology 4:944-951, (2018).

Armstrong, A. J. et al., Phase 3 prognostic analysis of the automated bone scan index (aBSI) in men with bone-metastatic castration-resistant prostate cancer (CRPC), Meeting Library ASC University (2017).

Belal, S. et al., Association of PET Index quantifying skeletal uptake in NaF PET/CT images with overall survival in prostate cancer patients, ASCO GU 2017, Poster 178, presented Feb. 16, 2017.

Belal, S. et al., PET Index quantifying skeletal uptake in NaF PET/CT images with overall survival in prostate cancer patients, ASCO GU 2017, Abstract (Feb. 13, 2017).

Belal, S. L. et al., 3D skeletal uptake of ^{18}F sodium fluoride in PET/CT images is associate with overall survival in patients with prostate cancer, EJNMMI Research, 7(15):1-8 (2017).

Belal, S.L. et al., Automated evaluation of normal uptake in different skeletal parts in 18F-sodium fluoride (NaF) PET/CT using a new convolutional neural network method, EJNMMI, EANM '17, 44(Suppl 2):S119-S956, Abstract EP-0116 (2017).

(56) **References Cited**

OTHER PUBLICATIONS

Bombardieri, E. et al., Bone scintigraphy: procedure guidelines for tumour imaging, Eur J. Nucl. Med. Mol. Imaging, 30:BP99-BP106, (2003).
Bushberg, J. T. et al., Essential Physics of Medical Imaging, Essential Physics of Medical Imaging, 19.3: p. 581 (table 15-3), p. 713 paragraph 6, section 19.3 and p. 720, (2011).
Dennis, E. et al., Bone Scan Index: A Quantitative Treatment Response Biomarker for Castration-Resistant Metastatic Prostate Cancer, Journal of Clinical Oncology, 30(5):519-524 (2012).
Eiber, M. et al., Prostate Cancer Molecular Imaging Standardized Evaluation (PROMISE): Proposed miTNM Classification for the Interpretation of PSMA-Ligand PET/CT, The Journal of Nuclear Medicine, 59(3):469-478, (2018).
GE Healthcare, SPECT/CT Cameras, retrieved Oct. 25, 2017: <http://www3.gehealthcare.com.sg/en-gb/products/categories/nuclear_medicine/spect-ct_cameras>.
Giesel, F. L. et al., F-18 labelled PSMA-1007: biodistribution, radiation dosimetry and histopathological validation of tumor lesions in prostate cancer patients, Eur. J. Nucl. Med. Mol. Imaging, 44:678-688 (2017).
Gjertsson, K., et al., A Novel Automated Deep Learning Algorithm for Segmentation of the Skeleton in Low-Dose CT for [(18)F] DCFPyL PET/CT Hybrid Imaging in Patients with Metastatic Prostate Cancer, Annual Congress of the European Association of Nuclear Medicine Oct. 12-16, 2019 Barcelona, Spain. Eur J Nucl Med Mol Imaging 46 (Suppl 1), S1-S952 (2019). Abstract EP-0823, p. S765.
Gjertsson, K., Segmentation in Skeletal Scintigraphy Images using Convolutional Neural Networks, Master's Theses in Mathematical Sciences, pp. 39-58, (2017), <https://lup.lub.lu.se/student-papers/search/publication/8916406>.
Goffin, K. E. et al., Phase 2 study of ^{99m}Tc-trofolastat SPECT/CT to identify and localize prostate cancer in intermediate- and high-risk patients undergoing radical prostatectomy and extended pelvic lymph node dissection, J. Nucl. Med., 27 pages (2017).
Guimond, A. et al., Average Brain Models: A Convergence Study, Computer Vision and Image Understanding, 77:192-210 (2000).
Hajnal, J. et al., 4.4 Intensity, Size, and Skew Correction; 7.1 Introduction; 7.2 Methods; 7.3 Image Interpretation—General, In: Medical Image Registration, CRC Press LLC, 80-81:144-148 (2001).
Hiller, S. M. et al., 99mTc-Labeled Small-Molecule Inhibitors of Prostate-Specific Membrane Antigen for Molecular Imaging of Prostate Cancer, Journal of Nuclear Medicine, 54(8):1369-1376 (2013) retrieved Oct. 25, 2017: <http://jnm.snmjournals.org/content/54/8/1369.full>.
Horikoshi, H. et al., Computer-aided diagnosis system for bone scintigrams from Japanese patients: importance of training database, Annals of Nuclear Medicine, 26(8):622-626 (2012).
Huang, J.-H. et al., A Set of Image Processing Algorithms for Computer-Aided Diagnosis in Nuclear Medicine Whole Body Bone Scan Images, IEEE Transactions on Nuclear Science, 54(3):514-522 (2007).
International Search Report for PCT/EP2020/050132, filed Jan. 6, 2020, 3 pages, dated Mar. 12, 2020.
Kaboteh R. et al., Progression of bone metastases in patients with prostate cancer—automated detection of new lesions and calculation of bone scan index, EJNMMI Research, 3:64 (2013).
Kaboteh, R. et al., Convolutional neural network based quantification of choline uptake in PET/CT studies is associated with overall survival in patents with prostate cancer, EJNMMI, EANM '17, 44(Suppl 2):S119-S956, Abstract EP-0642 (2017).
Keiss, et al., Prostate-specific membrane antigen and a target for cancer imaging and therapy, The Quarterly Journal of Nuclear Medicine and Molecular Imaging, 59(3):241-268 (2015).
Kikuchi, A. et al., Automated segmentation of the skeleton in whole-body bone scans: influence of difference in atlas, Nuclear Medicine Communications, 33(9):947-953 (2012).
Kinahan, P.E. et al., PET/CT Standardized Update Values (SUVs) in Clinical Practice and Assessing Response to Therapy, Semin Ultrasound CT MR 31(6):496-505 (2010) retrieved Oct. 25, 2017: <https://www.ncbi.nlm.nih.gov/pmc/articles/PMC3026294/>.
Knutsson, H., and Andersson, M., Morphons: Segmentation using Elastic Canvas and Paint on Priors, IEEE International Conference on Image Processing (ICIP 2005), Genova, Italy, 4 pages (2005).
Kopka, K. et al., Glu-Ureido-Based Inhibitors of Prostate-Specific Membrane Antigen: Lessons Learned During the Development of a Novel Class of Low-Molecular-Weight Theranostic Radiotracers, The Journal of Nuclear Medicine, 58(9)(Suppl. 2):17S-26S, (2017).
Litjens, G. et al., A survey on deep learning in medical image analysis, Medical Image Analysis, 42:60-88, (2017).
Liu, L. et al., Computer-Aided Detection of Prostate Cancer with MRI: Technology and Applications, Acad Radiol. Author manuscript, 50 pages 2016.
Ma, L. et al., Automatic segmentation of the prostate on CT images using deep learning and multi-atlas fusion, Proc. of SPIE vol. 10133:101332O-1-101332O-9 (2017).
Ma, L. et al., Combining Population and Patient-Specific Characteristics for Prostate Segmentation on 3D CT Images, Proc of SPIE 9784:978427-1-8 (2016).
Ma, L. et al., Random Walk Based Segmentation for the Prostate on 3D Transrectal Ultrasound Images, Proc SPIE Int Soc Opt Eng. Author manuscript, 13 pages (2016).
Mayo Clinic Staff, Choline C-11 PET scan, Overview, Mayo Clinic, 4 pages (2017), retrieved Oct. 25, 2017: <https://www.mayoclinic.org/tests-procedures/choline-c-11-pet-scan/home/ovc-20156994>.
Meyer, A., et al., Deep learning algorithm improves identification of men with low-risk prostate cancer using PSMA targeted 99mTc-MIP-1404 SPECT/CT, Journal of Clinical Oncology, 37:(15), (2019).
Nakajima, K. et al., Enhanced diagnostic accuracy for quantitative bone scan using an artificial neural network system: a Japanese multi-center database project, EJNMMI Research, 3:83 (2013).
National Cancer Institute, NCI Drug Dictionary: gallium Ga 68-labeled PSMA-11, retrieved Oct. 25, 2017: <https://www.cancer.gov/publications/dictionaries/cancer-drug?cdrid=766400>.
National Cancer Institute, NCI Drug Dictionary: technetium Tc 99m methylene diphosphonate, retrieved Oct. 25, 2017: <https://www.cancer.gov/publications/dictionaries/cancer-drug?cdrid=537722>.
Ohlsson, M., et al., Automated decision support for bone scintigraphy, Computer-based medical systems, pp. 1-6, (2009).
Peirui B. et al., Body region localization in whole-body low-dose CT images of PET/CT scans using virtual landmarks, Medical Physics Wiley USA, 46(3): 1286-1299 (2019).
Perera, M. et al., Sensitivity, Specificity, and Predictors of Positive 68Ga-Prostate-specific Membrane Antigen Positron Emission Tomography in Advanced Prostate Cancer: A Systematic Reviewand Meta-analysis, European Urology, 70(6):926-937 (2016).
Polymeri, E. et al., Analytical validation of an automated method for segmentation of the prostate gland in CT images, EJNMMI, EANM '17, 44(Suppl 2):S119-S956, Abstract EP-0641 (2017).
Pouliot, F., et al., Prospective evaluation of a Novel Deep Learning Algorithm (PSMA-AI) in the assessment of 99mTc-MIP-1404 SPECT/CT in patients with low or intermediate risk prostate cancer, Annual Congress of the European Association of Nuclear Medicine Oct. 12 -16, 2019 Barcelona, Spain. Eur J Nucl Med Mol Imaging 46 (Suppl 1), S1-S952 (2019). Abstract EP-0804, p. S765.
Radiologyinfo.org for Patients, Computed Tomography (CT), retrieved Oct. 25, 2017: <https://www.radiologyinfo.org/en/submenu.cfm?pg=ctscan>.
Rowe, S. P. et al., PET Imaging of prostate-specific membrane antigen in prostate cancer: current state of the art and future challenges, Prostate Cancer and Prostatic Diseases, 1-8 (2016).
Rowe, S. P. et al., PSMA-Based [^{18}F]DCFPyL PET/CT Is Superior to Conventional Imaging for Lesion Detection in Patients with Metastatic Prostate Cancer, Mol Imaging Biol, 18:411-419, (2016).
Sabbatini, P. et al., Prognostic Significance of Extent of Disease in Bone in Patients With Androgen-Independent Prostate Cancer, Journal of Clinical Oncology, 17(3):948-957 (1999).
Sadik, M. et al., 3D prostate gland uptake of 18F-choline-association with overall survival in patients with hormone-naïve prostate cancer, The Journal of Nuclear Medicine, 58(Suppl. 1):Abstract 544 (2017).

(56) **References Cited**

OTHER PUBLICATIONS

Sadik, M. et al., A new computer-based decision-support system for the interpretation of bone scans, Nuclear Medicine Communications, 27(5):417-423 (2006).
Sadik, M. et al., Automated 3D segmentation of the prostate gland in CT images—a first step towards objective measurements of prostate uptake in PET and SPECT images, Journal of Nuclear Medicine, 58(1):1074, (2017).
Sadik, M. et al., Automated quantification of reference levels in liver and mediastinum (blood pool) for the Deauville therapy response classification using FDG-PET/CT in lymphoma patients, EJNMMI, EANM '17, 44(Suppl 2):S119-S956, Abstract EP-0770 (2017).
Sadik, M. et al., Computer-assisted interpretation of planar whole-body bone scans, Journal Nuclear Medicine, 49(12):1958-65, 2008.
Sadik, M. et al., Convolutional neural networks for segmentation of 49 selected bones in CT images show high reproducibility, EJNMMI, EANM '17, 44(Suppl 2):S119-S956, Abstract OP-657 (2017).
Sadik, M. et al., Improved classifications of planar whole-body bone scans using a computer-assisted diagnosis system: a multicenter, multiple-reader, multiple-case study, Journal of Nuclear Medicine, 50(3): 368-75, 2009.
Sadik, M. et al., Variability in reference levels for Deauville classifications applied to lymphoma patients examined with 18F-FDG-PET/CT, EJNMMI, EANM '17, 44(Suppl 2):S119-S956, Abstract EP-0771 (2017).
Sajn, L. et al., Computerized segmentation of whole-body bone scintigrams and its use in automated diagnostics, Computer Methods and Programs in Biomedicine, 80:47-55 (2005).
Salerno, J. et al., Multiparametric magnetic resonance imaging for pre-treatment local staging of prostate cancer: A Cancer Care Ontario clinical practice guideline, Canadian Urological Association Journal, 10(9-10):332-339 (2016).
Sjöstrand K. et al., Statistical regularization of deformation fields for atlas-based segmentation of bone scintigraphy images, MICCAI 5761:664-671 (2009).
Sjöstrand, K., et al., Automated detection and quantification of Prostatic PSMA uptake in SPECT/CT using a Deep Learning Algorithm for Segmentation of Pelvic Anatomy, The Journal of Nuclear Medicine, 59(1):p. 30, (2018).
Sjostrand, K., et al., Automated Assessment of Prostatic PSMA Expression in SPECT/CT using Deep Convolutional Neural Networks—A Prospectively Planned Retrospective Analysis of Phase 3 Study MIP-1404-3301, The Journal of Nuclear Medicine, 60 (Supplement 1): Abstract 401, (2019).
Sluimer, I. et al., Toward Automated Segmentation of the Pathological Lung in CT, IEEE Transactions on Medical Imaging, 24(8):1025-1038 (2005).
Tian, Z. et al., A fully automatic multi-atlas based segmentation method for prostate MR images, Proc SPIE Int Soc Opt Eng. Author manuscript, 12 pages (2015).
Tian, Z. et al., A supervoxel-based segmentation method for prostate MR images, Med. Phys., 44(2):558-569 (2017).
Tian, Z. et al., Deep convolutional neural network for prostate MR segmentation, Proc. of SPIE 10135:101351L-1-101351L-6 (2017).
Tian, Z., et al., Superpixel-based Segmentation for 3D Prostate MR Images, IEEE Trans Med Imaging, Author manuscript, 32 pages, (2016).
Ulmert, D. et al., A Novel Automated Platform for Quantifying the Extent of Skeletal Tumour Involvement in Prostate Cancer Patients Using the Bone Scan Index, European Urology, 62(1):78-84 (2012).
Wrangsjo, A. et al., Non-rigid Registration Using Morphons, Proceedings of the 14th Scandinavian Conference on Image Analysis (SCIA '05), pp. 501-510 (2005).
Written Opinion for PCT/EP2020/050132, filed Jan. 6, 2020, 11 pages, dated Mar. 12, 2020.
Yin, T.-K., A Computer-Aided Diagnosis for Locating Abnormalities in Bone Scintigraphy by a Fuzzy System With a Three-Step Minimization Approach, IEEE Transactions on Medical Imaging, 23(5):639-654 (2004).
Ali, A. et al., The Automated Bone Scan Index as a Predictor of Response to Prostate Radiotherapy in Men with Newly Diagnosed Metastatic Prostate Cancer: An Exploratory Analysis of Stampede's "M1|RT Comparison", European Urology Oncology 3:412-419. (2020).
Ceci, F. et al., E-PSMA: the EANM standardized reporting guidelines v1.0 for PSMA-PET, European Journal of Nuclear Medicine and Molecular Imaging, 48:1626-1638, (2021).
Johnsson, K. et al., Analytical performance of aPROMISE: automated anatomic contextualization, detection, and quantification of [18F]DCFPyL (PSMA) imaging for standardized reporting, European Journal of Nuclear Medicin and Molecular Imaging, 11 pages, Aug. 31, 2021, doi: 10.1007/s00259-021-05497-8. Epub ahead of print. PMID: 34463809.
Matsubara, N. et al., A Phase II, Randomized, Open-Label, Multiarm Study of TAS-115 for Castration-Resistant Prostate Cancer Patients With Bone Metastases, Clinical Genitourinary Cancer, 000(xxx):1-10, (2021).
Nickols, N. et al., aPROMISE: A Novel Automated-PROMISE platform to Standardize Evaluation of Tumor Burden in 18F-DCFPyL (PSMA) images of Veterans with Prostate Cancer, Journal of Nuclear Medicine, 26 pages, May 28, 2021, doi: 10.2967/jnumed.120.261863.
Paschalis, A. et al., Prostate-specific Membrane Antigen Heterogeneity and DNA Repair Defects in Prostate Cancer, European Urology, 76(4):469-478, (2019).

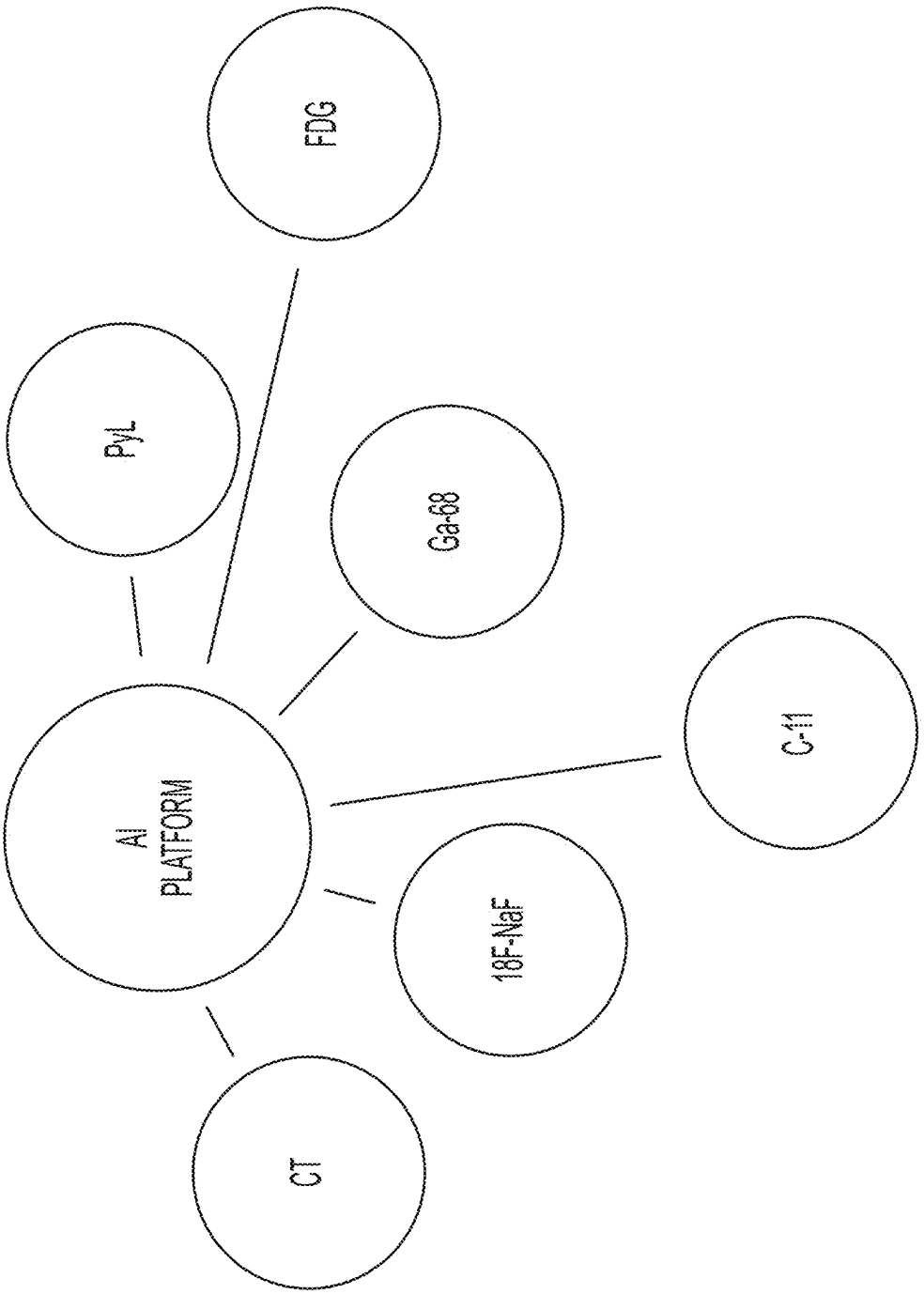


FIG. 1

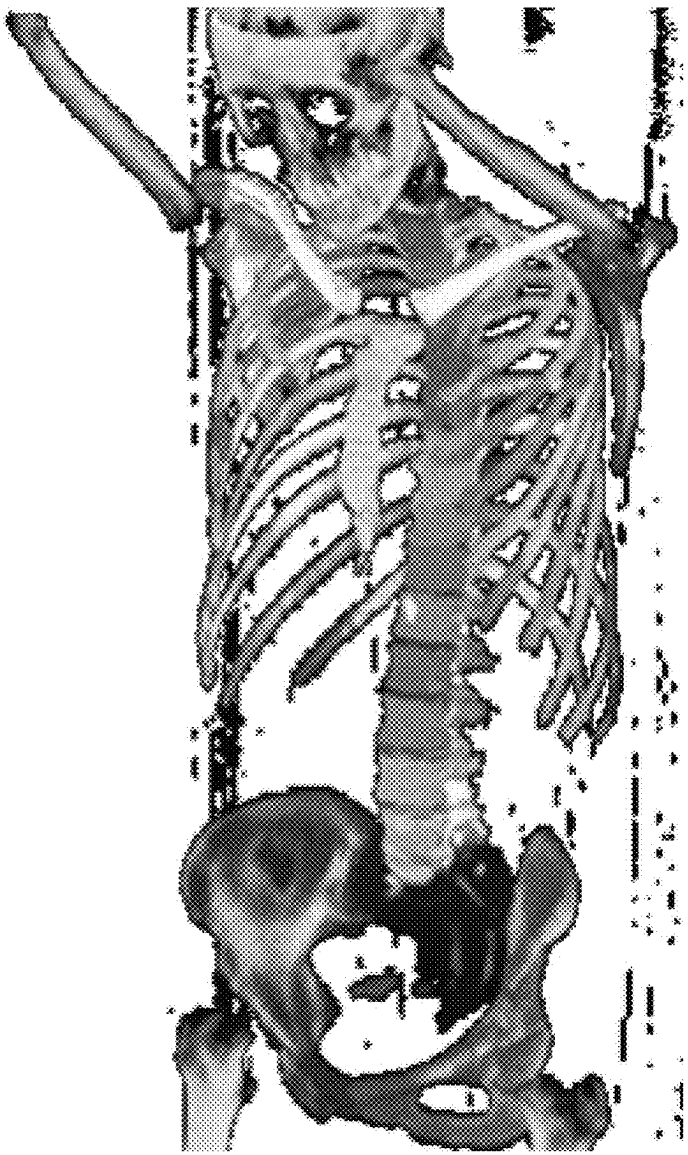


FIG. 2

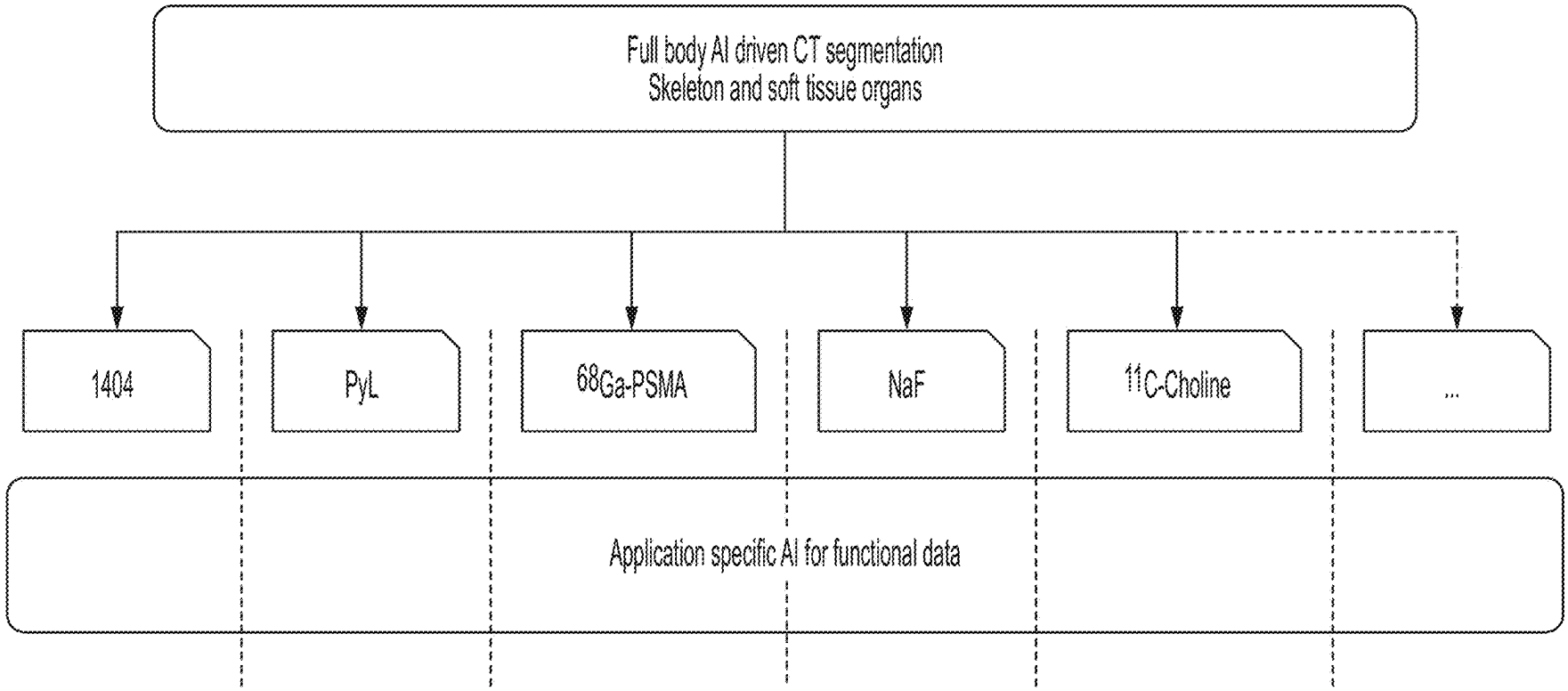

Full body AI driven CT segmentation
Skeleton and soft tissue organs
1404
PyL
68Ga-PSMA
NaF
11C-Choline
...
Application specific AI for functional data

FIG. 3

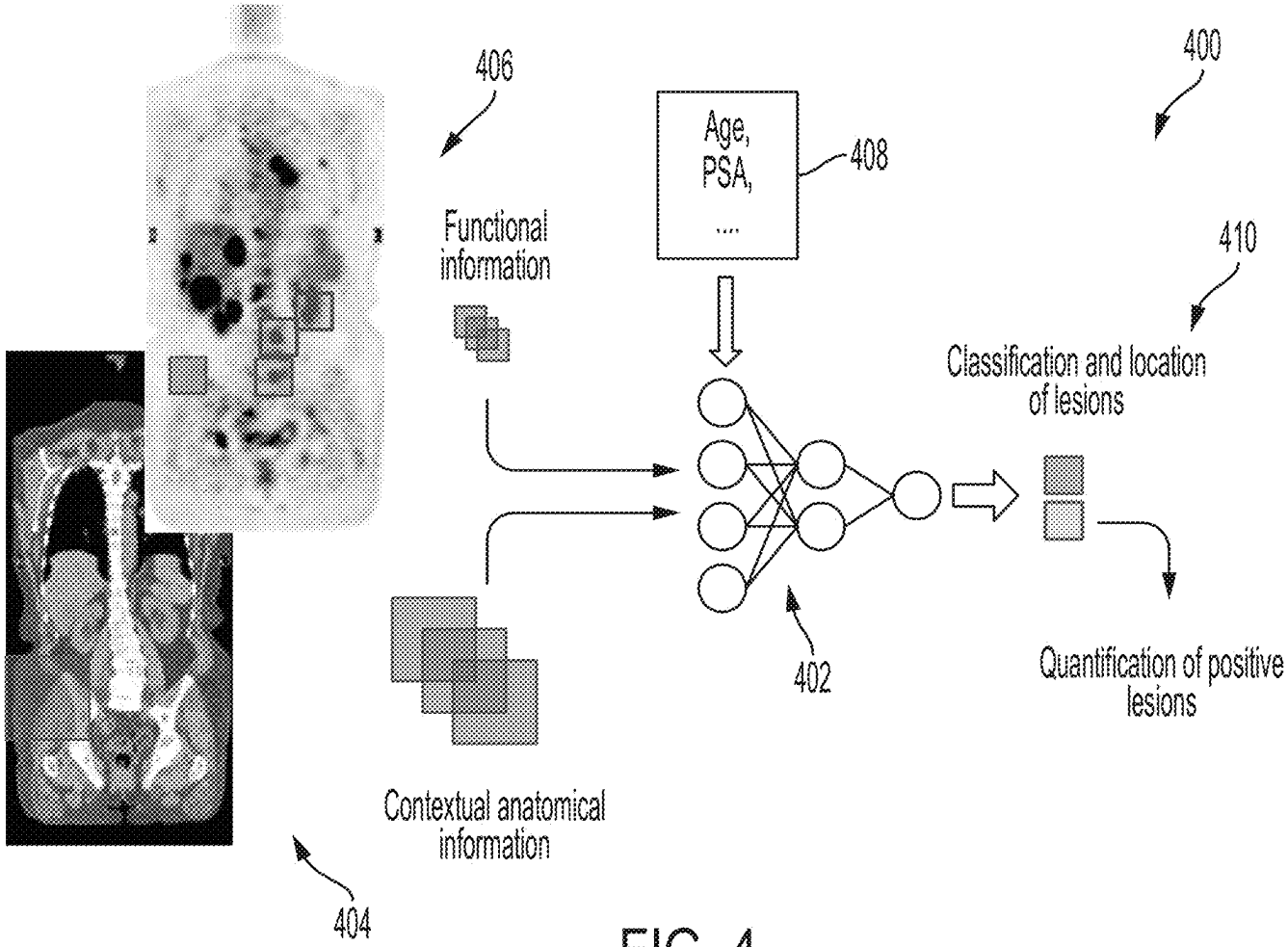

406
400
Age,
PSA,
....
408
Functional information
410
Classification and location of lesions
402
Quantification of positive lesions
Contextual anatomical information
404

FIG. 4

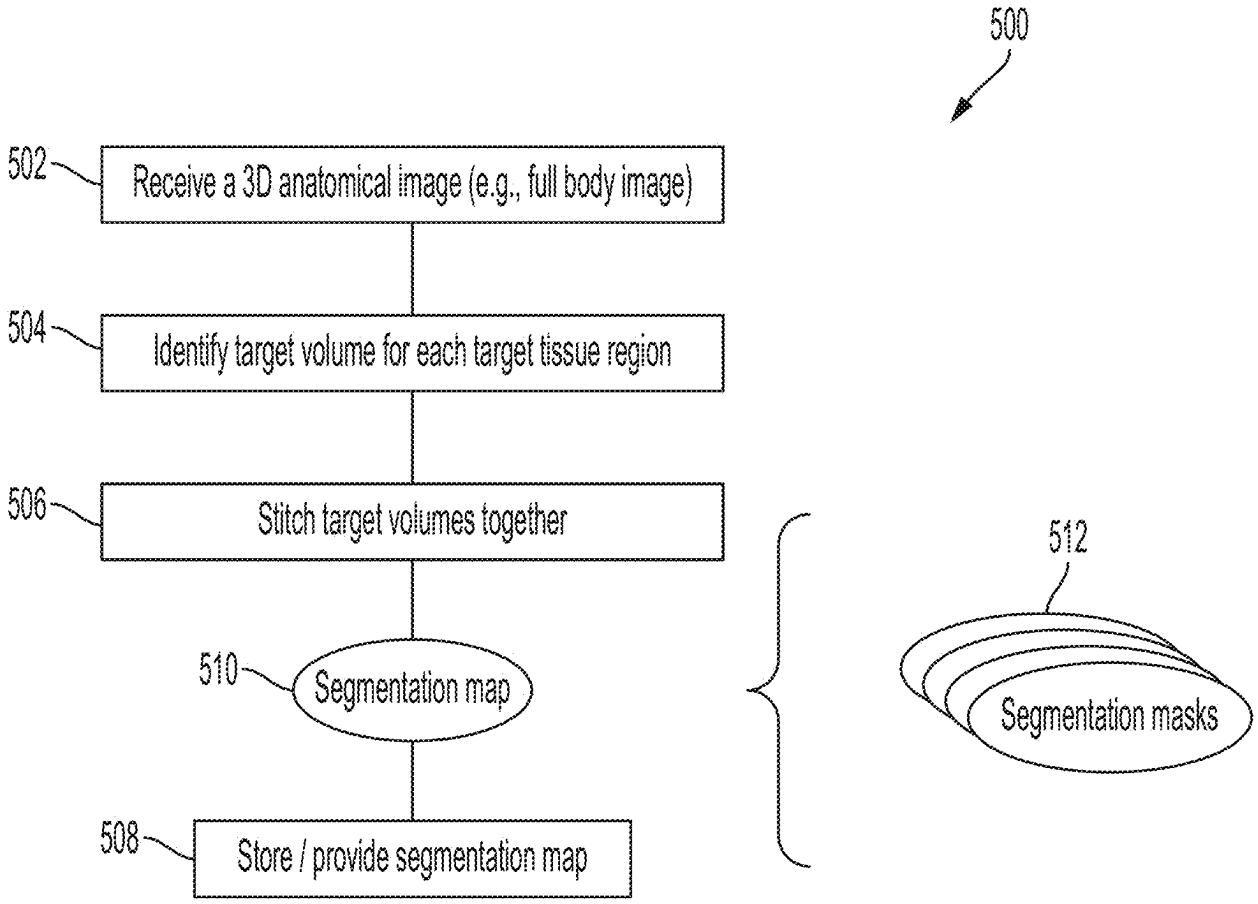

500
502
Receive a 3D anatomical image (e.g., full body image)
504
Identify target volume for each target tissue region
506
Stitch target volumes together
510
Segmentation map
508
Store / provide segmentation map
512
Segmentation masks

FIG. 5A

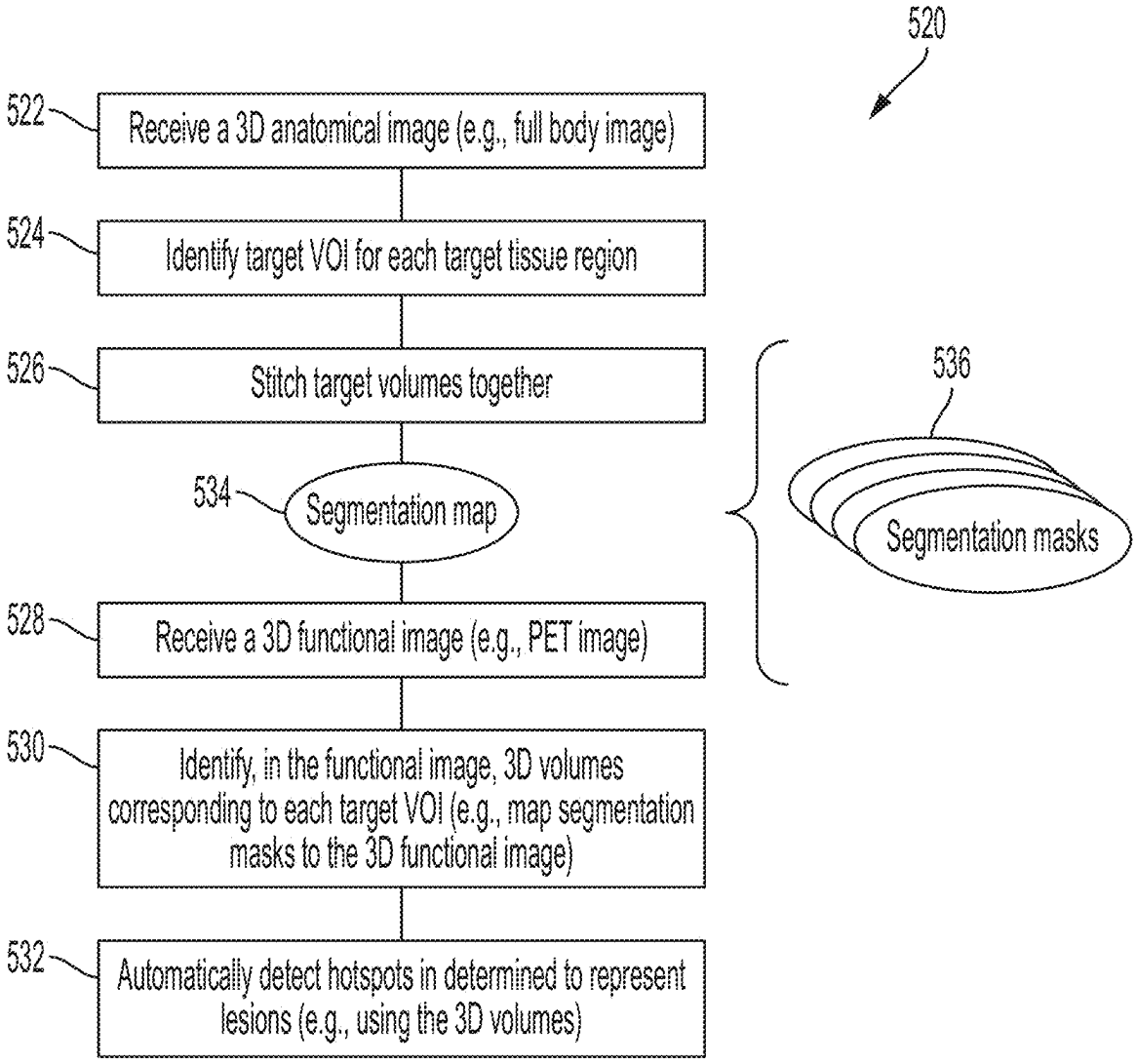

520
522
Receive a 3D anatomical image (e.g., full body image)
524
Identify target VOI for each target tissue region
526
Stitch target volumes together
534
Segmentation map
536
Segmentation masks
528
Receive a 3D functional image (e.g., PET image)
530
Identify, in the functional image, 3D volumes corresponding to each target VOI (e.g., map segmentation masks to the 3D functional image)
532
Automatically detect hotspots in determined to represent lesions (e.g., using the 3D volumes)

FIG. 5B

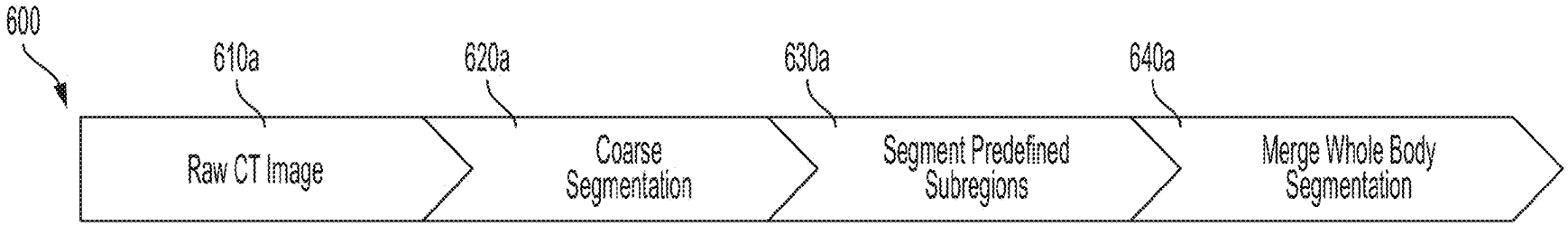

600
610a
620a
630a
640a
Raw CT Image
Coarse Segmentation
Segment Predefined Subregions
Merge Whole Body Segmentation

FIG. 6A

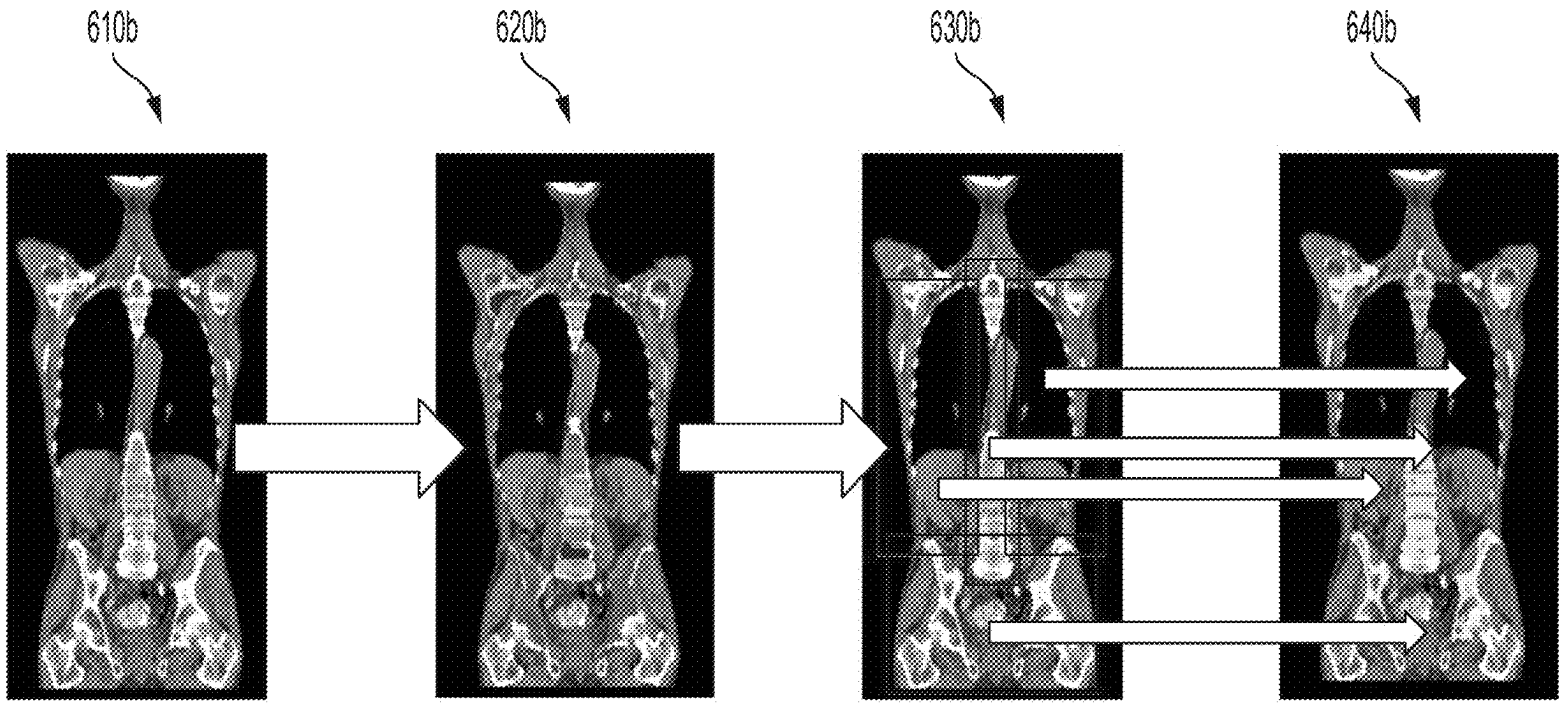

610b
620b
630b
640b

FIG. 6B

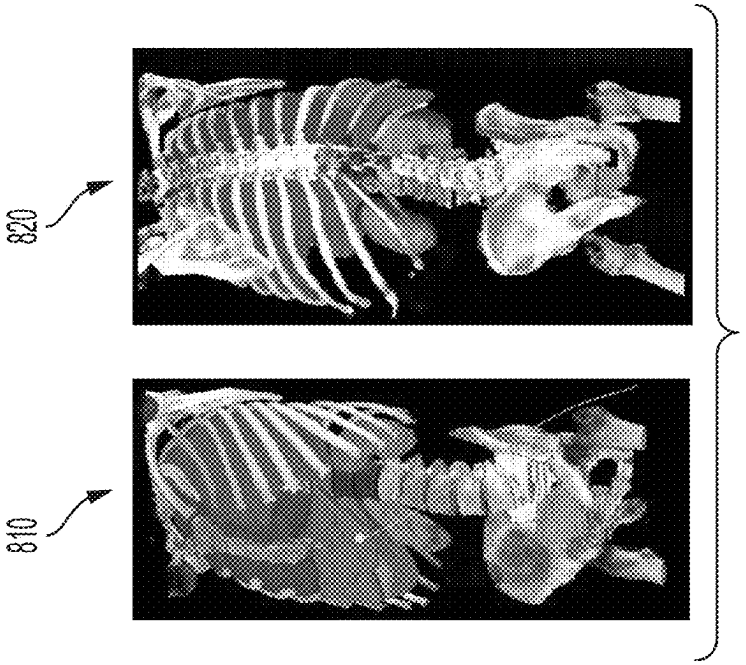


FIG. 8

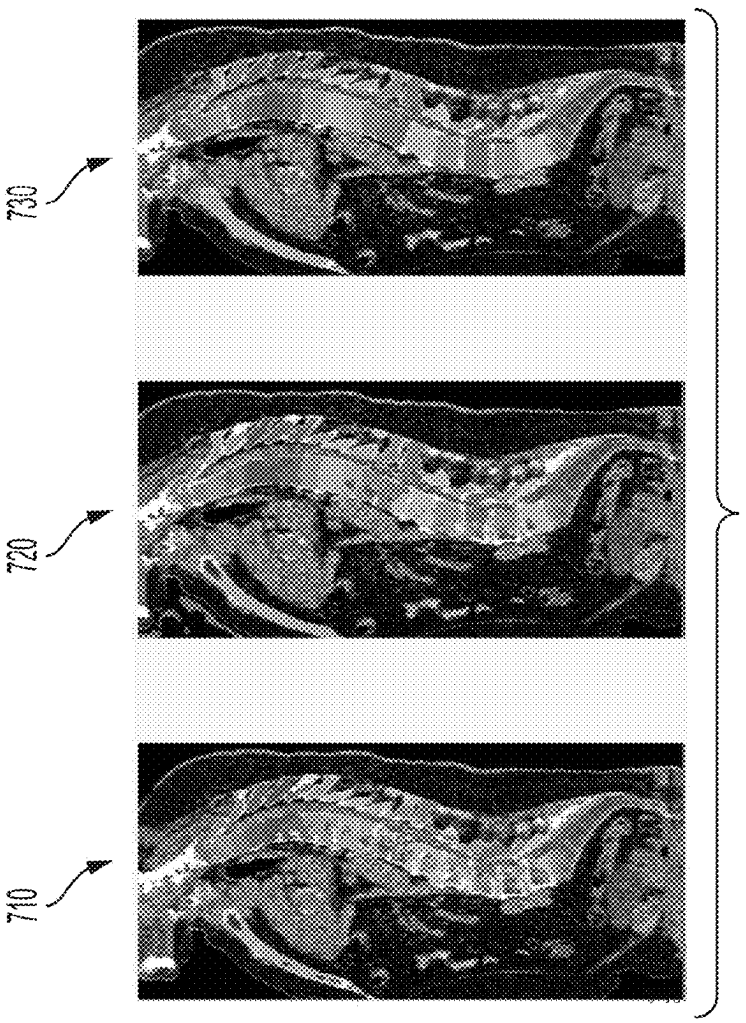


FIG. 7

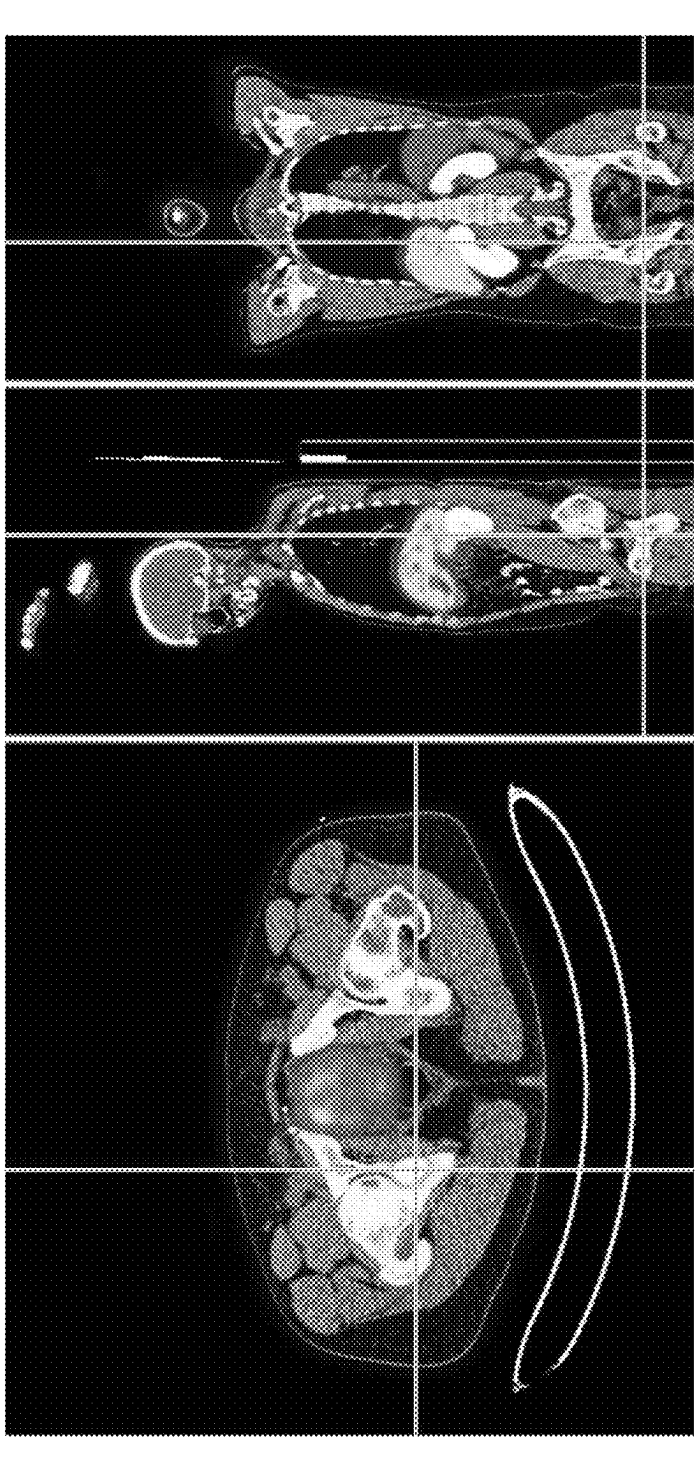


FIG. 9A

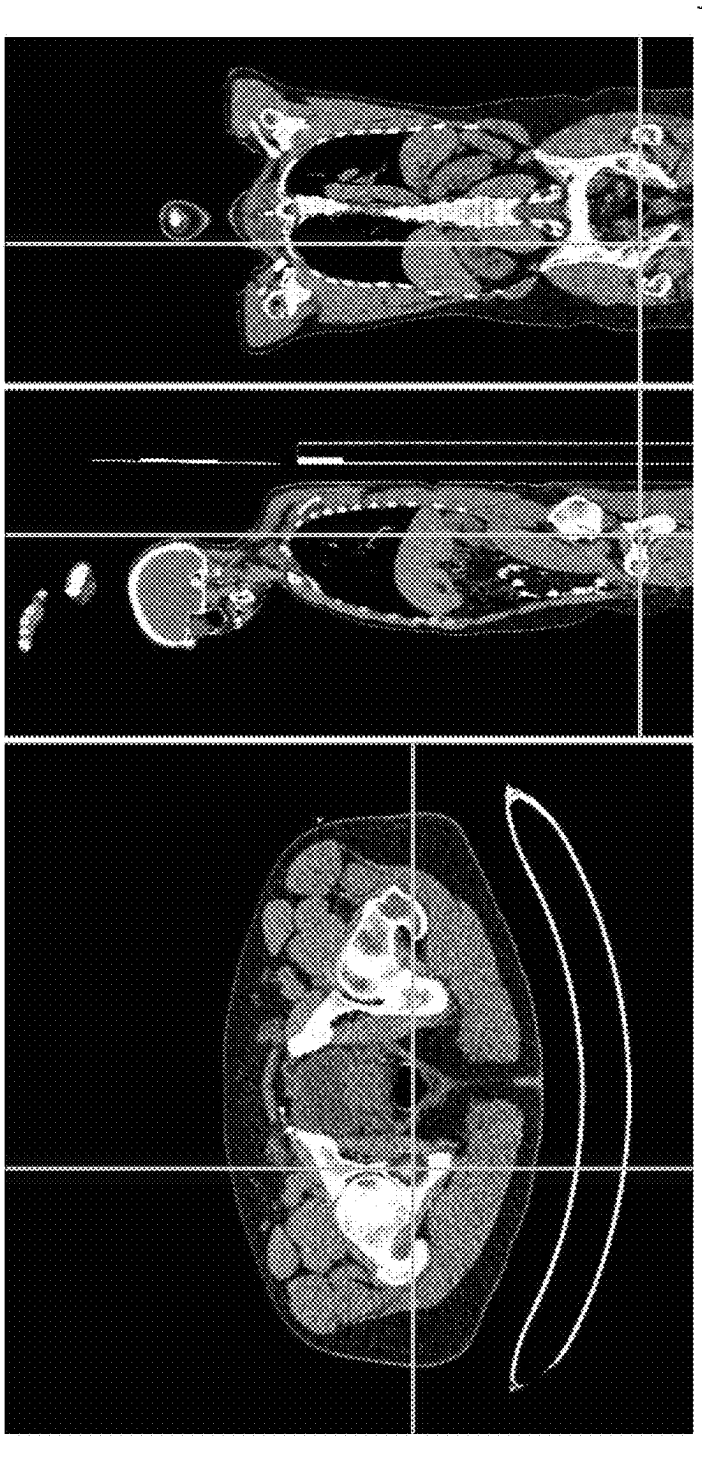


FIG. 9B

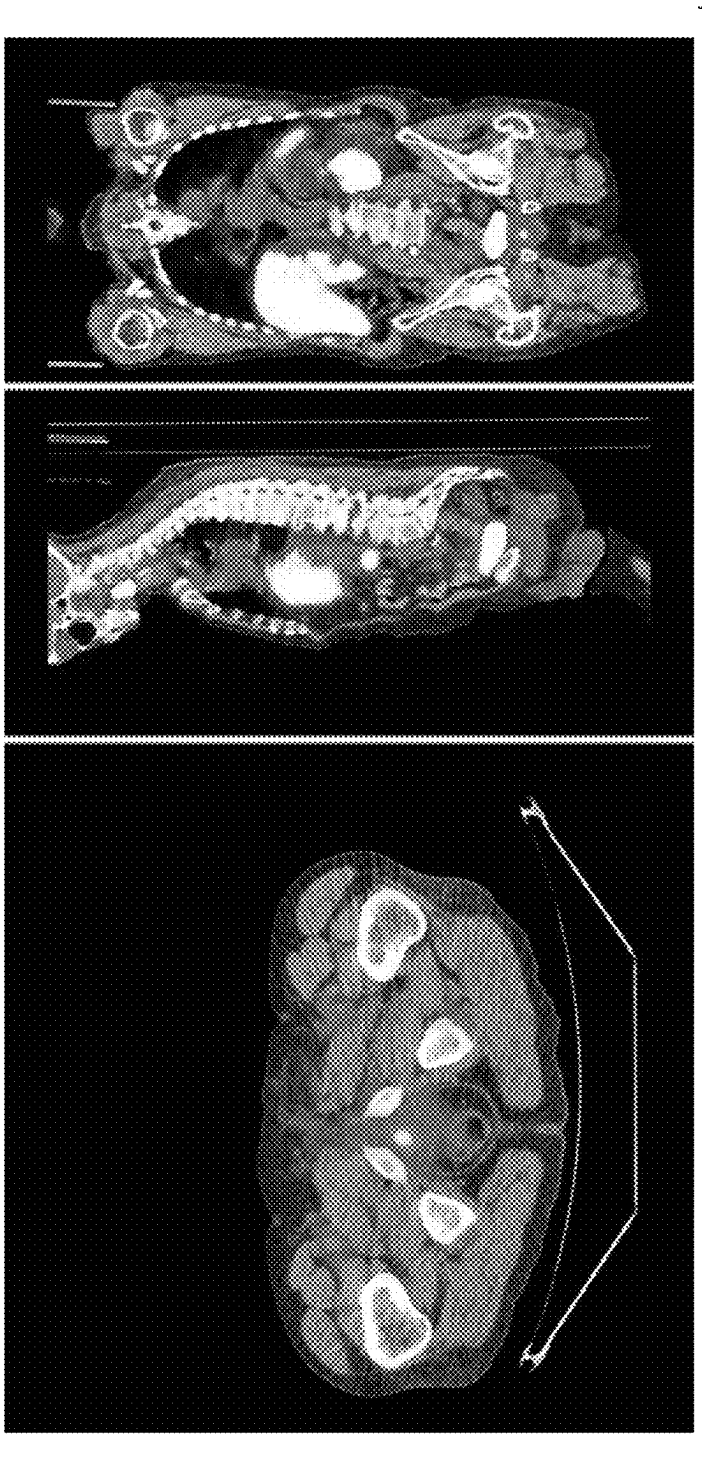


FIG. 9C

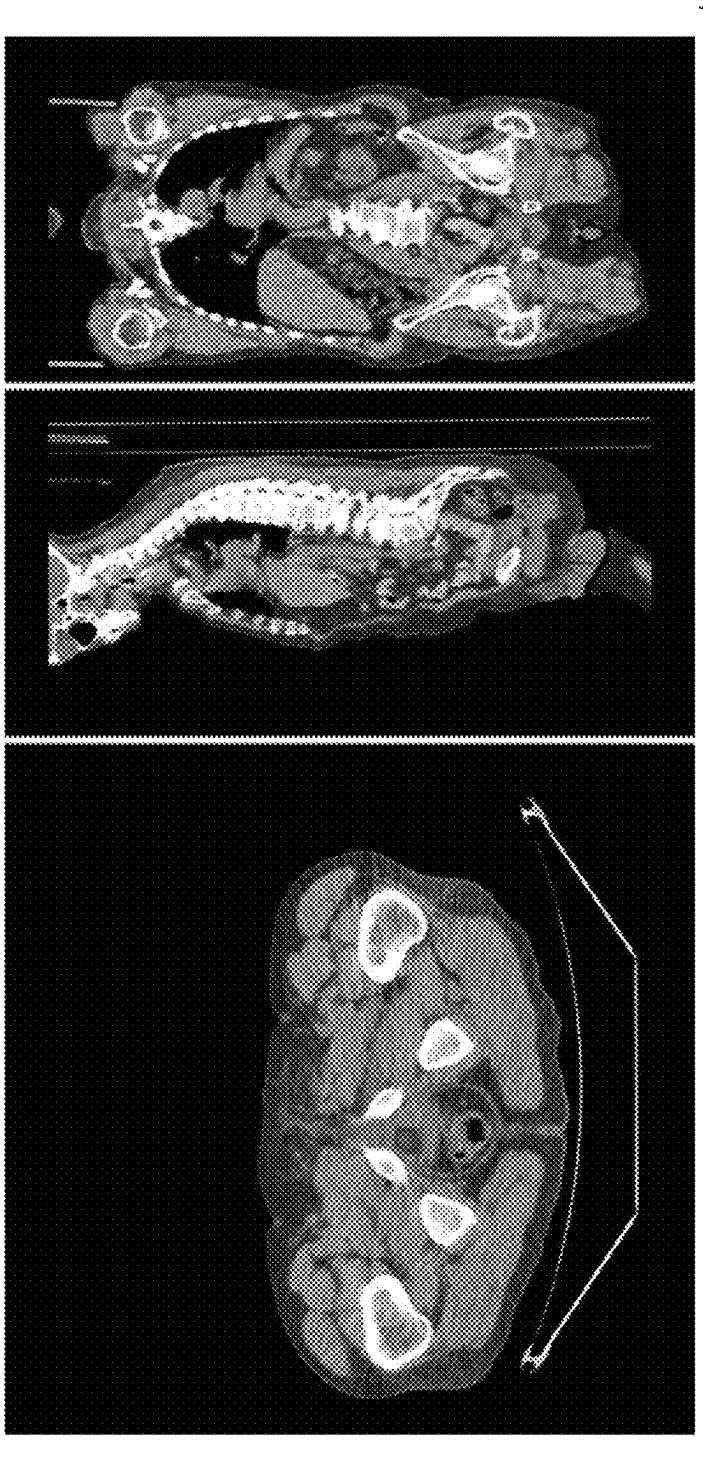


FIG. 9D

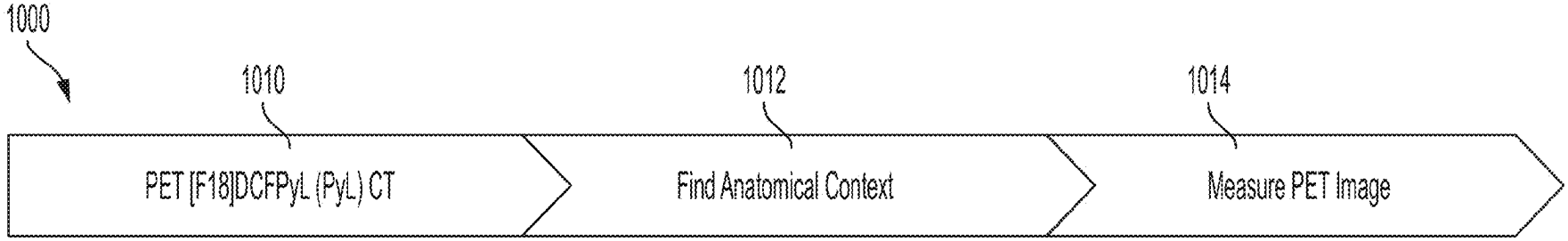


FIG. 10A

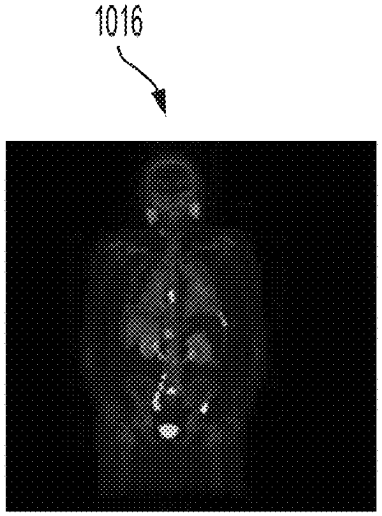


FIG. 10B

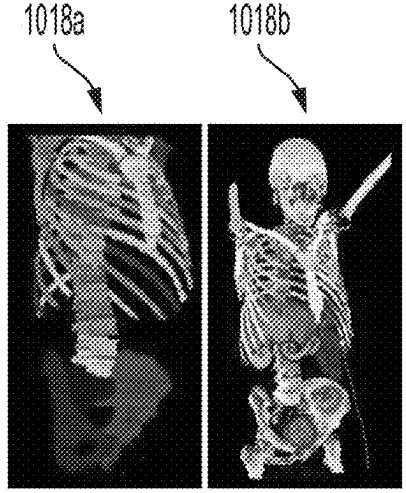


FIG. 10C

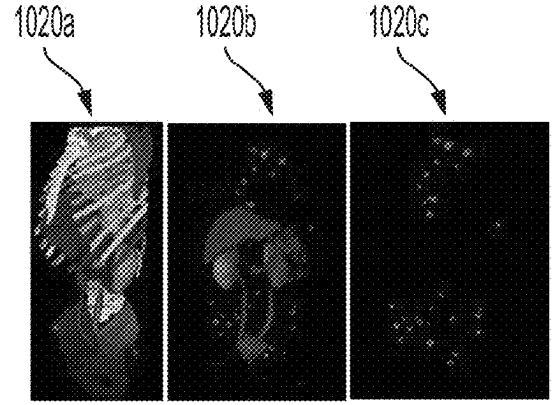


FIG. 10D

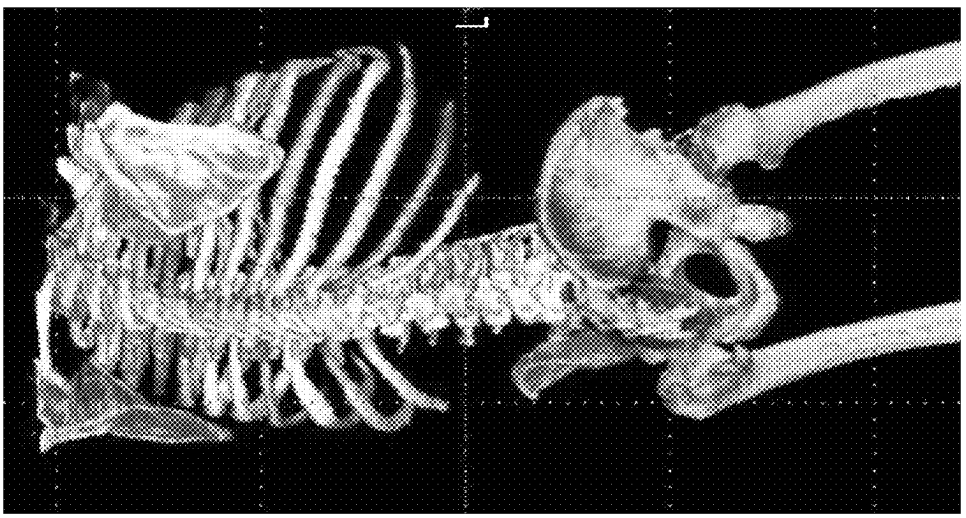


FIG. 11B

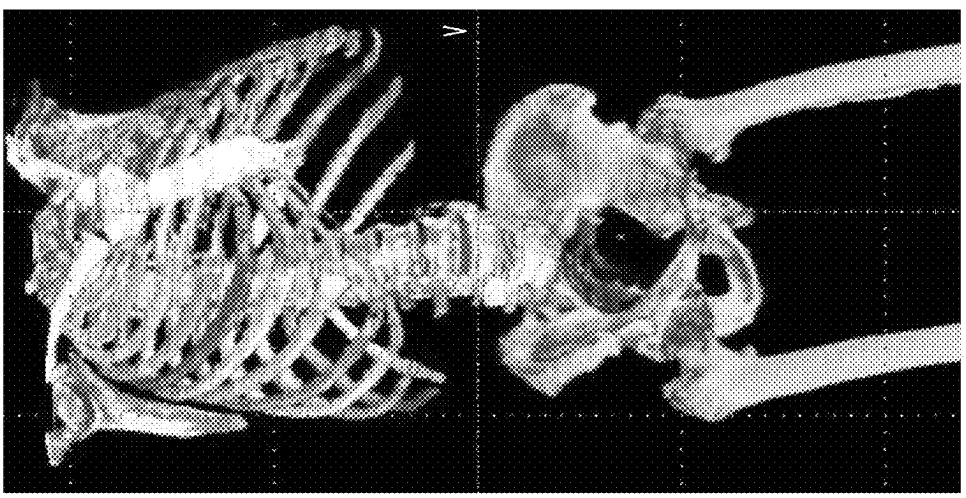


FIG. 11A

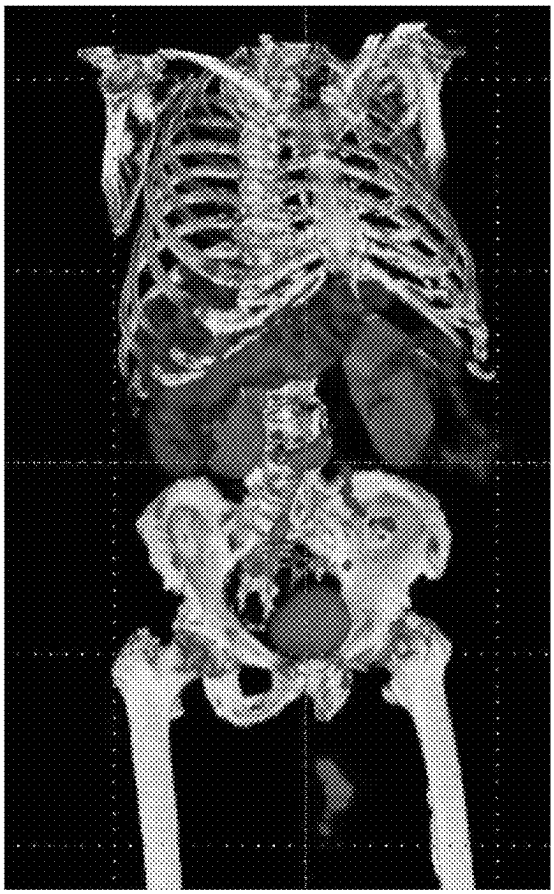


FIG. 12

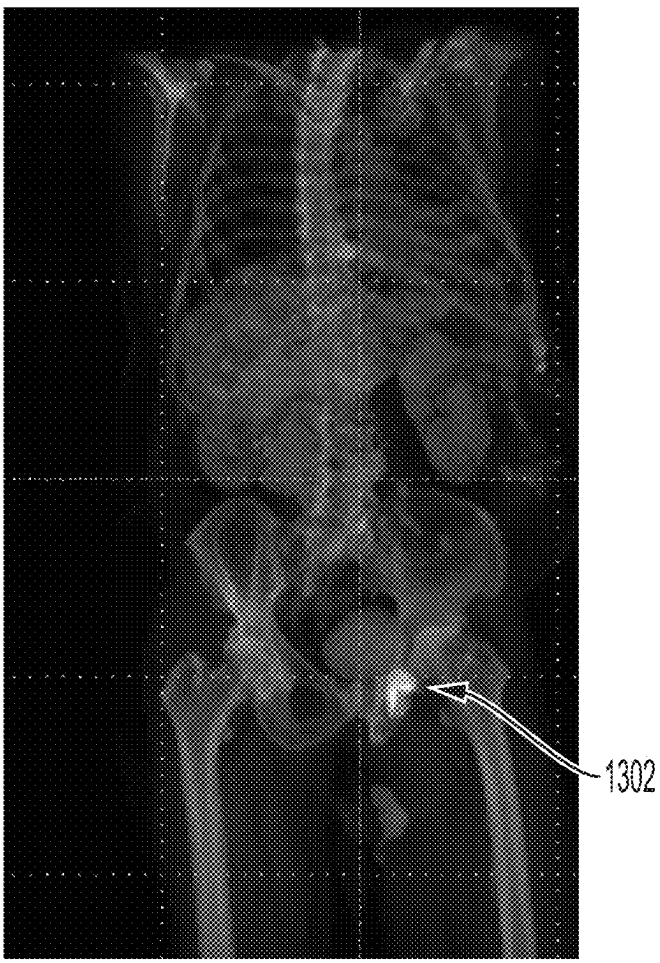


FIG. 13A

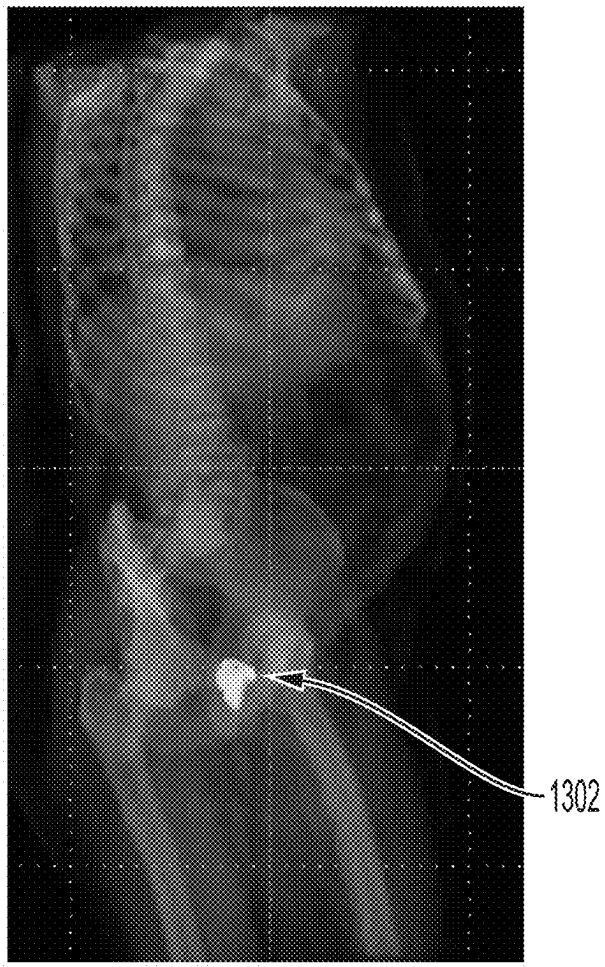


FIG. 13B

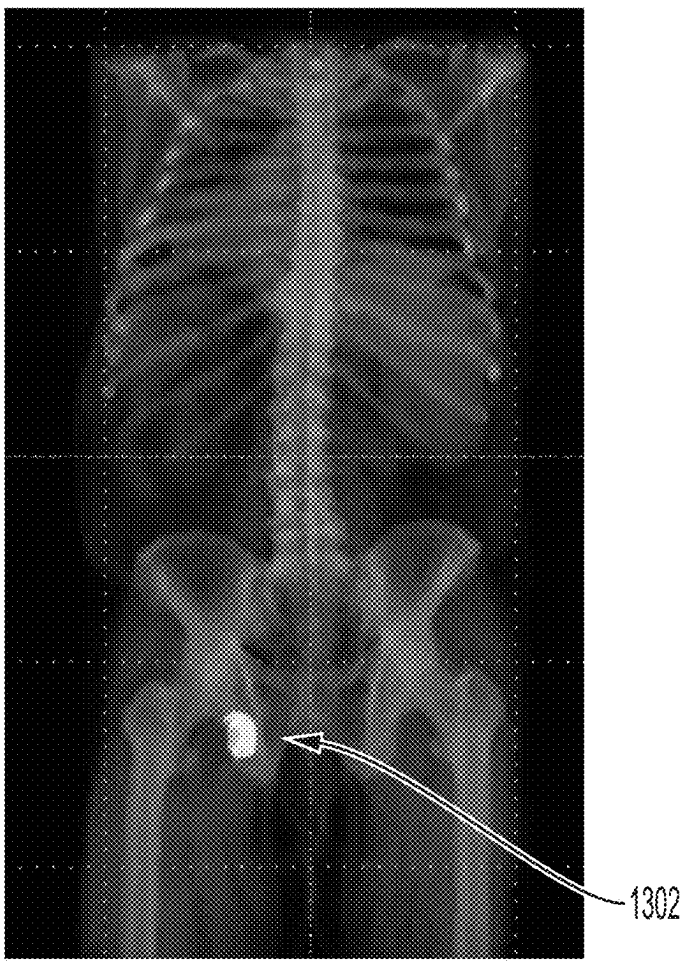


FIG. 13C

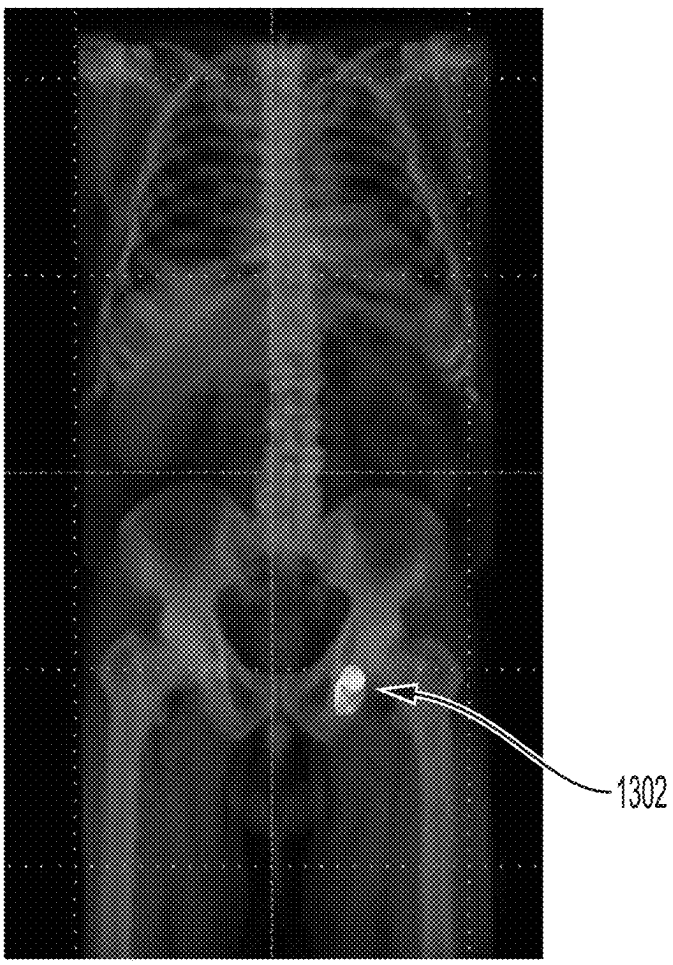


FIG. 13D

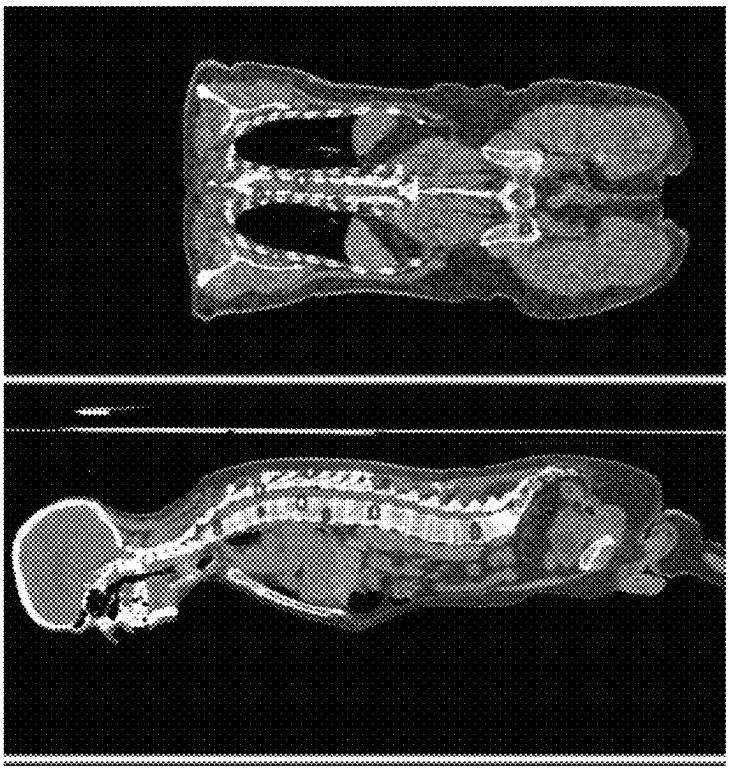


FIG. 14B

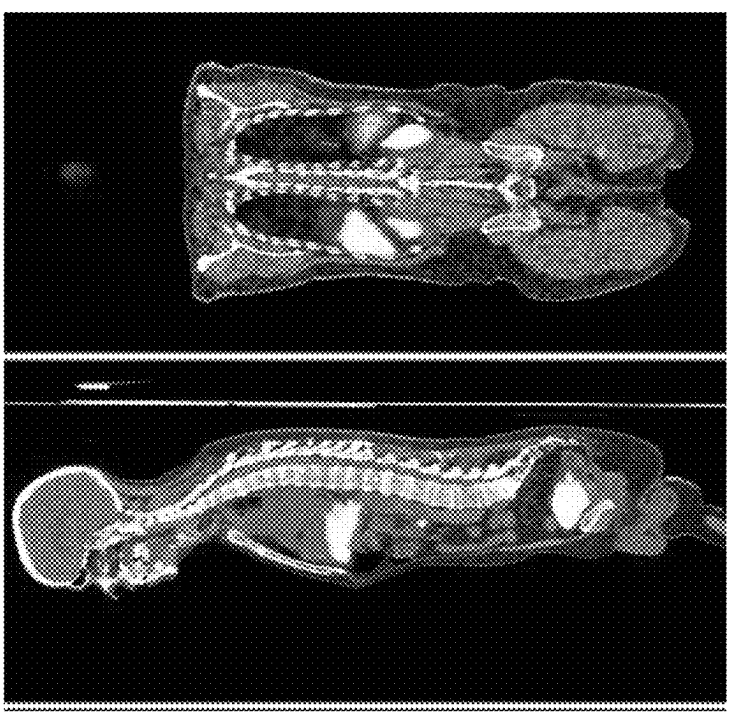


FIG. 14A

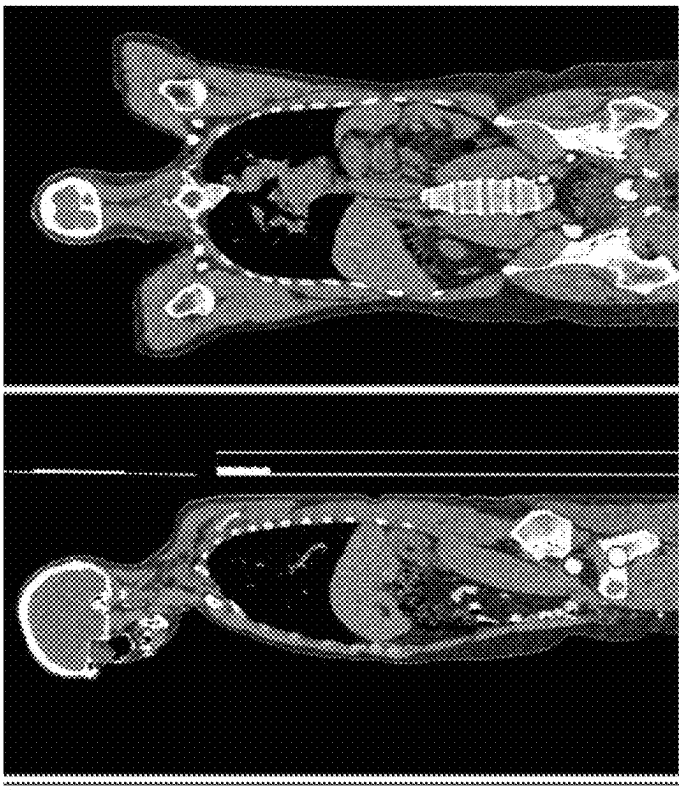


FIG. 15B

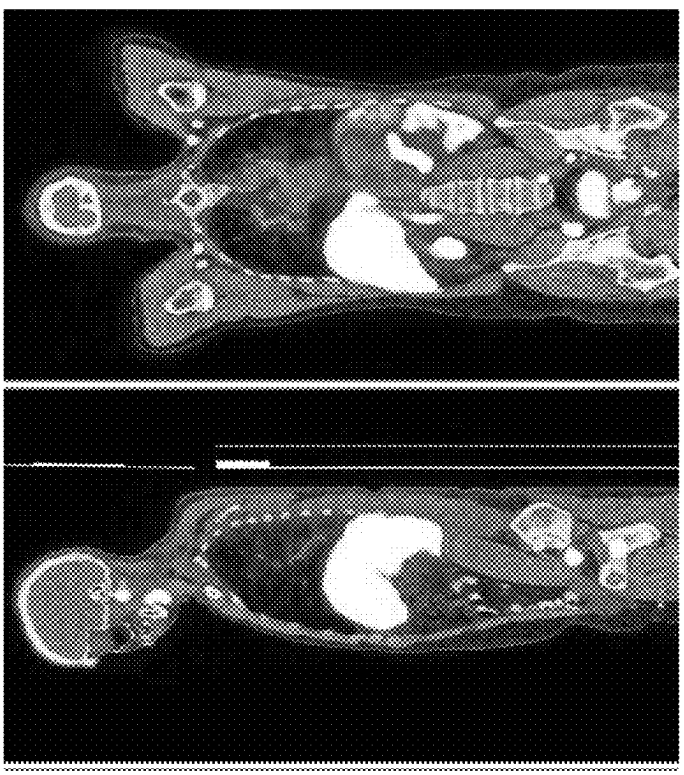


FIG. 15A

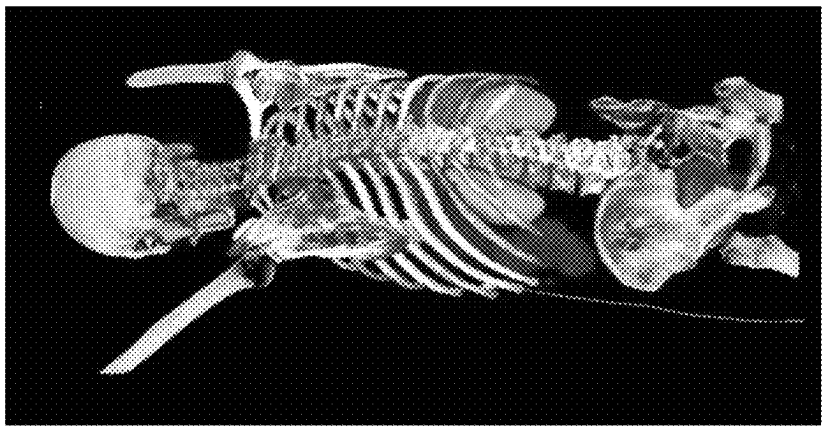


FIG. 16B



FIG. 16A

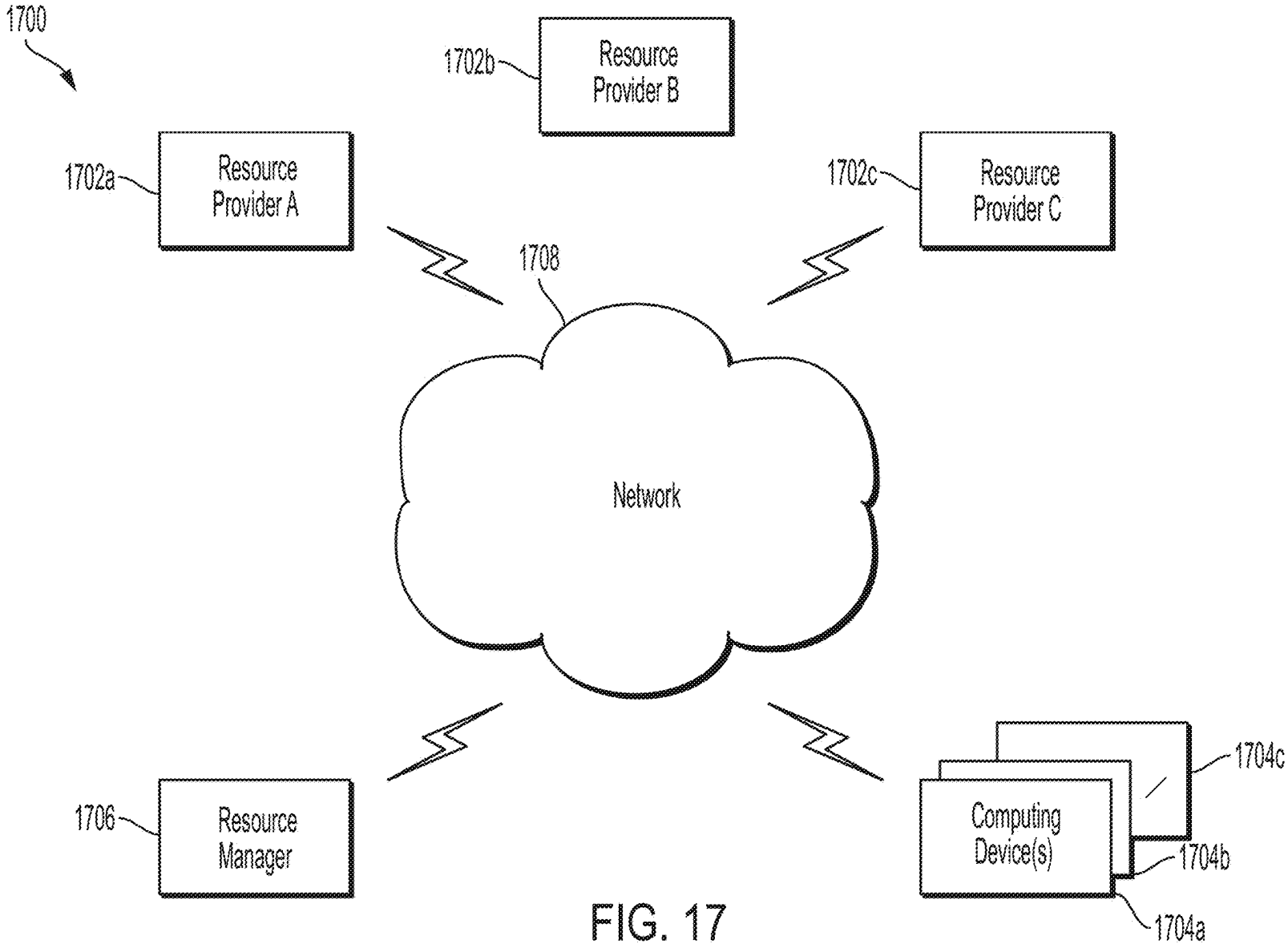

1700
1702b
Resource Provider B
1702a
Resource Provider A
1702c
Resource Provider C
1708
Network
1706
Resource Manager
Computing Device(s)
1704c
1704b
1704a

FIG. 17

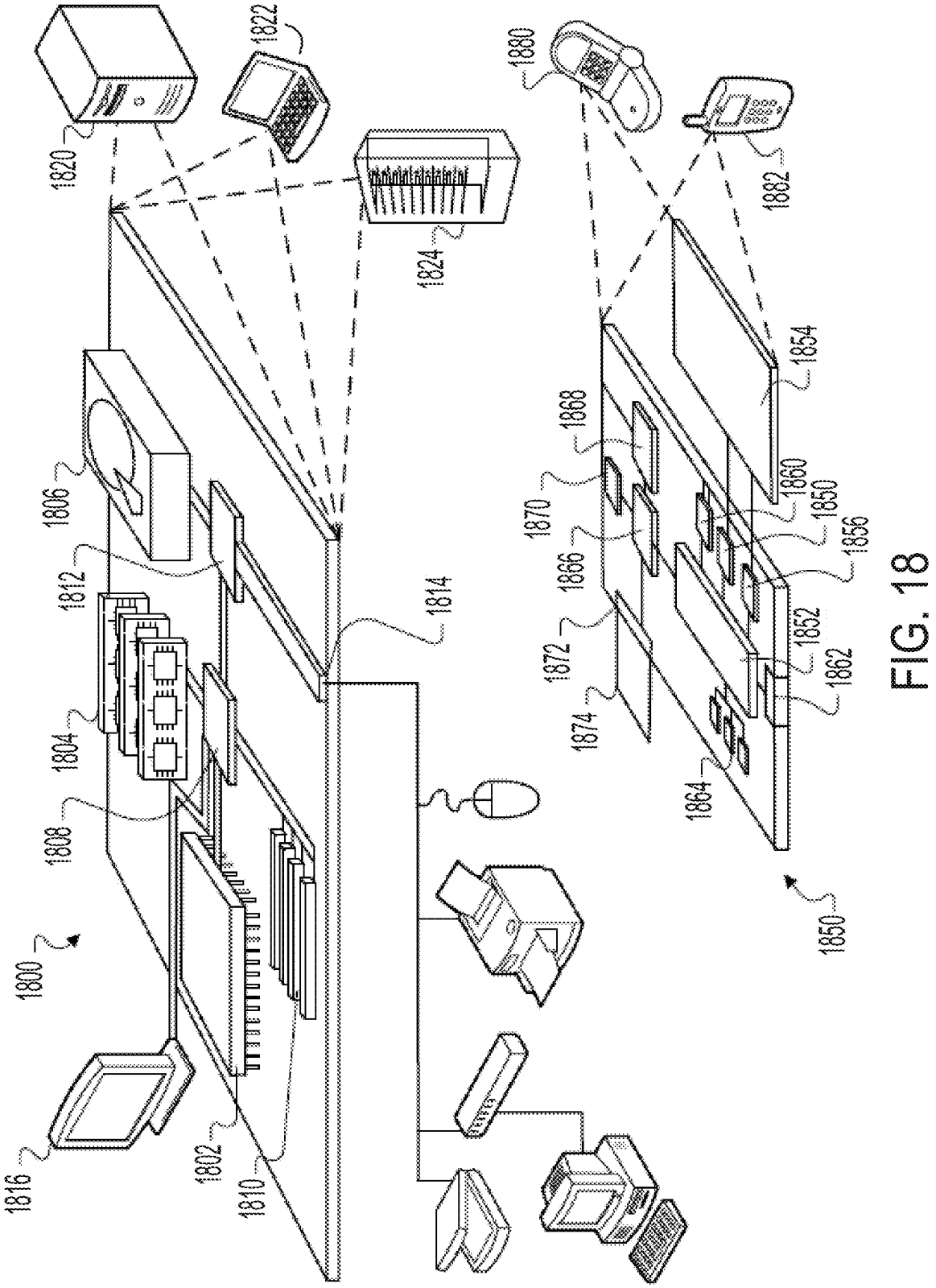

1820
1822
1824
1880
1882
1806
1812
1814
1804
1808
1800
1816
1802
1810
1854
1868
1870
1860
1850
1856
1866
1872
1852
1862
1874
1864
1850

FIG. 18

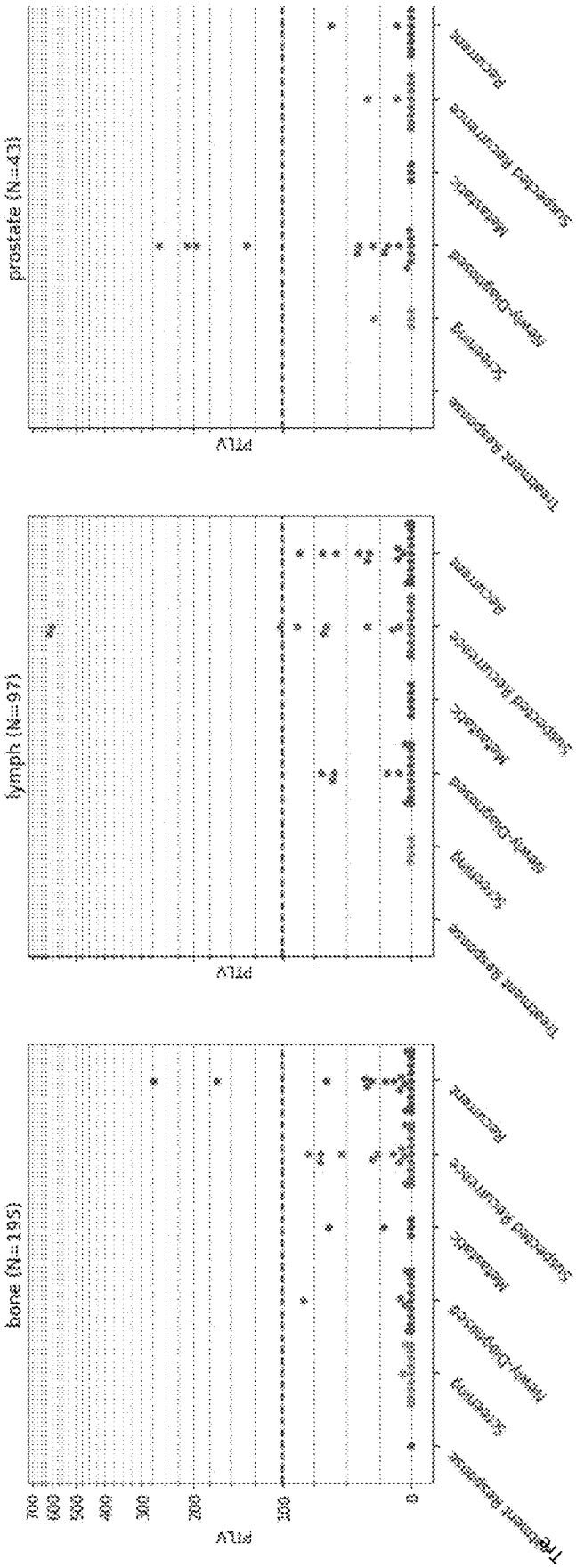

prostate (N=43)
lymph (N=97)
bone (N=195)
PSLV
Treatment Response
Kreatinin
Hemo-Dialyse
Metastasen
Suppressive Therapien
Recurrent
Treatment Response
Kreatinin
Hemo-Dialyse
Metastasen
Suppressive Therapien
Recurrent
Treatment Response
Kreatinin
Hemo-Dialyse
Metastasen
Suppressive Therapien
Recurrent

FIG. 19

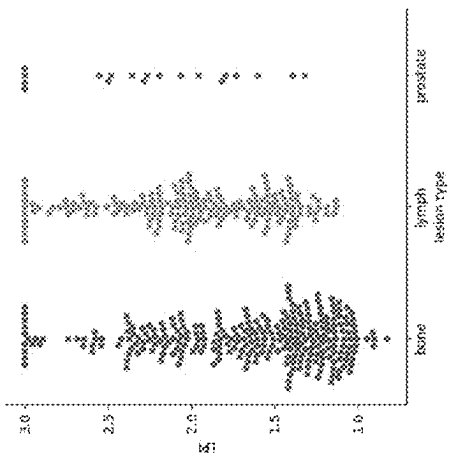

SI
3.0
2.5
2.0
1.5
1.0
bone
lymph
prostate
lesion type

FIG. 20

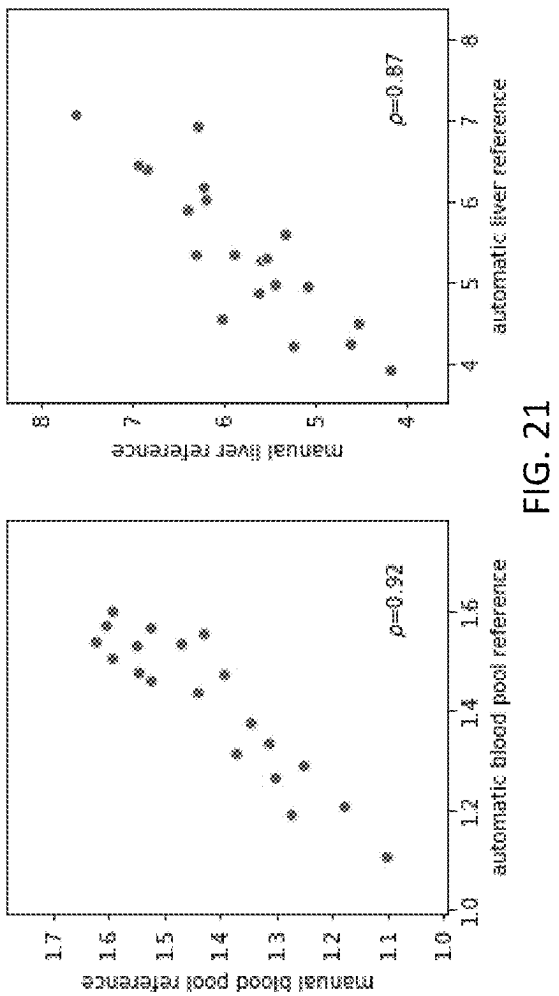

manual blood pool reference
automatic blood pool reference
ρ=0.92
manual liver reference
automatic liver reference
ρ=0.87

FIG. 21

SYSTEMS AND METHODS FOR PLATFORM AGNOSTIC WHOLE BODY IMAGE SEGMENTATION

CROSS-REFERENCE TO RELATED APPLICATIONS

This application claims priority to and benefit of U.S. Provisional Application No. 62/789,155, filed Jan. 7, 2019, U.S. Provisional Application No. 62/837,941, filed Apr. 24, 2019, U.S. Provisional Application No. 62/863,608, filed Jun. 19, 2019, U.S. Provisional Application No. 62/870,210, filed Jul. 3, 2019, U.S. Provisional Application No. 62/907,158, filed Sep. 27, 2019, U.S. Provisional Application No. 62/934,305, filed Nov. 12, 2019, the content of each of which are hereby incorporated by reference in their entirety.

FIELD OF THE INVENTION

This invention relates generally to methods, systems, and architectures for automated analysis of medical images. More particularly, in certain embodiments, the invention relates to automated identification of one or more particular regions of interest (e.g., corresponding to specific organs or tissue) within images of a subject.

BACKGROUND OF THE INVENTION

Targeted image analysis involves the use of radiolabeled small molecules that bind to specific receptors, enzymes and proteins in the body that are altered during the evolution of disease. After administration to a patient, these molecules circulate in the blood until they find their intended target. The bound radiopharmaceutical remains at the site of disease, while the rest of the agent clears from the body. The radioactive portion of the molecule serves as a beacon so that an image may be obtained depicting the disease location and concentration using commonly available nuclear medicine cameras, known as single-photon emission computerized tomography (SPECT) or positron emission tomography (PET) cameras, found in most hospitals throughout the world. Physicians can then use this information to determine the presence and the extent of disease in a patient. The physician can use this information to provide a recommended course of treatment to the patient and to track the progression of disease.

There are a variety of software-based analytical techniques available for analysis and enhancement of PET and SPECT images that can be used by a radiologist or physician. There are also a number of radiopharmaceuticals available for imaging particular kinds of cancer. Imaging agents used in the art include, among others include, without limitation ^{18}F-NaF, ^{11}C-Choline, 2-deoxy-2 [18F] fluoro-d-glucose (FDG), and the like. For example, the small molecule diagnostic 1404 targets the extracellular domain of prostate specific membrane antigen (PSMA), a protein amplified on the surface of >95% of prostate cancer cells and a validated target for the detection of primary and metastatic prostate cancer. 1404 is labeled with technetium-99m, a gamma-emitter isotope that is widely available, relatively inexpensive, facilitates efficient preparation, and has spectrum characteristics attractive for nuclear medicine imaging applications.

Another example radiopharmaceutical is PyL™ (also known as [^{18}F]DCFPyL, and 18F-PyL), which is a clinical-stage, fluorinated PSMA-targeted PET imaging agent for prostate cancer. A proof-of-concept study published in the

April 2016 issue of the Journal of Molecular Imaging and Biology demonstrated that PET imaging with PyL™ showed high levels of PyL™ uptake in sites of putative metastatic disease and primary tumors, suggesting the potential for high sensitivity and specificity in detecting prostate cancer.

An oncologist may use images from a targeted PET or SPECT study of a patient as input in her assessment of whether the patient has a particular disease, e.g., prostate cancer, what stage of the disease is evident, what the recommended course of treatment (if any) would be, whether surgical intervention is indicated, and likely prognosis. The oncologist may use a radiologist report in this assessment. A radiologist report is a technical evaluation of the PET or SPECT images prepared by a radiologist for a physician who requested the imaging study and includes, for example, the type of study performed, the clinical history, a comparison between images, the technique used to perform the study, the radiologist's observations and findings, as well as overall impressions and recommendations the radiologist may have based on the imaging study results. A signed radiologist report is sent to the physician ordering the study for the physician's review, followed by a discussion between the physician and patient about the results and recommendations for treatment.

Thus, the process involves having a radiologist perform an imaging study on the patient, analyzing the images obtained, creating a radiologist report, forwarding the report to the requesting physician, having the physician formulate an assessment and treatment recommendation, and having the physician communicate the results, recommendations, and risks to the patient. The process may also involve repeating the imaging study due to inconclusive results, or ordering further tests based on initial results.

If an imaging study shows that the patient has a particular disease or condition (e.g., cancer), the physician discusses various treatment options, including surgery, as well as risks of doing nothing or adopting a watchful waiting or active surveillance approach, rather than having surgery.

There are limitations associated with this process, both from the perspective of the physician and from the perspective of the patient. While the radiologist's report is certainly helpful, the physician must ultimately rely on her experience in formulating an assessment and recommendation for her patient. Furthermore, the patient must place a great deal of trust in his physician. The physician may show the patient his PET/SPECT images and may tell the patient a numerical risk associated with various treatment options or likelihood of a particular prognosis, but the patient may very well struggle to make sense of this information. Moreover, the patient's family will likely have questions, particularly if cancer is diagnosed but the patient opts not to have surgery. The patient and/or his family members may search online for supplemental information and may become misinformed about risks of the diagnosed condition. A difficult ordeal may become more traumatic.

Thus, there remains a need for systems and methods for improved automated analysis of medical imaging studies and communication of those results, diagnoses, prognoses, treatment recommendations, and associated risks to a patient. Of particular need is an image analysis system to consistently, efficiently, and accurately detect anatomical regions, including soft tissue organs, in the entire body.

SUMMARY OF THE INVENTION

Presented herein are systems and methods that provide for automated analysis of three-dimensional (3D) medical

images of a subject in order to automatically identify specific 3D volumes within the 3D images that correspond to specific anatomical regions e.g., organs and/or tissue). Notably, the image analysis approaches described herein are not limited to a single particular organ or portion of the body. Instead, they are robust and widely applicable, providing for consistent, efficient, and accurate detection of anatomical regions, including tissue and/or organs, in the entire body. In certain embodiments, the accurate identification of one or more such volumes is used to automatically determine quantitative metrics that represent uptake of radiopharmaceuticals in particular organs and/or tissue regions. These uptake metrics can be used to assess disease state in a subject, determine a prognosis for a subject, and/or determine efficacy of a treatment modality.

The capability of the approaches described herein to handle 3D images is an important advantage over certain other image analysis that only identify 2D regions in 2D images. For example, one approach relevant for cancer detection, EXINI Diagnostics AB's Bone Scan Index (BSI) software, detects regions of suspected bone cancer (see also U.S. Pat. No. 8,855,387, issued Oct. 7, 2014). However, the BSI analysis is carried out on two-dimensional scintigraphy images, as opposed to on three dimensional images.

Moreover, with the increase in the choices of imaging agents available to a physician to detect cancer, there remains a need for software with utility in analyzing images from any variety of imaging agents, using multiple detection modalities (SPECT/CT, PET/CT, and the like). Functional images such as SPECT and PET provide detailed and specific information on biological processes in the body, but their potential is only realized when combined with a detailed anatomical map so that function can be localized to individual organs and structures. Although CT and MRI provide detailed anatomical information, conventional (e.g., manual) identification of organs and structures is difficult, subjective and time consuming, making certain assessment infeasible without computer support. Accordingly, by providing platform agnostic image analysis approaches that allow for accurate and robust image segmentation applicable to a variety of imaging modalities, the systems and methods described herein facilitate image analysis of particular relevance to cancer detection, diagnosis, staging, and the like.

For example, the full body segmentation approaches described herein allow for automated analysis of combinations of anatomical and functional images in order to accurately identify and grade cancerous lesions within a subject. In particular, a PET/CT composite image can be acquired for a subject following administration of a radiopharmaceutical, such as a PSMA binding agent like PyL™. The automated, machine learning-based segmentation approaches described herein are used to identify, within the CT image of the PET/CT composite, target volumes of interest (VOIs) representing target tissue regions where cancerous lesions may be found. For example, a skeletal VOI corresponding to a graphical representation of one or more bones of the subject may be identified. Once the skeletal VOI is identified in the anatomical, CT, image, it can be mapped to the PET image to identify a corresponding skeletal volume therein. The corresponding skeletal volume in the PET image is then analyzed to detect one or more localized regions of relatively high intensity, referred to as hotspots. These hotspots correspond, physically, to local regions of increased radiopharmaceutical accumulation and, accordingly, prospective cancerous lesions.

In certain embodiments, the ability to accurately and rapidly perform full body segmentation via the approaches described herein is leveraged to provide a useful and uniform scale on which to evaluate and/or measure radiopharmaceutical uptake levels in physical lesions corresponding to detected hotspots (e.g., to thereby grade expression levels of particular biomolecules, such as PSMA). In particular, in addition to detecting target VOIs corresponding to specific target tissue regions in which cancerous lesions may occur, additional target VOIs corresponding to reference tissue regions are also detected. These reference VOIs are also mapped to the PET image, to identify corresponding reference volumes therein. Measures of intensity, such as a mean, peak, maximum, etc., within these reference volumes are then computed and used as reference points against which to evaluate intensities of individual detected hotspots and convert them to index values on the scale.

For example, in certain embodiments, an aorta and a liver VOI, corresponding to a representation of a portion of an aorta and liver, respectively, are identified within the anatomical image and mapped to the functional image to identify corresponding reference volumes therein. Intensity levels of each of these reference volumes are determined (e.g., as a mean, median, peak, etc. of intensities of voxels within each reference volume), and assigned corresponding index levels on a scale. Then, for each particular individual hotspot, a hotspot intensity level is determined (e.g., similarly, as a mean, median, peak, etc. of voxel intensities within the detected hotspot). A corresponding individual hotspot index value is then determined based individual hotspot intensity level, the aorta reference intensity level, and the liver reference intensity level. This approach provides a standardized scale on which to evaluate and measure uptake associated with hotspots across different images. This allows, for example, for comparison of multiple images obtained for a single subject at different time points, as well as comparison between images of different subjects.

In certain embodiments, individual hotspot indices are used to compute an overall index for the subject and/or particular target tissue region analyzed for presence of cancerous lesions. The overall index can serve as an indicator of disease severity and/or risk, for example by reflecting a total lesion volume within a particular target tissue region, with the weighting based on the hotspot index values for the individual detected hotspots to account for radiopharmaceutical uptake within the lesions. For example, a PSMA weighted total lesion volume within a skeletal volume can be computed as a weighted sum of individual detected hotspot volumes weighted by their corresponding index values. Such an index may reflect a level and/or aggressiveness of metastasis into bone.

Volumes corresponding to other tissue regions may be similarly identified and used to determine overall index values. For example, lymph node volumes may also be used to assess severity of metastases. Volumes corresponding to tissue regions where localized disease is initially found may also be identified and analyzed to detect lesions. For example, a prostate volume may be used to assess prostate cancer severity at its initial stages. Likewise, breast volumes representing breast tissue regions and lung volumes representing lung tissue regions can be used for assessment of localized breast and lung cancers, respectively.

According, by providing for full body segmentation and automated image-based analysis of cancerous lesions throughout various relevant target tissue regions throughout a subject's body, the AI-based systems and methods described herein allow for analysis of a variety of cancers at various stages. The techniques can be used to identify and stage localized disease in relevant tissue regions such as the

prostate, for example for early stage screening and monitoring, as well as to monitor regions such as bone and lymph nodes for metastasis as disease progresses. As such, the approaches described herein provide a complete set of tools for automated image-based detection of cancer, and tracking disease evolution, progression, and response to treatment.

In one aspect, the invention is directed to a method for automatically processing a 3D image to identify 3D volumes within the 3D image that correspond to particular target tissue regions, the method comprising: (a) receiving, by a processor of a computing device, a 3D anatomical image of a subject obtained using an anatomical imaging modality [e.g., x-ray computed tomography (CT); e.g., magnetic resonance imaging (MRI); e.g., ultra-sound], wherein the 3D anatomical image comprises a graphical representation of tissue (e.g., soft-tissue and/or bone) within the subject; (b) automatically identifying, by the processor, using one or more machine learning modules (e.g., wherein at least one of the one or more machine learning modules is a Convolutional Neural Network (CNN) module) for each of a plurality of target tissue regions, a corresponding target volume of interest (VOI) within the 3D anatomical image; (c) determining, by the processor, a 3D segmentation map representing a plurality of 3D segmentation masks, each 3D segmentation mask representing a particular identified target VOI (e.g., automatically, digitally stitching together the plurality of 3D segmentation masks to form the 3D segmentation map); and (d) storing and/or providing for display and/or further processing, the 3D segmentation map.

In certain embodiments, the 3D anatomical image is a full body image.

In certain embodiments, step (c) comprises digitally stitching together the plurality of 3D segmentation masks to form the 3D segmentation map {e.g., by creating an initially empty image volume (e.g., initializing all voxel values to zero) and then inserting labels from each segmentation mask into the image volume [e.g., by mapping labeled (e.g., as representing a particular target tissue region as determined by a machine learning module) voxels of input images to one or machine learning modules to voxels of the image volume (e.g., so as to match voxels of the image volume to voxels of the input images that represent a same physical location, thereby labeling voxels of the image volume correctly)]}.

In certain embodiments, step (b) comprises, for at least one specific target tissue region: determining, using a first module (e.g., a localization module) (e.g., a first machine learning module), an initial VOI within the 3D anatomical image, the initial VOI corresponding to an anatomical region (e.g., a group of related tissue, such as a pelvic region, a chest region, a head and/or neck region, and the like) containing the specific target tissue region (e.g., wherein the initial VOI excludes more voxels of the 3D anatomical image than it includes; e.g., wherein the initial VOI includes less than 25% of the voxels of the 3D anatomical image; e.g., wherein a majority of voxels within the initial VOI represent physical volumes within the anatomical region); and identifying, using a second module (e.g., a segmentation module) (e.g., a second machine learning module), the target VOI corresponding to the specific target tissue region within the initial VOI.

In certain embodiments, the second module is a CNN module that implements a CNN.

In certain embodiments, the first module is a CNN module that implements a CNN to perform a coarse segmentation to automatically identify the initial VOI corresponding to the anatomical region containing the specific target tissue region [e.g., by automatically identifying a graphical representation of a group of related tissue within the anatomical image (e.g., and, subsequently, determining the initial VOI as a rectangular region (e.g., rectangular prism or rectangular box) entirely enclosing the identified graphical representation of the group of related tissue)] [e.g., by, for each of one or more particular tissue regions anticipated to be located within the anatomical region, automatically identifying a corresponding VOI in the anatomical image (e.g., via the coarse segmentation), e.g., and determining the initial VOI as a rectangular region entirely enclosing all of the identified VOIs corresponding to the particular tissue regions].

In certain embodiments, the first module receives a sub-sampled [e.g., by a factor of two or more (e.g., four) along one or more dimensions] version of the anatomical image as input and identifies the initial VOI using the sub-sampled version of the anatomical image [e.g., and wherein the second module receives a full resolution version of the anatomical image, cropped to the initial VOI (e.g., such that the first module operates on an lower resolution image that represents a larger physical volume than the second module, while the second module operates on a higher resolution image but representing a smaller physical volume)].

In certain embodiments, the first module is a first CNN module and the second module is a second CNN module, and wherein the first CNN module comprises additional filters in order to account for increased variability in image size with respect to the second CNN module.

In certain embodiments, the 3D anatomical image is a full body image and step (b) comprises: automatically determining, using one or more localization modules implementing machine learning technique(s) (e.g., wherein each localization module is a CNN module that implements a CNN), a plurality of initial VOIs within the 3D anatomical image, each initial VOI corresponding to a particular anatomical region (e.g., a group of related tissue, such as a pelvic region, a chest region, a head and/or neck region, a spine region, an upper body region, a lower body region, etc.) and in which an associated subset of the target VOIs are located; and for each initial VOI, automatically identifying, using one or more segmentation modules implementing machine learning technique(s) (e.g., wherein each segmentation module is a CNN module that implements a CNN) the associated subset of target VOIs.

In certain embodiments, the plurality of initial VOIs comprises one or more members selected from the group consisting of: a pelvic region initial VOI corresponding to a pelvic region of the subject (e.g., wherein the subset of target VOIs located in the pelvic region initial VOI comprise one or more target VOIs corresponding to target tissue regions selected from the group consisting of a left and/or right ilium, a sacrum, and a coccyx); a spine region initial VOI corresponding to a spine of the subject (e.g., wherein the subset of target VOIs located in the pelvic region initial VOI comprise one or more target VOIs corresponding to target tissue regions selected from the group consisting of a thoracic vertebra, a lumber vertebra, and a sternum); a left upper body region initial VOI corresponding to a left side of the subject's upper body (e.g., wherein the subset of target VOIs located in the pelvic region initial VOI comprise one or more target VOIs corresponding to target tissue regions selected from the group consisting of one or more left rib(s), a left scapula, and a left clavicle); and a right upper body region initial VOI corresponding to a right side of the subject's upper body (e.g., wherein the subset of target VOIs located in the pelvic region initial VOI comprise one or more target VOIs corresponding to target tissue regions selected

from the group consisting of one or more right rib(s), a right scapula, and a right clavicle).

In certain embodiments, the method comprises: (e) receiving, by the processor, a 3D functional image of the subject obtained using a functional imaging modality [e.g., single-photon emission computed tomography (SPECT); e.g., positron emission tomography (PET)][e.g., wherein the 3D functional image comprises a plurality of voxels, each representing a particular physical volume within the subject and having an intensity value that represents detected radiation emitted from a the particular physical volume, wherein at least a portion of the plurality of voxels of the 3D functional image represent physical volumes within one or more of the target tissue regions of the subject]; and (f) identifying, by the processor, within the 3D functional image, one or more 3D volume(s), each corresponding to an identified target VOI, using the 3D segmentation map (e.g., by mapping 3D segmentation masks of the 3D segmentation map to the 3D functional image).

In certain embodiments, the method comprises: (g) determining, by the processor, a cancer status [(e.g., a prostate cancer status; e.g., a metastatic cancer status (e.g., metastatic cancer, including, e.g., metastatic prostate cancer, breast cancer, lung cancer, colon cancer, skin cancer, etc.)] for the subject (e.g., using intensities of voxels within the functional image and the one or more identified 3D volumes) (e.g., based on detected lesions) [e.g., a likelihood of the subject having and/or developing prostate cancer and/or a particular stage of prostate cancer (e.g., metastatic prostate cancer)] [e.g., a likelihood of the subject having and/or developing a metastatic cancer (including, e.g., metastatic prostate cancer, breast cancer, lung cancer, colon cancer, skin cancer, etc.)].

In certain embodiments, the method comprises performing steps (a)-(g) repeatedly for a plurality of anatomical and corresponding functional images collected at different time points to determine, at each time point, a cancer status of the subject, thereby tracking cancer status over time (e.g., to evaluate disease progression and/or treatment efficacy).

In certain embodiments, the method comprises (e.g., prior to step (g)): (h) automatically adjusting, by the processor, intensities of voxels of the 3D functional image to correct for background uptake (e.g., of the radiopharmaceutical) in one or more background tissue regions (e.g., correcting for uptake of the radiopharmaceutical that occurs in the one or more background tissue regions under normal circumstances, and which is not necessarily indicative of presence of cancerous lesions).

In certain embodiments, the target tissue regions comprise the one or more background tissue regions and step (h) comprises: using the 3D segmentation map to identify, within the 3D functional image, one or more 3D background tissue volume(s), each corresponding a particular background tissue region (e.g., by mapping 3D segmentation masks of the 3D segmentation map to the 3D functional image); and adjusting intensities of voxels of the 3D functional image based on intensities of voxels within the 3D background tissue volumes (e.g., by using intensities of voxels within the 3D background tissue volumes to estimate a contribution to intensities outside of the 3D background tissue volumes).

In certain embodiments, the one or more background tissue regions comprise one or more members selected from the group consisting of: a bladder (e.g., a urinary bladder), a kidney, a duodenum, a small intestine, a spleen, a liver, a pancreas, a stomach, an adrenal gland, a rectum, and testes.

In certain embodiments, the method comprises: (i) automatically detecting, by the processor, one or more hotspots within the 3D functional image determined to represent lesions based on intensities of voxels within the 3D functional image [e.g., based on a comparison of intensities within the 3D functional image with a threshold value (e.g., wherein the 3D functional image is a 3D PET image and the threshold is a particular standard uptake value (SUV) level)] (e.g., and also based on the one or more 3D volumes identified within the 3D functional image).

In certain embodiments, step (i) comprises using one or more thresholds [e.g., comparing intensities of voxels in the 3D functional image with the one or more thresholds (e.g., wherein the one or more thresholds comprises a plurality of region-specific thresholds, each used for a specific sub-set of the one or more 3D volumes identified within the 3D functional image)].

In certain embodiments, step (i) comprises applying one or more filters to the 3D functional image [e.g., as in a blob detection technique; e.g., wherein the one or more filters comprises one or more Gaussian filters (e.g., a high pass Gaussian filter and a low pass Gaussian filter, as in a Difference of Gaussians approach); e.g., wherein the one or more filters comprises a Laplacian filter (e.g., as in a Laplacian of a Gaussian technique); e.g., wherein different filter kernels are used for different sub-sets of the one or more 3D volumes identified within the 3D functional image].

In certain embodiments, step (i) comprises using a combination of two or more techniques for identification of hotspots in different sub-sets of the one or more 3D volumes identified within the 3D functional image [e.g., using a first filtering approach (e.g., as in the paragraph above) for a first sub-set of the one or more 3D volumes and using a second filtering approach for a second sub-set; e.g., using thresholding approach (e.g., as in the paragraphs above) for a first sub-set of the one or more 3D volumes and using a filtering approach (e.g., as in the paragraph above) for a second sub-set of the one or more 3D volumes].

In certain embodiments, step (i) comprises detecting an initial set of hotspots and, for at least a portion of the hotspots of the initial set, classifying each hotspot of at least a portion of the detected hotspots as either a cancerous lesion or not a cancerous lesion (e.g., as noise)[e.g., using a machine learning module; e.g., based on a shape and/or location of the hotspot (e.g., in combination with anatomical knowledge; e.g., wherein the location includes an identification of a particular target tissue region corresponding to the 3D volume in which the hotspot is located and/or a relative position of the hotspot within the particular target tissue region); e.g., and removing hotspots classified as not a cancerous lesion from the initial set, thereby obtaining a final set of hotspots determined to represent lesions].

In certain embodiments, the target tissue regions comprise one or more background tissue regions and the method comprises: using the 3D segmentation map to identify, within the 3D functional image, one or more 3D background tissue volume(s), each corresponding a particular background tissue region (e.g., a background tissue region in which significant radiopharmaceutical uptake occurs under normal circumstances and is not necessarily indicative of presence of cancerous lesions) (e.g., by mapping 3D segmentation masks of the 3D segmentation map to the 3D functional image); and excluding voxels of the 3D within the 3D background tissue from the voxels used to automatically detect the one or more hotspots at step (i).

In certain embodiments, the method comprises using the one or more detected hotspots (e.g., intensities of the one or more detected hotspots) to determine a cancer status for the subject.

In certain embodiments, the target tissue regions comprise one or more reference tissue regions and the method comprises: using the 3D segmentation map to identify, by the processor, within the 3D functional image, one or more 3D reference volume(s), each corresponding to a particular reference tissue region; determining, by the processor, one or more reference intensity values, each associated with a particular 3D reference volume of the one or more 3D reference volume(s) and corresponding to a measure of (e.g., an average/mean, a median, a maximum, etc.) intensity within the particular 3D reference volume; determining, by the processor, one or more individual hotspot intensity values, each associated with a particular hotspot of at least a portion of the detected one or more hotspots and corresponding to a measure of (e.g., an average/mean, a median, a maximum, etc.) intensity of the particular hotspot; and determining, by the processor, one or more individual hotspot index values using the one or more individual hotspot intensity values and the one or more reference intensity values [e.g., wherein each individual hotspot index value is associated with a particular hotspot of the at least a portion of the detected one or more hotspots and determined using (e.g., based on a comparison between) (i) the individual hotspot intensity value associated with the particular hotspot and (ii) the one or more reference intensity values].

In certain embodiments, the determining the one or more individual hotspot index values comprises mapping each of the one or more reference intensity values to a corresponding reference index value on a scale and, for each individual hotspot intensity value, using the reference intensity values and corresponding reference index values to interpolate a corresponding individual hotspot index value.

In certain embodiments, the reference tissue regions comprise one or more members selected from the group consisting of: a liver, an aorta (e.g., a thoracic aorta portion; e.g., an abdominal aorta portion), and a parotid gland.

In certain embodiments, a first reference intensity value (i) is a blood reference intensity value associated with a 3D reference volume corresponding to an aorta portion, and (ii) maps to a first reference index value; a second reference intensity value (i) is a liver reference intensity value associated with a 3D reference volume corresponding to a liver, and (ii) maps to a second reference index value; and the second reference intensity value is greater than the first reference intensity value and the second reference index value is greater than the first reference index value.

In certain embodiments, the reference intensity values comprises a maximum reference intensity value that maps to a maximum reference index value, and hotspots having associated hotspot intensity values greater than the maximum reference intensity value are assigned hotspot index values equal to the maximum reference index value.

In certain embodiments, the method comprises determining, by the processor, an overall index value indicative of a cancer status of the subject using at least a portion of the one or more hotspot index values.

In certain embodiments, the overall index value is determined as a weighted sum of at least a portion [e.g., located within a 3D volume of the functional image that corresponds to a skeletal region of the subject; e.g., located within a 3D volume of the functional image that corresponds to a lymph region of the subject] of the individual hotspot index values [e.g., wherein each hotspot index value in the sum is weighted by a measure of size (e.g., 3D volume; e.g., average diameter) of the associated hotspot].

In certain embodiments, the overall index value is associated with a particular target tissue region corresponding to a particular target VOI identified within the anatomical image; and the overall index value is determined using hotspot index values of a subset of hotspots located within a particular 3D volume in the 3D functional image that corresponds to the particular identified target VOI [e.g., and wherein the overall index value is computed as a weighted sum of the hotspot index values of the subset of hotspots (e.g., wherein the weighted sum is normalized by an estimated volume of the particular target tissue region (e.g., computed as a volume of the particular 3D volume in the function image and/or a volume of the particular target VOI))].

In certain embodiments, the particular target tissue region is selected from the group consisting of: a skeletal region comprising one or more bones of the subject, a lymph region, and a prostate region.

In certain embodiments, the 3D anatomical image is an x-ray computed tomography (CT) image, and the 3D functional image is a 3D single photon emission computed tomography (SPECT) image.

In certain embodiments, the 3D anatomical image is an x-ray computed tomography (CT) image, and the 3D functional image is a 3D positron emission tomography (PET) image.

In certain embodiments, the 3D PET image of the subject is obtained following administration to the subject of a radiopharmaceutical comprising a prostate-specific membrane antigen (PSMA) binding agent.

In certain embodiments, the radiopharmaceutical comprises [18F]DCFPyL.

In certain embodiments, step (b) comprises cropping, by the processor, the 3D anatomical image to remove voxels representing air [e.g., to create a cropped anatomical image, and using the cropped anatomical image to identify the one or more target VOIs (e.g., using the cropped anatomical image is used as input to one or more machine learning modules, as opposed to the original size 3D anatomical image)].

In certain embodiments, the target tissue regions comprise one or more members selected from the group consisting of: a left hip bone, a right hip bone, a sacrum and coccyx region, a left clavicle, a right clavicle, a left rib, a right rib, a left scapula, a right scapula, a sternum, a lumbar vertebra, a thoracic vertebra, a skull, a cervical vertebra, a left femur, a right femur, a left humerus, a right humerus, a prostate, a urinary bladder, a rectum, a left gluteus maximus, a right gluteus maximus, an aorta (e.g., a thoracic aorta portion; e.g., an abdominal aorta portion), a left kidney, a right kidney, a liver, a left lung, a right lung, a spleen, a ventricle, a left adrenal gland, a right adrenal gland, a gallbladder, a brain, a pancreas, a heart, a mandible, a left bronchi, a right bronchi, a trachea, a left common iliac artery, a right common iliac artery, and a parotid gland.

In certain embodiments, one or more of the target tissue regions comprise one or more specific bones selected from the group consisting of: a left clavicle, a right clavicle, a left femur, a right femur, a left fibula, a right fibula, a left hip bone, a right hip bone, a left humerus, a right humerus, a mandible, a left patella, a right patella, left radius, a right radius, a left tibia, a right tibia, a left ulna, a right ulna, a left rib (e.g., a first left rib, a second left rib, a third left rib, a fourth left rib, a fifth left rib, a sixth left rib, a seventh left rib, an eighth left rib, a ninth left rib, a tenth left rib, an

eleventh left rib, a twelfth left rib), a right rib (e.g., a first right rib, a second right rib, a third right rib, a fourth right rib, a fifth right rib, a sixth right rib, a seventh right rib, an eighth right rib, a ninth right rib, a tenth right rib, an eleventh right rib, a twelfth right rib), a sacrum and coccyx (e.g., a combined sacrum and coccyx region; e.g., a sacrum and a coccyx individually, so as to distinguish between the two), a left scapula, a right scapula, a skull, sternum, a vertebrae region [e.g., a cervical vertebrae region, comprising one or more (e.g., up to all) cervical vertebrae; e.g., a lumber vertebrae region, comprising one or more (e.g., up to all) lumbar vertebrae; e.g., a thoracic vertebrae region, comprising one or more (e.g., up to all) thoracic vertebrae], and an individual vertebra [e.g., e.g., an individual cervical vertebra (e.g., a first cervical vertebra, a second cervical vertebra, a third cervical vertebra, a fourth cervical vertebra, a fifth cervical vertebra, a sixth cervical vertebra, a seventh cervical vertebra); e.g., an individual lumbar vertebra (e.g., a first lumbar vertebra, a second lumbar vertebra, a third lumbar vertebra, a fourth lumbar vertebra, a fifth lumbar vertebra, a sixth lumbar vertebra); e.g., an individual thoracic vertebra (e.g., a first thoracic vertebra, a second thoracic vertebra, a third thoracic vertebra, a fourth, thoracic vertebra, a fifth thoracic vertebra, a sixth thoracic vertebra, a seventh thoracic vertebra, an eighth thoracic vertebra, a ninth thoracic vertebra, a tenth thoracic vertebra, an eleventh thoracic vertebra, an twelfth thoracic vertebra)].

In certain embodiments, one or more of the target tissue regions comprise one or more specific bones selected from the group consisting of: a left clavicle, a right clavicle, a left hip bone, a right hip bone, a left rib (e.g., a first left rib, a second left rib, a third left rib, a fourth left rib, a fifth left rib, a sixth left rib, a seventh left rib, an eighth left rib, a ninth left rib, a tenth left rib, an eleventh left rib, a twelfth left rib), a right rib (e.g., a first right rib, a second right rib, a third right rib, a fourth right rib, a fifth right rib, a sixth right rib, a seventh right rib, an eighth right rib, a ninth right rib, a tenth right rib, an eleventh right rib, a twelfth right rib), a sacrum and coccyx (e.g., a combined sacrum and coccyx region; e.g., a sacrum and a coccyx individually, so as to distinguish between the two), a left scapula, a right scapula, a sternum, a vertebrae region [e.g., a cervical vertebrae region, comprising one or more (e.g., up to all) cervical vertebrae; e.g., a lumber vertebrae region, comprising one or more (e.g., up to all) lumbar vertebrae; e.g., a thoracic vertebrae region, comprising one or more (e.g., up to all) thoracic vertebrae], and an individual vertebra [e.g., an individual lumbar vertebra (e.g., a first lumbar vertebra, a second lumbar vertebra, a third lumbar vertebra, a fourth lumbar vertebra, a fifth lumbar vertebra); e.g., an individual thoracic vertebra (e.g., a first thoracic vertebra, a second thoracic vertebra, a third thoracic vertebra, a fourth, thoracic vertebra, a fifth thoracic vertebra, a sixth thoracic vertebra, a seventh thoracic vertebra, an eighth thoracic vertebra, a ninth thoracic vertebra, a tenth thoracic vertebra, an eleventh thoracic vertebra, an twelfth thoracic vertebra)].

In certain embodiments, one or more of the target tissue regions comprise one or more soft-tissue regions (e.g., organs) selected from the group consisting of: a left adrenal gland, a right adrenal gland, an aorta (e.g., a thoracic aorta portion; e.g., an abdominal aorta portion), a brain, a left bronchi, a right bronchi, a gallbladder, a left gluteus maximus, a right gluteus maximus, a heart, a left common iliac artery, a right common iliac artery, a left kidney, a right kidney, a liver, a left lung, a right lung, a pancreas, a prostate, a rectum, a spleen, a trachea, a urinary bladder, a ventricle, and a parotid gland.

In certain embodiments, the one or more target tissue regions comprise one or more soft-tissue regions (e.g., organs) selected from the group consisting of: a gallbladder, a left kidney, a right kidney, a liver, a left lung, a right lung, a prostate, and a urinary bladder.

In certain embodiments, the target tissue regions comprise one or more bone regions, each corresponding to a specific bone [e.g., where the target tissue regions comprise at least a portion of (e.g., up to all) the bones listed in the paragraphs above] and one or more soft tissue regions, each corresponding to a specific soft-tissue region [e.g., where the target tissue regions comprise at least a portion of (e.g., up to all) the soft-tissue regions listed in the paragraphs above].

In another aspect, the invention is directed to a method for automatically processing 3D images to automatically identify cancerous lesions within a subject, the method comprising: (a) receiving, by a processor of a computing device, a 3D anatomical image of a subject obtained using an anatomical imaging modality [e.g., x-ray computed tomography (CT); e.g., magnetic resonance imaging (MRI); e.g., ultrasound], wherein the 3D anatomical image comprises a graphical representation of tissue (e.g., soft-tissue and/or bone) within the subject; (b) automatically identifying, by the processor, using one or more machine learning modules (e.g., wherein at least one of the one or more machine learning modules is a Convolutional Neural Network (CNN) module), for each of a plurality of target tissue regions, a corresponding target volume of interest (VOI) within the 3D anatomical image; (c) determining, by the processor, a 3D segmentation map representing a plurality of 3D segmentation masks, each 3D segmentation mask representing a particular identified target VOI (e.g., automatically, digitally stitching together the plurality of 3D segmentation masks to form the 3D segmentation map); (d) receiving, by the processor, a 3D functional image of the subject obtained using a functional imaging modality [e.g., single-photon emission computed tomography (SPECT); e.g., positron emission tomography (PET)][e.g., wherein the 3D functional image comprises a plurality of voxels, each representing a particular physical volume within the subject and having an intensity value that represents detected radiation emitted from a the particular physical volume, wherein at least a portion of the plurality of voxels of the 3D functional image represent physical volumes within one or more of the target tissue regions of the subject]; (e) identifying, within the 3D functional image, one or more 3D volume(s), each corresponding to an identified target VOI, using the 3D segmentation map (e.g., by mapping 3D segmentation masks of the 3D segmentation map to the 3D functional image); and (f) automatically detecting, by the processor, within at least a portion of the one or more 3D volumes identified within the 3D functional image, one or more hotspots determined to represent lesions based on intensities of voxels within the 3D functional image [e.g., based on a comparison of intensities within the 3D functional image with a threshold value (e.g., wherein the 3D functional image is a 3D PET image and the threshold is a particular standard uptake value (SUV) level)].

In certain embodiments, the method comprises using, by the processor, the one or more detected hotspots (e.g., intensities of the one or more detected hotspots) to determine a cancer status for the subject.

In certain embodiments, the target tissue regions comprise one or more reference tissue regions and wherein the method comprises: using the 3D segmentation map to identify, by the processor, within the 3D functional image, one or more 3D reference volume(s), each corresponding to a particular

reference tissue region; determining one or more reference intensity values, each associated with a particular 3D reference volume of the one or more 3D reference volume(s) and corresponding to a measure of (e.g., an average/mean, a median, a maximum, etc.) intensity within the particular 3D reference volume; determining, by the processor, one or more individual hotspot intensity values, each associated with a particular hotspot of at least a portion of the detected one or more hotspots and corresponding to a measure of (e.g., an average/mean, a median, a maximum, etc.) intensity of the particular hotspot; and determining, by the processor, one or more individual hotspot index values using the one or more individual hotspot intensity values and the one or more reference intensity values [e.g., wherein each individual hotspot index value is associated with a particular hotspot of the at least a portion of the detected one or more hotspots and determined using (e.g., based on a comparison between) (i) the individual hotspot intensity value associated with the particular hotspot and (ii) the one or more reference intensity values].

In certain embodiments, the reference tissue regions comprise one or more members selected from the group consisting of: a liver, an aorta (e.g., a thoracic aorta portion; e.g., an abdominal aorta portion), and a parotid gland.

In certain embodiments, the method comprises determining, by the processor, an overall index value indicative of a cancer status of the subject using at least a portion of the one or more hotspot index values.

In certain embodiments, the overall index value is determined as a weighted sum of at least a portion [e.g., located within a 3D volume of the functional image that corresponds to a skeletal region of the subject; e.g., located within a 3D volume of the functional image that corresponds to a lymph region of the subject] of the individual hotspot index values [e.g., wherein each hotspot index value in the sum is weighted by a measure of size (e.g., 3D volume; e.g., average diameter) of the associated hotspot].

In certain embodiments, the 3D anatomical image is an x-ray computed tomography (CT) image, and the 3D functional image is a 3D positron emission tomography (PET) image.

In certain embodiments, the 3D PET image of the subject is obtained following administration to the subject of a radiopharmaceutical comprising a prostate-specific membrane antigen (PSMA) binding agent.

In certain embodiments, the radiopharmaceutical comprises [18F]DCFPyL.

In another aspect, the invention is directed to a method for automatically processing 3D images to identify, and measure uptake of radiopharmaceutical in, cancerous lesions (e.g., metastases) within a subject having or at risk for a cancer (e.g., prostate cancer, breast cancer, lung cancer; e.g., a metastatic cancer, such as metastatic prostate cancer, metastatic breast cancer, metastatic lung cancer), the method comprising: (a) receiving, by a processor of a computing device, a 3D anatomical image of a subject obtained using an anatomical imaging modality [e.g., x-ray computed tomography (CT); e.g., magnetic resonance imaging (MRI); e.g., ultra-sound], wherein the 3D anatomical image comprises a graphical representation of tissue (e.g., soft-tissue and/or bone) within the subject; (b) automatically identifying, by the processor, using one or more machine learning modules (e.g., wherein at least one of the machine learning modules is a Convolutional Neural Network (CNN) module), within the 3D anatomical image: a first skeletal volume comprising a graphical representation of one or more bones of the subject; a first aorta volume comprising a graphical representation of at least a portion of an aorta of the subject; and a first liver volume comprising a graphical representation of a liver of the subject; (c) determining, by the processor, a 3D segmentation map representing a plurality of 3D segmentation masks, including a skeletal mask representing the identified first skeletal volume, an aorta mask representing the identified first aorta volume, and a liver mask representing the identified first liver volume; (d) receiving, by the processor, a 3D functional image of the subject obtained using a functional imaging modality [e.g., single-photon emission computed tomography (SPECT); e.g., positron emission tomography (PET)][e.g., wherein the 3D functional image comprises a plurality of voxels, each representing a particular physical volume within the subject and having an intensity value that represents detected radiation emitted from a the particular physical volume, wherein at least a portion of the plurality of voxels of the 3D functional image represent physical volumes within one or more bones, an aorta portion, and/or a liver of the subject]; (e) automatically identifying, within the 3D functional image, using the 3D segmentation map (e.g., by mapping the 3D segmentation masks of the 3D segmentation map to the 3D functional image): a second skeletal volume corresponding to the first identified skeletal volume, within the 3D anatomical image; a second aorta volume corresponding to the first aorta volume, identified within the 3D anatomical image; and a second liver volume corresponding to the first liver volume, identified within the 3D anatomical image; (f) automatically detecting, by the processor, within the second skeletal volume, one or more hotspots determined to represent lesions based on intensities of voxels within the second skeletal volume (e.g., the one or more hotspots corresponding to localized regions of relatively high intensity, e.g., identified based on a comparison of intensities of voxels located within the second skeletal volume with a threshold value); and (g) determining, by the processor, for each of the one or more detected hotspots, an individual hotspot index (e.g., indicative of a measure of radiopharmaceutical uptake in the lesions represented by the detected hotspot) value by: determining an aorta reference intensity level based on a measure (e.g., a mean, a maximum, a median, etc.) of intensity of voxels within the second aorta volume; determining a liver reference intensity level based on a measure (e.g., a mean, a maximum, a median, etc.) of intensity of voxels within the second liver volume; and for each individual detected hotspot: determining a corresponding individual hotspot intensity level based on a measure (e.g., a mean, a maximum, a median, etc.) of intensity of voxels of the detected hotspot; and determining a corresponding individual hotspot index level from the individual hotspot intensity level, the aorta reference intensity level, and the liver reference intensity level.

In certain embodiments, the method comprises determining, by the processor, an overall index value indicative of a cancer status of the subject based on the individual hotspot index values of at least a portion of the one or more detected hotspots.

In certain embodiments, the subject has or is at risk for prostate cancer.

In certain embodiments, step (b) comprises automatically identifying, within the 3D anatomical image, a first prostate volume comprising a graphical representation of a prostate of the subject, the 3D segmentation map determined at step (c) further includes a prostate mask representing the identified first prostate volume, step (e) comprises automatically identifying, within the 3D functional image, a second prostate volume corresponding to the first identified prostate

volume, within the 3D anatomical image, step (f) comprises automatically detecting one or more hotspots in the second prostate volume, and the method further comprises: determining, by the processor, (i) an overall bone index value indicative of a lesion content (e.g., and severity) in the one or more bones of the subject based on the individual hotspot index values of at least a portion of the one or more detected hotspots located in the second skeletal volume and (ii) an overall prostate index value indicative of a lesion content (e.g., and severity) in the prostate of the subject based on the individual hotspot index values of at least a portion of the one or more detected hotspots located in the second prostate volume.

In certain embodiments, the subject has or is at risk for metastatic cancer (e.g., metastatic prostate cancer, metastatic breast cancer, metastatic lung cancer, and other metastatic bone cancers).

In another aspect, the invention is directed to a method for automatically processing a set of full body 3D anatomical images of varying sizes to automatically identify, within each 3D anatomical image, a plurality of 3D volumes that correspond to particular target tissue regions, the method comprising: (a) receiving, by a processor of a computing device, the set of 3D anatomical images of one or more subject(s) obtained using an anatomical imaging modality [e.g., x-ray computed tomography (CT); e.g., magnetic resonance imaging (MRI); e.g., ultra-sound], wherein the 3D anatomical image comprises a graphical representation of tissue (e.g., soft-tissue and/or bone) within each of the one or more subject(s), wherein the set of 3D anatomical images has a mean x-dimension, a mean y-dimension, and a mean z-dimension, at least one of which (the mean x-, mean y-, or mean z-dimension) having a standard deviation at least 3% of the corresponding mean [e.g., at least one of which (the mean x-, mean y-, or mean z-dimension) having a relative standard deviation of at least 3%, at least 5%, at least 10%, at least 15%, or at least 20%]; and (b) automatically determining, by the processor, using a localization module that implements a CNN, within each image of the set of 3D anatomical images, at least one initial VOI corresponding to a particular anatomical region (e.g., a group of related tissue, such as a pelvic region and a spin region) that comprises one or more particular associated target tissue regions (e.g., one or more specific bones, e.g., one or more specific organs), thereby identifying at least one initial VOI for the corresponding 3D anatomical image; and (c) for each initial VOI, automatically identifying, by the processor, using one or more segmentation modules each implementing a CNN, for each of the one or more particular target tissue regions associated with the particular anatomical region to which the initial VOI corresponds, a corresponding target VOI (e.g., a graphical representation of the particular target tissue region).

In another aspect, the invention is directed to a system for automatically processing a 3D image to identify 3D volumes within the 3D image that correspond to particular target tissue regions, the system comprising: a processor of a computing device; and a memory having instructions stored thereon, wherein the instructions, when executed by the processor, cause the processor to: (a) receive a 3D anatomical image of a subject obtained using an anatomical imaging modality [e.g., x-ray computed tomography (CT); e.g., magnetic resonance imaging (MRI); e.g., ultra-sound], wherein the 3D anatomical image comprises a graphical representation of tissue (e.g., soft-tissue and/or bone) within the subject; (b) automatically identify, using one or more machine learning modules (e.g., wherein at least one of the one or more machine learning modules is a Convolutional Neural Network (CNN) module), for each of a plurality of target tissue regions, a corresponding target volume of interest (VOI) within the 3D anatomical image; (c) determine 3D segmentation map representing a plurality of 3D segmentation masks, each 3D segmentation mask representing a particular identified target VOI (e.g., automatically, digitally stitching together the plurality of 3D segmentation masks to form the 3D segmentation map); and (d) store and/or provide the 3D segmentation map for display and/or further processing.

In certain embodiments, the 3D anatomical image is a full body image.

In certain embodiments, at step (c) the instructions cause the processor to digitally stitch together the plurality of 3D segmentation masks to form the 3D segmentation map {e.g., by creating an initially empty image volume (e.g., initializing all voxel values to zero) and then inserting labels from each segmentation mask into the image volume [e.g., by mapping labeled (e.g., as representing a particular target tissue region as determined by a machine learning module) voxels of input images to one or machine learning modules to voxels of the image volume (e.g., so as to match voxels of the image volume to voxels of the input images that represent a same physical location, thereby labeling voxels of the image volume correctly)]}.

In certain embodiments, at step (b), the instructions cause the processor to, for at least one specific target tissue region: determine, using a first module (e.g., a localization module) (e.g., a first machine learning module), an initial VOI within the 3D anatomical image, the initial VOI corresponding to an anatomical region (e.g., a group of related tissue, such as a pelvic region, a chest region, a head and/or neck region, and the like) containing the specific target tissue region (e.g., wherein the initial VOI excludes more voxels of the 3D anatomical image than it includes; e.g., wherein the initial VOI includes less than 25% of the voxels of the 3D anatomical image; e.g., wherein a majority of voxels within the initial VOI represent physical volumes within the anatomical region); and identify, using a second module (e.g., a segmentation module) (e.g., a second machine learning module), the target VOI corresponding to the specific target tissue region within the initial VOI.

In certain embodiments, the second module is a CNN module that implements a CNN.

In certain embodiments, the first module is a CNN module that implements a CNN to perform a coarse segmentation to automatically identify the initial VOI corresponding to the anatomical region containing the specific target tissue region [e.g., by automatically identifying a graphical representation of a group of related tissue within the anatomical image (e.g., and, subsequently, determining the initial VOI as a rectangular region (e.g., rectangular prism or rectangular box) entirely enclosing the identified graphical representation of the group of related tissue)] [e.g., by, for each of one or more particular tissue regions anticipated to be located within the anatomical region, automatically identifying a corresponding VOI in the anatomical image (e.g., via the coarse segmentation), e.g., and determining the initial VOI as a rectangular region entirely enclosing all of the identified VOIs corresponding to the particular tissue regions].

In certain embodiments, the first module receives a sub-sampled [e.g., by a factor of two or more (e.g., four) along one or more dimensions] version of the anatomical image as input and identifies the initial VOI using the sub-sampled version of the anatomical image [e.g., and wherein the second module receives a full resolution version of the

anatomical image, cropped to the initial VOI (e.g., such that the first module operates on an lower resolution image that represents a larger physical volume than the second module, while the second module operates on a higher resolution image but representing a smaller physical volume)].

In certain embodiments, the first module is a first CNN module and the second module is a second CNN module, and wherein the first CNN module comprises additional filters in order to account for increased variability in image size with respect to the second CNN module.

In certain embodiments, the 3D anatomical image is a full body image and wherein, at step (b), the instructions cause the processor to: automatically determine, using one or more localization modules implementing machine learning technique(s) (e.g., wherein each localization module is a CNN module that implements a CNN), a plurality of initial VOIs within the 3D anatomical image, each initial VOI corresponding to a particular anatomical region (e.g., a group of related tissue, such as a pelvic region, a chest region, a head and/or neck region, a spine region, an upper body region, a lower body region, etc.) and in which an associated subset of the target VOIs are located; and for each initial VOI, automatically identify, using one or more segmentation modules implementing machine learning technique(s) (e.g., wherein each segmentation module is a CNN module that implements a CNN) the associated subset of target VOIs.

In certain embodiments, the plurality of initial VOIs comprises one or more members selected from the group consisting of: a pelvic region initial VOI corresponding to a pelvic region of the subject (e.g., wherein the subset of target VOIs located in the pelvic region initial VOI comprise one or more target VOIs corresponding to target tissue regions selected from the group consisting of a left and/or right ilium, a sacrum, and a coccyx); a spine region initial VOI corresponding to a spine of the subject (e.g., wherein the subset of target VOIs located in the pelvic region initial VOI comprise one or more target VOIs corresponding to target tissue regions selected from the group consisting of a thoracic vertebra, a lumber vertebra, and a sternum); a left upper body region initial VOI corresponding to a left side of the subject's upper body (e.g., wherein the subset of target VOIs located in the pelvic region initial VOI comprise one or more target VOIs corresponding to target tissue regions selected from the group consisting of one or more left rib(s), a left scapula, and a left clavicle); and a right upper body region initial VOI corresponding to a right side of the subject's upper body (e.g., wherein the subset of target VOIs located in the pelvic region initial VOI comprise one or more target VOIs corresponding to target tissue regions selected from the group consisting of one or more right rib(s), a right scapula, and a right clavicle).

In certain embodiments, the instructions cause the processor to: (e) receive a 3D functional image of the subject obtained using a functional imaging modality [e.g., single-photon emission computed tomography (SPECT); e.g., positron emission tomography (PET)][e.g., wherein the 3D functional image comprises a plurality of voxels, each representing a particular physical volume within the subject and having an intensity value that represents detected radiation emitted from a the particular physical volume, wherein at least a portion of the plurality of voxels of the 3D functional image represent physical volumes within one or more of the target tissue regions of the subject]; and (f) identify, within the 3D functional image, one or more 3D volume(s), each corresponding to an identified target VOI, using the 3D segmentation map (e.g., by mapping 3D segmentation masks of the 3D segmentation map to the 3D functional image).

In certain embodiments, the instructions cause the processor to: (g) determine a cancer status [(e.g., a prostate cancer status; e.g., a metastatic cancer status (e.g., metastatic cancer, including, e.g., metastatic prostate cancer, breast cancer, lung cancer, colon cancer, skin cancer, etc.)] for the subject (e.g., using intensities of voxels within the functional image and the one or more identified 3D volumes) (e.g., based on detected lesions) [e.g., a likelihood of the subject having and/or developing prostate cancer and/or a particular stage of prostate cancer (e.g., metastatic prostate cancer)] [e.g., a likelihood of the subject having and/or developing a metastatic cancer (including, e.g., metastatic prostate cancer, breast cancer, lung cancer, colon cancer, skin cancer, etc.)].

In certain embodiments, the instructions cause the processor to perform steps (a)-(g) repeatedly for a plurality of anatomical and corresponding functional images collected at different time points to determine, at each time point, a cancer status of the subject, thereby tracking cancer status over time (e.g., to evaluate disease progression and/or treatment efficacy).

In certain embodiments, the instructions cause the processor to (e.g., prior to step (g)): (h) automatically adjust intensities of voxels of the 3D functional image to correct for background uptake (e.g., of the radiopharmaceutical) in one or more background tissue regions (e.g., correcting for uptake of the radiopharmaceutical that occurs in the one or more background tissue regions under normal circumstances, and which is not necessarily indicative of presence of cancerous lesions).

In certain embodiments, the target tissue regions comprise the one or more background tissue regions and wherein, at step (h), the instructions cause the processor to: use the 3D segmentation map to identify, within the 3D functional image, one or more 3D background tissue volume(s), each corresponding a particular background tissue region (e.g., by mapping 3D segmentation masks of the 3D segmentation map to the 3D functional image); and adjust intensities of voxels of the 3D functional image based on intensities of voxels within the 3D background tissue volumes (e.g., by using intensities of voxels within the 3D background tissue volumes to estimate a contribution to intensities outside of the 3D background tissue volumes).

In certain embodiments, the one or more background tissue regions comprise one or more members selected from the group consisting of: a bladder (e.g., a urinary bladder), a kidney, a duodenum, a small intestine, a spleen, a liver, a pancreas, a stomach, an adrenal gland, a rectum, and testes.

In certain embodiments, the instructions cause the processor to: (i) automatically detect one or more hotspots within the 3D functional image determined to represent lesions based on intensities of voxels within the 3D functional image [e.g., based on a comparison of intensities within the 3D functional image with a threshold value (e.g., wherein the 3D functional image is a 3D PET image and the threshold is a particular standard uptake value (SUV) level)] (e.g., and also based on the one or more 3D volumes identified within the 3D functional image).

In certain embodiments, at step (i), the instructions cause the processor to use one or more thresholds [e.g., comparing intensities of voxels in the 3D functional image with the one or more thresholds (e.g., wherein the one or more thresholds comprises a plurality of region-specific thresholds, each used for a specific sub-set of the one or more 3D volumes identified within the 3D functional image)].

In certain embodiments, at step (i), the instructions cause the processor to apply one or more filters to the 3D functional image [e.g., as in a blob detection technique; e.g., wherein the one or more filters comprises one or more Gaussian filters (e.g., a high pass Gaussian filter and a low pass Gaussian filter, as in a Difference of Gaussians approach); e.g., wherein the one or more filters comprises a Laplacian filter (e.g., as in a Laplacian of a Gaussian technique); e.g., wherein different filter kernels are used for different sub-sets of the one or more 3D volumes identified within the 3D functional image].

In certain embodiments, at step (i), the instructions cause the processor to use a combination of two or more techniques for identification of hotspots in different sub-sets of the one or more 3D volumes identified within the 3D functional image [e.g., using a first filtering approach (e.g., as in the paragraph above) for a first sub-set of the one or more 3D volumes and using a second filtering approach for a second sub-set; e.g., using thresholding approach (e.g., as in the paragraphs above) for a first sub-set of the one or more 3D volumes and using a filtering approach (e.g., as in the paragraph above) for a second sub-set of the one or more 3D volumes].

In certain embodiments, at step (i), the instructions cause the processor to detect an initial set of hotspots and, for at least a portion of the hotspots of the initial set, classify each hotspot of at least a portion of the detected hotspots as either a cancerous lesion or not a cancerous lesion (e.g., as noise)[e.g., using a machine learning module; e.g., based on a shape and/or location of the hotspot (e.g., in combination with anatomical knowledge; e.g., wherein the location includes an identification of a particular target tissue region corresponding to the 3D volume in which the hotspot is located and/or a relative position of the hotspot within the particular target tissue region); e.g., and removing hotspots classified as not a cancerous lesion from the initial set, thereby obtaining a final set of hotspots determined to represent lesions].

In certain embodiments, the target tissue regions comprise one or more background tissue regions and the instructions cause the processor to: use the 3D segmentation map to identify, within the 3D functional image, one or more 3D background tissue volume(s), each corresponding a particular background tissue region (e.g., a background tissue region in which significant radiopharmaceutical uptake occurs under normal circumstances and is not necessarily indicative of presence of cancerous lesions) (e.g., by mapping 3D segmentation masks of the 3D segmentation map to the 3D functional image); and exclude voxels of the 3D within the 3D background tissue from the voxels used to automatically detect the one or more hotspots at step (i).

In certain embodiments, the instructions cause the processor to use the one or more detected hotspots (e.g., intensities of the one or more detected hotspots) to determine a cancer status for the subject.

In certain embodiments, the target tissue regions comprise one or more reference tissue regions and the instructions cause the processor to: use the 3D segmentation map to identify, within the 3D functional image, one or more 3D reference volume(s), each corresponding to a particular reference tissue region; determine one or more reference intensity values, each associated with a particular 3D reference volume of the one or more 3D reference volume(s) and corresponding to a measure of (e.g., an average/mean, a median, a maximum, etc.) intensity within the particular 3D reference volume; determine one or more individual hotspot intensity values, each associated with a particular hotspot of at least a portion of the detected one or more hotspots and corresponding to a measure of (e.g., an average/mean, a median, a maximum, etc.) intensity of the particular hotspot; and determine one or more individual hotspot index values using the one or more individual hotspot intensity values and the one or more reference intensity values [e.g., wherein each individual hotspot index value is associated with a particular hotspot of the at least a portion of the detected one or more hotspots and determined using (e.g., based on a comparison between) (i) the individual hotspot intensity value associated with the particular hotspot and (ii) the one or more reference intensity values].

In certain embodiments, the instructions cause the processor to determine the one or more individual hotspot index values by mapping each of the one or more reference intensity values to a corresponding reference index value on a scale and, for each individual hotspot intensity value, using the reference intensity values and corresponding reference index values to interpolate a corresponding individual hotspot index value.

In certain embodiments, the reference tissue regions comprise one or more members selected from the group consisting of: a liver, an aorta (e.g., a thoracic aorta portion; e.g., an abdominal aorta portion), and a parotid gland.

In certain embodiments, a first reference intensity value (i) is a blood reference intensity value associated with a 3D reference volume corresponding to an aorta portion, and (ii) maps to a first reference index value; a second reference intensity value (i) is a liver reference intensity value associated with a 3D reference volume corresponding to a liver, and (ii) maps to a second reference index value; and the second reference intensity value is greater than the first reference intensity value and the second reference index value is greater than the first reference index value.

In certain embodiments, the reference intensity values comprises a maximum reference intensity value that maps to a maximum reference index value, and wherein hotspots having associated hotspot intensity values greater than the maximum reference intensity value are assigned hotspot index values equal to the maximum reference index value.

In certain embodiments, the instructions cause the processor to determine an overall index value indicative of a cancer status of the subject using at least a portion of the one or more hotspot index values.

In certain embodiments, the overall index value is determined as a weighted sum of at least a portion [e.g., located within a 3D volume of the functional image that corresponds to a skeletal region of the subject; e.g., located within a 3D volume of the functional image that corresponds to a lymph region of the subject] of the individual hotspot index values [e.g., wherein each hotspot index value in the sum is weighted by a measure of size (e.g., 3D volume; e.g., average diameter) of the associated hotspot].

In certain embodiments, the overall index value is associated with a particular target tissue region corresponding to a particular target VOI identified within the anatomical image; and the overall index value is determined using hotspot index values of a subset of hotspots located within a particular 3D volume in the 3D functional image that corresponds to the particular identified target VOI [e.g., and wherein the overall index value is computed as a weighted sum of the hotspot index values of the subset of hotspots (e.g., wherein the weighted sum is normalized by an estimated volume of the particular target tissue region (e.g., computed as a volume of the particular 3D volume in the function image and/or a volume of the particular target VOI))].

In certain embodiments, the particular target tissue region is selected from the group consisting of: a skeletal region comprising one or more bones of the subject, a lymph region, and a prostate region.

In certain embodiments, the 3D anatomical image is an x-ray computed tomography (CT) image, and the 3D functional image is a 3D single photon emission computed tomography (SPECT) image.

In certain embodiments, the 3D anatomical image is an x-ray computed tomography (CT) image, and the 3D functional image is a 3D positron emission tomography (PET) image.

In certain embodiments, the 3D PET image of the subject is obtained following administration to the subject of a radiopharmaceutical comprising a prostate-specific membrane antigen (PSMA) binding agent.

In certain embodiments, the radiopharmaceutical comprises [18F]DCFPyL.

In certain embodiments, at step (b), the instructions cause the processor to crop the 3D anatomical image to remove voxels representing air [e.g., to create a cropped anatomical image, and using the cropped anatomical image to identify the one or more target VOIs (e.g., using the cropped anatomical image is used as input to one or more machine learning modules, as opposed to the original size 3D anatomical image)].

In certain embodiments, the target tissue regions comprise one or more members selected from the group consisting of: a left hip bone, a right hip bone, a sacrum and coccyx region, a left clavicle, a right clavicle, a left rib, a right rib, a left scapula, a right scapula, a sternum, a lumbar vertebra, a thoracic vertebra, a skull, a cervical vertebra, a left femur, a right femur, a left humerus, a right humerus, a prostate, a urinary bladder, a rectum, a left gluteus maximus, a right gluteus maximus, an aorta (e.g., a thoracic aorta portion; e.g., an abdominal aorta portion), a left kidney, a right kidney, a liver, a left lung, a right lung, a spleen, a ventricle, a left adrenal gland, a right adrenal gland, a gallbladder, a brain, a pancreas, a heart, a mandible, a left bronchi, a right bronchi, a trachea, a left common iliac artery, a right common iliac artery, and a parotid gland.

In certain embodiments, one or more of the target tissue regions comprise one or more specific bones selected from the group consisting of: a left clavicle, a right clavicle, a left femur, a right femur, a left fibula, a right fibula, a left hip bone, a right hip bone, a left humerus, a right humerus, a mandible, a left patella, a right patella, left radius, a right radius, a left tibia, a right tibia, a left ulna, a right ulna, a left rib (e.g., a first left rib, a second left rib, a third left rib, a fourth left rib, a fifth left rib, a sixth left rib, a seventh left rib, an eighth left rib, a ninth left rib, a tenth left rib, an eleventh left rib, a twelfth left rib), a right rib (e.g., a first right rib, a second right rib, a third right rib, a fourth right rib, a fifth right rib, a sixth right rib, a seventh right rib, an eighth right rib, a ninth right rib, a tenth right rib, an eleventh right rib, a twelfth right rib), a sacrum and coccyx (e.g., a combined sacrum and coccyx region; e.g., a sacrum and a coccyx individually, so as to distinguish between the two), a left scapula, a right scapula, a skull, sternum, a vertebrae region [e.g., a cervical vertebrae region, comprising one or more (e.g., up to all) cervical vertebrae; e.g., a lumber vertebrae region, comprising one or more (e.g., up to all) lumbar vertebrae; e.g., a thoracic vertebrae region, comprising one or more (e.g., up to all) thoracic vertebrae], and an individual vertebra [e.g., e.g., an individual cervical vertebra (e.g., a first cervical vertebra, a second cervical vertebra, a third cervical vertebra, a fourth cervical vertebra, a fifth cervical vertebra, a sixth cervical vertebra, a seventh cervical vertebra); e.g., an individual lumbar vertebra (e.g., a first lumbar vertebra, a second lumbar vertebra, a third lumbar vertebra, a fourth lumbar vertebra, a fifth lumbar vertebra, a sixth lumbar vertebra); e.g., an individual thoracic vertebra (e.g., a first thoracic vertebra, a second thoracic vertebra, a third thoracic vertebra, a fourth, thoracic vertebra, a fifth thoracic vertebra, a sixth thoracic vertebra, a seventh thoracic vertebra, an eighth thoracic vertebra, a ninth thoracic vertebra, a tenth thoracic vertebra, an eleventh thoracic vertebra, an twelfth thoracic vertebra)].

In certain embodiments, one or more of the target tissue regions comprise one or more specific bones selected from the group consisting of: a left clavicle, a right clavicle, a left hip bone, a right hip bone, a left rib (e.g., a first left rib, a second left rib, a third left rib, a fourth left rib, a fifth left rib, a sixth left rib, a seventh left rib, an eighth left rib, a ninth left rib, a tenth left rib, an eleventh left rib, a twelfth left rib), a right rib (e.g., a first right rib, a second right rib, a third right rib, a fourth right rib, a fifth right rib, a sixth right rib, a seventh right rib, an eighth right rib, a ninth right rib, a tenth right rib, an eleventh right rib, a twelfth right rib), a sacrum and coccyx (e.g., a combined sacrum and coccyx region; e.g., a sacrum and a coccyx individually, so as to distinguish between the two), a left scapula, a right scapula, a sternum, a vertebrae region [e.g., a cervical vertebrae region, comprising one or more (e.g., up to all) cervical vertebrae; e.g., a lumber vertebrae region, comprising one or more (e.g., up to all) lumbar vertebrae; e.g., a thoracic vertebrae region, comprising one or more (e.g., up to all) thoracic vertebrae], and an individual vertebra [e.g., an individual lumbar vertebra (e.g., a first lumbar vertebra, a second lumbar vertebra, a third lumbar vertebra, a fourth lumbar vertebra, a fifth lumbar vertebra); e.g., an individual thoracic vertebra (e.g., a first thoracic vertebra, a second thoracic vertebra, a third thoracic vertebra, a fourth, thoracic vertebra, a fifth thoracic vertebra, a sixth thoracic vertebra, a seventh thoracic vertebra, an eighth thoracic vertebra, a ninth thoracic vertebra, a tenth thoracic vertebra, an eleventh thoracic vertebra, an twelfth thoracic vertebra)].

In certain embodiments, one or more of the target tissue regions comprise one or more soft-tissue regions (e.g., organs) selected from the group consisting of: a left adrenal gland, a right adrenal gland, an aorta (e.g., a thoracic aorta portion; e.g., an abdominal aorta portion), a brain, a left bronchi, a right bronchi, a gallbladder, a left gluteus maximus, a right gluteus maximus, a heart, a left common iliac artery, a right common iliac artery, a left kidney, a right kidney, a liver, a left lung, a right lung, a pancreas, a prostate, a rectum, a spleen, a trachea, a urinary bladder, a ventricle, and a parotid gland.

In certain embodiments, the one or more target tissue regions comprise one or more soft-tissue regions (e.g., organs) selected from the group consisting of: a gallbladder, a left kidney, a right kidney, a liver, a left lung, a right lung, a prostate, and a urinary bladder.

In certain embodiments, the target tissue regions comprise one or more bone regions, each corresponding to a specific bone [e.g., where the target tissue regions comprise at least a portion of (e.g., up to all) the bones listed in the paragraphs above] and one or more soft tissue regions, each corresponding to a specific soft-tissue region [e.g., where the target tissue regions comprise at least a portion of (e.g., up to all) the soft-tissue regions listed in the paragraphs above].

In another aspect, the invention is directed to a system for automatically processing 3D images to automatically identify cancerous lesions within a subject, the system compris-

ing: a processor of a computing device; and a memory having instructions stored thereon, wherein the instructions, when executed by the processor, cause the processor to: (a) receive a 3D anatomical image of a subject obtained using an anatomical imaging modality [e.g., x-ray computed tomography (CT); e.g., magnetic resonance imaging (MRI); e.g., ultra-sound], wherein the 3D anatomical image comprises a graphical representation of tissue (e.g., soft-tissue and/or bone) within the subject; (b) automatically identify, using one or more machine learning modules (e.g., wherein at least one of the one or more machine learning modules is a Convolutional Neural Network (CNN) module), for each of a plurality of target tissue regions, a corresponding target volume of interest (VOI) within the 3D anatomical image; (c) determine a 3D segmentation map representing a plurality of 3D segmentation masks, each 3D segmentation mask representing a particular identified target VOI (e.g., automatically, digitally stitching together the plurality of 3D segmentation masks to form the 3D segmentation map); (d) receive a 3D functional image of the subject obtained using a functional imaging modality [e.g., single-photon emission computed tomography (SPECT); e.g., positron emission tomography (PET)][e.g., wherein the 3D functional image comprises a plurality of voxels, each representing a particular physical volume within the subject and having an intensity value that represents detected radiation emitted from a the particular physical volume, wherein at least a portion of the plurality of voxels of the 3D functional image represent physical volumes within one or more of the target tissue regions of the subject]; (e) identify, within the 3D functional image, one or more 3D volume(s), each corresponding to an identified target VOI, using the 3D segmentation map (e.g., by mapping 3D segmentation masks of the 3D segmentation map to the 3D functional image); and (f) automatically detect, within at least a portion of the one or more 3D volumes identified within the 3D functional image, one or more hotspots determined to represent lesions based on intensities of voxels within the 3D functional image [e.g., based on a comparison of intensities within the 3D functional image with a threshold value (e.g., wherein the 3D functional image is a 3D PET image and the threshold is a particular standard uptake value (SUV) level)].

In certain embodiments, the instructions cause the processor to use the one or more detected hotspots (e.g., intensities of the one or more detected hotspots) to determine a cancer status for the subject.

In certain embodiments, the target tissue regions comprise one or more reference tissue regions and wherein the instructions cause the processor to: use the 3D segmentation map to identify, within the 3D functional image, one or more 3D reference volume(s), each corresponding to a particular reference tissue region; determine one or more reference intensity values, each associated with a particular 3D reference volume of the one or more 3D reference volume(s) and corresponding to a measure of (e.g., an average/mean, a median, a maximum, etc.) intensity within the particular 3D reference volume; determine one or more individual hotspot intensity values, each associated with a particular hotspot of at least a portion of the detected one or more hotspots and corresponding to a measure of (e.g., an average/mean, a median, a maximum, etc.) intensity of the particular hotspot; and determine one or more individual hotspot index values using the one or more individual hotspot intensity values and the one or more reference intensity values [e.g., wherein each individual hotspot index value is associated with a particular hotspot of the at least a portion of the detected one or more hotspots and determined using (e.g., based on a comparison between) (i) the individual hotspot intensity value associated with the particular hotspot and (ii) the one or more reference intensity values].

In certain embodiments, the reference tissue regions comprise one or more members selected from the group consisting of: a liver, an aorta (e.g., a thoracic aorta portion; e.g., an abdominal aorta portion), and a parotid gland.

In certain embodiments, the instructions cause the processor to determine an overall index value indicative of a cancer status of the subject using at least a portion of the one or more hotspot index values.

In certain embodiments, the overall index value is determined as a weighted sum of at least a portion [e.g., located within a 3D volume of the functional image that corresponds to a skeletal region of the subject; e.g., located within a 3D volume of the functional image that corresponds to a lymph region of the subject] of the individual hotspot index values [e.g., wherein each hotspot index value in the sum is weighted by a measure of size (e.g., 3D volume; e.g., average diameter) of the associated hotspot].

In certain embodiments, the 3D anatomical image is an x-ray computed tomography (CT) image, and the 3D functional image is a 3D positron emission tomography (PET) image.

In certain embodiments, the 3D PET image of the subject is obtained following administration to the subject of a radiopharmaceutical comprising a prostate-specific membrane antigen (PSMA) binding agent.

In certain embodiments, the radiopharmaceutical comprises [18F]DCFPyL.

In another aspect, the invention is directed to a system for automatically processing 3D images to identify, and measure uptake of radiopharmaceutical in, cancerous lesions (e.g., metastases) within a subject having or at risk for a cancer (e.g., prostate cancer, breast cancer, lung cancer; e.g., a metastatic cancer, such as metastatic prostate cancer, metastatic breast cancer, metastatic lung cancer), the system comprising: a processor of a computing device; and a memory having instructions stored thereon, wherein the instructions, when executed by the processor, cause the processor to: (a) receive a 3D anatomical image of a subject obtained using an anatomical imaging modality [e.g., x-ray computed tomography (CT); e.g., magnetic resonance imaging (MRI); e.g., ultra-sound], wherein the 3D anatomical image comprises a graphical representation of tissue (e.g., soft-tissue and/or bone) within the subject; (b) automatically identify using one or more machine learning modules (e.g., wherein at least one of the machine learning modules is a Convolutional Neural Network (CNN) module), within the 3D anatomical image: a first skeletal volume comprising a graphical representation of one or more bones of the subject; a first aorta volume comprising a graphical representation of at least a portion of an aorta of the subject; and a first liver volume comprising a graphical representation of a liver of the subject; (c) determine a 3D segmentation map representing a plurality of 3D segmentation masks, including a skeletal mask representing the identified first skeletal volume, an aorta mask representing the identified first aorta volume, and a liver mask representing the identified first liver volume; (d) receive a 3D functional image of the subject obtained using a functional imaging modality [e.g., single-photon emission computed tomography (SPECT); e.g., positron emission tomography (PET)] [e.g., wherein the 3D functional image comprises a plurality of voxels, each representing a particular physical volume within the subject and having an intensity value that represents detected radiation emitted from a the particular physical volume, wherein

at least a portion of the plurality of voxels of the 3D functional image represent physical volumes within one or more bones, an aorta portion, and/or a liver of the subject]; (e) automatically identify, within the 3D functional image, using the 3D segmentation map (e.g., by mapping the 3D segmentation masks of the 3D segmentation map to the 3D functional image): a second skeletal volume corresponding to the first identified skeletal volume, within the 3D anatomical image; a second aorta volume corresponding to the first aorta volume, identified within the 3D anatomical image; and a second liver volume corresponding to the first liver volume, identified within the 3D anatomical image; (f) automatically detect, within the second skeletal volume, one or more hotspots determined to represent lesions based on intensities of voxels within the second skeletal volume (e.g., the one or more hotspots corresponding to localized regions of relatively high intensity, e.g., identified based on a comparison of intensities of voxels located within the second skeletal volume with a threshold value); and (g) determine, for each of the one or more detected hotspots, an individual hotspot index (e.g., indicative of a measure of radiopharmaceutical uptake in the lesions represented by the detected hotspot) value by: determining an aorta reference intensity level based on a measure (e.g., a mean, a maximum, a median, etc.) of intensity of voxels within the second aorta volume; determining a liver reference intensity level based on a measure (e.g., a mean, a maximum, a median, etc.) of intensity of voxels within the second liver volume; and for each individual detected hotspot: determining a corresponding individual hotspot intensity level based on a measure (e.g., a mean, a maximum, a median, etc.) of intensity of voxels of the detected hotspot; and determining a corresponding individual hotspot index level from the individual hotspot intensity level, the aorta reference intensity level, and the liver reference intensity level.

In certain embodiments, the instructions cause the processor to determine an overall index value indicative of a cancer status of the subject based on the individual hotspot index values of at least a portion of the one or more detected hotspots.

In certain embodiments, the subject has or is at risk for prostate cancer.

In certain embodiments, the instructions cause the processor to: at step (b), automatically identify, within the 3D anatomical image, a first prostate volume comprising a graphical representation of a prostate of the subject; at step (c), include a prostate mask representing the identified first prostate volume in the determined 3D segmentation map; at step (e), automatically identify, within the 3D functional image, a second prostate volume corresponding to the first identified prostate volume, within the 3D anatomical image, at step (f), automatically detect one or more hotspots in the second prostate volume; and determine (i) an overall bone index value indicative of a lesion content (e.g., and severity) in the one or more bones of the subject based on the individual hotspot index values of at least a portion of the one or more detected hotspots located in the second skeletal volume and (ii) an overall prostate index value indicative of a lesion content (e.g., and severity) in the prostate of the subject based on the individual hotspot index values of at least a portion of the one or more detected hotspots located in the second prostate volume.

In certain embodiments, the subject has or is at risk for metastatic cancer (e.g., metastatic prostate cancer, metastatic breast cancer, metastatic lung cancer, and other metastatic bone cancers).

In another aspect, the invention is directed to a system for automatically processing a set of full body 3D anatomical images of varying sizes to automatically identify, within each 3D anatomical image, a plurality of 3D volumes that correspond to particular target tissue regions, the system comprising: a processor of a computing device; and a memory having instructions stored thereon, wherein the instructions, when executed by the processor, cause the processor to: (a) receive the set of 3D anatomical images of one or more subject(s) obtained using an anatomical imaging modality [e.g., x-ray computed tomography (CT); e.g., magnetic resonance imaging (MRI); e.g., ultra-sound], wherein the 3D anatomical image comprises a graphical representation of tissue (e.g., soft-tissue and/or bone) within each of the one or more subject(s), wherein the set of 3D anatomical images has a mean x-dimension, a mean y-dimension, and a mean z-dimension, at least one of which (the mean x-, mean y-, or mean z-dimension) having a standard deviation at least 3% of the corresponding mean [e.g., at least one of which (the mean x-, mean y-, or mean z-dimension) having a relative standard deviation of at least 3%, at least 5%, at least 10%, at least 15%, or at least 20%]; and (b) automatically determine, using a localization module that implements a CNN, within each image of the set of 3D anatomical images, at least one initial VOI corresponding to a particular anatomical region (e.g., a group of related tissue, such as a pelvic region and a spin region) that comprises one or more particular associated target tissue regions (e.g., one or more specific bones, e.g., one or more specific organs), thereby identifying at least one initial VOI for the corresponding 3D anatomical image; and (c) for each initial VOI, automatically identify, using one or more segmentation modules each implementing a CNN, for each of the one or more particular target tissue regions associated with the particular anatomical region to which the initial VOI corresponds, a corresponding target VOI (e.g., a graphical representation of the particular target tissue region).

Features of embodiments described with respect to one aspect of the invention may be applied with respect to another aspect of the invention.

BRIEF DESCRIPTION OF THE FIGURES

The patent or application file contains at least one drawing executed in color. Copies of this patent or patent application publication with color drawing(s) will be provided by the Office upon request and payment of the necessary fee.

The foregoing and other objects, aspects, features, and advantages of the present disclosure will become more apparent and better understood by referring to the following description taken in conjunction with the accompanying drawings, in which:

FIG. **1** is a diagram showing integration of various imaging modalities with an artificial intelligence (AI) platform, according to an illustrative embodiment.

FIG. **2** is an image showing a skeleton of a subject with various specific bones identified, according to an illustrative embodiment.

FIG. **3** is a block diagram showing use of full body segmentation in various functional imaging modalities, for various applications, according to an illustrative embodiment.

FIG. **4** is a diagram showing processing flow of different informational datasets by an AI module to classify, locate, and quantify cancerous lesions, according to an illustrative embodiment.

FIG. **5**A is a block flow diagram of a process for automatically processing 3D images to identify 3D volumes within the 3D images that correspond to particular target tissue regions, according to an illustrative embodiment.

FIG. **5**B is a block flow diagram of a process for automatically processing 3D images to identify 3D volumes and use the 3D volumes to detect hotspots representing cancerous lesions, according to an illustrative embodiment.

FIG. **6**A is a block flow diagram of a process for automatically processing CT images for whole-body segmentation, according to an illustrative embodiment.

FIG. **6**B is a set of CT images showing processing results of various steps of the process shown in FIG. **6**A.

FIG. **7** is a set of three images used as training data for machine learning modules used to segment CT images, according to an illustrative embodiment.

FIG. **8** is a set of two images with identified volumes of interest overlaid.

FIG. **9**A is a set of 2D views of a 3D PET/CT image obtained from a subject following administration of PyL™.

FIG. **9**B is the same set of 2D views shown in FIG. **9**A, following background correction.

FIG. **9**C is a set of 2D views of a 3D PET/CT image obtained from a subject following administration of PyL™.

FIG. **9**D is the same set of 2D views shown in FIG. **9**C, following background correction.

FIG. **10**A is a block flow diagram showing an example process for analyzing PyL™-PET images, according to an illustrative embodiment.

FIG. **10**B is a PET/CT image obtained following administration of PyL™ to a subject.

FIG. **10**C is a set of two CT images showing volumes of interest identified via the machine learning approaches described herein.

FIG. **10**D is a set of 3 images illustrating background correction in PET images, according to an illustrative embodiment.

FIG. **11**A is a view of a 3D CT image with volumes of interest corresponding to specific bones labeled in color, according to an illustrative embodiment.

FIG. **11**B is another view of the 3D CT image with labeled volumes of interest shown in FIG. **11**A.

FIG. **12** is a CT image with an overlaid PET image showing identified background tissue regions.

FIG. **13**A is view a CT image with an overlaid PET image showing a detected lesion.

FIG. **13**B is another view of the CT image with overlaid PET image of FIG. **13**A, showing the detected lesion.

FIG. **13**C is another view of the CT image with overlaid PET image of FIG. **13**A, showing the detected lesion.

FIG. **13**D is another view of the CT image with overlaid PET image of FIG. **13**A, showing the detected lesion.

FIG. **14**A is a set of two views of a CT image with an overlaid PET image obtained for a subject following administration of PyL™.

FIG. **14**B shows the same views as FIG. **14**A, but following processing via the machine learning approaches described herein to provide for background correction and detection of lesions.

FIG. **15**A is a set of two views of a CT image with an overlaid PET image obtained for a subject following administration of PyL™.

FIG. **15**B shows the same views as FIG. **15**A, but following processing via the machine learning approaches described herein to provide for background correction and detection of lesions.

FIG. **16**A is a view of a 3D CT image with identified volumes of interest overlaid.

FIG. **16**B is another view of the 3D CT image with identified volumes of interest overlaid shown in FIG. **16**A.

FIG. **17** is a block diagram of an exemplary cloud computing environment, used in certain embodiments.

FIG. **18** is a block diagram of an example computing device and an example mobile computing device used in certain embodiments.

FIG. **19** is a set of three graph, each graphs showing overall index values quantifying PyL™-PSMA uptake in lesions identified in a particular tissue region based on PET/CT image analysis for six different cancer indications, according to an illustrative embodiment.

FIG. **20** is a graph showing individual lesion PSMA index (LPI) values determined for lesions detected in three different tissue regions (bone, lymph, and prostate) via PET/CT image analysis, according to an illustrative embodiment.

FIG. **21** is a set of two graphs comparing reference values determined via manual and automated image analysis for a blood pool reference value and a liver reference value according to an illustrative embodiment.

The features and advantages of the present disclosure will become more apparent from the detailed description set forth below when taken in conjunction with the drawings, in which like reference characters identify corresponding elements throughout. In the drawings, like reference numbers generally indicate identical, functionally similar, and/or structurally similar elements.

DETAILED DESCRIPTION

It is contemplated that systems, architectures, devices, methods, and processes of the claimed invention encompass variations and adaptations developed using information from the embodiments described herein. Adaptation and/or modification of the systems, architectures, devices, methods, and processes described herein may be performed, as contemplated by this description.

Throughout the description, where articles, devices, systems, and architectures are described as having, including, or comprising specific components, or where processes and methods are described as having, including, or comprising specific steps, it is contemplated that, additionally, there are articles, devices, systems, and architectures of the present invention that consist essentially of, or consist of, the recited components, and that there are processes and methods according to the present invention that consist essentially of, or consist of, the recited processing steps.

It should be understood that the order of steps or order for performing certain action is immaterial so long as the invention remains operable. Moreover, two or more steps or actions may be conducted simultaneously.

The mention herein of any publication, for example, in the Background section, is not an admission that the publication serves as prior art with respect to any of the claims presented herein. The Background section is presented for purposes of clarity and is not meant as a description of prior art with respect to any claim.

Documents are incorporated herein by reference as noted. Where there is any discrepancy in the meaning of a particular term, the meaning provided in the Definition section above is controlling.

Headers are provided for the convenience of the reader—the presence and/or placement of a header is not intended to limit the scope of the subject matter described herein.

i. Definitions

As used herein, "radionuclide" refers to a moiety comprising a radioactive isotope of at least one element. Exemplary suitable radionuclides include but are not limited to those described herein. In some embodiments, a radionuclide is one used in positron emission tomography (PET). In some embodiments, a radionuclide is one used in single-photon emission computed tomography (SPECT). In some embodiments, a non-limiting list of radionuclides includes ^{99m}Tc, ^{111}In, ^{64}Cu, ^{67}Ga, ^{68}Ga, ^{186}Re, ^{188}Re, ^{153}Sm, ^{177}Lu, ^{67}Cu, ^{123}I, ^{124}I, ^{125}I, ^{126}I, ^{131}I, ^{11}C, ^{13}N, ^{15}O, ^{18}F, ^{153}Sm, ^{166}Ho, ^{177}Lu, ^{149}Pm, ^{90}Y, ^{213}Bi, ^{103}Pd, ^{109}Pd, ^{159}Gd, ^{140}La, ^{198}Au, ^{199}Au, ^{169}Yb, ^{175}Yb, ^{165}Dy, ^{166}Dy, ^{105}Rh, ^{111}Ag, ^{89}Zr, ^{225}Ac, ^{82}Rb, ^{75}Br, ^{76}Br, ^{77}Br, ^{80}Br, ^{80m}Br, ^{82}Br, ^{83}Br, ^{211}At and ^{192}Ir.

As used herein, the term "radiopharmaceutical" refers to a compound comprising a radionuclide. In certain embodiments, radiopharmaceuticals are used for diagnostic and/or therapeutic purposes. In certain embodiments, radiopharmaceuticals include small molecules that are labeled with one or more radionuclide(s), antibodies that are labeled with one or more radionuclide(s), and antigen-binding portions of antibodies that are labeled with one or more radionuclide(s).

As used herein, "3D" or "three dimensional" with reference to an "image" means conveying information about three dimensions. A 3D image may be rendered as a dataset in three dimensions and/or may be displayed as a set of two-dimensional representations, or as a three-dimensional representation.

As used herein, an "image"—for example, a 3-D image of a subject—includes any visual representation, such as a photo, a video frame, streaming video, as well as any electronic, digital or mathematical analogue of a photo, video frame, or streaming video. Any apparatus described herein, in certain embodiments, includes a display for displaying an image or any other result produced by the processor. Any method described herein, in certain embodiments, includes a step of displaying an image or any other result produced via the method.

As used herein, a "subject" means a human or other mammal (e.g., rodent (mouse, rat, hamster), pig, cat, dog, horse, primate, rabbit, and the like).

As used herein, "administering" an agent means introducing a substance (e.g., an imaging agent) into a subject. In general, any route of administration may be utilized including, for example, parenteral (e.g., intravenous), oral, topical, subcutaneous, peritoneal, intraarterial, inhalation, vaginal, rectal, nasal, introduction into the cerebrospinal fluid, or instillation into body compartments.

As used herein, the terms "filter", and "filtering", as in a "filtering function" or a "filter", refer to a function that operates on localized portions of an input array (e.g., a multi-dimensional array) of data (e.g., image data, e.g., values computed by a layer of a CNN), referred to herein as "subpatches", computing, for a given subpatch, a response value. In general, a filter is applied in a sliding window fashion across the array to compute a plurality of response values for the array. In particular, for a given multidimensional array, a subpatch of the array can be a rectangular region of the array having a specific size (e.g., having the same number of dimensions as the array). For example, for a 6×3×3 array, a given 3×3×3 subpatch refers to a given 3×3×3 set of adjacent values (e.g., a neighborhood) of the array, such that there are five distinct 3×3×3 subpatches in the 6×3×3 array (each patch shifted one position over along the first dimension).

For example, a filtering function can compute, for a given subpatch of an array, a response value using the values of the subpatch. A filtering function can be applied in a sliding window fashion across an array, computing, for each of a plurality of subpatches of the array, a response value. The computed response values can be stored in an output array such that the positional correspondence between response values and the subpatches of the input array is maintained.

For example, at a first step, beginning with a subpatch in a corner of an input array, a filter can compute a first response value, and store the first response value in a corresponding corner of an output array. In certain embodiments, at a second step, the filter then computes a second response value for a second subpatch, shifted one position over along a specific dimension of the input array. The second response value can be stored in a corresponding position of the output array—that is, shifted one position over along a same dimension of the output array. The step of shifting position of the subpatch, computing a response value, and storing the response value in a corresponding position of the output array can be repeated for the full input array, along each dimension of the input array. In certain embodiments (e.g., a strided filtering approach), the subpatch for which the filter computes a response value is shifted more than one position at a time along a given dimension, such that response values are not computed for every possible subpatch of the input array.

As used herein, the term "convolutional neural network (CNN)" refers to a type of artificial neural network where at least one layer performs one or more filtering functions. As used herein, the term "convolution layer" refers to a layer of a CNN that receives as input an input array and computes an output array, wherein values of the output array are computed by applying one or more filters to the input array. In particular, in certain embodiments, a convolution layer receives as input an input array having n+1 dimensions and produces an output array also having n+1 dimensions. The first n dimensions of input and output arrays operated on by filtering layers of a CNN are referred to herein as "spatial dimensions". The (n+1)th dimension of the input is referred to herein as the "input channel" dimension. The size of the input channel dimension is referred to herein as the "number of input channels". The $(n+1)^{th}$ dimension of the output is referred to herein as the "output channel" dimension. The size of the input channel dimension is referred to herein as the "number of output channels".

In certain embodiments, a convolution layer computes response values by applying a filter that operates on subpatches that are smaller than the input array along the spatial dimensions, but extend across the full output channel dimension. For example, an $N\times M\times L\times K_0$ size input array, has three spatial dimensions and K_0 output channels. Filters of a convolution layer may operate on subpatches having sizes of $N_f\times M_f\times L_f\times K_0$, where $N_f\leq N$, $M_f\leq M$ and $L_f\leq L$. Often, a filter of a convolutional layer operates on subpatches having sizes where $N_f<N$, $M_f<M$ and/or $L_f<L$. For example, in certain embodiments, $N_f<<N$, $M_f<<M$ and/or $L_f<<L$.

Accordingly, for each of one or more filters applied by a convolution layer, response values computed by a given filter are stored in a corresponding output channel. Accordingly, a convolution layer that receives an input array having n+1 dimensions computes an output array also having n+1 dimensions, wherein the $(n+1)^{th}$ dimension represents the output channels corresponding to the one or more filters applied by the convolution layer. In this manner, an output array computed by a given convolution layer can be received as input by a subsequent convolution layer.

As used herein, the term "size" in reference to a filter of a convolution layer refers to a size along spatial dimensions of subpatches on which the filter operates (e.g., the subpatch size along the output channel dimension is taken as the full number of output channels). As used herein, the term "size", in reference to a convolution layer, as in "size of a convolution layer" refers to a size of filters of the convolution layer (e.g., each filter of the convolution layer having a same size). In certain embodiments, a filter of a convolution layer has a number of variable parameters that are determined via a machine learning training process. In certain embodiments, the number of parameters of a given filter equals the number of values in a subpatch that the given filter operates on. For example, a size $N_f \times M_f \times L_f$ filter that operates on an input array with K_0 output channels has $N_f \times M_f \times L_f \times K_0$ parameters. In certain embodiments, a filter is implemented as an array, and the response value determined by the filter for a given subpatch is computed as a dot product between the filter and the given subpatch.

As used herein, the term "fully convolutional neural network (FCNN)" refers to a CNN wherein each layer of the CNN is a convolution layer.

As used herein, the term "volume", as used in reference to an input or output of a layer of a CNN refers to an input array received or an output array computed by a CNN layer.

As used herein, the term "CNN module" refers to a computer implemented process that implements a specific CNN in order to determine, for a given input, such as an image (e.g., a 2D image; e.g., a 3D image) one or more output values. For example, a CNN module may receive as input a 3D image of a subject (e.g., a CT image; e.g., an MRI), and for each voxel of the image, determine a value that represents a likelihood that the voxel lies within a region of the 3D image that corresponds to a representation of a particular organ or tissue of the subject. A CNN module may be software and/or hardware. For example, a CNN module may be implemented entirely as software, or certain functions of a CNN module may be carried out via specialized hardware (e.g., via an application specific integrated circuit (ASIC)).

As used herein, the term "tissue" refers to bone (osseous tissue) as well as soft-tissue.

In certain embodiments, the approaches described herein can be used to segment and identify target tissue regions within a full body image of a subject. As used herein, the terms "full body" and "whole body" used (interchangeably) in the context of segmentation refer to approaches that evaluate a majority (e.g., greater than 50%) of a graphical representation of a subject's body in a 3D anatomical image to identify target tissue regions of interest. In certain embodiments, full body and whole body segmentation refers to identification of target tissue regions within at least an entire torso of a subject. In certain embodiments, portions of limbs are also included, along with a head of the subject.

A. Detecting and Assessing Cancer Status Via Nuclear Medicine Imaging and Automated Image Segmentation

Described herein are systems and methods that provide artificial intelligence (AI)-based segmentation technology that provides a basis for detecting, evaluating, and making predictions about cancer status of subjects. In particular, the AI-based segmentation techniques described herein allow for 3D representations of various tissue regions in medical images to be accurately and rapidly identified. The AI-based segmentation technologies described herein utilize machine learning techniques, such as Convolutional Neural Networks (CNNs) to automatically to identify a plurality of target 3D volumes of interest (VOIs) each corresponding to a specific target tissue region, such as one or more organs, portions of organs, particular bone(s), a skeletal region etc. Each identified 3D VOI may be represented via a segmentation mask. The multiple segmentation masks, identifying multiple target tissue regions across a patient's body, can be stitched together to form a segmentation map. The segmentation map, and/or various segmentation masks that it comprises, may be used compute various quantities from medical images, such as useful indices that serve as measures and/or predictions of cancer status, progression, and response to treatment. Segmentation maps and masks may also be displayed, for example as a graphical representation overlaid on a medical image to guide physicians and other medical practitioners.

In certain embodiments, AI-based segmentation is performed using an anatomical image that provides detailed structural information about locations and extent of tissue within a subject's body. Examples of anatomical images include, without limitation, x-ray computed tomography (CT) images, magnetic resonance images (MRI), and ultrasound. Image contrast in anatomical images is a function of physical properties of underlying tissue, such as density, water and fat content. As described in further detail herein, the AI-based segmentation techniques of the present disclosure analyze contrast variations and patterns in anatomical image to identify target 3D VOIs that correspond to different specific target tissue regions.

In certain embodiments, structural information and identified target VOIs from anatomical images are combined with and/or used to analyze images obtained via functional imaging modalities. Functional images reflect physiological properties and activity in a subject. They are often acquired using probes and have intensity variations that reflect a spatial distribution of the probes within an imaged portion of a subject. For example, nuclear medicine images (e.g., PET scans; e.g., SPECT scans; e.g., whole-body scans; e.g. composite PET-CT images; e.g., composite SPECT-CT images) detect radiation emitted from the radionuclides of radiopharmaceuticals to form an image. The distribution of a particular radiopharmaceutical within a patient may be determined by biological mechanisms such as blood flow or perfusion, as well as by specific enzymatic or receptor binding interactions. Different radiopharmaceuticals may be designed to take advantage of different biological mechanisms and/or particular specific enzymatic or receptor binding interactions and thus, when administered to a patient, selectively concentrate within particular types of tissue and/or regions within the patient. Greater amounts of radiation are emitted from regions within the patient that have higher concentrations of radiopharmaceutical than other regions, such that these regions appear brighter in nuclear medicine images. Accordingly, intensity variations within a nuclear medicine image can be used to map the distribution of radiopharmaceutical within the patient. This mapped distribution of radiopharmaceutical within the patient can be used to, for example, infer the presence of cancerous tissue within various regions of the patient's body.

Transferring a segmentation map to a functional image (e.g., a nuclear medicine image, such as a PET image or a SPECT image) provides valuable context for evaluating and deriving meaning from intensity fluctuations in the functional image. In particular, it allows for regions of the functional image to be identified as corresponding to particular tissue regions of the subject. In this manner, intensity values and fluctuations in and across voxels within a particular region can thus be understood as originating from

underlying accumulation of a radiopharmaceutical in a specific tissue region (e.g., organ or bone) of the subject.

As described in further detail herein, this anatomical context serves a variety of uses. For example, it allows for measures of radiopharmaceutical uptake in various specific target organs and tissue regions, such as prostate, lymph nodes, and bone, to be assessed, and used as an indicator of presence of cancerous tissue therein. Identifying a what particular region intensities of a functional image are associated with also allows them to be evaluated in proper context. For example intensities of a certain value, if associated with a prostate region, may be more likely to be indicative of cancer than intensities of the same value, when found within another organ, such as a bladder or kidney. In certain embodiments, reference regions are identified and used to compute normalization values and levels on a scale to which intensities in other regions are compared to evaluate a cancer status. Background regions, to either be excluded from the image or used to correct for artifacts may also be identified.

Accordingly, the AI-based segmentation approaches described herein can serve as a platform on which a variety of tools and techniques for detecting, evaluating, and predicting cancer status for patients can be built. Moreover, since the AI-based segmentation tools described herein can identify a variety of important tissue regions across an entire body of a patient, and then transfer those identifications (e.g., segmentation maps) from anatomical images to various functional images, they can be used as a building block for analysis techniques based on a variety of different imaging methods that obtain contrast via a variety of different radiopharmaceuticals.

FIGS. **1-3** illustrate this concept. In particular, FIG. **1** is a schematic illustrating how various anatomical and functional imaging modalities can be integrated in the context of a platform agnostic AI-based segmentation technology. As illustrated in FIG. **1**, the AI-segmentation platform described herein can be used as a basis for analysis of a variety of images, such as anatomical CT image themselves, 18NaF images, C-11 images, Ga-68 images, FDG image, and PyL™ images. FIG. **2** shows results of an example segmentation performed on a skeleton of a subject, with different specific bones identified by different colors. The segmentation shown in FIG. **2**, performed using a CT image, can be transferred to a functional image in order to identify 3D volumes in the functional image that correspond to the target VOIs identified within the CT image. Other VOIs, such as soft-tissue, may also be identified and used to identify corresponding 3D volumes in a functional image. For example, FIG. **3** is a block flow diagram illustrating how segmentation of various soft-tissue and bone regions based on an anatomical image (e.g., a CT image) can be used and mapped to images obtained via various functional imaging modalities using various probes (e.g., ^{99m}Tc-MIP-1404, ^{18}F-PyL, ^{68}Ga-PSMA-11, ^{18}F-NaF, ^{11}C-Choline, [18F]FDG, [18F]FACBC, etc.) to perform image based diagnosis and assessment of disease progression, state, and the like. As shown in FIG. **3**, the full body segmentation techniques described herein can serve as a platform that a variety of application specific image analysis techniques that utilize different functional imaging modalities and probes can leverage and be built upon.

FIG. **4** is a diagram showing how artificial intelligence-based image analysis **400** can be performed to classify and locate lesions, as well as quantify positive lesions, e.g., for assessing cancer state in a subject. As shown in FIG. **4**, a machine learning module **402**, such as a convolutional neural network (CNN), receives contextual anatomical information (e.g., a CT image or other anatomical imaging modality) **404** along with functional information (e.g., a functional image, such as a SPECT, PET, or other functional image obtained using a particular imaging probe) **406**. The machine learning module **402** then uses the functional **406** and anatomical **404** information to identify, classify, and/or quantify cancerous lesions in a subject **410**. The machine learning module **402** may also leverage additional information **408**, such as subject demographic data (e.g., age, weight, etc.) and other diagnostic test results (e.g., a biopsy, Gleason score, genetic testing results, a prostate specific antigen (PSA) test result), clinical treatment(s) (e.g., external beam radiation, brachytherapy, prostatectomy, antiandrogens, immunotherapy (e.g., Provenge), chemotherapy, etc.) as input and base the classification, identification, and/or quantification of cancerous lesions on this additional information as well.

FIG. **5** is a block flow diagram showing an example process **500** for performing segmentation to identify a plurality of target tissue regions. As shown in FIG. **5**, a machine learning module receives a 3D anatomical image (e.g., a full body image) as input **502**, and identifies, for each of a plurality of target tissue region, a target volume comprising a graphical representation of the target tissue region within the 3D anatomical image **504**. The target volumes are stitched together **506** to form a segmentation map **510** that comprises a plurality of segmentation masks **512**, with each segmentation mask representing an identified target volume. The segmentation map **510** can be stored and/or provided for display and/or further processing **508**.

i. Image Segmentation Using Convolutional Neural Networks (CNNs)

In certain embodiments, the AI-based image segmentation approaches described herein utilize machine learning techniques, such as CNNs to perform segmentation. As described herein, one or more machine learning modules may be used to perform intermediate analysis and processing of images, and ultimately identify target VOIs.

In certain embodiments, the AI-based image segmentation described herein utilizes a two-step approach to identify one or more of the 3D target VOIs representing target tissue regions of interest in an anatomical image. In this two-step approach, an initial volume of interest (VOI) that comprises one or more of the target VOIs is first identified. The initial VOI may be identified using a first module, referred to as a localization module. The localization module may be a first machine learning module, such as a first Convolutional Neural Network (CNN) module. Once the initial VOI is identified, a second module, referred to as a segmentation module [e.g., that implements a second machine learning network (e.g., a second CNN) to perform fine segmentation], is used to identify one or more target VOIs within the initial VOI. This approach is advantageous as allows the segmentation module to operate on a standardized input, of manageable size, without regard to variations in dimensions and boundaries of the original anatomical image received. This two-step approach is especially useful for performing accurate, finely resolved segmentation of tissue regions within a large image, such as a full body scan. The localization module may perform a rough analysis, such as by performing a coarse segmentation, to identify the initial VOI. Freed from having to accommodate varying image sizes, and analyze an entire image, the segmentation module can

devote resources to performing fine segmentation to accurately identify the target VOIs within the initial VOI.

Moreover, as described in further detail herein, for example in Example 1, to identify a set of target VOIs spread out across an entire body of a subject, multiple initial VOIs can be identified in order to partition a whole body image into multiple manageable initial VOIs, each comprising a subset of the desired target VOIs to be identified. The partitioning of a whole body image into multiple initial VOIs can be performed using a single localization module, such as a machine learning module that performs a coarse segmentation to identify general anatomical regions such as an upper body, a lower body, a spine, and a pelvic region. In certain embodiments, multiple localization modules (e.g., each tasked with identifying one or more initial VOIs) may be used. For each identified initial VOI, one or more segmentation modules may then be used to perform fine segmentation and identify the one or more desired target VOIs within the initial VOI.

Various localization and segmentation modules may be combined and implemented as a single module and/or a single software application, or may be implemented separately, e.g., as separate software applications.

A number of different approaches may be used by a localization module to identify a particular initial VOI. For example, in one approach, the localization module may implement a CNN that receives a grayscale CT image (e.g., a single input channel) as input and outputs coordinates of opposite corners of a rectangular VOI (e.g., a bounding box). In another approach, the localization module may implement a CNN that receives two input channels: (i) a grayscale CT image, and (ii) a pre-processed version of the CT image. The pre-processed version of the CT image may be a thresholded version of the CT image, wherein the thresholding provides a rough identification of the initial VOI to be identified. The CNN is trained to analyze both these input channels in order to output coordinates representing opposite corners of a rectangular initial VOI (e.g., a bounding box).

In a third approach, in order to identify a particular initial VOI comprising one or more specific target VOIs, the localization module performs a coarse segmentation to roughly identify the specific target VOIs. In this way, the localization module is essentially a rough version of the segmentation modules used to identify the specific target VOIs within the particular initial VOI. A rectangular initial VOI is then generated using the coarsely identified specific target VOIs (e.g., by drawing the smallest box that fits them, or maybe adding some buffer distance). A distinction here is that the output of the localization module in this case is not merely coordinates of cuboid vertices. In this approach, likelihood values are automatically determined for each voxel of the image that give the likelihood as to how the voxel is classified—e.g., whether the voxel is a particular initial VOI, or background, for example.

In certain embodiments, voxel classifications performed by the machine learning modules may be refined via an iterative process in order to mitigate noise in the classification process. In particular, in certain embodiments, a machine learning module such as a CNN module receives an entire image, or portion thereof as input, and outputs, for each particular voxel, a label classifying the particular voxel as (i) one of a set of pre-defined classes corresponding to anatomical regions or target tissue regions, or (ii) background. For example, a localization module trained to identify initial VOIs corresponding to a spine, a pelvic region, and a left and right upper body may label each voxel as 1, 2, 3, or 4 for spine, pelvic region, left upper body, and right upper body, respectively, or 0 for background.

A segmentation module that identifies one or more target tissue regions within a particular initial VOI may receive the particular initial VOI as input, and output an integer label for each voxel, with the integer label identifying that voxel as corresponding to one of the particular target tissue regions, or background. For example, a segmentation module that identifies different vertebrae may receive as input an initial VOI corresponding to the spine, and label each voxel in the initial VOI with an integer corresponding to a particular vertebra (e.g., **1** for a first lumbar vertebra, 2 for a second lumbar vertebra, 3 for a third lumbar vertebra, etc. with other integer labels for other bones).

The classification performed by machine learning modules as described above, may produce noisy results, with certain isolated voxels having different labels than their surroundings. For example, a CNN module may produce an output wherein a majority of voxels within a large volume are assigned a first label, with isolated voxels and/or small groups of voxels assigned different, e.g., second or third labels, identifying them as corresponding to different anatomical regions than their neighbors. Often such isolated voxels and/or islands appear on the edges of a large uniformly labeled region.

These small non-uniformities correspond to noise in the classification process, and can be removed via an iterative procedure as follows. First, for each label representing (i) a particular anatomical region or target tissue region, or (ii) background, an associated largest connected component of labeled voxels is identified. Second, for each particular label, differently labeled isolated voxels and/or voxel islands that are immediately adjacent to voxels of the largest connected component associated with the particular label are identified and re-assigned the particular label. In certain embodiments, in a third step, any remaining isolated differently labeled voxel islands can then be removed. In a fourth step, holes in segmentation regions—voxels that are labeled as background but are completely encapsulated by non-background labeled voxels are filled (e.g., by assigning voxels of the holes a label of the non-background region that encapsulates them). The second through fourth steps, in which isolated voxels and/or voxel islands are relabeled based on their surroundings are repeated until convergence—i.e., no change from on iteration to the next. This approach reduces and/or eliminates isolated voxels of a different label from their surrounding thereby mitigating noise in the classification process.

These various approaches for identifying initial VOIs may be used alone or in combination to identify multiple initial VOIs within an anatomical image of a subject. Once one or more initial VOIs are identified, one or more target VOIs within each initial VOI may be identified. For example, PCT Publication WO2019/136349, the content of which is hereby incorporated by reference in its entirety, provides further detail on how a single initial VOI corresponding to a pelvic region may be identified within a CT image, and how fine segmentation may be performed to identify target VOIs corresponding to organs such as a prostate, bladder, gluteal muscles, as well as various pelvic bones, such as a sacrum, coccyx, and left and right hip bones, may be identified. The approaches described herein, and in particular in Examples 1-4, show how multiple initial VOIs can be identified and used to identify a plurality of target VOIs across a subject's body, thereby providing for accurate whole-body image segmentation that can serve as a basis for detection and assessment of cancer status, progression, and response to

treatment at localized stages in various organs and tissue regions, as well as metastatic stages where it is present in multiple regions in a patient's body.

ii. Providing Anatomical Context to 3D Functional Images

Segmentation maps generated by automated AI-based analysis of anatomical images can be transferred to 3D functional images in order to identify, within the 3D functional image, 3D volumes corresponding to the target VOIs identified in the anatomical image. In particular, in certain embodiments, the individual segmentation masks (of the segmentation map) are mapped from the 3D anatomical image to the 3D functional image. The 3D volumes identified within the 3D functional image can be used for a variety of purposes in analyzing images for assessment of cancer status.

Certain identified 3D volumes and corresponding target VOIs correspond to tissue regions where cancer is suspected and/or may occur. Such regions may include, for example, a prostate, breast tissue, lung(s), brain, lymph nodes, and bone. Other regions may also be evaluated. Certain regions, such as prostate, breast, and lungs, are relevant for detecting cancer at earlier, localized stages, while others, such as lymph nodes and bone are relevant for assessing metastatic cancer. Since intensities of functional images, such as PET and SPECT images map spatial distribution of radiopharmaceutical accumulation in a patient's body, by accurately identifying specific 3D volumes in functional images that correspond to specific tissue regions intensities of voxels within those 3D volumes can be used determine a measure of uptake of radiopharmaceutical probes within the specific tissue regions to which they correspond. Since radiopharmaceutical probes can be designed to selectively accumulate in cancerous tissue (e.g., via enhanced affinity to biomolecules that are overexpressed in cancerous tissue, such as prostate specific membrane antigen (PSMA)), detecting and quantifying uptake of particular probes in certain target tissue regions and organs is of interest is indicative of and/or can be used to determining a cancer status for the subject. For example, as described in PCT Publication WO2019/136349, the content of which is hereby incorporated by reference in its entirety, assessing 1404 uptake in a prostate volume can be used to determine a prostate cancer status for a subject. Other probes may be used to assess metastatic cancer, present in a wide variety of other tissue regions, including bones. For example, Examples 2 to 6 describe segmentation used to identify accumulation of PyL™ in cancerous lesions throughout a patient's body.

Accordingly, in certain embodiments, segmentation performed on an anatomical image, such as CT image, is transferred (e.g., mapped) to a co-registered functional image, such as a PET or SPECT image, allowing for specific tissue volumes of interest within the functional image that correspond to particular tissue regions of interest to be identified. Accumulation of radiopharmaceutical within those particular tissue regions can then be quantified based on intensities of functional image voxels that lie within the specific tissue volumes of interest.

A variety of approaches can be used to analyze voxel intensities in functional images. For example, an average, a median, a total, a maximum, etc. intensity within a specific volume may be computed and used for quantification. This computed value may then be compared with other values, e.g., computed for other tissue regions (e.g., for normalization), and used to assign a cancer status to a patient (e.g., based on comparison with one or more predetermined threshold values). In certain embodiments, localized regions of high intensity—referred to as hotspots, are identified within particular 3D volumes. As described in further detail in section B, below, these localized hotspots can be identified as representing cancerous lesions, and used to determine cancer status of a subject. In certain embodiments, machine learning approaches can be used. For example, intensities of functional image voxels lying within one or more specific tissue volumes of interest can be used as inputs to machine learning modules that compute a risk index that can, in itself be used to quantify a risk of cancer, metastasis, or recurrence of cancer, etc. and/or compared with reference values, such as thresholds, to assign a particular cancer status.

In certain embodiments, in addition to identifying specific tissue regions in which cancerous tissue is may be present, e.g., in order to determine the presence and/or the state of cancer therein, other additional tissue regions may be identified. Such additional tissue regions may correspond to background regions in which a particular radiopharmaceutical probe accumulates under normal circumstances, without lesions necessarily being present.

In certain embodiments, identified background regions are used to normalize voxel intensities so as to standardize intensity values from image to image. For example, as described in PCT Publication WO2019/136349, the content of which is hereby incorporated by reference in its entirety, gluteal muscles can be identified and uptake in them can be used to normalize intensities in SPECT images obtained following administration of 1404.

Identification of certain background regions can also be used to account for high probe accumulation levels in these regions. In certain embodiments, certain background regions are identified and excluded from analysis. For example, as described in Example 3, certain probes, such as PyL™ may accumulate in certain background regions under normal circumstances, absent any cancerous lesions or tissue within those regions. Accordingly, these regions may be identified and excluded from, e.g., hotspot detection analysis. Examples of such regions include kidneys, duodenum, small intestines, spleen, liver, pancreas, stomach, adrenal gland, rectum, and testes.

In certain embodiments, identifying 3D volumes in a functional image that correspond to background regions can be used to correct for intensity bleed effects, where high accumulation of radiopharmaceutical in a particular region may produce high intensities in the functional image not only in the 3D volume that corresponds to the particular region, but also in its neighborhood. Such intensity bleed into other regions of functional images can mask useful signal. For example, radiopharmaceutical typically accumulates in high amounts in a patient's bladder. When imaged via a functional imaging modality, this high accumulation in the bladder may, via scattering effects, contribute to intensities in 3D volumes corresponding to tissue regions outside the bladder, such as a prostate. Accordingly, accounting for this intensity bleed or "cross-talk" can improve the accuracy with which intensities in a 3D functional image are used to measure underlying radiopharmaceutical uptake.

In certain embodiments, the 3D volume corresponding to the particular background region producing the intensity bleed is dilated. The dilated background region may be excluded from analysis, so as to avoid using intensities of regions directly adjacent to the background region to determine uptake metrics or identification of hotspots.

In certain embodiments, a suppression method which models the profile of the functional intensities may also be

used to adjust the intensity levels in neighboring regions to correct for the intensity bleed. In this approach, for a particular background region that produces intensity bleed, an amount of suppression, that is, intensity bleed, to remove from a particular voxel of the functional image is dependent on a distance from that voxel to a high intensity core region within a particular 3D background volume corresponding to the particular background region. The high intensity core region may be determined as a region comprising voxels having intensities above a predetermined value, or within a specific fraction of a maximum intensity in a specific region of the functional image.

In certain embodiments, this suppression is utilized if a maximum functional image intensity within a 3D volume identified as corresponding to the particular background region is more than a specific multiplier value times a determined background intensity value. Background intensity values may be determined based on intensities of voxels of the 3D functional image corresponding to specific reference volumes corresponding to specific tissue regions, such as gluteal muscles. The suppression approach may be applied to a sub-region of the 3D functional image in the vicinity of the particular background region producing intensity bleed. For example, it may be applied to a rectangular sub-region encompassing the particular region, plus a predetermined margin.

In certain embodiments, one or more intensity bleed functions are determined to perform suppression and thereby correct intensities of voxels of the 3D functional image for bleed (e.g., cross-talk). For example, the 3D functional image may be cropped to the aforementioned rectangular sub-region encompassing the particular region plus the predetermined margin. A determined background intensity value can be subtracted from intensities of voxels within the cropped image region. Sample intensities can then be collected to determine how intensity originating from radiopharmaceutical uptake within the particular background region decreases as one moves away from the particular background 3D volume corresponding to the particular background region. Samples beginning at an extreme top, right, left, and bottom, and then moving outwards up, right, left, and down, respectively, may be used. Other directions are also possible. The sampled intensities provide curves (e.g., sets of sampled intensity data points) showing intensity decrease from the high intensity core. Template functions, such as n-th degree polynomials can be fit to these sampled curves and used to compute intensity values to be used as correction factors in the vicinity of the particular 3D background volume.

For example, PCT Publication WO2019/136349, the content of which is hereby incorporated by reference in its entirety describes how identification of a bladder region can be used to adjust prostate voxel intensities for intensity bleed through due to high accumulation in the bladder in 1404-SPECT images. In certain embodiments, similar approaches can be used for other images obtained with other probes, which may accumulate in the bladder, and/or other regions (e.g., the liver, the kidneys, etc.).

In certain embodiments, the segmentation approaches described herein assume that the 3D anatomical image includes certain anatomical regions. For example, an embodiment of the systems and methods described herein may assume that its input anatomical images always include a pelvic region, and automatically attempts to segment the pelvic region. The systems and methods described herein may also, for other anatomical regions, only segment such regions if they are included in the anatomical image input, for example first performing a determination as to whether they are present.

Approaches for performing whole body segmentation to identify target tissue regions corresponding to bone and/or soft-tissue (e.g., organs) are described in further detail in Examples 1, 2, 3, and 4 below. Also described are approaches for using such whole body segmentation for assessment of disease state, in particular, cancer in a patient.

B. Hotspot and Lesion Detection

In certain embodiments, instead of, or in addition to, quantifying overall uptake in a particular volume within the functional image, localized hotspots (localized regions of relatively high intensity) are detected. In certain embodiments, hotspots are detected via a thresholding approach—by comparing intensities of voxels within the functional image to one or more thresholds values. Groupings of voxels with intensities above a threshold may be detected as hotspots. A single, global, threshold value may be used, or, in certain embodiments, multiple region specific thresholds may also be used. For example, segmentation of the co-registered anatomical image can be used to set different thresholds for different tissue regions used for hotspot detection. Segmentation of the co-registered image can also be used, as described herein, to remove effects of background signal, thereby facilitating hotspot detection (e.g., if a global threshold and/or multiple regional thresholds are used).

In certain embodiments, hotspots can additionally be detected using blob detection techniques. One approach is to use the Difference of Gaussians approach, where a PET image is filtered through a combination of high and low-pass filters approximated by Gaussian kernels. The filters reduce background noise and are invariant to changes in background levels in the different regions of the image (e.g. the thorax might have significantly higher background levels due to significant uptake in liver and kidneys compared to the pelvic region). This cascaded high/low-pass filter approach would allow for hotspot extraction without the utilization of fixed thresholds, but could instead identify local changes in the PET intensities. Another approach is to employ a Laplacian of a Gaussian blob detection method. The Laplacian of a Gaussian approach is a method for detecting edges in images using Laplacian and Gaussian filter kernels. By using different sizes of kernels, edges of structures of different sizes are detected. Choosing appropriate kernel sizes allows the method to detect structures that have properties common to lesions. The described approaches may be used in a stand-alone fashion where only one of the techniques is used for all regions of interest, or they may be used simultaneously, where different methods can be employed for different tissue regions as identified by the semantic segmentation of the co-registered anatomical image in conjunction with either a single global threshold or multiple local thresholds.

FIG. **5**B shows an example process **520** for using the segmentation approaches described herein to detect hotspots representing cancerous lesions. In a first step, a 3D anatomical image is received **522**. A one or more target VOIs corresponding to particular target tissue regions are identified within the 3D anatomical image **524** and the identifications of the target VOIs are stitched together **526** to create a segmentation map **534** comprising a plurality of segmentation masks **536**. Each segmentation mask of the segmentation map represents a particular target VOI. Next, a 3D functional image (e.g., a PET image) is received **528** and the segmentation map is transferred to the 3D functional image

to identify, for each target VOI, a corresponding 3D volume in the 3D functional image **530**. The identified 3D volumes are then used to detect **532**, within the 3D functional image, one or more hotspots corresponding to localized regions of high intensity relative to their surroundings. In particular, one or more specific 3D volumes may correspond to specific tissue regions where cancerous lesions may form, and be analyzed to detect hotspots therein. Other 3D volumes may be used to perform background correction, or intentionally be excluded from the hotspot detection process. As described in further detail herein, still other volumes may be relevant in that they are used as reference volumes for computing useful indices that can be assigned to hotspots in order to score them, e.g., to indicate risk/severity of the underlying lesions they represent.

Hotspots may also be classified following their initial detection, e.g., as cancerous or not, and/or assigned likelihood values representing their likelihood of being a metastases. Hotspot classification may be performed by extracting hotspot features (e.g., metrics that describe characteristics of a particular hotspot) and using the extracted hotspot features as a basis for classification, e.g., via a machine learning module.

In certain embodiments, hotspot classification can also be performed without the use of machine learning. In such embodiments, anatomical knowledge can be combined with information relating to the shape and location of a detected hotspot to classify the hotspot as either a cancerous lesion or noise. For example, if a detected hotspot is located on the edge of a rib facing the liver and the detected peak is not the global maximum in the area surrounding the hotspot, it is possible to estimate whether the hotspot is a tumor or not based on the given anatomical and spatial information. The segmentation of the co-registered anatomical image can additionally be used to create intensity models of background tissue regions known to not contain cancerous cells, but where exceptionally high functional image voxel intensities are common. Such background regions may cause intensity bleed outside of the boundaries of the background region itself and impact the neighboring regions where cancerous lesions might exist. Profiles of the intensity levels can be estimated and used to subtract the estimated additional intensity levels present in neighboring tissue regions harboring cancerous lesions to allow a more robust hotspot detection.

Hotspots representing lesions may be used to determine risk indices that provide an indication of disease presence and/or state (e.g., a cancer status, similar to a Gleason score) for a patient. For example, metrics such as number of hotspots, a total summed intensity of identified hotspots, area fraction of a particular body part or region (e.g., skeleton) occupied by hotspots, and the like, may be used themselves as, and/or in calculation of, such risk indices. In certain embodiments, regions identified via the segmentation approaches described herein may be used in computation of risk indices, for example in computing metrics such as area fractions. Examples of approaches for using identified hotspots to compute risk indices is provided herein, in Examples 5 and 7.

C. Example CNN-Based Whole Body Segmentation and Lesion Detection Approaches

The following examples demonstrate use of the AI-based segmentation and hotspot detection approaches described herein for whole-body segmentation, detecting cancerous lesions, and determining useful metrics for evaluating a cancer status of a subject.

i. Example 1—CNN Based Whole Body Segmentation

Example 1 describes an example approach for whole body segmentation. The implementation in this example uses five neural networks to segment bones within an entire torso. A first neural network is used to roughly localize different regions of the body. The results are used to divide the body into four regions. In each of these regions, a corresponding neural network is then used to perform segmentation into distinct bones. The results from all four regions are then combined into a finished result (e.g., a final segmentation map).

This approach is related to the two-step 'bounding box' approach described herein, wherein a first machine learning module (e.g., a localization module) is used to roughly localize an initial volume of interest (VOI) corresponding to an anatomical region that comprises one or more particular target tissue regions (e.g., a prostate). A second machine learning module (e.g., a segmentation module) then performs a fine segmentation within the initial VOI to identify target volume(s) corresponding to the target tissue region(s) within the initial VOI. In this case, for whole body segmentation, the first machine learning module (localization module) identifies multiple initial VOIs, each corresponding to a different anatomical region. Then, for each anatomical region, a corresponding secondary machine learning module (segmentation module) identifies one or more target volumes, each representing a particular target tissue region. The machine learning modules (e.g., neural networks) may be implemented as separate modules, or certain machine learning networks may be combined. For example, each secondary, segmentation network may be implemented as a separate module, or within a single module.

Accordingly, in this example, the first module (localization) is used for identifying the anatomical regions within the CT; that is, to find volumes of interest where networks of the second module can be applied to generate the segmentation map that is used for further analysis. The networks in the second module work with a full-resolution CT image, while the localization network works in low resolution, using a sub-sampled version of the CT image.

Three example versions of CNN networks used in software implementing whole-body segmentation in accordance with the approaches. Versions 1 and 2 segment 49 bones, and version 2 segments 49 bones and 8 soft-tissue regions.

CNN-Based Segmentation Platform Example Version 1

In a first example version of a CNN network used for whole body segmentation, the first machine learning module (localization module) in this example is referred to as "coarse-seg", and was trained to identify 49 bones in sub-sampled CT images (a sub-sampling factor of 4 along each dimension). The localization module was used to differentiate regions of the body in to a pelvic region, a spine, a left upper body, and a right upper body. The four fine segmentation networks were as follows:

- "fine-seg-pelvic": Trained to identify the left and right ilium and the sacrum and coccyx;
- "fine-seg-spine": Trained to identify 12 thoracic vertebrae, 5 lumbar vertebrae, and the sternum;
- "fine-seg-left-upper-body": Trained to identify 12 ribs on the left side of the body, the left scapula, and left clavicle; and
- "fine-seg-right-upper-body": Trained to identify 12 ribs on the right side of the body, the right scapula, and right clavicle.

The input image sizes for each network were as follows:

TABLE 1

Input image sizes for five neural networks.

Network Name	Input image size (no. slices, no. rows, no. columns)
coarse-seg	(81, 70, 104)
fine-seg-pelvic	(93, 146, 253)
fine-seg-spine	(194, 204, 94)
fine-seg-left-upper-body	(158, 187, 144)
fine-seg-right-upper-body	(158, 191, 146)

While the coarse-seg network of the localization module received, as an input image, an 3D anatomical image representing a large physical volume and comprising a majority of the subject's body, the actual number of voxels in its input image was lower than for the other networks due to the factor of 4 sub-sampling. The number of voxels and size of the input image to the localization module was also reduced by cropping (removing) regions of the image that did not include graphical representations of tissue, but instead represent air. Removing these voxels as a pre-processing step further reduced the size of the image input to the localization module (see e.g., first two columns of Table 4 below). Reducing the size of the image input to the localization module via sub-sampling allows the coarse-seg network to trade resolution of the image on which it operates for additional filters, which allow it to e.g., account for variability in images it receives and perform more accurate and robust coarse segmentation to identify the different initial volumes of interest.

The number of filters and parameters used in each neural network are listed in Tables 2-4, below:

TABLE 2

Number of convolutional filters in five neural networks.

Network Name	Total Number of Filters	Number of Filters in First Layer
coarse-seg	4096 + 49 (49 classes)	32
fine-seg-pelvic	4096 + 3	32
fine-seg-spine	2048 + 18	16
fine-seg-left-upper-body	2048 + 14	16
fine-seg-right-upper-body	2048 + 14	16

TABLE 3

Number of parameters in five neural networks

Network Name	Total params.	No. trainable params.	No. non-trainable params.
coarse-seg	5,881,978	5,878,678	3,300
fine-seg-pelvic	5,880,276	5,877,068	3,208
fine-seg-spine	1,472,815	1,471,177	1,638
fine-seg-left-upper-body	1,472,731	1,471,101	1,630
fine-seg-right-upper-body	1,472,731	1,471,101	1,630

Table 4 below also shows a variability in input image size for the raw data and five neural networks used in this example. As shown in the table, variability in input image size for the four secondary, fine segmentation networks is less than that for the first, localization network since the identification of the initial VOIs produces a more standardized input for the secondary machine learning modules.

TABLE 4

Input image size for raw data and five neural networks.

	Raw data	Coarse-seg (cropped by air)	Fine-seg-pelvic (cropped by coarse)	Fine-seg-spine (cropped by coarse)	Fine-seg-left-upper-body (cropped by coarse)	Fine-seg-right-upper-body (cropped by coarse)
rows mean px	512	390	121	151	126	129
rows std px	0	39	7	19	20	21
rows min px	512	255	97	107	72	88
rows max px	512	399	136	189	170	188
rows min mm	700	308	133	146	98	120
rows max mm	700	546	186	258	232	242
columns mean px	512	399	207	67	112	113
columns std px	0	61	14	10	13	15
columns min px	512	311	155	45	84	72
columns max px	512	512	236	130	164	215
columns min mm	700	425	212	62	115	98
columns max mm	700	700	322	178	224	294
slices mean px	342	340	74	158	110	111
slices std px	99	95	6	12	11	12
slices min px	274	274	48	125	85	85
slices max px	624	624	92	208	136	140
slices min mm	822	822	144	375	255	255
slices max mm	1872	1872	276	624	408	420

CNN-Based Segmentation Platform Example Version 2

An updated, second, example version of the CNN whole-body segmentation system as described above in this example included adjustments to input image sizes, number of convolutional filters, and parameters used in the neural networks used to perform the segmentation. Tables 5, 6, and 7, as seen below, show updated values for the various parameters used in the five neural networks. Table 5 shows updated values for the input image sizes shown in Table 1, Table 6 shows updated values for the number of convolutional filters for the neural networks shown in Table 2, and Table 7 shows updated values for the number of parameters used by the neural networks shown in Table 3.

TABLE 5

Updated values for input image sizes for five neural networks.

Network Name	Input image size (no. slices, no. rows, no. columns)
coarse-seg	(81, 77, 99)
fine-seg-pelvic	(92, 144, 251)
fine-seg-spine	(192, 183, 115)
fine-seg-left-upper-body	(154, 171, 140)
fine-seg-right-upper-body	(154, 170, 140)

TABLE 6

Updated values for number of convolutional filters in five neural networks.

Network Name	Total Number of Filters	Number of Filters in First Layer
coarse-seg	4096 + 49 (49 classes)	32
fine-seg-pelvic	3328 + 3	26
fine-seg-spine	2048 + 18	16
fine-seg-left-upper-body	2048 + 14	16
fine-seg-right-upper-body	2048 + 14	16

TABLE 7

Updated values for number of parameters in five neural networks

Network Name	Total params.	No. trainable params.	No. non-trainable params.
coarse-seg	5,882,423	5,879,132	3,300
fine-seg-pelvic	3,881,200	3,883,812	2,612
fine-seg-spine	1,472,815	1,471,177	1,638
fine-seg-left-upper-body	1,472,731	1,471,101	1,630
fine-seg-right-upper-body	1,472,731	1,471,101	1,630

CNN-Based Segmentation Platform Example Version 3

Another, 3rd, example version of the CNN whole body segmentation approach was used to segment soft-tissue regions as well as bones. As described herein, this 3rd version included two coarse segmentation modules, which were used in parallel, referred to herein as "coarse-seg-02" and "coarse-seg-03".

The "coarse-seg-02" module was trained to identify 49 bones in sub-sampled CT images. The "coarse-seg-03" module was trained to identify 49 bones and the liver, in sub-sampled CT images. The "coarse-seg-02" module outperformed the "coarse-seg-03" module for localization of bones and, to take advantage of the benefits of each module, both were used in parallel, to identify initial volumes of interest (e.g., "bounding boxes") for different fine segmentation networks. In particular, in the 3rd version, seven fine segmentation networks were used. Six out of the seven fine segmentation networks used "coarse-seg-02" for initial volume of interest identification and a seventh, "fine-seg-abdomen", used "coarse-seg-03" for the initial volume of interest identification.

The seven fine segmentation networks for this 3rd example version of the CNN whole-body segmentation system are as follows:

- "fine-seg-abdomen": Trained to identify the liver, left and right kidney, and gallbladder;
- "fine-seg-left-lung": Trained to identify the left lung;
- "fine-seg-right-lung": Trained to identify the right lung
- "fine-seg-pelvic-region-mixed": Trained to identify the left and right ilium, the prostate, the urinary bladder, and the sacrum and coccyx;
- "fine-seg-spine-bone": Trained to identify 12 thoracic vertebrae, 5 lumbar vertebrae, and the sternum;
- "fine-seg-left-upper-body-bone": Trained to identify 12 ribs on the left side of the body, the left scapula, and left clavicle; and
- "fine-seg-right-upper-body-bone": Trained to identify 12 ribs on the right side of the body, the right scapula, and right clavicle.

Tables 8, 9, and 10, below, show values for the various parameters used in seven neural networks in the 3rd version of the CNN-based segmentation system.

TABLE 8

Input image sizes for the seven neural networks and two localization networks.

Network Name	Input image size (Input image size (no. slices, no. rows, no. columns)
coarse-seg-02	(81, 77, 99)
coarse-seg-03	(81, 77, 99)
fine-seg-abdomen	(92, 176, 259)
fine-seg-left-lung	(154, 171, 140)
fine-seg-right-lung	(154, 171, 141)
fine-seg-left-upper-body-bone	(154, 171, 140)
fine-seg-right-upper-body-bone	(154, 170, 140)
fine-seg-pelvic-region-mixed	(92, 144, 251)
fine-seg-spine-bone	(192, 183, 115)

TABLE 9

Number of convolutional filters in the seven neural networks and two localization networks.

Network Name	Total Number of Filters	Number of Filters in First Layer
coarse-seg-02	2278 + 49 (49 classes)	32
coarse-seg-03	2278 + 50	32
fine-seg-abdomen	1142 + 16 (not all output classes are included in the complete segmentation platform)	16
fine-seg-left-lung	1142 + 15	16
fine-seg-right-lung	1142 + 15	16
fine-seg-left-upper-body	1142 + 14	16
fine-seg-right-upper-body	1142 + 14	16
fine-seg-pelvic-region-mixed	1852 + 5	26
fine-seg-spine-bone	1142 + 18	16

TABLE 10

Number of parameters in seven neural networks and two localization networks.

Network Name	Total Params	No. trainable params	No. non-trainable params
coarse-seg-02	5,882,432	5,879,132	3,300
coarse-seg-03	5,882,469	5,879,167	3,302
fine-seg-abdomen	1,473,003	1,471,369	1,634
fine-seg-left-lung	1,472,752	1,471,120	1,632
fine-seg-right-lung	1,472,752	1,471,120	1,632
fine-seg-left-upper-body	1,472,731	1,471,101	1,630
fine-seg-right-upper-body	1,472,731	1,471,101	1,630
fine-seg-pelvic-region-mixed	3,883,812	3,881,200	2,612
fine-seg-spine-bone	1,472,815	1,471,177	1,638

Accordingly, this example demonstrates how segmentation approaches described herein can be used to perform efficient whole body segmentation.

ii. Example 2: Automated Segmentation of the Skeleton in Low-Dose CT and Quantification of Metastatic Prostate Cancer in [^{18}F]DCFPyL PET

PSMA-PET/CT hybrid imaging is a promising diagnostic platform for prostate cancer patients. While manual delineation of organs in three dimensional CT images is often needed for accurate diagnostics and treatment planning, such manual delineation is a time consuming process. To address this challenge, this example demonstrates automating the process of accurate bone segmentation in whole body CT images using deep learning approaches in accordance with the whole body segmentation technology described herein. As described in this example, the anatomical information gained via such skeletal segmentation can be used to create a fully automated lesion detection algorithm in [^{18}F]DCFPyL (PyL™-PSMA) PET/CT images.

A deep learning algorithm based on cascaded deep learning convolutional neural networks for semantic segmentation of 12 skeletal regions was developed. In particular, the 12 skeletal regions were the thoracic and lumbar vertebrae, sinister (left)/dexter (right) ribs, sternum, sinister (left)/dexter (right) clavicle, sinister (left)/dexter (right) scapula, sinister (left)/dexter (right) ilium, and the sacrum. A training set (N=90) and validation set (N=22) of pairs of low-dose CT images and manually crafted segmentation maps were used to develop the deep learning algorithm. The algorithm's performance was assessed on a test set (N=10) of low-dose CT images obtained from a PyL™-PSMA study. In the test set of images, five representatively body parts: sinister (left) ilium, lumbar vertebrae, sinister (left) ribs, dexter (right) scapula, and sternum were manually segmented. These manual segmentations were used as ground truth for evaluation of the automated segmentation procedure.

The automated segmentation can be used for automated lesion detection. For example, automated lesion detection approach using a hard threshold of standard uptake value (SUV) based on PET image voxel intensities can be performed.

Sorensen-Dice scores were used to evaluate accuracy of the automated segmentation. The segmentation approach achieved a Sorensen-Dice score mean and standard deviation of 0.95 and 0.024, respectively, on the training set and a mean and standard deviation of 0.93 and 0.036, respectively, on the validation set. For the test set, mean values (with standard deviation values shown in parentheses) for each of the five regions are as follows: 0.94 (0.016) for dexter (right) clavicle, 0.90 (0.023) for sinister (left) ribs, 0.92 (0.019) for sternum, 0.94 (0.033) for lumbar vertebrae, and 0.97 (0.0033) for sinister (left) ilium. The overall mean (over all body parts) was 0.93, with a standard deviation of 0.030.

Accordingly, this example demonstrates the accuracy of a fully automated segmentation approach for 12 skeletal regions in whole body low-dose CT images and use of an automated lesion detection approach for PyL™-PSMA/CT hybrid imaging.

iii. Example 3: Automated Whole Body Segmentation for PyL™-PET Image Analysis and Lesion Detection

This example demonstrates automated segmentation of 49 bones and 27 soft-tissue regions in whole body CT images using deep learning approaches in accordance with the whole body segmentation technology described herein. This example also demonstrates how the anatomical information gained via such segmentation can be used to create a fully automated lesion detection algorithm in [^{18}F]DCFPyL (PyL™-PSMA) PET/CT images. This example also shows how the segmentation can be used to remove background signal from PET images to facilitate observation and detection of lesions in which PyL™ has accumulated.

FIG. **6**A shows a block flow diagram illustrating an embodiment of the segmentation processes described herein that is used in the PyL™-PET/CT image analysis described in this example. As in process **500**, shown in FIG. **5**, in process **600** an anatomical image is received. In particular, in process **600**, a CT image is received **610***a*. In this example, process **600** is used to identify and segment the CT image into target volumes of interest corresponding to 49 specific bones and 8 soft tissue regions (in this example, example version 3 of the CNN-based segmentation approach described in Example 1 is used). In order to identify the target volumes, a coarse segmentation is performed **620***a* to localize a set of initial volumes of interest, or sub-regions, e.g., as described in Example 1. A fine segmentation is then performed within each of the sub-regions to identify the specific target volumes of interest that correspond to the target 49 bone and 8 soft-tissue regions **630***a*. Segmentation masks representing the identified target volumes can be created, and merged **640***a*, for example to create a 3D whole body segmentation map.

As noted in Example 1 (CNN Network Version 3), the specific regions segmented are as follows:

49 Bones:
clavicle_left
clavicle_right
hip_bone_left
hip_bone_right
rib_left_1
rib_left_10
rib_left_11
rib_left_12
rib_left_2
rib_left_3
rib_left_4
rib_left_5
rib_left_6
rib_left_7
rib_left_8
rib_left_9

-continued

rib_right_1
rib_right_10
rib_right_11
rib_right_12
rib_right_2
rib_right_3
rib_right_4
rib_right_5
rib_right_6
rib_right_7
rib_right_8
rib_right_9
sacrum_and_coccyx
scapula_left
scapula_right
sternum
vertebra_lumbar_1
vertebra_lumbar_2
vertebra_lumbar_3
vertebra_lumbar_4
vertebra_lumbar_5
vertebra_thoracic_1
vertebra_thoracic_10
vertebra_thoracic_11
vertebra_thoracic_12
vertebra_thoracic_2
vertebra_thoracic_3
vertebra_thoracic_4
vertebra_thoracic_5
vertebra_thoracic_6
vertebra_thoracic_7
vertebra_thoracic_8
vertebra_thoracic_9
8 Soft-Tissue Regions:
gall_bladder
kidney_left
kidney_right
liver
lung_left
lung_right
prostate
urinary_bladder

FIG. **6**B shows a series of CT images overlaid with annotations illustrating the steps in the whole-body segmentation process **600** described in this example. An example raw CT image that is received at step **610***a* is shown in **610***b*. Image **620***b* shows results of a coarse segmentation (different regions identified are shown as colored regions) used to identify the initial volumes of interest in the CT image. Image **630***b* shows "bounding boxes" identifying initial volumes of interest in which fine segmentation is performed to identify the target volumes of interest corresponding to the 49 bones and 8 soft tissue regions. Image **640** illustrates the final, merged whole body segmentation.

Turning to FIG. **7**, in order to train the machine learning modules used to perform the segmentations, numerous pre-labeled sample images, such as the three images (**710**, **720**, **730**) shown in FIG. **7**, were used as a training data set. The machine learning modules were fine-tuned using 1000's of manually annotated labels along with 100's of models trained on dozens of GPUs over 1000's of hours before optimal configurations for the many components of the segmentation platform were discovered. Once trained, however, segmentation can be performed rapidly, with results such as those shown in FIGS. **8** (**810** and **820** are two example images) and FIGS. **16**A and **16**B obtained in a matter of seconds—typically under 180 seconds.

The anatomical context obtained by segmenting the CT image can be used to detect lesions in PET images that are co-registered with the CT image, for example, as in a typical PET/CT imaging modality in which CT and PET images are obtained for a subject in quick succession, with the subject remaining in a substantially same position as the images are recorded. In particular, as demonstrated in this example, segmentation of the CT image can be transferred to the PET image in order to identify regions of interest such as the prostate gland or the skeleton, where the entire functional image except for regions expected to carry either primary or secondary prostate cancer tumors can be excluded from the lesion detection algorithm. Without wishing to be bound to any particular theory, exclusion of regions from the lesion detection algorithm can be especially important for background regions where accumulation leads to high intensity in PET image voxels within and around the background tissue regions. The high intensities in background tissue regions may, if not excluded from the prostatic lesion detection process, lead to erroneous classification of background noise as cancerous lesions. In the regions that remain after the background exclusion process, a simple threshold (e.g., a SUV of 3) in conjunction with a lesion classification algorithm can be employed to find hotspots within the relevant tissue regions. The classification algorithm may be used as a simple check to confirm the hotspots position and to compare the intensity in the hotspot's neighborhood. If the hotspot is part of a larger hotspot and is located on the edge of a body part (e.g. a rib close to the liver), the lesion may be classified as noise and excluded. FIGS. **9**A-D illustrate the need for, and benefits obtained by, this background subtraction approach and lesion detection algorithm, where only regions of interest are included in the detection procedure, and portions of the image contains high intensity background voxels. FIGS. **9**A and **9**C show PET images as white-to-red-to-blue false color overlaid on CT images. Blue color indicates low PET image intensity, transitioning from red to white as intensity increases. FIGS. **9**B and **9**D show the same PET images as in **9**A and **9**C, but with all background uptake removed from the PET image. In FIGS. **9**B and **9**D, a few localized hotspots, corresponding to cancerous lesions are visible. In the PET images without background removal, these hotspots were overwhelmed and masked by the large background signal.

FIG. **10**A shows an example process **1000** for using the anatomical context provided by whole body CT segmentation for detecting lesions and determining useful risk indices that quantify a cancer status (e.g., prostate cancer status) of a subject using PET/CT images obtained following administration of PyL™ as a radiopharmaceutical. As shown in FIG. **10**A, PET/CT images are obtained **1010**, anatomical context is determined **1012** via segmentation of bones and soft tissue and used to obtain measurements (e.g., of lesions and/or risk indices) from the PET image **1014**. FIG. **10**B shows an example PET/CT image **1016** and FIG. **10**C shows example segmentations of bones and soft tissue **1018***a* and **1018***b*. As shown in FIG. **10**D, segmentation of bone and soft-tissue (e.g., shown in image **1020***a*) can be used to remove background signal (e.g., from background tissue regions, such as those shown in image **1020***b*), leaving only desired signal from hotspots indicative of cancerous lesions **1020***c*.

FIGS. **11-13** illustrate this process, showing how segmentation of a CT image can be transferred to a PET image, and are used to provide anatomical context for background removal and lesion detection. In particular, FIG. **11**A and FIG. **11**B show different views of a CT image, in which segmentation of bones has been performed. The various segmented bones are labeled with different colors in the views shown in FIG. **11**A and FIG. **11**B. Notably, by virtue of the "bounding box" approach described herein, even such

a complex and large scale segmentation can be performed extremely rapidly. The segmentation shown in FIGS. **11**A and **11**B was performed in less than 180 seconds.

As shown in FIG. **12**, segmentation of bones and soft tissue can be used to account for normal uptake in certain background tissue regions, which may occur under normal circumstances and mask useful hotspot signals that indicate presence of cancerous lesions. In PET/CT imaging performed with PyL™, normal uptake can occur in kidneys, duodenum, small intestines, spleen, liver, pancreas, stomach, adrenal gland, rectum, and testes. FIG. **12** shows the aforementioned regions identified in red. As shown in FIG. **13**A, once background intensities due to normal PyL™ accumulation in these regions is subtracted out, lesions become readily observable and can be detected. One such lesion **1302** is visible in FIGS. **13**A-D. Lesions such as lesion **1302** can be detected, for example via a thresholding approach, and classified as PyL™ positive (i.e., indicative of cancer) e.g., as described above. As with segmentation, lesion detection is also rapid. Lesion **1302** was detected in less than 5 seconds.

FIG. **14**A and FIG. **14**B show results of the PET image processing and lesion detection approach described above performed on PET/CT images obtained for a 65 year old male with metastatic castration resistant prostate cancer. The patient's prostate specific antigen (PSA) score was 6.8 ng/ml. The PET images were obtained following administration of PyL™ as the radiopharmaceutical. FIG. **14**A shows the initial, raw, PET/CT image. FIG. **14**B shows the image following the processing described herein. The background intensity is removed, and several small lesions are readily observable. The segmentation of the 49 bones and 8 soft-tissue regions (e.g., organs) was performed in less than 180 seconds.

FIG. **15**A and FIG. **15**B show results of the PET image processing and lesion detection approach performed on PET/CT images obtained for a 54 year old male with metastatic castration resistant prostate cancer. The patient's PSA score was 33.55 ng/ml. The PET images were obtained following administration of PyL™ as the radiopharmaceutical. FIG. **15**A shows the initial, raw, PET/CT image. FIG. **15**B shows the image following the processing described herein. The background intensity is removed, and several small lesions are readily observable. The segmentation of the 49 bones and 8 soft-tissue regions (e.g., organs) was again performed in less than or about 180 seconds.

Accordingly, this example demonstrates how the whole-body segmentation approach described herein contextualizing the PyL™ images, with automated segmentation of 27 soft-tissue organs and 49 bones, to detect, quantify and track PyL™ avid lesions. The approach would allow the clinicians/physicians to ask clinically relevant questions for better management of prostate cancer patients. Advantages such as increased diagnostic accuracy, precision, speed, and reproducibility, were demonstrated (statistically) in the context of artificial intelligence assisted 1404-SPECT image analysis (see, e.g., PCT Publication WO2019/136349, the content of which is hereby incorporated by reference in its entirety), may also be obtained for PyL™-PET images.

iv. Example 4: Example Bone and Soft-Tissue Segmentation Regions

This example provides a listing of a set of example bone and soft-tissue regions that a system developed using the approaches and embodiments described herein can identify via segmentation of CT images. In particular, listed below are 67 bones and 22 soft-tissue regions for that have been manually labeled (e.g., identified by one or more human experts) in a set of CT images. These manually labeled CT images can be used as training data for the machine learning approaches described herein. For example, while Examples 1-3 describe current versions of software implementing whole body segmentation approaches that segment 49 bones and 8 soft-tissue regions, their functionality can readily be updated to segment any number of the 67 bone and 22 soft-tissue regions listed in this example. Accordingly, this example shows that embodiments of the systems and methods described herein may be developed to identify similar regions, including, but not necessarily limited to the specific regions described in this example. Certain systems and methods may identify tissue regions not necessarily listed in this example. In certain embodiments, both bone and soft-tissue regions are identified. In certain embodiments, some systems and methods may identify only bones, or only soft-tissue.

As indicated in the listing below, certain left and right hand side bones are identified as separate tissue regions (e.g., a left clavicle and a right clavicle) and, in certain cases, individual members of large groups of bones are identified separately. For example, the example listing below shows that individual ribs and vertebrae are identified via the segmentation approach of this example (specific ribs and vertebrae are numbered in the listing). This example also should make clear that the approaches described herein can be used to segment a variety of regions throughout the body, including, but not necessarily limited to the regions listed herein.

Segmentation Regions:

Bones (67)
clavicle_left
clavicle_right
femur_left
femur_right
fibula_left
fibula_right
hip_bone_left
hip_bone_right
humerus_left
humerus_right
mandible
patella_left
patella_right
radius_left
radius_right
rib_left_1
rib_left_2
rib_left_3
rib_left_4
rib_left_5
rib_left_6
rib_left_7
rib_left_8
rib_left_9
rib_left_10
rib_left_11
rib_left_12
rib_right_1
rib_right_2
rib_right_3
rib_right_4
rib_right_5
rib_right_6
rib_right_7
rib_right_8
rib_right_9
rib_right_10
rib_right_11

-continued

rib_right_12
sacrum_and_coccyx
scapula_left
scapula_right
skull
sternum
tibia_left
tibia_right
ulna_left
ulna_right
vertebra_cervical_all
vertebra_lumbar_1
vertebra_lumbar_2
vertebra_lumbar_3
vertebra_lumbar_4
vertebra_lumbar_5
vertebra_lumbar_6
vertebra_thoracic_1
vertebra_thoracic_2
vertebra_thoracic_3
vertebra_thoracic_4
vertebra_thoracic_5
vertebra_thoracic_6
vertebra_thoracic_7
vertebra_thoracic_8
vertebra_thoracic_9
vertebra_thoracic_10
vertebra_thoracic_11
vertebra_thoracic_12
Soft tissue (22):
adrenal_gland_left
adrenal_gland_right
aorta_abdominal_part
aorta_thoracic_part
brain
bronchi_left
bronchi_right
gallbladder
gluteus_maximus_left
gluteus_maximus_right
heart
kidney_left
kidney_right
liver
lung_left
lung_right
pancreas
prostate
rectum
spleen
urinary_bladder
ventricle

v. Example 5: Computing Hotspot Indices for Radiopharmaceutical Uptake Quantification and Clinical Endpoint Assessment

Example 5 is an example approach that uses the segmentation and hotspot detection methods described herein to compute, for a particular detected hotspot, a hotpot index value that can be used to infer and/or quantify uptake of radiopharmaceutical within the lesion that the detected hotspot represents. The computed hotspot index can be related to clinical endpoints, including survival rate of a patient and to determine treatment strategy. When computed for multiple images, collected at different time points, the computed index values can be compared with each other for a particular patient, and the change in index used to evaluate efficacy of a treatment and to make a prognosis of how the index will change in the near future. In certain embodiments, the computed index can predict sensitivity towards treatment targeting the imaging-ligand. In certain embodiments, the computed index can also be included in nomograms for effective patient stratification.

The approach in this example uses a CT-PET image set obtained for a particular patient following administration of a radiopharmaceutical comprising a PSMA binding agent, for example, PyL™. However, the approaches described herein are agnostic to the particular radiopharmaceutical used for imaging, and can be utilized with a variety of different radiopharmaceuticals, e.g., ^{99m}Tc-MIP-1404, ^{18}F-PyL, ^{68}Ga-PSMA-11, ^{18}F-NaF, ^{11}C-Choline, [18F]FDG, [18F]FACBC, etc.

A machine learning-based approach in accordance with the systems and methods described herein is used to identify various target VOIs within the CT image. As described herein, the target VOIs are volumes in the CT image identified, automatically, by the segmentation approach, to correspond particular target tissue regions. In this example approach, target VOIs corresponding to a liver, an aorta portion, and a parotid gland are identified. As described herein, these particular tissue regions—the liver, aorta portion, and parotid gland—serve as reference regions for computation of the hotspot index. Other target VOIs corresponding to other target tissue regions, in addition to the reference regions, may also be identified. Segmentation masks representing the identified target VOIs are mapped to the PET image to identify corresponding 3D volumes within the PET image. In this manner, 3D reference volumes corresponding to the liver, aorta portion, and parotid gland are identified in the PET image. Once identified, each particular 3D reference volume is used to compute a corresponding reference intensity value that provides a measure of the intensities of voxels within the particular 3D reference volume. In this example, a mean intensity inside each volume is used, though other measures (e.g., a median, a maximum, a mode, etc.) are possible.

To compute an index value for a particular identified hotspot, a hotspot intensity value is computed for that particular hotspot and compared with the reference intensity values. Similar to the reference values, the hotspot intensity value provides a measure of intensity of voxels of the hotspot. In this example, a maximum value is computed, although, as with the reference values, other measures can be used. As this example shows, the particular measure used to compute the hotspot intensity value need not be the same as that used to compute the reference intensity values. To compute the hotspot index value, the reference intensity values can be mapped to reference index values on a scale, and the hotspot index value can then be computed based on whether the hotspot intensity value lies above, below, or in between the reference values.

For example, typically the reference intensity value computed from the reference volume corresponding to the aorta portion (this—aorta—region is used to provide a measure of uptake in the blood pool, and may also be referred to as a blood or blood pool reference value) is lowest in value, followed by the liver and then the parotid region. Accordingly, a hotspot whose hotspot intensity value is equal to the blood reference value will be assigned a hotspot index value equal to 100; a hotspot whose hotspot intensity value is equal to the liver reference value will be assigned a hotspot index value equal to 200; and a hotspot whose hotspot intensity value is equal to the parotid gland reference value will be assigned a hotspot index value equal to 300. Hotspot index values for hotspot intensity values lying in between two reference intensity values can be determined via interpolation (e.g., linear interpolation).

In this manner, a detected hotspot can be assigned an index value that quantifies, in a standardized fashion (e.g., so as to be comparable between different images) a level of

radiopharmaceutical uptake in the particular lesion that the hotspot represents. As described herein, these indices can be related to survival, which, in turn, makes them useful for treatment management. For example, depending on the expected outcome of the patient, a more or less aggressive treatment may be considered. Price of treatments can also be included as a factor. The index is especially useful when measured over time. When comparing indices across time and multiple imaging examinations for a patient, the change in index can be used to evaluate the efficacy of a treatment, and to make a prognosis how the index will change in the near future.

Notably, a significant advantage of the approach described in this example over previous approaches is the ability to compute reference intensity values (as well as hotspot intensity values) from automatically identified 3D volumes provided by the artificial intelligence based segmentation approaches described herein. Previous approaches that attempted to quantify regions of images representing lesions relied on hand marking—e.g., via placement of a circular marker—of regions in 2D slices to identify 2D regions of interest lying within a reference tissue region. In contrast to such small 2D regions, the 3D volume that are identified via the approaches used herein capture intensities throughout entire organs, and thereby offer increased accuracy and repeatability. Moreover, by using accurate automated segmentation, further increases in accuracy and repeatability are provided.

In addition, rather than classifying a detected lesion using one of a small number of values, the approach of this example uses a continuously varying index computed via interpolation. This approach provides more detailed information that can be utilized to manage treatment strategy and track disease progression and/or treatment efficacy over time in a finely grained and accurate fashion.

vi. Example 6: Automated Hotspot Detection and Uptake Quantification in Bone and Local Lymph

PyL™-PSMA PET/CT hybrid imaging (e.g., images PET/CT images acquired for a patient after administering PyL™ to the patient) is a promising tool for detection of metastatic prostate cancer. Image segmentation, hotspot detection, and quantification technologies of the present disclosure can be used as a basis for providing automated quantitative assessment of abnormal PyL™-PSMA uptake in bone and local lymph (i.e., lymph nodes localized within and/or in substantial proximity to a pelvic region of a patient). In particular, as shown in this example, image segmentation and hotspot detection techniques in accordance with the systems and methods described herein can be used to automatically analyze in PET images to detect hotspots that a physician might identify as malignant lesions.

In this example, PET/CT scans were evaluated to automatically identify, within the PET images of the scans, hotspots corresponding to potential bone and local lymph node lesions. For each scan, a semantic segmentation of the CT image was performed using the deep learning approaches described herein in order to identify a set of specific bone and soft-tissue regions (e.g., organs). Once obtained, the CT image segmentation was transferred (e.g., mapped) to the PET image of the PET/CT scan to identify corresponding 3D volumes in the PET image. In each PET image, intensities corresponding to background uptake were removed by suppressing intensities in identified volumes corresponding to a urinary bladder, a liver, and a kidney. The segmentation was also used to define relevant volumes in which to detect hotspots. Blob detection algorithms were then applied to identify abnormal hotspots representing either possible bone lesions or possible malignant local lymph nodes. Reference volumes corresponding to a liver and a thoracic part of an aorta were used to compute reference SUV values.

Accuracy of the hotspot detection approach in this example was validated by comparing detection of hotspots in PET images using the automated approach described herein with manual annotations identifying bone lesions and lymph node lesions from teams of physicians. A set of 157 PET/CT scans that were annotated for bone lesions (114 of the images did not have any lesions and 11 of the images had greater than three lesions) were used to evaluate accuracy in detecting hotspots corresponding to bone lesions and a set of 66 scans that were annotated for local lymph node lesions (40 images without lesions and six with greater than three lesions). The bone detection algorithm identified 97% of all annotated bone lesions, with on average 109 hotspots per image. The local lymph detection algorithm found 96% of all annotated malignant local lymph nodes, with on average 32 hotspots per scan.

Accuracy of the deep learning segmentation was also evaluated in this example. The segmentation algorithm was trained to segment a set of 52 bones and 7 soft tissue regions (e.g., organs) used either for defining the hotspot search region or as reference regions. Training and validation was performed and evaluated for each particular region (bone or soft tissue region) using a manual identification of that region in a CT image. For example, 140 manually identified livers were used to train the algorithm for liver segmentation, and 37 manually identified livers were used for validation. Similarly, 61 and 14 manually identified aortas were used for training and validation of the aorta region segmentation, respectively. For liver segmentation, Dice scores of 0.99 and 0.96 were obtained for the training and validation sets, respectively. For aorta segmentation, Dice scores of 0.96 and 0.89 were obtained for training and validation, respectively. Finally, a set of ten additional images that were not used development of the algorithm were used to assess generalization. For these ten images, Dice scores characterizing segmentation accuracy of the liver and aorta were 0.97±0.01 and 0.91±0.5, respectively.

A full listing of the specific 52 bone (the sacrum and coccyx are listed on a single line as “sacrum_and_coccyx”, but correspond to two segmented regions) and 7 soft-tissue regions used in this particular example is below.

Bone Regions:
capula_left
clavicle_left
clavicle_left
clavicle_right
hip_bone_left
hip_bone_right
rib_left_1
rib_left_10
rib_left_11
rib_left_12
rib_left_2
rib_left_3
rib_left_4
rib_left_5
rib_left_6
rib_left_7
rib_left_8
rib_left_9
rib_right_1

-continued

rib_right_10
rib_right_11
rib_right_12
rib_right_2
rib_right_3
rib_right_4
rib_right_5
rib_right_6
rib_right_7
rib_right_8
rib_right_9
sacrum_and_coccyx
scapula_left
scapula_right
sternum
vertebra_lumbar_1
vertebra_lumbar_2
vertebra_lumbar_3
vertebra_lumbar_4
vertebra_lumbar_5
vertebra_thoracic_1
vertebra_thoracic_10
vertebra_thoracic_11
vertebra_thoracic_12
vertebra_thoracic_2
vertebra_thoracic_3
vertebra_thoracic_4
vertebra_thoracic_5
vertebra_thoracic_6
vertebra_thoracic_7
vertebra_thoracic_8
vertebra_thoracic_9
Soft Tissue Regions:
aorta_abdominal_part
aorta_thoracic_part
kidney_left
kidney_right
liver
prostate
urinary_bladder

Accordingly, this example demonstrates use of deep learning based semantic segmentation for automated identification of hotspots and for computation of SUV reference values in [18F] DCFPyL (PyL™-PSMA) PET/CT images.

vii. Example 7: Lesion PSMA Score and PSMA Weighted Lesion Involvement

This example provides an approach for assigning detected hotspots hotspot indices, based on a comparison of individual hotspot intensities with reference levels, and then using the assigned individual hotspot indices to determine overall indices representing a weighted sum of measures of lesion size. The indices used in this example are used to assess cancer status for patients imaged using a PSMA binding agent and PET-CT imaging.

In particular, individual hotspot indices are determined via interpolation from our reference levels similar to the approach described in Example 5. In this example, reference VOIs corresponding to an aorta portion and a liver portion are segmented and mapped to corresponding 3D volumes in a PET image. The aorta portion volume is used to determine a blood reference intensity, and the liver volume is used to determine a liver reference intensity. In this example, each reference intensity is determined from its corresponding volume by taking an average intensity (SUV) in the corresponding volume, but other measures, such as a maximum, peak, or median value could also be used. Reference levels on a scale, referred to as a Lesion PSMA Score (LPS), are assigned to intensity values based on the blood and liver reference intensities (SUVs) as follows: a LPS of 0 is assigned to a 0 SUV level, an LPS of 1 is assigned to the blood reference intensity, an LPS of 2 is assigned to the liver reference intensity, and a maximum LPS of 3 is assigned to a reference intensity calculated as twice the liver reference intensity.

Individual hotspots are assigned LPS scores based on their individual intensities. For individual hotspots having intensities ranging from 0 to the maximum reference intensity (twice the liver reference intensity), the LPS score corresponding to the individual hotspot intensity is interpolated from the reference scale. Hotspots having intensities greater than the maximum reference intensity are assigned the maximum LPS of 3.

Two example overall risk indices that can be computed using detected hotspots and the individual hotspot indices (LPS scores) are calculated as weighted sums of hotspot sizes in particular volumes corresponding to tissue regions where cancerous lesions may occur. A first example index is a PSMA-weighted total bone/lymph/prostate lesion volume or ratio (PTLV or PTLR). This index is a weighted sum of lesion volumes, the weight being the lesion PSMA score. The sum is computed separately for 3D volumes corresponding to bone (e.g., a skeletal region), lymph nodes, and prostate as the weighted sum of hotspot volumes for hotspots found in each particular region. In particular, the weighted sum is computed as follows:

$$\Sigma(\text{lesion volume} \times \text{lesion psma score})$$

In certain case, a ratio may be preferable and can be computed by dividing the weighted sum by the total 3D volume of the particular region (e.g., in the PET image). Weighting summed hotspot volumes by LPS, as opposed to, for example SUV or normalized SUV is advantageous since it PSMA expression in the form of (normalized) SUV values may not relate to aggressiveness of the disease in a linear fashion. That is, for example, it is not a given that a hotspot with an intensity of 100 represents a lesion is five times worse than one represented by a hotpot having an intensity of 20. Calculating the LPS score and weighting hotspots by the LPS score provides a scale to compare different hotspots.

Another example index is a PSMA-weighted bone/lymph aggregated diameter (PLAD). This index is also a sum of a measure of lesion size, weighted by LPS score, but instead of volume this index uses an average diameter (e.g., averaged of x, y, and z-diameters) of each hotspot. Since volume is a three-dimensional quantity, a minor change in volume for a large lesion can dominate (e.g., cause large fluctuations in the sum) over changes in size of smaller lesions. Using the average diameter instead mitigates this effect. This index is calculated as follows:

$$\Sigma(\text{lesion average diameter} \times \text{lesion psma score})$$

The weighed aggregated diameter can be calculated for the bone and lymph.

vii. Example 8: Improved Performance in AI-Assisted Image Analysis for Patients with Low or Intermediate Risk Prostate Cancer

99mTc MIP-1404 (1404) is a PSMA targeted imaging agent for the detection and staging of clinically significant prostate cancer. Manual assessment of tracer uptake in SPECT/CT images introduces inherent limitations in inter- and intra-reader standardization. This example describes a study that evaluated the performance of PSMA-AI assisted reads, wherein automated segmentation of prostate volumes

and other target tissue regions are performed in accordance with the embodiments described herein, over manual assessment and known clinical predictors.

The study analyzed 464 evaluable patients with very low-, low-, or intermediate-risk prostate cancer, whose diagnostic biopsy indicated a Gleason grade of ≤3+4 and/or who were candidates for active surveillance (1404-3301). All subjects received an IV injection of 1404 and SPECT/CT imaging was performed 3-6 hours postdose. Three independent readers evaluated the images. All subjects underwent either voluntary RP (low- and intermediate-risk) or prostate biopsy (very low-risk) post dosing. Clinically significant disease was declared in subjects with Gleason grade 7 or higher. The PSMA-AI was developed and locked prior to the analysis. Three different independent readers used PSMA-AI to obtain quantitative expression of 1404 in the prostate against the background (PSMA-Index). PSMA-Index for all readers and subjects were compared to the histopathological reference, yielding 6 receiver operating characteristic (ROC) curves (3 manual reads+3 PSMA-AI assisted reads). The clinical performance of the 1404 PSMA-AI assisted read was also evaluated by comparing the Area Under the ROC Curve (AUC), of a multivariate model (PSA, clinical staging and diagnostic Gleason score) with and without PSMA-Index.

The manual reads demonstrated AUCs of 0.62, 0.62 and 0.63. The reads with PSMA-AI demonstrated AUCs of 0.65, 0.66 and 0.66. The PSMA-AI performance in terms of AUC was higher than manual in all 3*3=9 pairwise comparisons between the two reader groups, with statistically significant improvement observed in five cases (nominal $p<0.05$), not accounting for multiple comparisons. The predictive ability of the baseline multivariate model, without PSMA-Index, was at AUC 0.74. Upon adding of PSMA-Index, the model predictive ability increased to AUC 0.77. The logistic regression model indicated that PSMA-Index ($p=0.004$), pre-surgery PSA (0.018) and % positive cores ($p=<0.001$) were significantly associated with clinically significant disease. When measuring reproducibility, log (PSMA-Index) correlation coefficients for pairs of PSMAAI readers were 0.94, 0.97 and 0.98.

Accordingly, the study described in this example demonstrated that PSMA-AI provides a standardized platform to generate reproducible quantitative assessment of 1404. The PSMA-AI assisted read demonstrated an additive improvement over known predictors for identifying men with clinically significant disease.

ix. Example 9: Automated Calculation of PSMA Indices for Quantification of 18F-DCFPyL Uptake from PET/CT Images for Prostate Cancer Staging

This example demonstrates automated image segmentation, lesion detection, and calculation of a standardized index score based on hotspot indices assigned to detected lesions via embodiments of the approaches described herein. The automated image analysis procedures are used for evaluated cancer status of patients imaged via PET/CT scanning after being administered the radiopharmaceutical 18F-DCFPyL (PyL™).

In this example, a cascaded deep learning pipeline was used to segment relevant organs in the CT image, and segmentations are projected into PET image space. In particular, target regions corresponding to a bone volume corresponding to bones of the subject, a lymph volume corresponding to lymph regions, and a prostate volume corresponding to a prostate gland were segmented in the CT image and mapped to identify corresponding 3D volumes in the PET image. Likewise, aorta and liver volumes corresponding to an aorta portion and a liver were also segmented and mapped to the PET image for use as reference regions as described herein.

Hotspots were detected in the PET image. Hotspots that were considered to represent lesions are manually segmented, as well as additional lesions not detected by the algorithm. Each individual detected hotspot was quantified by calculating an individual hotspot index referred to as lesion miPSMA index (LPI). As described in Examples 6 and 7 above, the LPI used in this example is a continuous index computed using automatically segmented (as opposed to manually identified) volumes. Accordingly, it offers advantages over previous approaches that utilize manual identification of various organs in images, and which only classify lesions using a small, finite, number of enumerated values. Accordingly, this approach provides more detailed information that can be utilized to manage treatment strategy and track disease progression and/or treatment efficacy over time in a finely grained and accurate fashion.

The LPI for each detected hotspot was computed based on reference values determined from blood pool (as measured from an identified aorta volume) and liver reference regions, e.g., similar to that described in Example 7 above. In particular, a blood pool reference intensity (SUV value) was measured using an aorta volume within the PET image, and a liver reference intensity was measured from a liver volume identified in the PET image. Both the blood pool and liver reference intensity levels were measured as the mean SUV (SUV_{mean}) within the corresponding volume in a PET image. Reference LPI index values of 1 and 2 were assigned to the blood pool and liver reference intensities, respectively. A maximal reference index level of 3 was assigned to a reference intensity corresponding to twice the liver reference intensity value.

Each individual detected hotspots was assigned LPI scores based (i) a measured hotspot intensity value for the hotspot and (ii) comparison with the blood pool and liver reference intensity values and the aforementioned reference index levels. In particular, for each hotspot, an individual hotspot intensity value corresponding to a mean lesion uptake was calculated as a mean SUV across voxels of the hotspot. For an individual hotspot, an LPI equal to 1 was assigned if the mean lesion standard uptake value (SUV_{mean}) equal to the blood pool reference value; an LPI equal to 2 was assigned for hotspots having mean lesion uptake values equal to the liver reference uptake value; and an LPI equal to 3 was assigned to hotspots having a mean lesion uptake value is equal to or above twice the liver reference uptake. For hotspots having intensities in falling in between reference intensity values, individual hotspot LPIs were interpolated from based on the hotspot intensity value and reference intensity-index value pairs.

An aggregated lesion volume within the bone region was computed as a weighted sum of volumes of individual hotspots detected within the bone volume in the PET image, with the volume of each hotspot weighted by its corresponding LPI. In this manner a PSMA-weighted Total Lesion Volume (PLTV) index was computed for the bone region, denoted $PTLV_{bone}$. PLTV index values were also computed for the lymph ($PTLV_{lymph}$) and prostate ($PTLV_{prostate}$) regions analogously. For each of the three regions, PET/CT image data sets for subjects having various different indications were used to automatically determine PLTV index values.

Performance of the AI-based automated technique was evaluated based on comparison with manual organ segmentation and annotation of images to identify hotspots, and PLTV index values computed for different indications were compared across regions.

Using manual expert interpretation as a gold standard for comparison, the automated hotspot detection algorithm was determined to have sensitivity of 92.1% for bone lesions (97.2% in the 52 automatically segmented bones) and 96.2% for lymph lesions. On average, 17 bone hotspots were detected per scan and 23 lymph hotspots were detected per scan.

PLTV index values were computed using a sample dataset of 197 PET/CT images for the bone region, 99 PET/CT image for the lymph region, and 43 PET/CT images for the prostate region. In the data sets, 94% of individual hotspot LPI's determined were between 1 and 3, with minimum LPIs determined for bone, lymph, and prostate regions of 0.82, 1.1, and 1.3, respectively. Median LPI values for the bone, lymph, and prostate regions were 1.5, 2.0, and 2.3, respectively.

For each region, PLTV indices were computed for subjects having various different indications as follows: Treatment Response (TR), Screening (S), Newly Diagnosed (ND), Metastatic (M), Suspected Recurrence (SR), Recurrent (R). PLTV index values were compared across indications by calculating the means of the values in the interquartile range (IQR_{mean}), hence excluding outliers. Ordering indications by IQR_{mean} of the PLTV values yields TR<S<ND<R<SR<M for the bone region, S=M<R<ND<SR for lymph region, and M<SR<R<S<ND for prostate region, aligning well with clinical expectations of disease state.

FIG. **19** shows PLTV index values determined for the various indications for each region. FIG. **20** shows a scatter plot of individual hotspot LPI values for hotspots detected in each of the three regions.

In comparison with manual approaches for determining reference values for grading lesions, such as the of Eiber et al., 2017, the blood and liver automated reference values are based on a larger image volume compared to the manual reference method and are hence expected to be more robust. FIG. **21** compares reference values computed via the automated segmentation approaches described herein for the blood pool (left graph) and liver (right graph) regions with reference values computed using manual identification of organ boundaries. As shown in FIG. **21**, in a sample of 20 PET/CT scans, the correlation (Pearson's r) between automated and manual reference was 0.92 for blood and 0.87 for liver.

Accordingly, this example demonstrates use of the automated segmentation, hotspot detection, and index value calculation for detecting cancer and tracking cancer progression and/or response to treatment over time.

D. Imaging Agents

In certain embodiments, 3D functional images are nuclear medicine images that use imaging agents comprising radiopharmaceuticals. Nuclear medicine images are obtained following administration of a radiopharmaceutical to a patient, and provide information regarding the distribution of the radiopharmaceutical within the patient. Radiopharmaceuticals are compounds that comprise a radionuclide.

Nuclear medicine images (e.g., PET scans; e.g., SPECT scans; e.g., whole-body scans; e.g. composite PET-CT images; e.g., composite SPECT-CT images) detect radiation emitted from the radionuclides of radiopharmaceuticals to form an image. The distribution of a particular radiopharmaceutical within a patient may be determined by biological mechanisms such as blood flow or perfusion, as well as by specific enzymatic or receptor binding interactions. Different radiopharmaceuticals may be designed to take advantage of different biological mechanisms and/or particular specific enzymatic or receptor binding interactions and thus, when administered to a patient, selectively concentrate within particular types of tissue and/or regions within the patient. Greater amounts of radiation are emitted from regions within the patient that have higher concentrations of radiopharmaceutical than other regions, such that these regions appear brighter in nuclear medicine images. Accordingly, intensity variations within a nuclear medicine image can be used to map the distribution of radiopharmaceutical within the patient. This mapped distribution of radiopharmaceutical within the patient can be used to, for example, infer the presence of cancerous tissue within various regions of the patient's body.

For example, upon administration to a patient, technetium 99m methylenediphosphonate (^{99m}Tc MDP) selectively accumulates within the skeletal region of the patient, in particular at sites with abnormal osteogenesis associated with malignant bone lesions. The selective concentration of radiopharmaceutical at these sites produces identifiable hotspots—localized regions of high intensity in nuclear medicine images. Accordingly, presence of malignant bone lesions associated with metastatic prostate cancer can be inferred by identifying such hotspots within a whole-body scan of the patient. Risk indices that correlate with patient overall survival and other prognostic metrics indicative of disease state, progression, treatment efficacy, and the like, can be computed based on automated analysis of intensity variations in whole-body scans obtained following administration of ^{99m}Tc MDP to a patient. In certain embodiments, other radiopharmaceuticals can also be used in a similar fashion to ^{99m}Tc MDP.

In certain embodiments, the particular radiopharmaceutical used depends on the particular nuclear medicine imaging modality used. For example ^{18}F sodium fluoride (NaF) also accumulates in bone lesions, similar to ^{99m}Tc MDP, but can be used with PET imaging. In certain embodiments, PET

imaging may also utilize a radioactive form of the vitamin choline, which is readily absorbed by prostate cancer cells.

In certain embodiments, radiopharmaceuticals that selectively bind to particular proteins or receptors of interest—particularly those whose expression is increased in cancerous tissue may be used. Such proteins or receptors of interest include, but are not limited to tumor antigens, such as CEA, which is expressed in colorectal carcinomas, Her2/neu, which is expressed in multiple cancers, BRCA 1 and BRCA 2, expressed in breast and ovarian cancers; and TRP-1 and -2, expressed in melanoma.

For example, human prostate-specific membrane antigen (PSMA) is upregulated in prostate cancer, including metastatic disease. PSMA is expressed by virtually all prostate cancers and its expression is further increased in poorly differentiated, metastatic and hormone refractory carcinomas. Accordingly, radiopharmaceuticals corresponding to PSMA binding agents (e.g., compounds that a high affinity to PSMA) labelled with one or more radionuclide(s) can be used to obtain nuclear medicine images of a patient from which the presence and/or state of prostate cancer within a variety of regions (e.g., including, but not limited to skeletal regions) of the patient can be assessed. In certain embodiments, nuclear medicine images obtained using PSMA binding agents are used to identify the presence of cancerous tissue within the prostate, when the disease is in a localized state. In certain embodiments, nuclear medicine images obtained using radiopharmaceuticals comprising PSMA binding agents are used to identify the presence of cancerous tissue within a variety of regions that include not only the prostate, but also other organs and tissue regions such as lungs, lymph nodes, and bones, as is relevant when the disease is metastatic.

In particular, upon administration to a patient, radionuclide labelled PSMA binding agents selectively accumulate within cancerous tissue, based on their affinity to PSMA. In a similar manner to that described above with regard to ^{99m}Tc MDP, the selective concentration of radionuclide labelled PSMA binding agents at particular sites within the patient produces detectable hotspots in nuclear medicine images. As PSMA binding agents concentrate within a variety of cancerous tissues and regions of the body expressing PSMA, localized cancer within a prostate of the patient and/or metastatic cancer in various regions of the patient's body can be detected, and evaluated. As described in the following, risk indices that correlate with patient overall survival and other prognostic metrics indicative of disease state, progression, treatment efficacy, and the like, can be computed based on automated analysis of intensity variations in nuclear medicine images obtained following administration of a PSMA binding agent radiopharmaceutical to a patient.

A variety of radionuclide labelled PSMA binding agents may be used as radiopharmaceutical imaging agents for nuclear medicine imaging to detect and evaluate prostate cancer. In certain embodiments, the particular radionuclide labelled PSMA binding agent that is used depends on factors such as the particular imaging modality (e.g., PET; e.g., SPECT) and the particular regions (e.g., organs) of the patient to be imaged. For example, certain radionuclide labelled PSMA binding agents are suited for PET imaging, while others are suited for SPECT imaging. For example, certain radionuclide labelled PSMA binding agents facilitate imaging a prostate of the patient, and are used primarily when the disease is localized, while others facilitate imaging organs and regions throughout the patient's body, and are useful for evaluating metastatic prostate cancer.

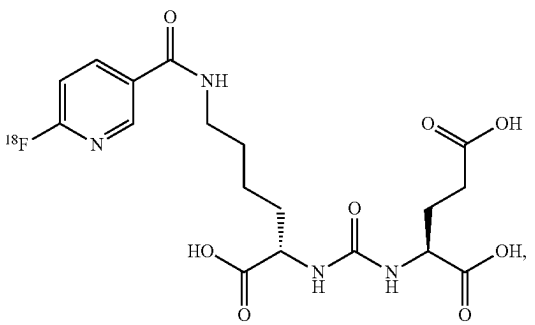
A variety of PSMA binding agents and radionuclide labelled versions thereof are described in U.S. Pat. Nos. 8,778,305, 8,211,401, and 8,962,799, each of which are incorporated herein by reference in their entireties.

i. PET Imaging Radionuclide Labelled PSMA Binding Agents

In certain embodiments, the radionuclide labelled PSMA binding agent is a radionuclide labelled PSMA binding agent appropriate for PET imaging.

In certain embodiments, the radionuclide labelled PSMA binding agent comprises [18F]DCFPyL (also referred to as PyL™; also referred to as DCFPyL-18F):

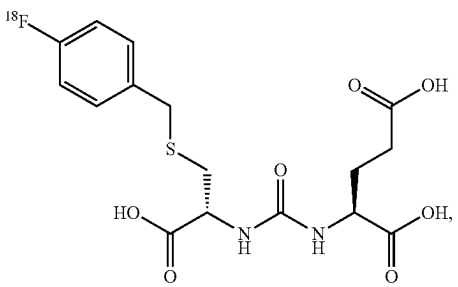
[18F]DCFPyL



or a pharmaceutically acceptable salt thereof.

In certain embodiments, the radionuclide labelled PSMA binding agent comprises [18F]DCFBC:

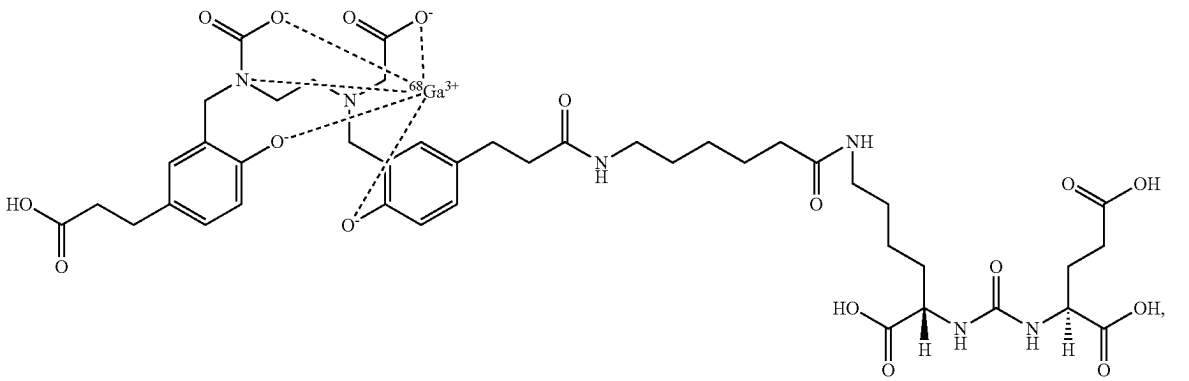
[18F]DCFBC



or a pharmaceutically acceptable salt thereof.

In certain embodiments, the radionuclide labelled PSMA binding agent comprises ^{68}Ga-PSMA-HBED-CC (also referred to as ^{68}Ga-PSMA-11):

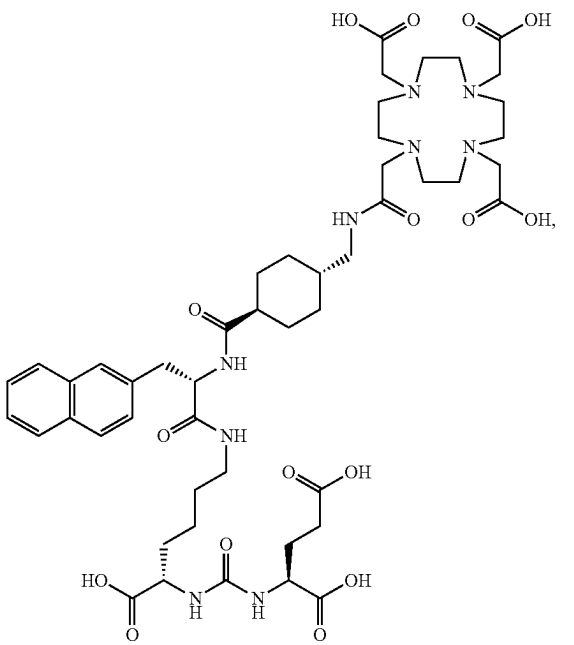
^{68}Ga-PSMA-HBED-CC



or a pharmaceutically acceptable salt thereof.

In certain embodiments, the radionuclide labelled PSMA binding agent comprises PSMA-617:

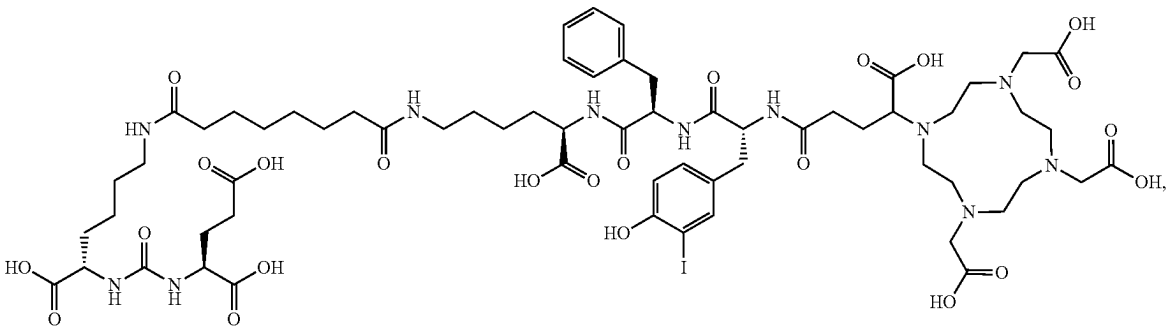
PSMA-617



or a pharmaceutically acceptable salt thereof. In certain embodiments, the radionuclide labelled PSMA binding agent comprises ^{68}Ga-PSMA-617, which is PSMA-617 labelled with ^{68}Ga, or a pharmaceutically acceptable salt thereof. In certain embodiments, the radionuclide labelled PSMA binding agent comprises ^{177}Lu-PSMA-617, which is PSMA-617 labelled with ^{177}Lu, or a pharmaceutically acceptable salt thereof.

In certain embodiments, the radionuclide labelled PSMA binding agent comprises PSMA-I&T:

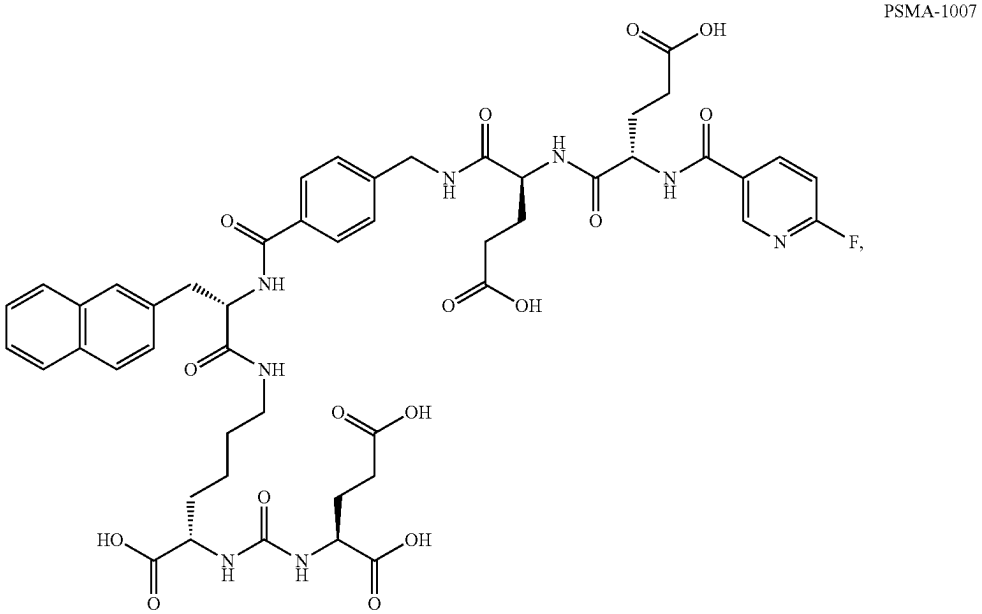
PSMA-I&T



or a pharmaceutically acceptable salt thereof. In certain embodiments, the radionuclide labelled PSMA binding agent comprises ^{68}Ga-PSMA-I&T, which is PSMA-I&T labelled with ^{68}Ga, or a pharmaceutically acceptable salt thereof.

In certain embodiments, the radionuclide labelled PSMA binding agent comprises PSMA-1007:

PSMA-1007



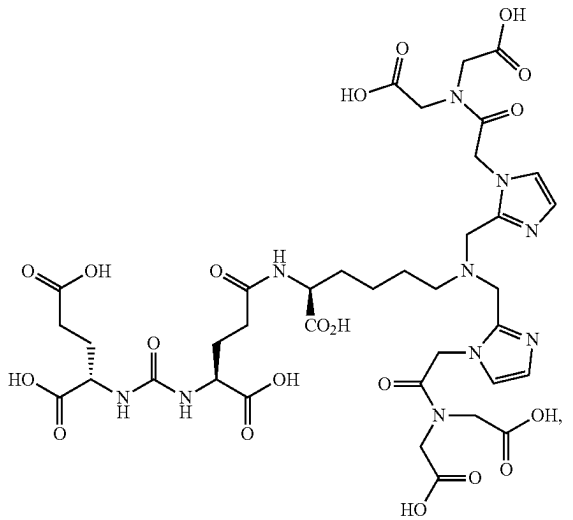
or a pharmaceutically acceptable salt thereof. In certain embodiments, the radionuclide labelled PSMA binding agent comprises ^{18}F-PSMA-1007, which is PSMA-1007 labelled with ^{18}F, or a pharmaceutically acceptable salt thereof.

ii. SPECT Imaging Radionuclide Labelled PSMA Binding Agents

In certain embodiments, the radionuclide labelled PSMA binding agent is a radionuclide labelled PSMA binding agent appropriate for SPECT imaging.

In certain embodiments, the radionuclide labelled PSMA binding agent comprises 1404 (also referred to as MIP-1404):

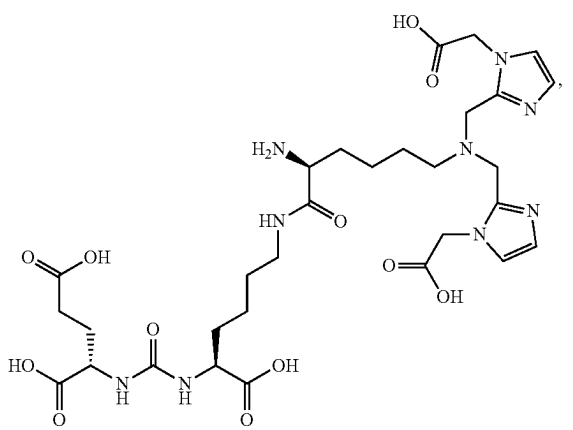
1404



or a pharmaceutically acceptable salt thereof.

In certain embodiments, the radionuclide labelled PSMA binding agent comprises 1405 (also referred to as MIP-1405):

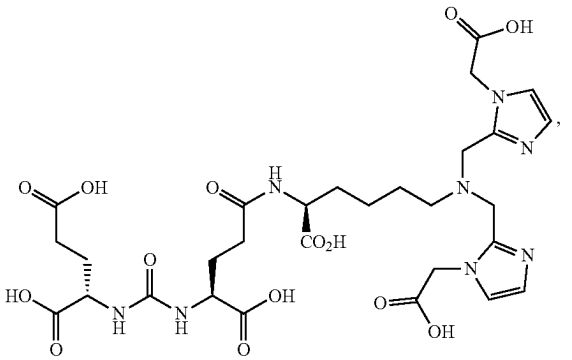
1405



or a pharmaceutically acceptable salt thereof.

In certain embodiments, the radionuclide labelled PSMA binding agent comprises 1427 (also referred to as MIP-1427):

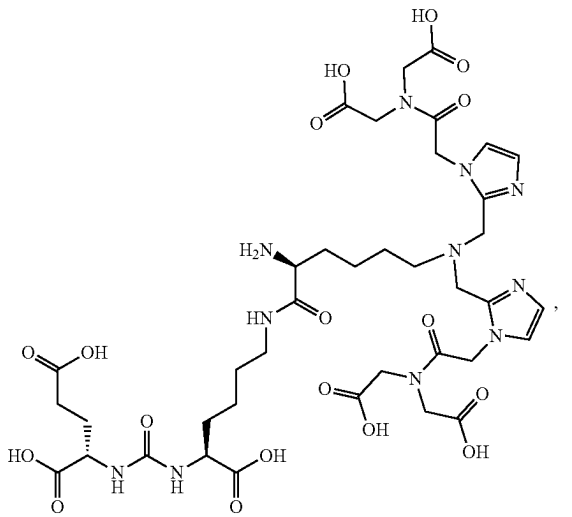
1427



or a pharmaceutically acceptable salt thereof.

In certain embodiments, the radionuclide labelled PSMA binding agent comprises 1428 (also referred to as MIP-1428):

1428

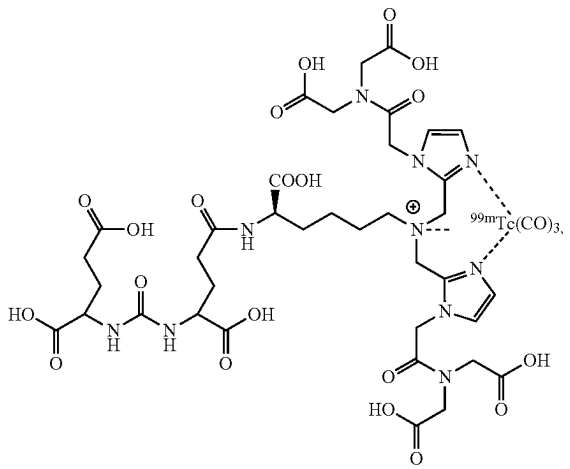


or a pharmaceutically acceptable salt thereof.

In certain embodiments, the PSMA binding agent is labelled with a radionuclide by chelating it to a radioisotope of a metal [e.g., a radioisotope of technetium (Tc) (e.g., technetium-99m (^{99m}Tc)); e.g., a radioisotope of rhenium (Re) (e.g., rhenium-188 (^{188}Re); e.g., rhenium-186 (^{186}Re)); e.g., a radioisotope of yttrium (Y) (e.g., ^{90}Y); e.g., a radioisotope of lutetium (Lu) (e.g., ^{177}Lu); e.g., a radioisotope of gallium (Ga) (e.g., ^{68}Ga; e.g., ^{67}Ga); e.g., a radioisotope of indium (e.g., ^{111}In); e.g., a radioisotope of copper (Cu) (e.g., ^{67}Cu)].

In certain embodiments, **1404** is labelled with a radionuclide (e.g., chelated to a radioisotope of a metal). In certain embodiments, the radionuclide labelled PSMA binding agent comprises ^{99m}Tc-MIP-1404, which is 1404 labelled with (e.g., chelated to) ^{99m}Tc:

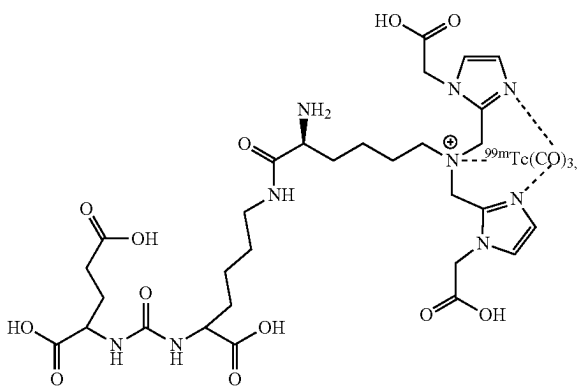
^{99m}Tc-MIP-1404



or a pharmaceutically acceptable salt thereof. In certain embodiments, 1404 may be chelated to other metal radioisotopes [e.g., a radioisotope of rhenium (Re) (e.g., rhenium-188 (^{188}Re); e.g., rhenium-186 (^{186}Re)); e.g., a radioisotope of yttrium (Y) (e.g., ^{90}Y); e.g., a radioisotope of lutetium (Lu) (e.g., ^{177}Lu); e.g., a radioisotope of gallium (Ga) (e.g., ^{68}Ga; e.g., ^{67}Ga); e.g., a radioisotope of indium (e.g., ^{111}In); e.g., a radioisotope of copper (Cu) (e.g., ^{67}Cu)] to form a compound having a structure similar to the structure shown above for ^{99m}Tc-MIP-1404, with the other metal radioisotope substituted for ^{99m}Tc.

In certain embodiments, 1405 is labelled with a radionuclide (e.g., chelated to a radioisotope of a metal). In certain embodiments, the radionuclide labelled PSMA binding agent comprises ^{99m}Tc-MIP-1405, which is 1405 labelled with (e.g., chelated to) ^{99m}Tc:

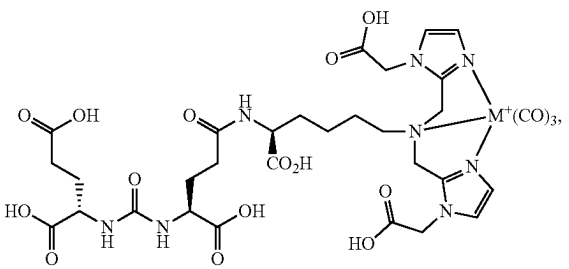
^{99m}Tc-MIP-1405



or a pharmaceutically acceptable salt thereof. In certain embodiments, 1405 may be chelated to other metal radioisotopes [e.g., a radioisotope of rhenium (Re) (e.g., rhenium-188 (^{188}Re); e.g., rhenium-186 (^{186}Re)); e.g., a radioisotope of yttrium (Y) (e.g., ^{90}Y); e.g., a radioisotope of lutetium (Lu) (e.g., ^{177}Lu); e.g., a radioisotope of gallium (Ga) (e.g., ^{68}Ga; e.g., ^{67}Ga); e.g., a radioisotope of indium (e.g., ^{111}In); e.g., a radioisotope of copper (Cu) (e.g., ^{67}Cu)] to form a compound having a structure similar to the structure shown above for ^{99m}Tc-MIP-1405, with the other metal radioisotope substituted for ^{99m}Tc.

In certain embodiments, 1427 is labelled with (e.g., chelated to) a radioisotope of a metal, to form a compound according to the formula below:

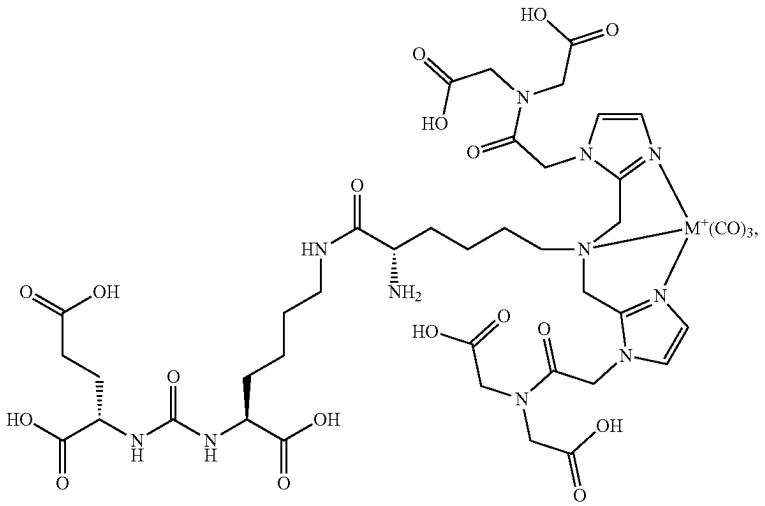
1427 chelated to a metal



or a pharmaceutically acceptable salt thereof, wherein M is a metal radioisotope [e.g., a radioisotope of technetium (Tc) (e.g., technetium-99m (^{99m}Tc)); e.g., a radioisotope of rhenium (Re) (e.g., rhenium-188 (^{188}Re); e.g., rhenium-186 (^{186}Re)); e.g., a radioisotope of yttrium (Y) (e.g., ^{90}Y); e.g., a radioisotope of lutetium (Lu) (e.g., ^{177}Lu); e.g., a radioisotope of gallium (Ga) (e.g., ^{68}Ga; e.g., ^{67}Ga); e.g., a radioisotope of indium (e.g., ^{111}In); e.g., a radioisotope of copper (Cu) (e.g., ^{67}Cu)] with which 1427 is labelled.

In certain embodiments, 1428 is labelled with (e.g., chelated to) a radioisotope of a metal, to form a compound according to the formula below:

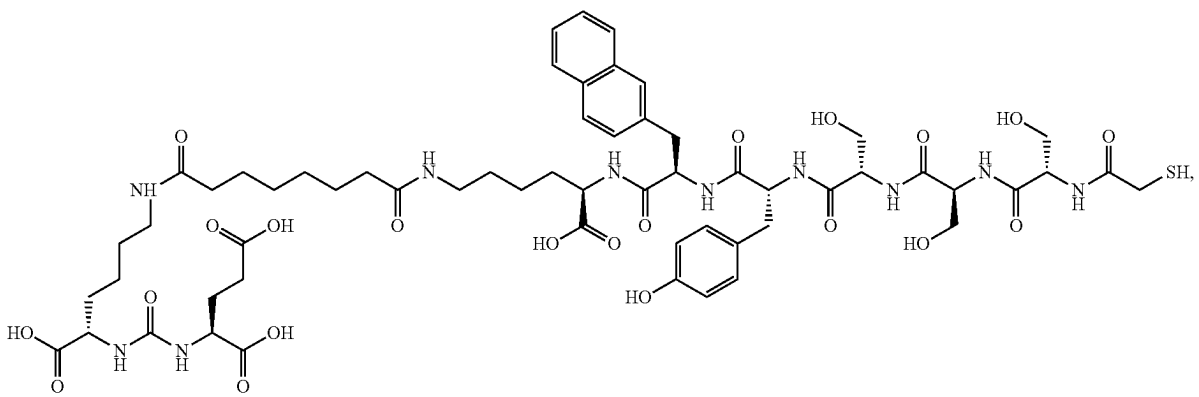
1428 chelated to a metal



or a pharmaceutically acceptable salt thereof, wherein M is a metal radioisotope [e.g., a radioisotope of technetium (Tc) (e.g., technetium-99m (^{99m}Tc)); e.g., a radioisotope of rhenium (Re) (e.g., rhenium-188 (^{188}Re); e.g., rhenium-186 (^{186}Re)); e.g., a radioisotope of yttrium (Y) (e.g., ^{90}Y); e.g., a radioisotope of lutetium (Lu) (e.g., ^{177}Lu); e.g., a radioisotope of gallium (Ga) (e.g., ^{68}Ga; e.g., ^{67}Ga); e.g., a radioisotope of indium (e.g., ^{111}In); e.g., a radioisotope of copper (Cu) (e.g., ^{67}Cu)] with which 1428 is labelled.

In certain embodiments, the radionuclide labelled PSMA binding agent comprises PSMA I&S:

PSMA I&S



or a pharmaceutically acceptable salt thereof. In certain embodiments, the radionuclide labelled PSMA binding agent comprises ^{99m}Tc-PSMA I&S, which is PSMA I&S labelled with ^{99m}Tc, or a pharmaceutically acceptable salt thereof.

E. Computer System and Network Architecture

As shown in FIG. **17**, an implementation of a network environment **1700** for use in providing systems, methods, and architectures described herein is shown and described. In brief overview, referring now to FIG. **17**, a block diagram of an exemplary cloud computing environment **1700** is shown and described. The cloud computing environment **1700** may include one or more resource providers **1702***a*, **1702***b*, **1702***c* (collectively, **1702**). Each resource provider **1702** may include computing resources. In some implementations, computing resources may include any hardware and/or software used to process data. For example, computing resources may include hardware and/or software capable of executing algorithms, computer programs, and/or computer applications. In some implementations, exemplary computing resources may include application servers and/or databases with storage and retrieval capabilities. Each resource provider **1702** may be connected to any other resource provider **1702** in the cloud computing environment **1700**. In some implementations, the resource providers **1702** may be connected over a computer network **1708**. Each resource provider **1702** may be connected to one or more computing device **1704***a*, **1704***b*, **1704***c* (collectively, **1704**), over the computer network **1708**.

The cloud computing environment **1700** may include a resource manager **1706**. The resource manager **1706** may be connected to the resource providers **1702** and the computing

devices **1704** over the computer network **1708**. In some implementations, the resource manager **1706** may facilitate the provision of computing resources by one or more resource providers **1702** to one or more computing devices **1704**. The resource manager **1706** may receive a request for a computing resource from a particular computing device **1704**. The resource manager **1706** may identify one or more resource providers **1702** capable of providing the computing resource requested by the computing device **1704**. The resource manager **1706** may select a resource provider **1702** to provide the computing resource. The resource manager **1706** may facilitate a connection between the resource provider **1702** and a particular computing device **1704**. In some implementations, the resource manager **1706** may establish a connection between a particular resource provider **1702** and a particular computing device **1704**. In some implementations, the resource manager **1706** may redirect a particular computing device **1704** to a particular resource provider **1702** with the requested computing resource.

FIG. **18** shows an example of a computing device **1800** and a mobile computing device **1850** that can be used to implement the techniques described in this disclosure. The computing device **1800** is intended to represent various forms of digital computers, such as laptops, desktops, workstations, personal digital assistants, servers, blade servers, mainframes, and other appropriate computers. The mobile computing device **1850** is intended to represent various forms of mobile devices, such as personal digital assistants, cellular telephones, smart-phones, and other similar computing devices. The components shown here, their connections and relationships, and their functions, are meant to be examples only, and are not meant to be limiting.

The computing device **1800** includes a processor **1802**, a memory **1804**, a storage device **1806**, a high-speed interface **1808** connecting to the memory **1804** and multiple high-speed expansion ports **1810**, and a low-speed interface **1812** connecting to a low-speed expansion port **1814** and the storage device **1806**. Each of the processor **1802**, the memory **1804**, the storage device **1806**, the high-speed interface **1808**, the high-speed expansion ports **1810**, and the low-speed interface **1812**, are interconnected using various busses, and may be mounted on a common motherboard or in other manners as appropriate. The processor **1802** can process instructions for execution within the computing device **1800**, including instructions stored in the memory **1804** or on the storage device **1806** to display graphical information for a GUI on an external input/output device, such as a display **1816** coupled to the high-speed interface **1808**. In other implementations, multiple processors and/or multiple buses may be used, as appropriate, along with multiple memories and types of memory. Also, multiple computing devices may be connected, with each device providing portions of the necessary operations (e.g., as a server bank, a group of blade servers, or a multi-processor system). Thus, as the term is used herein, where a plurality of functions are described as being performed by "a processor", this encompasses embodiments wherein the plurality of functions are performed by any number of processors (one or more) of any number of computing devices (one or more). Furthermore, where a function is described as being performed by "a processor", this encompasses embodiments wherein the function is performed by any number of processors (one or more) of any number of computing devices (one or more) (e.g., in a distributed computing system).

The memory **1804** stores information within the computing device **1800**. In some implementations, the memory **1804** is a volatile memory unit or units. In some implementations, the memory **1804** is a non-volatile memory unit or units. The memory **1804** may also be another form of computer-readable medium, such as a magnetic or optical disk.

The storage device **1806** is capable of providing mass storage for the computing device **1800**. In some implementations, the storage device **1806** may be or contain a computer-readable medium, such as a floppy disk device, a hard disk device, an optical disk device, or a tape device, a flash memory or other similar solid state memory device, or an array of devices, including devices in a storage area network or other configurations. Instructions can be stored in an information carrier. The instructions, when executed by one or more processing devices (for example, processor **1802**), perform one or more methods, such as those described above. The instructions can also be stored by one or more storage devices such as computer- or machine-readable mediums (for example, the memory **1804**, the storage device **1806**, or memory on the processor **1802**).

The high-speed interface **1808** manages bandwidth-intensive operations for the computing device **1800**, while the low-speed interface **1812** manages lower bandwidth-intensive operations. Such allocation of functions is an example only. In some implementations, the high-speed interface **1808** is coupled to the memory **1804**, the display **1816** (e.g., through a graphics processor or accelerator), and to the high-speed expansion ports **1810**, which may accept various expansion cards (not shown). In the implementation, the low-speed interface **1812** is coupled to the storage device **1806** and the low-speed expansion port **1814**. The low-speed expansion port **1814**, which may include various communication ports (e.g., USB, Bluetooth®, Ethernet, wireless Ethernet) may be coupled to one or more input/output devices, such as a keyboard, a pointing device, a scanner, or a networking device such as a switch or router, e.g., through a network adapter.

The computing device **1800** may be implemented in a number of different forms, as shown in the figure. For example, it may be implemented as a standard server **1820**, or multiple times in a group of such servers. In addition, it may be implemented in a personal computer such as a laptop computer **1822**. It may also be implemented as part of a rack server system **1824**. Alternatively, components from the computing device **1800** may be combined with other components in a mobile device (not shown), such as a mobile computing device **1850**. Each of such devices may contain one or more of the computing device **1800** and the mobile computing device **1850**, and an entire system may be made up of multiple computing devices communicating with each other.

The mobile computing device **1850** includes a processor **1852**, a memory **1864**, an input/output device such as a display **1854**, a communication interface **1866**, and a transceiver **1868**, among other components. The mobile computing device **1850** may also be provided with a storage device, such as a micro-drive or other device, to provide additional storage. Each of the processor **1852**, the memory **1864**, the display **1854**, the communication interface **1866**, and the transceiver **1868**, are interconnected using various buses, and several of the components may be mounted on a common motherboard or in other manners as appropriate.

The processor **1852** can execute instructions within the mobile computing device **1850**, including instructions stored in the memory **1864**. The processor **1852** may be implemented as a chipset of chips that include separate and multiple analog and digital processors. The processor **1852** may provide, for example, for coordination of the other

components of the mobile computing device **1850**, such as control of user interfaces, applications run by the mobile computing device **1850**, and wireless communication by the mobile computing device **1850**.

The processor **1852** may communicate with a user through a control interface **1858** and a display interface **1856** coupled to the display **1854**. The display **1854** may be, for example, a TFT (Thin-Film-Transistor Liquid Crystal Display) display or an OLED (Organic Light Emitting Diode) display, or other appropriate display technology. The display interface **1856** may comprise appropriate circuitry for driving the display **1854** to present graphical and other information to a user. The control interface **1858** may receive commands from a user and convert them for submission to the processor **1852**. In addition, an external interface **1862** may provide communication with the processor **1852**, so as to enable near area communication of the mobile computing device **1850** with other devices. The external interface **1862** may provide, for example, for wired communication in some implementations, or for wireless communication in other implementations, and multiple interfaces may also be used.

The memory **1864** stores information within the mobile computing device **1850**. The memory **1864** can be implemented as one or more of a computer-readable medium or media, a volatile memory unit or units, or a non-volatile memory unit or units. An expansion memory **1874** may also be provided and connected to the mobile computing device **1850** through an expansion interface **1872**, which may include, for example, a SIMM (Single In Line Memory Module) card interface. The expansion memory **1874** may provide extra storage space for the mobile computing device **1850**, or may also store applications or other information for the mobile computing device **1850**. Specifically, the expansion memory **1874** may include instructions to carry out or supplement the processes described above, and may include secure information also. Thus, for example, the expansion memory **1874** may be provide as a security module for the mobile computing device **1850**, and may be programmed with instructions that permit secure use of the mobile computing device **1850**. In addition, secure applications may be provided via the SIMM cards, along with additional information, such as placing identifying information on the SIMM card in a non-hackable manner.

The memory may include, for example, flash memory and/or NVRAM memory (non-volatile random access memory), as discussed below. In some implementations, instructions are stored in an information carrier. that the instructions, when executed by one or more processing devices (for example, processor **1852**), perform one or more methods, such as those described above. The instructions can also be stored by one or more storage devices, such as one or more computer- or machine-readable mediums (for example, the memory **1864**, the expansion memory **1874**, or memory on the processor **1852**). In some implementations, the instructions can be received in a propagated signal, for example, over the transceiver **1868** or the external interface **1862**.

The mobile computing device **1850** may communicate wirelessly through the communication interface **1866**, which may include digital signal processing circuitry where necessary. The communication interface **1866** may provide for communications under various modes or protocols, such as GSM voice calls (Global System for Mobile communications), SMS (Short Message Service), EMS (Enhanced Messaging Service), or MMS messaging (Multimedia Messaging Service), CDMA (code division multiple access), TDMA (time division multiple access), PDC (Personal Digital Cellular), WCDMA (Wideband Code Division Multiple Access), CDMA2000, or GPRS (General Packet Radio Service), among others. Such communication may occur, for example, through the transceiver **1868** using a radio-frequency. In addition, short-range communication may occur, such as using a Bluetooth®, Wi-Fi™, or other such transceiver (not shown). In addition, a GPS (Global Positioning System) receiver module **1870** may provide additional navigation- and location-related wireless data to the mobile computing device **1850**, which may be used as appropriate by applications running on the mobile computing device **1850**.

The mobile computing device **1850** may also communicate audibly using an audio codec **1860**, which may receive spoken information from a user and convert it to usable digital information. The audio codec **1860** may likewise generate audible sound for a user, such as through a speaker, e.g., in a handset of the mobile computing device **1850**. Such sound may include sound from voice telephone calls, may include recorded sound (e.g., voice messages, music files, etc.) and may also include sound generated by applications operating on the mobile computing device **1850**.

The mobile computing device **1850** may be implemented in a number of different forms, as shown in the figure. For example, it may be implemented as a cellular telephone **1880**. It may also be implemented as part of a smart-phone **1882**, personal digital assistant, or other similar mobile device.

Various implementations of the systems and techniques described here can be realized in digital electronic circuitry, integrated circuitry, specially designed ASICs (application specific integrated circuits), computer hardware, firmware, software, and/or combinations thereof. These various implementations can include implementation in one or more computer programs that are executable and/or interpretable on a programmable system including at least one programmable processor, which may be special or general purpose, coupled to receive data and instructions from, and to transmit data and instructions to, a storage system, at least one input device, and at least one output device.

These computer programs (also known as programs, software, software applications or code) include machine instructions for a programmable processor, and can be implemented in a high-level procedural and/or object-oriented programming language, and/or in assembly/machine language. As used herein, the terms machine-readable medium and computer-readable medium refer to any computer program product, apparatus and/or device (e.g., magnetic discs, optical disks, memory, Programmable Logic Devices (PLDs)) used to provide machine instructions and/or data to a programmable processor, including a machine-readable medium that receives machine instructions as a machine-readable signal. The term machine-readable signal refers to any signal used to provide machine instructions and/or data to a programmable processor.

To provide for interaction with a user, the systems and techniques described here can be implemented on a computer having a display device (e.g., a CRT (cathode ray tube) or LCD (liquid crystal display) monitor) for displaying information to the user and a keyboard and a pointing device (e.g., a mouse or a trackball) by which the user can provide input to the computer. Other kinds of devices can be used to provide for interaction with a user as well; for example, feedback provided to the user can be any form of sensory feedback (e.g., visual feedback, auditory feedback, or tactile feedback); and input from the user can be received in any form, including acoustic, speech, or tactile input.

The systems and techniques described here can be implemented in a computing system that includes a back end component (e.g., as a data server), or that includes a middleware component (e.g., an application server), or that includes a front end component (e.g., a client computer having a graphical user interface or a Web browser through which a user can interact with an implementation of the systems and techniques described here), or any combination of such back end, middleware, or front end components. The components of the system can be interconnected by any form or medium of digital data communication (e.g., a communication network). Examples of communication networks include a local area network (LAN), a wide area network (WAN), and the Internet.

The computing system can include clients and servers. A client and server are generally remote from each other and typically interact through a communication network. The relationship of client and server arises by virtue of computer programs running on the respective computers and having a client-server relationship to each other.

In some implementations, the various modules described herein can be separated, combined or incorporated into single or combined modules. The modules depicted in the figures are not intended to limit the systems described herein to the software architectures shown therein.

Elements of different implementations described herein may be combined to form other implementations not specifically set forth above. Elements may be left out of the processes, computer programs, databases, etc. described herein without adversely affecting their operation. In addition, the logic flows depicted in the figures do not require the particular order shown, or sequential order, to achieve desirable results. Various separate elements may be combined into one or more individual elements to perform the functions described herein.

Throughout the description, where apparatus and systems are described as having, including, or comprising specific components, or where processes and methods are described as having, including, or comprising specific steps, it is contemplated that, additionally, there are apparatus, and systems of the present invention that consist essentially of, or consist of, the recited components, and that there are processes and methods according to the present invention that consist essentially of, or consist of, the recited processing steps.

It should be understood that the order of steps or order for performing certain action is immaterial so long as the invention remains operable. Moreover, two or more steps or actions may be conducted simultaneously.

While the invention has been particularly shown and described with reference to specific preferred embodiments, it should be understood by those skilled in the art that various changes in form and detail may be made therein without departing from the spirit and scope of the invention as defined by the appended claims.

While the invention has been particularly shown and described with reference to specific preferred embodiments, it should be understood by those skilled in the art that various changes in form and detail may be made therein without departing from the spirit and scope of the invention as defined by the appended claims.

What is claimed is:

1. A method for automatically processing 3D images to identify, and measure uptake of radiopharmaceutical in, cancerous lesions within a subject having or at risk for a cancer, the method comprising:

(a) receiving, by a processor of a computing device, a 3D anatomical image of a subject obtained using an anatomical imaging modality, wherein the 3D anatomical image comprises a graphical representation of tissue within the subject;

(b) automatically identifying, by the processor, using one or more machine learning modules, within the 3D anatomical image:

a first skeletal volume comprising a graphical representation of one or more bones of the subject;

a first aorta volume comprising a graphical representation of at least a portion of an aorta of the subject; and

a first liver volume comprising a graphical representation of a liver of the subject;

(c) determining, by the processor, a 3D segmentation map representing a plurality of 3D segmentation masks, including a skeletal mask representing the identified first skeletal volume, an aorta mask representing the identified first aorta volume, and a liver mask representing the identified first liver volume;

(d) receiving, by the processor, a 3D functional image of the subject obtained using a functional imaging modality;

(e) automatically identifying, within the 3D functional image, using the 3D segmentation map:

a second skeletal volume corresponding to the first identified skeletal volume, within the 3D anatomical image;

a second aorta volume corresponding to the first aorta volume, identified within the 3D anatomical image; and

a second liver volume corresponding to the first liver volume, identified within the 3D anatomical image;

(f) automatically detecting, by the processor, within the second skeletal volume, one or more hotspots determined to represent lesions based on intensities of voxels within the second skeletal volume; and

(g) determining, by the processor, for each of the one or more detected hotspots, an individual hotspot index value by:

determining an aorta reference intensity level based on a measure of intensity of voxels within the second aorta volume;

determining a liver reference intensity level based on a measure of intensity of voxels within the second liver volume; and

for each individual detected hotspot:

determining a corresponding individual hotspot intensity level based on a measure of intensity of voxels of the detected hotspot; and

determining a corresponding individual hotspot index level from the individual hotspot intensity level, the aorta reference intensity level, and the liver reference intensity level.

2. The method of claim **1**, comprising determining, by the processor, an overall index value indicative of a cancer status of the subject based on the individual hotspot index values of at least a portion of the one or more detected hotspots.

3. The method of claim **1**, wherein the subject has or is at risk for prostate cancer.

4. The method of claim **1**, wherein:

step (b) comprises automatically identifying, within the 3D anatomical image, a first prostate volume comprising a graphical representation of a prostate of the subject,

the 3D segmentation map determined at step (c) further includes a prostate mask representing the identified first prostate volume,

step (e) comprises automatically identifying, within the 3D functional image, a second prostate volume corresponding to the first identified prostate volume, within the 3D anatomical image,

step (f) comprises automatically detecting one or more hotspots in the second prostate volume, and the method further comprises:

determining, by the processor, (i) an overall bone index value indicative of a lesion content in the one or more bones of the subject based on the individual hotspot index values of at least a portion of the one or more detected hotspots located in the second skeletal volume and (ii) an overall prostate index value indicative of a lesion content in the prostate of the subject based on the individual hotspot index values of at least a portion of the one or more detected hotspots located in the second prostate volume.

5. The method of claim **1**, wherein the subject has or is at risk for metastatic cancer.

6. A system for automatically processing 3D images to identify, and measure uptake of radiopharmaceutical in, cancerous lesions within a subject having or at risk for a cancer, the system comprising:

a processor of a computing device; and

a memory having instructions stored thereon, wherein the instructions, when executed by the processor, cause the processor to:

(a) receive a 3D anatomical image of a subject obtained using an anatomical imaging modality, wherein the 3D anatomical image comprises a graphical representation of tissue within the subject;

(b) automatically identify using one or more machine learning modules, within the 3D anatomical image:

a first skeletal volume comprising a graphical representation of one or more bones of the subject;

a first aorta volume comprising a graphical representation of at least a portion of an aorta of the subject; and

a first liver volume comprising a graphical representation of a liver of the subject;

(c) determine a 3D segmentation map representing a plurality of 3D segmentation masks, including a skeletal mask representing the identified first skeletal volume, an aorta mask representing the identified first aorta volume, and a liver mask representing the identified first liver volume;

(d) receive a 3D functional image of the subject obtained using a functional imaging modality;

(e) automatically identify, within the 3D functional image, using the 3D segmentation map:

a second skeletal volume corresponding to the first identified skeletal volume, within the 3D anatomical image;

a second aorta volume corresponding to the first aorta volume, identified within the 3D anatomical image; and

a second liver volume corresponding to the first liver volume, identified within the 3D anatomical image;

(f) automatically detect, within the second skeletal volume, one or more hotspots determined to represent lesions based on intensities of voxels within the second skeletal volume; and

(g) determine, for each of the one or more detected hotspots, an individual hotspot index value by:

determining an aorta reference intensity level based on a measure of intensity of voxels within the second aorta volume;

determining a liver reference intensity level based on a measure of intensity of voxels within the second liver volume; and

for each individual detected hotspot:

determining a corresponding individual hotspot intensity level based on a measure of intensity of voxels of the detected hotspot; and

determining a corresponding individual hotspot index level from the individual hotspot intensity level, the aorta reference intensity level, and the liver reference intensity level.

7. The system of claim **6**, wherein the instructions cause the processor to determine an overall index value indicative of a cancer status of the subject based on the individual hotspot index values of at least a portion of the one or more detected hotspots.

8. The system of claim **6**, wherein the subject has or is at risk for prostate cancer.

9. The system of claim **6**, wherein the instructions cause the processor to:

at step (b), automatically identify, within the 3D anatomical image, a first prostate volume comprising a graphical representation of a prostate of the subject;

at step (c), include a prostate mask representing the identified first prostate volume in the determined 3D segmentation map;

at step (e), automatically identify, within the 3D functional image, a second prostate volume corresponding to the first identified prostate volume, within the 3D anatomical image,

at step (f), automatically detect one or more hotspots in the second prostate volume; and

determine (i) an overall bone index value indicative of a lesion content in the one or more bones of the subject based on the individual hotspot index values of at least a portion of the one or more detected hotspots located in the second skeletal volume and (ii) an overall prostate index value indicative of a lesion content in the prostate of the subject based on the individual hotspot index values of at least a portion of the one or more detected hotspots located in the second prostate volume.

10. The system of claim **6**, wherein the subject has or is at risk for metastatic cancer.

* * * * *

EXHIBIT 6

US011721428B2

(12) **United States Patent**
Brynolfsson et al.

(10) **Patent No.: US 11,721,428 B2**
(45) **Date of Patent: Aug. 8, 2023**

(54) **SYSTEMS AND METHODS FOR ARTIFICIAL INTELLIGENCE-BASED IMAGE ANALYSIS FOR DETECTION AND CHARACTERIZATION OF LESIONS**

(71) Applicant: **EXINI Diagnostics AB**, Lund (SE)

(72) Inventors: **Johan Martin Brynolfsson**, Helsingborg (SE); **Kerstin Elsa Maria Johnsson**, Lund (SE); **Hannicka Maria Eleonora Sahlstedt**, Malmö (SE)

(73) Assignee: **EXINI Diagnostics AB**, Lund (SE)

(*) Notice: Subject to any disclaimer, the term of this patent is extended or adjusted under 35 U.S.C. 154(b) by 153 days.

(21) Appl. No.: **17/008,411**

(22) Filed: **Aug. 31, 2020**

(65) **Prior Publication Data**

US 2022/0005586 A1 Jan. 6, 2022

Related U.S. Application Data

(60) Provisional application No. 63/048,436, filed on Jul. 6, 2020.

(51) **Int. Cl.**
G16H 30/40 (2018.01)
G16H 50/20 (2018.01)
(Continued)

(52) **U.S. Cl.**
CPC ***G16H 30/40*** (2018.01); ***G06T 7/0012*** (2013.01); ***G06T 7/11*** (2017.01); ***G16H 50/20*** (2018.01);
(Continued)

(58) **Field of Classification Search**
None
See application file for complete search history.

(56) **References Cited**

U.S. PATENT DOCUMENTS

7,450,747 B2 11/2008 Jabri et al.
7,751,605 B2 7/2010 Gündel et al.
(Continued)

FOREIGN PATENT DOCUMENTS

CN 101528267 A 9/2009
CN 102361594 A 2/2012
(Continued)

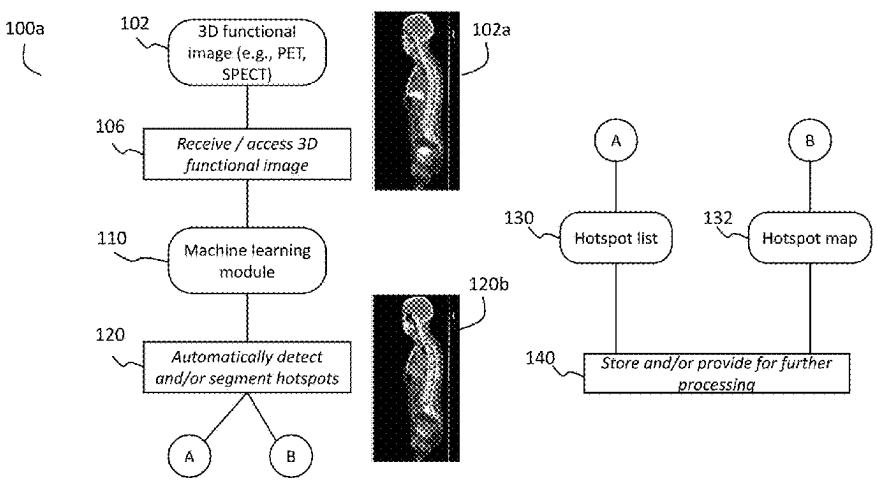
OTHER PUBLICATIONS

Ali, A. et al., The Automated Bone Scan Index as a Predictor of Response to Prostate Radiotherapy in Men with Newly Diagnosed Metastatic Prostate Cancer: An Exploratory Analysis of STAMPEDE's "M1|RT Comparison", European Urology Oncology 3:412-419. (2020).
(Continued)

Primary Examiner — Vu Le
Assistant Examiner — Courtney Joan Nelson
(74) *Attorney, Agent, or Firm* — Choate, Hall & Stewart LLP; William R. Haulbrook; Ronen Adato

(57) **ABSTRACT**

Presented herein are systems and methods that provide for improved detection and characterization of lesions within a subject via automated analysis of nuclear medicine images, such as positron emission tomography (PET) and single photon emission computed tomography (SPECT) images. In particular, in certain embodiments, the approaches described herein leverage artificial intelligence (AI) to detect regions of 3D nuclear medicine images corresponding to hotspots that represent potential cancerous lesions in the subject. The machine learning modules may be used not only to detect presence and locations of such regions within an image, but also to segment the region corresponding to the lesion and/or classify such hotspots based on the likelihood that they are indicative of a true, underlying cancerous lesion. This AI-based lesion detection, segmentation, and classification can
(Continued)



provide a basis for further characterization of lesions, overall tumor burden, and estimation of disease severity and risk.

24 Claims, 18 Drawing Sheets
(9 of 18 Drawing Sheet(s) Filed in Color)

(51) **Int. Cl.**
G16H 50/30 (2018.01)
G06T 7/11 (2017.01)
G06T 7/00 (2017.01)

(52) **U.S. Cl.**
CPC ... ***G16H 50/30*** (2018.01); *G06T 2207/10072* (2013.01); *G06T 2207/30056* (2013.01); *G06T 2207/30096* (2013.01)

(56) **References Cited**

U.S. PATENT DOCUMENTS

7,935,055	B2	5/2011	Burckhardt	
7,970,194	B2	6/2011	Kimura	
8,199,985	B2	6/2012	Jakobsson et al.	
8,211,401	B2	7/2012	Babich et al.	
8,467,856	B2	6/2013	Renisch et al.	
8,538,166	B2	9/2013	Gordon et al.	
8,705,887	B2	4/2014	Ma et al.	
8,778,305	B2	7/2014	Pomper et al.	
8,855,387	B2	10/2014	Hamadeh et al.	
8,962,799	B2	2/2015	Babich et al.	
9,002,081	B2	4/2015	Brown	
9,466,133	B2	10/2016	Sowards-Emmerd et al.	
9,710,915	B2	7/2017	Firouzian et al.	
9,721,340	B2	8/2017	Gillies et al.	
10,058,393	B2	8/2018	Bonutti et al.	
10,223,610	B1	3/2019	Akselrod-Ballin et al.	
10,311,971	B2	6/2019	Opfer et al.	
10,330,763	B2	6/2019	James et al.	
10,339,653	B2	7/2019	Gillies et al.	
10,340,044	B2	7/2019	Yao et al.	
10,340,046	B2	7/2019	Baker	
RE47,609	E	9/2019	Hamadeh et al.	
10,492,723	B2	12/2019	Madabhushi et al.	
10,600,184	B2	3/2020	Golden et al.	
10,665,346	B2	5/2020	Baker	
10,748,652	B2	8/2020	Yao et al.	
10,762,993	B2	9/2020	Baker	
10,818,386	B2	10/2020	Yao et al.	
10,943,681	B2	3/2021	Yao et al.	
10,973,486	B2	4/2021	Sjostrand et al.	
11,011,257	B2	5/2021	Lints et al.	
11,321,844	B2	5/2022	Johnsson et al.	
11,386,988	B2	7/2022	Johnsson et al.	
11,424,035	B2	8/2022	Baker	
2003/0215120	A1	11/2003	Uppaluri et al.	
2005/0281381	A1	12/2005	Guendel	
2006/0062425	A1	3/2006	Shen et al.	
2006/0064396	A1	3/2006	Wei et al.	
2006/0078183	A1	4/2006	deCharms	
2007/0081712	A1*	4/2007	Huang	G06T 7/38 382/128
2007/0081713	A1	4/2007	Jerebko	
2007/0100225	A1	5/2007	Maschke	
2007/0115204	A1	5/2007	Budz et al.	
2008/0027315	A1	1/2008	McGinnis	
2009/0309874	A1	12/2009	Salganicoff et al.	
2010/0215581	A1	8/2010	Hoffmann	
2010/0266170	A1*	10/2010	Khamene	G06T 7/149 382/128
2010/0322488	A1	12/2010	Virtue et al.	
2011/0063288	A1	3/2011	Valadez	
2011/0255763	A1	10/2011	Bogoni et al.	
2012/0123253	A1	5/2012	Renisch et al.	
2013/0038707	A1	2/2013	Cunningham et al.	
2013/0094704	A1	4/2013	Hamadeh et al.	
2013/0129168	A1	5/2013	Ross	
2013/0211231	A1	8/2013	Sundarapandian et al.	
2013/0281841	A1	10/2013	Everett et al.	
2015/0110716	A1	4/2015	Armor	
2015/0331995	A1	11/2015	Zhao et al.	
2016/0203263	A1	7/2016	Maier et al.	
2016/0335395	A1	11/2016	Wu et al.	
2017/0083682	A1	3/2017	McNutt et al.	
2018/0144828	A1	5/2018	Baker	
2018/0259608	A1	9/2018	Golden et al.	
2018/0360402	A1	12/2018	Carmi	
2019/0038239	A1	2/2019	Flohr et al.	
2019/0105009	A1	4/2019	Siemionow et al.	
2019/0209116	A1	7/2019	Sjostrand et al.	
2019/0388049	A1	12/2019	Gupta et al.	
2020/0027559	A1	1/2020	Baker	
2020/0051238	A1	2/2020	El Harouni et al.	
2020/0074634	A1	3/2020	Kecskemethy et al.	
2020/0085382	A1	3/2020	Taerum et al.	
2020/0126666	A1	4/2020	Baker	
2020/0170604	A1	6/2020	Yildirim et al.	
2020/0193594	A1	6/2020	Georgescu et al.	
2020/0193603	A1	6/2020	Golden et al.	
2020/0245960	A1	8/2020	Richter et al.	
2020/0315455	A1	10/2020	Lee et al.	
2020/0337658	A1	10/2020	Sjostrand et al.	
2020/0342600	A1	10/2020	Sjostrand et al.	
2020/0352518	A1	11/2020	Lyman et al.	
2020/0357117	A1	11/2020	Lyman et al.	
2020/0357118	A1	11/2020	Yao et al.	
2020/0357521	A1	11/2020	Baker	
2021/0032206	A1	2/2021	Neumaier et al.	
2021/0082547	A1	3/2021	Yao et al.	
2021/0093249	A1	4/2021	Anand et al.	
2021/0183485	A1	6/2021	Yao et al.	
2021/0233633	A1	7/2021	Lints et al.	
2021/0334974	A1	10/2021	Johnsson et al.	
2021/0335480	A1	10/2021	Johnsson et al.	

FOREIGN PATENT DOCUMENTS

CN	103607954	A	2/2014	
EP	1426903	A2	6/2004	
EP	1508872	A1	2/2005	
EP	3043318	A1	7/2016	
JP	2010-029481	A	2/2010	
JP	6013042	B2	10/2016	
JP	6170284	B2	7/2017	
SE	524500	C2	8/2004	
WO	WO-99/05503	A2	2/1999	
WO	WO-2007/062135	A2	5/2007	
WO	WO-2009/084995	A1	7/2009	
WO	WO-2011/077303	A1	6/2011	
WO	WO-2015/058151	A2	4/2015	
WO	WO-2018015953	A1 *	1/2018	G06T 5/002
WO	WO-2018/081354	A1	5/2018	
WO	WO-2018081354	A1 *	5/2018	A61B 6/037
WO	WO-2019/103912	A2	5/2019	
WO	WO-2019/136349	A2	7/2019	
WO	WO-2019136349	A2 *	7/2019	A61B 6/032
WO	WO-2020/144134	A1	7/2020	
WO	WO-2020/146032	A1	7/2020	
WO	WO-2020/190821	A1	9/2020	
WO	WO-2020/219619	A1	10/2020	
WO	WO-2020/219620	A1	10/2020	
WO	WO-2021/061315	A1	4/2021	
WO	WO-2022/008374	A1	1/2022	

OTHER PUBLICATIONS

Ceci, F. et al., E-PSMA: the EANM standardized reporting guidelines v1.0 for PSMA-PET, European Journal of Nuclear Medicine and Molecular Imaging, 48:1626-1638, (2021).
International Search Report, International Application No. PCT/EP2021/068337, 7 pages, (dated Dec. 9, 2021).

(56) **References Cited**

OTHER PUBLICATIONS

Johnsson, K. et al., Analytical performance of aPROMISE: automated anatomic contextualization, detection, and quantification of [18F]DCFPyL (PSMA) imaging for standardized reporting, European Journal of Nuclear Medicin and Molecular Imaging, 11 pages, Aug. 31, 2021, doi: 10.1007/s00259-021-05497-8. Epub ahead of print. PMID: 34463809.

Matsubara, N. et al, A Phase II, Randomized, Open-Label, Multiarm Study of TAS-115 for Castration-Resistant Prostate Cancer Patients With Bone Metastases, Clinical Genitourinary Cancer, 000(xxx):1-10, (2021).

Nickols, N. et al., aPROMISE: A Novel Automated-PROMISE platform to Standardize Evaluation of Tumor Burden in 18F-DCFPyL (PSMA) images of Veterans with Prostate Cancer, Journal of Nuclear Medicine, 26 pages, May 28, 2021, doi: 10.2967/jnumed.120.261863.

Partial Search Report and Provisional Opinion, International Application No. PCT/EP2021/068337, 8 pages, dated Oct. 18, 2021.

Paschalis, A. et al., Prostate-specific Membrane Antigen Heterogeneity and DNA Repair Defects in Prostate Cancer, European Urology, 76(4):469-478, (2019).

Written Opinion, International Application No. PCT/EP2021/068337, 13 pages, (dated Dec. 9, 2021).

American College of Radiology (ACR) and the Society for Pediatric Radiology (SPR), ACR-SPR Practice Parameter For The Performance Of Skeletal Scintigraphy (Bone Scan), Resolution 28, (2013-Revused2017), available from: <http://www.acr.org>, 9 pages (2017).

Anand, A. et al., A Pre-Analytical Validation Study of Automated Bone Scan Index: Effect on Accuracy and Reproducibility Due to the Procedural Variabilities in Bone Scan Image Acquisition. J Nucl Med. pp. 1865-1871, (2016).

Anand, A. et al., Analytic Validation of the Automated Bone Scan Index as an Imaging Biomarker to Standardize Quantitative Changes in Bone Scans of Patients with Metastatic Prostate Cancer, J. Nucl. Med., 57(1):41-45 (2016).

Anand, A. et al., Automated Bone Scan Index as a quantitative imaging biomarker in metastatic castration-resistant prostate cancer patients being treated with enzalutamide, EJNMMI Research, 6:23, 7 pages (2016).

Anand, A. et al., Translating Prostate Cancer Working Group 2 (PCWG2) Progression Criteria into a Quantitative Response Biomarker in Metastatic Castration Resistant Prostate Cancer (mCRPC), ASCO GU Conference, Poster, 1 page, presented Feb. 16, 2017.

Anand, A. et al., Translating Prostate Cancer Working Group 2 (PCWG2) progression criteria into a quantitative response biomarker in metastatic castration-resistant prostate cancer (mCRPC), Journal of Clinical Oncology, 35(6):170 (2017).

Armstrong, A. et al., Assessment of the bone scan index in a randomized placebo-controlled trial of tasquinimod in men with metastatic castration-resistant prostate cancer (mCRPC), Urologic Oncology: Seminars and Original Investigations, 32:1308-1316 (2014).

Armstrong, A. et al., Development and validation of a prognostic model for overall survival in chemotherapy-naive men with metastatic castration-resistant prostate cancer (mCRPC) from the phase 3 prevail clinical trial, Journal of Clinical Oncology, 35(Suppl.6) Abstract 138, 5 pages, (2017).

Armstrong, A. J. et al., Phase 3 Assessment of the Automated Bone Scan Index as a Prognostic Imaging Biomarker of Overall Survival in Men with Metastatic Castration-Resistant Prostate Cancer: A Secondary Analysis of a Randomized Clinical Trial. JAMA Oncology 4:944-951, (2018).

Armstrong, A. J. et al., Phase 3 prognostic analysis of the automated bone scan index (aBSI) in men with bone-metastatic castration-resistant prostate cancer (CRPC), Meeting Library ASC University, 11 pages (2017).

Bai, P. et. al., Body region localization in whole-body low-dose CT images of PET/CT scans using virtual landmarks, Medical Physics Wiley USA, 46(3): 1286-1299 (2019).

Belal, S. et al., Association of PET Index quantifying skeletal uptake in NaF PET/CT images with overall survival in prostate cancer patients, ASCO GU 2017, Poster 178, 1 page, presented Feb. 16, 2017.

Belal, S. et al., PET Index quantifying skeletal uptake in NaF PET/CT images with overall survival in prostate cancer patients, ASCO GU 2017, Abstract, 1 page, (Feb. 13, 2017).

Belal, S. L. et al, 3D skeletal uptake of ^{18}F sodium fluoride in PET/CT images is associate with overall survival in patients with prostate cancer, EJNMMI Research, 7(15):1-8 (2017).

Belal, S.L. et al., Automated evaluation of normal uptake in different skeletal parts in 18F-sodium fluoride (NaF) PET/CT using a new convolutional neural network method, EJNMMI, EANM '17, 44(Suppl 2):S119-S956, Abstract EP-0116 (2017).

Bombardieri, E. et al., Bone scintigraphy: procedure guidelines for tumour imaging, Eur J. Nucl. Med. Mol. Imaging, 30:BP99-BP106, (2003).

Brynolfsson, J., et. al., Deep Learning based urinary bladder segmentation using 18FDCFPyL (PyL-PSMA) PET/CT images, EPS-145, European Association of Nuclear Medicine, (2020), <http://link.springer.com/article/10.1007/s00259-020-04988-4>. pp. S1 and S403-S404, Retrieved Sep. 18, 2020.

Brynolfsson, J., et. al., Deep Learning-Enabled comprehensive detection and quantification of 18FDCFPyL (PyL-PSMA) PET/CT, OP-548, European Association of Nuclear Medicine, (2020), <http://link.springer.com/article/10.1007/s00259-020-04988-4>. pp. S1 and S273, Retrieved Sep. 18, 2020.

Bushberg, J. T. et al., Essential Physics of Medical Imaging, Essential Physics of Medical Imaging, 19.3: p. 581 (table 15-3), p. 713 paragraph 6, section 19.3 and p. 720, (2011).

Capobianco, N. et. al., Whole-body uptake classification and prostate cancer staging in ^{68}Ga-PSMA-11 PET/CT using dual-tracer learning, European Journal of Nuclear Medicine and Molecular Imaging, (2021), <https:/doi.org/10.1007/s00259-021-05473-2> 10 pages. Retrieved on Apr. 18, 2021.

Cha, K. H., et al. Urinary bladder segmentation in CT urography using deep-learning convolutional neural network and level sets, Medical physics, 43(4):1882-1896, (2016).

Ciernik, I. F., et al. 3D-segmentation of the 18F-choline PET signal for target volume definition in radiation therapy of the prostate, Technology in cancer research & treatment 6(1):23-30, (2007).

Dennis, E. et al., Bone Scan Index: A Quantitative Treatment Response Biomarker for Castration-Resistant Metastatic Prostate Cancer, Journal of Clinical Oncology, 30(5):519-524 (2012).

Dertat, A., Applied Depp Learning—{art 4: Convolutional Neural Networks, Towards Data Science, <http://towardsdatascience.com/applied-deep-learning-part-4-convolutional-neural-networks-584bc134de2> 26 pages, (2017).

Eiber, M. et al., Prostate Cancer Molecular Imaging Standardized Evaluation (PROMISE): Proposed miTNM Classification for the Interpretation of PSMA-Ligand PET/CT, The Journal of Nuclear Medicine, 59(3):469-478, (2018).

Fendler, W.P. et. al., 68Ga-PSMA PET/CT: Joint EANM and SNMMI procedure guideline for prostate cancer imaging: version 1.0, Eur J Nucl Med Mol Imaging, DOI 10.1007/s00259-017-3670-z, 11 pages, (2017).

GE Healthcare, SPECT/CT Cameras, 2 pages, retrieved Oct. 25, 2017: <http://www3.gehealthcare.com.sg/en-GB/products/categories/nuclear_medicine/spect-ct_cameras>.

Giesel, F. L. et al., F-18 labelled PSMA-1007: biodistribution, radiation dosimetry and histopathological validation of tumor lesions in prostate cancer patients, Eur. J. Nucl. Med. Mol. Imaging, 44:678-688 (2017).

Gjertsson, K., et. al., A Novel Automated Deep Learning Algorithm for Segmentation of the Skeleton in Low-Dose CT for [(18)F] DCFPyL PET/CT Hybrid Imaging in Patients with Metastatic Prostate Cancer, Annual Congress of the European Association of Nuclear Medicine Oct. 12-16, 2019 Barcelona, Spain. Eur J Nucl Med Mol Imaging 46 (Suppl 1), S1-S952 (2019). Abstract EP-0823, p. S765.

(56) **References Cited**

OTHER PUBLICATIONS

Gjertsson, K., Segmentation in Skeletal Scintigraphy Images using Convolutional Neural Networks, Master's Theses in Mathematical Sciences, pp. 39-58, (2017), <https://lup.lub.lu.se/student-papers/search/publication/8916406>.

Goffin, K. E. et al., Phase 2 study of ^{99m}Tc-trofolastat SPECT/CT to identify and localize prostate cancer in intermediate- and high-risk patients undergoing radical prostatectomy and extended pelvic lymph node dissection, J. Nucl. Med., 27 pages (2017).

Guimond, A. et al., Average Brain Models: A Convergence Study, Computer Vision and Image Understanding, 77:192-210 (2000).

Hajnal, J. et al., 4.4 Intensity, Size, and Skew Correction; 7.1 Introduction; 7.2 Methods; 7.3 Image Interpretation—General, In: Medical Image Registration, CRC Press LLC, 80-81:144-148 (2001).

Hiller, S. M. et al., 99mTc-Labeled Small-Molecule Inhibitors of Prostate-Specific Membrane Antigen for Molecular Imaging of Prostate Cancer, Journal of Nuclear Medicine, 54(8):1369-1376 (2013) retrieved Oct. 25, 2017: <http://jnm.snmjournals.org/content/54/8/1369.full>.

Horikoshi, H. et al., Computer-aided diagnosis system for bone scintigrams from Japanese patients: importance of training database, Annals of Nuclear Medicine, 26(8):622-626 (2012).

Huang, J.-H. et al., A Set of Image Processing Algorithms for Computer-Aided Diagnosis in Nuclear Medicine Whole Body Bone Scan Images, IEEE Transactions on Nuclear Science, 54(3):514-522 (2007).

Im, HJ, et. al., et al., Current Methods to Define Metabolic Tumor vol. in Positron Emission Tomography: Which One is Better?, Nucl. Med. Mol. Imaging, 52(1):5-15, (2018).

Johnsson, K., et. al., miPSMA Index: Comprehensive and Automated Quantification of 18F-DCFPyL (PyL-PSMA) PET/CT for Prostate Cancer Staging, J Nucl Med., 61: (Supplement 1):1435, 5 pages, (2020).

Kaboteh R. et al., Progression of bone metastases in patients with prostate cancer—automated detection of new lesions and calculation of bone scan index, EJNMMI Research, 3:64, 6 pages, (2013).

Kaboteh, R. et al., Convolutional neural network based quantification of choline uptake in PET/CT studies is associated with overall survival in patents with prostate cancer, EJNMMI, EANM '17, 44(Suppl 2):S119-S956, Abstract EP-0642 (2017).

Keiss, et al., Prostate-specific membrane antigen and a target for cancer imaging and therapy, The Quarterly Journal of Nuclear Medicine and Molecular Imaging, 59(3):241-268 (2015).

Kikuchi, A. et al., Automated segmentation of the skeleton in whole-body bone scans: influence of difference in atlas, Nuclear Medicine Communications, 33(9):947-953 (2012).

Kinahan, P.E. et al., PET/CT Standardized Update Values (SUVs) in Clinical Practice and Assessing Response to Therapy, Semin Ultrasound CT MR 31(6):496-505 (2010) retrieved Oct. 25, 2017: <https://www.ncbi.nlm.nih.gov/pmc/articles/PMC3026294/>.

Knutsson, H., and Andersson, M., Morphons: Segmentation using Elastic Canvas and Paint on Priors, IEEE International Conference on Image Processing (ICIP 2005), Genova, Italy, 4 pages (2005).

Kopka, K. et al., Glu-Ureido-Based Inhibitors of Prostate-Specific Membrane Antigen: Lessons Learned During the Development of a Novel Class of Low-Molecular-Weight Theranostic Radiotracers, The Journal of Nuclear Medicine, 58(9)(Suppl. 2):17S-26S, (2017).

Lin, T.Y. et. al., Feature Pyramid Networks for object detection, FAIR, 10 pages, (2016), <https://arxiv.org/abs/1612.03144v1>.

Litjens, G. et al., A survey on deep learning in medical image analysis, Medical Image Analysis, 42:60-88, (2017).

Liu, L. et al., Computer-Aided Detection of Prostate Cancer with MRI: Technology and Applications, Acad Radiol. Author manuscript, 50 pages 2016.

Ma, L. et al., Automatic segmentation of the prostate on CT images using deep learning and multi-atlas fusion, Proc. of SPIE vol. 10133:101332O-1-101332O-9 (2017).

Ma, L. et al., Combining Population and Patient-Specific Characteristics for Prostate Segmentation on 3D CT Images, Proc of SPIE 9784:978427-1-8 (2016).

Ma, L. et al., Random Walk Based Segmentation for the Prostate on 3D Transrectal Ultrasound Images, Proc SPIE Int Soc Opt Eng. Author manuscript, 13 pages (2016).

Mayo Clinic Staff, Choline C-11 PET scan, Overview, Mayo Clinic, 4 pages (2017), retrieved Oct. 25, 2017: <https://www.mayoclinic.org/tests-procedures/choline-c-11-pet-scan/home/ovc-20156994>.

Meyer, A., et. al., Deep learning algorithm improves identification of men with low-risk prostate cancer using PSMA targeted 99mTc-MIP-1404 SPECT/CT, Journal of Clinical Oncology, 37:(15), (2019).

Nakajima, K. et al., Enhanced diagnostic accuracy for quantitative bone scan using an artificial neural network system: a Japanese multi-center database project, EJNMMI Research, 3:83, 9 pages, (2013).

National Cancer Institute, NCI Drug Dictionary: gallium Ga 68-labeled PSMA-11, 1 page, retrieved Oct. 25, 2017: <https://www.cancer.gov/publications/dictionaries/cancer-drug?cdrid=766400>.

National Cancer Institute, NCI Drug Dictionary: technetium Tc 99m methylene diphosphonate, 1 page, retrieved Oct. 25, 2017: <https://www.cancer.gov/publications/dictionaries/cancer-drug?cdrid=537722>.

Nickols, N.G., et. al., A deep learning algorithm to predict coexisting metastatic disease using intraprostatic [F18]DCFPYL PSMA image alone in veterans with prostate cancer, Journal of Clinical Oncology 38, (Supplement 6), 2020.

Ohlsson, M., et. al., Automated decision support for bone scintigraphy, Computer-based medical systems, pp. 1-6, (2009).

Perera, M. et al., Sensitivity, Specificity, and Predictors of Positive 68Ga-Prostate-specific Membrane Antigen Positron Emission Tomography in Advanced Prostate Cancer: A Systematic Review and Meta-analysis, European Urology, 70(6):926-937 (2016).

Polymeri, E. et al., Analytical validation of an automated method for segmentation of the prostate gland in CT images, EJNMMI, EANM '17, 44(Suppl 2):S119-S956, Abstract EP-0641 (2017).

Polymeri, E., et. al., Deep learning-based quantification of PET/CT prostate gland uptake: association with overall survival, Clinical Physiology Functional Imaging, DOI: 10.1111/cpf.12611, 40(2):106-113, (2019).

Pouliot, F., et. al., Prospective evaluation of a Novel Deep Learning Algorithm (PSMA-AI) in the assessment of 99mTc-MIP-1404 SPECT/CT in patients with low or intermediate risk prostate cancer, Annual Congress of the European Association of Nuclear Medicine Oct. 12-16, 2019 Barcelona, Spain. Eur J Nucl Med Mol Imaging 46 (Suppl 1), S1-S952 (2019). Abstract EP-0804, p. S765.

radiologyinfo.org for Patients, Computed Tomography (CT), 2 pages, retrieved Oct. 25, 2017: <https://www.radiologyinfo.org/en/submenu.cfm?pg=ctscan>.

Ren, S., et. al., Faster R-CNN: Towards Real-Time Object Detection with Region Proposal Networks, 14 pages, (2015), <http://image-net.org/challenges/LSVRC/2015/results>.

Ronneberger, O., et. al., U-Net: Convolutional Networks for Biomedical Image Segmentation, Springer International Publishing, pp. 234-241, (2015), <http://lmb.informatik.uni-freiburg.de/>. Published online on Nov. 18, 2015.

Rowe, S. P. et al., PET Imaging of prostate-specific membrane antigen in prostate cancer: current state of the art and future challenges, Prostate Cancer and Prostatic Diseases, pp. 1-8 (2016).

Rowe, S. P. et al., PSMA-Based [^{18}F]DCFPyL PET/CT Is Superior to Conventional Imaging for Lesion Detection in Patients with Metastatic Prostate Cancer, Mol Imaging Biol, 18:411-419, (2016).

Sabbatini, P. et al., Prognostic Significance of Extent of Disease in Bone in Patients With Androgen-Independent Prostate Cancer, Journal of Clinical Oncology, 17(3):948-957 (1999).

Sadik, M. et al., 3D prostate gland uptake of 18F-choline-association with overall survival in patients with hormone-naïve prostate cancer, The Journal of Nuclear Medicine, 58(Suppl. 1):Abstract 544, 2 pages, (2017).

Sadik, M. et al., A new computer-based decision-support system for the interpretation of bone scans, Nuclear Medicine Communications, 27(5):417-423 (2006).

Sadik, M. et al., Automated 3D segmentation of the prostate gland in CT images—a first step towards objective measurements of prostate uptake in PET and SPECT images, Journal of Nuclear Medicine, 58(1):1074, (2017).

(56) **References Cited**

OTHER PUBLICATIONS

Sadik, M. et al., Automated quantification of reference levels in liver and mediastinum (blood pool) for the Deauville therapy response classification using FDG-PET/CT in lymphoma patients, EJNMMI, EANM '17, 44(Suppl 2):S119-S956, Abstract EP-0770 (2017).
Sadik, M. et al., Computer-assisted interpretation of planar whole-body bone scans, Journal Nuclear Medicine, 49(12):1958-65, 2008.
Sadik, M. et al., Convolutional neural networks for segmentation of 49 selected bones in CT images show high reproducibility, EJNMMI, EANM '17, 44(Suppl 2):S119-S956, Abstract OP-657 (2017).
Sadik, M. et al., Improved classifications of planar whole-body bone scans using a computer-assisted diagnosis system: a multicenter, multiple-reader, multiple-case study, Journal of Nuclear Medicine, 50(3): 368-75, 2009.
Sadik, M. et al., Variability in reference levels for Deauville classifications applied to lymphoma patients examined with 18F-FDG-PET/CT, EJNMMI, EANM '17, 44(Suppl 2):S119-S956, Abstract EP-0771 (2017).
Sajn, L. et al., Computerized segmentation of whole-body bone scintigrams and its use in automated diagnostics, Computer Methods and Programs in Biomedicine, 80:47-55 (2005).
Salerno, J. et al., Multiparametric magnetic resonance imaging for pre-treatment local staging of prostate cancer: A Cancer Care Ontario clinical practice guideline, Canadian Urological Association Journal, 10(9-10):332-339 (2016).
Santos-Cuevas, C. et al. 99mTc-labeled PSMA inhibitor: Biokinetics and radiation dosimetry in healthy subjects and imaging of prostate cancer tumors in patients, Nuclear Medicine and Biology 52:1-6, (2017).
Sjöstrand K. et al., Statistical regularization of deformation fields for atlas-based segmentation of bone scintigraphy images, MICCAI 5761:664-671 (2009).
Sjöstrand, K., et al., Automated detection and quantification of Prostatic PSMA uptake in SPECT/CT using a Deep Learning Algorithm for Segmentation of Pelvic Anatomy, The Journal of Nuclear Medicine, 59(1):p. 30, (2018).
Sjostrand, K., et. al., Automated Assessment of Prostatic PSMA Expression in SPECT/CT using Deep Convolutional Neural Networks—A Prospectively Planned Retrospective Analysis of Phase 3 Study MIP-1404-3301, The Journal of Nuclear Medicine, 60 (Supplement 1): Abstract 401, 1 page, (2019).
Sluimer, I. et al., Toward Automated Segmentation of the Pathological Lung in CT, IEEE Transactions on Medical Imaging, 24(8):1025-1038 (2005).
Tian, Z. et al., A fully automatic multi-atlas based segmentation method for prostate MR images, Proc SPIE Int Soc Opt Eng. Author manuscript, 12 pages (2015).
Tian, Z. et al., A supervoxel-based segmentation method for prostate MR images, Med. Phys., 44(2):558-569 (2017).
Tian, Z. et al., Deep convolutional neural network for prostate MR segmentation, Proc. of SPIE 10135:101351L-1-101351L-6 12 pages, (2017).
Tian, Z., et al., Superpixel-based Segmentation for 3D Prostate MR Images, IEEE Trans Med Imaging, Author manuscript, pp. 558-569, (2016).
Trägärdh, E., et. al., RECOMIA—a cloud-based platform for artificial intelligence research in nuclear medicine and radiology, EJNMMI Physics, <https://doi.org/10.1186/s40658-020-00316-9>, 7:51, 12 pages, (2020).
Ulmert, D. et al., A Novel Automated Platform for Quantifying the Extent of Skeletal Tumour Involvement in Prostate Cancer Patients Using the Bone Scan Index, European Urology, 62(1):78-84 (2012).
Wallis, J.W. et. al., Three-dimensional display in nuclear medicine, IEEE Trans Med Imaging, 8(4):297-230, (1989).
Wrangsjo, A. et al., Non-rigid Registration Using Morphons, Proceedings of the 14th Scandinavian Conference on Image Analysis (SCIA '05), pp. 501-510 (2005).
Yin, T.-K., A Computer-Aided Diagnosis for Locating Abnormalities in Bone Scintigraphy by a Fuzzy System With a Three-Step Minimization Approach, IEEE Transactions on Medical Imaging, 23(5):639-654 (2004).
Christ, P.F. et al., Automatic Liver and Tumor Segmentation of CT and MRI Volumes Using Cascaded Fully Convolutional Neural Networks, Arxiv.org, Cornell University Library, 20 pages, (2017).

* cited by examiner

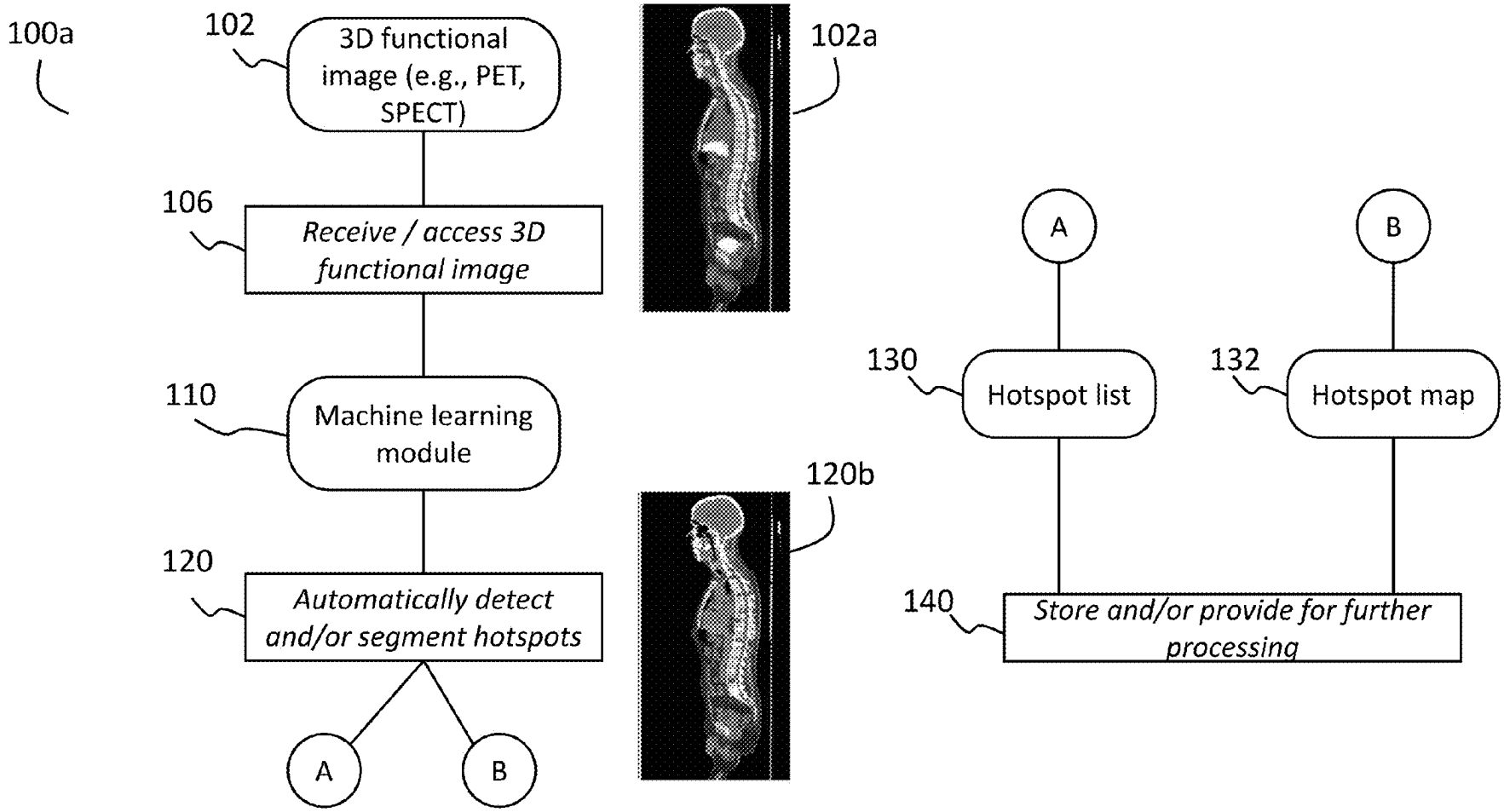

100a
102
3D functional image (e.g., PET, SPECT)
102a
106
Receive / access 3D functional image
110
Machine learning module
120
Automatically detect and/or segment hotspots
A
B
120b
A
B
130
Hotspot list
132
Hotspot map
140
Store and/or provide for further processing

FIG. 1A

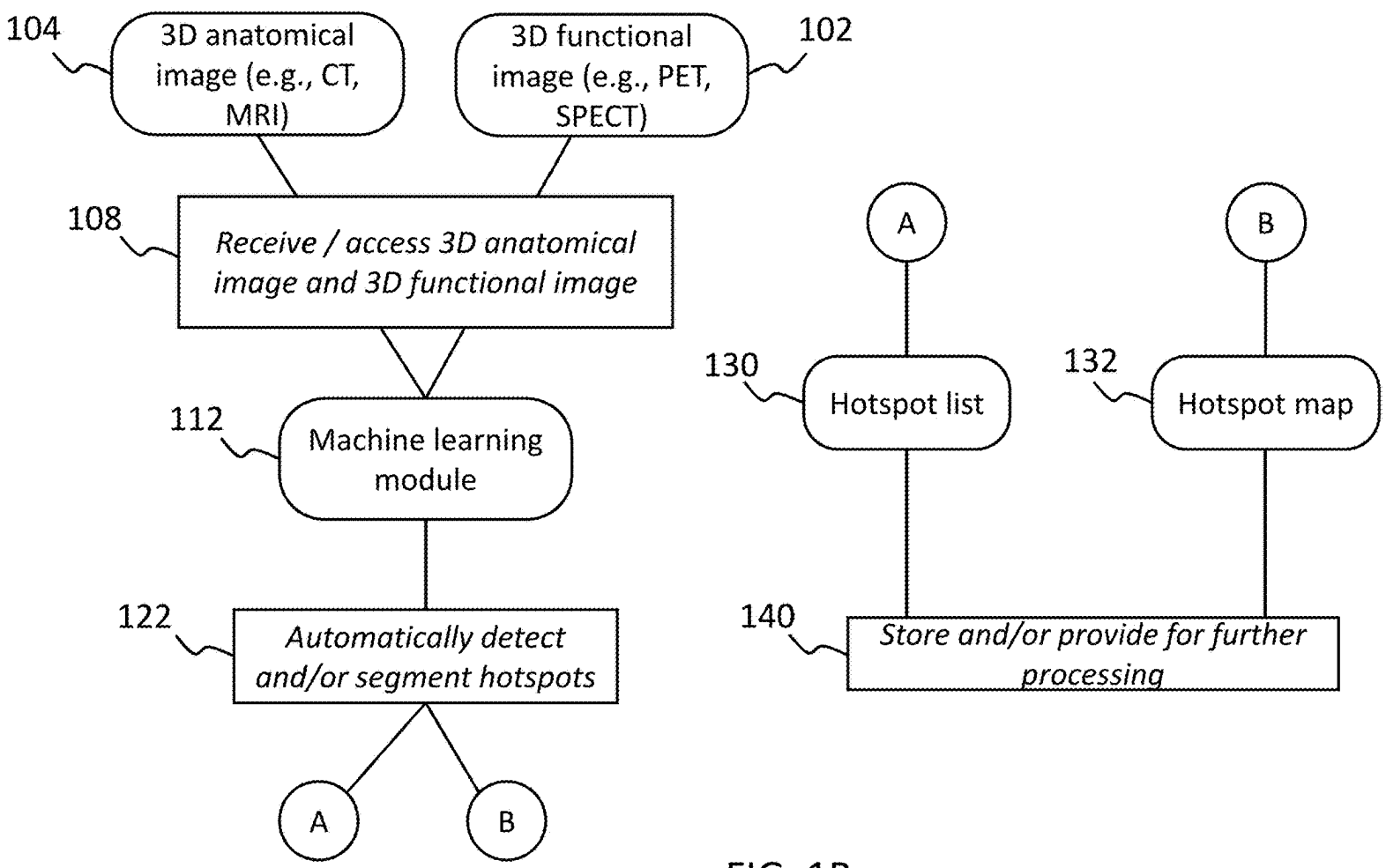

100b
104
3D anatomical image (e.g., CT, MRI)
102
3D functional image (e.g., PET, SPECT)
108
Receive / access 3D anatomical image and 3D functional image
112
Machine learning module
122
Automatically detect and/or segment hotspots
A
B
A
B
130
Hotspot list
132
Hotspot map
140
Store and/or provide for further processing

FIG. 1B

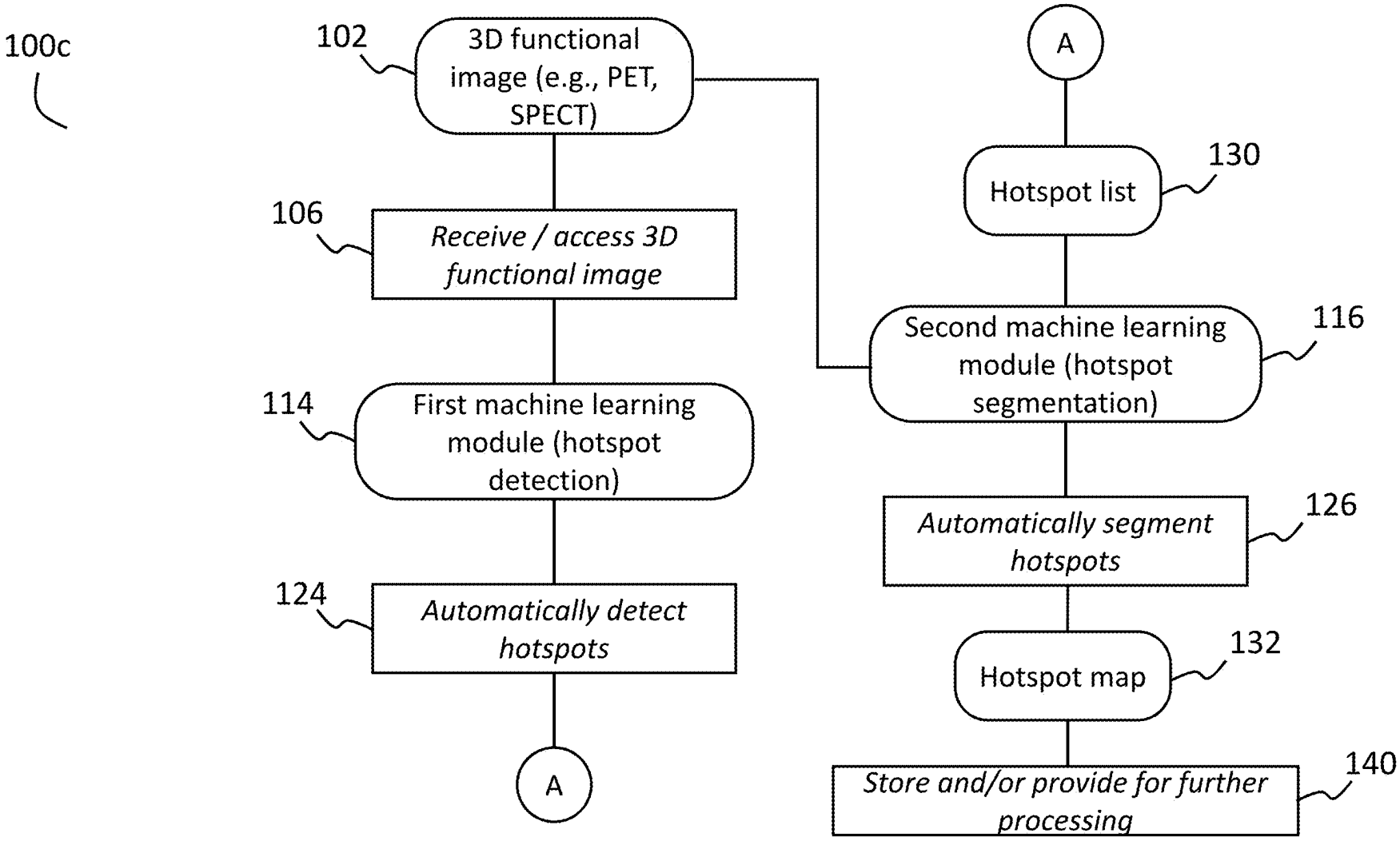

100c
102
3D functional image (e.g., PET, SPECT)
106
Receive / access 3D functional image
114
First machine learning module (hotspot detection)
124
Automatically detect hotspots
A
A
130
Hotspot list
116
Second machine learning module (hotspot segmentation)
126
Automatically segment hotspots
132
Hotspot map
140
Store and/or provide for further processing

FIG. 1C

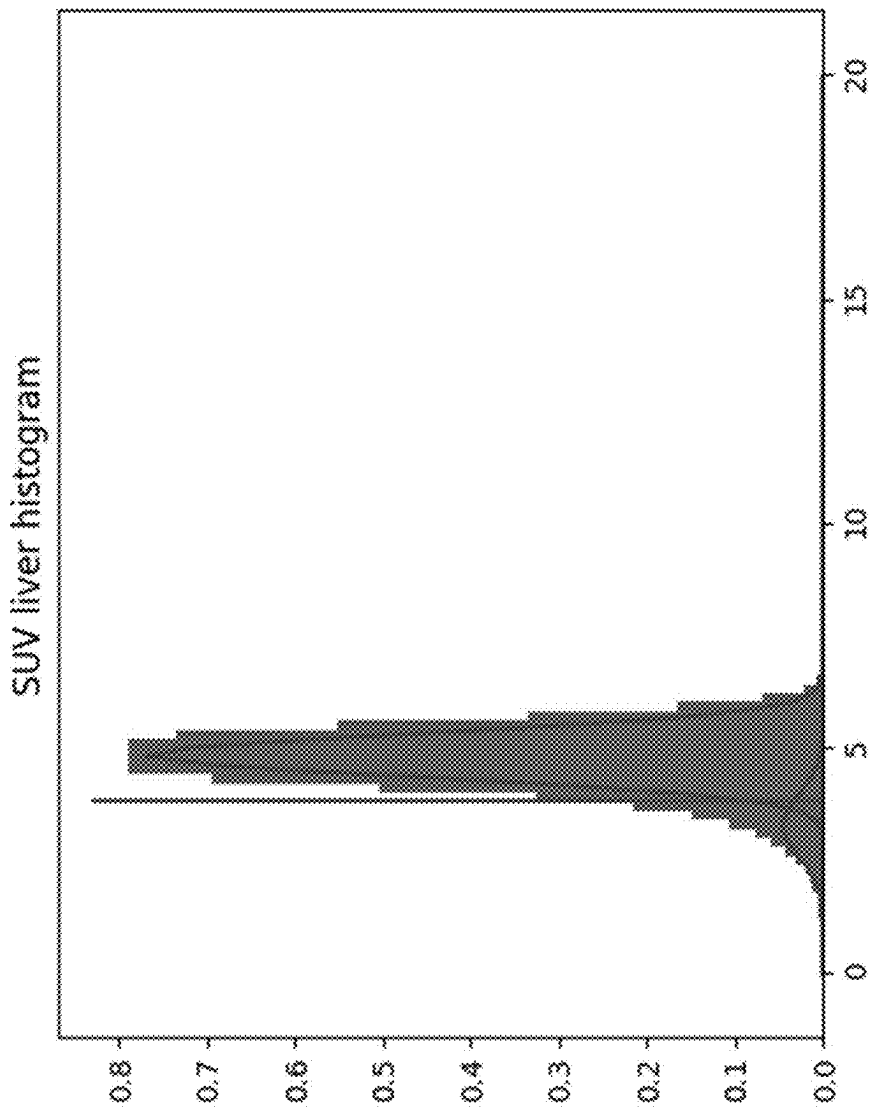


FIG. 2A

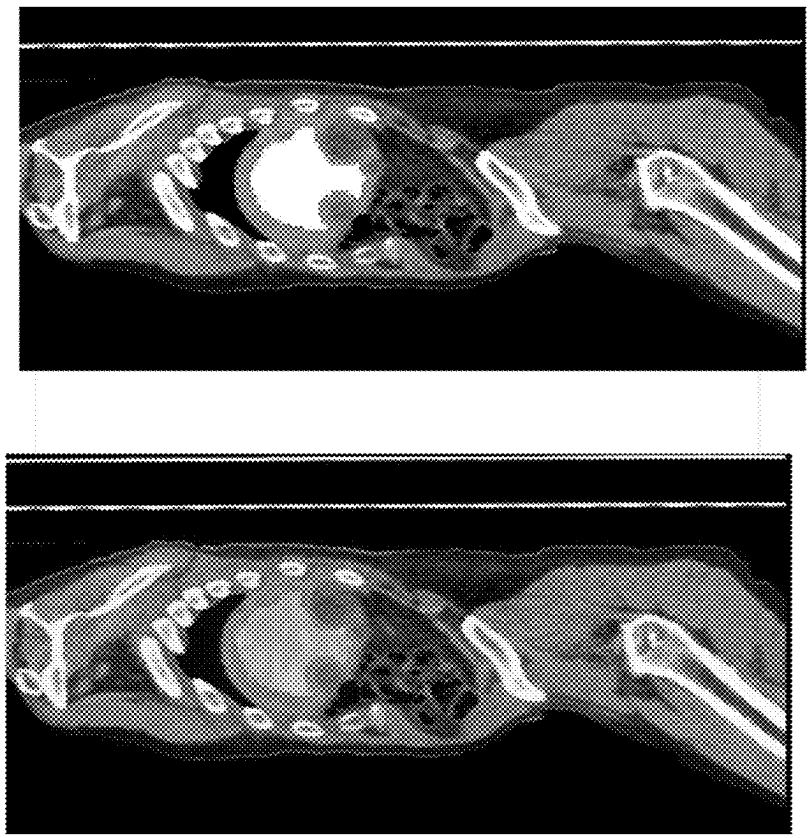


FIG. 2B

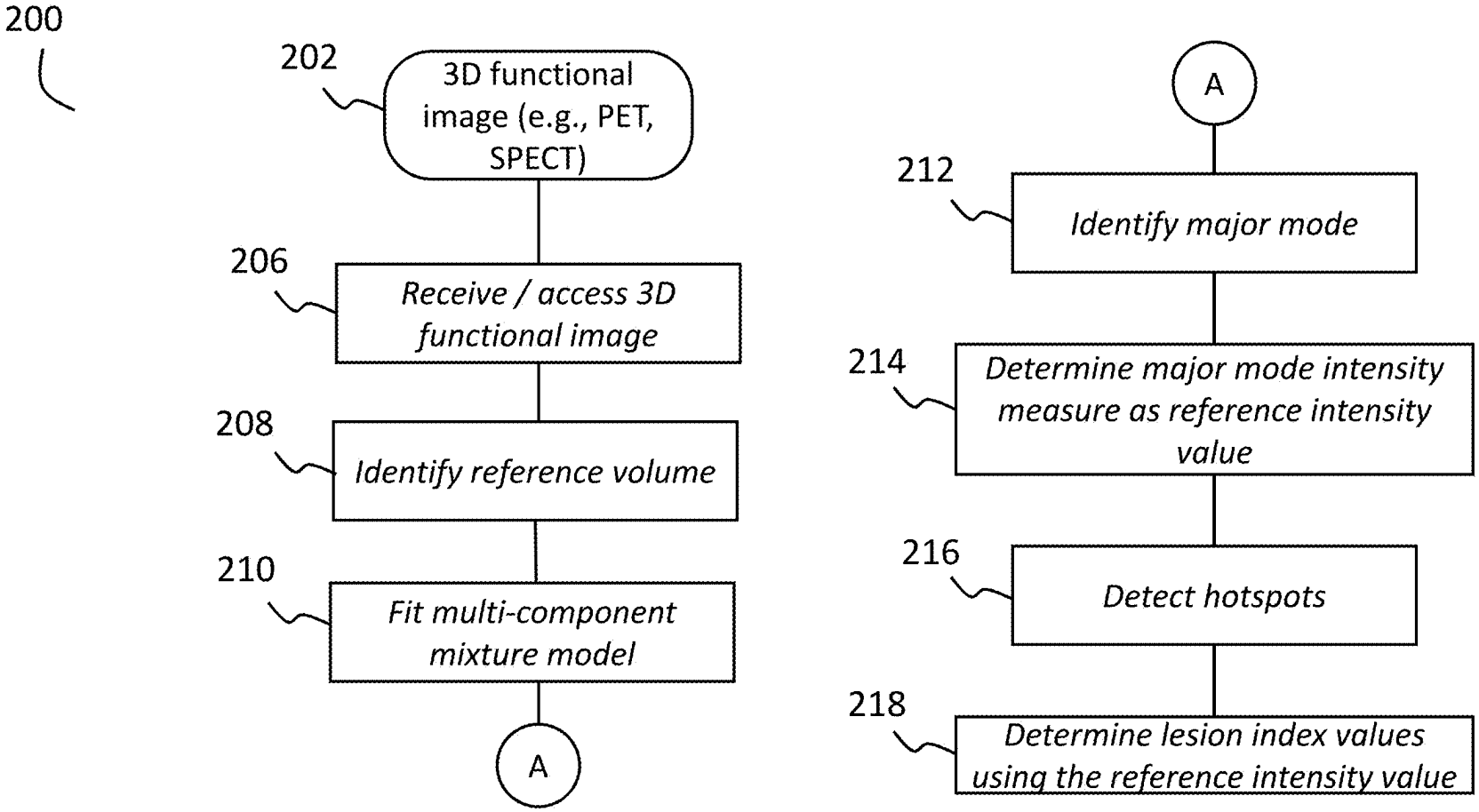

200
202
3D functional image (e.g., PET, SPECT)
206
Receive / access 3D functional image
208
Identify reference volume
210
Fit multi-component mixture model
A
A
212
Identify major mode
214
Determine major mode intensity measure as reference intensity value
216
Detect hotspots
218
Determine lesion index values using the reference intensity value

FIG. 2C

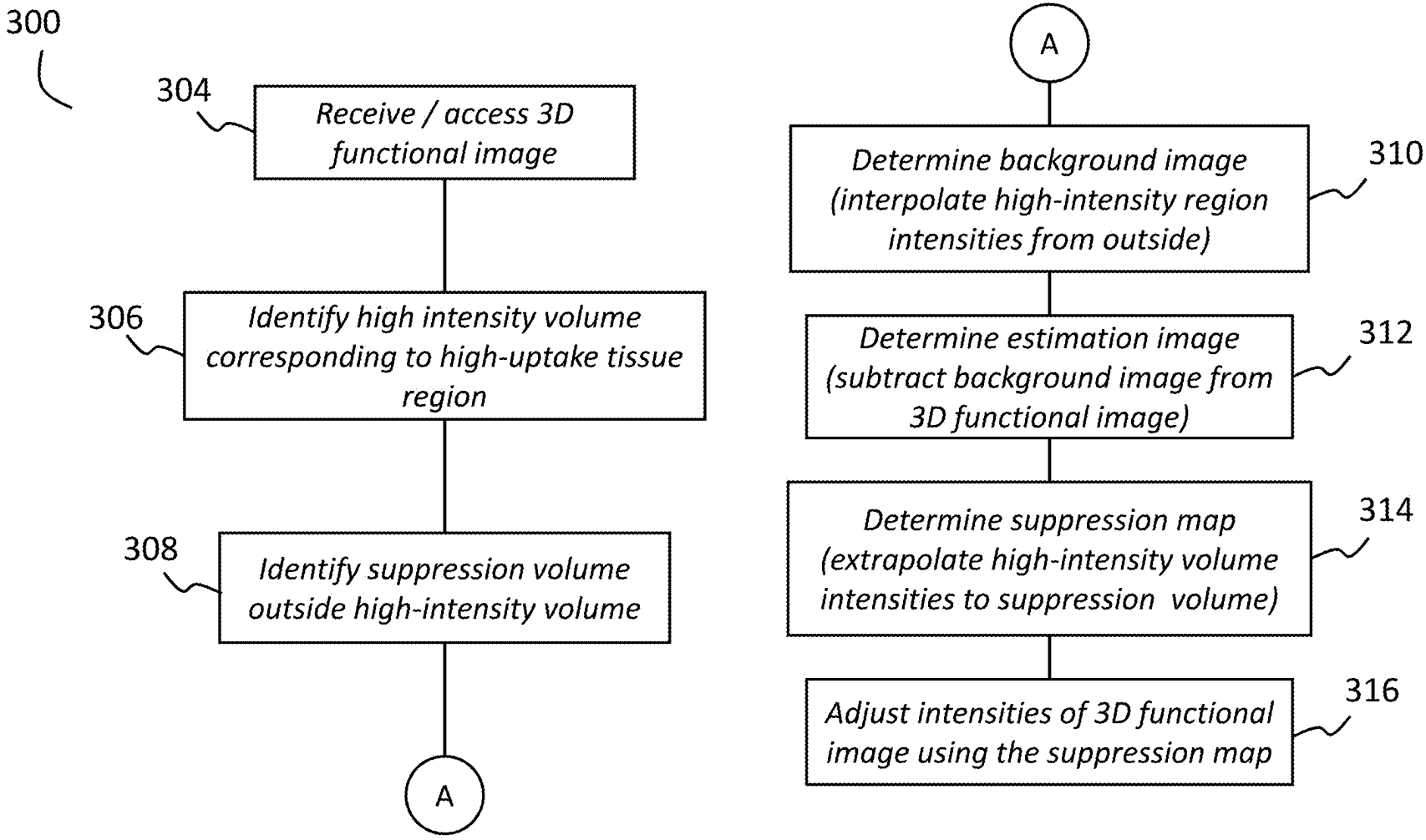

300
304
Receive / access 3D functional image
306
Identify high intensity volume corresponding to high-uptake tissue region
308
Identify suppression volume outside high-intensity volume
A
A
Determine background image (interpolate high-intensity region intensities from outside)
310
Determine estimation image (subtract background image from 3D functional image)
312
Determine suppression map (extrapolate high-intensity volume intensities to suppression volume)
314
Adjust intensities of 3D functional image using the suppression map
316

FIG. 3

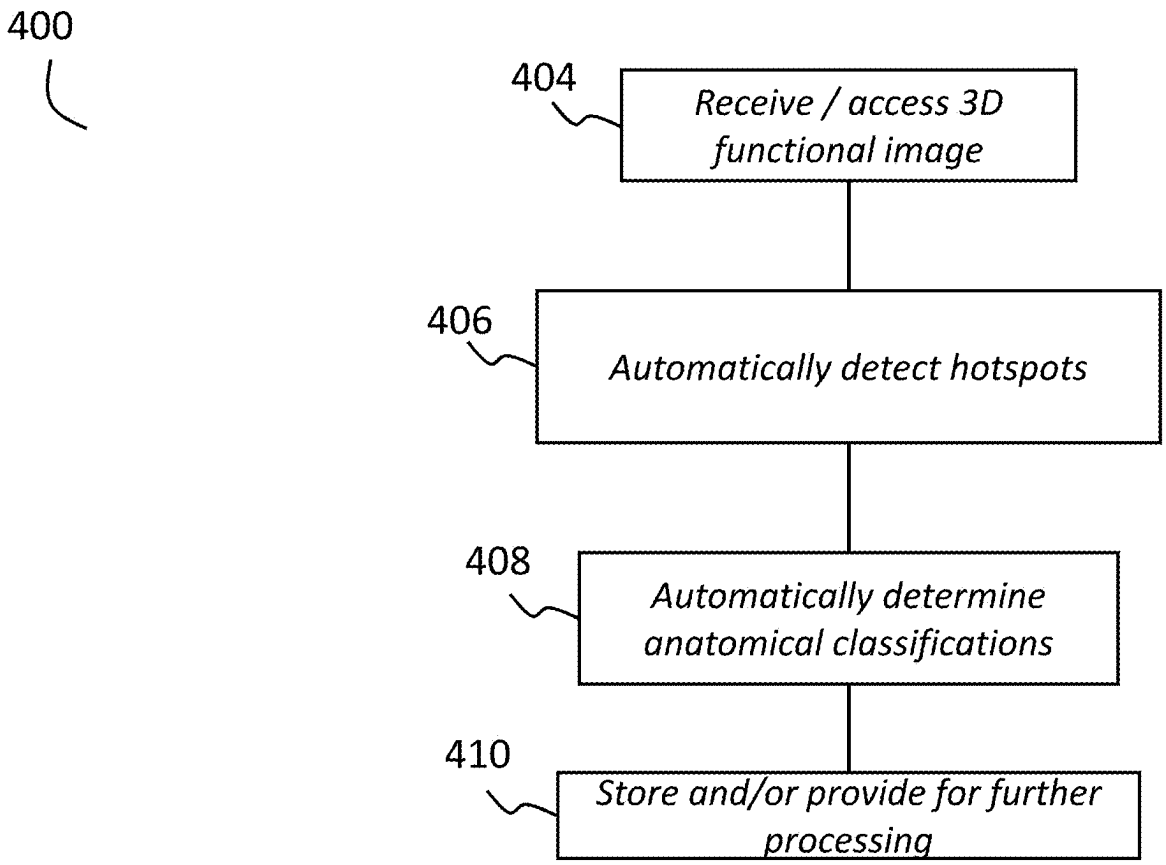

400
404
Receive / access 3D functional image
406
Automatically detect hotspots
408
Automatically determine anatomical classifications
410
Store and/or provide for further processing

FIG. 4

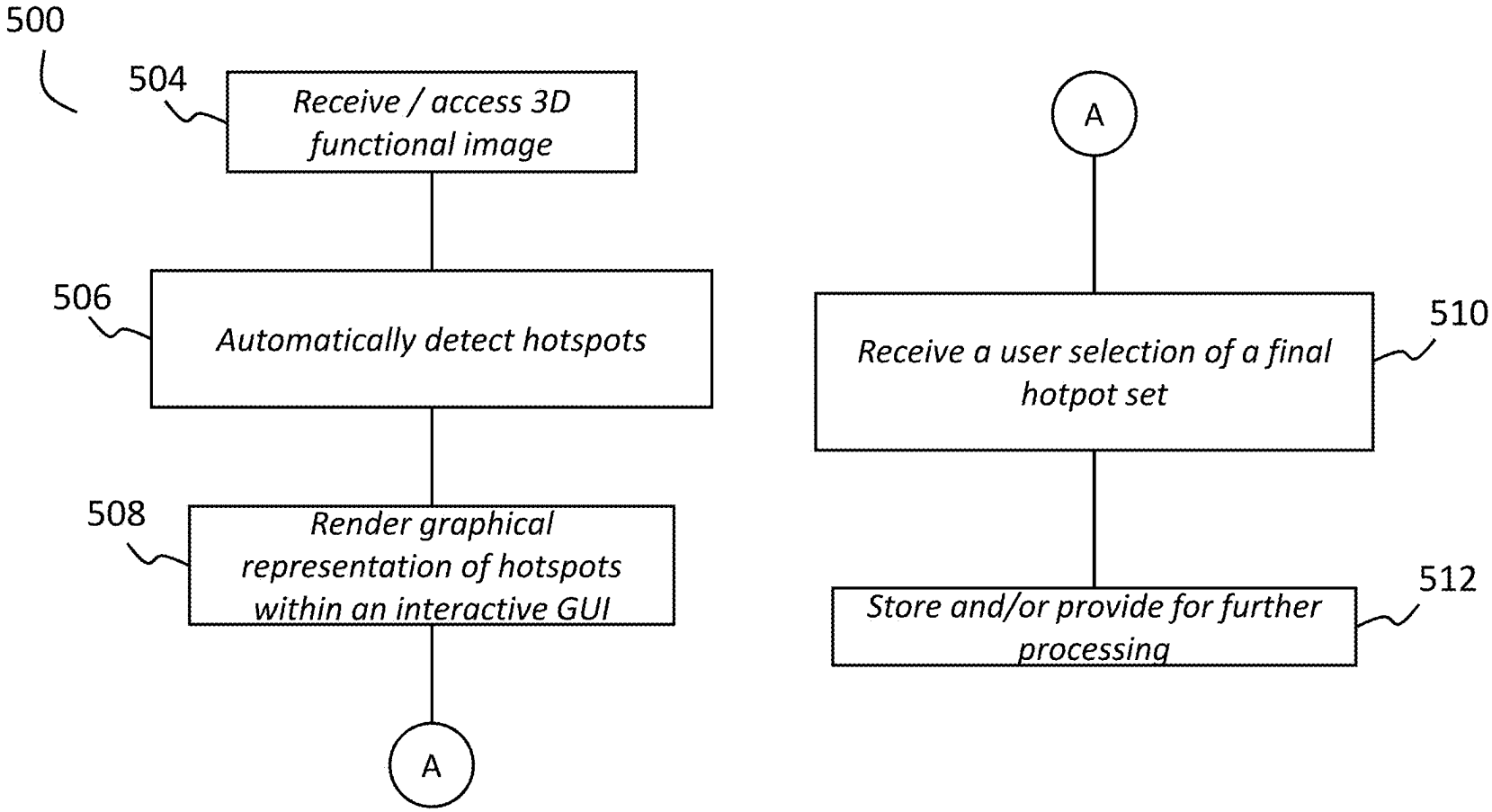

500
504
Receive / access 3D functional image
506
Automatically detect hotspots
508
Render graphical representation of hotspots within an interactive GUI
A
A
510
Receive a user selection of a final hotpot set
512
Store and/or provide for further processing

FIG. 5A

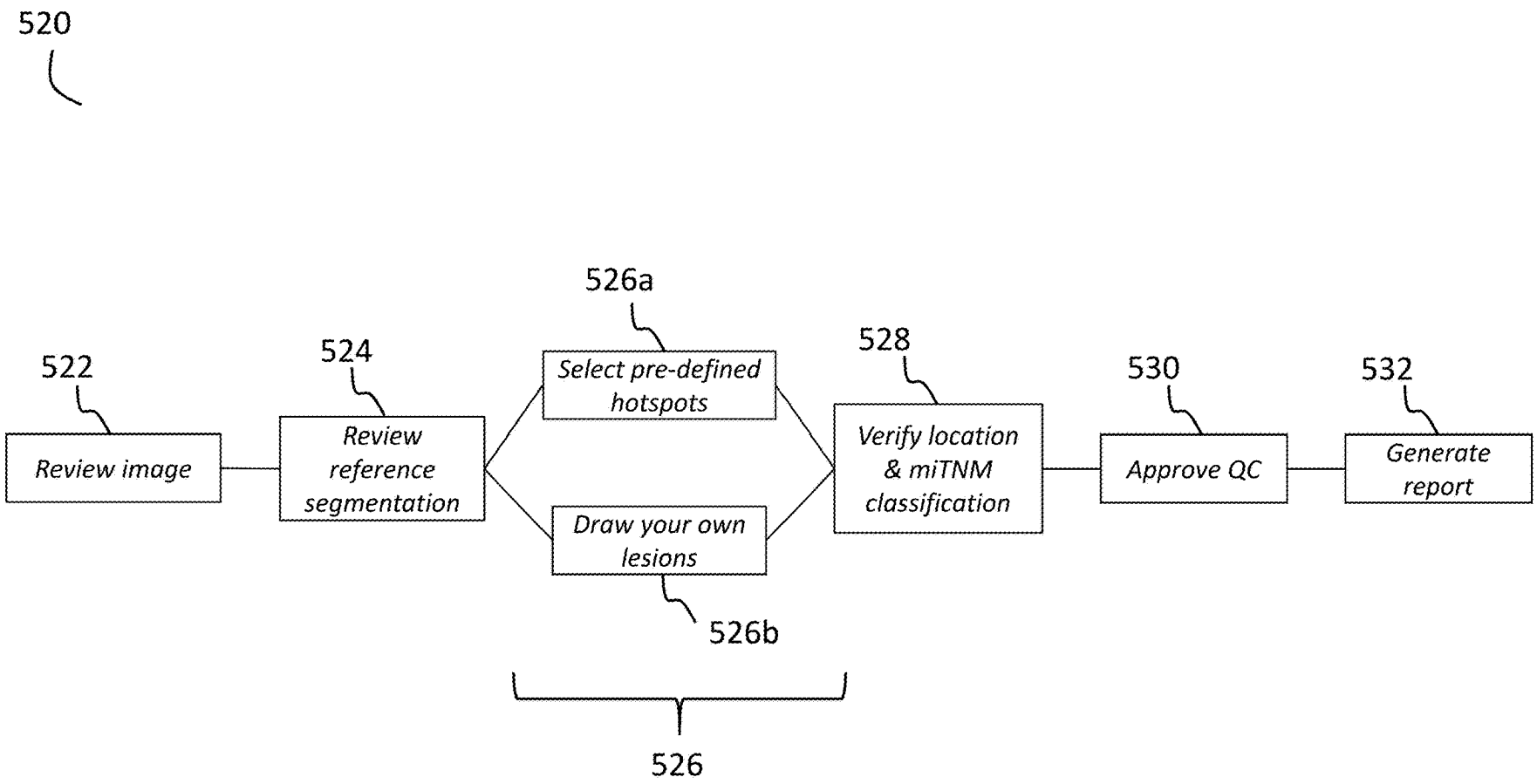

520
522
Review image
524
Review reference segmentation
526a
Select pre-defined hotspots
Draw your own lesions
526b
526
528
Verify location & miTNM classification
530
Approve QC
532
Generate report

FIG. 5B

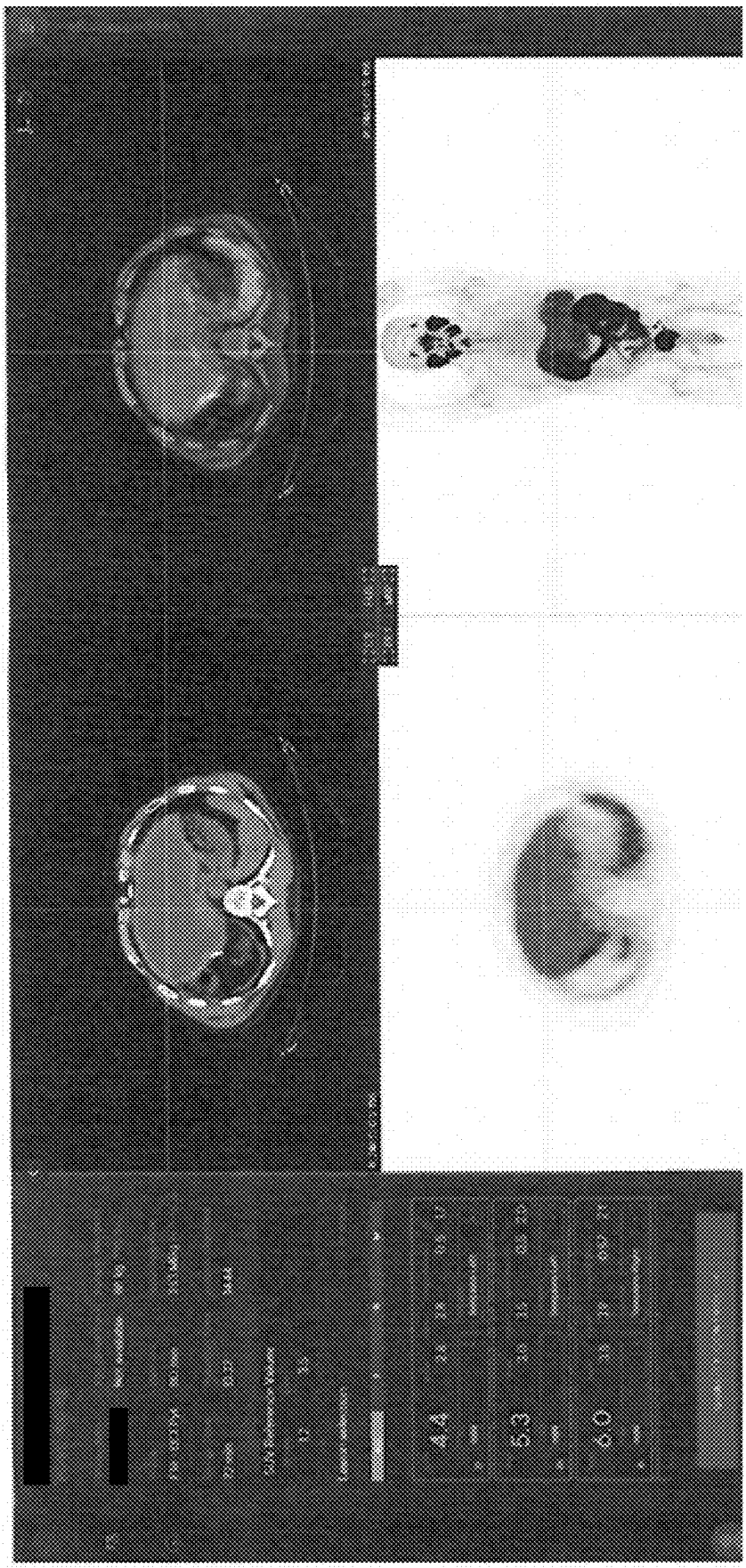


FIG. 6A

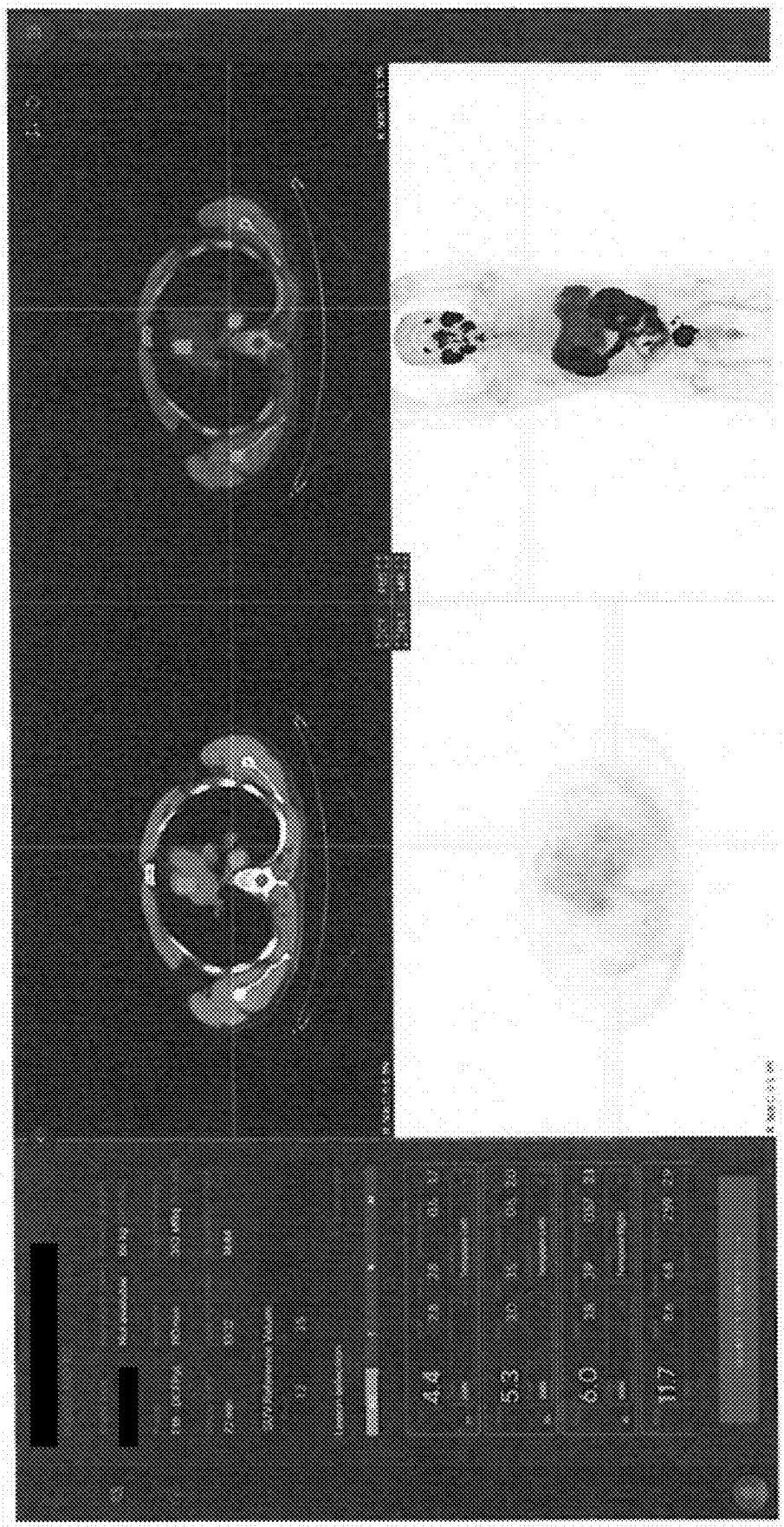


FIG. 6B

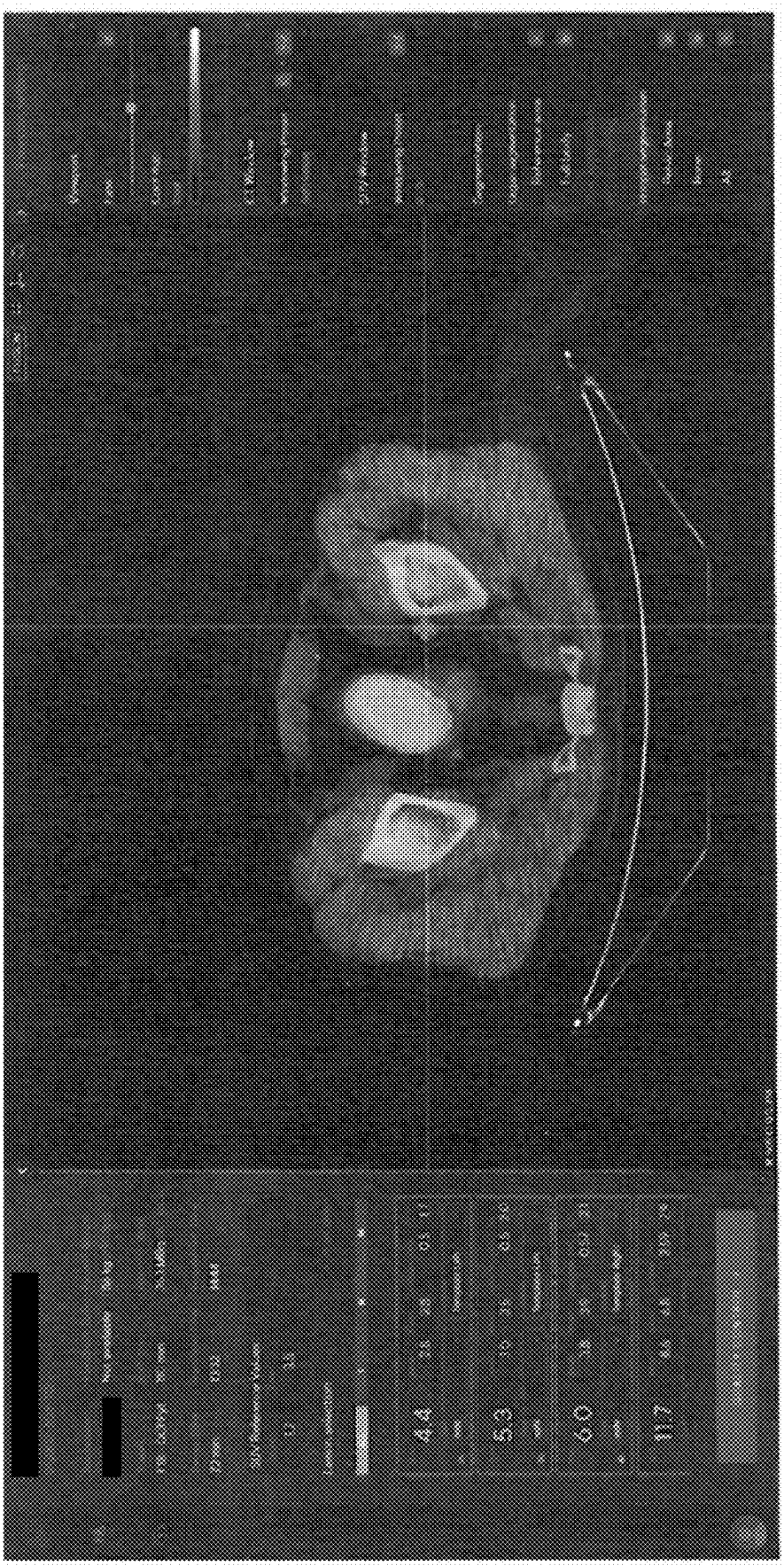


FIG. 6C

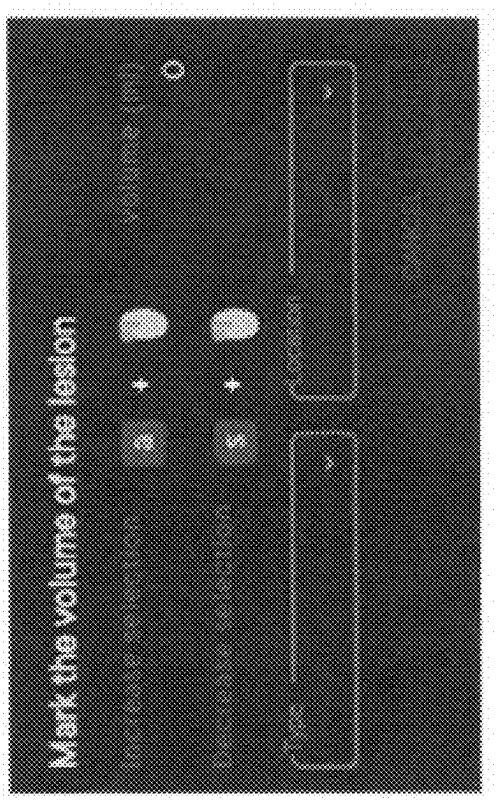


FIG. 6E

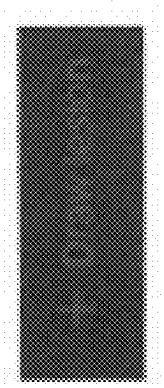


FIG. 6D

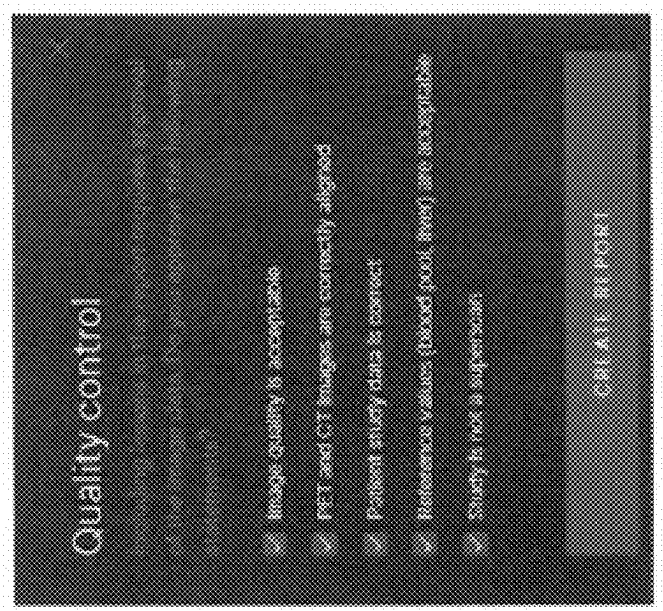


FIG. 6F

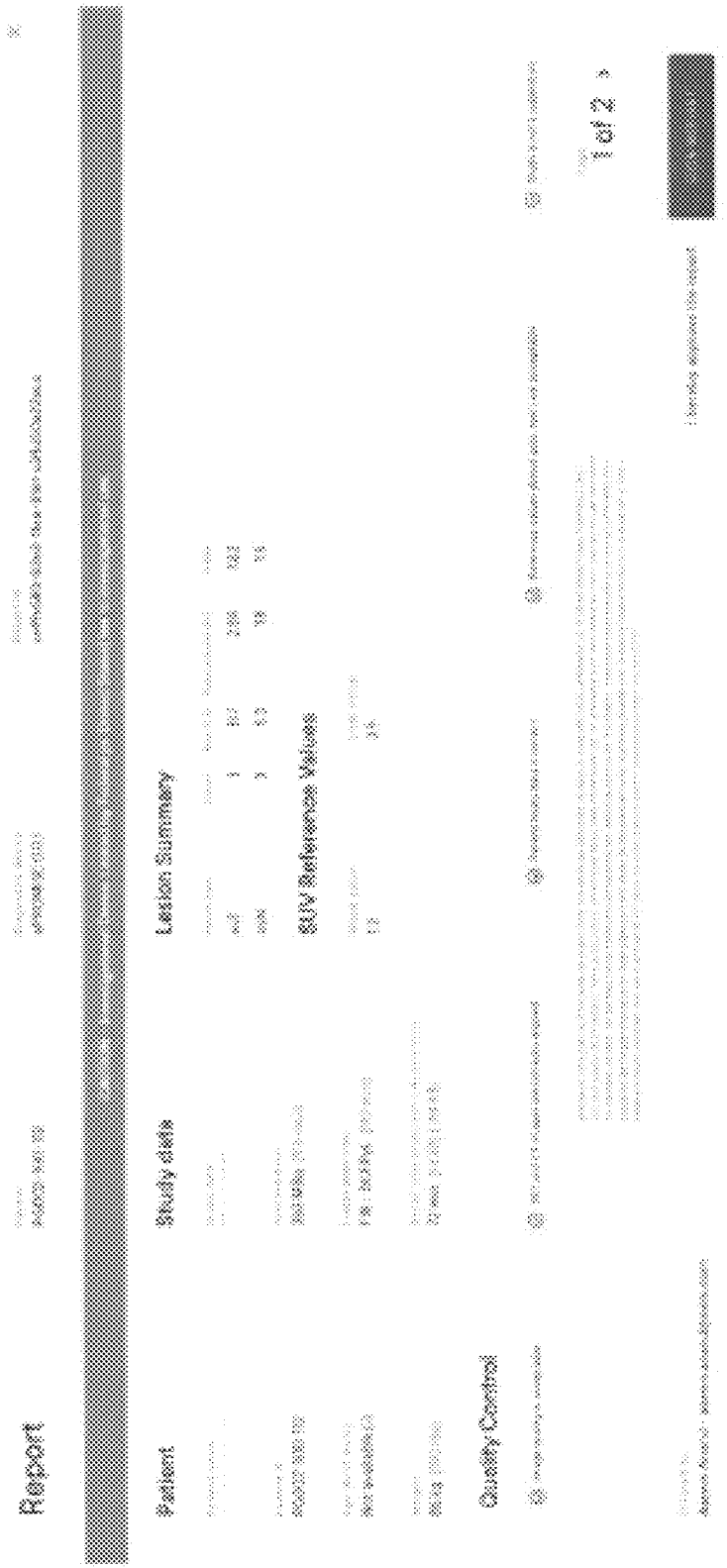

Report
Patient
Study data
Lesion Summary
SUV Reference Values
Quality Control
Top 2 ›

FIG. 6G

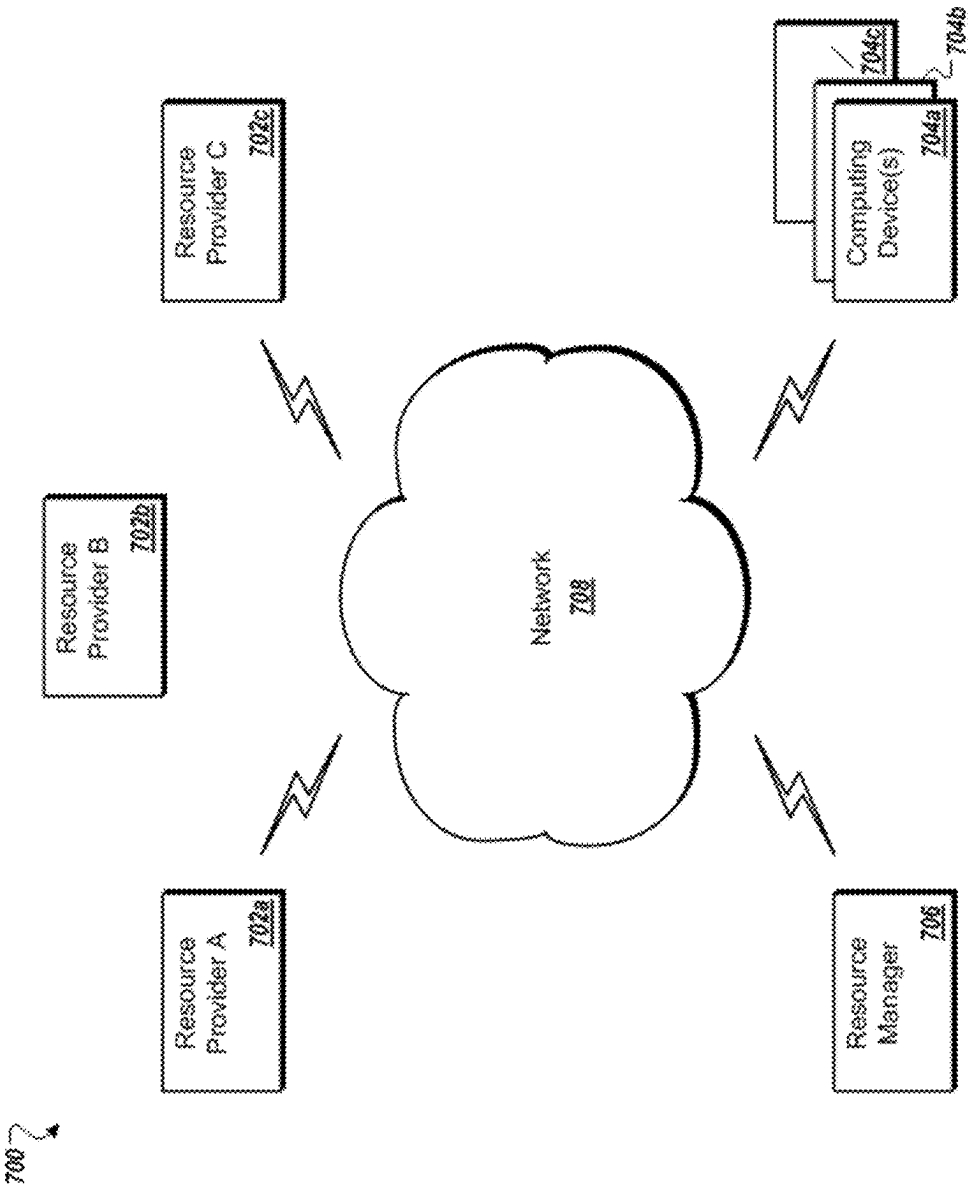

700
Resource Provider A
702a
Resource Provider B
702b
Resource Provider C
702c
Network
708
Computing Device(s)
704a
704c
704b
Resource Manager
706

FIG. 7

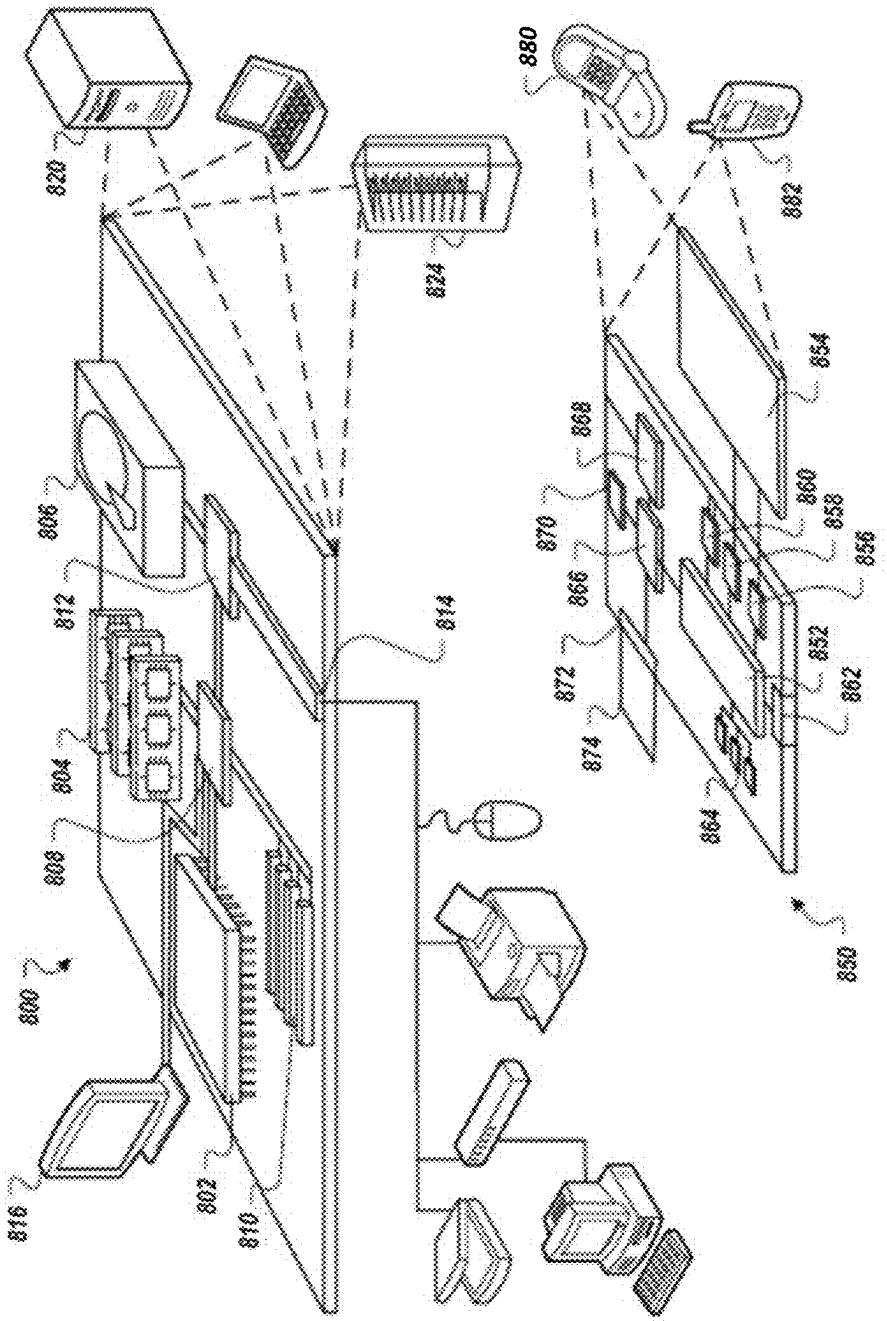

820
824
806
812
814
804
808
800
816
802
810
880
882
854
868
870
866
872
874
864
860
858
856
852
862
850

FIG. 8

SYSTEMS AND METHODS FOR ARTIFICIAL INTELLIGENCE-BASED IMAGE ANALYSIS FOR DETECTION AND CHARACTERIZATION OF LESIONS

CROSS-REFERENCE TO RELATED APPLICATION

This application claims priority to and benefit of U.S. Provisional Application No. 63/048,436, filed Jul. 6, 2020, the content of which is hereby incorporated by reference in its entirety.

TECHNICAL FIELD

This invention relates generally to systems and methods for creation, analysis, and/or presentation of medical image data. More particularly, in certain embodiments, the invention relates to systems and methods for automated analysis of medical images to identify and/or characterize cancerous lesions.

BACKGROUND

Nuclear medicine imaging involves the use of radiolabeled compounds, referred to as radiopharmaceuticals. Radiopharmaceuticals are administered to patients and accumulate in various regions in the body in manner that depends on, and is therefore indicative of, biophysical and/or biochemical properties of tissue therein, such as those influenced by presence and/or state of disease, such as cancer. For example, certain radiopharmaceuticals, following administration to a patient, accumulate in regions of abnormal osteogenesis associated with malignant bone lesions, which are indicative of metastases. Other radiopharmaceuticals may bind to specific receptors, enzymes, and proteins in the body that are altered during evolution of disease. After administration to a patient, these molecules circulate in the blood until they find their intended target. The bound radiopharmaceutical remains at the site of disease, while the rest of the agent clears from the body.

Nuclear medicine imaging techniques capture images by detecting radiation emitted from the radioactive portion of the radiopharmaceutical. The accumulated radiopharmaceutical serves as a beacon so that an image may be obtained depicting the disease location and concentration using commonly available nuclear medicine modalities. Examples of nuclear medicine imaging modalities include bone scan imaging (also referred to as scintigraphy), single-photon emission computerized tomography (SPECT), and positron emission tomography (PET). Bone scan, SPECT, and PET imaging systems are found in most hospitals throughout the world. Choice of a particular imaging modality depends on and/or dictates the particular radiopharmaceutical used. For example, technetium 99m (^{99m}Tc) labeled compounds are compatible with bone scan imaging and SPECT imaging, while PET imaging often uses fluorinated compounds labeled with 18F. The compound ^{99m}Tc methylenediphosphonate (^{99m}Tc MDP) is a popular radiopharmaceutical used for bone scan imaging in order to detect metastatic cancer. Radiolabeled prostate-specific membrane antigen (PSMA) targeting compounds such as ^{99m}Tc labeled **1404** and PyL™ (also referred to as [18F]DCFPyL) can be used with SPECT and PET imaging, respectively, and offer the potential for highly specific prostate cancer detection.

Accordingly, nuclear medicine imaging is a valuable technique for providing physicians with information that can be used to determine the presence and the extent of disease in a patient. The physician can use this information to provide a recommended course of treatment to the patient and to track the progression of disease.

For example, an oncologist may use nuclear medicine images from a study of a patient as input in her assessment of whether the patient has a particular disease, e.g., prostate cancer, what stage of the disease is evident, what the recommended course of treatment (if any) would be, whether surgical intervention is indicated, and likely prognosis. The oncologist may use a radiologist report in this assessment. A radiologist report is a technical evaluation of the nuclear medicine images prepared by a radiologist for a physician who requested the imaging study and includes, for example, the type of study performed, the clinical history, a comparison between images, the technique used to perform the study, the radiologist's observations and findings, as well as overall impressions and recommendations the radiologist may have based on the imaging study results. A signed radiologist report is sent to the physician ordering the study for the physician's review, followed by a discussion between the physician and patient about the results and recommendations for treatment.

Thus, the process involves having a radiologist perform an imaging study on the patient, analyzing the images obtained, creating a radiologist report, forwarding the report to the requesting physician, having the physician formulate an assessment and treatment recommendation, and having the physician communicate the results, recommendations, and risks to the patient. The process may also involve repeating the imaging study due to inconclusive results, or ordering further tests based on initial results. If an imaging study shows that the patient has a particular disease or condition (e.g., cancer), the physician discusses various treatment options, including surgery, as well as risks of doing nothing or adopting a watchful waiting or active surveillance approach, rather than having surgery.

Accordingly, the process of reviewing and analyzing multiple patient images, over time, plays a critical role in the diagnosis and treatment of cancer. There is a significant need for improved tools that facilitate and improve accuracy of image review and analysis for cancer diagnosis and treatment. Improving the toolkit utilized by physicians, radiologists, and other healthcare professionals in this manner provides for significant improvements in standard of care and patient experience.

SUMMARY OF THE INVENTION

Presented herein are systems and methods that provide for improved detection and characterization of lesions within a subject via automated analysis of nuclear medicine images, such as positron emission tomography (PET) and single photon emission computed tomography (SPECT) images. In particular, in certain embodiments, the approaches described herein leverage artificial intelligence (AI) techniques to detect regions of 3D nuclear medicine images that represent potential cancerous lesions in the subject. In certain embodiments, these regions correspond to localized regions of elevated intensity with relative to their surroundings—hotspots—due to increased uptake of radiopharmaceutical within lesions. The systems and methods described herein may use one or more machine learning modules not only to detect presence and locations of such hotspots within an image, but also to segment the region corresponding to the hotspot and/or classify hotspots based on the likelihood that they indeed correspond to a true, underlying cancerous

lesion. These AI-based lesion detection, segmentation, and classification approaches can provide a basis for further characterization of lesions, overall tumor burden, and estimation of disease severity and risk.

For example, once image hotspots representing lesions are detected, segmented, and classified, lesion index values can be computed to provide a measure of radiopharmaceutical uptake within and/or a size (e.g., volume) of the underlying lesion. The computed lesion index values can, in turn, be aggregated to provide an overall estimate of tumor burden, disease severity, metastasis risk, and the like, for the subject. In certain embodiments, lesion index values are computed by comparing measures of intensities within segmented hotspot volumes to intensities of specific reference organs, such as liver and aorta portions. Using reference organs in this manner allows for lesion index values to be measured on a normalized scale that can be compared between images of different subjects. In certain embodiments, the approaches described herein include techniques for suppressing intensity bleed from multiple image regions that correspond to organs and tissue regions in which radiopharmaceutical accumulates at high-levels under normal circumstances, such as a kidney, liver, and a bladder (e.g., urinary bladder). Intensities in regions of nuclear medicine images corresponding to these organs are typically high even for normal, healthy subjects, and not necessarily indicative of cancer. Moreover, high radiopharmaceutical accumulation in these organs results in high levels of emitted radiation. The increased emitted radiation can scatter, resulting not just in high intensities within regions of nuclear medicine images corresponding to the organs themselves, but also at nearby outside voxels. This intensity bleed, into regions of an image outside and around regions corresponding to an organ associated with high uptake, can hinder detection of nearby lesions and cause inaccuracies in measuring uptake therein. Accordingly, correcting such intensity bleed effects improves accuracy of lesion detection and quantification.

In certain embodiments, the AI-based lesion detection technique described herein augment the functional information obtained from nuclear medicine images with anatomical information obtained from anatomical images, such as x-ray computed tomography (CT) images. For example, machine learning modules utilized in the approaches described herein may receive multiple channels of input, including a first channel corresponding to a portion of a functional, nuclear medicine, image (e.g., a PET image; e.g., a SPECT image), as well as additional channels corresponding to a portion of a co-aligned anatomical (e.g., CT) image and/or anatomical information derived therefrom. Adding anatomical context in this manner may improve accuracy of lesion detection approaches. Anatomical information may also be incorporated into lesion classification approaches applied following detection. For example, in addition to computing lesion index values based on intensities of detected hotspots, hotspots may also be assigned an anatomical label based on their location. For example, detected hotspots may be automatically assigned an label (e.g., an alphanumeric label) based on whether their locations correspond to locations within a prostate, pelvic lymph node, non-pelvic lymph node, bone, or a soft-tissue region outside the prostate and lymph nodes.

In certain embodiments, detected hotspots and associated information, such as computed lesion index values and anatomical labeling, are displayed with an interactive graphical user interface (GUI) so as to allow for review by a medical professional, such as a physician, radiologist, technician, etc. Medical professionals may thus use the GUI to review and confirm accuracy of detected hotspots, as well as corresponding index values and/or anatomical labeling. In certain embodiments, the GUI may also allow users to identify, and segment (e.g., manually) additional hotspots within medical images, thereby allowing a medical professional to identify additional potential lesions that he/she believes the automated detection process may have missed. Once identified, lesion index values and/or anatomical labeling may also be determined for these manually identified and segmented lesions. Once a user is satisfied with the set of detected hotspots and information computed therefrom, they may confirm their approval and generate a final, signed, report that can, for example, be reviewed and used to discuss outcomes and diagnosis with a patient, and assess prognosis and treatment options.

In this manner, the approaches described herein provide AI-based tools for lesion detection and analysis that can improve accuracy of and streamline assessment of disease (e.g., cancer) state and progression in a subject. This facilitates diagnosis, prognosis, and assessment of response to treatment, thereby improving patient outcomes.

In one aspect, the invention is directed to a method for automatically processing 3D images of a subject to identify and/or characterize (e.g., grade) cancerous lesions within the subject, the method comprising: (a) receiving (e.g., and/or accessing), by a processor of a computing device, a 3D functional image of the subject obtained using a functional imaging modality [e.g., positron emission tomography (PET); e.g., single-photon emission computed tomography (SPECT)][e.g., wherein the 3D functional image comprises a plurality of voxels, each representing a particular physical volume within the subject and having an intensity value (e.g., standard uptake value (SUV)) that represents detected radiation emitted from the particular physical volume, wherein at least a portion of the plurality of voxels of the 3D functional image represent physical volumes within the target tissue region]; (b) automatically detecting, by the processor, using a machine learning module [e.g., a pre-trained machine learning module (e.g., having pre-determined (e.g., and fixed) parameters having been determined via a training procedure)], one or more hotspots within the 3D functional image, each hotspot corresponding to a local region of elevated intensity with respect to its surrounding and representing (e.g., indicative of) a potential cancerous lesion within the subject, thereby creating one or both of (i) and (ii) as follows: (i) a hotspot list [e.g., a list of coordinates (e.g., image coordinates; e.g., physical space coordinates); e.g., a mask identifying voxels of the 3D functional image corresponding to a location (e.g., a center of mass) of a detected hotspot] identifying, for each hotspot, a location of the hotspot, and (ii) a 3D hotspot map, identifying, for each hotspot, a corresponding 3D hotspot volume within the 3D functional image {e.g., wherein, the 3D hotspot map is a segmentation map (e.g., comprising one or more segmentation masks) identifying, for each hotspot, voxels within the 3D functional image corresponding to the 3D hotspot volume of each hotspot [e.g., wherein the 3D hotspot map is obtained via artificial intelligence-based segmentation of the functional image (e.g., using a machine-learning module that receives, as input, at least the 3D functional image and generates the 3D hotspot map as output, thereby segmenting hotspots)]; e.g., wherein the 3D hotspot map delineates, for each hotspot, a 3D boundary (e.g., an irregular boundary) of the hotspot (e.g., the 3D boundary enclosing the 3D hotspot volume, e.g., and distinguishing voxels of the 3D functional image that make up the 3D hotspot volume from other

voxels of the 3D functional image)}; and (c) storing and/or providing, for display and/or further processing, the hotspot list and/or the 3D hotspot map.

In certain embodiments, the machine learning module receives, as input, at least a portion of the 3D functional image and automatically detects the one or more hotspots based at least in part on intensities of voxels of the received portion of the 3D functional image. In certain embodiments, the machine learning module receives, as input, a 3D segmentation map that identifies one or more volumes of interest (VOIs) within the 3D functional image, each VOI corresponding to a particular target tissue region and/or a particular anatomical region within the subject [e.g., a soft-tissue region (e.g., a prostate, a lymph node, a lung, a breast); e.g., one or more particular bones; e.g., an overall skeletal region].

In certain embodiments, the method comprises receiving (e.g., and/or accessing), by the processor, a 3D anatomical image of the subject obtained using an anatomical imaging modality [e.g., x-ray computed tomography (CT); e.g., magnetic resonance imaging (Mill); e.g., ultra-sound], wherein the 3D anatomical image comprises a graphical representation of tissue (e.g., soft-tissue and/or bone) within the subject, and the machine learning module receives at least two channels of input, said input channels comprising a first input channel corresponding to at least a portion of the 3D anatomical image and a second input channel corresponding to at least a portion of the 3D functional image [e.g., wherein the machine learning module receives a PET image and a CT image as separate channels (e.g., separate channels representative of the same volume) (e.g., analogous to receipt by a machine learning module of two color channels (RGB) of a photographic color image)].

In certain embodiments, the machine learning module receives, as input, a 3D segmentation map that identifies, within the 3D functional image and/or the 3D anatomical image, one or more volumes of interest (VOIs), each VOI corresponding to a particular target tissue region and/or a particular anatomical region. In certain embodiments, the method comprises automatically segmenting, by the processor, the 3D anatomical image, thereby creating the 3D segmentation map.

In certain embodiments, the machine learning module is a region-specific machine learning module that receives, as input, a specific portion of the 3D functional image corresponding to one or more specific tissue regions and/or anatomical regions of the subject.

In certain embodiments, the machine learning module generates, as output, the hotspot list [e.g., wherein the machine learning module implements a machine learning algorithm (e.g., an artificial neural network (ANN)) trained to determine, based on intensities of voxels of at least a portion of the 3D functional image, one or more locations (e.g., 3D coordinates), each corresponding to a location of one of the one or more hotspots].

In certain embodiments, the machine learning module generates, as output, the 3D hotspot map [e.g., wherein the machine learning module implements a machine learning algorithm (e.g., an artificial neural network (ANN)) trained to segment the 3D functional image (e.g., based at least in part on intensities of voxels of the 3D functional image) to identify the 3D hotspot volumes of the 3D hotspot map (e.g., the 3D hotspot map delineating, for each hotspot, a 3D boundary (e.g., an irregular boundary) of the hotspot, thereby identifying the 3D hotspot volumes (e.g., enclosed by the 3D hotspot boundaries)); e.g., wherein the machine learning module implements a machine learning algorithm trained to determine, for each voxel of at least a portion of the 3D functional image, a hotspot likelihood value representing a likelihood that the voxel corresponds to a hotspot (e.g., and step (b) comprises performing one or more subsequent post-processing steps, such as thresholding, to identify the 3D hotspot volumes of the 3D hotspot map using the hotspot likelihood values (e.g., the 3D hotspot map delineating, for each hotspot, a 3D boundary (e.g., an irregular boundary) of the hotspot, thereby identifying the 3D hotspot volumes (e.g., enclosed by the 3D hotspot boundaries)))].

In certain embodiments, the method comprises: (d) determining, by the processor, for each hotspot of at least a portion of the hotspots, a lesion likelihood classification corresponding to a likelihood of the hotspot representing a lesion within the subject [e.g., a binary classification indicative of whether the hotspot is a true lesion or not; e.g., a likelihood value on a scale (e.g., a floating point value ranging from zero to one) representing a likelihood of the hotspot representing a true lesion].

In certain embodiments, step (d) comprises using a second machine learning module to determine, for each hotspot of the portion, the lesion likelihood classification [e.g., wherein the machine learning module implements a machine learning algorithm trained to detect hotspots (e.g., to generate, as output, the hotspot list and/or the 3D hotspot map) and to determine, for each hotspot, the lesion likelihood classification for the hotpot]. In certain embodiments, step (d) comprises using a second machine learning module (e.g., a hotspot classification module) to determine the lesion likelihood classification for each hotspot [e.g., based at least in part on one or more members selected from the group consisting of: intensities of the 3D functional image, the hotspot list, the 3D hotspot map, intensities of a 3D anatomical image, and a 3D segmentation map; e.g., wherein the second machine learning module receives one or more channels of input corresponding to one or more members selected from the group consisting of intensities of the 3D functional image, the hotspot list, the 3D hotspot map, intensities of a 3D anatomical image, and a 3D segmentation map].

In certain embodiments, the method comprises determining, by the processor, for each hotspot, a set of one or more hotspot features and using the set of the one or more hotspot features as input to the second machine learning module.

In certain embodiments, the method comprises: (e) selecting, by the processor, based at least in part on the lesion likelihood classifications for the hotspots, a subset of the one or more hotspots corresponding to hotspots having a high likelihood of corresponding to cancerous lesions (e.g., for inclusion in a report; e.g., for use in computing one or more risk index values for the subject).

In certain embodiments, the method comprises: (f) [e.g., prior to step (b)] adjusting intensities of voxels of the 3D functional image, by the processor, to correct for intensity bleed (e.g., cross-talk) from one or more high-intensity volumes of the 3D functional image, each of the one or more high-intensity volumes corresponding to a high-uptake tissue region within the subject associated with high radiopharmaceutical uptake under normal circumstances (e.g., not necessarily indicative of cancer). In certain embodiments, step (f) comprises correcting for intensity bleed from a plurality of high-intensity volumes one at a time, in a sequential fashion [e.g., first adjusting intensities of voxels of the 3D functional image to correct for intensity bleed from a first high-intensity volume to generate a first corrected image, then adjusting intensities of voxels of the first corrected image to correct for intensity bleed from a second

high-intensity volume, and so on]. In certain embodiments, the one or more high-intensity volumes correspond to one or more high-uptake tissue regions selected from the group consisting of a kidney, a liver, and a bladder (e.g., a urinary bladder).

In certain embodiments, the method comprises: (g) determining, by the processor, for each of at least a portion of the one or more hotspots, a corresponding lesion index indicative of a level of radiopharmaceutical uptake within and/or size (e.g., volume) of an underlying lesion to which the hotspot corresponds. In certain embodiments, step (g) comprises comparing an intensity (intensities) (e.g., corresponding to standard uptake values (SUVs)) of one or more voxels associated with the hotspot (e.g., at and/or about a location of the hotspot; e.g., within a volume of the hotspot) with one or more reference values, each reference value associated with a particular reference tissue region (e.g., a liver; e.g., an aorta portion) within the subject and determined based on intensities (e.g., SUV values) of a reference volume corresponding to the reference tissue region [e.g., as an average (e.g., a robust average, such as a mean of values in an interquartile range)]. In certain embodiments, the one or more reference values comprise one or more members selected from the group consisting of an aorta reference value associated with an aorta portion of the subject and a liver reference value associated with a liver of the subject.

In certain embodiments, for at least one particular reference value associated with a particular reference tissue region, determining the particular reference value comprises fitting intensities of voxels [e.g., fitting an distribution of intensities of voxels (e.g., fitting a histogram of voxel intensities)] within a particular reference volume corresponding to the particular reference tissue region to a multi-component mixture model (e.g., a two-component Gaussian model)[e.g., and identifying one or more minor peaks in a distribution of voxel intensities, said minor peaks corresponding to voxels associated with anomalous uptake, and excluding those voxels from the reference value determination (e.g., thereby accounting for effects of abnormally low radiopharmaceutical uptake in certain portions of reference tissue regions, such as portions of the liver)].

In certain embodiments, the method comprises using the determined lesion index values compute (e.g., automatically, by the processor) an overall risk index for the subject, indicative of a caner status and/or risk for the subject.

In certain embodiments, the method comprises determining, by the processor (e.g., automatically), for each hotspot, an anatomical classification corresponding to a particular anatomical region and/or group of anatomical regions within the subject in which the potential cancerous lesion that the hotspot represents is determined [e.g., by the processor (e.g., based on a received and/or determined 3D segmentation map)] to be located [e.g., within a prostate, a pelvic lymph node, a non-pelvic lymph node, a bone (e.g., a bone metastatic region), and a soft tissue region not situated in prostate or lymph node].

In certain embodiments, the method comprise: (h) causing, by the processor, for display within a graphical user interface (GUI), graphical representation of at least a portion of the one or more hotspots for review by a user. In certain embodiments, the method comprises: (i) receiving, by the processor, via the GUI, a user selection of a subset of the one or more hotspots confirmed via user review as likely to represent underlying cancerous lesions within the subject.

In certain embodiments, the 3D functional image comprises a PET or SPECT image obtained following administration of an agent (e.g., a radiopharmaceutical; e.g., an imaging agent) to the subject. In certain embodiments, the agent comprises a PSMA binding agent. In certain embodiments, the agent comprises [18F]DCFPyL. In certain embodiments, the agent comprises ^{99m}Tc.

In certain embodiments, the machine learning module implements a neural network [e.g., an artificial neural network (ANN); e.g., a convolutional neural network (CNN)].

In certain embodiments, the processor is a processor of a cloud-based system.

In another aspect, the invention is directed to a method for automatically processing 3D images of a subject to identify and/or characterize (e.g., grade) cancerous lesions within the subject, the method comprising: (a) receiving (e.g., and/or accessing), by a processor of a computing device, a 3D functional image of the subject obtained using a functional imaging modality [e.g., positron emission tomography (PET); e.g., single-photon emission computed tomography (SPECT)][e.g., wherein the 3D functional image comprises a plurality of voxels, each representing a particular physical volume within the subject and having an intensity value that represents detected radiation emitted from the particular physical volume, wherein at least a portion of the plurality of voxels of the 3D functional image represent physical volumes within the target tissue region]; (b) receiving (e.g., and/or accessing), by the processor, a 3D anatomical image of the subject obtained using an anatomical imaging modality [e.g., x-ray computed tomography (CT); e.g., magnetic resonance imaging (MRI); e.g., ultra-sound], wherein the 3D anatomical image comprises a graphical representation of tissue (e.g., soft-tissue and/or bone) within the subject; (c) automatically detecting, by the processor, using a machine learning module, one or more hotspots within the 3D functional image, each hotspot corresponding to a local region of elevated intensity with respect to its surrounding and representing (e.g., indicative of) a potential cancerous lesion within the subject, thereby creating one or both of (i) and (ii) as follows: (i) a hotspot list identifying, for each hotspot, a location of the hotspot, and (ii) a 3D hotspot map, identifying, for each hotspot, a corresponding 3D hotspot volume within the 3D functional image {e.g., wherein, the 3D hotspot map is a segmentation map (e.g., comprising one or more segmentation masks) identifying, for each hotspot, voxels within the 3D functional image corresponding to the 3D hotspot volume of each hotspot [e.g., wherein the 3D hotspot map is obtained via artificial intelligence-based segmentation of the functional image (e.g., using a machine-learning module that receives, as input, at least the 3D functional image and generates the 3D hotspot map as output, thereby segmenting hotspots)]; e.g., wherein the 3D hotspot map delineates, for each hotspot, a 3D boundary (e.g., an irregular boundary) of the hotspot (e.g., the 3D boundary enclosing the 3D hotspot volume, e.g., and distinguishing voxels of the 3D functional image that make up the 3D hotspot volume from other voxels of the 3D functional image)}, wherein the machine learning module receives at least two channels of input, said input channels comprising a first input channel corresponding to at least a portion of the 3D anatomical image and a second input channel corresponding to at least a portion of the 3D functional image [e.g., wherein the machine learning module receives a PET image and a CT image as separate channels (e.g., separate channels representative of the same volume) (e.g., analogous to receipt by a machine learning module of two color channels (RGB) of a photographic color image)] and/or anatomical information derived therefrom [e.g., a 3D segmentation map that identifies, within the 3D functional image, one or more volumes of interest

(VOIs), each VOI corresponding to a particular target tissue region and/or a particular anatomical region]; and (d) storing and/or providing for display and/or further processing, the hotspot list and/or the 3D hotspot map.

In another aspect, the invention is directed to a method for automatically processing 3D images of a subject to identify and/or characterize (e.g., grade) cancerous lesions within the subject, the method comprising: (a) receiving (e.g., and/or accessing), by a processor of a computing device, a 3D functional image of the subject obtained using a functional imaging modality [e.g., positron emission tomography (PET); e.g., single-photon emission computed tomography (SPECT)][e.g., wherein the 3D functional image comprises a plurality of voxels, each representing a particular physical volume within the subject and having an intensity value that represents detected radiation emitted from the particular physical volume, wherein at least a portion of the plurality of voxels of the 3D functional image represent physical volumes within the target tissue region]; (b) automatically detecting, by the processor, using a first machine learning module, one or more hotspots within the 3D functional image, each hotspot corresponding to a local region of elevated intensity with respect to its surrounding and representing (e.g., indicative of) a potential cancerous lesion within the subject, thereby creating a hotspot list identifying, for each hotspot, a location of the hotspot [e.g., wherein the machine learning module implements a machine learning algorithm (e.g., an artificial neural network (ANN)) trained to determine, based on intensities of voxels of at least a portion of the 3D functional image, one or more locations (e.g., 3D coordinates), each corresponding to a location of one of the one or more hotspots]; (c) automatically determining, by the processor, using a second machine learning module and the hotspot list, for each of the one or more hotspots, a corresponding 3D hotspot volume within the 3D functional image, thereby creating a 3D hotspot map [e.g., wherein the second machine learning module implements a machine learning algorithm (e.g., an artificial neural network (ANN)) trained to segment the 3D functional image based at least in part on the hotspot list along with intensities of voxels of the 3D functional image to identify the 3D hotspot volumes of the 3D hotspot map; e.g., wherein the machine learning module implements a machine learning algorithm trained to determine, for each voxel of at least a portion of the 3D functional image, a hotspot likelihood value representing a likelihood that the voxel corresponds to a hotspot (e.g., and step (b) comprises performing one or more subsequent post-processing steps, such as thresholding, to identify the 3D hotspot volumes of the 3D hotspot map using the hotspot likelihood values][e.g., wherein, the 3D hotspot map is a segmentation map (e.g., comprising one or more segmentation masks) generated using (e.g., based on and/or corresponding to output from) the second machine learning module, the 3D hotspot map identifying, for each hotspot, voxels within the 3D functional image corresponding to the 3D hotspot volume of each hotspot); e.g., wherein the 3D hotspot map delineates, for each hotspot, a 3D boundary (e.g., an irregular boundary) of the hotspot (e.g., the 3D boundary enclosing the 3D hotspot volume, e.g., and distinguishing voxels of the 3D functional image that make up the 3D hotspot volume from other voxels of the 3D functional image)]; and (d) storing and/or providing for display and/or further processing, the hotspot list and/or the 3D hotspot map.

In certain embodiments, the method comprises: (e) determining, by the processor, for each hotspot of at least a portion of the hotspots, a lesion likelihood classification corresponding to a likelihood of the hotspot representing a lesion within the subject. In certain embodiments, step (e) comprises using a third machine learning module (e.g., a hotspot classification module) to determine the lesion likelihood classification for each hotspot [e.g., based at least in part on one or more members selected from the group consisting of intensities of the 3D functional image, the hotspot list, the 3D hotspot map, intensities of a 3D anatomical image, and a 3D segmentation map; e.g., wherein the third machine learning module receives one or more channels of input corresponding to one or more members selected from the group consisting of intensities of the 3D functional image, the hotspot list, the 3D hotspot map, intensities of a 3D anatomical image, and a 3D segmentation map].

In certain embodiments, the method comprises: (f) selecting, by the processor, based at least in part on the lesion likelihood classifications for the hotspots, a subset of the one or more hotspots corresponding to hotspots having a high likelihood of corresponding to cancerous lesions (e.g., for inclusion in a report; e.g., for use in computing one or more risk index values for the subject).

In another aspect, the invention is directed to a method of measuring intensity values within a reference volume corresponding to a reference tissue region (e.g., a liver volume associated with a liver of a subject) so as to avoid impact from tissue regions associated with low (e.g., abnormally low) radiopharmaceutical uptake (e.g., due to tumors without tracer uptake), the method comprising: (a) receiving (e.g., and/or accessing), by a processor of a computing device, the 3D functional image of a subject, said 3D functional image obtained using a functional imaging modality [e.g., positron emission tomography (PET); e.g., single-photon emission computed tomography (SPECT)] [e.g., wherein the 3D functional image comprises a plurality of voxels, each representing a particular physical volume within the subject and having an intensity value that represents detected radiation emitted from the particular physical volume, wherein at least a portion of the plurality of voxels of the 3D functional image represent physical volumes within the target tissue region]; (b) identifying, by the processor, the reference volume within the 3D functional image; (c) fitting, by the processor, a multi-component mixture model (e.g., a two-component Gaussian mixture model) to intensities of voxels within the reference volume [e.g., fitting the multi-component mixture model to a distribution (e.g., a histogram) of intensities of voxels within the reference volume]; (d) identifying, by the processor, a major mode of the multi-component model; (e) determining, by the processor, a measure of (e.g., a mean, a maximum, a mode, a median, etc.) intensities corresponding to the major mode, thereby determining a reference intensity value corresponding to a measure of intensity of voxels that are (i) within the reference tissue volume and (ii) associated with the major mode (e.g., and excluding, from the reference value calculation, voxels having intensities associated with minor modes) (e.g., thereby avoiding impact from tissue regions associated with low radiopharmaceutical uptake); (f) detecting, by the processor, within the functional image, one or more hotspots corresponding potential cancerous lesions; and (g) determining, by the processes or, for each hotspot of at least a portion of the detected hotspots, a lesion index value, using at least the reference intensity value [e.g., the lesion index value based on (i) a measure of intensities of voxels corresponding to the detected hotspot and (ii) the reference intensity value].

In another aspect, the invention is directed to a method of correcting for intensity bleed (e.g., cross-talk) from due to high-uptake tissue regions within the subject that are associated with high radiopharmaceutical uptake under normal circumstances (e.g., and not necessarily indicative of cancer), the method comprising: (a) receiving (e.g., and/or accessing), by a processor of a computing device, the 3D functional image of the subject, said 3D functional image obtained using a functional imaging modality [e.g., positron emission tomography (PET); e.g., single-photon emission computed tomography (SPECT)][e.g., wherein the 3D functional image comprises a plurality of voxels, each representing a particular physical volume within the subject and having an intensity value that represents detected radiation emitted from the particular physical volume, wherein at least a portion of the plurality of voxels of the 3D functional image represent physical volumes within the target tissue region]; (b) identifying, by the processor, a high-intensity volume within the 3D functional image, said high intensity volume corresponding to a particular high-uptake tissue region (e.g., a kidney; e.g., a liver; e.g., a bladder) in which high radiopharmaceutical uptake occurs under normal circumstances; (c) identifying, by the processor, based on the identified high-intensity volume, a suppression volume within the 3D functional image, said suppression volume corresponding to a volume lying outside and within a predetermined decay distance from a boundary of the identified high intensity volume; (d) determining, by the processor, a background image corresponding to the 3D functional image with intensities of voxels within the high-intensity volume replaced with interpolated values determined based on intensities of voxels of the 3D functional image within the suppression volume; (e) determining, by the processor, an estimation image by subtracting intensities of voxels of the background image from intensities of voxels from the 3D functional image (e.g., performing a voxel-by-voxel subtraction); (f) determining, by the processor, a suppression map by: extrapolating intensities of voxels of the estimation image corresponding to the high-intensity volume to locations of voxels within the suppression volume to determine intensities of voxels of the suppression map corresponding to the suppression volume; and setting intensities of voxels of the suppression map corresponding to locations outside the suppression volume to zero; and (g) adjusting, by the processor, intensities of voxels of the 3D functional image based on the suppression map (e.g., by subtracting intensities of voxels of the suppression map from intensities of voxels of the 3D functional image), thereby correcting for intensity bleed from the high-intensity volume.

In certain embodiments, the method comprises performing steps (b) through (g) for each of a plurality of high-intensity volumes in a sequential manner, thereby correcting for intensity bleed from each of the plurality of high-intensity volumes.

In certain embodiments, the plurality of high-intensity volumes comprise one or more members selected from the group consisting of a kidney, a liver, and a bladder (e.g., a urinary bladder).

In another aspect, the invention is directed to a method for automatically processing 3D images of a subject to identify and/or characterize (e.g., grade) cancerous lesions within the subject, the method comprising: (a) receiving (e.g., and/or accessing), by a processor of a computing device, a 3D functional image of the subject obtained using a functional imaging modality [e.g., positron emission tomography (PET); e.g., single-photon emission computed tomography (SPECT)][e.g., wherein the 3D functional image comprises a plurality of voxels, each representing a particular physical volume within the subject and having an intensity value that represents detected radiation emitted from the particular physical volume, wherein at least a portion of the plurality of voxels of the 3D functional image represent physical volumes within the target tissue region]; (b) automatically detecting, by the processor, one or more hotspots within the 3D functional image, each hotspot corresponding to a local region of elevated intensity with respect to its surrounding and representing (e.g., indicative of) a potential cancerous lesion within the subject; (c) causing, by the processor, rendering of a graphical representation of the one or more hotspots for display within an interactive graphical user interface (GUI) (e.g., a quality control and reporting GUI); (d) receiving, by the processor, via the interactive GUI, a user selection of a final hotspot set comprising at least a portion (e.g., up to all) of the one or more automatically detected hotspots (e.g., for inclusion in a report); and (e) storing and/or providing for display and/or further processing, the final hotspot set.

In certain embodiments, the method comprises: (f) receiving, by the processor, via the GUI, a user selection of one or more additional, user-identified, hotspots for inclusion in the final hotspot set; and (g) updating, by the processor, the final hotspot set to include the one or more additional user-identified hotspots.

In certain embodiments, step (b) comprises using one or more machine learning modules.

In another aspect, the invention is directed to a method for automatically processing 3D images of a subject to identify and characterize (e.g., grade) cancerous lesions within the subject, the method comprising: (a) receiving (e.g., and/or accessing), by a processor of a computing device, a 3D functional image of the subject obtained using a functional imaging modality [e.g., positron emission tomography (PET); e.g., single-photon emission computed tomography (SPECT)][e.g., wherein the 3D functional image comprises a plurality of voxels, each representing a particular physical volume within the subject and having an intensity value that represents detected radiation emitted from the particular physical volume, wherein at least a portion of the plurality of voxels of the 3D functional image represent physical volumes within the target tissue region]; (b) automatically detecting, by the processor, one or more hotspots within the 3D functional image, each hotspot corresponding to a local region of elevated intensity with respect to its surrounding and representing (e.g., indicative of) a potential cancerous lesion within the subject; (c) automatically determining, by the processor, for each of at least a portion of the one or more hotspots, an anatomical classification corresponding to a particular anatomical region and/or group of anatomical regions within the subject in which the potential cancerous lesion that the hotspot represents is determined [e.g., by the processor (e.g., based on a received and/or determined 3D segmentation map)] to be located [e.g., within a prostate, a pelvic lymph node, a non-pelvic lymph node, a bone (e.g., a bone metastatic region), and a soft tissue region not situated in prostate or lymph node]; and (d) storing and/or providing for display and/or further processing, an identification of the one or more hotspots along with, for each hotspot, the anatomical classification corresponding to the hotspot.

In certain embodiments, step (b) comprises using one or more machine learning modules.

In another aspect, the invention is directed to a system for automatically processing 3D images of a subject to identify and/or characterize (e.g., grade) cancerous lesions within the

subject, the system comprising: a processor of a computing device; and a memory having instructions stored thereon, wherein the instructions, when executed by the processor, cause the processor to: (a) receive (e.g., and/or access) a 3D functional image of the subject obtained using a functional imaging modality [e.g., positron emission tomography (PET); e.g., single-photon emission computed tomography (SPECT)][e.g., wherein the 3D functional image comprises a plurality of voxels, each representing a particular physical volume within the subject and having an intensity value (e.g., standard uptake value (SUV)) that represents detected radiation emitted from the particular physical volume, wherein at least a portion of the plurality of voxels of the 3D functional image represent physical volumes within the target tissue region]; (b) automatically detect, using a machine learning module [e.g., a pre-trained machine learning module (e.g., having pre-determined (e.g., and fixed) parameters having been determined via a training procedure)], one or more hotspots within the 3D functional image, each hotspot corresponding to a local region of elevated intensity with respect to its surrounding and representing (e.g., indicative of) a potential cancerous lesion within the subject, thereby creating one or both of (i) and (ii) as follows: (i) a hotspot list [e.g., a list of coordinates (e.g., image coordinates; e.g., physical space coordinates); e.g., a mask identifying voxels of the 3D functional image, each voxel corresponding to a location (e.g., a center of mass) of a detected hotspot] identifying, for each hotspot, a location of the hotspot, and (ii) a 3D hotspot map, identifying, for each hotspot, a corresponding 3D hotspot volume within the 3D functional image {e.g., wherein, the 3D hotspot map is a segmentation map (e.g., comprising one or more segmentation masks) identifying, for each hotspot, voxels within the 3D functional image corresponding to the 3D hotspot volume of each hotspot [e.g., wherein the 3D hotspot map is obtained via artificial intelligence-based segmentation of the functional image (e.g., using a machine-learning module that receives, as input, at least the 3D functional image and generates the 3D hotspot map as output, thereby segmenting hotspots)]; e.g., wherein the 3D hotspot map delineates, for each hotspot, a 3D boundary (e.g., an irregular boundary) of the hotspot (e.g., the 3D boundary enclosing the 3D hotspot volume, e.g., and distinguishing voxels of the 3D functional image that make up the 3D hotspot volume from other voxels of the 3D functional image)}; and (c) store and/or provide, for display and/or further processing, the hotspot list and/or the 3D hotspot map.

In certain embodiments, the machine learning module receives, as input, at least a portion of the 3D functional image and automatically detects the one or more hotspots based at least in part on intensities of voxels of the received portion of the 3D functional image.

In certain embodiments, the machine learning module receives, as input, a 3D segmentation map that identifies one or more volumes of interest (VOIs) within the 3D functional image, each VOI corresponding to a particular target tissue region and/or a particular anatomical region within the subject [e.g., a soft-tissue region (e.g., a prostate, a lymph node, a lung, a breast); e.g., one or more particular bones; e.g., an overall skeletal region].

In certain embodiments, the instructions cause the processor to: receive (e.g., and/or access) a 3D anatomical image of the subject obtained using an anatomical imaging modality [e.g., x-ray computed tomography (CT); e.g., magnetic resonance imaging (Mill); e.g., ultra-sound], wherein the 3D anatomical image comprises a graphical representation of tissue (e.g., soft-tissue and/or bone) within the subject, and the machine learning module receives at least two channels of input, said input channels comprising a first input channel corresponding to at least a portion of the 3D anatomical image and a second input channel corresponding to at least a portion of the 3D functional image [e.g., wherein the machine learning module receives a PET image and a CT image as separate channels (e.g., separate channels representative of the same volume) (e.g., analogous to receipt by a machine learning module of two color channels (RGB) of a photographic color image)].

In certain embodiments, the machine learning module receives, as input, a 3D segmentation map that identifies, within the 3D functional image and/or the 3D anatomical image, one or more volumes of interest (VOIs), each VOI corresponding to a particular target tissue region and/or a particular anatomical region.

In certain embodiments, the instructions cause the processor to automatically segment the 3D anatomical image, thereby creating the 3D segmentation map.

In certain embodiments, the machine learning module is a region-specific machine learning module that receives, as input, a specific portion of the 3D functional image corresponding to one or more specific tissue regions and/or anatomical regions of the subject.

In certain embodiments, the machine learning module generates, as output, the hotspot list [e.g., wherein the machine learning module implements a machine learning algorithm (e.g., an artificial neural network (ANN)) trained to determine, based on intensities of voxels of at least a portion of the 3D functional image, one or more locations (e.g., 3D coordinates), each corresponding to a location of one of the one or more hotspots].

In certain embodiments, the machine learning module generates, as output, the 3D hotspot map [e.g., wherein the machine learning module implements a machine learning algorithm (e.g., an artificial neural network (ANN)) trained to segment the 3D functional image (e.g., based at least in part on intensities of voxels of the 3D functional image) to identify the 3D hotspot volumes of the 3D hotspot map (e.g., the 3D hotspot map delineating, for each hotspot, a 3D boundary (e.g., an irregular boundary) of the hotspot, thereby identifying the 3D hotspot volumes (e.g., enclosed by the 3D hotspot boundaries)); e.g., wherein the machine learning module implements a machine learning algorithm trained to determine, for each voxel of at least a portion of the 3D functional image, a hotspot likelihood value representing a likelihood that the voxel corresponds to a hotspot (e.g., and step (b) comprises performing one or more subsequent post-processing steps, such as thresholding, to identify the 3D hotspot volumes of the 3D hotspot map using the hotspot likelihood values (e.g., the 3D hotspot map delineating, for each hotspot, a 3D boundary (e.g., an irregular boundary) of the hotspot, thereby identifying the 3D hotspot volumes (e.g., enclosed by the 3D hotspot boundaries)))].

In certain embodiments, the instructions cause the processor to: (d) determine, for each hotspot of at least a portion of the hotspots, a lesion likelihood classification corresponding to a likelihood of the hotspot representing a lesion within the subject [e.g., a binary classification indicative of whether the hotspot is a true lesion or not; e.g., a likelihood value on a scale (e.g., a floating point value ranging from zero to one) representing a likelihood of the hotspot representing a true lesion].

In certain embodiments, at step (d) the instructions cause the processor to use the machine learning module to determine, for each hotspot of the portion, the lesion likelihood classification [e.g., wherein the machine learning module

implements a machine learning algorithm trained to detect hotspots (e.g., to generate, as output, the hotspot list and/or the 3D hotspot map) and to determine, for each hotspot, the lesion likelihood classification for the hotpot].

In certain embodiments, at step (d) the instructions cause the processor to use a second machine learning module (e.g., a hotspot classification module) to determine the lesion likelihood classification for each hotspot [e.g., based at least in part on one or more members selected from the group consisting of intensities of the 3D functional image, the hotspot list, the 3D hotspot map, intensities of a 3D anatomical image, and a 3D segmentation map; e.g., wherein the second machine learning module receives one or more channels of input corresponding to one or more members selected from the group consisting of: intensities of the 3D functional image, the hotspot list, the 3D hotspot map, intensities of a 3D anatomical image, and a 3D segmentation map].

In certain embodiments, the instructions cause the processor to determine, for each hotspot, a set of one or more hotspot features and using the set of the one or more hotspot features as input to the second machine learning module.

In certain embodiments, 55 to 58, wherein the instructions cause the processor to: (e) select, based at least in part on the lesion likelihood classifications for the hotspots, a subset of the one or more hotspots corresponding to hotspots having a high likelihood of corresponding to cancerous lesions (e.g., for inclusion in a report; e.g., for use in computing one or more risk index values for the subject).

In certain embodiments, the instructions cause the processor to: (f) [e.g., prior to step (b)] adjust intensities of voxels of the 3D functional image, by the processor, to correct for intensity bleed (e.g., cross-talk) from one or more high-intensity volumes of the 3D functional image, each of the one or more high-intensity volumes corresponding to a high-uptake tissue region within the subject associated with high radiopharmaceutical uptake under normal circumstances (e.g., not necessarily indicative of cancer).

In certain embodiments, at step (f) the instructions cause the processor to correct for intensity bleed from a plurality of high-intensity volumes one at a time, in a sequential fashion [e.g., first adjusting intensities of voxels of the 3D functional image to correct for intensity bleed from a first high-intensity volume to generate a first corrected image, then adjusting intensities of voxels of the first corrected image to correct for intensity bleed from a second high-intensity volume, and so on].

In certain embodiments, the one or more high-intensity volumes correspond to one or more high-uptake tissue regions selected from the group consisting of a kidney, a liver, and a bladder (e.g., a urinary bladder).

In certain embodiments, the instructions cause the processor to: (g) determine, for each of at least a portion of the one or more hotspots, a corresponding lesion index indicative of a level of radiopharmaceutical uptake within and/or size (e.g., volume) of an underlying lesion to which the hotspot corresponds.

In certain embodiments, at step (g) the instructions cause the processor to compare an intensity (intensities) (e.g., corresponding to standard uptake values (SUVs)) of one or more voxels associated with the hotspot (e.g., at and/or about a location of the hotspot; e.g., within a volume of the hotspot) with one or more reference values, each reference value associated with a particular reference tissue region (e.g., a liver; e.g., an aorta portion) within the subject and determined based on intensities (e.g., SUV values) of a reference volume corresponding to the reference tissue region [e.g., as an average (e.g., a robust average, such as a mean of values in an interquartile range)].

In certain embodiments, the one or more reference values comprise one or more members selected from the group consisting of an aorta reference value associated with an aorta portion of the subject and a liver reference value associated with a liver of the subject.

In certain embodiments, for at least one particular reference value associated with a particular reference tissue region, the instructions cause the processor to determine the particular reference value by fitting intensities of voxels [e.g., by fitting an distribution of intensities of voxels (e.g., fitting a histogram of voxel intensities)] within a particular reference volume corresponding to the particular reference tissue region to a multi-component mixture model (e.g., a two-component Gaussian model)[e.g., and identifying one or more minor peaks in a distribution of voxel intensities, said minor peaks corresponding to voxels associated with anomalous uptake, and excluding, from the reference value determination, those voxels from the reference value determination (e.g., thereby accounting for effects of abnormally low radiopharmaceutical uptake in certain portions of reference tissue regions, such as portions of the liver)].

In certain embodiments, the instructions cause the processor to use the determined lesion index values compute (e.g., automatically) an overall risk index for the subject, indicative of a caner status and/or risk for the subject.

In certain embodiments, the instructions cause the processor to determine (e.g., automatically), for each hotspot, an anatomical classification corresponding to a particular anatomical region and/or group of anatomical regions within the subject in which the potential cancerous lesion that the hotspot represents is determined [e.g., by the processor (e.g., based on a received and/or determined 3D segmentation map)] to be located [e.g., within a prostate, a pelvic lymph node, a non-pelvic lymph node, a bone (e.g., a bone metastatic region), and a soft tissue region not situated in prostate or lymph node].

In certain embodiments, the instructions cause the processor to: (h) causing, for display within a graphical user interface (GUI), rendering of a graphical representation of at least a portion of the one or more hotspots for review by a user.

In certain embodiments, the instructions cause the processor to: (i) receiving, via the GUI, a user selection of a subset of the one or more hotspots confirmed via user review as likely to represent underlying cancerous lesions within the subject.

In certain embodiments, the 3D functional image comprises a PET or SPECT image obtained following administration of an agent (e.g., a radiopharmaceutical; e.g., an imaging agent) to the subject. In certain embodiments, the agent comprises a PSMA binding agent. In certain embodiments, the agent comprises [18F]DCFPyL. In certain embodiments, the agent comprises ^{99m}Tc.

In certain embodiments, the machine learning module implements a neural network [e.g., an artificial neural network (ANN); e.g., a convolutional neural network (CNN)].

In certain embodiments, the processor is a processor of a cloud-based system.

In another aspect, the invention is directed to a system for automatically processing 3D images of a subject to identify and/or characterize (e.g., grade) cancerous lesions within the subject, the system comprising: a processor of a computing device; and a memory having instructions stored thereon, wherein the instructions, when executed by the processor, cause the processor to: (a) receive (e.g., and/or access) a 3D

functional image of the subject obtained using a functional imaging modality [e.g., positron emission tomography (PET); e.g., single-photon emission computed tomography (SPECT)][e.g., wherein the 3D functional image comprises a plurality of voxels, each representing a particular physical volume within the subject and having an intensity value that represents detected radiation emitted from the particular physical volume, wherein at least a portion of the plurality of voxels of the 3D functional image represent physical volumes within the target tissue region]; (b) receive (e.g., and/or access) a 3D anatomical image of the subject obtained using an anatomical imaging modality [e.g., x-ray computed tomography (CT); e.g., magnetic resonance imaging (MRI); e.g., ultra-sound], wherein the 3D anatomical image comprises a graphical representation of tissue (e.g., soft-tissue and/or bone) within the subject; (c) automatically detect, using a machine learning module, one or more hotspots within the 3D functional image, each hotspot corresponding to a local region of elevated intensity with respect to its surrounding and representing (e.g., indicative of) a potential cancerous lesion within the subject, thereby creating one or both of (i) and (ii) as follows: (i) a hotspot list identifying, for each hotspot, a location of the hotspot, and (ii) a 3D hotspot map, identifying, for each hotspot, a corresponding 3D hotspot volume within the 3D functional image {e.g., wherein, the 3D hotspot map is a segmentation map (e.g., comprising one or more segmentation masks) identifying, for each hotspot, voxels within the 3D functional image corresponding to the 3D hotspot volume of each hotspot [e.g., wherein the 3D hotspot map is obtained via artificial intelligence-based segmentation of the functional image (e.g., using a machine-learning module that receives, as input, at least the 3D functional image and generates the 3D hotspot map as output, thereby segmenting hotspots)]; e.g., wherein the 3D hotspot map delineates, for each hotspot, a 3D boundary (e.g., an irregular boundary) of the hotspot (e.g., the 3D boundary enclosing the 3D hotspot volume, e.g., and distinguishing voxels of the 3D functional image that make up the 3D hotspot volume from other voxels of the 3D functional image)}, wherein the machine learning module receives at least two channels of input, said input channels comprising a first input channel corresponding to at least a portion of the 3D anatomical image and a second input channel corresponding to at least a portion of the 3D functional image [e.g., wherein the machine learning module receives a PET image and a CT image as separate channels (e.g., separate channels representative of the same volume) (e.g., analogous to receipt by a machine learning module of two color channels (RGB) of a photographic color image)] and/or anatomical information derived therefrom [e.g., a 3D segmentation map that identifies, within the 3D functional image, one or more volumes of interest (VOIs), each VOI corresponding to a particular target tissue region and/or a particular anatomical region]; and (d) store and/or provide, for display and/or further processing, the hotspot list and/or the 3D hotspot map.

In another aspect, the invention is directed to a system for automatically processing 3D images of a subject to identify and/or characterize (e.g., grade) cancerous lesions within the subject, the system comprising: a processor of a computing device; and a memory having instructions stored thereon, wherein the instructions, when executed by the processor, cause the processor to: (a) receive (e.g., and/or access) a 3D functional image of the subject obtained using a functional imaging modality [e.g., positron emission tomography (PET); e.g., single-photon emission computed tomography (SPECT)][e.g., wherein the 3D functional image comprises a plurality of voxels, each representing a particular physical volume within the subject and having an intensity value that represents detected radiation emitted from the particular physical volume, wherein at least a portion of the plurality of voxels of the 3D functional image represent physical volumes within the target tissue region]; (b) automatically detect, using a first machine learning module, one or more hotspots within the 3D functional image, each hotspot corresponding to a local region of elevated intensity with respect to its surrounding and representing (e.g., indicative of) a potential cancerous lesion within the subject, thereby creating a hotspot list identifying, for each hotspot, a location of the hotspot [e.g., wherein the machine learning module implements a machine learning algorithm (e.g., an artificial neural network (ANN)) trained to determine, based on intensities of voxels of at least a portion of the 3D functional image, one or more locations (e.g., 3D coordinates), each corresponding to a location of one of the one or more hotspots]; (c) automatically determine, using a second machine learning module and the hotspot list, for each of the one or more hotspots, a corresponding 3D hotspot volume within the 3D functional image, thereby creating a 3D hotspot map [e.g., wherein the second machine learning module implements a machine learning algorithm (e.g., an artificial neural network (ANN)) trained to segment the 3D functional image based at least in part on the hotspot list along with intensities of voxels of the 3D functional image to identify the 3D hotspot volumes of the 3D hotspot map; e.g., wherein the machine learning module implements a machine learning algorithm trained to determine, for each voxel of at least a portion of the 3D functional image, a hotspot likelihood value representing a likelihood that the voxel corresponds to a hotspot (e.g., and step (b) comprises performing one or more subsequent post-processing steps, such as thresholding, to identify the 3D hotspot volumes of the 3D hotspot map using the hotspot likelihood values] [e.g., wherein, the 3D hotspot map is a segmentation map (e.g., comprising one or more segmentation masks) generated using (e.g., based on and/or corresponding to output from) the second machine learning module, the 3D hotspot map identifying, for each hotspot, voxels within the 3D functional image corresponding to the 3D hotspot volume of each hotspot); e.g., wherein the 3D hotspot map delineates, for each hotspot, a 3D boundary (e.g., an irregular boundary) of the hotspot (e.g., the 3D boundary enclosing the 3D hotspot volume, e.g., and distinguishing voxels of the 3D functional image that make up the 3D hotspot volume from other voxels of the 3D functional image)]; and (d) store and/or provide, for display and/or further processing, the hotspot list and/or the 3D hotspot map.

In certain embodiments, the instructions cause the processor to: (e) determine, for each hotspot of at least a portion of the hotspots, a lesion likelihood classification corresponding to a likelihood of the hotspot representing a lesion within the subject.

In certain embodiments, at step (e) the instructions cause the processor to use a third machine learning module (e.g., a hotspot classification module) to determine the lesion likelihood classification for each hotspot [e.g., based at least in part on one or more members selected from the group consisting of intensities of the 3D functional image, the hotspot list, the 3D hotspot map, intensities of a 3D anatomical image, and a 3D segmentation map; e.g., wherein the third machine learning module receives one or more channels of input corresponding to one or more members selected from the group consisting of intensities of the 3D

functional image, the hotspot list, the 3D hotspot map, intensities of a 3D anatomical image, and a 3D segmentation map].

In certain embodiments, the instructions cause the processor to: (f) select, based at least in part on the lesion likelihood classifications for the hotspots, a subset of the one or more hotspots corresponding to hotspots having a high likelihood of corresponding to cancerous lesions (e.g., for inclusion in a report; e.g., for use in computing one or more risk index values for the subject).

In another aspect, the invention is directed to a system for measuring intensity values within a reference volume corresponding to a reference tissue region (e.g., a liver volume associated with a liver of a subject) so as to avoid impact from tissue regions associated with low (e.g., abnormally low) radiopharmaceutical uptake (e.g., due to tumors without tracer uptake), the system comprising: a processor of a computing device; and a memory having instructions stored thereon, wherein the instructions, when executed by the processor, cause the processor to: (a) receive (e.g., and/or access) a 3D functional image of a subject, said 3D functional image obtained using a functional imaging modality [e.g., positron emission tomography (PET); e.g., single-photon emission computed tomography (SPECT)][e.g., wherein the 3D functional image comprises a plurality of voxels, each representing a particular physical volume within the subject and having an intensity value that represents detected radiation emitted from the particular physical volume, wherein at least a portion of the plurality of voxels of the 3D functional image represent physical volumes within the target tissue region]; (b) identify the reference volume within the 3D functional image; (c) fit a multi-component mixture model (e.g., a two-component Gaussian mixture model) to intensities of voxels within the reference volume [e.g., fitting the multi-component mixture model to a distribution (e.g., a histogram) of intensities of voxels within the reference volume]; (d) identify a major mode of the multi-component model; (e) determine a measure of (e.g., a mean, a maximum, a mode, a median, etc.) intensities corresponding to the major mode, thereby determining a reference intensity value corresponding to a measure of intensity of voxels that are (i) within the reference tissue volume and (ii) associated with the major mode, (e.g., and excluding, from the reference value calculation, voxels having intensities associated with minor modes) (e.g., thereby avoiding impact from tissue regions associated with low radiopharmaceutical uptake); (f) detect, within the 3D functional image, one or more hotspots corresponding potential cancerous lesions; and (g) determine, for each hotspot of at least a portion of the detected hotspots, a lesion index value, using at least the reference intensity value [e.g., the lesion index value based on (i) a measure of intensities of voxels corresponding to the detected hotspot and (ii) the reference intensity value]. In another aspect, the invention is directed to a system for correcting for intensity bleed (e.g., cross-talk) from due to high-uptake tissue regions within the subject that are associated with high radiopharmaceutical uptake under normal circumstances (e.g., and not necessarily indicative of cancer), the method comprising: (a) receive (e.g., and/or access) a 3D functional image of the subject, said 3D functional image obtained using a functional imaging modality [e.g., positron emission tomography (PET); e.g., single-photon emission computed tomography (SPECT)][e.g., wherein the 3D functional image comprises a plurality of voxels, each representing a particular physical volume within the subject and having an intensity value that represents detected radiation emitted from the particular physical volume, wherein at least a portion of the plurality of voxels of the 3D functional image represent physical volumes within the target tissue region]; (b) identify a high-intensity volume within the 3D functional image, said high intensity volume corresponding to a particular high-uptake tissue region (e.g., a kidney; e.g., a liver; e.g., a bladder) in which high radiopharmaceutical uptake occurs under normal circumstances; (c) identify, based on the identified high-intensity volume, a suppression volume within the 3D functional image, said suppression volume corresponding to a volume lying outside and within a predetermined decay distance from a boundary of the identified high intensity volume; (d) determine a background image corresponding to the 3D functional image with intensities of voxels within the high-intensity volume replaced with interpolated values determined based on intensities of voxels of the 3D functional image within the suppression volume; (e) determine an estimation image by subtracting intensities of voxels of the background image from intensities of voxels from the 3D functional image (e.g., performing a voxel-by-voxel subtraction); (f) determine a suppression map by: extrapolating intensities of voxels of the estimation image corresponding to the high-intensity volume to locations of voxels within the suppression volume to determine intensities of voxels of the suppression map corresponding to the suppression volume; and setting intensities of voxels of the suppression map corresponding to locations outside the suppression volume to zero; and (g) adjust intensities of voxels of the 3D functional image based on the suppression map (e.g., by subtracting intensities of voxels of the suppression map from intensities of voxels of the 3D functional image), thereby correcting for intensity bleed from the high-intensity volume.

In certain embodiments, the instructions cause the processor to perform steps (b) through (g) for each of a plurality of high-intensity volumes in a sequential manner, thereby correcting for intensity bleed from each of the plurality of high-intensity volumes.

In certain embodiments, the plurality of high-intensity volumes comprise one or more members selected from the group consisting of a kidney, a liver, and a bladder (e.g., a urinary bladder).

In another aspect, the invention is directed to a system for automatically processing 3D images of a subject to identify and/or characterize (e.g., grade) cancerous lesions within the subject, the system comprising: a processor of a computing device; and a memory having instructions stored thereon, wherein the instructions, when executed by the processor, cause the processor to: (a) receive (e.g., and/or access), a 3D functional image of the subject obtained using a functional imaging modality [e.g., positron emission tomography (PET); e.g., single-photon emission computed tomography (SPECT)][e.g., wherein the 3D functional image comprises a plurality of voxels, each representing a particular physical volume within the subject and having an intensity value that represents detected radiation emitted from the particular physical volume, wherein at least a portion of the plurality of voxels of the 3D functional image represent physical volumes within the target tissue region]; (b) automatically detect one or more hotspots within the 3D functional image, each hotspot corresponding to a local region of elevated intensity with respect to its surrounding and representing (e.g., indicative of) a potential cancerous lesion within the subject; (c) cause rendering of a graphical representation of the one or more hotspots for display within an interactive graphical user interface (GUI) (e.g., a quality control and reporting GUI); (d) receive, via the interactive GUI, a user

selection of a final hotspot set comprising at least a portion (e.g., up to all) of the one or more automatically detected hotspots (e.g., for inclusion in a report); and (e) store and/or provide, for display and/or further processing, the final hotspot set.

In certain embodiments, the instructions cause the processor to: (f) receive, via the GUI, a user selection of one or more additional, user-identified, hotspots for inclusion in the final hotspot set; and (g) update, the final hotspot set to include the one or more additional user-identified hotspots.

In certain embodiments, at step (b) the instructions cause the processor to use one or more machine learning modules.

In another aspect, the invention is directed to a system for automatically processing 3D images of a subject to identify and characterize (e.g., grade) cancerous lesions within the subject, the system comprising: a processor of a computing device; and a memory having instructions stored thereon, wherein the instructions, when executed by the processor, cause the processor to: (a) receive (e.g., and/or access) a 3D functional image of the subject obtained using a functional imaging modality [e.g., positron emission tomography (PET); e.g., single-photon emission computed tomography (SPECT)][e.g., wherein the 3D functional image comprises a plurality of voxels, each representing a particular physical volume within the subject and having an intensity value that represents detected radiation emitted from the particular physical volume, wherein at least a portion of the plurality of voxels of the 3D functional image represent physical volumes within the target tissue region]; (b) automatically detect one or more hotspots within the 3D functional image, each hotspot corresponding to a local region of elevated intensity with respect to its surrounding and representing (e.g., indicative of) a potential cancerous lesion within the subject; (c) automatically determine, for each of at least a portion of the one or more hotspots, an anatomical classification corresponding to a particular anatomical region and/or group of anatomical regions within the subject in which the potential cancerous lesion that the hotspot represents is determined [e.g., by the processor (e.g., based on a received and/or determined 3D segmentation map)] to be located [e.g., within a prostate, a pelvic lymph node, a non-pelvic lymph node, a bone (e.g., a bone metastatic region), and a soft tissue region not situated in prostate or lymph node]; and (d) store and/or provide, for display and/or further processing, an identification of the one or more hotspots along with, for each hotspot, the anatomical classification corresponding to the hotspot.

In certain embodiments, the instructions cause the processor to perform step (b) using one or more machine learning modules.

Features of embodiments described with respect to one aspect of the invention may be applied with respect to another aspect of the invention.

BRIEF DESCRIPTION OF THE DRAWINGS

The patent or application file contains at least one drawing executed in color. Copies of this patent or patent application publication with color drawing(s) will be provided by the Office upon request and payment of the necessary fee.

The foregoing and other objects, aspects, features, and advantages of the present disclosure will become more apparent and better understood by referring to the following description taken in conjunction with the accompanying drawings, in which:

FIG. **1**A is a block flow diagram of an example process for artificial intelligence (AI)-based lesion detection, according to an illustrative embodiment.

FIG. **1**B is a block flow diagram of an example process for AI-based lesion detection, according to an illustrative embodiment.

FIG. **1**C is a block flow diagram of an example process for AI-based lesion detection, according to an illustrative embodiment.

FIG. **2**A is a graph showing a histogram of liver SUV values overlaid with a two-component Gaussian mixture model, according to an illustrative embodiment.

FIG. **2**B is a PET image overlaid on a CT images showing a portion of a liver volume used for calculation of a liver reference value, according to an illustrative embodiment.

FIG. **2**C is a block flow diagram of an example process for computing reference intensity values that avoids/reduces impact from tissue regions associated with low radiopharmaceutical uptake, according to an illustrative embodiment.

FIG. **3** is a block flow diagram of an example process for correcting for intensity bleed from one or more tissue regions associated with high radiopharmaceutical uptake, according to an illustrative embodiment.

FIG. **4** is block flow diagram of an example process for anatomically labeling hotspots corresponding to detected lesions, according to an illustrative embodiment.

FIG. **5**A is a block flow diagram of an example process for interactive lesion detection, allowing for user feedback and review via a graphical user interface (GUI), according to an illustrative embodiment.

FIG. **5**B is an example process for user review, quality control, and reporting of automatically detected lesions, according to an illustrative embodiment.

FIG. **6**A is a screenshot of a GUI used for confirming accurate segmentation of a liver reference volume, according to an illustrative embodiment.

FIG. **6**B is a screenshot of a GUI used for confirming accurate segmentation of an aorta portion (blood pool) reference volume, according to an illustrative embodiment.

FIG. **6**C is a screenshot of a GUI used for user selection and/or validation of automatically segmented hotspots corresponding to detected lesions within a subject, according to an illustrative embodiment.

FIG. **6**D is a screenshot of a portion of a GUI allowing a user to manually identify lesions within an image, according to an illustrative embodiment.

FIG. **6**E is a screenshot of another portion of a GUI allowing a user to manually identify lesions within an image, according to an illustrative embodiment.

FIG. **6**F is a screenshot of a portion of a GUI showing a quality control checklist, according to an illustrative embodiment.

FIG. **6**G is a screenshot of a report generated by a user, using an embodiment of the automated lesion detection tools described herein, according to an illustrative embodiment.

FIG. **7** is a block diagram of an exemplary cloud computing environment, used in certain embodiments.

FIG. **8** is a block diagram of an example computing device and an example mobile computing device used in certain embodiments

The features and advantages of the present disclosure will become more apparent from the detailed description set forth below when taken in conjunction with the drawings, in which like reference characters identify corresponding elements throughout. In the drawings, like reference numbers generally indicate identical, functionally similar, and/or structurally similar elements.

DETAILED DESCRIPTION

It is contemplated that systems, devices, methods, and processes of the claimed invention encompass variations and adaptations developed using information from the embodiments described herein. Adaptation and/or modification of the systems, devices, methods, and processes described herein may be performed by those of ordinary skill in the relevant art.

Throughout the description, where articles, devices, and systems are described as having, including, or comprising specific components, or where processes and methods are described as having, including, or comprising specific steps, it is contemplated that, additionally, there are articles, devices, and systems of the present invention that consist essentially of, or consist of, the recited components, and that there are processes and methods according to the present invention that consist essentially of, or consist of, the recited processing steps.

It should be understood that the order of steps or order for performing certain action is immaterial so long as the invention remains operable. Moreover, two or more steps or actions may be conducted simultaneously.

The mention herein of any publication, for example, in the Background section, is not an admission that the publication serves as prior art with respect to any of the claims presented herein. The Background section is presented for purposes of clarity and is not meant as a description of prior art with respect to any claim.

Headers are provided for the convenience of the reader—the presence and/or placement of a header is not intended to limit the scope of the subject matter described herein.

A. Nuclear Medicine Images

Nuclear medicine images are obtained using a nuclear imaging modality such as bone scan imaging, Positron Emission Tomography (PET) imaging, and Single-Photon Emission Tomography (SPECT) imaging.

As used herein, an "image"—for example, a 3-D image of mammal—includes any visual representation, such as a photo, a video frame, streaming video, as well as any electronic, digital or mathematical analogue of a photo, video frame, or streaming video. Any apparatus described herein, in certain embodiments, includes a display for displaying an image or any other result produced by the processor. Any method described herein, in certain embodiments, includes a step of displaying an image or any other result produced via the method.

As used herein, "3-D" or "three-dimensional" with reference to an "image" means conveying information about three dimensions. A 3-D image may be rendered as a dataset in three dimensions and/or may be displayed as a set of two-dimensional representations, or as a three-dimensional representation.

In certain embodiments, nuclear medicine images use imaging agents comprising radiopharmaceuticals. Nuclear medicine images are obtained following administration of a radiopharmaceutical to a patient (e.g., a human subject), and provide information regarding the distribution of the radiopharmaceutical within the patient. Radiopharmaceuticals are compounds that comprise a radionuclide.

As used herein, "administering" an agent means introducing a substance (e.g., an imaging agent) into a subject. In general, any route of administration may be utilized including, for example, parenteral (e.g., intravenous), oral, topical, subcutaneous, peritoneal, intraarterial, inhalation, vaginal, rectal, nasal, introduction into the cerebrospinal fluid, or instillation into body compartments

As used herein, "radionuclide" refers to a moiety comprising a radioactive isotope of at least one element. Exemplary suitable radionuclides include but are not limited to those described herein. In some embodiments, a radionuclide is one used in positron emission tomography (PET). In some embodiments, a radionuclide is one used in single-photon emission computed tomography (SPECT). In some embodiments, a non-limiting list of radionuclides includes ^{99m}Tc, ^{64}Cu, ^{67}Ga, ^{68}Ga, ^{186}Re, ^{188}Re, ^{153}Sm, ^{177}Lu, ^{67}Cu, ^{123}I, ^{124}I, ^{125}I, ^{126}I, ^{131}I, ^{11}C, ^{13}N, ^{15}O, ^{18}F, ^{153}Sm, ^{166}Ho, ^{177}Lu, ^{149}Pm, ^{90}Y, ^{213}Bi, ^{103}Pd, ^{109}Pd, ^{159}Gd, ^{140}La, ^{198}Au, ^{199}Au, ^{169}Yb, ^{175}Yb, ^{165}Dy, ^{166}Dy, ^{105}Rh, ^{111}Ag, ^{89}Zr, ^{225}AC, ^{82}Rb, ^{75}Br, ^{76}Br, ^{77}Br, ^{80}Br, ^{80m}Br, ^{82}Br, ^{83}Br, ^{211}At and ^{192}Ir.

As used herein, the term "radiopharmaceutical" refers to a compound comprising a radionuclide. In certain embodiments, radiopharmaceuticals are used for diagnostic and/or therapeutic purposes. In certain embodiments, radiopharmaceuticals include small molecules that are labeled with one or more radionuclide(s), antibodies that are labeled with one or more radionuclide(s), and antigen-binding portions of antibodies that are labeled with one or more radionuclide(s).

Nuclear medicine images (e.g., PET scans; e.g., SPECT scans; e.g., whole-body bone scans; e.g. composite PET-CT images; e.g., composite SPECT-CT images) detect radiation emitted from the radionuclides of radiopharmaceuticals to form an image. The distribution of a particular radiopharmaceutical within a patient may be determined by biological mechanisms such as blood flow or perfusion, as well as by specific enzymatic or receptor binding interactions. Different radiopharmaceuticals may be designed to take advantage of different biological mechanisms and/or particular specific enzymatic or receptor binding interactions and thus, when administered to a patient, selectively concentrate within particular types of tissue and/or regions within the patient. Greater amounts of radiation are emitted from regions within the patient that have higher concentrations of radiopharmaceutical than other regions, such that these regions appear brighter in nuclear medicine images. Accordingly, intensity variations within a nuclear medicine image can be used to map the distribution of radiopharmaceutical within the patient. This mapped distribution of radiopharmaceutical within the patient can be used to, for example, infer the presence of cancerous tissue within various regions of the patient's body.

For example, upon administration to a patient, technetium 99m methylenediphosphonate (^{99m}Tc MDP) selectively accumulates within the skeletal region of the patient, in particular at sites with abnormal osteogenesis associated with malignant bone lesions. The selective concentration of radiopharmaceutical at these sites produces identifiable hotspots—localized regions of high intensity in nuclear medicine images. Accordingly, presence of malignant bone lesions associated with metastatic prostate cancer can be inferred by identifying such hotspots within a whole-body scan of the patient. As described in the following, risk indices that correlate with patient overall survival and other prognostic metrics indicative of disease state, progression, treatment efficacy, and the like, can be computed based on automated analysis of intensity variations in whole-body scans obtained following administration of ^{99m}Tc MDP to a patient. In certain embodiments, other radiopharmaceuticals can also be used in a similar fashion to ^{99m}Tc MDP.

In certain embodiments, the particular radiopharmaceutical used depends on the particular nuclear medicine imaging modality used. For example 18F sodium fluoride (NaF) also accumulates in bone lesions, similar to ^{99m}Tc MDP, but can

be used with PET imaging. In certain embodiments, PET imaging may also utilize a radioactive form of the vitamin choline, which is readily absorbed by prostate cancer cells.

In certain embodiments, radiopharmaceuticals that selectively bind to particular proteins or receptors of interest—particularly those whose expression is increased in cancerous tissue may be used. Such proteins or receptors of interest include, but are not limited to tumor antigens, such as CEA, which is expressed in colorectal carcinomas, Her2/neu, which is expressed in multiple cancers, BRCA 1 and BRCA 2, expressed in breast and ovarian cancers; and TRP-1 and -2, expressed in melanoma.

For example, human prostate-specific membrane antigen (PSMA) is upregulated in prostate cancer, including metastatic disease. PSMA is expressed by virtually all prostate cancers and its expression is further increased in poorly differentiated, metastatic and hormone refractory carcinomas. Accordingly, radiopharmaceuticals corresponding to PSMA binding agents (e.g., compounds that a high affinity to PSMA) labelled with one or more radionuclide(s) can be used to obtain nuclear medicine images of a patient from which the presence and/or state of prostate cancer within a variety of regions (e.g., including, but not limited to skeletal regions) of the patient can be assessed. In certain embodiments, nuclear medicine images obtained using PSMA binding agents are used to identify the presence of cancerous tissue within the prostate, when the disease is in a localized state. In certain embodiments, nuclear medicine images obtained using radiopharmaceuticals comprising PSMA binding agents are used to identify the presence of cancerous tissue within a variety of regions that include not only the prostate, but also other organs and tissue regions such as lungs, lymph nodes, and bones, as is relevant when the disease is metastatic.

In particular, upon administration to a patient, radionuclide labelled PSMA binding agents selectively accumulate within cancerous tissue, based on their affinity to PSMA. In a similar manner to that described above with regard to ^{99m}Tc MDP, the selective concentration of radionuclide labelled PSMA binding agents at particular sites within the patient produces detectable hotspots in nuclear medicine images. As PSMA binding agents concentrate within a variety of cancerous tissues and regions of the body expressing PSMA, localized cancer within a prostate of the patient and/or metastatic cancer in various regions of the patient's body can be detected, and evaluated. Risk indices that correlate with patient overall survival and other prognostic metrics indicative of disease state, progression, treatment efficacy, and the like, can be computed based on automated analysis of intensity variations in nuclear medicine images obtained following administration of a PSMA binding agent radiopharmaceutical to a patient.

A variety of radionuclide labelled PSMA binding agents may be used as radiopharmaceutical imaging agents for nuclear medicine imaging to detect and evaluate prostate cancer. In certain embodiments, the particular radionuclide labelled PSMA binding agent that is used depends on factors such as the particular imaging modality (e.g., PET; e.g., SPECT) and the particular regions (e.g., organs) of the patient to be imaged. For example, certain radionuclide labelled PSMA binding agents are suited for PET imaging, while others are suited for SPECT imaging. For example, certain radionuclide labelled PSMA binding agents facilitate imaging a prostate of the patient, and are used primarily when the disease is localized, while others facilitate imaging organs and regions throughout the patient's body, and are useful for evaluating metastatic prostate cancer.

A variety of PSMA binding agents and radionuclide labelled versions thereof are described in U.S. Pat. Nos. 8,778,305, 8,211,401, and 8,962,799, each of which are incorporated herein by reference in their entireties. Several PSMA binding agents and radionuclide labelled versions thereof are also described in PCT Application PCT/US2017/058418, filed Oct. 26, 2017 (PCT publication WO 2018/081354), the content of which is incorporated herein by reference in its entirety. Section C, below, describes several example PSMA binding agents and radionuclide labelled versions thereof, as well.

B. Automated Lesion Detection and Analysis

i. Automated Lesion Detection

In certain embodiments, the systems and methods described herein utilize machine learning techniques for automated image segmentation and detection of hotspots corresponding to and indicative of possible cancerous lesions within a subject.

In certain embodiments, the systems and methods described herein may be implemented in a cloud-based platform, for example as described in PCT/US2017/058418, filed Oct. 26, 2017 (PCT publication WO 2018/081354), the content of which is hereby incorporated by reference in its entirety.

In certain embodiments, as described herein, machine learning modules implement one or more machine learning techniques, such as random forest classifiers, artificial neural networks (ANNs), convolutional neural networks (CNNs), and the like. In certain embodiments, machine learning modules implementing machine learning techniques are trained, for example using manually segmented and/or labeled images, to identify and/or classify portions of images. Such training may be used to determine various parameters of machine learning algorithms implemented by a machine learning module, such as weights associated with layers in neural networks. In certain embodiments, once a machine learning module is trained, e.g., to accomplish a specific task such as identifying certain target regions within images, values of determined parameters are fixed and the (e.g., unchanging, static) machine learning module is used to process new data (e.g., different from the training data) and accomplish its trained task without further updates to its parameters (e.g., the machine learning module does not receive feedback and/or update). In certain embodiments, machine learning modules may receive feedback, e.g., based on user review of accuracy, and such feedback may be used as additional training data, to dynamically update the machine learning module. In some embodiments, the trained machine learning module is a classification algorithm with adjustable and/or fixed (e.g., locked) parameters, e.g., a random forest classifier.

In certain embodiments, machine learning techniques are used to automatically segment anatomical structures in anatomical images, such as CT, Mill, ultra-sound, etc. images, in order to identify volumes of interest corresponding to specific target tissue regions such as specific organs (e.g., a prostate, lymph node regions, a kidney, a liver, a bladder, an aorta portion) as well as bones. In this manner, machine learning modules may be used to generate segmentation masks and/or segmentation maps (e.g., comprising a plurality of segmentation masks, each corresponding to and identifying a particular target tissue region) that can be mapped to (e.g., projected onto) functional images, such as PET or SPECT images, to provide anatomical context for evaluating intensity fluctuations therein. Approaches for segmenting images and using the obtained anatomical context for analysis of nuclear medicine images are described,

for example, in further detail in PCT/US2019/012486, filed Jan. 7, 2019 (PCT publication WO 2019/136349) and PCT/EP2020/050132, filed Jan. 6, 2020 (PCT publication WO 2020/144134), the contents of each of which is hereby incorporated by reference in their entirety.

In certain embodiments, potential lesions are detected as regions of locally high intensity in functional images, such as PET images. These localized regions of elevated intensity, also referred to as hotspots, can be detected using image processing techniques not necessarily involving machine learning, such as filtering and thresholding, and segmented using approaches such as the fast marching method. Anatomical information established from the segmentation of anatomical images allows for anatomical labeling of detected hotspots representing potential lesions. Anatomical context may also be useful in allowing different detection and segmentation techniques to be used for hotspot detection in different anatomical regions, which can increase sensitivity and performance.

In certain embodiments, automatically detected hotspots may be presented to a user via an interactive graphical user interface (GUI). In certain embodiments, to account for target lesions detected by the user (e.g., physician), but that are missed or poorly segmented by the system, a manual segmentation tool is included in the GUI, allowing the user to manually "paint" regions of images that they perceive as corresponding to lesions of any shape and size. These manually segmented lesions may then be included, along with selected automatically detected target lesions, in subsequently generated reports.

ii. AI-Based Lesion Detection

In certain embodiments, the systems and methods described herein utilize one or more machine learning modules to analyze intensities of 3D functional images and detect hotspot representing potential lesions. For example, by collecting a dataset of PET/CT images in which hotspots that represent lesions have been manually detected and segmented, training material for AI-based lesion detection algorithms can be obtained. These manually labeled images can be used to train one or more machine learning algorithms to automatically analyze functional images (e.g., PET images) to accurately detect and segment hotspots corresponding to cancerous lesions.

FIG. **1**A shows an example process **100***a* for automated lesion detection and/or segmentation using machine learning modules that implement machine learning algorithms, such as ANNs, CNNs, and the like. As shown in FIG. **1**A, a 3D functional image **102**, such as a PET or SPECT image, is received **106** and used as input to a machine learning module **110**. FIG. **1**A shows an example PET image, obtained using PyL™ as a radiopharmaceutical **102***a*. The PET image **102***a* is shown overlaid on a CT image (e.g., as a PET/CT image), but the machine learning module **110** may receive the PET (e.g., or other functional image) itself (e.g., not including the CT, or other anatomical image) as input. In certain embodiments, as described below, an anatomical image may also be received as input. The machine learning module automatically detects and/or segments hotspots **120** determined (by the machine learning module) to represent potential cancerous lesions. An example image showing hotspots appearing in a PET image **120***b* is shown in FIG. **1**A as well. Accordingly, the machine learning module generates, as output, one or both of (i) a hotspot list **130** and (ii) a hotspot map **132**. In certain embodiments, the hotspot list identifies locations (e.g., centers of mass) of the detected hotspots. In certain embodiments, the hotspot map is identifies 3D volumes and/or delineates 3D boundaries of detected hotspots, as determined via image segmentation performed by the machine learning module **110**. The hotspot list and/or hotspot map may be stored and/or provided (e.g., to other software modules) for display and/or further processing **140**.

In certain embodiments, machine learning-based lesion detection algorithms may be trained on, and utilize, not only functional image information (e.g., from a PET image), but also anatomical information. For example, in certain embodiments, one or more machine learning modules used for lesion detection and segmentation may be trained on, and receive as input, two channels—a first channel corresponding to a portion of a PET image, and a second channel corresponding to a portion of a CT image. In certain embodiments, information derived from an anatomical (e.g., CT) image may also be used as input to machine learning modules for lesion detection and/or segmentation. For example, in certain embodiments, 3D segmentation maps identifying various tissue regions within an anatomical and/or functional image can also be used to provide anatomical context.

FIG. **1**B shows an example process **100***b* in which both a 3D anatomical image **104**, such as a CT or MR image, and a 3D functional image **102** are received **108** and used as input to a machine learning module **112** that performs hotspot detection and/or segmentation **122** based on information (e.g., voxel intensities) from both the 3D anatomical image **104** and the 3D functional image **102** as described herein. A hotspot list **130** and/or hotspot map **132** may be generated as output from the machine learning module, and stored/provided for further processing (e.g., graphical rendering for display, subsequent operations by other software modules, etc.) **140**.

In certain embodiments, automated lesion detection and analysis (e.g., for inclusion in a report) includes three tasks: (i) detection of hotspots corresponding to lesions, (ii) segmentation of detected hotspots (e.g., to identify, within a functional image, a 3D volume corresponding to each lesion), and (iii) classification of detected hotspots as having high or low probability of corresponding to a true lesion within the subject (e.g., and thus appropriate for inclusion in a radiologist report or not). In certain embodiments, one or more machine learning modules may be used to accomplish these three tasks, e.g., one by one (e.g., in sequence) or in combination. For example, in certain embodiments, a first machine learning module is trained to detect hotspots and identify hotspot locations, a second machine learning module is trained to segment hotspots, and a third machine learning module is trained to classify detected hotspots, for example using information obtained from the other two machine learning modules.

For example, as shown in the example process **100***c* of FIG. **1**C, a 3D functional image **102** may be received **106** and used as input to a first machine learning module **114** that performs automated hotspot detection. The first machine learning module **114** automatically detects one or more hotspots **124** in the 3D functional image and generates a hotspot list **130** as output. A second machine learning module **116** may receive the hotspot list **130** as input along with the 3D functional image, and perform automated hotspot segmentation, **126** to generate a hotspot map **132**. As previously described, the hotspot map **132**, as well as the hotspot list **130**, may be stored and/or provided for further processing **140**.

In certain embodiments, a single machine learning module is trained to directly segment hotspots within images (e.g., 3D functional images; e.g., to generate a 3D hotspot map identifying volumes corresponding to detected hot-

spots), thereby combining the first two steps of detection and segmentation of hotspots. A second machine learning module may then be used to classify detected hotspots, for example based on the segmented hotspots determined previously. In certain embodiments, a single machine learning module may be trained to accomplish all three tasks—detection, segmentation, and classification—in a single step.

iii. Lesion Index Values

In certain embodiments, lesion index values are calculated for detected hotspots to provide a measure of, for example, relative uptake within and/or size of the corresponding physical lesion. In certain embodiments, lesion index values are computed for a particular hotspot based (i) on a measure of intensity for the hotspot and (ii) reference values corresponding to measures of intensity within one or more reference volumes, each corresponding to a particular reference tissue region. For example, in certain embodiments, reference values include an aorta reference value that measures intensity within an aorta volume corresponding to a portion of an aorta and a liver reference value that measures intensity within a liver volume corresponding to a liver of the subject. In certain embodiments, intensities of voxels of a nuclear medicine image, for example a PET image, represent standard uptake values (SUVs) (e.g., having been calibrated for injected radiopharmaceutical dose and/or patient weight), and measures of hotspot intensity and/or measures reference values are SUV values. Use of such reference values in computing lesion index values is described in further detail, for example, in PCT/EP2020/050132, filed Jan. 6, 2020, the contents of which is hereby incorporated by reference in its entirety.

In certain embodiments, a segmentation mask is used to identify a particular reference volume in, for example a PET image. For a particular reference volume, a segmentation mask identifying the reference volume may be obtained via segmentation of an anatomical, e.g., CT, image. To identify voxels of the reference volume to be used for computation of the corresponding reference value, the mask may be eroded a fixed distance (e.g., at least one voxel), to create a reference organ mask that identifies a reference volume corresponding to a physical region entirely within the reference tissue region. For example, erosion distances of 3 mm and 9 mm have been used for aorta and liver reference volumes, respectively. Additional mask refinement may also be performed (e.g., to select a specific, desired, set of voxels for use in computing the reference value), for example as described below with respect to the liver reference volume.

Various measures of intensity within reference volumes may be used. For example, in certain embodiments, a robust average of voxels inside the reference volume (e.g., as defined by the reference volume segmentation mask, following erosion) may be determined as a mean of values in an interquartile range of voxel intensities (IQR_{mean}) Other measures, such as a peak, a maximum, a median, etc. may also be determined. In certain embodiments, an aorta reference value is determined as a robust average of SUV from voxels inside the aorta mask. The robust average is computed as the mean of the values in the interquartile range, IQR_{mean}.

In certain embodiments, a subset of voxels within a reference volume is selected in order to avoid impact from reference tissue regions that may have abnormally low radiopharmaceutical uptake. Although the automated segmentation techniques described and referenced herein can provide an accurate outline (e.g., identification) of regions of images corresponding to specific tissue regions, there are often areas of abnormally low uptake in the liver which should be excluded from the reference value calculation. For example, liver reference value (e.g., a liver SUV value) is computed so as to avoid impact from regions in the liver with very low tracer (radiopharmaceutical) activity, that might appear e.g., due to tumors without tracer uptake. In certain embodiments, to account for effects of abnormally low uptake in reference tissue regions the reference value calculation for the liver analyzes a histogram of intensities of voxels corresponding to the liver (e.g., voxels within an identified liver reference volume) and removes (e.g., excludes) intensities if they form a second histogram peak of lower intensities, thereby only including intensities associated with a higher intensity value peak.

For example, for the liver, the reference SUV may be computed as a mean SUV of a major mode in a two-component Gaussian Mixture Model fitted to a histogram of SUV's of voxels within the liver reference volume (e.g., as identified by a liver segmentation mask, e.g., following the above-described erosion procedure). In certain embodiments, if the minor component has a larger mean SUV than the major component, and the minor component has at least 0.33 of the weight, an error is thrown and no reference value for the liver is determined. In certain embodiments, if the minor component has a larger mean than the major peak, the liver reference mask is kept as it is. Otherwise a separation SUV threshold is computed, defined by that the probability to belong to the major component for a SUV that is at the threshold or is larger is the same as the probability to belong to the minor component for a SUV that is at the separation threshold or is smaller. The reference liver mask is then refined by removing voxels with SUV smaller than the separation threshold. A liver reference value may then be determined as a measure of intensity (e.g., SUV) values of voxels identified by the liver reference mask, for example as described herein with respect to the aorta reference. FIG. **2**A illustrates an example liver reference computation, showing a histogram of liver SUV values with Gaussian mixture components shown in red and the separation threshold marked in green.

FIG. **2**B shows the resulting portion of the liver volume used to calculate the liver reference value, with voxels corresponding to the lower value peak excluded from the reference value calculation. As shown in the figure, lower intensity areas towards the bottom of the liver have been excluded, as well as regions close to the liver edge.

FIG. **2**C shows an example process **200** where a multi-component mixture model is used to avoid impact from regions with low tracer uptake, as described herein with respect to liver reference volume computation. The process shown in FIG. **2**C and described herein with regard to the liver may also be applied, similarly, to computation of intensity measures of other organs and tissue regions of interest as well, such as an aorta (e.g., aorta portion, such as the thoracic aorta portion or abdominal aorta portion), a parotid gland, a gluteal muscle. As shown, in FIG. **2**C and described herein, in a first step, a 3D functional image **202** is received, and a reference volume corresponding to a specific reference tissue region (e.g., liver, aorta, parotid gland) is identified therein **208**. A multi-component mixture model **210** is then fit to a distribution intensities (e.g., a histogram of intensities) of (e.g., within) the reference volume, and a major mode of the mixture model is identified **212**. A measure of intensities associated with the major mode (e.g., and excluding contributions from intensities associated with other, minor, modes) is determined **214** and used as the reference intensity value for the identified reference volume. In certain embodiments, hotspots are

detected **216** and the reference intensity value determined in this manner can be used to determine lesion index values for the detected hotspots **218**, for example via approaches such as those described in PCT/US2019/012486, filed Jan. 7, 2019 and PCT/EP2020/050132, filed Jan. 6, 2020, the content of each of which is hereby incorporated by reference in its entirety.

iv. Suppression of Intensity Bleed Associated with Normal Uptake in High-Uptake Organs

In certain embodiments, intensities of voxels of a functional image are adjusted in order to suppress/correct for intensity bleed associated with certain organs in which high-uptake occurs under normal circumstances. This approach may be used, for example, for organs such as a kidney, a liver, and a urinary bladder. In certain embodiments, correcting for intensity bleed associated with multiple organs is performed one organ at a time, in a step-wise fashion. For example, in certain embodiments, first kidney uptake is suppressed, then liver uptake, then urinary bladder uptake. Accordingly, the input to liver suppression is an image where kidney uptake has been corrected for (e.g., and input to bladder suppression is an image wherein kidney and liver uptake have been corrected for).

FIG. **3** shows an example process **300** for correcting intensity blead from a high-uptake tissue region. As shown in FIG. **3**, a 3D functional image is received **304** and a high intensity volume corresponding to the high-uptake tissue region is identified **306**. In another step, a suppression volume outside the high-intensity volume is identified **308**. In certain embodiments, as described herein, the suppression volume may be determined as a volume enclosing regions outside of, but within a pre-determined distance from, the high-intensity volume. In another step, a background image is determined **310**, for example by assigning voxels within the high-intensity volume intensities determined based on intensities outside the high-intensity volume (e.g., within the suppression volume), e.g., via interpolation (e.g., using convolution). In another step, an estimation image is determined **312** by subtracting the background image from the 3D functional image (e.g., via a voxel-by-voxel intensity subtraction). In another step, a suppression map is determined **314**. As described herein, in certain embodiments, the suppression map is determined using the estimation image, by extrapolating intensity values of voxels within the high-intensity volume to locations outside the high intensity volume. In certain embodiments, intensities are only extrapolated to locations within the suppression volume, and intensities of voxels outside the suppression volume are set to 0. The suppression map is then used to adjust intensities of the 3D functional image **316**, for example by subtracting the suppression map from the 3D functional image (e.g., performing a voxel-by-voxel intensity subtraction).

An example approach for suppression/correction of intensity bleed from a particular organ (in certain embodiments, kidneys are treated together) for a PET/CT composite image is as follows:

1. The projected CT organ mask segmentation is adjusted to high-intensity regions of the PET image, in order to handle PET/CT misalignment. If the PET-adjusted organ mask is less than 10 pixels, no suppression is made for this organ.
2. A "background image" is computed, replacing all high uptake with interpolated background uptake within the decay distance from the PET-adjusted organ mask. This is done using convolution with Gaussian kernels.
3. Intensities that should be accounted for when estimating suppression are computed as the difference between the input PET and the background image. This "estimation image" has high intensities inside the given organ and zero intensity at locations farther than the decay distance from the given organ.
4. A suppression map is estimated from the estimation image using an exponential model. The suppression map is only non-zero in the region within the decay distance of the PET-adjusted organ segmentation.
5. The suppression map is subtracted from the original PET image.

As described above, these five steps may be repeated, for each of a set of multiple organs, in a sequential fashion.

v. Anatomical Labeling of Detected Lesions

In certain embodiments, detected hotspots are (e.g., automatically) assigned anatomical labels that identify particular anatomical regions and/or groups of regions in which the lesions that they represent are determined to be located. For example, as shown in the example process **400** of FIG. **4**, a 3D functional image may be received **404** an used to automatically detect hotspots **406**, for example via any of the approaches described herein. Once hotspots are detected, anatomical classifications for each hotspot can be automatically determined **408** and each hotspot labeled with the determined anatomical classification. Automated anatomical labeling may, for example, be performed using automatically determined locations of detected hotspots along with anatomical information provided by, for example, a 3D segmentation map identifying image regions corresponding to particular tissue regions and/or an anatomical image. The hotspots and anatomical labeling of each may be stored and/or provided for further processing **410**.

For example, detected hotspots may be automatically classified into one of five classes as follows:

T (prostate tumor)

N (pelvic lymph node)

Ma (non-pelvic lymph)

Mb (bone metastasis)

Mc (soft tissue metastasis not situated in prostate or lymphe node)

Table 1, below, lists tissue regions associated with each of the five classes. Hotspots corresponding to locations within any of the tissue regions associated with a particular class may, accordingly, be automatically assigned to that class.

TABLE 1

List of Tissue Regions Corresponding to Five Classes in a Lesion Anatomical Labeling Approach

Bone Mb	Lymph nodes Ma	Pelvic lymph nodes N	Prostate T	Soft tissue Mc
Skull	Cervical	Template right	Prostate	Brain
Thorax	Supraclavicular	Template left		Neck
Vertebrae lumbar	Axillary	Presacral		Lung
Vertebrae thoracic	Mediastinal	Other, pelvic		Esophageal
Pelvis	Hilar			Liver
Extremities	Mesenteric			Gallbladder
	Elbow			Spleen
	Popliteal			Pancreas
	Peri-/para-aortic			Adrenal
	Other, non-pelvic			Kidney
				Bladder
				Skin
				Muscle
				Other

vi. Graphical User Interface and Quality Control and Reporting

In certain embodiments, detected hotspots and associated information, such as computed lesion index values and anatomical labeling are displayed with an interactive graphical user interface (GUI) so as to allow for review by a medical professional, such as a physician, radiologist, technician, etc. Medical professionals may thus use the GUI to review and confirm accuracy of detected hotspots, as well as corresponding index values and/or anatomical labeling. In certain embodiments, the GUI may also allow users to identify, and segment (e.g., manually) additional hotspots within medical images, thereby allowing a medical professional to identify additional potential lesions that he/she believes the automated detection process may have missed. Once identified, lesion index values and/or anatomical labeling may also be determined for these manually identified and segmented lesions. For example, as indicated in FIG. **3**, the user may review locations determined for each hotspot, as well as anatomical labeling, such as a (e.g., automatically determined) miTNM classification. The miTNM classification scheme is described in further detail, for example, in Eiber et al., "Prostate Cancer Molecular Imaging Standardized Evaluation (PROMISE): Proposed miTNM Classification for the Interpretation of PSMA-Ligand PET/CT," *J. Nucl. Med.*, vol. 59, pg. 469-78 (2018), the content of which is hereby incorporated by reference in its entirety. Once a user is satisfied with the set of detected hotspots and information computed therefrom, they may confirm their approval and generate a final, signed report that can be reviewed and used to discuss outcomes and diagnosis with a patient, and assess prognosis and treatment options.

For example, as shown in FIG. **5**A, in an example process **500** for interactive hotspot review and detection, a 3D functional image is received **504** and hotspots are automatically detected **506**, for example using any of the automated detection approaches described herein. The set of automated hotspots is represented and rendered graphically within an interactive GUI **508** for user review. The user may select at least a portion (e.g., up to all) of the automatically determined hotspots for inclusion in a final hotspot set **510**, which may then be used for further calculations **512**, e.g., to determine risk index values for the patient.

FIG. **5**B shows an example workflow **520** for user review of detected lesions and lesion index values for quality control and reporting. The example workflow allows for user review of segmented lesions as well as liver and aorta segmentation used for calculation of lesion index values as described herein. For example, in a first step, a user reviews images (e.g., a CT image) for quality **522** and accuracy of automated segmentation used to obtain liver and blood pool (e.g., aorta) reference values **524**. As shown in FIGS. **6**A, and **6**B the GUI allows a user evaluates images and overlaid segmentation to ensure that the automated segmentation of the liver (purple color in FIG. **6**A) is within healthy liver tissue and that automated segmentation of blood pool (aorta portion, shown as salmon color in FIG. **6**B is within the aorta and left ventricle.

In another step **526**, a user validates automatically detected hotspots and/or identifies additional hotspots, e.g., to create a final set of hotspots corresponding to lesions, for inclusion in a generated report. As shown in FIG. **6**C, a user may select an automatically identified hotspot by hovering over a graphical representation of the hotspot displayed within the GUI (e.g., as an overlay and/or marked region on a PET and/or CT image). To facilitate hotspot selection, the particular hotspot selected may be indicated to the user, via a color change (e.g., turning green). The user may then click on the hotspot to select it, which may be visually confirmed to the user via another color change. For example, as shown in FIG. **4**C, upon selection the hotspot turns pink. Upon user selection, quantitatively determined values, such as a lesion index and/or anatomical labeling may be displayed to the user, allowing them to verify the automatically determined values **528**.

In certain embodiments, the GUI allows a user to select hotspots from the set of (automatically) pre-identified hotspots to confirm they indeed represent lesions **526***a* and also to identify additional hotspots **562***b* corresponding to lesions, not having been automatically detected.

As shown in FIG. **6**D and FIG. **6**E, the user may use GUI tools to draw on slices of images (e.g., PET images and/or CT images; e.g., a PET image overlaid on a CT image) to mark regions corresponding to a new, manually identified lesion. Quantitative information, such as a lesion index and/or anatomical labeling may be determined for the manually identified lesion automatically, or may be manually entered by the user.

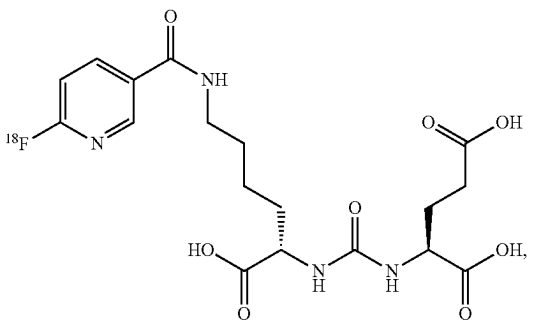
In another step, e.g., once the user has selected and/or manually identified all lesions, the GUI displays a quality control checklist for the user to review **530**, as shown in FIG. **6**F. Once the user reviews and completes the checklist, they may click "Create Report" to sign and generate a final report **532**. An example of a generated report is shown in FIG. **6**G.

C. Imaging Agents

i. PET Imaging Radionuclide Labelled PSMA Binding Agents

In certain embodiments, the radionuclide labelled PSMA binding agent is a radionuclide labelled PSMA binding agent appropriate for PET imaging.

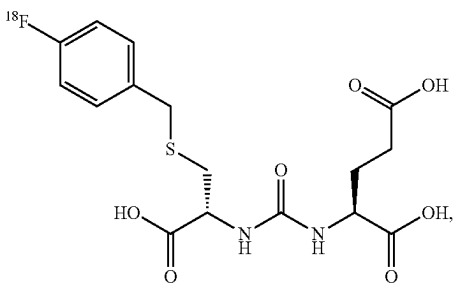
In certain embodiments, the radionuclide labelled PSMA binding agent comprises [18F]DCFPyL (also referred to as PyL™; also referred to as DCFPyL-18F):



[18F]DCFPyL

or a pharmaceutically acceptable salt thereof.

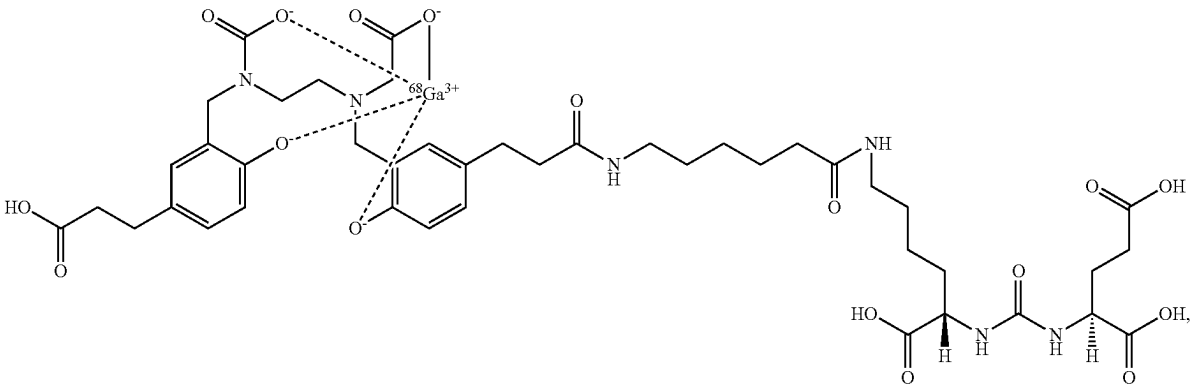
In certain embodiments, the radionuclide labelled PSMA binding agent comprises [18F]DCFBC:



[18F]DCFBC

or a pharmaceutically acceptable salt thereof.

In certain embodiments, the radionuclide labelled PSMA binding agent comprises ^{68}Ga-PSMA-HBED-CC (also referred to as ^{68}Ga-PSMA-11):

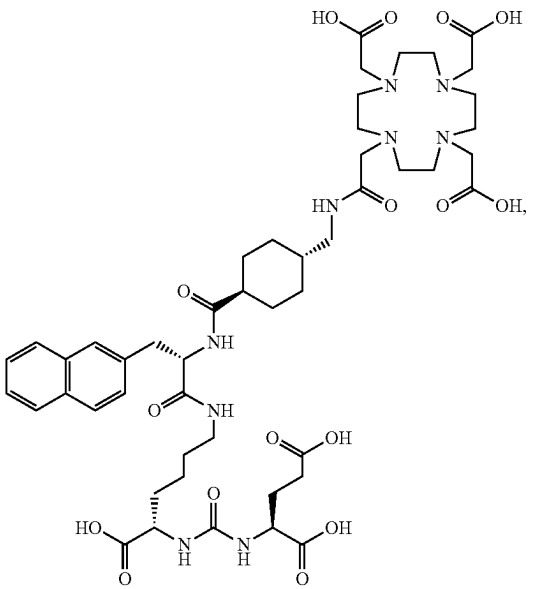


^{68}Ga-PSMA-HBED-CC

or a pharmaceutically acceptable salt thereof.

In certain embodiments, the radionuclide labelled PSMA binding agent comprises PSMA-617:

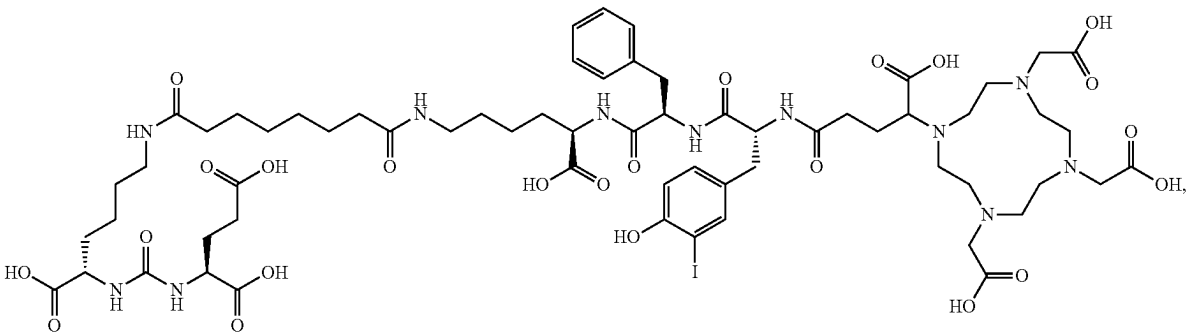
PSMA-617



or a pharmaceutically acceptable salt thereof. In certain embodiments, the radionuclide labelled PSMA binding agent comprises ^{68}Ga-PSMA-617, which is PSMA-617 labelled with ^{68}Ga, or a pharmaceutically acceptable salt thereof. In certain embodiments, the radionuclide labelled PSMA binding agent comprises ^{177}Lu-PSMA-617, which is PSMA-617 labelled with ^{177}Lu, or a pharmaceutically acceptable salt thereof.

In certain embodiments, the radionuclide labelled PSMA binding agent comprises PSMA-I&T:

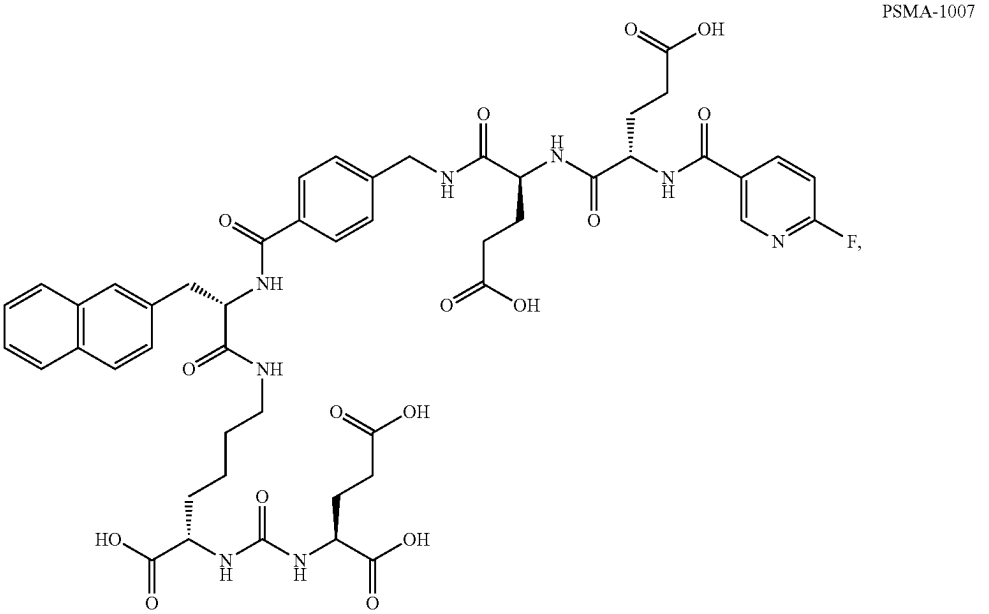
PSMA-I&T



or a pharmaceutically acceptable salt thereof. In certain embodiments, the radionuclide labelled PSMA binding agent comprises ^{68}Ga-PSMA-I&T, which is PSMA-I&T labelled with ^{68}Ga, or a pharmaceutically acceptable salt thereof.

In certain embodiments, the radionuclide labelled PSMA binding agent comprises PSMA-1007:

PSMA-1007



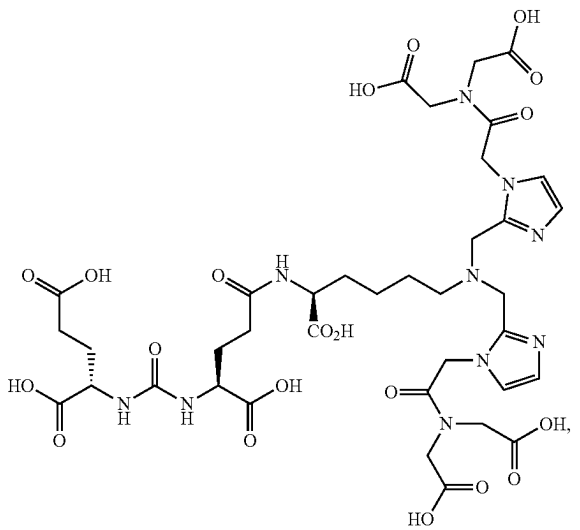
or a pharmaceutically acceptable salt thereof. In certain embodiments, the radionuclide labelled PSMA binding agent comprises ^{18}F-PSMA-1007, which is PSMA-1007 labelled with ^{18}F, or a pharmaceutically acceptable salt thereof.

ii. SPECT Imaging Radionuclide Labelled PSMA Binding Agents

In certain embodiments, the radionuclide labelled PSMA binding agent is a radionuclide labelled PSMA binding agent appropriate for SPECT imaging.

In certain embodiments, the radionuclide labelled PSMA binding agent comprises 1404 (also referred to as MIP-1404):

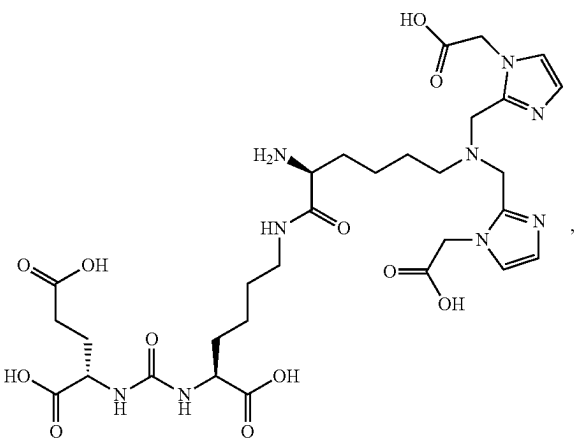
1404



or a pharmaceutically acceptable salt thereof.

In certain embodiments, the radionuclide labelled PSMA binding agent comprises 1405 (also referred to as MIP-1405):

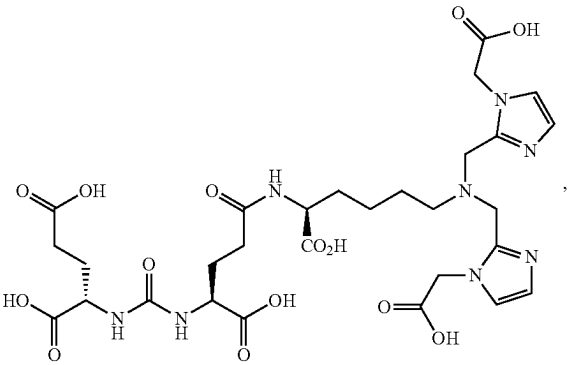
1405



or a pharmaceutically acceptable salt thereof.

In certain embodiments, the radionuclide labelled PSMA binding agent comprises 1427 (also referred to as MIP-1427):

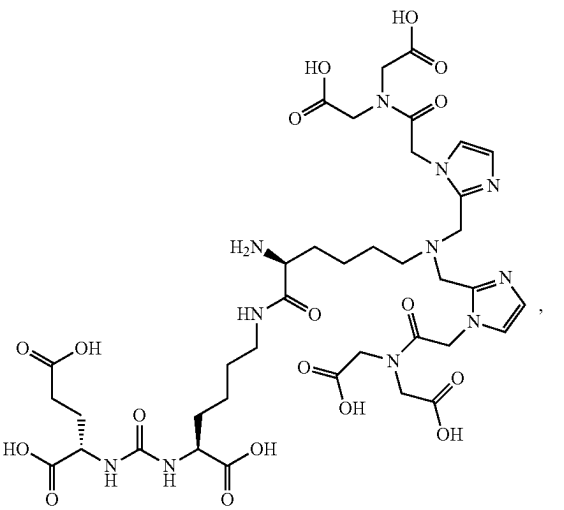
1427



or a pharmaceutically acceptable salt thereof.

In certain embodiments, the radionuclide labelled PSMA binding agent comprises 1428 (also referred to as MIP-1428):

1428

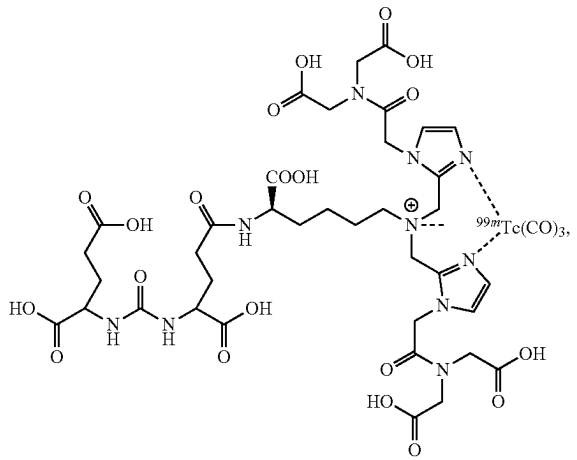


or a pharmaceutically acceptable salt thereof.

In certain embodiments, the PSMA binding agent is labelled with a radionuclide by chelating it to a radioisotope of a metal [e.g., a radioisotope of technetium (Tc) (e.g., technetium-99m (^{99m}Tc)); e.g., a radioisotope of rhenium (Re) (e.g., rhenium-188 (^{188}Re); e.g., rhenium-186 (^{186}Re)); e.g., a radioisotope of yttrium (Y) (e.g., ^{90}Y); e.g., a radioisotope of lutetium (Lu)(e.g., ^{177}Lu); e.g., a radioisotope of gallium (Ga) (e.g., ^{68}Ga; e.g., ^{67}Ga); e.g., a radioisotope of indium (e.g., ^{111}In); e.g., a radioisotope of copper (Cu) (e.g., ^{67}Cu)].

In certain embodiments, 1404 is labelled with a radionuclide (e.g., chelated to a radioisotope of a metal). In certain embodiments, the radionuclide labelled PSMA binding agent comprises ^{99m}Tc-MIP-1404, which is 1404 labelled with (e.g., chelated to) ^{99m}Tc:

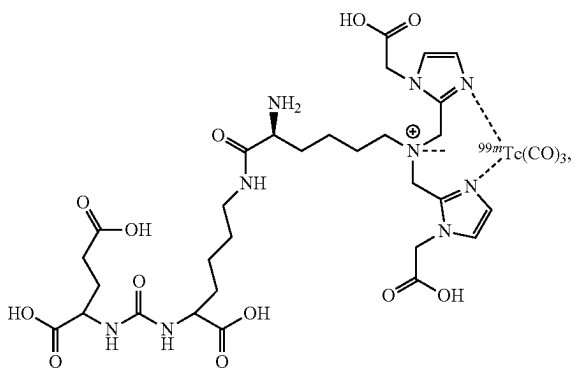
^{99m}Tc-MIP-1404



or a pharmaceutically acceptable salt thereof. In certain embodiments, 1404 may be chelated to other metal radioisotopes [e.g., a radioisotope of rhenium (Re) (e.g., rhenium-188 (^{188}Re); e.g., rhenium-186 (^{186}Re)); e.g., a radioisotope of yttrium (Y) (e.g., ^{90}Y); e.g., a radioisotope of lutetium (Lu) (e.g., ^{177}Lu); e.g., a radioisotope of gallium (Ga) (e.g., ^{68}Ga; e.g., ^{67}Ga); e.g., a radioisotope of indium (e.g., ^{111}In); e.g., a radioisotope of copper (Cu) (e.g., ^{67}Cu)] to form a compound having a structure similar to the structure shown above for ^{99m}Tc-MIP-1404, with the other metal radioisotope substituted for ^{99m}Tc.

In certain embodiments, 1405 is labelled with a radionuclide (e.g., chelated to a radioisotope of a metal). In certain embodiments, the radionuclide labelled PSMA binding agent comprises ^{99m}Tc-MIP-1405, which is 1405 labelled with (e.g., chelated to) ^{99m}Tc:

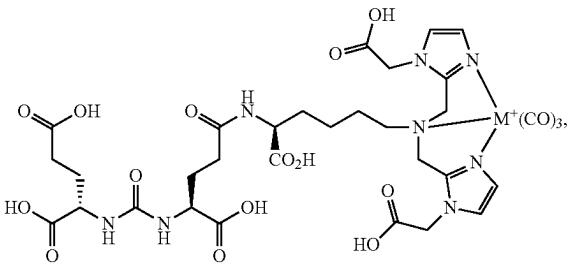
^{99m}Tc-MIP-1405



or a pharmaceutically acceptable salt thereof. In certain embodiments, 1405 may be chelated to other metal radioisotopes [e.g., a radioisotope of rhenium (Re) (e.g., rhenium-188 (^{188}Re); e.g., rhenium-186 (^{186}Re)); e.g., a radioisotope of yttrium (Y) (e.g., ^{90}Y); e.g., a radioisotope of lutetium (Lu)(e.g., ^{177}Lu); e.g., a radioisotope of gallium (Ga) (e.g., ^{68}Ga; e.g., ^{67}Ga); e.g., a radioisotope of indium (e.g., ^{111}In); e.g., a radioisotope of copper (Cu) (e.g., ^{67}Cu)] to form a compound having a structure similar to the structure shown above for ^{99m}Tc-MIP-1405, with the other metal radioisotope substituted for ^{99m}Tc.

In certain embodiments, 1427 is labelled with (e.g., chelated to) a radioisotope of a metal, to form a compound according to the formula below:

1427

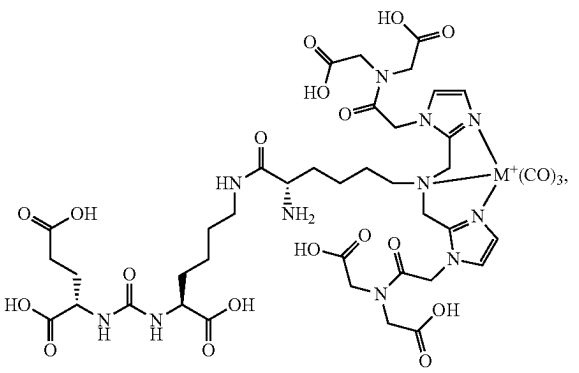


chelated to a metal

or a pharmaceutically acceptable salt thereof, wherein M is a metal radioisotope [e.g., a radioisotope of technetium (Tc) (e.g., technetium-99m (^{99m}Tc)); e.g., a radioisotope of rhenium (Re) (e.g., rhenium-188 (^{188}Re); e.g., rhenium-186 (^{186}Re)); e.g., a radioisotope of yttrium (Y) (e.g., ^{90}Y); e.g., a radioisotope of lutetium (Lu)(e.g., ^{177}Lu); e.g., a radioisotope of gallium (Ga) (e.g., ^{68}Ga; e.g., ^{67}Ga); e.g., a radioisotope of indium (e.g., ^{111}In); e.g., a radioisotope of copper (Cu) (e.g., ^{67}Cu)] with which 1427 is labelled.

In certain embodiments, **1428** is labelled with (e.g., chelated to) a radioisotope of a metal, to form a compound according to the formula below:

1428

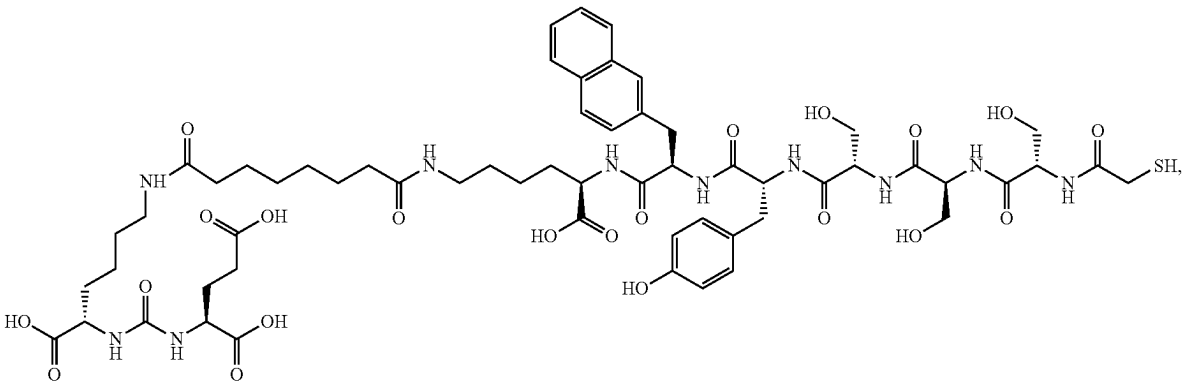


chelated to a metal

or a pharmaceutically acceptable salt thereof, wherein M is a metal radioisotope [e.g., a radioisotope of technetium (Tc) (e.g., technetium-99m (^{99m}Tc)); e.g., a radioisotope of rhenium (Re) (e.g., rhenium-188 (^{188}Re); e.g., rhenium-186 (^{186}Re)); e.g., a radioisotope of yttrium (Y) (e.g., ^{90}Y); e.g., a radioisotope of lutetium (Lu)(e.g., ^{177}Lu); e.g., a radioisotope of gallium (Ga) (e.g., ^{68}Ga; e.g., ^{67}Ga); e.g., a radioisotope of indium (e.g., ^{111}In); e.g., a radioisotope of copper (Cu) (e.g., ^{67}Cu)] with which 1428 is labelled.

In certain embodiments, the radionuclide labelled PSMA binding agent comprises PSMA I&S:

PSMA I&S



or a pharmaceutically acceptable salt thereof. In certain embodiments, the radionuclide labelled PSMA binding agent comprises ^{99m}Tc-PSMA I&S, which is PSMA I&S labelled with ^{99m}Tc, or a pharmaceutically acceptable salt thereof.

D. Computer System and Network Architecture

As shown in FIG. **7**, an implementation of a network environment **700** for use in providing systems, methods, and architectures described herein is shown and described. In brief overview, referring now to FIG. **7**, a block diagram of an exemplary cloud computing environment **700** is shown and described. The cloud computing environment **700** may include one or more resource providers **702***a*, **702***b*, **702***c* (collectively, **702**). Each resource provider **702** may include computing resources. In some implementations, computing resources may include any hardware and/or software used to process data. For example, computing resources may include hardware and/or software capable of executing algorithms, computer programs, and/or computer applications. In some implementations, exemplary computing resources may include application servers and/or databases with storage and retrieval capabilities. Each resource provider **702** may be connected to any other resource provider **702** in the cloud computing environment **700**. In some implementations, the resource providers **702** may be connected over a computer network **708**. Each resource provider **702** may be connected to one or more computing device **704***a*, **704***b*, **704***c* (collectively, **704**), over the computer network **708**.

The cloud computing environment **700** may include a resource manager **706**. The resource manager **706** may be connected to the resource providers **702** and the computing devices **704** over the computer network **708**. In some implementations, the resource manager **706** may facilitate the provision of computing resources by one or more resource providers **702** to one or more computing devices **704**. The resource manager **706** may receive a request for a computing resource from a particular computing device **704**. The resource manager **706** may identify one or more resource providers **702** capable of providing the computing resource requested by the computing device **704**. The resource manager **706** may select a resource provider **702** to provide the computing resource. The resource manager **706** may facilitate a connection between the resource provider **702** and a particular computing device **704**. In some implementations, the resource manager **706** may establish a connection between a particular resource provider **702** and a particular computing device **704**. In some implementations, the resource manager **706** may redirect a particular computing device **704** to a particular resource provider **702** with the requested computing resource.

FIG. **8** shows an example of a computing device **800** and a mobile computing device **850** that can be used to implement the techniques described in this disclosure. The computing device **800** is intended to represent various forms of digital computers, such as laptops, desktops, workstations, personal digital assistants, servers, blade servers, mainframes, and other appropriate computers. The mobile computing device **850** is intended to represent various forms of mobile devices, such as personal digital assistants, cellular telephones, smart-phones, and other similar computing devices. The components shown here, their connections and relationships, and their functions, are meant to be examples only, and are not meant to be limiting.

The computing device **800** includes a processor **802**, a memory **804**, a storage device **806**, a high-speed interface **808** connecting to the memory **804** and multiple high-speed expansion ports **810**, and a low-speed interface **812** connecting to a low-speed expansion port **814** and the storage device **806**. Each of the processor **802**, the memory **804**, the storage device **806**, the high-speed interface **808**, the high-speed expansion ports **810**, and the low-speed interface **812**, are interconnected using various busses, and may be mounted on a common motherboard or in other manners as appropriate. The processor **802** can process instructions for execution within the computing device **800**, including instructions stored in the memory **804** or on the storage device **806** to display graphical information for a GUI on an external input/output device, such as a display **816** coupled to the high-speed interface **808**. In other implementations, multiple processors and/or multiple buses may be used, as appropriate, along with multiple memories and types of memory. Also, multiple computing devices may be connected, with each device providing portions of the necessary operations (e.g., as a server bank, a group of blade servers, or a multi-processor system). Thus, as the term is used herein, where a plurality of functions are described as being performed by "a processor", this encompasses embodiments wherein the plurality of functions are performed by any number of processors (one or more) of any number of computing devices (one or more). Furthermore, where a function is described as being performed by "a processor",

this encompasses embodiments wherein the function is performed by any number of processors (one or more) of any number of computing devices (one or more) (e.g., in a distributed computing system).

The memory **804** stores information within the computing device **800**. In some implementations, the memory **804** is a volatile memory unit or units. In some implementations, the memory **804** is a non-volatile memory unit or units. The memory **804** may also be another form of computer-readable medium, such as a magnetic or optical disk.

The storage device **806** is capable of providing mass storage for the computing device **800**. In some implementations, the storage device **806** may be or contain a computer-readable medium, such as a floppy disk device, a hard disk device, an optical disk device, or a tape device, a flash memory or other similar solid state memory device, or an array of devices, including devices in a storage area network or other configurations. Instructions can be stored in an information carrier. The instructions, when executed by one or more processing devices (for example, processor **802**), perform one or more methods, such as those described above. The instructions can also be stored by one or more storage devices such as computer- or machine-readable mediums (for example, the memory **804**, the storage device **806**, or memory on the processor **802**).

The high-speed interface **808** manages bandwidth-intensive operations for the computing device **800**, while the low-speed interface **812** manages lower bandwidth-intensive operations. Such allocation of functions is an example only. In some implementations, the high-speed interface **808** is coupled to the memory **804**, the display **816** (e.g., through a graphics processor or accelerator), and to the high-speed expansion ports **810**, which may accept various expansion cards (not shown). In the implementation, the low-speed interface **812** is coupled to the storage device **806** and the low-speed expansion port **814**. The low-speed expansion port **814**, which may include various communication ports (e.g., USB, Bluetooth®, Ethernet, wireless Ethernet) may be coupled to one or more input/output devices, such as a keyboard, a pointing device, a scanner, or a networking device such as a switch or router, e.g., through a network adapter.

The computing device **800** may be implemented in a number of different forms, as shown in the figure. For example, it may be implemented as a standard server **820**, or multiple times in a group of such servers. In addition, it may be implemented in a personal computer such as a laptop computer **822**. It may also be implemented as part of a rack server system **824**. Alternatively, components from the computing device **800** may be combined with other components in a mobile device (not shown), such as a mobile computing device **850**. Each of such devices may contain one or more of the computing device **800** and the mobile computing device **850**, and an entire system may be made up of multiple computing devices communicating with each other.

The mobile computing device **850** includes a processor **852**, a memory **864**, an input/output device such as a display **854**, a communication interface **866**, and a transceiver **868**, among other components. The mobile computing device **850** may also be provided with a storage device, such as a micro-drive or other device, to provide additional storage. Each of the processor **852**, the memory **864**, the display **854**, the communication interface **866**, and the transceiver **868**, are interconnected using various buses, and several of the components may be mounted on a common motherboard or in other manners as appropriate.

The processor **852** can execute instructions within the mobile computing device **850**, including instructions stored in the memory **864**. The processor **852** may be implemented as a chipset of chips that include separate and multiple analog and digital processors. The processor **852** may provide, for example, for coordination of the other components of the mobile computing device **850**, such as control of user interfaces, applications run by the mobile computing device **850**, and wireless communication by the mobile computing device **850**.

The processor **852** may communicate with a user through a control interface **858** and a display interface **856** coupled to the display **854**. The display **854** may be, for example, a TFT (Thin-Film-Transistor Liquid Crystal Display) display or an OLED (Organic Light Emitting Diode) display, or other appropriate display technology. The display interface **856** may comprise appropriate circuitry for driving the display **854** to present graphical and other information to a user. The control interface **858** may receive commands from a user and convert them for submission to the processor **852**. In addition, an external interface **862** may provide communication with the processor **852**, so as to enable near area communication of the mobile computing device **850** with other devices. The external interface **862** may provide, for example, for wired communication in some implementations, or for wireless communication in other implementations, and multiple interfaces may also be used.

The memory **864** stores information within the mobile computing device **850**. The memory **864** can be implemented as one or more of a computer-readable medium or media, a volatile memory unit or units, or a non-volatile memory unit or units. An expansion memory **874** may also be provided and connected to the mobile computing device **850** through an expansion interface **872**, which may include, for example, a SIMM (Single In Line Memory Module) card interface. The expansion memory **874** may provide extra storage space for the mobile computing device **850**, or may also store applications or other information for the mobile computing device **850**. Specifically, the expansion memory **874** may include instructions to carry out or supplement the processes described above, and may include secure information also. Thus, for example, the expansion memory **874** may be provide as a security module for the mobile computing device **850**, and may be programmed with instructions that permit secure use of the mobile computing device **850**. In addition, secure applications may be provided via the SIMM cards, along with additional information, such as placing identifying information on the SIMM card in a non-hackable manner.

The memory may include, for example, flash memory and/or NVRAM memory (non-volatile random access memory), as discussed below. In some implementations, instructions are stored in an information carrier. that the instructions, when executed by one or more processing devices (for example, processor **852**), perform one or more methods, such as those described above. The instructions can also be stored by one or more storage devices, such as one or more computer- or machine-readable mediums (for example, the memory **864**, the expansion memory **874**, or memory on the processor **852**). In some implementations, the instructions can be received in a propagated signal, for example, over the transceiver **868** or the external interface **862**.

The mobile computing device **850** may communicate wirelessly through the communication interface **866**, which may include digital signal processing circuitry where necessary. The communication interface **866** may provide for

communications under various modes or protocols, such as GSM voice calls (Global System for Mobile communications), SMS (Short Message Service), EMS (Enhanced Messaging Service), or MMS messaging (Multimedia Messaging Service), CDMA (code division multiple access), TDMA (time division multiple access), PDC (Personal Digital Cellular), WCDMA (Wideband Code Division Multiple Access), CDMA2000, or GPRS (General Packet Radio Service), among others. Such communication may occur, for example, through the transceiver **868** using a radio-frequency. In addition, short-range communication may occur, such as using a Bluetooth®, Wi-Fi™, or other such transceiver (not shown). In addition, a GPS (Global Positioning System) receiver module **870** may provide additional navigation- and location-related wireless data to the mobile computing device **850**, which may be used as appropriate by applications running on the mobile computing device **850**.

The mobile computing device **850** may also communicate audibly using an audio codec **860**, which may receive spoken information from a user and convert it to usable digital information. The audio codec **860** may likewise generate audible sound for a user, such as through a speaker, e.g., in a handset of the mobile computing device **850**. Such sound may include sound from voice telephone calls, may include recorded sound (e.g., voice messages, music files, etc.) and may also include sound generated by applications operating on the mobile computing device **850**.

The mobile computing device **850** may be implemented in a number of different forms, as shown in the figure. For example, it may be implemented as a cellular telephone **880**. It may also be implemented as part of a smart-phone **882**, personal digital assistant, or other similar mobile device.

Various implementations of the systems and techniques described here can be realized in digital electronic circuitry, integrated circuitry, specially designed ASICs (application specific integrated circuits), computer hardware, firmware, software, and/or combinations thereof. These various implementations can include implementation in one or more computer programs that are executable and/or interpretable on a programmable system including at least one programmable processor, which may be special or general purpose, coupled to receive data and instructions from, and to transmit data and instructions to, a storage system, at least one input device, and at least one output device.

These computer programs (also known as programs, software, software applications or code) include machine instructions for a programmable processor, and can be implemented in a high-level procedural and/or object-oriented programming language, and/or in assembly/machine language. As used herein, the terms machine-readable medium and computer-readable medium refer to any computer program product, apparatus and/or device (e.g., magnetic discs, optical disks, memory, Programmable Logic Devices (PLDs)) used to provide machine instructions and/or data to a programmable processor, including a machine-readable medium that receives machine instructions as a machine-readable signal. The term machine-readable signal refers to any signal used to provide machine instructions and/or data to a programmable processor.

To provide for interaction with a user, the systems and techniques described here can be implemented on a computer having a display device (e.g., a CRT (cathode ray tube) or LCD (liquid crystal display) monitor) for displaying information to the user and a keyboard and a pointing device (e.g., a mouse or a trackball) by which the user can provide input to the computer. Other kinds of devices can be used to provide for interaction with a user as well; for example, feedback provided to the user can be any form of sensory feedback (e.g., visual feedback, auditory feedback, or tactile feedback); and input from the user can be received in any form, including acoustic, speech, or tactile input.

The systems and techniques described here can be implemented in a computing system that includes a back end component (e.g., as a data server), or that includes a middleware component (e.g., an application server), or that includes a front end component (e.g., a client computer having a graphical user interface or a Web browser through which a user can interact with an implementation of the systems and techniques described here), or any combination of such back end, middleware, or front end components. The components of the system can be interconnected by any form or medium of digital data communication (e.g., a communication network). Examples of communication networks include a local area network (LAN), a wide area network (WAN), and the Internet.

The computing system can include clients and servers. A client and server are generally remote from each other and typically interact through a communication network. The relationship of client and server arises by virtue of computer programs running on the respective computers and having a client-server relationship to each other.

In some implementations, the various modules described herein can be separated, combined or incorporated into single or combined modules. The modules depicted in the figures are not intended to limit the systems described herein to the software architectures shown therein.

Elements of different implementations described herein may be combined to form other implementations not specifically set forth above. Elements may be left out of the processes, computer programs, databases, etc. described herein without adversely affecting their operation. In addition, the logic flows depicted in the figures do not require the particular order shown, or sequential order, to achieve desirable results. Various separate elements may be combined into one or more individual elements to perform the functions described herein.

Throughout the description, where apparatus and systems are described as having, including, or comprising specific components, or where processes and methods are described as having, including, or comprising specific steps, it is contemplated that, additionally, there are apparatus, and systems of the present invention that consist essentially of, or consist of, the recited components, and that there are processes and methods according to the present invention that consist essentially of, or consist of, the recited processing steps.

It should be understood that the order of steps or order for performing certain action is immaterial so long as the invention remains operable. Moreover, two or more steps or actions may be conducted simultaneously.

While the invention has been particularly shown and described with reference to specific preferred embodiments, it should be understood by those skilled in the art that various changes in form and detail may be made therein without departing from the spirit and scope of the invention as defined by the appended claims.

What is claimed is:

1. A method of measuring intensity values within a reference volume corresponding to a reference tissue region so as to avoid impact from tissue regions associated with low radiopharmaceutical uptake, the method comprising:

(a) receiving, by a processor of a computing device, a 3D functional image of a subject, said 3D functional image

obtained using positron emission tomography (PET) and/or single-photon emission computed tomography (SPECT);

(b) identifying, by the processor, the reference volume within the 3D functional image;

(c) fitting, by the processor, a multi-component mixture model to a distribution of intensities of voxels within the reference volume;

(d) identifying, by the processor, a major mode of the multi-component model;

(e) determining, by the processor, a measure of intensities corresponding to the major mode, thereby determining a reference intensity value corresponding to a measure of intensity of voxels that are (i) within the reference tissue volume and (ii) associated with the major mode;

(f) detecting, by the processor, within the functional image, one or more hotspots corresponding potential cancerous lesions; and

(g) determining, by the processor, for each particular hotspot of at least a portion of the detected hotspots, a lesion index value indicative of: (I) a level of radiopharmaceutical uptake within and underlying lesion to which the particular hotspot corresponds and/or (II) a size of an underlying lesion to which the particular hotspot corresponds, wherein the lesion index value is determined based on (i) a measure of intensity of the particular hotspot and (ii) the reference intensity value.

2. The method of claim **1**, wherein step (e) comprises:

determining a separation threshold based on the distribution of the intensities of voxels within the reference volume and the mixture model fit;

refining the reference volume to remove voxels having intensities smaller than the separation threshold, thereby obtaining a refined reference volume; and

determining the measure of intensities corresponding to the major mode using intensities of voxels of the refined reference volume.

3. The method of claim **1**, wherein step (b) comprises:

receiving, by the processor, a 3D anatomical image of the subject obtained using x-ray Computed Tomography (CT) and/or magnetic resonance imaging (MRI), wherein the 3D anatomical image comprises a graphical representation of the reference tissue region within the subject;

automatically segmenting the 3D anatomical image, to generate a 3D segmentation mask that identifies, within the 3D anatomical image, a 3D volume corresponding to the reference tissue region; and

mapping the 3D segmentation mask onto the 3D functional image to identify the reference volume within the 3D functional image.

4. The method of claim **3**, comprising using a first set of one or more machine learning modules to automatically segment the 3D anatomical image.

5. The method of claim **1**, wherein step (f) comprises using a second machine learning module to automatically detect the one or more hotspots within the 3D functional image.

6. The method of claim **5**, wherein the second machine learning module receives, as input, at least a portion of the 3D functional image and generates, as output, a 3D hotspot map identifying, for each hotspot, a corresponding 3D hotspot volume within the 3D functional image.

7. The method of claim **1**, further comprising adjusting intensities of voxels of the 3D functional image, by the processor, to correct for intensity bleed from one or more high-intensity volumes of the 3D functional image, each of the one or more high-intensity volumes corresponding to a high-uptake tissue region within the subject associated with high radiopharmaceutical uptake under normal circumstances.

8. The method of claim **1**, wherein the reference tissue region comprises one or more members selected from the group consisting of an aorta portion of the subject and a liver of the subject.

9. The method of claim **1**, comprising using the determined lesion index values to compute an overall risk index for the subject, indicative of a cancer status and/or risk for the subject.

10. The method of claim **1**, wherein the 3D functional image comprises a PET or SPECT image obtained following administration of an agent to the subject.

11. The method of claim **10**, wherein the agent comprises a PSMA binding agent.

12. The method of claim **11**, wherein the agent comprises [18F]DCFPyL.

13. A system for measuring intensity values within a reference volume corresponding to a reference tissue region so as to avoid impact from tissue regions associated with low radiopharmaceutical uptake, the system comprising:

a processor of a computing device; and

memory having instructions stored thereon, wherein the instructions, when executed by the processor, cause the processor to:

(a) receive a 3D functional image of a subject, said 3D functional image obtained using positron emission tomography (PET) and/or single-photon emission computed tomography (SPECT);

(b) identify the reference volume within the 3D functional image;

(c) fit a multi-component mixture model to a distribution of intensities of voxels within the reference volume;

(d) identify a major mode of the multi-component model;

(e) determine a measure of intensities corresponding to the major mode, thereby determining a reference intensity value corresponding to a measure of intensity of voxels that are (i) within the reference tissue volume and (ii) associated with the major mode;

(f) detect, within the functional image, one or more hotspots corresponding potential cancerous lesions; and

(g) determine, for each particular hotspot of at least a portion of the detected hotspots, a lesion index value indicative of: (I) a level of radiopharmaceutical uptake within and underlying lesion to which the particular hotspot corresponds and/or (II) a size of an underlying lesion to which the particular hotspot corresponds, wherein the lesion index value is determined based on (i) a measure of intensity of the particular hotspot and (ii) the reference intensity value.

14. The system of claim **13**, wherein step (e) comprises:

determining a separation threshold based on the distribution of the intensities of voxels within the reference volume and the mixture model fit;

refining the reference volume to remove voxels having intensities smaller than the separation threshold, thereby obtaining a refined reference volume; and

determining the measure of intensities corresponding to the major mode using intensities of voxels of the refined reference volume.

15. The system of claim 13, wherein step (b) comprises:

receiving a 3D anatomical image of the subject obtained using x-ray Computed Tomography (CT) and/or magnetic resonance imaging (MRI), wherein the 3D anatomical image comprises a graphical representation of the reference tissue region within the subject;

automatically segmenting the 3D anatomical image, to generate a 3D segmentation mask that identifies, within the 3D anatomical image, a 3D volume corresponding to the reference tissue region; and

mapping the 3D segmentation mask onto the 3D functional image to identify the reference volume within the 3D functional image.

16. The system of claim 15, wherein the instructions, when executed by the processor, cause the processor to use a first set of one or more machine learning modules to automatically segment the 3D anatomical image.

17. The system of claim 13, wherein step (f) comprises using a second machine learning module to automatically detect the one or more hotspots within the 3D functional image.

18. The system of claim 17, wherein the second machine learning module receives, as input, at least a portion of the 3D functional image and generates, as output, a 3D hotspot map identifying, for each hotspot, a corresponding 3D hotspot volume within the 3D functional image.

19. The system of claim 13, wherein the instructions, when executed by the processor, cause the processor to adjust intensities of voxels of the 3D functional image to correct for intensity bleed from one or more high-intensity volumes of the 3D functional image, each of the one or more high-intensity volumes corresponding to a high-uptake tissue region within the subject associated with high radiopharmaceutical uptake under normal circumstances.

20. The system of claim 13, wherein the reference tissue region comprises one or more members selected from the group consisting of an aorta portion of the subject and a liver of the subject.

21. The system of claim 13, wherein the instructions, when executed by the processor, cause the processor to use the determined lesion index values to compute an overall risk index for the subject, indicative of a cancer status and/or risk for the subject.

22. The system of claim 13, wherein the 3D functional image comprises a PET or SPECT image obtained following administration of an agent to the subject.

23. The system of claim 22, wherein the agent comprises a PSMA binding agent.

24. The system of claim 23, wherein the agent comprises [18F]DCFPyL.

* * * * *

EXHIBIT 7

US011941817B2

(12) **United States Patent**
Richter et al.

(10) **Patent No.: US 11,941,817 B2**
(45) **Date of Patent: Mar. 26, 2024**

(54) **SYSTEMS AND METHODS FOR PLATFORM AGNOSTIC WHOLE BODY IMAGE SEGMENTATION**

(71) Applicant: **EXINI Diagnostics AB**, Lund (SE)

(72) Inventors: **Jens Filip Andreas Richter**, Lund (SE); **Kerstin Elsa Maria Johnsson**, Lund (SE); **Erik Konrad Gjertsson**, Lund (SE); **Aseem Undvall Anand**, Queens, NY (US)

(73) Assignee: **EXINI Diagnostics AB**, Lund (SE)

(*) Notice: Subject to any disclaimer, the term of this patent is extended or adjusted under 35 U.S.C. 154(b) by 0 days.

(21) Appl. No.: **18/127,991**

(22) Filed: **Mar. 29, 2023**

(65) **Prior Publication Data**

US 2023/0316530 A1 Oct. 5, 2023

Related U.S. Application Data

(62) Division of application No. 16/734,599, filed on Jan. 6, 2020, now Pat. No. 11,657,508.
(Continued)

(51) **Int. Cl.**
G06T 7/00 (2017.01)
A61B 6/00 (2006.01)
(Continued)

(52) **U.S. Cl.**
CPC ***G06T 7/11*** (2017.01); ***A61B 6/032*** (2013.01); ***A61B 6/037*** (2013.01); ***A61B 6/463*** (2013.01);
(Continued)

(58) **Field of Classification Search**
CPC G06T 7/11
See application file for complete search history.

(56) **References Cited**

U.S. PATENT DOCUMENTS

5,762,608 A 6/1998 Warne et al.
7,450,747 B2 11/2008 Jabri et al.
(Continued)

FOREIGN PATENT DOCUMENTS

CN 1200520 A 12/1998
CN 101528267 A 9/2009
(Continued)

OTHER PUBLICATIONS

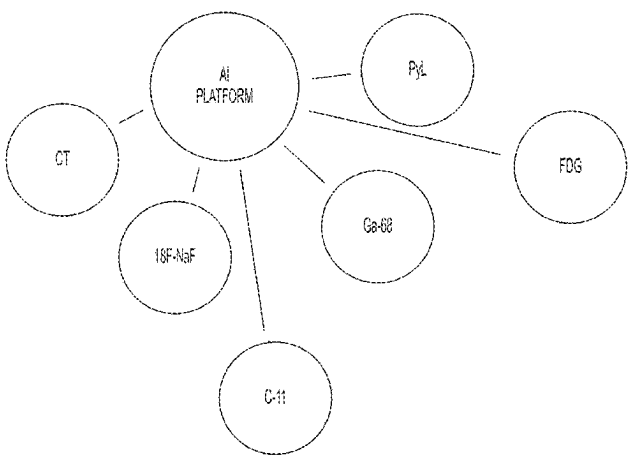
Ali, A. et al., The Automated Bone Scan Index as a Predictor of Response to Prostate Radiotherapy in Men with Newly Diagnosed Metastatic Prostate Cancer: An Exploratory Analysis of Stampede's "M1|RT Comparison", European Urology Oncology 3:412-419, (2020).
(Continued)

Primary Examiner — Joseph M Santos Rodriguez
(74) *Attorney, Agent, or Firm* — Choate, Hall & Stewart LLP; William R. Haulbrook; Ronen Adato

(57) **ABSTRACT**

Presented herein are systems and methods that provide for automated analysis of three-dimensional (3D) medical images of a subject in order to automatically identify specific 3D volumes within the 3D images that correspond to specific anatomical regions (e.g., organs and/or tissue). Notably, the image analysis approaches described herein are not limited to a single particular organ or portion of the body. Instead, they are robust and widely applicable, providing for consistent, efficient, and accurate detection of anatomical regions, including soft tissue organs, in the entire body. In certain embodiments, the accurate identification of one or more such volumes is used to automatically determine quantitative metrics that represent uptake of radiopharmaceuticals in particular organs and/or tissue regions. These uptake metrics can be used to assess disease state in a subject, determine a prognosis for a subject, and/or determine efficacy of a treatment modality.

32 Claims, 26 Drawing Sheets
(20 of 26 Drawing Sheet(s) Filed in Color)



Related U.S. Application Data

(60) Provisional application No. 62/934,305, filed on Nov. 12, 2019, provisional application No. 62/907,158, filed on Sep. 27, 2019, provisional application No. 62/870,210, filed on Jul. 3, 2019, provisional application No. 62/863,608, filed on Jun. 19, 2019, provisional application No. 62/837,941, filed on Apr. 24, 2019, provisional application No. 62/789,155, filed on Jan. 7, 2019.

(51) **Int. Cl.**

A61B 6/03	(2006.01)
A61K 51/04	(2006.01)
G06F 18/214	(2023.01)
G06T 7/11	(2017.01)
G06V 20/64	(2022.01)
G06V 20/69	(2022.01)
G06V 30/24	(2022.01)
G16H 30/20	(2018.01)
G16H 30/40	(2018.01)
G16H 50/20	(2018.01)
G16H 50/30	(2018.01)
G16H 50/50	(2018.01)

(52) **U.S. Cl.**

CPC ***A61B 6/466*** (2013.01); ***A61B 6/481*** (2013.01); ***A61B 6/505*** (2013.01); ***A61B 6/507*** (2013.01); ***A61B 6/5205*** (2013.01); ***A61B 6/5241*** (2013.01); ***A61B 6/5247*** (2013.01); ***A61K 51/0455*** (2013.01); ***G06F 18/214*** (2023.01); ***G06V 20/64*** (2022.01); ***G06V 20/695*** (2022.01); ***G06V 20/698*** (2022.01); ***G06V 30/2504*** (2022.01); ***G16H 30/20*** (2018.01); ***G16H 30/40*** (2018.01); ***G16H 50/20*** (2018.01); ***G16H 50/30*** (2018.01); ***G16H 50/50*** (2018.01); *G06V 2201/031* (2022.01); *G06V 2201/033* (2022.01)

(56) **References Cited**

U.S. PATENT DOCUMENTS

7,751,605	B2	7/2010	Gündel et al.
7,935,055	B2	5/2011	Burckhardt
7,970,194	B2	6/2011	Kimura
8,199,985	B2	6/2012	Jakobsson et al.
8,211,401	B2	7/2012	Babich et al.
8,467,856	B2	6/2013	Renisch et al.
8,538,166	B2	9/2013	Gordon et al.
8,705,887	B2	4/2014	Ma et al.
8,778,305	B2	7/2014	Pomper et al.
8,855,387	B2	10/2014	Hamadeh et al.
8,962,799	B2	2/2015	Babich et al.
8,995,736	B2	3/2015	Kaufman et al.
9,002,081	B2	4/2015	Brown
9,466,133	B2	10/2016	Sowards-Emmerd et al.
9,710,915	B2	7/2017	Firouzian et al.
9,721,340	B2	8/2017	Gillies et al.
10,058,393	B2	8/2018	Bonutti et al.
10,223,610	B1	3/2019	Akselrod-Ballin et al.
10,311,971	B2	6/2019	Opfer et al.
10,330,763	B2	6/2019	James et al.
10,339,653	B2	7/2019	Gillies et al.
10,340,044	B2	7/2019	Yao et al.
10,340,046	B2	7/2019	Baker
RE47,609	E	9/2019	Hamadeh et al.
10,492,723	B2	12/2019	Madabhushi et al.
10,600,184	B2	3/2020	Golden et al.
10,665,346	B2	5/2020	Baker
10,748,652	B2	8/2020	Yao et al.
10,762,993	B2	9/2020	Baker
10,818,386	B2	10/2020	Yao et al.
10,943,681	B2	3/2021	Yao et al.
10,973,486	B2	4/2021	Sjostrand et al.
11,011,257	B2	5/2021	Lints et al.
11,321,844	B2	5/2022	Johnsson et al.
11,386,988	B2	7/2022	Johnsson et al.
11,424,035	B2	8/2022	Baker
11,534,125	B2	12/2022	Sjöstrand et al.
11,564,621	B2	1/2023	Anand et al.
11,657,508	B2	5/2023	Richter et al.
11,721,428	B2	8/2023	Brynolfsson et al.
2003/0215120	A1	11/2003	Uppaluri et al.
2005/0281381	A1	12/2005	Guendel
2006/0062425	A1	3/2006	Shen et al.
2006/0064396	A1	3/2006	Wei et al.
2006/0078183	A1	4/2006	deCharms
2007/0081712	A1	4/2007	Huang et al.
2007/0081713	A1	4/2007	Jerebko
2007/0100225	A1	5/2007	Maschke
2007/0115204	A1	5/2007	Budz et al.
2008/0027315	A1	1/2008	McGinnis
2009/0309874	A1	12/2009	Salganicoff et al.
2009/0311182	A1	12/2009	Wang et al.
2010/0215581	A1	8/2010	Hoffmann
2010/0266170	A1	10/2010	Khamene et al.
2010/0322488	A1	12/2010	Virtue et al.
2011/0063288	A1	3/2011	Valadez
2011/0255763	A1	10/2011	Bogoni et al.
2012/0123253	A1	5/2012	Renisch et al.
2013/0038707	A1	2/2013	Cunningham et al.
2013/0094704	A1	4/2013	Hamadeh et al.
2013/0129168	A1	5/2013	Ross
2013/0211231	A1	8/2013	Sundarapandian et al.
2013/0281841	A1	10/2013	Everett et al.
2014/0193336	A1	7/2014	Rousso et al.
2015/0110716	A1	4/2015	Armor
2015/0119704	A1	4/2015	Roth et al.
2015/0331995	A1	11/2015	Zhao et al.
2016/0203263	A1	7/2016	Maier et al.
2016/0335395	A1	11/2016	Wu et al.
2017/0083682	A1	3/2017	McNutt et al.
2017/0112577	A1	4/2017	Bonutti et al.
2018/0144828	A1	5/2018	Baker
2018/0259608	A1	9/2018	Golden et al.
2018/0360402	A1	12/2018	Carmi
2019/0038239	A1	2/2019	Flohr et al.
2019/0105009	A1	4/2019	Siemionow et al.
2019/0209116	A1	7/2019	Sjostrand et al.
2019/0388049	A1	12/2019	Gupta et al.
2020/0027559	A1	1/2020	Baker
2020/0051238	A1	2/2020	El Harouni et al.
2020/0074634	A1	3/2020	Kecskemethy et al.
2020/0085382	A1	3/2020	Taerum et al.
2020/0126666	A1	4/2020	Baker
2020/0170604	A1	6/2020	Yildirim et al.
2020/0193594	A1	6/2020	Georgescu et al.
2020/0193603	A1	6/2020	Golden et al.
2020/0245960	A1	8/2020	Richter et al.
2020/0311919	A1	10/2020	Grimmer et al.
2020/0315455	A1	10/2020	Lee et al.
2020/0337658	A1	10/2020	Sjostrand et al.
2020/0342600	A1	10/2020	Sjostrand et al.
2020/0352518	A1	11/2020	Lyman et al.
2020/0357117	A1	11/2020	Lyman et al.
2020/0357118	A1	11/2020	Yao et al.
2020/0357521	A1	11/2020	Baker
2020/0410672	A1	12/2020	Katscher et al.
2021/0032206	A1	2/2021	Neumaier et al.
2021/0082547	A1	3/2021	Yao et al.
2021/0093249	A1	4/2021	Anand et al.
2021/0183485	A1	6/2021	Yao et al.
2021/0233633	A1	7/2021	Lints et al.
2021/0334974	A1	10/2021	Johnsson et al.
2021/0335480	A1	10/2021	Johnsson et al.
2022/0005586	A1	1/2022	Brynolfsson et al.
2022/0375612	A1	11/2022	Baker
2022/0398724	A1	12/2022	Anand et al.

(56) **References Cited**

U.S. PATENT DOCUMENTS

2023/0115732	A1	4/2023	Brynolfsson et al.
2023/0148980	A1	5/2023	Sjöstrand et al.

FOREIGN PATENT DOCUMENTS

CN	102361594	A	2/2012
CN	102947840	A	2/2013
CN	103607954	A	2/2014
CN	106558045	A	4/2017
CN	107644421	A	1/2018
EP	1426903	A2	6/2004
EP	1508872	A1	2/2005
EP	3043318	A1	7/2016
GB	2457577	A	8/2009
JP	2010-029481	A	2/2010
JP	2011-067594	A	4/2011
JP	2014-006130	A	1/2014
JP	2015-513083	A	4/2015
JP	6013042	B2	10/2016
JP	2017067489	A	4/2017
JP	6170284	B2	7/2017
SE	524500	C2	8/2004
TW	201201847	A	1/2012
WO	WO-99/05503	A2	2/1999
WO	WO-2007/062135	A2	5/2007
WO	WO-2009/084995	A1	7/2009
WO	WO-2011/077303	A1	6/2011
WO	WO-2011/091378	A1	7/2011
WO	WO-2011/095580	A1	8/2011
WO	WO-2013/126147	A2	8/2013
WO	WO-2015/058151	A2	4/2015
WO	WO-2018/014475	A1	1/2018
WO	WO-2018/015953	A1	1/2018
WO	WO-2018/081354	A1	5/2018
WO	WO-2019/005722	A1	1/2019
WO	WO-2019/103912	A2	5/2019
WO	WO-2019/136349	A2	7/2019
WO	WO-2020/144134	A1	7/2020
WO	WO-2020/146032	A1	7/2020
WO	WO-2020/190821	A1	9/2020
WO	WO-2020/219619	A1	10/2020
WO	WO-2020/219620	A1	10/2020
WO	WO-2021/061315	A1	4/2021
WO	WO-2022/008374	A1	1/2022
WO	WO-2023/057411	A1	4/2023

OTHER PUBLICATIONS

American College of Radiology (ACR) and the Society for Pediatric Radiology (SPR), ACR-SPR Practice Parameter For The Performance Of Skeletal Scintigraphy (Bone Scan), Resolution 28, (2013—Revused2017), available from: <http://www.acr.org>, 9 pages (2017).

Anand, A. et al., A Pre-Analytical Validation Study of Automated Bone Scan Index: Effect on Accuracy and Reproducibility Due to the Procedural Variabilities in Bone Scan Image Acquisition. J Nucl Med. pp. 1865-1871, (2016).

Anand, A. et al., Analytic Validation of the Automated Bone Scan Index as an Imaging Biomarker to Standardize Quantitative Changes in Bone Scans of Patients with Metastatic Prostate Cancer, J. Nucl. Med., 57(1):41-45 (2016).

Anand, A. et al., Automated Bone Scan Index as a quantitative imaging biomarker in metastatic castration-resistant prostate cancer patients being treated with enzalutamide, EJNMMI Research, 6:23, 7 pages (2016).

Anand, A. et al., Translating Prostate Cancer Working Group 2 (PCWG2) Progression Criteria into a Quantitative Response Biomarker in Metastatic Castration Resistant Prostate Cancer (mCRPC), ASCO GU Conference, Poster, 1 page, presented Feb. 16, 2017.

Anand, A. et al., Translating Prostate Cancer Working Group 2 (PCWG2) progression criteria into a quantitative response biomarker in metastatic castration-resistant prostate cancer (mCRPC), Journal of Clinical Oncology, 35(6):170 (2017).

Armstrong, A. et al., Assessment of the bone scan index in a randomized placebo-controlled trial of tasquinimod in men with metastatic castration-resistant prostate cancer (mCRPC), Urologic Oncology: Seminars and Original Investigations, 32:1308-1316 (2014).

Armstrong, A. et al., Development and validation of a prognostic model for overall survival in chemotherapy-naive men with metastatic castration-resistant prostate cancer (mCRPC) from the phase 3 prevail clinical trial, Journal of Clinical Oncology, 35(Suppl.6): Abstract 138, 5 pages, (2017).

Armstrong, A. J. et al., Phase 3 Assessment of the Automated Bone Scan Index as a Prognostic Imaging Biomarker of Overall Survival in Men with Metastatic Castration-Resistant Prostate Cancer: A Secondary Analysis of a Randomized Clinical Trial. JAMA Oncology 4:944-951, (2018).

Armstrong, A. J. et al., Phase 3 prognostic analysis of the automated bone scan index (aBSI) in men with bone-metastatic castration-resistant prostate cancer (CRPC), Meeting Library ASC University, 11 pages (2017).

Bai, P. et. al., Body region localization in whole-body low-dose CT images of PET/CT scans using virtual landmarks, Medical Physics Wiley USA, 46(3): 1286-1299 (2019).

Belal, S. et al., Association of PET Index quantifying skeletal uptake in NaF PET/CT images with overall survival in prostate cancer patients, ASCO GU 2017, Poster 178, 1 page, presented Feb. 16, 2017.

Belal, S. et al., PET Index quantifying skeletal uptake in NaF PET/CT images with overall survival in prostate cancer patients, ASCO GU 2017, Abstract, 1 page, (Feb. 13, 2017).

Belal, S. L. et al, 3D skeletal uptake of ^{18}F sodium fluoride in PET/CT images is associate with overall survival in patients with prostate cancer, EJNMMI Research, 7(15):1-8 (2017).

Belal, S.L. et al., Automated evaluation of normal uptake in different skeletal parts in 18F-sodium fluoride (NaF) PET/CT using a new convolutional neural network method, EJNMMI, EANM '17, 44(Suppl 2):S119-S956, Abstract EP-0116 (2017).

Bombardieri, E. et al., Bone scintigraphy: procedure guidelines for tumour imaging, Eur J. Nucl. Med. Mol. Imaging, 30:BP99-BP106, (2003).

Brynolfsson, J., et. al., Deep Learning based urinary bladder segmentation using 18FDCFPyL (PyL-PSMA) PET/CT images, EPS-145, European Association of Nuclear Medicine, (2020), <http://link.springer.com/article/10.1007/s00259-020-04988-4>. pp. S1 and S403-404, Retrieved Sep. 18, 2020.

Brynolfsson, J., et. al., Deep Learning-Enabled comprehensive detection and quantification of 18FDCFPyL (PyL-PSMA) PET/CT, OP-548, European Association of Nuclear Medicine, (2020), <http://link.springer.com/article/10.1007/s00259-020-04988-4>. pp. S1 and S273, Retrieved Sep. 18, 2020.

Bushberg, J. T. et al., Essential Physics of Medical Imaging, Essential Physics of Medical Imaging, 19.3: p. 581 (table 15-3), p. 713 paragraph 6, section 19.3 and p. 720, (2011).

Capobianco, N. et al., Whole-body uptake classification and prostate cancer staging in ^{68}Ga-PSMA-11 PET/CT using dual-tracer learning, European Journal of Nuclear Medicine and Molecular Imaging, (2021), <https:/doi.org/10.1007/s00259-021-05473-2> 10 pages. Retrieved on Apr. 18, 2021.

Ceci, F. et al., E-PSMA: the EANM standardized reporting guidelines v1.0 for PSMA-PET, European Journal of Nuclear Medicine and Molecular Imaging, 48:1626-1638, (2021).

Cha, K. H., et al. Urinary bladder segmentation in CT urography using deep-learning convolutional neural network and level sets, Medical physics, 43(4):1882-1896, (2016).

Christ, P.F. et al., Automatic Liver and Tumor Segmentation of CT and MRI Volumes Using Cascaded Fully Convolutional Neural Networks, Arxiv.org, Cornell University Library, 20 pages, (2017).

Ciernik, I. F., et al. 3D-segmentation of the 18F-choline PET signal for target volume definition in radiation therapy of the prostate, Technology in cancer research & treatment 6(1): 23-30, (2007).

Dennis, E. et al., Bone Scan Index: A Quantitative Treatment Response Biomarker for Castration-Resistant Metastatic Prostate Cancer, Journal of Clinical Oncology, 30(5):519-524 (2012).

(56) **References Cited**

OTHER PUBLICATIONS

Dertat, A., Applied Deep Learning—Part 4: Convolutional Neural Networks, Towards Data Science,<http://towardsdatascience.com/applied-deep-learning-part-4-convolutional-neural-networks-584bc134c1e2> 26 pages, (2017).

Eiber, M. et al., Prostate Cancer Molecular Imaging Standardized Evaluation (PROMISE): Proposed miTNM Classification for the Interpretation of PSMA-Ligand PET/CT, The Journal of Nuclear Medicine, 59(3):469-478, (2018).

Fendler, W.P. et. al., ^{68}Ga-PSMA PET/CT: Joint EANM and SNMMI procedure guideline for prostate cancer imaging: version 1.0, Eur J Nucl Med Mol Imaging, DOI 10.1007/s00259-017-3670-z, 11 pages, (2017).

GE Healthcare, SPECT/CT Cameras, 2 pages, retrieved Oct. 25, 2017: <http://www3.gehealthcare.com.sg/en-gb/products/categories/nuclear_medicine/spect-ct_cameras>.

Giesel, F. L. et al., F-18 labelled PSMA-1007: biodistribution, radiation dosimetry and histopathological validation of tumor lesions in prostate cancer patients, Eur. J. Nucl. Med. Mol. Imaging, 44:678-688 (2017).

Gjertsson, K., et. al., A Novel Automated Deep Learning Algorithm for Segmentation of the Skeleton in Low-Dose CT for [(18)F] DCFPyL PET/CT Hybrid Imaging in Patients with Metastatic Prostate Cancer, Annual Congress of the European Association of Nuclear Medicine Oct. 12-16, 2019 Barcelona, Spain. Eur J Nucl Med Mol Imaging 46 (Suppl 1), S1-S952 (2019). Abstract EP-0823, p. S765.

Gjertsson, K., Segmentation in Skeletal Scintigraphy Images using Convolutional Neural Networks, Master's Theses in Mathematical Sciences, pp. 39-58, (2017), <https://lup.lub.lu.se/student-papers/search/publication/8916406>.

Goffin, K. E. et al., Phase 2 study of ^{99m}Tc-trofolastat SPECT/CT to identify and localize prostate cancer in intermediate- and high-risk patients undergoing radical prostatectomy and extended pelvic lymph node dissection, J. Nucl. Med., 27 pages (2017).

Gorthi, S. et al., Segmentation of Head and Neck Lymph Node Regions for Radiotherapy Planning Using Active Contour-Based Atlas Registration, IEEE Journal of Selected Topics in Signal Processing, 3(1):135-147 (2009).

Grahovac, M. et al., Machine learning predictive performance evaluation of conventional and fuzzy radiomics in clinical cancer imaging cohorts, Eur. J. Med. Mol. Imaging, 50(6):1607-1620 (2023).

Guimond, A. et al., Average Brain Models: A Convergence Study, Computer Vision and Image Understanding, 77:192-210 (2000).

Hajnal, J. et al., 4.4 Intensity, Size, and Skew Correction; 7.1 Introduction; 7.2 Methods; 7.3 Image Interpretation—General, In: Medical Image Registration, CRC Press LLC, 80-81:144-148 (2001).

Hiller, S. M. et al., 99mTc-Labeled Small-Molecule Inhibitors of Prostate-Specific Membrane Antigen for Molecular Imaging of Prostate Cancer, Journal of Nuclear Medicine, 54(8):1369-1376 (2013) retrieved Oct. 25, 2017: <http://jnm.snmjournals.org/content/54/8/1369.full>.

Horikoshi, H. et al., Computer-aided diagnosis system for bone scintigrams from Japanese patients: importance of training database, Annals of Nuclear Medicine, 26(8):622-626 (2012).

Huang, J.-H. et al., A Set of Image Processing Algorithms for Computer-Aided Diagnosis in Nuclear Medicine Whole Body Bone Scan Images, IEEE Transactions on Nuclear Science, 54(3):514-522 (2007).

IM, HJ, et. al., et. al., Current Methods to Define Metabolic Tumor Volume in Positron Emission Tomography: Which One is Better?, Nucl. Med. Mol. Imaging, 52(1):5-15, (2018).

Inoue, T., What cancers can be understood and not known by "PET"?—Effects of PET scanning by site, Medical Note Interview, 4 pages, (2015), retrieved from the internet at: https://medicalnote.jp/contents/150715-000003-CYJIZE.

International Search Report for PCT/EP2020/050132, filed Jan. 6, 2020, 3 pages, dated Mar. 12, 2020.

Johnsson, K. et al., Analytical performance of aPROMISE: automated anatomic contextualization, detection, and quantification of [18F]DCFPyL (PSMA) imaging for standardized reporting, European Journal of Nuclear Medicin and Molecular Imaging, 11 pages, Aug. 31, 2021, doi: 10.1007/s00259-021-05497-8. Epub ahead of print. PMID: 34463809.

Johnsson, K., et. al., miPSMA Index: Comprehensive and Automated Quantification of 18F-DCFPyL (PyL-PSMA) PET/CT for Prostate Cancer Staging, J Nucl Med., 61: (Supplement 1): 1435, 5 pages, (2020).

Kaboteh R. et al., Progression of bone metastases in patients with prostate cancer—automated detection of new lesions and calculation of bone scan index, EJNMMI Research, 3:64, 6 pages, (2013).

Kaboteh, R. et al., Convolutional neural network based quantification of choline uptake in PET/CT studies is associated with overall survival in patents with prostate cancer, EJNMMI, EANM '17, 44(Suppl 2):S119-S956, Abstract EP-0642 (2017).

Kertesz, H. et al., Implementation of a Spatially-Variant and Tissue-Dependent Positron Range Correction for PET/CT Imaging, Front. Physiol., 13:818463 (2022).

Kertesz, H. et al., Positron range in combination with point-spread-function correction: an evaluation of different implementations for [124I]-PET imaging, ENJMMI Phys., 9(1):56 (2022).

Khurshid, Z. et al., Role of textural heterogeneity parameters in patient selection for 177Lu-PSMA therapy via response prediction, Oncotarget., 9(70):33312-33321 (2018).

Kiess, et al., Prostate-specific membrane antigen and a target for cancer imaging and therapy, The Quarterly Journal of Nuclear Medicine and Molecular Imaging, 59(3):241-268 (2015).

Kikuchi, A. et al., Automated segmentation of the skeleton in whole-body bone scans: influence of difference in atlas, Nuclear Medicine Communications, 33(9):947-953 (2012).

Kinahan, P.E. et al., PET/CT Standardized Update Values (SUVs) in Clinical Practice and Assessing Response to Therapy, Semin Ultrasound CT MR 31(6):496-505 (2010) retrieved Oct. 25, 2017: <https://www.ncbi.nlm.nih.gov/pmc/articles/PMC3026294/>.

Knutsson, H., and Andersson, M., Morphons: Segmentation using Elastic Canvas and Paint on Priors, IEEE International Conference on Image Processing (ICIP 2005), Genova, Italy, 4 pages (2005).

Kopka, K. et al., Glu-Ureido-Based Inhibitors of Prostate-Specific Membrane Antigen: Lessons Learned During the Development of a Novel Class of Low-Molecular-Weight Theranostic Radiotracers, The Journal of Nuclear Medicine, 58(9)(Suppl. 2):17S-26S, (2017).

Krajnc, D. et al., Automated data preparation for in vivo tumor characterization with machine learning, Front. Oncol., 12:1017911 (2022).

Lin, T.Y. et. al., Feature Pyramid Networks for object detection, FAIR, 10 pages, (2016), <https://arxiv.org/abs/1612.03144v1>.

Litjens, G. et al., A survey on deep learning in medical image analysis, Medical Image Analysis, 42:60-88, (2017).

Liu, L. et al., Computer-Aided Detection of Prostate Cancer with MRI: Technology and Applications, Acad Radiol. Author manuscript, 50 pages 2016.

Ma, L. et al., Automatic segmentation of the prostate on CT images using deep learning and multi-atlas fusion, Proc. of SPIE vol. 10133:101332O-1-101332O-9 (2017).

Ma, L. et al., Combining Population and Patient-Specific Characteristics for Prostate Segmentation on 3D CT Images, Proc of SPIE 9784:978427-1-8 (2016).

Ma, L. et al., Random Walk Based Segmentation for the Prostate on 3D Transrectal Ultrasound Images, Proc SPIE Int Soc Opt Eng. Author manuscript, 13 pages (2016).

Matsubara, N. et al, A Phase II, Randomized, Open-Label, Multi-arm Study of TAS-115 for Castration-Resistant Prostate Cancer Patients With Bone Metastases, Clinical Genitourinary Cancer, 000(xxx):1-10, (2021).

Mayo Clinic Staff, Choline C-11 PET scan, Overview, Mayo Clinic, 4 pages (2017), retrieved Oct. 25, 2017: <https://www.mayoclinic.org/tests-procedures/choline-c-11-pet-scan/home/ovc-20156994>.

Meyer, A., et. al., Deep learning algorithm improves identification of men with low-risk prostate cancer using PSMA targeted 99mTc-MIP-1404 SPECT/CT, Journal of Clinical Oncology, 37:(15), (2019).

(56) **References Cited**

OTHER PUBLICATIONS

Nakajima, K. et al., Enhanced diagnostic accuracy for quantitative bone scan using an artificial neural network system: a Japanese multi-center database project, EJNMMI Research, 3:83, 9 pages, (2013).
National Cancer Institute, NCI Drug Dictionary: gallium Ga 68-labeled PSMA-11, 1 page, retrieved Oct. 25, 2017: <https://www.cancer.gov/publications/dictionaries/cancer-drug?cdrid=766400>.
National Cancer Institute, NCI Drug Dictionary: technetium Tc 99m methylene diphosphonate, 1 page, retrieved Oct. 25, 2017: <https://www.cancer.gov/publications/dictionaries/cancer-drug?cdrid=537722>.
Nickols, N. et al., aPROMISE: A Novel Automated-PROMISE platform to Standardize Evaluation of Tumor Burden in 18F-DCFPyL (PSMA) images of Veterans with Prostate Cancer, Journal of Nuclear Medicine, 26 pages, May 28, 2021, doi: 10.2967/jnumed.120.261863.
Nickols, N.G., et. al., A deep learning algorithm to predict coexisting metastatic disease using intraprostatic [F18]DCFPYL PSMA image alone in veterans with prostate cancer, Journal of Clinical Oncology 38, (Supplement 6), 2020.
Ohlsson, M., et. al., Automated decision support for bone scintigraphy, Computer-based medical systems, pp. 1-6, (2009).
Papp, L. et al., Glioma Survival Prediction with Combined Analysis of In Vivo 11C-MET PET Features, Ex Vivo Features, and Patient Features by Supervised Machine Learning, J. Nucl. Med., 59(6):892-899 (2018).
Papp, L. et al., Optimized Feature Extraction for Radiomics Analysis of 18F-FDG PET Imaging, J. Nucl. Med., 60(6):864-872 (2019).
Papp, L. et al., Supervised machine learning enables non-invasive lesion characterization in primary prostate cancer with [68Ga]Ga-PSMA-11 PET/MRI, Eur. J. Nucl. Mol. Imaging, 48(6): 1795-1805 (2021).
Paschalis, A. et al., Prostate-specific Membrane Antigen Heterogeneity and DNA Repair Defects in Prostate Cancer, European Urology, 76(4):469-478, (2019).
Perera, M. et al., Sensitivity, Specificity, and Predictors of Positive 68Ga-Prostate-specific Membrane Antigen Positron Emission Tomography in Advanced Prostate Cancer: A Systematic Review and Meta-analysis, European Urology, 70(6):926-937 (2016).
Polymeri, E. et al., Analytical validation of an automated method for segmentation of the prostate gland in CT images, EJNMMI, EANM '17, 44(Suppl 2):S119-S956, Abstract EP-0641 (2017).
Polymeri, E., et. al., Deep learning-based quantification of PET/CT prostate gland uptake: association with overall survival, Clinical Physiology Functional Imaging, DOI: 10.1111/cpf.12611, 40(2):106-113, (2019).
Pouliot, F., et. al., Prospective evaluation of a Novel Deep Learning Algorithm (PSMA-AI) in the assessment of 99mTc-MIP-1404 SPECT/CT in patients with low or intermediate risk prostate cancer, Annual Congress of the European Association of Nuclear Medicine Oct. 12-16, 2019 Barcelona, Spain. Eur J Nucl Med Mol Imaging 46 (Suppl 1), S1-S952 (2019). Abstract EP-0804, p. S765.
radiologyinfo.org for Patients, Computed Tomography (CT), 2 pages, retrieved Oct. 25, 2017: <https://www.radiologyinfo.org/en/submenu.cfm?pg=ctscan>.
Ren, S., et. al., Faster R-CNN: Towards Real-Time Object Detection with Region Proposal Networks, 14 pages, (2015), <http://image-net.org/challenges/LSVRC/2015/results>.
Ronneberger, O., et. al., U-Net: Convolutional Networks for Biomedical Image Segmentation, Springer International Publishing, pp. 234-241, (2015), <http://lmb.informatik.uni-freiburg.de/>. Published online on Nov. 18, 2015.
Rowe, S. P. et al., PET Imaging of prostate-specific membrane antigen in prostate cancer: current state of the art and future challenges, Prostate Cancer and Prostatic Diseases, pp. 1-8 (2016).
Rowe, S. P. et al., PSMA-Based [^{18}F]DCFPyL PET/CT Is Superior to Conventional Imaging for Lesion Detection in Patients with Metastatic Prostate Cancer, Mol Imaging Biol, 18:411-419, (2016).
Sabbatini, P. et al., Prognostic Significance of Extent of Disease in Bone in Patients With Androgen-Independent Prostate Cancer, Journal of Clinical Oncology, 17(3):948-957 (1999).
Sadik, M. et al., 3D prostate gland uptake of 18F-choline—association with overall survival in patients with hormone-naïve prostate cancer, The Journal of Nuclear Medicine, 58(Suppl. 1):Abstract 544, 2 pages, (2017).
Sadik, M. et al., A new computer-based decision-support system for the interpretation of bone scans, Nuclear Medicine Communications, 27(5):417-423 (2006).
Sadik, M. et al., Automated 3D segmentation of the prostate gland in CT images—a first step towards objective measurements of prostate uptake in PET and SPECT images, Journal of Nuclear Medicine, 58(1):1074, (2017).
Sadik, M. et al., Automated quantification of reference levels in liver and mediastinum (blood pool) for the Deauville therapy response classification using FDG-PET/CT in lymphoma patients, EJNMMI, EANM '17, 44(Suppl 2):S119-S956, Abstract EP-0770 (2017).
Sadik, M. et al., Computer-assisted interpretation of planar whole-body bone scans, Journal Nuclear Medicine, 49(12):1958-65, 2008.
Sadik, M. et al., Convolutional neural networks for segmentation of 49 selected bones in CT images show high reproducibility, EJNMMI, EANM '17, 44(Suppl 2):S119-S956, Abstract OP-657 (2017).
Sadik, M. et al., Improved classifications of planar whole-body bone scans using a computer-assisted diagnosis system: a multicenter, multiple-reader, multiple-case study, Journal of Nuclear Medicine, 50(3): 368-75, 2009.
Sadik, M. et al., Variability in reference levels for Deauville classifications applied to lymphoma patients examined with 18F-FDG-PET/CT, EJNMMI, EANM '17, 44(Suppl 2):S119-S956, Abstract EP-0771 (2017).
Sajn, L. et al., Computerized segmentation of whole-body bone scintigrams and its use in automated diagnostics, Computer Methods and Programs in Biomedicine, 80:47-55 (2005).
Salerno, J. et al., Multiparametric magnetic resonance imaging for pre-treatment local staging of prostate cancer: A Cancer Care Ontario clinical practice guideline, Canadian Urological Association Journal, 10(9-10):332-339 (2016).
Santos-Cuevas, C. et al. 99mTc-labeled PSMA inhibitor: Biokinetics and radiation dosimetry in healthy subjects and imaging of prostate cancer tumors in patients, Nuclear Medicine and Biology 52:1-6, (2017).
Shi, F. et al., Deep learning empowered volume delineation of whole-body organs-at-risk for accelerated radiotherapy, Nat. Commun., 13(1):6566 (2022).
Sjöstrand K. et al., Statistical regularization of deformation fields for atlas-based segmentation of bone scintigraphy images, MICCAI 5761:664-671 (2009).
Sjöstrand, K., et al., Automated detection and quantification of Prostatic PSMA uptake in SPECT/CT using a Deep Learning Algorithm for Segmentation of Pelvic Anatomy, The Journal of Nuclear Medicine, 59(1):p. 30, (2018).
Sjostrand, K., et. al., Automated Assessment of Prostatic PSMA Expression in SPECT/CT using Deep Convolutional Neural Networks—A Prospectively Planned Retrospective Analysis of Phase 3 Study MIP-1404-3301, The Journal of Nuclear Medicine, 60 (Supplement 1): Abstract 401, 1 page, (2019).
Sluimer, I. et al., Toward Automated Segmentation of the Pathological Lung in CT, IEEE Transactions on Medical Imaging, 24(8):1025-1038 (2005).
Teng, C. et al., Head and neck lymph node region delineation using a hybrid image registration method, 3rd IEEE International Symposium on Biomedical Imaging: Nano to Macro, 4 pages, (2006).
Tian, Z. et al., A fully automatic multi-atlas based segmentation method for prostate MR images, Proc SPIE Int Soc Opt Eng. Author manuscript, 12 pages (2015).
Tian, Z. et al., A supervoxel-based segmentation method for prostate MR images, Med. Phys., 44(2):558-569 (2017).
Tian, Z. et al., Deep convolutional neural network for prostate MR segmentation, Proc. of SPIE 10135:101351L-1-101351L-6 12 pages, (2017).

(56) **References Cited**

OTHER PUBLICATIONS

Tian, Z., et al., Superpixel-based Segmentation for 3D Prostate MR Images, IEEE Trans Med Imaging, Author manuscript, pp. 558-569, (2016).
Trägärdh, E., et. al., RECOMIA—a cloud-based platform for artificial intelligence research in nuclear medicine and radiology, EJNMMI Physics, <https://doi.org/10.1186/s40658-020-00316-9>, 7:51, 12 pages, (2020).
Ulmert, D. et al., A Novel Automated Platform for Quantifying the Extent of Skeletal Tumour Involvement in Prostate Cancer Patients Using the Bone Scan Index, European Urology, 62(1):78-84 (2012).
Valladares, A. et al., A multi-modality physical phantom for mimicking tumor heterogeneity patterns in PET/CT and PET/MRI, Med. Phys., 49(9):5819-5829 (2022).
Wallis, J.W. et. al., Three-dimensional display in nuclear medicine, IEEE Trans Med Imaging, 8(4):297-303, (1989).
Washino, H., Injectable for bone scintigraphy: Technetium hydroxymethylenediphosphonate (99mTc) injection solution (Revised Edition), 9 pages, (2007), retrieved from the internet at:https://rada.or.jp/database/home4/normal/ht-docs/member/synopsis/030292.html#:%7E:text=%E6%A6%82%E8%A6%81).
Wrangsjo, A. et al., Non-rigid Registration Using Morphons, Proceedings of the 14th Scandinavian Conference on Image Analysis (SCIA '05), pp. 501-510 (2005).
Written Opinion for PCT/EP2020/050132, filed Jan. 6, 2020, 11 pages, dated Mar. 12, 2020.
Yin, T.-K., and Chiu, N.T., A Computer-Aided Diagnosis for Locating Abnormalities in Bone Scintigraphy by a Fuzzy System With a Three-Step Minimization Approach, IEEE Transactions on Medical Imaging, 23(5):639-654 (2004).
Gafita, A. et al., Novel Framework for Treatment Response Evaluation Using PSMA PET/CT in Patients with Metastatic Castration-Resistant Prostate Cancer (RECIP 1.0): An International Multicenter Study, J. Nucl. Med., 63(11): 1651-1658 (2022).
Guan, H. et al., Automatic Hot Spot Detection and Segmentation in Whole Body FDG-PET Images, IEEE International Conference on Image Processing, 4 pages, (2006).
Kawakami, K. et al., Introduction of bone scintigraphy diagnosis support software "Bonenavi" (Topics), Journal of Nuclear Medicine (Japanese), 63:41-51 (2011).
Kawakami, K., Evaluation of bone metastasis by bone scintigraphy diagnostic support software BONENAVI, Communication of the Imaging Group of the JSRT, 36(1):74-77 (2013).
Nogi, S. et al., Metastatic bone tumor quantified by computer-assisted diagnosis system of bone scintigraphy, Nuclear Medicine in Clinic, 45(3):35-37 (2012).
Partin, A.W. et al., Combination of prostate-specific antigen, clinical stage, and Gleason score to predict pathological stage of localized prostate cancer. A multi-institutional update, JAMA, 277(18):1445-1451 (1997).
Partin, A.W. et al., The use of prostate specific antigen, clinical stage and Gleason score to predict pathological stage in men with localized prostate cancer, J. Urol., 150(1):110-114 (1993).
Poulakis, V. et al., Preoperative neural network using combined magnetic resonance imaging variables, prostate specific antigen, and Gleason score to predict prostate cancer recurrence after radical prostatectomy, Eur. Urol., 46(5):571-578 (2004).
Seifert, R. et al., Second Version of the Prostate Cancer Molecular Imaging Standardized Evaluation Framework Including Response Evaluation for Clinical Trials (Promise V2), Eur. Urol., 83(5):405-412 (2023).
US Food and Drug Administration, Clinical Trial Endpoints for the Approval of Cancer Drugs and Biologics, 21 pages, (2018).

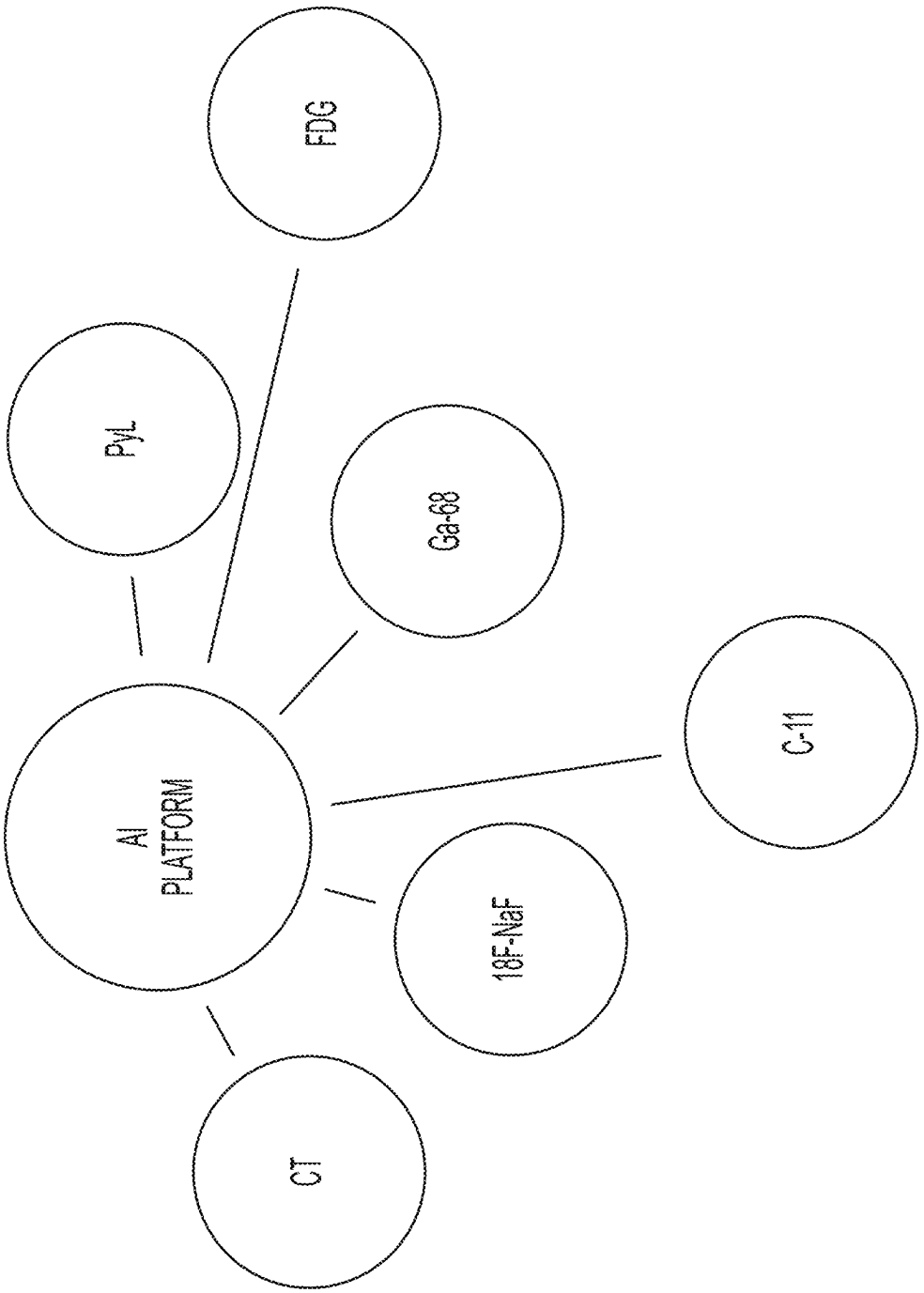


FIG. 1

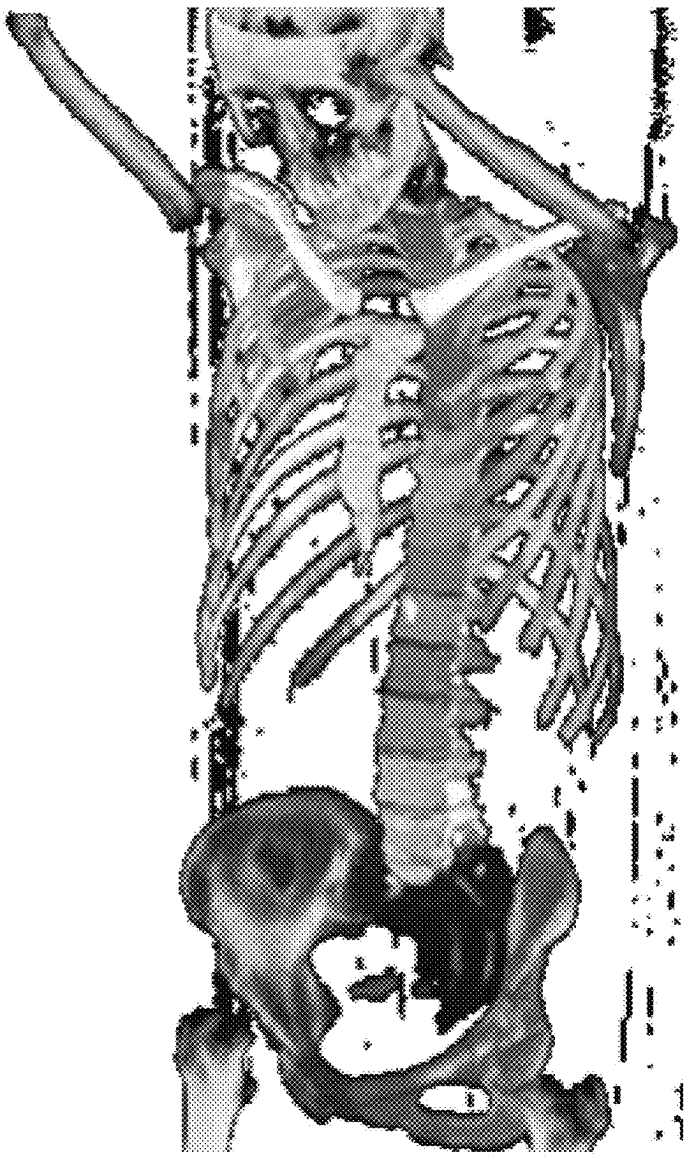


FIG. 2

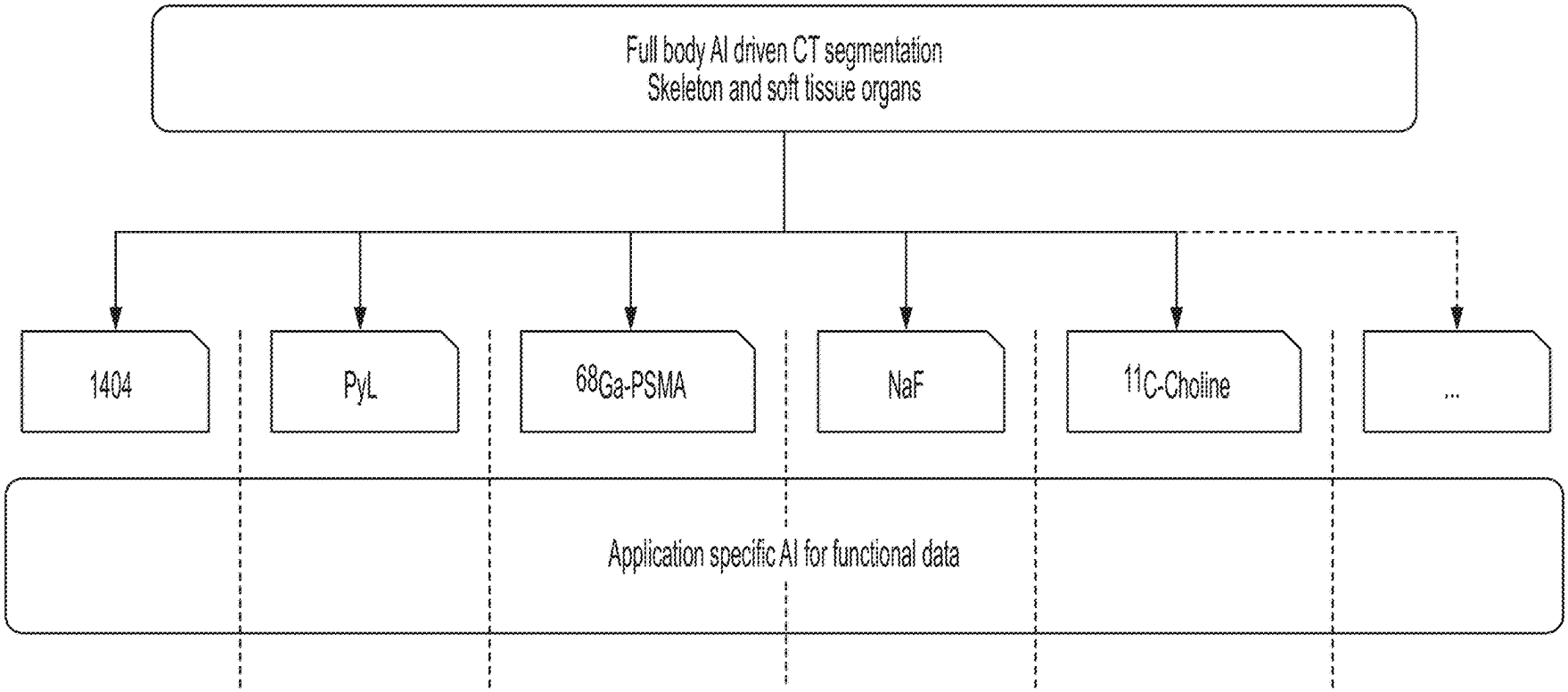

Full body AI driven CT segmentation
Skeleton and soft tissue organs
1404
PyL
68Ga-PSMA
NaF
11C-Choline
...
Application specific AI for functional data

FIG. 3

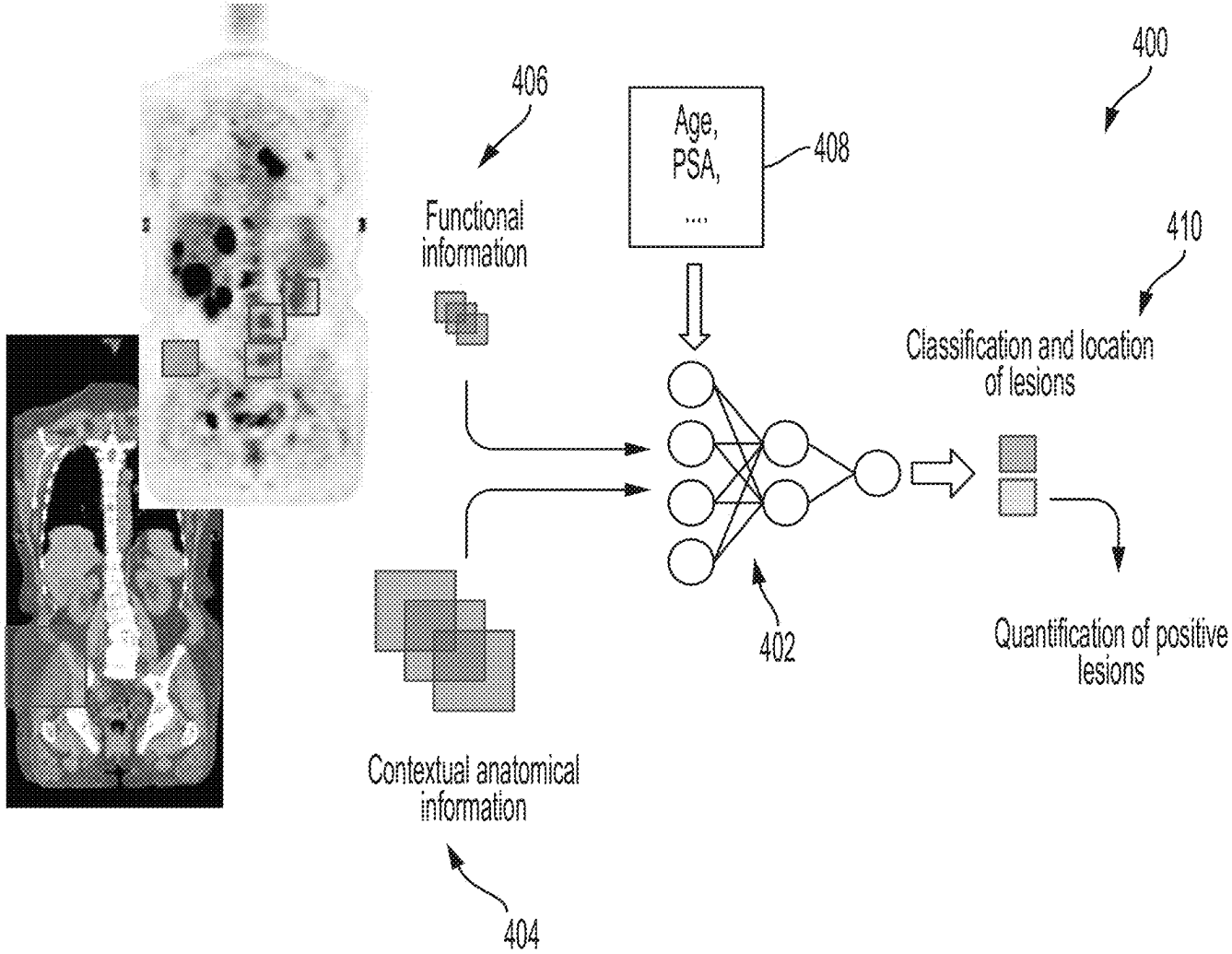

400
406
Functional information
Age, PSA, ...
408
410
Classification and location of lesions
402
Quantification of positive lesions
Contextual anatomical information
404

FIG. 4

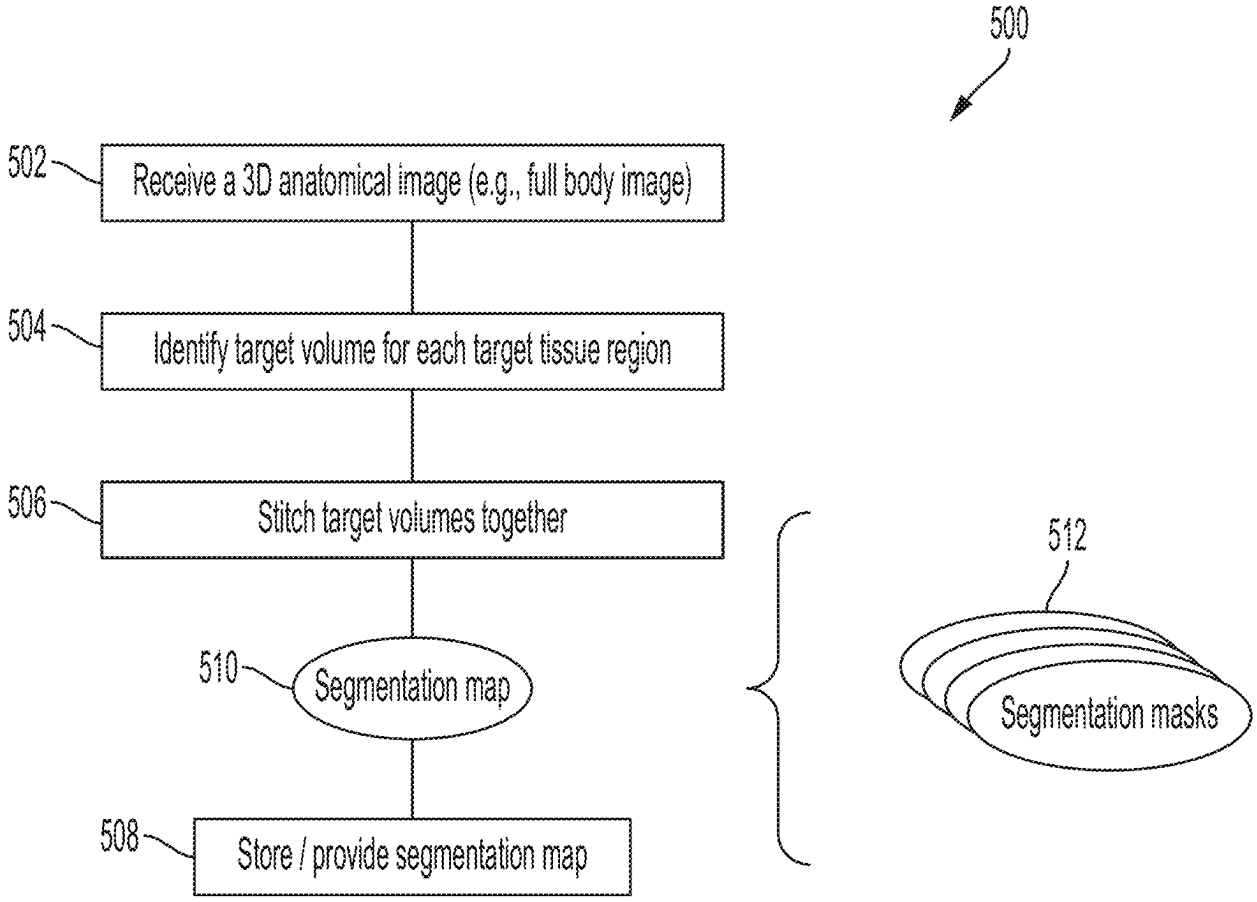

500
502
Receive a 3D anatomical image (e.g., full body image)
504
Identify target volume for each target tissue region
506
Stitch target volumes together
510
Segmentation map
508
Store / provide segmentation map
512
Segmentation masks

FIG. 5A

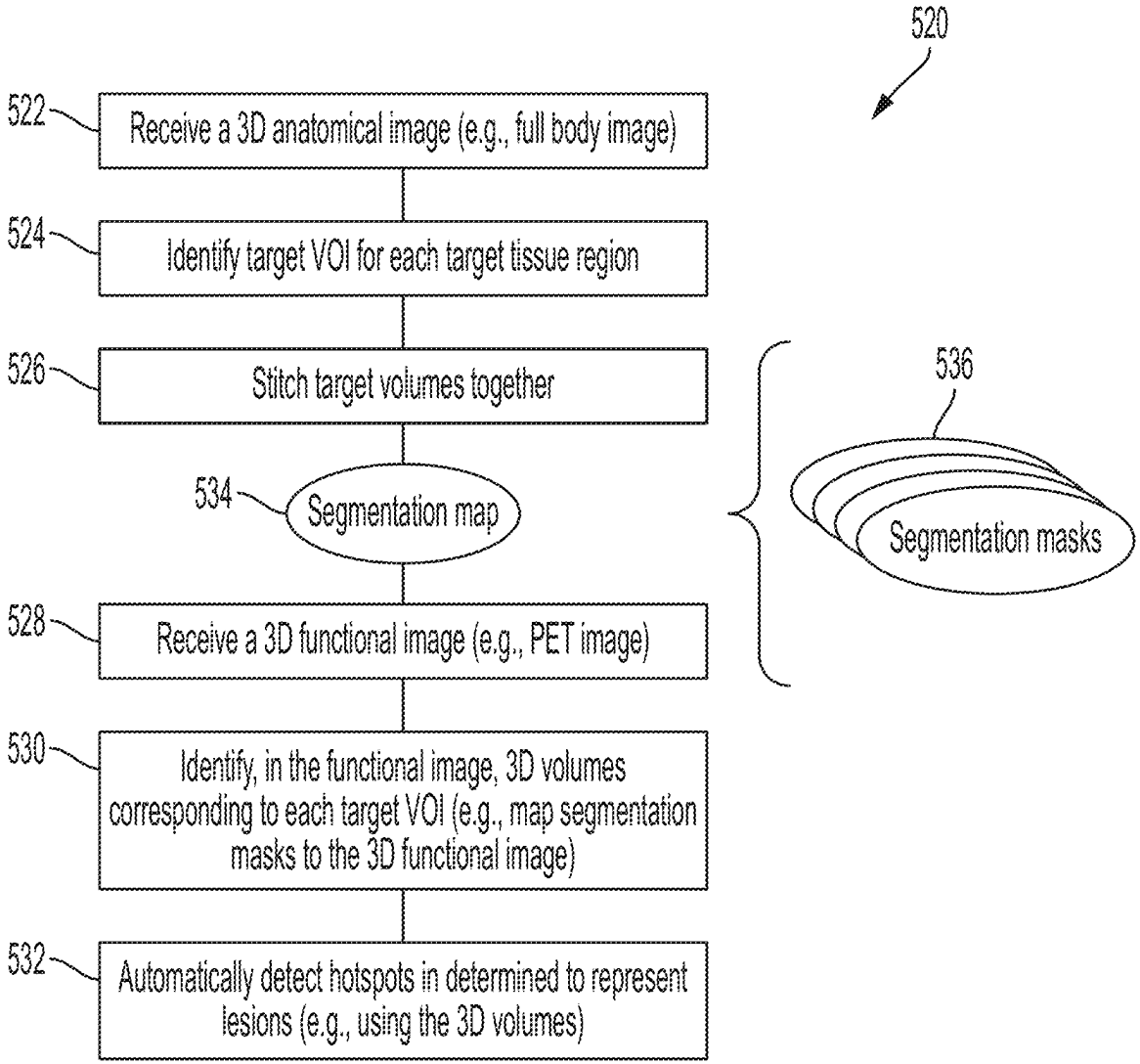

520
522
Receive a 3D anatomical image (e.g., full body image)
524
Identify target VOI for each target tissue region
526
Stitch target volumes together
534
Segmentation map
536
Segmentation masks
528
Receive a 3D functional image (e.g., PET image)
530
Identify, in the functional image, 3D volumes corresponding to each target VOI (e.g., map segmentation masks to the 3D functional image)
532
Automatically detect hotspots in determined to represent lesions (e.g., using the 3D volumes)

FIG. 5B

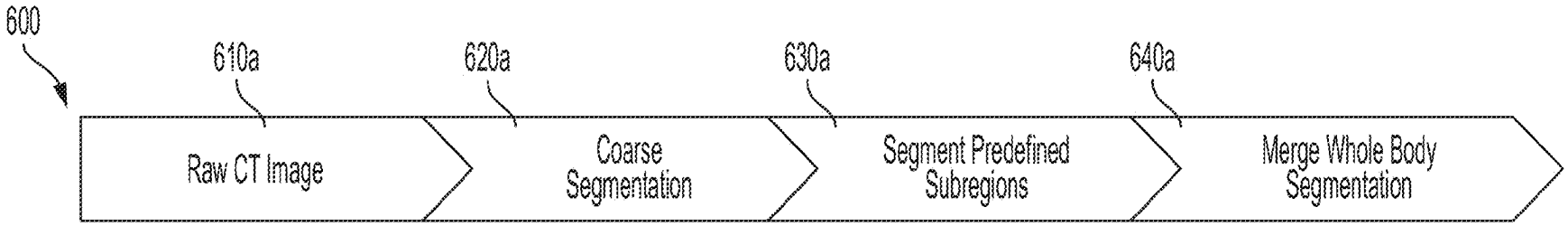

600
610a
620a
630a
640a
Raw CT Image
Coarse Segmentation
Segment Predefined Subregions
Merge Whole Body Segmentation

FIG. 6A

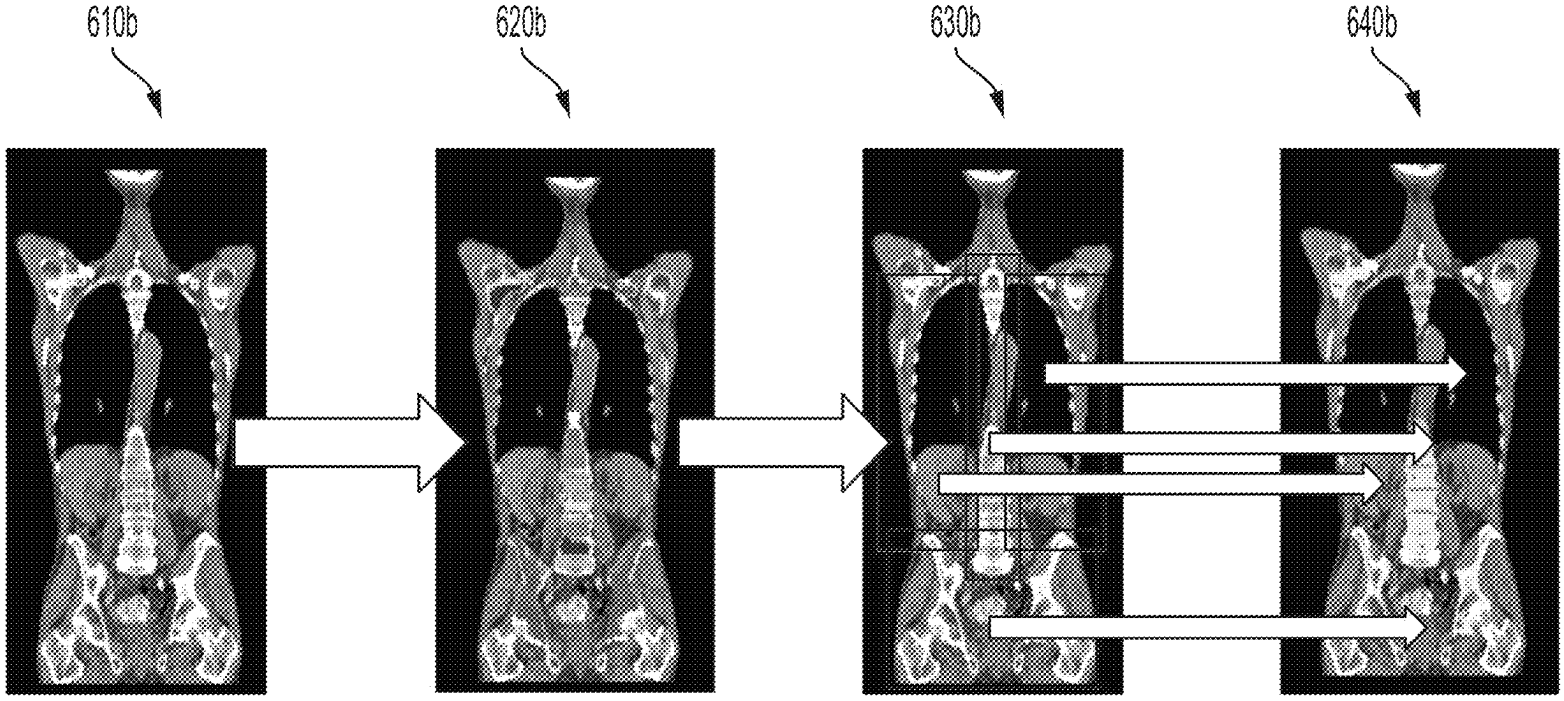

610b
620b
630b
640b

FIG. 6B

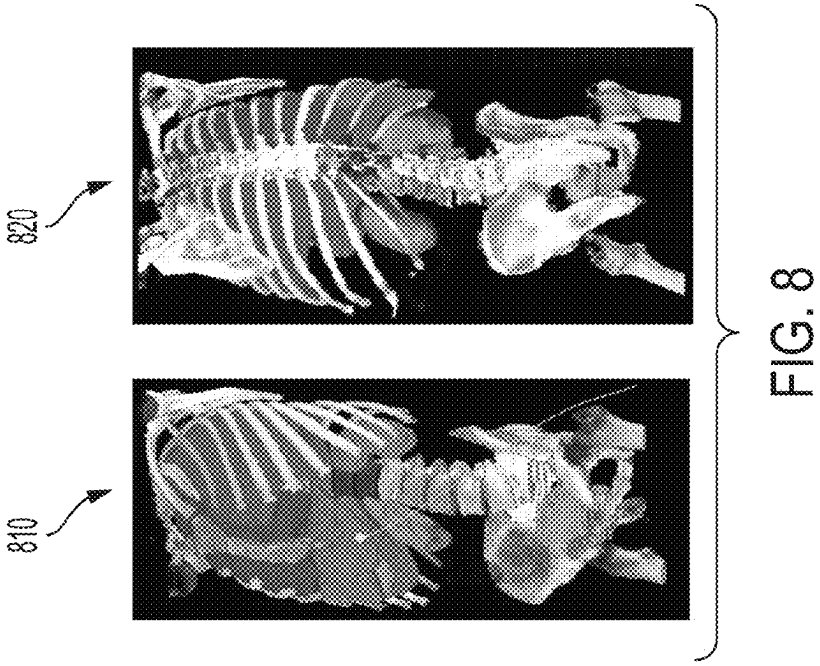


FIG. 8

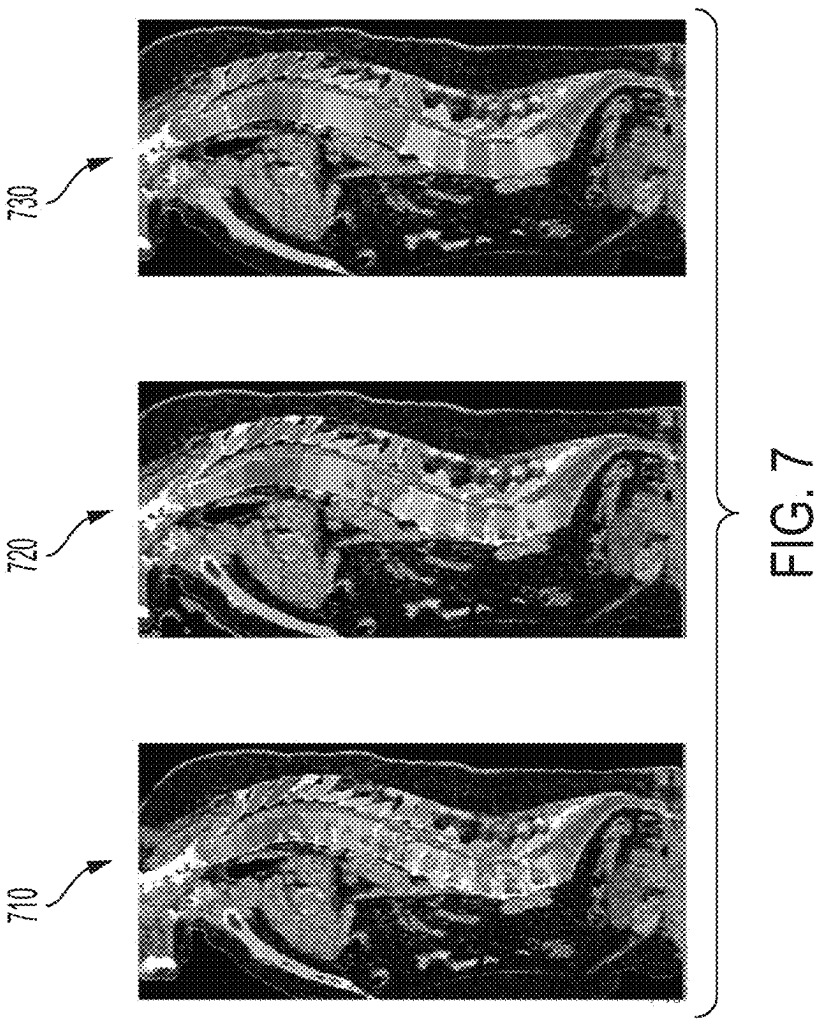


FIG. 7



FIG. 9A

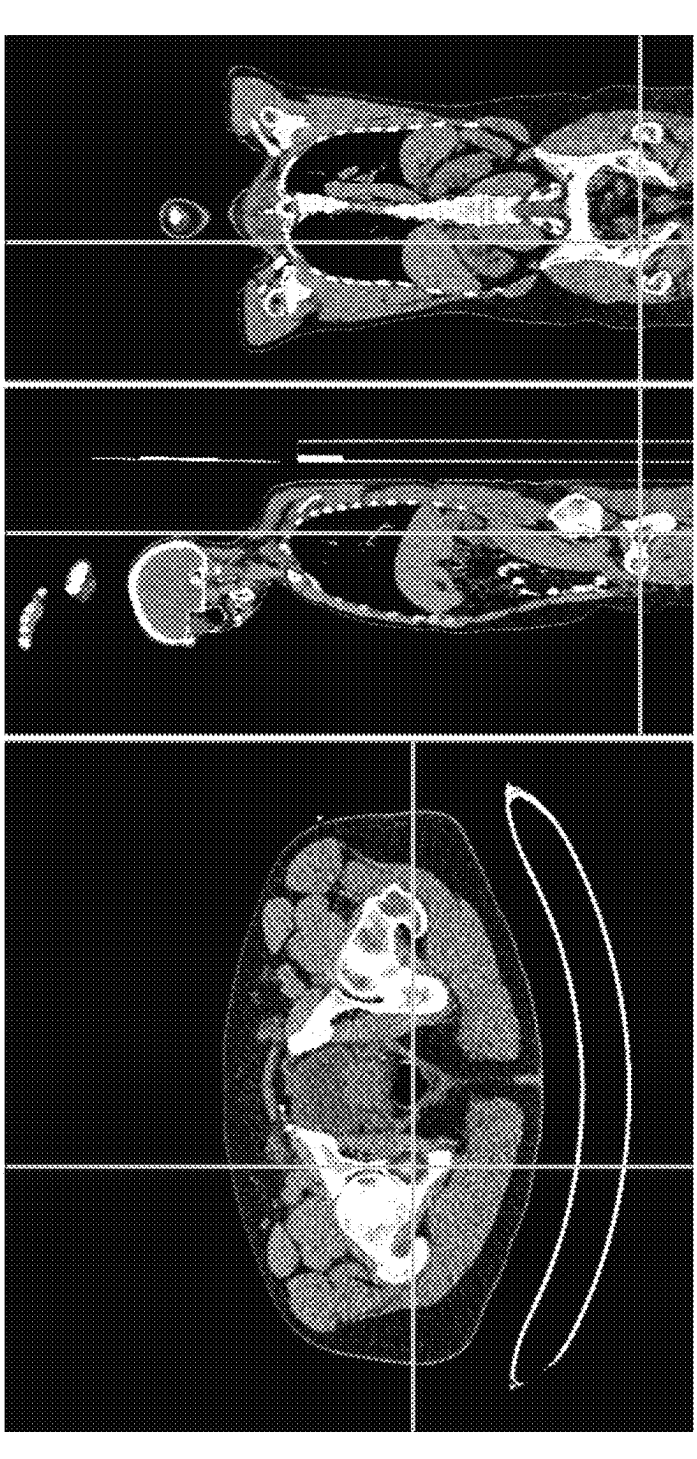


FIG. 9B

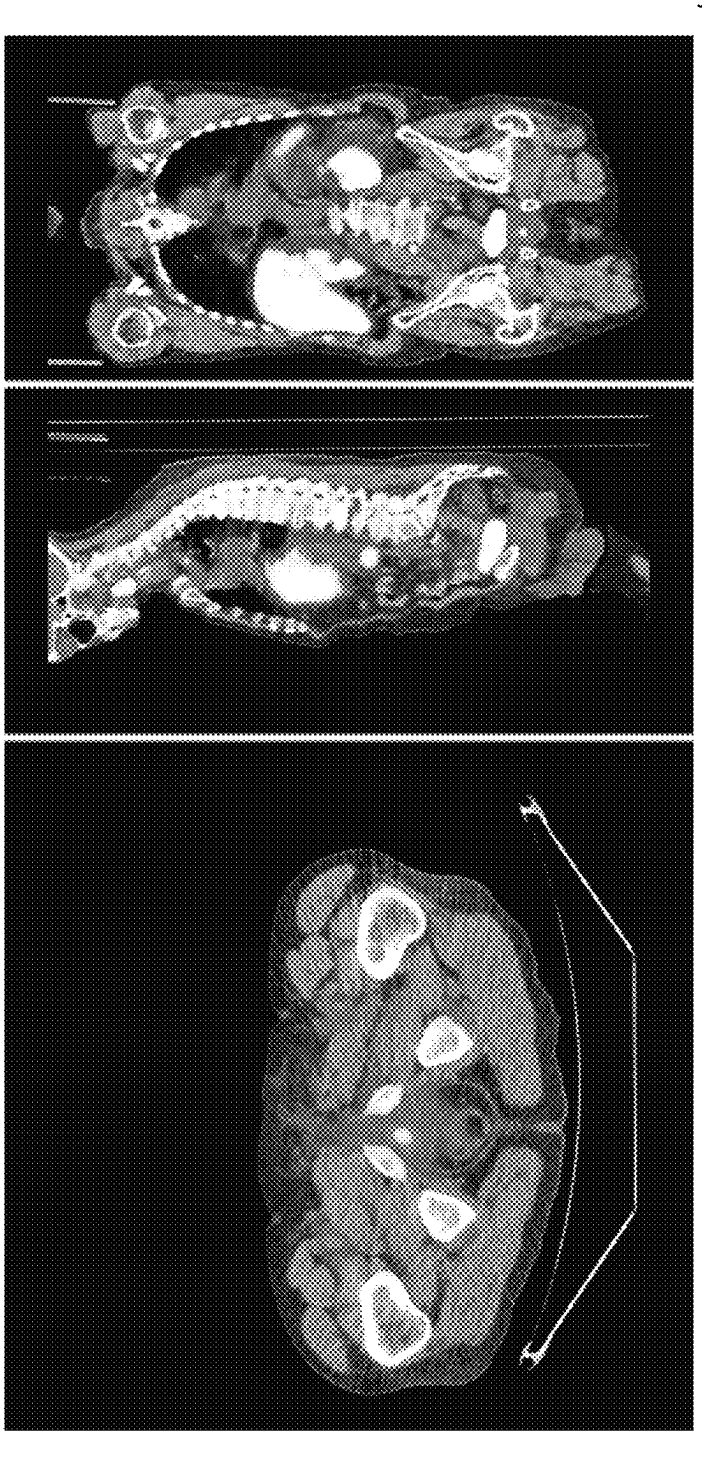


FIG. 9C

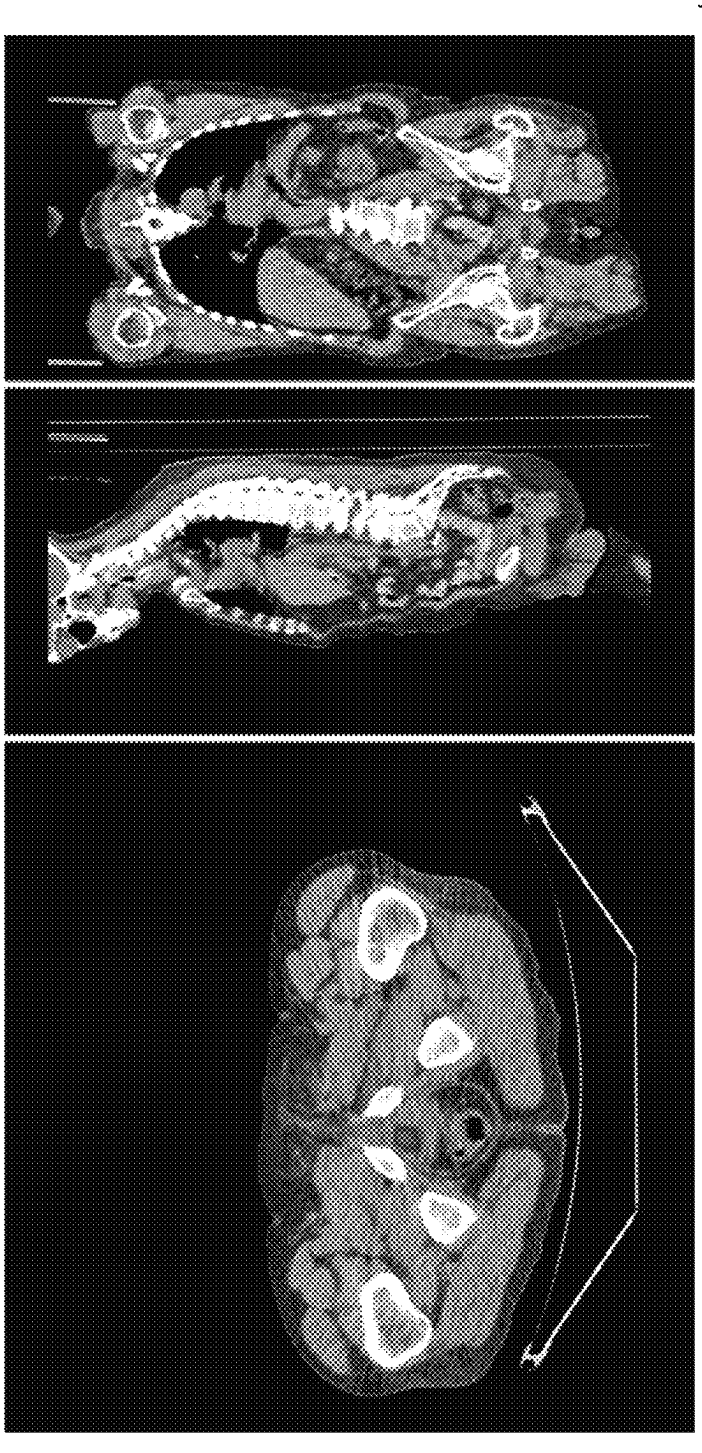


FIG. 9D

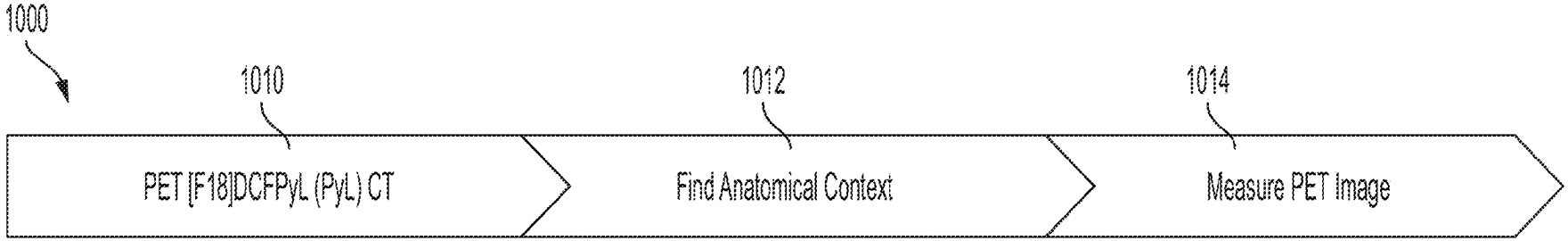


FIG. 10A

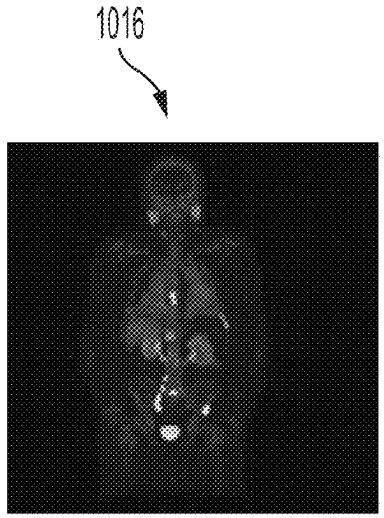


FIG. 10B

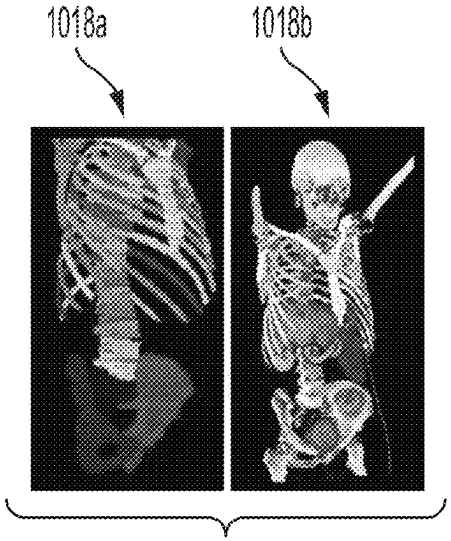


FIG. 10C

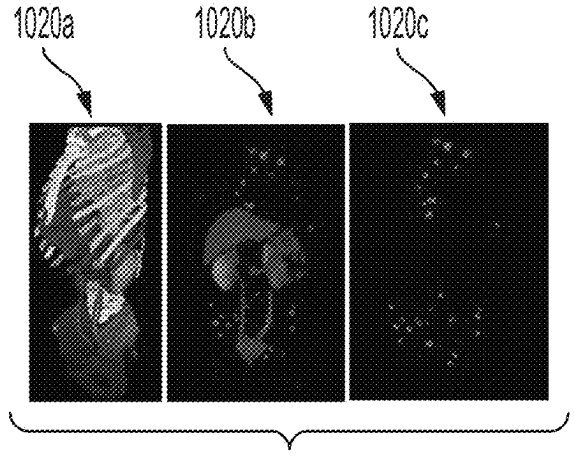


FIG. 10D

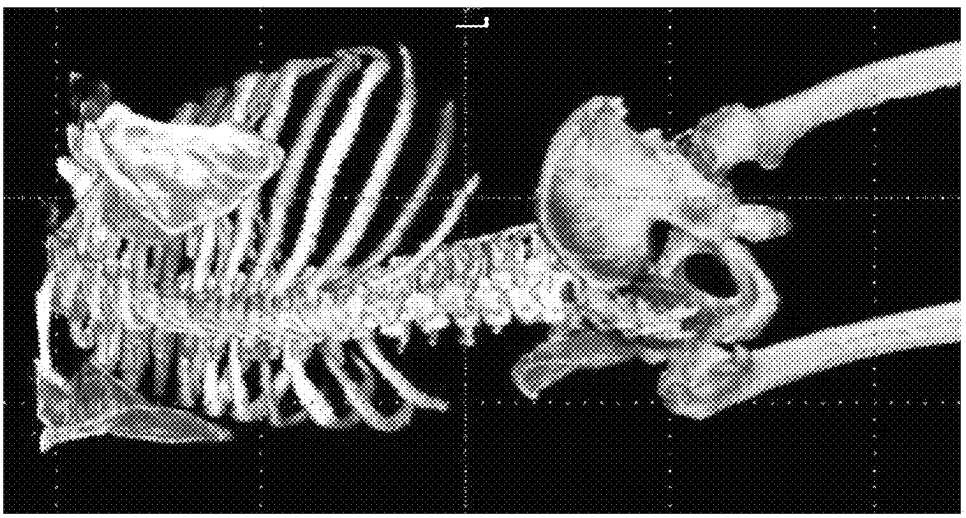


FIG. 11B

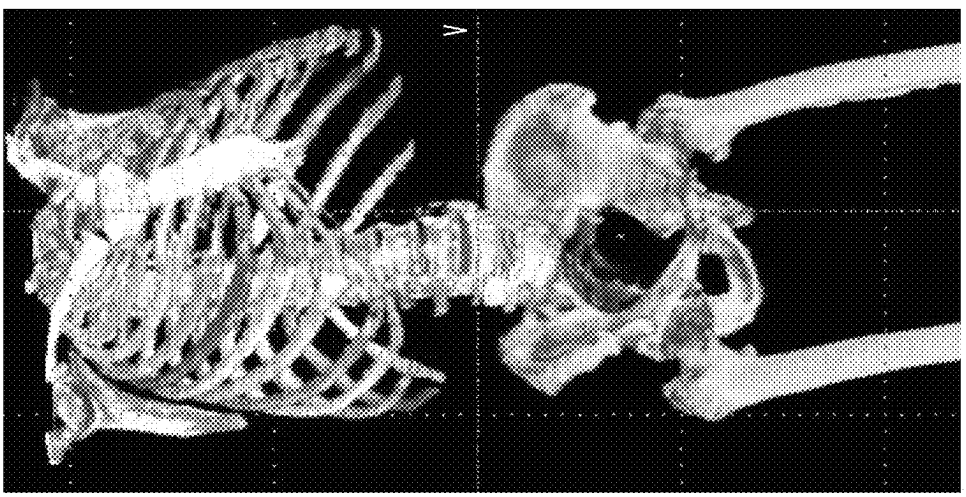


FIG. 11A

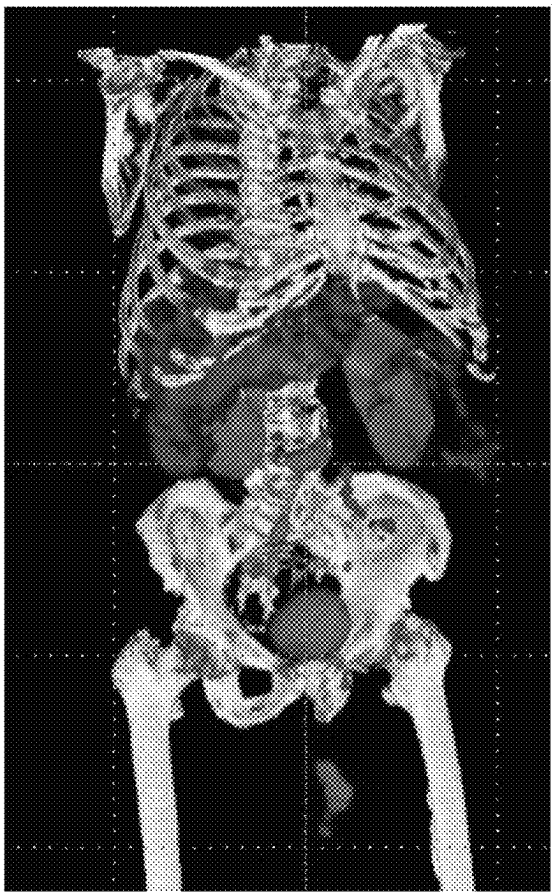


FIG. 12

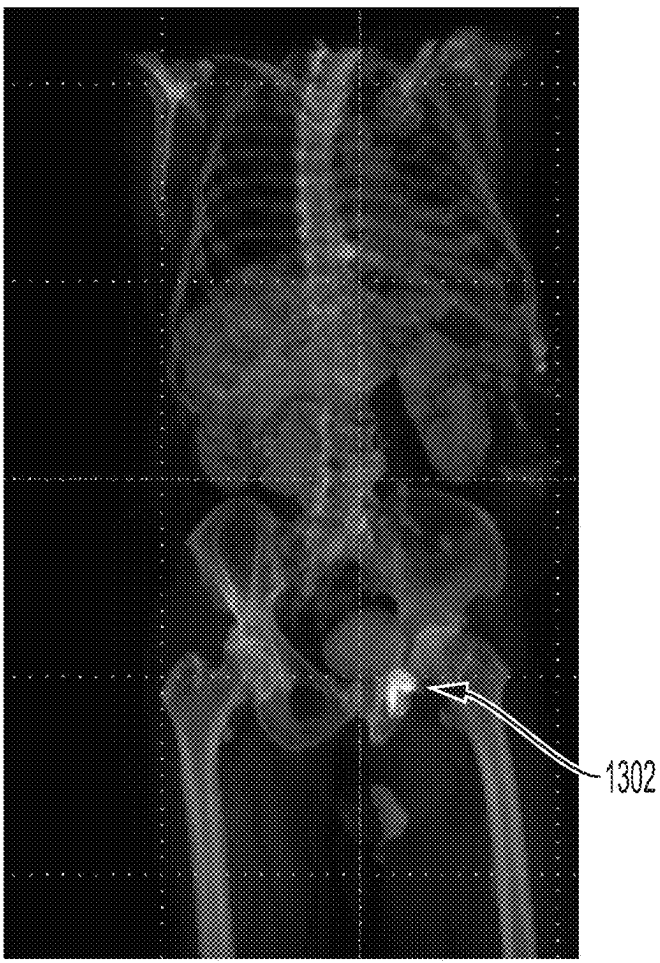


FIG. 13A

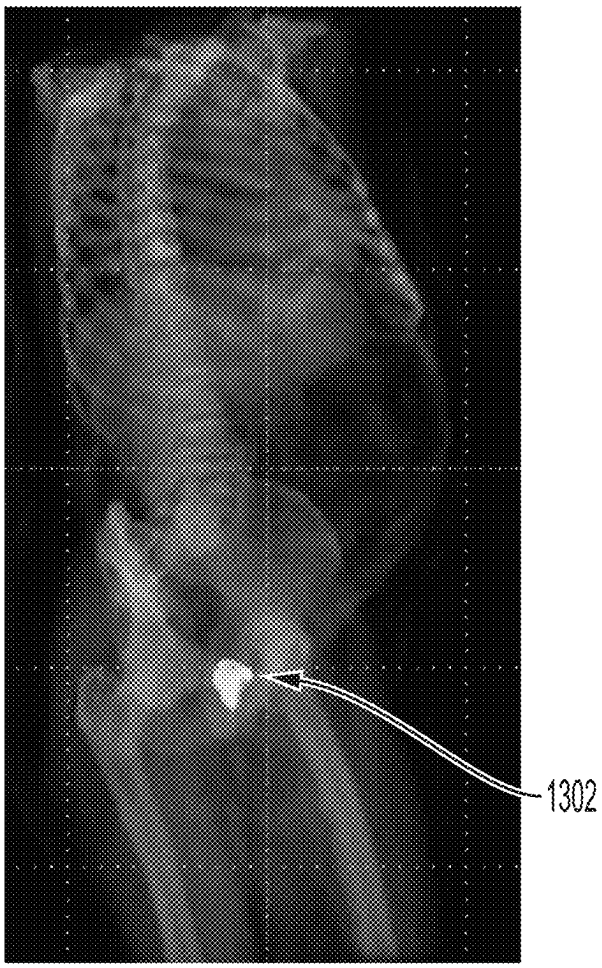


FIG. 13B

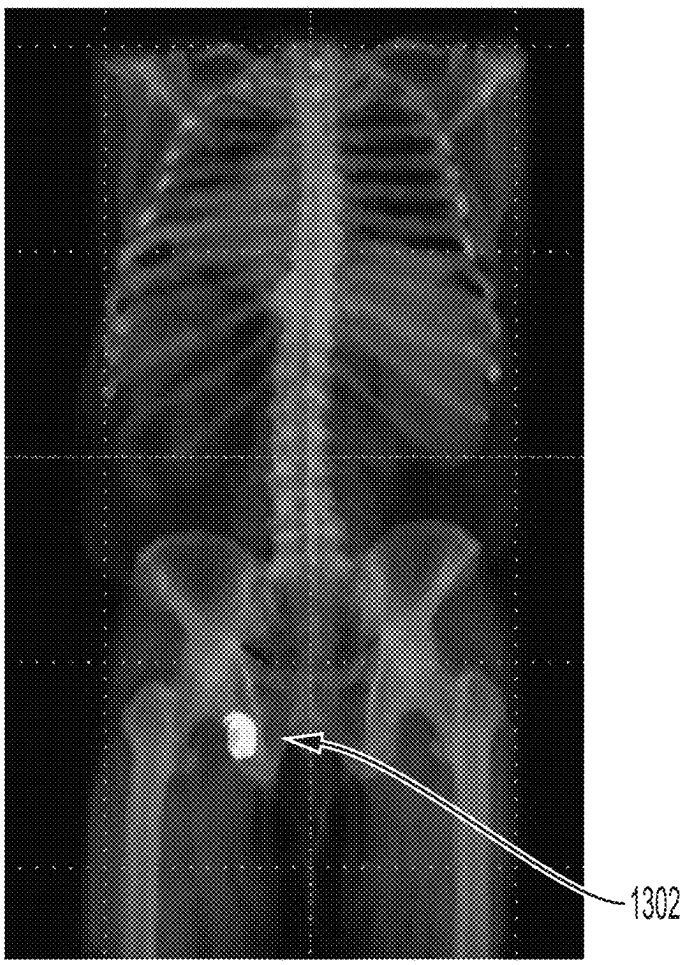


FIG. 13C

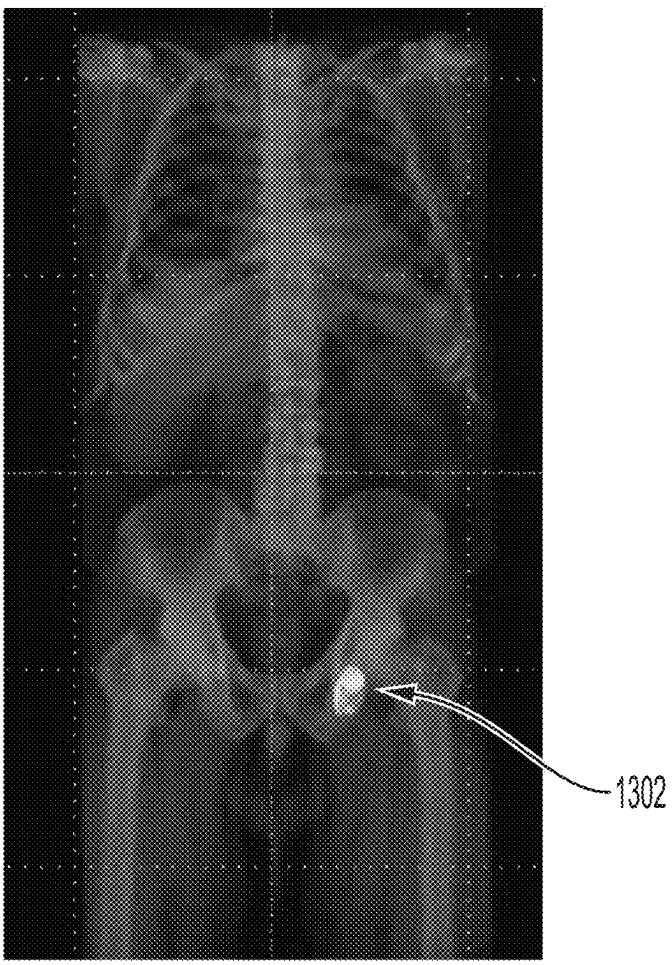


FIG. 13D



FIG. 14B

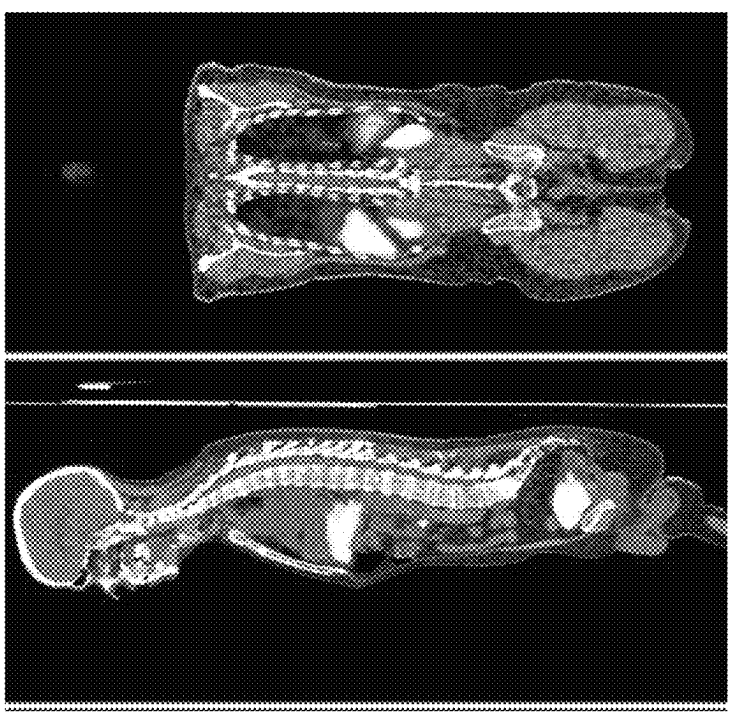


FIG. 14A

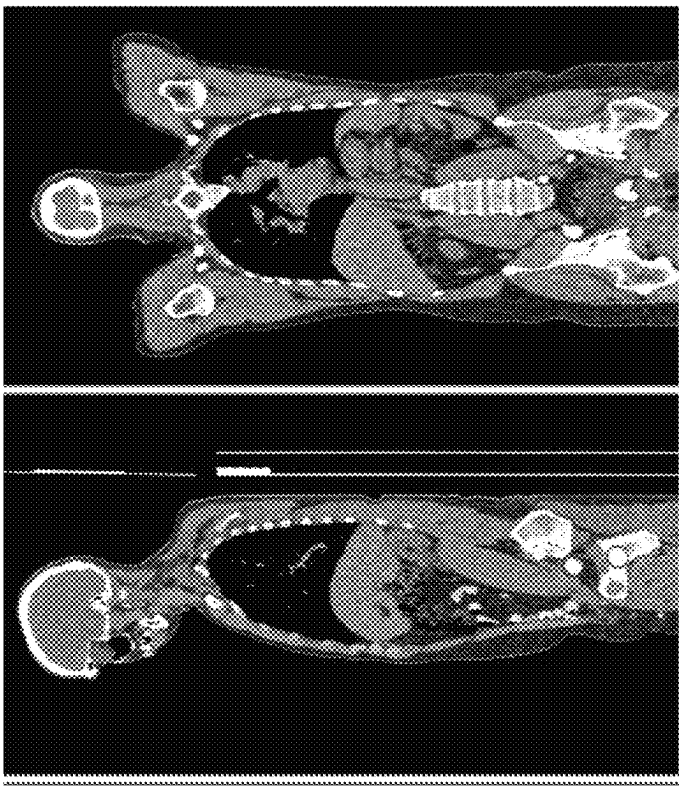


FIG. 15B

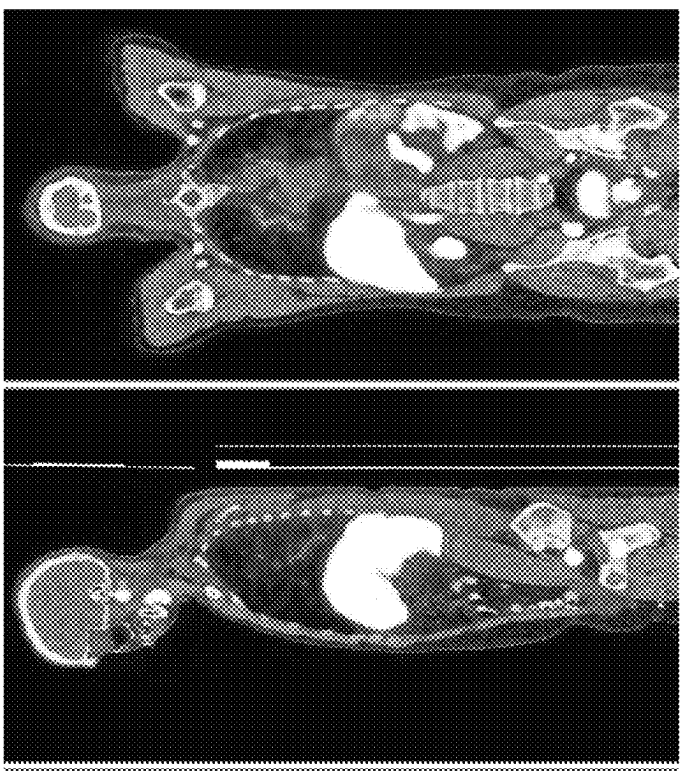


FIG. 15A

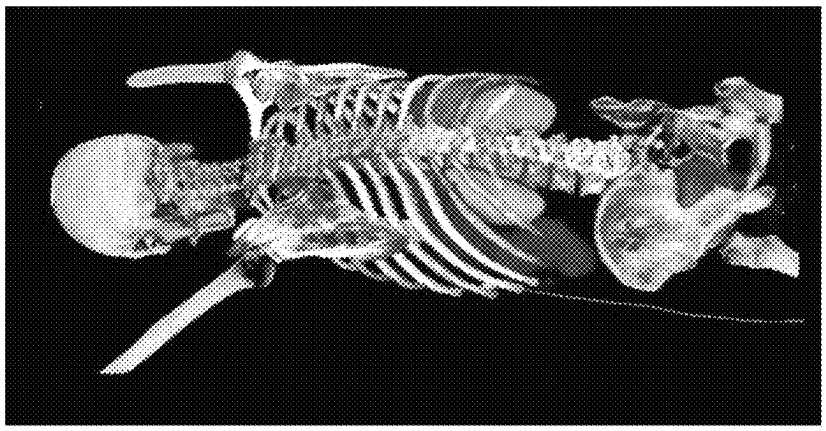


FIG. 16B

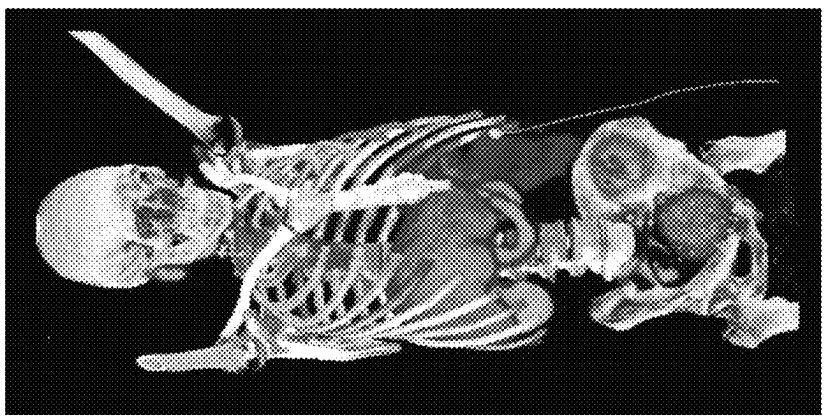


FIG. 16A

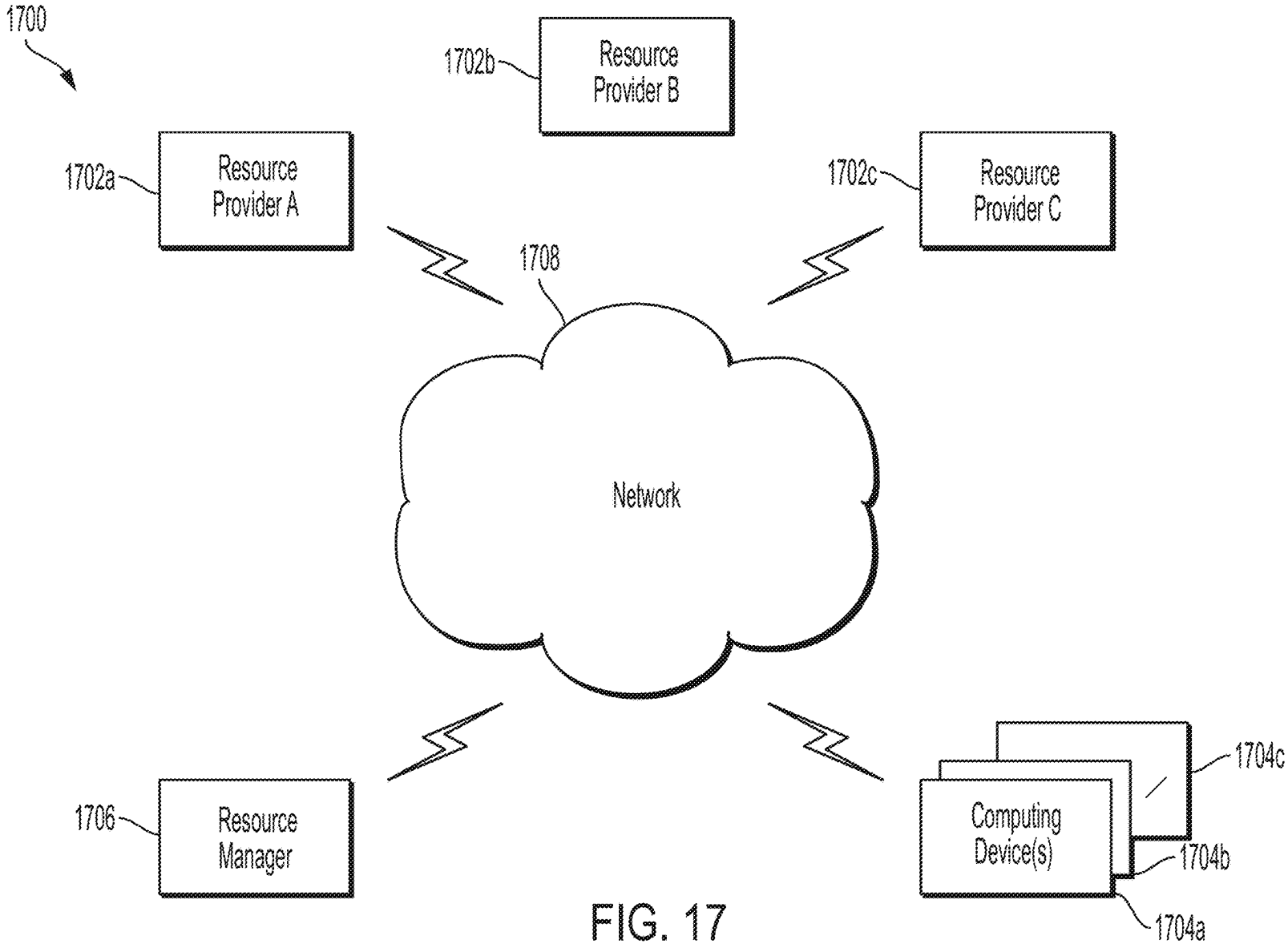

1700
1702b
Resource Provider B
1702a
Resource Provider A
1702c
Resource Provider C
1708
Network
1706
Resource Manager
Computing Device(s)
1704c
1704b
1704a

FIG. 17

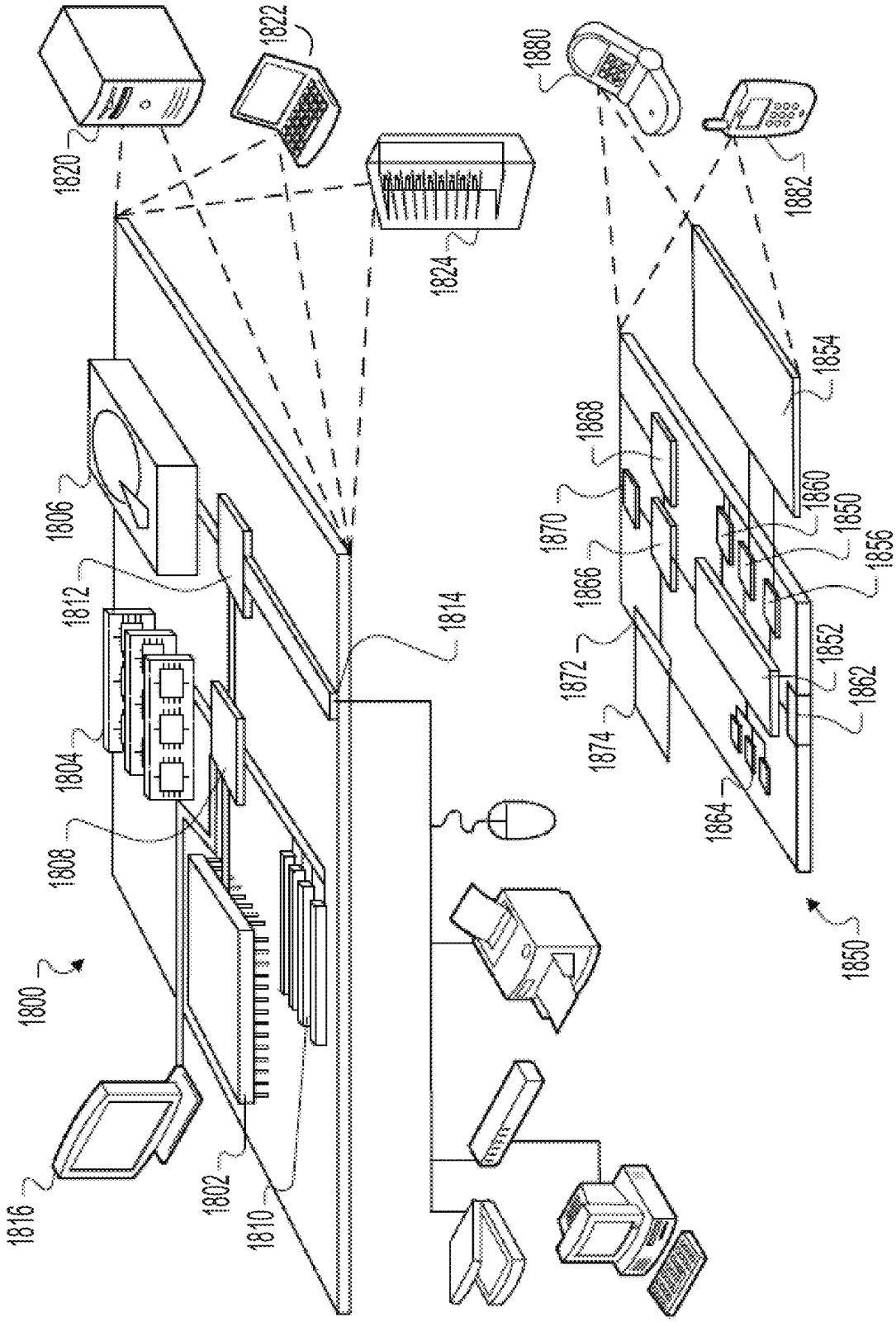

1820
1822
1824
1880
1882
1806
1812
1814
1804
1808
1800
1816
1802
1810
1854
1868
1870
1860
1850
1856
1866
1852
1872
1862
1874
1864
1850

FIG. 18

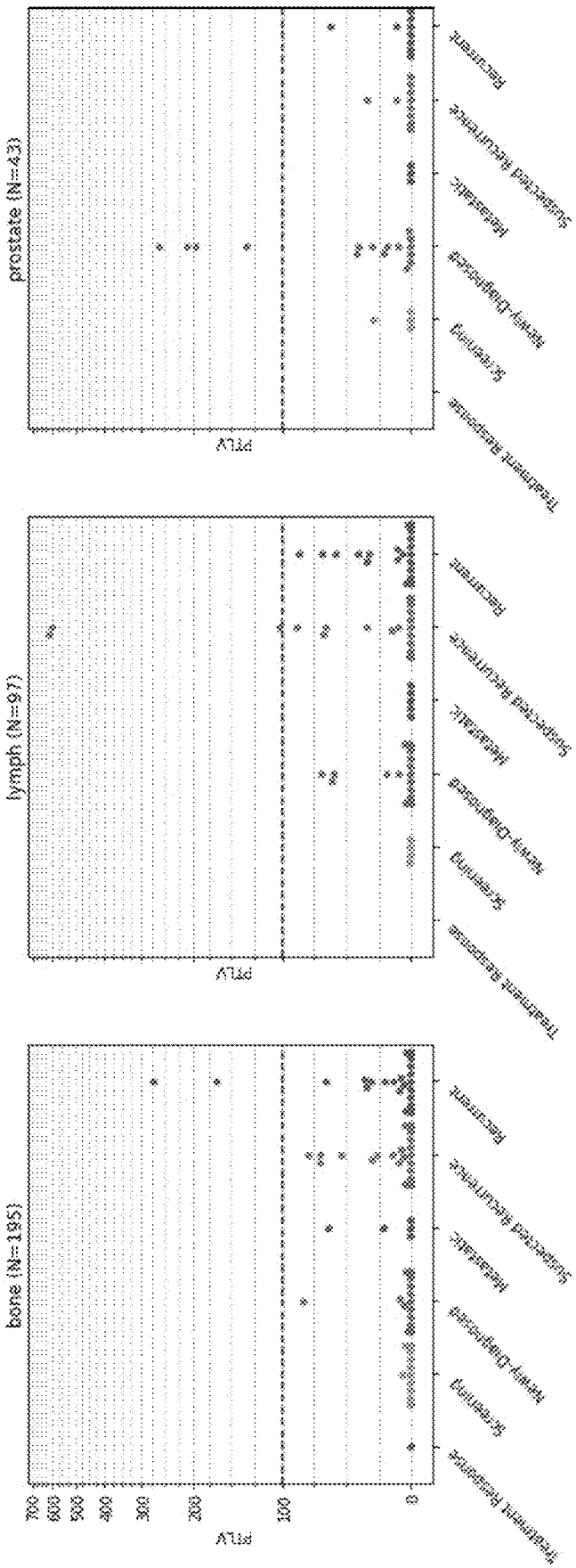

prostate (N=43)
lymph (N=97)
bone (N=195)
PSLV
Treatment Response
Kinetics
Tumor Burden
Metastatic
Suppressed Recurrence
Recurrent

FIG. 19

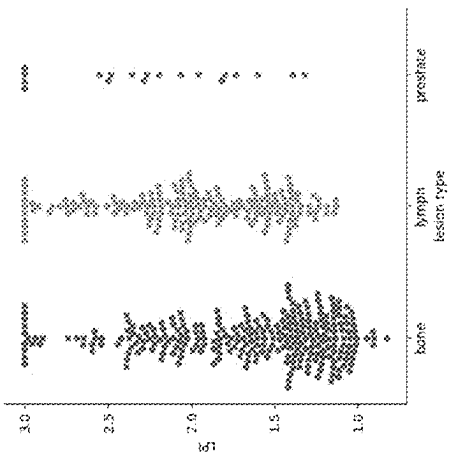

bone
lymph
prostate
lesion type

FIG. 20

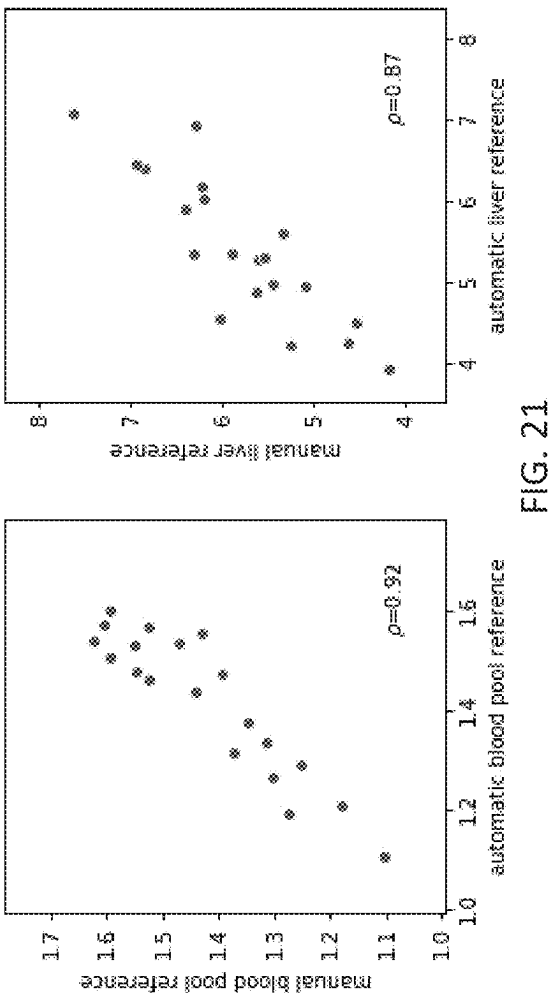

manual blood pool reference
automatic blood pool reference
ρ=0.92
manual liver reference
automatic liver reference
ρ=0.87

FIG. 21

SYSTEMS AND METHODS FOR PLATFORM AGNOSTIC WHOLE BODY IMAGE SEGMENTATION

CROSS-REFERENCE TO RELATED APPLICATIONS

This application is a divisional of U.S. Non-Provisional application Ser. No. 16/734,599 (now U.S. Pat. No. 11,657,508), filed Jan. 6, 2020, which claims priority to and benefit of U.S. Provisional Application No. 62/789,155, filed Jan. 7, 2019, U.S. Provisional Application No. 62/837,941, filed Apr. 24, 2019, U.S. Provisional Application No. 62/863,608, filed Jun. 19, 2019, U.S. Provisional Application No. 62/870,210, filed Jul. 3, 2019, U.S. Provisional Application No. 62/907,158, filed Sep. 27, 2019, U.S. Provisional Application No. 62/934,305, filed Nov. 12, 2019, the content of each of which are hereby incorporated by reference in their entirety.

FIELD OF THE INVENTION

This invention relates generally to methods, systems, and architectures for automated analysis of medical images. More particularly, in certain embodiments, the invention relates to automated identification of one or more particular regions of interest (e.g., corresponding to specific organs or tissue) within images of a subject.

BACKGROUND OF THE INVENTION

Targeted image analysis involves the use of radiolabeled small molecules that bind to specific receptors, enzymes and proteins in the body that are altered during the evolution of disease. After administration to a patient, these molecules circulate in the blood until they find their intended target. The bound radiopharmaceutical remains at the site of disease, while the rest of the agent clears from the body. The radioactive portion of the molecule serves as a beacon so that an image may be obtained depicting the disease location and concentration using commonly available nuclear medicine cameras, known as single-photon emission computerized tomography (SPECT) or positron emission tomography (PET) cameras, found in most hospitals throughout the world. Physicians can then use this information to determine the presence and the extent of disease in a patient. The physician can use this information to provide a recommended course of treatment to the patient and to track the progression of disease.

There are a variety of software-based analytical techniques available for analysis and enhancement of PET and SPECT images that can be used by a radiologist or physician. There are also a number of radiopharmaceuticals available for imaging particular kinds of cancer. Imaging agents used in the art include, among others include, without limitation ^{18}F—NaF, ^{11}C-Choline, 2-deoxy-2 [18F] fluoro-d-glucose (FDG), and the like. For example, the small molecule diagnostic 1404 targets the extracellular domain of prostate specific membrane antigen (PSMA), a protein amplified on the surface of >95% of prostate cancer cells and a validated target for the detection of primary and metastatic prostate cancer. 1404 is labeled with technetium-99m, a gamma-emitter isotope that is widely available, relatively inexpensive, facilitates efficient preparation, and has spectrum characteristics attractive for nuclear medicine imaging applications.

Another example radiopharmaceutical is PyL™ (also known as [^{18}F]DCFPyL, and 18F-PyL), which is a clinical-stage, fluorinated PSMA-targeted PET imaging agent for prostate cancer. A proof-of-concept study published in the April 2016 issue of the Journal of Molecular Imaging and Biology demonstrated that PET imaging with PyL™ showed high levels of PyL™ uptake in sites of putative metastatic disease and primary tumors, suggesting the potential for high sensitivity and specificity in detecting prostate cancer.

An oncologist may use images from a targeted PET or SPECT study of a patient as input in her assessment of whether the patient has a particular disease, e.g., prostate cancer, what stage of the disease is evident, what the recommended course of treatment (if any) would be, whether surgical intervention is indicated, and likely prognosis. The oncologist may use a radiologist report in this assessment. A radiologist report is a technical evaluation of the PET or SPECT images prepared by a radiologist for a physician who requested the imaging study and includes, for example, the type of study performed, the clinical history, a comparison between images, the technique used to perform the study, the radiologist's observations and findings, as well as overall impressions and recommendations the radiologist may have based on the imaging study results. A signed radiologist report is sent to the physician ordering the study for the physician's review, followed by a discussion between the physician and patient about the results and recommendations for treatment.

Thus, the process involves having a radiologist perform an imaging study on the patient, analyzing the images obtained, creating a radiologist report, forwarding the report to the requesting physician, having the physician formulate an assessment and treatment recommendation, and having the physician communicate the results, recommendations, and risks to the patient. The process may also involve repeating the imaging study due to inconclusive results, or ordering further tests based on initial results.

If an imaging study shows that the patient has a particular disease or condition (e.g., cancer), the physician discusses various treatment options, including surgery, as well as risks of doing nothing or adopting a watchful waiting or active surveillance approach, rather than having surgery.

There are limitations associated with this process, both from the perspective of the physician and from the perspective of the patient. While the radiologist's report is certainly helpful, the physician must ultimately rely on her experience in formulating an assessment and recommendation for her patient. Furthermore, the patient must place a great deal of trust in his physician. The physician may show the patient his PET/SPECT images and may tell the patient a numerical risk associated with various treatment options or likelihood of a particular prognosis, but the patient may very well struggle to make sense of this information. Moreover, the patient's family will likely have questions, particularly if cancer is diagnosed but the patient opts not to have surgery. The patient and/or his family members may search online for supplemental information and may become misinformed about risks of the diagnosed condition. A difficult ordeal may become more traumatic.

Thus, there remains a need for systems and methods for improved automated analysis of medical imaging studies and communication of those results, diagnoses, prognoses, treatment recommendations, and associated risks to a patient. Of particular need is an image analysis system to consistently, efficiently, and accurately detect anatomical regions, including soft tissue organs, in the entire body.

SUMMARY OF THE INVENTION

Presented herein are systems and methods that provide for automated analysis of three-dimensional (3D) medical images of a subject in order to automatically identify specific 3D volumes within the 3D images that correspond to specific anatomical regions e.g., organs and/or tissue). Notably, the image analysis approaches described herein are not limited to a single particular organ or portion of the body. Instead, they are robust and widely applicable, providing for consistent, efficient, and accurate detection of anatomical regions, including tissue and/or organs, in the entire body. In certain embodiments, the accurate identification of one or more such volumes is used to automatically determine quantitative metrics that represent uptake of radiopharmaceuticals in particular organs and/or tissue regions. These uptake metrics can be used to assess disease state in a subject, determine a prognosis for a subject, and/or determine efficacy of a treatment modality.

The capability of the approaches described herein to handle 3D images is an important advantage over certain other image analysis that only identify 2D regions in 2D images. For example, one approach relevant for cancer detection, EXINI Diagnostics AB's Bone Scan Index (BSI) software, detects regions of suspected bone cancer (see also U.S. Pat. No. 8,855,387, issued Oct. 7, 2014). However, the BSI analysis is carried out on two-dimensional scintigraphy images, as opposed to on three dimensional images.

Moreover, with the increase in the choices of imaging agents available to a physician to detect cancer, there remains a need for software with utility in analyzing images from any variety of imaging agents, using multiple detection modalities (SPECT/CT, PET/CT, and the like). Functional images such as SPECT and PET provide detailed and specific information on biological processes in the body, but their potential is only realized when combined with a detailed anatomical map so that function can be localized to individual organs and structures. Although CT and MRI provide detailed anatomical information, conventional (e.g., manual) identification of organs and structures is difficult, subjective and time consuming, making certain assessment infeasible without computer support. Accordingly, by providing platform agnostic image analysis approaches that allow for accurate and robust image segmentation applicable to a variety of imaging modalities, the systems and methods described herein facilitate image analysis of particular relevance to cancer detection, diagnosis, staging, and the like.

For example, the full body segmentation approaches described herein allow for automated analysis of combinations of anatomical and functional images in order to accurately identify and grade cancerous lesions within a subject. In particular, a PET/CT composite image can be acquired for a subject following administration of a radiopharmaceutical, such as a PSMA binding agent like PyL™. The automated, machine learning-based segmentation approaches described herein are used to identify, within the CT image of the PET/CT composite, target volumes of interest (VOIs) representing target tissue regions where cancerous lesions may be found. For example, a skeletal VOI corresponding to a graphical representation of one or more bones of the subject may be identified. Once the skeletal VOI is identified in the anatomical, CT, image, it can be mapped to the PET image to identify a corresponding skeletal volume therein. The corresponding skeletal volume in the PET image is then analyzed to detect one or more localized regions of relatively high intensity, referred to as hotspots. These hotspots correspond, physically, to local regions of increased radiopharmaceutical accumulation and, accordingly, prospective cancerous lesions.

In certain embodiments, the ability to accurately and rapidly perform full body segmentation via the approaches described herein is leveraged to provide a useful and uniform scale on which to evaluate and/or measure radiopharmaceutical uptake levels in physical lesions corresponding to detected hotspots (e.g., to thereby grade expression levels of particular biomolecules, such as PSMA). In particular, in addition to detecting target VOIs corresponding to specific target tissue regions in which cancerous lesions may occur, additional target VOIs corresponding to reference tissue regions are also detected. These reference VOIs are also mapped to the PET image, to identify corresponding reference volumes therein. Measures of intensity, such as a mean, peak, maximum, etc., within these reference volumes are then computed and used as reference points against which to evaluate intensities of individual detected hotspots and convert them to index values on the scale.

For example, in certain embodiments, an aorta and a liver VOI, corresponding to a representation of a portion of an aorta and liver, respectively, are identified within the anatomical image and mapped to the functional image to identify corresponding reference volumes therein. Intensity levels of each of these reference volumes are determined (e.g., as a mean, median, peak, etc. of intensities of voxels within each reference volume), and assigned corresponding index levels on a scale. Then, for each particular individual hotspot, a hotspot intensity level is determined (e.g., similarly, as a mean, median, peak, etc. of voxel intensities within the detected hotspot). A corresponding individual hotspot index value is then determined based individual hotspot intensity level, the aorta reference intensity level, and the liver reference intensity level. This approach provides a standardized scale on which to evaluate and measure uptake associated with hotspots across different images. This allows, for example, for comparison of multiple images obtained for a single subject at different time points, as well as comparison between images of different subjects.

In certain embodiments, individual hotspot indices are used to compute an overall index for the subject and/or particular target tissue region analyzed for presence of cancerous lesions. The overall index can serve as an indicator of disease severity and/or risk, for example by reflecting a total lesion volume within a particular target tissue region, with the weighting based on the hotspot index values for the individual detected hotspots to account for radiopharmaceutical uptake within the lesions. For example, a PSMA weighted total lesion volume within a skeletal volume can be computed as a weighted sum of individual detected hotspot volumes weighted by their corresponding index values. Such an index may reflect a level and/or aggressiveness of metastasis into bone.

Volumes corresponding to other tissue regions may be similarly identified and used to determine overall index values. For example, lymph node volumes may also be used to assess severity of metastases. Volumes corresponding to tissue regions where localized disease is initially found may also be identified and analyzed to detect lesions. For example, a prostate volume may be used to assess prostate cancer severity at its initial stages. Likewise, breast volumes representing breast tissue regions and lung volumes representing lung tissue regions can be used for assessment of localized breast and lung cancers, respectively.

According, by providing for full body segmentation and automated image-based analysis of cancerous lesions

throughout various relevant target tissue regions throughout a subject's body, the AI-based systems and methods described herein allow for analysis of a variety of cancers at various stages. The techniques can be used to identify and stage localized disease in relevant tissue regions such as the prostate, for example for early stage screening and monitoring, as well as to monitor regions such as bone and lymph nodes for metastasis as disease progresses. As such, the approaches described herein provide a complete set of tools for automated image-based detection of cancer, and tracking disease evolution, progression, and response to treatment.

In one aspect, the invention is directed to a method for automatically processing a 3D image to identify 3D volumes within the 3D image that correspond to particular target tissue regions, the method comprising: (a) receiving, by a processor of a computing device, a 3D anatomical image of a subject obtained using an anatomical imaging modality [e.g., x-ray computed tomography (CT); e.g., magnetic resonance imaging (MRI); e.g., ultra-sound], wherein the 3D anatomical image comprises a graphical representation of tissue (e.g., soft-tissue and/or bone) within the subject; (b) automatically identifying, by the processor, using one or more machine learning modules (e.g., wherein at least one of the one or more machine learning modules is a Convolutional Neural Network (CNN) module) for each of a plurality of target tissue regions, a corresponding target volume of interest (VOI) within the 3D anatomical image; (c) determining, by the processor, a 3D segmentation map representing a plurality of 3D segmentation masks, each 3D segmentation mask representing a particular identified target VOI (e.g., automatically, digitally stitching together the plurality of 3D segmentation masks to form the 3D segmentation map); and (d) storing and/or providing for display and/or further processing, the 3D segmentation map.

In certain embodiments, the 3D anatomical image is a full body image.

In certain embodiments, step (c) comprises digitally stitching together the plurality of 3D segmentation masks to form the 3D segmentation map {e.g., by creating an initially empty image volume (e.g., initializing all voxel values to zero) and then inserting labels from each segmentation mask into the image volume [e.g., by mapping labeled (e.g., as representing a particular target tissue region as determined by a machine learning module) voxels of input images to one or machine learning modules to voxels of the image volume (e.g., so as to match voxels of the image volume to voxels of the input images that represent a same physical location, thereby labeling voxels of the image volume correctly)]}.

In certain embodiments, step (b) comprises, for at least one specific target tissue region: determining, using a first module (e.g., a localization module)(e.g., a first machine learning module), an initial VOI within the 3D anatomical image, the initial VOI corresponding to an anatomical region (e.g., a group of related tissue, such as a pelvic region, a chest region, a head and/or neck region, and the like) containing the specific target tissue region (e.g., wherein the initial VOI excludes more voxels of the 3D anatomical image than it includes; e.g., wherein the initial VOI includes less than 25% of the voxels of the 3D anatomical image; e.g., wherein a majority of voxels within the initial VOI represent physical volumes within the anatomical region); and identifying, using a second module (e.g., a segmentation module)(e.g., a second machine learning module), the target VOI corresponding to the specific target tissue region within the initial VOI.

In certain embodiments, the second module is a CNN module that implements a CNN.

In certain embodiments, the first module is a CNN module that implements a CNN to perform a coarse segmentation to automatically identify the initial VOI corresponding to the anatomical region containing the specific target tissue region [e.g., by automatically identifying a graphical representation of a group of related tissue within the anatomical image (e.g., and, subsequently, determining the initial VOI as a rectangular region (e.g., rectangular prism or rectangular box) entirely enclosing the identified graphical representation of the group of related tissue)] [e.g., by, for each of one or more particular tissue regions anticipated to be located within the anatomical region, automatically identifying a corresponding VOI in the anatomical image (e.g., via the coarse segmentation), e.g., and determining the initial VOI as a rectangular region entirely enclosing all of the identified VOIs corresponding to the particular tissue regions].

In certain embodiments, the first module receives a sub-sampled [e.g., by a factor of two or more (e.g., four) along one or more dimensions] version of the anatomical image as input and identifies the initial VOI using the sub-sampled version of the anatomical image [e.g., and wherein the second module receives a full resolution version of the anatomical image, cropped to the initial VOI (e.g., such that the first module operates on an lower resolution image that represents a larger physical volume than the second module, while the second module operates on a higher resolution image but representing a smaller physical volume)].

In certain embodiments, the first module is a first CNN module and the second module is a second CNN module, and wherein the first CNN module comprises additional filters in order to account for increased variability in image size with respect to the second CNN module.

In certain embodiments, the 3D anatomical image is a full body image and step (b) comprises: automatically determining, using one or more localization modules implementing machine learning technique(s) (e.g., wherein each localization module is a CNN module that implements a CNN), a plurality of initial VOIs within the 3D anatomical image, each initial VOI corresponding to a particular anatomical region (e.g., a group of related tissue, such as a pelvic region, a chest region, a head and/or neck region, a spine region, an upper body region, a lower body region, etc.) and in which an associated subset of the target VOIs are located; and for each initial VOI, automatically identifying, using one or more segmentation modules implementing machine learning technique(s) (e.g., wherein each segmentation module is a CNN module that implements a CNN) the associated subset of target VOIs.

In certain embodiments, the plurality of initial VOIs comprises one or more members selected from the group consisting of: a pelvic region initial VOI corresponding to a pelvic region of the subject (e.g., wherein the subset of target VOIs located in the pelvic region initial VOI comprise one or more target VOIs corresponding to target tissue regions selected from the group consisting of a left and/or right ilium, a sacrum, and a coccyx); a spine region initial VOI corresponding to a spine of the subject (e.g., wherein the subset of target VOIs located in the pelvic region initial VOI comprise one or more target VOIs corresponding to target tissue regions selected from the group consisting of a thoracic vertebra, a lumber vertebra, and a sternum); a left upper body region initial VOI corresponding to a left side of the subject's upper body (e.g., wherein the subset of target VOIs located in the pelvic region initial VOI comprise one or more target VOIs corresponding to target tissue regions selected from the group consisting of one or more left rib(s), a left scapula, and a left clavicle); and a right upper body

region initial VOI corresponding to a right side of the subject's upper body (e.g., wherein the subset of target VOIs located in the pelvic region initial VOI comprise one or more target VOIs corresponding to target tissue regions selected from the group consisting of one or more right rib(s), a right scapula, and a right clavicle).

In certain embodiments, the method comprises: (e) receiving, by the processor, a 3D functional image of the subject obtained using a functional imaging modality [e.g., single-photon emission computed tomography (SPECT); e.g., positron emission tomography (PET)] [e.g., wherein the 3D functional image comprises a plurality of voxels, each representing a particular physical volume within the subject and having an intensity value that represents detected radiation emitted from a the particular physical volume, wherein at least a portion of the plurality of voxels of the 3D functional image represent physical volumes within one or more of the target tissue regions of the subject]; and (f) identifying, by the processor, within the 3D functional image, one or more 3D volume(s), each corresponding to an identified target VOI, using the 3D segmentation map (e.g., by mapping 3D segmentation masks of the 3D segmentation map to the 3D functional image).

In certain embodiments, the method comprises: (g) determining, by the processor, a cancer status [(e.g., a prostate cancer status; e.g., a metastatic cancer status (e.g., metastatic cancer, including, e.g., metastatic prostate cancer, breast cancer, lung cancer, colon cancer, skin cancer, etc.)] for the subject (e.g., using intensities of voxels within the functional image and the one or more identified 3D volumes)(e.g., based on detected lesions) [e.g., a likelihood of the subject having and/or developing prostate cancer and/or a particular stage of prostate cancer (e.g., metastatic prostate cancer)] [e.g., a likelihood of the subject having and/or developing a metastatic cancer (including, e.g., metastatic prostate cancer, breast cancer, lung cancer, colon cancer, skin cancer, etc.)].

In certain embodiments, the method comprises performing steps (a)-(g) repeatedly for a plurality of anatomical and corresponding functional images collected at different time points to determine, at each time point, a cancer status of the subject, thereby tracking cancer status over time (e.g., to evaluate disease progression and/or treatment efficacy).

In certain embodiments, the method comprises (e.g., prior to step (g)): (h) automatically adjusting, by the processor, intensities of voxels of the 3D functional image to correct for background uptake (e.g., of the radiopharmaceutical) in one or more background tissue regions (e.g., correcting for uptake of the radiopharmaceutical that occurs in the one or more background tissue regions under normal circumstances, and which is not necessarily indicative of presence of cancerous lesions).

In certain embodiments, the target tissue regions comprise the one or more background tissue regions and step (h) comprises: using the 3D segmentation map to identify, within the 3D functional image, one or more 3D background tissue volume(s), each corresponding a particular background tissue region (e.g., by mapping 3D segmentation masks of the 3D segmentation map to the 3D functional image); and adjusting intensities of voxels of the 3D functional image based on intensities of voxels within the 3D background tissue volumes (e.g., by using intensities of voxels within the 3D background tissue volumes to estimate a contribution to intensities outside of the 3D background tissue volumes).

In certain embodiments, the one or more background tissue regions comprise one or more members selected from the group consisting of: a bladder (e.g., a urinary bladder), a kidney, a duodenum, a small intestine, a spleen, a liver, a pancreas, a stomach, an adrenal gland, a rectum, and testes.

In certain embodiments, the method comprises: (i) automatically detecting, by the processor, one or more hotspots within the 3D functional image determined to represent lesions based on intensities of voxels within the 3D functional image [e.g., based on a comparison of intensities within the 3D functional image with a threshold value (e.g., wherein the 3D functional image is a 3D PET image and the threshold is a particular standard uptake value (SUV) level)] (e.g., and also based on the one or more 3D volumes identified within the 3D functional image).

In certain embodiments, step (i) comprises using one or more thresholds [e.g., comparing intensities of voxels in the 3D functional image with the one or more thresholds (e.g., wherein the one or more thresholds comprises a plurality of region-specific thresholds, each used for a specific sub-set of the one or more 3D volumes identified within the 3D functional image)].

In certain embodiments, step (i) comprises applying one or more filters to the 3D functional image [e.g., as in a blob detection technique; e.g., wherein the one or more filters comprises one or more Gaussian filters (e.g., a high pass Gaussian filter and a low pass Gaussian filter, as in a Difference of Gaussians approach); e.g., wherein the one or more filters comprises a Laplacian filter (e.g., as in a Laplacian of a Gaussian technique); e.g., wherein different filter kernels are used for different sub-sets of the one or more 3D volumes identified within the 3D functional image].

In certain embodiments, step (i) comprises using a combination of two or more techniques for identification of hotspots in different sub-sets of the one or more 3D volumes identified within the 3D functional image [e.g., using a first filtering approach (e.g., as in paragraphs above) for a first sub-set of the one or more 3D volumes and using a second filtering approach for a second sub-set; e.g., using thresholding approach (e.g., as paragraphs above) for a first sub-set of the one or more 3D volumes and using a filtering approach (e.g., as paragraphs above) for a second sub-set of the one or more 3D volumes].

In certain embodiments, step (i) comprises detecting an initial set of hotspots and, for at least a portion of the hotspots of the initial set, classifying each hotspot of at least a portion of the detected hotspots as either a cancerous lesion or not a cancerous lesion (e.g., as noise) [e.g., using a machine learning module; e.g., based on a shape and/or location of the hotspot (e.g., in combination with anatomical knowledge; e.g., wherein the location includes an identification of a particular target tissue region corresponding to the 3D volume in which the hotspot is located and/or a relative position of the hotspot within the particular target tissue region); e.g., and removing hotspots classified as not a cancerous lesion from the initial set, thereby obtaining a final set of hotspots determined to represent lesions].

In certain embodiments, the target tissue regions comprise one or more background tissue regions and the method comprises: using the 3D segmentation map to identify, within the 3D functional image, one or more 3D background tissue volume(s), each corresponding a particular background tissue region (e.g., a background tissue region in which significant radiopharmaceutical uptake occurs under normal circumstances and is not necessarily indicative of presence of cancerous lesions)(e.g., by mapping 3D segmentation masks of the 3D segmentation map to the 3D functional image); and excluding voxels of the 3D within the

3D background tissue from the voxels used to automatically detect the one or more hotspots at step (i).

In certain embodiments, the method comprises using the one or more detected hotspots (e.g., intensities of the one or more detected hotspots) to determine a cancer status for the subject.

In certain embodiments, the target tissue regions comprise one or more reference tissue regions and the method comprises: using the 3D segmentation map to identify, by the processor, within the 3D functional image, one or more 3D reference volume(s), each corresponding to a particular reference tissue region; determining, by the processor, one or more reference intensity values, each associated with a particular 3D reference volume of the one or more 3D reference volume(s) and corresponding to a measure of (e.g., an average/mean, a median, a maximum, etc.) intensity within the particular 3D reference volume; determining, by the processor, one or more individual hotspot intensity values, each associated with a particular hotspot of at least a portion of the detected one or more hotspots and corresponding to a measure of (e.g., an average/mean, a median, a maximum, etc.) intensity of the particular hotspot; and determining, by the processor, one or more individual hotspot index values using the one or more individual hotspot intensity values and the one or more reference intensity values [e.g., wherein each individual hotspot index value is associated with a particular hotspot of the at least a portion of the detected one or more hotspots and determined using (e.g., based on a comparison between) (i) the individual hotspot intensity value associated with the particular hotspot and (ii) the one or more reference intensity values].

In certain embodiments, the determining the one or more individual hotspot index values comprises mapping each of the one or more reference intensity values to a corresponding reference index value on a scale and, for each individual hotspot intensity value, using the reference intensity values and corresponding reference index values to interpolate a corresponding individual hotspot index value.

In certain embodiments, the reference tissue regions comprise one or more members selected from the group consisting of: a liver, an aorta (e.g., a thoracic aorta portion; e.g., an abdominal aorta portion), and a parotid gland.

In certain embodiments, a first reference intensity value (i) is a blood reference intensity value associated with a 3D reference volume corresponding to an aorta portion, and (ii) maps to a first reference index value; a second reference intensity value (i) is a liver reference intensity value associated with a 3D reference volume corresponding to a liver, and (ii) maps to a second reference index value; and the second reference intensity value is greater than the first reference intensity value and the second reference index value is greater than the first reference index value.

In certain embodiments, the reference intensity values comprises a maximum reference intensity value that maps to a maximum reference index value, and hotspots having associated hotspot intensity values greater than the maximum reference intensity value are assigned hotspot index values equal to the maximum reference index value.

In certain embodiments, the method comprises determining, by the processor, an overall index value indicative of a cancer status of the subject using at least a portion of the one or more hotspot index values.

In certain embodiments, the overall index value is determined as a weighted sum of at least a portion [e.g., located within a 3D volume of the functional image that corresponds to a skeletal region of the subject; e.g., located within a 3D volume of the functional image that corresponds to a lymph region of the subject] of the individual hotspot index values [e.g., wherein each hotspot index value in the sum is weighted by a measure of size (e.g., 3D volume; e.g., average diameter) of the associated hotspot].

In certain embodiments, the overall index value is associated with a particular target tissue region corresponding to a particular target VOI identified within the anatomical image; and the overall index value is determined using hotspot index values of a subset of hotspots located within a particular 3D volume in the 3D functional image that corresponds to the particular identified target VOI [e.g., and wherein the overall index value is computed as a weighted sum of the hotspot index values of the subset of hotspots (e.g., wherein the weighted sum is normalized by an estimated volume of the particular target tissue region (e.g., computed as a volume of the particular 3D volume in the function image and/or a volume of the particular target VOI))].

In certain embodiments, the particular target tissue region is selected from the group consisting of: a skeletal region comprising one or more bones of the subject, a lymph region, and a prostate region.

In certain embodiments, the 3D anatomical image is an x-ray computed tomography (CT) image, and the 3D functional image is a 3D single photon emission computed tomography (SPECT) image.

In certain embodiments, the 3D anatomical image is an x-ray computed tomography (CT) image, and the 3D functional image is a 3D positron emission tomography (PET) image.

In certain embodiments, the 3D PET image of the subject is obtained following administration to the subject of a radiopharmaceutical comprising a prostate-specific membrane antigen (PSMA) binding agent.

In certain embodiments, the radiopharmaceutical comprises [18F]DCFPyL.

In certain embodiments, step (b) comprises cropping, by the processor, the 3D anatomical image to remove voxels representing air [e.g., to create a cropped anatomical image, and using the cropped anatomical image to identify the one or more target VOIs (e.g., using the cropped anatomical image is used as input to one or more machine learning modules, as opposed to the original size 3D anatomical image)].

In certain embodiments, the target tissue regions comprise one or more members selected from the group consisting of: a left hip bone, a right hip bone, a sacrum and coccyx region, a left clavicle, a right clavicle, a left rib, a right rib, a left scapula, a right scapula, a sternum, a lumbar vertebra, a thoracic vertebra, a skull, a cervical vertebra, a left femur, a right femur, a left humerus, a right humerus, a prostate, a urinary bladder, a rectum, a left gluteus maximus, a right gluteus maximus, an aorta (e.g., a thoracic aorta portion; e.g., an abdominal aorta portion), a left kidney, a right kidney, a liver, a left lung, a right lung, a spleen, a ventricle, a left adrenal gland, a right adrenal gland, a gallbladder, a brain, a pancreas, a heart, a mandible, a left bronchi, a right bronchi, a trachea, a left common iliac artery, a right common iliac artery, and a parotid gland.

In certain embodiments, one or more of the target tissue regions comprise one or more specific bones selected from the group consisting of: a left clavicle, a right clavicle, a left femur, a right femur, a left fibula, a right fibula, a left hip bone, a right hip bone, a left humerus, a right humerus, a mandible, a left patella, a right patella, left radius, a right radius, a left tibia, a right tibia, a left ulna, a right ulna, a left rib (e.g., a first left rib, a second left rib, a third left rib, a

fourth left rib, a fifth left rib, a sixth left rib, a seventh left rib, an eighth left rib, a ninth left rib, a tenth left rib, an eleventh left rib, a twelfth left rib), a right rib (e.g., a first right rib, a second right rib, a third right rib, a fourth right rib, a fifth right rib, a sixth right rib, a seventh right rib, an eighth right rib, a ninth right rib, a tenth right rib, an eleventh right rib, a twelfth right rib), a sacrum and coccyx (e.g., a combined sacrum and coccyx region; e.g., a sacrum and a coccyx individually, so as to distinguish between the two), a left scapula, a right scapula, a skull, sternum, a vertebrae region [e.g., a cervical vertebrae region, comprising one or more (e.g., up to all) cervical vertebrae; e.g., a lumber vertebrae region, comprising one or more (e.g., up to all) lumbar vertebrae; e.g., a thoracic vertebrae region, comprising one or more (e.g., up to all) thoracic vertebrae], and an individual vertebra [e.g., e.g., an individual cervical vertebra (e.g., a first cervical vertebra, a second cervical vertebra, a third cervical vertebra, a fourth cervical vertebra, a fifth cervical vertebra, a sixth cervical vertebra, a seventh cervical vertebra); e.g., an individual lumbar vertebra (e.g., a first lumbar vertebra, a second lumbar vertebra, a third lumbar vertebra, a fourth lumbar vertebra, a fifth lumbar vertebra, a sixth lumbar vertebra); e.g., an individual thoracic vertebra (e.g., a first thoracic vertebra, a second thoracic vertebra, a third thoracic vertebra, a fourth, thoracic vertebra, a fifth thoracic vertebra, a sixth thoracic vertebra, a seventh thoracic vertebra, an eighth thoracic vertebra, a ninth thoracic vertebra, a tenth thoracic vertebra, an eleventh thoracic vertebra, an twelfth thoracic vertebra)].

In certain embodiments, one or more of the target tissue regions comprise one or more specific bones selected from the group consisting of: a left clavicle, a right clavicle, a left hip bone, a right hip bone, a left rib (e.g., a first left rib, a second left rib, a third left rib, a fourth left rib, a fifth left rib, a sixth left rib, a seventh left rib, an eighth left rib, a ninth left rib, a tenth left rib, an eleventh left rib, a twelfth left rib), a right rib (e.g., a first right rib, a second right rib, a third right rib, a fourth right rib, a fifth right rib, a sixth right rib, a seventh right rib, an eighth right rib, a ninth right rib, a tenth right rib, an eleventh right rib, a twelfth right rib), a sacrum and coccyx (e.g., a combined sacrum and coccyx region; e.g., a sacrum and a coccyx individually, so as to distinguish between the two), a left scapula, a right scapula, a sternum, a vertebrae region [e.g., a cervical vertebrae region, comprising one or more (e.g., up to all) cervical vertebrae; e.g., a lumber vertebrae region, comprising one or more (e.g., up to all) lumbar vertebrae; e.g., a thoracic vertebrae region, comprising one or more (e.g., up to all) thoracic vertebrae], and an individual vertebra [e.g., an individual lumbar vertebra (e.g., a first lumbar vertebra, a second lumbar vertebra, a third lumbar vertebra, a fourth lumbar vertebra, a fifth lumbar vertebra); e.g., an individual thoracic vertebra (e.g., a first thoracic vertebra, a second thoracic vertebra, a third thoracic vertebra, a fourth, thoracic vertebra, a fifth thoracic vertebra, a sixth thoracic vertebra, a seventh thoracic vertebra, an eighth thoracic vertebra, a ninth thoracic vertebra, a tenth thoracic vertebra, an eleventh thoracic vertebra, an twelfth thoracic vertebra)].

In certain embodiments, one or more of the target tissue regions comprise one or more soft-tissue regions (e.g., organs) selected from the group consisting of: a left adrenal gland, a right adrenal gland, an aorta (e.g., a thoracic aorta portion; e.g., an abdominal aorta portion), a brain, a left bronchi, a right bronchi, a gallbladder, a left gluteus maximus, a right gluteus maximus, a heart, a left common iliac artery, a right common iliac artery, a left kidney, a right kidney, a liver, a left lung, a right lung, a pancreas, a prostate, a rectum, a spleen, a trachea, a urinary bladder, a ventricle, and a parotid gland.

In certain embodiments, the one or more target tissue regions comprise one or more soft-tissue regions (e.g., organs) selected from the group consisting of: a gallbladder, a left kidney, a right kidney, a liver, a left lung, a right lung, a prostate, and a urinary bladder.

In certain embodiments, the target tissue regions comprise one or more bone regions, each corresponding to a specific bone [e.g., where the target tissue regions comprise at least a portion of (e.g., up to all) the bones listed in paragraphs above] and one or more soft tissue regions, each corresponding to a specific soft-tissue region [e.g., where the target tissue regions comprise at least a portion of (e.g., up to all) the soft-tissue regions listed in paragraphs above].

In another aspect, the invention is directed to a method for automatically processing 3D images to automatically identify cancerous lesions within a subject, the method comprising: (a) receiving, by a processor of a computing device, a 3D anatomical image of a subject obtained using an anatomical imaging modality [e.g., x-ray computed tomography (CT); e.g., magnetic resonance imaging (MRI); e.g., ultrasound], wherein the 3D anatomical image comprises a graphical representation of tissue (e.g., soft-tissue and/or bone) within the subject; (b) automatically identifying, by the processor, using one or more machine learning modules (e.g., wherein at least one of the one or more machine learning modules is a Convolutional Neural Network (CNN) module), for each of a plurality of target tissue regions, a corresponding target volume of interest (VOI) within the 3D anatomical image; (c) determining, by the processor, a 3D segmentation map representing a plurality of 3D segmentation masks, each 3D segmentation mask representing a particular identified target VOI (e.g., automatically, digitally stitching together the plurality of 3D segmentation masks to form the 3D segmentation map); (d) receiving, by the processor, a 3D functional image of the subject obtained using a functional imaging modality [e.g., single-photon emission computed tomography (SPECT); e.g., positron emission tomography (PET)][e.g., wherein the 3D functional image comprises a plurality of voxels, each representing a particular physical volume within the subject and having an intensity value that represents detected radiation emitted from a the particular physical volume, wherein at least a portion of the plurality of voxels of the 3D functional image represent physical volumes within one or more of the target tissue regions of the subject]; (e) identifying, within the 3D functional image, one or more 3D volume(s), each corresponding to an identified target VOI, using the 3D segmentation map (e.g., by mapping 3D segmentation masks of the 3D segmentation map to the 3D functional image); and (f) automatically detecting, by the processor, within at least a portion of the one or more 3D volumes identified within the 3D functional image, one or more hotspots determined to represent lesions based on intensities of voxels within the 3D functional image [e.g., based on a comparison of intensities within the 3D functional image with a threshold value (e.g., wherein the 3D functional image is a 3D PET image and the threshold is a particular standard uptake value (SUV) level)].

In certain embodiments, the method comprises using, by the processor, the one or more detected hotspots (e.g., intensities of the one or more detected hotspots) to determine a cancer status for the subject.

In certain embodiments, the target tissue regions comprise one or more reference tissue regions and wherein the method

comprises: using the 3D segmentation map to identify, by the processor, within the 3D functional image, one or more 3D reference volume(s), each corresponding to a particular reference tissue region; determining one or more reference intensity values, each associated with a particular 3D reference volume of the one or more 3D reference volume(s) and corresponding to a measure of (e.g., an average/mean, a median, a maximum, etc.) intensity within the particular 3D reference volume; determining, by the processor, one or more individual hotspot intensity values, each associated with a particular hotspot of at least a portion of the detected one or more hotspots and corresponding to a measure of (e.g., an average/mean, a median, a maximum, etc.) intensity of the particular hotspot; and determining, by the processor, one or more individual hotspot index values using the one or more individual hotspot intensity values and the one or more reference intensity values [e.g., wherein each individual hotspot index value is associated with a particular hotspot of the at least a portion of the detected one or more hotspots and determined using (e.g., based on a comparison between) (i) the individual hotspot intensity value associated with the particular hotspot and (ii) the one or more reference intensity values].

In certain embodiments, the reference tissue regions comprise one or more members selected from the group consisting of: a liver, an aorta (e.g., a thoracic aorta portion; e.g., an abdominal aorta portion), and a parotid gland.

In certain embodiments, the method comprises determining, by the processor, an overall index value indicative of a cancer status of the subject using at least a portion of the one or more hotspot index values.

In certain embodiments, the overall index value is determined as a weighted sum of at least a portion [e.g., located within a 3D volume of the functional image that corresponds to a skeletal region of the subject; e.g., located within a 3D volume of the functional image that corresponds to a lymph region of the subject] of the individual hotspot index values [e.g., wherein each hotspot index value in the sum is weighted by a measure of size (e.g., 3D volume; e.g., average diameter) of the associated hotspot].

In certain embodiments, the 3D anatomical image is an x-ray computed tomography (CT) image, and the 3D functional image is a 3D positron emission tomography (PET) image.

In certain embodiments, the 3D PET image of the subject is obtained following administration to the subject of a radiopharmaceutical comprising a prostate-specific membrane antigen (PSMA) binding agent.

In certain embodiments, the radiopharmaceutical comprises [18F]DCFPyL.

In another aspect, the invention is directed to a method for automatically processing 3D images to identify, and measure uptake of radiopharmaceutical in, cancerous lesions (e.g., metastases) within a subject having or at risk for a cancer (e.g., prostate cancer, breast cancer, lung cancer; e.g., a metastatic cancer, such as metastatic prostate cancer, metastatic breast cancer, metastatic lung cancer), the method comprising: (a) receiving, by a processor of a computing device, a 3D anatomical image of a subject obtained using an anatomical imaging modality [e.g., x-ray computed tomography (CT); e.g., magnetic resonance imaging (MRI); e.g., ultra-sound], wherein the 3D anatomical image comprises a graphical representation of tissue (e.g., soft-tissue and/or bone) within the subject; (b) automatically identifying, by the processor, using one or more machine learning modules (e.g., wherein at least one of the machine learning modules is a Convolutional Neural Network (CNN) module), within the 3D anatomical image: a first skeletal volume comprising a graphical representation of one or more bones of the subject; a first aorta volume comprising a graphical representation of at least a portion of an aorta of the subject; and a first liver volume comprising a graphical representation of a liver of the subject; (c) determining, by the processor, a 3D segmentation map representing a plurality of 3D segmentation masks, including a skeletal mask representing the identified first skeletal volume, an aorta mask representing the identified first aorta volume, and a liver mask representing the identified first liver volume; (d) receiving, by the processor, a 3D functional image of the subject obtained using a functional imaging modality [e.g., single-photon emission computed tomography (SPECT); e.g., positron emission tomography (PET)][e.g., wherein the 3D functional image comprises a plurality of voxels, each representing a particular physical volume within the subject and having an intensity value that represents detected radiation emitted from a the particular physical volume, wherein at least a portion of the plurality of voxels of the 3D functional image represent physical volumes within one or more bones, an aorta portion, and/or a liver of the subject]; (e) automatically identifying, within the 3D functional image, using the 3D segmentation map (e.g., by mapping the 3D segmentation masks of the 3D segmentation map to the 3D functional image): a second skeletal volume corresponding to the first identified skeletal volume, within the 3D anatomical image; a second aorta volume corresponding to the first aorta volume, identified within the 3D anatomical image; and a second liver volume corresponding to the first liver volume, identified within the 3D anatomical image; (f) automatically detecting, by the processor, within the second skeletal volume, one or more hotspots determined to represent lesions based on intensities of voxels within the second skeletal volume (e.g., the one or more hotspots corresponding to localized regions of relatively high intensity, e.g., identified based on a comparison of intensities of voxels located within the second skeletal volume with a threshold value); and (g) determining, by the processor, for each of the one or more detected hotspots, an individual hotspot index (e.g., indicative of a measure of radiopharmaceutical uptake in the lesions represented by the detected hotspot) value by: determining an aorta reference intensity level based on a measure (e.g., a mean, a maximum, a median, etc.) of intensity of voxels within the second aorta volume; determining a liver reference intensity level based on a measure (e.g., a mean, a maximum, a median, etc.) of intensity of voxels within the second liver volume; and for each individual detected hotspot: determining a corresponding individual hotspot intensity level based on a measure (e.g., a mean, a maximum, a median, etc.) of intensity of voxels of the detected hotspot; and determining a corresponding individual hotspot index level from the individual hotspot intensity level, the aorta reference intensity level, and the liver reference intensity level.

In certain embodiments, the method comprises determining, by the processor, an overall index value indicative of a cancer status of the subject based on the individual hotspot index values of at least a portion of the one or more detected hotspots.

In certain embodiments, the subject has or is at risk for prostate cancer.

In certain embodiments, step (b) comprises automatically identifying, within the 3D anatomical image, a first prostate volume comprising a graphical representation of a prostate of the subject, the 3D segmentation map determined at step (c) further includes a prostate mask representing the iden-

tified first prostate volume, step (e) comprises automatically identifying, within the 3D functional image, a second prostate volume corresponding to the first identified prostate volume, within the 3D anatomical image, step (f) comprises automatically detecting one or more hotspots in the second prostate volume, and the method further comprises: determining, by the processor, (i) an overall bone index value indicative of a lesion content (e.g., and severity) in the one or more bones of the subject based on the individual hotspot index values of at least a portion of the one or more detected hotspots located in the second skeletal volume and (ii) an overall prostate index value indicative of a lesion content (e.g., and severity) in the prostate of the subject based on the individual hotspot index values of at least a portion of the one or more detected hotspots located in the second prostate volume.

In certain embodiments, the subject has or is at risk for metastatic cancer (e.g., metastatic prostate cancer, metastatic breast cancer, metastatic lung cancer, and other metastatic bone cancers).

In another aspect, the invention is directed to a method for automatically processing a set of full body 3D anatomical images of varying sizes to automatically identify, within each 3D anatomical image, a plurality of 3D volumes that correspond to particular target tissue regions, the method comprising: (a) receiving, by a processor of a computing device, the set of 3D anatomical images of one or more subject(s) obtained using an anatomical imaging modality [e.g., x-ray computed tomography (CT); e.g., magnetic resonance imaging (MRI); e.g., ultra-sound], wherein the 3D anatomical image comprises a graphical representation of tissue (e.g., soft-tissue and/or bone) within each of the one or more subject(s), wherein the set of 3D anatomical images has a mean x-dimension, a mean y-dimension, and a mean z-dimension, at least one of which (the mean x-, mean y-, or mean z-dimension) having a standard deviation at least 3% of the corresponding mean [e.g., at least one of which (the mean x-, mean y-, or mean z-dimension) having a relative standard deviation of at least 3%, at least 5%, at least 10%, at least 15%, or at least 20%]; and (b) automatically determining, by the processor, using a localization module that implements a CNN, within each image of the set of 3D anatomical images, at least one initial VOI corresponding to a particular anatomical region (e.g., a group of related tissue, such as a pelvic region and a spin region) that comprises one or more particular associated target tissue regions (e.g., one or more specific bones, e.g., one or more specific organs), thereby identifying at least one initial VOI for the corresponding 3D anatomical image; and (c) for each initial VOI, automatically identifying, by the processor, using one or more segmentation modules each implementing a CNN, for each of the one or more particular target tissue regions associated with the particular anatomical region to which the initial VOI corresponds, a corresponding target VOI (e.g., a graphical representation of the particular target tissue region).

In another aspect, the invention is directed to a system for automatically processing a 3D image to identify 3D volumes within the 3D image that correspond to particular target tissue regions, the system comprising: a processor of a computing device; and a memory having instructions stored thereon, wherein the instructions, when executed by the processor, cause the processor to: (a) receive a 3D anatomical image of a subject obtained using an anatomical imaging modality [e.g., x-ray computed tomography (CT); e.g., magnetic resonance imaging (MRI); e.g., ultra-sound], wherein the 3D anatomical image comprises a graphical representation of tissue (e.g., soft-tissue and/or bone) within the subject; (b) automatically identify, using one or more machine learning modules (e.g., wherein at least one of the one or more machine learning modules is a Convolutional Neural Network (CNN) module), for each of a plurality of target tissue regions, a corresponding target volume of interest (VOI) within the 3D anatomical image; (c) determine 3D segmentation map representing a plurality of 3D segmentation masks, each 3D segmentation mask representing a particular identified target VOI (e.g., automatically, digitally stitching together the plurality of 3D segmentation masks to form the 3D segmentation map); and (d) store and/or provide the 3D segmentation map for display and/or further processing.

In certain embodiments, the 3D anatomical image is a full body image.

In certain embodiments, at step (c) the instructions cause the processor to digitally stitch together the plurality of 3D segmentation masks to form the 3D segmentation map {e.g., by creating an initially empty image volume (e.g., initializing all voxel values to zero) and then inserting labels from each segmentation mask into the image volume [e.g., by mapping labeled (e.g., as representing a particular target tissue region as determined by a machine learning module) voxels of input images to one or machine learning modules to voxels of the image volume (e.g., so as to match voxels of the image volume to voxels of the input images that represent a same physical location, thereby labeling voxels of the image volume correctly)]}.

In certain embodiments, at step (b), the instructions cause the processor to, for at least one specific target tissue region: determine, using a first module (e.g., a localization module) (e.g., a first machine learning module), an initial VOI within the 3D anatomical image, the initial VOI corresponding to an anatomical region (e.g., a group of related tissue, such as a pelvic region, a chest region, a head and/or neck region, and the like) containing the specific target tissue region (e.g., wherein the initial VOI excludes more voxels of the 3D anatomical image than it includes; e.g., wherein the initial VOI includes less than 25% of the voxels of the 3D anatomical image; e.g., wherein a majority of voxels within the initial VOI represent physical volumes within the anatomical region); and identify, using a second module (e.g., a segmentation module)(e.g., a second machine learning module), the target VOI corresponding to the specific target tissue region within the initial VOI.

In certain embodiments, the second module is a CNN module that implements a CNN.

In certain embodiments, the first module is a CNN module that implements a CNN to perform a coarse segmentation to automatically identify the initial VOI corresponding to the anatomical region containing the specific target tissue region [e.g., by automatically identifying a graphical representation of a group of related tissue within the anatomical image (e.g., and, subsequently, determining the initial VOI as a rectangular region (e.g., rectangular prism or rectangular box) entirely enclosing the identified graphical representation of the group of related tissue)] [e.g., by, for each of one or more particular tissue regions anticipated to be located within the anatomical region, automatically identifying a corresponding VOI in the anatomical image (e.g., via the coarse segmentation), e.g., and determining the initial VOI as a rectangular region entirely enclosing all of the identified VOIs corresponding to the particular tissue regions].

In certain embodiments, the first module receives a subsampled [e.g., by a factor of two or more (e.g., four) along one or more dimensions] version of the anatomical image as

input and identifies the initial VOI using the sub-sampled version of the anatomical image [e.g., and wherein the second module receives a full resolution version of the anatomical image, cropped to the initial VOI (e.g., such that the first module operates on an lower resolution image that represents a larger physical volume than the second module, while the second module operates on a higher resolution image but representing a smaller physical volume)].

In certain embodiments, the first module is a first CNN module and the second module is a second CNN module, and wherein the first CNN module comprises additional filters in order to account for increased variability in image size with respect to the second CNN module.

In certain embodiments, the 3D anatomical image is a full body image and wherein, at step (b), the instructions cause the processor to: automatically determine, using one or more localization modules implementing machine learning technique(s) (e.g., wherein each localization module is a CNN module that implements a CNN), a plurality of initial VOIs within the 3D anatomical image, each initial VOI corresponding to a particular anatomical region (e.g., a group of related tissue, such as a pelvic region, a chest region, a head and/or neck region, a spine region, an upper body region, a lower body region, etc.) and in which an associated subset of the target VOIs are located; and for each initial VOI, automatically identify, using one or more segmentation modules implementing machine learning technique(s) (e.g., wherein each segmentation module is a CNN module that implements a CNN) the associated subset of target VOIs.

In certain embodiments, the plurality of initial VOIs comprises one or more members selected from the group consisting of: a pelvic region initial VOI corresponding to a pelvic region of the subject (e.g., wherein the subset of target VOIs located in the pelvic region initial VOI comprise one or more target VOIs corresponding to target tissue regions selected from the group consisting of a left and/or right ilium, a sacrum, and a coccyx); a spine region initial VOI corresponding to a spine of the subject (e.g., wherein the subset of target VOIs located in the pelvic region initial VOI comprise one or more target VOIs corresponding to target tissue regions selected from the group consisting of a thoracic vertebra, a lumber vertebra, and a sternum); a left upper body region initial VOI corresponding to a left side of the subject's upper body (e.g., wherein the subset of target VOIs located in the pelvic region initial VOI comprise one or more target VOIs corresponding to target tissue regions selected from the group consisting of one or more left rib(s), a left scapula, and a left clavicle); and a right upper body region initial VOI corresponding to a right side of the subject's upper body (e.g., wherein the subset of target VOIs located in the pelvic region initial VOI comprise one or more target VOIs corresponding to target tissue regions selected from the group consisting of one or more right rib(s), a right scapula, and a right clavicle).

In certain embodiments, the instructions cause the processor to: (e) receive a 3D functional image of the subject obtained using a functional imaging modality [e.g., single-photon emission computed tomography (SPECT); e.g., positron emission tomography (PET)] [e.g., wherein the 3D functional image comprises a plurality of voxels, each representing a particular physical volume within the subject and having an intensity value that represents detected radiation emitted from a the particular physical volume, wherein at least a portion of the plurality of voxels of the 3D functional image represent physical volumes within one or more of the target tissue regions of the subject]; and (f) identify, within the 3D functional image, one or more 3D volume(s), each corresponding to an identified target VOI, using the 3D segmentation map (e.g., by mapping 3D segmentation masks of the 3D segmentation map to the 3D functional image).

In certain embodiments, the instructions cause the processor to: (g) determine a cancer status [(e.g., a prostate cancer status; e.g., a metastatic cancer status (e.g., metastatic cancer, including, e.g., metastatic prostate cancer, breast cancer, lung cancer, colon cancer, skin cancer, etc.)] for the subject (e.g., using intensities of voxels within the functional image and the one or more identified 3D volumes)(e.g., based on detected lesions) [e.g., a likelihood of the subject having and/or developing prostate cancer and/or a particular stage of prostate cancer (e.g., metastatic prostate cancer)] [e.g., a likelihood of the subject having and/or developing a metastatic cancer (including, e.g., metastatic prostate cancer, breast cancer, lung cancer, colon cancer, skin cancer, etc.)].

In certain embodiments, the instructions cause the processor to perform steps (a)-(g) repeatedly for a plurality of anatomical and corresponding functional images collected at different time points to determine, at each time point, a cancer status of the subject, thereby tracking cancer status over time (e.g., to evaluate disease progression and/or treatment efficacy).

In certain embodiments, the instructions cause the processor to (e.g., prior to step (g)): (h) automatically adjust intensities of voxels of the 3D functional image to correct for background uptake (e.g., of the radiopharmaceutical) in one or more background tissue regions (e.g., correcting for uptake of the radiopharmaceutical that occurs in the one or more background tissue regions under normal circumstances, and which is not necessarily indicative of presence of cancerous lesions).

In certain embodiments, the target tissue regions comprise the one or more background tissue regions and wherein, at step (h), the instructions cause the processor to: use the 3D segmentation map to identify, within the 3D functional image, one or more 3D background tissue volume(s), each corresponding a particular background tissue region (e.g., by mapping 3D segmentation masks of the 3D segmentation map to the 3D functional image); and adjust intensities of voxels of the 3D functional image based on intensities of voxels within the 3D background tissue volumes (e.g., by using intensities of voxels within the 3D background tissue volumes to estimate a contribution to intensities outside of the 3D background tissue volumes).

In certain embodiments, the one or more background tissue regions comprise one or more members selected from the group consisting of: a bladder (e.g., a urinary bladder), a kidney, a duodenum, a small intestine, a spleen, a liver, a pancreas, a stomach, an adrenal gland, a rectum, and testes.

In certain embodiments, the instructions cause the processor to: (i) automatically detect one or more hotspots within the 3D functional image determined to represent lesions based on intensities of voxels within the 3D functional image [e.g., based on a comparison of intensities within the 3D functional image with a threshold value (e.g., wherein the 3D functional image is a 3D PET image and the threshold is a particular standard uptake value (SUV) level)] (e.g., and also based on the one or more 3D volumes identified within the 3D functional image).

In certain embodiments, at step (i), the instructions cause the processor to use one or more thresholds [e.g., comparing intensities of voxels in the 3D functional image with the one or more thresholds (e.g., wherein the one or more thresholds comprises a plurality of region-specific thresholds, each

used for a specific sub-set of the one or more 3D volumes identified within the 3D functional image)].

In certain embodiments, at step (i), the instructions cause the processor to apply one or more filters to the 3D functional image [e.g., as in a blob detection technique; e.g., wherein the one or more filters comprises one or more Gaussian filters (e.g., a high pass Gaussian filter and a low pass Gaussian filter, as in a Difference of Gaussians approach); e.g., wherein the one or more filters comprises a Laplacian filter (e.g., as in a Laplacian of a Gaussian technique); e.g., wherein different filter kernels are used for different sub-sets of the one or more 3D volumes identified within the 3D functional image].

In certain embodiments, at step (i), the instructions cause the processor to use a combination of two or more techniques for identification of hotspots in different sub-sets of the one or more 3D volumes identified within the 3D functional image [e.g., using a first filtering approach (e.g., as in paragraphs above) for a first sub-set of the one or more 3D volumes and using a second filtering approach for a second sub-set; e.g., using thresholding approach (e.g., as in paragraphs above) for a first sub-set of the one or more 3D volumes and using a filtering approach (e.g., as in paragraphs above) for a second sub-set of the one or more 3D volumes].

In certain embodiments, at step (i), the instructions cause the processor to detect an initial set of hotspots and, for at least a portion of the hotspots of the initial set, classify each hotspot of at least a portion of the detected hotspots as either a cancerous lesion or not a cancerous lesion (e.g., as noise) [e.g., using a machine learning module; e.g., based on a shape and/or location of the hotspot (e.g., in combination with anatomical knowledge; e.g., wherein the location includes an identification of a particular target tissue region corresponding to the 3D volume in which the hotspot is located and/or a relative position of the hotspot within the particular target tissue region); e.g., and removing hotspots classified as not a cancerous lesion from the initial set, thereby obtaining a final set of hotspots determined to represent lesions].

In certain embodiments, the target tissue regions comprise one or more background tissue regions and the instructions cause the processor to: use the 3D segmentation map to identify, within the 3D functional image, one or more 3D background tissue volume(s), each corresponding a particular background tissue region (e.g., a background tissue region in which significant radiopharmaceutical uptake occurs under normal circumstances and is not necessarily indicative of presence of cancerous lesions)(e.g., by mapping 3D segmentation masks of the 3D segmentation map to the 3D functional image); and exclude voxels of the 3D within the 3D background tissue from the voxels used to automatically detect the one or more hotspots at step (i).

In certain embodiments, the instructions cause the processor to use the one or more detected hotspots (e.g., intensities of the one or more detected hotspots) to determine a cancer status for the subject.

In certain embodiments, the target tissue regions comprise one or more reference tissue regions and the instructions cause the processor to: use the 3D segmentation map to identify, within the 3D functional image, one or more 3D reference volume(s), each corresponding to a particular reference tissue region; determine one or more reference intensity values, each associated with a particular 3D reference volume of the one or more 3D reference volume(s) and corresponding to a measure of (e.g., an average/mean, a median, a maximum, etc.) intensity within the particular 3D reference volume; determine one or more individual hotspot intensity values, each associated with a particular hotspot of at least a portion of the detected one or more hotspots and corresponding to a measure of (e.g., an average/mean, a median, a maximum, etc.) intensity of the particular hotspot; and determine one or more individual hotspot index values using the one or more individual hotspot intensity values and the one or more reference intensity values [e.g., wherein each individual hotspot index value is associated with a particular hotspot of the at least a portion of the detected one or more hotspots and determined using (e.g., based on a comparison between) (i) the individual hotspot intensity value associated with the particular hotspot and (ii) the one or more reference intensity values].

In certain embodiments, the instructions cause the processor to determine the one or more individual hotspot index values by mapping each of the one or more reference intensity values to a corresponding reference index value on a scale and, for each individual hotspot intensity value, using the reference intensity values and corresponding reference index values to interpolate a corresponding individual hotspot index value.

In certain embodiments, the reference tissue regions comprise one or more members selected from the group consisting of: a liver, an aorta (e.g., a thoracic aorta portion; e.g., an abdominal aorta portion), and a parotid gland.

In certain embodiments, a first reference intensity value (i) is a blood reference intensity value associated with a 3D reference volume corresponding to an aorta portion, and (ii) maps to a first reference index value; a second reference intensity value (i) is a liver reference intensity value associated with a 3D reference volume corresponding to a liver, and (ii) maps to a second reference index value; and the second reference intensity value is greater than the first reference intensity value and the second reference index value is greater than the first reference index value.

In certain embodiments, the reference intensity values comprises a maximum reference intensity value that maps to a maximum reference index value, and wherein hotspots having associated hotspot intensity values greater than the maximum reference intensity value are assigned hotspot index values equal to the maximum reference index value.

In certain embodiments, the instructions cause the processor to determine an overall index value indicative of a cancer status of the subject using at least a portion of the one or more hotspot index values.

In certain embodiments, the overall index value is determined as a weighted sum of at least a portion [e.g., located within a 3D volume of the functional image that corresponds to a skeletal region of the subject; e.g., located within a 3D volume of the functional image that corresponds to a lymph region of the subject] of the individual hotspot index values [e.g., wherein each hotspot index value in the sum is weighted by a measure of size (e.g., 3D volume; e.g., average diameter) of the associated hotspot].

In certain embodiments, the overall index value is associated with a particular target tissue region corresponding to a particular target VOI identified within the anatomical image; and the overall index value is determined using hotspot index values of a subset of hotspots located within a particular 3D volume in the 3D functional image that corresponds to the particular identified target VOI [e.g., and wherein the overall index value is computed as a weighted sum of the hotspot index values of the subset of hotspots (e.g., wherein the weighted sum is normalized by an estimated volume of the particular target tissue region (e.g.,

computed as a volume of the particular 3D volume in the function image and/or a volume of the particular target VOI))].

In certain embodiments, the particular target tissue region is selected from the group consisting of: a skeletal region comprising one or more bones of the subject, a lymph region, and a prostate region.

In certain embodiments, the 3D anatomical image is an x-ray computed tomography (CT) image, and the 3D functional image is a 3D single photon emission computed tomography (SPECT) image.

In certain embodiments, the 3D anatomical image is an x-ray computed tomography (CT) image, and the 3D functional image is a 3D positron emission tomography (PET) image.

In certain embodiments, the 3D PET image of the subject is obtained following administration to the subject of a radiopharmaceutical comprising a prostate-specific membrane antigen (PSMA) binding agent.

In certain embodiments, the radiopharmaceutical comprises [18F]DCFPyL.

In certain embodiments, at step (b), the instructions cause the processor to crop the 3D anatomical image to remove voxels representing air [e.g., to create a cropped anatomical image, and using the cropped anatomical image to identify the one or more target VOIs (e.g., using the cropped anatomical image is used as input to one or more machine learning modules, as opposed to the original size 3D anatomical image)].

In certain embodiments, the target tissue regions comprise one or more members selected from the group consisting of: a left hip bone, a right hip bone, a sacrum and coccyx region, a left clavicle, a right clavicle, a left rib, a right rib, a left scapula, a right scapula, a sternum, a lumbar vertebra, a thoracic vertebra, a skull, a cervical vertebra, a left femur, a right femur, a left humerus, a right humerus, a prostate, a urinary bladder, a rectum, a left gluteus maximus, a right gluteus maximus, an aorta (e.g., a thoracic aorta portion; e.g., an abdominal aorta portion), a left kidney, a right kidney, a liver, a left lung, a right lung, a spleen, a ventricle, a left adrenal gland, a right adrenal gland, a gallbladder, a brain, a pancreas, a heart, a mandible, a left bronchi, a right bronchi, a trachea, a left common iliac artery, a right common iliac artery, and a parotid gland.

In certain embodiments, one or more of the target tissue regions comprise one or more specific bones selected from the group consisting of: a left clavicle, a right clavicle, a left femur, a right femur, a left fibula, a right fibula, a left hip bone, a right hip bone, a left humerus, a right humerus, a mandible, a left patella, a right patella, left radius, a right radius, a left tibia, a right tibia, a left ulna, a right ulna, a left rib (e.g., a first left rib, a second left rib, a third left rib, a fourth left rib, a fifth left rib, a sixth left rib, a seventh left rib, an eighth left rib, a ninth left rib, a tenth left rib, an eleventh left rib, a twelfth left rib), a right rib (e.g., a first right rib, a second right rib, a third right rib, a fourth right rib, a fifth right rib, a sixth right rib, a seventh right rib, an eighth right rib, a ninth right rib, a tenth right rib, an eleventh right rib, a twelfth right rib), a sacrum and coccyx (e.g., a combined sacrum and coccyx region; e.g., a sacrum and a coccyx individually, so as to distinguish between the two), a left scapula, a right scapula, a skull, sternum, a vertebrae region [e.g., a cervical vertebrae region, comprising one or more (e.g., up to all) cervical vertebrae; e.g., a lumber vertebrae region, comprising one or more (e.g., up to all) lumbar vertebrae; e.g., a thoracic vertebrae region, comprising one or more (e.g., up to all) thoracic vertebrae], and an individual vertebra [e.g., e.g., an individual cervical vertebra (e.g., a first cervical vertebra, a second cervical vertebra, a third cervical vertebra, a fourth cervical vertebra, a fifth cervical vertebra, a sixth cervical vertebra, a seventh cervical vertebra); e.g., an individual lumbar vertebra (e.g., a first lumbar vertebra, a second lumbar vertebra, a third lumbar vertebra, a fourth lumbar vertebra, a fifth lumbar vertebra, a sixth lumbar vertebra); e.g., an individual thoracic vertebra (e.g., a first thoracic vertebra, a second thoracic vertebra, a third thoracic vertebra, a fourth, thoracic vertebra, a fifth thoracic vertebra, a sixth thoracic vertebra, a seventh thoracic vertebra, an eighth thoracic vertebra, a ninth thoracic vertebra, a tenth thoracic vertebra, an eleventh thoracic vertebra, an twelfth thoracic vertebra)].

In certain embodiments, one or more of the target tissue regions comprise one or more specific bones selected from the group consisting of: a left clavicle, a right clavicle, a left hip bone, a right hip bone, a left rib (e.g., a first left rib, a second left rib, a third left rib, a fourth left rib, a fifth left rib, a sixth left rib, a seventh left rib, an eighth left rib, a ninth left rib, a tenth left rib, an eleventh left rib, a twelfth left rib), a right rib (e.g., a first right rib, a second right rib, a third right rib, a fourth right rib, a fifth right rib, a sixth right rib, a seventh right rib, an eighth right rib, a ninth right rib, a tenth right rib, an eleventh right rib, a twelfth right rib), a sacrum and coccyx (e.g., a combined sacrum and coccyx region; e.g., a sacrum and a coccyx individually, so as to distinguish between the two), a left scapula, a right scapula, a sternum, a vertebrae region [e.g., a cervical vertebrae region, comprising one or more (e.g., up to all) cervical vertebrae; e.g., a lumber vertebrae region, comprising one or more (e.g., up to all) lumbar vertebrae; e.g., a thoracic vertebrae region, comprising one or more (e.g., up to all) thoracic vertebrae], and an individual lumbar vertebra (e.g., a first lumbar vertebra, a second lumbar vertebra, a third lumbar vertebra, a fourth lumbar vertebra, a fifth lumbar vertebra); e.g., an individual thoracic vertebra (e.g., a first thoracic vertebra, a second thoracic vertebra, a third thoracic vertebra, a fourth, thoracic vertebra, a fifth thoracic vertebra, a sixth thoracic vertebra, a seventh thoracic vertebra, an eighth thoracic vertebra, a ninth thoracic vertebra, a tenth thoracic vertebra, an eleventh thoracic vertebra, an twelfth thoracic vertebra)].

In certain embodiments, one or more of the target tissue regions comprise one or more soft-tissue regions (e.g., organs) selected from the group consisting of: a left adrenal gland, a right adrenal gland, an aorta (e.g., a thoracic aorta portion; e.g., an abdominal aorta portion), a brain, a left bronchi, a right bronchi, a gallbladder, a left gluteus maximus, a right gluteus maximus, a heart, a left common iliac artery, a right common iliac artery, a left kidney, a right kidney, a liver, a left lung, a right lung, a pancreas, a prostate, a rectum, a spleen, a trachea, a urinary bladder, a ventricle, and a parotid gland.

In certain embodiments, the one or more target tissue regions comprise one or more soft-tissue regions (e.g., organs) selected from the group consisting of: a gallbladder, a left kidney, a right kidney, a liver, a left lung, a right lung, a prostate, and a urinary bladder.

In certain embodiments, the target tissue regions comprise one or more bone regions, each corresponding to a specific bone [e.g., where the target tissue regions comprise at least a portion of (e.g., up to all) the bones listed in paragraphs above] and one or more soft tissue regions, each corresponding to a specific soft-tissue region [e.g., where the target tissue regions comprise at least a portion of (e.g., up to all) the soft-tissue regions listed in paragraphs above].

In another aspect, the invention is directed to a system for automatically processing 3D images to automatically identify cancerous lesions within a subject, the system comprising: a processor of a computing device; and a memory having instructions stored thereon, wherein the instructions, when executed by the processor, cause the processor to: (a) receive a 3D anatomical image of a subject obtained using an anatomical imaging modality [e.g., x-ray computed tomography (CT); e.g., magnetic resonance imaging (MRI); e.g., ultra-sound], wherein the 3D anatomical image comprises a graphical representation of tissue (e.g., soft-tissue and/or bone) within the subject; (b) automatically identify, using one or more machine learning modules (e.g., wherein at least one of the one or more machine learning modules is a Convolutional Neural Network (CNN) module), for each of a plurality of target tissue regions, a corresponding target volume of interest (VOI) within the 3D anatomical image; (c) determine a 3D segmentation map representing a plurality of 3D segmentation masks, each 3D segmentation mask representing a particular identified target VOI (e.g., automatically, digitally stitching together the plurality of 3D segmentation masks to form the 3D segmentation map); (d) receive a 3D functional image of the subject obtained using a functional imaging modality [e.g., single-photon emission computed tomography (SPECT); e.g., positron emission tomography (PET)][e.g., wherein the 3D functional image comprises a plurality of voxels, each representing a particular physical volume within the subject and having an intensity value that represents detected radiation emitted from a the particular physical volume, wherein at least a portion of the plurality of voxels of the 3D functional image represent physical volumes within one or more of the target tissue regions of the subject]; (e) identify, within the 3D functional image, one or more 3D volume(s), each corresponding to an identified target VOI, using the 3D segmentation map (e.g., by mapping 3D segmentation masks of the 3D segmentation map to the 3D functional image); and (f) automatically detect, within at least a portion of the one or more 3D volumes identified within the 3D functional image, one or more hotspots determined to represent lesions based on intensities of voxels within the 3D functional image [e.g., based on a comparison of intensities within the 3D functional image with a threshold value (e.g., wherein the 3D functional image is a 3D PET image and the threshold is a particular standard uptake value (SUV) level)].

In certain embodiments, the instructions cause the processor to use the one or more detected hotspots (e.g., intensities of the one or more detected hotspots) to determine a cancer status for the subject.

In certain embodiments, the target tissue regions comprise one or more reference tissue regions and wherein the instructions cause the processor to: use the 3D segmentation map to identify, within the 3D functional image, one or more 3D reference volume(s), each corresponding to a particular reference tissue region; determine one or more reference intensity values, each associated with a particular 3D reference volume of the one or more 3D reference volume(s) and corresponding to a measure of (e.g., an average/mean, a median, a maximum, etc.) intensity within the particular 3D reference volume; determine one or more individual hotspot intensity values, each associated with a particular hotspot of at least a portion of the detected one or more hotspots and corresponding to a measure of (e.g., an average/mean, a median, a maximum, etc.) intensity of the particular hotspot; and determine one or more individual hotspot index values using the one or more individual hotspot intensity values and the one or more reference intensity values [e.g., wherein each individual hotspot index value is associated with a particular hotspot of the at least a portion of the detected one or more hotspots and determined using (e.g., based on a comparison between) (i) the individual hotspot intensity value associated with the particular hotspot and (ii) the one or more reference intensity values].

In certain embodiments, the reference tissue regions comprise one or more members selected from the group consisting of: a liver, an aorta (e.g., a thoracic aorta portion; e.g., an abdominal aorta portion), and a parotid gland.

In certain embodiments, the instructions cause the processor to determine an overall index value indicative of a cancer status of the subject using at least a portion of the one or more hotspot index values.

In certain embodiments, the overall index value is determined as a weighted sum of at least a portion [e.g., located within a 3D volume of the functional image that corresponds to a skeletal region of the subject; e.g., located within a 3D volume of the functional image that corresponds to a lymph region of the subject] of the individual hotspot index values [e.g., wherein each hotspot index value in the sum is weighted by a measure of size (e.g., 3D volume; e.g., average diameter) of the associated hotspot].

In certain embodiments, the 3D anatomical image is an x-ray computed tomography (CT) image, and the 3D functional image is a 3D positron emission tomography (PET) image.

In certain embodiments, the 3D PET image of the subject is obtained following administration to the subject of a radiopharmaceutical comprising a prostate-specific membrane antigen (PSMA) binding agent.

In certain embodiments, the radiopharmaceutical comprises [18F]DCFPyL.

In another aspect, the invention is directed to a system for automatically processing 3D images to identify, and measure uptake of radiopharmaceutical in, cancerous lesions (e.g., metastases) within a subject having or at risk for a cancer (e.g., prostate cancer, breast cancer, lung cancer; e.g., a metastatic cancer, such as metastatic prostate cancer, metastatic breast cancer, metastatic lung cancer), the system comprising: a processor of a computing device; and a memory having instructions stored thereon, wherein the instructions, when executed by the processor, cause the processor to: (a) receive a 3D anatomical image of a subject obtained using an anatomical imaging modality [e.g., x-ray computed tomography (CT); e.g., magnetic resonance imaging (MRI); e.g., ultra-sound], wherein the 3D anatomical image comprises a graphical representation of tissue (e.g., soft-tissue and/or bone) within the subject; (b) automatically identify using one or more machine learning modules (e.g., wherein at least one of the machine learning modules is a Convolutional Neural Network (CNN) module), within the 3D anatomical image: a first skeletal volume comprising a graphical representation of one or more bones of the subject; a first aorta volume comprising a graphical representation of at least a portion of an aorta of the subject; and a first liver volume comprising a graphical representation of a liver of the subject; (c) determine a 3D segmentation map representing a plurality of 3D segmentation masks, including a skeletal mask representing the identified first skeletal volume, an aorta mask representing the identified first aorta volume, and a liver mask representing the identified first liver volume; (d) receive a 3D functional image of the subject obtained using a functional imaging modality [e.g., single-photon emission computed tomography (SPECT); e.g., positron emission tomography (PET)] [e.g., wherein the 3D functional image comprises a plurality of voxels, each

representing a particular physical volume within the subject and having an intensity value that represents detected radiation emitted from a the particular physical volume, wherein at least a portion of the plurality of voxels of the 3D functional image represent physical volumes within one or more bones, an aorta portion, and/or a liver of the subject]; (e) automatically identify, within the 3D functional image, using the 3D segmentation map (e.g., by mapping the 3D segmentation masks of the 3D segmentation map to the 3D functional image): a second skeletal volume corresponding to the first identified skeletal volume, within the 3D anatomical image; a second aorta volume corresponding to the first aorta volume, identified within the 3D anatomical image; and a second liver volume corresponding to the first liver volume, identified within the 3D anatomical image; (f) automatically detect, within the second skeletal volume, one or more hotspots determined to represent lesions based on intensities of voxels within the second skeletal volume (e.g., the one or more hotspots corresponding to localized regions of relatively high intensity, e.g., identified based on a comparison of intensities of voxels located within the second skeletal volume with a threshold value); and (g) determine, for each of the one or more detected hotspots, an individual hotspot index (e.g., indicative of a measure of radiopharmaceutical uptake in the lesions represented by the detected hotspot) value by: determining an aorta reference intensity level based on a measure (e.g., a mean, a maximum, a median, etc.) of intensity of voxels within the second aorta volume; determining a liver reference intensity level based on a measure (e.g., a mean, a maximum, a median, etc.) of intensity of voxels within the second liver volume; and for each individual detected hotspot: determining a corresponding individual hotspot intensity level based on a measure (e.g., a mean, a maximum, a median, etc.) of intensity of voxels of the detected hotspot; and determining a corresponding individual hotspot index level from the individual hotspot intensity level, the aorta reference intensity level, and the liver reference intensity level.

In certain embodiments, the instructions cause the processor to determine an overall index value indicative of a cancer status of the subject based on the individual hotspot index values of at least a portion of the one or more detected hotspots.

In certain embodiments, the subject has or is at risk for prostate cancer.

In certain embodiments, the instructions cause the processor to: at step (b), automatically identify, within the 3D anatomical image, a first prostate volume comprising a graphical representation of a prostate of the subject; at step (c), include a prostate mask representing the identified first prostate volume in the determined 3D segmentation map; at step (e), automatically identify, within the 3D functional image, a second prostate volume corresponding to the first identified prostate volume, within the 3D anatomical image, at step (f), automatically detect one or more hotspots in the second prostate volume; and determine (i) an overall bone index value indicative of a lesion content (e.g., and severity) in the one or more bones of the subject based on the individual hotspot index values of at least a portion of the one or more detected hotspots located in the second skeletal volume and (ii) an overall prostate index value indicative of a lesion content (e.g., and severity) in the prostate of the subject based on the individual hotspot index values of at least a portion of the one or more detected hotspots located in the second prostate volume.

In certain embodiments, the subject has or is at risk for metastatic cancer (e.g., metastatic prostate cancer, metastatic breast cancer, metastatic lung cancer, and other metastatic bone cancers).

In another aspect, the invention is directed to a system for automatically processing a set of full body 3D anatomical images of varying sizes to automatically identify, within each 3D anatomical image, a plurality of 3D volumes that correspond to particular target tissue regions, the system comprising: a processor of a computing device; and a memory having instructions stored thereon, wherein the instructions, when executed by the processor, cause the processor to: (a) receive the set of 3D anatomical images of one or more subject(s) obtained using an anatomical imaging modality [e.g., x-ray computed tomography (CT); e.g., magnetic resonance imaging (MRI); e.g., ultra-sound], wherein the 3D anatomical image comprises a graphical representation of tissue (e.g., soft-tissue and/or bone) within each of the one or more subject(s), wherein the set of 3D anatomical images has a mean x-dimension, a mean y-dimension, and a mean z-dimension, at least one of which (the mean x-, mean y-, or mean z-dimension) having a standard deviation at least 3% of the corresponding mean [e.g., at least one of which (the mean x-, mean y-, or mean z-dimension) having a relative standard deviation of at least 3%, at least 5%, at least 10%, at least 15%, or at least 20%]; and (b) automatically determine, using a localization module that implements a CNN, within each image of the set of 3D anatomical images, at least one initial VOI corresponding to a particular anatomical region (e.g., a group of related tissue, such as a pelvic region and a spin region) that comprises one or more particular associated target tissue regions (e.g., one or more specific bones, e.g., one or more specific organs), thereby identifying at least one initial VOI for the corresponding 3D anatomical image; and (c) for each initial VOI, automatically identify, using one or more segmentation modules each implementing a CNN, for each of the one or more particular target tissue regions associated with the particular anatomical region to which the initial VOI corresponds, a corresponding target VOI (e.g., a graphical representation of the particular target tissue region).

Features of embodiments described with respect to one aspect of the invention may be applied with respect to another aspect of the invention.

BRIEF DESCRIPTION OF THE FIGURES

The patent or application file contains at least one drawing executed in color. Copies of this patent or patent application publication with color drawing(s) will be provided by the Office upon request and payment of the necessary fee.

The foregoing and other objects, aspects, features, and advantages of the present disclosure will become more apparent and better understood by referring to the following description taken in conjunction with the accompanying drawings, in which:

FIG. **1** is a diagram showing integration of various imaging modalities with an artificial intelligence (AI) platform, according to an illustrative embodiment.

FIG. **2** is an image showing a skeleton of a subject with various specific bones identified, according to an illustrative embodiment.

FIG. **3** is a block diagram showing use of full body segmentation in various functional imaging modalities, for various applications, according to an illustrative embodiment.

FIG. **4** is a diagram showing processing flow of different informational datasets by an AI module to classify, locate, and quantify cancerous lesions, according to an illustrative embodiment.

FIG. **5**A is a block flow diagram of a process for automatically processing 3D images to identify 3D volumes within the 3D images that correspond to particular target tissue regions, according to an illustrative embodiment.

FIG. **5**B is a block flow diagram of a process for automatically processing 3D images to identify 3D volumes and use the 3D volumes to detect hotspots representing cancerous lesions, according to an illustrative embodiment.

FIG. **6**A is a block flow diagram of a process for automatically processing CT images for whole-body segmentation, according to an illustrative embodiment.

FIG. **6**B is a set of CT images showing processing results of various steps of the process shown in FIG. **6**A.

FIG. **7** is a set of three images used as training data for machine learning modules used to segment CT images, according to an illustrative embodiment.

FIG. **8** is a set of two images with identified volumes of interest overlaid.

FIG. **9**A is a set of 2D views of a 3D PET/CT image obtained from a subject following administration of PyL™.

FIG. **9**B is the same set of 2D views shown in FIG. **9**A, following background correction.

FIG. **9**C is a set of 2D views of a 3D PET/CT image obtained from a subject following administration of PyL™.

FIG. **9**D is the same set of 2D views shown in FIG. **9**C, following background correction.

FIG. **10**A is a block flow diagram showing an example process for analyzing PyL™-PET images, according to an illustrative embodiment.

FIG. **10**B is a PET/CT image obtained following administration of PyL™ to a subject.

FIG. **10**C is a set of two CT images showing volumes of interest identified via the machine learning approaches described herein.

FIG. **10**D is a set of 3 images illustrating background correction in PET images, according to an illustrative embodiment.

FIG. **11**A is a view of a 3D CT image with volumes of interest corresponding to specific bones labeled in color, according to an illustrative embodiment.

FIG. **11**B is another view of the 3D CT image with labeled volumes of interest shown in FIG. **11**A.

FIG. **12** is a CT image with an overlaid PET image showing identified background tissue regions.

FIG. **13**A is view a CT image with an overlaid PET image showing a detected lesion.

FIG. **13**B is another view of the CT image with overlaid PET image of FIG. **13**A, showing the detected lesion.

FIG. **13**C is another view of the CT image with overlaid PET image of FIG. **13**A, showing the detected lesion.

FIG. **13**D is another view of the CT image with overlaid PET image of FIG. **13**A, showing the detected lesion.

FIG. **14**A is a set of two views of a CT image with an overlaid PET image obtained for a subject following administration of PyL™.

FIG. **14**B shows the same views as FIG. **14**A, but following processing via the machine learning approaches described herein to provide for background correction and detection of lesions.

FIG. **15**A is a set of two views of a CT image with an overlaid PET image obtained for a subject following administration of PyL™.

FIG. **15**B shows the same views as FIG. **15**A, but following processing via the machine learning approaches described herein to provide for background correction and detection of lesions.

FIG. **16**A is a view of a 3D CT image with identified volumes of interest overlaid.

FIG. **16**B is another view of the 3D CT image with identified volumes of interest overlaid shown in FIG. **16**A.

FIG. **17** is a block diagram of an exemplary cloud computing environment, used in certain embodiments.

FIG. **18** is a block diagram of an example computing device and an example mobile computing device used in certain embodiments.

FIG. **19** is a set of three graph, each graphs showing overall index values quantifying PyL™-PSMA uptake in lesions identified in a particular tissue region based on PET/CT image analysis for six different cancer indications, according to an illustrative embodiment.

FIG. **20** is a graph showing individual lesion PSMA index (LPI) values determined for lesions detected in three different tissue regions (bone, lymph, and prostate) via PET/CT image analysis, according to an illustrative embodiment.

FIG. **21** is a set of two graphs comparing reference values determined via manual and automated image analysis for a blood pool reference value and a liver reference value according to an illustrative embodiment.

The features and advantages of the present disclosure will become more apparent from the detailed description set forth below when taken in conjunction with the drawings, in which like reference characters identify corresponding elements throughout. In the drawings, like reference numbers generally indicate identical, functionally similar, and/or structurally similar elements.

DETAILED DESCRIPTION

It is contemplated that systems, architectures, devices, methods, and processes of the claimed invention encompass variations and adaptations developed using information from the embodiments described herein. Adaptation and/or modification of the systems, architectures, devices, methods, and processes described herein may be performed, as contemplated by this description.

Throughout the description, where articles, devices, systems, and architectures are described as having, including, or comprising specific components, or where processes and methods are described as having, including, or comprising specific steps, it is contemplated that, additionally, there are articles, devices, systems, and architectures of the present invention that consist essentially of, or consist of, the recited components, and that there are processes and methods according to the present invention that consist essentially of, or consist of, the recited processing steps.

It should be understood that the order of steps or order for performing certain action is immaterial so long as the invention remains operable. Moreover, two or more steps or actions may be conducted simultaneously.

The mention herein of any publication, for example, in the Background section, is not an admission that the publication serves as prior art with respect to any of the claims presented herein. The Background section is presented for purposes of clarity and is not meant as a description of prior art with respect to any claim.

Documents are incorporated herein by reference as noted. Where there is any discrepancy in the meaning of a particular term, the meaning provided in the Definition section above is controlling.

Headers are provided for the convenience of the reader—the presence and/or placement of a header is not intended to limit the scope of the subject matter described herein.

i. Definitions

As used herein, "radionuclide" refers to a moiety comprising a radioactive isotope of at least one element. Exemplary suitable radionuclides include but are not limited to those described herein. In some embodiments, a radionuclide is one used in positron emission tomography (PET). In some embodiments, a radionuclide is one used in single-photon emission computed tomography (SPECT). In some embodiments, a non-limiting list of radionuclides includes ^{99m}Tc, ^{111}In, ^{64}Cu, ^{67}Ga, ^{68}Ga, ^{186}Re, ^{188}Re, ^{153}Sm, ^{177}Lu, ^{67}Cu, ^{123}I, ^{124}I, ^{125}I, ^{126}I, ^{131}I, ^{11}C, ^{13}N, ^{15}O, ^{18}F, ^{153}Sm, ^{166}Ho, ^{177}Lu, ^{149}Pm, ^{90}Y, ^{213}Bi, ^{103}Pd, ^{109}Pd, ^{159}Gd, ^{140}La, ^{198}Au, ^{199}Au, ^{169}Yb, ^{175}Yb, ^{165}Dy, ^{166}Dy, ^{105}Rh, ^{111}Ag, ^{89}Zr, ^{225}Ac, ^{82}Rb, ^{75}Br, ^{76}Br, ^{77}Br, ^{80}Br, ^{80m}Br, ^{82}Br, ^{83}Br, ^{211}At and ^{192}Ir.

As used herein, the term "radiopharmaceutical" refers to a compound comprising a radionuclide. In certain embodiments, radiopharmaceuticals are used for diagnostic and/or therapeutic purposes. In certain embodiments, radiopharmaceuticals include small molecules that are labeled with one or more radionuclide(s), antibodies that are labeled with one or more radionuclide(s), and antigen-binding portions of antibodies that are labeled with one or more radionuclide(s).

As used herein, "3D" or "three dimensional" with reference to an "image" means conveying information about three dimensions. A 3D image may be rendered as a dataset in three dimensions and/or may be displayed as a set of two-dimensional representations, or as a three-dimensional representation.

As used herein, an "image"—for example, a 3-D image of a subject—includes any visual representation, such as a photo, a video frame, streaming video, as well as any electronic, digital or mathematical analogue of a photo, video frame, or streaming video. Any apparatus described herein, in certain embodiments, includes a display for displaying an image or any other result produced by the processor. Any method described herein, in certain embodiments, includes a step of displaying an image or any other result produced via the method.

As used herein, a "subject" means a human or other mammal (e.g., rodent (mouse, rat, hamster), pig, cat, dog, horse, primate, rabbit, and the like).

As used herein, "administering" an agent means introducing a substance (e.g., an imaging agent) into a subject. In general, any route of administration may be utilized including, for example, parenteral (e.g., intravenous), oral, topical, subcutaneous, peritoneal, intraarterial, inhalation, vaginal, rectal, nasal, introduction into the cerebrospinal fluid, or instillation into body compartments.

As used herein, the terms "filter", and "filtering", as in a "filtering function" or a "filter", refer to a function that operates on localized portions of an input array (e.g., a multi-dimensional array) of data (e.g., image data, e.g., values computed by a layer of a CNN), referred to herein as "subpatches", computing, for a given subpatch, a response value. In general, a filter is applied in a sliding window fashion across the array to compute a plurality of response values for the array. In particular, for a given multidimensional array, a subpatch of the array can be a rectangular region of the array having a specific size (e.g., having the same number of dimensions as the array). For example, for a 6×3×3 array, a given 3×3×3 subpatch refers to a given 3×3×3 set of adjacent values (e.g., a neighborhood) of the array, such that there are five distinct 3×3×3 subpatches in the 6×3×3 array (each patch shifted one position over along the first dimension).

For example, a filtering function can compute, for a given subpatch of an array, a response value using the values of the subpatch. A filtering function can be applied in a sliding window fashion across an array, computing, for each of a plurality of subpatches of the array, a response value. The computed response values can be stored in an output array such that the positional correspondence between response values and the subpatches of the input array is maintained.

For example, at a first step, beginning with a subpatch in a corner of an input array, a filter can compute a first response value, and store the first response value in a corresponding corner of an output array. In certain embodiments, at a second step, the filter then computes a second response value for a second subpatch, shifted one position over along a specific dimension of the input array. The second response value can be stored in a corresponding position of the output array—that is, shifted one position over along a same dimension of the output array. The step of shifting position of the subpatch, computing a response value, and storing the response value in a corresponding position of the output array can be repeated for the full input array, along each dimension of the input array. In certain embodiments (e.g., a strided filtering approach), the subpatch for which the filter computes a response value is shifted more than one position at a time along a given dimension, such that response values are not computed for every possible subpatch of the input array.

As used herein, the term "convolutional neural network (CNN)" refers to a type of artificial neural network where at least one layer performs one or more filtering functions. As used herein, the term "convolution layer" refers to a layer of a CNN that receives as input an input array and computes an output array, wherein values of the output array are computed by applying one or more filters to the input array. In particular, in certain embodiments, a convolution layer receives as input an input array having n+1 dimensions and produces an output array also having n+1 dimensions. The first n dimensions of input and output arrays operated on by filtering layers of a CNN are referred to herein as "spatial dimensions". The (n+1)th dimension of the input is referred to herein as the "input channel" dimension. The size of the input channel dimension is referred to herein as the "number of input channels". The (n+1)th dimension of the output is referred to herein as the "output channel" dimension. The size of the input channel dimension is referred to herein as the "number of output channels".

In certain embodiments, a convolution layer computes response values by applying a filter that operates on subpatches that are smaller than the input array along the spatial dimensions, but extend across the full output channel dimension. For example, an $N \times M \times L \times K_0$ size input array, has three spatial dimensions and K_0 output channels. Filters of a convolution layer may operate on subpatches having sizes of $N_f \times M_f \times L_f \times K_0$, where $N_f \leq N$, $M_f \leq M$ and $L_f \leq L$. Often, a filter of a convolutional layer operates on subpatches having sizes where $N_f < N$, $M_f < M$ and/or $L_f < L$. For example, in certain embodiments, $N_f << N$, $M_f << M$ and/or $L_f << L$.

Accordingly, for each of one or more filters applied by a convolution layer, response values computed by a given filter are stored in a corresponding output channel. Accordingly, a convolution layer that receives an input array having n+1 dimensions computes an output array also having n+1 dimensions, wherein the (n+1)th dimension represents the

output channels corresponding to the one or more filters applied by the convolution layer. In this manner, an output array computed by a given convolution layer can be received as input by a subsequent convolution layer.

As used herein, the term "size" in reference to a filter of a convolution layer refers to a size along spatial dimensions of subpatches on which the filter operates (e.g., the subpatch size along the output channel dimension is taken as the full number of output channels). As used herein, the term "size", in reference to a convolution layer, as in "size of a convolution layer" refers to a size of filters of the convolution layer (e.g., each filter of the convolution layer having a same size). In certain embodiments, a filter of a convolution layer has a number of variable parameters that are determined via a machine learning training process. In certain embodiments, the number of parameters of a given filter equals the number of values in a subpatch that the given filter operates on. For example, a size $N_f \times M_f \times L_f$ filter that operates on an input array with K_0 output channels has $N_f \times M_f \times L_f \times K_0$ parameters. In certain embodiments, a filter is implemented as an array, and the response value determined by the filter for a given subpatch is computed as a dot product between the filter and the given subpatch.

As used herein, the term "fully convolutional neural network (FCNN)" refers to a CNN wherein each layer of the CNN is a convolution layer.

As used herein, the term "volume", as used in reference to an input or output of a layer of a CNN refers to an input array received or an output array computed by a CNN layer.

As used herein, the term "CNN module" refers to a computer implemented process that implements a specific CNN in order to determine, for a given input, such as an image (e.g., a 2D image; e.g., a 3D image) one or more output values. For example, a CNN module may receive as input a 3D image of a subject (e.g., a CT image; e.g., an MRI), and for each voxel of the image, determine a value that represents a likelihood that the voxel lies within a region of the 3D image that corresponds to a representation of a particular organ or tissue of the subject. A CNN module may be software and/or hardware. For example, a CNN module may be implemented entirely as software, or certain functions of a CNN module may be carried out via specialized hardware (e.g., via an application specific integrated circuit (ASIC)).

As used herein, the term "tissue" refers to bone (osseous tissue) as well as soft-tissue.

In certain embodiments, the approaches described herein can be used to segment and identify target tissue regions within a full body image of a subject. As used herein, the terms "full body" and "whole body" used (interchangeably) in the context of segmentation refer to approaches that evaluate a majority (e.g., greater than 50%) of a graphical representation of a subject's body in a 3D anatomical image to identify target tissue regions of interest. In certain embodiments, full body and whole body segmentation refers to identification of target tissue regions within at least an entire torso of a subject. In certain embodiments, portions of limbs are also included, along with a head of the subject.

A. Detecting and Assessing Cancer Status Via Nuclear Medicine Imaging and Automated Image Segmentation

Described herein are systems and methods that provide artificial intelligence (AI)-based segmentation technology that provides a basis for detecting, evaluating, and making predictions about cancer status of subjects. In particular, the AI-based segmentation techniques described herein allow for 3D representations of various tissue regions in medical images to be accurately and rapidly identified. The AI-based segmentation technologies described herein utilize machine learning techniques, such as Convolutional Neural Networks (CNNs) to automatically to identify a plurality of target 3D volumes of interest (VOIs) each corresponding to a specific target tissue region, such as one or more organs, portions of organs, particular bone(s), a skeletal region etc. Each identified 3D VOI may be represented via a segmentation mask. The multiple segmentation masks, identifying multiple target tissue regions across a patient's body, can be stitched together to form a segmentation map. The segmentation map, and/or various segmentation masks that it comprises, may be used compute various quantities from medical images, such as useful indices that serve as measures and/or predictions of cancer status, progression, and response to treatment. Segmentation maps and masks may also be displayed, for example as a graphical representation overlaid on a medical image to guide physicians and other medical practitioners.

In certain embodiments, AI-based segmentation is performed using an anatomical image that provides detailed structural information about locations and extent of tissue within a subject's body. Examples of anatomical images include, without limitation, x-ray computed tomography (CT) images, magnetic resonance images (MRI), and ultrasound. Image contrast in anatomical images is a function of physical properties of underlying tissue, such as density, water and fat content. As described in further detail herein, the AI-based segmentation techniques of the present disclosure analyze contrast variations and patterns in anatomical image to identify target 3D VOIs that correspond to different specific target tissue regions.

In certain embodiments, structural information and identified target VOIs from anatomical images are combined with and/or used to analyze images obtained via functional imaging modalities. Functional images reflect physiological properties and activity in a subject. They are often acquired using probes and have intensity variations that reflect a spatial distribution of the probes within an imaged portion of a subject. For example, nuclear medicine images (e.g., PET scans; e.g., SPECT scans; e.g., whole-body scans; e.g. composite PET-CT images; e.g., composite SPECT-CT images) detect radiation emitted from the radionuclides of radiopharmaceuticals to form an image. The distribution of a particular radiopharmaceutical within a patient may be determined by biological mechanisms such as blood flow or perfusion, as well as by specific enzymatic or receptor binding interactions. Different radiopharmaceuticals may be designed to take advantage of different biological mechanisms and/or particular specific enzymatic or receptor binding interactions and thus, when administered to a patient, selectively concentrate within particular types of tissue and/or regions within the patient. Greater amounts of radiation are emitted from regions within the patient that have higher concentrations of radiopharmaceutical than other regions, such that these regions appear brighter in nuclear medicine images. Accordingly, intensity variations within a nuclear medicine image can be used to map the distribution of radiopharmaceutical within the patient. This mapped distribution of radiopharmaceutical within the patient can be used to, for example, infer the presence of cancerous tissue within various regions of the patient's body.

Transferring a segmentation map to a functional image (e.g., a nuclear medicine image, such as a PET image or a SPECT image) provides valuable context for evaluating and

deriving meaning from intensity fluctuations in the functional image. In particular, it allows for regions of the functional image to be identified as corresponding to particular tissue regions of the subject. In this manner, intensity values and fluctuations in and across voxels within a particular region can thus be understood as originating from underlying accumulation of a radiopharmaceutical in a specific tissue region (e.g., organ or bone) of the subject.

As described in further detail herein, this anatomical context serves a variety of uses. For example, it allows for measures of radiopharmaceutical uptake in various specific target organs and tissue regions, such as prostate, lymph nodes, and bone, to be assessed, and used as an indicator of presence of cancerous tissue therein. Identifying a what particular region intensities of a functional image are associated with also allows them to be evaluated in proper context. For example intensities of a certain value, if associated with a prostate region, may be more likely to be indicative of cancer than intensities of the same value, when found within another organ, such as a bladder or kidney. In certain embodiments, reference regions are identified and used to compute normalization values and levels on a scale to which intensities in other regions are compared to evaluate a cancer status. Background regions, to either be excluded from the image or used to correct for artifacts may also be identified.

Accordingly, the AI-based segmentation approaches described herein can serve as a platform on which a variety of tools and techniques for detecting, evaluating, and predicting cancer status for patients can be built. Moreover, since the AI-based segmentation tools described herein can identify a variety of important tissue regions across an entire body of a patient, and then transfer those identifications (e.g., segmentation maps) from anatomical images to various functional images, they can be used as a building block for analysis techniques based on a variety of different imaging methods that obtain contrast via a variety of different radiopharmaceuticals.

FIGS. **1-3** illustrate this concept. In particular, FIG. **1** is a schematic illustrating how various anatomical and functional imaging modalities can be integrated in the context of a platform agnostic AI-based segmentation technology. As illustrated in FIG. **1**, the AI-segmentation platform described herein can be used as a basis for analysis of a variety of images, such as anatomical CT image themselves, 18NaF images, C-11 images, Ga-68 images, FDG image, and PyL™ images. FIG. **2** shows results of an example segmentation performed on a skeleton of a subject, with different specific bones identified by different colors. The segmentation shown in FIG. **2**, performed using a CT image, can be transferred to a functional image in order to identify 3D volumes in the functional image that correspond to the target VOIs identified within the CT image. Other VOIs, such as soft-tissue, may also be identified and used to identify corresponding 3D volumes in a functional image. For example, FIG. **3** is a block flow diagram illustrating how segmentation of various soft-tissue and bone regions based on an anatomical image (e.g., a CT image) can be used and mapped to images obtained via various functional imaging modalities using various probes (e.g., ^{99m}Tc-MIP-1404, ^{18}F-PyL, ^{68}Ga-PSMA-11, ^{18}F—NaF, ^{11}C-Choline, [18F]FDG, [18F]FACBC, etc.) to perform image based diagnosis and assessment of disease progression, state, and the like. As shown in FIG. **3**, the full body segmentation techniques described herein can serve as a platform that a variety of application specific image analysis techniques that utilize different functional imaging modalities and probes can leverage and be built upon.

FIG. **4** is a diagram showing how artificial intelligence-based image analysis 400 can be performed to classify and locate lesions, as well as quantify positive lesions, e.g., for assessing cancer state in a subject. As shown in FIG. **4**, a machine learning module **402**, such as a convolutional neural network (CNN), receives contextual anatomical information (e.g., a CT image or other anatomical imaging modality) 404 along with functional information (e.g., a functional image, such as a SPECT, PET, or other functional image obtained using a particular imaging probe) 406. The machine learning module **402** then uses the functional 406 and anatomical 404 information to identify, classify, and/or quantify cancerous lesions in a subject 410. The machine learning module **402** may also leverage additional information 408, such as subject demographic data (e.g., age, weight, etc.) and other diagnostic test results (e.g., a biopsy, Gleason score, genetic testing results, a prostate specific antigen (PSA) test result), clinical treatment(s) (e.g., external beam radiation, brachytherapy, prostatectomy, antiandrogens, immunotherapy (e.g., Provenge), chemotherapy, etc.) as input and base the classification, identification, and/or quantification of cancerous lesions on this additional information as well.

FIG. **5** is a block flow diagram showing an example process **500** for performing segmentation to identify a plurality of target tissue regions. As shown in FIG. **5**, a machine learning module receives a 3D anatomical image (e.g., a full body image) as input **502**, and identifies, for each of a plurality of target tissue region, a target volume comprising a graphical representation of the target tissue region within the 3D anatomical image **504**. The target volumes are stitched together **506** to form a segmentation map **510** that comprises a plurality of segmentation masks **512**, with each segmentation mask representing an identified target volume. The segmentation map **510** can be stored and/or provided for display and/or further processing **508**.

i. Image Segmentation Using Convolutional Neural Networks (CNNs)

In certain embodiments, the AI-based image segmentation approaches described herein utilize machine learning techniques, such as CNNs to perform segmentation. As described herein, one or more machine learning modules may be used to perform intermediate analysis and processing of images, and ultimately identify target VOIs.

In certain embodiments, the AI-based image segmentation described herein utilizes a two-step approach to identify one or more of the 3D target VOIs representing target tissue regions of interest in an anatomical image. In this two-step approach, an initial volume of interest (VOI) that comprises one or more of the target VOIs is first identified. The initial VOI may be identified using a first module, referred to as a localization module. The localization module may be a first machine learning module, such as a first Convolutional Neural Network (CNN) module. Once the initial VOI is identified, a second module, referred to as a segmentation module [e.g., that implements a second machine learning network (e.g., a second CNN) to perform fine segmentation], is used to identify one or more target VOIs within the initial VOL This approach is advantageous as allows the segmentation module to operate on a standardized input, of manageable size, without regard to variations in dimensions and boundaries of the original anatomical image received. This

two-step approach is especially useful for performing accurate, finely resolved segmentation of tissue regions within a large image, such as a full body scan. The localization module may perform a rough analysis, such as by performing a coarse segmentation, to identify the initial VOI. Freed from having to accommodate varying image sizes, and analyze an entire image, the segmentation module can devote resources to performing fine segmentation to accurately identify the target VOIs within the initial VOI.

Moreover, as described in further detail herein, for example in Example 1, to identify a set of target VOIs spread out across an entire body of a subject, multiple initial VOIs can be identified in order to partition a whole body image into multiple manageable initial VOIs, each comprising a subset of the desired target VOIs to be identified. The partitioning of a whole body image into multiple initial VOIs can be performed using a single localization module, such as a machine learning module that performs a coarse segmentation to identify general anatomical regions such as an upper body, a lower body, a spine, and a pelvic region. In certain embodiments, multiple localization modules (e.g., each tasked with identifying one or more initial VOIs) may be used. For each identified initial VOI, one or more segmentation modules may then be used to perform fine segmentation and identify the one or more desired target VOIs within the initial VOI.

Various localization and segmentation modules may be combined and implemented as a single module and/or a single software application, or may be implemented separately, e.g., as separate software applications.

A number of different approaches may be used by a localization module to identify a particular initial VOL For example, in one approach, the localization module may implement a CNN that receives a grayscale CT image (e.g., a single input channel) as input and outputs coordinates of opposite corners of a rectangular VOI (e.g., a bounding box). In another approach, the localization module may implement a CNN that receives two input channels: (i) a grayscale CT image, and (ii) a pre-processed version of the CT image. The pre-processed version of the CT image may be a thresholded version of the CT image, wherein the thresholding provides a rough identification of the initial VOI to be identified. The CNN is trained to analyze both these input channels in order to output coordinates representing opposite corners of a rectangular initial VOI (e.g., a bounding box).

In a third approach, in order to identify a particular initial VOI comprising one or more specific target VOIs, the localization module performs a coarse segmentation to roughly identify the specific target VOIs. In this way, the localization module is essentially a rough version of the segmentation modules used to identify the specific target VOIs within the particular initial VOL A rectangular initial VOI is then generated using the coarsely identified specific target VOIs (e.g., by drawing the smallest box that fits them, or maybe adding some buffer distance). A distinction here is that the output of the localization module in this case is not merely coordinates of cuboid vertices. In this approach, likelihood values are automatically determined for each voxel of the image that give the likelihood as to how the voxel is classified—e.g., whether the voxel is a particular initial VOI, or background, for example.

In certain embodiments, voxel classifications performed by the machine learning modules may be refined via an iterative process in order to mitigate noise in the classification process. In particular, in certain embodiments, a machine learning module such as a CNN module receives an entire image, or portion thereof as input, and outputs, for each particular voxel, a label classifying the particular voxel as (i) one of a set of pre-defined classes corresponding to anatomical regions or target tissue regions, or (ii) background. For example, a localization module trained to identify initial VOIs corresponding to a spine, a pelvic region, and a left and right upper body may label each voxel as 1, 2, 3, or 4 for spine, pelvic region, left upper body, and right upper body, respectively, or 0 for background.

A segmentation module that identifies one or more target tissue regions within a particular initial VOI may receive the particular initial VOI as input, and output an integer label for each voxel, with the integer label identifying that voxel as corresponding to one of the particular target tissue regions, or background. For example, a segmentation module that identifies different vertebrae may receive as input an initial VOI corresponding to the spine, and label each voxel in the initial VOI with an integer corresponding to a particular vertebra (e.g., 1 for a first lumbar vertebra, 2 for a second lumbar vertebra, 3 for a third lumbar vertebra, etc. with other integer labels for other bones).

The classification performed by machine learning modules as described above, may produce noisy results, with certain isolated voxels having different labels than their surroundings. For example, a CNN module may produce an output wherein a majority of voxels within a large volume are assigned a first label, with isolated voxels and/or small groups of voxels assigned different, e.g., second or third labels, identifying them as corresponding to different anatomical regions than their neighbors. Often such isolated voxels and/or islands appear on the edges of a large uniformly labeled region.

These small non-uniformities correspond to noise in the classification process, and can be removed via an iterative procedure as follows. First, for each label representing (i) a particular anatomical region or target tissue region, or (ii) background, an associated largest connected component of labeled voxels is identified. Second, for each particular label, differently labeled isolated voxels and/or voxel islands that are immediately adjacent to voxels of the largest connected component associated with the particular label are identified and re-assigned the particular label. In certain embodiments, in a third step, any remaining isolated differently labeled voxel islands can then be removed. In a fourth step, holes in segmentation regions—voxels that are labeled as background but are completely encapsulated by non-background labeled voxels are filled (e.g., by assigning voxels of the holes a label of the non-background region that encapsulates them). The second through fourth steps, in which isolated voxels and/or voxel islands are relabeled based on their surroundings are repeated until convergence—i.e., no change from on iteration to the next. This approach reduces and/or eliminates isolated voxels of a different label from their surrounding thereby mitigating noise in the classification process.

These various approaches for identifying initial VOIs may be used alone or in combination to identify multiple initial VOIs within an anatomical image of a subject. Once one or more initial VOIs are identified, one or more target VOIs within each initial VOI may be identified. For example, PCT Publication WO2019/136349, the content of which is hereby incorporated by reference in its entirety, provides further detail on how a single initial VOI corresponding to a pelvic region may be identified within a CT image, and how fine segmentation may be performed to identify target VOIs corresponding to organs such as a prostate, bladder, gluteal muscles, as well as various pelvic bones, such as a sacrum,

coccyx, and left and right hip bones, may be identified. The approaches described herein, and in particular in Examples 1-4, show how multiple initial VOIs can be identified and used to identify a plurality of target VOIs across a subject's body, thereby providing for accurate whole-body image segmentation that can serve as a basis for detection and assessment of cancer status, progression, and response to treatment at localized stages in various organs and tissue regions, as well as metastatic stages where it is present in multiple regions in a patient's body.

ii. Providing Anatomical Context to 3D Functional Images

Segmentation maps generated by automated AI-based analysis of anatomical images can be transferred to 3D functional images in order to identify, within the 3D functional image, 3D volumes corresponding to the target VOIs identified in the anatomical image. In particular, in certain embodiments, the individual segmentation masks (of the segmentation map) are mapped from the 3D anatomical image to the 3D functional image. The 3D volumes identified within the 3D functional image can be used for a variety of purposes in analyzing images for assessment of cancer status.

Certain identified 3D volumes and corresponding target VOIs correspond to tissue regions where cancer is suspected and/or may occur. Such regions may include, for example, a prostate, breast tissue, lung(s), brain, lymph nodes, and bone. Other regions may also be evaluated. Certain regions, such as prostate, breast, and lungs, are relevant for detecting cancer at earlier, localized stages, while others, such as lymph nodes and bone are relevant for assessing metastatic cancer. Since intensities of functional images, such as PET and SPECT images map spatial distribution of radiopharmaceutical accumulation in a patient's body, by accurately identifying specific 3D volumes in functional images that correspond to specific tissue regions intensities of voxels within those 3D volumes can be used determine a measure of uptake of radiopharmaceutical probes within the specific tissue regions to which they correspond. Since radiopharmaceutical probes can be designed to selectively accumulate in cancerous tissue (e.g., via enhanced affinity to biomolecules that are overexpressed in cancerous tissue, such as prostate specific membrane antigen (PSMA)), detecting and quantifying uptake of particular probes in certain target tissue regions and organs is of interest is indicative of and/or can be used to determining a cancer status for the subject. For example, as described in PCT Publication WO2019/136349, the content of which is hereby incorporated by reference in its entirety, assessing 1404 uptake in a prostate volume can be used to determine a prostate cancer status for a subject. Other probes may be used to assess metastatic cancer, present in a wide variety of other tissue regions, including bones. For example, Examples 2 to 6 describe segmentation used to identify accumulation of PyL™ in cancerous lesions throughout a patient's body.

Accordingly, in certain embodiments, segmentation performed on an anatomical image, such as CT image, is transferred (e.g., mapped) to a co-registered functional image, such as a PET or SPECT image, allowing for specific tissue volumes of interest within the functional image that correspond to particular tissue regions of interest to be identified. Accumulation of radiopharmaceutical within those particular tissue regions can then be quantified based on intensities of functional image voxels that lie within the specific tissue volumes of interest.

A variety of approaches can be used to analyze voxel intensities in functional images. For example, an average, a median, a total, a maximum, etc. intensity within a specific volume may be computed and used for quantification. This computed value may then be compared with other values, e.g., computed for other tissue regions (e.g., for normalization), and used to assign a cancer status to a patient (e.g., based on comparison with one or more predetermined threshold values). In certain embodiments, localized regions of high intensity—referred to as hotspots, are identified within particular 3D volumes. As described in further detail in section B, below, these localized hotspots can be identified as representing cancerous lesions, and used to determine cancer status of a subject. In certain embodiments, machine learning approaches can be used. For example, intensities of functional image voxels lying within one or more specific tissue volumes of interest can be used as inputs to machine learning modules that compute a risk index that can, in itself be used to quantify a risk of cancer, metastasis, or recurrence of cancer, etc. and/or compared with reference values, such as thresholds, to assign a particular cancer status.

In certain embodiments, in addition to identifying specific tissue regions in which cancerous tissue is may be present, e.g., in order to determine the presence and/or the state of cancer therein, other additional tissue regions may be identified. Such additional tissue regions may correspond to background regions in which a particular radiopharmaceutical probe accumulates under normal circumstances, without lesions necessarily being present.

In certain embodiments, identified background regions are used to normalize voxel intensities so as to standardize intensity values from image to image. For example, as described in PCT Publication WO2019/136349, the content of which is hereby incorporated by reference in its entirety, gluteal muscles can be identified and uptake in them can be used to normalize intensities in SPECT images obtained following administration of 1404.

Identification of certain background regions can also be used to account for high probe accumulation levels in these regions. In certain embodiments, certain background regions are identified and excluded from analysis. For example, as described in Example 3, certain probes, such as PyL™ may accumulate in certain background regions under normal circumstances, absent any cancerous lesions or tissue within those regions. Accordingly, these regions may be identified and excluded from, e.g., hotspot detection analysis. Examples of such regions include kidneys, duodenum, small intestines, spleen, liver, pancreas, stomach, adrenal gland, rectum, and testes.

In certain embodiments, identifying 3D volumes in a functional image that correspond to background regions can be used to correct for intensity bleed effects, where high accumulation of radiopharmaceutical in a particular region may produce high intensities in the functional image not only in the 3D volume that corresponds to the particular region, but also in its neighborhood. Such intensity bleed into other regions of functional images can mask useful signal. For example, radiopharmaceutical typically accumulates in high amounts in a patient's bladder. When imaged via a functional imaging modality, this high accumulation in the bladder may, via scattering effects, contribute to intensities in 3D volumes corresponding to tissue regions outside the bladder, such as a prostate. Accordingly, accounting for this intensity bleed or "cross-talk" can improve the accuracy with which intensities in a 3D functional image are used to measure underlying radiopharmaceutical uptake.

In certain embodiments, the 3D volume corresponding to the particular background region producing the intensity bleed is dilated. The dilated background region may be excluded from analysis, so as to avoid using intensities of regions directly adjacent to the background region to determine uptake metrics or identification of hotspots.

In certain embodiments, a suppression method which models the profile of the functional intensities may also be used to adjust the intensity levels in neighboring regions to correct for the intensity bleed. In this approach, for a particular background region that produces intensity bleed, an amount of suppression, that is, intensity bleed, to remove from a particular voxel of the functional image is dependent on a distance from that voxel to a high intensity core region within a particular 3D background volume corresponding to the particular background region. The high intensity core region may be determined as a region comprising voxels having intensities above a predetermined value, or within a specific fraction of a maximum intensity in a specific region of the functional image.

In certain embodiments, this suppression is utilized if a maximum functional image intensity within a 3D volume identified as corresponding to the particular background region is more than a specific multiplier value times a determined background intensity value. Background intensity values may be determined based on intensities of voxels of the 3D functional image corresponding to specific reference volumes corresponding to specific tissue regions, such as gluteal muscles. The suppression approach may be applied to a sub-region of the 3D functional image in the vicinity of the particular background region producing intensity bleed. For example, it may be applied to a rectangular sub-region encompassing the particular region, plus a predetermined margin.

In certain embodiments, one or more intensity bleed functions are determined to perform suppression and thereby correct intensities of voxels of the 3D functional image for bleed (e.g., cross-talk). For example, the 3D functional image may be cropped to the aforementioned rectangular sub-region encompassing the particular region plus the predetermined margin. A determined background intensity value can be subtracted from intensities of voxels within the cropped image region. Sample intensities can then be collected to determine how intensity originating from radiopharmaceutical uptake within the particular background region decreases as one moves away from the particular background 3D volume corresponding to the particular background region. Samples beginning at an extreme top, right, left, and bottom, and then moving outwards up, right, left, and down, respectively, may be used. Other directions are also possible. The sampled intensities provide curves (e.g., sets of sampled intensity data points) showing intensity decrease from the high intensity core. Template functions, such as n-th degree polynomials can be fit to these sampled curves and used to compute intensity values to be used as correction factors in the vicinity of the particular 3D background volume.

For example, PCT Publication WO2019/136349, the content of which is hereby incorporated by reference in its entirety describes how identification of a bladder region can be used to adjust prostate voxel intensities for intensity bleed through due to high accumulation in the bladder in 1404-SPECT images. In certain embodiments, similar approaches can be used for other images obtained with other probes, which may accumulate in the bladder, and/or other regions (e.g., the liver, the kidneys, etc.).

In certain embodiments, the segmentation approaches described herein assume that the 3D anatomical image includes certain anatomical regions. For example, an embodiment of the systems and methods described herein may assume that its input anatomical images always include a pelvic region, and automatically attempts to segment the pelvic region. The systems and methods described herein may also, for other anatomical regions, only segment such regions if they are included in the anatomical image input, for example first performing a determination as to whether they are present.

Approaches for performing whole body segmentation to identify target tissue regions corresponding to bone and/or soft-tissue (e.g., organs) are described in further detail in Examples 1, 2, 3, and 4 below. Also described are approaches for using such whole body segmentation for assessment of disease state, in particular, cancer in a patient.

B. Hotspot and Lesion Detection

In certain embodiments, instead of, or in addition to, quantifying overall uptake in a particular volume within the functional image, localized hotspots (localized regions of relatively high intensity) are detected. In certain embodiments, hotspots are detected via a thresholding approach—by comparing intensities of voxels within the functional image to one or more thresholds values. Groupings of voxels with intensities above a threshold may be detected as hotspots. A single, global, threshold value may be used, or, in certain embodiments, multiple region specific thresholds may also be used. For example, segmentation of the co-registered anatomical image can be used to set different thresholds for different tissue regions used for hotspot detection. Segmentation of the co-registered image can also be used, as described herein, to remove effects of background signal, thereby facilitating hotspot detection (e.g., if a global threshold and/or multiple regional thresholds are used).

In certain embodiments, hotspots can additionally be detected using blob detection techniques. One approach is to use the Difference of Gaussians approach, where a PET image is filtered through a combination of high and low-pass filters approximated by Gaussian kernels. The filters reduce background noise and are invariant to changes in background levels in the different regions of the image (e.g. the thorax might have significantly higher background levels due to significant uptake in liver and kidneys compared to the pelvic region). This cascaded high/low-pass filter approach would allow for hotspot extraction without the utilization of fixed thresholds, but could instead identify local changes in the PET intensities. Another approach is to employ a Laplacian of a Gaussian blob detection method. The Laplacian of a Gaussian approach is a method for detecting edges in images using Laplacian and Gaussian filter kernels. By using different sizes of kernels, edges of structures of different sizes are detected. Choosing appropriate kernel sizes allows the method to detect structures that have properties common to lesions. The described approaches may be used in a stand-alone fashion where only one of the techniques is used for all regions of interest, or they may be used simultaneously, where different methods can be employed for different tissue regions as identified by the semantic segmentation of the co-registered anatomical image in conjunction with either a single global threshold or multiple local thresholds.

FIG. **5**B shows an example process **520** for using the segmentation approaches described herein to detect hotspots

representing cancerous lesions. In a first step, a 3D anatomical image is received **522**. A one or more target VOIs corresponding to particular target tissue regions are identified within the 3D anatomical image **524** and the identifications of the target VOIs are stitched together **526** to create a segmentation map **534** comprising a plurality of segmentation masks **536**. Each segmentation mask of the segmentation map represents a particular target VOL Next, a 3D functional image (e.g., a PET image) is received **528** and the segmentation map is transferred to the 3D functional image to identify, for each target VOI, a corresponding 3D volume in the 3D functional image **530**. The identified 3D volumes are then used to detect **532**, within the 3D functional image, one or more hotspots corresponding to localized regions of high intensity relative to their surroundings. In particular, one or more specific 3D volumes may correspond to specific tissue regions where cancerous lesions may form, and be analyzed to detect hotspots therein. Other 3D volumes may be used to perform background correction, or intentionally be excluded from the hotspot detection process. As described in further detail herein, still other volumes may be relevant in that they are used as reference volumes for computing useful indices that can be assigned to hotspots in order to score them, e.g., to indicate risk/severity of the underlying lesions they represent.

Hotspots may also be classified following their initial detection, e.g., as cancerous or not, and/or assigned likelihood values representing their likelihood of being a metastases. Hotspot classification may be performed by extracting hotspot features (e.g., metrics that describe characteristics of a particular hotspot) and using the extracted hotspot features as a basis for classification, e.g., via a machine learning module.

In certain embodiments, hotspot classification can also be performed without the use of machine learning. In such embodiments, anatomical knowledge can be combined with information relating to the shape and location of a detected hotspot to classify the hotspot as either a cancerous lesion or noise. For example, if a detected hotspot is located on the edge of a rib facing the liver and the detected peak is not the global maximum in the area surrounding the hotspot, it is possible to estimate whether the hotspot is a tumor or not based on the given anatomical and spatial information. The segmentation of the co-registered anatomical image can additionally be used to create intensity models of background tissue regions known to not contain cancerous cells, but where exceptionally high functional image voxel intensities are common. Such background regions may cause intensity bleed outside of the boundaries of the background region itself and impact the neighboring regions where cancerous lesions might exist. Profiles of the intensity levels can be estimated and used to subtract the estimated additional intensity levels present in neighboring tissue regions harboring cancerous lesions to allow a more robust hotspot detection.

Hotspots representing lesions may be used to determine risk indices that provide an indication of disease presence and/or state (e.g., a cancer status, similar to a Gleason score) for a patient. For example, metrics such as number of hotspots, a total summed intensity of identified hotspots, area fraction of a particular body part or region (e.g., skeleton) occupied by hotspots, and the like, may be used themselves as, and/or in calculation of, such risk indices. In certain embodiments, regions identified via the segmentation approaches described herein may be used in computation of risk indices, for example in computing metrics such as area fractions. Examples of approaches for using identified hotspots to compute risk indices is provided herein, in Examples 5 and 7.

C. Example CNN-Based Whole Body Segmentation and Lesion Detection Approaches

The following examples demonstrate use of the AI-based segmentation and hotspot detection approaches described herein for whole-body segmentation, detecting cancerous lesions, and determining useful metrics for evaluating a cancer status of a subject.

i. Example 1—CNN Based Whole Body Segmentation

Example 1 describes an example approach for whole body segmentation. The implementation in this example uses five neural networks to segment bones within an entire torso. A first neural network is used to roughly localize different regions of the body. The results are used to divide the body into four regions. In each of these regions, a corresponding neural network is then used to perform segmentation into distinct bones. The results from all four regions are then combined into a finished result (e.g., a final segmentation map).

This approach is related to the two-step 'bounding box' approach described herein, wherein a first machine learning module (e.g., a localization module) is used to roughly localize an initial volume of interest (VOI) corresponding to an anatomical region that comprises one or more particular target tissue regions (e.g., a prostate). A second machine learning module (e.g., a segmentation module) then performs a fine segmentation within the initial VOI to identify target volume(s) corresponding to the target tissue region(s) within the initial VOL In this case, for whole body segmentation, the first machine learning module (localization module) identifies multiple initial VOIs, each corresponding to a different anatomical region. Then, for each anatomical region, a corresponding secondary machine learning module (segmentation module) identifies one or more target volumes, each representing a particular target tissue region. The machine learning modules (e.g., neural networks) may be implemented as separate modules, or certain machine learning networks may be combined. For example, each secondary, segmentation network may be implemented as a separate module, or within a single module.

Accordingly, in this example, the first module (localization) is used for identifying the anatomical regions within the CT; that is, to find volumes of interest where networks of the second module can be applied to generate the segmentation map that is used for further analysis. The networks in the second module work with a full-resolution CT image, while the localization network works in low resolution, using a sub-sampled version of the CT image.

Three example versions of CNN networks used in software implementing whole-body segmentation in accordance with the approaches. Versions 1 and 2 segment 49 bones, and version 2 segments 49 bones and 8 soft-tissue regions.

CNN-Based Segmentation Platform Example Version 1

In a first example version of a CNN network used for whole body segmentation, the first machine learning module (localization module) in this example is referred to as "coarse-seg", and was trained to identify 49 bones in sub-sampled CT images (a sub-sampling factor of 4 along each dimension). The localization module was used to differentiate regions of the body in to a pelvic region, a spine, a left

upper body, and a right upper body. The four fine segmentation networks were as follows:

"fine-seg-pelvic": Trained to identify the left and right ilium and the sacrum and coccyx;

"fine-seg-spine": Trained to identify 12 thoracic vertebrae, 5 lumbar vertebrae, and the sternum;

"fine-seg-left-upper-body": Trained to identify 12 ribs on the left side of the body, the left scapula, and left clavicle; and

"fine-seg-right-upper-body": Trained to identify 12 ribs on the right side of the body, the right scapula, and right clavicle.

The input image sizes for each network were as follows:

TABLE 1

Input image sizes for five neural networks.

Network Name	Input image size (no. slices, no. rows, no. columns)
coarse-seg	(81, 70, 104)
fine-seg-pelvic	(93, 146, 253)
fine-seg-spine	(194, 204, 94)
fine-seg-left-upper-body	(158, 187, 144)
fine-seg-right-upper-body	(158, 191, 146)

While the coarse-seg network of the localization module received, as an input image, an 3D anatomical image representing a large physical volume and comprising a majority of the subject's body, the actual number of voxels in its input image was lower than for the other networks due to the factor of 4 sub-sampling. The number of voxels and size of the input image to the localization module was also reduced by cropping (removing) regions of the image that did not include graphical representations of tissue, but instead represent air. Removing these voxels as a pre-processing step further reduced the size of the image input to the localization module (see e.g., first two columns of Table 4 below). Reducing the size of the image input to the localization module via sub-sampling allows the coarse-seg network to trade resolution of the image on which it operates for additional filters, which allow it to e.g., account for variability in images it receives and perform more accurate and robust coarse segmentation to identify the different initial volumes of interest.

The number of filters and parameters used in each neural network are listed in Tables 2-4, below:

TABLE 2

Number of convolutional filters in five neural networks.

Network Name	Total Number of Filters	Number of Filters in First Layer
coarse-seg	4096 + 49 (49 classes)	32
fine-seg-pelvic	4096 + 3	32
fine-seg-spine	2048 + 18	16
fine-seg-left-upper-body	2048 + 14	16
fine-seg-right-upper-body	2048 + 14	16

TABLE 3

Number of parameters in five neural networks

Network Name	Total params.	No. trainable params.	No. non-trainable params.
coarse-seg	5,881,978	5,878,678	3,300
fine-seg-pelvic	5,880,276	5,877,068	3,208
fine-seg-spine	1,472,815	1,471,177	1,638
fine-seg-left-upper-body	1,472,731	1,471,101	1,630
fine-seg-right-upper-body	1,472,731	1,471,101	1,630

Table 4 below also shows a variability in input image size for the raw data and five neural networks used in this example. As shown in the table, variability in input image size for the four secondary, fine segmentation networks is less than that for the first, localization network since the identification of the initial VOIs produces a more standardized input for the secondary machine learning modules.

TABLE 4

Input image size for raw data and five neural networks.

	Raw data	Coarse-seg (cropped by air)	Fine-seg-pelvic (cropped by coarse)	Fine-seg-spine (cropped by coarse)	Fine-seg-left-upper-body (cropped by coarse)	Fine-seg-right-upper-body (cropped by coarse)
rows mean px	512	390	121	151	126	129
rows std px	0	39	7	19	20	21
rows min px	512	255	97	107	72	88
rows max px	512	399	136	189	170	188
rows min mm	700	308	133	146	98	120
rows max mm	700	546	186	258	232	242
columns mean px	512	399	207	67	112	113
columns std px	0	61	14	10	13	15
columns min px	512	311	155	45	84	72
columns max px	512	512	236	130	164	215
columns min mm	700	425	212	62	115	98
columns max mm	700	700	322	178	224	294
slices mean px	342	340	74	158	110	111
slices std px	99	95	6	12	11	12
slices min px	274	274	48	125	85	85

TABLE 4-continued

Input image size for raw data and five neural networks.

	Raw data	Coarse-seg (cropped by air)	Fine-seg-pelvic (cropped by coarse)	Fine-seg-spine (cropped by coarse)	Fine-seg-left-upper-body (cropped by coarse)	Fine-seg-right-upper-body (cropped by coarse)
slices max px	624	624	92	208	136	140
slices min mm	822	822	144	375	255	255
slices max mm	1872	1872	276	624	408	420

CNN-Based Segmentation Platform Example Version 2

An updated, second, example version of the CNN whole-body segmentation system as described above in this example included adjustments to input image sizes, number of convolutional filters, and parameters used in the neural networks used to perform the segmentation. Tables 5, 6, and 7, as seen below, show updated values for the various parameters used in the five neural networks. Table 5 shows updated values for the input image sizes shown in Table 1, Table 6 shows updated values for the number of convolutional filters for the neural networks shown in Table 2, and Table 7 shows updated values for the number of parameters used by the neural networks shown in Table 3.

TABLE 5

Updated values for input image sizes for five neural networks.

Network Name	Input image size (no. slices, no. rows, no. columns)
coarse-seg	(81, 77, 99)
fine-seg-pelvic	(92, 144, 251)
fine-seg-spine	(192, 183, 115)
fine-seg-left-upper-body	(154, 171, 140)
fine-seg-right-upper-body	(154, 170, 140)

TABLE 6

Updated values for number of convolutional filters in five neural networks.

Network Name	Total Number of Filters	Number of Filters in First Layer
coarse-seg	4096 + 49 (49 classes)	32
fine-seg-pelvic	3328 + 3	26
fine-seg-spine	2048 + 18	16
fine-seg-left-upper-body	2048 + 14	16
fine-seg-right-upper-body	2048 + 14	16

TABLE 7

Updated values for number of parameters in five neural networks

Network Name	Total params.	No. trainable params.	No. non-trainable params.
coarse-seg	5,882,423	5,879,132	3,300
fine-seg-pelvic	3,881,200	3,883,812	2,612
fine-seg-spine	1,472,815	1,471,177	1,638
fine-seg-left-upper-body	1,472,731	1,471,101	1,630
fine-seg-right-upper-body	1,472,731	1,471,101	1,630

CNN-Based Segmentation Platform Example Version 3

Another, 3rd, example version of the CNN whole body segmentation approach was used to segment soft-tissue regions as well as bones. As described herein, this 3rd version included two coarse segmentation modules, which were used in parallel, referred to herein as "coarse-seg-02" and "coarse-seg-03".

The "coarse-seg-02" module was trained to identify 49 bones in sub-sampled CT images. The "coarse-seg-03" module was trained to identify 49 bones and the liver, in sub-sampled CT images. The "coarse-seg-02" module outperformed the "coarse-seg-03" module for localization of bones and, to take advantage of the benefits of each module, both were used in parallel, to identify initial volumes of interest (e.g., "bounding boxes") for different fine segmentation networks. In particular, in the 3rd version, seven fine segmentation networks were used. Six out of the seven fine segmentation networks used "coarse-seg-02" for initial volume of interest identification and a seventh, "fine-seg-abdomen", used "coarse-seg-03" for the initial volume of interest identification.

The seven fine segmentation networks for this 3rd example version of the CNN whole-body segmentation system are as follows:

- "fine-seg-abdomen": Trained to identify the liver, left and right kidney, and gallbladder;
- "fine-seg-left-lung": Trained to identify the left lung;
- "fine-seg-right-lung": Trained to identify the right lung
- "fine-seg-pelvic-region-mixed": Trained to identify the left and right ilium, the prostate, the urinary bladder, and the sacrum and coccyx;
- "fine-seg-spine-bone": Trained to identify 12 thoracic vertebrae, 5 lumbar vertebrae, and the sternum;
- "fine-seg-left-upper-body-bone": Trained to identify 12 ribs on the left side of the body, the left scapula, and left clavicle; and
- "fine-seg-right-upper-body-bone": Trained to identify 12 ribs on the right side of the body, the right scapula, and right clavicle.

Tables 8, 9, and 10, below, show values for the various parameters used in seven neural networks in the 3rd version of the CNN-based segmentation system.

TABLE 8

Input image sizes for the seven neural networks and two localization networks.

Network Name	Input image size (Input image size (no. slices, no. rows, no. columns)
coarse-seg-02	(81, 77, 99)
coarse-seg-03	(81, 77, 99)
fine-seg-abdomen	(92, 176, 259)
fine-seg-left-lung	(154, 171, 140)
fine-seg-right-lung	(154, 171, 141)

TABLE 8-continued

Input image sizes for the seven neural networks and two localization networks.

Network Name	Input image size (Input image size (no. slices, no. rows, no. columns)
fine-seg-left-upper-body-bone	(154, 171, 140)
fine-seg-right-upper-body-bone	(154, 170, 140)
fine-seg-pelvic-region-mixed	(92, 144, 251)
fine-seg-spine-bone	(192, 183, 115)

TABLE 9

Number of convolutional filters in the seven neural networks and two localization networks.

Network Name	Total Number of Filters	Number of Filters in First Layer
coarse-seg-02	2278 + 49 (49 classes)	32
coarse-seg-03	2278 + 50	32
fine-seg-abdomen	1142 + 16 (not all output classes are included in the complete segmentation platform)	16
fine-seg-left-lung	1142 + 15	16
fine-seg-right-lung	1142+ 15	16
fine-seg-left-upper-body	1142 + 14	16
fine-seg-right-upper-body	1142 + 14	16
fine-seg-pelvic-region-mixed	1852 + 5	26
fine-seg-spine-bone	1142 + 18	16

TABLE 10

Number of parameters in seven neural networks and two localization networks.

Network Name	Total Params	No. trainable params	No. non-trainable params
coarse-seg-02	5,882,432	5,879,132	3,300
coarse-seg-03	5,882,469	5,879,167	3,302
fine-seg-abdomen	1,473,003	1,471,369	1,634
fine-seg-left-lung	1,472,752	1,471,120	1,632
fine-seg-right-lung	1,472,752	1,471,120	1,632
fine-seg-left-upper-body	1,472,731	1,471,101	1,630
fine-seg-right-upper-body	1,472,731	1,471,101	1,630
fine-seg-pelvic-region-mixed	3,883,812	3,881,200	2,612
fine-seg-spine-bone	1,472,815	1,471,177	1,638

Accordingly, this example demonstrates how segmentation approaches described herein can be used to perform efficient whole body segmentation.

ii. Example 2: Automated Segmentation of the Skeleton in Low-Dose CT and Quantification of Metastatic Prostate Cancer in [^{18}F]DCFPyL PET

PSMA-PET/CT hybrid imaging is a promising diagnostic platform for prostate cancer patients. While manual delineation of organs in three dimensional CT images is often needed for accurate diagnostics and treatment planning, such manual delineation is a time consuming process. To address this challenge, this example demonstrates automating the process of accurate bone segmentation in whole body CT images using deep learning approaches in accordance with the whole body segmentation technology described herein. As described in this example, the anatomical information gained via such skeletal segmentation can be used to create a fully automated lesion detection algorithm in [^{18}F]DCFPyL (PyL™-PSMA) PET/CT images.

A deep learning algorithm based on cascaded deep learning convolutional neural networks for semantic segmentation of 12 skeletal regions was developed. In particular, the 12 skeletal regions were the thoracic and lumbar vertebrae, sinister (left)/dexter (right) ribs, sternum, sinister (left)/dexter (right) clavicle, sinister (left)/dexter (right) scapula, sinister (left)/dexter (right) ilium, and the sacrum. A training set (N=90) and validation set (N=22) of pairs of low-dose CT images and manually crafted segmentation maps were used to develop the deep learning algorithm. The algorithm's performance was assessed on a test set (N=10) of low-dose CT images obtained from a PyL™—PSMA study. In the test set of images, five representatively body parts: sinister (left) ilium, lumbar vertebrae, sinister (left) ribs, dexter (right) scapula, and sternum were manually segmented. These manual segmentations were used as ground truth for evaluation of the automated segmentation procedure.

The automated segmentation can be used for automated lesion detection. For example, automated lesion detection approach using a hard threshold of standard uptake value (SUV) based on PET image voxel intensities can be performed.

Sorensen-Dice scores were used to evaluate accuracy of the automated segmentation. The segmentation approach achieved a Sorensen-Dice score mean and standard deviation of 0.95 and 0.024, respectively, on the training set and a mean and standard deviation of 0.93 and 0.036, respectively, on the validation set. For the test set, mean values (with standard deviation values shown in parentheses) for each of the five regions are as follows: 0.94 (0.016) for dexter (right) clavicle, 0.90 (0.023) for sinister (left) ribs, 0.92 (0.019) for sternum, 0.94 (0.033) for lumbar vertebrae, and 0.97 (0.0033) for sinister (left) ilium. The overall mean (over all body parts) was 0.93, with a standard deviation of 0.030.

Accordingly, this example demonstrates the accuracy of a fully automated segmentation approach for 12 skeletal regions in whole body low-dose CT images and use of an automated lesion detection approach for PyL™-PSMA/CT hybrid imaging.

iii. Example 3: Automated Whole Body Segmentation for PyL™-PET Image Analysis and Lesion Detection

This example demonstrates automated segmentation of 49 bones and 27 soft-tissue regions in whole body CT images using deep learning approaches in accordance with the whole body segmentation technology described herein. This example also demonstrates how the anatomical information gained via such segmentation can be used to create a fully automated lesion detection algorithm in [^{18}F]DCFPyL (PyL™-PSMA) PET/CT images. This example also shows how the segmentation can be used to remove background signal from PET images to facilitate observation and detection of lesions in which PyL™ has accumulated.

FIG. **6**A shows a block flow diagram illustrating an embodiment of the segmentation processes described herein that is used in the PyL™-PET/CT image analysis described in this example. As in process **500**, shown in FIG. **5**, in process **600** an anatomical image is received. In particular, in process **600**, a CT image is received **610***a*. In this example, process **600** is used to identify and segment the CT image into target volumes of interest corresponding to 49 specific bones and 8 soft tissue regions (in this example, example version 3 of the CNN-based segmentation approach

described in Example 1 is used). In order to identify the target volumes, a coarse segmentation is performed **620***a* to localize a set of initial volumes of interest, or sub-regions, e.g., as described in Example 1. A fine segmentation is then performed within each of the sub-regions to identify the specific target volumes of interest that correspond to the target 49 bone and 8 soft-tissue regions **630***a*. Segmentation masks representing the identified target volumes can be created, and merged **640***a*, for example to create a 3D whole body segmentation map.

As noted in Example 1 (CNN Network Version 3), the specific regions segmented are as follows:

49 Bones:
- clavicle_left
- clavicle_right
- hip_bone_left
- hip_bone_right
- rib_left_1
- rib_left_10
- rib_left_11
- rib_left_12
- rib_left_2
- rib_left_3
- rib_left_4
- rib_left_5
- rib_left_6
- rib_left_7
- rib_left_8
- rib_left_9
- rib_right_1
- rib_right_10
- rib_right_11
- rib_right_12
- rib_right_2
- rib_right_3
- rib_right_4
- rib_right_5
- rib_right_6
- rib_right_7
- rib_right_8
- rib_right_9
- sacrum_and_coccyx
- scapula_left
- scapula_right
- sternum
- vertebra_lumbar_1
- vertebra_lumbar_2
- vertebra_lumbar_3
- vertebra_lumbar_4
- vertebra_lumbar_5
- vertebra_thoracic_1
- vertebra_thoracic_10
- vertebra_thoracic_11
- vertebra_thoracic_12
- vertebra_thoracic_2
- vertebra_thoracic_3
- vertebra_thoracic_4
- vertebra_thoracic_5
- vertebra_thoracic_6
- vertebra_thoracic_7
- vertebra_thoracic_8
- vertebra_thoracic_9

8 Soft-Tissue Regions:
- gallbladder
- kidney_left
- kidney_right
- liver
- lung_left
- lung_right
- prostate
- urinary_bladder

FIG. **6**B shows a series of CT images overlaid with annotations illustrating the steps in the whole-body segmentation process **600** described in this example. An example raw CT image that is received at step **610***a* is shown in **610***b*. Image **620***b* shows results of a coarse segmentation (different regions identified are shown as colored regions) used to identify the initial volumes of interest in the CT image. Image **630***b* shows "bounding boxes" identifying initial volumes of interest in which fine segmentation is performed to identify the target volumes of interest corresponding to the 49 bones and 8 soft tissue regions. Image **640** illustrates the final, merged whole body segmentation.

Turning to FIG. **7**, in order to train the machine learning modules used to perform the segmentations, numerous pre-labeled sample images, such as the three images (**710**, **720**, **730**) shown in FIG. **7**, were used as a training data set. The machine learning modules were fine-tuned using 1000's of manually annotated labels along with 100's of models trained on dozens of GPUs over 1000's of hours before optimal configurations for the many components of the segmentation platform were discovered. Once trained, however, segmentation can be performed rapidly, with results such as those shown in FIGS. **8** (**810** and **820** are two example images) and FIGS. **16**A and **16**B obtained in a matter of seconds—typically under 180 seconds.

The anatomical context obtained by segmenting the CT image can be used to detect lesions in PET images that are co-registered with the CT image, for example, as in a typical PET/CT imaging modality in which CT and PET images are obtained for a subject in quick succession, with the subject remaining in a substantially same position as the images are recorded. In particular, as demonstrated in this example, segmentation of the CT image can be transferred to the PET image in order to identify regions of interest such as the prostate gland or the skeleton, where the entire functional image except for regions expected to carry either primary or secondary prostate cancer tumors can be excluded from the lesion detection algorithm. Without wishing to be bound to any particular theory, exclusion of regions from the lesion detection algorithm can be especially important for background regions where accumulation leads to high intensity in PET image voxels within and around the background tissue regions. The high intensities in background tissue regions may, if not excluded from the prostatic lesion detection process, lead to erroneous classification of background noise as cancerous lesions. In the regions that remain after the background exclusion process, a simple threshold (e.g., a SUV of 3) in conjunction with a lesion classification algorithm can be employed to find hotspots within the relevant tissue regions. The classification algorithm may be used as a simple check to confirm the hotspots position and to compare the intensity in the hotspot's neighborhood. If the hotspot is part of a larger hotspot and is located on the edge of a body part (e.g. a rib close to the liver), the lesion may be classified as noise and excluded. FIGS. **9**A-D illustrate the need for, and benefits obtained by, this background subtraction approach and lesion detection algorithm, where only regions of interest are included in the detection

procedure, and portions of the image contains high intensity background voxels. FIGS. **9**A and **9**C show PET images as white-to-red-to-blue false color overlaid on CT images. Blue color indicates low PET image intensity, transitioning from red to white as intensity increases. FIGS. **9**B and **9**D show the same PET images as in **9**A and **9**C, but with all background uptake removed from the PET image. In FIGS. **9**B and **9**D, a few localized hotspots, corresponding to cancerous lesions are visible. In the PET images without background removal, these hotspots were overwhelmed and masked by the large background signal.

FIG. **10**A shows an example process **1000** for using the anatomical context provided by whole body CT segmentation for detecting lesions and determining useful risk indices that quantify a cancer status (e.g., prostate cancer status) of a subject using PET/CT images obtained following administration of PyL™ as a radiopharmaceutical. As shown in FIG. **10**A, PET/CT images are obtained **1010**, anatomical context is determined **1012** via segmentation of bones and soft tissue and used to obtain measurements (e.g., of lesions and/or risk indices) from the PET image **1014**. FIG. **10**B shows an example PET/CT image **1016** and FIG. **10**C shows example segmentations of bones and soft tissue **1018***a* and **1018***b*. As shown in FIG. **10**D, segmentation of bone and soft-tissue (e.g., shown in image **1020***a*) can be used to remove background signal (e.g., from background tissue regions, such as those shown in image **1020***b*), leaving only desired signal from hotspots indicative of cancerous lesions **1020***c*.

FIGS. **11**-**13** illustrate this process, showing how segmentation of a CT image can be transferred to a PET image, and are used to provide anatomical context for background removal and lesion detection. In particular, FIG. **11**A and FIG. **11**B show different views of a CT image, in which segmentation of bones has been performed. The various segmented bones are labeled with different colors in the views shown in FIG. **11**A and FIG. **11**B. Notably, by virtue of the "bounding box" approach described herein, even such a complex and large scale segmentation can be performed extremely rapidly. The segmentation shown in FIGS. **11**A and **11**B was performed in less than 180 seconds.

As shown in FIG. **12**, segmentation of bones and soft tissue can be used to account for normal uptake in certain background tissue regions, which may occur under normal circumstances and mask useful hotspot signals that indicate presence of cancerous lesions. In PET/CT imaging performed with PyL™, normal uptake can occur in kidneys, duodenum, small intestines, spleen, liver, pancreas, stomach, adrenal gland, rectum, and testes. FIG. **12** shows the aforementioned regions identified in red. As shown in FIG. **13**A, once background intensities due to normal PyL™ accumulation in these regions is subtracted out, lesions become readily observable and can be detected. One such lesion **1302** is visible in FIGS. **13**A-D. Lesions such as lesion **1302** can be detected, for example via a thresholding approach, and classified as PyL™ positive (i.e., indicative of cancer) e.g., as described above. As with segmentation, lesion detection is also rapid. Lesion **1302** was detected in less than 5 seconds.

FIG. **14**A and FIG. **14**B show results of the PET image processing and lesion detection approach described above performed on PET/CT images obtained for a 65 year old male with metastatic castration resistant prostate cancer. The patient's prostate specific antigen (PSA) score was 6.8 ng/ml. The PET images were obtained following administration of PyL™ as the radiopharmaceutical. FIG. **14**A shows the initial, raw, PET/CT image. FIG. **14**B shows the image following the processing described herein. The background intensity is removed, and several small lesions are readily observable. The segmentation of the 49 bones and 8 soft-tissue regions (e.g., organs) was performed in less than 180 seconds.

FIG. **15**A and FIG. **15**B show results of the PET image processing and lesion detection approach performed on PET/CT images obtained for a 54 year old male with metastatic castration resistant prostate cancer. The patient's PSA score was 33.55 ng/ml. The PET images were obtained following administration of PyL™ as the radiopharmaceutical. FIG. **15**A shows the initial, raw, PET/CT image. FIG. **15**B shows the image following the processing described herein. The background intensity is removed, and several small lesions are readily observable. The segmentation of the 49 bones and 8 soft-tissue regions (e.g., organs) was again performed in less than or about 180 seconds.

Accordingly, this example demonstrates how the whole-body segmentation approach described herein contextualizing the PyL™ images, with automated segmentation of 27 soft-tissue organs and 49 bones, to detect, quantify and track PyL™ avid lesions. The approach would allow the clinicians/physicians to ask clinically relevant questions for better management of prostate cancer patients. Advantages such as increased diagnostic accuracy, precision, speed, and reproducibility, were demonstrated (statistically) in the context of artificial intelligence assisted 1404-SPECT image analysis (see, e.g., PCT Publication WO2019/136349, the content of which is hereby incorporated by reference in its entirety), may also be obtained for PyL™-PET images.

iv. Example 4: Example Bone and Soft-Tissue Segmentation Regions

This example provides a listing of a set of example bone and soft-tissue regions that a system developed using the approaches and embodiments described herein can identify via segmentation of CT images. In particular, listed below are 67 bones and 22 soft-tissue regions for that have been manually labeled (e.g., identified by one or more human experts) in a set of CT images. These manually labeled CT images can be used as training data for the machine learning approaches described herein. For example, while Examples 1-3 describe current versions of software implementing whole body segmentation approaches that segment 49 bones and 8 soft-tissue regions, their functionality can readily be updated to segment any number of the 67 bone and 22 soft-tissue regions listed in this example. Accordingly, this example shows that embodiments of the systems and methods described herein may be developed to identify similar regions, including, but not necessarily limited to the specific regions described in this example. Certain systems and methods may identify tissue regions not necessarily listed in this example. In certain embodiments, both bone and soft-tissue regions are identified. In certain embodiments, some systems and methods may identify only bones, or only soft-tissue.

As indicated in the listing below, certain left and right hand side bones are identified as separate tissue regions (e.g., a left clavicle and a right clavicle) and, in certain cases, individual members of large groups of bones are identified separately. For example, the example listing below shows that individual ribs and vertebrae are identified via the segmentation approach of this example (specific ribs and vertebrae are numbered in the listing). This example also should make clear that the approaches described herein can

be used to segment a variety of regions throughout the body, including, but not necessarily limited to the regions listed herein.

Segmentation Regions:

- Bones (67)
  - clavicle_left
  - clavicle_right
  - femur_left
  - femur_right
  - fibula left
  - fibula_right
  - hip_bone_left
  - hip_bone_right
  - humerus_left
  - humerus_right
  - mandible
  - patella_left
  - patella_right
  - radius left
  - radius_right
  - rib_left_1
  - rib_left_2
  - rib_left_3
  - rib_left_4
  - rib_left_5
  - rib_left_6
  - rib_left_7
  - rib_left_8
  - rib_left_9
  - rib_left_10
  - rib_left_11
  - rib_left_12
  - rib_right_1
  - rib_right_2
  - rib_right_3
  - rib_right_4
  - rib_right_5
  - rib_right_6
  - rib_right_7
  - rib_right_8
  - rib_right_9
  - rib_right_10
  - rib_right_11
  - rib_right_12
  - sacrum_and_coccyx
  - scapula_left
  - scapula_right
  - skull
  - sternum
  - tibia left
  - tibia_right
  - ulna_left
  - ulna_right
  - vertebra_cervical_all
  - vertebra_lumbar_1
  - vertebra_lumbar_2
  - vertebra_lumbar_3
  - vertebra_lumbar_4
  - vertebra_lumbar_5
  - vertebra_lumbar_6
  - vertebra_thoracic_1
  - vertebra_thoracic_2
  - vertebra_thoracic_3
  - vertebra_thoracic_4
  - vertebra_thoracic_5
  - vertebra_thoracic_6
  - vertebra_thoracic_7
  - vertebra_thoracic_8
  - vertebra_thoracic_9
  - vertebra_thoracic_10
  - vertebra_thoracic_11
  - vertebra_thoracic_12
- Soft tissue (22):
  - adrenal_gland_left
  - adrenal_gland_right
  - aorta_abdominal_part
  - aorta_thoracic_part
  - brain
  - bronchi left
  - bronchi_right
  - gallbladder
  - gluteus_maximus_left
  - gluteus_maximus_right
  - heart
  - kidney_left
  - kidney_right
  - liver
  - lung_left
  - lung_right
  - pancreas
  - prostate
  - rectum
  - spleen
  - urinary_bladder
  - ventricle

v. Example 5: Computing Hotspot Indices for Radiopharmaceutical Uptake Quantification and Clinical Endpoint Assessment

Example 5 is an example approach that uses the segmentation and hotspot detection methods described herein to compute, for a particular detected hotspot, a hotpot index value that can be used to infer and/or quantify uptake of radiopharmaceutical within the lesion that the detected hotspot represents. The computed hotspot index can be related to clinical endpoints, including survival rate of a patient and to determine treatment strategy. When computed for multiple images, collected at different time points, the computed index values can be compared with each other for a particular patient, and the change in index used to evaluate efficacy of a treatment and to make a prognosis of how the index will change in the near future. In certain embodiments, the computed index can predict sensitivity towards treatment targeting the imaging-ligand. In certain embodiments, the computed index can also be included in nomograms for effective patient stratification.

The approach in this example uses a CT-PET image set obtained for a particular patient following administration of a radiopharmaceutical comprising a PSMA binding agent, for example, PyL™. However, the approaches described herein are agnostic to the particular radiopharmaceutical used for imaging, and can be utilized with a variety of different radiopharmaceuticals, e.g., ^{99m}Tc-MIP-1404, ^{18}F-PyL, ^{68}Ga-PSMA-11, ^{18}F—NaF, ^{11}C-Choline, [18F]FDG, [18F]FACBC, etc.

A machine learning-based approach in accordance with the systems and methods described herein is used to identify various target VOIs within the CT image. As described herein, the target VOIs are volumes in the CT image identified, automatically, by the segmentation approach, to correspond particular target tissue regions. In this example approach, target VOIs corresponding to a liver, an aorta portion, and a parotid gland are identified. As described

herein, these particular tissue regions—the liver, aorta portion, and parotid gland—serve as reference regions for computation of the hotspot index. Other target VOIs corresponding to other target tissue regions, in addition to the reference regions, may also be identified. Segmentation masks representing the identified target VOIs are mapped to the PET image to identify corresponding 3D volumes within the PET image. In this manner, 3D reference volumes corresponding to the liver, aorta portion, and parotid gland are identified in the PET image. Once identified, each particular 3D reference volume is used to compute a corresponding reference intensity value that provides a measure of the intensities of voxels within the particular 3D reference volume. In this example, a mean intensity inside each volume is used, though other measures (e.g., a median, a maximum, a mode, etc.) are possible.

To compute an index value for a particular identified hotspot, a hotspot intensity value is computed for that particular hotspot and compared with the reference intensity values. Similar to the reference values, the hotspot intensity value provides a measure of intensity of voxels of the hotspot. In this example, a maximum value is computed, although, as with the reference values, other measures can be used. As this example shows, the particular measure used to compute the hotspot intensity value need not be the same as that used to compute the reference intensity values. To compute the hotspot index value, the reference intensity values can be mapped to reference index values on a scale, and the hotspot index value can then be computed based on whether the hotspot intensity value lies above, below, or in between the reference values.

For example, typically the reference intensity value computed from the reference volume corresponding to the aorta portion (this—aorta—region is used to provide a measure of uptake in the blood pool, and may also be referred to as a blood or blood pool reference value) is lowest in value, followed by the liver and then the parotid region. Accordingly, a hotspot whose hotspot intensity value is equal to the blood reference value will be assigned a hotspot index value equal to 100; a hotspot whose hotspot intensity value is equal to the liver reference value will be assigned a hotspot index value equal to 200; and a hotspot whose hotspot intensity value is equal to the parotid gland reference value will be assigned a hotspot index value equal to 300. Hotspot index values for hotspot intensity values lying in between two reference intensity values can be determined via interpolation (e.g., linear interpolation).

In this manner, a detected hotspot can be assigned an index value that quantifies, in a standardized fashion (e.g., so as to be comparable between different images) a level of radiopharmaceutical uptake in the particular lesion that the hotspot represents. As described herein, these indices can be related to survival, which, in turn, makes them useful for treatment management. For example, depending on the expected outcome of the patient, a more or less aggressive treatment may be considered. Price of treatments can also be included as a factor. The index is especially useful when measured over time. When comparing indices across time and multiple imaging examinations for a patient, the change in index can be used to evaluate the efficacy of a treatment, and to make a prognosis how the index will change in the near future.

Notably, a significant advantage of the approach described in this example over previous approaches is the ability to compute reference intensity values (as well as hotspot intensity values) from automatically identified 3D volumes provided by the artificial intelligence based segmentation approaches described herein. Previous approaches that attempted to quantify regions of images representing lesions relied on hand marking—e.g., via placement of a circular marker—of regions in 2D slices to identify 2D regions of interest lying within a reference tissue region. In contrast to such small 2D regions, the 3D volume that are identified via the approaches used herein capture intensities throughout entire organs, and thereby offer increased accuracy and repeatability. Moreover, by using accurate automated segmentation, further increases in accuracy and repeatability are provided.

In addition, rather than classifying a detected lesion using one of a small number of values, the approach of this example uses a continuously varying index computed via interpolation. This approach provides more detailed information that can be utilized to manage treatment strategy and track disease progression and/or treatment efficacy over time in a finely grained and accurate fashion.

vi. Example 6: Automated Hotspot Detection and Uptake Quantification in Bone and Local Lymph

PyL™-PSMA PET/CT hybrid imaging (e.g., images PET/CT images acquired for a patient after administering PyL™ to the patient) is a promising tool for detection of metastatic prostate cancer. Image segmentation, hotspot detection, and quantification technologies of the present disclosure can be used as a basis for providing automated quantitative assessment of abnormal PyL™-PSMA uptake in bone and local lymph (i.e., lymph nodes localized within and/or in substantial proximity to a pelvic region of a patient). In particular, as shown in this example, image segmentation and hotspot detection techniques in accordance with the systems and methods described herein can be used to automatically analyze in PET images to detect hotspots that a physician might identify as malignant lesions.

In this example, PET/CT scans were evaluated to automatically identify, within the PET images of the scans, hotspots corresponding to potential bone and local lymph node lesions. For each scan, a semantic segmentation of the CT image was performed using the deep learning approaches described herein in order to identify a set of specific bone and soft-tissue regions (e.g., organs). Once obtained, the CT image segmentation was transferred (e.g., mapped) to the PET image of the PET/CT scan to identify corresponding 3D volumes in the PET image. In each PET image, intensities corresponding to background uptake were removed by suppressing intensities in identified volumes corresponding to a urinary bladder, a liver, and a kidney. The segmentation was also used to define relevant volumes in which to detect hotspots. Blob detection algorithms were then applied to identify abnormal hotspots representing either possible bone lesions or possible malignant local lymph nodes. Reference volumes corresponding to a liver and a thoracic part of an aorta were used to compute reference SUV values.

Accuracy of the hotspot detection approach in this example was validated by comparing detection of hotspots in PET images using the automated approach described herein with manual annotations identifying bone lesions and lymph node lesions from teams of physicians. A set of 157 PET/CT scans that were annotated for bone lesions (114 of the images did not have any lesions and 11 of the images had greater than three lesions) were used to evaluate accuracy in detecting hotspots corresponding to bone lesions and a set of 66 scans that were annotated for local lymph node lesions (40 images without lesions and six with greater than three

lesions). The bone detection algorithm identified 97% of all annotated bone lesions, with on average 109 hotspots per image. The local lymph detection algorithm found 96% of all annotated malignant local lymph nodes, with on average 32 hotspots per scan.

Accuracy of the deep learning segmentation was also evaluated in this example. The segmentation algorithm was trained to segment a set of 52 bones and 7 soft tissue regions (e.g., organs) used either for defining the hotspot search region or as reference regions. Training and validation was performed and evaluated for each particular region (bone or soft tissue region) using a manual identification of that region in a CT image. For example, 140 manually identified livers were used to train the algorithm for liver segmentation, and 37 manually identified livers were used for validation. Similarly, 61 and 14 manually identified aortas were used for training and validation of the aorta region segmentation, respectively. For liver segmentation, Dice scores of 0.99 and 0.96 were obtained for the training and validation sets, respectively. For aorta segmentation, Dice scores of 0.96 and 0.89 were obtained for training and validation, respectively. Finally, a set of ten additional images that were not used development of the algorithm were used to assess generalization. For these ten images, Dice scores characterizing segmentation accuracy of the liver and aorta were 0.97±0.01 and 0.91±0.5, respectively.

A full listing of the specific 52 bone (the sacrum and coccyx are listed on a single line as "sacrum and coccyx", but correspond to two segmented regions) and 7 soft-tissue regions used in this particular example is below.

Bone Regions:
- capula_left
- clavicle_left
- clavicle_right
- hip_bone_left
- hip_bone_right
- rib_left_1
- rib_left_10
- rib_left_11
- rib_left_12
- rib_left_2
- rib_left_3
- rib_left_4
- rib_left_5
- rib_left_6
- rib_left_7
- rib_left_8
- rib_left_9
- rib_right_1
- rib_right_10
- rib_right_11
- rib_right_12
- rib_right_2
- rib_right_3
- rib_right_4
- rib_right_5
- rib_right_6
- rib_right_7
- rib_right_8
- rib_right_9
- sacrum_and_coccyx
- scapula_left
- scapula_right
- sternum
- vertebra_lumbar_1
- vertebra_lumbar_2
- vertebra_lumbar_3
- vertebra_lumbar_4
- vertebra_lumbar_5
- vertebra_thoracic_1
- vertebra_thoracic_10
- vertebra_thoracic_11
- vertebra_thoracic_12
- vertebra_thoracic_2
- vertebra_thoracic_3
- vertebra_thoracic_4
- vertebra_thoracic_5
- vertebra_thoracic_6
- vertebra_thoracic_7
- vertebra_thoracic_8
- vertebra_thoracic_9

Soft Tissue Regions:
- aorta_abdominal_part
- aorta_thoracic_part
- kidney_left
- kidney_right
- liver
- prostate
- urinary_bladder

Accordingly, this example demonstrates use of deep learning based semantic segmentation for automated identification of hotspots and for computation of SUV reference values in [18^F] DCFPyL (PyL™-PSMA) PET/CT images.

vii. Example 7: Lesion PSMA Score and PSMA Weighted Lesion Involvement

This example provides an approach for assigning detected hotspots hotspot indices, based on a comparison of individual hotspot intensities with reference levels, and then using the assigned individual hotspot indices to determine overall indices representing a weighted sum of measures of lesion size. The indices used in this example are used to assess cancer status for patients imaged using a PSMA binding agent and PET-CT imaging.

In particular, individual hotspot indices are determined via interpolation from our reference levels similar to the approach described in Example 5. In this example, reference VOIs corresponding to an aorta portion and a liver portion are segmented and mapped to corresponding 3D volumes in a PET image. The aorta portion volume is used to determine a blood reference intensity, and the liver volume is used to determine a liver reference intensity. In this example, each reference intensity is determined from its corresponding volume by taking an average intensity (SUV) in the corresponding volume, but other measures, such as a maximum, peak, or median value could also be used. Reference levels on a scale, referred to as a Lesion PSMA Score (LPS), are assigned to intensity values based on the blood and liver reference intensities (SUVs) as follows: a LPS of 0 is assigned to a 0 SUV level, an LPS of 1 is assigned to the blood reference intensity, an LPS of 2 is assigned to the liver reference intensity, and a maximum LPS of 3 is assigned to a reference intensity calculated as twice the liver reference intensity.

Individual hotspots are assigned LPS scores based on their individual intensities. For individual hotspots having intensities ranging from 0 to the maximum reference intensity (twice the liver reference intensity), the LPS score corresponding to the individual hotspot intensity is interpolated from the reference scale. Hotspots having intensities greater than the maximum reference intensity are assigned the maximum LPS of 3.

Two example overall risk indices that can be computed using detected hotspots and the individual hotspot indices (LPS scores) are calculated as weighted sums of hotspot sizes in particular volumes corresponding to tissue regions where cancerous lesions may occur. A first example index is a PSMA-weighted total bone/lymph/prostate lesion volume or ratio (PTLV or PTLR). This index is a weighted sum of lesion volumes, the weight being the lesion PSMA score. The sum is computed separately for 3D volumes corresponding to bone (e.g., a skeletal region), lymph nodes, and prostate as the weighted sum of hotspot volumes for hotspots found in each particular region. In particular, the weighted sum is computed as follows:

$$\Sigma(\text{lesion volume} \times \text{lesion psma score})$$

In certain case, a ratio may be preferable and can be computed by dividing the weighted sum by the total 3D volume of the particular region (e.g., in the PET image). Weighting summed hotspot volumes by LPS, as opposed to, for example SUV or normalized SUV is advantageous since it PSMA expression in the form of (normalized) SUV values may not relate to aggressiveness of the disease in a linear fashion. That is, for example, it is not a given that a hotspot with an intensity of 100 represents a lesion is five times worse than one represented by a hotpot having an intensity of 20. Calculating the LPS score and weighting hotspots by the LPS score provides a scale to compare different hotspots.

Another example index is a PSMA-weighted bone/lymph aggregated diameter (PLAD). This index is also a sum of a measure of lesion size, weighted by LPS score, but instead of volume this index uses an average diameter (e.g., averaged of x, y, and z-diameters) of each hotspot. Since volume is a three-dimensional quantity, a minor change in volume for a large lesion can dominate (e.g., cause large fluctuations in the sum) over changes in size of smaller lesions. Using the average diameter instead mitigates this effect. This index is calculated as follows:

$$\Sigma(\text{lesion average diameter} \times \text{lesion psma score})$$

The weighed aggregated diameter can be calculated for the bone and lymph.

vii. Example 8: Improved Performance in AI-Assisted Image Analysis for Patients with Low or Intermediate Risk Prostate Cancer

99mTc MIP-1404 (1404) is a PSMA targeted imaging agent for the detection and staging of clinically significant prostate cancer. Manual assessment of tracer uptake in SPECT/CT images introduces inherent limitations in inter- and intra-reader standardization. This example describes a study that evaluated the performance of PSMA-AI assisted reads, wherein automated segmentation of prostate volumes and other target tissue regions are performed in accordance with the embodiments described herein, over manual assessment and known clinical predictors.

The study analyzed 464 evaluable patients with very low-, low-, or intermediate-risk prostate cancer, whose diagnostic biopsy indicated a Gleason grade of ≤3+4 and/or who were candidates for active surveillance (1404-3301). All subjects received an IV injection of 1404 and SPECT/CT imaging was performed 3-6 hours postdose. Three independent readers evaluated the images. All subjects underwent either voluntary RP (low- and intermediate-risk) or prostate biopsy (very low-risk) post dosing. Clinically significant disease was declared in subjects with Gleason grade 7 or higher. The PSMA-AI was developed and locked prior to the analysis. Three different independent readers used PSMA-AI to obtain quantitative expression of 1404 in the prostate against the background (PSMA-Index). PSMA-Index for all readers and subjects were compared to the histopathological reference, yielding 6 receiver operating characteristic (ROC) curves (3 manual reads+3 PSMA-AI assisted reads). The clinical performance of the 1404 PSMA-AI assisted read was also evaluated by comparing the Area Under the ROC Curve (AUC), of a multivariate model (PSA, clinical staging and diagnostic Gleason score) with and without PSMA-Index.

The manual reads demonstrated AUCs of 0.62, 0.62 and 0.63. The reads with PSMA-AI demonstrated AUCs of 0.65, 0.66 and 0.66. The PSMA-AI performance in terms of AUC was higher than manual in all 3*3=9 pairwise comparisons between the two reader groups, with statistically significant improvement observed in five cases (nominal $p<0.05$), not accounting for multiple comparisons. The predictive ability of the baseline multivariate model, without PSMA-Index, was at AUC 0.74. Upon adding of PSMA-Index, the model predictive ability increased to AUC 0.77. The logistic regression model indicated that PSMA-Index ($p=0.004$), pre-surgery PSA (0.018) and % positive cores ($p=<0.001$) were significantly associated with clinically significant disease. When measuring reproducibility, log (PSMA-Index) correlation coefficients for pairs of PSMAAI readers were 0.94, 0.97 and 0.98.

Accordingly, the study described in this example demonstrated that PSMA-AI provides a standardized platform to generate reproducible quantitative assessment of 1404. The PSMA-AI assisted read demonstrated an additive improvement over known predictors for identifying men with clinically significant disease.

ix. Example 9: Automated Calculation of PSMA Indices for Quantification of 18F-DCFPyL Uptake from PET/CT Images for Prostate Cancer Staging

This example demonstrates automated image segmentation, lesion detection, and calculation of a standardized index score based on hotspot indices assigned to detected lesions via embodiments of the approaches described herein. The automated image analysis procedures are used for evaluated cancer status of patients imaged via PET/CT scanning after being administered the radiopharmaceutical 18F-DCFPyL (PyL™).

In this example, a cascaded deep learning pipeline was used to segment relevant organs in the CT image, and segmentations are projected into PET image space. In particular, target regions corresponding to a bone volume corresponding to bones of the subject, a lymph volume corresponding to lymph regions, and a prostate volume corresponding to a prostate gland were segmented in the CT image and mapped to identify corresponding 3D volumes in the PET image. Likewise, aorta and liver volumes corresponding to an aorta portion and a liver were also segmented and mapped to the PET image for use as reference regions as described herein.

Hotspots were detected in the PET image. Hotspots that were considered to represent lesions are manually segmented, as well as additional lesions not detected by the algorithm. Each individual detected hotspot was quantified by calculating an individual hotspot index referred to as lesion miPSMA index (LPI). As described in Examples 6 and 7 above, the LPI used in this example is a continuous index computed using automatically segmented (as opposed to manually identified) volumes. Accordingly, it offers

advantages over previous approaches that utilize manual identification of various organs in images, and which only classify lesions using a small, finite, number of enumerated values. Accordingly, this approach provides more detailed information that can be utilized to manage treatment strategy and track disease progression and/or treatment efficacy over time in a finely grained and accurate fashion.

The LPI for each detected hotspot was computed based on reference values determined from blood pool (as measured from an identified aorta volume) and liver reference regions, e.g., similar to that described in Example 7 above. In particular, a blood pool reference intensity (SUV value) was measured using an aorta volume within the PET image, and a liver reference intensity was measured from a liver volume identified in the PET image. Both the blood pool and liver reference intensity levels were measured as the mean SUV (SUV_{mean}) within the corresponding volume in a PET image. Reference LPI index mean, values of 1 and 2 were assigned to the blood pool and liver reference intensities, respectively. A maximal reference index level of 3 was assigned to a reference intensity corresponding to twice the liver reference intensity value.

Each individual detected hotspots was assigned LPI scores based (i) a measured hotspot intensity value for the hotspot and (ii) comparison with the blood pool and liver reference intensity values and the aforementioned reference index levels. In particular, for each hotspot, an individual hotspot intensity value corresponding to a mean lesion uptake was calculated as a mean SUV across voxels of the hotspot. For an individual hotspot, an LPI equal to 1 was assigned if the mean lesion standard uptake value (SUV_{mean}) equal to the blood pool reference value; an LPI equal to 2 was assigned for hotspots having mean lesion uptake values equal to the liver reference uptake value; and an LPI equal to 3 was assigned to hotspots having a mean lesion uptake value is equal to or above twice the liver reference uptake. For hotspots having intensities in falling in between reference intensity values, individual hotspot LPIs were interpolated from based on the hotspot intensity value and reference intensity-index value pairs.

An aggregated lesion volume within the bone region was computed as a weighted sum of volumes of individual hotspots detected within the bone volume in the PET image, with the volume of each hotspot weighted by its corresponding LPI. In this manner a PSMA-weighted Total Lesion Volume (PLTV) index was computed for the bone region, denoted $PTLV_{bone}$. PLTV index values were also computed for the lymph ($PTLV_{lymph}$) and prostate ($PTLV_{prostate}$) regions analogously. For each of the three regions, PET/CT image data sets for subjects having various different indications were used to automatically determine PLTV index values.

Performance of the AI-based automated technique was evaluated based on comparison with manual organ segmentation and annotation of images to identify hotspots, and PLTV index values computed for different indications were compared across regions.

Using manual expert interpretation as a gold standard for comparison, the automated hotspot detection algorithm was determined to have sensitivity of 92.1% for bone lesions (97.2% in the 52 automatically segmented bones) and 96.2% for lymph lesions. On average, 17 bone hotspots were detected per scan and 23 lymph hotspots were detected per scan.

PLTV index values were computed using a sample dataset of 197 PET/CT images for the bone region, 99 PET/CT image for the lymph region, and 43 PET/CT images for the prostate region. In the data sets, 94% of individual hotspot LPI's determined were between 1 and 3, with minimum LPIs determined for bone, lymph, and prostate regions of 0.82, 1.1, and 1.3, respectively. Median LPI values for the bone, lymph, and prostate regions were 1.5, 2.0, and 2.3, respectively.

For each region, PLTV indices were computed for subjects having various different indications as follows: Treatment Response (TR), Screening (S), Newly Diagnosed (ND), Metastatic (M), Suspected Recurrence (SR), Recurrent (R). PLTV index values were compared across indications by calculating the means of the values in the interquartile range (IQR_{mean}), hence excluding outliers. Ordering indications by IQR_{mean} of the PLTV values yields TR<S<ND<R<SR<M for the bone region, S=M<R<ND<SR for lymph region, and M<SR<R<S<ND for prostate region, aligning well with clinical expectations of disease state.

FIG. **19** shows PLTV index values determined for the various indications for each region. FIG. **20** shows a scatter plot of individual hotspot LPI values for hotspots detected in each of the three regions.

In comparison with manual approaches for determining reference values for grading lesions, such as the of Eiber et al., 2017, the blood and liver automated reference values are based on a larger image volume compared to the manual reference method and are hence expected to be more robust. FIG. **21** compares reference values computed via the automated segmentation approaches described herein for the blood pool (left graph) and liver (right graph) regions with reference values computed using manual identification of organ boundaries. As shown in FIG. **21**, in a sample of 20 PET/CT scans, the correlation (Pearson's r) between automated and manual reference was 0.92 for blood and 0.87 for liver.

Accordingly, this example demonstrates use of the automated segmentation, hotspot detection, and index value calculation for detecting cancer and tracking cancer progression and/or response to treatment over time.

D. Imaging Agents

In certain embodiments, 3D functional images are nuclear medicine images that use imaging agents comprising radiopharmaceuticals. Nuclear medicine images are obtained following administration of a radiopharmaceutical to a patient, and provide information regarding the distribution of the radiopharmaceutical within the patient. Radiopharmaceuticals are compounds that comprise a radionuclide.

Nuclear medicine images (e.g., PET scans; e.g., SPECT scans; e.g., whole-body scans; e.g. composite PET-CT images; e.g., composite SPECT-CT images) detect radiation emitted from the radionuclides of radiopharmaceuticals to form an image. The distribution of a particular radiopharmaceutical within a patient may be determined by biological mechanisms such as blood flow or perfusion, as well as by specific enzymatic or receptor binding interactions. Different radiopharmaceuticals may be designed to take advantage of different biological mechanisms and/or particular specific enzymatic or receptor binding interactions and thus, when administered to a patient, selectively concentrate within particular types of tissue and/or regions within the patient. Greater amounts of radiation are emitted from regions within the patient that have higher concentrations of radiopharmaceutical than other regions, such that these regions appear brighter in nuclear medicine images. Accordingly, intensity variations within a nuclear medicine image can be

used to map the distribution of radiopharmaceutical within the patient. This mapped distribution of radiopharmaceutical within the patient can be used to, for example, infer the presence of cancerous tissue within various regions of the patient's body.

For example, upon administration to a patient, technetium 99m methylenediphosphonate (^{99m}Tc MDP) selectively accumulates within the skeletal region of the patient, in particular at sites with abnormal osteogenesis associated with malignant bone lesions. The selective concentration of radiopharmaceutical at these sites produces identifiable hotspots—localized regions of high intensity in nuclear medicine images. Accordingly, presence of malignant bone lesions associated with metastatic prostate cancer can be inferred by identifying such hotspots within a whole-body scan of the patient. Risk indices that correlate with patient overall survival and other prognostic metrics indicative of disease state, progression, treatment efficacy, and the like, can be computed based on automated analysis of intensity variations in whole-body scans obtained following administration of ^{99m}Tc MDP to a patient. In certain embodiments, other radiopharmaceuticals can also be used in a similar fashion to ^{99m}Tc MDP.

In certain embodiments, the particular radiopharmaceutical used depends on the particular nuclear medicine imaging modality used. For example 18F sodium fluoride (NaF) also accumulates in bone lesions, similar to ^{99m}Tc MDP, but can be used with PET imaging. In certain embodiments, PET imaging may also utilize a radioactive form of the vitamin choline, which is readily absorbed by prostate cancer cells.

In certain embodiments, radiopharmaceuticals that selectively bind to particular proteins or receptors of interest—particularly those whose expression is increased in cancerous tissue may be used. Such proteins or receptors of interest include, but are not limited to tumor antigens, such as CEA, which is expressed in colorectal carcinomas, Her2/neu, which is expressed in multiple cancers, BRCA 1 and BRCA 2, expressed in breast and ovarian cancers; and TRP-1 and -2, expressed in melanoma.

For example, human prostate-specific membrane antigen (PSMA) is upregulated in prostate cancer, including metastatic disease. PSMA is expressed by virtually all prostate cancers and its expression is further increased in poorly differentiated, metastatic and hormone refractory carcinomas. Accordingly, radiopharmaceuticals corresponding to PSMA binding agents (e.g., compounds that a high affinity to PSMA) labelled with one or more radionuclide(s) can be used to obtain nuclear medicine images of a patient from which the presence and/or state of prostate cancer within a variety of regions (e.g., including, but not limited to skeletal regions) of the patient can be assessed. In certain embodiments, nuclear medicine images obtained using PSMA binding agents are used to identify the presence of cancerous tissue within the prostate, when the disease is in a localized state. In certain embodiments, nuclear medicine images obtained using radiopharmaceuticals comprising PSMA binding agents are used to identify the presence of cancerous tissue within a variety of regions that include not only the prostate, but also other organs and tissue regions such as lungs, lymph nodes, and bones, as is relevant when the disease is metastatic.

In particular, upon administration to a patient, radionuclide labelled PSMA binding agents selectively accumulate within cancerous tissue, based on their affinity to PSMA. In a similar manner to that described above with regard to ^{99m}Tc MDP, the selective concentration of radionuclide labelled PSMA binding agents at particular sites within the patient produces detectable hotspots in nuclear medicine images. As PSMA binding agents concentrate within a variety of cancerous tissues and regions of the body expressing PSMA, localized cancer within a prostate of the patient and/or metastatic cancer in various regions of the patient's body can be detected, and evaluated. As described in the following, risk indices that correlate with patient overall survival and other prognostic metrics indicative of disease state, progression, treatment efficacy, and the like, can be computed based on automated analysis of intensity variations in nuclear medicine images obtained following administration of a PSMA binding agent radiopharmaceutical to a patient.

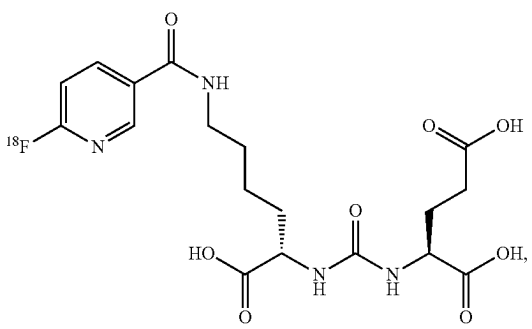
A variety of radionuclide labelled PSMA binding agents may be used as radiopharmaceutical imaging agents for nuclear medicine imaging to detect and evaluate prostate cancer. In certain embodiments, the particular radionuclide labelled PSMA binding agent that is used depends on factors such as the particular imaging modality (e.g., PET; e.g., SPECT) and the particular regions (e.g., organs) of the patient to be imaged. For example, certain radionuclide labelled PSMA binding agents are suited for PET imaging, while others are suited for SPECT imaging. For example, certain radionuclide labelled PSMA binding agents facilitate imaging a prostate of the patient, and are used primarily when the disease is localized, while others facilitate imaging organs and regions throughout the patient's body, and are useful for evaluating metastatic prostate cancer.

A variety of PSMA binding agents and radionuclide labelled versions thereof are described in U.S. Pat. Nos. 8,778,305, 8,211,401, and 8,962,799, each of which are incorporated herein by reference in their entireties.

i. PET Imaging Radionuclide Labelled PSMA Binding Agents

In certain embodiments, the radionuclide labelled PSMA binding agent is a radionuclide labelled PSMA binding agent appropriate for PET imaging.

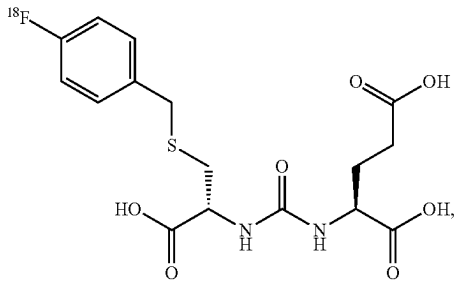
In certain embodiments, the radionuclide labelled PSMA binding agent comprises [18F]DCFPyL (also referred to as PyL™; also referred to as DCFPyL-18F):



[18F]DCFPyL

or a pharmaceutically acceptable salt thereof.

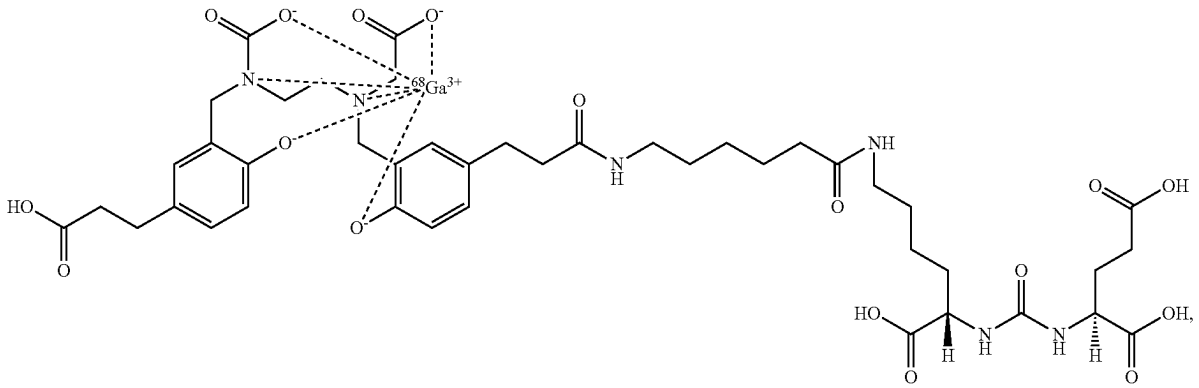
In certain embodiments, the radionuclide labelled PSMA binding agent comprises [18F]DCFBC:



[18F]DCFBC

or a pharmaceutically acceptable salt thereof.

In certain embodiments, the radionuclide labelled PSMA binding agent comprises ^{68}Ga-PSMA-HBED-CC (also referred to as ^{68}Ga-PSMA-11):

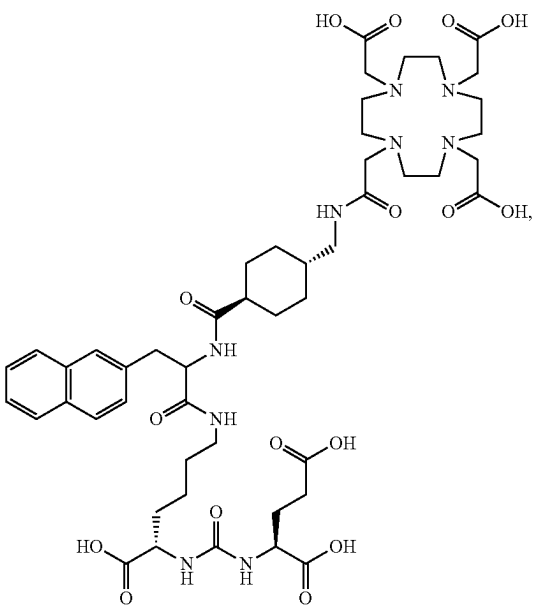


^{68}Ga-PSMA-HBED-CC

or a pharmaceutically acceptable salt thereof.

In certain embodiments, the radionuclide labelled PSMA binding agent comprises PSMA-617:

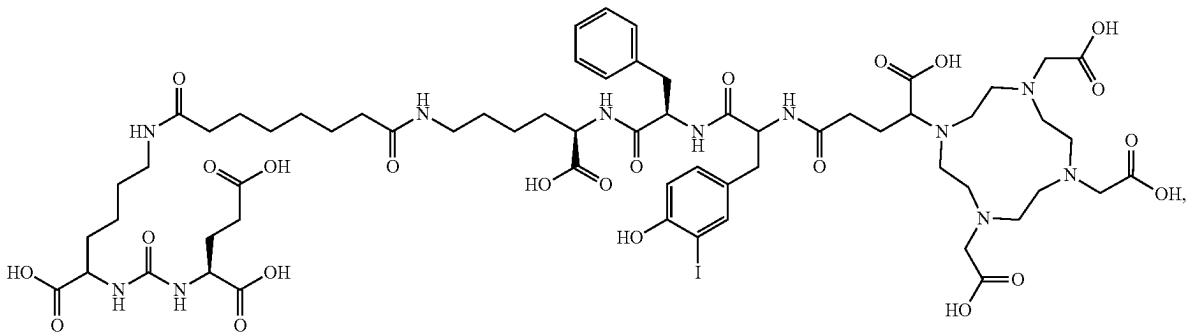
PSMA-617



or a pharmaceutically acceptable salt thereof. In certain embodiments, the radionuclide labelled PSMA binding agent comprises ^{68}Ga-PSMA-617, which is PSMA-617 labelled with ^{68}Ga, or a pharmaceutically acceptable salt thereof. In certain embodiments, the radionuclide labelled PSMA binding agent comprises ^{177}Lu-PSMA-617, which is PSMA-617 labelled with ^{177}Lu, or a pharmaceutically acceptable salt thereof.

In certain embodiments, the radionuclide labelled PSMA binding agent comprises PSMA-I&T:

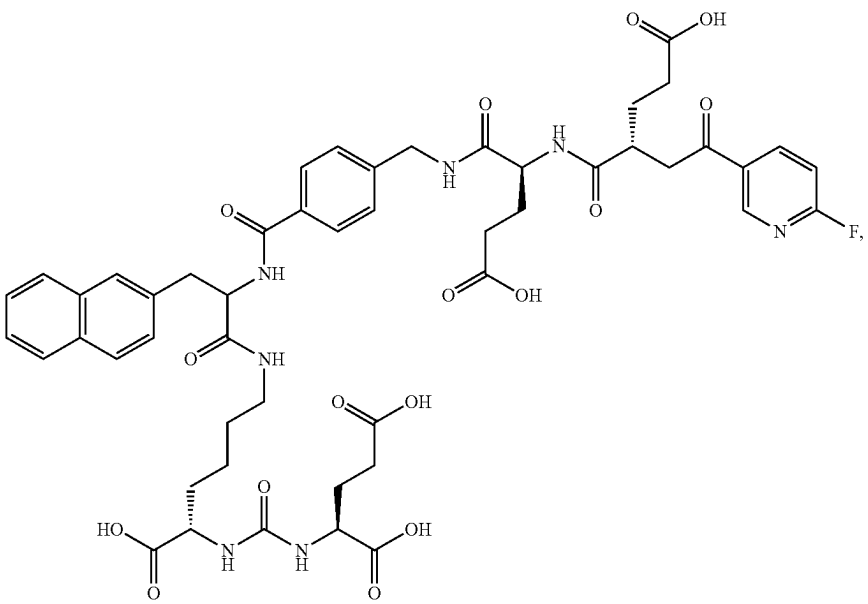
PSMA I&T



or a pharmaceutically acceptable salt thereof. In certain embodiments, the radionuclide labelled PSMA binding agent comprises ^{68}Ga-PSMA-I&T, which is PSMA-I&T labelled with ^{68}Ga, or a pharmaceutically acceptable salt thereof.

In certain embodiments, the radionuclide labelled PSMA binding agent comprises PSMA-1007:

PSMA-1007



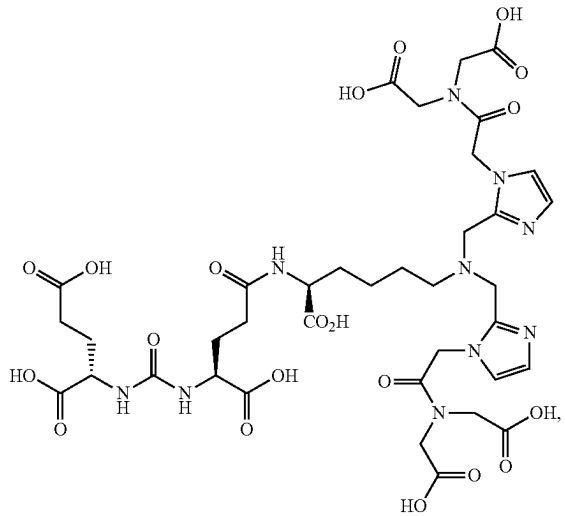
or a pharmaceutically acceptable salt thereof. In certain embodiments, the radionuclide labelled PSMA binding agent comprises ^{18}F-PSMA-1007, which is PSMA-1007 labelled with ^{18}F, or a pharmaceutically acceptable salt thereof.

ii. SPECT Imaging Radionuclide Labelled PSMA Binding Agents

In certain embodiments, the radionuclide labelled PSMA binding agent is a radionuclide labelled PSMA binding agent appropriate for SPECT imaging.

In certain embodiments, the radionuclide labelled PSMA binding agent comprises 1404 (also referred to as MIP-1404):

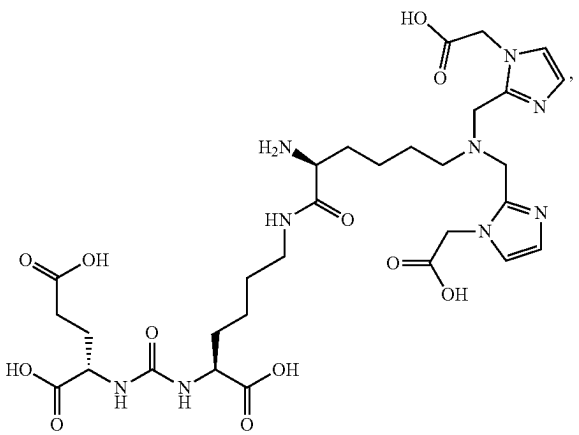
1404



or a pharmaceutically acceptable salt thereof.

In certain embodiments, the radionuclide labelled PSMA binding agent comprises 1405 (also referred to as MIP-1405):

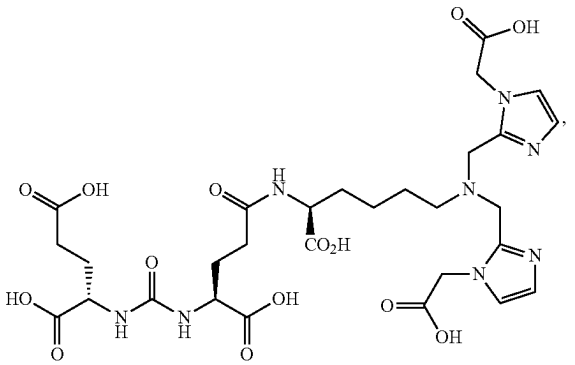
1405



or a pharmaceutically acceptable salt thereof.

In certain embodiments, the radionuclide labelled PSMA binding agent comprises 1427 (also referred to as MIP-1427):

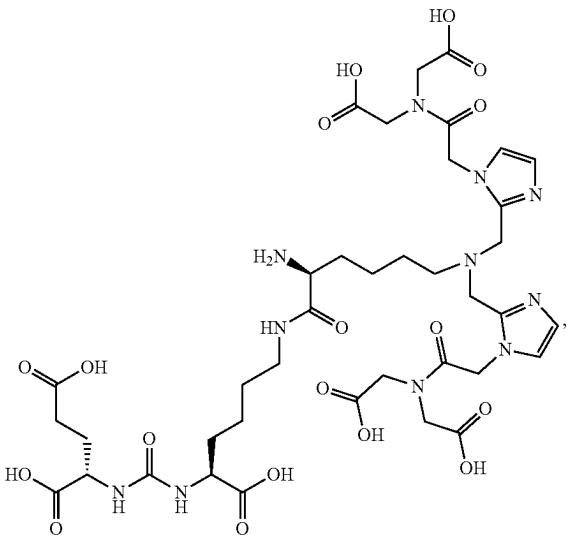
1427



or a pharmaceutically acceptable salt thereof.

In certain embodiments, the radionuclide labelled PSMA binding agent comprises 1428 (also referred to as MIP-1428):

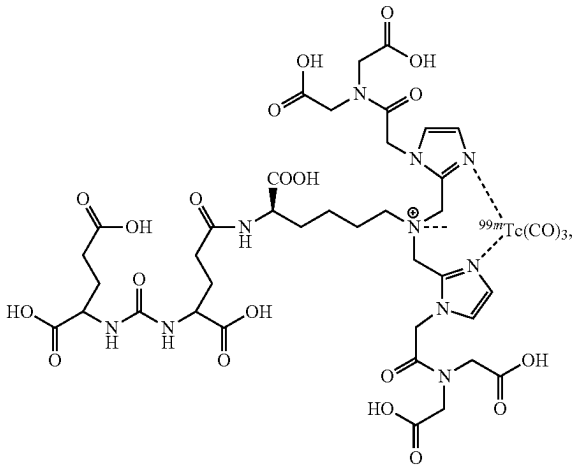
1428



or a pharmaceutically acceptable salt thereof.

In certain embodiments, the PSMA binding agent is labelled with a radionuclide by chelating it to a radioisotope of a metal [e.g., a radioisotope of technetium (Tc) (e.g., technetium-99m (^{99m}Tc)); e.g., a radioisotope of rhenium (Re) (e.g., rhenium-188 (^{188}Re); e.g., rhenium-186 (^{186}Re)); e.g., a radioisotope of yttrium (Y) (e.g., ^{90}Y); e.g., a radioisotope of lutetium (Lu) (e.g., ^{177}Lu); e.g., a radioisotope of gallium (Ga) (e.g., ^{68}Ga; e.g., ^{67}Ga); e.g., a radioisotope of indium (e.g., ^{111}In); e.g., a radioisotope of copper (Cu) (e.g., ^{67}Cu)].

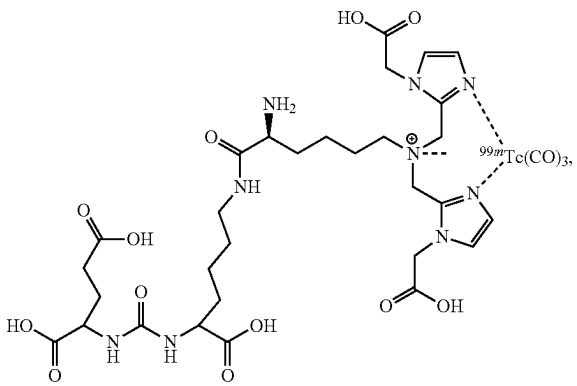
In certain embodiments, 1404 is labelled with a radionuclide (e.g., chelated to a radioisotope of a metal). In certain embodiments, the radionuclide labelled PSMA binding agent comprises ^{99m}Tc-MIP-1404, which is 1404 labelled with (e.g., chelated to) ^{99m}Tc:



^{99m}Tc-MIP-1404

or a pharmaceutically acceptable salt thereof. In certain embodiments, 1404 may be chelated to other metal radioisotopes [e.g., a radioisotope of rhenium (Re) (e.g., rhenium-188 (^{188}Re); e.g., rhenium-186 (^{186}Re)); e.g., a radioisotope of yttrium (Y) (e.g., ^{90}Y); e.g., a radioisotope of lutetium (Lu) (e.g., ^{177}Lu); e.g., a radioisotope of gallium (Ga) (e.g., ^{68}Ga; e.g., ^{67}Ga); e.g., a radioisotope of indium (e.g., ^{111}In); e.g., a radioisotope of copper (Cu) (e.g., ^{67}Cu)] to form a compound having a structure similar to the structure shown above for ^{99m}Tc-MIP-1404, with the other metal radioisotope substituted for ^{99m}Tc.

In certain embodiments, 1405 is labelled with a radionuclide (e.g., chelated to a radioisotope of a metal). In certain embodiments, the radionuclide labelled PSMA binding agent comprises ^{99m}Tc-MIP-1405, which is 1405 labelled with (e.g., chelated to) ^{99m}Tc:

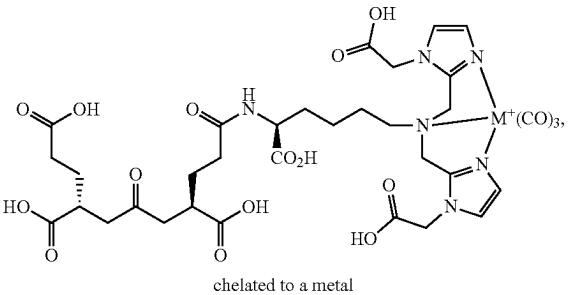


^{99m}Tc-MIP-1405

or a pharmaceutically acceptable salt thereof. In certain embodiments, 1405 may be chelated to other metal radioisotopes [e.g., a radioisotope of rhenium (Re) (e.g., rhenium-188 (^{188}Re); e.g., rhenium-186 (^{186}Re)); e.g., a radioisotope of yttrium (Y) (e.g., ^{90}Y); e.g., a radioisotope of lutetium (Lu) (e.g., ^{177}Lu); e.g., a radioisotope of gallium (Ga) (e.g., ^{68}Ga; e.g., ^{67}Ga); e.g., a radioisotope of indium (e.g., ^{111}In); e.g., a radioisotope of copper (Cu) (e.g., ^{67}Cu)] to form a compound having a structure similar to the structure shown above for ^{99m}Tc-MIP-1405, with the other metal radioisotope substituted for ^{99m}Tc.

In certain embodiments, 1427 is labelled with (e.g., chelated to) a radioisotope of a metal, to form a compound according to the formula below:

1427

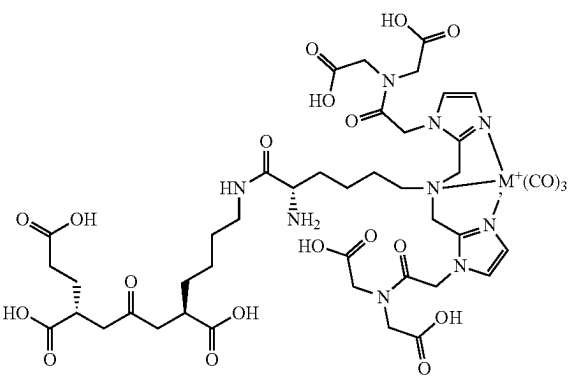


chelated to a metal

or a pharmaceutically acceptable salt thereof, wherein M is a metal radioisotope [e.g., a radioisotope of technetium (Tc) (e.g., technetium-99m (^{99m}Tc)); e.g., a radioisotope of rhenium (Re) (e.g., rhenium-188 (^{188}Re); e.g., rhenium-186 (^{186}Re)) e.g., a radioisotope of yttrium (Y) (e.g., ^{90}Y); e.g., a radioisotope of lutetium (Lu) (e.g., ^{177}Lu); e.g., a radioisotope of gallium (Ga) (e.g., ^{68}Ga; e.g., ^{67}Ga); e.g., a radioisotope of indium (e.g., ^{111}In); e.g., a radioisotope of copper (Cu) (e.g., ^{67}Cu)] with which 1427 is labelled.

In certain embodiments, 1428 is labelled with (e.g., chelated to) a radioisotope of a metal, to form a compound according to the formula below:

1428

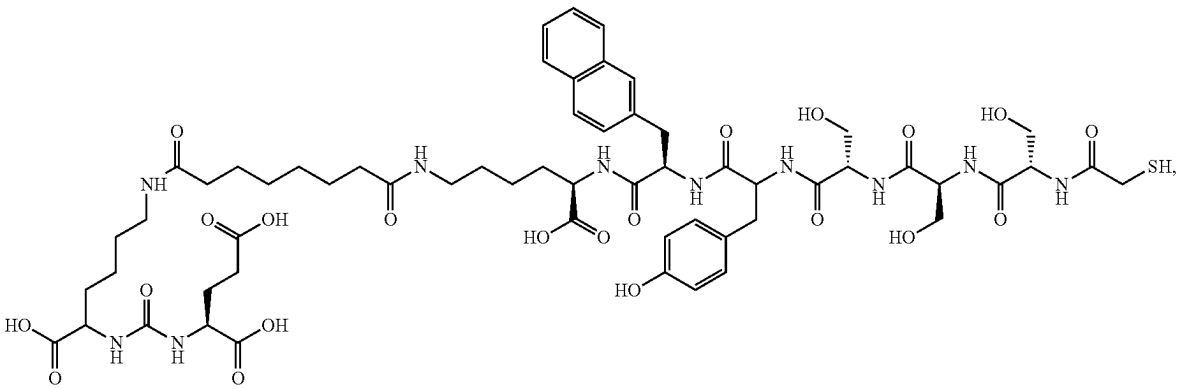


chelated to a metal

or a pharmaceutically acceptable salt thereof, wherein M is a metal radioisotope [e.g., a radioisotope of technetium (Tc) (e.g., technetium-99m (^{99m}Tc)); e.g., a radioisotope of rhenium (Re) (e.g., rhenium-188 (^{188}Re); e.g., rhenium-186 (^{186}Re)) e.g., a radioisotope of yttrium (Y) (e.g., ^{90}Y); e.g., a radioisotope of lutetium (Lu) (e.g., ^{177}Lu); e.g., a radioisotope of gallium (Ga) (e.g., ^{68}Ga; e.g., ^{67}Ga); e.g., a radioisotope of indium (e.g., ^{111}In); e.g., a radioisotope of copper (Cu) (e.g., ^{67}Cu)] with which 1428 is labelled.

In certain embodiments, the radionuclide labelled PSMA binding agent comprises PSMA I&S:

PSMA I&S



or a pharmaceutically acceptable salt thereof. In certain embodiments, the radionuclide labelled PSMA binding agent comprises ^{99m}Tc-PSMA I&S, which is PSMA I&S labelled with ^{99m}Tc, or a pharmaceutically acceptable salt thereof.

E. Computer System and Network Architecture

As shown in FIG. **17**, an implementation of a network environment **1700** for use in providing systems, methods, and architectures described herein is shown and described. In brief overview, referring now to FIG. **17**, a block diagram of an exemplary cloud computing environment **1700** is shown and described. The cloud computing environment **1700** may include one or more resource providers **1702***a*, **1702***b*, **1702***c* (collectively, **1702**). Each resource provider **1702** may include computing resources. In some implementations, computing resources may include any hardware and/or software used to process data. For example, computing resources may include hardware and/or software capable of executing algorithms, computer programs, and/or computer applications. In some implementations, exemplary computing resources may include application servers and/or databases with storage and retrieval capabilities. Each resource provider **1702** may be connected to any other resource provider **1702** in the cloud computing environment **1700**. In some implementations, the resource providers **1702** may be connected over a computer network **1708**. Each resource provider **1702** may be connected to one or more computing device **1704***a*, **1704***b*, **1704***c* (collectively, **1704**), over the computer network **1708**.

The cloud computing environment **1700** may include a resource manager **1706**. The resource manager **1706** may be connected to the resource providers **1702** and the computing devices **1704** over the computer network **1708**. In some implementations, the resource manager **1706** may facilitate the provision of computing resources by one or more resource providers **1702** to one or more computing devices **1704**. The resource manager **1706** may receive a request for a computing resource from a particular computing device **1704**. The resource manager **1706** may identify one or more resource providers **1702** capable of providing the computing resource requested by the computing device **1704**. The resource manager **1706** may select a resource provider **1702** to provide the computing resource. The resource manager **1706** may facilitate a connection between the resource provider **1702** and a particular computing device **1704**. In some implementations, the resource manager **1706** may establish a connection between a particular resource provider **1702** and a particular computing device **1704**. In some implementations, the resource manager **1706** may redirect a particular computing device **1704** to a particular resource provider **1702** with the requested computing resource.

FIG. **18** shows an example of a computing device **1800** and a mobile computing device **1850** that can be used to implement the techniques described in this disclosure. The computing device **1800** is intended to represent various forms of digital computers, such as laptops, desktops, workstations, personal digital assistants, servers, blade servers, mainframes, and other appropriate computers. The mobile computing device **1850** is intended to represent various forms of mobile devices, such as personal digital assistants, cellular telephones, smart-phones, and other similar computing devices. The components shown here, their connections and relationships, and their functions, are meant to be examples only, and are not meant to be limiting.

The computing device **1800** includes a processor **1802**, a memory **1804**, a storage device **1806**, a high-speed interface **1808** connecting to the memory **1804** and multiple high-speed expansion ports **1810**, and a low-speed interface **1812** connecting to a low-speed expansion port **1814** and the storage device **1806**. Each of the processor **1802**, the memory **1804**, the storage device **1806**, the high-speed interface **1808**, the high-speed expansion ports **1810**, and the low-speed interface **1812**, are interconnected using various busses, and may be mounted on a common motherboard or in other manners as appropriate. The processor **1802** can process instructions for execution within the computing device **1800**, including instructions stored in the memory **1804** or on the storage device **1806** to display graphical information for a GUI on an external input/output device, such as a display **1816** coupled to the high-speed interface **1808**. In other implementations, multiple processors and/or multiple buses may be used, as appropriate, along with multiple memories and types of memory. Also, multiple computing devices may be connected, with each device providing portions of the necessary operations (e.g., as a server bank, a group of blade servers, or a multi-processor system). Thus, as the term is used herein, where a plurality of functions are described as being performed by "a processor", this encompasses embodiments wherein the plurality of functions are performed by any number of processors (one or more) of any number of computing devices (one or more). Furthermore, where a function is described as being

performed by "a processor", this encompasses embodiments wherein the function is performed by any number of processors (one or more) of any number of computing devices (one or more) (e.g., in a distributed computing system).

The memory **1804** stores information within the computing device **1800**. In some implementations, the memory **1804** is a volatile memory unit or units. In some implementations, the memory **1804** is a non-volatile memory unit or units. The memory **1804** may also be another form of computer-readable medium, such as a magnetic or optical disk.

The storage device **1806** is capable of providing mass storage for the computing device **1800**. In some implementations, the storage device **1806** may be or contain a computer-readable medium, such as a floppy disk device, a hard disk device, an optical disk device, or a tape device, a flash memory or other similar solid state memory device, or an array of devices, including devices in a storage area network or other configurations. Instructions can be stored in an information carrier. The instructions, when executed by one or more processing devices (for example, processor **1802**), perform one or more methods, such as those described above. The instructions can also be stored by one or more storage devices such as computer- or machine-readable mediums (for example, the memory **1804**, the storage device **1806**, or memory on the processor **1802**).

The high-speed interface **1808** manages bandwidth-intensive operations for the computing device **1800**, while the low-speed interface **1812** manages lower bandwidth-intensive operations. Such allocation of functions is an example only. In some implementations, the high-speed interface **1808** is coupled to the memory **1804**, the display **1816** (e.g., through a graphics processor or accelerator), and to the high-speed expansion ports **1810**, which may accept various expansion cards (not shown). In the implementation, the low-speed interface **1812** is coupled to the storage device **1806** and the low-speed expansion port **1814**. The low-speed expansion port **1814**, which may include various communication ports (e.g., USB, Bluetooth®, Ethernet, wireless Ethernet) may be coupled to one or more input/output devices, such as a keyboard, a pointing device, a scanner, or a networking device such as a switch or router, e.g., through a network adapter.

The computing device **1800** may be implemented in a number of different forms, as shown in the figure. For example, it may be implemented as a standard server **1820**, or multiple times in a group of such servers. In addition, it may be implemented in a personal computer such as a laptop computer **1822**. It may also be implemented as part of a rack server system **1824**. Alternatively, components from the computing device **1800** may be combined with other components in a mobile device (not shown), such as a mobile computing device **1850**. Each of such devices may contain one or more of the computing device **1800** and the mobile computing device **1850**, and an entire system may be made up of multiple computing devices communicating with each other.

The mobile computing device **1850** includes a processor **1852**, a memory **1864**, an input/output device such as a display **1854**, a communication interface **1866**, and a transceiver **1868**, among other components. The mobile computing device **1850** may also be provided with a storage device, such as a micro-drive or other device, to provide additional storage. Each of the processor **1852**, the memory **1864**, the display **1854**, the communication interface **1866**, and the transceiver **1868**, are interconnected using various buses, and several of the components may be mounted on a common motherboard or in other manners as appropriate.

The processor **1852** can execute instructions within the mobile computing device **1850**, including instructions stored in the memory **1864**. The processor **1852** may be implemented as a chipset of chips that include separate and multiple analog and digital processors. The processor **1852** may provide, for example, for coordination of the other components of the mobile computing device **1850**, such as control of user interfaces, applications run by the mobile computing device **1850**, and wireless communication by the mobile computing device **1850**.

The processor **1852** may communicate with a user through a control interface **1858** and a display interface **1856** coupled to the display **1854**. The display **1854** may be, for example, a TFT (Thin-Film-Transistor Liquid Crystal Display) display or an OLED (Organic Light Emitting Diode) display, or other appropriate display technology. The display interface **1856** may comprise appropriate circuitry for driving the display **1854** to present graphical and other information to a user. The control interface **1858** may receive commands from a user and convert them for submission to the processor **1852**. In addition, an external interface **1862** may provide communication with the processor **1852**, so as to enable near area communication of the mobile computing device **1850** with other devices. The external interface **1862** may provide, for example, for wired communication in some implementations, or for wireless communication in other implementations, and multiple interfaces may also be used.

The memory **1864** stores information within the mobile computing device **1850**. The memory **1864** can be implemented as one or more of a computer-readable medium or media, a volatile memory unit or units, or a non-volatile memory unit or units. An expansion memory **1874** may also be provided and connected to the mobile computing device **1850** through an expansion interface **1872**, which may include, for example, a SIMM (Single In Line Memory Module) card interface. The expansion memory **1874** may provide extra storage space for the mobile computing device **1850**, or may also store applications or other information for the mobile computing device **1850**. Specifically, the expansion memory **1874** may include instructions to carry out or supplement the processes described above, and may include secure information also. Thus, for example, the expansion memory **1874** may be provide as a security module for the mobile computing device **1850**, and may be programmed with instructions that permit secure use of the mobile computing device **1850**. In addition, secure applications may be provided via the SIMM cards, along with additional information, such as placing identifying information on the SIMM card in a non-hackable manner.

The memory may include, for example, flash memory and/or NVRAM memory (non-volatile random access memory), as discussed below. In some implementations, instructions are stored in an information carrier. that the instructions, when executed by one or more processing devices (for example, processor **1852**), perform one or more methods, such as those described above. The instructions can also be stored by one or more storage devices, such as one or more computer- or machine-readable mediums (for example, the memory **1864**, the expansion memory **1874**, or memory on the processor **1852**). In some implementations, the instructions can be received in a propagated signal, for example, over the transceiver **1868** or the external interface **1862**.

The mobile computing device **1850** may communicate wirelessly through the communication interface **1866**, which

may include digital signal processing circuitry where necessary. The communication interface **1866** may provide for communications under various modes or protocols, such as GSM voice calls (Global System for Mobile communications), SMS (Short Message Service), EMS (Enhanced Messaging Service), or MMS messaging (Multimedia Messaging Service), CDMA (code division multiple access), TDMA (time division multiple access), PDC (Personal Digital Cellular), WCDMA (Wideband Code Division Multiple Access), CDMA2000, or GPRS (General Packet Radio Service), among others. Such communication may occur, for example, through the transceiver **1868** using a radio-frequency. In addition, short-range communication may occur, such as using a Bluetooth®, Wi-Fi™, or other such transceiver (not shown). In addition, a GPS (Global Positioning System) receiver module **1870** may provide additional navigation- and location-related wireless data to the mobile computing device **1850**, which may be used as appropriate by applications running on the mobile computing device **1850**.

The mobile computing device **1850** may also communicate audibly using an audio codec **1860**, which may receive spoken information from a user and convert it to usable digital information. The audio codec **1860** may likewise generate audible sound for a user, such as through a speaker, e.g., in a handset of the mobile computing device **1850**. Such sound may include sound from voice telephone calls, may include recorded sound (e.g., voice messages, music files, etc.) and may also include sound generated by applications operating on the mobile computing device **1850**.

The mobile computing device **1850** may be implemented in a number of different forms, as shown in the figure. For example, it may be implemented as a cellular telephone **1880**. It may also be implemented as part of a smart-phone **1882**, personal digital assistant, or other similar mobile device.

Various implementations of the systems and techniques described here can be realized in digital electronic circuitry, integrated circuitry, specially designed ASICs (application specific integrated circuits), computer hardware, firmware, software, and/or combinations thereof. These various implementations can include implementation in one or more computer programs that are executable and/or interpretable on a programmable system including at least one programmable processor, which may be special or general purpose, coupled to receive data and instructions from, and to transmit data and instructions to, a storage system, at least one input device, and at least one output device.

These computer programs (also known as programs, software, software applications or code) include machine instructions for a programmable processor, and can be implemented in a high-level procedural and/or object-oriented programming language, and/or in assembly/machine language. As used herein, the terms machine-readable medium and computer-readable medium refer to any computer program product, apparatus and/or device (e.g., magnetic discs, optical disks, memory, Programmable Logic Devices (PLDs)) used to provide machine instructions and/or data to a programmable processor, including a machine-readable medium that receives machine instructions as a machine-readable signal. The term machine-readable signal refers to any signal used to provide machine instructions and/or data to a programmable processor.

To provide for interaction with a user, the systems and techniques described here can be implemented on a computer having a display device (e.g., a CRT (cathode ray tube) or LCD (liquid crystal display) monitor) for displaying information to the user and a keyboard and a pointing device (e.g., a mouse or a trackball) by which the user can provide input to the computer. Other kinds of devices can be used to provide for interaction with a user as well; for example, feedback provided to the user can be any form of sensory feedback (e.g., visual feedback, auditory feedback, or tactile feedback); and input from the user can be received in any form, including acoustic, speech, or tactile input.

The systems and techniques described here can be implemented in a computing system that includes a back end component (e.g., as a data server), or that includes a middleware component (e.g., an application server), or that includes a front end component (e.g., a client computer having a graphical user interface or a Web browser through which a user can interact with an implementation of the systems and techniques described here), or any combination of such back end, middleware, or front end components. The components of the system can be interconnected by any form or medium of digital data communication (e.g., a communication network). Examples of communication networks include a local area network (LAN), a wide area network (WAN), and the Internet.

The computing system can include clients and servers. A client and server are generally remote from each other and typically interact through a communication network. The relationship of client and server arises by virtue of computer programs running on the respective computers and having a client-server relationship to each other.

In some implementations, the various modules described herein can be separated, combined or incorporated into single or combined modules. The modules depicted in the figures are not intended to limit the systems described herein to the software architectures shown therein.

Elements of different implementations described herein may be combined to form other implementations not specifically set forth above. Elements may be left out of the processes, computer programs, databases, etc. described herein without adversely affecting their operation. In addition, the logic flows depicted in the figures do not require the particular order shown, or sequential order, to achieve desirable results. Various separate elements may be combined into one or more individual elements to perform the functions described herein.

Throughout the description, where apparatus and systems are described as having, including, or comprising specific components, or where processes and methods are described as having, including, or comprising specific steps, it is contemplated that, additionally, there are apparatus, and systems of the present invention that consist essentially of, or consist of, the recited components, and that there are processes and methods according to the present invention that consist essentially of, or consist of, the recited processing steps.

It should be understood that the order of steps or order for performing certain action is immaterial so long as the invention remains operable. Moreover, two or more steps or actions may be conducted simultaneously.

While the invention has been particularly shown and described with reference to specific preferred embodiments, it should be understood by those skilled in the art that various changes in form and detail may be made therein without departing from the spirit and scope of the invention as defined by the appended claims.

While the invention has been particularly shown and described with reference to specific preferred embodiments, it should be understood by those skilled in the art that various changes in form and detail may be made therein

without departing from the spirit and scope of the invention as defined by the appended claims.

What is claimed is:

1. A method for automatically processing 3D images to automatically identify cancerous lesions within a subject, the method comprising:

(a) receiving, by a processor of a computing device, a 3D anatomical image of a subject obtained using an anatomical imaging modality, wherein the 3D anatomical image comprises a graphical representation of tissue within the subject;

(b) automatically identifying, by the processor, using one or more machine learning modules, for each of a plurality of target tissue regions, a corresponding target volume of interest (VOI) within the 3D anatomical image;

(c) determining, by the processor, a 3D segmentation map representing a plurality of 3D segmentation masks, each 3D segmentation mask representing a particular identified target VOI;

(d) receiving, by the processor, a 3D functional image of the subject obtained using a functional imaging modality;

(e) identifying, within the 3D functional image, one or more 3D volume(s), each corresponding to an identified target VOI, using the 3D segmentation map; and

(f) automatically detecting, by the processor, within at least a portion of the one or more 3D volumes identified within the 3D functional image, one or more hotspots determined to represent lesions based on intensities of voxels within the 3D functional image.

2. The method of claim **1**, comprising using, by the processor, the one or more detected hotspots to determine a cancer status for the subject.

3. The method of claim **1**, wherein the target tissue regions comprise one or more reference tissue regions and wherein the method comprises:

using the 3D segmentation map to identify, by the processor, within the 3D functional image, one or more 3D reference volume(s), each corresponding to a particular reference tissue region;

determining, by the processor, one or more reference intensity values, each associated with a particular 3D reference volume of the one or more 3D reference volume(s) and corresponding to a measure of intensity within the particular 3D reference volume;

determining, by the processor, one or more individual hotspot intensity values, each associated with a particular hotspot of at least a portion of the detected one or more hotspots and corresponding to a measure of intensity of the particular hotspot; and

determining, by the processor, one or more individual hotspot index values using the one or more individual hotspot intensity values and the one or more reference intensity values.

4. The method of claim **3**, wherein the reference tissue regions comprise one or more members selected from the group consisting of: a liver, an aorta, and a parotid gland.

5. The method of claim **2**, comprising, determining, by the processor, an overall index value indicative of a cancer status of the subject using at least a portion of the one or more hotspot index values.

6. The method of claim **5**, wherein the overall index value is determined as a weighted sum of at least a portion of the individual hotspot index values.

7. The method of claim **1**, wherein:

the 3D anatomical image is an x-ray computed tomography (CT) image, and

the 3D functional image is a 3D positron emission tomography (PET) image.

8. The method of claim **7**, wherein the 3D PET image of the subject is obtained following administration to the subject of a radiopharmaceutical comprising a prostate-specific membrane antigen (PSMA) binding agent.

9. The method of claim **8**, wherein the radiopharmaceutical comprises [^{18}F]DCFPyL.

10. A system for automatically processing 3D images to automatically identify cancerous lesions within a subject, the system comprising:

a processor of a computing device; and

a memory having instructions stored thereon, wherein the instructions, when executed by the processor, cause the processor to:

(a) receive a 3D anatomical image of a subject obtained using an anatomical imaging modality, wherein the 3D anatomical image comprises a graphical representation of tissue within the subject;

(b) automatically identify, using one or more machine learning modules, for each of a plurality of target tissue regions, a corresponding target volume of interest (VOI) within the 3D anatomical image;

(c) determine a 3D segmentation map representing a plurality of 3D segmentation masks, each 3D segmentation mask representing a particular identified target VOI;

(d) receive a 3D functional image of the subject obtained using a functional imaging modality;

(e) identify, within the 3D functional image, one or more 3D volume(s), each corresponding to an identified target VOI, using the 3D segmentation map; and

(f) automatically detect, within at least a portion of the one or more 3D volumes identified within the 3D functional image, one or more hotspots determined to represent lesions based on intensities of voxels within the 3D functional image.

11. The system of claim **10**, wherein the instructions cause the processor to use the one or more detected hotspots to determine a cancer status for the subject.

12. The system of claim **10**, wherein the target tissue regions comprise one or more reference tissue regions and wherein the instructions cause the processor to:

use the 3D segmentation map to identify, within the 3D functional image, one or more 3D reference volume(s), each corresponding to a particular reference tissue region;

determine one or more reference intensity values, each associated with a particular 3D reference volume of the one or more 3D reference volume(s) and corresponding to a measure of intensity within the particular 3D reference volume;

determine one or more individual hotspot intensity values, each associated with a particular hotspot of at least a portion of the detected one or more hotspots and corresponding to a measure of intensity of the particular hotspot; and

determine one or more individual hotspot index values using the one or more individual hotspot intensity values and the one or more reference intensity values.

13. The system of claim **12**, wherein the reference tissue regions comprise one or more members selected from the group consisting of: a liver, an aorta, and a parotid gland.

14. The system of claim 11, wherein the instructions cause the processor to determine an overall index value indicative of a cancer status of the subject using at least a portion of the one or more hotspot index values.

15. The system of claim 14, wherein the overall index value is determined as a weighted sum of at least a portion of the individual hotspot index values.

16. The system of claim 10, wherein:

the 3D anatomical image is an x-ray computed tomography (CT) image, and

the 3D functional image is a 3D positron emission tomography (PET) image.

17. The system of claim 16, wherein the 3D PET image of the subject is obtained following administration to the subject of a radiopharmaceutical comprising a prostate-specific membrane antigen (PSMA) binding agent.

18. The system of claim 17, wherein the radiopharmaceutical comprises [^{18}F]DCFPyL.

19. The method of claim 1, wherein the target tissue regions comprise one or more background tissue regions and wherein the method comprises:

at step (e), using the 3D segmentation map to identify, within the 3D functional image, as at least a portion of the one or more 3D volumes, one or more 3D background tissue volume(s), each corresponding a particular background tissue region; and

excluding voxels of the 3D within the 3D background tissue from the voxels used to automatically detect the one or more hotspots at step (f).

20. The method of claim 5, wherein:

the overall index value is associated with a particular target tissue region corresponding to a particular target VOI identified within the anatomical image; and

the overall index value is determined using hotspot index values of a subset of hotspots located within a particular 3D volume in the 3D functional image that corresponds to the particular identified target VOI.

21. The method of claim 20, wherein the particular target tissue region is selected from the group consisting of: a skeletal region comprising one or more bones of the subject, a lymph region, and a prostate region.

22. The method of claim 8, wherein the radiopharmaceutical comprises ^{68}Ga-PSMA-11.

23. The method of claim 8, wherein the radiopharmaceutical comprises ^{68}Ga-PSMA-617.

24. The method of claim 8, wherein the radiopharmaceutical comprises ^{68}Ga-PSMA-I&T.

25. The method of claim 8, wherein the radiopharmaceutical comprises ^{18}F-PSMA-1007.

26. The system of claim 10, wherein the target tissue regions comprise one or more background tissue regions and wherein the instructions cause the processor to:

at step (e), using the 3D segmentation map to identify, within the 3D functional image, as at least a portion of the one or more 3D volumes, one or more 3D background tissue volume(s), each corresponding a particular background tissue region; and

exclude voxels of the 3D within the 3D background tissue from the voxels used to automatically detect the one or more hotspots at step (f).

27. The system of claim 14, wherein:

the overall index value is associated with a particular target tissue region corresponding to a particular target VOI identified within the anatomical image; and

the overall index value is determined using hotspot index values of a subset of hotspots located within a particular 3D volume in the 3D functional image that corresponds to the particular identified target VOI.

28. The system of claim 26, wherein the particular target tissue region is selected from the group consisting of: a skeletal region comprising one or more bones of the subject, a lymph region, and a prostate region.

29. The system of claim 17, wherein the radiopharmaceutical comprises ^{68}Ga-PSMA-11.

30. The method of claim 17, wherein the radiopharmaceutical comprises ^{68}Ga-PSMA-617.

31. The method of claim 17, wherein the radiopharmaceutical comprises ^{68}Ga-PSMA-I&T.

32. The method of claim 17, wherein the radiopharmaceutical comprises ^{18}F-PSMA-1007.

* * * * *